~~CONFIDENTIAL~~

RM E54I07

NACA RM E54I07

UNCLASSIFIED

UNAVAILABLE

Downgraded at 3 year intervals
Declassified after 12 years

Stamped by auth. NASA ltr
dtd Aug. 9, 1963, s/ H.G. Maines

AGR-9-25-63

NACA

RESEARCH MEMORANDUM

ADAPTATION OF COMBUSTION PRINCIPLES TO AIRCRAFT PROPULSION

VOLUME I - BASIC CONSIDERATIONS IN THE COMBUSTION OF HYDROCARBON FUELS WITH AIR

By Fuels and Combustion Research Division

Lewis Flight Propulsion Laboratory
Cleveland, Ohio

Declassified by authority of NASA
Classification Change Notice
No. 113 dated June 28, 1967.

UNAVAILABLE

UNCLASSIFIED

CLASSIFIED DOCUMENT

This material contains information affecting the National Defense of the United States within the meaning of the espionage laws, Title 18, U.S.C., Secs. 793 and 794, the transmission or revelation of which in any manner to an unauthorized person is prohibited by law.

NATIONAL ADVISORY COMMITTEE
FOR AERONAUTICS

WASHINGTON
April 1, 1955

~~CONFIDENTIAL~~

UNCLASSIFIED

~~CONFIDENTIAL~~

UNCLASSIFIED

UNAVAILABLE

NASA Technical Library
3 1176 01435 7306

3073

ADAPTATION OF COMBUSTION PRINCIPLES TO AIRCRAFT PROPULSION

Vol. I - BASIC CONSIDERATIONS IN THE COMBUSTION OF HYDROCARBON FUELS WITH AIR

By Fuels and Combustion Research Division

Lewis Flight Propulsion Laboratory
Cleveland, Ohio

Edited by

Henry C. Barnett
Robert R. Hibbard

CLASSIFICATION CHANGED

To UNCLASSIFIED

By authority of NASA CCN 1113 Date 6-28-62
amp
7-31-67

GROUP 4
Downgraded at 3 year intervals;
declassified after 12 years

UNAVAILABLE

~~CONFIDENTIAL~~

UNCLASSIFIED

Technical information herein has been compiled from data of the NACA and other organizations. Data originating outside the NACA cannot be reproduced for further dissemination without the permission of the originating organization.

ADAPTATION OF COMBUSTION PRINCIPLES TO AIRCRAFT PROPULSION

FOREWORD

During the past ten years, investigations within the broad area of combustion research have been conducted by government, industry, and university. Much of this research has been sponsored and financed by the Federal Government, usually to further some application of combustion such as flight propulsion. As a result, extensive data have been published by a variety of sources. The greatest benefit can be derived by collecting, collating, and interpreting this information. Accordingly, the NACA has herein integrated and interpreted information on combustion with a view to its application to flight propulsion.

3073

The principal problem of interest in this study is that of burning fuel continuously and efficiently in a small volume and at high rates. Heat-release rates must be large and combustion efficiency nearly perfect in order to obtain high thrust and low specific fuel consumption from a small, lightweight engine. Wide ranges of speed, altitude, and climate are generally encountered in flight, and these factors often change rapidly. Thus, the combustion system must perform over wide ranges of fuel flow, inlet-air flow, pressure, and temperature.

In addition to burning fuel efficiently and at high rates, the performance required of a combustion system depends on the particular engine and its operation. In general, the following conditions are desirable: Pressure loss through the combustion system should be kept to a minimum, since high pressure loss causes increased engine specific fuel consumption. Mixing of burned and unburned gases upstream of the combustor outlet must provide a preferred temperature distribution at the outlet. This requirement may result either from turbine stress-strength considerations or from the need of a nearly uniform jet velocity profile for high propulsive efficiency. Deposition of coke and formation of smoke are both undesirable in the operation of combustors. Of the two factors, coke deposition presents the more serious problem because of its adverse effect on combustor performance and life. The combustion system should be durable, yet lightweight. Reliable ignition is also necessary. Unfortunately, some of these requirements are conflicting with respect to design. Specifically, then, the combustion problem for a high-performance aircraft engine such as the jet or turbine type arises from two factors: (1) the extreme range and rapid variations of operating conditions encountered, and (2) the many requirements of the combustor, some of which necessitate compromise in the design.

Many sources of basic and background information are available to the designer of high-speed combustion systems. The volume of literature concerning this subject, which was large before World War II, has since expanded tremendously with the expenditure of millions of dollars by the Federal Government. These funds have supported both fundamental and applied combustion research in laboratories throughout the nation.

A large number of recent research papers on the fundamentals of combustion are compiled in the Third and Fourth Symposia on Combustion published by the Williams & Wilkins Company; and there are a few very useful texts on basic aspects of combustion, such as Explosion and Combustion Processes in Gases by Jost, Combustion, Flames, and Explosions of Gases by Lewis and von Elbe, and Flames by Gaydon and Wolfhard. Much additional information exists in technical journals, symposia, and house organs such as progress reports on military projects.

Published information on the application of combustion research to flight propulsion is less comprehensive. Although many individual papers on the subject appear in the classified literature, there are only a few summary papers. Discussions relating combustion fundamentals to the problem of design principles for jet-engine combustors have appeared in NACA conferences for industry (e.g., NACA Conference on Turbojet Engines for Supersonic Propulsion, Oct. 8-9, 1953; NACA Conference on Supersonic Missile Propulsion, Mar. 13, 1952), but these discussions are necessarily brief. The Applied Physics Laboratory of Johns Hopkins University is summarizing and integrating its own information pertinent to ram-jet engine design. The Princeton University Press is preparing a twelve-volume treatise on High-Speed Aerodynamics and Jet Propulsion that will include a treatment of both basic and applied combustion, although it will be limited to the unclassified literature. 3073

As can be seen, no adequate summary of the source material on combustion is available to the flight-propulsion engineer. Such a summary should reduce design effort by organizing pertinent information on both basic and applied combustion and extracting those principles and ideas which are useful or significant in aircraft engine design. The purpose of this report is to present such a study.

First, several chapters review such fundamental processes as fuel-air mixture preparation, gas flow and mixing, flammability and ignition, flame propagation in both homogeneous and heterogeneous mediums, flame stabilization, combustion oscillations, and smoke and carbon formation. The practical significance and the relation of these processes to theory are presented. A second series of chapters describes the observed performance and design problems of engine combustors of the principal types. An attempt is made to interpret performance in terms of the fundamental processes and theories previously reviewed. Third, the design of high-speed combustion systems is discussed. Combustor design principles that can be established from basic considerations and from experience with actual combustors are described. Finally, future requirements for aircraft engine combustion systems are examined.

Certain limitations have been necessary. The references were selected from a complete review of the field in order to illustrate points that were pertinent to the subject at the date of writing. Thus, the references cited are a thorough bibliography, but not a complete one. Some important topics may have been omitted. Also, the study is one of air-breathing engines and hydrocarbon fuels; rocket engines and fuels other than hydrocarbons, such as the so-called high energy fuels, are considered outside the scope of this report.

Because of continuing progress both in fundamental combustion research and in the adaptation of combustion principles to aircraft propulsion, this report is not intended as a final summary of developments in the field; however, it may be of assistance in future work.

Walter T. Olson

TABLE OF CONTENTS

Chapter Page

I - ATOMIZATION AND EVAPORATION OF LIQUID FUELS I-1

INTRODUCTION I-1

SYMBOLS I-1

ATOMIZATION OF FUEL I-4
Basic Relations for Fuel Atomization I-4
Atomization theory I-4
Drop-size distribution in sprays I-8
Air Atomization I-11
Pressure-Atomizing Nozzles I-15
Summary Comments on Utility of Fuel-Atomization Data I-20

FUEL EVAPORATION I-21
Equilibrium Flash Vaporization I-21
Drop Evaporation into Static Surroundings I-23
Drop evaporation theory I-23
Evaporation into low-temperature surroundings I-24
Evaporation into high-temperature surroundings I-26
Drop Evaporation under Forced Convection I-26
Heat-transfer correlations I-27
Mass-transfer correlations I-29
Unsteady-State Drop Evaporation I-30
Additional Drop-Evaporation Considerations I-31
Drop Surface Temperature Determination I-32
Recommended Drop-Evaporation Relations I-32

EVAPORATION OF SPRAYS I-33
Theory I-33
Experiment I-33

SIGNIFICANCE OF ATOMIZATION AND EVAPORATION RESEARCH IN APPLICATION TO JET-ENGINE DESIGN I-34

REFERENCES I-36

II - FLOW AND MIXING PROCESSES IN COMBUSTION CHAMBERS II-1

INTRODUCTION II-1

SYMBOLS II-2

AERODYNAMIC FLOW II-8

COMBUSTOR APPROACH-STREAM PARAMETERS II-8
Turbojet Combustion Chambers II-8
Generalized parameters II-9
Compressor wake effects II-11
Ram-Jet Combustion Chambers - Generalized Parameters II-11

[redacted]

Chapter Page

COMBUSTOR PRESSURE LOSSES II-13
Effect on Over-All Cycle Performance II-13
Causes II-13
Changes in flow cross-sectional area due to expansion II-14
Changes in flow cross-sectional area due to contraction II-15
Body shape and blocked area II-15
Fluid friction II-16
Momentum II-18
Isothermal flow behind bluff bodies II-19
Flow behind bluff bodies with heat addition II-20
Eddy formation II-20
Estimation and Correlation II-21

AIR DISTRIBUTION II-23

GAS JETS II-24
Theoretical Background II-25
Free jets II-25
Coaxial jets II-31
Normal jets II-32
Multiple jets II-33
Experimental Data II-33
Free jets II-33
Coaxial jets II-37
Normal jets II-39
Oblique jets II-41
Multiple jets II-41
Orifice coefficients II-42

AERODYNAMIC MIXING II-45

DIFFUSION II-45
Fundamental Equations II-45
Empirical laws of heat, mass, and momentum transfer II-45
Differential equations of diffusion II-47
Homogeneous, Isotropic, Turbulent Fields II-48
Diffusion by continuous movements II-48
Correlation coefficient II-50
Turbulence spectrum II-52
Comparison of turbulent and molecular diffusion II-53
Generalized form of differential equations of diffusion II-54
Point source II-55
Standard square deviation II-57
Line, plane, surface, and volume sources II-57
Nonisotropic Turbulent Flow Fields II-58
Homogeneous fields II-58
Nonhomogenous fields II-58
Turbulent Flow Fields Containing Periodic Flow Fluctuations II-59
Superimposed discrete periodicities II-60
Superimposed velocity fluctuations with finite band width II-60
Summary II-61

Chapter Page

FUEL-AIR MIXING II-61
Experiments on Diffusion from Simple Point and Line Sources II-62
Fuel Droplet Trajectories and Impingement II-62
Turbulent Spreading of Evaporating Liquid Fuel Droplets from Fuel Injectors II-64
Combined Spreading of Liquid and Vapor Fuel in High-Velocity Air Streams II-66
Effect of Solid Boundaries and Flow-Area Changes on Fuel Spreading . II-69
Summary II-69

JET MIXING II-69

REFERENCES II-73

III - IGNITION AND FLAMMABILITY OF HYDROCARBON FUELS III-1

INTRODUCTION III-1

SYMBOLS III-2

FLAME QUENCHING III-3
Effect of Variables on Flame Quenching III-3
Geometry of quenching surface III-4
Hydrocarbon type III-4
Inert diluents III-4
Temperature III-5
Pressure III-5
Oxygen concentration III-6
Dead Space III-6
Homogeneous Quenching III-7
Interpretations of Wall Quenching III-8
Quenching in Flammability and Spark-Ignition Measurements III-11
Flammability measurements III-11
Spark-ignition energy measurements III-12

FLAMMABILITY LIMITS III-13
Effects of Variables on Flammability Limits at Atmospheric Pressure . III-13
Hydrocarbon type III-14
Petroleum fuels III-14
Mists and sprays III-15
Diluents III-16
Temperature III-17
Velocity and turbulence III-17
Effects of Variables on Flammability Limits at Nonatmospheric Pressures III-18
Hydrocarbon type III-19
Petroleum fuels III-19
Significance of Flammability Limits III-20
Limits of flame propagation III-20
True flammability limits III-20

Chapter Page

IGNITION III-21
Ignition by Heated Surfaces III-22
Mixture composition III-23
Ignition lag III-23
Heated spheres and rods III-23
Turbulence III-24
Surface condition and composition III-24
Surface area III-25
Fuel composition III-25
Pressure III-26
Diluents III-27
Ignition by Flames III-27
Pilot flames III-27
Propagating flames through constrictions III-28
Ignition by Hot Gases III-28
Heated air III-28
Vitiated air III-31
Ignition by Chemical Means III-32
Spontaneously flammable compounds III-33
Catalytic metals III-34
Ignition by Shock Waves III-35
Ignition by Capacitance Sparks III-37
Mixutre composition III-39
Fuel type III-40
Electrode spacing III-41
Electrode type III-41
Condenser voltage III-41
Spark duration III-41
Oscillation frequency III-41
Sparking rate III-42
Mixture velocity III-42
Turbulence III-43
Pressure III-43
Temperature III-45
Diluents III-46
Ignition by Inductance Sparks III-46
Mixture composition, pressure, and temperature III-46
Electrode spacing III-47
Electrode material III-47
Circuit inductance and voltage III-47
Current type III-48

SIGNIFICANCE OF BASIC QUENCHING, FLAMMABILITY, AND IGNITION DATA IN RELATION TO AIRCRAFT PROPULSION PROBLEMS III-48
Quenching III-48
Flammability III-49
Ignition III-49

REFERENCES III-50

3073

Chapter Page

IV - LAMINAR FLAME PROPAGATION IV-1

INTRODUCTION IV-1

SYMBOLS IV-1

CHARACTERISTICS OF LAMINAR FLAMES IV-4
Temperature Profile IV-4
Relation of Various Images to Temperature Profile IV-6
Luminous zone IV-6
Schlieren image IV-6
Shadow image IV-7

FLAME VELOCITY IV-8
Methods of Measuring IV-8
Stationary flame or burner IV-8
Transparent tube IV-12
Soap-bubble or constant-pressure bomb IV-13
Constant-volume bomb IV-14
Evaluation of methods IV-16
Effects of Chemical Variables IV-16
Fuel-oxidant ratio IV-16
Molecular structure of hydrocarbon IV-18
Additives, antiknocks, and fuel blending IV-19
Effects of Physical Variables IV-22
Pressure IV-22
Temperature IV-23
Electric fields IV-23
Acoustical and mechanical disturbances IV-24

THEORIES OF LAMINAR FLAME PROPAGATION IV-24
Comprehensive Equations IV-26
Approximate Equations IV-28
Thermal mechanism IV-28
Diffusional mechanism IV-33
Miscellaneous approximate equations IV-37
Evaluation of thermal and diffusional mechanisms IV-38

APPLICATION OF LAMINAR FLAME RESEARCH TO PRACTICAL COMBUSTION PROBLEMS . IV-40

REFERENCES IV-42

V - TURBULENT FLAMES V-1

INTRODUCTION V-1

SYMBOLS V-1

CHARACTERISTICS OF TURBULENT FLAMES V-3
Bunsen Flames V-3
Flame height V-3
Brush width V-3
Flames in Tubes V-4
Flames Supported on Rods (V-Flames) V-4

3073

Chapter Page

TURBULENT FLAME VELOCITY V-4
Measurement V-4
Open burner flames V-4
Flames in tubes V-5
Spherical flames V-5
Flames supported on rods (V-flames) V-5
Dependence of flame velocity on location of measurement V-6
Effects of Chemical Variables V-6
Fuel concentration V-6
Fuel type V-7
Effects of Physical Variables V-7
Pressure V-7
Temperature V-8
Velocity and turbulence promotion V-8

THEORIES OF TURBULENT FLAME PROPAGATION V-9
Turbulent Flames V-9
Damköhler theory V-9
Shelkin theory V-11
Delbourg theory V-12
Karlovitz theory V-14
Leason theory V-15
Scurlock and Grover theory V-16
Flame-Induced Turbulence V-19

APPLICABILITY OF TURBULENT FLAME STUDIES TO JET-ENGINE COMBUSTION V-20

REFERENCES V-21

VI - FLAME STABILIZATION VI-1

INTRODUCTION VI-1

SYMBOLS VI-1

STABILITY DIAGRAMS: VELOCITY-CONCENTRATION LIMITS VI-3
Open Flames with Secondary Air VI-3
Flames Deprived of Secondary Air VI-3

MECHANISMS OF FLAME STABILIZATION VI-4
Critical Boundary Velocity Gradient VI-4
Flames stabilized on burner VI-4
Flames supported on wires or rods VI-6
Penetration distance VI-6
Stabilization by Eddies VI-7

EFFECT OF VARIABLES ON STABILITY LIMITS VI-7
Flow Variables at Constant Pressure and Temperature VI-7
Characteristic dimension of burner or flame holder VI-7
Turbulence VI-9
Boundary-layer thickness VI-9
Electric fields VI-9
Acoustical disturbances VI-10

3073

[redacted]

Chapter Page

Pressure and Temperature Variation VI-10
Pressure VI-10
Mixture temperature VI-11
Liquid fuel VI-12
Flame-holder temperature VI-13
Chemical Variables VI-13
Fuel type VI-13
Additives and fuel blending VI-14
Water vapor VI-15
Diluent concentration VI-15

THERMAL THEORIES OF FLAME STABILIZATION VI-15
Burner Flames - Critical Boundary Velocity Gradients VI-15
Flames Supported on Flame Holders - Eddy Stabilization VI-17

NONISOTROPIC FLAMES VI-19
Cell Formation and Surface Break-Up of Open Flames VI-19
Cellular Flames in Tubes VI-20

SIGNIFICANCE OF FLAME STABILIZATION TO JET-ENGINE COMBUSTION VI-21

REFERENCES VI-24

VII - DIFFUSION FLAMES VII-1

INTRODUCTION VII-1

SYMBOLS VII-1

GASEOUS DIFFUSION FLAMES VII-3
Appearance VII-3
Structure VII-4
Laminar flames VII-4
Turbulent flames VII-5
Theory VII-5
Laminar flames VII-6
Turbulent flames VII-10
Effect of Variables on Flame Height VII-11
Laminar flames VII-11
Turbulent flames VII-14
Stability VII-15

LIQUID DIFFUSION FLAMES VII-16
Single Drop Combustion VII-16
Theory VII-16
Combustion in quiescent air VII-20
Combustion in air streams VII-22
Fuel Sprays and Mists VII-24
Theory of combustion VII-25
Experimental observation VII-25

APPLICABILITY OF RESEARCH DATA ON DIFFUSION FLAMES TO JET-ENGINE COMBUSTOR DESIGN VII-27

REFERENCES VII-28

3073

Chapter Page

VIII - OSCILLATIONS IN COMBUSTORS VIII-1

INTRODUCTION VIII-1

MODES OF OSCILLATION VIII-2
The Burner as a Resonant Room VIII-2
The Burner as a Helmholtz Resonator VIII-5
Systems of Oscillation with Nonacoustic Elements VIII-8

INTERACTIONS VIII-10
Elements Disturbed by Velocity and Pressure Oscillations VIII-10
Effects of Feedback Loops on Pressure and Velocity VIII-13

SIGNIFICANCE OF RESONANCE STUDIES IN DESIGN OF JET-ENGINE COMBUSTORS . VIII-14
Design Criteria Based on Mode of Resonance VIII-14
Design Criteria Based on Sensitivity of Disturbed Elements VIII-15
The Future for Combustion Oscillation VIII-15

REFERENCES VIII-16

IX - SMOKE AND COKE FORMATION IN THE COMBUSTION OF HYDROCARBON-AIR MIXTURES IX-1

INTRODUCTION IX-1

PHYSICAL AND CHEMICAL NATURE OF SMOKE AND COKE IX-2
Smoke IX-2
Coke IX-3

EFFECT OF OPERATING VARIABLES ON SMOKING TENDENCY IX-3
Burner Geometry IX-3
Diffusion flames IX-3
Bunsen flames IX-5
Fuel-Air Ratio IX-5
Diffusion flames IX-5
Bunsen flames IX-5
Temperature IX-6
Diffusion flames IX-6
Bunsen flames IX-6
Pressure IX-6
Diffusion flames IX-6
Bunsen flames IX-6

EFFECT OF FUEL VARIABLES ON SMOKING TENDENCY IX-7
Effect of Hydrocarbon Type on Diffusion Flames IX-7
Aromatics IX-7
Alkynes IX-8
Monoolefins IX-8
Diolefins IX-8
Cycloolefins IX-8
Paraffins IX-8
Cycloparaffins IX-8
Summary IX-9
Hydrocarbon blends and refinery streams IX-9

Chapter Page

Effect of Hydrocarbon Type on Bunsen Flames IX-9
Methods of Correlating Smoking Tendency with Hydrocarbon Structure in Diffusion Flames IX-10
Effect of Nonhydrocarbon Components IX-11
Diffusion flames IX-11
Bunsen flames IX-11
Effect of Additives IX-11
Diffusion flames IX-11
Bunsen flames IX-12

THEORIES OF SMOKE AND COKE FORMATION IX-12
Smoke IX-12
Coke IX-15

EFFECT OF SOLIDS ON RADIANT HEAT TRANSFER IX-16

SIGNIFICANCE OF BASIC SMOKE AND COKE STUDIES IN DESIGN OF JET-ENGINE COMBUSTORS IX-17

REFERENCES IX-17

APPENDIX - PHYSICAL AND COMBUSTION PROPERTIES OF SELECTED FUELS i

CHAPTER I

ATOMIZATION AND EVAPORATION OF LIQUID FUELS

By Charles C. Graves and Donald W. Bahr

INTRODUCTION

In both turbojet and ram-jet engines, the fuel is usually fed into the combustion chamber either as a well-atomized liquid spray or as a vapor (prevaporizing-type combustor). Accordingly, the formation of liquid sprays, the evaporation of both single drops and entire sprays, and the conditions required for various degrees of fuel flash vaporization are of interest to the combustion-chamber designer. Theoretical and experimental work on most of these factors is not sufficiently complete to permit much direct application to particular combustion chambers. However, even if used only in a qualitative sense, knowledge of the principles and trends involved is required for good combustion-chamber design.

The factors involved in the atomization and evaporation of liquid fuel are discussed herein primarily in their own light and not in relation to their effect on other processes contributing to over-all combustion-chamber performance. The application of this knowledge to actual combustion-chamber design is discussed in subsequent chapters. A detailed discussion of the mixing of the liquid and vapor fuel with the combustion air is presented in chapter II.

SYMBOLS

The following symbols are used in this chapter:

a	constant
b	constant
$b_{g,w}$	mass diffusion coefficient
$\bar{c}$	root mean square molecular velocity or surrounding fluid
c_p	specific heat at constant pressure
$\bar{c}_v$	root mean square molecular velocity of diffusing vapor
D_v	diffusion coefficient of vapor in surrounding fluid
d	drop diameter
d_{ab}	mean drop diameter
d_h	orifice diameter
d_j	diameter of undisturbed jet
d_m	mass or volume median drop diameter
d_t	air-atomizer throat diameter

d_{32}	Sauter mean drop diameter
F	flow number
F_v	ventilation factor
f	fuel-air ratio
g	gravitational constant
H	latent heat of vaporization
h	specific enthalpy
K	constant
l	mean free molecular path of surrounding fluid
M	molecular weight
m	constant
$\frac{dm}{dt}$	evaporation rate of drop
N	number of drops
Nu	Nusselt number for heat transfer
Nu'	Nusselt number for mass transfer
n	distribution constant
P	nozzle pressure drop
Pr	Prandtl number
p	ambient pressure
p_{BM}	log mean pressure of surrounding fluid
Q	volume-flow rate
q	constant
R	universal gas constant
Re	Reynolds number
$ReSc'$	$dU_r\rho_g/b_{g,w}$
R_s	weight fraction of fuel spray containing drops of diameter larger than d
r	radius
r_h	orifice radius
S	1/2 film thickness

3073

Sc	Schmidt number
T	static temperature
$T_{a,w}$	air temperature at which water has same drop-surface temperature as given liquid
T_{bp}	normal boiling point of evaporating liquid
t	time
t_o	breakup time of liquid jet
U_a	air velocity
U_r	relative velocity between drop and air or liquid film and air
U_{rc}	relative velocity between drop and air at instant of breakup
$U_{l,h}$	velocity of liquid at orifice
W	weight-flow rate
We	Weber number
x	fraction of fuel vaporized
$\bar{x}$	size constant in drop-distribution functions
x_m	maximum stable drop diameter
y	variable in logarithmic-normal distribution function
z	axial distance downstream of fuel injector
Z	$\mu_l/\sqrt{\rho_l \sigma d_j}$
α	accommodation coefficient
β	spray-cone angle
Γ	gamma function
$\varkappa$	thermal conductivity
λ	wavelength of surface disturbance
λ_{max}	wavelength of surface disturbance producing maximum film or jet instability
μ	absolute viscosity
ν	kinematic viscosity
ρ	density
σ	surface tension
ψ	distance between liquid surface and surface where diffusion starts

3073

Subscripts:

a	air
f	fuel
g	surrounding fluid
l	liquid
m	vapor-air mixture
o	drop surface
v	vapor
1	condition prior to vaporization
2	condition at end of vaporization
∞	infinite distance from drop

ATOMIZATION OF FUEL

Basic Relations for Fuel Atomization

Atomization theory. - In order to provide the rapid liquid fuel evaporation rates required in jet-engine combustors, the fuel must be finely atomized and well distributed. The mechanism of atomization is not well understood, and no general theory has been evolved to predict degree of atomization for particular nozzle designs, fuel properties, and operating conditions. However, a general picture of the atomization process can be drawn from considerable experimental work and some limited theoretical work performed in previous years.

The atomization of liquid fuel can be considered to occur in six steps:

(1) Stretching of fuel into sheets or streams as a result of accelerating the liquid through the nozzle orifice

(2) Appearance of small local ripples and protuberances at the liquid surface as a result of initial liquid turbulence and the action of the air on the liquid stream

(3) Formation of ligaments as a result of air pressure and shearing forces (ligaments are torn from main body of liquid or result from additional stretching of fuel sheets or streams)

(4) Collapse of ligaments into drops as a result of surface tension

(5) Further breakup of these drops

(6) Agglomeration of drops

Combinations of part or of all these steps would appear to occur whether atomization is effected by injecting fuel at high velocity into relatively quiescent air (pressure atomization) or by the action of a high-velocity air stream on a relatively

low-velocity fuel stream (air atomization). The relative importance of each step varies with application, depending upon such factors as relative velocity between fuel and air, and fuel-air ratio. The various factors involved in the atomization process might be best considered by following the changes occurring in atomization as the relative velocity between the fuel and the air is increased from low to high values.

Rayleigh (ref. 1) treated the effect of rotationally symmetric disturbances (fig. I-1(a)) on the breakup of a liquid jet. The flow was assumed to be incompressible and irrotational. It was shown that a liquid jet subject to surface disturbances becomes unstable when $\lambda/d_j > \pi$. Here, λ is the wavelength of the surface disturbance and d_j is the diameter of the undisturbed jet. The surface disturbances increase and finally result in the breakup of the jet into drops. When λ/d_j is equal to 4.51, the surface disturbances increase at the maximum rate and result in the maximum degree of jet instability. In experiments on a free-falling jet, Tyler (ref. 2) obtained a value for λ/d_j equal to 4.65. On the basis of these tests, Tyler concluded that the breakup of such jets occurs under the condition of maximum degree of instability as given by the Rayleigh theory.

Weber (ref. 3) extended the Rayleigh analysis to viscous liquids moving at low velocities. For the case where the air and fuel have the same velocity, the breakup time t_o of a liquid jet caused by rotationally symmetric disturbances (fig. I-1(a)) could be expressed by the equation

$$t_o = K\left[\left(\frac{\rho_l}{\sigma}\right)^{0.5} d_j^{1.5} + 3\left(\frac{\mu_l}{\sigma}\right) d_j\right] \tag{1}$$

where

d_j diameter of undisturbed jet

K constant

μ_l absolute viscosity

ρ_l liquid density

σ surface tension

The value of λ/d_j for the maximum degree of jet instability is given by the equation

$$\frac{\lambda_{max}}{d_j} = \pi\sqrt{2}\left[1 + 3\left(\frac{\mu_l^2}{\sigma\rho_l d_j}\right)^{\frac{1}{2}}\right]^{\frac{1}{2}} \tag{2}$$

From these equations, it can be seen that both breakup time and the optimum value of λ/d_j for breakup increase with increasing viscosity and decrease with increasing surface tension. The trends predicted by the Weber analysis (ref. 3) are in agreement with the experiments of Haenlein (ref. 4).

At higher relative velocities, wave formation (fig. I-1(b)) is encountered as a result of air effects. Weber showed that a minimum relative velocity must exist for the onset of wave formation. As this velocity is exceeded, the required distance for breakup decreases.

The various stages of atomization for simple jets were separated by Ohnesorge (ref. 5) into three groups, as shown in figure I-2. Here, a dimensionless parameter Z, equal to $\mu_l/\sqrt{\rho_l \sigma d_j}$, is plotted against the jet Reynolds number. In region I, the jet broke up in accordance with the Rayleigh-type disturbances (fig. I-1(a)). In region II, the jet breakup occurred in the form of helicoidal waves. In region III, complete disruption of the jet occurred at the orifice.

Jet breakup resulting from wave formation has also been considered for the case of swirl-type pressure-atomizing nozzles. For swirl-type nozzles operating under a moderate pressure differential, the liquid emerges from the orifice in the form of a conical film. Waves and holes appear in the film which eventually disintegrates to form the spray. Two theoretical investigations (refs. 6 and 7) have been made in an attempt to explain the breakup of the film as the result of wave formation. The analyses follow the classical treatments given by Lamb (ref. 8). Viscous, inertial, and gravitational forces are neglected. The flow is considered to be potential. The relative velocity between the film and surrounding medium is assumed constant and the film is treated as two-dimensional. Provided the film is flat (fig. I-3(a)), it is not subject to disturbing or restoring forces. However, if there is a slight surface bulge, the film is subject to both aerodynamic and surface-tension forces. At the bulge, a local decrease in pressure occurs which tends to increase the surface disturbance. This force is opposed by restoring forces resulting from surface tension. Under certain conditions, where aerodynamic forces predominate, the film becomes unstable and eventually breaks up. 3073

In reference 6, the analysis is concerned with film breakup resulting from antisymmetrical oscillations. For this type of oscillation, the cross section of the film is as shown in figure I-3(b). The thickness of the disturbed film is considered to be constant. It was found that the film is unstable for

$$We = \frac{\rho_l U_r^2 S}{\sigma} > 1 \tag{3}$$

where

S 1/2 film thickness

U_r relative velocity between film and air

We Weber number

For $We >> 1$, the wavelength λ of the surface disturbance resulting in maximum instability of the film is

$$\lambda_{max} = \frac{4\pi\sigma}{\rho_a U_r^2} \tag{4}$$

where ρ_a is the air density. Equation (4) can be expressed as

$$\frac{\lambda_{max}}{S} = \frac{4\pi}{We}\left(\frac{\rho_l}{\rho_a}\right) \tag{5}$$

Fair agreement was found between predicted and calculated values of λ_{max} obtained from photographs of swirl atomizer sprays (ref. 9). Symmetrical oscillations, in which the mean surface of the film remains flat, would also result in an unstable film. However, the degree of instability was stated to be much less than for the antisymmetrical oscillation considered in reference 6.

In reference 7, a similar type of analysis was made independently. In this treatment, the film cross section was considered to have the form shown in figure I-3(c). Only the upper surface of the film was considered to be disturbed. The case of exponential increase in wave amplitude was considered in detail.

At high relative velocities between liquid and air, complete disruption of the liquid jet occurs close to the fuel orifice and results in the formation of large numbers of drops. This type of atomization occurs particularly in the case of air atomization and is also found with pressure-atomizing nozzles operating under high injection-pressure differentials. An analytical study of this type of atomization was made by Castleman (ref. 10) who applied the Rayleigh analysis (ref. 1) to the case of air atomization in which ligaments are torn from the liquid jet surface. According to the Castleman picture of atomization, ligaments are drawn from the main mass and collapse, because of their instability, into a number of drops. At the higher air speeds, finer ligaments are formed which break up to form smaller drops. Higher surface tension would cause quicker collapse of the ligaments before they are drawn too finely and would result in larger drops. These trends are verified by experiment.

3073

At high relative velocities between fuel and air, the drops formed from the breakup of the ligaments, may, in turn, be broken up as a result of air effects. This mechanism was studied by Hinze (ref. 11) and Lane (ref. 12). Hinze showed that the criterion for drop breakup is the appropriate value of the Weber number We as given by

$$We = \frac{\rho_a U_r^2 d}{2\sigma} \tag{6}$$

where

d drop diameter

The predicted value of We for breakup varied between 6 for low-viscosity liquids and 10 for high-viscosity liquids for the case where the liquid drop is exposed suddenly to a constant-velocity air stream. Under most atomization conditions, however, the relative velocity between drop and air stream decreases rapidly. If the viscosity appreciably decreases the rate of drop deformation, the relative velocity may therefore be reduced below the critical value before the drop is appreciably deformed. Consequently, the critical initial value of velocity for drop breakup under actual atomizing conditions may be much higher than the steady-state critical velocity obtained from equation (6). In addition, the actual effect of drop viscosity on drop breakup may be much higher than that predicted from theory.

Lane (ref. 12) investigated the breakup of individual drops when exposed to steady and transient air streams. In one set of experiments, water drops having initial diameters ranging from 0.5 to 5.0 millimeters were dropped into a constant-velocity air stream. At a critical relative velocity between drop and air, the freely falling drops assumed the form of hollow bags which subsequently burst and produced a shower of drops. The relation between drop velocity and diameter at breakup could be expressed by the equation

$$U_{rc}^2 d = 612 \tag{7}$$

where

d drop diameter, mm

U_{rc} relative velocity between drop and air at instant of breakup, m/sec

Additional tests using liquids having surface tensions σ varying from approximately 28 to 475 dynes per centimeter established the relation

$$U_{rc} \propto \sqrt{\frac{\sigma}{d}} \tag{8}$$

These results are in agreement with the prediction of Hinze that drop breakup is associated with a critical value of Weber number. Experiments conducted with high-velocity transient air blasts showed that under these conditions thin layers were stripped from the drop surface before it was appreciably deformed. Drop-size measurements indicated that equation (7) would predict too great a rate of decrease in drop size at the very-high-velocity conditions. On the basis of the Hinze and Lane results, average spray drop size, as affected by drop breakup, would be expected to be larger for fuels having higher surface tensions and viscosities. The results might also be used to estimate maximum expected drop sizes to be obtained with air atomizers.

Collision of drops with resulting agglomeration may cause an appreciable increase in average drop size. Under the high turbulence levels in jet-engine combustors, the collision rate might be expected to be large, particularly where there is a large number of drops per unit volume of combustion space. Where pressure-atomizing nozzles are used, collisions also occur as a result of the difference in velocities of the various size drops. Under high nozzle-pressure-drop conditions, atomization occurs close to the nozzle orifice. Small drops decrease rapidly in velocity and tend to collect near the nozzle. The larger drops, which retain their velocity over longer distances, overtake and collide with smaller drops in their flight path.

The effect of agglomeration is indicated for pressure-atomizing nozzles from determination of mean drop sizes at various distances from the nozzle orifice (ref. 13). Agglomeration was believed to have caused the observed increase in mean drop size with increase in distance from the nozzle. In tests using the molten-wax method (ref. 14), agglomeration was found to be quite pronounced for low-cone-angle swirl nozzles operating at high-pressure drops.

The effect of agglomeration on mean drop size for the case of air atomization is suggested from the experiments described in references 15 and 16. In reference 15, it was found that the volume ratio of air to fuel had a pronounced effect on the Sauter mean diameter if the value of this ratio was less than 5000. For a hydrocarbon fuel sprayed into air at room temperature and pressure, this value corresponds to a fuel-air weight ratio of 0.012. Since fuel-air ratios near the fuel nozzles in turbojet and ram-jet engines can easily exceed this value, agglomeration may be an important factor in the determination of mean drop size. In reference 16, the volume median drop size for air atomization at sonic air velocities was found to be primarily a function of air-to-liquid mass-flow ratios.

Drop-size distribution in sprays. - One of the liquid fuel spray characteristics of direct interest to the combustion-chamber designer is the fractional weight of the spray distributed among the various drop sizes. Drop-size distribution relations have been used in the calculation of theoretical evaporation rates of liquid fuel sprays (ref. 17). Eventually, when the process of fuel spray evaporation is better understood, knowledge of drop-size distribution will be of use to the designer in the determination of fuel spray evaporation rates for particular designs and operating conditions.

A typical example of the drop-size distribution for a liquid fuel spray is shown in figure I-4(a). Here, the distribution is given in the cumulative mass-fraction form; that is, the weight fraction R_s of the total spray containing drops of diameter larger than d. In figure I-4(b), the same distribution is given in the differential form. Here, the area under the curve between two values of d represents the weight fraction of the total spray containing that particular range of drop diameters.

Since the theory of atomization is still not completely understood, recourse has been made to empirically fitted mathematical expressions for drop-size distributions, such as presented in table I-I. Four of the more well-known relations, Nukiyama-Tanasawa (ref. 15), Rosin-Rammler (ref. 18), logarithmic-normal (ref. 19) and upper-limit (ref. 20), are presented in table I-I. The relations are given in both the cumulative mass-fraction and differential forms. In addition, expressions are given for the Sauter mean diameter, one of the more common measures of mean drop size (ref. 20). The Sauter or surface mean diameter is the diameter of the drop having the same surface-to-volume ratio as the sum total of all drops in the spray.

3073

The general expression for a mean drop diameter d_{ab} is given by

$$d_{ab} = \left[\frac{\int_0^N d^a \, d(N)}{\int_0^N d^b \, d(N)}\right]^{\frac{1}{a-b}} = \left[\frac{\int_0^1 d^{a-3} \, d(R_s)}{\int_0^1 d^{b-3} \, d(R_s)}\right]^{\frac{1}{a-b}} \tag{9}$$

a,b constants

N number of drops

R_s weight fraction of fuel spray containing drops of diameter larger than d

For example, the Sauter mean diameter d_{32}, which involves a ratio of volume d^3 and surface d^2, is obtained by setting $a = 3$ and $b = 2$.

The median drop diameter d_m may also be used. Median drop diameters are defined as diameters dividing the spray into two equal parts, in terms of such properties as volume, surface area, or number. A commonly used median diameter is the mass or volume median.

The Rosin-Rammler expression (table I-I) is a special form of the more general Nukiyama-Tanasawa expression in which the exponents b and q have values such that the differential form is readily integrated to the cumulative mass-fraction form. Both the logarithmic-normal and upper-limit relations (see table I-I) use the following expression in the normal-probability distribution curve:

$$y = \ln [f(d)] \tag{10}$$

In the logarithmic-normal relation, $f(d)$ has the form $d/\bar{x}$, where $\bar{x}$ is a constant obtained from experimental data and is related to mean drop size. In the upper-limit relation, $f(d)$ has the form Kd/x_m-d, where K is a constant and x_m is the maximum stable drop diameter. This form of $f(x)$ was chosen in order to make the predicted frequency of distribution approach zero at a finite drop size, in accordance with experimental data.

With the exception of the logarithmic-normal relation, the expressions in table I-I are not based on a physical model of size reduction. Epstein (ref. 19) has shown that the size distribution of crushed solids approaches the logarithmic-normal distribution law asymptotically as the crushing process is continued, provided certain conditions of the breakup mechanism are satisfied. However, since none of the relations are derived on the basis of a physical model of the atomization of a fuel spray, the choice of which relation to use must depend upon the ability of the relation to represent accurately the experimental drop-size distribution data. In some cases, the choice based on accuracy of representation may be tempered by ease of use of the relation in application to such processes as fuel spray evaporation and combustion.

The expressions in table I-I require evaluation of two constants, one a measure of mean drop size and the other a measure of spray uniformity. The upper-limit equation requires evaluation of an additional constant, the maximum stable drop diameter. Determination of the constants in the relations of table I-I, as required for the best fitting of the relations to experimentally determined drop-size distributions, is readily accomplished by graphical methods. Functional scales are employed (e.g., probability paper) so that the data approximate a straight line when plotted. Values of the constants are obtained from the slopes and the intercepts of best straight-lines through the data. However, it is noted that the use of such graphical procedures may result in appreciable error (ref. 21).

Of the four relations in table I-I, the Rosin-Rammler expression is the easiest to use in the cumulative mass-fraction form. In this form, it is a simple exponential function, whereas the other relations require use of tables of the incomplete gamma function or probability integral. The upper-limit and logarithmic-probability relations have the simplest form in terms of the Sauter mean diameter. The upper-limit relation follows the trends of experimentally determined drop-size distribution data more closely in that it is based on the existence of a maximum stable drop diameter. While the other relations predict existence of drops of infinite diameter, the predicted frequency of occurrence of the larger-diameter drops becomes quite small. Accordingly, errors associated with the predicted occurrence of infinite-diameter drops may be insignificant for the case where such relations are used in theoretical analyses of fuel spray evaporation or combustion rates, particularly for the case of finely atomized sprays. Under these conditions, the Rosin-Rammler relation appears to be the most convenient to use. It should be noted, however, that appreciable differences between calculated and actual mean drop sizes may be encountered in the application of the first three relations of table I-I, particularly the Nukiyama-Tanasawa relation, to experimental drop-size distribution data (ref. 20). For example, the Nukiyama-Tanasawa relation may give a Sauter mean diameter larger than that of the largest drop found in the sample. References 20 to 22 give a more complete discussion of the application, advantages, and disadvantages of the relations of table I-I.

Several other methods of treating experimental drop-size distribution data have been reported in the recent literature. Since these methods have not had much use up to the present time, only a brief description will be given. In reference 23, an adjustment factor (a function of drop diameter) was applied to the logarithmic-normal relation to correct for deviation of the experimental data from the probability curve. The primary purpose of this adjustment factor appears to be correction for the deviation between the experimental and logarithmic-probability distribution in the larger drop-size ranges. In reference 24, for data from a pressure-atomizing nozzle, it was found that a plot of the square root of drop diameter gave a better straight-line plot on probability paper than a plot of the diameter to the first power. In reference 25, for data from an air-atomizing nozzle, the following distribution function gave satisfactory representation of the experimental data:

$$\frac{d(N)}{d(d)} = mNe^{-md} \tag{11}$$

where

d drop diameter

m constant

N number of drops counted

3073

Air Atomization

One of the most extensive series of experiments on air atomization was conducted by Nukiyama and Tanasawa (refs. 15 and 26 to 28). Drop-size distribution and average drop size were determined for a range of liquid properties, flow conditions, and atomizer sizes and configurations. With the exception of a few scattered tests, all data were obtained at subsonic air velocities. All tests were conducted with the atomizer exhausting into room air. Drop sizes were determined by collecting samples of the spray on small oil-coated glass slides. The experimental results were expressed in terms of the Sauter mean diameter d_{32} calculated directly from the data by the equation

$$d_{32} = \frac{\Sigma d^3 \Delta N}{\Sigma d^2 \Delta N} \tag{12}$$

where ΔN is the number of droplets having diameters between $d - \Delta d/2$ and $d + \Delta d/2$. The degree of accuracy of drop-size measurements was estimated to be on the order of ±15 percent.

In reference 26, experiments were conducted using water and a converging air nozzle as shown in figure I-5(a). The Sauter mean diameter was essentially independent of the size of the air and water nozzles for water-nozzle diameters from 0.2 to 1.0 millimeter and air-nozzle diameters from 2 to 5 millimeters. Transition from laminar to turbulent flow conditions in the water jet appeared to have little effect on drop size. The Sauter mean diameter was found to be a function of (1) the relative velocity U_r between water and air, and (2) the ratio of volume-flow rates of air and water Q_a/Q_l. The volume-flow rate of air was computed on the basis of the density at the throat of the air nozzle. The relative velocity U_r was calculated from the volume-flow rates and the cross-sectional areas at the throats of the water and air nozzles. Drop size decreased with increasing Q_a/Q_l. However, for $Q_a/Q_l > 5000$, the effect of Q_a/Q_l became negligible, and d_{32} was inversely proportional to the relative velocity.

In reference 27, similar experiments were conducted with water and two atomizers, as shown in figures I-5(b) and (c). The data covered a range of nozzle sizes and flow conditions. It was concluded that, providing the air velocity is based on the cross-sectional area of the vena contracta, there is no effect of atomizer configuration on average drop size. Relative position of the water and air nozzles had a negligible effect on average drop size, even when the water nozzle was well into the vena contracta region of the air jet. However, at greater distances downstream of the air jet where lower air velocities would exist, an increase in average drop size was obtained. The sizes of air and water nozzles were again found to have little effect on average drop size.

In reference 15, the Nukiyama-Tanasawa distribution function (table I-I) was developed and applied to data from references 26 and 27. For high values of Q_a/Q_l and U_r, the values of b and q in this relation were found to have values of 2 and 1, respectively, for all nozzles. At low values of either Q_a/Q_l or U_r, $b = 2$ and $q < 1$.

In reference 28, drop-size distributions and average drop sizes were determined for the nozzle type of figure I-5(c) over a range of atomizer sizes, flow conditions, and liquid properties. A range of liquid surface tensions σ from 30 to 73 dynes per centimeter, densities ρ_l from 0.8 to 1.2 grams per cubic centimeter, and viscosities μ_l from 0.01 to 0.3 poise were obtained by varying the proportions of an alcohol-glycerin-water solution. The effects of flow conditions and liquid properties on average drop size were correlated by the expression

$$d_{32} = 585 \frac{\sqrt{\sigma}}{U_r\sqrt{\rho_l}} + 597 \left(\frac{\mu_l}{\sqrt{\sigma\rho_l}}\right)^{0.45} \left(1000 \frac{Q_l}{Q_a}\right)^{1.5} \text{ microns} \tag{13}$$

where the fuel properties have the units given previously and U_r is in meters per second. The air velocity was calculated by assuming the vena contracta area to be 0.8 that of the air orifice. From this relation, it is seen that, for large values of Q_a/Q_l, atomization is a function of only relative velocity, surface tension, and liquid density. At lower values of Q_a/Q_l, drop size increases and liquid viscosity influences atomization.

The experiments of Nukiyama and Tanasawa did not cover the effects of gas properties on atomization. However, in reference 29, some limited experimental results are presented which indicate the general effect of gas temperature, viscosity, and density on median drop size for venturi atomizers. Comparison of data obtained with nitrogen and ethene as the atomizing gases indicated that at constant gas velocity, density, and ratio of liquid-to-gas volume-flow rate, a 60-percent decrease in gas viscosity resulted in approximately the same percentage increase in median diameter. The effect of gas density on atomization was indicated from comparison of data obtained with nitrogen and helium as the atomizing gases. At constant gas viscosity and ratio of liquid-to-gas volume-flow rates, a decrease in gas density at the atomizer throat from 1.18 to 0.169 gram per liter resulted in an approximately twofold increase in median drop diameter despite an increase in velocity. Results obtained with an exhaust-gas venturi atomizer indicated that at high liquid-to-gas volume-flow ratios, improved atomization would be expected with the use of high atomizing-gas temperatures. At low ratios of liquid-to-gas volume-flow rates, the improvement would be small. This result is consistent with trends suggested by consideration of the Nukiyama-Tanasawa drop-size correlation (eq. (8)) and effects of increased temperature on fuel viscosity. Heating of the fuel by the high-temperature atomizing gas would result in lowered fuel viscosity. As indicated by equation (8), this reduced viscosity would appreciably affect drop size only at the large ratios of liquid-to-gas volume-flow rates. The effect would be expected to be greater for liquids having high viscosity indices.

In reference 30, drop-size measurements were made for the atomization of molten sulfur in a venturi-type atomizer. A sketch of the atomizer is presented in figure I-6. The throat had a diameter of 0.25 inch. A flared diverging section was provided to reduce wall wetting. The air temperature for all experiments was held at approximately 293° F.

For subsonic throat velocities, the Sauter mean diameter d_{32} in microns was given by

$$d_{32} = \frac{26,100}{U_r} + 75 \left(1000 \frac{Q_l}{Q_a}\right)^{1.5} \tag{14}$$

where the volume-flow rate of air was based on conditions at the venturi throat. The Sauter mean diameter was given in terms of weight flow by

$$d_{32} = 687 \frac{\left(1.5 + \frac{W_l}{W_a}\right)}{W_a^{0.90}} \tag{15}$$

where U_r is in feet per second and W_a and W_l are the weight-flow rates of air and sulfur, respectively, in pounds per hour.

For a limited set of data at sonic throat velocities,

$$d_{32} = 29,900 \frac{\left(1.5 + \frac{W_l}{W_a}\right)}{W_a^{1.63}} \tag{16}$$

It was suggested that equations (15) and (16) could be applied to other atomizers by multiplying W_a and W_l for the new atomizer by $(0.25/d_t)^2$ where d_t is the new throat diameter in inches.

It was noted that the data at subsonic air velocities were in approximate agreement with the predictions of the Nukiyama-Tanasawa equation if approximate corrections were made for the effect of air temperature on atomization as found in reference 29.

Air atomization at sonic air velocities was also studied in reference 16. All tests were conducted for the atomizers exhausting to room air. Drop samples were collected by swinging a transparent, oil-coated plastic slide across the spray. The drop samples were analyzed by photomicrographing the slides and counting the number of drops contained within 5-micron intervals of drop diameter. Results were expressed in terms of the volume median drop diameter, that is, the drop diameter that divides the spray into two groups of equal volume. Three convergent nozzles and one divergent nozzle were tested. The three convergent nozzles were scaled in proportion, as indicated in figure I-7(a). A sketch of the divergent nozzle is shown in figure I-7(b).

The results of the tests for water atomization are presented in figure I-8, where the volume median diameter is plotted against the water-to-air weight-flow ratio. The atomization was found to be independent of either air pressure or water-flow rate for a constant value of water-to-air weight-flow ratio. The volume median diameter increased with increase in nozzle size and water-to-air weight-flow ratio. The nozzle-size effects were considered to be mainly a function of the air-orifice size. As indicated in figure I-8, the divergent nozzle produced larger median drop diameters than the convergent nozzle having the same throat diameter. This result might be attributed to wall wetting, since the divergent portion of the nozzle had a small included angle. It is noted that the results of reference 16 are not in accord with those of reference 30, where it was found that drop size was a function of air-flow rate as well as the ratio of liquid-to-air weight-flow rates.

Additional tests were conducted with the small convergent nozzle using ethylene glycol and a mixture of methanol and glycerin. The results are shown in figure I-9,

where volume median drop diameter is again plotted against the liquid-to-air weight-flow ratio. It is seen that use of ethylene glycol, a dense, viscous liquid, produced appreciably larger volume median drop diameters than water or the methanol-glycerin mixture. For purposes of comparison, the properties of the three liquids at the conditions used are also presented in figure I-9. On the basis of the results shown in figure I-9, viscosity is of greater importance than surface tension in the determination of the median drop size for sonic atomizers.

In figure I-10, the volume median drop diameter is plotted on log-log paper against the air-orifice diameter of the three convergent nozzles for several values of the ratio of water-to-air weight-flow rate. From the average value of the slopes of best straight lines through the data, the volume median drop diameter is approximately proportional to the 0.4 power of the air-orifice diameter. 3073

In reference 25, tests were conducted to determine flow characteristics and drop-size distribution for a particular design high-pressure air atomizer to be used with highly viscous fuels in gas-turbine combustors. The general features of the atomizer are presented in figure I-11(a). A high rotational speed was imparted to the air by means of the helical swirler in the inner body. Fuel entered the atomizing section in a radial direction through a narrow gap formed between the end of the inner body and the outer casing. This type of design presented the fuel as a thin film to a high-speed, swirling air stream. Tests were made for two fuel-gap widths (0.005 and 0.010 in.), air pressures from 20 to 100 pounds per square inch gage, and fuel pressures from 10 to 50 pounds per square inch gage. All data were obtained with the atomizer exhausting to room air. Drop sizes were determined by the molten-wax method, with the wax preheated to simulate fuels having kinematic viscosities of 10 and 20 centistokes, respectively. In order to minimize effects of changes in viscosity with cooling on the initial phase of atomization, the supply temperatures of the atomizing air and wax were held at the same value. The experimental drop-size data were satisfactorily represented by equation (11). Although the information obtained was insufficient to determine definite correlations, the data indicated that average drop size increased with (1) increase in fuel flow, (2) decrease in air flow, (3) increase in fuel gap, and (4) increase in fuel viscosity. It is noted that the range of ratios of fuel-to-air mass-flow rates were appreciably larger (0.8 to >400) than those investigated in reference 16 (0.1 to 0.9).

In reference 31, additional tests were conducted on a larger version of the N.G.T.E. air-blast atomizer of reference 25. A sketch of the larger atomizer is presented in figure I-11(b). There is some difference in the general features of the two atomizers of figure I-11. However, the actual atomizing sections were considered to have sufficient geometric similarity to permit some confidence to be placed on conclusions as to the effect of atomizer size on mean drop size. The experimental drop-size data were again found to be satisfactorily represented by equation (11).

In figure I-12, the data of reference 31 are plotted as the Sauter mean diameter against fuel-air ratios for fuel viscosities of 20 and 40 centistokes. An approximate correlation is indicated. However, it was noted in reference 31 that, at a given fuel-air ratio, smaller mean drop sizes were obtained at the higher fuel- (or air-) flow rates. This trend is in agreement with the results obtained in reference 30.

From comparison of the drop-size data obtained with the 1/4- and 1/8-inch-orifice-diameter atomizers, it was concluded that mean drop size was approximately proportional to the square root of the air-orifice diameter. This is in reasonable agreement with the data obtained in reference 16 (see fig. I-10).

3073

Pressure-Atomizing Nozzles

The consideration of pressure-atomizing nozzles in this section is limited to the centrifugal-type, continuous-spray nozzle. This type of nozzle, which is widely used in gas-turbine combustors, can produce well-atomized sprays without the high efflux velocities and, hence, long penetration distances of the simple-orifice nozzles such as used in Diesel engines. In addition, its wide dispersion of fuel is conducive to better mixing of fuel and air.

Unfortunately, much of the experimental work on fuel sprays reported in the literature has been concerned with the intermittent fuel spray of the Diesel engine. It is only within recent years that much work has been devoted to the swirl-type nozzle as a result of the impetus given by its use in aircraft gas-turbine combustors and for such industrial purposes as spray drying. The two general types of the fixed-configuration centrifugal pressure-atomizing nozzle used might be classified as the grooved-core and the whirl-chamber types. In the grooved-core-type nozzle, the swirl required for the hollow-cone spray is obtained by using spiral grooves in the nozzle insert. In the whirl-chamber-type nozzle, this swirl is imparted by injecting the liquid tangentially into a whirl chamber. The major portion of data reported on drop-size distribution has been obtained with the whirl-type nozzle. With the exception of some limited data on the spill-flow nozzle (refs. 32 and 33), no published data are available for wide-flow-range nozzles such as the duplex and variable-area atomizers.

It is emphasized that only a few of the investigations have been of such scope as to offer hope of predicting reasonably accurate atomization characteristics for nozzles, fuels, or operating conditions other than the particular ones tested. Appreciably different variation in trends and, sometimes, opposite trends have been obtained or suggested by different investigators. In addition, all values for average drop size and spray uniformity for centrifugal atomizers have been obtained for fuel injected into quiescent air at room temperature and pressure. Under actual combustor conditions, the fuel spray is generally subjected to a blast of highly turbulent hot gases covering a range of pressure, temperatures, and velocities. Quantitative knowledge of the effect of such variables on fuel sprays from swirl-type nozzles is lacking. However, some trends may be assumed from results of several of the investigations reported in the literature. In general, data available in the literature on fuel sprays is sufficient to give the combustor designer a rough idea of the spray-atomization characteristics required for fuel-spray-burning and evaporation-rate calculations.

An extensive study of atomization for centrifugal pressure nozzles operating with fuel oil was made by Longwell (ref. 34). Drop-size distribution was determined by freezing part of the spray and sieving drops into various size groups. The drop-size distribution data were correlated by the following equations:

$$d_m = \frac{0.72 \times 10^4 \, r_h}{\sin \frac{\beta}{2}} \frac{e^{0.70\,v}}{p^{0.37}} \tag{17}$$

$$R_s = e^{-0.693\left(\frac{d}{d_m}\right)^n} \tag{18}$$

where

d drop diameter, microns

d_m mass median drop diameter, microns

n distribution constant

P nozzle pressure drop (50 to 300 lb/sq in.)

R_s fractional weight of spray containing drops of diameter larger than d

r_h nozzle-orifice radius, cm (0.04 to 1.4)

β spray-cone angle (60° to 120°)

ν kinematic viscosity, cm^2/sec (0.08 to 0.8)

A plot of the distribution constant is presented in figure I-13. The distribution constant is a measure of the weight fraction of the spray contained within a given range of drop diameters about the most probable drop diameter. Larger values of n are associated with large fractions of the spray contained within the given drop-size range and consequently with a more uniform spray.

Several correlations have been presented that were based on drop-size data obtained by Bowen and Joyce with the molten-wax method (ref. 35). Needham (ref. 32) obtained the following correlations:

(1) For Joseph Lucas and Company simplex atomizers of optimum cone angle (80° to 90°), pressure drops from 6 to 125 pounds per square inch, flow numbers from 0.5 to 4.15, and a molten-wax viscosity of 2.2 centistokes,

$$\bar{x} = 270 \frac{W_l^{0.25}}{P^{0.4}} \text{ microns} \tag{19}$$

$$d_{32} = 182 \frac{W_l^{0.25}}{P^{0.4}} \text{ microns} \tag{20}$$

where

W_l flow rate, lb/hr

$\bar{x}$ size constant in Rosin-Rammler distribution function (table I-I)

(2) For a limited set of data with a Power Jets Limited spill flow atomizer,

$$\bar{x} = 510 \frac{W_l^{0.3}}{P^{0.5}} \text{ microns} \tag{21}$$

$$d_{32} = 360 \frac{W_l^{0.3}}{P^{0.5}} \text{ microns} \tag{22}$$

From a dimensional analysis and the correlation based on the Lucas atomizers, Needham suggested a general relation for particle size given by

$$\text{Average drop size} \propto \frac{d_h^{0.5}\ \mu_l^{0.45}\ \sigma^{0.05}}{P^{0.275}\ \rho_l^{0.225}} \tag{23}$$

where d_h is the nozzle-orifice diameter. This relation was not verified experimentally.

Hopkins (ref. 14) used dimensional analysis to obtain the following dimensionless relation:

3073

$$\bar{x} = \frac{\mu_l^2}{\rho_l \sigma} f\left(\frac{d_h U_{l,h}}{\mu_l}, \frac{\sigma}{\mu_l U_{l,h}}, \beta\right) \tag{24}$$

where

d_h orifice diameter

$U_{l,h}$ velocity of liquid at orifice

β spray cone angle

The Needham correlation (ref. 32) was considered to be a special case of this relation. No experimental verification of the relation was given.

In reference 36, the drop-size data for two Monarch nozzles having rated capacities of 3.0 and 17.5 gallons per hour were correlated in terms of the Rosin-Rammler distribution function. Molten wax, simulating kerosene, was sprayed into room air. Nozzle pressure drops ranged from 25 to 150 pounds per square inch. Drop sizes were determined by measuring photographs of representative samples of the solidified droplets. The final results were expressed by the following equations:

3.0-gallon-per-hour Monarch nozzle,

$$\bar{x} = 494\ P^{-0.368}\ \text{microns} \tag{25}$$

$$d_{32} = 392\ P^{-0.368}\ \text{microns} \tag{26}$$

17.5-gallon-per-hour Monarch nozzle,

$$\bar{x} = 342\ P^{-0.17}\ \text{microns} \tag{27}$$

$$d_{32} = 251\ P^{-0.17}\ \text{microns} \tag{28}$$

The spray cone angles of the nozzles were not reported.

Bowen and Joyce (ref. 35) obtained correlations based on the complete set of molten-wax data up to that time. All the data were obtained with the molten wax having a viscosity simulating that of kerosene (approximately 2.0 centistokes). The major portion of the data was obtained with Joseph Lucas and Company whirl-type centrifugal atomizers. The general features of the swirl chambers of these atomizers are given in reference 37. The following correlations were given:

$$\log d_{32} = 2.6164 - (0.3712 - 0.0258\ F) \log P \tag{29}$$

$$\log \bar{x} = (2.7008 + 0.02162\ F) - (0.3358 - 0.02427\ F) \log P \tag{30}$$

where

F flow number; equals 1.2 times nozzle output in gal/hr divided by square root of pressure drop in lb/sq in.; usually determined at a nozzle pressure drop of 100 lb/sq in.

The distribution constant n in the Rosin-Rammler distribution law (table I-I) can be obtained from the equation

$$\log \left[\Gamma \left(1 - \frac{1}{n}\right)\right] = \log \bar{x} - \log d_{32} \tag{31}$$

where

Γ gamma function

The effects of cone angle on atomization were not appreciable for pressure drops above approximately 30 pounds per square inch. For low pressure drops (approximately 10 lb/sq in.) and for cone angles less than approximately 75°, there was a rapid increase in drop size with decrease in cone angle. Cone-angle effects predominated in this operating region. Use of the preceding relations for estimates of atomization in the low-pressure-drop range was recommended only for atomizers of optimum cone angle. The relations would give too low an estimate of drop size for narrow-cone-angle atomizers in this region. No estimate of the accuracy of the correlations was given.

In reference 38, the drop-size data considered by Bowen and Joyce (ref. 35) was reanalyzed using the multiple-regression technique. An equation for the Sauter mean diameter of the form used by Bowen and Joyce was obtained and is given by

$$\log d_{32} = 2.6447 - (0.3970 - 0.03153\ F) \log P \tag{32}$$

This equation gave an accuracy of ±22.9 percent.

The data were also correlated in terms of an equation of simpler form given by

$$\log d_{32} = 2.6219 - 0.3395 \log P + 0.1979 \log F \tag{33}$$

This equation gave an accuracy of ±23.3 percent. An additional correlation including the effects of cone angle was given by

$$\log d_{32} = 3.5060 - 0.5853 \log P + 0.08171 \log F + 0.02331\ F \log P - 0.01743\ \beta + 0.00008236\ \beta^2 + 0.002467\ \beta \log P \tag{34}$$

β cone angle, deg

This equation gave an accuracy of ±18.1 percent. Use of this complicated equation was not considered warranted except under exceptional circumstances.

All the data of Joyce and Hopkins considered in the foregoing correlations were obtained for a molten-wax viscosity of approximately 2.0 centistokes. However, Joyce (ref. 39) has presented a graph giving the results of some preliminary tests on the effect of viscosity on surface mean diameter. At a nozzle pressure drop of 100 pounds per square inch, an increase in kinematic viscosity from 2 to 18.5 centistokes increased the surface mean diameter from approximately 97 to 140 microns.

3073

A study of spatial spray distribution, drop-size distribution, and capacity of centrifugal pressure-atomizing nozzles was reported by Tate and Marshall (ref. 24). The drop-size distribution data were obtained with grooved-core-type commercial nozzles and dyed water. Spray samples were collected in glass-bottom collecting cells filled with a solution immiscible with water. Drop sizes were determined from a visual count of photomicrographs of the samples. Mean drop size and spray uniformity were expressed in terms of orifice diameter and calculated tangential and vertical velocities of the sprayed liquid. These velocity components were "superficial average" velocities, the tangential component being based on conditions just upstream of the orifice, and the vertical component on the assumption of a full-flowing orifice. Graphs and equations were presented that permit the calculation of drop-size distribution for the particular nozzles and operating conditions investigated. A method was suggested that might permit use of the correlation for whirl-chamber-type centrifugal nozzles. However, no confirmation of this method was given. No data were obtained to permit estimation of drop-size distribution for liquids other than water. However, a limited set of data was obtained giving the effect of viscosity on mean drop size for one grooved-core nozzle operating at constant pressure. When kinematic viscosity was increased from 1 to 7 centistokes, mean drop size increased from approximately 54 to 78 microns. The relation of Longwell (ref. 34) for the effect of pressure drop, orifice diameter, cone angle, and viscosity on mean drop size did not fit the data obtained in this investigation (ref. 24).

Turner and Moulton (ref. 23) obtained drop-size distribution data for several commercial grooved-core and whirl-chamber-type centrifugal pressure nozzles. Organic materials that solidified well above room temperature were sprayed into room air. The solidified droplets from the entire spray were collected, and a representative sample was analyzed by visual count under high magnification. Graphs and equations are presented (ref. 23) that permit calculation of drop-size distribution for the particular nozzles and operating conditions investigated. Data were obtained over a limited range of surface tensions and viscosities. The data indicated that mean drop size was proportional to (1) surface tension to powers from approximately 0.6 to 1.0, (2) viscosity to the 0.25 power or less, (3) weight-flow rate to the -0.38 to -0.58 power, and (4) orifice diameter to approximately the 1.5 power. The effect of liquid density on atomization was not determined. If the correlation is expressed in terms of injection pressure differential as a variable, the mean drop size would be approximately proportional to the square root of the orifice diameter, a result in agreement with references 32 and 35. The correlations of reference 23 predict surface tension effects that are appreciably greater than expected (e.g., ref. 39). However, in reference 40, tests on a swirl-type pressure atomizer indicated that the changes in surface tension to be found among the various hydrocarbon-type fuels would have a negligible effect on average drop size. Viscosity was considered to be the dominant fuel property in the determination of fineness of atomization. Since the tests covered a three-fold change in surface tension, the conclusions of reference 40 appear to be more justified than those of reference 23, which were based on data for a very small change in surface tension.

In reference 41 some drop-size measurements are reported for hollow-cone and solid-cone commercial nozzles spraying into room air. Water was used for all tests. With one exception, the nozzle-pressure drop was 50 pounds per square inch. Spray samples were collected on greased glass slides and were photographed and measured under magnification. Reasonable agreement was found between the observed drop-size distribution and values obtained by other investigators (ref. 42) with the same type nozzles. The results indicated no significant difference in mean drop sizes produced by the hollow-cone and solid-cone-type nozzles. On the basis of the combined data for both type nozzles, it was concluded that the mass median diameter was approximately proportional to the orifice diameter. This would be in agreement with the conclusion of Longwell (ref. 34). However, it is noted that, if the data were restricted to those obtained with the hollow-cone nozzles, the mass median diameter would be approximately proportional to the 0.6 power of the orifice diameter, a result similar to that reported in references 23, 32, and 35.

The major portion of the drop-size distribution data for centrifugal pressure-atomizing nozzles was obtained by some version of the molten-wax method. In this method, a wax or other material that melts well above room temperature is sprayed into room air. By appropriate choice of material and preheat temperature, the initial viscosity of the sprayed liquid at the nozzle can be set at the desired value. The droplets freeze in flight and are collected. Drop-size distribution is determined by the filtration or sedimentation method or by microscopic measurement of a representative sample (ref. 43). There is some question as to the validity of data obtained by the molten-wax method. A limited set of data by Longwell (ref. 34) suggests that this method may give a higher mean drop size than would be obtained by using the actual liquid the molten wax is intended to simulate. In these tests, two oils were sprayed into still air. One oil was preheated in order to reduce its viscosity to that of the less viscous oil. The tests indicated that the preheated oil gave a higher mean drop size. This was attributed by Longwell to the increase in viscosity of the preheated oil as it was cooled during atomization. A similar effect would be expected for the molten-wax method.

Summary Comments on Utility of Fuel-Atomization Data

For estimates of drop size to be expected with air atomizers operating at subsonic velocities, equation (13) is recommended. It is noted, however, that this relation is limited to the case of air at 77° F and atmospheric pressure in the atomizing section. Rough corrections for changes in temperature, density, and viscosity of the atomizing gas may be made on the basis of the data of reference 29.

For air atomizers operating at sonic velocities, the results of references 16 and 31 indicate that average drop size may be approximately correlated in terms of the ratio of liquid-to-air weight-flow rate W_l/W_a, average drop size decreasing with decrease in W_l/W_a. The data of references 16 and 31 indicate that average drop size is approximately proportional to the square root of the air-orifice diameter, for atomizers of similar shape. The data of reference 16 suggest that fuel viscosity has a greater effect than surface tension for sonic air atomizers. Air atomizers appear to be a particularly effective means for obtaining fine sprays with highly viscous fuels (20 to 40 centistokes).

The major portion of the drop-size data obtained with swirl-type pressure atomizers indicates that average drop size is approximately proportional to the square root of the orifice diameter and to the pressure drop to the -0.4 power. At constant atomizer size, the average drop size increases with decrease in spray-cone angle from the optimum value (80° to 100°). This increase in drop size becomes more pronounced at the lower nozzle-pressure drops.

For swirl-type atomizers operating with kerosene-type fuels and having optimum cone angles, equation (33) gives an approximate indication of the average drop size to be expected. The accuracy and limitations of the available correlations for drop size do not appear to warrant their use for more than rough estimates of atomization for atomizers other than the ones investigated.

The available data indicate that average drop size is approximately proportional to the fourth root of the fuel viscosity. Insufficient data are available to indicate quantitative effects of fuel surface tension on atomization. In reference 23, the average drop size was found to be proportional to fuel surface tension to the 0.6 to 0.7 power. However, in reference 40, the surface-tension effects appear to be minor. Since the surface-tension range for most hydrocarbon fuels is quite narrow, the effect of surface tension on average drop size can probably be neglected.

3073

FUEL EVAPORATION

The evaporation of the atomized fuel is the second major step of the fuel-preparation process in jet engines. Both combustor performance and required combustor length are influenced by the rate of vapor formation. A knowledge of how the spray evaporation process is affected by the air-flow conditions, fuel-injection conditions, and fuel type is therefore important. In this section, the steady-state evaporation of single drops and sprays into static and dynamic surroundings and into both low- and high-temperature surroundings is considered. The unsteady-state process existing during the initial period of drop evaporation is also discussed.

In addition to rate considerations, the vapor-liquid phase-equilibrium conditions must be included in an analysis of spray evaporation. Although the fuel injected into jet engines seldom attains phase equilibrium, the maximum amount of spray evaporation is represented by such conditions. For low-temperature operating conditions and for fuels of low volatility, the phase-equilibrium conditions are important factors to be considered in an evaluation of the fuel spray evaporation process in jet engines.

Equilibrium Flash Vaporization

Under some operating conditions and for the lower-volatility fuels, the fraction of fuel evaporated may be limited to a low value regardless of the time allowed for evaporation (ref. 44). Such conditions are reached when the vapor concentration of the fuel-air mixture reaches its saturation value. For multicomponent fuels, the calculation of this limiting value of percentage evaporated is based on the equilibrium flash-vaporization curve, which may also be used to estimate conditions required for partial or complete vaporization of fuel in the fuel - lubricating-oil heat exchanger.

For fuels having known constituents, the equilibrium flash-vaporization curve at a given pressure and temperature may be calculated by simultaneous solution of material balance equations and equilibrium relations for the individual constituents. Such a calculation procedure might be applied to the case of petroleum fractions by assuming the fuel to be composed of a finite number of individual constituents. However, such methods are generally impractical for petroleum fractions, and recourse has been made to empirical correlations that permit estimation of the equilibrium flash-vaporization curve from distillation curves. In references 45 and 46, graphs are presented that relate the atmospheric equilibrium flash-vaporization curve to the true boiling point and the A.S.T.M. analytical distillation curves. Two methods are available for correcting the atmospheric equilibrium flash-vaporization curve to other pressures. For vapor pressures below and slightly above

atmospheric pressure, the flash-vaporization curve is assumed to shift parallel to itself. The shift is based on a particular point on the atmospheric flash-vaporization curves, which is treated as a pure compound on a vapor-pressure chart. In reference 45, the base point is taken as the intersection between the atmospheric flash and distillation curves. In reference 47 the base point is taken as the 40-percent-vaporized point on the atmospheric flash-vaporization curve. For correction of the atmospheric flash-vaporization curve to higher pressures, the recommended procedure is based on the construction of a phase diagram on a Cox-type vapor-pressure chart (refs. 45 and 47).

In order to relate initial and final conditions for the cases of evaporation with or without the presence of air, the energy equation is applied, assuming an adiabatic mixing process. If kinetic energy is neglected, the energy equation is given by 3073

$$h_{1,f,l} + \frac{h_{1,a}}{f} = (1-x)\ h_{2,f,l} + x\ h_{2,f,v} + \frac{h_{2,a}}{f} \tag{35}$$

where

f	fuel-air ratio
$h_{1,a}$	enthalpy of air prior to vaporization
$h_{1,f,l}$	enthalpy of fuel prior to vaporization
$h_{2,a}$	enthalpy of air at end of vaporization
$h_{2,f,l}$	enthalpy of liquid fuel at end of vaporization
$h_{2,f,v}$	enthalpy of vapor fuel at end of vaporization
x	fraction of fuel vaporized

For petroleum fractions, the enthalpies required in the use of the energy equations may be estimated from empirical relations available in reference 45.

From Dalton's law, the fuel vapor pressure $p_{f,v}$, ambient pressure p, and fraction of fuel vaporized may be related by

$$\frac{p_{f,v}}{p} = \frac{xf\ \frac{M_a}{M_f}}{1 + xf\ \frac{M_a}{M_f}} \tag{36}$$

where M_f and M_a are the molecular weights of the fuel vapor and air, respectively. From equations (35) and (36) and the equilibrium flash-vaporization curves, the final temperature and percentage of fuel vaporized may be related to the fuel-air ratio, the total pressure, and the inlet temperatures of the fuel and air.

Within the specification limits of jet fuels, there may be rather wide variations in the A.S.T.M. distillation curve. These variations are reflected in the equilibrium flash-vaporization curves and, consequently, may result in appreciable changes in the conditions required to obtain various degrees of flash vaporization in the combustor or heat exchanger. In order to illustrate the effect of fuel

variations on flash vaporization, the preceding calculation procedures were applied to the A.S.T.M. distillation curves for JP-4 fuel presented in figure 6(c) of reference 48. This figure is reproduced in figure I-14. The atmospheric equilibrium flash-vaporization curves corresponding to the three A.S.T.M. distillation curves of figure I-14 were calculated by the method of reference 45. The fuel vapor pressures and the temperature-enthalpy curves corresponding to the three fuels were also calculated by the method of reference 45.

In figure I-15, the percent fuel evaporated is plotted against the inlet air temperature for several values of ambient pressure and a fuel-air ratio of 0.06. The curves were calculated from equation (35), assuming the inlet temperatures of fuel and air to be equal. It is seen that inlet air temperatures on the order of 250° F are required to achieve complete vaporization of the fuel. At lower air temperatures, the limitations imposed by equilibrium considerations would have a pronounced effect on the vaporization rate. The limitations could result in appreciable differences between actual evaporation rates and those calculated on the basis of the common assumption of zero fuel vapor pressure in the atmosphere surrounding individual drops.

3073

Drop Evaporation into Static Surroundings

Drop evaporation theory. - Steady-state evaporation from drops into static surroundings provides a simple illustration of the principles involved in evaporation over wide ranges of conditions. The evaporation rates so determined may be applied to conditions of low relative velocity between the fuel drops and the air stream in combustors. The assumed physical model is shown in figure I-16. Vapor at the saturation pressure for the drop-surface temperature diffuses to the surrounding atmosphere. The drop-surface temperature is at a value below that of the surroundings such that heat is transferred to the drop at a rate which is just adequate to supply the necessary heat for the evaporation.

The evaporation rate of the droplet can be expressed in terms of either mass- or heat-transfer equations. In the derivation of these equations, it is assumed that a quasi-stationary state exists such that the vapor concentration and temperature gradients around the drop are, at every instant, those corresponding to equilibrium values for the existing drop size. This assumption has been shown to be correct to a high degree of approximation in reference 49. It is also assumed that the temperature in the drop interior is constant at its equilibrium value. For the condition of spherical symmetry, the differential heat- and mass-transfer equations for a spherical surface at a distance r from the drop center are given by

$$\frac{dm}{dt} = \left[\frac{1}{H + c_{p,v}\left(T - T_o\right)}\right] \varkappa_m \, 4\pi r^2 \frac{dT}{dr} \tag{37}$$

$$\frac{dm}{dt} = \frac{D_v p M_v 4\pi r^2}{RT} \frac{d}{dr}\left[\ln\left(1 - \frac{p_{f,v}}{p}\right)\right] \tag{38}$$

where

$c_{p,v}$ specific heat of diffusing vapor

D_v diffusivity of diffusing vapor in air

H latent heat of vaporization at drop-surface temperature

M_v molecular weight of diffusing vapor

$\frac{dm}{dt}$ evaporation rate of drop

p ambient pressure

$p_{f,v}$ vapor pressure of diffusing vapor

R universal gas constant

r radial distance from drop center

T temperature

T_o drop-surface temperature

$\varkappa_m$ thermal conductivity of vapor-air mixture

In equation (37), the term $c_{p,v}(T - T_o)$ represents the enthalpy change of the fuel vapor between the drop surface and the surface considered. This relation equates the heat transferred by mass movement of the vapor to that transferred by thermal conductivity. Equation (38) is the application of the Stefan diffusion equation (ref. 50) to drop evaporation.

For evaporation in static surroundings, these equations are integrated between the drop surface and infinity to obtain the following equation:

$$\frac{dm}{dt} = \frac{2\pi\varkappa_m d}{c_{p,v}} \ln\left[1 + c_{p,v}\frac{(T_\infty - T_o)}{L}\right] \tag{39}$$

$$\frac{dm}{dt} = \frac{-2\pi D_v p M_v d}{RT} \ln\left(1 - \frac{p_{f,v,o}}{p}\right) \tag{40}$$

where

$p_{f,v,o}$ vapor pressure of diffusing vapor at drop surface

T_∞ temperature at an infinite distance from drop

For these integrations, $c_{p,v}$, $\varkappa_m$, and D_v/T were assumed independent of temperature, and represent mean values between the drop surface and the surroundings. The vapor partial pressure in the surrounding atmosphere was assumed to be zero for the integration of equation (38).

Evaporation into low-temperature surroundings. - For evaporation into low-temperature surroundings where the sensible heat change of the vapor between the drop surface and surroundings is small compared with the latent heat of vaporization, equation (37) reduces to the following relation:

$$\frac{dm}{dt} = \frac{2\pi\varkappa_m d}{H}(T - T_o) \tag{41}$$

This equation is similar in form to that of simple heat transfer to a sphere in quiescent surroundings. Similarly, for evaporation where the vapor pressure at the drop surface is small compared with the total pressure, equation (40) reduces to

$$\frac{dm}{dt} = \frac{2\pi D_v M_v}{RT} d\,(p_{f,v,o}) \tag{42}$$

This relation is the Langmuir equation (ref. 51). Equations (41) and (42) are of similar form, illustrating the analogy between heat and mass transfer. Equation (42) has been experimentally verified with drops of several relatively low-volatility liquids evaporating into low-temperature surroundings (refs. 52 to 56). The equation was found to be valid at total pressures near atmospheric.

3073

From equation (42), the drop-evaporation rate per unit drop-surface area is inversely proportional to the drop diameter. In addition, this rate is inversely proportional to pressure as determined by the pressure dependency of the diffusion coefficient. Therefore, for sufficiently small drops or low total pressures, the evaporation rate per unit area as obtained from equation (42) becomes greater than the theoretical maximum evaporation rate in a vacuum, as determined by gas kinetics (ref. 57). The maximum evaporation rate for a drop evaporating isothermally in a vacuum is given by the following equation:

$$\frac{dm}{dt} = \frac{\pi M_v d^2 \bar{c}_v \alpha}{RT} p_{f,v,o} \tag{43}$$

where

$\bar{c}_v$ mean molecular velocity of vapor

α accommodation coefficient

The accommodation coefficient represents the fraction of vapor molecules which condense as they strike the liquid surface.

The case of evaporation of very small drops was treated theoretically by Fuchs (ref. 58). In this analysis, diffusion was considered to start at a distance approximately one mean free path from the drop surface. The drop-evaporation rate according to this model is described by the following equation:

$$\frac{dm}{dt} = \frac{\dfrac{2\pi D_v M_v d p_{f,v,o}}{RT}}{\dfrac{2D_v}{d\bar{c}_v\alpha} + \dfrac{d}{d + 2\psi}} \tag{44}$$

where

ψ distance between drop surface and surface where diffusion is assumed to start

For drop diameters large compared with ψ, this equation reduces to the Langmuir equation. For very small drops, the second term in the denominator approaches zero, and the evaporation rate approaches that of a drop evaporating in a vacuum as given by equation (43). Similarly, for the larger size drops, this theoretical maximum evaporation rate is approached at sufficiently low pressures where ψ again is large compared with the drop diameter.

This theory has been verified experimentally at low pressures (refs. 59 to 61). Evaporation rates of dibutyl phthalate, butyl stearate, and straight-chain paraffin hydrocarbon drops approximately 500 microns in diameter were determined over a range of temperature from 60° to 105° F and at pressures down to 0.1 millimeter of mercury absolute. However, for most applications, the use of equation (44) is not necessary. At atmospheric pressure, the effect predicted by Fuchs would be negligible for drops larger than 1 micron.

Other factors which affect predicted values of drop-evaporation rate are the drop surface tension and free convection. The correction for the effect of surface tension on the saturation vapor pressure of the drop has been shown to be insignificant for drops larger than 1 micron (ref. 59). For evaporation in low-temperature surroundings, the influence of free convection on the experimental results is also minor, if the drop diameters and containing vessel are small (ref. 55).

Evaporation into high-temperature surroundings. - Drop evaporation into high-temperature static surroundings has not been studied extensively. Most of the applicable experimental work in this region has been done with single burning drops in quiescent atmospheres. The burning drop has been considered theoretically as a special case of evaporation, where the heat for vaporization is supplied from a burning zone surrounding the drop.

For the high-temperature evaporation case of burning drops, the heat-transfer equation is used. The drop surface temperature is assumed to be that of the fuel boiling point at the given total pressure. The error involved in this assumption is minor because of the large temperature differences. A detailed discussion of the burning of single drops, together with the available experimental data, is presented in chapter VII.

The sensible heat change of the diffusing vapor may be large compared with the latent heat of vaporization for evaporation into high-temperature surroundings. Consequently, serious errors in the drop-evaporation rate may result if this enthalpy term is neglected. In figure I-17, the ratio of the evaporation rate predicted by the simple heat-transfer equation to that predicted by the equation accounting for the fuel vapor enthalpy is plotted for isooctane and water droplets evaporating in quiescent surroundings at various temperatures. A large difference between the two rates is obtained with isooctane drops at the higher temperatures. The effect is much less with water droplets since water has a high latent heat of vaporization.

Drop Evaporation under Forced Convection

Drop evaporation under forced-convection conditions differs from evaporation into quiescent surroundings in two important respects. The assumptions of infinite film thickness and spherical symmetry are not applicable to the case of drop evaporation into moving fluids.

As is shown in figure I-18, the local transfer rates change over the drop surface. In this figure, local transfer rate expressed as a fraction of the transfer rate at the forward stagnation point is plotted against the angle from the forward stagnation point. These data were obtained by Fröessling (ref. 62) for the sublimation of a naphthalene bead. From boundary-layer considerations, the local transfer rate would be expected to be a maximum at the forward stagnation point and decrease gradually to a minimum at the separation point. The data of figure I-18 appear to follow this type of change. Ranz and Marshall (ref. 63) determined the temperature profile around an evaporating water drop. These measurements also indicate a gradual decrease in the local transfer rate from the maximum value at the forward stagnation point.

Correlations of the drop-evaporation rate under forced-convection conditions neglect the changes in the local transfer rate and use an average value for the entire sphere. The total drop in either temperature or partial pressure of diffusing vapor is assumed to take place across a stagnant film. These correlations are based on heat-transfer as well as mass-transfer relations. For the case where the drop temperature is at its equilibrium value, the heat- and mass-transfer equations generally used are, respectively, as follows:

3073

$$\frac{dm}{dt} = \frac{\pi \varkappa_m d \left(T_g - T_o\right)}{H} Nu \tag{45}$$

$$\frac{dm}{dt} = \frac{\pi D_v M_v p d \left(p_{f,v,o} - p_{f,v,g}\right)}{RT\, p_{BM}} Nu' \tag{46}$$

where

Nu Nusselt number for heat transfer

Nu' Nusselt number for mass transfer

p_{BM} logarithmic mean pressure of nondiffusing gas

$p_{v,g}$ partial pressure of diffusing vapor in fluid stream

T_g temperature of fluid stream

Heat-transfer correlations. - Several theoretical treatments of the heat transfer to spheres in fluid streams have been reported. Johnstone, Pigford, and Chapin (ref. 64) assumed that the velocity of the fluid around the sphere is tangential to the surface and equal to the approach velocity. For Reynolds numbers greater than 200, the resulting equation is

$$Nu = 0.714\ (Re)^{1/2}\ (Pr)^{1/2} \tag{47}$$

where

$c_{p,g}$ specific heat of surrounding fluid

Pr Prandtl number, $c_{p,g}\mu_g/\varkappa_g$

Re Reynolds number, $dU_r\rho_g/\mu_g$

U_r velocity of fluid stream relative to the sphere

$\varkappa_g$ thermal conductivity of surrounding fluid

μ_g viscosity of surrounding fluid

ρ_g density of surrounding fluid

For Reynolds numbers approaching zero, the solution for this model results in a limiting Nusselt number equal to 2, as is required for heat transfer from a sphere into static surroundings.

Drake, Sauer, and Schaaf (ref. 65) followed the assumptions described in reference 64, but used a different method for obtaining the solution. For Reynolds numbers below 1000, the two solutions differ. Kudryashev (ref. 66) also obtained an

analytical solution based on the thermal boundary layer. The values of Nusselt number predicted by the various theoretical treatments are compared in figure I-19 over a range of Reynolds numbers from 30 to 2000.

An extensive survey of published data on heat and mass transfer to spheres was described by Williams (ref. 67). The suggested empirical correlation of the heat-transfer data is given by the following equation:

$$Nu = 0.37\ (Re)^{0.6}\ (Pr)^{1/3} \tag{48}$$

In the range of Reynolds numbers less than 1000, the data showed considerable scatter. This range was recently investigated by Tang, Duncan, and Schweyer (ref. 68). In this study, heat-transfer rates for steel spheres in air streams were determined. The resulting correlation is as follows: 3078

$$Nu = 2.1 + 0.37\ (Re)^{1/2} \tag{49}$$

A similar investigation has been described by Kramers (ref. 69).

Ranz and Marshall (ref. 63) determined the evaporation rates of suspended water and benzene drops over a range of Reynolds numbers from zero to 200 and at air temperatures from 80° to 400° F. For evaporating water drops, the data were correlated by the following relation:

$$Nu = 2.0 + 0.6\ (Re)^{1/2}\ (Pr)^{1/3} \tag{50}$$

Ingebo (ref. 70) determined evaporation rates of nine pure liquids in air streams having temperatures ranging from approximately 80° to 1000° F. A liquid drop was simulated by means of a wetted cork sphere having an average diameter of 0.69 centimeter. Reynolds numbers ranged from 1600 to 5700. Nusselt number was correlated in terms of Reynolds number, Schmidt number, and ratio of thermal conductivity of the air and the diffusing vapor. In a later report (ref. 71) data were obtained in air for static pressures from approximately 1/2 to 2 atmospheres. The majority of these experiments were conducted at room temperature. In order to extend the correlation, an additional limited set of data was obtained for evaporation into streams of helium, argon, and carbon dioxide. The final correlation (ref. 71) is given by

$$Nu = 2.0 + 2.58\ (10)^6 \left[ReSc'\left(\frac{gl}{\bar{c}^2}\right)\right]^{0.6} \left[\left(\frac{\varkappa_g}{\varkappa_v}\right)^{1/2}\right] \tag{51}$$

where

$b_{g,w}$ mass diffusion coefficient, pM_vD_v/RT

$\bar{c}$ root mean square molecular velocity of surrounding fluid

D_v diffusion coefficient

d drop diameter

g gravitational constant

l mean free molecular path of surrounding fluid

M_v molecular weight of diffusing vapor

R gas constant

ReSc' $dU_r\rho_g/b_{g,w}$

T temperature

U_r velocity of gas stream relative to drop

$\varkappa_v$ thermal conductivity of diffusing vapor

3073

In equation (51), ρ_g is evaluated at the bulk temperature of the surrounding fluid. The thermal conductivity terms and $b_{g,w}$ are evaluated at the average temperature between the drop surface temperature and the fluid bulk temperature. The terms l and $\bar{c}$ are evaluated at the drop surface temperature.

In figure I-20, a comparison of the various predicted and experimental data for heat transfer to spheres in air is presented. The Prandtl number of the Ranz and Marshall (ref. 63) and Williams correlations (ref. 67) is that of dry air. In the correlation of reference 70, Sc' and the ratio $\varkappa_g/\varkappa_v$ were assumed equal to unity. The correlation factor $gl/\bar{c}^2$ was calculated for air.

Another investigation of drop evaporation in high-temperature air streams was reported by Gohrbandt (ref. 72). The evaporation rate of camphor spheres was determined over a range of Reynolds numbers from 100 to 2000 and air temperatures from about 85° to 930° F. The evaporation rate was found to be proportional to the drop diameter and the square root of the Reynolds number.

Mass-transfer correlations. - A theoretical approach to mass transfer for spheres in moving fluids was described by Johnstone and Kleinschmidt (ref. 73). In this analysis, it was assumed that the sphere contacts a cylindrical tube having an inner diameter equal to that of the sphere and a thickness equal to the distance a diffusing molecule could travel in the time the sphere moves 1 diameter. Increasing the relative velocity between the sphere and surrounding gas decreases the available diffusion time and, therefore, the thickness of the imaginary tube. All molecules contained within the tube are considered to be absorbed. The Nusselt number for mass transfer obtained from this approach is

$$Nu' = (p_{BM}/p)^{1/2} (Re)^{1/2} (Sc)^{1/2} \tag{52}$$

where

p_{BM} log mean pressure of surrounding fluid

Sc Schmidt number, $\mu_g/\rho_g D_v$

Use of the diffusion equation in correlations of drop-evaporation data is limited to evaporation in relatively low-temperature surroundings, since this equation is very sensitive to experimental errors in the drop surface temperature at the higher surface vapor pressures. However, several mass-transfer correlations for the evaporation rate of droplets in room-temperature air have been reported.

Williams (ref. 67) correlated the mass-transfer data of Fröessling (ref. 62), Johnstone and Williams (ref. 74), Powell (ref. 75), and McInness (see ref. 67). The recommended equations for the mass-transfer Nusselt number are as follows:

$$Nu' = 1.5\ (Re)^{0.35}\ (Sc)^{1/3}\quad 5 < Re < 400$$
$$Nu' = 0.43\ (Re)^{0.56}\ (Sc)^{1/3}\quad 400 < Re < 10^5 \tag{53}$$

Maisel and Sherwood (ref. 76) reported data on the evaporation of water and of benzene from porous spheres. The data for water were in good agreement with equation (53). Deviation of the data for benzene was attributed to incomplete wetting of the sphere.

Fröessling (ref. 62) correlated data for evaporation of water, aniline, naphthalene, and nitrobenzene into air streams at room temperature. The data were obtained over a range of Reynolds numbers from 2.4 to 750. This correlation may be written in the following form: 3073

$$Nu' = 2 + 0.55\ (Re)^{1/2}\ (Sc)^{1/3} \tag{54}$$

The mass-transfer correlation of Ranz and Marshall (ref. 63) is as follows:

$$Nu' = 2 + 0.60\ (Re)^{1/2}\ (Sc)^{1/3} \tag{55}$$

This correlation is of the same form as their heat-transfer correlation, but with the Prandtl number replaced with the Schmidt number. In reference 63 it is illustrated that the data of Fröessling (ref. 62) and of Maisel and Sherwood (ref. 76) agree closely with this correlation.

Another correlation on drop evaporation has been described by Kinzer and Gunn (ref. 77):

$$Nu' = 2 + 0.564\ F_v\ (Re)^{1/2}\ (Sc)^{1/2} \tag{56}$$

where F_v is the ventilation factor. This equation was used to express evaporation-rate data obtained for water drops falling freely at their terminal velocities through air at room temperature. Drops with diameters from 20 to 4200 microns were studied. Application of the experimental data to equation (56) indicated that the ventilation factor F_v varied from zero to a value greater than 2 in the range of Reynolds numbers smaller than 100. For Reynolds numbers greater than 100, F was approximately equal to 1. As noted in reference 77, the water drop evaporation data for the higher Reynolds number range would be adequately correlated by equation (54) if the constant were reduced from 0.55 to 0.505. This represents a difference in the calculated Nusselt number of approximately 7 percent for Reynolds numbers from 100 to 750.

Unsteady-State Drop Evaporation

The final case of single-drop evaporation to be considered is that of unsteady-state evaporation. Here, the initial drop temperature is above or below its equilibrium value and consequently changes with time. Both theoretical and experimental work has been reported for this case.

Topps (ref. 78) studied evaporation rates of small drops falling through a high-temperature atmosphere. Initial drop diameters ranged from approximately 300 to 550 microns. The results for this rather narrow range of drop diameters indicated that the evaporation rate varied approximately as the 4.5 power of the initial drop diameter. This large reduction in evaporation rate with decrease in initial drop diameter was attributed by Topps to the conduction of heat to the drop interior, which reduced the heat available for evaporation of the smaller drops.

Kinzer and Gunn (ref. 77) have described an investigation of the time-rate of change in the average temperature of falling water drops. A simplified theoretical expression was obtained for the time required for the drops to reach 63 percent of the equilibrium-temperature difference. Thermal conductivity of the drop interior was assumed to be infinite. Satisfactory agreement was found between the predicted and experimental values.

Recently, El Wakil, Uyehara, and Myers (ref. 79) described an analytical study of the unsteady-state evaporation of pure liquid drops for conditions similar to those existing in jet-engine combustors. In this analysis, the thermal conductivity of the drop interior was also assumed to be infinite. Motion pictures of the circulation of metallic powders within the evaporating drops disclosed appreciable internal circulation currents and indicated that the assumption of infinite thermal conductivity is substantially correct. Temperature-time, mass-time, and penetration-time histories were calculated for drops evaporating in air. This type of calculation involves the simultaneous solution of the heat-transfer, mass-transfer, and drop-motion equations.

3073

A typical set of results is presented in figure I-21. In this figure, percent evaporated, relative velocity, and drop temperature are plotted against time in milliseconds. The calculations are for an isooctane drop having an initial diameter of 50 microns, initial temperature of 50° F, and initial velocity relative to air of 100 feet per second. The air was assumed to be at a pressure of 1/2 atmosphere and at a temperature of 1000° F. For this fuel, the amount of heat going to the drop interior far exceeded that supplying latent heat of vaporization during the major portion of the unsteady-state period. Calculations of this type indicate that, at high air temperatures and for high-volatility fuels, the unsteady-state period represents a large part of the vaporization time.

Additional Drop-Evaporation Considerations

Ranz and Marshall (ref. 63) have investigated the evaporation rate of water drops containing dissolved and suspended solids. For drops containing solids in solution, the initial evaporation rates were those to be expected for saturated solutions even though the average concentrations in the drops were below the saturation value. For drops containing solids in suspension, the initial drop-evaporation rates were those corresponding to pure water.

The contribution of radiant energy in the evaporation of liquid drops was analytically investigated in reference 80. The results of this study demonstrated that, under the conditions normally encountered in jet-engine combustors, the transfer of radiant energy to the fuel drops is negligible unless solid particles are added to the fuel to increase its emissivity.

In references 81 and 82, equations are presented to determine the time required for complete vaporization of liquid drops injected into gaseous streams. In these analyses, the relations describing the drag forces are combined with the heat-transfer equations. During the acceleration period, preheating of the drop is assumed to occur. No vaporization is assumed to occur until the drop reaches stream velocity. The drop-evaporation-rate relations used in these treatments, therefore, correspond to that of a drop evaporating in still air.

An investigation of the effect of turbulence on the evaporation of water from spheres has been reported by Maisel and Sherwood (ref. 83). The influence of both scale and intensity of turbulence were studied. The results indicate that increased turbulence intensity influences the buffer and laminar layers where most of the

resistance to diffusion is located and therefore increases the evaporation rate. The scale of turbulence affects only the eddy diffusivity in the fully turbulent region, which represents a small fraction of the total resistance to diffusion. Thus, increasing the scale of turbulence does not appreciably influence the evaporation rate.

Drop Surface Temperature Determination

Drop-evaporation rates are treated in terms of either heat-transfer or mass-transfer relations. The use of either type of equation requires an accurate knowledge of the drop surface temperature. For steady-state evaporation, this temperature is the wet-bulb temperature. Psychrometric data for some vapors, in addition to that for water, are available in reference 84.

A correlation of drop surface temperature data in terms of the normal boiling point of the evaporating liquid is described in reference 70. This equation may be written as follows:

$$T_{a,w} = T_a - 0.80\ T_{bp} + 75 \tag{57}$$

where

T_a temperature of air into which the liquid is evaporating, °C

$T_{a,w}$ air temperature at which water has same drop surface temperature as given liquid, °C

T_{bp} normal boiling point of evaporating liquid, °C

The term $T_{a,w}$ is computed from equation (57) and the wet-bulb temperature for water corresponding to $T_{a,w}$ is determined from a psychrometric chart. This wet-bulb temperature is equal to the drop surface temperature of the evaporating liquid. The data for this correlation were obtained with nine pure liquids and at a total pressure equal to atmospheric and with air temperatures from 80° to 675° F.

The drop surface temperature may also be determined from a simultaneous solution of the appropriate heat- and mass-transfer equations. This approach was employed in references 63 and 85 for the case of drop evaporation under forced-convection conditions. In these treatments, Nusselt number correlations for heat and mass transfer were used to express the influence of the forced convection on the drop-evaporation rate.

Recommended Drop-Evaporation Relations

Either heat-transfer or mass-transfer equations may be used to predict drop-evaporation rates. For evaporation in high-temperature surroundings, however, the heat-transfer equation is preferred because of the sensitivity of the vapor-pressure term in the diffusion equation at the higher surface vapor pressures. For evaporation in very-high-temperature surroundings, drop-evaporation rates may be predicted by using the heat-transfer equation and assuming the drop surface temperature to be at the liquid boiling point for the given total pressure.

Drop-evaporation rates in quiescent surroundings may be obtained by use of equations (39) and (40). Equation (39) may be used in the simplified form of equation (41) for evaporation in low-temperature surroundings. Equation (40) may also be used in the simplified form of equation (42) for low-volatility liquids.

For evaporation under forced-convection conditions and low-temperature surroundings, equations (45) and (50) have been shown to give accurate predictions of drop-evaporation rates. For evaporation into high-temperature fluid streams, equation (51) should be employed.

EVAPORATION OF SPRAYS

Theory

3073

Extension of single-drop data to sprays is difficult, since both drop-size distribution of the spray and relative velocities between the air and drops must be known. In addition, there are such complicating factors as drop distortion, unsteady-state evaporation, and interaction between drops.

Several theoretical analyses of spray evaporation have been made by using single-drop relations in conjunction with assumed drop-size distributions. One such analysis is that described by Probert (ref. 17). In this treatment, all drops were assumed to have zero relative velocity with respect to the air. The spray was assumed to follow the Rosin-Rammler distribution equation (ref. 18). The evaporation rate of the single drops was defined by an equation similar to that of Langmuir (ref. 51). With this analysis, the fraction of unevaporated spray after a given period of time was calculated but was not checked experimentally.

Another theoretical treatment of spray vaporization has been presented by Tribus, Klein, and Rembowski (ref. 86). Zero relative velocity between the air and droplets was assumed. The spray-evaporation rate in this analysis is expressed in terms of the wet-bulb depression of the injected liquid. It is shown that, given an initial drop-size spectrum, successive spectra may be deduced by calculating the variation in drop size of the largest drop and relating all other drop sizes to this maximum.

Experiment

Because of the lack of experimental data on both drop-size distribution and relative velocity between drops and air, it is generally impractical to apply evaporation-rate relations for single drops to spray evaporation. Some attempts to measure directly the spray-vaporization rate in air streams have been made. An investigation of this type has been described by Fledderman and Hanson (ref. 87). The influence of turbulence and air velocity on the spray-vaporization rate was studied. A theoretical analysis of spray vaporization was also included in this study. Fröessling's equation for single-drop evaporation (ref. 62) was combined with the drop-size distribution equation of Nukiyama and Tanasawa (ref. 15). The resulting expression, however, is very complex.

The experimental measurements were obtained by sampling hexane sprays at various distances downstream of a hollow-cone spray nozzle. The percentage of evaporated spray was determined over a limited range of air velocities. The results indicated a strong dependence of evaporation rate on the relative velocity between the drops and the air stream. Increased turbulence intensity was also found to increase the spray-vaporization rate. The test results, however, did not provide conclusive information on the effect of scale of turbulence on the evaporation rate.

The results of a few measurements of the evaporation rate of kerosene sprays in essentially still air have been reported by Sacks (ref. 88). In this program, kerosene was injected from a swirl-chamber fuel nozzle at pressures of 50 and 80 pounds per square inch. Over this range of conditions, 0.2 to 0.3 percent of the spray was found to evaporate per second, compared with a value of approximately 50 percent

per second as calculated by using the Langmuir equation (ref. 51) and the relation of Probert (ref. 17). This large difference between predicted and experimental values was attributed primarily to the inability of the Langmuir equation to predict evaporation rates for single drops when in a cloud of drops.

The evaporation of fuel sprays in high-velocity air streams has also been discussed in reference 89. In this investigation, the fuel was injected contra-stream from a simple orifice, and the evaporation rates were determined by sampling the sprays. The influences of air temperature, air velocity, ambient air pressure, fuel temperature, and axial distance from the fuel orifice on the percentage of spray evaporation were investigated. In most of these measurements, a hydrocarbon fuel with a narrow boiling range of 317° to 346° F was used.

A study of the effect of the air-flow and fuel-injection parameters on the evaporation of gasoline-type fuel sprays has recently been reported in reference 90. This program was conducted by injecting isooctane contrastream from a simple orifice into air flowing through a duct 8 inches in diameter. Both the total-fuel and liquid-fuel distribution across the test duct were determined by sampling measurements.

The measurements were made over ranges of air temperature, air velocity, air pressure, fuel-injection pressure, fuel-orifice size, and axial distance from the fuel orifice. These ranges and the resulting correlation of the measurements are illustrated in figure I-22. The measurements were correlated by the following expression:

$$\frac{x}{1-x} = 9.35\left[\left(\frac{T_a}{1000}\right)^{4.4}\left(\frac{U_a}{100}\right)^{0.80}(p)^{-1.2}(P)^{0.42}(z)^{0.84}\right] \tag{58}$$

where

P fuel-injection pressure drop, lb/sq in.

p air pressure, in. Hg abs

T_a air temperature, °R

U_a air velocity, ft/sec

x fraction of spray evaporated

z axial distance from fuel orifice, in.

The relative effects of the variables on the spray-evaporation rate are indicated by the exponents. The large influence of air temperature is evident. In comparison, the effects of the other variables are minor. The evaporation rate was essentially unaffected by changes in the diameter of the fuel orifice.

SIGNIFICANCE OF ATOMIZATION AND EVAPORATION RESEARCH IN APPLICATION TO JET-ENGINE DESIGN

The two general types of fuel-atomizing system considered for gas-turbine or ram-jet application are the air atomizer and the centrifugal pressure-atomizing nozzle. Of the two systems, the air atomizer is capable of producing much smaller average drop sizes. The air atomizer has also been considered for the atomization of highly viscous fuels.

A correlation (eq. (13)) is available for a venturi-type air atomizer. However, no data are available for atomization under the high-turbulence-level conditions

found in ram-jet-type installations. If used as a rough first estimate of drop size for a ram-jet installation, equation (13) would probably give a somewhat larger average drop size than the actual value. Equation (13) was obtained for air at approximately room pressure and temperature. Rough estimates of drop size for other gas conditions may be obtained from the data of reference 29, which indicate that average drop size increases with a decrease in gas density, viscosity, and temperature.

The experiments on sonic-velocity air atomizers indicate that the average drop size is a function primarily of the ratio W_l/W_a of liquid-to-air mass-flow rates, the average drop size decreasing with decrease in W_l/W_a. Sauter mean diameters below 100 microns were obtained, even for an initial liquid viscosity of 40 centistokes (see ref. 31 and fig. I-12(b)). The data of references 16 and 31 indicate that the average drop size is approximately proportional to the square root of the orifice diameter for atomizers of similar geometry.

3073

The major portion of drop-size data for centrifugal pressure-atomizing nozzles has been obtained for fixed-configuration nozzles by use of some version of the molten-wax method. Correlations have been obtained (eqs. (29) to (34)) that permit rough estimates of atomization for fixed-configuration, whirl-chamber-type nozzles over a range of nozzle sizes and operating pressures. However, these correlations were for molten wax simulating kerosene and having a kinematic viscosity of approximately 2.0 centistokes. Data of references 23, 34, and 38 indicate that average drop size generally increases rather slowly with increase in viscosity. In reference 23, mean drop size was found to be proportional to viscosity to the 0.25 power or less. A limited set of data in reference 23 indicated that mean drop size was proportional to surface tension to powers from approximately 0.6 to unity. However, data of reference 40 for a wide range of surface tension indicate that the effect of surface tension on average drop size is minor. Since the range of surface tension covered by hydrocarbon-type fuels is quite narrow, it would appear that the effects of surface tension on the atomization of such fuels can be neglected.

Data of reference 36 show that there is an optimum cone angle which gives the smallest average drop size for a given nozzle size, operating pressure, and fuel. This optimum cone angle is generally between 80° and 90°. At low nozzle-operating pressures, the cone angle exerts a predominant influence on average drop size. In this operating range, there is a large increase in average drop size as the cone angle is decreased from its optimum value.

All drop-size data for the centrifugal pressure-atomizing nozzles were obtained for the nozzles spraying into quiescent room air. Accordingly, estimates of average drop size obtained from these investigations would be higher than the actual values for a turbojet installation where fuel is sprayed into high-temperature, turbulent gases.

The effect of various ambient conditions on the steady-state evaporation of pure liquid drops may be readily predicted. Little work has been done on the evaporation of multicomponent liquid drops. The unsteady-state period of drop evaporation has also been investigated (refs. 77 to 79). The analysis of reference 79 indicated that, at high air temperatures and with high-volatility fuels, the unsteady-state period represents a significant part of the evaporation time.

Either heat- or mass-transfer equations may be used for the prediction of single-drop-evaporation rates under steady-state conditions. For evaporation in high-temperature surroundings, however, the heat-transfer equation is preferred in view of the sensitivity of the vapor-pressure term in the diffusion equation at the higher surface vapor pressures. For evaporation into very-high-temperature surroundings, the drop surface temperature may be assumed equal to the liquid boiling point for the given total pressure.

Single-drop-evaporation rates in static surroundings may be obtained by use of equations (39) and (40). Equation (39) may be used in the simplified form of equation (41) for evaporation in low-temperature surroundings. Equation (40) may also be used in the simplified form of equation (42) for low-volatility liquids.

For evaporation under forced-convection conditions and low-temperature surroundings, equations (45) and (50) have been shown to give accurate prediction of drop-evaporation rates. For evaporation into high-temperature and varying pressure fluid streams, equation (51) should be used.

The evaporation of fuel sprays has been investigated both theoretically and experimentally. The theoretical analyses are generally not applicable, since they assume zero relative velocity between drops and air. Experimental results for spray evaporation in air streams are quite limited. The most complete study was for contrastream injection of isooctane from a simple orifice into air streams. For this case, the weight percent of the spray evaporated may be predicted with equation (58). This correlation indicates the relative importance of the air-flow and fuel-flow parameters on the evaporation of volatile-fuel sprays in air streams. 3073

REFERENCES

1. Rayleigh: On the Instability of Jets. Proc. London Math. Soc., vol. X, Nov. 14, 1878, pp. 4-13.

2. Tyler, E.: Instability of Liquid Jets. Phil. Mag., vol. 16, Aug. 1933, pp. 504-518.

3. Weber, Constantin: Zum Zerfall eines Flussigkeitsstrahles. Z.a.M.M., Bd. 11, Heft 2, Apr. 1931, pp. 136-145.

4. Haenlein, A.: The Disintegration of a Liquid Jet. NACA TM 659, 1932.

5. Ohnesorge, Wolfgang: Die Bildung von Tropfen Düsen und die Auflösung flussiger Strahlen. Z.a.M.M.; Bd. 16, Heft 6, Dec. 1936, pp. 355-358.

6. Squire, H. B.: Investigation of the Instability of a Moving Liquid Film. Combustion and Fuels Sub-committee, British A.R.C., Jan. 25, 1952.

7. York, J. L., and Stubbs, H. E.: The Mechanism of Disintegration of Liquid Sheets. Trans. A.S.M.E., vol. 75, no. 7, July 1953, pp. 1279-1286.

8. Lamb, Horace: Hydrodynamics. Sixth ed., Dover Pub., 1932.

9. Colburn, A. J. and Heath, H. H.: Swirl Atomiser Sprays in Partial Vacuum. Memo. No. M.86 British N.G.T.E., May 1950.

10. Castleman, R. A., Jr.: The Mechanism of the Atomization of Liquids. Nat. Bur. Standards Jour. Res., vol. 7, 1931, pp. 369-376.

11. Hinze, J. O.: Critical Speeds and Sizes of Liquid Globules. Appl. Sci. Res., vol. AI, 1949, pp. 273-288.

12. Lane, W. R.: Shatter of Drops in an Air Stream. Ind. and Eng. Chem., vol. 43, no. 6, 1951, pp. 1312-1317.

13. Rupe, Jack H.: A Technique for the Investigation of Spray Characteristics of Constant Flow Nozzles. Third Symposium on Combustion and Flame and Explosion Phenomena, The Williams & Wilkins Co. (Baltimore), 1949, pp. 680-694.

14. Hopkins, J. L.: The Effect of Spray Cone Angle on Atomisation. Tech. Rep. No. I.T.C./4, Shell Petroleum Co. (London), 1946.

15. Nukiyama, Shirō, and Tanasawa, Yasushi (E. Hope, trans.): Experiments on the Atomization of Liquids in an Air Stream. Rep. No. 3, On the Droplet-Size Distribution in an Atomized Jet, Defence Res. Board, Dept. Nat. Defence, Ottawa (Canada), Mar. 18, 1950.

16. Golitzine, N., Sharp, C. R., and Badham, L. G.: Spray Nozzles for the Simulation of Cloud Conditions in Icing Tests of Jet Engines. Rep. No. 14, Nat. Aero. Est. (Canada). 1951.

17. Probert, R. P.: The Influence of Spray Particle Size and Distribution in the Combustion of Oil Droplets. Phil. Mag., sec. 7, vol. 37, no. 265, Feb. 1946, pp. 94-105.

18. Rosin, P., and Rammler, E.: The Laws Governing the Fineness of Powdered Coal. Jour. Inst. Fuel, vol. 7, no. 31, Oct. 1933, pp. 29-36.

19. Epstein, Benjamin: Logarithmico-Normal Distribution in Breakage of Solids. Ind. and Eng. Chem., vol. 40, no. 12, Dec. 1948, pp. 2289-2291.

20. Mugele, R. A., and Evans, H. D.: Droplet Size Distribution in Sprays. Ind. and Eng. Chem., vol. 43, no. 6, June 1951, p. 1317.

21. Bowen, I. G., and Davies, G. P.: Particle Size Distribution and Estimation of Sauter Mean Diameter. Rep. No. I.C.T./28, Shell Petroleum Co. (London), Oct. 1951.

22. Bevans, Rowland S.: Mathematical Expressions for Drop Size Distribution in Sprays. Conf. on Fuel Sprays, Univ. of Mich., Mar. 30-31, 1949.

23. Turner, G. M., and Moulton, R. W.: Drop Size Distribution from Spray Nozzles. Chem. Eng. Prog., vol. 49, no. 4, Apr. 1953, pp. 185-190.

24. Tate, R. W., and Marshall, W. R.: Atomization by Centrifugal Pressure Nozzles. Chem. Eng. Prog., vol. 49, no. 4, Apr. 1953, pp. 169-174.

25. Heath, H. H., and Radcliffe, A.: The Performance of an Air Blast Atomizer. Rep. No. 71, British N.G.T.E., June 1950.

26. Nukiyama, Shirō, and Tanasawa, Yasushi (E. Hope, trans.): Experiments on the Atomization of Liquids in an Air Stream. Rep. No. 1, Defence Res. Board, Dept. Nat. Defence, Ottawa (Canada), Mar. 18, 1950.

27. Nukiyama, Shirō, and Tanasawa, Yasushi (E. Hope, trans.): Experiments on the Atomization of Liquids in an Air Stream. Rep. No. 2, Defence Res. Board, Dept. Nat. Defence, Ottawa (Canada), Mar. 18, 1950.

28. Nukiyama, Shirō, and Tanasawa, Yasushi (E. Hope, trans.): Experiments on the Atomization of Liquids in an Air Stream. Rep. No. 4, The Influence of the Characteristics of the Liquid on the Diameter of the Atomized Droplets. Defence Res. Board, Dept. Nat. Defence, Ottawa (Canada), Mar. 18, 1950.

29. Lewis, H. C., et al.: Atomization of Liquids in High Velocity Gas Streams. Ind. and Eng. Chem., vol. 40, no. 1, Jan. 1948, pp. 67-74.

30. Conroy, E. H., and Johnstone, H. F.: Combustion of Sulfur in a Venturi Spray Burner. Ind. and Eng. Chem., vol. 41, no. 12, 1949, pp. 2741-2748.

31. Radcliffe, A., and Clare, H.: A Correlation of the Performance of Two Air Blast Atomizers with Mixing Sections of Different Size. Rep. No. R.144, British N.G.T.E., Oct. 1953.

32. Needham, H. C.: Correlation of Particle Size Data on Pressure Jet Atomisers. Power Jets Rep. No. R. 1209, British N.G.T.E., May 1946.

33. Radcliffe, A.: On the Performance of a Type of Swirl Atomizer. Rep. No. R.83, British N.G.T.E., Jan. 1951.

34. Longwell, J. P.: Fuel Oil Atomization. D. Sc. Thesis, M.I.T., 1943.

35. Bowen, I. G., and Joyce, J. R.: The Effects of Cone Angle, Pressure, and Flow Number on the Particle Size of a Pressure Jet Atomiser. Tech. Rep. No. I.C.T./17, Shell Petroleum Co. (London), 1948.

36. Needham, H. C., and Starmer, R.: Particle Size Measurement. Spec. Rep. No. S.1, British N.G.T.E., July 1946.

37. Bowen, I. G., and Joyce, J. R.: Swirl Pressure Jet Atomisers. Tech. Rep. No. I.C.T./16, Shell Petroleum Co. (London), Dec. 1947.

38. Davies, G. P.: Correlation Between Sauter Mean Diameter and the Pressure, Flow Number, and Cone Angle from Pressure Jet Atomizers. Tech. Rep. No. I.C.T./29, Shell Petroleum Co. (London), Nov. 1951.

39. Joyce, J. R.: The Atomisation of Liquid Fuels for Combustion. Jour. Inst. Fuel, vol. 22, no. 124, Feb. 1949, pp. 150-156.

40. Giffen, E.: Atomisation of Fuel Sprays. Engineering, vol. 174, no. 4510, July 4, 1952, pp. 6-10.

41. Pigford, Robert L., and Pyle, Cyrus: Performance Characteristics of Spray-Type Absorption Equipment. Ind. and Eng. Chem., vol. 43, no. 7, 1951, pp. 1649-1662.

42. Houghton, H. G.: Spray Nozzles. Chemical Engineers' Handbook, John H. Perry, ed., Third ed., McGraw-Hill Book Co., Inc., 1950, pp. 1170-1175.

43. Tipler, W.: The Application of Optical and Sedimentation Methods to Particle Size Analysis of Wax Sprays. Tech. Rep. No. I.C.T./12, Shell Petroleum Co. (London), May 27, 1947.

44. Gilbert, Mitchell, Howard, John N., and Hicks, Bruce L.: An Analysis of the Factors Affecting the State of Fuel and Air Mixtures. NACA TN 1078, 1946.

45. Maxwell, J. B.: Data Book on Hydrocarbons. D. Van Nostrand Co., Inc., 1950.

46. Edmister, Wayne C.: Application of Thermodynamics to Hydrocarbon Processing. Pt. XXIII - Equilibrium Flash Vaporization Correlations for Petroleum Fractions. Petroleum Refiner, vol. 28, no. 10, Oct. 1949, pp. 143-150.

3073

47. Edmister, Wayne C.: Application of Thermodynamics to Hydrocarbon Processing. Pt. XXIV - Effect of Pressure on Phase Relationship for Petroleum Fractions. Petroleum Eng., vol. 28, no. 11, Nov. 1949, pp. 149-155.

48. Barnett, Henry C., and Hibbard, R. R.: Fuel Characteristics Pertinent to the Design of Aircraft Fuel Systems. NACA RM E53A21, 1953.

49. Luchak, G., and Langstroth, G. O.: Applications of Diffusion Theory to Evaporation from Droplets and Flat Surfaces. Suffield Rep. 171, Def. Res. Board (Canada), July 21, 1950.

50. Jakob, Max: Heat Transfer. Vol. I. John Wiley & Sons, Inc., 1949, p. 601.

51. Langmuir, I.: The Evaporation of Small Spheres. Phys. Rev., ser. 2, vol. XII, no. 5, Nov. 1918, pp. 368-370.

52. Topley, Bryan, and Whytlaw-Gray, Robert: Experiments on the Rate of Evaporation of Small Spheres as a Method of Determining Diffusion Coefficients - The Diffusion Coefficients of Iodine. Phil. Mag. and Jour. Sci., ser. 7, vol. 4, no. 7, Nov. 1927, pp. 873-888.

53. Houghton, H. G.: A Study of the Evaporation of Small Water Drops. Phys., vol. 4, 1933, pp. 419-424.

54. Whytlaw-Gray, R. W., and Patterson, H. S.: Smoke. Arnold (London), 1932.

55. Woodland, Dorothy J., and Mack, Edward, Jr.: The Effect of Curvature of Surface on Surface Energy. Rate of Evaporation of Liquid Droplets. Thickness of Saturated Vapor Films. Jour. Am. Chem. Soc., vol. 55, no. 8, Aug. 1933, pp. 3149-3161.

56. Langstroth, G. O., Diehl, C. H. H., and Winhold, E. J.: The Evaporation of Droplets in Still Air. Canadian Jour. Res., sec. A, vol. 28, Nov. 1950, pp. 580-595.

57. Kennard, E. H.: Kinetic Theory of Gases. McGraw-Hill Book Co., Inc., 1939, pp. 68-71.

58. Fuchs, N.: Concerning the Velocity of Evaporation of Small Droplets in a Gas Atmosphere. NACA TN 1160, 1947.

59. Bradley, R. S., Evans, M. G., and Whytlaw-Gray, R. W.: The Rate of Evaporation of Droplets. I. - Evaporation and Diffusion Coefficients, and Vapour Pressures of Dibutyl Phthalate and Butyl Stearate. Proc. Roy. Soc. (London), ser. A, vol. 186, no. A1006, Sept. 1946, pp. 368-390.

60. Birks, J., and Bradley, R. S.: The Rate of Evaporation of Droplets. II. - The Influence of Changes of Temperature and of the Surrounding Gas on the Rate of Evaporation of Drops of Di-n-butyl Phthalate. Proc. Roy. Soc. (London), ser. A, vol. 198, no. A1053, Aug. 1949, pp. 226-239.

61. Bradley, R. S., and Shellard, A. D.: The Rate of Evaporation of Droplets. III. - Vapour Pressures and Rates of Evaporation of Straight-Chain Paraffin Hydrocarbons. Proc. Roy. Soc. (London), ser. A, vol. 198, no. A1053, Aug. 1949, pp. 239-251.

62. Fröessling, Nils: On the Evaporation of Falling Droplets. Beitrage zur Geophysik, vol. 52, 1938, pp. 170-216.

63. Ranz, W. E., and Marshall, W. R., Jr.: Evaporation from Drops. Chem. Eng. Prog., vol. 48, no. 3, Mar. 1952, pp. 141-146; vol. 48, no. 4. Apr. 1952, pp. 173-180.

64. Johnstone, H. Fraser, Pigford, Robert L., and Chapin, John H.: Heat Transfer to Clouds of Falling Particles. Bull. No. 330, vol. 38, no. 43, Eng. Exp. Station, Univ. Ill., June 17, 1941.

65. Drake, R. M., Jr., Sauer, F. M., Jr., and Schaaf, S. A.: Forced Convection Heat Transfer from Cylinders and Spheres in a Rarefied Gas. Rep. No. He-150-74, Inst. Eng. Res., Univ. Calif., Nov. 15, 1950. (Contract No. N7-onr-295-Task 3.)

66. Kudryashev, L. I. (M. Gayer, trans.): A Refinement of the Calculation of the Heat Transfer Coefficient Between Gas and Suspended Particles by Application of the Thermal Boundary Layer Method. Trans. No. 368, British R.A.E., Mar. 1951.

67. Williams, Glenn Carber: Heat Transfer, Mass Transfer and Friction for Spheres. D. Sc. Thesis, M.I.T., 1942.

68. Tang, Y. S., Duncan, J. M., and Schweyer, H. E.: Heat and Momentum Transfer Between a Spherical Particle and Air Streams. NACA TN 2867, 1953.

69. Kramers, H.: Heat Transfer from Spheres to Flowing Media. Physica, vol. 12, no. 2-3, June 1946, pp. 61-80.

70. Ingebo, Robert D.: Vaporization Rates and Heat Transfer Coefficients for Pure Liquid Drops. NACA TN 2368, 1951.

71. Ingebo, Robert D.: Effect of Pressure on Evaporation Rate of Drops in Gas Streams. NACA TN 2580, 1953.

72. Gohrbandt, W.: The Evaporation of Spheres in a Hot Air Stream. Memo. No. M.110, British N.G.T.E., Apr. 1951.

73. Johnstone, H. F., and Kleinschmidt, R. V.: The Absorption of Gases in Wet Cyclone Scrubbers. Trans. Am. Inst. Chem. Eng., ser. A, vol. 34, no. 2, Apr. 25, 1938, pp. 181-198.

74. Johnstone, H. F., and Williams, G. C.: Absorption of Gases by Liquid Droplets. Ind. and Eng. Chem., vol. 31, no. 8, Aug. 1939, pp. 993-1001.

75. Powell, R. W.: Further Experiments on the Evaporation of Water from Saturated Surfaces. Trans. Inst. Chem. Eng., vol. 18, 1940, pp. 36-50; discussion, pp. 51-55.

76. Maisel, D. S., and Sherwood, T. K.: Evaporation of Liquids into Turbulent Gas Streams. Chem. Eng. Prog., vol. 46, no. 3, Mar. 1950, pp. 131-138.

77. Kinzer, Gilbert D., and Gunn, Ross: The Evaporation, Temperature and Thermal Relaxation-Time of Freely Falling Waterdrops. Jour. Meteorology, vol. 8, no. 2, Apr. 1951, pp. 71-83.

3073

78. Topps, J. E. C.: An Experimental Study of the Evaporation and Combustion of Falling Droplets. Memo. M-105, British N.G.T.E., Feb. 1951.

79. El Wakil, M. M., Uyehara, O. A., and Myers, P. S.: A Theoretical Investigation of the Heating up Period of Injected Fuel Droplets Vaporizing in Air. NACA TN 3179, 1954.

80. Berlad, A. L., and Hibbard, R. R.: Effect of Radiant Energy on Vaporization and Combustion of Liquid Fuels. NACA RM E52I09, 1952.

81. Kumm, E. L.: Calculations on the Evaporation Rate of Sprays in Rapidly Moving Gases. Rep. No. AL-916, North Am. Aviation, Inc., June 1949.

82. Wagner, C.: Calculations of the Flight Path of Fuel Droplets in the Air Stream of a Ram-Jet. Tech. Rep. No. 52, Ord. Res. and Dev. Div., Oct. 1948.

83. Maisel, D. S., and Sherwood, T. K.: Effect of Air Turbulence on Rate of Evaporation of Water. Chem. Eng. Prog., vol. 46, no. 4, Apr. 1950, pp. 172-175.

84. Perry, J. H., ed.: Chemical Engineers' Handbook. Third ed., Mc-Graw-Hill Book Co., Inc., 1950, pp. 812-816.

85. Johnstone, H. F., and Eads, Daniel K.: Vaporization of Small Sulfur Droplets. Ind. and Eng. Chem., vol. 42, no. 11, Nov. 1950, pp. 2293-2298.

86. Tribus, M., Klein, J. S., and Rembowski, J.: A Method for Calculating the Rate of Evaporation and the Change in Drop Size Distribution for Pure Sprays Injected into Unsaturated Air. Proj. M992-C, Eng. Res. Inst., Univ. of Mich., May 1952.

87. Fledderman, R. G., and Hanson, A. R.: The Effects of Turbulence and Wind Speed on the Rate of Evaporation of a Fuel Spray. Rep. No. CM667, Eng. Res. Inst., Univ. of Mich., June 20, 1951. (Contract NOrd 7924, Task UMH-3D, Proj. M604-3, U. S. Navy Dept., Bur. Ord.)

88. Sacks, W.: The Rate of Evaporation of a Kerosine Spray. Note 7, Nat. Aero. Establishment (Canada), 1951.

89. Longwell, J. P., Van Swerinhgen, R. A., Jr., Weiss, M. A., and Hatt, F. G.: Preparation of Air-Fuel Mixtures for Ramjet Combustors. Bumblebee Ser. Rep. No. 168, Esso Labs., Standard Oil Dev. Co., Nov. 1951. (Contract NORD 9233, with Bur. Ord., U. S. Navy.)

90. Bahr, Donald W.: Evaporation and Spreading of Isooctane Sprays in High-Velocity Air Streams. NACA RM E53I14, 1953.

3073

TABLE I-I. - MATHEMATICAL EXPRESSIONS FOR DROP-SIZE DISTRIBUTION

Expression	R_s	$\frac{dR_s}{dd}$	Sauter mean diameter	Reference
Nukiyama-Tanasawa	$1 - \frac{\Gamma_{bd^q}\left(\frac{6}{q}\right)}{\Gamma\left(\frac{6}{q}\right)}$	$\frac{-b^{6/q}}{\Gamma\left(\frac{6}{q}\right)} d^5 e^{-bd^q}$	$\frac{b^{-1/q}\,\Gamma\left(\frac{6}{q}\right)}{\Gamma\left(\frac{5}{q}\right)}$	15
Rosin-Rammler	e^{-bd^q} or $e^{-(d/\bar{x})^n}$	$-bqd^{q-1} e^{-bd^q}$ or $-\frac{n}{\bar{x}^n} d^{n-1} e^{-(d/\bar{x})^n}$	$\frac{b^{-1/q}}{\Gamma\left(1 - \frac{1}{q}\right)}$ or $\frac{\bar{x}}{\Gamma\left(1 - \frac{1}{n}\right)}$	18
Logarithmic-normal[a]	$1 - \frac{1}{\sqrt{\pi}} \int_{-\infty}^{qy} e^{-q^2y^2}\, d(qy)$	$\frac{-q}{d\sqrt{\pi}} e^{-q^2y^2}$	$\frac{\bar{x}}{e^{1/4q^2}}$	19
Upper-limit[b]	$1 - \frac{1}{\sqrt{\pi}} \int_{-\infty}^{qy} e^{-q^2y^2}\, d(qy)$	$\frac{-qx_m}{(x_m - d)\sqrt{\pi}} e^{-q^2y^2}$	$\frac{x_m}{1 + ke^{1/4q^2}}$	20

[a]Where $y = \ln \frac{d}{\bar{x}}$

[b]Where $y = \ln \frac{kd}{x_m - d}$

3073

(a) Rotationally symmetric oscillations.

(b) Wave formation.

Figure I-1. - Disturbance of low-velocity liquid jet.

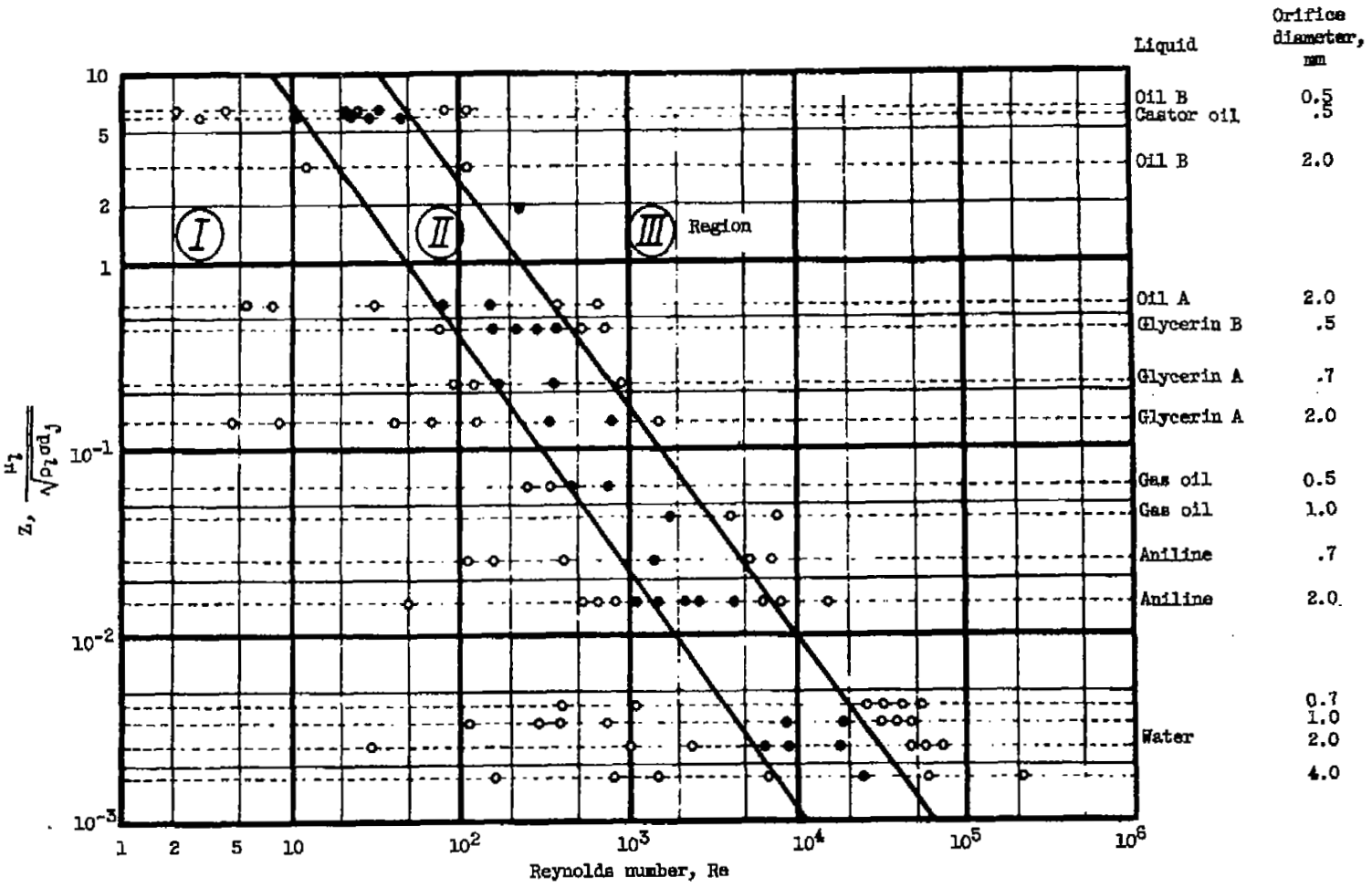

Figure I-2. - Stages of atomization with simple orifice.

3073

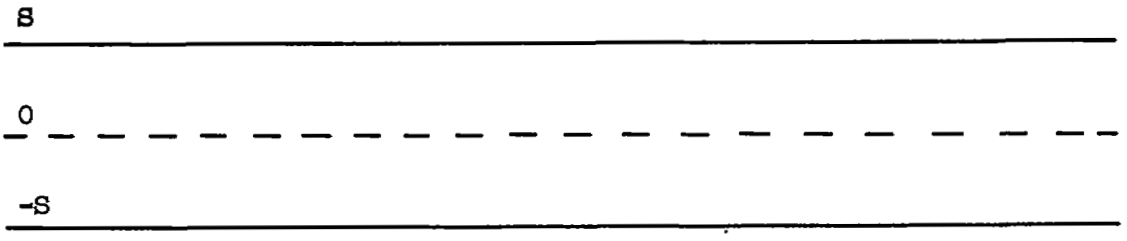

(a) Undisturbed film.

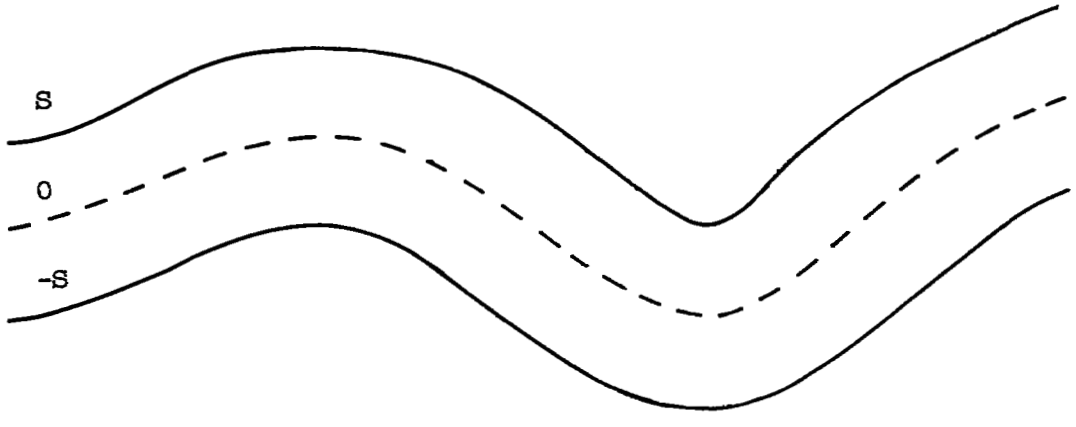

(b) Antisymmetric wave formation (ref. 6).

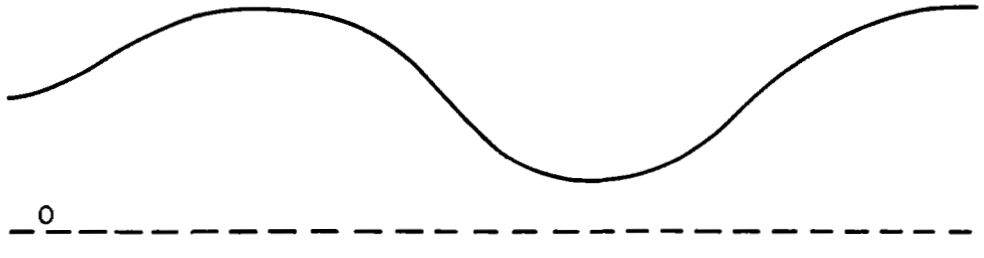

(c) Symmetric wave formation (ref. 7).

Figure I-3. - Wave formation for liquid sheets.

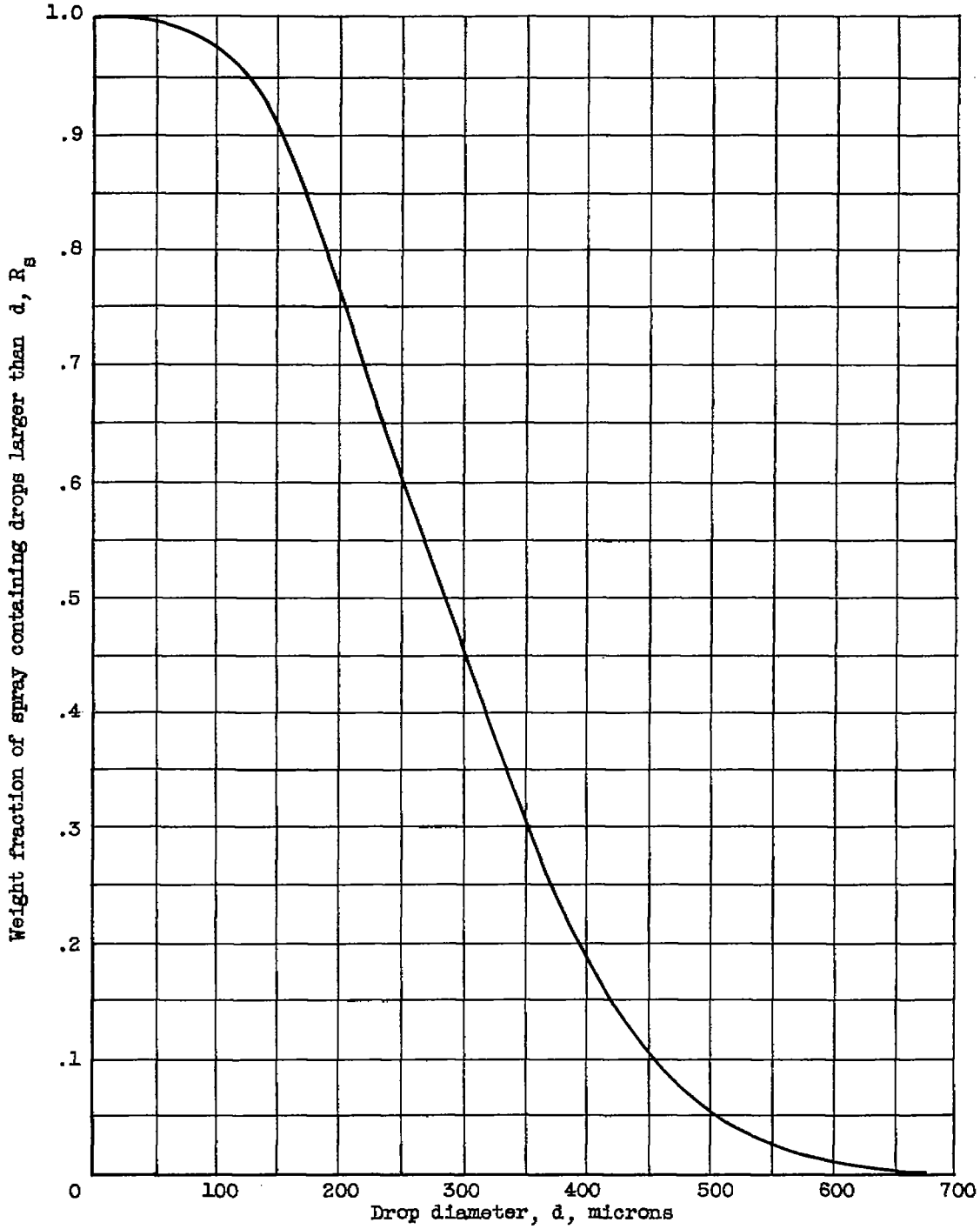

(a) Cumulative form.

Figure I-4. - Fuel spray drop-size distribution.

3073

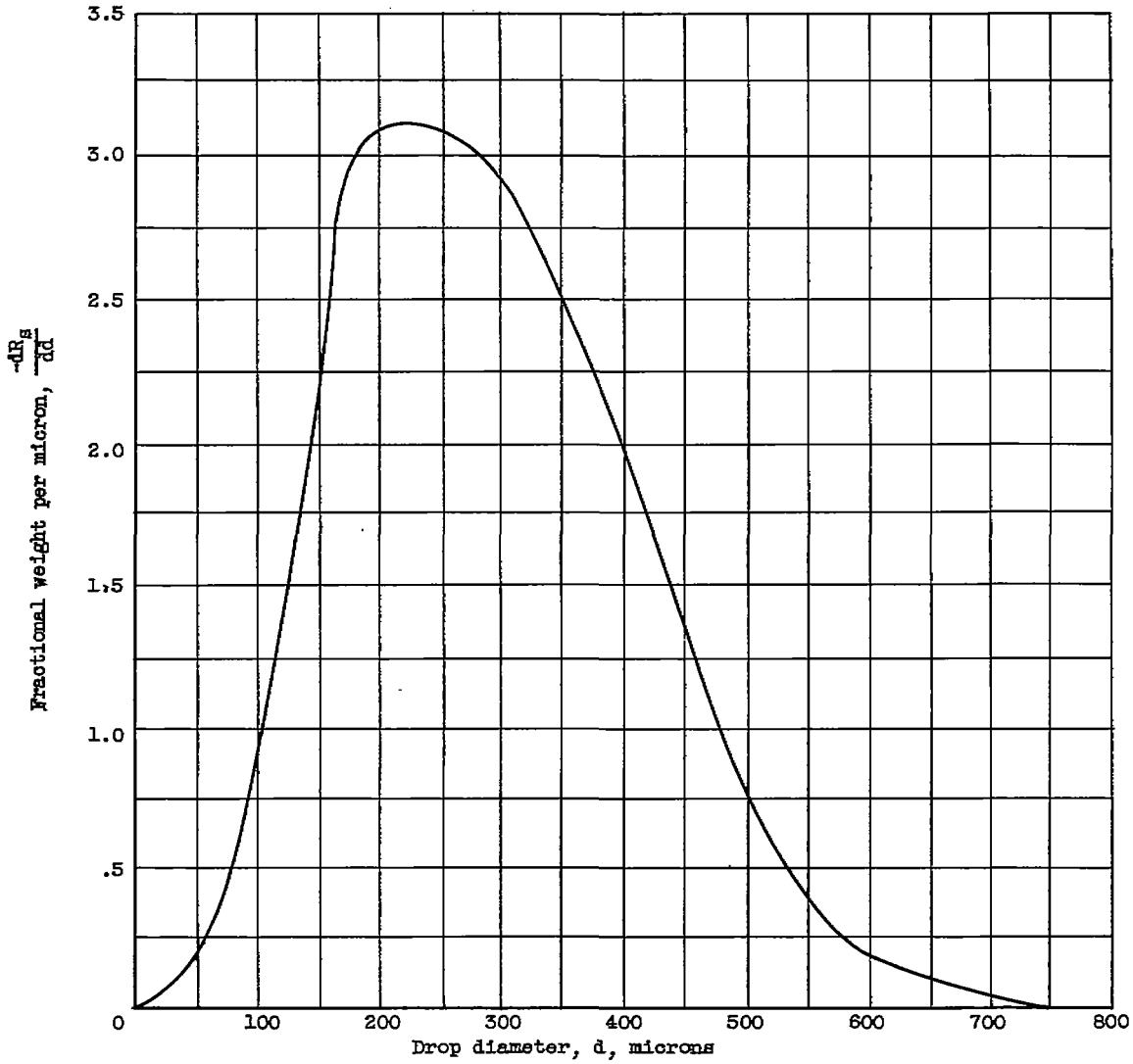

(b) Differential form.

Figure I-4. - Concluded. Fuel spray drop-size distribution.

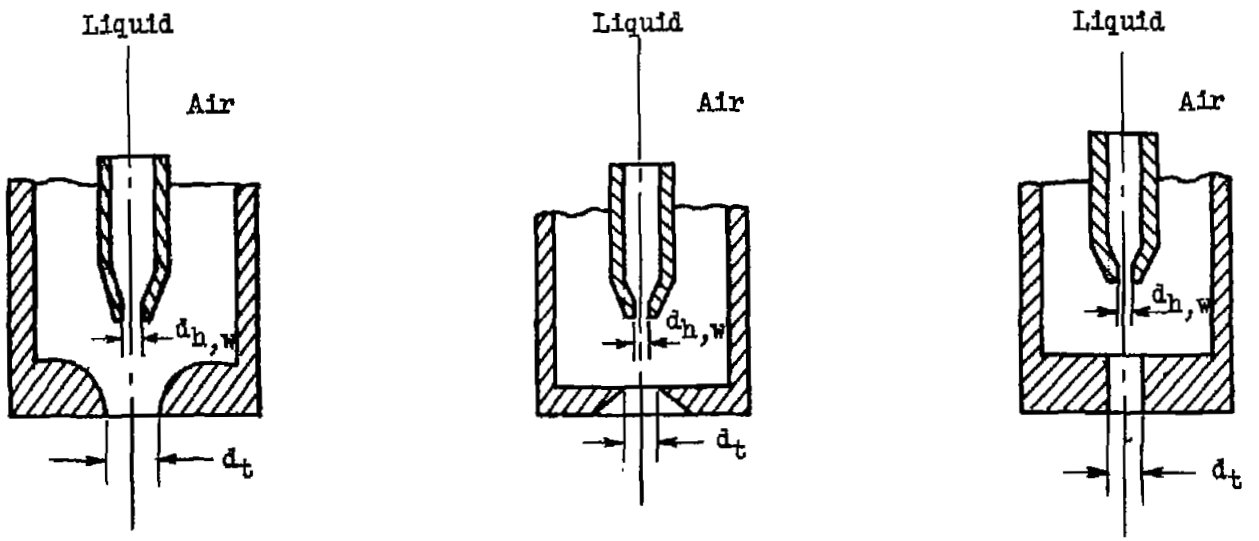

(a) Converging nozzle. (b) 120° Knife-edge nozzle. (c) Straight-bored nozzle.

Figure I-5. - Air-atomizing nozzles (refs. 15 and 26 to 28).

3073

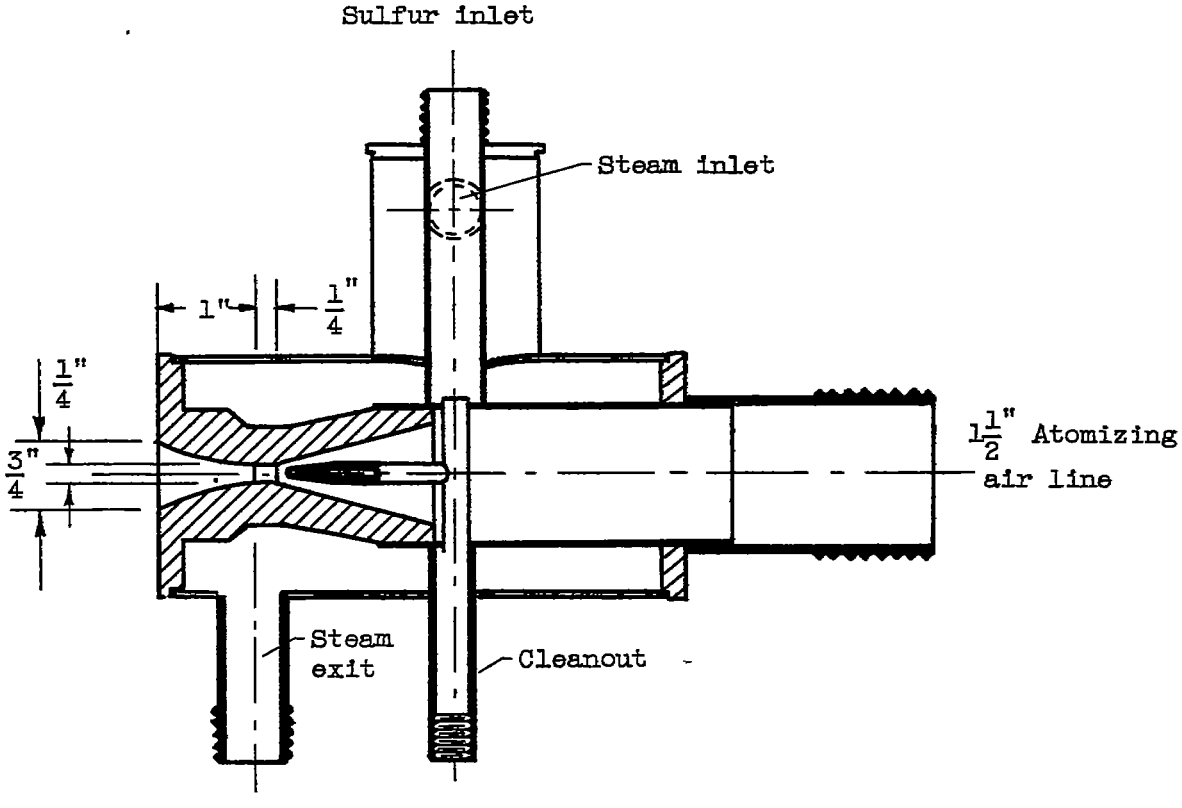

Figure I-6. - Venturi-type sulfur atomizer (reprinted by permission from ref. 30).

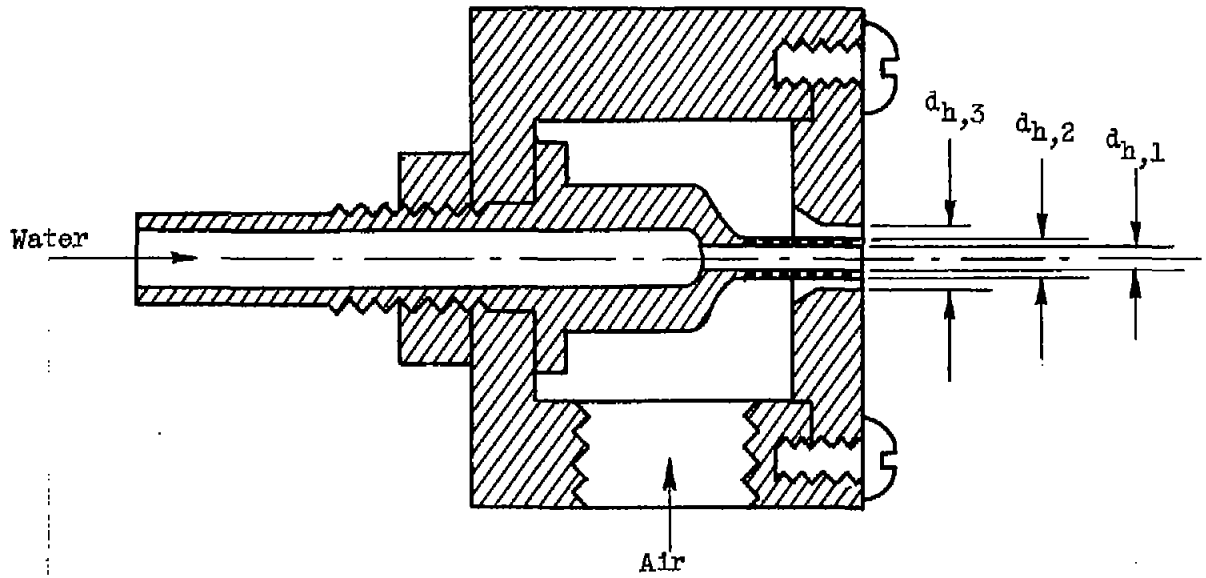

Atomizer	$d_{h,1}$, in.	$d_{h,2}$, in.	$d_{h,3}$, in.
Small	0.064	0.077	0.125
Medium	.104	.125	.203
Large	.152	.183	.297

(a) Convergent nozzles.

Figure I-7. - Sonic air-atomizing nozzles (ref. 16).

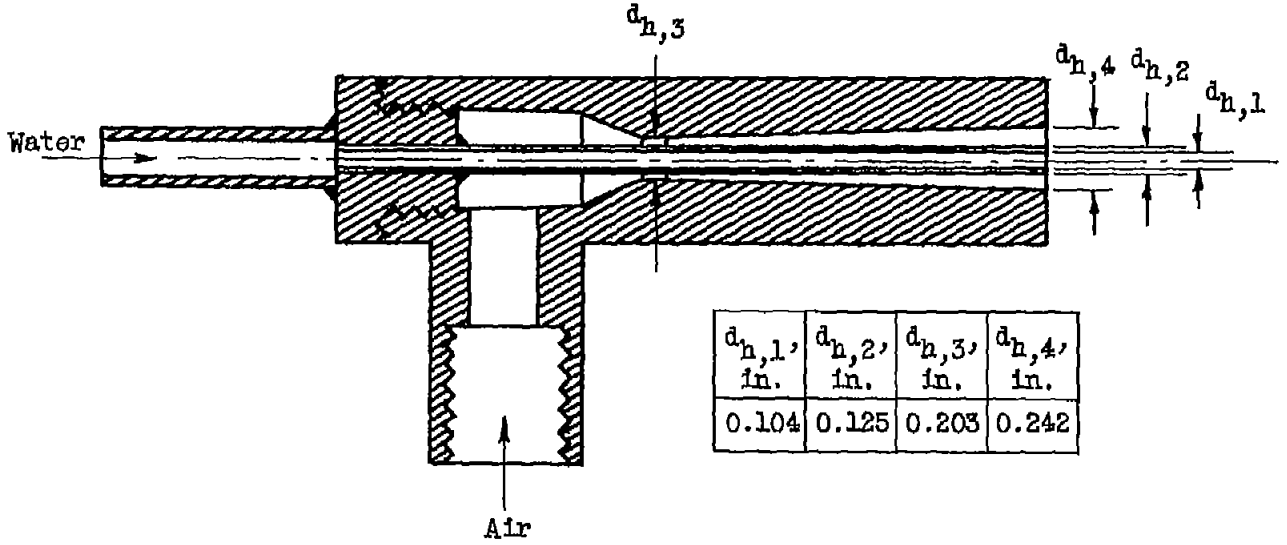

$d_{h,1}$, in.	$d_{h,2}$, in.	$d_{h,3}$, in.	$d_{h,4}$, in.
0.104	0.125	0.203	0.242

(b) Medium divergent.

Figure I-7. - Concluded. Sonic air-atomizing nozzles (ref. 16).

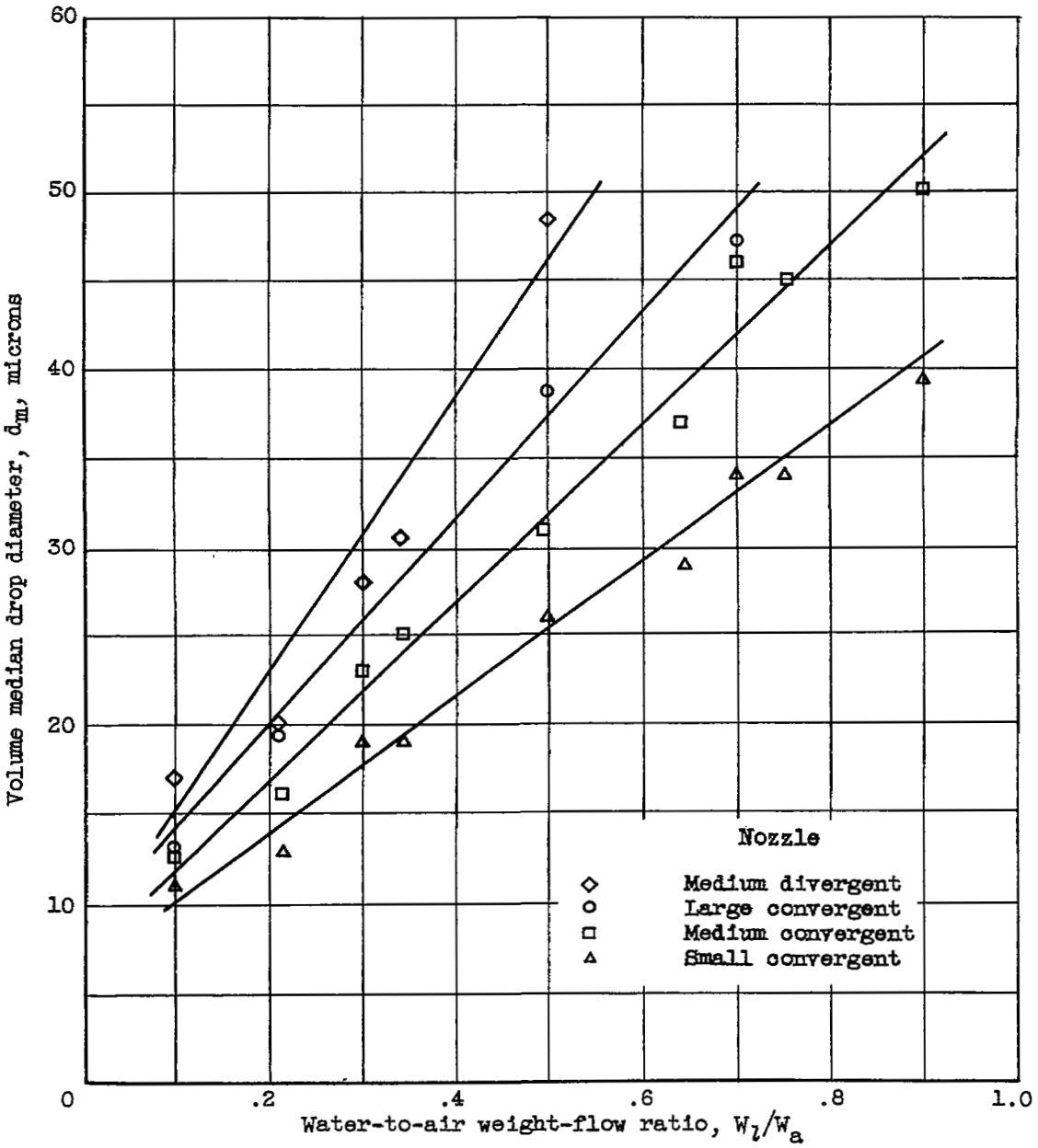

Figure I-8. - Effect of water-to-air weight-flow ratio on volume median drop diameter (ref. 16).

3073

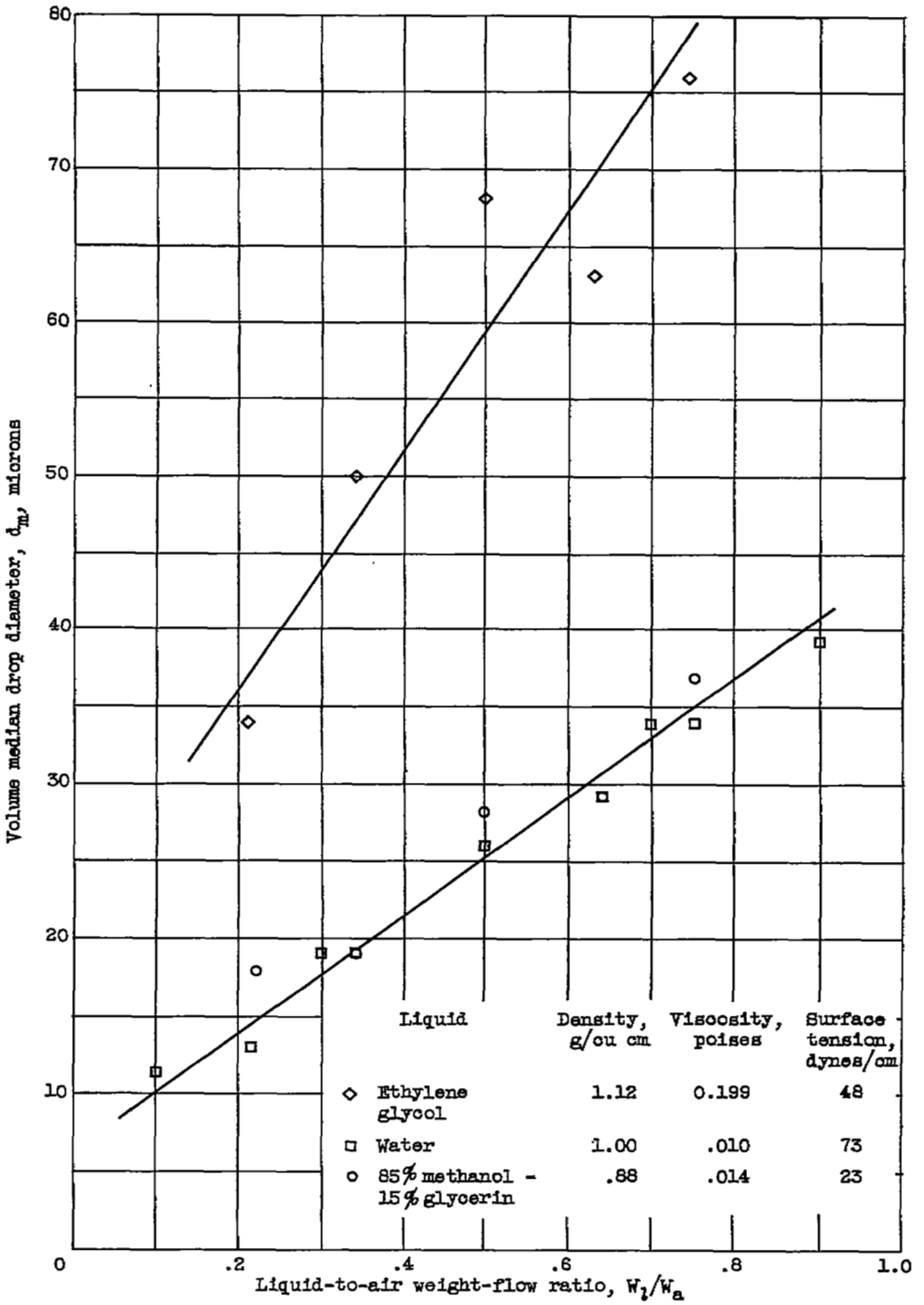

Figure I-9. - Volume median drop diameter obtained with sonic air atomization (ref. 16).

3073

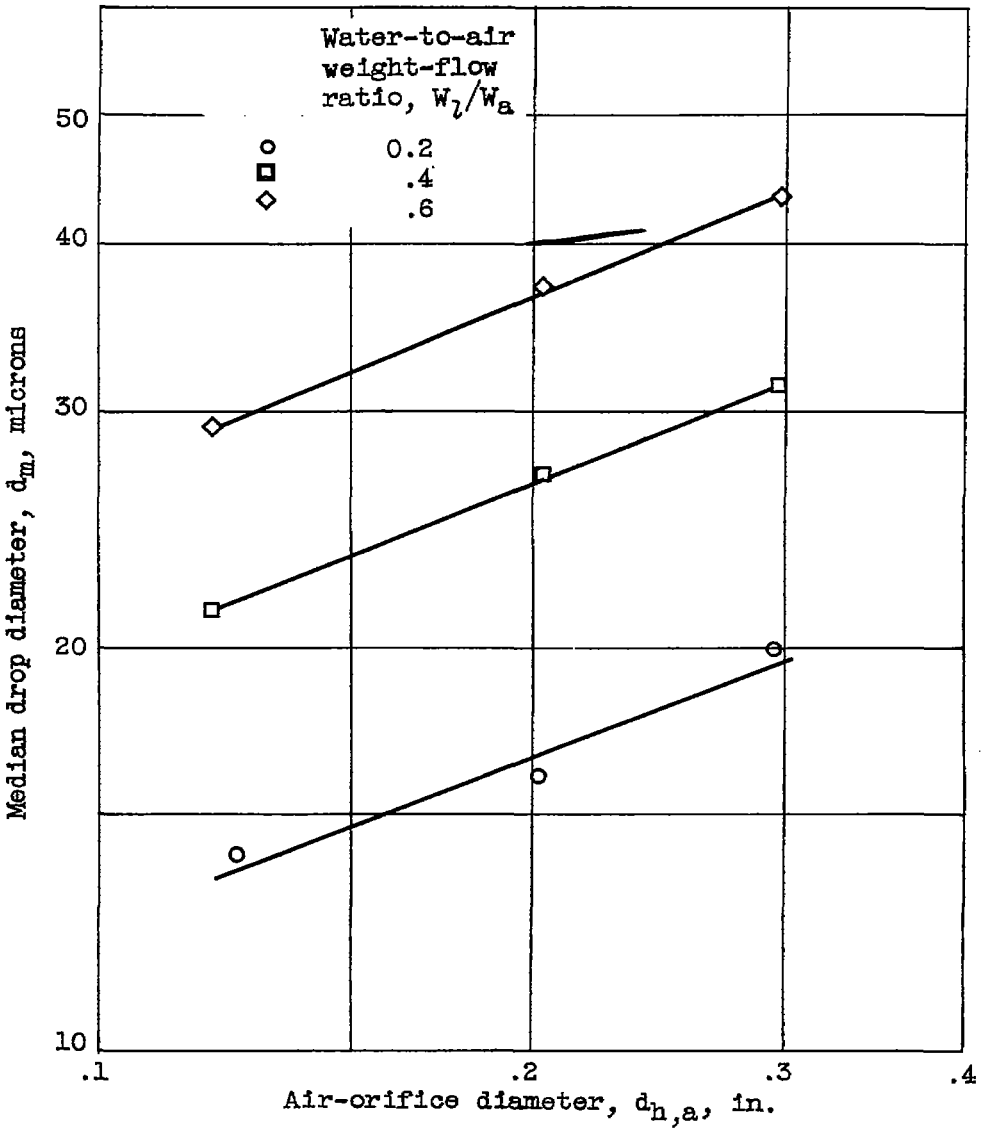

Figure I-10. - Effect of air-orifice diameter of sonic air atomizer on median drop diameter (ref. 16).

3073

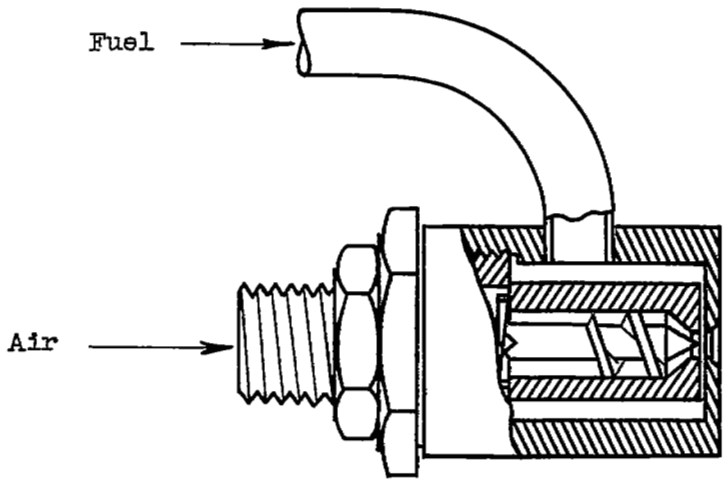

(a) 1/8-Inch orifice.

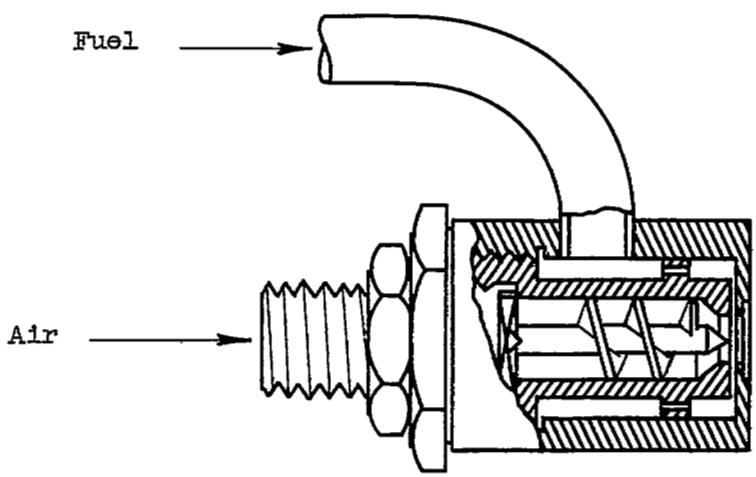

(b) 1/4-Inch orifice.

Figure I-11. - High-pressure air atomizers. (refs. 25 and 31).

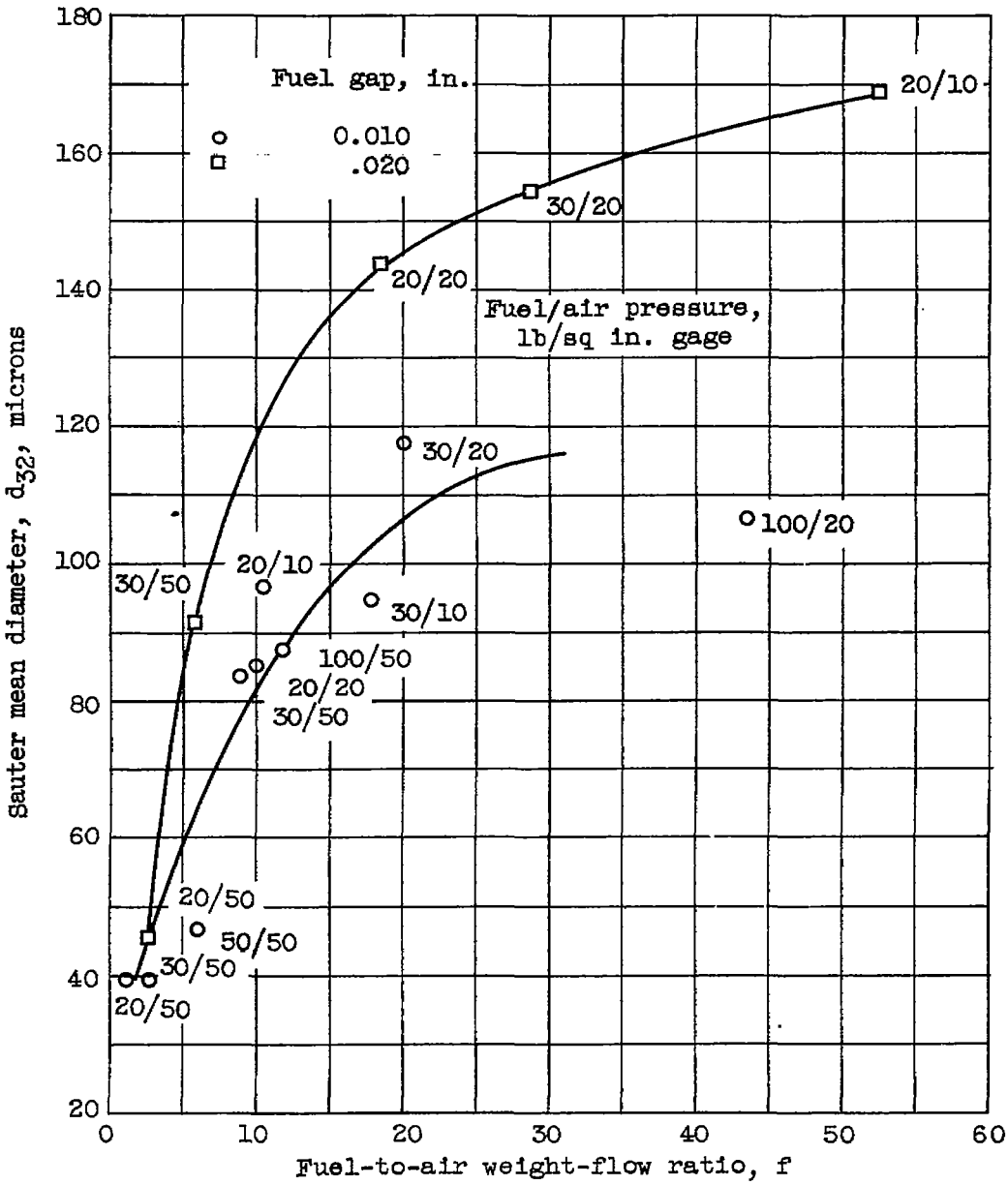

(a) Fuel viscosity, 20 centistokes.

Figure I-12. - Sauter mean diameter against fuel-air ratio for 0.25-inch atomizer (ref. 31).

3073

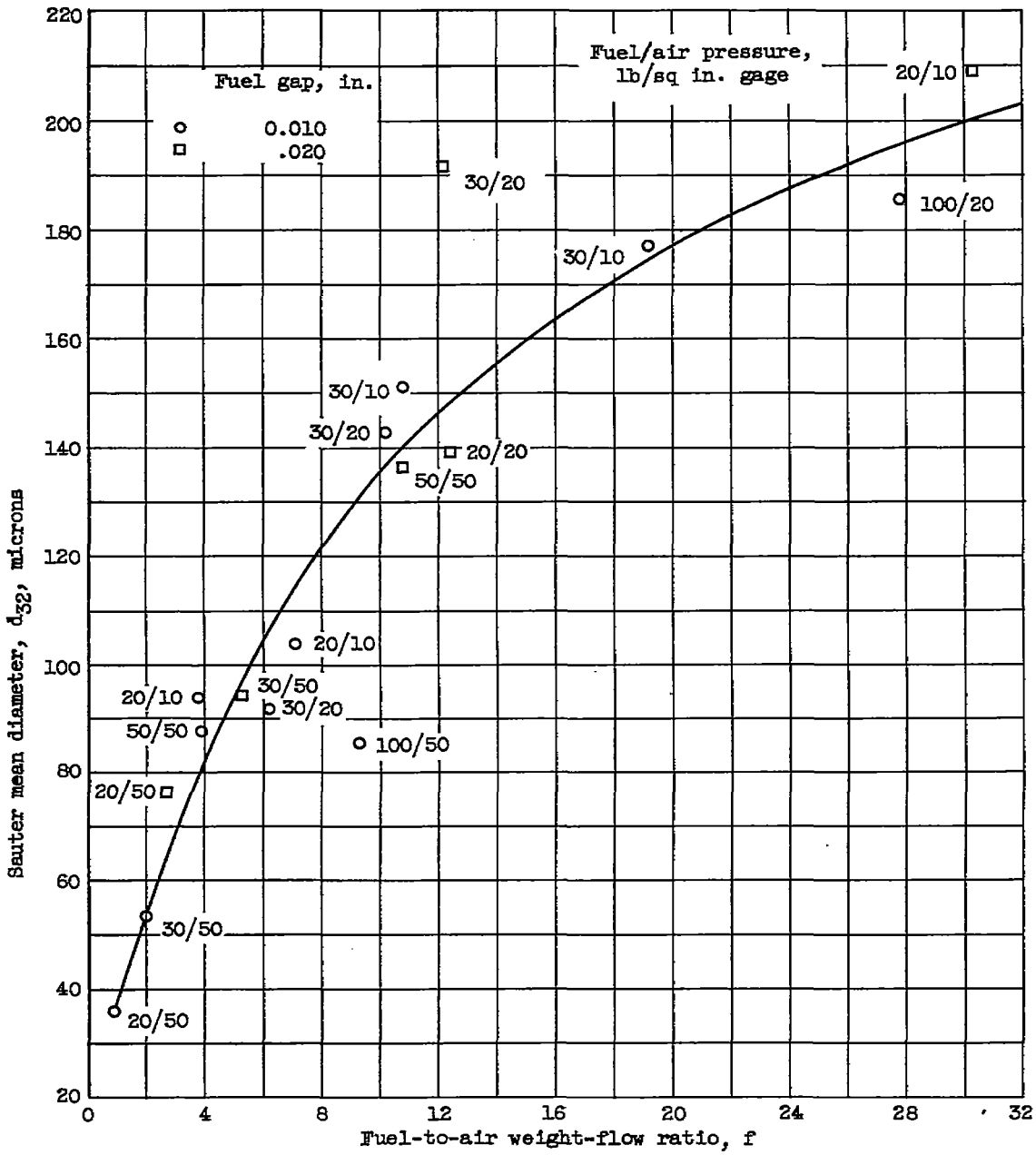

(b) Fuel viscosity, 40 centistokes.

Figure I-12. - Concluded. Sauter mean diameter against fuel-air ratio for 0.25-inch atomizer (ref. 31).

3073

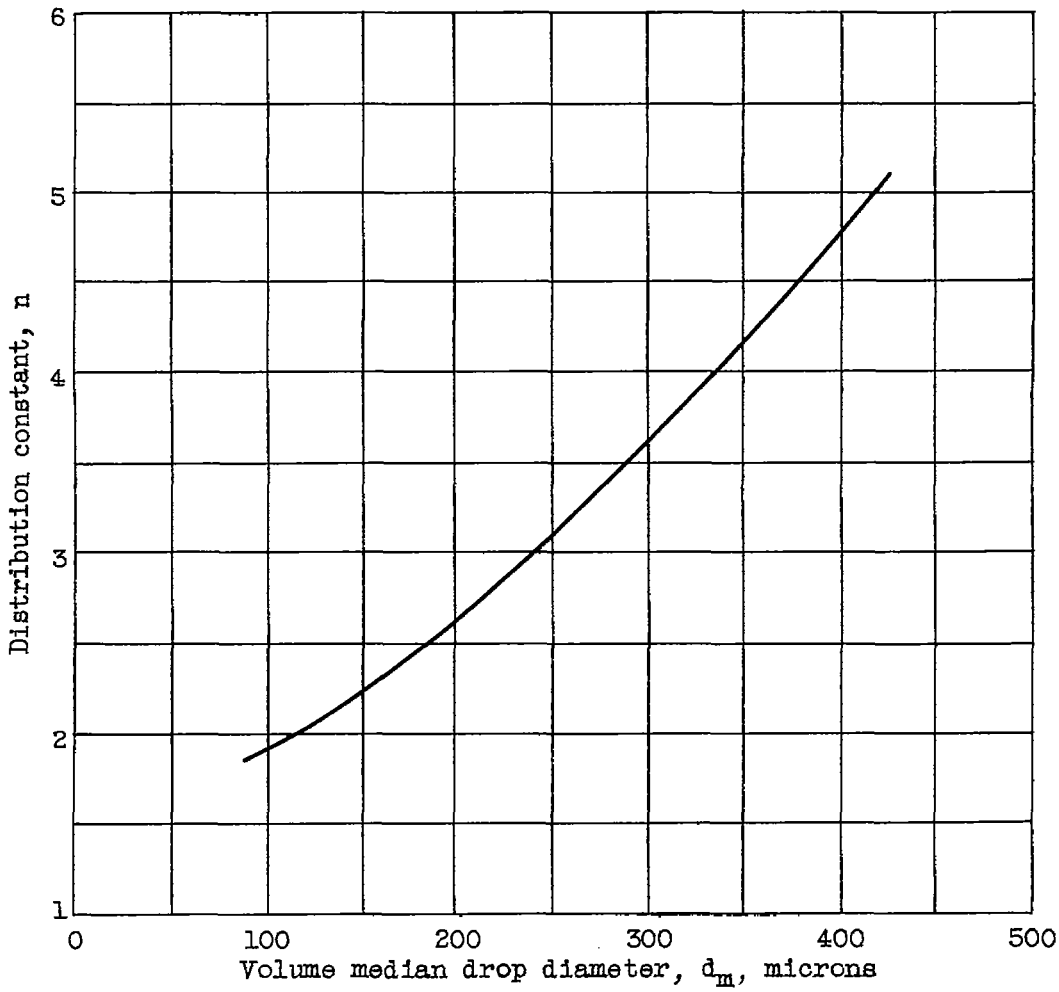

Figure I-13. - Distribution constant for a fuel-oil spray (ref. 34).

3073

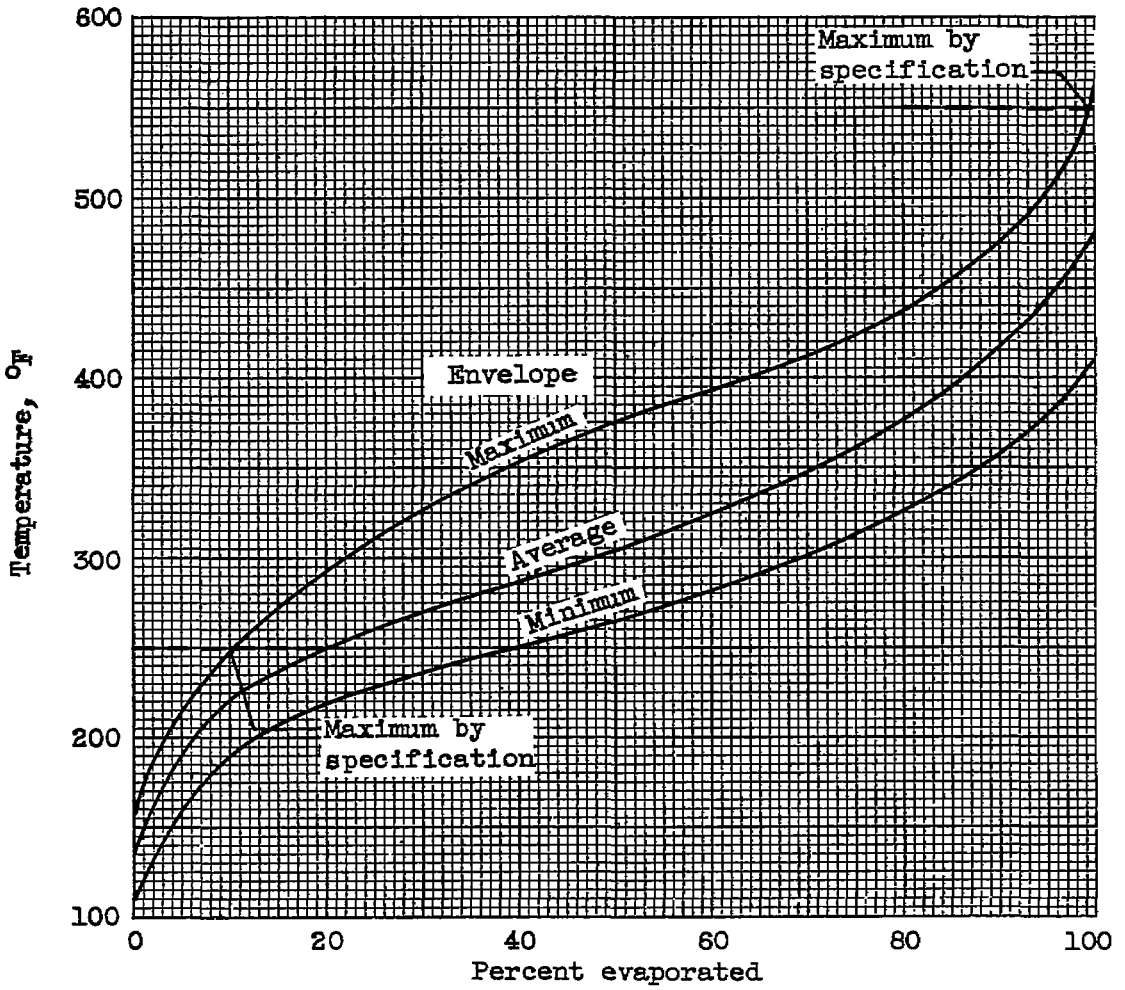

Figure I-14. - Variation of A.S.T.M. distillation temperatures for MIL-F-5624A grade JP-4 fuel.

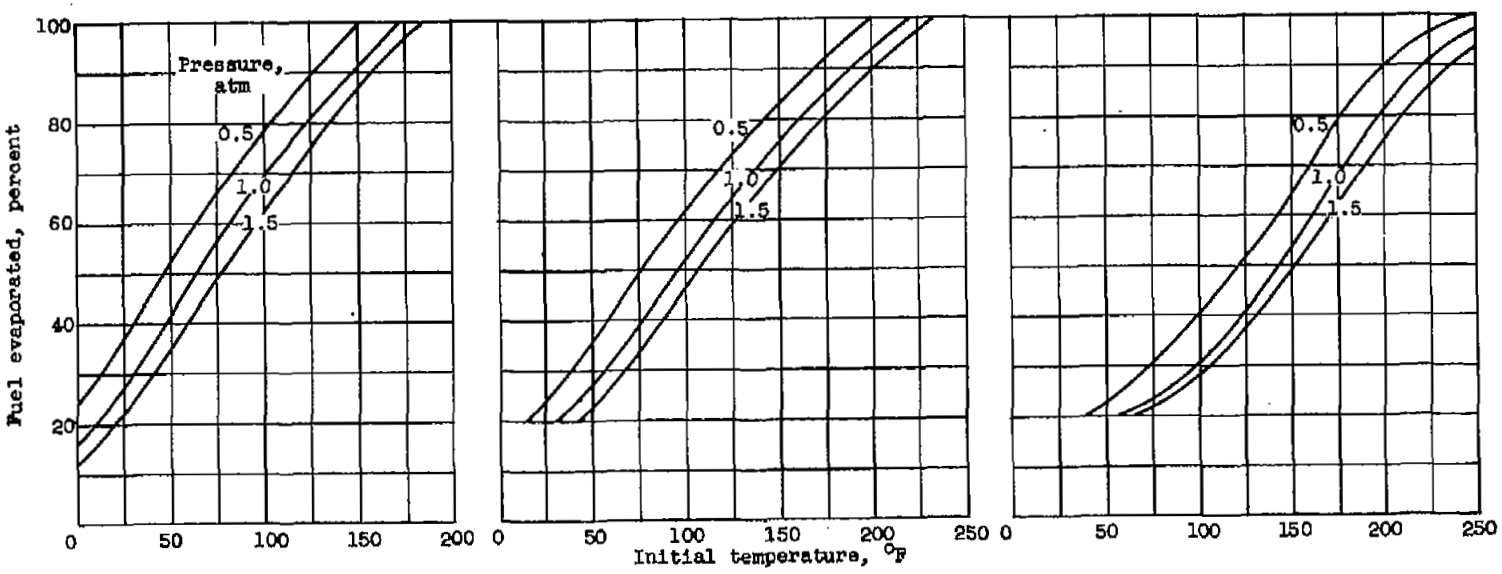

(a) Minimum envelope of figure I-14. (b) Average curve of figure I-14. (c) Maximum envelope of figure I-14.

Figure I-15. - Equilibrium vaporization of grade JP-4 fuel; fuel-air ratio, 0.06.

3073

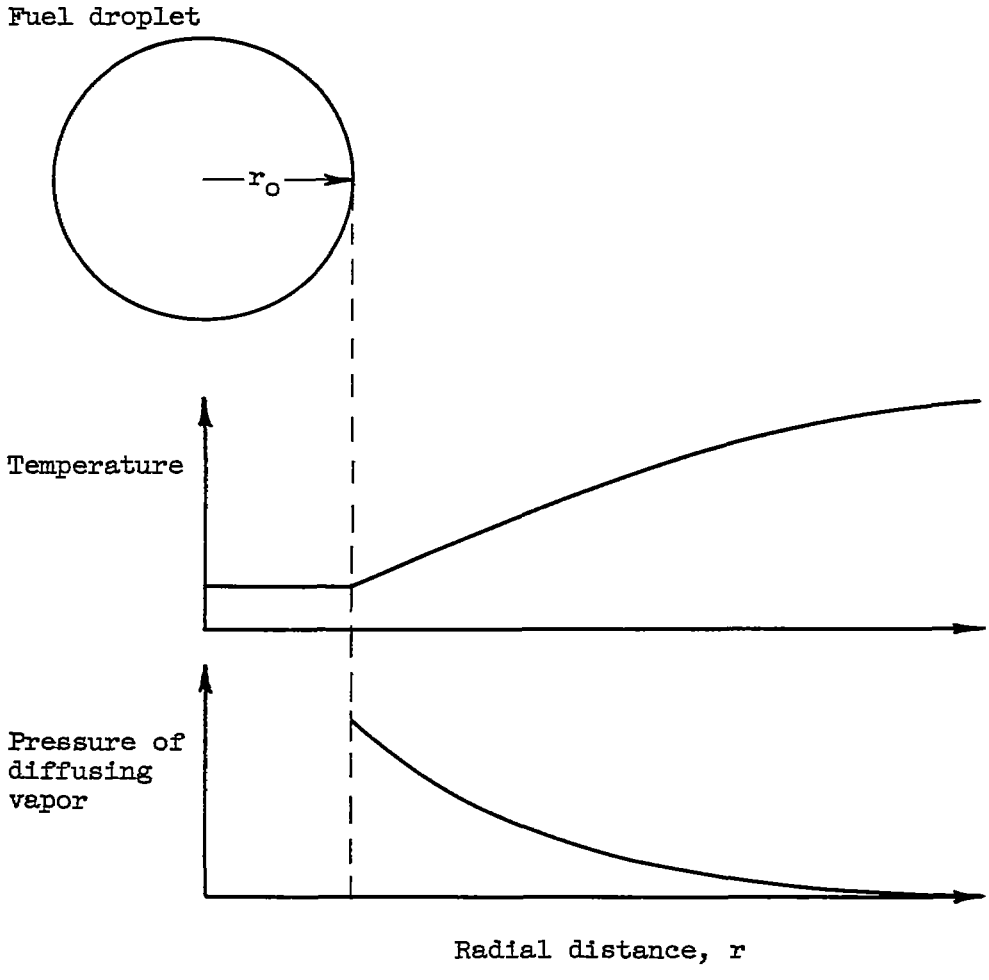

Figure I-16. - Model for evaporation of droplet under static conditions.

3073

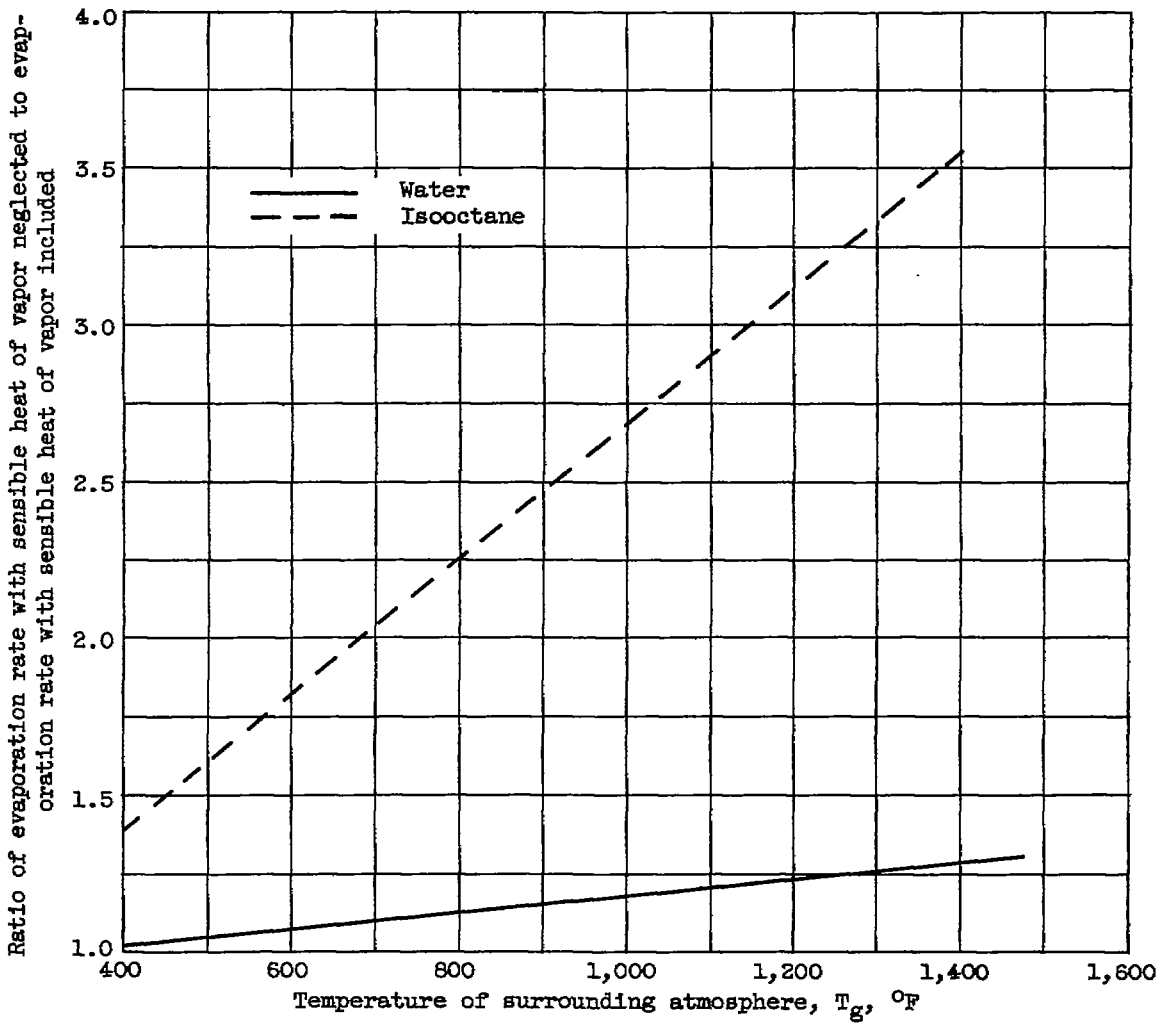

Figure I-17. - Effect of enthalpy change of diffusing vapor on calculated evaporation rates of water and isooctane drops.

3073

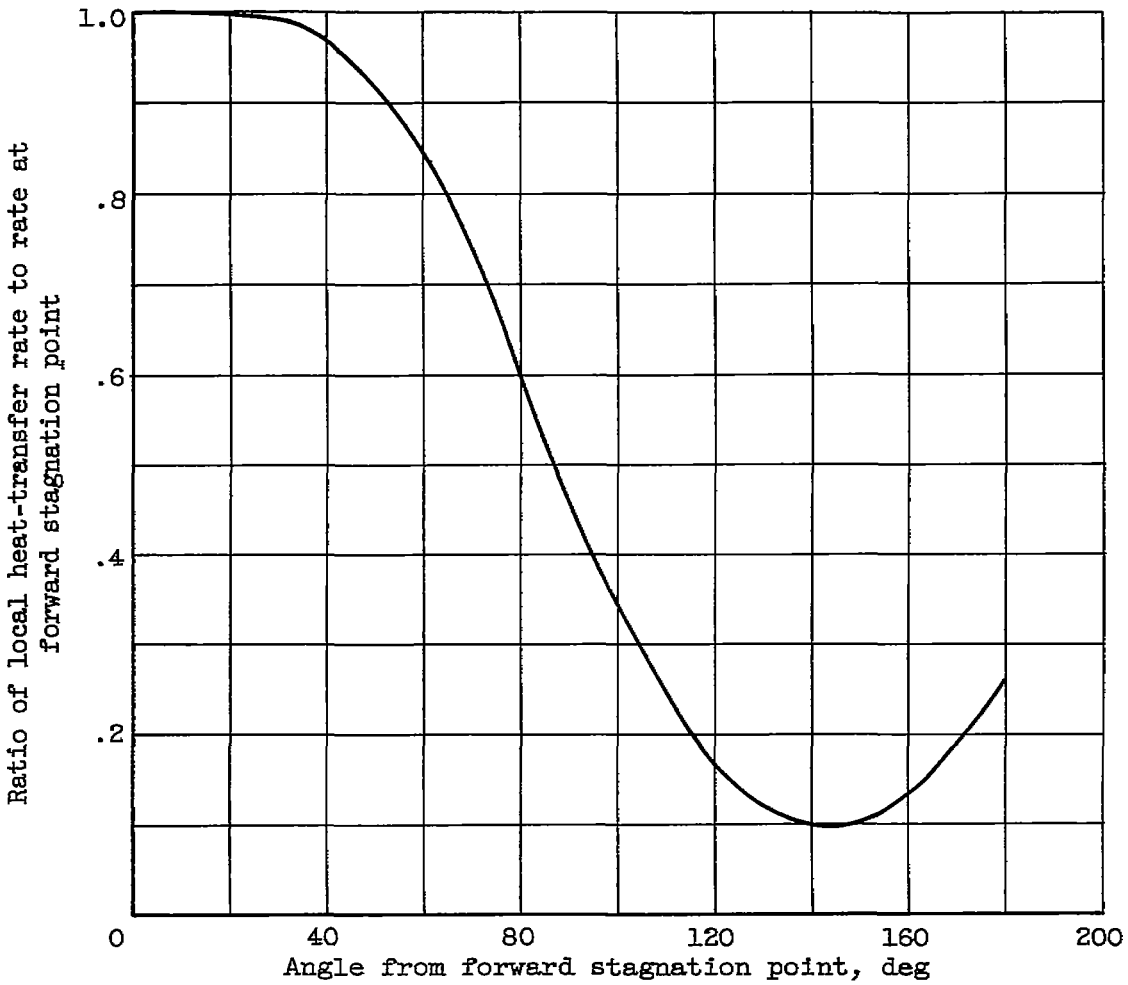

Figure I-18. - Change in local heat-transfer rate over surface of a sphere in air stream. Reynolds number, 136 (ref. 62).

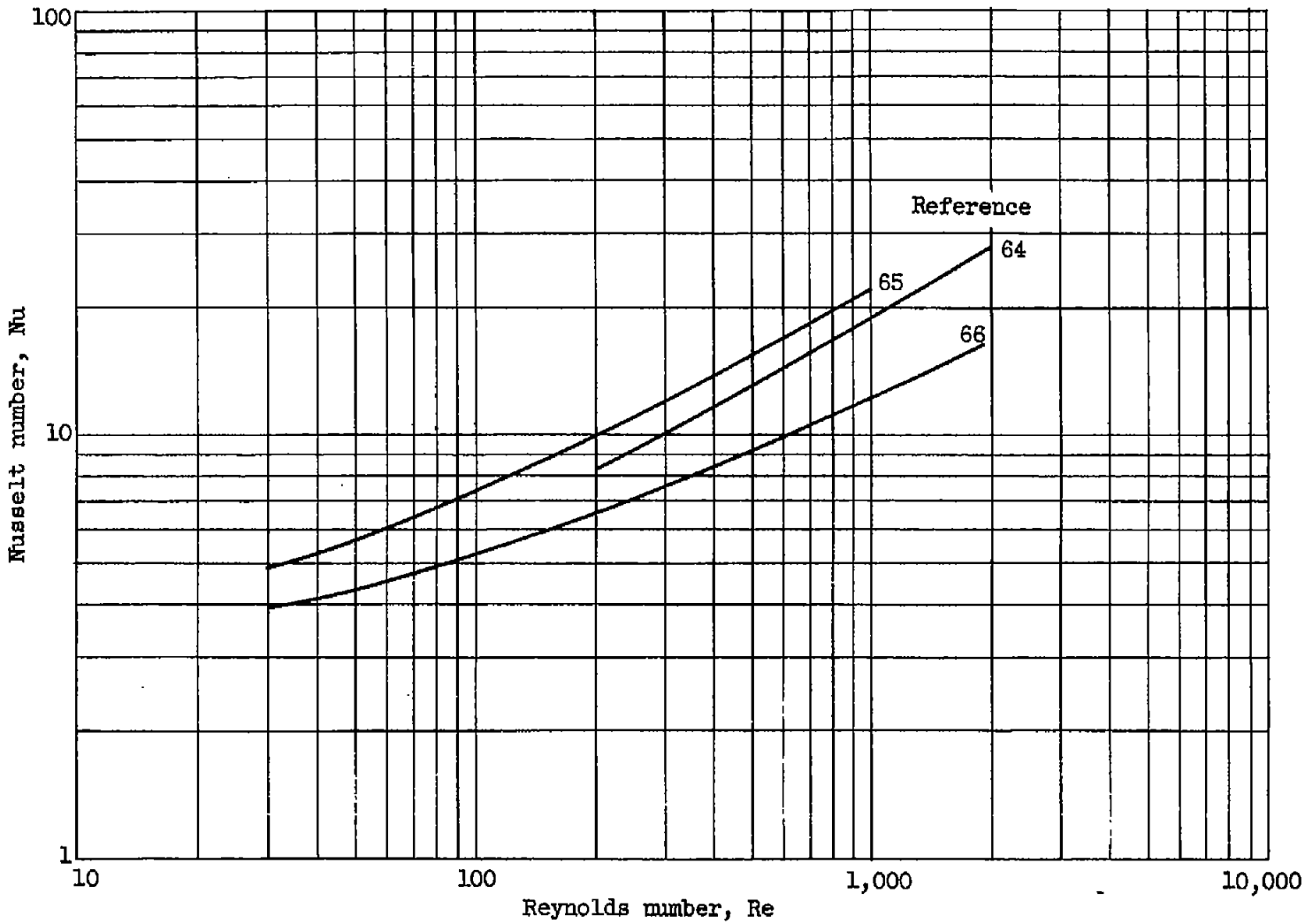

Figure I-19. - Predicted Nusselt numbers for heat transfer for spheres in air.

[redacted]

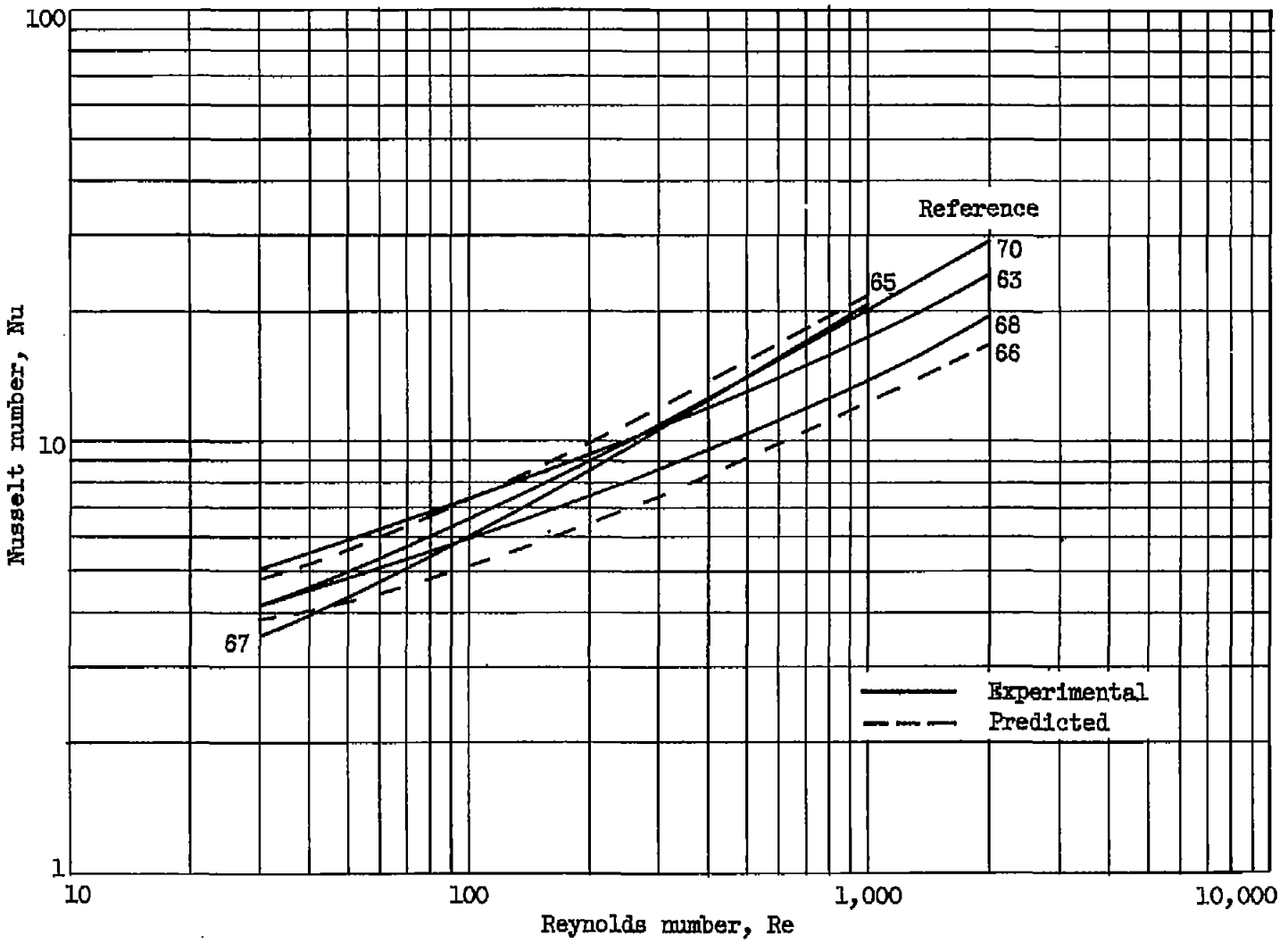

Figure I-20. - Predicted and experimental Nusselt numbers for heat transfer for spheres in air.

[redacted]

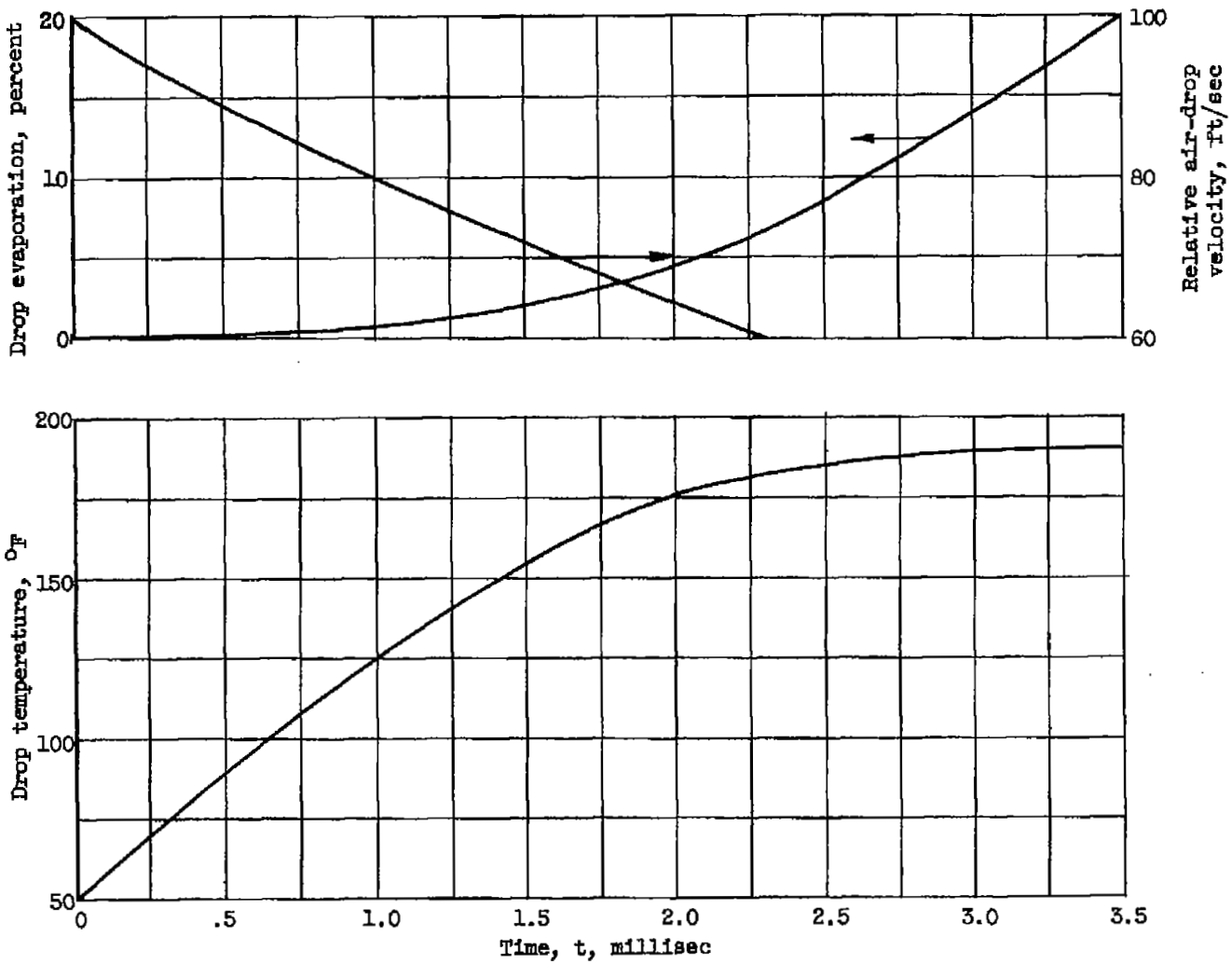

Figure I-21. - Unsteady-state evaporation of isooctane drop into air at 1000° F and 0.5 atmosphere. Drop diameter, 50 microns; initial drop temperature, 50° F; initial drop velocity, 100 feet per second (ref. 79).

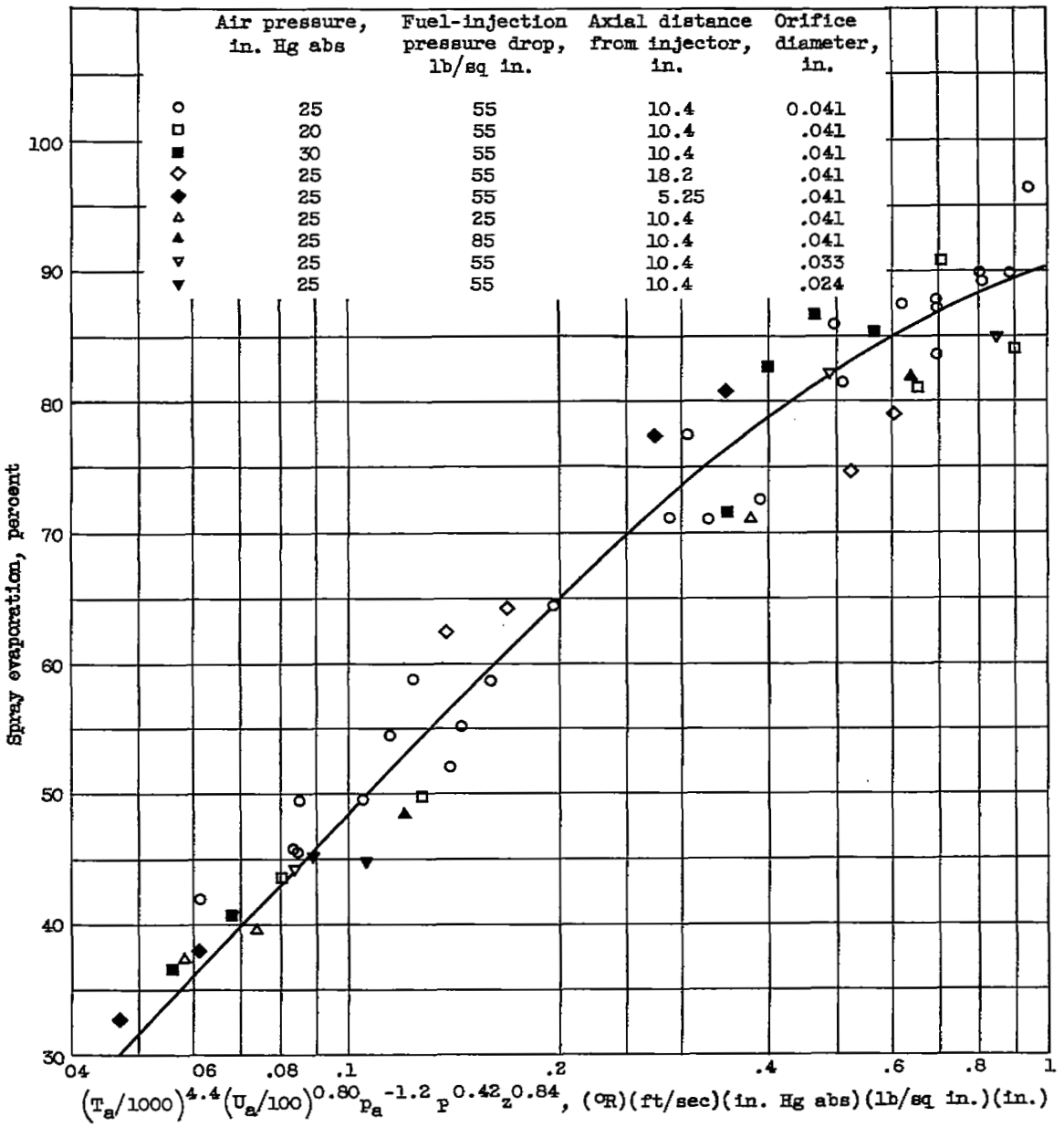

Figure I-22. - Correlation of percentage fuel spray evaporated for contrastream injection of isooctane from a simple orifice. Air velocity, 100 to 350 feet per second; air temperature, 80° to 390° F (ref. 89).

Chapter II

FLOW AND MIXING PROCESSES IN COMBUSTION CHAMBERS

By Wilfred E. Scull and William R. Mickelsen

INTRODUCTION

3267

The principal purpose of the combustion chamber in a jet engine is the efficient conversion of chemical energy contained in a fuel into the heat and kinetic energy of the exhaust gases. The energy conversion must occur efficiently not only in terms of the completeness of the combustion reaction, but also in an aerodynamic sense. Aerodynamic efficiency implies an efficient introduction and distribution of air in a combustion chamber for the purposes of burning a fuel-air mixture, and a dilution of the combustion products to the desired temperature level and proper temperature profile. In many instances, combustion efficiency may be sacrificed for aerodynamic efficiency, and vice versa.

According to various authors, the combustion problem may be quite largely aerodynamic in character. This was recognized in some of the earliest research on turbojet engines for aircraft propulsion (ref. 1), in which it was found that differences in combustor performance in engine tests and single-combustor tests could be traced directly to differences in the manner in which air flowed into the combustion chamber. In similar tests (ref. 2) with a sector of an annular combustor in a stationary test facility and the entire combustor installed in a full-scale engine, differences in air flow at the combustor inlet resulted in variations in combustion efficiency and poor temperature distribution at the combustor outlet.

The importance of aerodynamics in the problem of combustion is further emphasized by the fact that a finely dispersed spray of liquid fuel or a portion of combustible gas well mixed with stoichiometric proportions of air will not ignite and form a stable flame front at velocities greater than the velocity of laminar flame propagation (approximately 1 to 2 ft/sec for most hydrocarbon fuels), unless the aerodynamic flow pattern is such that localized vortices, zones of flow reversal, or a slowly moving boundary layer exists in the combustion zone. To stabilize the flame at the high velocities encountered in jet engines, it is therefore necessary to create low-velocity regions in which the flame can originate or else establish an aerodynamic flow pattern such that localized vortices or zones of flow reversal are created. Such vortices or zones of reverse flow allow the combustible mixture to attain local velocities necessary for high mass flow without exceeding translational velocities that could cause instability of the flame front.

The object of this discussion is the consideration of aerodynamic relations applicable to the design of combustion chambers of jet engines. Experimental and theoretical data relating combustor approach-stream parameters, combustor pressure losses, gas jets of many types, and orifice coefficients are included. Aerodynamic mixing is discussed in terms of fundamental turbulent diffusion theories relating heat, mass, and momentum transfer from different sources in various types of flow fields. The effect of periodic flow fluctuations on diffusion is discussed. Fuel-air mixing is presented in terms of spreading of liquid and vapor fuel from several different sources.

SYMBOLS

The following symbols are used in this chapter:

A	cross-sectional area
A^*	ratio of one of two parallel-jet areas to total mixed-jet area
a	distance between vortices in single row
a^*	flame-holder width
B,B'	dimensionless quantities
B^*	function of flow rates, velocities, areas, and angles between two mixing jets
b	constant
C	concentration
C_D	drag coefficient of droplet
C_{fr}	dimensionless friction coefficient
C_h	orifice discharge coefficient
C^*	function of flow rates, areas, and total temperatures of two mixing jets
c	mixing-length parameter
c_p	isobaric specific heat
D	turbulent diffusion coefficient
D_H	coefficient of turbulent diffusion of heat
$D_{l,f}$	diffusion coefficient for liquid fuel droplets
D_M	coefficient of turbulent diffusion of mass
D_U	coefficient of turbulent diffusion of momentum
d	diameter
d_M	molecular diffusion coefficient (mass)
d'	duct width
E,E',E''	functions of ϵ
F	drag
$F(f)$	spectrum density function of turbulent kinetic energy

f	fuel-air ratio
$\mathscr{f}$	frequency of vortex shedding
$\mathscr{f}_T$	frequency of turbulent fluctuations
G	weight-flow rate per unit area
g	gravitational constant
H	specific enthalpy
h	depth of rectangular duct
I	combustion intensity
i	lateral spacing between vortex rows
J	total fuel-spreading parameter
j	fraction of fuel evaporated before reaching point at which f_l is measured
K	strength of individual vortex
K^*	strength of point source
$k_1, k_2, \ldots$	constants
L	length
L^*	length of duct between station where Mach number is taken and station where choking would occur
$\mathscr{L}$	Lagrangian scale of turbulence
$\mathscr{L}'$	Eulerian scale of turbulence
l	penetration of jet
M	Mach number
m	momentum of jet at any cross section
N	engine rotational speed
n	number
P, P'	functions of W, U, α and W, T_t
Pr	Prandtl number
p	absolute pressure
$p_{t,2}/p_{t,\infty}$	diffuser total-pressure recovery factor

3267

$p_{t,3}/p_{t,2}$	compressor total-pressure ratio
Δp	pressure loss
$\Delta p_t/p_t$	total-pressure loss ratio
$\Delta p_t/q_r$	total-pressure loss coefficient
p^*	absolute pressure with choked flow
Q	total quantity of heat transferred
q	velocity pressure
R	gas constant
Re	Reynolds number
$\mathscr{R}$	Lagrangian double velocity correlation coefficient
$\mathscr{R}'$	Eulerian double velocity correlation coefficient
r	radial distance
r_c	compressor total-pressure ratio, $p_{t,3}/p_{t,2}$
r_{hy}	hydraulic radius
$r_{1/2}$	half-radius of axially symmetric jet at longitudinal distance x
r'	radial distance in disk source of radius S
r^*	inside radius of contrastream fuel injector
S	disk source radius
Sc	Schmidt number
s	longitudinal distance from jet center line
$s(\sigma)$	function of y/y_o
T	absolute temperature
$\overline{T}$	mean absolute temperature
T'	fluctuating value of absolute temperature
t	time
$t_{\mathscr{L}}$	characteristic time related to Lagrangian scale
t'	time, controlling rate of fuel injection

3267

U	velocity component in x-direction
u	turbulent velocity in x-direction
$\bar{u}$	time-average of u
$\sqrt{\overline{u^2}}$	turbulent intensity in x-direction
V	velocity component in r- or y-direction
v	turbulent velocity in y-direction
$\bar{v}$	time-average of v
$\sqrt{\overline{v^2}}$	turbulent intensity in y-direction
W	weight-flow rate
W'	weight-flow rate of diffusing quantity as function of time t'
W^*	weight-flow rate of diffusing quantity
w	turbulent velocity in z-direction
$\bar{w}$	time-average of w
$\sqrt{\overline{w^2}}$	turbulent intensity in z-direction
X	distance normal to A, or rectangular coordinate
x	longitudinal distance
x^*	distance from junction of two parallel jets
$\bar{Y}$	mean displacement
y	distance from center line of plane-parallel jet
$z(\sigma)$	function of r/r_o
α	angle between gas streams
β	function of $p_{t,j}$ and p_j
Γ	fluid shearing stress
γ	ratio of specific heats
δ	ratio of absolute pressure to NACA standard sea-level pressure, p/2116.2
$\delta(f-f_{per})$	Dirac delta function
ϵ	r/x
ζ	function of $p_{t,j}$ and p_j

3267

η	adiabatic efficiency
θ	ratio of absolute temperature to NACA standard sea-level temperature, $T/518.7$
$\varkappa$	thermal conductivity
Λ	range of droplet
λ	Lagrangian microscale of turbulence
μ	absolute viscosity of fluid
ν	kinematic viscosity of fluid
ξ	function of m, r, x, ν, and ρ in laminar free jet
ρ	fluid weight per unit volume
$\sqrt{\frac{\rho u^2}{\rho}}$	momentum flux velocity
σ	y/y_o or r/r_o
τ	temperature coefficient in jet
Φ	approximate mean vorticity
φ	dimensionless quantity
Ψ	stream function
ψ	function of U, D_x, r, r'
Ω	function of B^*, C^*, γ_3, M_3
ω	standard square deviation
ω'	standard square deviation evaluated at time $t - t'$

Subscripts:

A	known combustor conditions
a	air
an	annulus
B	new combustor conditions
C	cylinder
c	compressor
cf	crossflow

3267

cor	corrected
D	first
d	diffusion
dr	droplet
dt	duct
E	second
e	external
F	in plane of flame holder
f	fuel
fr	friction
G	third
H	heat
h	orifice
i	rectangular coordinates
ib	inner body
j	jet
L	molecular motion
$\mathscr{L}$	Lagrangian characteristic
l	liquid
M	mass
m	mixing
max	on axis of jet
no	normal
o	outer boundary of jet
ob	oblique
op	open
ov	over-all
p	potential core
per	periodic

2267

r	reference
rel	relative to free stream
S	Stokes' law
s	finite band width
T	turbulent
t	total
tu	turbine
U	momentum
u	pertaining to x-direction
v	pertaining to y-direction
w	pertaining to z-direction
x	position relative to x-direction
y	position relative to y-direction
z	position relative to z-direction
0	time zero
1	in space surrounding jet
2	compressor inlet
3	combustor inlet
3'	longitudinal position between combustor inlet and combustor outlet
4	combustor outlet
∞	free stream

3267

AERODYNAMIC FLOW

COMBUSTOR APPROACH-STREAM PARAMETERS

Turbojet Combustion Chambers

The more important combustor approach-stream parameters for a turbojet engine consist of inlet-air velocity, temperature, and pressure. A less important parameter is the combustor-inlet velocity profile. Each of these parameters may vary over a wide range dependent upon the operational variables of engine speed, flight Mach number, and flight altitude. The following table indicates the range of the combustor operating variables encountered during operation of a turbojet engine with a sea-level static compression ratio of 11 at a flight Mach number of 0.8 at various engine speeds and altitudes:

Altitude, ft	Engine speed	Inlet pressure, in. Hg abs	Inlet temperature, °F	Air flow, lb/sec
Sea level	Rated	376.5	708	197.9
	Idle	64.1	215	54.7
	Windmill	42.5	120	44.0
60,000	Rated	40.3	625	18.1
	Idle	6.1	113	4.7
	Windmill	2.2	30	2.7

In addition, supersonic flight speeds tend to increase the range of operating variables still further. For example, a supersonic turbojet engine which has a sea-level static compression ratio of 7.0 would have a combustor-inlet total temperature of 964° F during rated engine speed operation at a flight Mach number of 2.8 in the stratosphere.

Generalized parameters. - Sanders (ref. 3) developed performance parameters for jet engines from concepts of flow similarity, inertia, elastic and viscous forces, and thermal expansions of the working fluid. Dimensionless and corrected dimensional generalizing parameters were employed to relate engine performance to the geometry of the engine boundaries, the Mach number, the Reynolds number, and the total-temperature ratio of the engine. For turbojet engines, it was shown that

$$\frac{W_a\sqrt{\theta_t}}{\delta_t} = f\left(\frac{p_t}{\delta_t}, \frac{T_t}{\theta_t}, \frac{N}{\sqrt{\theta_t}}\right) \tag{1}$$

where

N engine rotational speed

p_t absolute total pressure

T_t absolute total temperature

W_a weight-flow rate of air

In equation (1),

$$\theta_t = \frac{T_t}{518.7} \tag{2}$$

and

$$\delta_t = \frac{p_t}{2116.2} \tag{3}$$

with T_t in °R, p_t in pounds per square foot absolute, and θ_t and δ_t usually evaluated in terms of the total temperature and pressure at the compressor inlet.

From equation (1), it is apparent that the corrected weight-flow rate of air $W_a\sqrt{\theta_t}/\delta_t$, the corrected absolute total pressure p_t/δ_t, and the corrected absolute

total temperature T_t/θ_t at any position in the engine are substantially constant for a constant corrected engine speed $N/\sqrt{\theta_t}$. These generalizations are valid at altitudes up to 40,000 feet. At higher altitudes, the effect of Reynolds number becomes apparent in the performance of the compressor. As a result, the corrected air flow $W_a\sqrt{\theta_t}/\delta_t$ does not remain constant for a constant corrected engine speed $N/\sqrt{\theta_t}$, but begins to diminish slightly with increasing altitudes. This decrease is a function of the particular engine under consideration (ref. 4). However, it has been shown that Reynolds number has very little or no effect on the compressor total-pressure ratio at extreme altitudes if the corrected engine speed remains constant (ref. 5).

New combustor-inlet conditions can be calculated as follows: Let subscripts A and B indicate the known and new inlet conditions, respectively, while subscripts 2 and 3 denote the compressor inlet and the combustor inlet, respectively. Then 3267

$$N_B = N_A\left(\sqrt{\frac{\theta_{t,B}}{\theta_{t,A}}}\right)_2 \tag{4}$$

$$W_{a,B} = W_{a,A}\left(\frac{\delta_{t,B}}{\delta_{t,A}}\sqrt{\frac{\theta_{t,A}}{\theta_{t,B}}}\right)_2 \tag{5}$$

$$p_{t,B,3} = p_{t,A,3}\left(\frac{\delta_{t,B}}{\delta_{t,A}}\right)_2 \tag{6}$$

where θ_t and δ_t are evaluated at the stations indicated by the subscripts. The value of the compressor-inlet absolute total temperature $T_{t,2}$ used in the determination of θ_t in equation (2) can be obtained from the expression

$$T_{t,2} = T_\infty\left(1 + \frac{\gamma-1}{2}M_\infty^2\right) \tag{7}$$

where

M_∞ flight Mach number

T_∞ ambient absolute temperature

γ specific heat ratio

Determination of the compressor-inlet absolute total pressure $p_{t,2}$ used in determination of δ_t in equation (3) requires a knowledge of the diffuser total-pressure recovery factor. Losses in total pressure in the engine inlet diffuser can occur as the result of friction, inefficient diffusion, or possible shock formation. Typical total-pressure recovery factors that can be used for current engine diffusers are presented in figure II-1 (ref. 6). The sharp decrease in recovery factors at high Mach numbers is due to shock formation at the diffuser inlet. The value of $p_{t,2}$ can be calculated from

$$p_{t,2} = \frac{p_{t,2}}{p_{t,\infty}} p_\infty \left(1 + \frac{\gamma-1}{2} M_\infty^2\right)^{\frac{\gamma}{\gamma-1}} \tag{8}$$

As mentioned previously, the combustor-inlet total temperature can be determined from the constancy of T_t/θ_t with a constant $N/\sqrt{\theta_t}$. However, if the compressor total-pressure ratio and adiabatic efficiency are known as a function of corrected engine speed and altitude, a better determination is

3267

$$T_{t,3} = T_{t,2}\left[1 + \frac{(r_c)^{\frac{\gamma-1}{\gamma}} - 1}{\eta_c}\right] \tag{9}$$

where

r_c compressor total-pressure ratio, $p_{t,3}/p_{t,2}$

η_c compressor adiabatic efficiency

The combustor-inlet absolute total pressure can be determined from the relation

$$p_{t,3} = p_{t,2} \frac{p_{t,3}}{p_{t,2}} = p_{t,2}\, r_c \tag{10}$$

Compressor wake effects. - The aerodynamic design of the turbojet combustor is closely related to the air-flow pattern at the compressor exit. Ideally, the optimum combustor-inlet air-flow pattern might have a uniform velocity profile with an average velocity determined by the preceding equations. However, especially in engines with centrifugal compressors, the velocity profile at the inlet may be nonuniform. Two combustor-inlet velocity profiles for an axial-flow turbojet engine are presented in figure II-2. These particular profiles show wider variations with engine operating speed than are usually found in current engines.

Uneven velocity profiles can be significant in terms of combustor total-pressure losses and operating problems. Lloyd (ref. 7) indicates that one of the major sources of combustor total-pressure loss is the entry loss associated with the diffusing and evening of the high-velocity air stream from the compressor. In addition to total-pressure losses, uneven inlet velocity profiles with accompanying uneven secondary-air distribution and unequal liner cooling might result in distortion and cracking of the combustor liner (ref. 8). Maldistribution of the air flow at the combustor inlet might also be responsible for asymmetric fuel sprays and noncentralized burning.

Ram-Jet Combustion Chambers - Generalized Parameters

Combustor approach-stream parameters (inlet-air velocity, temperature, and pressure) for a ram-jet combustor are the same as for a turbojet combustor. As with a turbojet combustor, these parameters may vary over a wide range; however, the range is dependent only upon flight Mach number and flight altitude for the ram jet. Determination of the approach-stream parameters is, in general, simpler for the ram-jet combustor than for the turbojet. Since there is no compressor in a

ram-jet engine, all the compression occurs in the diffuser. Combustor-inlet absolute total temperature and pressure can be determined by the following equations:

$$T_{t,3} = T_\infty\left(1 + \frac{\gamma-1}{2} M_\infty^2\right) \tag{11}$$

$$p_{t,3} = \frac{p_{t,2}}{p_{t,\infty}} \times p_\infty\left(1 + \frac{\gamma-1}{2} M_\infty^2\right)^{\frac{\gamma}{\gamma-1}} \tag{12}$$

As with the turbojet, the diffuser total-pressure recovery factor must be known in order to determine the combustor-inlet pressure. The data in figure II-1 are applicable to both types of engines. 3267

As a rule, combustor inlet-air velocity is selected to satisfy the thrust requirements of the engine. Thus, for a known combustor-inlet area, flight altitude, and flight Mach number, the combustor mass air flow can be determined from

$$W_a = \frac{A_3 U_3}{R_a} \frac{p_{t,3}}{T_{t,3}\left(1 + \frac{\gamma-1}{2} M_3^2\right)^{\frac{1}{\gamma-1}}} \tag{13}$$

where

A_3 combustor-inlet area

M_3 combustor-inlet Mach number

R_a gas constant for air

U_3 combustor-inlet air velocity

and

$$M_3 = \frac{U_3}{\sqrt{\gamma g R_a T_{t,3} - \frac{(\gamma-1)\, U_3^2}{2}}} \tag{14}$$

where

g gravitational constant

Data which can be used for rapid determination of the inlet conditions in a ram-jet engine are presented in figure II-3. This figure is based on the diffuser total-pressure recoveries of figure II-1.

COMBUSTOR PRESSURE LOSSES

In any type of combustion chamber, regions of low gas velocity must be present if stable combustion is to be maintained. Liners and flame holders are used in turbojet and ram-jet combustors, respectively, to provide stabilizing regions of low velocity. Advantages gained by use of such stabilizing mechanisms may be balanced by combustor pressure losses, which result in losses in over-all cycle efficiency.

Effect on Over-All Cycle Performance

The effect of combustor pressure loss on cycle efficiency has been expressed in reference 9 as

$$\frac{d\eta}{d\left(\frac{\Delta p_t}{p_{t,3}}\right)} = -\frac{\eta_c \eta_{tu}\left(\frac{\gamma-1}{\gamma}\right)\left(1-\frac{\Delta p_t}{p_{t,3}}\right)^{\frac{1-2\gamma}{\gamma}} r_c^{\frac{1-\gamma}{\gamma}}}{\eta_c\left(1-\frac{T_{t,2}}{T_{t,4}}\right)-\frac{T_{t,2}}{T_{t,4}}\left(r_c^{\frac{\gamma-1}{\gamma}}-1\right)} \tag{15}$$

where

Δp_t combustor total-pressure loss

$T_{t,4}$ combustor-outlet total temperature

η_{tu} turbine adiabatic efficiency

The denominator of the right side of equation (15) is always positive and proportional to the heat added in the combustor. As shown by figure II-4, total-pressure losses in turbojet engines are important, especially when operating at very low or very high over-all pressure ratios. For compressor total-pressure ratios less than 9, increases in compressor total-pressure ratios resulted in decreased effects of combustor total-pressure losses. With higher pressure ratios, combustor pressure losses caused greater thrust losses. These increases in thrust loss are caused by the greatly increased power required to operate the compressor at the high pressure ratios. Increasing pressure losses with accompanying decreases in cycle efficiency result in increases in fuel consumption. Likewise, increases in unit size become necessary, since higher rotative speeds and accompanying higher turbine stresses are required to obtain the higher compression ratios needed to maintain maximum cycle efficiencies with increasing pressure losses (ref. 10).

Causes

Pressure losses in combustors occur as the result of several factors: (1) abrupt changes in flow cross-sectional areas, (2) bluff bodies or flame-stabilizing devices in the combustion zone causing partial blockage of the open cross-sectional area, (3) frictional forces exerted upon the gas stream by flame-stabilizing devices and the walls of the combustion chamber, (4) increases in

momentum imparted to the gas stream as it flows through the combustor, and (5) the high degree of turbulence necessary to mix gases in a restricted combustion volume.

Changes in flow cross-sectional area due to expansion. - Pressure losses in the combustor-inlet diffuser, which partially slows the high-velocity air stream from the compressor, may be attributed to the combustor. For the case of sudden enlargements, which is the condition approached by some very short combustor-inlet diffusers, the following diagram is considered:

3267

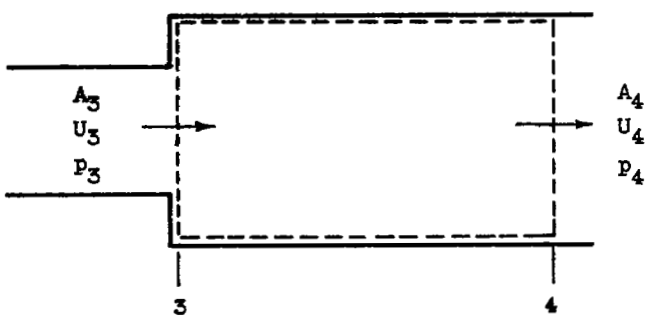

Application of Newton's second law to the control volume shown by the dotted lines yields the total-pressure loss Δp_t due to sudden enlargements as

$$\Delta p_t = \frac{\rho_3 U_3^2}{2g}\left(1 - 2\frac{A_3}{A_4}\right) + \frac{\rho_4 U_4^2}{2g} \tag{16}$$

where

ρ weight of fluid per unit volume

If the assumption is made that the fluid or gases are incompressible, which, for gas velocities of less than 400 feet per second, incurs an error less than the probable error of data for computing friction losses in pipe flow, the equation reduces to (ref. 11)

$$\Delta p_t = \frac{\rho_3 U_3^2}{2g}\left(1 - \frac{A_3}{A_4}\right)^2 \tag{17}$$

This equation can be used for any shape of cross section, and for fluids or gases in turbulent flow.

Obviously, a sudden enlargement is undesirable. However, length limitations in ram-jet or turbojet engines generally necessitate short diffusers. As a result, diffuser included angles are usually large. Figure II-5 (refs. 12 and 13) presents the pressure loss of diffusers as a function of the included angle. An optimum included angle of 7° to 10° is indicated for minimum pressure loss. Reductions in total-pressure loss for large angles of diffusion can be accomplished by introduction of a spiral flow or rotation into the gas flow upon entry to the diffuser (ref. 12). Reductions in total-pressure loss, with spiral flow or rotation

in the gas flowing in the diffuser, of as much as 45 to 60 percent are reported in reference 12. Similar results are expressed in reference 14 in terms of the increase in static pressure rise through a short 2:1 area ratio diffuser by use of rectangular vortex generators.

Changes in flow cross-sectional area due to contraction. - Liners or flame holders in the combustion volume serve not only as flame stabilizers but also house the combustion zone, proportion the air flow, and introduce turbulence necessary for good mixing of hot and cold gases during the combustion process. Insertion of a liner or flame holder in the combustion volume results in pressure losses, which, though unavoidable, can often be minimized. Blockage of the open cross-sectional area of a combustor may be considered somewhat similar to a sudden contraction in the flow area in a pipe. For sudden contractions, the following diagram is considered:

3267

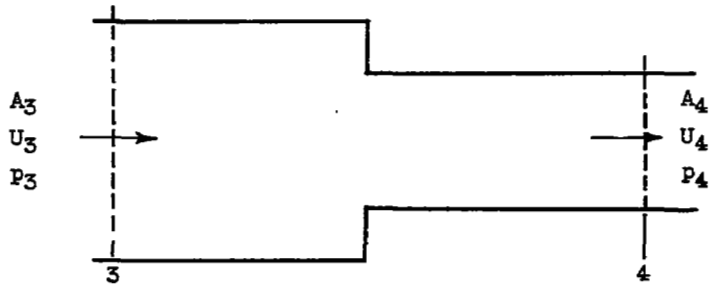

Assuming incompressibility, reference 15 indicates the total-pressure loss in this case to be

$$\Delta p_t = k_1 \frac{\rho_4 U_4^2}{2g} \tag{18}$$

where k_1 depends on the ratio of areas at stations 3 and 4 and is defined by

$$k_1 = 0.4\left(1.25 - \frac{A_4}{A_3}\right) \quad \text{for} \quad \frac{A_4}{A_3} < 0.715 \tag{19a}$$

and

$$k_1 = 0.75\left(1 - \frac{A_4}{A_3}\right) \quad \text{for} \quad \frac{A_4}{A_3} > 0.715 \tag{19b}$$

Total-pressure losses due to sudden contractions may be greatly reduced by using a conical or well-rounded transition section between areas 3 and 4. The value of k_1 for conical or well-rounded transition sections is reduced to approximately 0.05. This value of k_1 is applicable for all values of A_4/A_3, provided that the flow in the smaller area is turbulent.

Body shape and blocked area. - Ram-jet combustion chambers and afterburners utilize a flame-holding mechanism consisting of gutters or similar devices to provide a recirculatory zone of low velocity for flame stabilization. Usually, such devices in the combustion chamber provide more turbulence and better mixing, with

resultant increases in combustion efficiency. However, such devices create an unavoidable pressure loss with an accompanying adverse effect on over-all cycle efficiency. A theoretical analysis of the total-pressure losses in a combustion chamber using V-gutter flame holders is presented in reference 16. Compressible, nonviscous, one-dimensional flow was assumed. Data showing the theoretical total-pressure loss coefficient $\Delta p_t/q_r$ are presented in figure II-6, in which

A_F open flow area in plane of flame holders

k_2 area contraction coefficient, equal to flow area of vena contracta downstream of a flame holder divided by A_F

3267

q_r reference velocity pressure based on combustor-inlet air density and maximum cross-sectional area of combustor

For most purposes, k_2 may be assumed between 0.8 and 0.9. The data of figure II-6 have been replotted in figure II-7 at an inlet Mach number of 0.20 to show the effect of area blockage on the total-pressure loss coefficient. Also included are the theoretical loss coefficients for staggered flame holders (ref. 17). The data for staggered flame holders are valid only when the baffles at each plane provide approximately the same blockage. Total-pressure losses increase with increases in blocked area. In addition, total-pressure losses do not seem to be greatly affected by baffle geometry, being dependent more on blocked area.

For sloping-gutter flame holders, the projected area of the flame holders should be used to determine the area blockage.

For combustion chambers having center bodies in addition to gutter flame holders, the following equation (ref. 17) may apply:

$$\frac{\Delta p_t}{q_r} = \left[0.9\left(1 - \frac{A_F}{A_3}\right) + 0.45\left(\frac{A_{ib}}{A_3}\right)\right] \frac{q_F}{q_r} \tag{20}$$

where

A_{ib} area of inner body

q_F velocity pressure in flame-holder plane

Fluid friction. - Frictional total-pressure losses in combustors are generally small enough to be neglected in comparison with other factors causing pressure losses. However, in ram-jet engines and afterburners in which high-velocity gases scrub relatively long walls of the combustion chamber, frictional total-pressure losses may not be negligible. The total-pressure loss due to friction of a fluid flowing in a duct can be expressed by the Fanning friction equation (ref. 18):

$$\Delta p_{t,fr} = \frac{\rho U^2}{2g} C_{fr} \frac{L}{r_{hy}} \tag{21}$$

where

C_{fr} dimensionless friction coefficient

L duct length

$\Delta p_{t,fr}$ total-pressure loss due to friction

r_{hy} duct hydraulic radius

and ρ and U are average values. In figure II-8 (ref. 19), values of C_{fr} are presented for a range of Reynolds numbers from 10^4 to 10^7. The value of C_{fr} varies from 0.004 to 0.0035 for Reynolds numbers from 2.5×10^5 to 5.0×10^5. Reference 20 includes data from which the effect of wall friction alone upon a fluid flowing in a cylindrical duct can be estimated if the Mach number at the entrance and the friction coefficient of the chamber are known. Figure II-9 presents data showing the total-pressure loss in terms of these variables. Use of the figure can be demonstrated best by an example. Consider air flowing in a 6-inch-diameter duct at an inlet Mach number of 0.25 at sea level. The duct is 30 inches in length and the total-pressure loss is required.

Average air velocity in duct = $0.25\times1120 = 280$ ft/sec

Air density = 0.0766 lb/cu ft

Air viscosity = 3.723×10^{-7} slugs/(ft)(sec)

$$\text{Reynolds number} = \frac{\frac{0.0766}{32.2} \times 280 \times 0.5}{3.723\times10^{-7}} = 8.95\times10^5$$

For this Reynolds number, $C_{fr} = 0.0032$, while

$$r_{hy} = \frac{1}{4}\,(\text{duct diameter}) = \frac{0.5}{4} = 0.125 \text{ ft and}$$

$$\frac{C_{fr}L}{r_{hy}} = \frac{0.0032 \times 2.5}{0.125} = 0.064$$

For an inlet Mach number of 0.25,

$$\left(\frac{C_{fr}L^*}{r_{hy}}\right)_3 = 8.6$$

where

L^* duct length between station at which Mach number is taken and station at which choking would occur

and

$$\frac{p_{t,3}}{p_t^*} = 2.39 \text{ (fig. II-9)}$$

where

p_t^* total pressure with choked flow

$$\left(\frac{C_{fr}L^*}{r_{hy}}\right)_4 = \left(\frac{C_{fr}L^*}{r_{hy}}\right)_3 - \frac{C_{fr}L}{r_{hy}} = 8.6 - 0.064 = 8.536$$

For $\left(\frac{C_{fr}L^*}{r_{hy}}\right)_4 = 8.536$,

$M_4 = 0.255$,

$$\frac{p_{t,4}}{p_t^*} = 2.38$$

and

$$\frac{\Delta p_{t,fr}}{p_{t,3}} = 1 - \left(\frac{\frac{p_{t,4}}{p_t^*}}{\frac{p_{t,3}}{p_t^*}}\right) = 1 - \frac{2.38}{2.39} = 0.004$$

Momentum. - The momentum pressure loss in combustion chambers, which is inherent in any system in which heat is added to a moving gas stream, can be determined simply in terms of temperature ratios and Mach numbers by the following analysis:

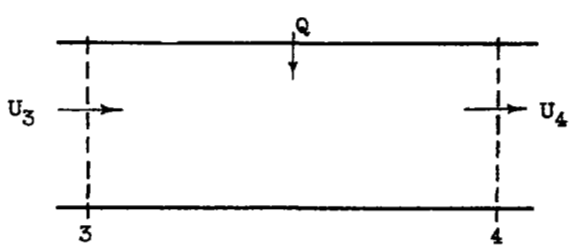

It is assumed that the gases are evenly mixed with respect to temperature and pressure at the entrance and exit of the combustor, that the gases are perfect and nonviscous, and that one-dimensional flow applies. Application of Newton's second law and the continuity equation leads to

$$\frac{\Delta p_t}{p_{t,3}} = 1 - \frac{1 + \gamma_3 M_3^2}{1 + \gamma_4 M_4^2}\left(\frac{1 + \frac{\gamma_4 - 1}{2} M_4^2}{1 + \frac{\gamma_3 - 1}{2} M_3^2}\right)^{\frac{\gamma}{\gamma - 1}} \tag{22}$$

and

$$\frac{T_{t,4}}{T_{t,3}} = \left(\frac{\gamma_4 R_3}{\gamma_3 R_4}\right)\left[\frac{M_4(1 + \gamma_3 M_3^2)}{M_3(1 + \gamma_4 M_4^2)}\right]^2\left(\frac{1 + \frac{\gamma_4 - 1}{2} M_4^2}{1 + \frac{\gamma_3 - 1}{2} M_3^2}\right) \tag{23}$$

where γ is an average value determined from γ_3 and γ_4. For critical or choked flow through an opening, the Mach number at the opening equals 1.0. For the condition of choking at the combustor exit, since M_4 equals 1.0,

3267

$$\frac{\Delta p_t}{p_{t,3}} = 1 - \frac{1 + \gamma_3 M_3^2}{1 + \gamma_4}\left[\frac{\gamma_4 + 1}{2 + (\gamma_3 - 1)M_3^2}\right]^{\frac{\gamma}{\gamma - 1}} \tag{24}$$

and

$$\frac{T_{t,4}}{T_{t,3}} = \left(\frac{\gamma_4 - 1}{\gamma_3 - 1}\right)\left(\frac{R_3}{R_4 M_3}\right)^2\left[\frac{(1 + \gamma_3 M_3^2)^2}{(1 + \gamma_4)\left(1 + \frac{\gamma_3 - 1}{2} M_3^2\right)}\right] \tag{25}$$

According to equation (23), the addition of heat or the increase of total temperature of any fluid in frictionless flow in a duct will result in an increase in M_4 if M_3 is subsonic, and a decrease in M_4 if M_3 is supersonic. The subsonic case only is considered here. Choking at the combustor exit does not mean that more fuel cannot be burned, provided sufficient air is present. It does mean, however, that if more fuel is burned, the combustor-inlet conditions will adjust to compensate for the increase in total-temperature ratio. The preceding equations are expressed in figure II-10 in terms of the effect of inlet and outlet conditions upon the total-pressure loss in a duct due to heat addition for $\gamma = 1.4$ and constant R. Total-pressure loss due to combustion decreases with decreases in combustor-inlet Mach number for a given temperature ratio.

Isothermal flow behind bluff bodies. - The flow behind bluff bodies such as flame holders in ram-jet combustion chambers may have noticeable effects on the combustor performance. Introduction of a cylindrical rod or a V-gutter flame holder into a moving gas stream results in the formation of vortices in the region immediately downstream. These vortices can be explained as follows: At extremely low Reynolds numbers (using the width of the bluff body as the length dimension), the streamlines of the flow broaden out behind the obstacle. As the Reynolds number is increased, the streamlines widen more and more, forming a closed region behind the object, within which there is an inflow along the axis of the wake and a flow in the general direction of motion in the outer portions. These motions form a pair of vortices, and exist at low Reynolds numbers, but become more prominent as the Reynolds number increases. With further increases in Reynolds number, the vortices become more elongated and asymmetrical, break off, and move downstream. This vortex shedding occurs at some critical Reynolds number which depends upon flame-holder shape, turbulence of the gas stream, and any wall effects from the combustion chamber. Reference 21 reports visual observation of the formation and shedding of vortices by the use of balsa dust injected upstream of various type flame holders.

The asymmetric arrangement of vortex pairs behind the bluff object alters the pressure distribution around the body, and vortices are discharged alternately from the two sides. In this way, a definite frequency of eddy motion, which depends upon the Reynolds number, is begun. Downstream of the bluff-object, the vortices arrange themselves in a double row in which each vortex is midway between the vortices in an opposite row; this arrangement is known as the Kármán vortex street. According to reference 22, regular vortex shedding occurs until Reynolds numbers approach 4 to 5×10^5. Above these values, flow is turbulent.

Flow behind bluff bodies with heat addition. - During combustion stabilized behind a flame holder in a flowing homogeneous fuel-air mixture, unburned mixture diffuses into the eddy region behind the flame holder and is burned, with accompanying diffusion of the combustion products and heat into the main stream to ignite the mixture flowing past. With a liquid fuel spray, heat from the burning mixture in the eddy region is transferred to the liquid fuel accumulated on the flame holder directly by radiation and convection, and indirectly by conduction through the flame holder itself. The amount of heat transferred controls the evaporation rate of the fuel. It is believed that the fuel vaporized by this heat mixes with air diffusing from the main stream and maintains the pilot flame in the eddy region. One of the differences noted in flow behind bluff bodies with and without heat addition is that no eddies are shed during combustion (ref. 23). One explanation of this fact is that the static pressure downstream of the bluff body is lower with combustion occurring. As a result of the reduced pressure, the eddy region becomes smaller and seems to attach itself to the bluff body. 3267

Eddy formation. - Small pressure losses induced by eddies downstream of flame holders may be estimated if data showing the strength, frequency of shedding, and longitudinal spacing between vortices in a row are known. Goldstein (ref. 22) states that the average drag per unit length of a cylindrical obstacle perpendicular to a flowing fluid can be expressed by

$$F = \frac{K^2\rho}{2\pi ag} + \frac{K\rho i}{ag}\left(U_\infty - 2U_{rel}\right) \tag{26}$$

where

a distance between vortices in row

F drag of flame holder per unit flame-holder length

i lateral spacing between vortex rows

K strength of individual vortex

U_{rel} velocity of vortex system relative to free stream

U_∞ fluid velocity upstream

According to reference 24, the strength of vortices of stable rows can be expressed as

$$K = 2\sqrt{2}\, aU_{rel} \tag{27a}$$

and

$$\sinh(\pi i/a) = 1 \tag{27b}$$

$$i/a = 0.281 \tag{27c}$$

Use of these data allows reduction of equation (26) to

$$F = \frac{\rho U_\infty^2}{2g} a\left[1.587 \frac{U_{rel}}{U_\infty} - 0.628\left(\frac{U_{rel}}{U_\infty}\right)^2\right] \tag{28}$$

3287

This equation does not include wall effects of the combustor. A similar equation which includes wall effects is derived in reference 22. Reference 21 presents data for the shedding frequency and strength of vortices from 14 different flame holders, including a cylinder and a flat plate. From data such as these, necessary values for equation (28) can be determined, since a can be determined from equation (27a), and

$$\frac{U_{rel}}{U_\infty} = 1 - \frac{af}{U_\infty} = 1 - \frac{\left(\frac{Kf}{2\sqrt{2}\,U_{rel}}\right)}{U_\infty} \tag{29}$$

where

f frequency of vortex shedding from flame holder

or

$$U_{rel} = \frac{U_\infty}{2} - \frac{\sqrt{U_\infty^2 - \sqrt{2}\,Kf}}{2} \tag{30}$$

(The negative sign must be used in eq. (30), since a vortex of zero strength would not exist and U_{rel} would equal zero.) The magnitude of the eddy drag is quite small as shown by the fact that a U-shaped flame holder, 3/4 inch wide, would cause a drag of approximately 0.12 pound per foot of length of flame holder in an air stream flowing at 55 feet per second at sea level.

The isothermal total-pressure loss coefficient for a flame holder due to vortex formation can be expressed essentially as

$$\frac{\Delta p_t}{q_r} = \frac{a\left[1.587 \frac{U_{rel}}{U_\infty} - 0.628\left(\frac{U_{rel}}{U_\infty}\right)^2\right]}{a^*} \tag{31}$$

where

a^* flame holder width

This total-pressure loss would be additive to the theoretical pressure loss obtained in reference 16.

Estimation and Correlation

Data for estimation of the total-pressure losses in a combustor for known isothermal pressure loss are presented in reference 25. This method, however, requires an isothermal test of the combustor before an estimation of the pressure losses at other operating conditions can be made.

A correlation has been developed (ref. 26) for various combustors and experimental configurations in which

$$\frac{\Delta p_t}{p_t} \propto I^{1.5} \tag{32}$$

where

I combustion intensity, Btu/(hr)(cu ft)(atm)

$\frac{\Delta p_t}{p_t}$ total-pressure loss ratio for system

3267

The value of I is preferably assessed on the size of the primary combustion zone only. This correlation was for use in combustion-chamber design. Using a design $\Delta p_t/p_t$, an intensity could be found, from which primary zone size could be determined. Values of the ratio L/d for cylindrical combustors were taken as 1.25 to 2.0. According to reference 26, the degree of combustion intensity is determined by the air-mixing pattern, the degree of turbulence, and the combustion properties of the fuel-air mixture, all of which contribute to pressure losses. Use of this correlation involves an arbitrary assumption as to the size of the primary zone.

A better correlation, and one which is generally used, is

$$\frac{\Delta p_t}{q_r} = k_3 + k_4\left(\frac{\rho_3}{\rho_4}\right) \tag{33}$$

where

k_3, k_4 dimensionless constants

q_r reference velocity pressure, defined by

$$q_r = \frac{R_3 T_3}{p_3}\left(\frac{1}{2g}\right)\left(\frac{W_a}{A_r}\right)^2 \tag{34}$$

A_r reference area of combustor, equal to maximum open cross-sectional area of combustor housing

ρ gas density

This correlation (ref. 27) indicates that the total-pressure losses in a combustor are a function of the previously mentioned factors, friction and pressure losses associated with the introduction of a flame-stabilizing device in a gas stream $(k_3 + k_4)q_r$, and pressure losses due to heat absorption (or density changes) of high-velocity gases $k_4\left(\frac{\rho_3}{\rho_4} - 1\right)q_r$. Pressure losses of a typical turbojet combustor are presented in figure II-11. As indicated by equation (33), total-pressure

losses increase linearly with increases in gas-density ratios. Friction pressure losses, the losses which would be found essentially by an isothermal test, are indicated at a density ratio of 1.0. Momentum pressure losses at any density ratio are the difference between the total-pressure losses and the friction pressure loss.

A theoretical analysis of isothermal total-pressure losses in a combustor having straight housing and liner walls has been made (unpublished NACA data). The following assumptions or effects were considered in the analysis:

3267

(1) Sudden contractions or enlargements in flow cross-sectional areas

(2) Incompressible, isothermal flow

(3) Ratio of total area of openings in liner to maximum cross-sectional (reference) area of housing

(4) Ratio of area of annulus between liner and housing to maximum cross-sectional (reference) area of housing

(5) Zero wall friction

(6) Variable orifice coefficients for openings in liner

The effect of external crossflow on the orifice coefficients was included. The effect of internal crossflow was assumed negligible for the range of operating conditions considered. Variable orifice coefficients are discussed later.

Theoretical total-pressure losses are presented in figure II-12 for several ratios of annulus-reference areas. Total-pressure losses decrease rapidly with increases in both annulus-reference area ratios and total liner opening - reference area ratios. Minimum total-pressure losses can be obtained essentially with a ratio of total liner open area to the reference area of the housing of 1.3. Additional data indicate the optimum ratio of annulus-reference areas for obtaining minimum total-pressure losses to be approximately 0.5. At present, increased interest is shown in the use of $\Delta p_t/p_t$, a total-pressure-loss ratio which is more useful for comparisons of combustor performance. However, this ratio is not unique in that it involves a different curve for each combustor-inlet velocity.

AIR DISTRIBUTION

The distribution of air flow within a combustor depends upon many factors, several of which are interrelated. In general, the simplest assumption regarding distribution of air flow in a combustor liner is that the air flow is proportional to the liner open area. However, such an assumption does not account for the effect of previously discussed pressure losses, the ratio of annular area between the combustor housing and liner to the total cross-sectional area, orifice coefficients, friction, or the rate of heat addition.

Experimental data showing air-flow distribution are rather meager in the literature. However, several theoretical analyses of the distribution are available. One of the most usable analyses has been made by the NACA for the air-flow distribution within the liner of a straight-wall tubular combustor. The same assumptions or effects listed in the section on estimating or correlating pressure-drop data were considered. With the proper corrections, these data should apply to other combustors, for example, annular combustors or combustors with housings and liners having nonparallel walls.

Isothermal air-flow distributions in a tubular straight-wall combustor are presented in figure II-13 as functions of liner open area, total-pressure losses, and ratios of the annular area between combustor housing and liner to the reference area of the combustor housing. Figure II-13(a) indicates that the percentage of the total air flow into the liner upstream of any longitudinal position is less than if it were proportional to the percentage of liner total open area available for flow, especially with low combustor total-pressure-loss coefficients. Figure II-13(b) indicates a similar effect on air-flow distribution for several ratios of the area of the annulus between liner and housing to the housing reference area. The effect is more pronounced at small values of annulus-reference area ratios.

Other methods of estimating air-flow distribution are available. However, most of these methods are stepwise, laborious, and less convenient than this method. References 28 and 29 present methods of evaluating the air-flow distribution that involve trial-and-error solutions beginning at the combustor inlet or outlet, and specification of effective flow areas or static pressures at any position in the combustor. Reference 30 presents an alternative method based upon arbitrarily assigned inlet flows or static pressures at each station, in addition to assumed jet-stream Mach numbers and inlet total temperatures. The method assumes combustion in a constant cross-sectional area, isentropic expansion of gases between stations, and radial mixing of gas jets at each station. After stepwise determination of internal flow, the upstream total pressure can be selected by assigning an over-all pressure loss or a pressure drop over a particular station. Either method fixes the inlet total pressure and allows a static-pressure evaluation over the external portion of the liner. Required open areas at each station are then determined from mass flows, orifice coefficients, and calculated orifice pressure drops. This method seems superior to the methods of references 28 and 29 in that only one trial-and-error solution may be necessary.

3267

GAS JETS

Mixing of gas streams or jets is an important problem in the design and operation of combustion chambers. For example, air needed to create the turbulence required for rapid mixing and burning in the primary zone of a turbojet combustor usually enters in the form of air jets through small openings in the combustor liner. Also, adequate penetration of the dilution or secondary air must occur in order to attain the degree of mixing and temperature uniformity required by turbojet combustors, in which exhaust-temperature profiles suitable for entry of the exhaust gases into the turbine are necessary. Such penetration is usually obtained by introduction of the secondary air through various openings in the downstream portion of the combustor. Similar problems also exist in the design and operation of ram-jet combustors and afterburners. Adequate mixing of gases of different temperatures, which exist downstream of flame holders, may result in higher propulsive efficiencies.

As shown in the following sketch, a jet consists essentially of a uniform stream of fluid emanating from an orifice:

3267

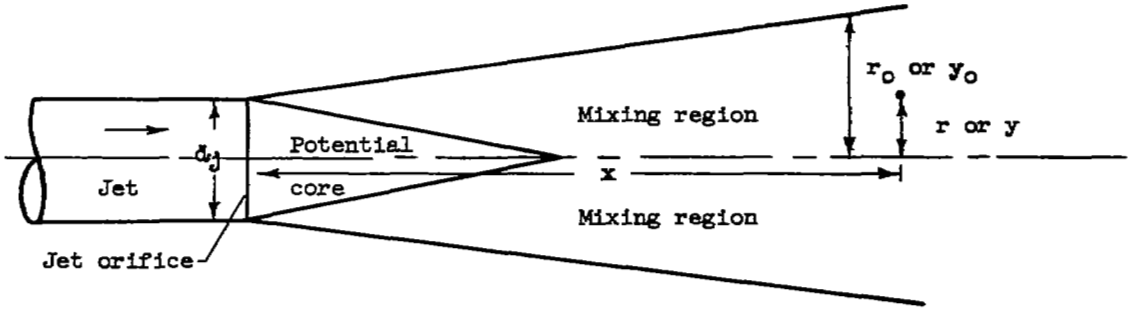

Within a certain region (the potential core) outside the orifice, the jet velocity and temperature are maintained. Outside and downstream of the potential core, a mixing region exists, in which the jet expands and interaction may occur between the jet fluid and any surrounding atmosphere. Jet parameters of interest are usually the velocity and the temperature at any position within the jet, the width and penetration of the jet, and any interaction of the jet with adjacent jets. Gas jets and mixing problems can be classified into two general categories: free jets and jets issuing into fluids which are not at rest. Each of these categories can be further subdivided into laminar and turbulent flow.

Theoretical Background

Free jets. - Unless specifically stated otherwise, all jets discussed as free jets have a single fluid composition.

Laminar flow: The study of a jet in laminar flow is usually only of academic interest. However, the results of such studies may be of value in fundamental combustion investigations. An analysis of the spread of a free, laminar, two-dimensional jet and a circular jet is given in reference 31. For a laminar jet issuing from a small circular hole in a wall, the equation of motion can be written as

$$U \frac{\partial U}{\partial x} + V \frac{\partial U}{\partial r} = \frac{\nu}{r} \frac{\partial}{\partial r}\left(r \frac{\partial U}{\partial r}\right) \tag{35}$$

where

U,V velocity components in x- and r-directions

x,r longitudinal and radial measurements

ν kinematic viscosity of jet fluid

The following assumptions are made:

(1) $\partial^2 U/\partial x^2$ is small compared with $\partial^2 U/\partial r^2$, and can be neglected.

(2) No pressure gradients or lateral fluid limitations exist across the jet.

(3) Flow is steady.

(4) The momentum at any section of the jet is assumed constant, since no pressure gradients exist and motion is steady.

(5) $U = \frac{1}{r}\frac{\partial \Psi}{\partial r}$ and $V = -\frac{1}{r}\frac{\partial \Psi}{\partial x}$, where Ψ is a stream function such that U and V satisfy the continuity equation.

3267

A solution of this equation for values of U and V is

$$U = \frac{3m}{8\pi\mu}\left(\frac{1}{x}\right)\frac{1}{\left(1 + \frac{1}{4}\xi^2\right)^2} \tag{36a}$$

and

$$V = \frac{1}{4}\left(\frac{3mg}{\pi\rho}\right)^{\frac{1}{2}}\left(\frac{1}{x}\right)\left[\frac{\xi\left(1 - \frac{1}{4}\xi^2\right)}{\left(1 + \frac{1}{4}\xi^2\right)^2}\right] \tag{36b}$$

where

m momentum of jet at any cross section = a constant = $\frac{2\pi\rho}{g}\int_0^\infty U^2 r\, dr$

μ absolute viscosity of jet fluid

ξ $(1/4\nu)(3mg/\pi\rho)^{1/2}(r/x)$

This solution is applicable for large values of $mg/\rho\nu^2$.

Turbulent flow velocity profiles: In practice, the motion in jets is usually turbulent in nature. One of the simplest cases of turbulent mixing is the plane-parallel mixing of a jet with gases at rest, with the mixing occurring along a single boundary between the gases. Reference 32 reports an early analysis of this type of mixing, with a free-turbulence or momentum-transfer theory based on the semiempirical, general turbulence theory of Prandtl. The momentum-transfer theory indicated the temperature and velocity profiles to be identical in a free jet. Good experimental verification of the theoretical velocity profiles of reference 32 was obtained by various investigators. However, experimental measurements of temperature profiles downstream of free jets indicated discrepancies between theory and experiment and no similarity of velocity and temperature profiles. Thus, the momentum-transfer theory was suitable for solution of mechanical flow problems of velocity profiles or fluid friction, but was ineffective for solution of problems involving temperature profiles or heat transfer.

Reference 33 presents a theory in which the tangential turbulent stresses in flow are a function of the transverse transport of vorticity. That is, the stresses

are a function of the correlation between vorticity fluctuations and transverse velocity components. Conservation of the vorticity of a fluid element until mixing occurred was assumed. It was also noted that the Prandtl theory did not account for local pressure gradients, which appreciably affect momentum interchange but not vorticity transport. The vorticity-transport theory of reference 33 gave velocity profiles almost as accurately as the momentum-transfer theory and, in addition, gave better agreement of theoretical and experimental temperature profiles. The vorticity-transport theory was extended to plane-parallel free jets in references 34 and 35.

3267

For two-dimensional compressible flow, Abramovich (ref. 34) indicated the equation of motion to be

$$\rho \frac{\partial U}{\partial t} + \rho U \frac{\partial U}{\partial x} + \rho V \frac{\partial U}{\partial y} = - \mu \frac{\partial^2 U}{\partial y^2} - \frac{\partial p}{\partial x} \tag{37}$$

where

t time

V velocity component in y-direction

y lateral measurement

and all values are instantaneous. By use of an approximate mean vorticity Φ where

$$\Phi = \frac{1}{2}\left(\frac{\partial \overline{U}}{\partial y}\right)$$

and a defined value L_m, which is a mixing length or mean free path of a fluid particle in turbulent flow, equation (37) reduces to

$$\overline{\rho}\overline{U} \frac{\partial \overline{U}}{\partial x} + \overline{\rho}\overline{V} \frac{\partial \overline{U}}{\partial y} = L_m^2 \frac{\partial \overline{U}}{\partial y} \frac{\partial}{\partial y}\left(\overline{\rho} \frac{\partial \overline{U}}{\partial y}\right) \tag{38}$$

where the bars indicate mean values. For incompressible flow, equation (38) reduces to

$$U \frac{\partial U}{\partial x} + V \frac{\partial U}{\partial y} = L_m^2 \frac{\partial U}{\partial y} \frac{\partial^2 U}{\partial y^2} \tag{39}$$

Equation (39) is similar to the equation found in reference 32 by use of the momentum-transfer theory, differing only in the definition of L_m. Equation (39) was solved by use of the same assumptions used in reference 32: constant momentum in the x-direction at any section of the jet; proportionality of L_m to x in an x-direction; and constancy of L_m across any section in a y-direction. That is

$$U_{max} \propto x^{-1/2}$$

$$L_m \propto y_o \propto x$$

where

U_{max} velocity on jet axis

y_o maximum jet spread on one side of jet

Equation (39) yields the same distribution for velocity as the momentum-transfer theory of reference 32:

$$U = 1.31 \frac{k_5 s(\sigma)}{(y_o)^{1/2}} \tag{40a}$$

3267

$$y_o = 3.02 k_6^{1/3} x \tag{40b}$$

where

k_5, k_6 constants

$s(\sigma)$ function of (y/y_o)

σ y/y_o

This solution is expressed in figure II-14 in terms of dimensionless ratios of U/U_{max} for any cross section. Good agreement of experimental and theoretical profiles has been found.

The theory of plane-parallel jet mixing was extended by Howarth (ref. 35) to the case of axially symmetric free jets. For these jets, the equations of motion for each of two theories are

Momentum-transfer theory:

$$U \frac{\partial U}{\partial x} + V \frac{\partial U}{\partial r} = \frac{1}{r} \frac{\partial}{\partial r}\left(-L_m^2 \frac{\partial U}{\partial r} r \frac{\partial U}{\partial r}\right) \tag{41}$$

Modified vorticity-transport theory:

$$U \frac{\partial U}{\partial x} + V \frac{\partial U}{\partial r} = -L_m^2 \frac{\partial U}{\partial r}\left(\frac{\partial^2 U}{\partial r^2} + \frac{1}{r} \frac{\partial U}{\partial r}\right) \tag{42}$$

These equations were solved by use of the same assumptions as used in equation (39). Although the two different theories yield approximately the same result, slightly better agreement with experiment was obtained with the momentum-transfer theory. The solution of equation (41) involved use of the stream function Ψ, defined in assumption (5) of equation (35). The value of U at any radius r was determined as

$$U = 4.65 \frac{k_7}{r_o} z(\sigma) \tag{43a}$$

$$r_o = 3.4k_8^{1/3}\ x \tag{43b}$$

where

k_7, k_8 constants

r_o maximum spread of jet at any cross section

$z(\sigma)$ function of (r/r_o)

σ r/r_o

This solution is expressed in figure II-14 in terms of dimensionless ratios for any cross section. According to Howarth, these results are fairly accurate, at least over the central portion of the jet, at distances downstream from the nozzle greater than 8 jet nozzle diameters.

Turbulent flow temperature profiles: Abramovich (ref. 34) indicates the differential equation of heat balance for plane-parallel free jets emanating into fluids of different temperatures to be

$$\rho \frac{\partial T}{\partial t} + \rho U \frac{\partial T}{\partial x} + \rho V \frac{\partial T}{\partial y} = 0 \tag{44}$$

Equation (44) neglects molecular heat conduction and conversion of the energy of viscous forces into heat with respect to turbulent heat transfer in the same manner as friction due to viscosity was disregarded in equation (38) relative to turbulent friction. By use of instantaneous and fluctuating values of variables and by assuming

$$\overline{\frac{\rho \partial T}{\partial t}} = 0 \text{ (steady flow)}$$

and

$$T' = L_m \frac{\partial \overline{T}}{\partial y}$$

where

$\overline{T}$ mean absolute temperature

T' fluctuating value of absolute temperature

equation (44) becomes

$$\rho U \frac{\partial T}{\partial x} + \rho V \frac{\partial T}{\partial y} = L_m^2\left[\frac{\partial \rho}{\partial y}\frac{\partial U}{\partial y}\frac{\partial T}{\partial y} + \frac{\partial}{\partial y}\left(\rho \frac{\partial U}{\partial y}\frac{\partial T}{\partial y}\right)\right] \tag{45}$$

which, for incompressible flow, reduces to

$$U \frac{\partial T}{\partial x} + V \frac{\partial T}{\partial y} = L_m^2 \frac{\partial}{\partial y}\left(\frac{\partial U}{\partial y}\frac{\partial T}{\partial y}\right) \tag{46}$$

Reference 34 presents a correlation of the solution of equation (46) in terms of a dimensionless parameter

$$\tau = \frac{T - T_1}{T_j - T_1}$$

where

T temperature at any point in jet mixing region

T_j temperature at any point in region of undisturbed flow in jet, or in potential core

T_1 temperature of fluid at rest in space surrounding jet

τ temperature coefficient in jet

This parameter has been used by other authors. Howarth (ref. 35), however, presents a solution of equation (46) as

$$\frac{T}{T_{max}} = [s(\sigma)]^{1/2}$$

where

$s(\sigma)$ function of (y/y_o)

T_{max} temperature on jet axis

σ y/y_o

and T_{max} and $U_{max} \propto \left(\frac{1}{x}\right)^{1/2}$

This solution is presented in figure II-15.

For axially symmetric free jets, the differential equation of heat transfer becomes (ref. 35)

$$U \frac{\partial T}{\partial x} + V \frac{\partial T}{\partial r} = \frac{1}{r} \frac{\partial}{\partial r}\left(-L_m^2 \frac{\partial U}{\partial r} r \frac{\partial T}{\partial r}\right) \tag{47}$$

Similar boundary conditions apply for velocity and temperature distributions based on the momentum transfer theory. Also, equation (47) differs from equation (41) only in a change of variable. Therefore, the solution of equation (47) based upon the momentum-transfer theory yields a temperature profile similar to that of the velocity. The boundary conditions used for temperature distribution with the vorticity-transport theory are unequal to those used for velocity distribution. Howarth (ref. 35) presents a solution of equation (47) as

$$\frac{T}{T_{max}} = e^{\int_0^{r/xk_8^{1/3}} \frac{E_1}{E_1'' - E'/\varepsilon} d\varepsilon} \tag{48}$$

where

3267

E, E', E'' $f(\varepsilon)$

k_8 constant

ε r/x

A comparison of experimental and theoretical temperature distributions based upon the momentum-transfer and vorticity-transport theories is presented in figure II-15. The experimental temperature distribution more closely follows that predicted by the vorticity-transport theory over most of the range.

Occasionally, a knowledge of lines of constant temperature or velocity in free jets is required. Solutions of the equations to determine constant velocity and temperature distributions in free jets indicated that isothermal and constant-velocity lines are straight lines emanating from the center of the jet orifice. According to the existing data, turbulent-flow velocity profiles in free jets can be determined best by use of the momentum-transfer theory, expressed in equations (39) and (41) and figure II-14. Turbulent-flow temperature profiles in free jets can be determined best by use of the vorticity-transport theory, expressed in equation (47) and figure II-15.

Coaxial jets. - In contrast to a jet issuing into a fluid at rest, many applications exist in which a jet emanates into a stream flowing parallel to the jet axis. Reference 36 presents a solution to an isothermal mixing problem of this type in terms of the momentum-transfer theory. The equations of motion for the region of fully developed flow and the region containing a uniform velocity potential core were solved by use of proper boundary conditions with the requirement that continuous values of jet radii and velocities exist at the intersection of the two regions. The following assumptions were made in the solution:

(1) Incompressible flow

(2) Pressure gradients near jet small enough to be neglected

(3) Constant velocity throughout potential core

(4) Constant momentum in x-direction at any jet section

(5) Mixing length L_m proportional to width of mixing region

(6) Lateral distribution of velocity in region containing potential core equal to

$$U = U_1 + \frac{U_j - U_1}{2}\left[1 - \cos \pi\left(\frac{r_o - r}{r_o - r_p}\right)\right] \tag{49}$$

(7) Lateral velocity distribution in fully developed jet equal to

$$U = U_1 + \frac{U_{max} - U_1}{2}\left(1 + \cos \pi \frac{r}{r_o}\right) \tag{50}$$

where all velocities are in the x-direction, and

r radial distance from jet axis to point where U is measured

r_o outer radius of fully developed jet

r_p radius of potential core

U velocity at any position in jet

U_j velocity of jet

U_{max} velocity on jet axis

U_1 velocity of coaxial stream

(8) Mixing length parameter c equal to $(0.0067)^{1/2}$ (differs slightly, approximately 10 percent, from a value found in another reference)

A diagram of the jet and the results of the analysis are presented in figures II-16 and -17. Results of the analysis indicated that: (1) length of the potential core decreases with decreasing ratios of stream-to-jet velocity to approximately 3.1 jet diameters for a free jet, and (2) similar to free jets, constant-velocity lines are approximately straight, emanating from the center of the jet orifice. Similar results have been found by other investigators.

Normal jets. - No theoretical data expressing the distribution of temperature or velocity in a fluid jet entering a fluid stream flowing normal to the jet were found. However, a theoretical analysis for the penetration of the jet into the stream is presented in reference 37. Velocity and temperature distributions for free jets and a negligible pressure gradient at the mixing section were assumed. Results of the analysis indicated that penetration of normal jets could be expressed as

$$\text{Penetration, } l = f\left[\left(\frac{\text{Momentum of jet}}{\text{Momentum of fluid stream}}\right)\left(\frac{\text{Volume flow of fluid stream}}{\text{Total volume flow of fluid stream and jet}}\right)^2\right] \tag{51}$$

For penetration of circular normal jets into fluid streams in rectangular ducts of width d' and depth h, penetration at a distance x/h from the orifice is suggested as

$$\text{Relative penetration, } \frac{l}{h} = f\left(\frac{\frac{d_j}{h}\frac{U_j}{U_1}\sqrt{\frac{T_1}{T_j}}}{1 + \frac{\pi}{4}\frac{d_j^2}{hd'}\frac{U_j}{U_1}}\right) \tag{52}$$

where

d_j jet orifice diameter

T_j temperature of jet fluid

T_1 temperature of fluid stream

U_j jet velocity

3267 U_1 fluid stream velocity

Multiple jets. - Two expressions for the penetration of multiple jets into fluid streams are presented in reference 37. For the penetration of n jets entering a fluid stream at right angles through n circular orifices spaced laterally across a rectangular duct of width d' and depth h, penetration at a distance x/h from the orifice is suggested as

$$\text{Relative penetration, } \frac{l}{h} = f\left(\frac{\frac{d_j}{h}\frac{U_j}{U_1}\sqrt{\frac{T_1}{T_j}}}{1 + n\frac{\pi}{4}\frac{d_j^2}{hd'}\frac{U_j}{U_1}}\right) \tag{53}$$

No experimental data using this parameter were included in reference 37. For the penetration of n jets entering a fluid stream at right angles through n circular orifices equally spaced circumferentially around a duct of diameter d_{dt}, the expression suggested for a distance x/d_{dt} from the orifice is

$$\text{Relative penetration, } \frac{l}{d_{dt}} = f\left[\frac{\frac{d_j}{d_{dt}}\frac{U_j}{U_1}\sqrt{\frac{T_1}{T_j}}}{1 + n\left(\frac{d_j}{d_{dt}}\right)^2\frac{U_j}{U_1}}\right] \tag{54}$$

No experimental data using this parameter were included.

Experimental Data

Despite an abundance of theoretical analyses of jets issuing into gases at rest or in motion, many disagreements exist between theoretical and experimental results. Likewise, application of fundamental jet-penetration data to jet-engine combustors has given results in disagreement with theory. Disagreements may be attributed to various factors such as direction, size, shape, and orientation of the jets relative to the main fluid, and the presence of other jets resulting in possible jet interaction.

Free jets. - Turbulent flow velocity profiles: Much of the extant experimental data relative to gas jets concern free jets mixing with air. In general, data are presented in terms of velocity distributions in both the potential core in axially symmetric jets and the region of fully developed jet flow. Equations written to

fit the experimental data for isothermal free jets mixing with air are presented in reference 38. Data are expressed in terms of momentum flux velocity ratios, in which

$$\text{Momentum flux velocity} = \sqrt{\frac{\overline{\rho U^2}}{\bar{\rho}}} \tag{55}$$

where

U instantaneous velocity in jet in x-direction at any radius r and longitudinal distance x

ρ instantaneous density of fluid

The value of $\overline{\rho U^2}$ is determined from impact tube measurements, and ρ is determined from static temperature and pressure. For incompressible flow, the momentum flux velocity is approximately $\sqrt{\overline{U^2}}$. Momentum flux velocity ratios of an isothermal free jet are presented in figure II-18 for the potential core, a transition region at the end of the potential core, and the region of fully developed flow. Many of the data are presented, as in many references, in terms of a half-radius, that is, the jet radius at which the momentum flux velocity equals one-half the momentum flux velocity on the jet axis at the same longitudinal distance from the jet orifice. The data indicate that

(1) The potential core within which the flux velocity ratios are constant radially is approximately 3.5 jet orifice diameters in length.

(2) The radius of the potential core could be expressed as

$$\frac{r_p}{d_j} = \frac{3.5 - x/d_j}{7.0} \tag{56}$$

where

r_p potential core radius at any longitudinal distance x

x longitudinal distance from jet orifice

Velocity ratios within the potential core (less than 3.5 diameters downstream) closely approached a single generalized curve. Within the transition region, however, a different curve could be drawn than for distances farther downstream. Radial flux velocity ratios, covering a range of jet velocities from 166 to 801 feet per second and distances from 10 to 30 jet diameters downstream of the jet orifice, were correlated by the following expression:

$$\sqrt{\frac{\overline{U^2}}{\overline{U_{max}^2}}} = e^{-\ln 2(r/r_{1/2})^2} \tag{57}$$

where

$r_{1/2}$ half-radius at longitudinal distance x

U_{max} velocity in x-direction on axis at longitudinal distance x

Some data have been reported in reference 39 from an investigation of momentum and mass transfer in coaxial jets. Isothermal experiments were conducted with homogeneous mixtures of air and helium flowing from 1/4-inch- and 1-inch-diameter nozzles into a coaxial stream of air in a 4-inch-diameter duct. Extrapolation of the results to the case of a free jet, that is, zero coaxial stream velocity, shows that:

(1) The potential core is 4.0 jet orifice diameters in length.

(2) The velocity in the fully developed flow region (downstream of the potential core) can be represented by

3267

$$\frac{U}{U_{max}} = \frac{1}{2}\left(1 + \cos \frac{\pi r}{2r_{1/2}}\right) \tag{58}$$

The potential core length is slightly larger than the experimental value (3.5 diameters) of reference 38 and the theoretical value (3.1 diameters) of reference 36. However, the lateral velocity distribution agrees approximately with the theoretical distribution of Squire and Trouncer (eq. (50)) and fairly well with the experimental curve of reference 38 (eq. (57)), as shown in figure II-18(c).

Axial velocity distribution within the fully developed flow region of the circular isothermal free jets of reference 38 could be closely approximated by

$$\frac{\sqrt{\overline{U_{max}^2}}}{\overline{U_j}} = \frac{1}{0.1508\ x/d_j} \tag{59}$$

where

$\overline{U_j}$ velocity of jet

The curve of figure II-19 and the experimental data agree closely with the previously discussed theoretical analysis of a symmetrical jet in which it was assumed, because of a constancy of momentum at any jet section, that

$$U_{max} \propto \frac{1}{x} \tag{60}$$

This expression for axial velocity distribution agrees closely with an expression of Squire (ref. 40), who recommended use of the relation

$$\frac{U_{max}}{U_j} = \frac{6.5}{x/d_j} \tag{61}$$

Extrapolation of the data of reference 39 for coaxial jets to a free jet gives the axial velocity distribution as

$$\frac{U_{max}}{U_j} = \frac{4}{x/d_j} \tag{62}$$

The large discrepancy between equation (62) and equations (59) and (61) may be due in part to the experimental configuration of reference 39.

Much data relative to axially symmetric free jets in air have been summarized in reference 40. Half-velocity radii in the fully developed flow region of a free

jet in air are presented in figure II-20. Experimental data from references 38 and 41 and theoretical data from references 36 and 42 are also included. Reichardt (ref. 42) expressed the half-radius at any longitudinal position as

$$r_{1/2} = 0.0725x\sqrt{\ln 4} \tag{63}$$

This expression and the experimental data of reference 38 agree closely with the data of figure II-20, which indicate the lines of half-velocity radius to lie on a cone of half-angle of 5°, with the apex of cone at the center of the jet orifice, for distances greater than 10 jet diameters from the orifice.

3267

A small amount of data included in reference 40 for 0.1-velocity radii is also presented in figure II-20. For the 0.1-velocity radii, straight lines emanate from the center of the jet orifice at an angle of 9.2°.

A small amount of experimental data pertaining to the velocity distribution in two-dimensional jets is available. For two-dimensional and axially symmetric free jets, theoretical analyses have indicated that:

(1) For two-dimensional jets, $U_{max} \propto \frac{1}{x^{1/2}}$

(2) For axially symmetric jets, $U_{max} \propto 1/x$

Using these relations, Squire (ref. 40) infers that expressions applicable to axially symmetric jets may be applied to two-dimensional jets by replacing (x/d_j) with $(x/y)^{1/2}$ wherever (x/d_j) appears. Howarth (ref. 35) presents some experimental data from a previous investigator on the velocity profiles in a two-dimensional free jet and compares them with the theoretical distribution derived from the momentum-transfer and modified vorticity-transport theories, both of which give the same theoretical velocity profile. Excellent agreement of experimental and theoretical data is indicated. The large amount of data on free jets includes many expressions for velocity distributions. For free jets (excluding the jets of ref. 39), recommended expressions for the radius of the potential core, and lateral and axial velocity distributions are equations (56), (57), and (59), respectively. Half- and 0.1-velocity radii can be determined from figure II-20.

Turbulent-flow temperature profiles: Experimental distributions of temperature in axially symmetric free jets are expressed in figure II-21. Results are expressed in terms of half-temperature and 0.1-temperature ratio radii. In the same manner as the velocity ratios, the temperature ratios are defined as the ratio of the temperature coefficient τ at any point to the temperature coefficient τ_{max} at a point on the axis in the same longitudinal plane. The temperature coefficient τ has been defined in the theoretical section considering temperature profiles in turbulent flow. For distances greater than 5 jet orifice diameters downstream, straight lines of half-temperature ratios lie on a cone of half-angle of 6.7° with the apex of the cone at the center of the jet orifice. For 0.1-temperature ratios, the distance downstream must be greater than 10 jet orifice diameters, and the half-angle is 11.7°.

Longitudinal distribution of temperature in axially symmetric free jets is shown in figure II-22. The temperature of the jet remains approximately constant for a distance of about 5 diameters, or the length of the potential core. For distances from 10 to 50 jet orifice diameters from the orifice,

$$\tau_{max} = \frac{4.8}{x/d_j} \tag{64}$$

This equation is recommended by Squire (ref. 40) as representative of the temperature distribution on the jet axis. A better expression for axial temperature distribution, for distances from 5 to 20 jet orifice diameters from the orifice, is

3267

$$\tau_{max} = 3\left(\frac{x}{d_j}\right)^{-0.845} \tag{65}$$

No experimental data showing the temperature distribution in two-dimensional free jets were found. However, Howarth (ref. 35) assumes that the agreement of experimental and theoretical temperature distributions in two-dimensional free jets is as good as with axially symmetric jets.

Coaxial jets. - Velocity measurements: In general, only a free jet spreads conically. Also, a boundary layer from the tube or nacelle containing the jet may have an important influence on the jet when the stream velocity is an appreciable fraction of the jet velocity. As a result, correlation of experimental data has led to general empirical rules concerning the characteristics of coaxial jets.

Squire (ref. 40) states that

$$\left\{\begin{matrix}\text{Increase in radii of half-velocity or} \\ \text{0.1-velocity circles above radius of} \\ \text{jet orifice}\end{matrix}\right\} \propto \left(\frac{U_j - U_1}{U_j}\right) \tag{66}$$

This expression should not be applied for longitudinal distances greater than 30 jet orifice diameters downstream. For the same longitudinal distances and for values of U_1/U_j less than 0.6, the velocity on the axis can be approximated by

$$\left(\frac{U_{max} - U_1}{U_j - U_1}\right)\frac{x}{d_j} = \frac{6.5}{1 - 0.6(U_1/U_j)} \tag{67}$$

An approximation for the length of the potential core is

$$\text{Potential core length} \propto \left(\frac{U_j}{U_j - U_1}\right) \tag{68}$$

Forstall and Shapiro (ref. 39) present the following empirical equations for coaxial jets:

$$L_p = 4 + 12\frac{U_1}{U_j} \tag{69}$$

$$\left(\frac{U_{max} - U_1}{U_j - U_1}\right)\frac{x}{d_j} = 4 + 12\left(\frac{U_1}{U_j}\right) \tag{70}$$

$$\frac{r_{1/2}}{d_j} = 0.5\left[\frac{4 + 12\left(\frac{U_1}{U_j}\right)}{x/d_j}\right]^{\frac{U_1 - U_j}{U_j}} \tag{71}$$

$$\left(\frac{U - U_1}{U_{max} - U_1}\right) = 0.5\left[1 + \cos\frac{\pi}{2}\left(\frac{r}{r_{1/2}}\right)\right] \tag{72}$$

3267

$$r_{1/2} \sim (x)^{\frac{U_j - U_1}{U_j}} \tag{73}$$

$$r_o \sim (x)^{\frac{U_j - U_1}{U_j}} \tag{74}$$

where

L_p potential core length

r radial distance from jet axis

r_o outer radius of jet

$r_{1/2}$ radius at which $U = 0.5\ (U_{max} + U_1)$

Discrepancies exist between these equations and the empirical correlations of reference 40. However, equation (72) approximates a similar theoretical equation of reference 36.

Temperature measurements: In general, temperature measurements in coaxial jets are less extensive than velocity measurements. However, Squire (ref. 40) suggests the following empirical relation based largely on the previous corresponding velocity relation:

$$\left\{\begin{matrix}\text{Increase in radii of half-temperature ratio} \\ \text{or 0.1-temperature ratio circles above} \\ \text{radius of jet orifice}\end{matrix}\right\} \propto \left(\frac{U_j - U_1}{U_j}\right) \tag{75}$$

This approximation applies at longitudinal distances of less than 30 jet orifice diameters from the jet orifice.

The temperature coefficient τ_{max} at any point on the jet axis can be approximated by

$$\left(\frac{x}{d_j}\right)\tau_{max} = \frac{4.8}{1 - 0.6(U_1/U_j)} \tag{76}$$

The use of the velocity basis for the preceding temperature approximations reflects the inadequacy of experimental data. As indicated in the theoretical discussion of coaxial jets, there is little agreement of velocity and temperature profiles. For coaxial jets, recommended expressions for correlation of jet size and velocity parameters are equations (69) to (74) (ref. 39). Recommended expressions for temperature parameters are equations (75) and (76) (ref. 40).

Normal jets. - The penetration of gas jets into gases moving normal to the jet are of special interest in the design of combustion chambers of turbojet engines in which the openings for air admission are normal to the flow direction of the hot gases. In general, the definition of jet penetration and the degree of mixing have been arbitrarily specified by different investigators. As a result, different correlations of experimental data have been developed.

3267

Penetration: Experimental data indicating the relative penetration and mixing of jets of cold air (temperature, approximately 575° R) with a normal flowing stream of hot air (temperature, approximately 1350° R) are presented in reference 37. Penetration was defined as the normal distance from the plane of the cold-air orifice to the point of minimum temperature 1.5 duct widths downstream of the orifice center line. It is concluded in reference 37 that:

(1) For circular cold-air jets of different diameters and a range of velocities and temperatures of the two streams,

$$\frac{l}{h}, \text{ Relative penetration, or } \frac{\text{Penetration}}{\text{Duct depth}} = k_9 + k_{10}\left[\frac{\left(\dfrac{\text{Momentum, cold stream}}{\text{Momentum, hot stream}}\right)^{1/2}}{\left(\dfrac{\Sigma\ \text{Volumetric flow rate}}{\text{Volume flow rate, hot stream}}\right)}\right] \tag{77}$$

where k_9 and k_{10} are constants. This relation holds until the relative penetration becomes approximately 0.6, at which time the cold-air jet approaches the opposite wall of the duct.

(2) For the same open area, circular and square holes give approximately the same penetration, while longitudinal and transverse rectangular holes give better and worse penetration, respectively (fig. II-23).

(3) In general, main-stream turbulence reduces jet penetration. Data expressing the effect of turbulence on jet penetration are very meager in the literature. The qualitative results quoted herein may depend to some extent on how the main-stream turbulence is generated.

(4) Pressure losses are less for a given penetration by use of a small number of large holes than by use of a large number of small holes.

Results from a similar investigation in a $1\frac{7}{8}$-inch-square duct in which hot-air jets (temperature, approximately 1040° R) entered normal flowing streams of cold air (temperature, approximately 600° R) through different shaped openings have been presented in reference 43. Penetration was defined in the same manner as in reference 37, except that no limitations were imposed on the distance downstream of the orifice center line. Relative penetration data were satisfactorily correlated in

terms of either mass or momentum ratios of the hot stream to the cold stream. Relative penetration increased with increases in either mass or momentum ratios. The effect of hole shape on relative penetration was generalized by dividing the relative penetration of jets from equal-area holes of circular, square, and longitudinally rectangular shape (ref. 37) by the longitudinal length of the hole (fig. II-23).

Penetration data for heated circular jets of air (temperature, approximately 860° R) entering normally a 2- by 20-inch duct filled with a stream of cold air (temperature, ambient) flowing at velocities of 260 or 360 feet per second are presented in reference 44. Penetration was defined as the distance to the point at which the temperature was 1° R greater than the free-stream total temperature. Data expressing the penetration were correlated by the expression

$$\left(\frac{l}{d_j}\right)^{1.65} = 2.91\left(\frac{\rho_j U_j}{\rho_1 U_1}\right)\sqrt{\frac{s}{d_j}} \tag{78}$$

where

s longitudinal distance from jet orifice center line

U_j velocity of jet at vena contracta

U_1 velocity of normal stream

ρ_j density of jet fluid at vena contracta

ρ_1 density of normal stream

Penetration was unaffected by variations of Reynolds number from 0.6×10^5 to 5.0×10^5, viscosity ratios of the two streams from 1.5 to 1.9, and ratios of duct width to jet diameter from 3.2 to 8.0.

A similar relation was found (ref. 45) for the penetration of liquid jets of water injected normally from small, simple, orifice-type nozzles into a high-velocity stream of air (velocity, approximately 700 ft/sec). Penetration, defined as the maximum penetration of liquid at any longitudinal position, was determined photographically. The data were correlated by the following empirical expression:

$$\left(\frac{l}{d_j}\right) = 0.450\left(\frac{U_j}{U_1}\right)^{0.95}\left(\frac{\rho_j}{\rho_1}\right)^{0.74}\left(\frac{s}{d_j}\right)^{0.22} \tag{79}$$

Temperature distribution: No data indicative of the temperature profiles of a cold jet entering a normal moving stream of hot gases were found. However, the entry of hot gases into a normal moving stream of cold air has been investigated (ref. 46). Temperatures of the hot gases ranged from 660° to 860° R; orifice diameters ranged from 0.250 to 0.625 inch; and free-stream velocities ranged from 160 to 390 feet per second. Orifice pressure differentials, which were much higher than would be encountered in turbojet combustors, ranged from 1.20 to 3.70. A method was presented for simple determination of the temperature profile downstream of the jet orifice. The procedure involves determination of the penetration of the

jet at two positions and determination of the upper and lower slopes of the profile. The slopes of the profile are functions of several dimensionless exponential ratios in which the exponents are functions of the test equipment and conditions. The maximum temperature difference at any downstream position was found to be a function of the difference between jet and main-stream temperatures, and the ratios of jet orifice diameter to main-stream width and longitudinal distance downstream.

Figure II-23 is recommended for determining the penetration of single cold-air jets entering a flowing stream of hot gases. This figure is more applicable to the design or analysis of turbojet combustors which have low orifice pressure ratios. For penetration of gas jets from orifices having high pressure ratios, equation (78) is recommended.

Oblique jets. - Penetration: Data expressing the effect of fluid jets mixing with fluids flowing at angles other than 0° or 90° are meager. The investigators of reference 35 varied the entrance angle of hot circular jets to include angles of $22\frac{1}{2}^{\circ}$, 45°, 90°, and 135° with the direction of flow of the main stream. In general, maximum and minimum penetrations were obtained with jets at 90° and $22\frac{1}{2}^{\circ}$ to the direction of flow of the main stream for all momentum ratios and distances downstream of the jet orifice center line. For angles of 135° or 45°, the better angle for penetration was dependent upon the position downstream and the momentum ratio of the two streams. Representative data are presented in figure II-24 (ref. 43) in terms of relative penetration of the jets.

Temperature distribution: Data expressing the temperature distribution in oblique jets are meager. However, Squire (ref. 40) presents general data for the distribution of temperature in a hot jet entering a cold stream from a 1-inch-diameter circular orifice in the wall of a 3-inch-diameter duct. The angle between streams was 15°. Representative data for this configuration are presented in figure II-25. With increasing main-stream velocities, the spread of the jet is reduced and the center line of the temperature profiles is bent downstream. In addition, at a stream-to-jet velocity ratio of approximately 0.4, the center line of the jet becomes parallel to the main-stream flow at approximately 8 inches downstream of the center of the jet orifice.

Multiple jets. - Multiple jets and their interaction or combination are of special interest in the design of combustion chambers in which air openings are generally closely spaced. In addition, the interaction or coalescence of jets may be important in the design of several jet engines mounted together to form a single propulsive unit.

Free-jet velocity distribution: Qualitative data are presented by Squire (ref. 40) for two 0.6-inch-diameter jets, with centers 2 inches apart exhausting into still air. At a distance of 17 jet orifice diameters downstream of the plane of the orifices, the velocity distribution indicated the separate jet origins. At 45 jet diameters downstream, the jets had coalesced, and a single jet-velocity distribution existed. As a rough approximation to determine the velocity at any point in a field of two adjacent free jets, Squire suggests that

$$U^2 = U_D^2 + U_E^2 \tag{80}$$

where

U velocity at point with both jets

U_D velocity at point in first jet

U_E velocity at point in second jet

In addition, Squire states that a row of jets coalesces and behaves as a two-dimensional jet at sufficient distances from the orifices. At distances greater than 10 times the distance between the centers of the individual orifices, the flow will approximate the flow for a two-dimensional jet of the same momentum per unit length.

3267

Free-jet spreading and interaction: Spreading and interaction of adjacent free jets from circular orifices have been investigated by the NACA (unpublished data). Pressure differentials across the orifices were much higher than those usually found across orifices in combustion chambers of jet engines. The jet boundary was arbitrarily defined as the point at which the ratio of the Mach number at that point to the Mach number of the jet expanded isentropically to exhaust ambient pressure was 0.11. Figures II-26(a) to (d) include data showing the jet boundaries at various positions downstream for several orifice pressure differentials and jet spacings. From these data, it is apparent that the distance before interaction of adjacent jets occurs decreases with increasing pressure differentials and decreasing spacings between jets. For some low orifice pressure differentials and large spacings between jets, interaction of the jets does not appear to occur within the region of the potential core.

Free-jet temperature distribution: A small amount of data showing the temperature distribution in the wake of two adjacent jets is also available (unpublished NACA data). Radial distribution of temperature of two jets at temperatures of 1410° and 540° R are shown in figure II-26(e). At an axial distance of 6 jet diameters, the generalized temperature profiles of the hot jets were approximately the same as those of the cold jets. Figure II-26(f) includes temperature profiles of two hot parallel jets from the exhaust of a rocket. The data have been generalized in terms of the previously defined temperature coefficient τ. For the particular jet spacing, the spread of the high-temperature jets at any axial position decreases with increasing jet temperatures. Radial distances for constant values of τ increase to a maximum before decreasing with increasing longitudinal distances from the plane of the nozzles. Similar data were found by Sloop and Morrell (ref. 47).

Normal jets: Multiple gas jets entering normal flowing gas streams are discussed briefly in reference 37. No qualitative data are presented. However, included schlieren photographs indicate that two orifices in line in the flow direction give better penetration than orifices staggered in position. In reference 37, it is suggested that the mixing with circular openings in line is similar to that with longitudinal slots. For longitudinal slots, it is hypothesized that the wake of the upstream half of the jet allows the downstream half to penetrate farther into the hot stream than would be possible otherwise. It is also suggested that the optimum distance between jet center lines should be approximately 2 jet orifice diameters.

Orifice coefficients. - Determination of mass flows through openings in combustion chambers requires a knowledge of the orifice pressure differentials and

discharge coefficients. Much data are available pertaining to the discharge coefficients of orifices in a plane normal to a fluid flowing in a duct. However, in combustion chambers of ram-jet or turbojet engines, the relative position of openings and the presence of flame and crossflow of gases generally limit the applicability of such data. As a result, various investigators have attempted to simulate the flow conditions in combustors for experimental determination of orifice coefficients.

Some of the parameters investigated in the experimental study of flow coefficients are orifice sizes, shapes, and pressure differentials, and velocities and Reynolds numbers of the gas streams. Callaghan and Bowden (ref. 48) determined the discharge coefficients of gas jets normal to air streams as a function of orifice pressure differentials and jet Reynolds numbers for circular, square, and elliptical orifices. The effect of air-stream velocity was also investigated. However, most of the data presented are for much higher orifice pressure differentials than would normally be encountered in jet-engine combustors. For orifices of the same area, elliptical orifices (with the major axis parallel to the direction of flow of the main stream) had higher discharge coefficients, followed by square and circular orifices. The discharge coefficient increased with increases in major-to-minor axis ratios. These results agree in general with the results of reference 37, in which maximum penetration of jets from longitudinal slots was compared with that of circles and squares of the same area.

3267

The experimental data of reference 48 were correlated in terms of jet Reynolds numbers and orifice pressure ratios. For jet Reynolds numbers from 0.3×10^5 to 3.6×10^5 and orifice pressure ratios from 1.15 to 2.09, the following correlations were obtained for jets emanating from sharp-edged orifices into still air:

Circular orifices:

$$\frac{C_h}{\zeta} = 0.948 + 4.83\,(Re_j\times10^{-4} + 53.8)^{-1} \tag{81}$$

$$\zeta = 0.151\,\frac{p_{t,j}}{p_j} + 0.44$$

Square orifices:

$$\frac{C_h}{\zeta} = 0.916 + 7.50\,(Re_j\times10^{-4} + 74.0)^{-1} \tag{82}$$

$$\zeta = 0.150\,\frac{p_{t,j}}{p_j} + 0.467$$

Elliptical orifices:

$$\frac{C_h}{\zeta} = 0.964 + 0.130\left(\frac{Re_j\times10^{-4}}{\beta} + 0.63\right)^{-1} \tag{83}$$

$$\zeta = 0.149\,\frac{p_{t,j}}{p_j} + 0.469$$

$$\beta = 5.97\,\frac{p_{t,j}}{p_j} - 4.17$$

where

C_h orifice discharge coefficient

p_j static pressure of jet

$p_{t,j}$ total pressure of jet

Re_j Reynolds number of jet

In addition, discharge coefficients for jets entering main streams having velocities as great as 380 feet per second can be calculated from the preceding formulas. However, the static pressure of the jet must be calculated from the static pressure of the main stream by use of the Bernoulli and continuity equations based on orifice open area, using the main-stream width minus the maximum width of the jet.

Some data are available indicating the effect of hole diameter, jet Mach number, and internal or external crossflow on the flow coefficients of orifices in a 6-inch-diameter tubular combustor liner. Typical data from reference 49 are presented in figure II-27. For 3/4-inch-diameter orifices in the 6-inch-diameter tubular liner, a linear variation of discharge coefficient from 0.605 to 0.64 was observed as jet Mach number varied from 0.10 to 0.42. These data are applicable for zero crossflow and a maximum of 12 orifices. The variation is greater than observed in reference 48; however, such differences may be attributed to different experimental apparatus. With external crossflow, corrected discharge coefficients decrease rapidly for orifice-to-crossflow Mach number ratios less than 5.0 (fig. II-27(b)). Corrected discharge coefficients increase with increases in orifice diameter, with the increase becoming less marked with increasing orifice-to-crossflow Mach number ratios. The effect of internal or external crossflow on corrected orifice discharge coefficients is presented in figure II-29 as a fraction of the corrected discharge coefficient for zero crossflow. Over a large range of orifice-to-external or -internal crossflow Mach number ratios, the orifice discharge coefficient is greater with internal crossflow.

Additional data indicating the effect of internal or external crossflow and orifice pressure ratios are available in reference 50. Representative data for zero internal flow and various external velocities with 3/8-inch-diameter orifices are presented in figure II-30. For zero external crossflow, the orifice is similar to a normal A.S.M.E. orifice in a straight pipe with a discharge coefficient of approximately 0.6. The discharge coefficient decreases with increasing external velocities and decreasing orifice pressure ratios. These trends agree qualitatively with the results of reference 48.

Much data within the range of orifice pressure ratios in the combustion chambers of jet engines are presented in reference 50. Representative discharge coefficients of two circular orifices are presented in figure II-31 in terms of $\Delta p/q_e$ and various external-internal flow velocity ratios. In general, orifice discharge coefficients increased with decreases in external-internal flow velocity ratios and orifice diameters. The change in slope of the curves of figure II-31 is hypothesized to be the result of opposite influences exerted by the internal and external lateral velocities. That is, an interaction which is dependent upon the velocity ratio occurs. For external-internal velocity ratios less than approximately 2, the internal velocity is more important, with the external velocity being more important at velocity ratios greater than 2.

As a first approximation for use in combustion chambers of jet engines, 0.6 should be used for orifice coefficients unless appreciable internal or external crossflow exists. In such cases, a corrected orifice discharge coefficient can be determined from figure II-28 for the proper orifice crossflow Mach number ratio and orifice diameter, or can be determined from figure II-29 by multiplying by 0.6 the ratio $C_{h,cf}/C_{h,cor}$ for the proper orifice crossflow Mach number ratio. Either of these two values should then be corrected for the effect of jet Mach number by multiplying by $C_h/0.6$ where C_h is read from figure II-27.

43267

AERODYNAMIC MIXING

The aerodynamic mixing of mass, heat, and momentum is of fundamental importance to many of the processes involved in converting the heat energy of fuel to an optimum distribution of momentum in the working fluid stream of jet engines. The processes involving aerodynamic mixing include fuel-air mixing, combustion, and jet mixing, all of which occur under turbulent flow conditions. For this reason, the discussion of mixing emphasizes turbulent transport in high-velocity gas streams.

The mixing of quantities such as mass, heat, and momentum in turbulent gas streams is accomplished by the gross transport of large groups of gas molecules by means of the turbulent fluid motion, with local mixing proceeding by means of molecular motion. The turbulent and molecular mixing of heat and mass follow the same general laws, from which differential equations may be formed for use in the solution of problems in the diffusion of mass and heat in turbulent streams. Solution of the differential equations of diffusion is complicated by the dependence of the molecular diffusion coefficients on temperature and pressure, and the dependence of the turbulent diffusion coefficients upon time. For applications where the molecular diffusion coefficient is constant or negligible compared with the turbulent diffusion coefficient, a generalized form of the differential equation of diffusion may be used to obtain exact or graphical solutions for a wide variety of transport problems encountered in jet-engine combustor design. The following sections include a general discussion of the theory of turbulent diffusion, a discussion of the solution of the differential equations of diffusion, a tabulation of solutions of transport problems for a wide variety of boundary conditions, a discussion of the effect of periodic flow fluctuations on transport, and applications of turbulent diffusion theory to problems in fuel-air mixing.

DIFFUSION

Fundamental Equations

Empirical laws of heat, mass, and momentum transfer. - The differential equations describing the transfer of heat, mass, and momentum arise from a set of similar empirical laws, each of which state that the flux of a quantity being transferred through a unit area is equal to the concentration gradient of the diffusing quantity multiplied by a coefficient. As shown in reference 39, these laws may be tabulated for comparison between the molecular and turbulent cases as follows:

Empirical law	Diffusion of	Laminar flow (molecular)	Turbulent flow
Fick	Mass	$\frac{W}{A} = d_M \frac{\partial C}{\partial X}$	$\frac{W}{A} = D_M \frac{\partial C}{\partial X}$
Biot-Fourier	Heat	$\frac{Q}{\rho c_p A} = \frac{\varkappa}{\rho c_p} \frac{\partial T}{\partial X}$	$\frac{Q}{\rho c_p A} = D_H \frac{\partial T}{\partial X}$
	Momentum	$\frac{\Gamma g}{\rho} = \frac{\mu}{\rho} \frac{\partial U}{\partial X}$	$\frac{\Gamma g}{\rho} = D_U \frac{\partial U}{\partial X}$

where

C concentration

c_p isobaric specific heat

D_H coefficient of turbulent diffusion of heat

D_M coefficient of turbulent diffusion of mass

D_U coefficient of turbulent diffusion of momentum

d_M molecular diffusion coefficient (mass)

U mean stream velocity

X distance normal to A

Γ fluid shearing stress

$\varkappa$ thermal conductivity

These empirical laws may be correlated by the Prandtl and Schmidt numbers, for both the laminar and turbulent flow cases:

Number	Laminar	Turbulent
Prandtl	$Pr = \left(\frac{\mu}{\rho}\right) \Big/ \frac{\varkappa}{\rho c_p}$	$Pr_T = \frac{D_U}{D_H}$
Schmidt	$Sc = \left(\frac{\mu}{\rho}\right) \Big/ (d_M)$	$Sc_T = \frac{D_U}{D_M}$

Experimental data on the diffusion of mass, heat, and momentum are summarized in reference 39 as follows:

Fluid flowing	Diffusing material	Laminar flow		Turbulent flow	
		Pr	Sc	Pr_T	Sc_T
Air	Warm air	0.74		0.76	
Air	Helium		0.34		0.70
Water	Salt water		785		.64

3267

From the preceding experimental results, it may be concluded that the turbulent diffusion of heat and mass occur at equal rates, since the turbulent Prandtl and Schmidt numbers are essentially equal for the separate cases of mass and heat transfer. The latter conclusion is in agreement with the statistical theory of turbulent diffusion, which is discussed in the next section. A necessary prerequisite to the use of the empirically determined turbulent diffusion coefficients is that the turbulent flow fields to be correlated must have proportional turbulence levels and similar turbulent velocity autocorrelation coefficients. A further limitation to the use of the dimensionless Prandtl and Schmidt numbers arises from the assumption of a constant coefficient of diffusion, which in subsequent sections is shown to be a function of time.

Differential equations of diffusion. - The differential equations of diffusion may be derived from the empirical Fick and Biot-Fourier laws by equating the amount of the diffusing quantity entering an infinitesimal volume to the time-rate of change of the total amount of the diffusing quantity in that infinitesimal volume (refs. 51 and 52, p. 7). For the case of the combined turbulent and molecular diffusion of mass without local sources or sinks, the differential equation becomes

$$\frac{\partial c}{\partial t} = \frac{\partial}{\partial X_i}\left[(D_{M_i} + d_{M_i}) \frac{\partial c}{\partial X_i}\right] \quad (i = 1,2,3) \tag{84}$$

where t is time, and the X_i are rectangular coordinates. If the turbulent field is homogeneous and isotropic, equation (84) may be simplified to

$$\frac{\partial c}{\partial t} = (D_M + d_M) \frac{\partial^2 c}{\partial X_i^2} \quad (i = 1,2,3) \tag{85}$$

The differential equation for the combined turbulent and molecular transport of heat without local sources or sinks is

$$\rho c_p \frac{\partial T}{\partial t} = \frac{\partial}{\partial X_i}\left[(\rho c_p D_{H_i} + \varkappa_i) \frac{\partial T}{\partial X_i}\right] \quad (i = 1,2,3) \tag{86}$$

A transformation of the independent variable T (temperature) similar to that presented in reference 53 may be employed:

$$H = \int_{T_r}^{T} \rho c_p \, dT \tag{87}$$

where H is the specific enthalpy and T_r is a base, or reference, temperature. With the use of this transformation, equation (86) may be written as

$$\frac{\partial H}{\partial t} = \frac{\partial}{\partial X_i}\left[\left(D_{H_i} + \frac{\varkappa_i}{\rho c_p}\right)\frac{\partial H}{\partial X_i}\right] \quad (i = 1,2,3) \tag{88}$$

If the turbulent field is homogeneous and isotropic, and if the molecular diffusivity $\varkappa_i/\rho c_p$ is small, or nearly constant, and equal in all directions, equation (88) may be simplifed to

$$\frac{\partial H}{\partial t} = \left(D_H + \frac{\varkappa}{\rho c_p}\right)\frac{\partial^2 H}{\partial X_i^2} \quad (i = 1,2,3) \tag{89}$$

3287

Exact solutions of the preceding differential equations can be made for a variety of transport problems only if the functional forms of the diffusion coefficients are known. The effect of temperature and pressure on the molecular transport coefficients d_M and $\varkappa/\rho c_p$ for most gaseous systems can be found in the literature. The turbulent diffusion coefficients D_M and D_H can be determined expermentally, or may be predicted theoretically from knowledge of two fundamental parameters of the turbulent field. The relation between the turbulent diffusion coefficient and the parameters of the turbulent field is found in the Taylor theory of diffusion by continuous movements, which is summarized in the following section.

Homogeneous, Isotropic, Turbulent Fields

Diffusion by continuous movements. - The theory of diffusion by continuous movements, first presented in reference 54, is generally considered to give a fundamental description of the mechanism of turbulent diffusion. The theory provides a coefficient of turbulent diffusion which may be used directly in equations (84), (85), (88), and (89). As will be shown in subsequent paragraphs, this diffusion coefficient is a function of two parameters that characterize all turbulent fields.

The first of the two turbulence parameters is called the intensity $\sqrt{\overline{u^2}}$, $\sqrt{\overline{v^2}}$, or $\sqrt{\overline{w^2}}$, which defines the magnitude of the turbulent velocities in the three Cartesian coordinate directions:

where U is the mean stream velocity, and the time averages $\overline{u}$, $\overline{v}$, and $\overline{w}$ are all zero. The second turbulence parameter used in the Taylor theory is the Lagrangian double velocity correlation coefficient $\mathcal{R}$ (sometimes called the autocorrelation coefficient) which describes the degree of correlation between the turbulent velocities of a particular fluid particle at time zero and at time t:

$$\mathscr{R}_u = \frac{\overline{\overline{u_0 u_t}}}{\sqrt{\overline{u_0^2}}\sqrt{\overline{u_t^2}}}$$

$$\mathscr{R}_v = \frac{\overline{\overline{v_0 v_t}}}{\sqrt{\overline{v_0^2}}\sqrt{\overline{v_t^2}}}$$

3267

$$\mathscr{R}_w = \frac{\overline{\overline{w_0 w_t}}}{\sqrt{\overline{w_0^2}}\sqrt{\overline{w_t^2}}} .$$

where the $\mathscr{R}$'s are functions of the time interval t, and where the double bar over the product of instantaneous velocities denotes an average of a large number of particle motions.

When the turbulent field is homogeneous ($\sqrt{\overline{u_0^2}} = \sqrt{\overline{u_t^2}}$, etc.), the Lagrangian correlation coefficients may be written as

$$\mathscr{R}_u = \frac{\overline{\overline{u_0 u_t}}}{\overline{u^2}}$$

$$\mathscr{R}_v = \frac{\overline{\overline{v_0 v_t}}}{\overline{v^2}}$$

$$\mathscr{R}_w = \frac{\overline{\overline{w_0 w_t}}}{\overline{w^2}}$$

From the definition of the correlation coefficient $\mathscr{R}_v$, an integral equation may be written:

$$\overline{\overline{v_0 \int_0^t v_t \, dt}} = \overline{v^2} \int_0^t \mathscr{R}_v \, dt \tag{90}$$

Since the mean displacement $\overline{Y}$ of a large number of fluid particles is given by

$$\overline{Y} = \overline{\overline{\int_0^t v \, dt}}$$

and since

$$\overline{Y \, v_0} = \overline{Y \frac{dY}{dt}} = \frac{1}{2} \frac{d\overline{Y^2}}{dt}$$

equation (90) may be written as

$$\frac{1}{2}\frac{d\overline{Y^2}}{dt} = \overline{v^2}\int_0^t \mathscr{R}_v \, dt \tag{91}$$

As shown in references 55 and 56, the quantity $\frac{1}{2}\frac{d\overline{Y^2}}{dt}$ corresponds directly to the turbulent diffusion coefficient D, so that

$$D_u = \overline{u^2}\int_0^t \mathscr{R}_u \, dt \tag{92}$$

$$D_v = \overline{v^2}\int_0^t \mathscr{R}_v \, dt \tag{93}$$

$$D_w = \overline{w^2}\int_0^t \mathscr{R}_w \, dt \tag{94}$$

The turbulent diffusion coefficients derived in the previous equations make no distinction between the transport of heat and mass, and are therefore considered to be applicable to both equations (85) and (89). It is of particular significance to note that the Taylor theory assumes a homogeneous turbulent field where the values of the various intensities and correlation coefficients do not change with position in the field.

Correlation coefficient. - Direct measurements of the Lagrangian correlation coefficient $\mathscr{R}$ does not appear to be feasible by conventional anemometry techniques, since by definition the motion of a particular particle must be observed over a finite length of time. An Eulerian double velocity correlation coefficient $\mathscr{R}'$ has been defined by Taylor in reference 57 and generalized by von Kármán and Howarth in reference 58. The Eulerian correlation coefficient $\mathscr{R}'$ describes the degree of correlation between fluid particle turbulent velocities at two different points in the field at the same instant. For a homogeneous turbulent field, the Eulerian correlation coefficients of interest in the present discussion are those relating the turbulent velocity components at the point (0,0,0) and (x,0,0):

$$\mathscr{R}'_u = \frac{\overline{u_0 u_x}}{\overline{u^2}}$$

$$\mathscr{R}'_v = \frac{\overline{v_0 v_x}}{\overline{v^2}}$$

$$\mathscr{R}'_w = \frac{\overline{w_0 w_x}}{\overline{w^2}}$$

The correlation coefficient $\mathscr{R}'$ can be measured directly by conventional anemometry techniques (refs. 59 and 60), but to date a relation has not been found between the

Lagrangian and Eulerian correlation coefficients. The distinction between the two correlation coefficients is illustrated in the following diagram of particle position and turbulent velocity components:

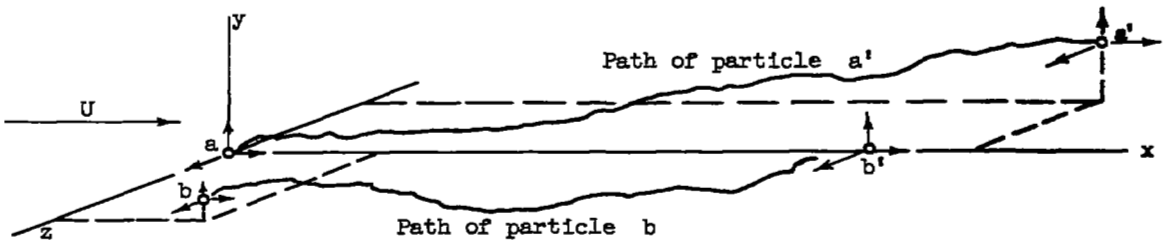

3267

It is evident from this diagram that measurement of velocity components at the points (0,0,0) and (x,0,0) cannot result in the true Lagrangian correlation $\mathscr{R}$ of either particle a or b.

A turbulent diffusion experiment reported in reference 61 has indicated that the Eulerian scale of turbulence $\mathscr{L}'$ may be roughly equal to the Lagrangian scale of turbulence $\mathscr{L}$ for turbulence Reynolds numbers $\left(\sqrt{\overline{u^2}}\,\mathscr{L}'\right)/\nu > 100$, where the Eulerian and Lagrangian scales are defined by

$$\mathscr{L}'_u = \int_0^\infty \mathscr{R}'_u \, dx$$

$$\mathscr{L}'_v = \int_0^\infty \mathscr{R}'_v \, dy$$

$$\mathscr{L}'_w = \int_0^\infty \mathscr{R}'_w \, dz$$

$$\mathscr{L}_u = \sqrt{\overline{u^2}} \int_0^\infty \mathscr{R}_u \, dt$$

$$\mathscr{L}_v = \sqrt{\overline{v^2}} \int_0^\infty \mathscr{R}_v \, dt$$

$$\mathscr{L}_w = \sqrt{\overline{w^2}} \int_0^\infty \mathscr{R}_w \, dt$$

While the equivalence of the Lagrangian and the Eulerian scales has not been fully established, it appears to be a fair approximation and will be used herein for purposes of illustration. Dryden has noted (ref. 62) that measured correlation coefficients commonly follow the exponential form, and suggests that the Lagrangian correlation coefficient might have the form

$$\mathscr{R}_v = e^{-t/t_{\mathscr{L}}} \tag{95}$$

where $t_{\mathscr{L}}$ is a characteristic time related to the Lagrangian scale by definition:

$$t_{\mathscr{L}} = \frac{\mathscr{L}_v}{\sqrt{\overline{v^2}}}$$

The exponential form of the Lagrangian correlation coefficient was found in a diffusion experiment reported in reference 63, and is used for illustration herein. An exponential correlation coefficient is shown in figure II-32 for typical ram-jet combustor approach-stream conditions of 300 feet per second mean stream velocity, 15 feet per second turbulence intensity, and 0.15 foot Lagrangian scale. 3267

In practice, the Lagrangian microscale of turbulence λ may have an appreciable effect on the form of the correlation coefficient (ref. 61). The microscale is defined by the relation

$$\mathscr{R} = 1 - \frac{t^2}{\lambda 2} \quad (t << \lambda_t) \tag{96}$$

and its effect on the correlation coefficient is shown in figure II-32 for a microscale value of 0.0416 foot.

The turbulent diffusion coefficient D_v, which results from the correlation coefficient $\mathscr{R}_v$ shown in figure II-32, is plotted in figure II-33 as a function of time t and of the distance downstream x through the transformation $x = Ut$. In order to illustrate the effect of turbulence scale on the turbulent diffusion coefficient, curves are also shown in figure II-33 for a range of scale values, all other parameters remaining the same. The curves show two characteristics of the turbulent diffusion coefficient:

(1) For small times $(t << t_{\mathscr{L}})$, or short distances $(x << Ut_{\mathscr{L}})$, the eddy diffusion coefficient follows the form

$$D_v = \overline{v^2}\, t$$

(2) For large times $(t >> t_{\mathscr{L}})$, or large distances $(x >> Ut_{\mathscr{L}})$, the eddy diffusion coefficient follows the form

$$D_v = \sqrt{\overline{v^2}}\, \mathscr{L}_v$$

It is of particular significance to note that the turbulent diffusion coefficient is not constant, as assumed in empirical treatments of diffusion, but is in reality a function of time, which may have a very large variation in the range of interest of processes such as fuel-air mixing.

Turbulence spectrum. - Taylor has shown (ref. 64) that the Eulerian correlation coefficient $\mathscr{R}'$ is related to the one-dimensional turbulence energy spectrum by the Fourier transform integral

$$\mathscr{R}' = \int_0^\infty F(f) \cos \frac{2\pi f x}{U} \, df \tag{97}$$

where the spectrum density function $F(f)$ represents the fraction of the total kinetic energy which lies between the frequencies f and $f + df$, so that

$$\int_0^\infty \overline{u^2}(f) \, F(f) \, df = \overline{u^2} \tag{98}$$

3267

The spectrum density function $F_v(f)$ shown in figure II-34 corresponds to an Eulerian correlation coefficient of the exponential form

$$\mathscr{R}'_v = e^{-\frac{y}{\mathscr{L}'_v}} \tag{99}$$

This short discussion of the relation between the correlation coefficient and the spectrum density function is presented to serve as a possible insight into the nature of the Lagrangian correlation coefficient in cases where flow fluctuations are present in addition to those due to turbulence proper. The effect of abnormal spectra on turbulent diffusion is discussed in a succeeding section.

Comparison of turbulent and molecular diffusion. - An excellent measure of diffusion is given by the quantity ω, which is equivalent to the square of the standard deviation used in the theory of statistics. The standard square deviation ω due to turbulence is related to the turbulent diffusion coefficient by the expression

$$\omega_T = \frac{\overline{Y_T^2}}{2} = \int_0^t D_v \, dt \tag{100}$$

In a similar manner, the standard square deviation due to molecular motion is related to the molecular diffusion coefficient by (ref. 55)

$$\omega_L = \frac{\overline{Y_L^2}}{2} = \int_0^t d_M \, dt \tag{101}$$

Methods for the determination of the total standard square deviation ω, where

$$\omega = \omega_T + \omega_L$$

are discussed in a subsequent section on the standard square deviation. At present, it will suffice to note that the greater the value of the parameter ω, the greater will be the degree of mixing. Comparison of the turbulent and molecular standard square deviations must be based on the form of the correlation coefficient, since the turbulent diffusion coefficient depends directly on the correlation coefficient as shown by equations (92) to (94). For purposes of comparison, a correlation coefficient of the form given by equation (95) has been assumed, and the turbulent and molecular mean square deviations are plotted in figure II-35 as a function of time for various values of the parameters $d_M/\mathscr{L}_v^2$ and $\sqrt{\overline{v^2}}/\mathscr{L}_v$.

On the basis of the preceding discussion, a comparison can be made for a model of practical interest: the diffusion of isooctane in a turbulent air stream. For this comparison, the molecular diffusion coefficient has been optimized by assuming a low static pressure of 0.25 atmosphere and a high static temperature of 1100° R. At these conditions, the molecular diffusion coefficient d has a value of 0.000774 square foot per second. The turbulent standard square deviation ω_T for a mean stream velocity U of 300 feet per second, a turbulence intensity $\sqrt{\overline{v^2}}$ of 15 feet per second, and a Lagrangian scale of 0.15 foot, was calculated from equation (100) using the turbulent diffusion coefficient shown in figure II-33. The turbulent and molecular standard square deviations are shown in figure II-36 as a function of time. While the molecular standard square deviation is negligible in this diffusion model over the range of interest, this may not always be the case. For example, the times and distances over which diffusion occurs in flame fronts are so small that the molecular diffusion coefficient might become significant. 3267

Generalized form of differential equations of diffusion. - Solutions of the differential equation of diffusion with constant coefficients have been treated for a wide variety of boundary conditions in references 52 and 65. Equations (85) and (89) for the combined turbulent and molecular diffusion of mass and heat, respectively, have coefficients that are functions of the independent variable time t, but may be transformed to equations with constant coefficients through the relations

$$\omega_L = \int_0^t (D_L + d_L)\, dt \tag{102}$$

$$\omega_H = \int_0^t \left(D_H + \frac{\varkappa}{\rho c_p}\right) dt \tag{103}$$

Methods for the determination of the standard square deviation ω are discussed in a subsequent section on the standard square deviation ω. With the transformations (102) and (103), equations (85) and (89) become, respectively,

$$\frac{\partial C}{\partial \omega_L} = \frac{\partial^2 C}{\partial x_i^2} \tag{104}$$

$$\frac{\partial H}{\partial \omega_H} = \frac{\partial^2 H}{\partial x_i^2} \tag{105}$$

which are amenable to the same solutions as the differential equations of diffusion with constant coefficients.

Several methods have been evolved for the solution of the differential equations of diffusion for the various boundary conditions corresponding to the type of diffusion source. The method to be followed herein is that which utilizes the instantaneous point source in derivations for all source configurations. In addition to its value in the more complex derivations, the point source model adequately describes some diffusion systems of practical interest, and is therefore treated in more detail than the complex models. Since equations (104) and (105) are identical except for the symbols defining the dependent variables, their solutions are also identical. Hereinafter, the equation for the diffusion of mass will be used, with the understanding that its solutions and those for the diffusion of heat are identical in form.

Point source. - The solution for a point source of diffusion is given in reference 65 (p. 338):

$$C = \frac{K^*}{(4\pi\omega)^{3/2}} e^{-\frac{\left[(x-Ut)^2 + r^2\right]}{4\omega}} \tag{106}$$

where

3267

C concentration of diffusing quantity at point (x,r) and time t, lb/cu ft

K^* strength of point source, lb

r radial distance from streamline passing through point source, ft

x distance downstream from point source, ft

ω standard square deviation of fluid particles, sq ft

The value ω is a function of time as illustrated in figure II-36(a) and may be determined from equation (102), or by methods discussed in the next section.

As shown in reference 56, the instantaneous point source solution may be used to solve for the case of a continuous point source. The concentration C at a point (x,r) is obtained by a summation of contributions to that point by instantaneous point sources located at the point ((x - Ut),0,0):

$$C = \frac{W^*}{(4\pi)^{3/2}} \int_0^\infty \frac{1}{\omega^{3/2}} e^{-\frac{(x-Ut)^2 + r^2}{4\omega}} dt \tag{107}$$

where W^* is the weight-flow rate (lb/sec) of material issuing from the point source. With the exception of the limiting cases of very small and very large distances from the point source, the functional form of ω does not permit direct integration of equation (107). To permit comparison with several approximate forms to be discussed, equation (107) has been solved graphically and plotted in figure II-37 for the following conditions:

Fluid	Air
Mean velocity, U, ft/sec	300
Static pressure, atm	0.25
Static temperature, °R	1100
Turbulence intensity, $\sqrt{\overline{u^2}} = \sqrt{\overline{v^2}} = \sqrt{\overline{w^2}}$, ft/sec	15
Turbulence scale, $\mathscr{L}_u = \mathscr{L}_v = \mathscr{L}_w$, ft	0.15
Correlation coefficient, $\mathscr{R}_u = \mathscr{R}_v = \mathscr{R}_w$	$e^{-t/t_{\mathscr{L}}}$
Fuel	Isooctane
Molecular diffusion coefficient, sq ft/sec	0.000774

For small times $t << t_{\mathscr{L}}$, $\frac{\sqrt{\overline{v^2}}}{U} << \frac{x}{\sqrt{x^2 + r^2}}$ and $x >> y,z$, equation (107) can be approximated by (ref. 56)

$$\frac{C}{W^*} = \frac{U}{2\pi\overline{v^2}x^2} e^{-\frac{U^2r^2}{2\overline{v^2}x^2}} \tag{108}$$

3267

For large times $t >> t_{\mathscr{L}}$, neglecting diffusion in the x-direction, equation (107) has the approximate solution (refs. 56 and 66):

$$\frac{C}{W^*} = \frac{1}{4\pi\sqrt{\overline{v^2}}\,\mathscr{L}_v\,(x^2 + r^2)^{1/2}} e^{\frac{U\left[x - (x^2+r^2)^{1/2}\right]}{2\sqrt{\overline{v^2}}\,\mathscr{L}_v}} \tag{109}$$

Another solution for large times $t >> t_{\mathscr{L}}$ and for $x > y,z$ is given in reference 67:

$$\frac{C}{W^*} = \frac{1}{4\pi\sqrt{\overline{v^2}}\,\mathscr{L}_v x} e^{-\frac{Ur^2}{4\sqrt{\overline{v^2}}\,\mathscr{L}_v x}} \tag{110}$$

The approximate solutions given by equations (108) to (110) are compared with the exact graphical solution in figure II-37, and it is evident that these solutions hold only for extreme values of x or t.

An approximate solution which is apparently more nearly exact than the preceding ones is given in reference 68:

$$\frac{C}{W^*} = \frac{1}{4\pi U\omega} e^{-\frac{r^2}{4\omega}} \tag{111}$$

where ω is evaluated at $t = x/U$. Equation (111) is shown in figure II-37, and follows the exact graphical solution throughout the range of interest. Through the use of equation (111), the effect of the scale and intensity of turbulence on fuel-air ratio profiles downstream of a point source may be shown as in figure II-38.

When the rate of fuel injection is a function of time $W_f(t')$, the diffusion problem becomes that of a transient point source with a solution as given in reference 65 (p. 339):

$$C = \frac{1}{(4\pi)^{3/2}} \int_0^t \frac{W_f'}{(\omega')^{3/2}} e^{-\frac{\left[(x-Ut')^2 + r^2\right]}{4\omega'}} dt' \tag{112}$$

where ω' is the standard square deviation evaluated at the time $t - t'$ by the use of equation (102) and methods described in the following section. The possibility of an analytic solution to equation (112) depends upon the functional form of W_f', even when diffusion in the x-direction is neglected, with the integration performed over x. In cases where analytic solutions are impossible, recourse must be made to graphical integration or to differential analyzers (analog computers) such as described in reference 69.

3267

Standard square deviation. - As discussed in a preceding section entitled Correlation coefficient, the Lagrangian parameters of turbulence cannot be measured by existing anemometry techniques, and further, a relation between the Lagrangian and Eulerian parameters has not yet been found. This state of the science does not allow direct mathematical or graphical determination of the standard square deviation ω through equations (92), (93), (94), (102), and (103). Two alternatives are possible, the first of which is based on the assumption of equality between the Lagrangian and Eulerian scales of turbulence $\mathscr{L}$ and $\mathscr{L}'$, and similarity in form between the Lagrangian and Eulerian correlation coefficients $\mathscr{R}$ and $\mathscr{R}'$. If this alternative were used, the Lagrangian parameter $\mathscr{R}$ could be estimated from Eulerian measurements of the turbulent field under consideration, and the standard square deviation could then be determined analytically or graphically from equations (92), (93), (94), (102), and (103).

The second alternative involves the indirect measurement of the standard square deviation ω in the field of turbulence by utilizing known solutions for continuous point or line sources. This method has essentially been employed in references 61 and 63, and is described briefly herein for the case of a continuous point source of diffusion. Inspection of equation (111) reveals that if the concentration C of a gas were known at a number of points (x,r) downstream of a point source emitting the gas at a continuous known rate W_f into a turbulent stream flowing at a known velocity U, the standard square deviation ω could be determined as a function of $t = x/U$. The instrumentation and equipment for such measurements would consist of a gas supply and tube injector, sampling probe(s), and a gas-concentration sensing instrument. The standard square deviation ω determined from such measurements could then be used in any equation shown in table II-I for the solution of diffusion problems having more complex source configurations, boundary conditions, or both. Of the two alternatives, this method seems to offer the best promise for accurate results and is recommended until more is known about the relation between the Lagrangian and Eulerian parameters of turbulence.

Line, plane, surface, and volume sources. - As mentioned previously, the instantaneous point source solution may be used in the solution of all diffusion source configurations. The concentration C at a point (x,r) is found by summing the contributions to that point from the infinite number of point sources which form the particular source configuration under study. Derivations of solutions for the various source configurations are not given herein, but a summary of equations is given in table II-I. Detailed derivations of these equations can be found in the references listed in the table. Many of the equations in table II-I do not have analytic solutions; hence, resort must be made to simplifying assumptions, graphical solution, or analog computers before direct solutions can be obtained.

Nonisotropic Turbulent Flow Fields

The preceding discussion on the theory of turbulent diffusion and solution of the differential diffusion has assumed that the turbulent field is homogeneous and isotropic, which may reduce the applicability of the results in most jet-engine flow fields. Several methods for treating fields other than isotropic or homogeneous have been found and are discussed in following paragraphs.

Homogeneous fields. - Frenkiel has suggested (ref. 56) solutions to diffusion problems for cases where the turbulent diffusion coefficients are linearly related by

$$D_u = k_v^2 D_v = k_w^2 D_w$$

where k_v and k_w are constants of proportionality. If the molecular diffusion coefficient is negligible, equation (84) may be written

$$\frac{1}{D_u}\frac{\partial C}{\partial t} = \frac{\partial^2 C}{\partial x^2} + \frac{1}{k_v^2}\frac{\partial^2 C}{\partial y^2} + \frac{1}{k_w^2}\frac{\partial^2 C}{\partial z^2} \tag{113}$$

which may be transformed by the relation

$$\omega_u = \int_0^t D_u \, dt$$

into a generalized form

$$\frac{\partial C}{\partial \omega_u} = \frac{\partial^2 C}{\partial x^2} + \frac{\partial^2 C}{\partial (k_v y)^2} + \frac{\partial^2 C}{\partial (k_w z)^2} \tag{114}$$

The solution to equation (114) for an instantaneous point source of diffusion is

$$C = \frac{W^* k_v k_w}{(4\pi\omega_u)^{3/2}} e^{-\frac{\left[(x-Ut)^2 + k_v^2 y^2 + k_w^2 z^2\right]}{4\omega_u}} \tag{115}$$

Solutions for other source configurations may be obtained by the summation method described in the preceding sections.

Nonhomogeneous fields. - Diffusion processes may occur in portions of the jet-engine stream having appreciable turbulence intensity and velocity gradients, so that the turbulent diffusion coefficient may be a function of both time and space (assuming neglible molecular diffusion):

$$D_u = f_u(t)F_u(x)$$

$$D_v = f_v(t)F_v(y)$$

$$D_w = f_w(t)F_v(z)$$

In this case, the differential equation of diffusion becomes

$$\frac{\partial c}{\partial t} = f_u(t)\frac{\partial}{\partial x}\left[F_u(x)\frac{\partial c}{\partial x}\right] + f_v(t)\frac{\partial}{\partial y}\left[F_v(y)\frac{\partial c}{\partial y}\right] + f_w(t)\frac{\partial}{\partial z}\left[F_w(z)\frac{\partial c}{\partial z}\right] \tag{116}$$

Successful solution of equation (111) depends on the complexity of the space-time equations for the diffusion coefficients D_u, D_v, and D_w.

3267

Turbulent Flow Fields Containing Periodic Flow Fluctuations

As mentioned in preceding sections of this chapter, flow fields encountered in jet engines may be substantially different from those found in fully developed turbulent flow in pipes or in turbulent flow behind grids. Since theoretical and experimental work in turbulent diffusion has mainly been confined to turbulent pipe flow, or flow fields behind grids, it is of interest to consider the effect of abnormal flow fields on diffusion.

Measurements of axial and lateral kinetic energy spectra (ref. 70, fig. 14) and of sound spectra (ref. 70 and discussion in ch. VIII) have indicated that flow fluctuations may be present in the form of discrete periodicities or in finite frequency bands. The spectrum density function for such turbulent fields may be written as

$$F(f) = \frac{\overline{v^2}}{\overline{v_t^2}} F(f)_T + \frac{\overline{v_{per}^2}}{\overline{v_t^2}} \delta(f - f_{per}) + \frac{\overline{v_s^2}}{\overline{v_t^2}} F(f)_{per} \tag{117}$$

where

$F(f)_T$ spectrum density function of turbulent kinetic energy

$\delta(f - f_{per})$ Dirac delta function

$F(f)_{per}$ spectrum density function of periodic flow fluctuation of finite band width

$\overline{v_{per}^2}$ mean square of periodic velocity fluctuation

$\overline{v_s^2}$ mean square of periodic velocity fluctuations having finite band width

$\overline{v_t^2}$ total mean square of all velocity fluctuations:

$$\overline{v_t^2} = \overline{v^2} + \overline{v_{per}^2} + \overline{v_s^2} \tag{118}$$

If the energy spectrum of a flow field is known, and can be represented by an equation such as equation (117), the Eulerian correlation coefficient can be calculated from equation (97). Although a direct relation has not been determined between the Eulerian correlation coefficient $\mathscr{R}'$ and the Lagrangian correlation coefficient $\mathscr{R}$, it will be assumed herein that they are of the same form, so that the coefficient $\mathscr{R}$ can be estimated for turbulent fields having abnormal spectra.

Superimposed discrete periodicities. - To illustrate the possible effect of a discrete periodic velocity fluctuation at a particular frequency on turbulent diffusion, the flow field used for figure II-37 is assumed to have an additional discrete velocity fluctuation contribution at 100 cycles per second with a magnitude of 30 feet per second. The spectrum density function for this field is

$$F_v(f) = \frac{4\frac{\mathscr{L}_v'}{U}}{1 + \left(\frac{2\pi\mathscr{L}_v'}{U}\right)^2 f^2} \frac{\overline{v^2}}{v_t^2} + \frac{\overline{v_{per}^2}}{v_t^2} \delta(f - 100) \tag{119}$$

so that the Eulerian correlation coefficient becomes

$$\mathscr{R}_v' = \frac{\overline{v^2}}{v_t^2} e^{-\frac{x}{\mathscr{L}_v'}} + \frac{\overline{v_{per}^2}}{v_t^2} \cos \frac{2\pi f x}{U} \tag{120}$$

It will be assumed that the Lagrangian correlation coefficient has the same form as the Eulerian correlation coefficient:

$$\mathscr{R}_v = \frac{\overline{v^2}}{v_t^2} e^{-t/t_{\mathscr{L}}} + \frac{\overline{v_{per}^2}}{v_t^2} \cos 2\pi f t \tag{121}$$

from which the standard square deviation ω may be obtained:

$$\omega = 2.24\ t + 0.0225\ (e^{-100\ t} - 1) + 0.00057\ (1 - \cos 200\ \pi t) \tag{122}$$

The standard square deviation as given by equation (122) is shown in figure II-39 for two cases:

(1) Assuming that the turbulent diffusion coefficient may have negative values

(2) Assuming that the turbulent diffusion coefficient cannot have negative values, and that where the theoretical relations have negative values, the turbulent diffusion coefficient is zero

The standard square deviation shown in figure II-36 is shown again in figure II-39 for comparison. The concentration downstream of a point source of diffusion in the turbulent field containing the discrete velocity fluctuation has been calculated from equation (111) and is shown in figure II-40 for both of the preceding cases, along with the concentration for the turbulent field without periodic velocity fluctuations.

Superimposed velocity fluctuations with finite band width. - By assuming that the Lagrangian and Eulerian correlation coefficients have the same form, the standard square deviation may be evaluted for a turbulent field having periodic velocity fluctuations of a constant mean square value distributed over a finite band width of frequencies. For illustration, the same turbulent field is taken, except that a band of turbulent velocities of constant amplitude is assumed to lie between 100 and 130 cps. The standard square deviation for this assumed field is shown in figure II-41, and the concentration downstream of a point source of diffusion is shown in figure II-42, along with the concentration profile that results from the turbulent field with no periodic velocity fluctuations.

Summary

A comparison has been made between the empirical treatment of turbulent diffusion and the Taylor theory of diffusion by continuous movements. It has been pointed out that the empirical treatment does not fully describe the process of turbulent diffusion, and may give misleading information when fundamental data are applied to full-scale engine design. The Taylor theory of diffusion requires quantitative knowledge of the Lagrangian parameters of the turbulent field under consideration before solution to particular mixing problems can be made. Since only the Eulerian parameters of the turbulent field can be measured by conventional anemometry techniques, an alternative instrumentation is suggested to obtain the Lagrangian parameters. This method would employ a simple point or line source of diffusion of mass or heat, respectively, installed in the flow region of interest, and concentration sensing instrumentation at points downstream of the diffusion source. The Lagrangian parameters could then be obtained from the measured concentration profiles, and used in the solution of mixing problems having more complex source configurations. If future research provides a direct relation between the Lagrangian and Eulerian parameters, the required data could be obtained by the simpler anemometry instrumentation.

3267

As pointed out in the preceding sections, periodic flow disturbances may seriously affect the diffusive character of jet-engine flow streams. For the present at least, this may make generalization of the diffusion process impossible. It is strongly recommended that turbulence measurements be made in full-scale engine test installations whenever possible so that realistic fundamental experiments on diffusion may be made. In addition to periodic flow disturbances, another complication of the mixing problem is found in nonhomogeneity of turbulent fields. The differential equations of diffusion are given for this case, but their solution depends upon the particular mixing problem. Further practical experience in these cases may provide reliable simplifying assumptions to the equations. A compilation is presented in table II-I for a variety of diffusion source configurations. Accompanying each equation are notes to assist the choosing of an equation for a particular mixing problem. A number of the source configurations and boundary conditions do not allow analytic solutions to the differential equations of diffusion; hence, recourse must be made to numerical, graphical, or differential analyzer methods of solution.

FUEL-AIR MIXING

The mixing of fuel with the flowing stream in jet engines is of considerable importance in design practice. The fuel-air-ratio distribution at flame stabilizers in ram-jet combustors and turbojet afterburners has often been found to affect the engine performance strongly. The initial mixing of fuel and air, with subsequent introduction of dilution air, has been found to be one of the most important processes in turbojet combustors. The application of the diffusion equations to the mixing of vapor with flowing air and heat with flowing air to some of the simple source configurations have met with substantial success, but much remains to be done in this field. In particular, suitable relations between the Eulerian and the Lagrangian turbulence parameters are needed in order to predict the standard square deviation of a given turbulent flow field. Solutions for the more complex source configurations and detailed knowledge of the turbulent field in all types of jet-engine combustor would be of considerable utility to both design practice and research. The following sections discuss the current status of practical application of theory to fuel-air mixing, and present suggested extensions to existing information on the fuel-air mixing of evaporating sprays in high-velocity air streams.

Experiments on Diffusion from Simple Point and Line Sources

The turbulent diffusion of hydrogen and carbon dioxide from a point source in a flowing air stream has been found to conform to equations (109) or (110) as reported in reference 68. As predicted by the Taylor theory of diffusion by continuous movements, the turbulent diffusion coefficient was found (1) to approach an asymptotic value with increase in distance downstream, (2) to be approximately directly proportional to the mean stream velocity U (and hence $\sqrt{\overline{v^2}}$, since $\sqrt{\overline{v^2}}/U$ is substantially constant in fully developed pipe flow), and (3) to be proportional to duct size (and hence $\mathscr{L}_v$, since $\mathscr{L}_v$ is proportional to pipe diameter in fully developed pipe flow). A similar experiment, reported in reference 63, has shown that the diffusion of salt water from a point source in a turbulent water stream follows equation (111), and that the Lagrangian correlation coefficient follows the form given by equation (95). 3267

The diffusion of naphtha injected at low velocity from a small tube into a high-velocity gas stream is reported in reference 71, and was found to follow equation (110) when an empirically determined turbulent diffusion coefficient was used. The turbulent diffusion coefficient was found to be independent of stream static pressure (over a range of 4 to 55 lb/sq in. abs), as predicted by the theory of diffusion by continuous movements.

The diffusion of heat from a line source has been reported in reference 72, and was found to follow equation (153), table II-I, where

$$\omega = \frac{1}{\rho c_p} \left(\overline{u^2}t + \varkappa\right) t \tag{123}$$

which is in agreement with the theoretical standard square deviation for $t \ll t_{\mathscr{L}}$, as discussed previously herein.

The diffusion of heat from a line source in a turbulent stream has also been investigated (ref. 61) through a range of time such that the Lagrangian correlation coefficient could be evaluated. The mean temperatures in the heat wake behind the line source were found to follow a simple form of equation (153), table II-I:

$$\frac{\Delta T}{(\Delta T)_0} = e^{-\frac{y^2}{4\omega}} \tag{124}$$

where the mean square deviation ω was found to be a function of time, which asymptotically approached a constant value.

Fuel Droplet Trajectories and Impingement

Aerodynamic mixing includes not only diffusion mixing of unlike gases, but also the contact of liquid fuel droplets with a gaseous medium into which the fuel may vaporize. In a turbojet combustor, liquid fuel generally is introduced in the form of a hollow-cone spray composed of fuel droplets that vary widely in size. The fuel is rapidly disintegrated by recirculatory currents induced in the primary combustion zone. In ram-jet combustors, however, liquid fuel may be in the form of a fine spray introduced longitudinally into a high-velocity air stream. Much of the spray may be deposited upon the flame holders, the amount depending on the

fineness of the spray and the gas stream velocity. It is suggested in reference 73 that the stability of flames behind a flame holder depends, among other things, upon the liquid fuel that collects upon the bluff object. A possible explanation of the entry of the collected fuel into the recirculatory zone downstream of the flame holder is the rearward flow of the liquid fuel to a downstream point on the flame holder, at which point the fuel is either sheared from the rod surface by the high-velocity air stream or is partially vaporized by heat conducted from the flame holder. Under either condition, much of the fuel is swept into the recirculatory zone. With such a combustion system, the rate at which fuel collects upon the bluff object, or the manner in which it is carried past (fuel droplet trajectories) can be important in stable and efficient combustion.

3267

Reference 74 presents data for the trajectories of small water droplets moving at high velocities past a cylinder in air. Data were calculated from the differential equations of motion of a particle. Variables included cylinder radius, air velocity, viscosity, and density, and the droplet velocity, diameter, density, Reynolds number, and drag coefficient. Data showing the maximum collection efficiency of a cylinder, the angle beyond which no droplets strike, and the velocity of impact of the droplets on the rod are presented. These data were calculated for droplets of uniform size. In general, however, droplets in a combustor are not of uniform size. Thus, although the data of reference 74 may not allow quantitative answers, qualitative comparisons of different flame holders may possibly be determined.

A detailed description of the method of calculating the data of reference 74 is beyond the scope of this report. In general, however, it was found that (ref. 75), for fuel collected on a cylindrical rod, the thickness of the fuel film decreases with decreasing fuel-air ratios and decreasing fuel viscosity, the point of maximum film thickness moves rearward and the film shape undergoes a marked change with increasing air-stream velocity, and the average velocity of fuel in the film at a position on the rod 90° from the stagnation point increases with increasing air velocity and fuel-air ratio, and decreasing fuel viscosity.

In reference 76, the families of curves of reference 74 are generalized into a narrow range of curves by the use of several simplifying assumptions. The total collection efficiency of the cylinder, the angle beyond which no droplet impingement occurs, and the droplet impact velocity at the stagnation point are presented in figures II-43, II-44, and II-45 in terms of B and φ as follows:

$$B = \frac{A_{dr}}{A_S} B' \tag{125a}$$

$$\varphi = \frac{Re_a^2}{B'} \tag{125b}$$

$$B' = \frac{4r_{dr}^2 U_a \rho_{dr}}{9d_c \mu_a} \tag{125c}$$

$$\frac{A_{dr}}{A_S} = \frac{1}{Re_a} \int_0^{Re_a} \frac{24}{C_D Re_{dr}} \, d(Re_{dr}) \tag{125d}$$

where

B, B', Φ	dimensionless quantities
C_D	drag coefficient of droplet
d_C	cylinder diameter
Re_a	Reynolds number of droplet based on air velocity U_a
Re_{dr}	Reynolds number of droplet based on velocity of droplet relative to air
r_{dr}	radius of droplet
U_a	velocity of air
Λ_{dr}	range of droplet in still air
Λ_S	Stokes' law range of droplet in still air
μ_a	viscosity of air
ρ_{dr}	density of droplet

3267

These data, as the data of reference 74, can be used best for qualitative comparisons of different flame holders.

Turbulent Spreading of Evaporating Liquid Fuel Droplets from Fuel Injectors

Information pertaining to the liquid fuel distribution in fuel sprays in high-velocity air streams is limited mainly to simple-orifice contrastream injectors. References 77 and 78 relate the boundary geometry of liquid sprays from simple-orifice injectors to spray variables such as injection angle, injection pressure, liquid density, and jet velocity; to injector variables such as strut shape and orifice diameter; and to air-stream variables such as stream velocity and density. Liquid concentration profiles resulting from oblique injectors and from complex fuel injectors have not been reported.

The initial spreading of the fuel spray is due to the radial momentum imparted to the fuel droplets by the injector, and is dependent on the variables discussed in chapter I. Further spreading takes place by virtue of the mixing action of the turbulent field, and has been found to follow the same general laws as the diffusion of vapor or gas when initial spreading has been accounted for by assigning an appropriate source configuration. Diesel oil concentration profiles downstream of a simple-orifice contrastream fuel injector and of a hollow-cone spray nozzle are reported in reference 71. For a low liquid jet velocity, the concentration profiles follow the equation

$$f_l = \frac{W_f U}{4\pi G_a D x} e^{-\frac{Ur^2}{4Dx}} \tag{126}$$

(where f_l is liquid fuel-air ratio) which is identical to equation (110), table II-I, if $D = \sqrt{\overline{v^2}}\,\mathscr{L}_v$ as assumed in the reference. For a higher liquid jet velocity with the simple-orifice contrastream injector, the data of reference 71 fit the diffusion equation for a disk source:

$$f_t = \frac{W_f}{G_a S^2}\,\psi \tag{127}$$

3267

where f_t is total fuel-air ratio, and where

$$\psi = \frac{U}{2\pi Dx}\,e^{-\frac{Ur^2}{4Dx}}\int_0^S r'e^{-\frac{Ur'^2}{4Dx}}\,I_0\left(\frac{Ur'r}{2Dx}\right)dr'$$

so that equation (127) is identical to equation (168), table II-I, if $\omega = D\frac{x}{U}$. The function ψ is plotted in reference 71 for a range of values of r/S and $US^2/2Dx$, and the disk source radius S was found to follow the empirical relation

$$\frac{S}{r} = 11.2\left(\frac{\rho_a U^2}{\rho_f U_f^2}\right)^{-1/3} \tag{128}$$

Concentration profiles downstream of the hollow-cone spray nozzle also followed equation (127) when an appropriate disk radius was used. It was found that the empirically determined diffusion coefficient for liquid fuel droplets was identical for the three fuel-injection systems when air-stream conditions were held constant.

The experimental work discussed in the preceding paragraph suggests that liquid fuel spreading proceeded at a rate independent of fuel droplet size, since the concentration profiles conform to equations derived for continuous mediums. A detailed photgraphic study of isooctane fuel sprays reported in reference 79 has shown that the acceleration of evaporating fuel droplets to stream velocity was independent of drop size for the stream conditions investigated. Analysis of the data reported in reference 79 shows that, for the spray system studied, the droplet velocity conformed to the equation

$$U_{dr} = U(1 - e^{-337\,t}) \tag{129}$$

The time required for a fuel droplet to reach any station x downstream of the fuel injector was

$$x = U\left[t - \frac{1}{337}\left(1 - e^{-337\,t}\right)\right] \tag{130}$$

Two such distance-time curves based on the data from reference 79 are shown in figure II-46, together with the linear time-distance curves $x = Ut$ corresponding to the two stream velocities investigated in the reference.

The significance of equation (130) is shown by further analysis of liquid fuel concentration profiles measured in the same fuel-injection system as the data of

reference 79. This liquid fuel concentration data is unpublished, and was obtained during the fuel-spreading program reported in reference 80. The liquid fuel concentration profiles follow a form based on equation (111), table II-I:

$$f_l = \frac{W_f(1-j)}{4\pi\rho_a U\omega_{l,f}} e^{-\frac{r^2}{4\omega_{l,f}}} \tag{131}$$

where

j fraction of total fuel evaporated before reaching point at which f_l is measured

$\omega_{l,f}$ liquid fuel standard square deviation

Values of $\omega_{l,f}$ were determined from the liquid fuel profiles at three different stations downstream of the fuel injector for the same stream conditions used in reference 79. Through the use of figure II-46, the liquid fuel standard square deviation can be plotted as a function of time, as shown in figure II-47(a). As seen from the figure, the diffusion coefficient $D_{l,f}$ for the liquid fuel droplets is independent of both time and stream velocity over the range investigated. The experimental data of reference 71 include values of the Diesel oil droplet diffusion coefficient $D_{l,f}$ at a fixed station downstream of the point source injector for a range of stream velocities from 200 to 460 feet per second. The droplet diffusion coefficient $D_{l,f}$ was found to be constant over this velocity range, which corroborates the data of figure II-47(a). At the present time, no straightforward analysis is available for explanation of the independence of the liquid fuel droplet diffusion coefficient from stream velocity.

A summary of unpublished data obtained in conjunction with the research reported in reference 80 is shown in figure II-47(b), where the isooctane liquid fuel droplet standard square deviation is plotted as a function of time. The time t was found from equation (130) for each data point, with the assumption that the liquid droplet acceleration was independent of stream pressure and temperature. The data scatter indicates that either the liquid droplet diffusion coefficient $D_{l,f}$ or the liquid droplet axial acceleration, or both, may have a relation to stream temperature and pressure. Further experimental data on the acceleration of evaporating fuel droplets over a range of stream pressures and temperatures would be of great utility in evaluation of the numerical constant in equations such as (129) and (130).

Combined Spreading of Liquid and Vapor Fuel in High-Velocity Air Streams

The spreading of evaporating liquid fuel sprays is treated in reference 80, where isooctane was injected from a simple-orifice contrastream injector into a high-velocity air stream. The stream pressure and temperatures were varied over wide ranges, and vaporization rates (ch. I) and total fuel-spreading parameters J were evaluated from the total fuel-concentration profiles which followed the form

$$f_t = \frac{f_{ov}S^2}{J} e^{-\frac{r^2}{J}} \tag{132}$$

where f_{ov} is the over-all fuel-air ratio. Equation (132) is identical to equation (111), table II-I, if $J = 4\omega$. The total fuel-spreading parameter J was found to follow the correlation

$$J = 0.0598\left(\frac{T}{1000}\right)^{0.67} p_f^{0.49}\, d^{0.79}\left(\frac{U}{100}\right)^{-0.85} p_a^{-0.57}\, x^{0.76} + 0.0042 \qquad (133)$$

While the correlations presented in reference 80 hold for fuel injectors and air-stream conditions used in the investigation, a more general analysis would apply to any source configuration. The remainder of this section is devoted to a suggested general analysis.

3267

The diffusion model of an evaporating spray may be considered to have a source configuration consisting of an infinite number of point sources of vapor fixed in space at the coordinates (x',y',z'):

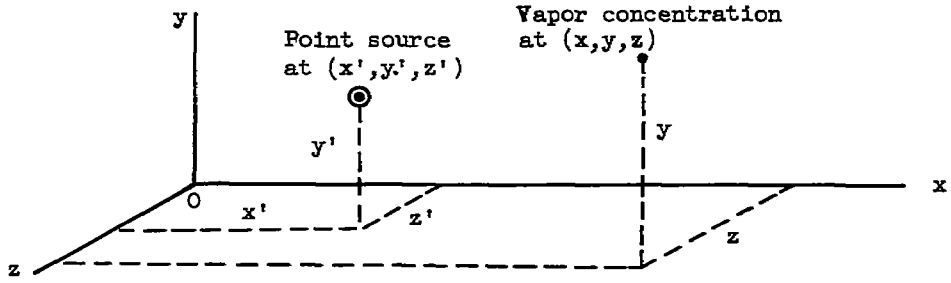

The point sources form a volume corresponding to the space swept out by the liquid fuel droplets as they are swept downstream, and each point source releases vapor at a rate determined by the liquid fuel concentration and the vaporization rate at the coordinates (x',y',z'). The rate of release of vapor, or point source strength, is given by

$$W_f^* = \rho_a U f_l \frac{\partial j}{\partial t} \qquad (134)$$

The liquid fuel - air ratio f_l is a function of the coordinates (x',y',z'), and its form will depend on the particular fuel-injection system under consideration. For the simple-orifice contrastream injector studied in reference 80, the liquid fuel - air ratio was of the form given by equation (131), which may be rewritten as

$$f_l = \frac{W_f^*(1-j)}{4\pi\rho_a U \omega_{l,f}}\, e^{-\frac{(x'^2 + y'^2)}{4\omega_{l,f}}} \qquad (135)$$

The vaporization rate $\partial j/\partial t$ appearing in equation (134) is discussed in chapter I. If the drop-size distribution is constant across a particular station, as was the case for the fuel sprays investigated in references 79 and 80 (and apparently in ref. 71), the vaporization rate $\partial j/\partial t$ is a function only of the distance x'. The functional relation between $\partial j/\partial t$ may be found by the equation

$$\frac{\partial j}{\partial t} = \frac{\partial j}{\partial x'}\frac{\partial x'}{\partial t} = U_{dr}\frac{\partial j}{\partial x'} \tag{136}$$

where the droplet velocity U_{dr} may be obtained from data such as those of reference 79 (shown in eq. (129)) and the axial gradient of the evaporated fraction $\partial j/\partial x'$ from data such as those of reference 80. The fraction of the total fuel which has been evaporated at any particular station can be obtained as a function of the distance x' from data such as those of reference 85, as discussed in chapter I.

The vapor concentration at a point (x,y,z) (see preceding sketch) is given by equation (177), table II-I, which may be written in terms of vapor fuel - air ratio as follows: 3267

$$f = \frac{1}{(4\pi)^{3/2}\rho_a}\int_0^\infty \frac{1}{\omega^{3/2}}\left(\int_0^\infty e^{-\frac{[(x-Ut)-x']^2}{4\omega}}\left\{\int_{-\infty}^\infty e^{-\frac{(y-y')^2}{4\omega}}\left[\int_{-\infty}^\infty W_f^* e^{-\frac{(z-z')^2}{4\omega}} dz'\right] dy'\right\} dx'\right) dt \tag{137}$$

For the fuel-injection system described in reference 80, the relations given by equations (134) to (136) may be applied to equation (137):

$$f = \frac{W_f}{(4\pi)^{5/2}\rho_a}\int_0^\infty \frac{1}{\omega^{3/2}}\left(\int_0^\infty \frac{(1-j)U_{dr}}{\omega_{l,f}}\frac{\partial j}{\partial x'} e^{-\frac{[(x-Ut)^2-x']^2}{4\omega}}\left\{\int_{-\infty}^\infty e^{-\frac{y'^2}{4\omega_{l,f}}-\frac{(y-y')^2}{4\omega}}\left[\int_{-\infty}^\infty e^{-\frac{z'}{4\omega_{l,f}}-\frac{(z-z')^2}{4\omega}} dz'\right] dy'\right\} dx'\right) dt \tag{138}$$

which may be reduced to

$$f = \frac{W_f}{2\pi^{\frac{3}{2}}\rho_a}\int_0^\infty \frac{1}{\omega^{\frac{3}{2}}} e^{-\frac{(y^2+z^2)}{4\omega}}\left\{\int_0^\infty \frac{(1-j)U_{dr}}{(\omega_{l,f}+\omega)}\frac{\partial j}{\partial x'} e^{-\frac{[(x-Ut)-x']^2}{4\omega}} e^{-\frac{\omega_{l,f}(y^2+z^2)}{\omega(\omega_{l,f}+\omega)}} dx'\right\} dt \tag{139}$$

While j and $\omega_{l,f}$ are known functions of x', the integration over x' must be carried out for a number of values of t for each particular point (x,y,z), so that the graphical solution of equation (139) would be tedious, even with the aid of a differential analyzer.

Effect of Solid Boundaries and Flow-Area Changes on Fuel Spreading

The effect of duct walls or other solid boundaries on both liquid fuel droplet and fuel vapor concentrations is discussed in reference 71. The effect of walls on the liquid fuel concentration is indeterminant, since the liquid may either adhere to the walls, or reatomize back into the stream (ref. 71). For the vapor case, an exact solution has been obtained (ref. 71) for the vapor fuel concentration profiles downstream of a point source located on the center line of a circular duct. A graphical method for wall correction is proposed in the same reference, which compares well with both experimental data and the exact theoretical solution. The method essentially assumes that vapor is reflected from the walls and is directly additive to the theoretical concentration profile for an infinite duct. An empirical method for graphically determining fuel concentration profiles in ducts of changing area is discussed in reference 71.

Summary

Experiments on the diffusion of vapor and of heat from simple point and line sources have substantiated many points in the Taylor theory of diffusion and in the analytic solutions of the differential equations of diffusion for such source configurations. The mean square deviation ϖ has been found to be a function of time asymptotically approaching a constant value, and to be independent of local static pressure.

In addition to the liquid fuel droplet spreading due to initial momentum imparted by the injection and atomization processes, liquid fuel sprays have been found to further mix with the air stream by virtue of turbulence present in the stream. Little work has been done on this subject to date, and available information seems to indicate that the turbulent mixing of fuel droplets follows the same general laws as those for vapor if special consideration is given to the aerodynamics of the droplet. Data taken over a limited range of stream and vaporization rate conditions seem to indicate that the turbulent diffusion coefficient for liquid fuel droplets is constant, but no general laws have been substantiated by experiment. A suggested model for the combined spreading of liquid and vapor fuel is presented, and the mathematical analysis is carried to an integral form not subject to analytic solution in its present form.

JET MIXING

Mixing of gases having different temperatures or different components may occur in laminar flow or in flow having a turbulence that is either microscopic or macroscopic in character. In laminar flow, mixing is usually slow and depends upon molecular diffusion. In turbulent flow, mixing depends upon eddy diffusion, whereby eddies in one stream diffuse into the other streams, with a resulting increase in the mixing rate. Microscopic turbulence arises from flow in a smooth pipe at Reynolds numbers greater than the critical value, while macroscopic turbulence results from obstruction or path changes in the mixing chamber. Mixing in turbulent flow, especially macroscopic mixing, is probably of greater importance in combustor design than any of the other forms of mixing. In general, mixing of gases can be achieved by two major methods:

(1) Subdivision of streams

(2) Creation of turbulence

Mixing of gas streams by stream subdivision is discussed by Minchin in reference 81. For two parallel streams of gases having equal velocities but different temperatures, the lateral temperature gradient due to microscopic mixing alone could be approximated by

$$\text{Temperature gradient} \approx 500(x)^{-0.61} \tag{140}$$

where x equals the distance from the junction of the two streams, and the temperature gradient, expressed in percentage of the maximum temperature difference per inch, is measured over a distance of 0.04 x. These results were found to be independent of the absolute velocities of the gas stream, as long as the velocities were equal and the Reynolds numbers were above the critical value. For mixing between parallel streams varying both in temperature and velocity, little change was discerned in the mixing near the mixing origin. However, the effect of the different velocity became marked at distances farther downstream. It was immaterial which of the different temperature streams was the faster.

Variation of the angle of mixing between jets has been found to influence mixing. However, as shown in the following table, the effect of the angle is negligible for included angles of less than 45°:

Total angle between jets, deg	Temperature gradients, percent/in.			
	Distance downstream from junction, in.			
	2.5	5.5	8.5	11.5
0	---	157	114	95
10	309	160	114	92.5
20	279	159	141	102.0
30	254	163	122	100.5
45	205	131	95.5	60.0
60	197	101	72	41.0
75	172	67	37	18.0
90	164	54	31.7	11.7

In general, mixing due to microscopic turbulence between parallel streams of gases is quite slow. Mixing can be accelerated either by creation of macroscopic turbulence in the entering streams, for example, by use of sharp S-bends before junction of the stream, or by use of a turbulence-producing device at the stream junctions. With the latter method, turbulence-producing devices introduced at the interface between streams to cause interlacing of the streams produced best results. Such devices are similar to flame holders used in some ram-jet engines.

A possible method of mixing discussed in reference 81 is the use of a cylindrical obstacle at the interface between two parallel gas streams. This mixing roll creates a vortex trail composed alternately of gases from the two different streams and provides gaps for penetration of gases from the opposite stream. Some data are reported in which the diameter of a cylinder between two parallel streams of gases at different temperatures was varied. Increasing mixing was obtained with diameter increases from 1/4 to 3/4 inch. However, the increased mixing was obtained at the expense of an increased pressure loss. Cylinders larger than 3/4 inch in diameter caused no improvements in mixing.

The absolute velocity of the two streams with the mixing roll affects the degree of mixing in that similar temperature distributions require the same time interval for mixing. Differences in velocities of the two parallel streams hindered formation of the vortex trail and reduced the degree of mixing, although little effect was noted at velocity ratios greater than 2:1. As with mixing with parallel streams alone, it is immaterial which stream is the faster.

Some data have been recorded in which macroscopic turbulence was created in each of the individual gas streams before mixing. Data in which 1/2-inch-diameter cylinders or sharp S-bends were installed upstream of the junction of parallel gas streams indicate that large-scale upstream macroturbulence reduces the mixing when the mixing roll method is employed. However, in plain mixing between parallel gas streams, mixing was improved by the introduction of upstream turbulence-producing obstructions. Mixing between two concentric gas streams differing in temperature has been found to be similar to the mixing of two parallel gas streams. However, the mixing roll method seems to be more effective with concentric gas streams than with parallel streams.

Pressure losses due to mixing of gas streams in the following three configurations are discussed in reference 82 (complete mixing of the two streams after their junction is assumed):

(1) For normal gas streams, expressions similar to those defining pressure losses due to heat addition can be utilized if the total-temperature ratio $T_{t,4}/T_{t,3}$ in equation (23) and figure II-10 is replaced by

$$\frac{T_{t,4}}{T_{t,3}} = \left(1 + \frac{W_3'}{W_3}\right)\left(1 + \frac{W_3'T_{t,3}'}{W_3T_{t,3}}\right) \tag{141}$$

where W_3 and W_3' are defined in table II-II. By use of this new value of overall total-temperature ratio, total-pressure losses due to complete mixing of two perpendicular gas streams can be determined, from either equation (22) or figure II-10.

(2) The mixing of oblique gas streams is somewhat more complicated than the mixing of perpendicular gas streams. Additional parameters derived in reference 82 include

$$B^* = \left(1 + \frac{W_3'}{W_3}\frac{U_3'}{U_3}\cos\alpha\right) \tag{142a}$$

$$C^* = \left(1 + \frac{W_3'}{W_3}\right)\sqrt{\frac{T_{t,4}}{T_{t,3}}} = \sqrt{\left(1 + \frac{W_3'}{W_3}\right)\left(1 + \frac{W_3'}{W_3}\frac{T_{t,3}'}{T_{t,3}}\right)} \tag{142b}$$

where α is the included angle between the gas streams. A new parameter Ω, which is a function of B^* and C^*, is also defined. Values of Ω/C^* for various inlet Mach numbers and values of B^* are presented in figure II-48. The value of exit Mach number M_4 can be found by substitution of Ω^2 for $T_{t,4}/T_{t,3}$ in figure II-10. Total-pressure losses due to mixing of the two oblique streams can be found from the same figure by use of the following equation:

$$\left(\frac{\Delta p_t}{p_{t,3}}\right)_{ob} = 1 - C^*\left(\frac{M_3}{M_4}\right)\left(\frac{1 + \gamma_4 M_4^2}{1 + \gamma_3 M_3^2}\right)\left[\frac{(\gamma_3-1)\left(1 + \frac{\gamma_3-1}{2} M_3^2\right)}{(\gamma_4-1)\left(1 + \frac{\gamma_4-1}{2} M_4^2\right)}\right]^{1/2}\left[1 - \left(\frac{\Delta p_t}{p_{t,3}}\right)_{no}\right] \tag{142c}$$

where M_4 and $(\Delta p_t/p_{t,3})_{no}$ are determined from figure II-10 as if for normal jets.

(3) Mixing of parallel gas streams is treated in reference 82 in much the same manner as oblique streams, except that a term which includes the area ratio is added. For mixing of parallel gas streams as shown in table II-II, the parameters B^* and C^* are defined as

$$B^* = A^*\left(1 + \frac{W_3'}{W_3}\frac{U_3'}{U_3}\right) \tag{143a}$$

$$C^* = A^*\left(1 + \frac{W_3'}{W_3}\right)\sqrt{\frac{T_{t,4}}{T_{t,3}}} = A^*\sqrt{\left(1 + \frac{W_3'}{W_3}\right)\left(1 + \frac{W_3'}{W_3}\cdot\frac{T_{t,3}'}{T_{t,3}}\right)} \tag{143b}$$

(A^* = ratio of jet flow area A_3 to mixed-jet flow area A_4.) The parameter Ω of figure II-48 applies to the case of parallel mixing as well as the mixing of oblique jets. As with other methods of mixing, the exit Mach number and total-pressure losses can be found by substitution of Ω^2 for $T_{t,4}/T_{t,3}$, and use of figure II-10 and equation (142c), which also applies for parallel gas streams.

REFERENCES

1. Whittle, F.: The Early History of the Whittle Jet-Propulsion Gas Turbine, Pt. II. The Aeroplane, vol. LXIX, no. 1797, Nov. 2, 1945, pp. 503-507.

2. Mark, Herman, and Zettle, Eugene V.: Axial-Slot Air Admission for Controlling Performance of a One-Quarter-Annulus Turbojet Combustor and Comparison with Complete Engine. NACA RM E52A21, 1952.

3. Sanders, Newell D.: Performance Parameters for Jet-Propulsion Engines. NACA TN 1106, 1946.

4. Fleming, William A.: Effects of Altitude on Turbojet Engine Performance. NACA RM E51J15, 1951.

5. Walker, Curtis L., Huntley, S. C., and Braithwaite, W. M.: Component and Over-All Performance Evaluation of an Axial-Flow Turbojet Engine over a Range of Engine-Inlet Reynolds Numbers. NACA RM E52B08, 1952.

6. Krebs, Richard P., and Wilcox, E. Clinton: Analysis of the Turbojet Engine for Propulsion of Supersonic Bombers. NACA RM E54A21, 1954.

7. Lloyd, Peter: Combustion in the Gas Turbine - A Survey of War-time Research and Development. R.&M. No. 2579, British A.R.C., May 1946.

8. Lovesey, A. C.: Modern Methods of Testing Aero-Engines and Power Plants. Jour. Roy. Aero. Soc., vol. 54, no. 474, June 1950, pp. 327-358.

9. DeZubay, E. A.: Combustion Processes and Their Application in Gas Turbines. Gas Turbine Lectures, Dept. Mech. and Ind. Eng., Univ. Michigan, June 29-July 10, 1953, pp. 510-558.

10. Yellott, J. I., and Lype, E. F.: Some Effects of Pressure Loss on the Open-Cycle Gas-Turbine Power Plant. Trans. A.S.M.E., vol. 69, no. 8, Nov. 1947, pp. 903-911.

11. Committee A-9, Aircraft Air Conditioning Equipment: Airplane Heating and Ventilating Equipment-Engineering Data - Fluid Dynamics. Aero. Info. Rep. No. 23, SAE, 1951, p. 7.

12. Patterson, G. N.: Modern Diffuser Design. Aircraft Eng., vol. X, no. 115, 1938, pp. 267-273.

13. Sänger, E., and Bredt, I.: A Ram-Jet Engine for Fighters. NACA TM 1106, 1947.

14. Valentine, E. Floyd, and Carroll, Raymond B.: Effects of Several Arrangements of Rectangular Vortex Generators on the Static-Pressure Rise Through a Short 2:1 Diffuser. NACA RM L50L04, 1951.

15. Perry, John H., ed.: Chemical Engineers' Handbook. Third ed., McGraw-Hill Book Co., Inc., 1950, pp. 387-388.

16. Sterbentz, William H.: Analysis and Experimental Observation of Pressure Losses in Ram-Jet Combustion Chambers. NACA RM E9H19, 1949.

17. Frost, E. E., Morris, K. G., Petrin, R. J., and Weiss, M. A.: Progress Report on Study of Combustors for Supersonic Ram-Jet. Rep. No. PDN 5740, Oct. 1, 1951-Mar. 31, 1952. Process Div. Esso Labs., Standard Oil Development Co., June 30, 1952. (Contract NOrd-9233 SOD/CM-735.)

18. McAdams, W. H.: Heat Transmission. Second ed., McGraw-Hill Book Co., Inc., 1942, p. 119.

19. Knight, H. A., and Walker, R. B.: The Component Pressure Losses in Combustion Chambers. Rep. No. R.143, British N.G.T.E., Nov. 1953.

20. Shapiro, Ascher H., and Hawthorne, W. R.: The Mechanics and Thermodynamics of Steady One-Dimensional Gas Flow. Jour. Appl. Mech., vol. 14, no. 4, Dec. 1947, pp. A-317-A-336.

21. Younger, George G., Gabriel, David S., and Mickelsen, William R.: Experimental Study of Isothermal Wake-Flow Characteristics of Various Flame-Holder Shapes. NACA RM E51K07, 1952.

22. Goldstein, Sidney, ed.: Modern Developments in Fluid Dynamics. Vol. II. The Clarendon Press (Oxford), 1938, pp. 556-557.

23. Williams, G. C., Hottel, H. C., and Scurlock, A. C.: Flame Stabilization and Propagation in High Velocity Gas Streams. Third Symposium on Combustion and Flame and Explosion Phenomena, The Williams & Wilkins Co., 1949, pp. 21-40.

24. Prandtl, L., and Tietjens, O. G.: Applied Hydro- and Aeromechanics. McGraw-Hill Book Co., Inc., 1934, pp. 130-136.

25. Pinkel, I. Irving, and Shames, Harold: Analysis of Jet-Propulsion-Engine Combustion-Chamber Pressure Losses. NACA Rep. 880, 1947. (Supersedes NACA TN 1180.)

26. Lubbock, I.: Combustion Problems of the Gas Turbine. Aircraft Eng., vol. XXIII, no. 269, July 1951, pp. 196-202; 213.

27. Childs, J. Howard, McCafferty, Richard J., and Surine, Oakley W.: Effect of Combustor-Inlet Conditions on Performance of an Annular Turbojet Combustor. NACA Rep. 881, 1947. (Supersedes NACA TN 1357.)

28. Leeper, C. K.: Analytical Treatment of Flow in Can Type Combustors. Rep. TB-15, Consolidated Vultee Aircraft Corp., Sept. 20, 1948.

29. Wead, R. K.: Theoretical Characteristics of Can Burners. Rep. TB-52, Consolidated Vultee Aircraft Corp., Nov. 22, 1949. (Contract NOrd 9028.)

30. Bader, Frank: A Convenient Method for Calculation of Flow Conditions within a Can-Type Burner Using Assigned Flow and Cross-Sectional Area Distributions. Rep. CM-642, Appl. Phys. Lab., The Johns Hopkins Univ., Sept. 28, 1950. (NOrd Contract 7386 with Bur. Ord., U.S. Navy.)

31. Goldstein, Sidney, ed.: Modern Developments in Fluid Dynamics. Vol. I. The Clarendon Press (Oxford), 1938, pp. 145-148.

32. Tollmien, Walter: Calculation of Turbulent Expansion Processes. NACA TM 1085, 1945.

33. Taylor, G. I.: The Transport of Vorticity and Heat Through a Fluid in Turbulent Motion. Proc. Roy. Soc. (London), ser. A, vol. 135, no. A828, Apr. 1, 1932. pp. 685-702.

34. Abramovich, G. N.: The Theory of a Free Jet of a Compressible Gas. NACA TM 1058, 1944.

3267

35. Howarth, L.: Concerning the Velocity and Temperature Distributions in Plane and Axially Symmetric Jets. Proc. Cambridge Phil. Soc., vol. 34, 1938, pp. 185-203.

36. Squire, H. B., and Trouncer, J.: Round Jets in a General Stream. R.&M. No. 1974, British A.R.C., 1944.

37. Hawthorne, W. R., Rogers, G. F. C., and Zaczek, B. Y.: Mixing of Gas Streams - The Penetration of a Jet of Cold Air into a Hot Stream. Tech. Note No. Eng. 271, British R.A.E., Mar. 1944.

38. Taylor, J. F., Grimmett, H. L., and Comings, E. W.: Isothermal Free Jets of Air Mixing with Air. Chem. Eng. Prog., vol. 47, no. 4, Apr. 1951, pp. 175-180.

39. Forstall, Walton, Jr., and Shapiro, Ascher H.: Momentum and Mass Transfer in Coaxial Gas Jets. Meteor Rep. No. 39, Dept. Mech. Eng., M.I.T., July 1949. (Bur. Ord. Contract NOrd 9661.)

40. Squire, H. B.: Jet Flow and Its Effects on Aircraft. Aircraft Eng., vol. XXII, no. 253, Mar. 1950, pp. 62-67.

41. Corrsin, Stanley: Investigation of Flow in an Axially Symmetrical Heated Jet of Air. NACA WR-94, 1943. (Supersedes NACA ACR 3L23.)

42. Reichardt, H.: On a New Theory of Free Turbulence. R.T.P. Trans. No. 1686, British M.A.P. (See also Z.a.M.M., Bd. 21. Heft 5, Oct. 1941, pp. 257-264.)

43. Pfeiffer, Arthur, Murati, George T., and Engel, Arthur B.: Mixing of Gas Streams. M.S. Thesis, M.I.T., 1945.

44. Callaghan, Edmund E., and Ruggeri, Robert S.: Investigation of the Penetration of an Air Jet Directed Perpendicularly to an Air Stream. NACA TN 1615, 1948.

45. Chelko, Louis J.: Penetration of Liquid Jets into a High-Velocity Air Stream. NACA RM E50F21, 1950.

46. Callaghan, Edmund E., and Ruggeri, Robert S.: A General Correlation of Temperature Profiles Downstream of a Heated-Air Jet Directed Perpendicularly to an Air Stream. NACA TN 2466, 1951.

47. Sloop, John L., and Morrell, Gerald: Temperature Survey of the Wake of Two Closely Located Parallel Jets. NACA RM E9I21, 1950.

48. Callaghan, Edmund E., and Bowden, Dean T.: Investigation of Flow Coefficient of Circular, Square, and Elliptical Orifices at High Pressure Ratios. NACA TN 1947, 1949.

49. Anon.: Bumblebee Semi-Annual Survey. Convair Rep. 5001-9, July-Dec. 1950, Consolidated Vultee Aircraft Corp. (Contract NOrd 9028.)

50. Seglem, Clifford E.: The Discharge Coefficient of a Combustor Air Inlet Hole. M.S. Thesis, Univ. of Pittsburgh, 1952.

51. Churchill, Ruel V.: Fourier Series and Boundary Value Problems. McGraw-Hill Book Co., Inc., 1941.

52. Carslaw, H. S., and Jaeger, J. C.: Conduction of Heat in Solids. Univ. Press (Oxford), 1947.

53. Van Dusen, M. S.: Note on the Theory of Heat Conduction. Bur. Standards Jour. Res., RP 178, vol. 4, no. 6, June 1930, pp. 753-756.

54. Taylor, G. I.: Diffusion by Continuous Movements. Proc. London Math. Soc., vol. 20, 1922, pp. 196-212.

55. Glasstone, Samuel: Textbook of Physical Chemistry. Second ed., D. Van Nostrand Co., Inc., 1946, p. 260.

56. Frenkiel, F. N.: Turbulent Diffusion: Mean Concentration Distribution in a Flow Field of Homogeneous Turbulence. Vol. III. Advances in Appl. Mech., Academic Press, Inc., 1953, pp. 61-107.

57. Taylor, G. I.: The Statistical Theory of Turbulence, Pt. II. Proc. Roy. Soc. (London), ser. A, vol. 151, no. 833, 1935, pp. 444-454.

58. von Kármán, Theodore, and Howarth, Leslie: On the Statistical Theory of Isotropic Turbulence. Proc. Roy. Soc. (London), ser. A, vol. 164, Jan. 1938, pp. 192-215.

59. Laurence, James C., and Landes, L. Gene: Auxiliary Equipment and Techniques for Adapting the Constant-Temperature Hot-Wire Anemometer to Specific Problems in Air-Flow Measurements. NACA TN 2843, 1952.

60. Kovásznay, Leslie S. G.: Development of Turbulence-Measuring Equipment. NACA TN 2839, 1953.

61. Uberoi, Mahinder S., and Corrsin, Stanley: Diffusion of Heat from a Line Source in Isotropic Turbulence. NACA TN 2710, 1952.

62. Dryden, Hugh L.: A Review of the Statistical Theory of Turbulence. Quart. Appl. Math., vol. 1, no. 1, Apr. 1943, pp. 7-42.

63. Kalinske, A. A., and Pien, C. C.: Eddy Diffusion. Ind. and Eng. Chem., vol. 36, no. 3, Mar. 7, 1944, pp. 220-222.

64. Taylor, G. I.: The Spectrum of Turbulence. Proc. Roy. Soc. (London), ser. A, vol. 164, Feb. 18, 1938, pp. 476-490.

65. Jakob, M.: Heat Transfer. Vol. 1. John Wiley & Sons, Inc., 1949.

3267

66. Wilson, H. A.: Convection of Heat. Proc. Cambridge Phil. Soc., vol. 12, Apr. 1904, pp. 406-423.

67. Roberts, D. F. T.: The Theoretical Scattering of Smoke in a Turbulent Atmosphere. Proc. Roy. Soc. (London), ser. A, vol. 104, 1923, pp. 640-654.

68. Towle, W. L., and Sherwood, T. K.: Eddy Diffusion - Mass Transfer in the Central Portion of a Turbulent Air Stream. Ind. and Eng. Chem., vol. 31, no. 4, Apr. 1939, pp. 457-462.

3267

69. Bush, V., and Caldwell, S. H.: A New Type of Differential Analyser. Jour. Franklin Inst., vol. 240, no. 4, Oct. 1945, pp. 255-326.

70. Mickelsen, William R., and Laurence, James C.: Measurement and Analysis of Turbulent Flow Containing Periodic Flow Fluctuations. NACA RM E53F19, 1953.

71. Longwell, John P., and Weiss, Malcolm A.: Mixing and Distribution of Liquids in High-Velocity Air Streams. Ind. and Eng. Chem., vol. 45, no. 3, Mar. 1953, pp. 667-677.

72. Schubauer, G. B.: A Turbulence Indicator Utilizing the Diffusion of Heat. NACA Rep. 524, 1935.

73. Scurlock, A. C.: Flame Stabilization and Propagation in High-Velocity Gas Streams. Meteor Rep. No. 19, M.I.T., May 1948. (Contract NOrd 9661.)

74. Langmuir, Irving, and Blodgett, Katherine B.: A Mathematical Investigation of Water Droplet Trajectories. Tech. Rep. No. 5418, Air Materiel Command, AAF, Feb. 19, 1946. (Contract No. W-33-038-ac-9151 with General Electric Co.)

75. Scull, Wilfred E.: Measurements of Liquid Fuel Films on a Rod Flame-Holder. Rep. of Exp. Res. Problem in Chem. Eng., M.I.T., Jan. 19, 1951.

76. Sherman, P., Klein, J. S., and Tribus, M.: Determination of Drop Trajectories by Means of an Extension of Stokes' Law. Eng. Res. Inst., Air Res. and Dev. Command, USAF, Univ. Michigan, Apr. 1952. (Contract AF 18(600)-51, Proj. M992-D.)

77. Robbins, George W., and Wiggins, J. W.: Investigation of Ramjet Fuel Sprays. USCAL Rep. 4-6, Aero. Lab., Univ. Southern Calif., July 16, 1947. (Navy Contract NOa(s)8257.)

78. Chelko, Louis J.: Penetration of Liquid Jets into a High-Velocity Air Stream. NACA RM E50F21, 1950.

79. Ingebo, Robert D.: Vaporization Rates and Drag Coefficients for Isooctane Sprays in Turbulent Air Streams. NACA TN 3265, 1954.

80. Bahr, Donald W.: Evaporation and Spreading of Isooctane Sprays in High-Velocity Air Streams. NACA RM E53I14, 1953.

81. Minchin, L. T.: The Mixing of Gas Streams. Rep. No. E.3965, British R.A.E., Jan. 1943.

82. Hawthorne, W. R., and Cohen, H.: Pressure Losses and Velocity Changes Due to Heat Release and Mixing in Frictionless, Compressible Flow. Rep. No. E.3997, British R.A.E., Jan. 1944.

TABLE II-I. - EQUATIONS FOR CONCENTRATION OF HEAT OR MASS DOWNSTREAM OF VARIOUS SOURCES

Source configuration	Type solution	Reference	Conditions	Range	Equation (a)
Point 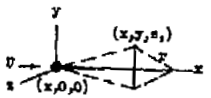	(b,c)	65 (p.388)	----------	All t	$C = \frac{K^*}{(4\pi\alpha)^{3/2}} \exp\left\{-\frac{1}{4\alpha}\left[(x-Ut)^2 + r^2\right]\right\}$ (106)
	(c,d)	56	----------	All t	$C = \frac{W^*}{(4\pi)^{3/2}} \int_0^\infty \alpha^{-3/2} \exp\left\{-\frac{1}{4\alpha}\left[(x-Ut)^2 + r^2\right]\right\} dt$ (107)
	(c,d)	56	----------	$t \ll t_g$	$C = \frac{W^* \exp\left(-\frac{U^2}{2\nu^2}\right)}{(2\pi)^{3/2}\sqrt{\nu^2}\,(x^2+r^2)} \left\{1 + \frac{\pi}{2} \exp\left[\frac{x^2U^2}{2\nu^2\,(x^2+r^2)}\right] \operatorname{erfc}\left[-\frac{xU}{\sqrt{2}\sqrt{\nu^2}\,(x^2+r^2)^{1/2}}\right]\right\}$ (144)
	(d,e)	56	$\frac{\sqrt{\nu^2}}{U} \ll \frac{x}{\sqrt{x^2+r^2}}$ $0 < x \gg y,z$	$t \ll t_g$	$C = \frac{W^*U}{2\pi\,\nu^2\,x^2} \exp\left(-\frac{U^2r^2}{2\nu^2\,x^2}\right)$ (108)
	(d,e)	52,66	$\frac{\partial c}{\partial x} \doteq 0$	$t \gg t_g$	$C = \frac{W^*}{4\pi\sqrt{\nu^2}\,g_y\,(x^2+r^2)^{1/2}} \exp\left\{\frac{U\left[x-(x^2+r^2)^{1/2}\right]}{2\sqrt{\nu^2}\,g_y}\right\}$ (109)
	(d,e)	67	$\frac{\partial c}{\partial x} \doteq 0, x > y,z$	$t \gg t_g$	$C = \frac{W^*}{4\pi\sqrt{\nu^2}\,g_x} \exp\left(-\frac{Ur^2}{4\sqrt{\nu^2}\,g_x}\right)$ (110)
	(d,e)	66	$\frac{\partial c}{\partial x} = 0$	All t	$C = \frac{W^*}{4\pi U\alpha} \exp\left(-\frac{r^2}{4\alpha}\right)$ (111)
	(c,f)	65 (p.559)	----------	All t	$C^* = \frac{1}{(4\pi)^{3/2}} \int_0^t \frac{W'}{(\alpha')^{3/2}} \exp\left\{-\frac{1}{4\alpha'}\left[(x-Ut')^2 + r^2\right]\right\} dt'$ (112)
Line 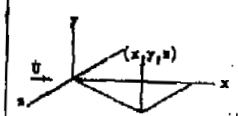	(b,c)	--	Line source lying between $z=1, z=-1$ K^* variable	All t	$C = \frac{1}{(4\pi)^{3/2}} \int_{-1}^{1} \frac{K^*(z')}{\alpha^{3/2}} \exp\left\{-\frac{1}{4\alpha}\left[(x-Ut)^2 + y^2 + (z-z')^2\right]\right\} dz'$ (145)
	(b,c)	--	Line source lying between $z=1, z=-1$	All t	$C = \frac{K^*}{8\pi\alpha} \exp\left\{-\frac{1}{4\alpha}\left[(x-Ut)^2 + y^2\right]\right\} \left[\operatorname{erf}\left(\frac{z+1}{2\sqrt{\alpha}}\right) - \operatorname{erf}\left(\frac{z-1}{2\sqrt{\alpha}}\right)\right]$ (146)
	(b,c)	--	Infinite length or bounded	All t	$C = \frac{K^*}{4\pi\alpha} \exp\left\{-\frac{1}{4\alpha}\left[(x-Ut)^2 + y^2\right]\right\}$ (147)

[a]Symbols are explained as follows:

$\exp(a) = e^a$

$\operatorname{erf}(a) = \frac{2}{\sqrt{\pi}} \int_0^a e^{-\alpha^2}\, d\alpha$

$\operatorname{erfc}(a) = 1 - \operatorname{erf}(a)$

$K_0(a)$ = modified Bessel function, second kind, zero order

$I_0(a)$ = modified Bessel function, first kind, zero order

$r^2 = y^2 + z^2$, $\alpha^2 = (x - Ut)^2 + y^2 + z^2$

K^*, W^*, and W' are independent of x, y, and z except where noted.

[b]Instantaneous.

[c]Exact.

[d]Continuous.

[e]Approximate.

[f]Transient.

TABLE II-I. - Continued. EQUATIONS FOR CONCENTRATION OF HEAT OR MASS DOWNSTREAM OF VARIOUS SOURCES

Source configuration	Type solution	Reference	Conditions	Range	Equation (a)
Line (continued)	(c,d)	--	Line source lying between $z=1, z=-1$	All t	$C = \frac{W^*}{8\pi}\int_0^\infty \frac{1}{\alpha}\exp\left\{-\frac{1}{4\alpha}\left[(x-Ut)^2+y^2\right]\right\}\left[\operatorname{erf}\left(\frac{z+1}{2\sqrt{\alpha}}\right)-\operatorname{erf}\left(\frac{z-1}{2\sqrt{\alpha}}\right)\right]dt$ (148)
	(c,d)	--	Infinite length or bounded	All t	$C = \frac{W^*}{4\pi}\int_0^\infty \frac{1}{\alpha}\exp\left\{-\frac{1}{4\alpha}\left[(x-Ut)^2+y^2\right]\right\}dt$ (149)
	(d,e)	56	$\frac{y}{x}, \frac{\sqrt{\nu^2}}{U} \ll 1$	$t \ll t_{\mathscr{L}}$	$C = \frac{W^*}{\sqrt{2\pi}\,U\mathscr{L}x}\exp\left(-\frac{U^2y^2}{2\nu^2 x^2}\right)$ (150)
	(d,e)	56	----------	$t \gg t_{\mathscr{L}}$	$C = \frac{W^*}{2\pi U\mathscr{L}^2}\exp\left(\frac{Ux}{2\nu^2/\sqrt{\nu^2\mathscr{L}}}\right)K_0\left(\frac{U\sqrt{x^2+y^2}}{2\nu^2/\sqrt{\nu^2\mathscr{L}}}\right)$ (151)
	(d,e)	56	$\frac{y}{x} \ll 1$	$t \gg t_{\mathscr{L}}$	$C = \frac{W^*\left(\sqrt{\nu^2}\right)^{1/2}}{2\sqrt{\pi}\,(U\mathscr{L})^{3/2}x^{1/2}}\exp\left(-\frac{Uy^2}{4\nu^2\mathscr{L}x}\right)$ (152)
	(d,e)	56	$\frac{y}{x}, \frac{\sqrt{\nu^2}}{U} \ll 1$	All t	$C = \frac{W^*\sqrt{\nu^2}}{\sqrt{4\pi\alpha}\,U^2\mathscr{L}}\exp\left(-\frac{x^2}{4\alpha}\right)$ (153)
	(c,f)	--	Line source lying between $z=1, z=-1$	All t	$C = \frac{1}{(4\pi)^{3/2}}\int_0^t\left(\int_{-1}^{1}\frac{W'(z',t')}{(\alpha')^{3/2}}\exp\left\{-\frac{1}{4\alpha'}\left[(x-Ut')^2+y^2+(z-z')^2\right]dz'\right\}\right)dt'$ (154)
	(c,f)	--	Line source lying between $z=1, z=-1$	All t	$C = \frac{1}{8\pi}\int_0^t\frac{W'}{\alpha'}\exp\left\{-\frac{1}{4\alpha'}\left[(x-Ut')^2+y^2\right]\right\}\left[\operatorname{erf}\left(\frac{z+1}{2\sqrt{\alpha'}}\right)-\operatorname{erf}\left(\frac{z-1}{2\sqrt{\alpha'}}\right)\right]dt'$ (155)
	(c,f)	--	Infinite length or bounded	All t	$C = \frac{1}{4\pi}\int_0^{t'}\frac{W'}{\alpha'}\exp\left\{-\frac{1}{4\alpha'}\left[(x-Ut')^2+y^2\right]\right\}dt'$ (156)
	(b,c)	52	Ring source of radius r	All t	$C = \frac{K^*R}{4\sqrt{\pi}\,\alpha^{3/2}}\exp\left\{-\frac{1}{4\alpha}\left[(x-Ut)^2+r^2+R^2\right]\right\}I_0\left(\frac{Rr}{2\alpha}\right)$ (157)
	(e,d)	--	Ring source of radius r	All t	$C = \frac{W^*R}{4\sqrt{\pi}}\int_0^\infty\frac{1}{\alpha^{3/2}}\exp\left\{-\frac{1}{4\alpha}\left[(x-Ut)^2+r^2+R^2\right]\right\}I_0\left(\frac{Rr}{2\alpha}\right)dt$ (158)

[a] Symbols are explained as follows:

$\exp(a) = e^a$

$\operatorname{erf}(a) = \frac{2}{\sqrt{\pi}}\int_0^a e^{-\alpha^2}\,d\alpha$

$\operatorname{erfc}(a) = 1 - \operatorname{erf}(a)$

$K_0(a)$ = modified Bessel function, second kind, zero order

$I_0(a)$ = modified Bessel function, first kind, zero order

$r^2 = y^2 + z^2$, $\sigma^2 = (x - Ut)^2 + y^2 + z^2$

K^*, W^*, and W' are independent of x, y, and z except where noted.

[b] Instantaneous.

[c] Exact.

[d] Continuous.

[e] Approximate.

[f] Transient.

TABLE II-1. - Continued. EQUATIONS FOR CONCENTRATION OF HEAT OR MASS DOWNSTREAM OF VARIOUS SOURCES

Source configuration	Type solution	Reference	Conditions	Range	Equation (a)	
Line (concluded)	(c,f)	--	Ring source of radius r	All t	$C = \frac{R}{4\sqrt{\pi}}\int_0^t \frac{W'}{(\sigma')^{3/2}} \exp\left\{-\frac{1}{4\sigma}r\left[(x-Ut')^2 + r^2 + R^2\right]\right\} I_0\left(\frac{Rr}{2\sigma}\right)dt'$	(159)
	(d,e)	71	Ring source of radius r; $\partial C/\partial x = 0$	All t	$C = \frac{W^*}{4\pi U\sigma} \exp\left[-\frac{1}{4\sigma}(R^2 + r^2)\right] I_0\left(\frac{Rr}{2\sigma}\right)$	(160)
Plane	(b,c)	--	Plane lying between $y'=-a$, $z'=-b$	All t	$C = \frac{K^*}{4\sqrt{4\pi\sigma}} \exp\left[-\frac{(x-Ut)^2}{4\sigma}\right]\left[\operatorname{erf}\left(\frac{y+a}{2\sqrt{\sigma}}\right) - \operatorname{erf}\left(\frac{y-a}{2\sqrt{\sigma}}\right)\right]\left[\operatorname{erf}\left(\frac{z+b}{2\sqrt{\sigma}}\right) - \operatorname{erf}\left(\frac{z-b}{2\sqrt{\sigma}}\right)\right]$	(161)
	(b,c)	--	Infinite plane; $(y+a),(z+b) \gg \sqrt{4\sigma}$	All t	$C = \frac{K^*}{\sqrt{4\pi\sigma}} \exp\left[-\frac{(x-Ut)^2}{4\sigma}\right]$	(162)
	(c,d)	--	Infinite plane	All t	$C = \frac{W^*}{\sqrt{4\pi}}\int_0^\infty \frac{1}{\sigma^{1/2}} \exp\left[-\frac{(x-Ut)^2}{4\sigma}\right]dt$	(163)
	(c,f)	--	Infinite plane	All t	$C = \frac{1}{\sqrt{4\pi}}\int_0^t \frac{W'}{(\sigma')^{1/2}} \exp\left[-\frac{(x-Ut)^2}{4\sigma}\right]dt'$	(164)
	(b,c)	--	Disk source of radius r	All t	$C = \frac{K^*}{4\sqrt{\pi\sigma}} \exp\left\{-\frac{1}{4\sigma}\left[(x-Ut)^2 + r^2\right]\right\}\left[\int_0^{R^2/4\sigma} e^{-\alpha} I_0\left(r\sqrt{\frac{\alpha}{\sigma}}\right)d\alpha\right]$	(165)
	(c,d)	--	Disk source of radius r	All t	$C = \frac{W^*}{4\pi^{1/2}}\int_0^\infty \frac{1}{\sigma^{1/2}} \exp\left\{-\frac{1}{4\sigma}\left[(x-Ut)^2 + r^2\right]\right\}\left[\int_0^{R^2/4\sigma} e^{-\alpha} I_0\left(r\sqrt{\frac{\alpha}{\sigma}}\right)d\alpha\right]dt$	(166)
	(c,f)	--	Disk source of radius r	All t	$C = \frac{1}{4\pi^{1/2}}\int_0^t \frac{W'}{(\sigma')^{1/2}} \exp\left\{-\frac{1}{4\sigma}r\left[(x-Ut')^2 + r^2\right]\right\}\left[\int_0^{R^2/4\sigma'} e^{-\alpha} I_0\left(r\sqrt{\frac{\alpha}{\sigma}}\right)d\alpha\right]dt'$	(167)
	(d,e)	71	Disk source of radius r; $\partial C/\partial x = 0$	All t	$C = \frac{W^*}{2\pi UR^2\sigma} \exp\left(-\frac{r^2}{4\sigma}\right)\int_0^R r' \exp\left(-\frac{r'^2}{4\sigma}\right) I_0\left(\frac{r'r}{2\sigma}\right)dr'$	(168)

[a]Symbols are explained as follows:

$\exp(z) = e^z$

$\operatorname{erf}(z) = \frac{2}{\sqrt{\pi}}\int_0^z e^{-\alpha^2}\,d\alpha$

$\operatorname{erfc}(z) = 1 - \operatorname{erf}(z)$

$K_0(z)$ = modified Bessel function, second kind, zero order

$I_0(z)$ = modified Bessel function, first kind, zero order

$r^2 = y^2 + z^2$, $\sigma^2 = (x - Ut)^2 + y^2 + z^2$

K^*, W^*, and W' are independent of x, y, and z except where noted.

[b]Instantaneous.

[c]Exact.

[d]Continuous.

[e]Approximate.

[f]Transient.

TABLE II-I. - Concluded. EQUATIONS FOR CONCENTRATION OF HEAT OR MASS DOWNSTREAM OF VARIOUS SOURCES

Source configuration	Type solution	Reference	Conditions	Range	Equation (a)	
Surface	(b,c)	--	Cylindrical surface of radius r between x=a, x=-a	All t	$C = \frac{K^*R}{4\omega} \exp\left(-\frac{r^2+R^2}{4\omega}\right) I_0\left(\frac{rR}{2\omega}\right) \left\{\operatorname{erf}\left[\frac{(x-Ut)+a}{\sqrt{4\omega}}\right] - \operatorname{erf}\left[\frac{(x-Ut)-a}{\sqrt{4\omega}}\right]\right\}$	(169)
	(b,c)	--	Cylindrical surface of radius r with infinite length	All t	$C = \frac{W^*R}{2\omega} \exp\left(-\frac{r^2+R^2}{4}\right) I_0\left(\frac{rR}{2\omega}\right)$	(170)
	(c,d)	--	Cylindrical surface of radius r with infinite length	All t	$C = \frac{W^*R}{2} \int_0^\infty \frac{1}{\omega} \exp\left(-\frac{r^2+R^2}{4\omega}\right) I_0\left(\frac{rR}{2\omega}\right)$	(171)
	(c,f)	--	Cylindrical surface of radius r with infinite length	All t	$C = \frac{R}{2} \int_0^t \frac{W'}{\omega'} \exp\left(-\frac{r^2+R^2}{4\omega'}\right) I_0\left(\frac{rR}{2\omega'}\right) dt'$	(172)
	(b,c)	--	Spherical surface of radius r	All t	$C = \frac{K^*R}{\sigma(4\pi\omega)^{1/2}} \left\{\exp\left[-\frac{(\sigma-R)^2}{4\omega}\right] - \exp\left[-\frac{(\sigma-R)^2}{4\omega}\right]\right\}$	(173)
	(c,d)	--	Spherical surface of radius r	All t	$C = \frac{W^*R}{(4\pi)^{1/2}} \int_0^\infty \frac{1}{\sigma\omega^{1/2}} \left\{\exp\left[-\frac{(\sigma-R)^2}{4\omega}\right] - \exp\left[-\frac{(\sigma-R)^2}{4\omega}\right]\right\} dt$	(174)
	(c,f)	--	Spherical surface of radius r	All t	$C = \frac{R}{(4\pi)^{1/2}} \int_0^\infty \frac{W'}{\sigma'(\omega')^{1/2}} \left\{\exp\left[-\frac{(\sigma'-R)^2}{4\omega'}\right] - \exp\left[-\frac{(\sigma'-R)^2}{4\omega'}\right]\right\} dt'$	(175)
Volume	(b,c)	88, p. 338	K^* variable over volume V'	All t	$C = \frac{1}{(4\pi\omega)^{3/2}} \iiint_{V'} K^* \exp\left\{-\frac{1}{4\omega}\left[(x-x')^2 + (y-y')^2 + (z-z')^2\right]\right\} dV'$	(176)
	(c,d)	--	W' variable over volume V'	All t	$C = \frac{1}{(4\pi)^{3/2}} \int_0^\infty \frac{1}{\omega^{3/2}} \left(\iiint_{V'} W' \exp\left\{-\frac{1}{4\omega}\left[(x-x')^2 + (y-y')^2 + (z-z')^2\right]\right\} dV'\right) dt$	(177)

[a]Symbols are explained as follows:

$\exp(a) = e^a$

$\operatorname{erf}(a) = \frac{2}{\sqrt{\pi}} \int_0^a e^{-\alpha^2} d\alpha$

$\operatorname{erfc}(a) = 1 - \operatorname{erf}(a)$

$K_0(a)$ = modified Bessel function, second kind, zero order

$I_0(a)$ = modified Bessel function, first kind, zero order

$r^2 = y^2 + z^2$, $\sigma^2 = (x - Ut)^2 = y^2 + z^2$

K^*, W^*, and W' are independent of x, y, and z except where noted.

[b]Instantaneous.

[c]Exact.

[d]Continuous.

[e]Approximate.

[f]Transient.

TABLE II-II. - ARRANGEMENTS FOR MIXING OF GAS STREAMS

[Ref. 82.]

Gas stream	Arrangement	B^*	C^*	$\frac{\Omega}{C^*}$
Normal	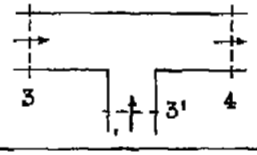	1	$\sqrt{\left(1 + \frac{W_{3'}}{W_3}\right)\left(1 + \frac{W_{3'}}{W_3} \cdot \frac{T_{t,3'}}{T_{t,3}}\right)}$	1
Oblique	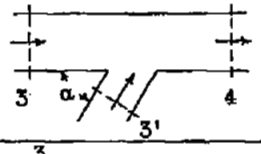	$\left(1 + \frac{W_{3'}}{W_3} \cdot \frac{U_{3'}}{U_3} \cos \alpha\right)$	$\sqrt{\left(1 + \frac{W_{3'}}{W_3}\right)\left(1 + \frac{W_{3'}}{W_3} \cdot \frac{T_{t,3'}}{T_{t,3}}\right)}$	From figure II-48
Parallel	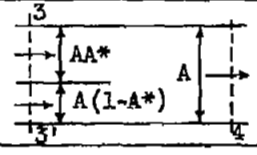	$A^*\left(1 + \frac{W_{3'}}{W_3} \cdot \frac{U_{3'}}{U_3}\right)$	$A^* \sqrt{\left(1 + \frac{W_{3'}}{W_3}\right)\left(1 + \frac{W_{3'}}{W_3} \cdot \frac{T_{t,3'}}{T_{t,3}}\right)}$	From figure II-48

3267

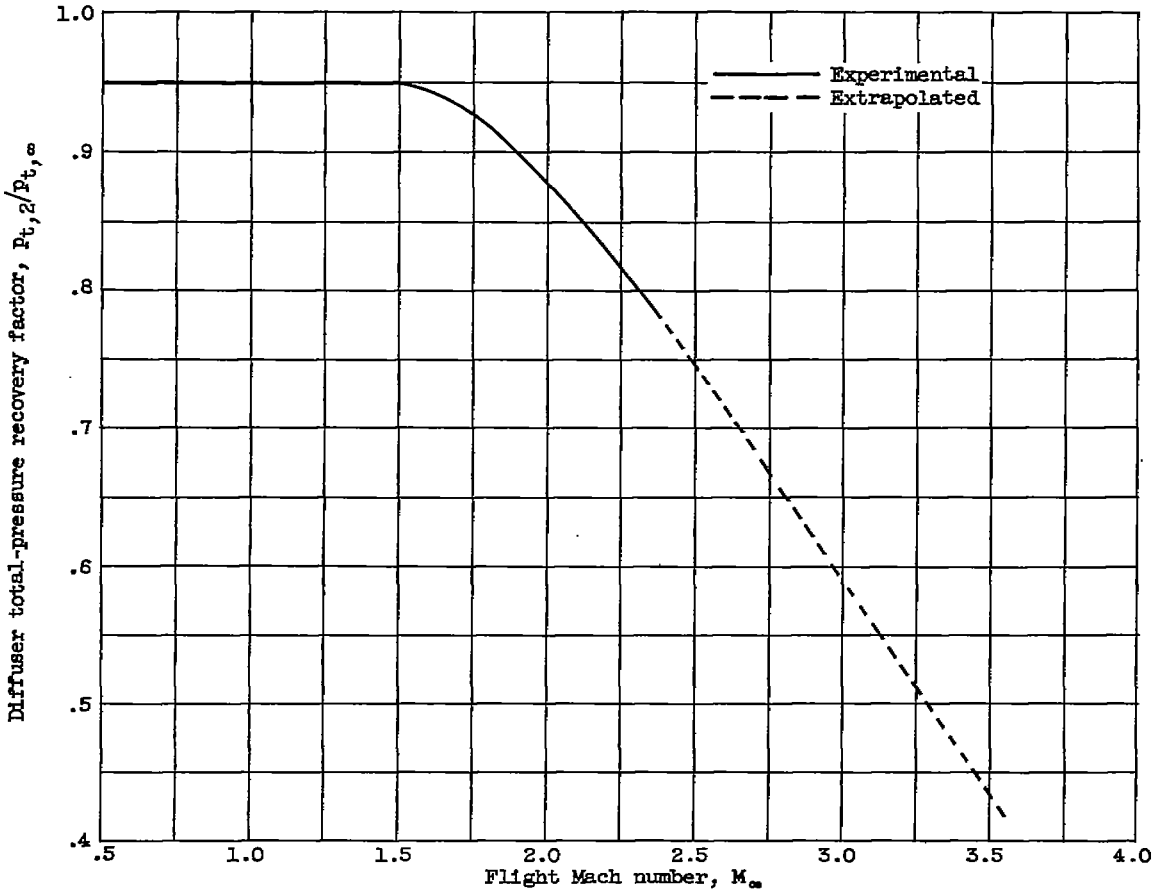

Figure II-1. - Diffuser total-pressure recovery factors (ref. 6).

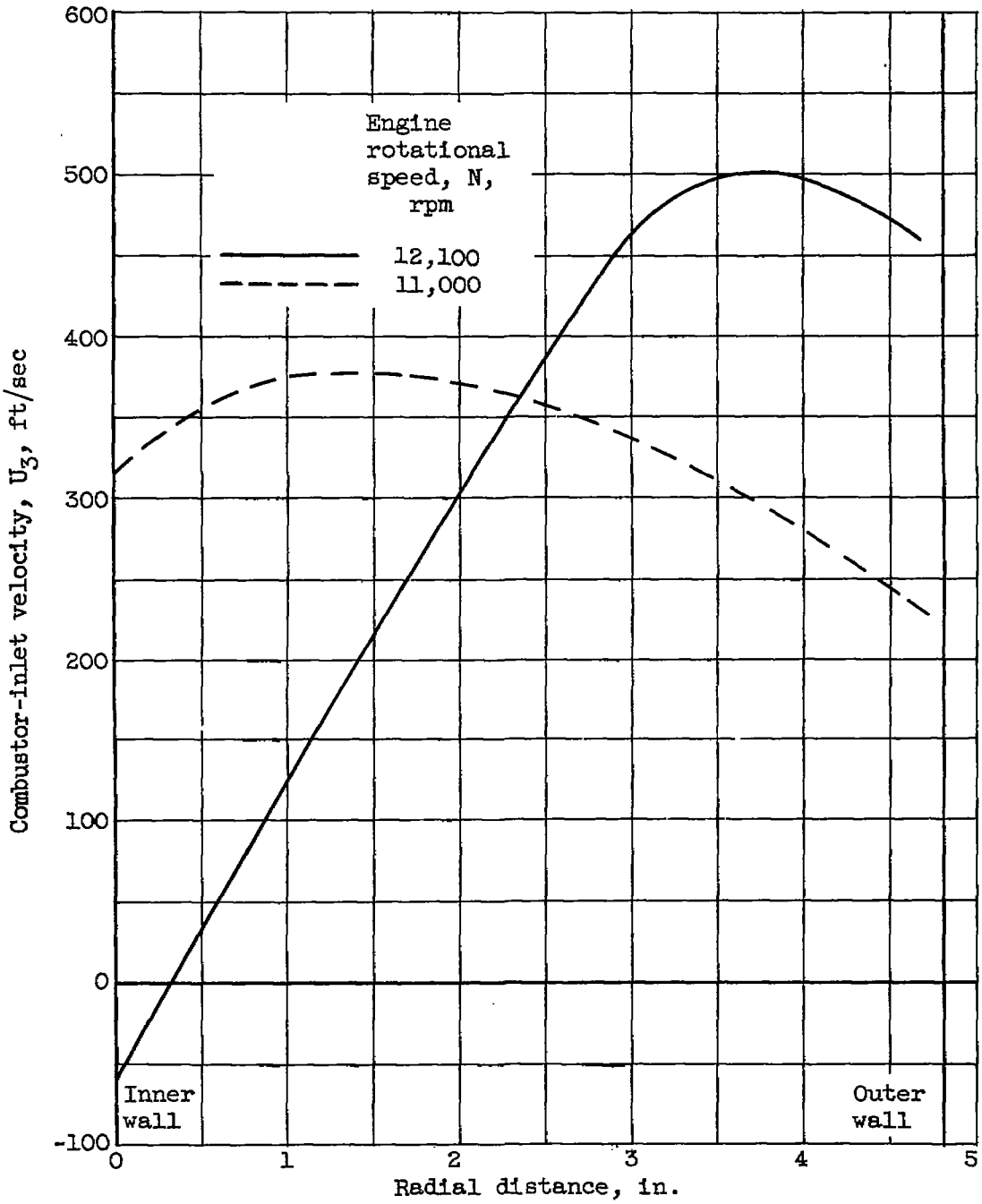

Figure II-2. - Variation of combustor-inlet velocity profile with engine speed (ref. 2).

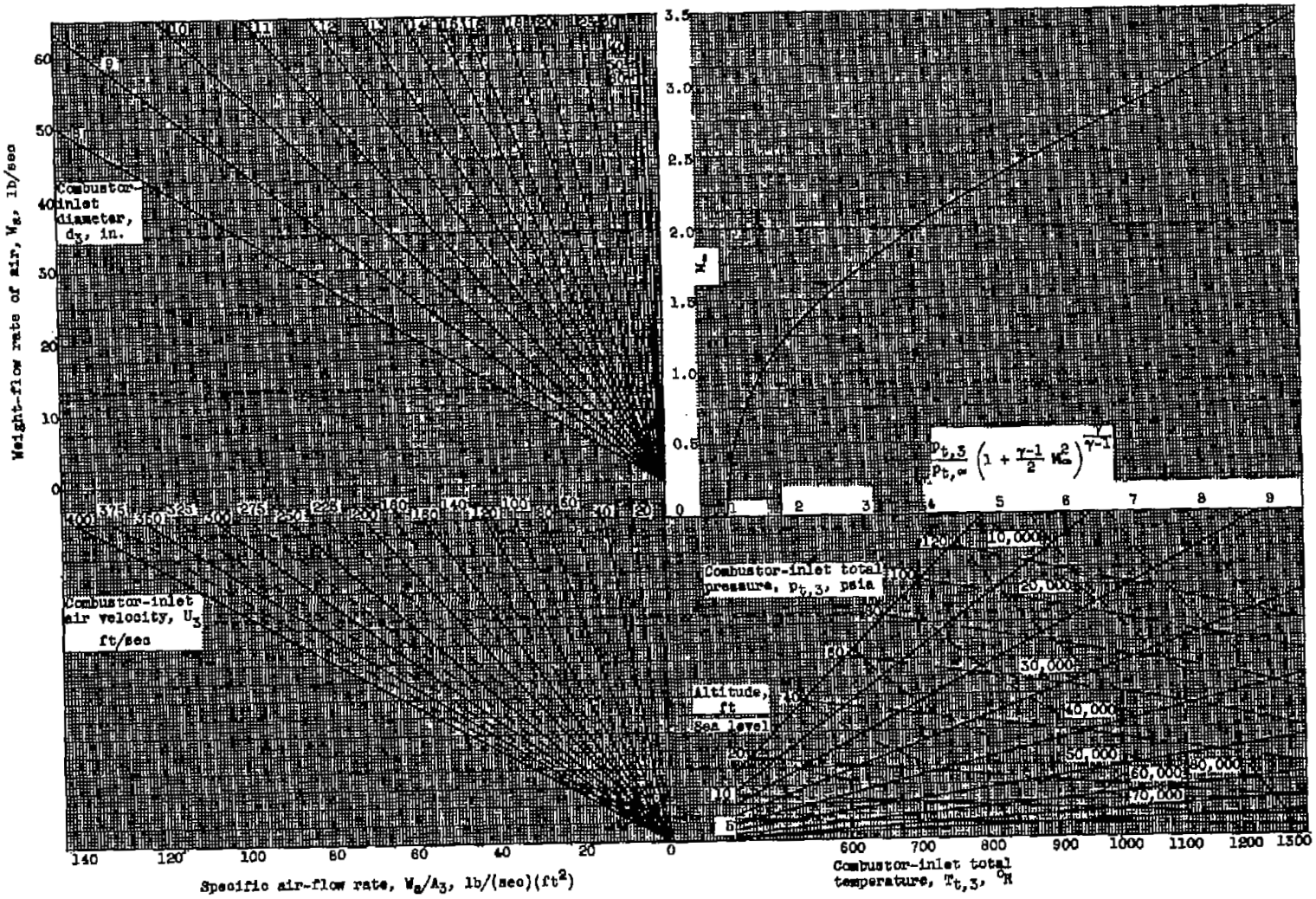

Figure II-3. - Ram-jet-combustor inlet conditions.

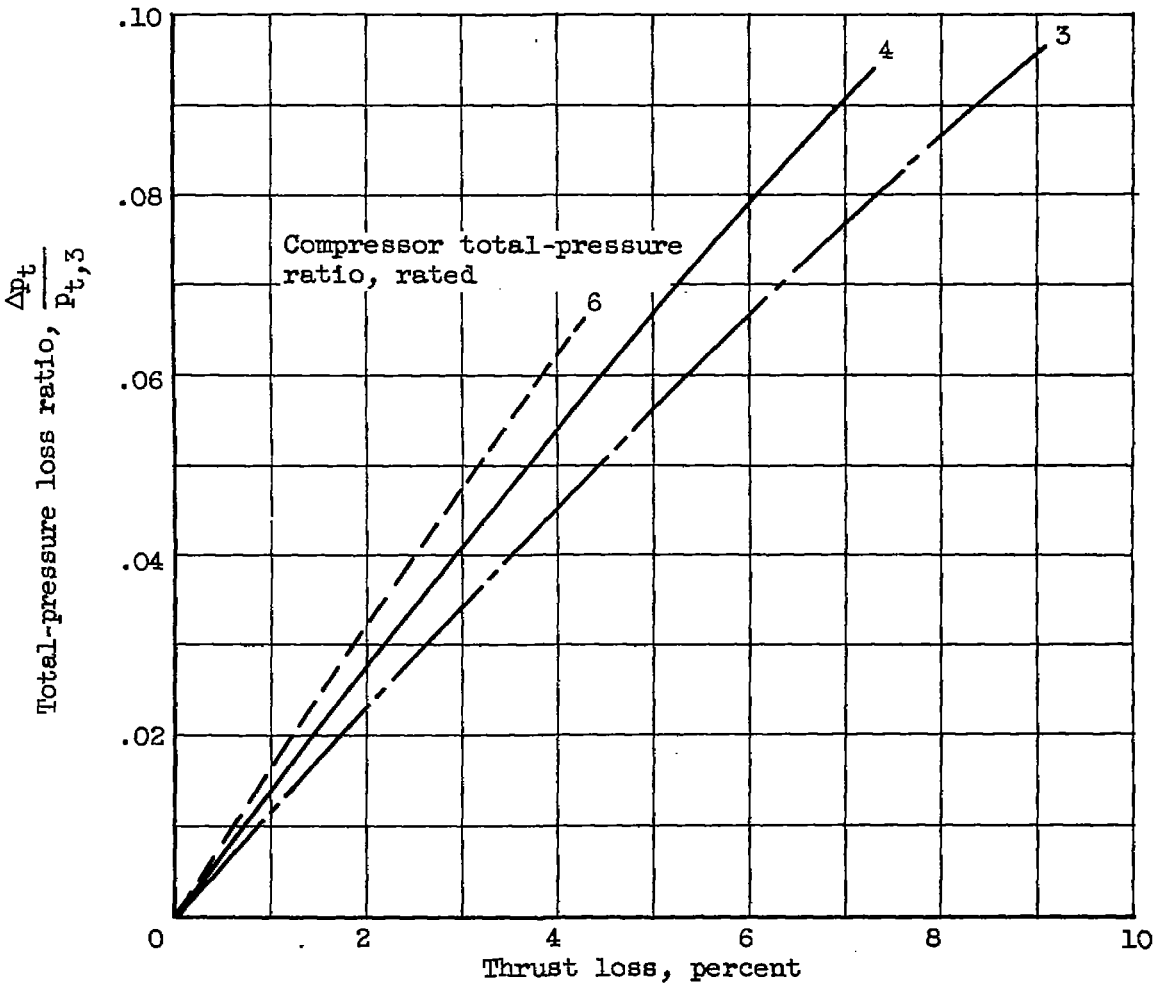

(a) Sea-level, static conditions (ref. 7).

Figure II-4. - Calculated thrust loss of turbojet engine as function of combustor total-pressure loss.

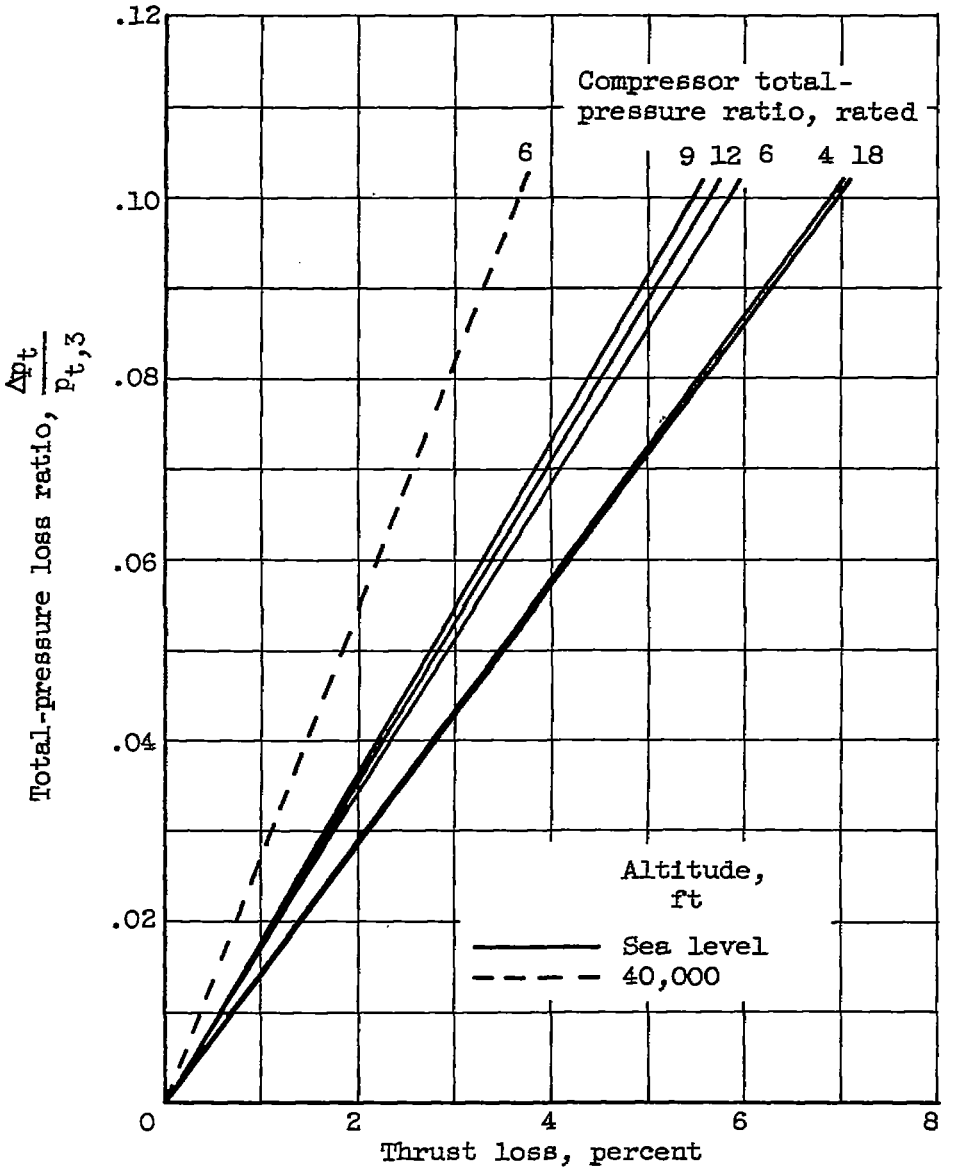

(b) Flight Mach number, 0.6; nozzle coefficient, 0.96; lower heating value of fuel, 18,700 Btu per pound; combustor-outlet total temperature, 1960° R; compressor efficiency, 85 percent; turbine efficiency, 90 percent; combustion efficiency, 97 percent.

Figure II-4. - Concluded. Calculated thrust loss of turbojet engine as function of combustor total-pressure loss.

[redacted]

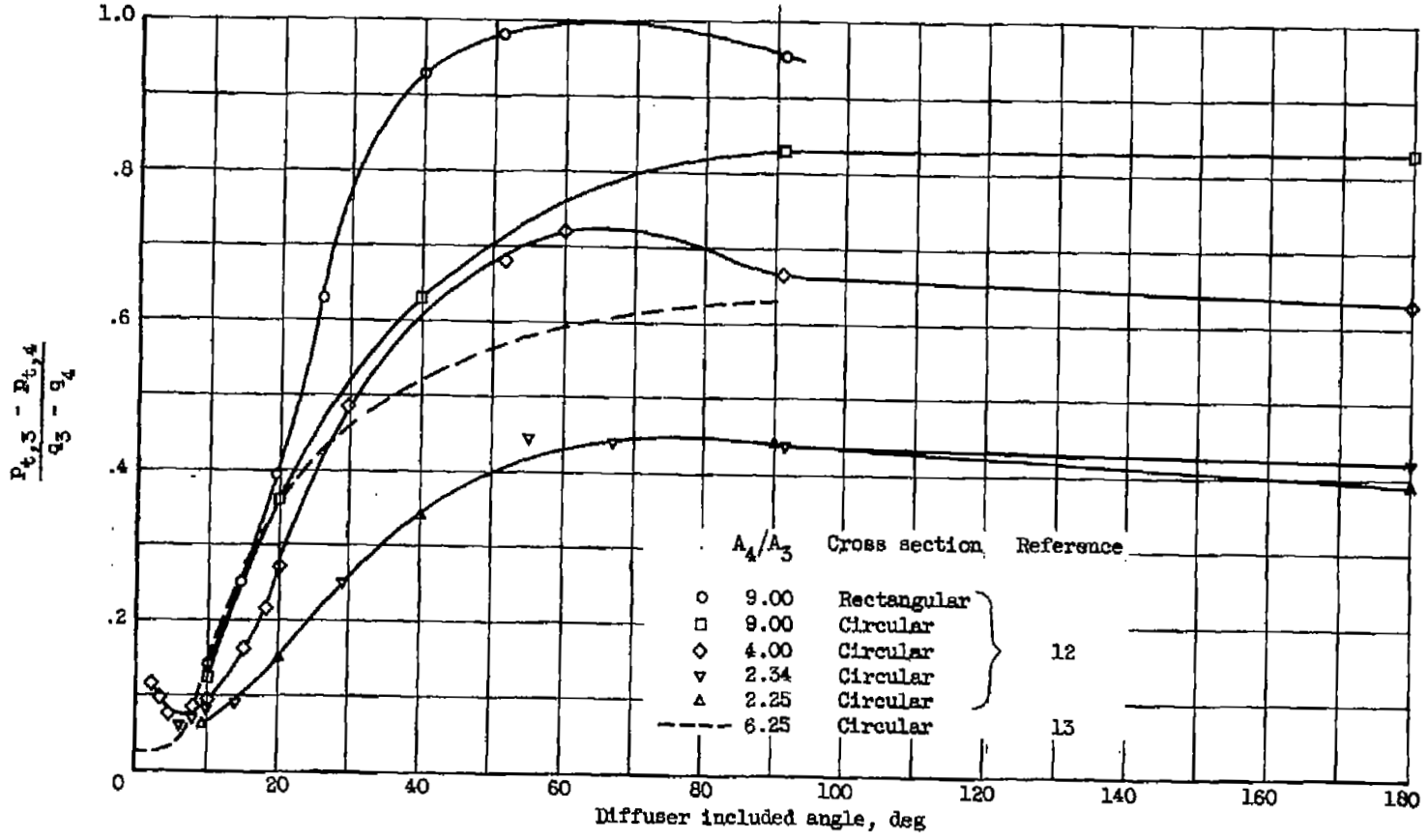

Figure II-5. - Effect of diffuser included angle on diffuser total-pressure losses.

[redacted]

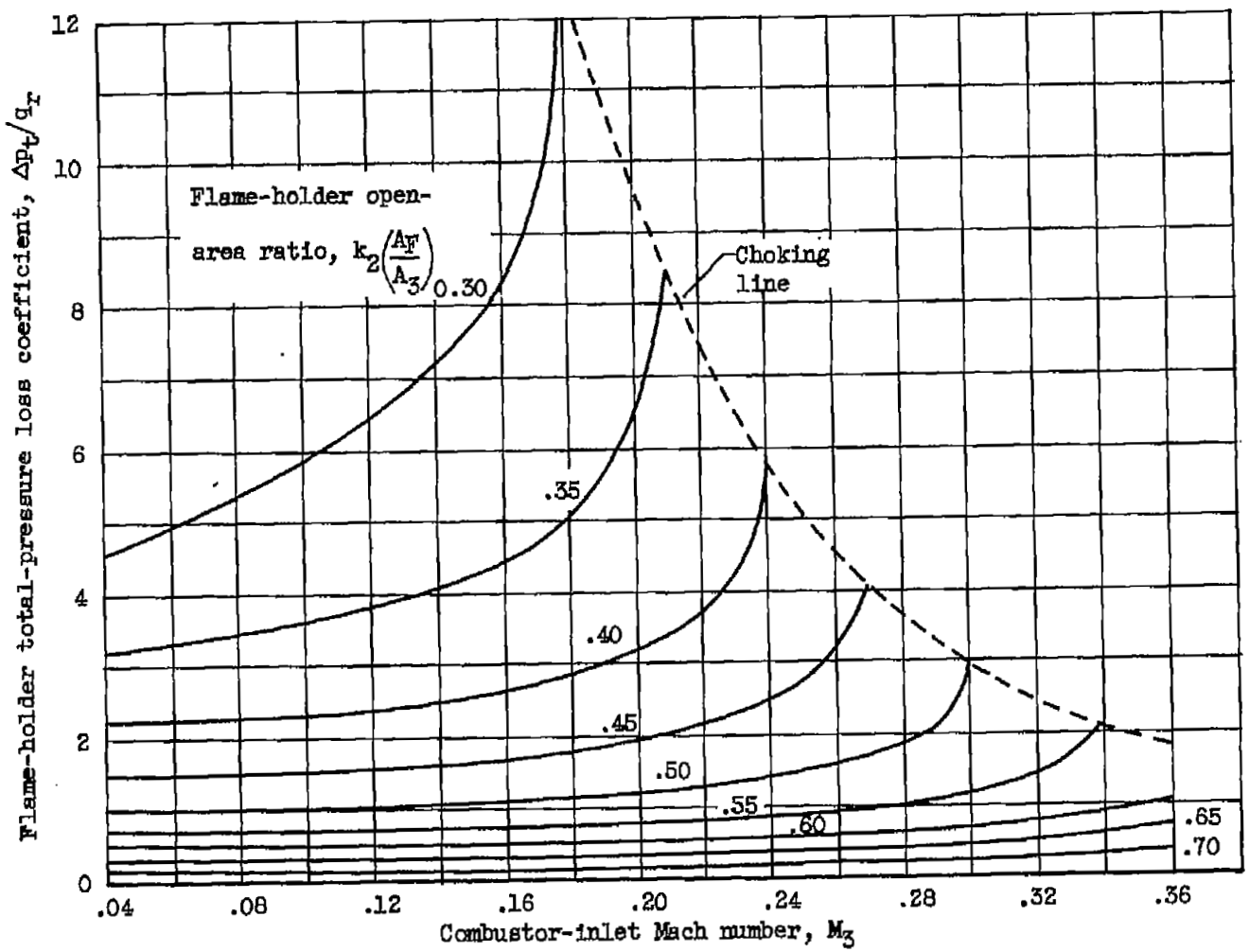

Figure II-6. - Variation of theoretical isothermal flame-holder total-pressure loss coefficient with combustor-inlet Mach number for various values of effective flame-holder open-area ratio. Specific heat ratios, $\gamma_3 = \gamma_4 = 1.4$ (ref. 16).

3267

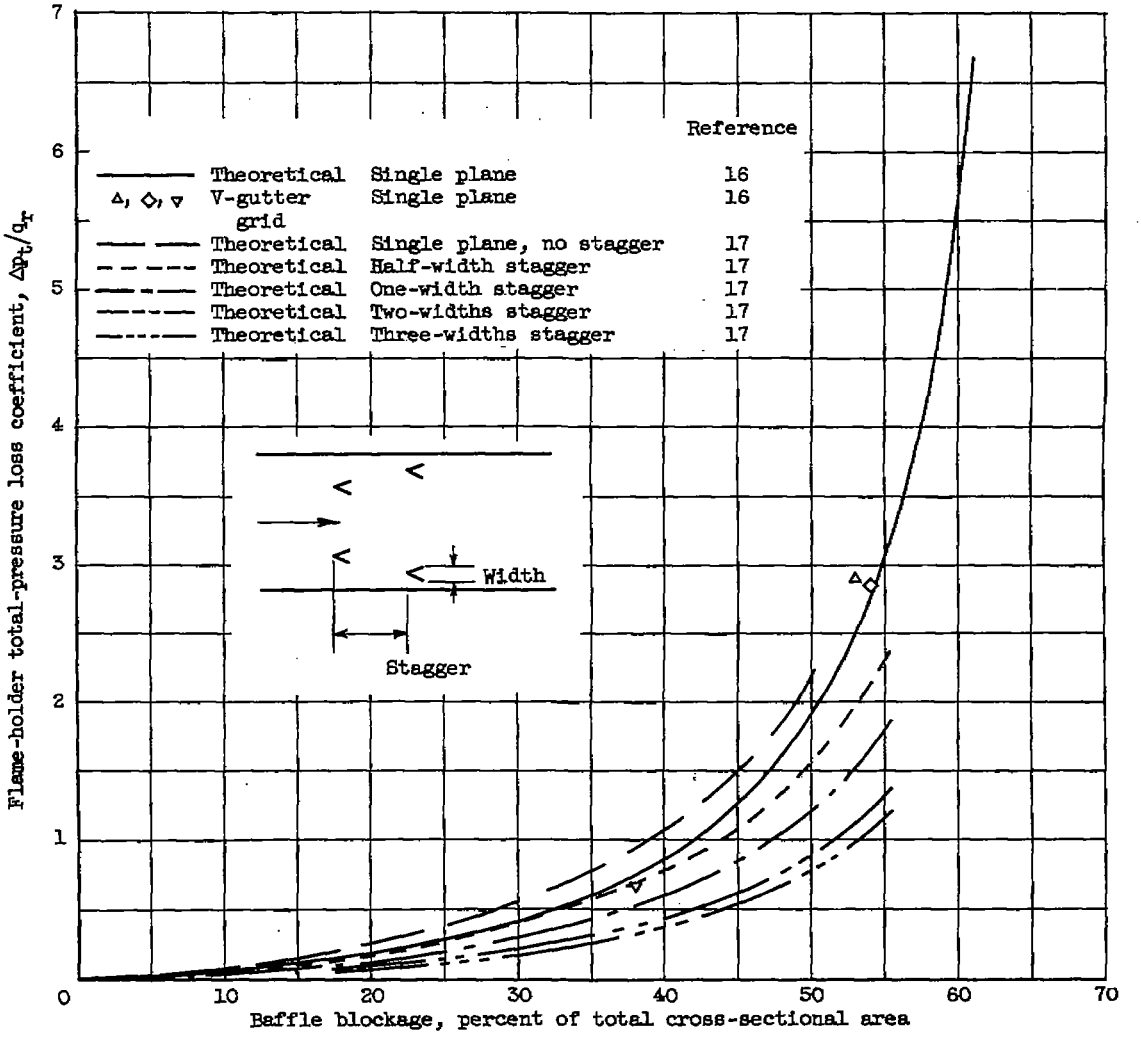

Figure II-7. - Effect of area blockage on combustor isothermal total-pressure losses. Combustor-inlet Mach number, 0.2.

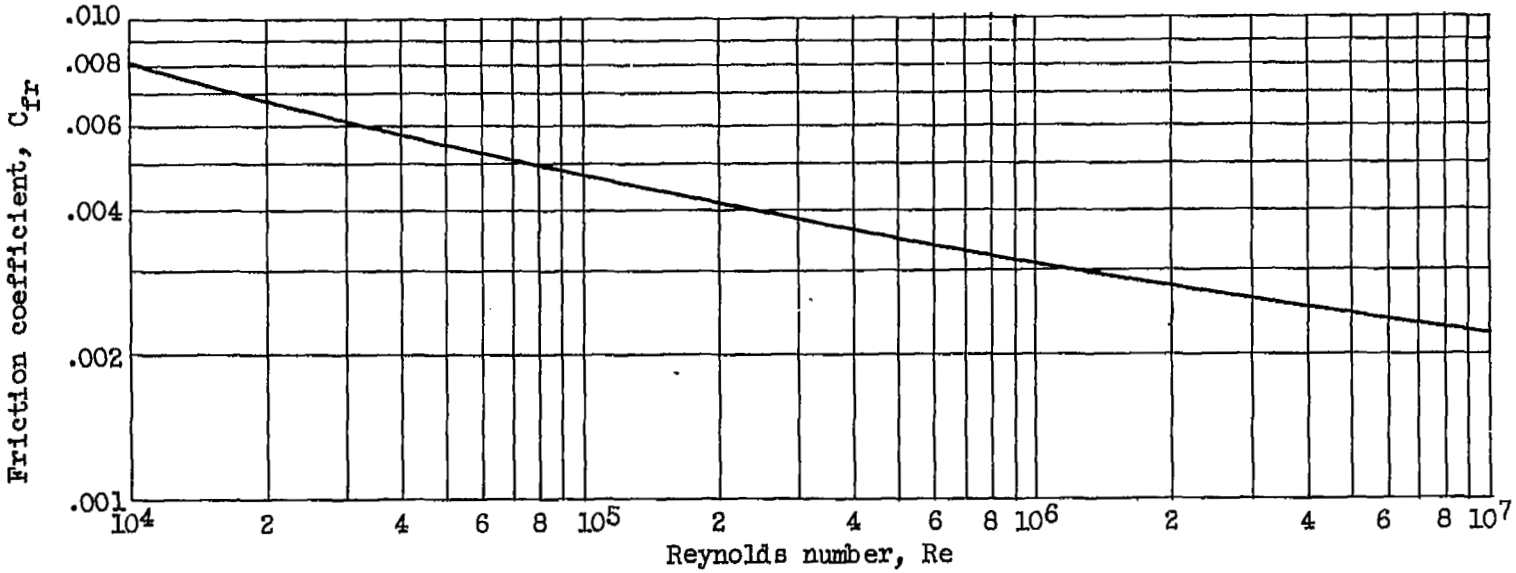

Figure II-8. - Friction coefficients for sheet metal surfaces as a function of Reynolds number (ref. 19).

3267

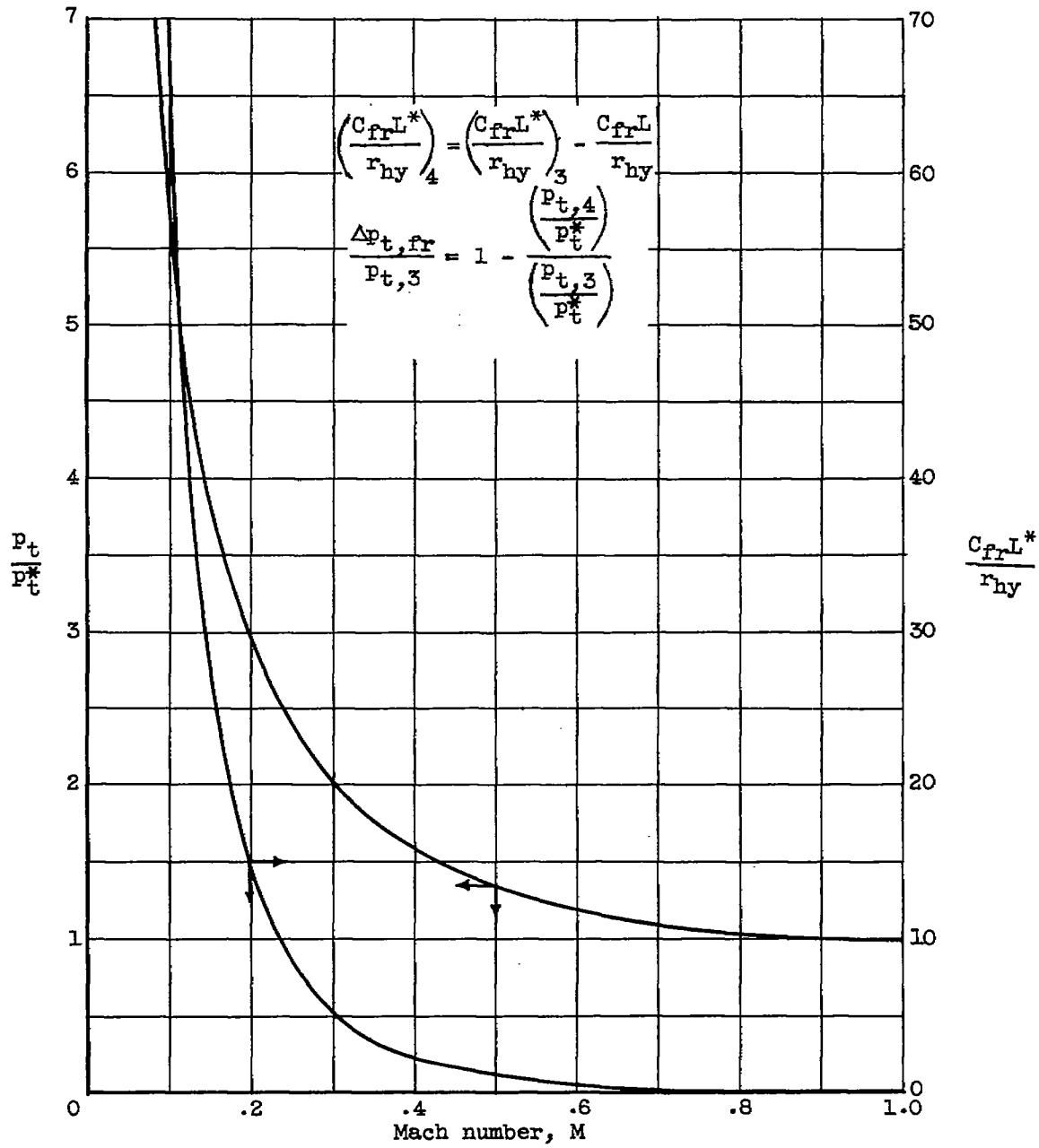

Figure II-9. - Data for estimation of frictional total-pressure losses in cylindrical ducts (where p_t^* is total pressure with choked flow and L^* is length of duct between station where Mach number is taken and station where choking would occur, ref. 20).

3267

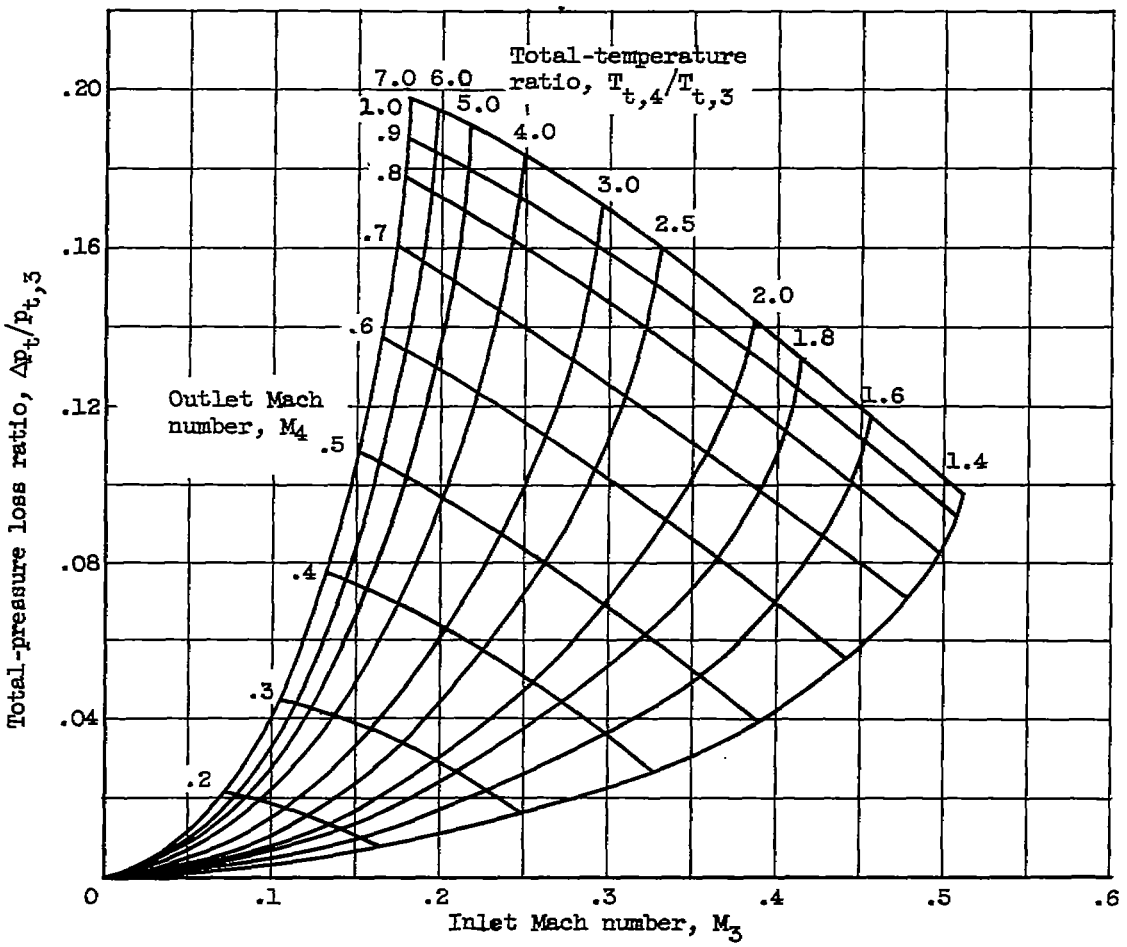

Figure II-10. - Total-pressure loss due to heat addition in flowing air stream ($\gamma_4 = \gamma_3 = 1.4$; R = 53.35 ft-lb/lb-°R)(ref. 82).

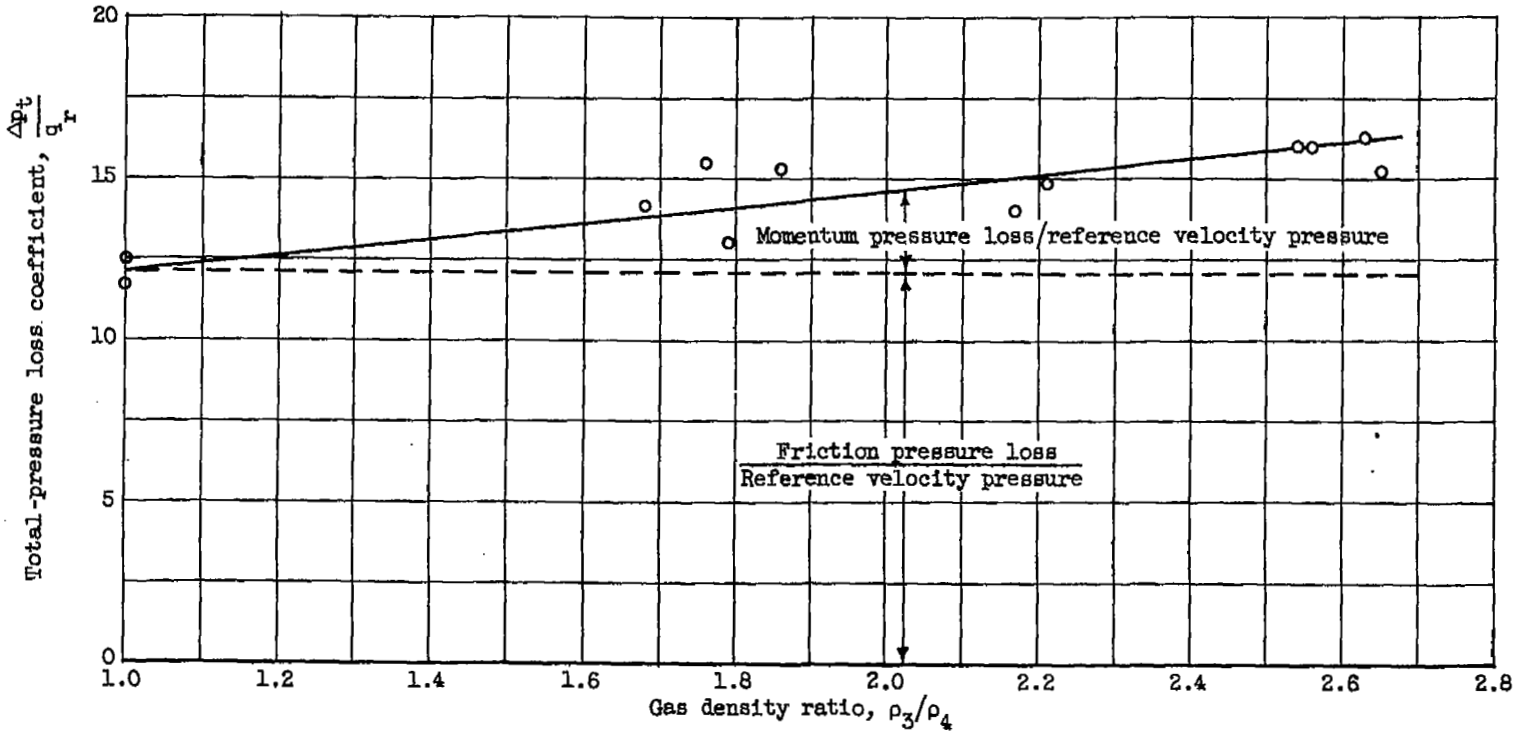

Figure II-11. - Total-pressure losses as function of reference velocity pressures of typical turbojet combustor.

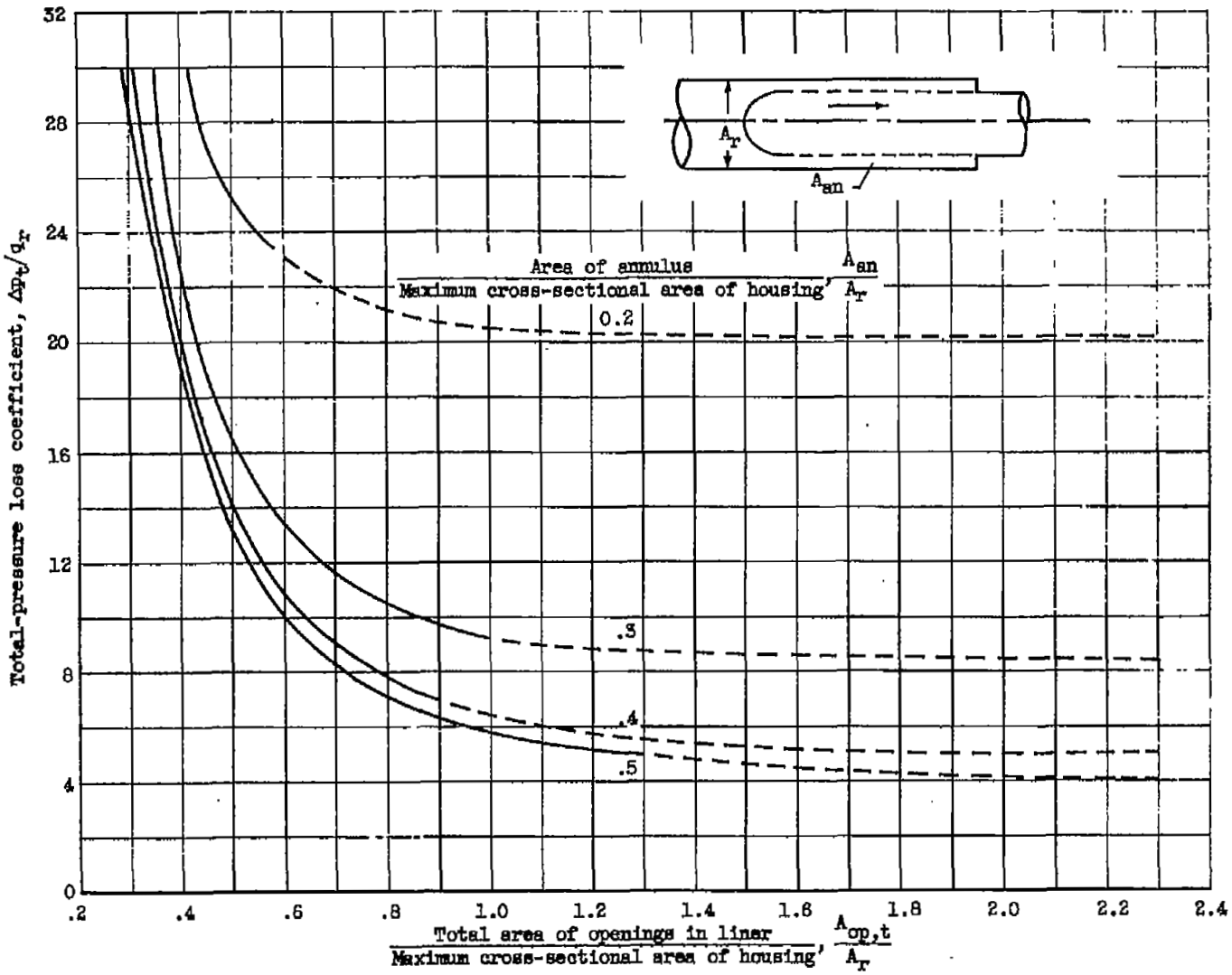

Figure II-12. - Theoretical isothermal total-pressure losses in combustor having straight liner and housing walls.

3267

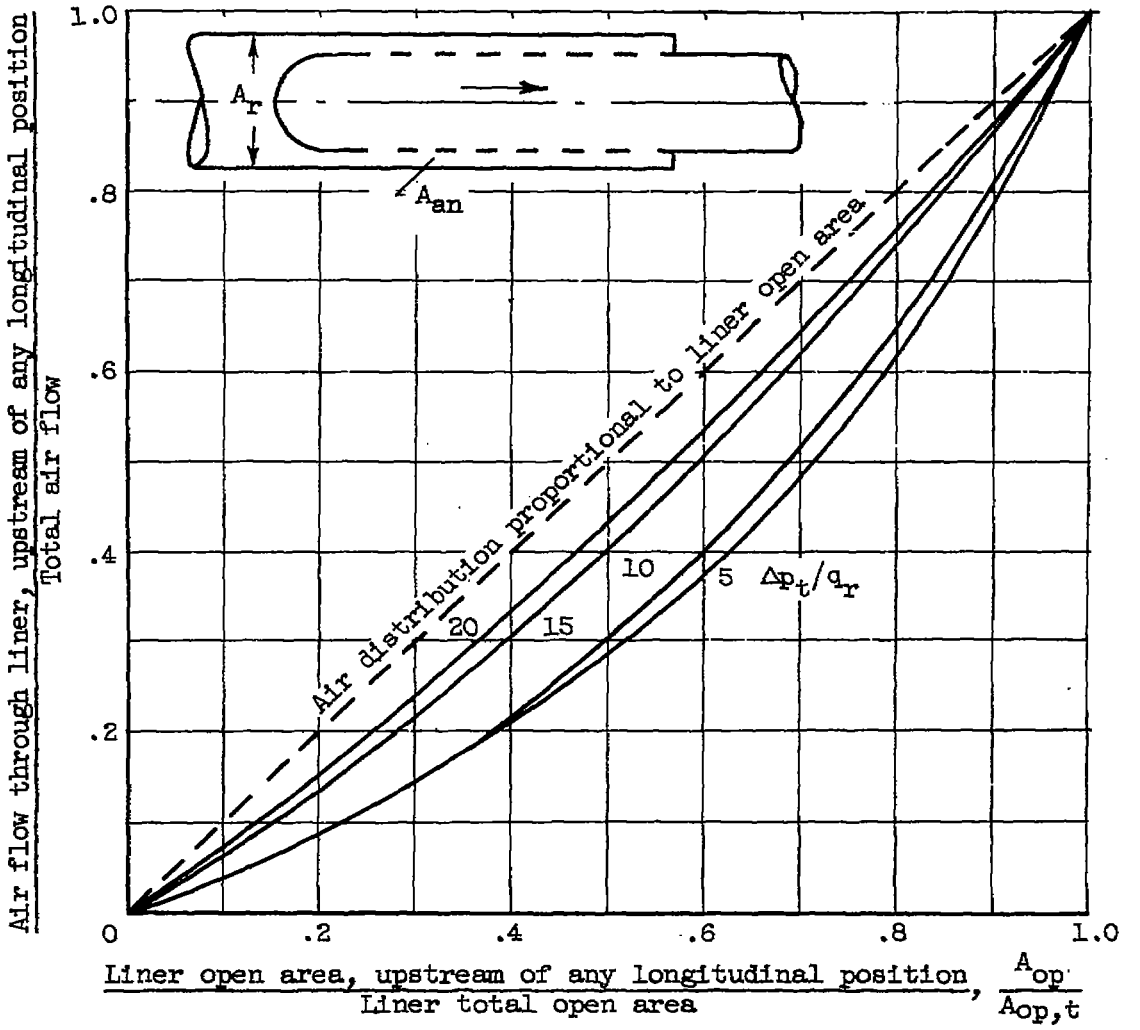

(a) Ratio of area of annulus to reference area, 0.3.

Figure II-13. - Air-flow distribution (theoretical) in tubular combustor. Frictionless, isothermal, incompressible flow. Combustor housing and liner cross-sectional areas constant.

3267

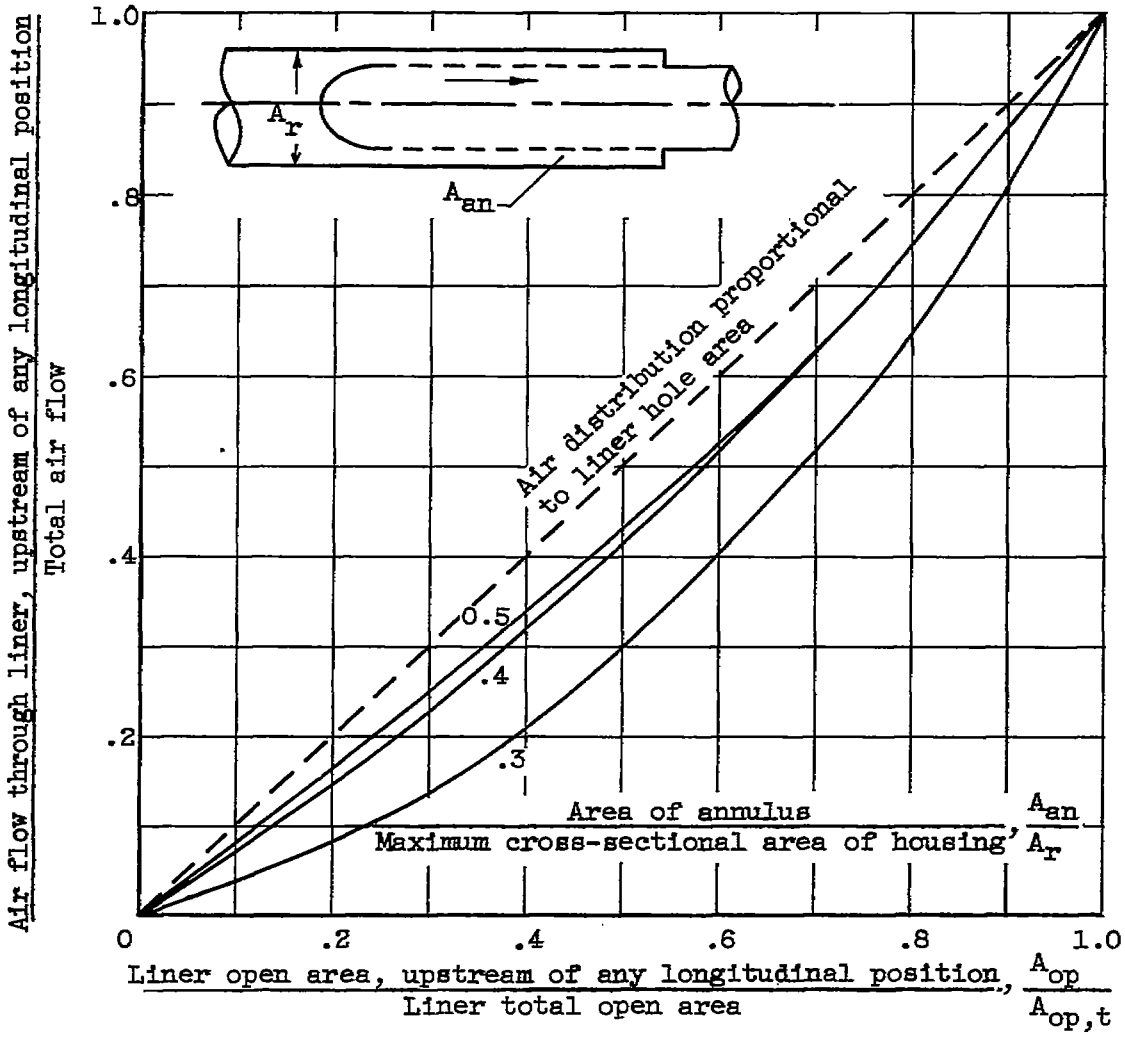

(b) Ratio of total-pressure loss to reference velocity pressure, 10.0.

Figure II-13. - Concluded. Air-flow distribution (theoretical) in tubular combustor. Frictionless, isothermal, incompressible flow. Combustor housing and liner cross-sectional areas constant.

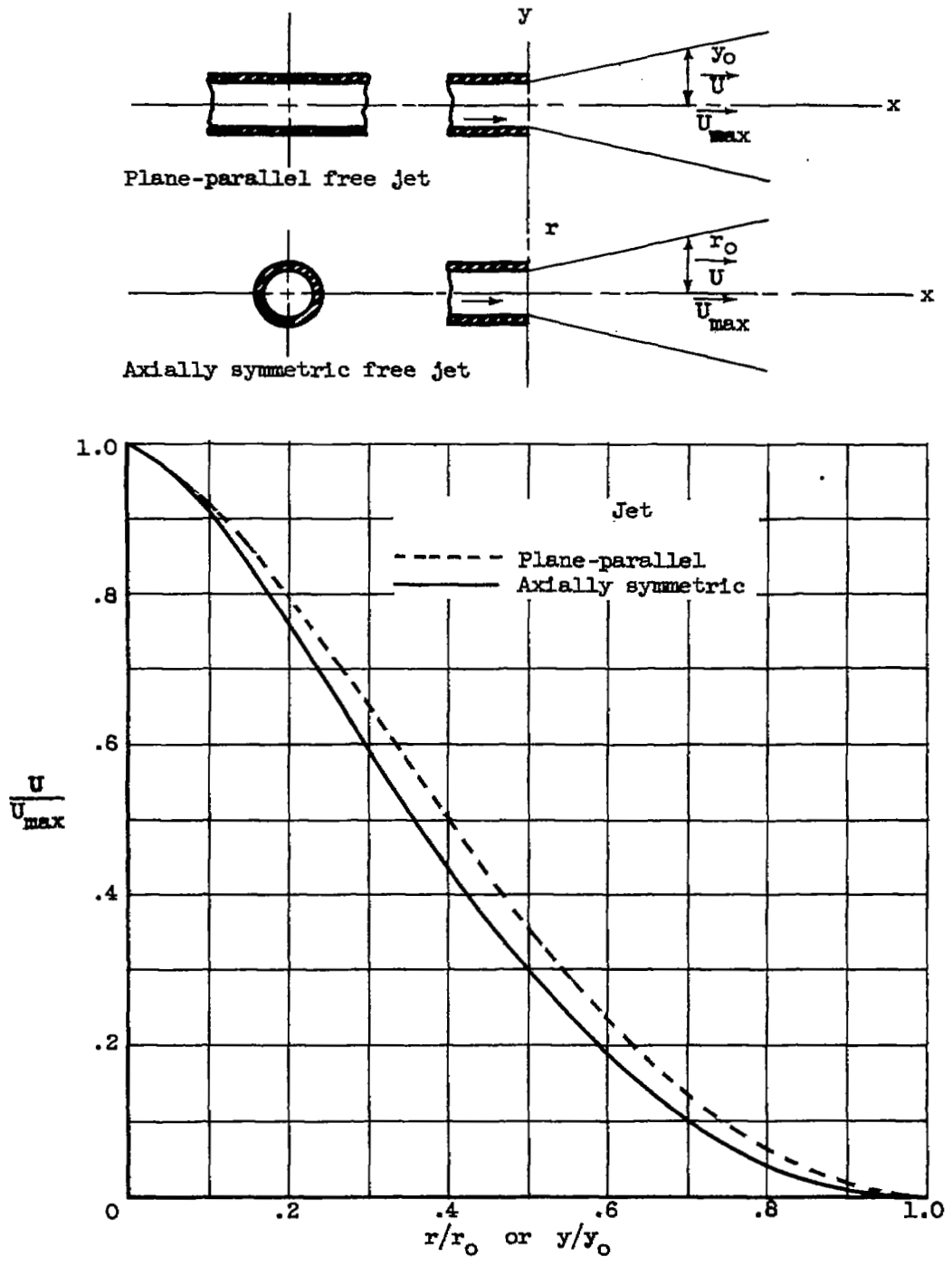

Figure II-14. - Theoretical velocity distributions based on momentum-transfer theory in plane-parallel and axially symmetric free jets (ref. 35).

3267

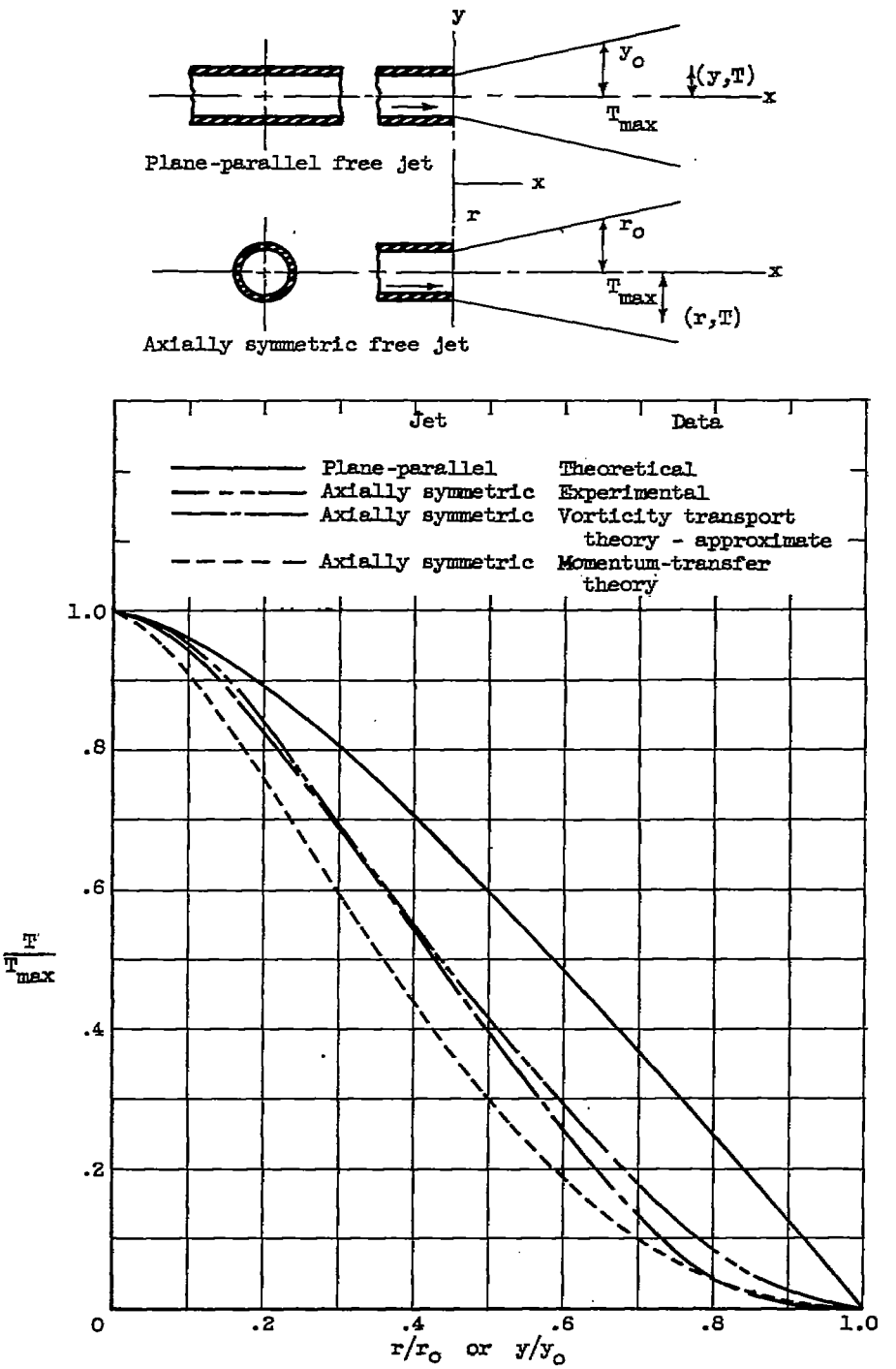

Figure II-15. - Theoretical and experimental temperature distributions in plane-parallel and axially symmetric free jets (ref. 35).

3267

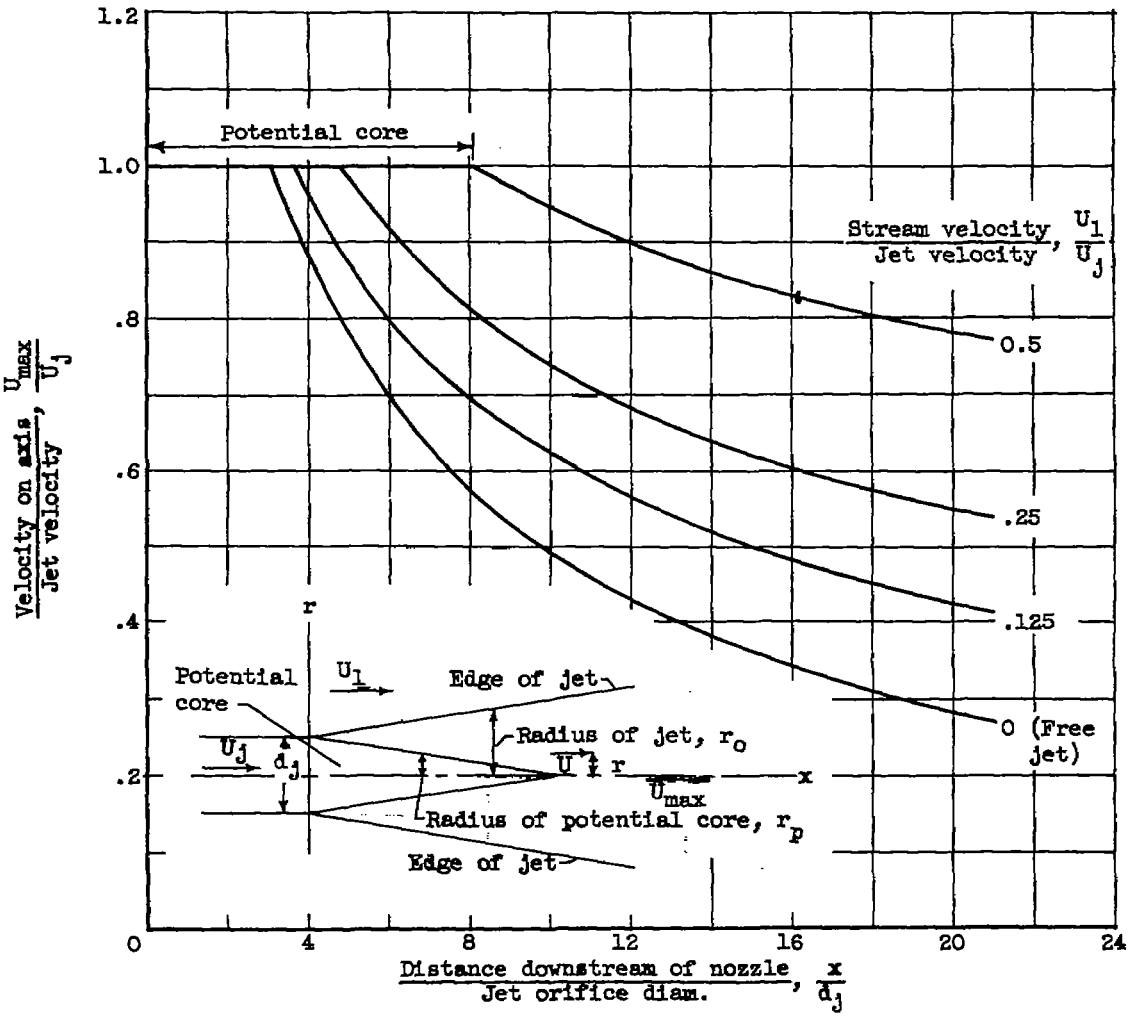

Figure II-16. - Axial distribution of velocity on axis in circular coaxial jets (ref. 36).

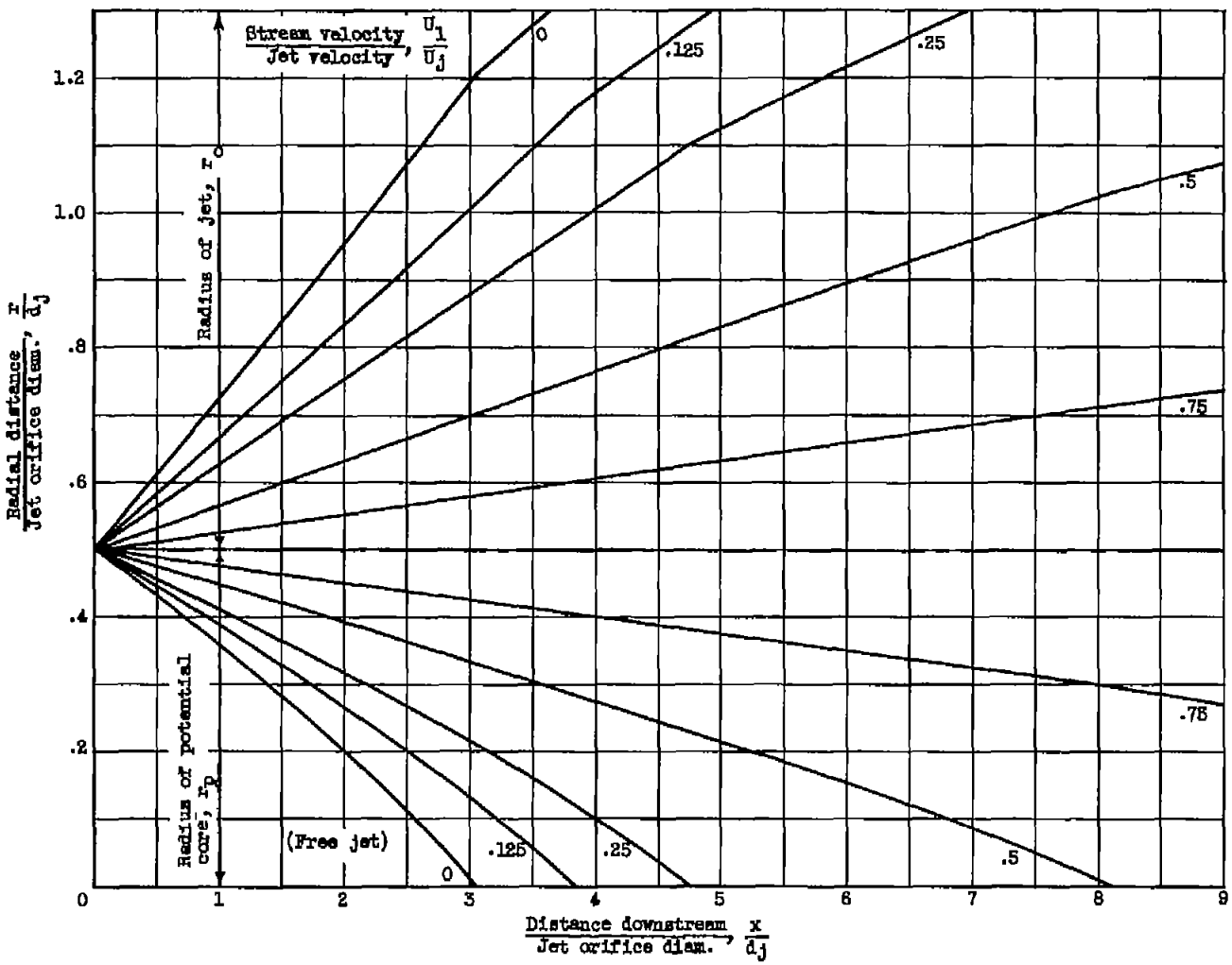

Figure II-17. - Boundaries of jet and potential core in circular coaxial jets (ref. 36).

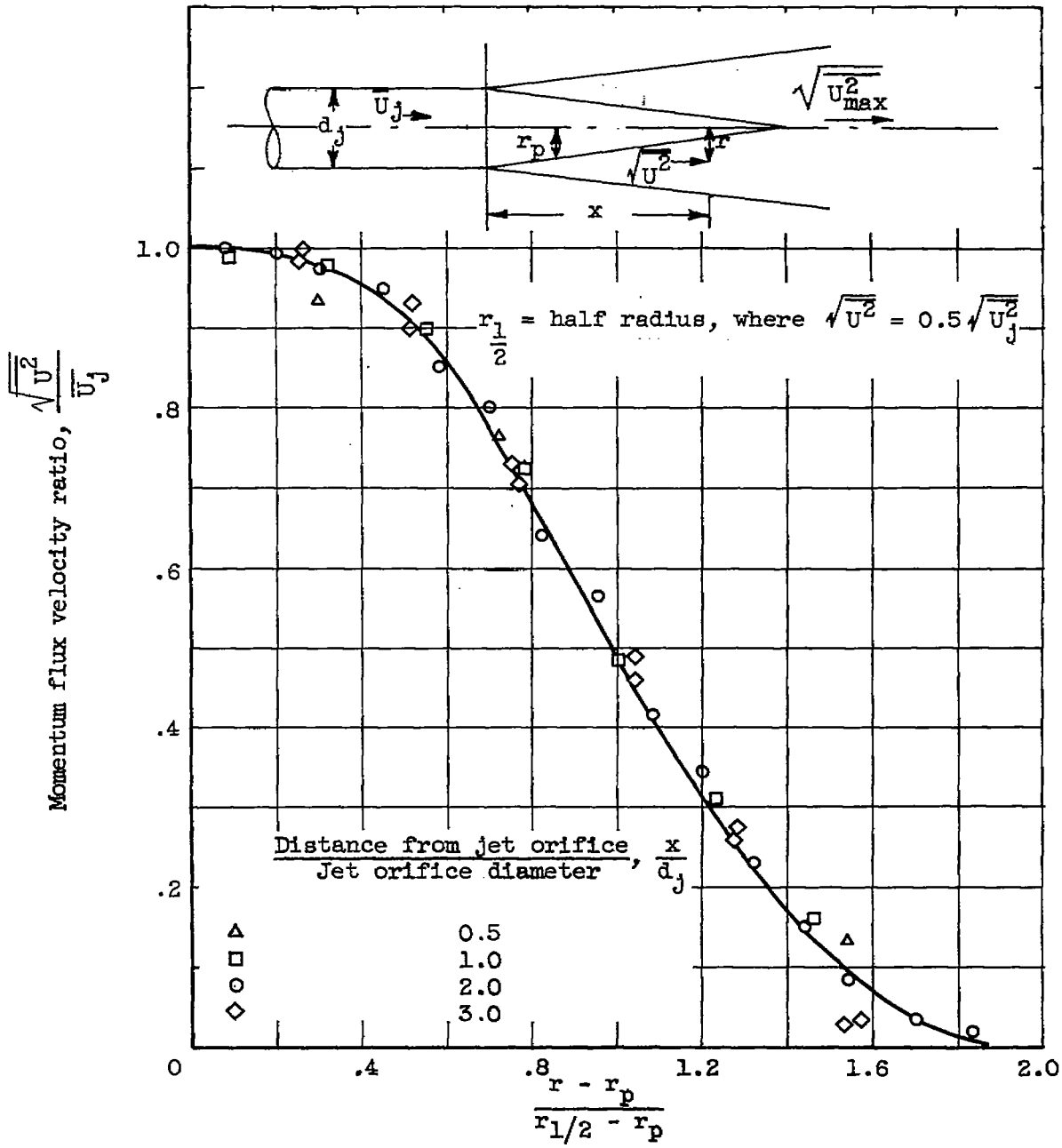

(a) Potential core region.

Figure II-18. - Radial distribution of momentum flux ratios in isothermal, axially symmetric free jets of air. 0.9-Inch-diameter, long-throat nozzle; mean jet velocity, 390 feet per second (ref. 38).

3267

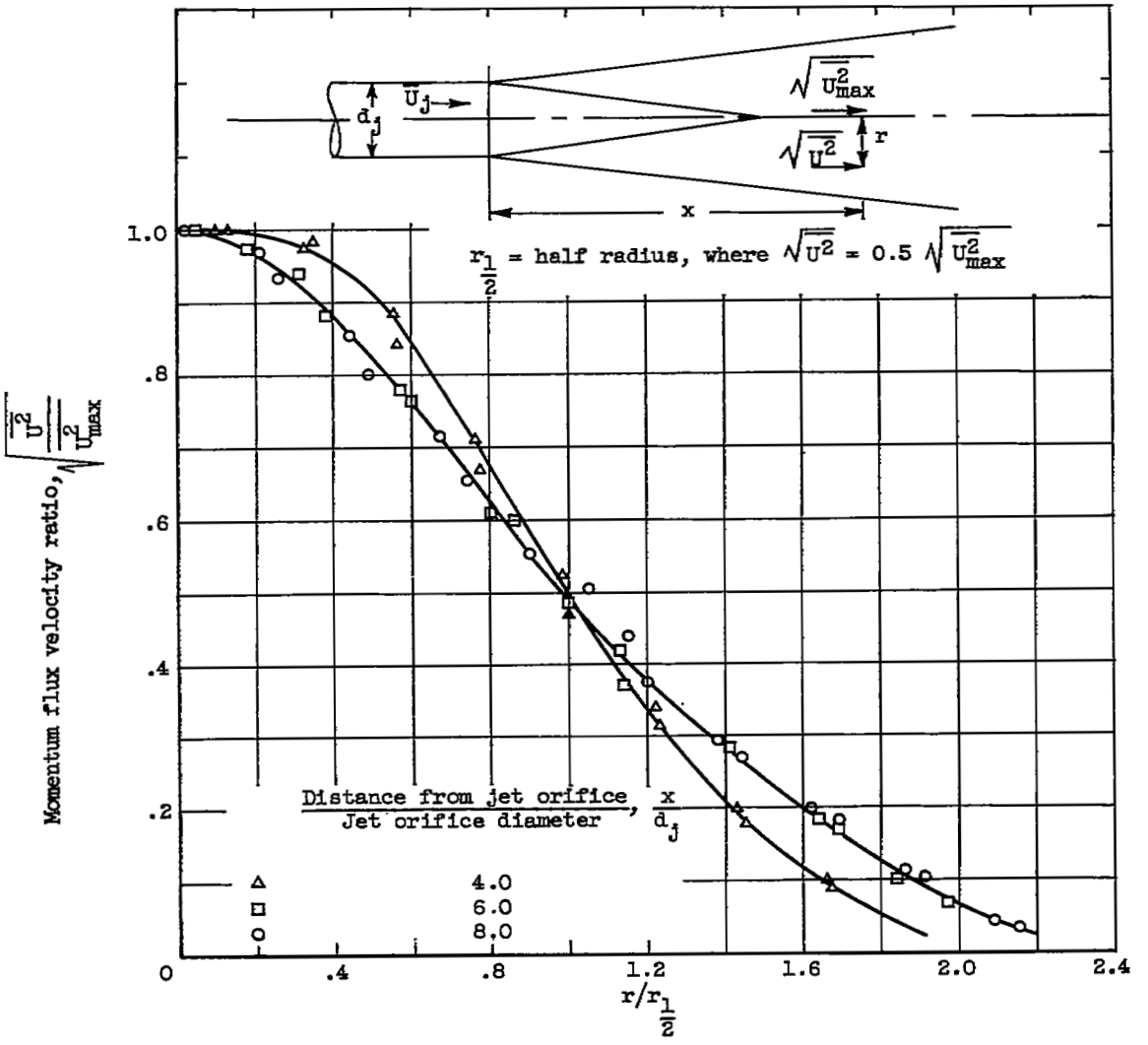

(b) Transition region.

Figure II-18. - Continued. Radial distribution of momentum flux ratios in isothermal, axially symmetric free jets of air. 0.9-Inch-diameter, long-throat nozzle; mean jet velocity, 390 feet per second (ref. 38).

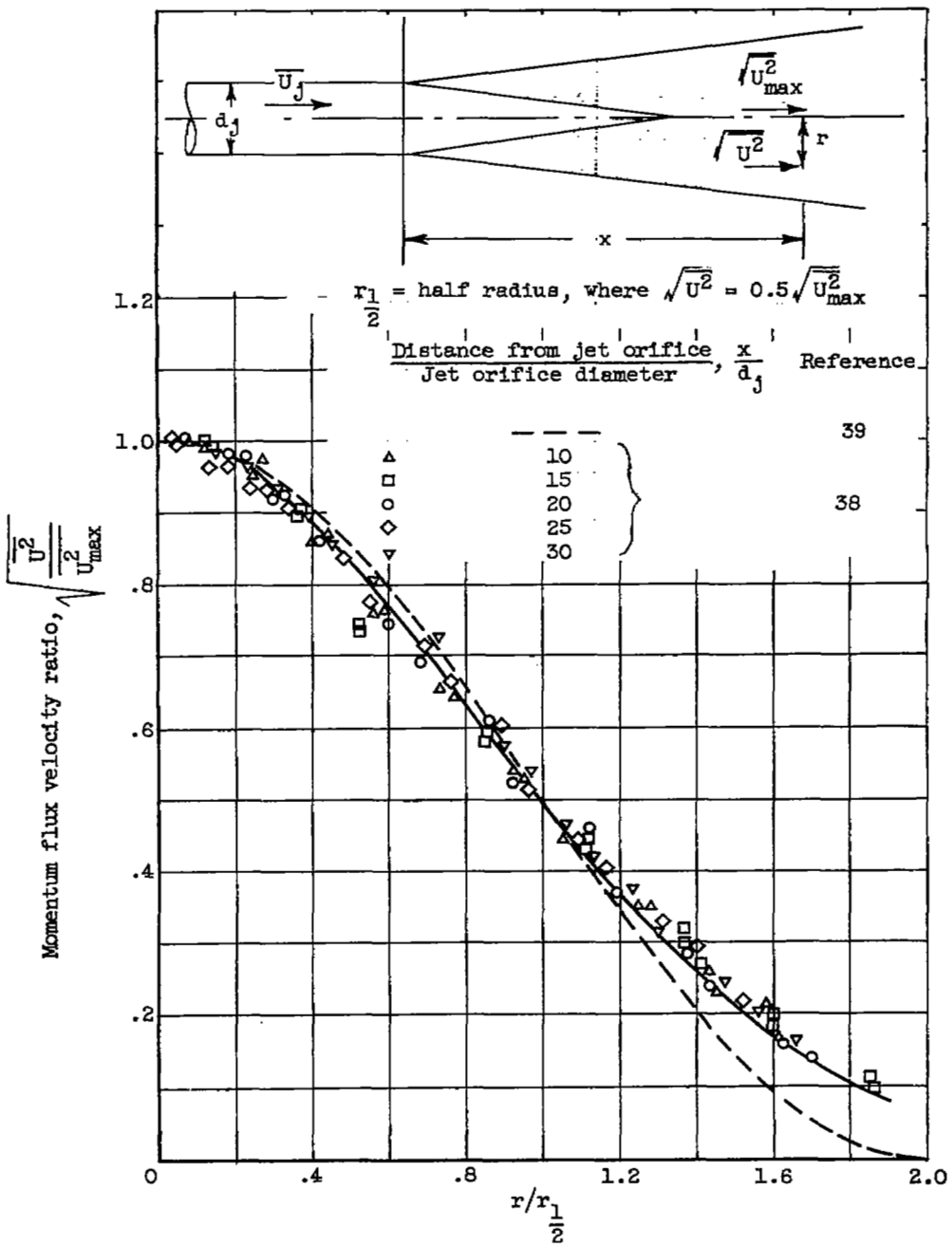

(c) Fully developed flow region.

Figure II-18. - Concluded. Radial distribution of momentum flux ratios in isothermal, axially symmetric free jets of air. 0.9-Inch-diameter, long-throat nozzle; mean jet velocity, 390 feet per second (ref. 38).

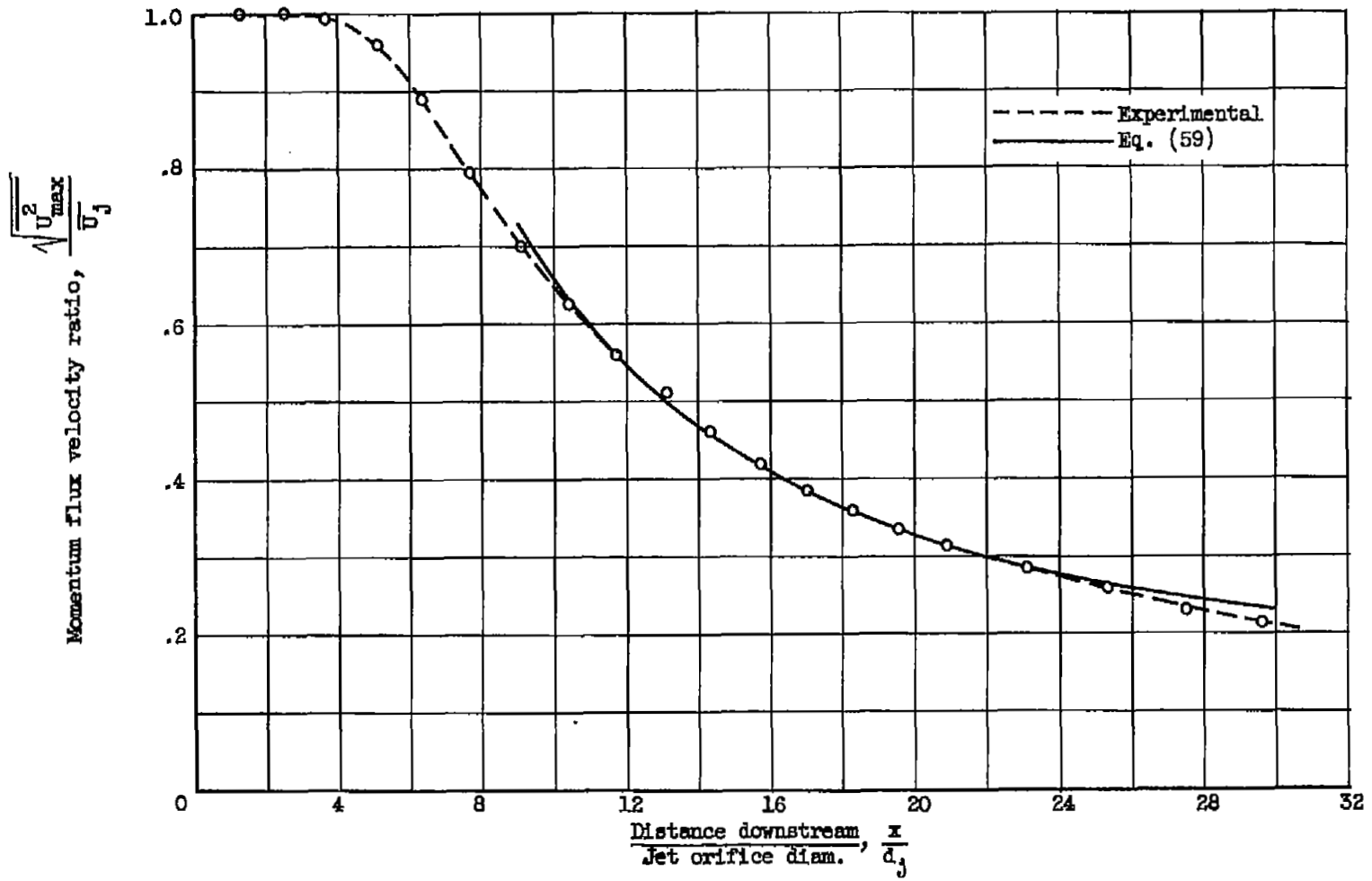

Figure II-19. - Axial velocity distribution in axially symmetric isothermal free jet in air. 0.9-Inch-diameter, long-throat nozzle; mean jet velocity, 390 feet per second (ref. 38).

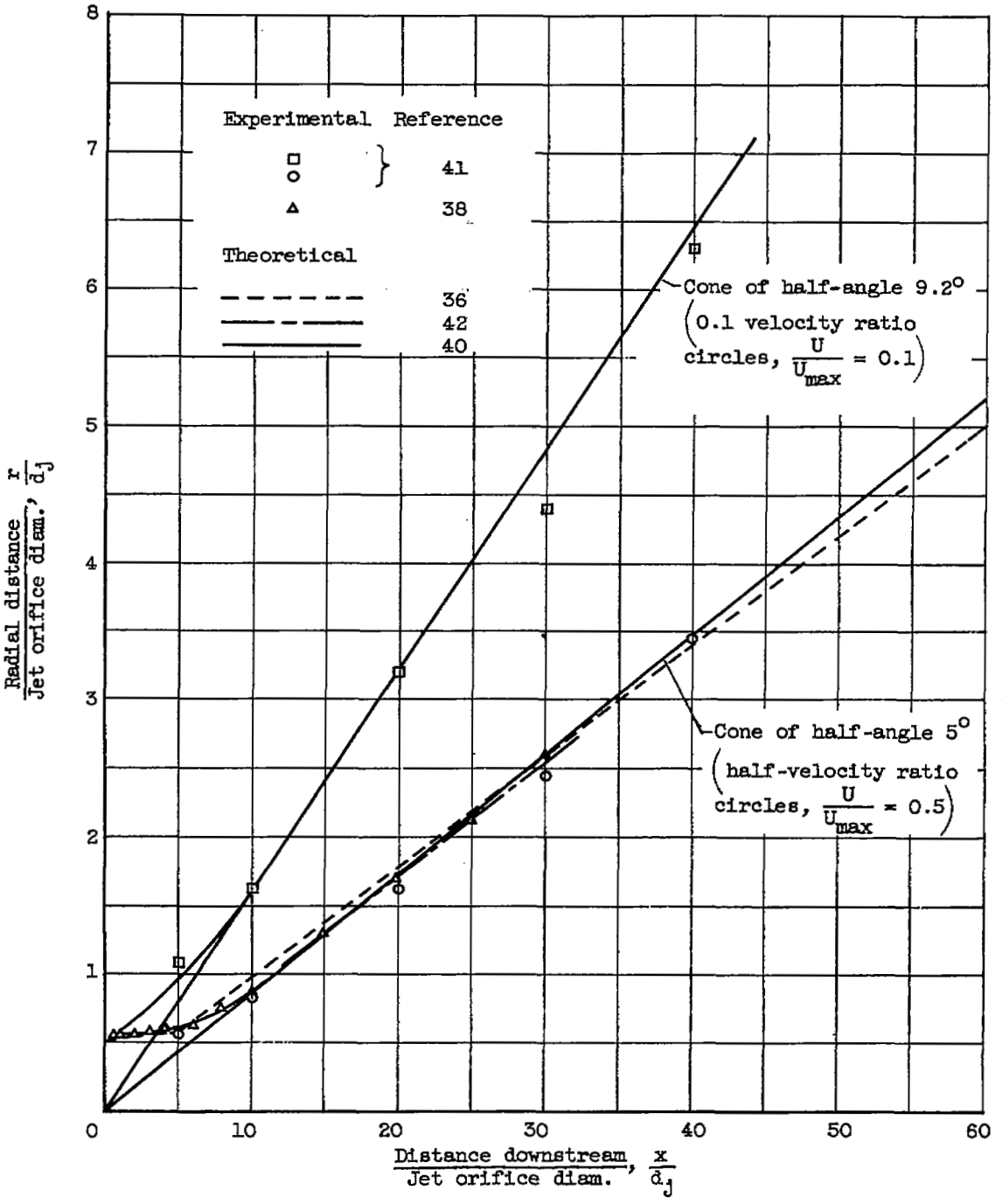

Figure II-20. - Velocity distributions in axially symmetric free jets in air.

3267

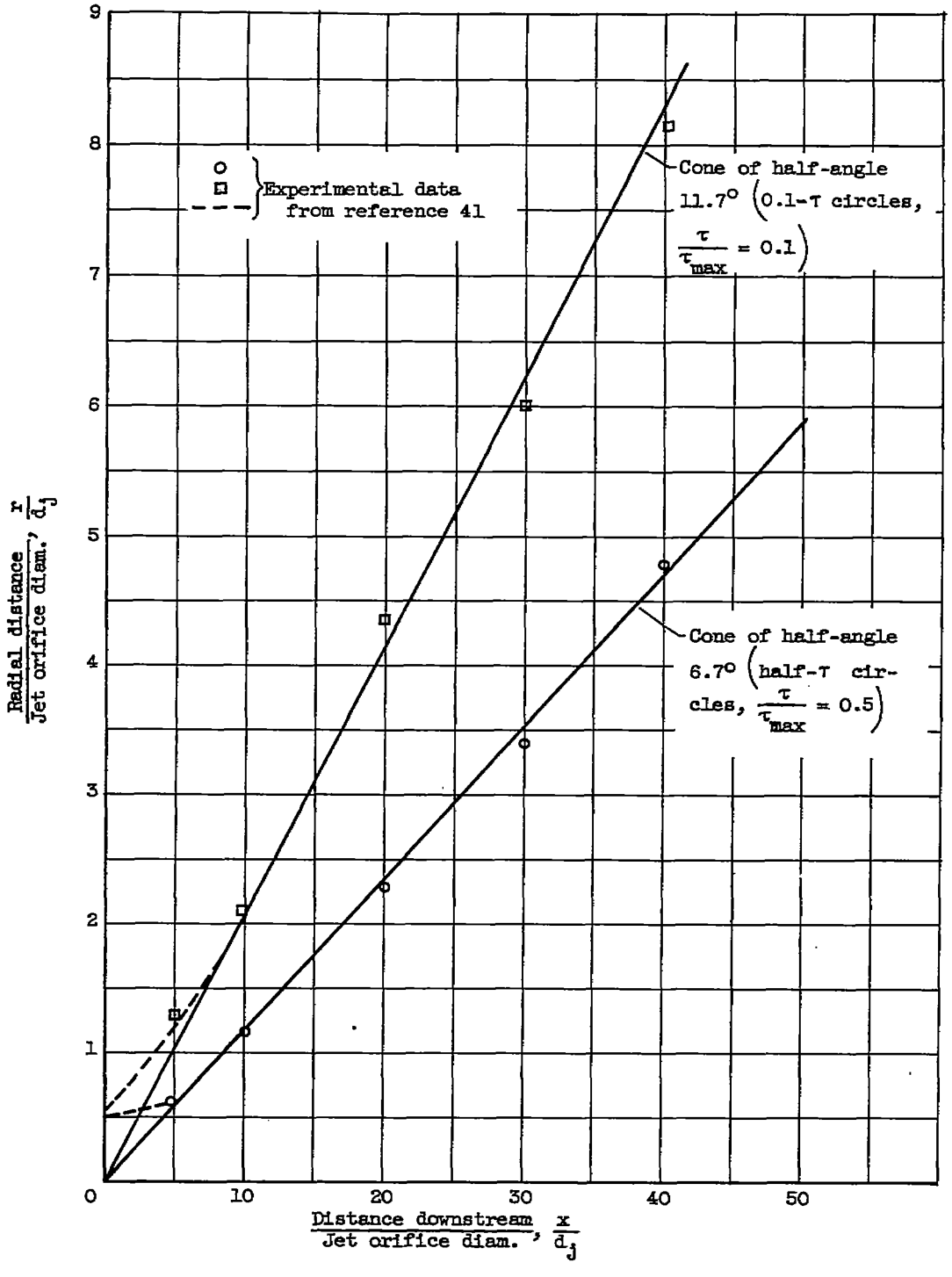

Figure II-21. - Temperature distributions in axially symmetric free jets in air (ref. 40).

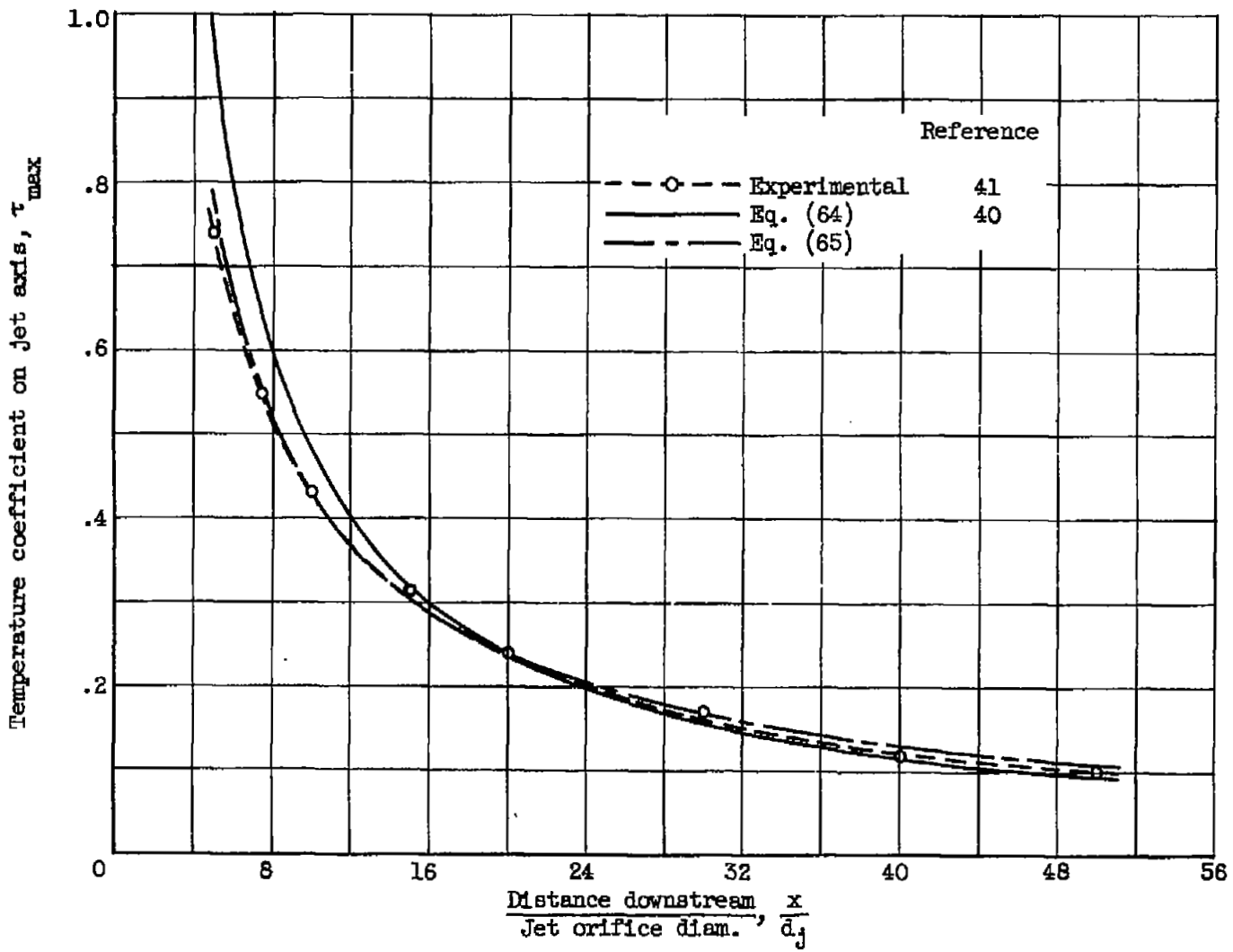

Figure II-22. - Axial temperature distribution in axially symmetric free jets in air.

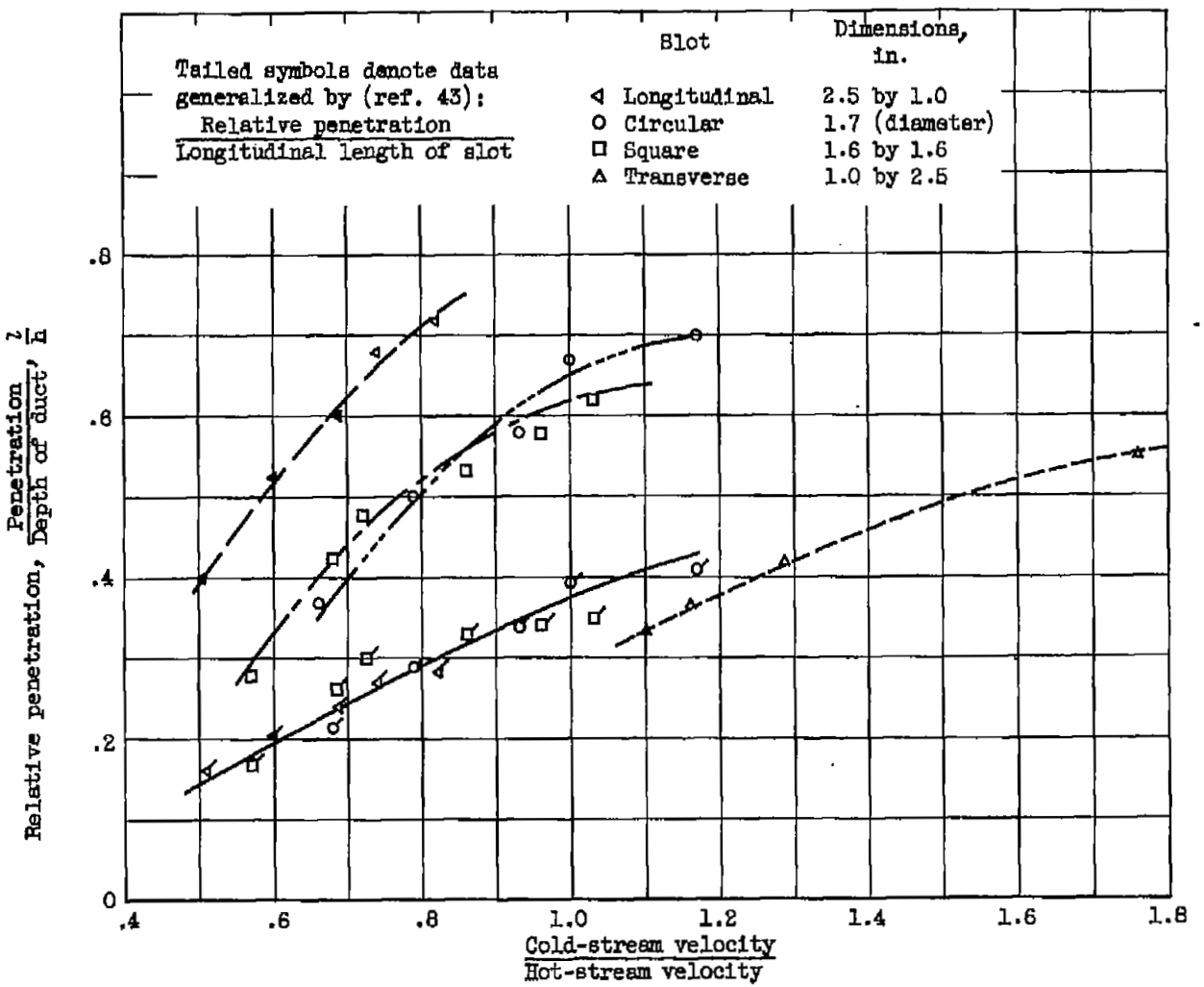

Figure II-23. - Effect of opening shape on penetration of cold-air jets (temperature, 575° R) into normal hot-air stream (temperature, 1350° R)(ref. 37).

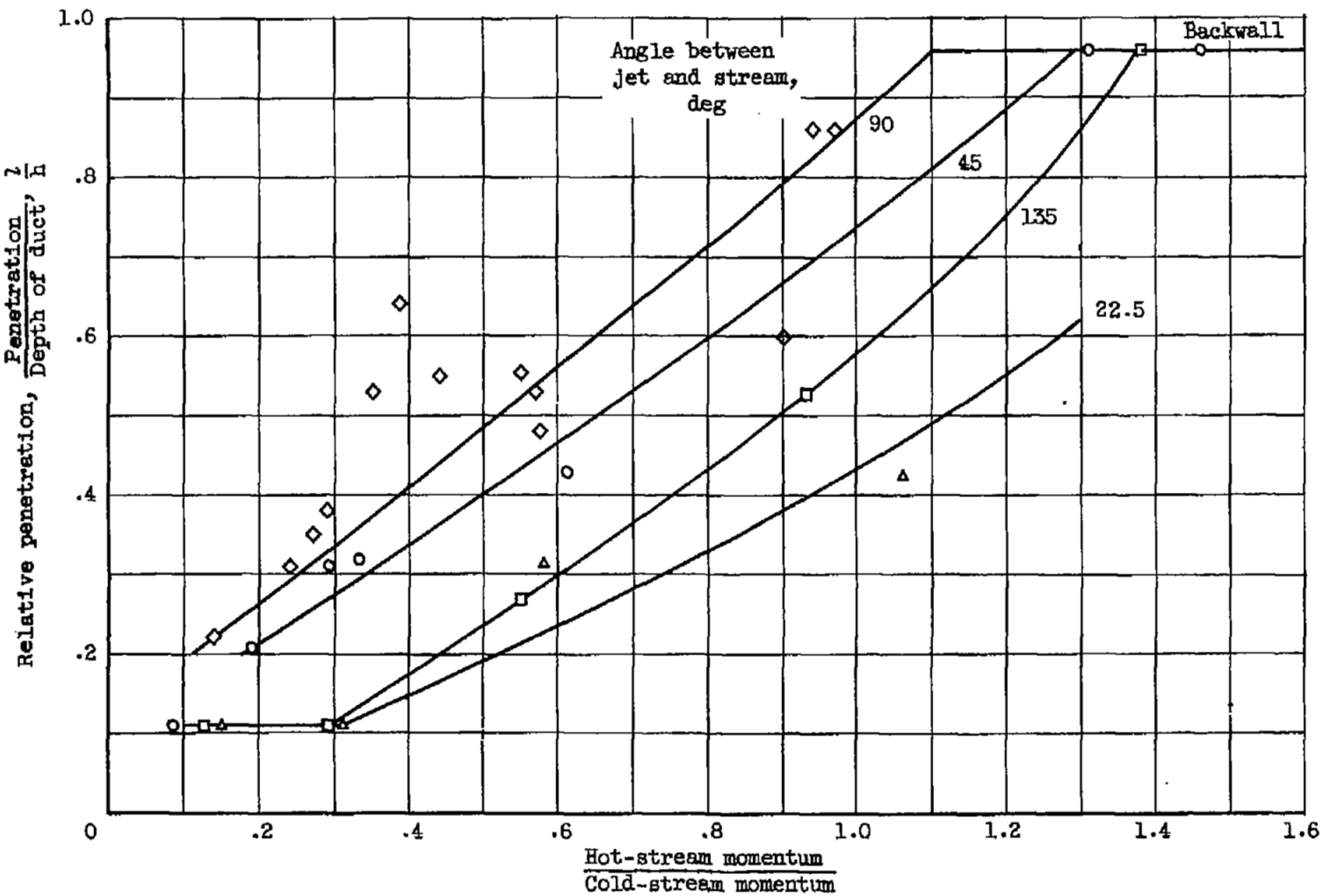

Figure II-24. - Effect of angle between hot-air (temperature, 1040° R) jets and cold-air (temperature, 600° R) streams on penetration of 0.824-inch-diameter jets (ref. 43).

3267

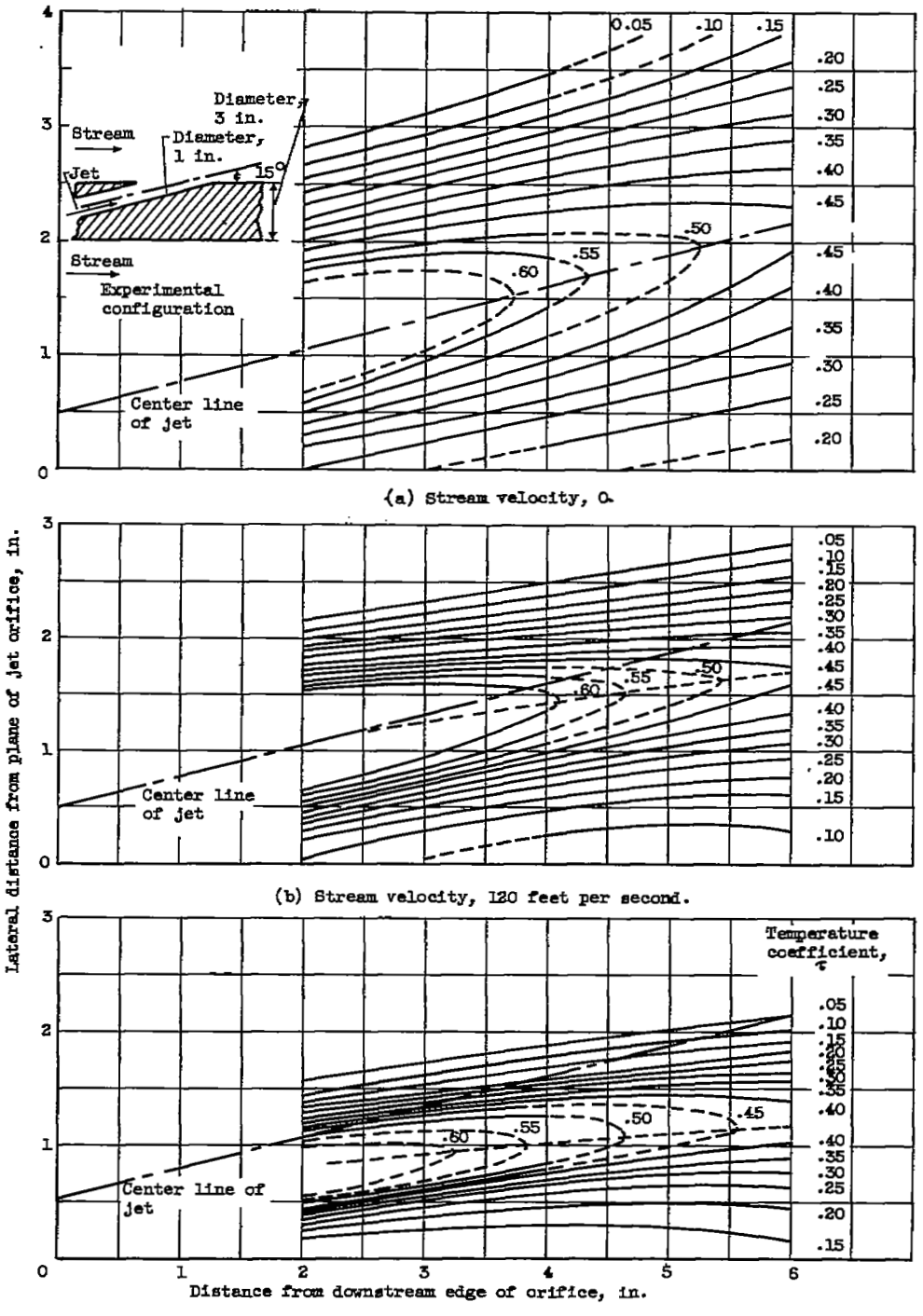

(a) Stream velocity, 0.

(b) Stream velocity, 120 feet per second.

(c) Stream velocity, 240 feet per second.

Figure II-25. - Temperature distributions downstream of axially symmetric oblique jet. Jet velocity, 615 feet per second; jet temperature, 834° R (ref. 40).

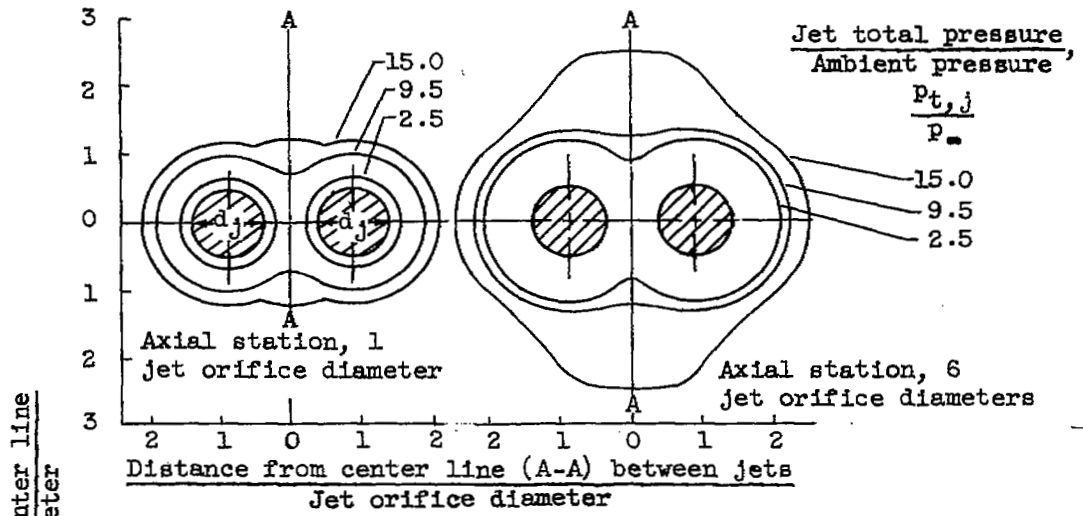

(a) Function of axial position. Nozzle spacing, 1.74 jet orifice diameters.

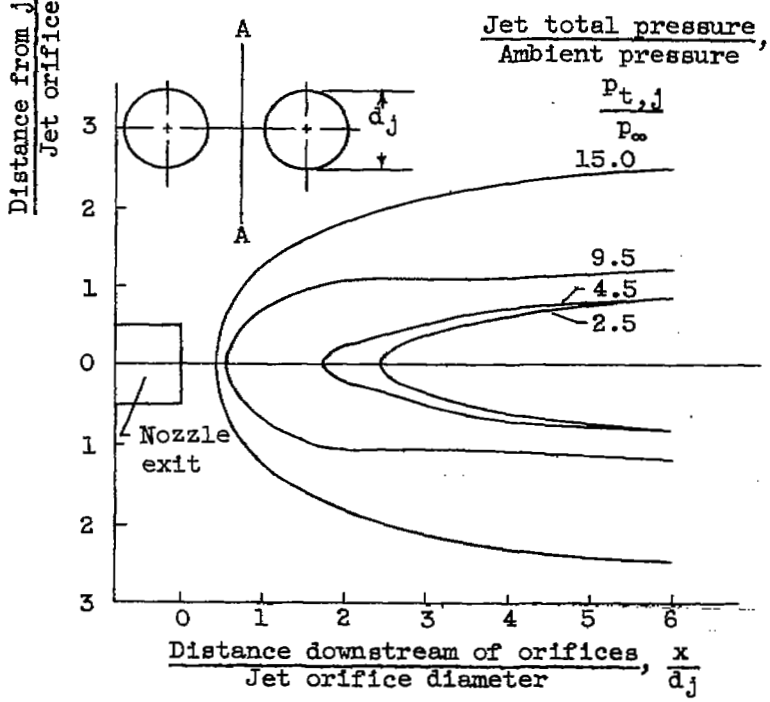

(b) Vertical plane through section A-A. Nozzle spacing, 1.74 jet orifice diameters.

Figure II-26. - Jet boundaries (twin jets).

3267

3267

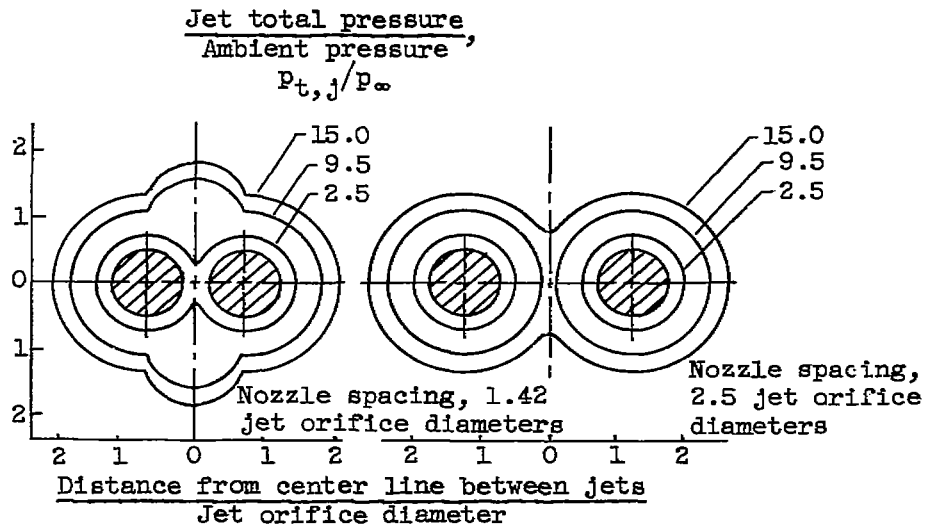

(c) Function of nozzle spacing. Axial station, 2 jet orifice diameters from orifice.

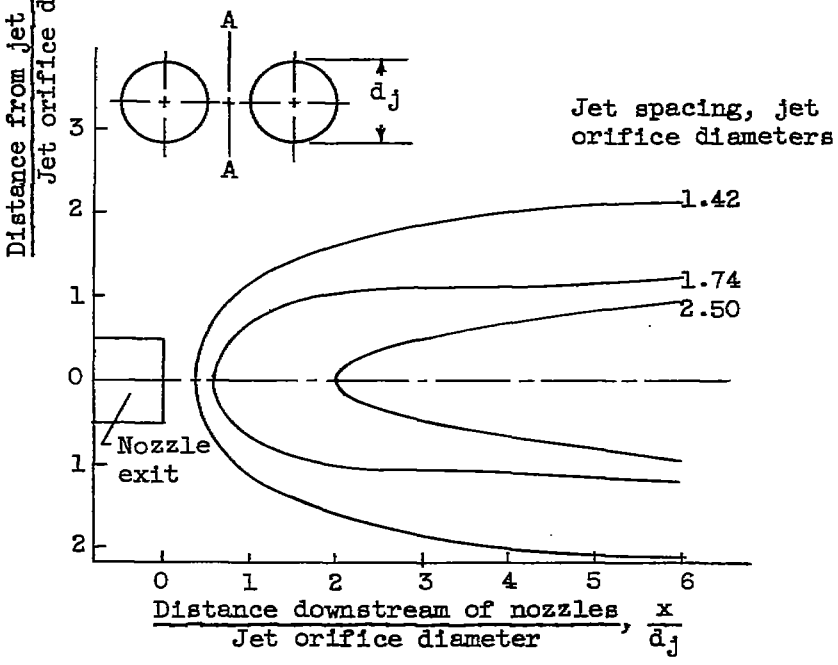

(d) Vertical plane through section A-A; $p_{t,j}/p_\infty$, 9.5.

Figure II-26. - Continued. Jet boundaries (twin jets).

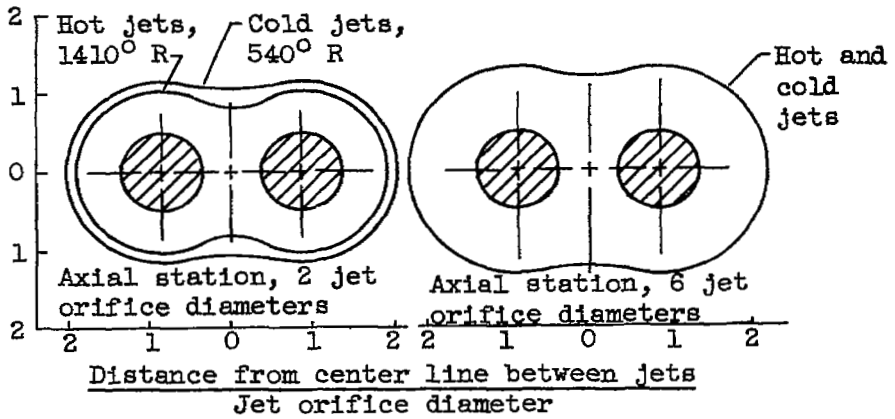

(e) Function of jet temperature. Orifice spacing, 1.74 jet orifice diameters; $p_{j,t}/p_\infty$, 9.5.

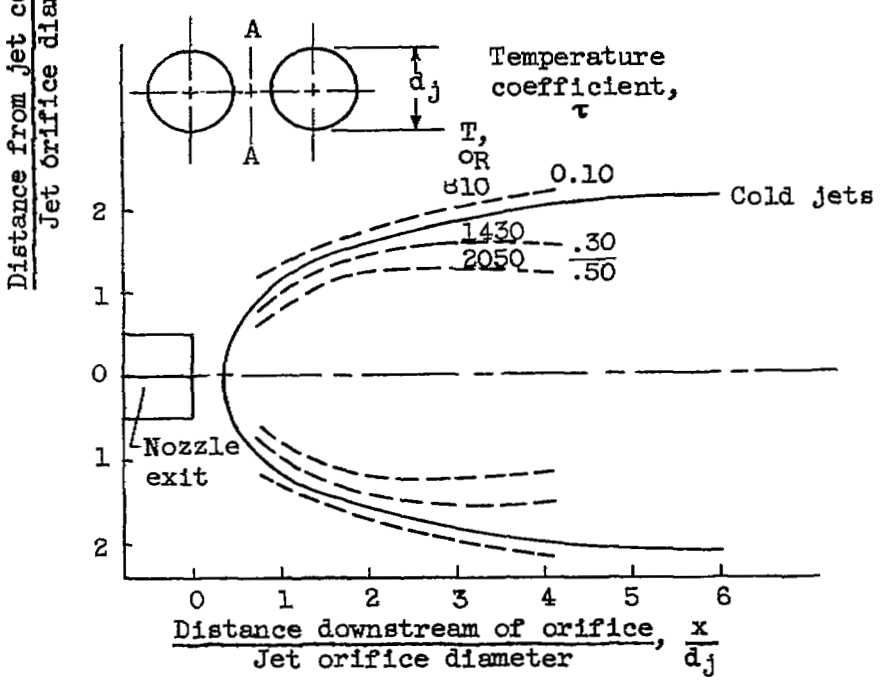

(f) Vertical plane through section A-A. Orifice spacing, 1.42 jet orifice diameters; $p_{t,j}/p_\infty$, 9.5.

Figure II-26. - Concluded. Jet boundaries (twin jets).

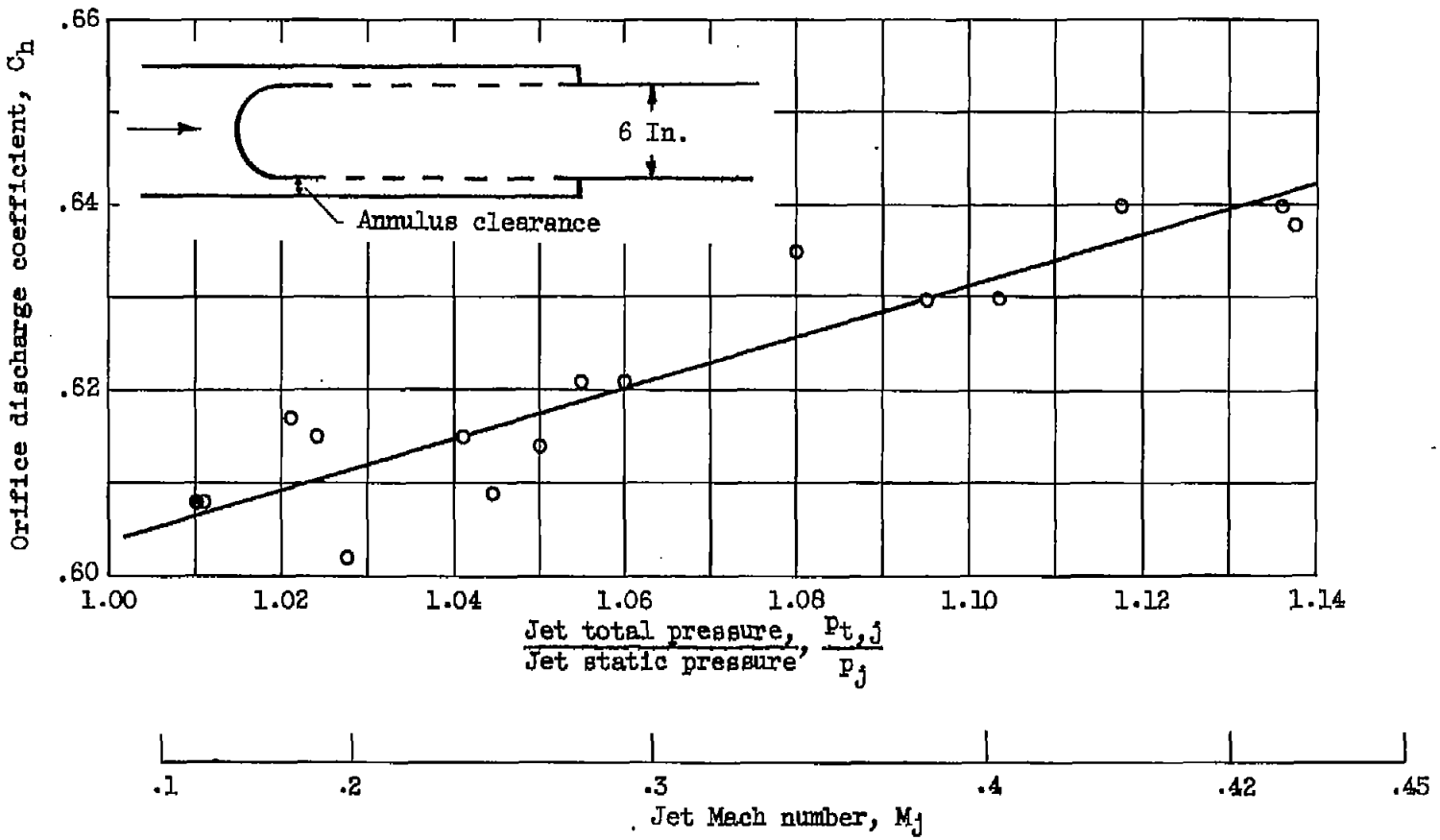

(a) Zero crossflow; maximum of 12 orifices; wall thickness, 0.064 inch; annulus clearance, 1 inch to ∞.

Figure II-27. - Orifice discharge coefficients of 0.752-inch-diameter orifices in 6-inch-diameter tubular liner (ref. 49).

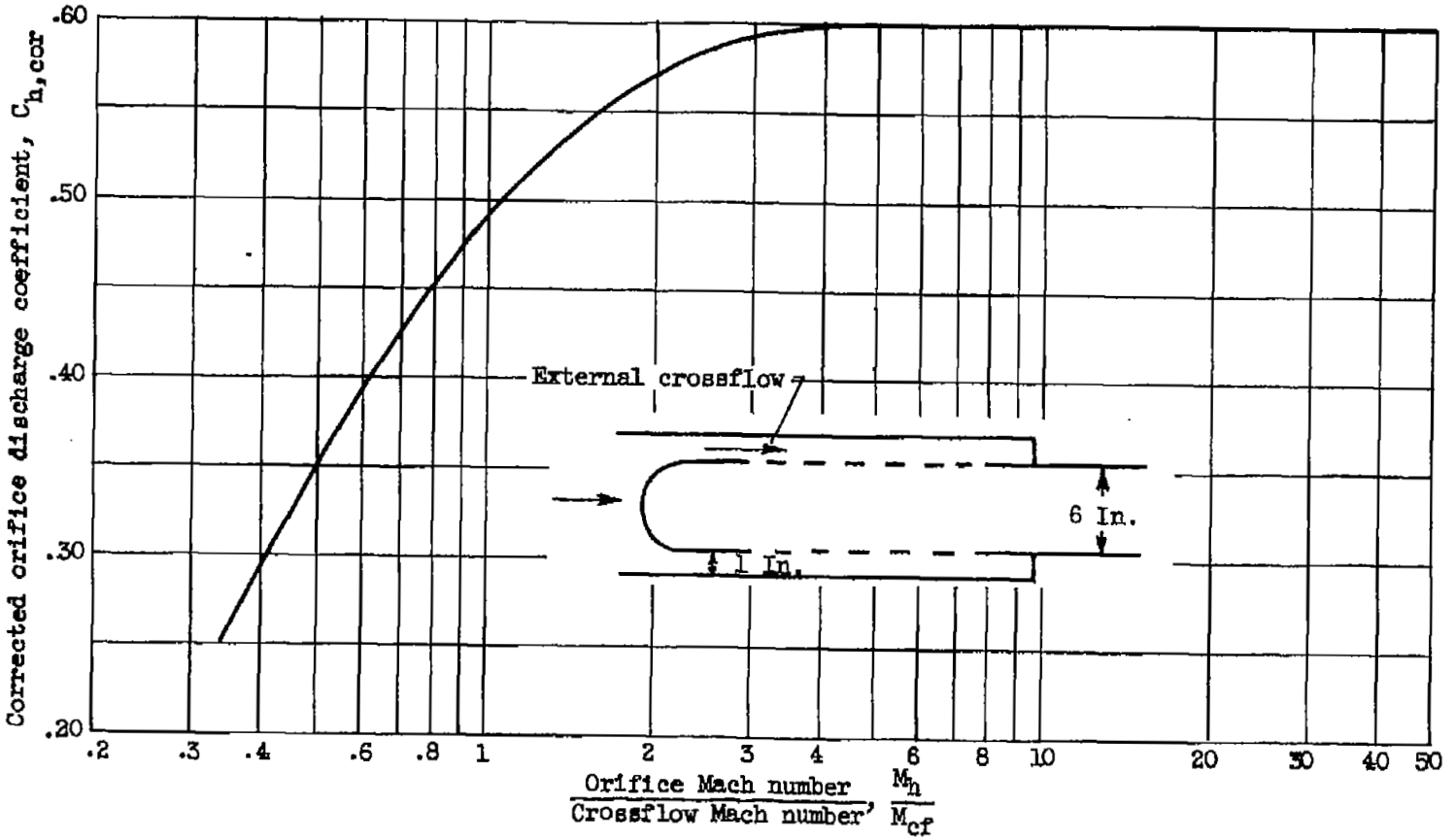

(b) External crossflow; coefficient corrected to 0.60 for $p_{t,j}/p_j = 1.00$ with zero crossflow; annulus clearance, 1 inch.

Figure II-27. - Concluded. Orifice discharge coefficients of 0.752-inch-diameter orifices in 6-inch-diameter tubular liner (ref. 49).

3267

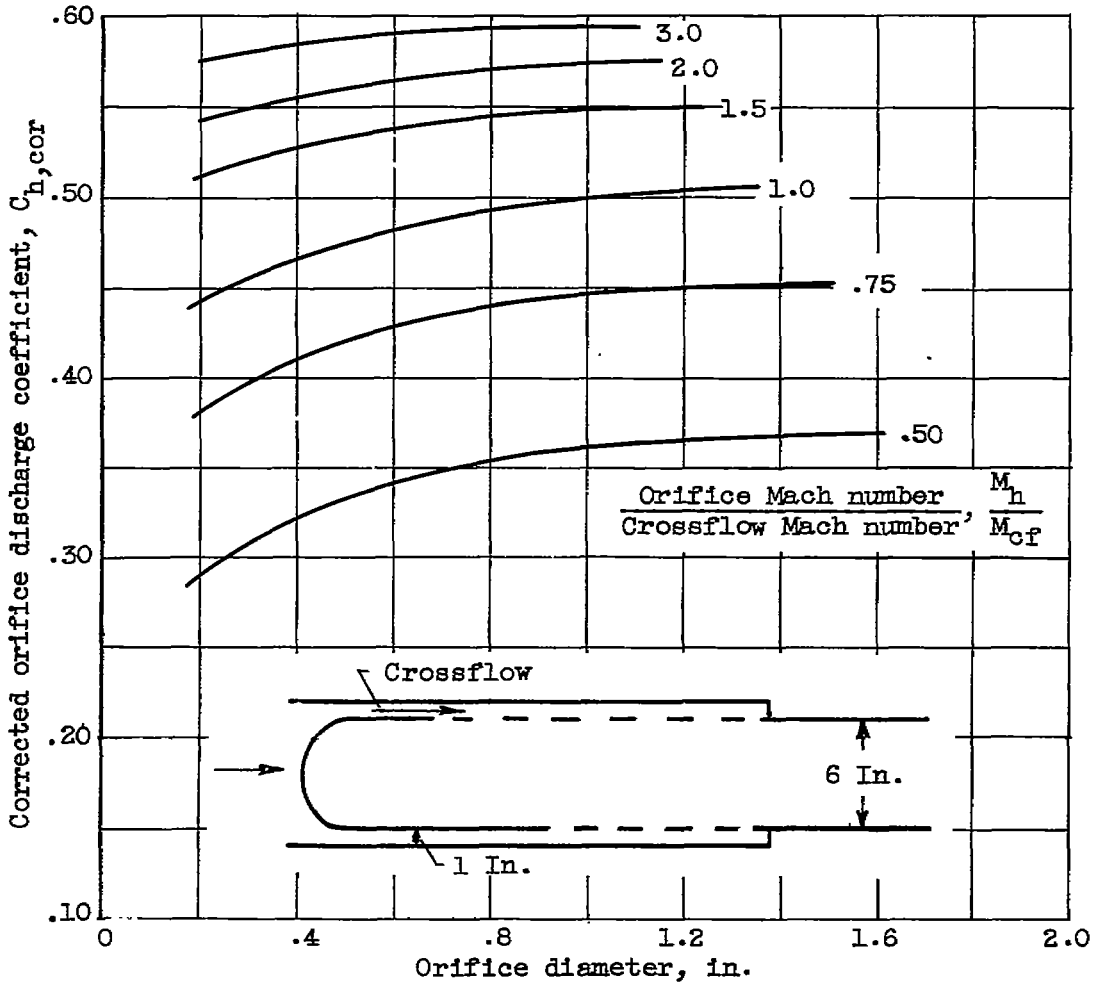

Figure II-28. - Effect of orifice diameter on corrected orifice discharge coefficients with external crossflow. Liner diameter, 6 inches; wall thickness, 0.064 inch; coefficient corrected to 0.60 for $p_{t,j}/p_j = 1.00$ with zero crossflow; annulus clearance, 1 inch (ref. 49).

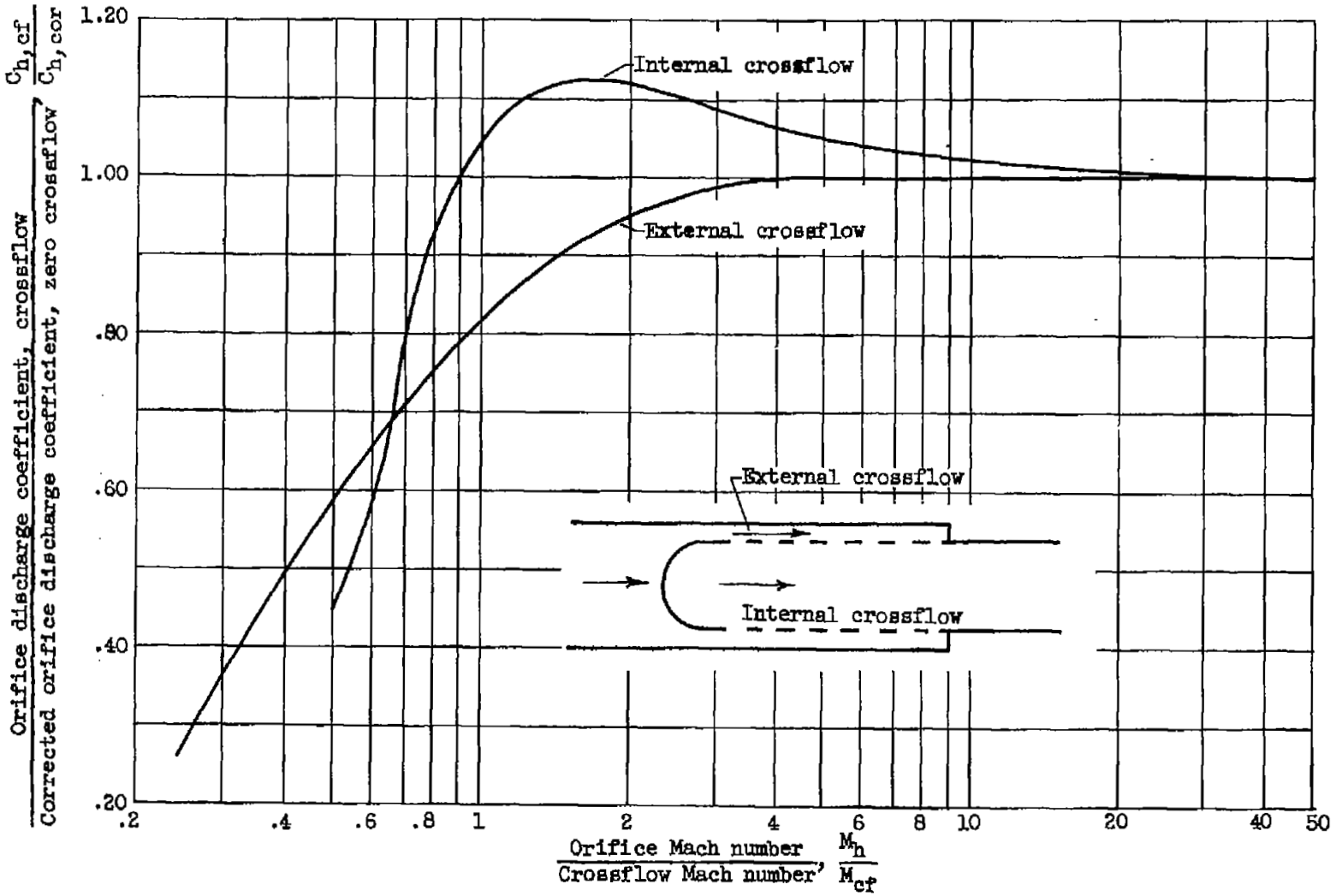

Figure II-29. - Effect of internal and external crossflow on orifice discharge coefficients (ref. 49).

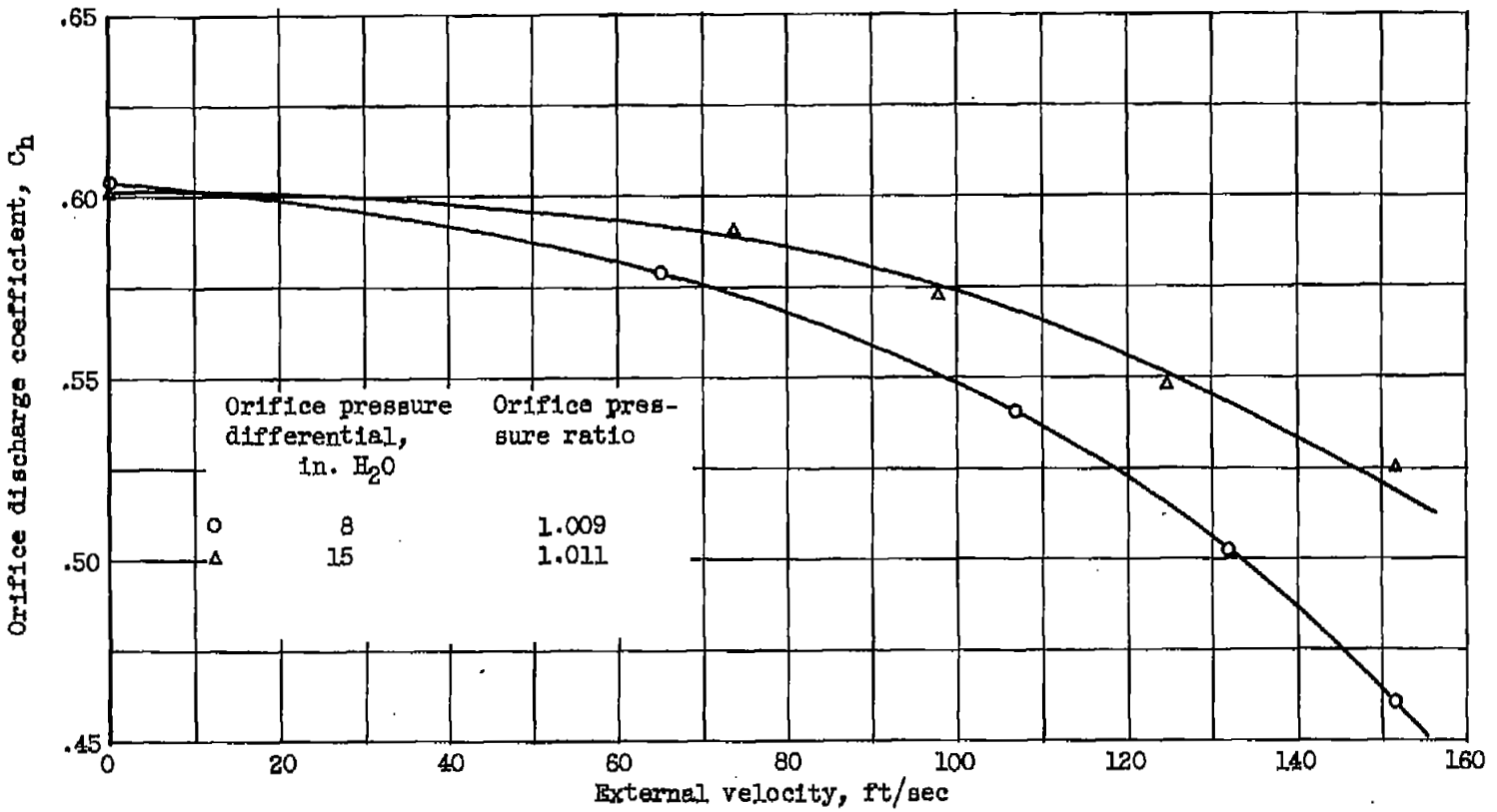

Figure II-30. - Effect of external velocity and orifice pressure ratio on discharge coefficient of 3/8-inch-diameter orifice. Zero internal velocity; external static pressure, 44.2 pounds per square inch absolute (ref. 50).

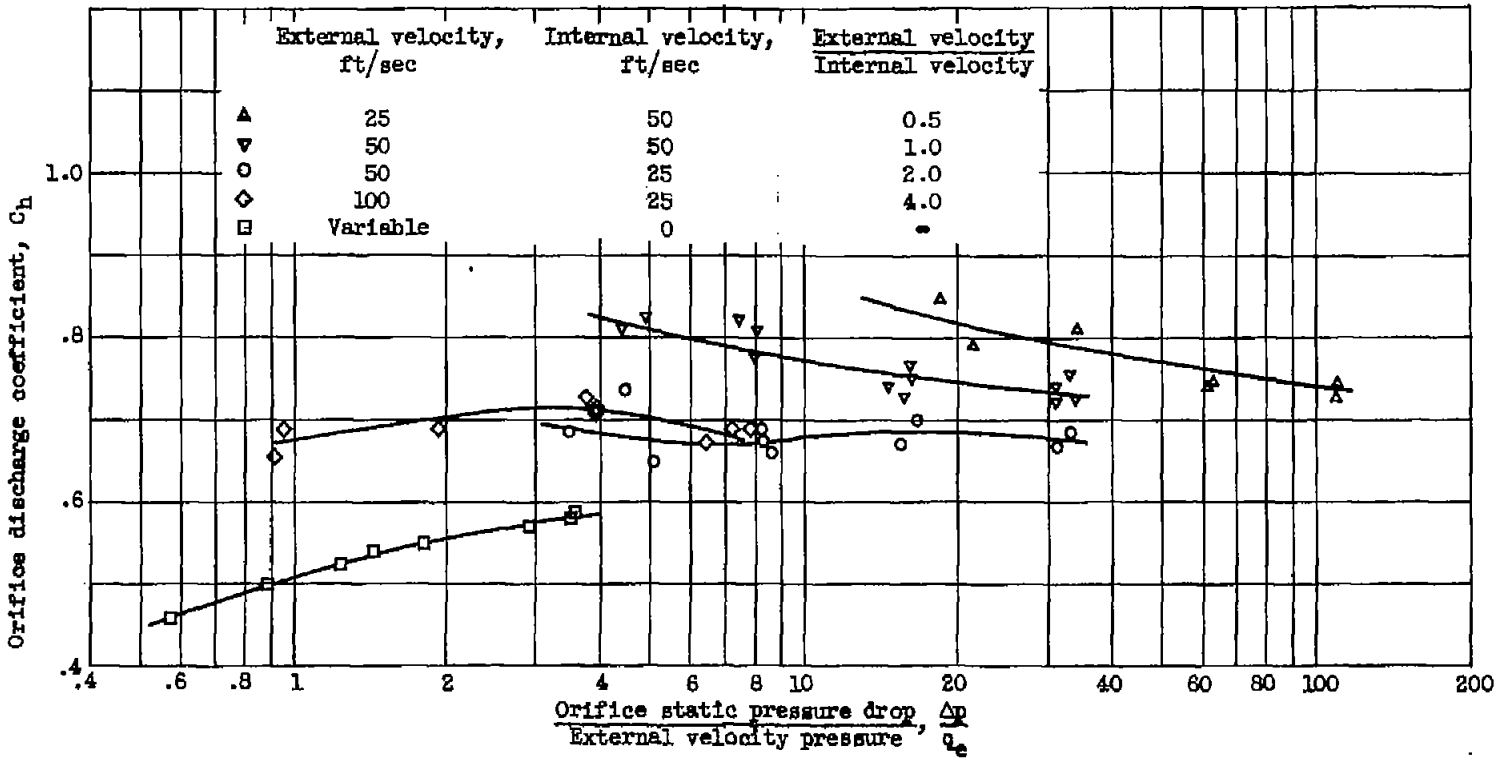

(a) Orifice diameter, 0.375 inch.

Figure II-31. - Orifice discharge coefficients. Internal static pressure, 45 pounds per square inch absolute (ref. 50).

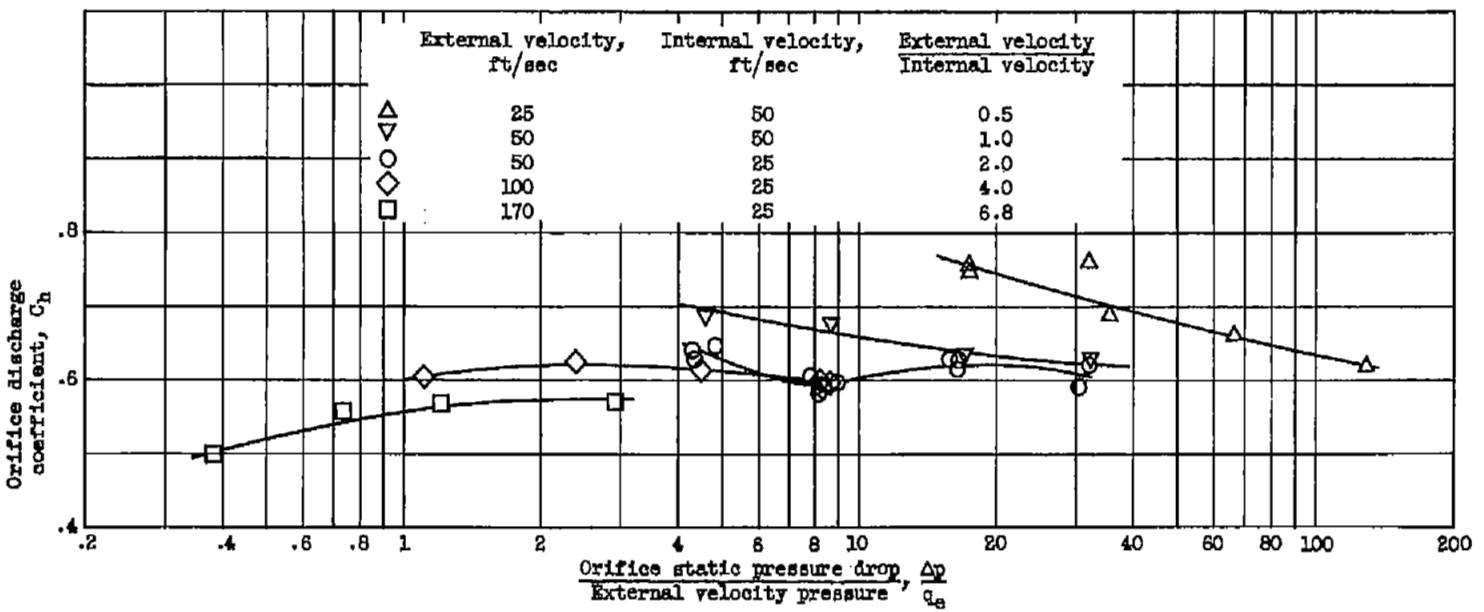

(b) Orifice diameter, 0.750 inch.

Figure II-31. - Concluded. Orifice discharge coefficients. Internal static pressure, 45 pounds per square inch absolute (ref. 50).

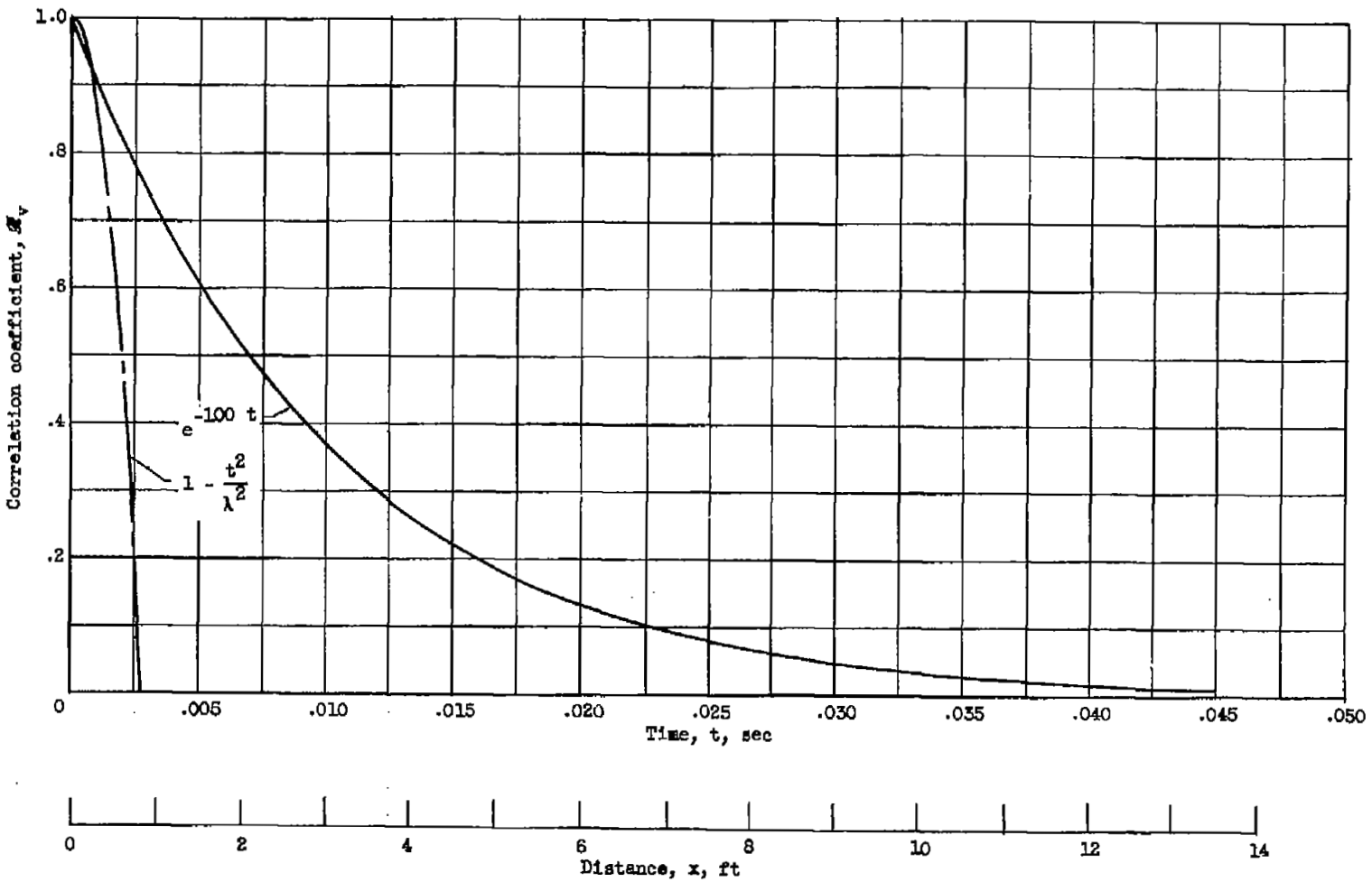

Figure II-32. - Correlation coefficient $\mathcal{R}_v$ of form $\mathcal{R}_v = e^{-t/t_{\mathcal{L}}}$. Mean stream velocity, 300 feet per second; turbulence intensity, 15 feet per second; turbulence scale, 0.15 foot; turbulence microscale, 0.0416 foot.

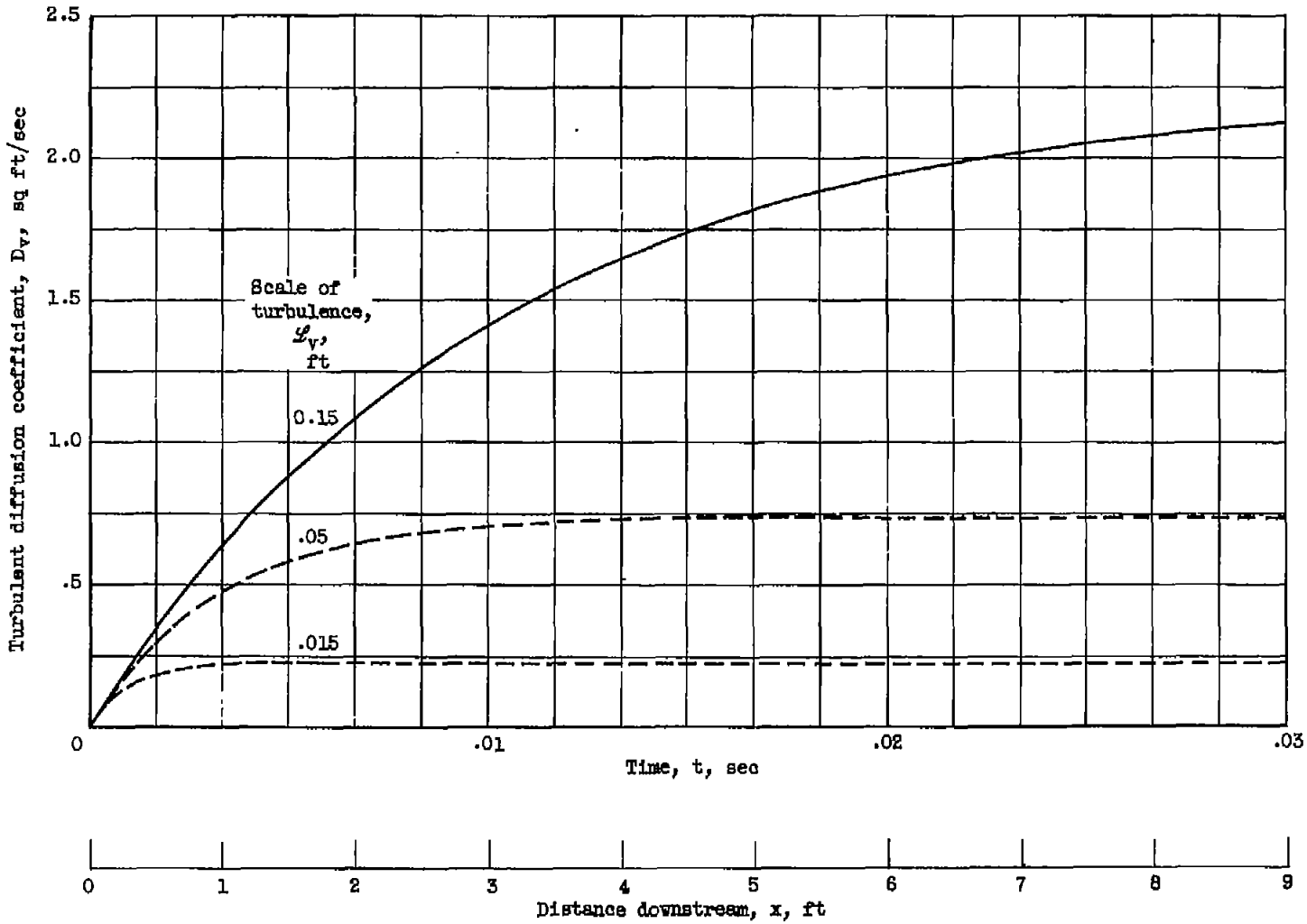

Figure II-33. - Theoretical turbulent diffusion coefficient D_v corresponding to Lagrangian correlation coefficient $\mathscr{L}_v = e^{-t/t_{\mathscr{L}}}$. Mean stream velocity, 300 feet per second; turbulence intensity, 15 feet per second; Lagrangian scale of turbulence as noted.

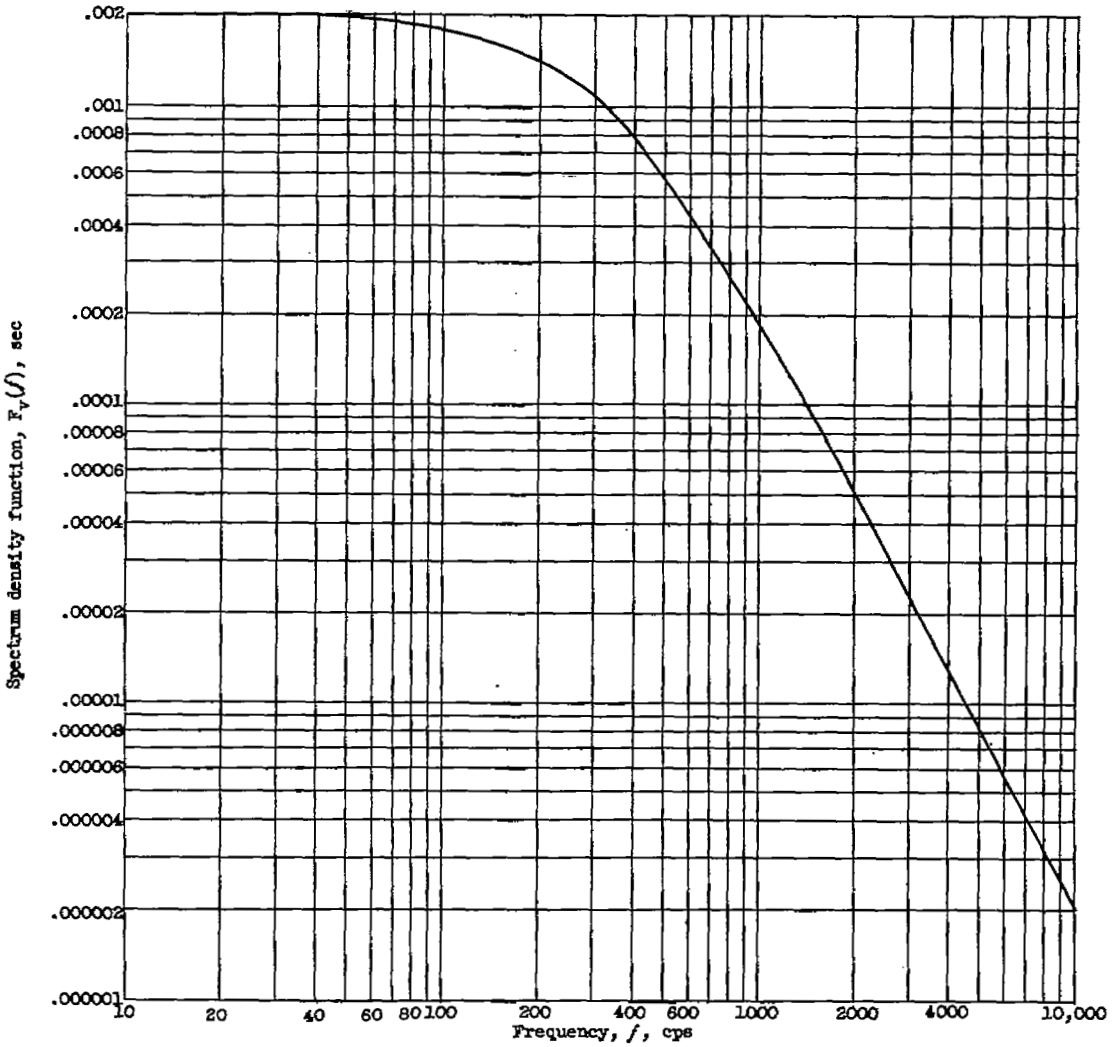

Figure II-34. - One-dimensional spectrum of turbulence when $\mathcal{R}'_v = e^{-\frac{y}{\mathcal{L}'_v}}$. Mean stream velocity, 300 feet per second; Eulerian scale $\mathcal{L}'_u$, 0.15 foot; negligible microscale.

3267

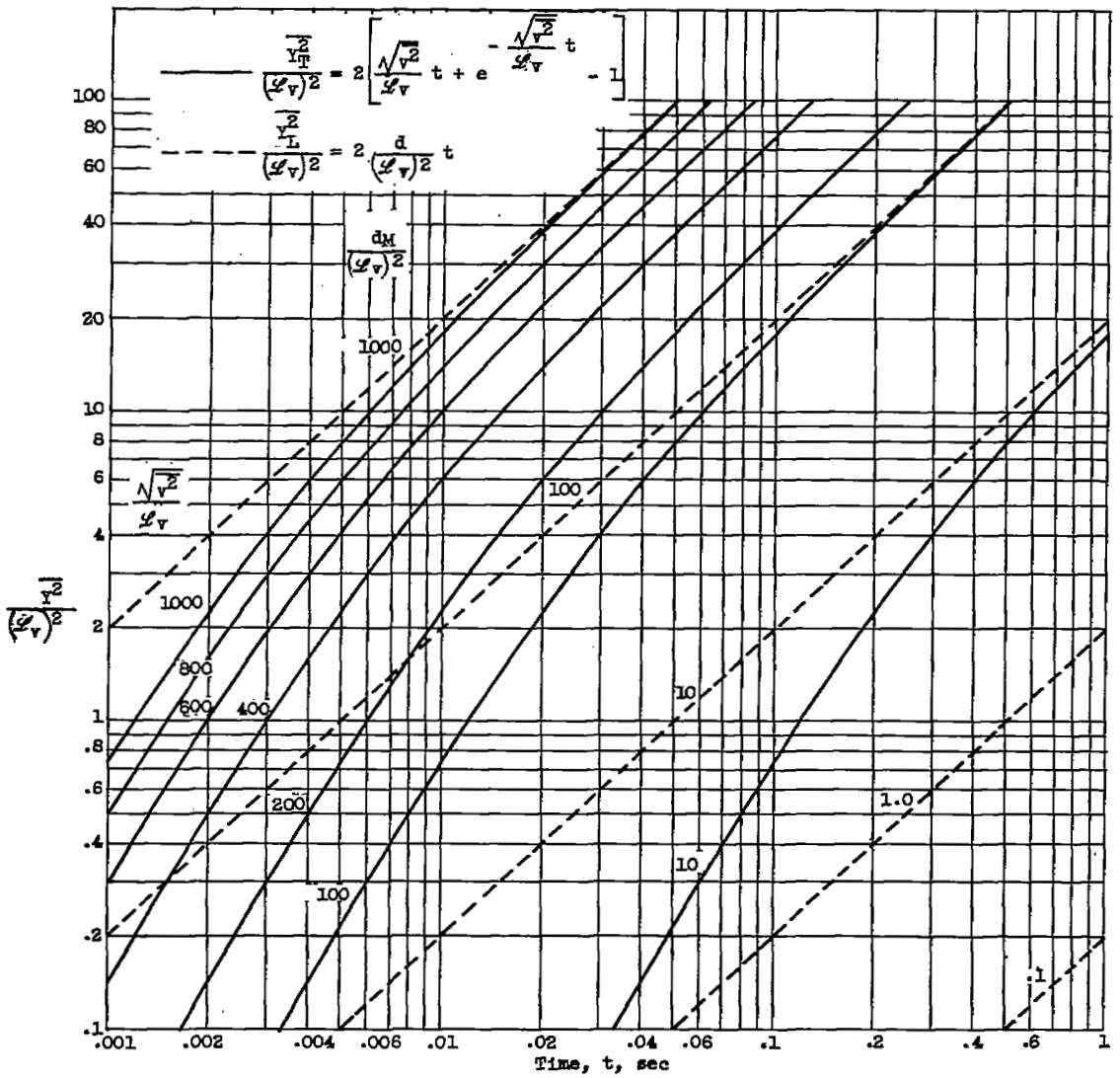

Figure II-35. - Comparison of turbulent and molecular standard square deviations, based on $\mathscr{R} = e^{-\frac{\sqrt{\overline{Y^2}}}{\mathscr{L}_V} t}$

3267

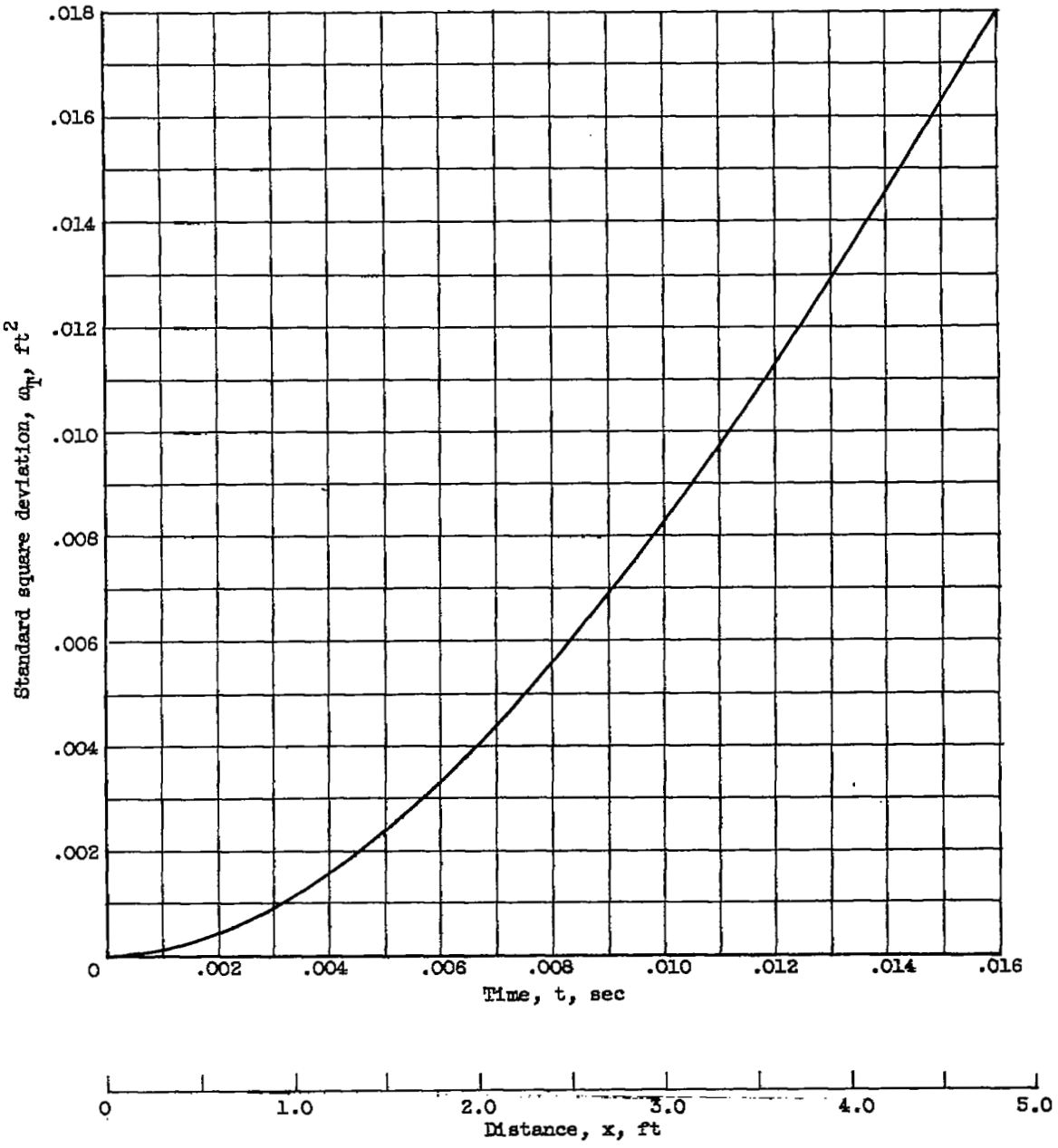

(a) Standard square deviation over a range of interest in jet-engine applications.

Figure II-36. - Standard square deviation based on turbulent diffusion coefficient shown in figure II-33 for Lagrangian scale of turbulence $\mathscr{L}_v$ = 0.15 foot.

3267

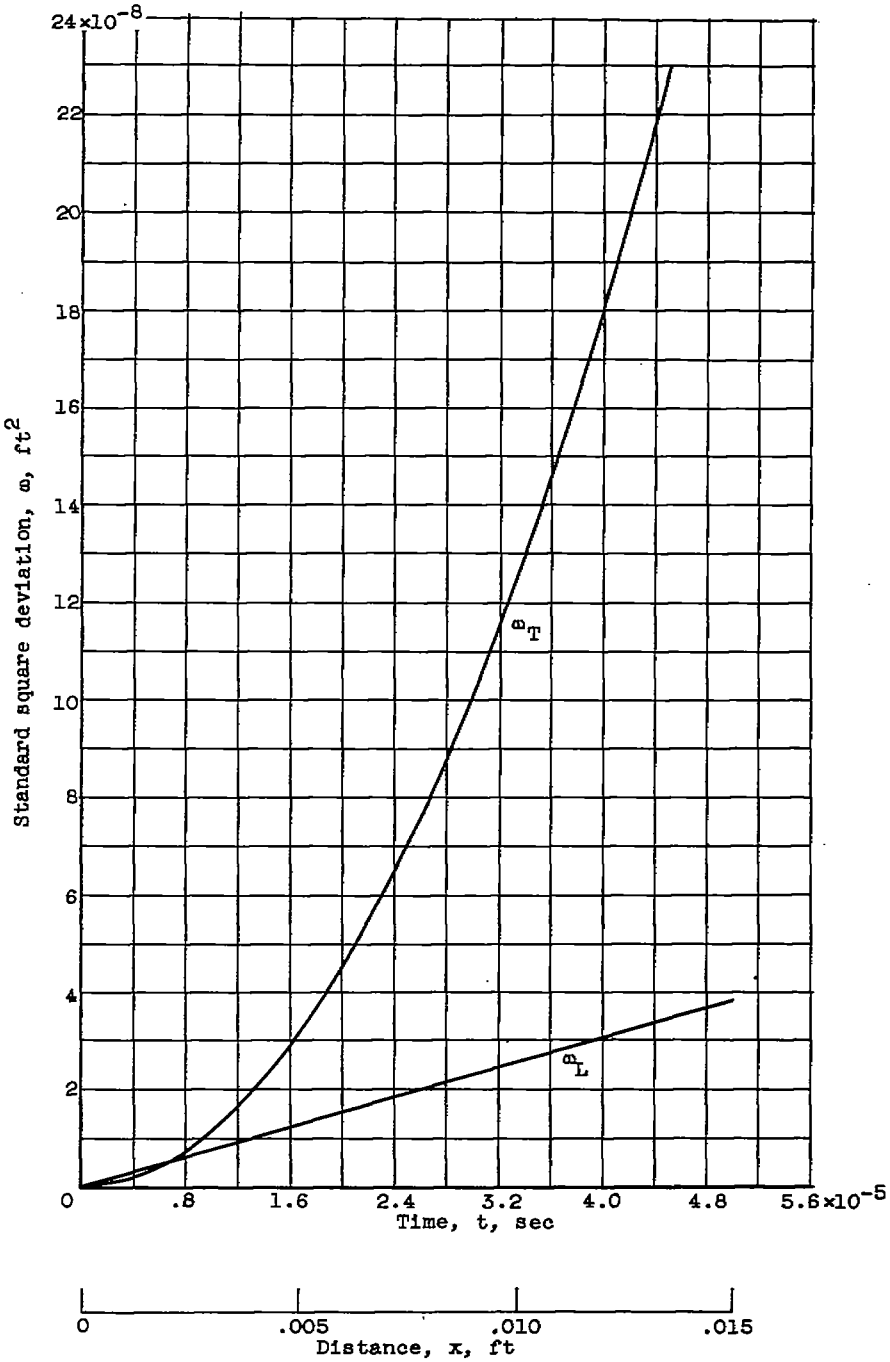

(b) Comparison of turbulent and molecular standard square deviations.

Figure II-36. - Concluded. Standard square deviation based on turbulent diffusion coefficient shown in figure II-33 for Lagrangian scale of turbulence $\mathscr{L}_v = 0.15$ foot.

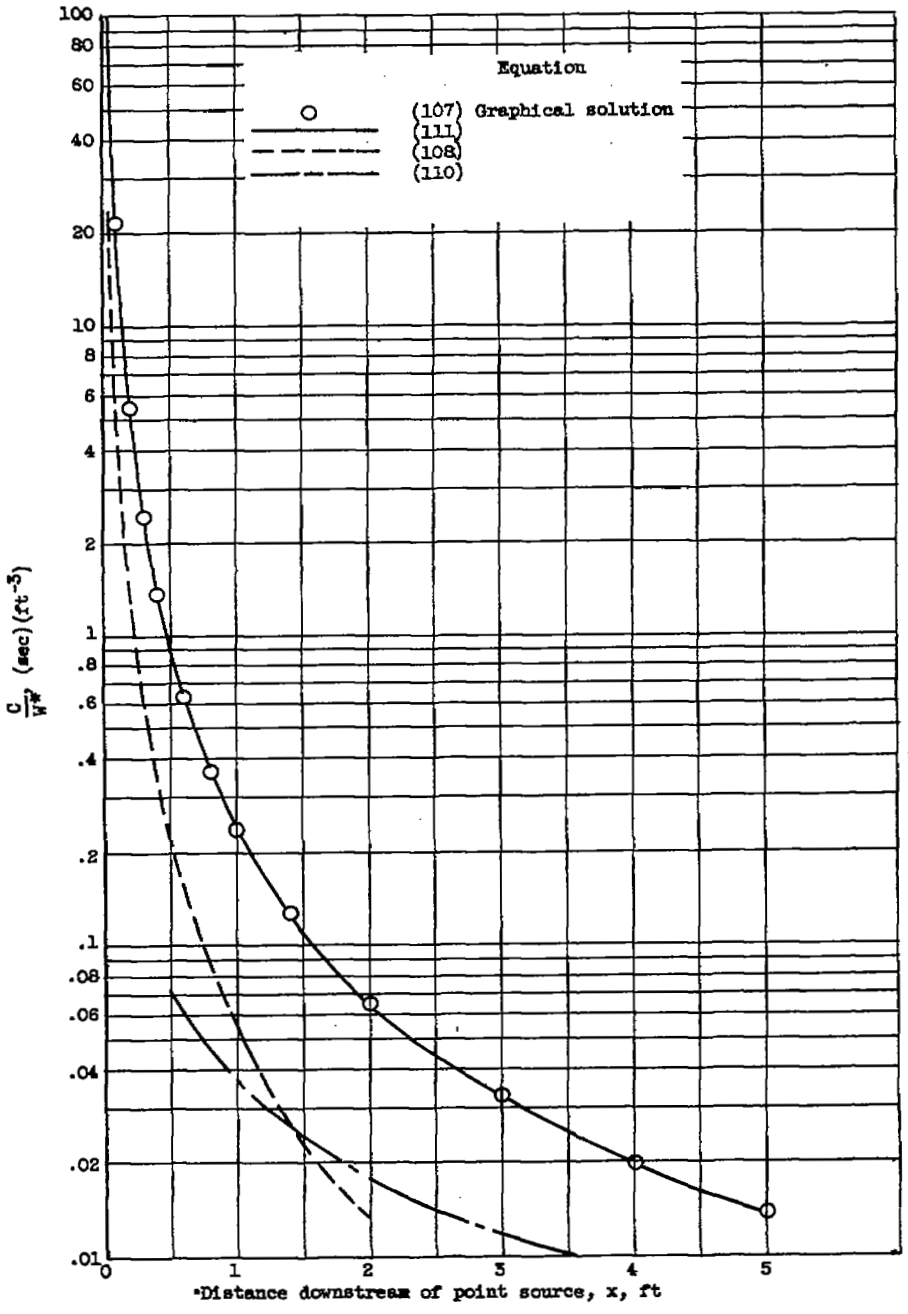

(a) Mean concentrations along x-axis.

Figure II-37. - Comparison of solutions for point source of diffusion. Mean stream velocity, 300 feet per second; turbulence intensity, 15 feet per second; turbulence scale, 0.15 foot; correlation coefficient, $e^{-\frac{t}{t}}$; stream static pressure, 0.25 atmosphere; stream temperature, 1100° R; isooctane vapor diffusing through air.

3267

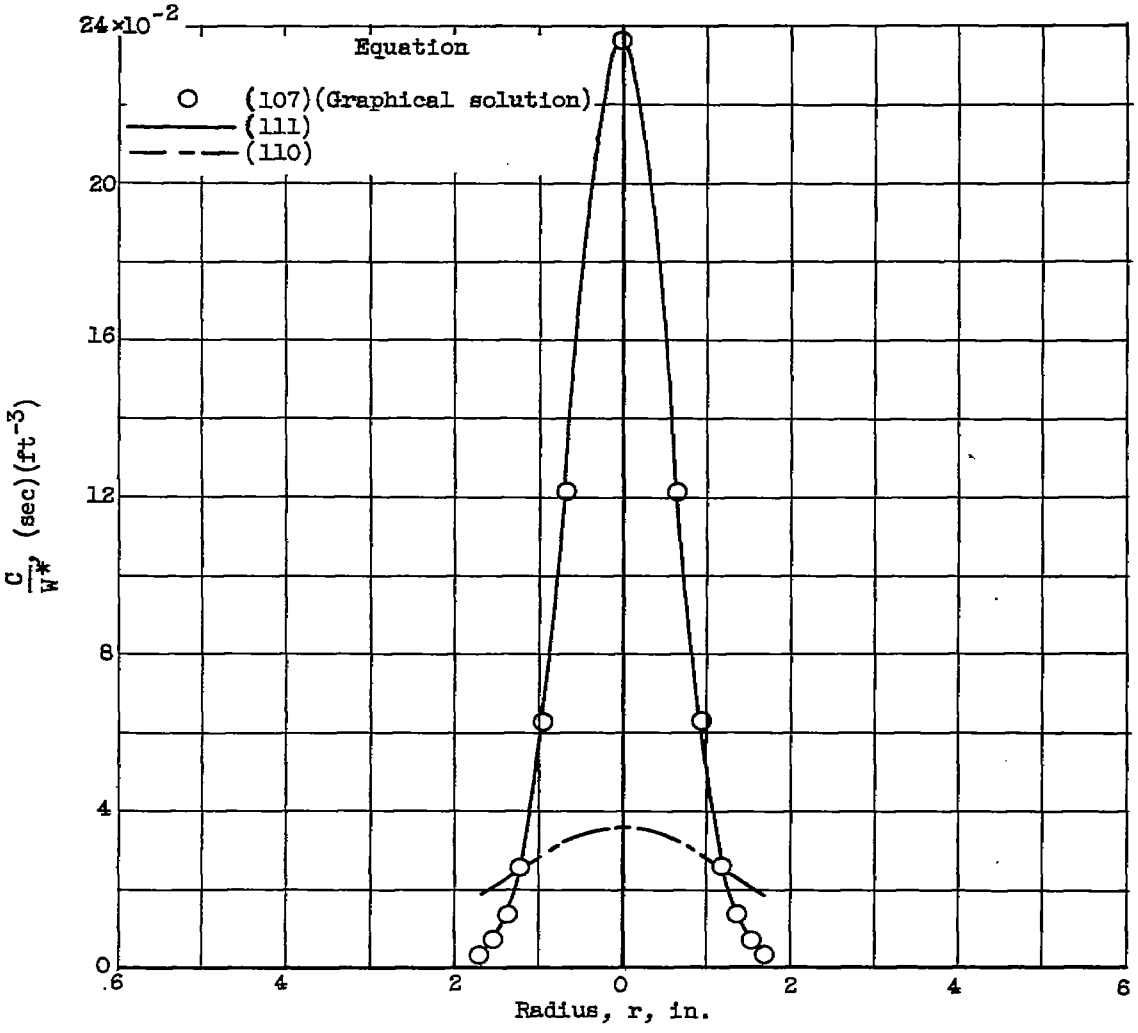

(b) Radial concentration profile at $x = 1.0$ foot.

Figure II-37. - Continued. Comparison of solutions for point source of diffusion. Mean stream velocity, 300 feet per second; turbulence intensity, 15 feet per second; turbulence scale, 0.15 foot; correlation coefficient, $e^{-\frac{t}{t_{\mathcal{L}}}}$; stream static pressure, 0.25 atmosphere; stream temperature, 1100° R; isooctane vapor diffusing through air.

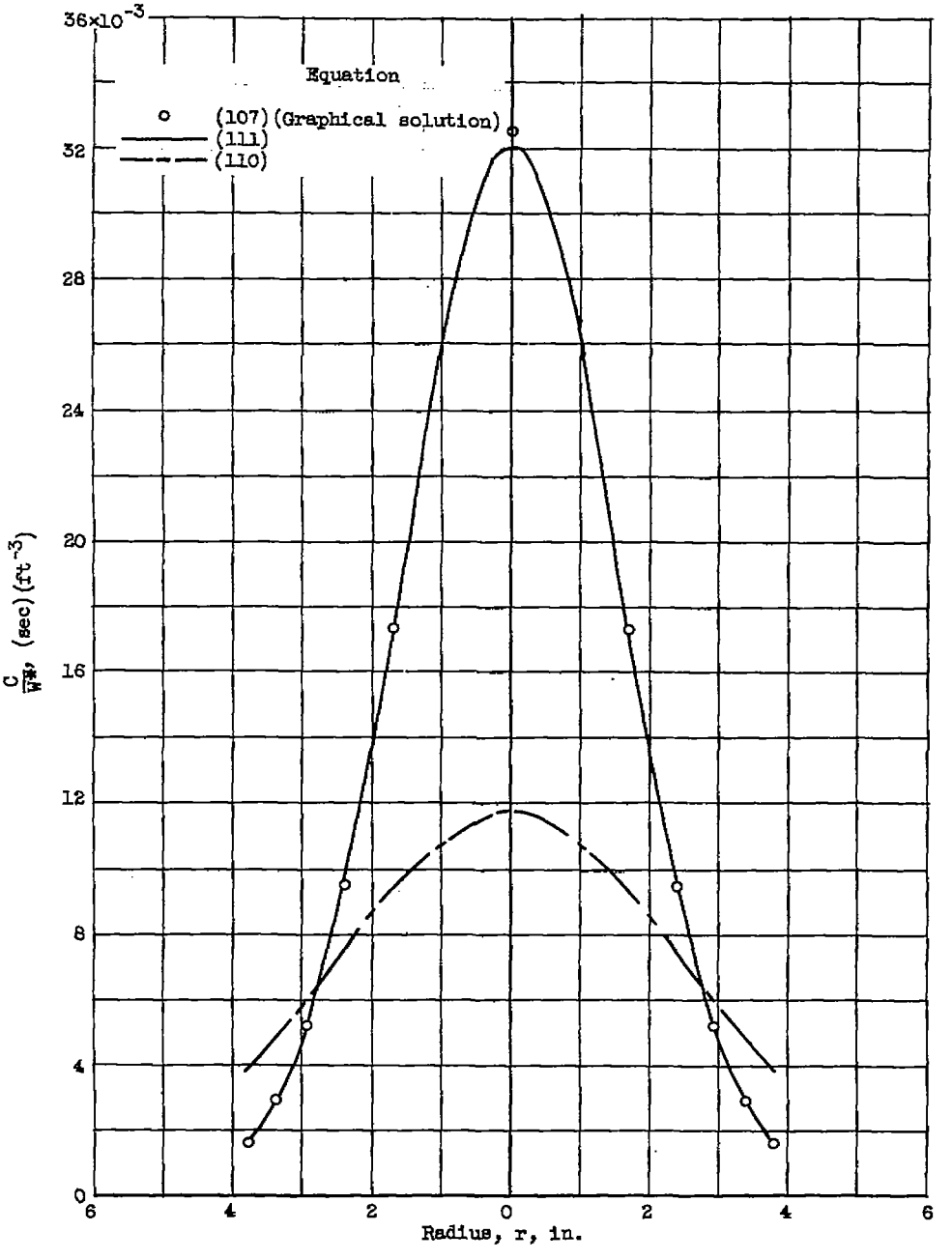

(c) Radial concentration profile at x = 3.0 feet.

Figure II-37. - Continued. Comparison of solutions for point source of diffusion. Mean stream velocity, 300 feet per second; turbulence intensity, 15 feet per second; turbulence scale, 0.15 foot; correlation coefficient, $e^{-\frac{t}{t_{\varphi}}}$; stream static pressure, 0.25 atmosphere; stream temperature, 1100° R; isooctane vapor diffusing through air.

3267

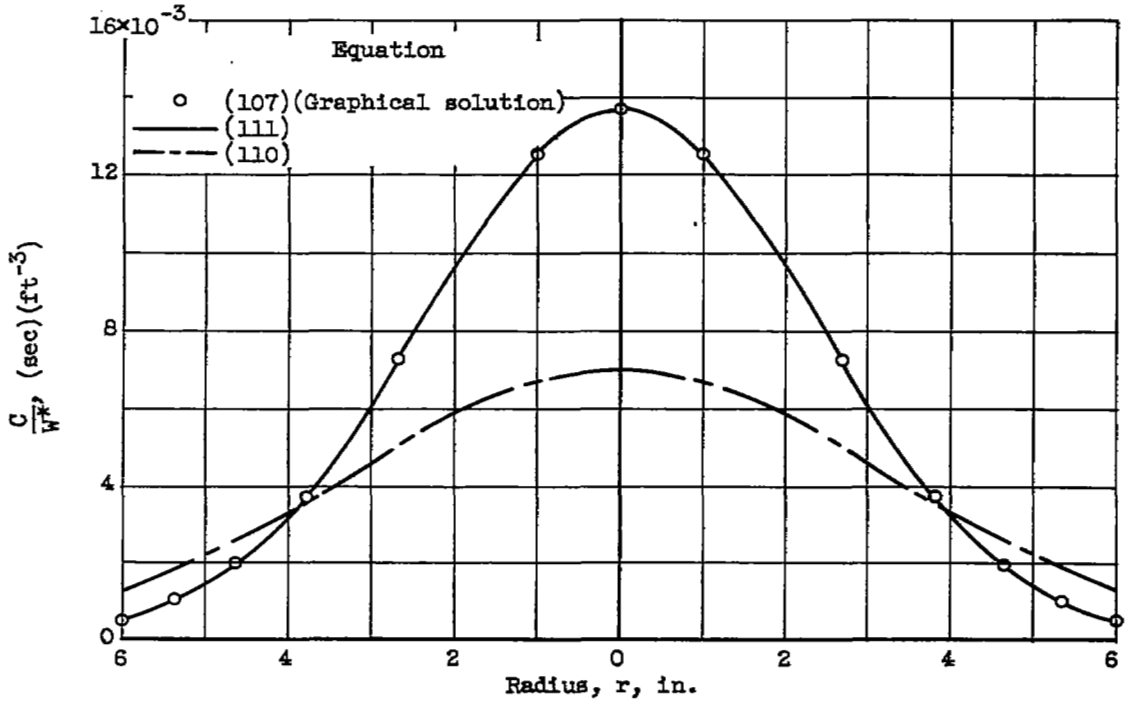

(d) Radial concentration profile at $x = 5.0$ feet.

Figure II-37. - Concluded. Comparison of solutions for point source of diffusion. Mean stream velocity, 300 feet per second; turbulence intensity, 15 feet per second; turbulence scale, 0.15 foot; correlation coefficient, $e^{-\frac{t}{t}}$; stream static pressure, 0.25 atmosphere; stream temperature, 1100° R; isooctane vapor diffusing through air.

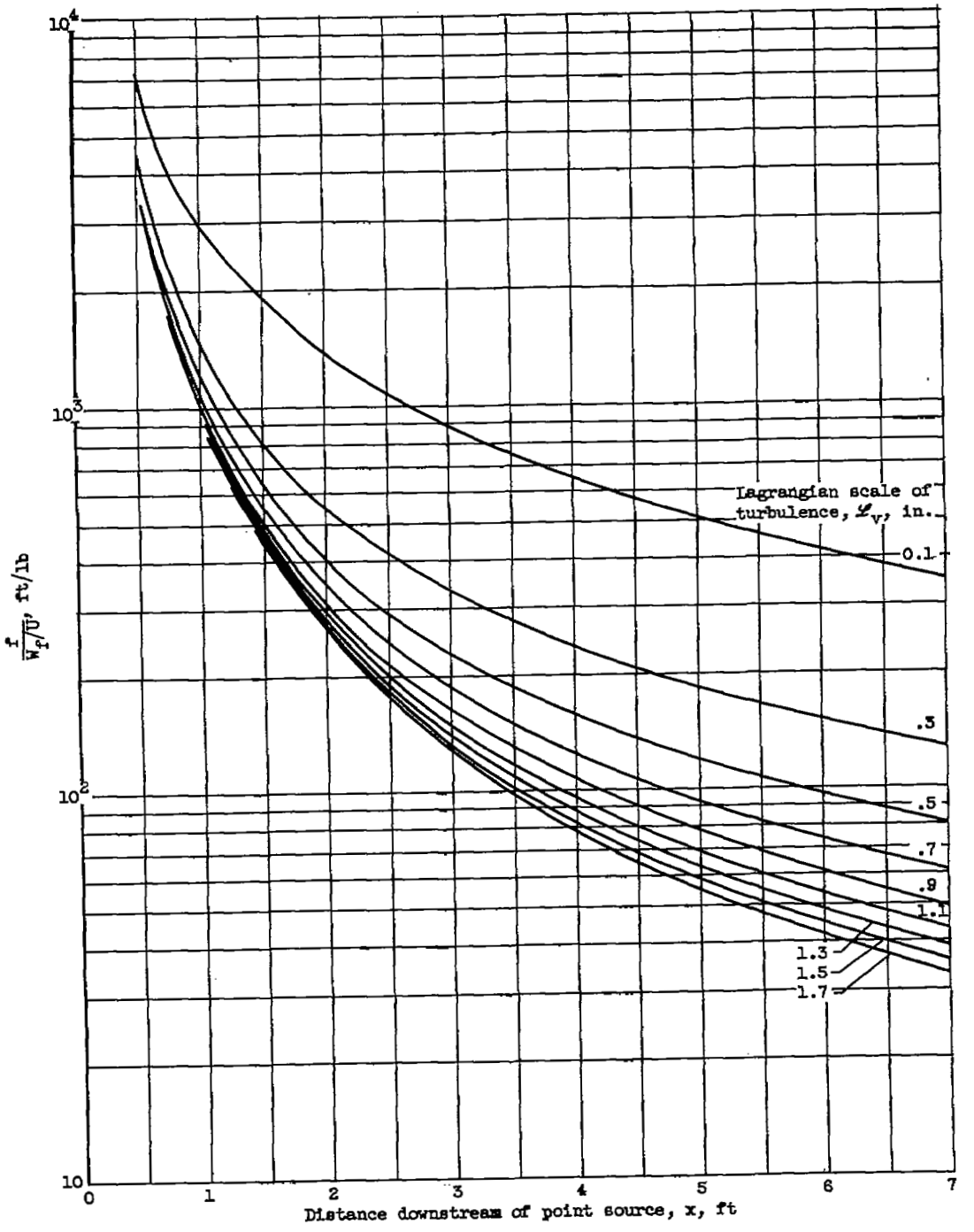

(a) Turbulence intensity, 0.05.

Figure II-38. - Effect of scale of turbulence on axial fuel-air ratio profile downstream of continuous point source of diffusion. Profiles based on equation (111); air density, 0.0764 pound per cubic foot.

3267

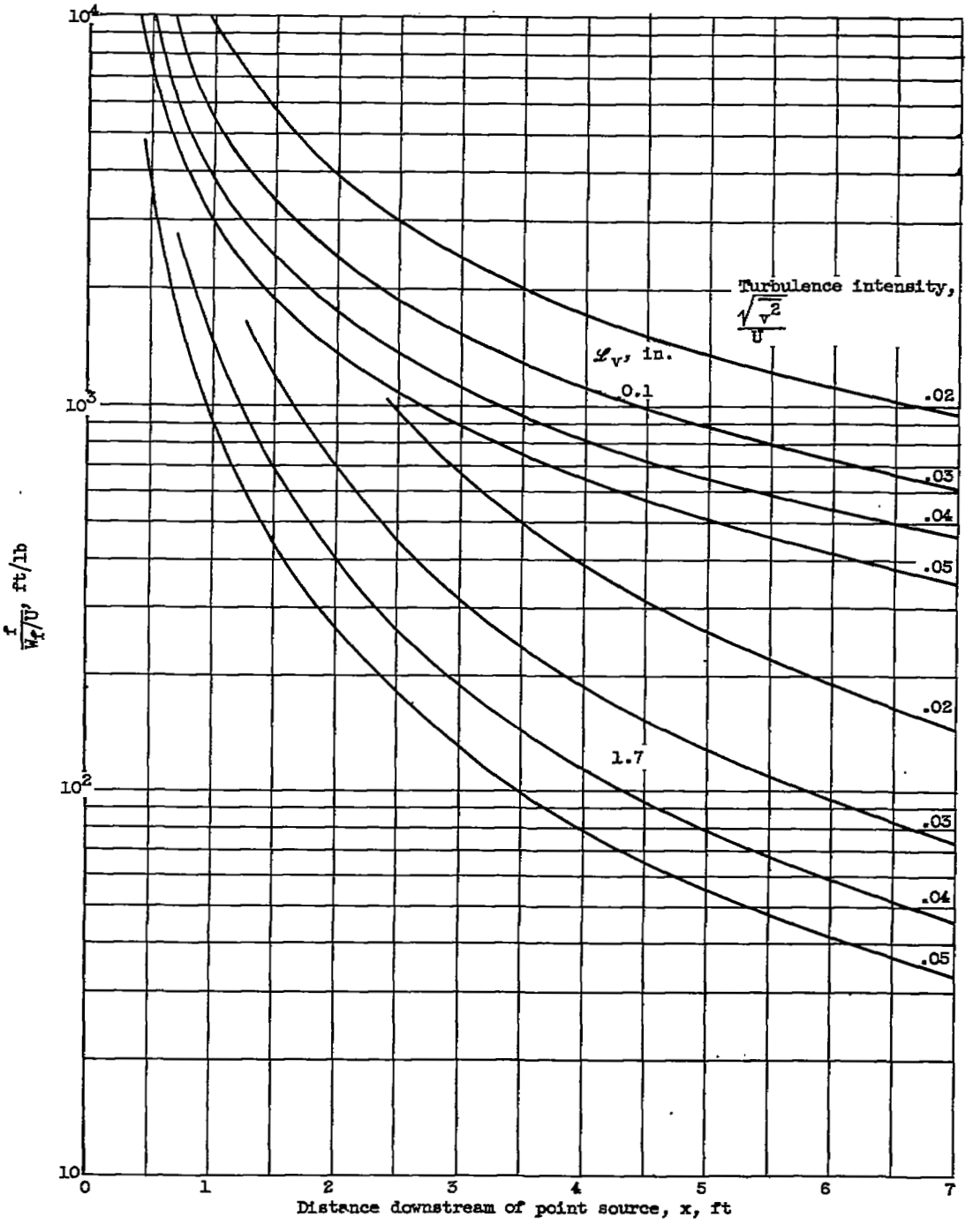

(b) Turbulence intensity as noted.

Figure II-38. - Concluded. Effect of scale of turbulence on axial fuel-air ratio profile downstream of continuous point source of diffusion. Profiles based on equation (111); air density, 0.0764 pound per cubic foot.

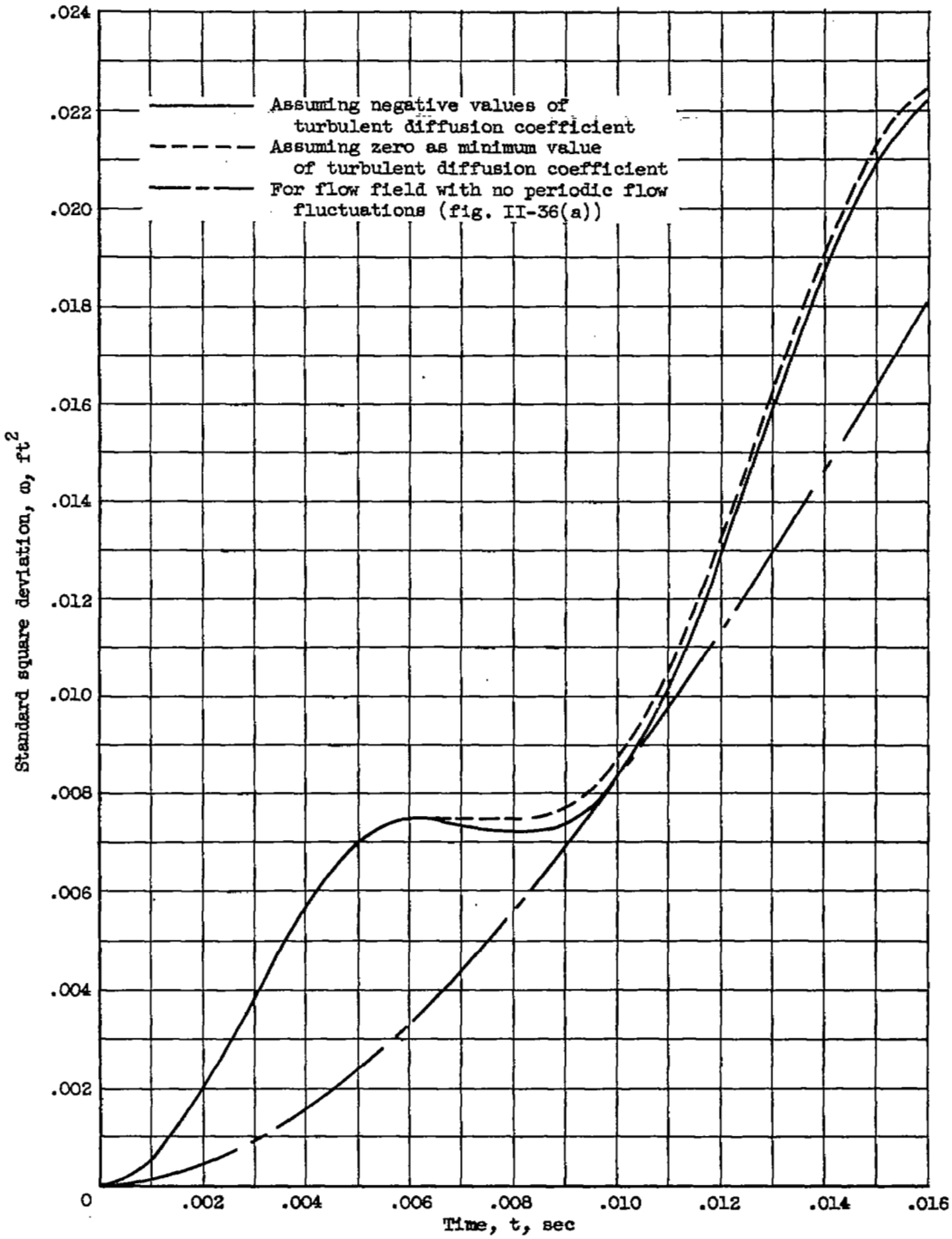

Figure II-39. - Standard square deviation for turbulent flow field with superimposed discrete velocity fluctuation.

3267

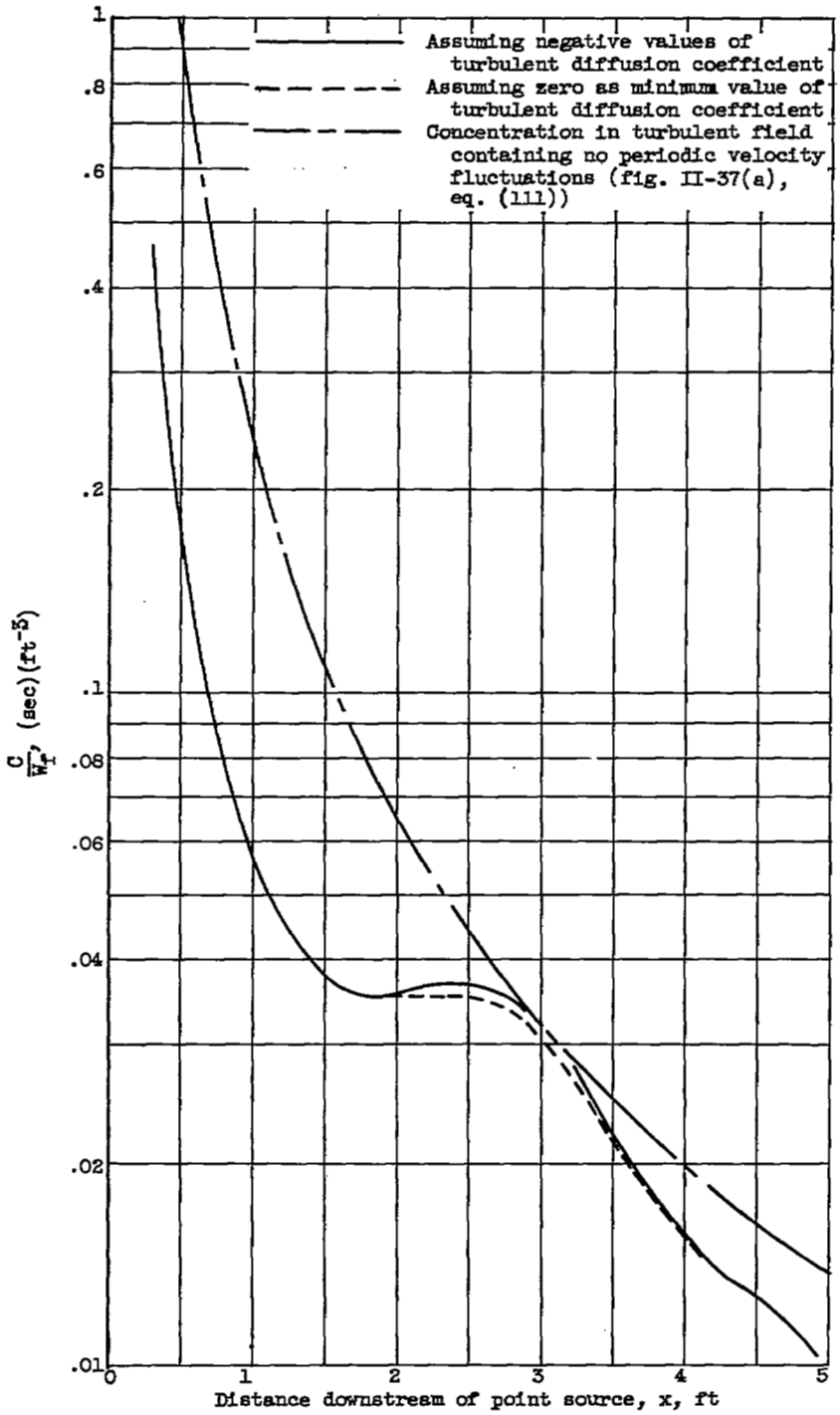

Figure II-40. - Concentration downstream of point source of diffusion in turbulent flow field with superimposed discrete periodic velocity fluctuation.

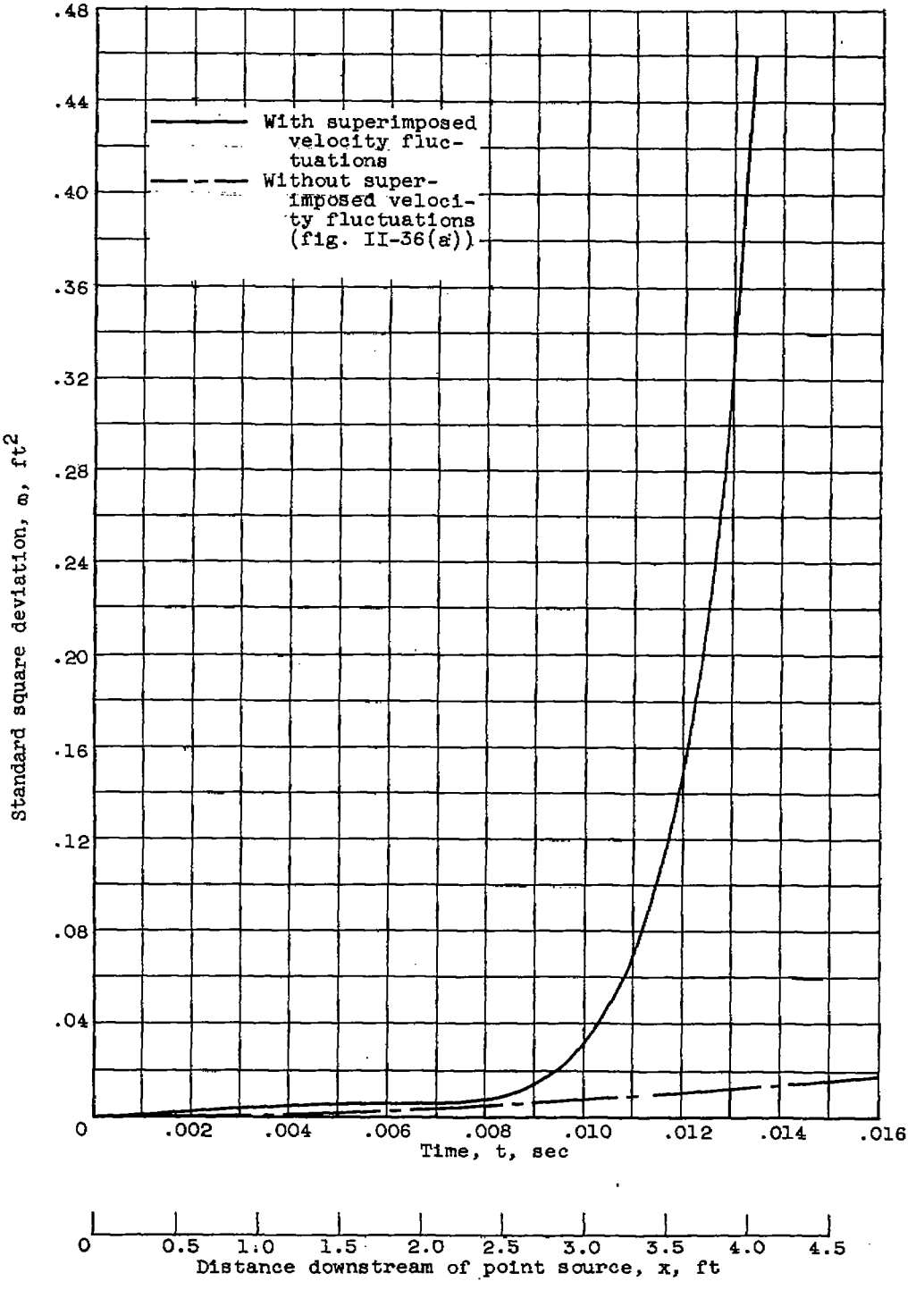

Figure II-41. - Standard square deviation for turbulent flow field with superimposed velocity fluctuations over finite band width.

[redacted]

3267

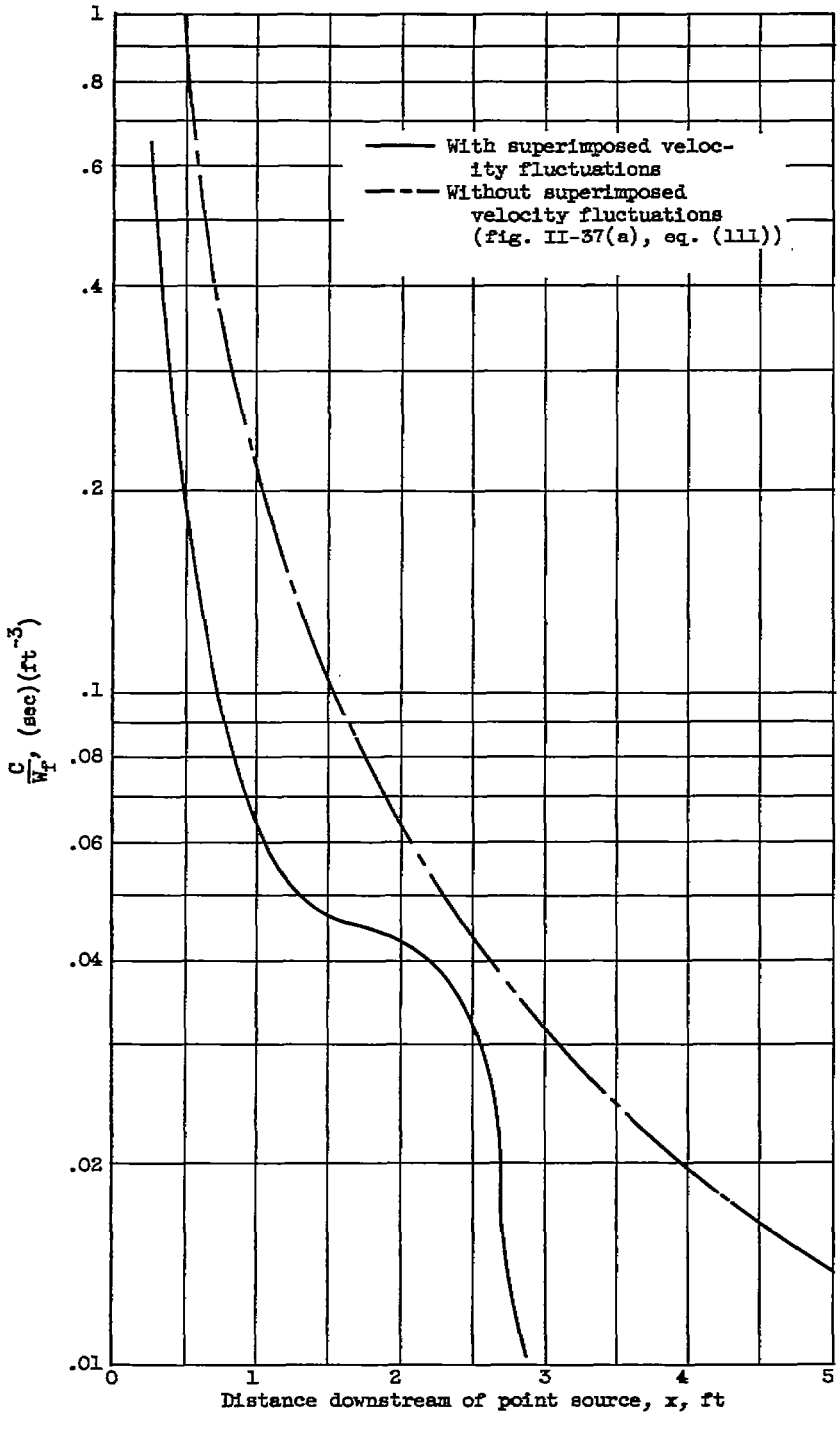

Figure II-42. - Concentration downstream of point source of diffusion in turbulent flow field with superimposed velocity fluctuations over finite band width.

[redacted]

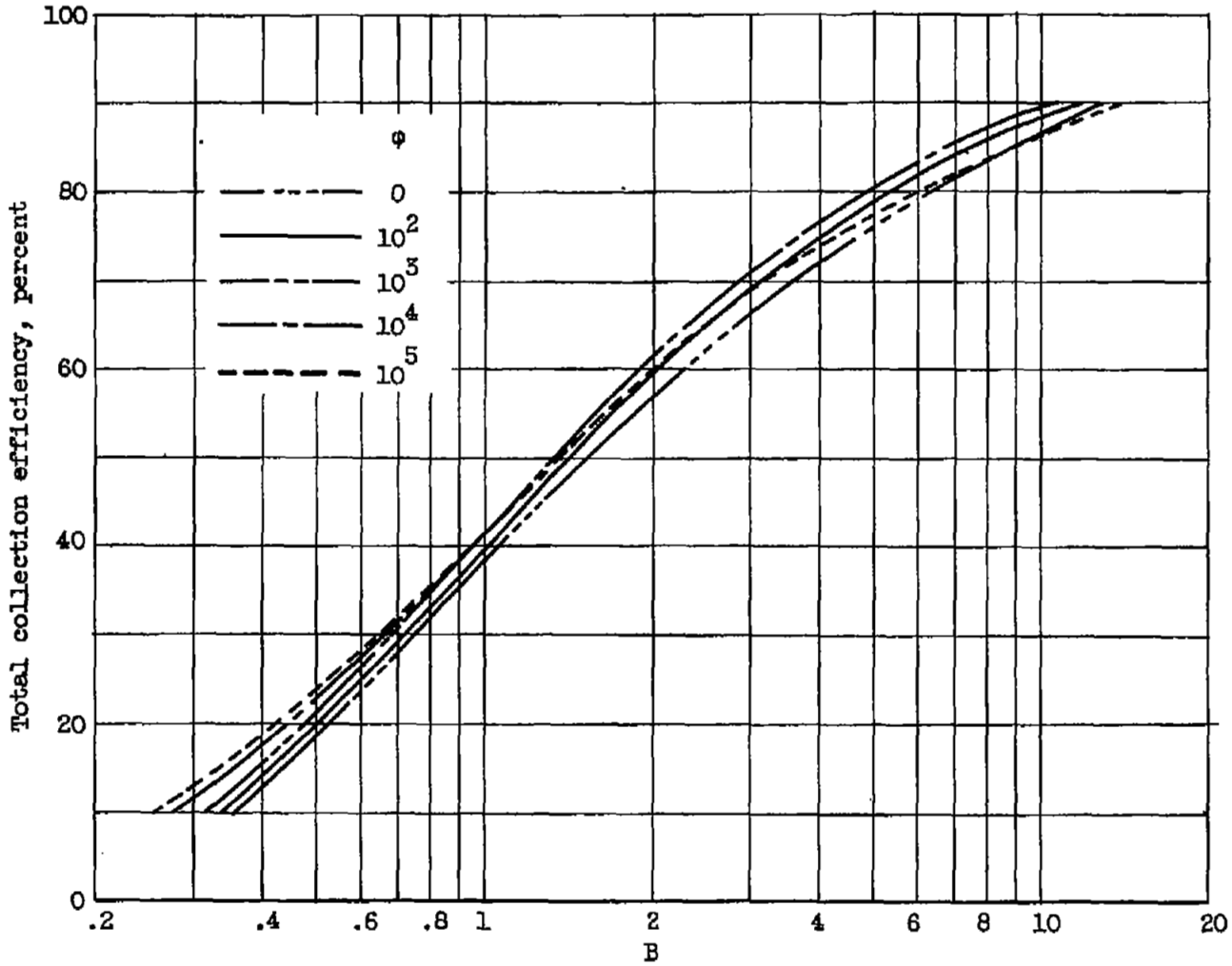

Figure II-43. - Total liquid droplet collection efficiency of cylindrical rod in moving air stream (ref. 76).

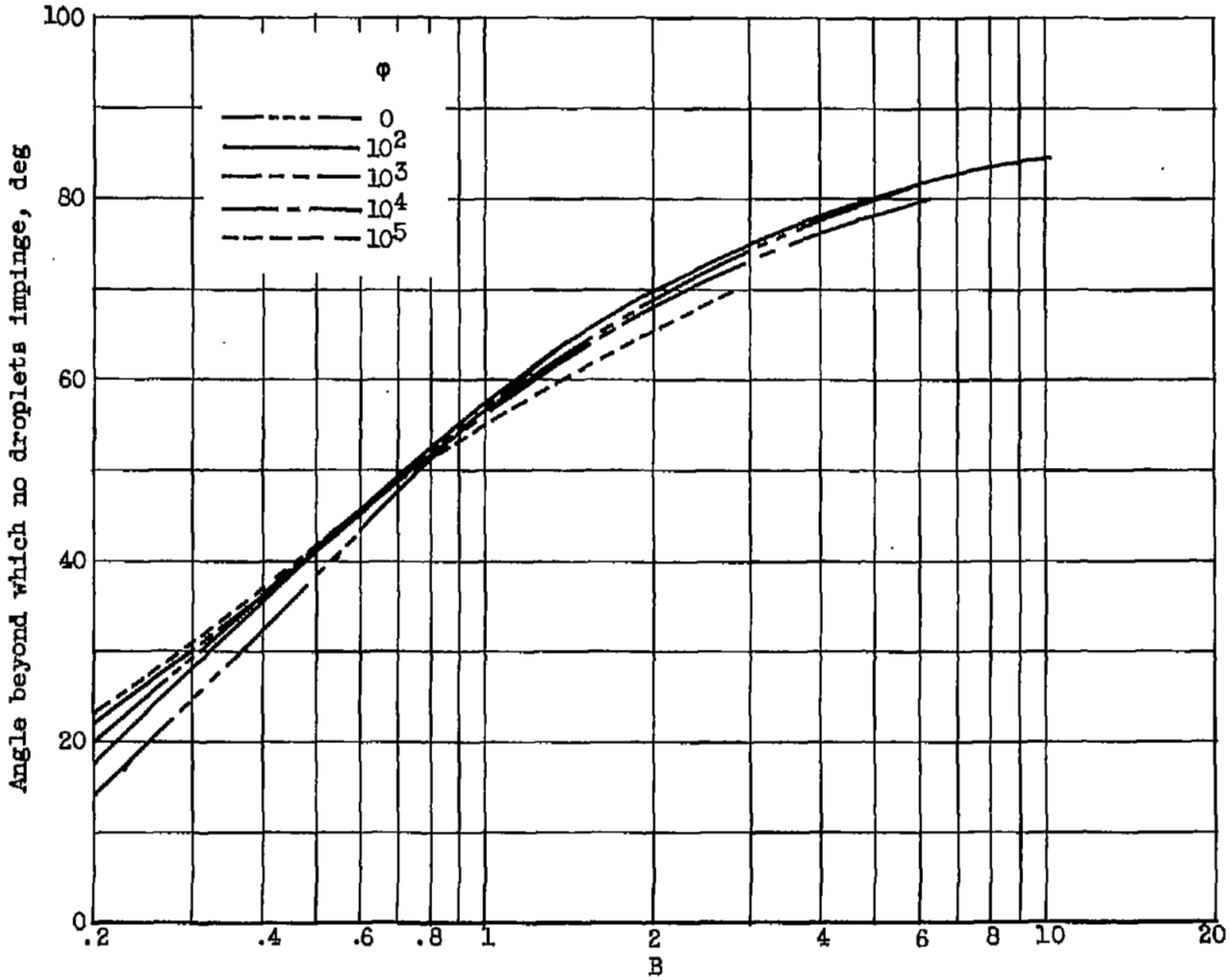

Figure II-44. - Angle beyond which no liquid droplets impinge on cylindrical rod in moving air stream (ref. 76).

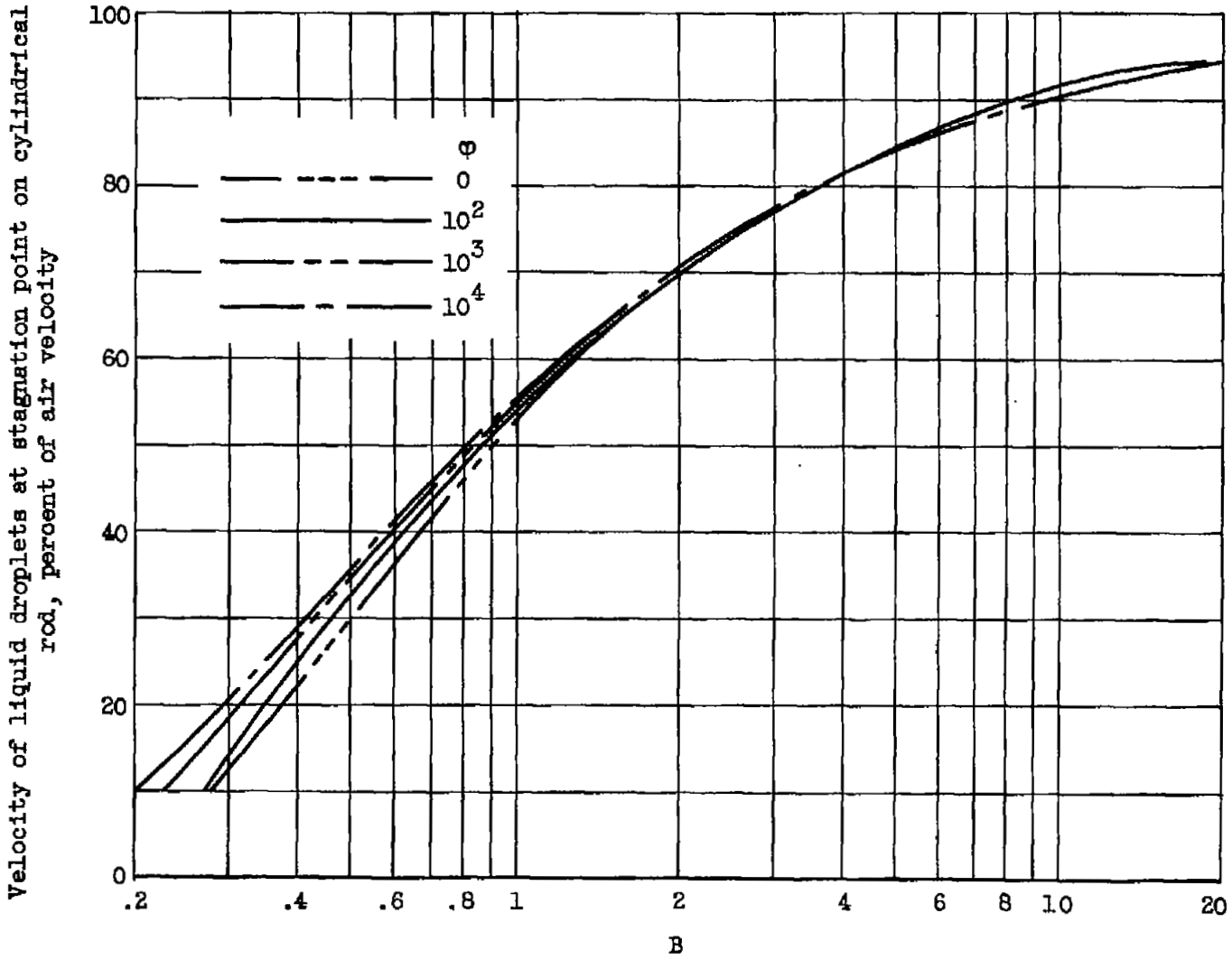

Figure 11-45. - Impact velocity of liquid droplets at stagnation point on cylindrical rod in moving air stream (ref. 76).

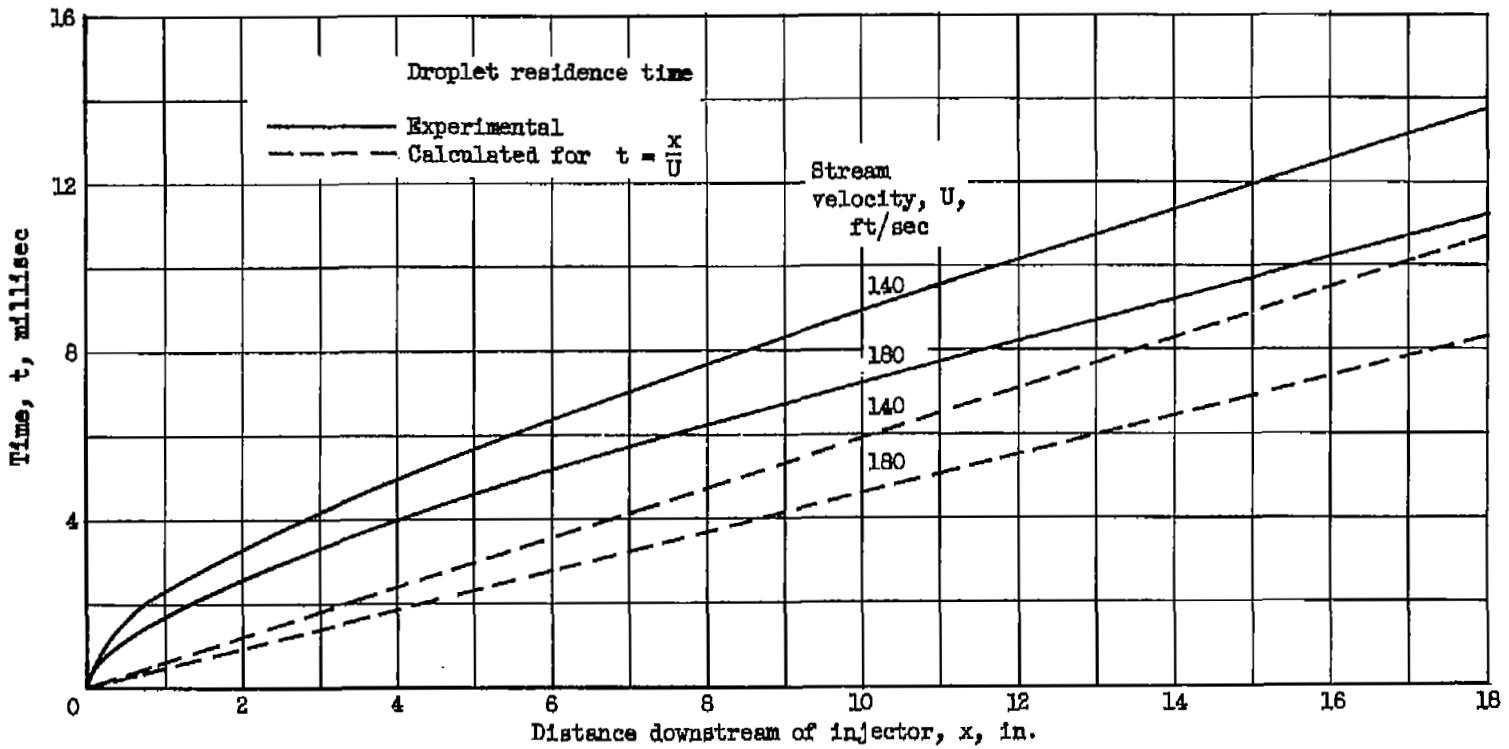

Figure II-46. - Fuel droplet residence time in simple-orifice, contrastream, isooctane evaporating spray.

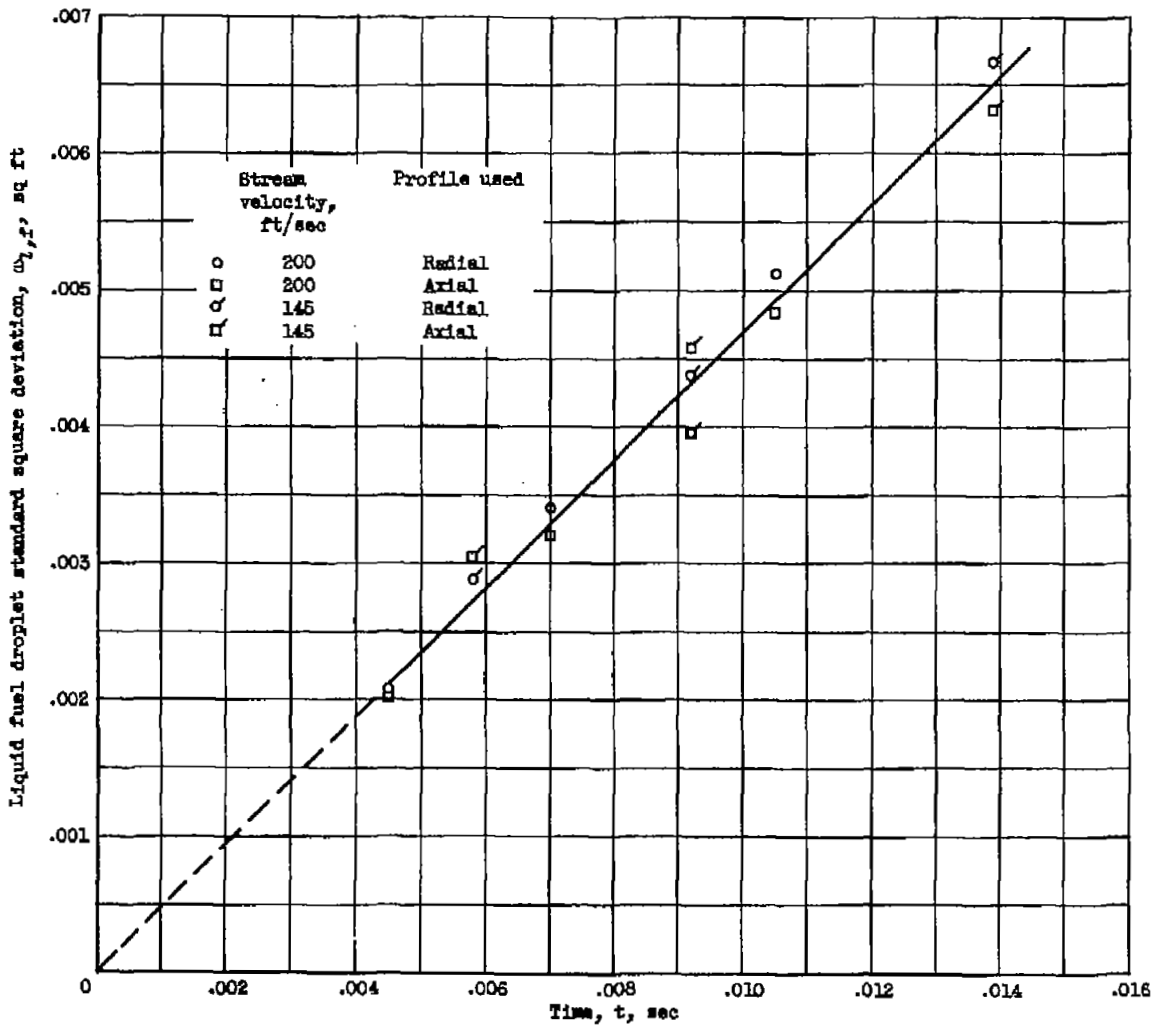

(a) Variation of stream velocity.

Figure II-47. - Isooctane liquid fuel droplet standard square deviation downstream of simulated point source.

3267

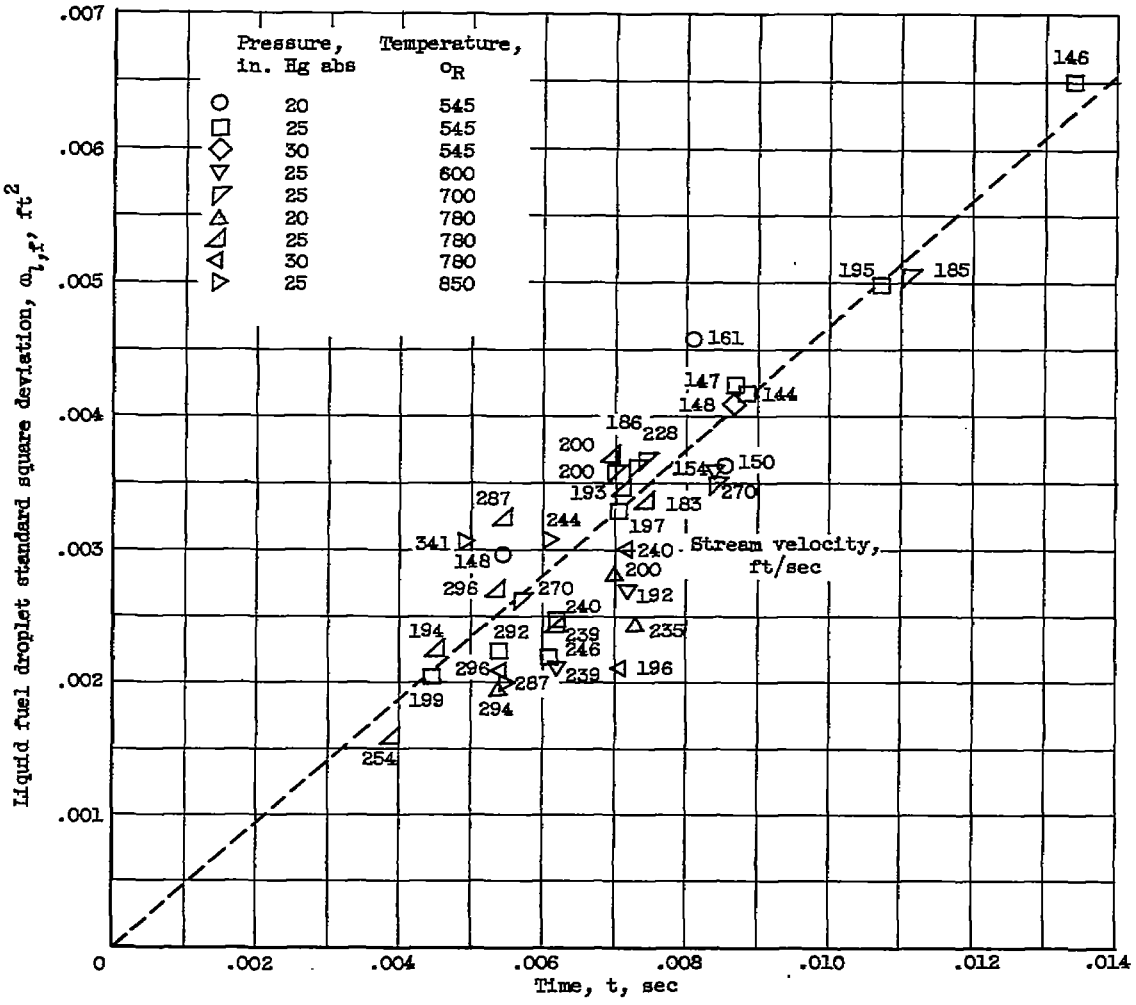

(b) Variation of pressure and temperature.

Figure II-47. - Concluded. Isooctane liquid fuel droplet standard square deviation downstream of simulated point source.

[redacted]

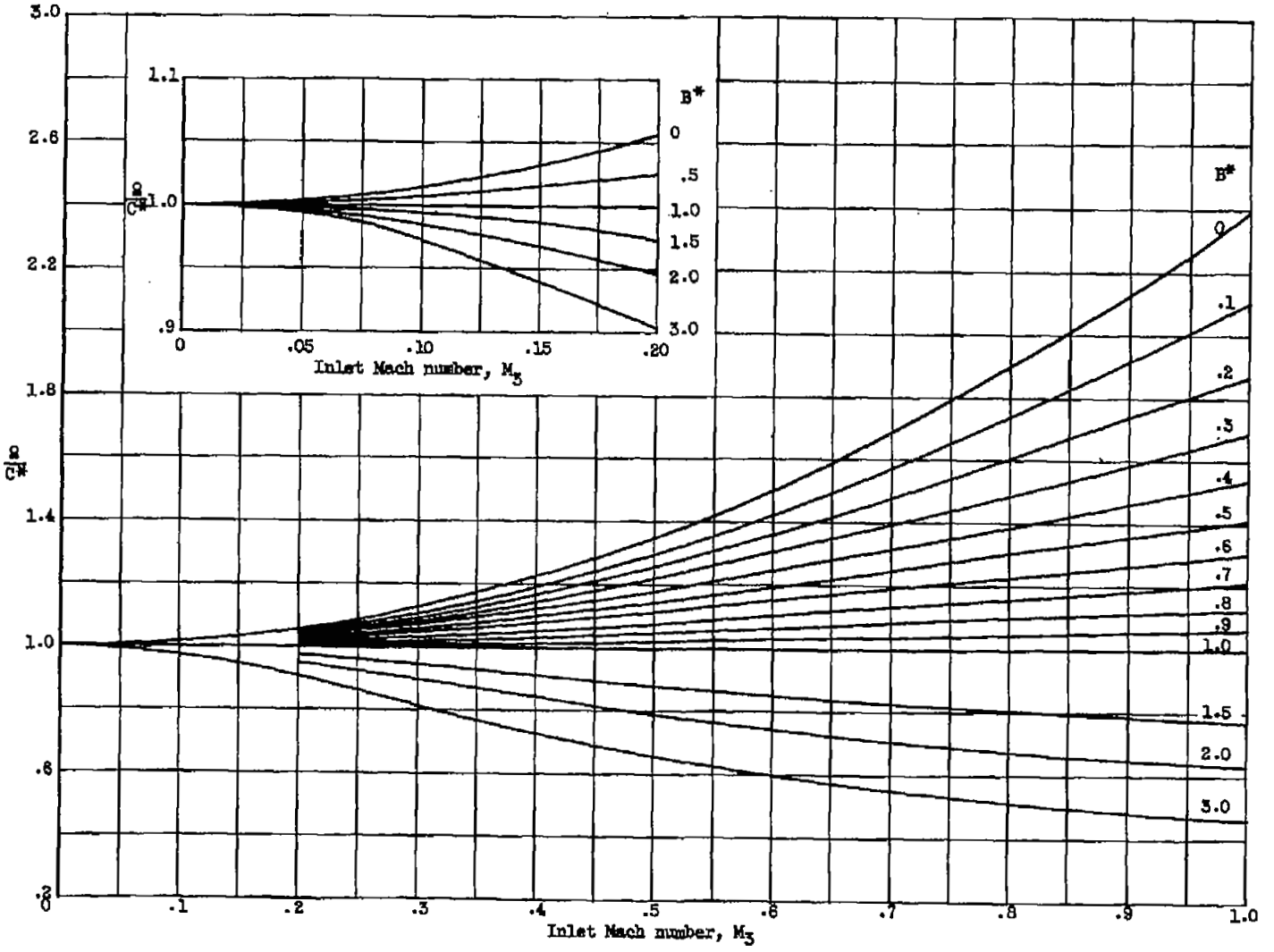

Figure II-48. - Values of parameter Ω for determination of mixing pressure losses of oblique and parallel gas streams (ref. 82).

CHAPTER III

IGNITION AND FLAMMABILITY OF HYDROCARBON FUELS

By Frank E. Belles and Clyde C. Swett

INTRODUCTION

There are many influences, both physical and chemical, that may act to set limits on ignition or flame propagation in fuel-air mixtures. The importance of these limits in high-speed combustors is evident; they may give rise to conditions in which the mixture cannot be ignited, or, if ignited, is incapable of sustained burning. It is the purpose of this chapter to discuss the experimental observations of flame quenching and of the limits of flammability, flame propagation, and ignition, and to draw from them some insight into the basic mechanisms that set the limits. Although most of the results in the literature have been obtained for homogeneous mixtures and for single fuels rather than multicomponent fuels such as those used in practical engines, there are many applications of both the data and the ideas to the operating problems of high-speed combustors.

A flammable mixture is defined as one capable of propagating flame indefinitely away from, and in the absence of, a source of ignition. That is, an ignition source such as an electric spark must be provided initially, but a flammable mixture will continue to propagate the flame even after the spark has been turned off, while a nonflammable one will not. In the nonflammable case, emission of light or some other evidence of chemical reaction may be observed, but this persists only while the ignition source is in operation.

A flammable mixture of fuel and air may be progressively diluted with either constituent until eventually a mixture results that is nonflammable. The limit of flammability is the borderline composition that separates mixtures capable of propagating a flame from those that are not. If the diluting agent is air, the limit mixture contains too little fuel to be capable of sustained flame propagation, and the borderline concentration is termed the lean or lower flammability limit. Conversely, if the diluting agent is fuel, the rich or upper flammability limit is reached. The flammability limits at a particular temperature and pressure obtained in this manner are often called the concentration limits. They may be made independent of any apparatus effects; therefore, these limits are physicochemical constants for each fuel. Mixtures of fuel concentrations between the lean and rich limits are said to lie within the flammable range.

It is sometimes observed that a flame in a mixture well within the flammable range will be extinguished if it is forced to propagate through a constriction. The walls are evidently able to exert some repressive influence on the flame. The effect is observable in Bunsen burners when the flow of mixture is suddenly stopped; if the burner tube is sufficiently wide, the flame will flash back and propagate into the stationary mixture, whereas with a smaller tube, it will be extinguished at the port. This effect of the walls on flame propagation is termed quenching. It is possible to determine a minimum diameter or a minimum rectangular opening through which a flame will travel, and such a dimension is a quenching distance.

Although the walls are able to set limits of flame propagation, these limits are not flammability limits in the true sense, since they are not physicochemical constants of the fuel. Rather, they are conditioned by the presence of walls.

SYMBOLS

The following symbols are used in this chapter:

B	geometrical factor
b	constant
C	fraction of molecules
C	constant
c	capacitance of condenser
c_p	heat capacity
D	diffusion coefficient
d	rod diameter
d_1	critical tube diameter
d_2	critical slit opening
E	apparent energy of activation
$f\sqrt{\overline{u^2}}$	function of intensity of turbulence
H	total ignition energy
H_L	energy in line source
i	current
j	energy from capacitance
K	constant
k	average rate constant
L	electrode spacing
L_q	quenching distance
l	inductance
N_f	number of fuel molecules per unit volume
p	pressure
R	gas constant
r	sphere radius

T temperature

T_F equilibrium adiabatic flame temperature

T_0 mixture temperature

t ignition lag

t_s spark duration

U gas velocity

U_F burning velocity

v voltage

$\varkappa$ thermal conductivity

FLAME QUENCHING

Before a discussion of flammability and ignition is begun, it is desirable to consider flame quenching. This phenomenon affects the process of flame propagation, with which flammability is concerned, and also that of ignition. The effects of quenching must either be taken into account or eliminated in the measurement of limits of flammability and of ignition energies, if meaningful interpretations of the data are to be made. In older literature, the importance of flame quenching was not understood, with the result that many misleading conclusions were reached.

As stated in the INTRODUCTION, quenching may be observed when a Bunsen flame is allowed to flash back into the burner tube. This fact serves as the basis for a standard means of measuring quenching distance. A flame is established on the burner port, and the mixture flow is then suddenly stopped. If the flame flashes back and propagates down the burner tube, a smaller one is substituted until the tube will just permit the flame to propagate. The diameter of the tube is thus the quenching distance for the given fuel-oxidant mixture under the specified conditions of temperature and pressure. In practice, a rectangular burner with a continuously variable width is often used, to avoid the frequent changes of tubes and to improve the precision of the measurements. An alternative procedure is to employ a fixed burner opening, and to change one of the conditions, such as pressure or mixture composition, until the condition corresponding to the specified quenching distance is determined.

It will be shown that quenching distances may be measured by entirely different means from the ones just described. This is possible because of the existence of quenching effects in measurements of flammability and spark-ignition energies of fuel-oxidant mixtures. Before these aspects are discussed, however, some of the data on the effects of variables on straightforward quenching-distance measurements will be presented.

Effects of Variables on Flame Quenching

All the experiments described in this section were conducted with homogeneous mixtures of gaseous or vapor fuel and air or some other oxidant. In addition, all the quenching distances were measured by means of the flash-back of burner flames into quiescent mixtures.

Geometry of quenching surface. - Reference 1 reports quenching distances measured by establishing a flame on a burner and then suddenly stopping the mixture flow. The flame either flashed back through the burner or was quenched at the port, depending upon the size of the burner. A variety of cylindrical and rectangular tubes was used, and the fuels were methane and propane in air at room temperature and atmospheric pressure.

The critical tube diameters and critical slit openings for flame propagation, that is, the quenching distances, were not the same. The critical diameters were larger than the critical slit openings. A geometrical factor B may be defined as

$$B = d_1/d_2 \tag{1}$$

where

d_1 critical diameter

d_2 critical slit opening

The data of reference 1 show that, for lean to stoichiometric mixtures, the average value of B is 1.25 for methane-air mixtures and 1.45 for propane-air mixtures.

Hydrocarbon type. - Friedman and Johnston have measured the quenching distances of mixtures of propane, benzene, n-heptane, and isooctane in air by determining the smallest opening of a rectangular burner that will permit a flame to flash back when the mixture flow is stopped (ref. 2). The data are presented in figure III-1, where quenching distance is plotted against percent stoichiometric fuel-air ratio. The experiments were carried out at 1 atmosphere pressure and 212° F ambient temperature.

Figure III-1 shows that mixtures slightly richer than stoichiometric are able to propagate flame through the narrowest channels. For lean and stoichiometric mixtures, the quenching distances decrease in the order: isooctane > n-heptane > propane > benzene. Reference 2 notes that this order is the same as the order of increasing burning velocities for the four compounds. In the case of rich mixtures, there are changes in the order of quenching distances, and it is not certain that there is any simple relation with burning velocity.

Although in all cases, the quenching distances are small under the conditions of the experiment, there are considerable percentage differences from fuel to fuel. For example, the quenching distance of a stoichiometric mixture of benzene in air at 1 atmosphere and 212° F is about 80 percent of that of a stoichiometric isooctane-air mixture.

Inert diluents. - For his work on the effects of inert gases on quenching, Friedman (ref. 3) used hydrogen as the fuel and conducted the experiments at ambient pressure and temperature. The inert gases used were helium, argon, nitrogen, and carbon dioxide. Mixtures of hydrogen, oxygen, and inert gas were prepared with a quantity of inert gas such that the calculated flame temperature of the stoichiometric mixture was 4244° F in all four cases.

Some of the data of reference 3 are shown in figure III-2. It is seen that, for a given mixture, the quenching distance decreases with the inert diluent used in the order: He > A > N_2 > CO_2, that is, the quenching effect of the walls on the flame is greater if the diluent is helium than if it is carbon dioxide. Although the combustible used was hydrogen, analogous results would almost certainly be obtained with a hydrocarbon fuel.

The results in reference 3 were interpreted on the basis of a thermal model of quenching, in which heat is conducted away from the flame by the walls. This analysis indicated that the quenching distance should be proportional to the factor

$$\varkappa/U_F c_p \tag{2}$$

where

c_p heat capacity per unit volume of unburned gas

U_F burning velocity of mixture

$\varkappa$ thermal conductivity of mixture

This parameter correlated the quenching-distance data for various inert diluents in a satisfactory manner. However, it is emphasized (ref. 3) that no conclusion could be drawn as to the true mechanism of quenching, and that diffusion of active particles to the walls might be important.

Temperature. - Friedman and Johnston (ref. 4) have studied the effects of temperature on quenching distance. Increased temperature decreases the quenching distance; that is, the flame is able to pass through smaller openings. The results shown in figure III-3 for propane-air mixtures at about 1 atmosphere pressure are consistent with the general observation that chemical reactions are promoted by increase in temperature. No quantitative interpretation of the data has yet been made. The magnitude of the temperature effect varies with mixture composition; for rich and stoichiometric propane-air mixtures, quenching distance is approximately proportional to the -0.5 power of the absolute temperature, while for lean mixtures, the exponent increases.

Pressure. - Friedman and Johnston have also studied the effects of pressure on the quenching distances of propane-air flames (ref. 4) and of benzene-, n-heptane-, and isooctane-air flames (ref. 2). A rectangular burner was employed, as previously described.

Some of the data of reference 4 are presented in figure III-4. Quenching distance increases as pressure decreases. That is, the quenching effect of the walls on the flames becomes greater when the pressure is reduced.

A logarithmic cross plot of the data of figure III-4 for several propane concentrations is shown in figure III-5. Straight lines result, so that the pressure dependence of the quenching distance is of the form

$$d_2 \propto p^{-b} \tag{3}$$

where

b constant

p pressure

Reference 4 gave the value of the exponent b for the propane concentration corresponding to the minimum quenching distance as 0.91. Reference 2 subsequently showed that the pressure dependence of the minimum quenching distances of benzene-, n-heptane-, and isooctane-air flames is almost identical to that of propane-air flames. It therefore appears that, as a rough approximation for hydrocarbons burning in air,

$$d_2(\text{minimum}) \propto 1/p \tag{4}$$

In the case of propane-air mixtures, however, the value of the exponent of the pressure is slightly dependent on the propane concentration, and increases from lean to rich mixtures. The effect was noted in reference 5, using the data of reference 4, and also in reference 6. The following table shows the variation of the pressure dependence of quenching distance of propane-air flames with fuel concentration:

Stoichiometric fuel-air ratio, percent	Negative exponent of pressure, b	Reference
74	0.83	5[a]
74	.85	6
86	.84	6
87	.85	5[a]
100	.88	5[a]
100	.89	6
110	.91	4
124	.95	6
149	.98	6

[a]Using data of ref. 4.

The variations in b shown by this table do not appear very large, but, as can be seen in figure III-5, they are quite apparent in a logarithmic plot of quenching distance against pressure.

Oxygen concentration. - Reference 6 describes the effects of pressure on the quenching distances of flames in various propane-oxygen-nitrogen systems. The measurements were made with a variable-width rectangular burner over a pressure range from 2.99 to 29.92 inches of mercury absolute. Five oxidant atmospheres were used, containing 17, 21, 30, 50, and 70 volume percent oxygen. The effects of pressure on the quenching distances of flames in any given oxidant were very similar to those described in the preceding section.

At any given pressure and percent stoichiometric propane, it was found that the quenching distance decreased as the oxygen concentration of the oxidant increased. The effects are shown graphically in figure III-6, where data for stoichiometric mixtures and two pressures are presented. The decrease in quenching distance with increase in the amount of oxygen in the oxidant atmosphere is very rapid up to about 25 percent oxygen (air = 21 percent), and then becomes more gradual.

Dead Space

When a flame is adjacent to a surface, it is observed that the luminous zone does not extend completely to the surface. There is a region, the width of which depends on the experimental conditions, where the reactions appear to be quenched by the wall. The distance from the end of the luminous zone to the wall is called dead space. The dead space may easily be observed, for example, by sighting across the top of a Bunsen burner; it is seen that the base of the flame cone is situated a small distance above the burner port.

Thus, it is evident that the wall quenches the flame reactions in the gas adjacent to it. It is therefore logical to consider the topic of dead space in connection with a discussion of quenching distance.

It might at first appear that, if the dead space associated with a flame propagating through a rectangular duct were measured, the dead space should be equal to one-half the quenching distance under the same conditions. This interpretation is based on the idea that the quenching distance corresponds to a situation in which the flame has zero width, because of the merging of the dead spaces associated with two walls when the walls are brought sufficiently close together.

The fact is, however, that the quenching distance is considerably larger than twice the dead space (ref. 7). Part of the difference may be attributed to the fact that the measurement of dead space is complicated by uncertainty as to the boundary of the flame. For example, in visual measurements, the boundary is chosen as the farthest extent of the luminous flame zone; on the other hand, if photographs are taken, the boundary will almost certainly appear to be in a somewhat different position because of the differences in sensitivity between the optical system and the human eye.

Aside from these experimental uncertainties, however, it is still reasonable that the quenching distance between parallel walls should not be equal to twice the dead space associated with one wall. This is because the same flame is not observed in the two cases: the dead space is associated with a propagating flame, while the quenching distance, by definition, is the smallest opening that will just permit a flame to propagate, or, equivalently, the opening that will just prevent propagation. Furthermore, it has been observed in connection with the measurement of quenching distances in circular tubes that above the critical diameter the flame appears to fill the cross-section tube; at the quenching condition, the flame is extinguished at the mouth of the tube (ref. 5). In other words, there does not appear to be any marked diminution in the size of the flame as the quenching condition is approached.

Thus, the dead space is a characteristic distance associated with a flame, and it arises through the quenching action of the walls, but it is not equivalent to the quenching distance.

There have not been many experimental studies of dead space. Reference 7 contains a summary of the work. Qualitatively, dead space varies with fuel concentration and with pressure in much the same way as does quenching distance. For example, the minimum dead space occurs in butane-air mixtures that are slightly richer than stoichiometric, and increases as the pressure is decreased (ref. 7).

Homogeneous Quenching

The discussion of quenching has heretofore been concerned with the effects of walls on the flame. The effects must occur because the walls absorb heat or free-radical chain carriers of the flame reactions, one or both of which must be transferred ahead of the flame to the unburned gas in sufficient quantity if the flame is to continue propagating (see ch. IV). These considerations suggest the possibility that a flame might be quenched by the combustible gas itself. Such homogeneous quenching might occur, for example, with a flame propagating in a turbulent mixture. If the turbulent intensity were sufficiently high, the dilution of the flame zone with cold unburned gas might overwhelm the transfer of heat and chain carriers from the burning zone to the surrounding fresh gas, and the flame would then be extinguished.

The situation described has received very limited experimental attention. In the only available literature concerning this phenomenon (ref. 8), the spread of flame from a nucleus in a flowing turbulent stream through a tube was studied. The turbulence was pipe turbulence, and the mixture of propane and air was periodically

ignited by a spark across the full width of flow. Inasmuch as there was no flame holder, the flame traveled downstream with the flow and was observed stroboscopically. At the limits of flame propagation, the mixture was ignited at the spark, but the flame nucleus decreased in size and was finally extinguished as it traversed the test section. The range of propane concentrations over which propagating flames were obtained was determined for flow velocities up to 250 feet per second. Typical curves, obtained at a static pressure of 30.7 inches of mercury absolute, are shown in figure III-7, where the concentration range of propagation is seen to narrow with increasing flow velocity. The lean limit of flame propagation changes less rapidly than the rich when the data are plotted in terms of percent stoichiometric, and the two limits tend to converge on the stoichiometric propane concentration. A Reynolds number of 2000 in these tests corresponded to about 12 feet per second flow velocity; therefore, the data apply to the turbulent regime. In one series of experiments, a screen was inserted upstream of the spark; this reduced the turbulent scale, but there was no appreciable effect on the range of mixtures capable of propagating flame at a given velocity. Reference 8 offers no conclusive explanation of the behavior of the lean limit curve at flow velocities less than 50 feet per second.

Inasmuch as the turbulent intensity increases with increasing flow velocity, the experiments indicate that the idea of homogeneous quenching by dilution with a combustible mixture may have some physical reality; reference 8 suggests this mechanism to explain curves similar to those of figure III-7.

Interpretations of Wall Quenching

In order to interpret the observed ability of walls to quench flames in terms of fundamental processes, it is first necessary to decide upon the mechanism by which a flame is presumed to propagate, and then to examine the influence of the presence of walls upon this mechanism. Inasmuch as a flame is a zone of intense chemical reaction accompanied by the evolution of heat and the formation of new products from the reacting fuel and air, there exist steep gradients of temperature and concentration from the flame to the unburned gas.

It is possible to set up differential equations that govern the flow of heat and of various molecular species that must occur as a result of these gradients. In order to use the equations and to obtain solutions by ordinary means, however, it is necessary to make certain assumptions. This matter is discussed in chapter IV. At this point, it may suffice to say that, although both heat and matter must flow from the flame because of the gradients that exist, and although the transfer of both heat and matter are probably essential features of the basic mechanism of flame propagation, in the past, one or the other of these two types of transfer has been chosen as most important. In other words, in order to make the basic differential equations amenable to solution in closed form, it was sometimes assumed that the transfer of heat from the flame to the unburned gas is the most important process in flame propagation, and that the diffusion of matter is much less important. In other cases, the opposite point of view was adopted. In either case, the assumption made can be justified in various ways.

As a result of the considerations discussed, two schools of thought have arisen concerning the most important mechanism responsible for flame propagation. One emphasizes the importance of heat conduction from the hot to the cold gas, since it is known that chemical reactions can be started and accelerated by an increase in temperature. The other stresses the importance of the diffusion of certain active particles (free radicals and atoms) known to be produced in flames; because of their highly reactive and energetic nature, these active particles are supposed to be able to initiate chemical reactions in the cold gas. Actually, as stated previously, both features may be important.

Thus, interpretations of the quenching effect start with the assumption of one of these two processes as the more important one, and then identify the walls as a sink for either heat or active particles. On the basis of these models, the flame is quenched if the walls abstract more than some critical amount of heat or active particles. The resulting interpretations may be described as either thermal or diffusional interpretations.

Actually, the distinction is not as clear as might be inferred. For example, references 3 and 9 describe interpretations of quenching distance that are based on heat transfer to the cold walls, but in both cases, the equations involve the experimental burning velocity of the mixture (see ch. IV). Consequently, there is the possibility that, if the burning velocity depends upon diffusion of active particles, these quenching theories are not uniquely thermal.

The theory developed in reference 3 was used, as described, to correlate data on the effects of various inert diluents on the quenching distances of hydrogen-oxygen-diluent mixtures. The correlating parameter (eq. (2)) was quite successful; it has not been applied to other types of quenching data.

The theory of reference 9 is based on the combustion-wave theory of Lewis and von Elbe (ref. 10), and has been applied to quenching distances of methane-oxygen-nitrogen mixtures at atmospheric pressure. With the use of an experimental burning velocity, it is possible to solve the equations to obtain an estimate of the absolute value of the quenching distance of a mixture. In reference 9, these calculations are made and the results compared with experimental values. Quenching by tubes and by rectangular burners was considered. Some of the results are reproduced in the following table:

Mixture, percent by volume										
Methane	10	15	25	40	50	52.5	10.0	16.3	21.5	26.4
Oxygen	90	85	75	60	50	47.5	18.8	29.3	39.8	49.1
Nitrogen	0	0	0	0	0	0	71.2	54.4	39.7	24.5
Quenching distance										
Critical slit openings, d_2										
Experimental	0.086	0.046	0.028	0.043	0.15	0.22	0.28	0.079	0.053	0.045
Calculated	.086	.039	.019	.033	.09	.14	.17	.056	.038	.039
Percent deviation	0	-15	-32	-23	-40	-36	-39	-29	-28	-13
Critical diameters, d_1										
Experimental	0.118	0.068	0.048	0.069	0.215	0.325	0.335	0.142	0.092	0.070
Calculated	.190	.094	.039	.065	.190	.340	.354	.117	.075	.061
Percent deviation	61	38	-19	-6	-12	5	6	-18	-18	-13
$B = d_1/d_2$										
Experimental	1.37	1.48	1.71	1.61	1.43	1.48	1.20	1.80	1.74	1.56
Calculated	2.21	2.41	2.05	1.97	2.11	2.43	2.08	2.09	1.97	1.56

From these data, it may be seen that the theory of reference 9 is capable of predicting reasonably well the observed values of d_1, d_2, and B.

In contrast to the two thermal treatments of quenching described, reference 5 presents a diffusional interpretation based on the destruction of active particles at the wall. It was assumed that the diffusion of active particles ahead of the flame, where they react with fuel molecules, is responsible for flame propagation, and that when the flame is near a wall, a certain proportion of the active particles is lost by collision with the surface. On this basis, it was possible to set up a balance between the number of collisions of active particles and fuel molecules required to propagate the flame, and the number of active particles lost by diffusion to the wall. The important active particles were assumed to be the light, rapidly diffusing species H, O, and OH. The quenching distances for lean to stoichiometric mixtures could be calculated from the resulting equations with surprisingly good accuracy. Separate equations were developed for two cases: (1) The critical diameter for flame propagation in a cylindrical tube:

$$d_1 = \left\{\left[\frac{32T_F^2}{(298)^2\ N_f}\right]\left(\frac{C}{k}\right)\left(\frac{1}{\frac{p_H}{D_H} + \frac{p_O}{D_O} + \frac{p_{OH}}{D_{OH}}}\right)\right\}^{\frac{1}{2}} \tag{5}$$

where

C fraction of molecules present in gas phase which must react for flame to continue to propagate

D_H, D_O, D_{OH} diffusion coefficients of H, O, and OH at 77° F and 1 atm

d_1 critical tube diameter for propagation in a given fuel-air mixture at a particular pressure

k average rate constant for reaction of active particles with fuel molecules

N_f number of fuel molecules per unit volume

p_H, p_O, p_{OH} equilibrium partial pressures of H, O, and OH in flame

T_F equilibrium adiabatic flame temperature

(2) The minimum width of the opening for propagation through a rectangular slit:

$$d_2 = \left\{\left[\frac{12T_F^2}{(298)^2\ N_f}\right]\left(\frac{C}{k}\right)\left(\frac{1}{\frac{p_H}{D_H} + \frac{p_O}{D_O} + \frac{p_{OH}}{D_{OH}}}\right)\right\}^{\frac{1}{2}} \tag{6}$$

where

d_2 critical opening of rectangular slit for propagation

Equations (5) and (6) were used to make absolute calculations of quenching distances for propane-air mixtures over a range of concentrations from lean to stoichiometric and pressures less than 1 atmosphere, and for stoichiometric ethene-air and isooctane-air mixtures in a similar pressure range (ref. 5). All quantities in the

equations were calculated or estimated, except the constants C and k. It was found that C could be approximated by the lean concentration limit of flammability measured at atmospheric pressure, and that a suitable value of k could be derived from burning-velocity data. These constants have specific values for a given fuel and oxidant; therefore, it is not required to use a separate experimental value for the calculation of quenching distance at each condition. It will be recalled that the theory of reference 9 requires a value of the burning velocity for each condition at which an absolute calculation of quenching distance is made. The agreement between observed and calculated quenching distances shown in reference 5 was quite striking, with an average difference of ±3 percent. The agreement was probably in some degree fortuitous, and depended in part on the choice of the diffusion coefficients and the choice of the temperature dependence of the diffusion coefficients.

However, equations (5) and (6) may be used to correlate quenching-distance data if the ratio C/k is left as an undetermined constant. This was done in reference 5, and also in reference 6, where the effects of pressure, propane concentration, and oxygen concentration in the oxidant were found to be correlated. In reference 6, it was found that the choice of diffusion coefficients and temperature dependence did not affect the result.

In addition, this treatment predicts the following value for the geometrical factor B:

$$B = \frac{d_1}{d_2} = \left(\frac{32}{13}\right)^{\frac{1}{2}} = 1.64 \tag{7}$$

This result is in agreement with experiment. Finally, it was found that the pressure exponent b (eq. (3)) and its variation with fuel concentration are reasonably well predicted (refs. 5 and 6).

All three of the interpretations discussed have had some success. No two have been applied to the same set of experimental data; hence, direct comparisons cannot be made at present. The diffusional treatment has been used in more widely varying situations than the others, with good success, but it does not hold in its present form in the case of mixtures richer than stoichiometric.

Quenching in Flammability and Spark-Ignition Measurements

It was stated at the beginning of the discussion of quenching that measurements of flammability and spark-ignition energy may be affected by quenching. It is therefore sometimes possible to determine quenching distances from such measurements. It will now be shown briefly how these effects appear.

Flammability measurements. - The concentration limits of flammability are, if measured properly, true physicochemical constants for each fuel. Limits of this type are discussed in the following section. Determination of these limits has generally been limited to work at atmospheric pressure. However, some work has been done at lower pressures. Most of the observations at reduced pressures have indicated that the lean and rich limits of homogeneous mixtures progressively converge and finally meet at some pressure below which no flame will propagate. Most of the older literature on low-pressure limits should be regarded critically. In most cases, insufficient cognizance was taken of the effects of the size of the test vessel and the need for a powerful ignition source. Thus, many of the limits recorded are actually ignition limits for the particular source used, or are the result of quenching by the walls. For example, it was believed that mixtures of

ordinary hydrocarbon fuels in air could not sustain flame propagation below a pressure of about 1.2 inches mercury; it is now known that this minimum pressure is actually set by quenching due to the walls of the usual 2-inch-diameter tubes used in the experiments. The minimum pressure is lowered if larger tubes are used. Another difficulty in measuring limits at pressures other than atmospheric is the need to maintain the pressure constant during the propagation of the flame.

Recent work has avoided these difficulties, and has clarified the meaning of the limits at reduced pressures (ref. 5). Care was taken to eliminate any effects of the ignition source, and the flame tubes were connected to a large plenum so that the flames propagated at essentially constant pressure. The limits were measured for homogeneous fuel-air mixtures in flame tubes of several diameters. Typical results for propane-air are shown in figure III-8 (ref. 5). It is seen that the lean-limit concentration is lower for the larger tubes, as is the minimum pressure for flame propagation. The rich limit, although not shown in figure III-8, also increases with increasing tube diameter; therefore, the flammable range at a given pressure is wider for the larger tubes.

Inasmuch as the diameter of the flame tube affects the results, it is evident that these limits are not true flammability limits. That is, they are not physicochemical constants of the fuel. They are better termed limits of flame propagation at reduced pressures. The behavior of the data suggests that the limits are set by quenching action of the tube walls, and in order to test this idea, logarithmic cross plots of the data of figure III-8 were made at constant propane concentrations on the lean side of stoichiometric (fig. III-9).

Friedman and Johnston (ref. 4) measured quenching distances for propane-air flames in terms of the critical width of a rectangular slit that would allow flashback of a Bunsen flame when the mixture flow was reduced. Some of their data are also shown in figure III-9; the critical slit widths have been multiplied by an empirical factor of 1.4 to account for the geometrical differences between the experiments. Figure III-9 shows that the two types of data nearly coincide. Therefore, it was concluded that the measured pressure limit of flame propagation of a given mixture in a tube of a particular size is actually a measurement of the critical diameter, or quenching distance, for flame propagation in the mixture at the pressure of the limit (ref. 5).

Spark-ignition energy measurements. - Spark-ignition energy is measured by determining the minimum amount of energy that must be dissipated in the gap between two electrodes in order to produce a flame. It has been found that, for a given temperature, pressure, and fuel-air mixture, this energy depends upon the length of the gap (refs. 11 and 12). Typical results are shown in figure III-10 for natural gas at 1.0 atmosphere pressure and in figure III-11 for propane at 3.0 inches of mercury absolute. It should be noted that, regardless of the electrode geometry, the curves converge at some minimum ignition energy as the electrode gap is increased from low values. The most striking curve is the one shown in figure III-10 for flanged electrodes; it is seen that the minimum spark-ignition energy increases with extreme rapidity if the electrodes are closer than about 0.08 inch. In other words, the flanged electrodes have the effect of suppressing ignition altogether if the gap is less than some critical width.

The function of the ignition spark is to supply the energy required to initiate the chemical reactions of a self-propagating flame. From the preceding discussion of wall quenching, it is evident that a flame cannot propagate through the gap formed by the flanged electrodes if the distance is less than the quenching distance. Consequently, if the gap is less than the quenching distance, the mixture cannot be ignited regardless of the amount of energy supplied.

In the experiments with unflanged electrodes, the quenching distance is not so well defined; increasing the energy supplied to the gap overpowers the quenching effects, and a propagating flame can be obtained. However, it is significant that, in figure III-10, the start of the rising portion of the curve obtained with unflanged electrodes coincides with the quenching distance.

Finally, it will be shown that the quenching distance obtained from spark-ignition experiments is the same or very nearly the same as that obtained by the usual means, that is, by determining the critical slit opening for flash-back of a Bunsen flame. It is also the same as the critical diameter obtained from low-pressure limits of flame propagation, as described in the preceding section, multiplied by a constant to account for the geometrical differences in quenching effect by cylindrical and plane-parallel surfaces. Data of all three types are plotted in figure III-12, and it is seen that the points conform very well to a single line (ref. 5).

Thus, it has been shown that the same quenching effects that have been studied by means of flash-back also extend to measurements of flammability at reduced pressures, and to measurements of spark-ignition energy. Wall quenching is therefore an important phenomenon at all stages of the combustion process, and must be considered if unambiguous interpretations of combustion data are to be made.

FLAMMABILITY LIMITS

Effects of Variables on Flammability Limits at Atmospheric Pressure

It is necessary in the measurement of lean and rich concentration limits of flammability to eliminate all external effects, so that the limit is a property only of the fuel at a given temperature and pressure. Coward and Jones (ref. 13) have critically reviewed the literature on flammability limits and have recommended the experimental procedure that will lead to the determination of true limits.

It has already been stated in the definition of flammable mixtures that the ignition source must not affect the results. If a weak source is used, some mixtures may not inflame, especially if they are near the limit concentration, while a stronger source would succeed in igniting them. The limits determined with the weak igniter would consequently not be limits of flammability, but merely limits of ignitibility for the particular source used. Thus, it is essential to use a strong source, such as a spark several millimeters long or a small naked flame.

In order to minimize quenching action by the walls, the vessel in which the flame is observed should be at least 2 inches in diameter for observations at atmospheric pressure. It should also be long enough (4 ft) to allow the observer to judge whether the mixture is truly capable of propagating a flame indefinitely away from the ignition source. A glass tube of these dimensions is a suitable vessel.

The ignition end of the tube should be open during the test, to avoid a change in pressure. Finally, it is important to specify the direction of flame propagation. Since it may be stated as a rough approximation that a flame cannot propagate downward in a mixture if the convection current it produces is faster than the speed of the flame, the limits for upward propagation are usually slightly wider than for downward or horizontal propagation.

The experimental results discussed are limited to those obtained with upward propagation, and subject to the precautions described, unless otherwise noted. In addition, only concentration limits of flammability at atmospheric pressure will be discussed; the effects of pressure will be considered later.

Hydrocarbon type. - The flammability limits of various hydrocarbon types in air at atmospheric pressure and room temperature are listed in table III-I (ref. 13). For the comparison shown in this table, the limits are expressed in terms of the percent of stoichiometric fuel-air ratio (by weight).

Although the results of table III-I indicate no striking effects of hydrocarbon type (above propane and propene) on the lean flammability limits, considerable variation among the rich limits is apparent. Among the saturated compounds (normal and isoparaffins), the rich limit tends to increase with molecular weight. Inasmuch as the lean limits are about the same for all the fuels, the range of flammability increases with molecular weight. Ranges of flammability calculated from the data of table III-I have been plotted to show this increase graphically (fig. III-13). A more complete set of data (ref. 14) indicates that the flammable range for normal paraffins passes through a maximum at n-heptane and decreases to n-decane. However, these data (ref. 14) are less accurate than those of table III-I because the work was done at reduced pressures, and extrapolations must be made to estimate the limits at 1 atmosphere pressure. In spite of these extrapolations, it is believed that the proper trends are indicated.

The branched-chain hydrocarbons (isoparaffins) have somewhat smaller flammable ranges than the corresponding straight-chain fuels (fig. III-13).

Among the three monoolefins listed, ethene stands out because of its extremely wide range of flammability (45.8 to 676 percent stoichiometric). The results for propene and 1-butene are similar to those for the corresponding saturated compounds. Figure III-13 emphasizes the anomalous nature of ethene. An extension of the curve for olefins, by means of the data of reference 14, would show that the flammable range increases rapidly from propene to 1-hexene, and then levels off through 1-decene.

The data for aromatic compounds are incomplete. The flammable range for benzene is smaller than that for a six-carbon-atom branched-chain fuel.

The flammability limits for cycloparaffins are not included in table III-I, but reference 13 shows them to be very similar to the limits of normal paraffins with the same number of carbon atoms.

Petroleum fuels. - The discussion thus far has been concerned with the flammability limits of pure hydrocarbons. On the other hand, practical aircraft fuels are complex mixtures of many hydrocarbons, each with its own effect on the limits of the mixed fuel. The limits of such fuels, however, may be measured in the manner previously described, if the apparatus is maintained at a temperature high enough to keep all constituents in the vapor phase.

Inspection of the data in table III-II (ref. 15) shows that, in order to obtain a consistent set of flammability limits for these four fuels, the limits of all would have to be determined at a rather high temperature. Perhaps the closest approach to the required conditions is found in experiments reported in reference 16. The limits determined at 300° F and atmospheric pressure for three fuels are listed in table III-III. The data of reference 16 were reported only in terms of fuel-air ratios; in order to express the limits in volume percent fuel vapor in air, it was necessary to estimate some average molecular weight for each fuel. This was done by the methods described in reference 14, with the following results: average molecular weight of 100/130 grade gasoline, 100; JP-1, 150; JP-3, 114. Assuming that the fuels are mainly composed of paraffin hydrocarbons, these molecular weights correspond approximately to heptane, decane, and octane, respectively. The limits for these compounds (table III-I) compare fairly well with the limits in table III-III, considering the approximations and the differences in temperature involved.

It seems definite, from these and other data, that the flammable range of aircraft fuels completely vaporized and mixed with air is about 1 to 7 percent by volume.

If multicomponent liquid fuels are not completely vaporized, quite different results may be obtained. Thus, if the tests are carried out at low temperatures and only part of the liquid sample is vaporized, the vapors will be composed mainly of the lower-boiling constituents. Mixtures of these vapors with air may be prepared, and the limits determined in the manner previously described. Both lean and rich limits should lie at higher concentrations (volume percent) than if the entire sample were vaporized, because the limits of the lighter hydrocarbons behave in this manner (table III-I). This expectation is verified by experiment; the lower the temperature, and hence the smaller the fraction of liquid fuel that serves as the source of vapor for making fuel-air mixtures, the higher the concentrations of the limits (ref. 16).

It is evident that the history of an aircraft fuel has an effect on its limits of flammability. For example, a fuel containing quantities of volatile hydrocarbons may be stored under conditions that permit their gradual escape and the limits will be more and more controlled by the heavier compounds. Consequently, it is difficult to predict the flammability of a given sample, and even more difficult to obtain reproducible results if the supply of fuel vapor is obtained from, for example, the first 10 percent of the liquid to evaporate.

The preceding discussion refers to unsaturated vapor-air mixtures. If a liquid fuel and its vapors are allowed to come to equilibrium in a volume of air, so that the air is saturated at the given temperature, the temperature itself sets the lean and rich limits. For example, grade 100/130 gasoline and JP-3 jet fuel have such high equilibrium vapor pressures at a temperature of about 78° F that saturated vapor-air mixtures are beyond the rich limit and are therefore nonflammable. As the temperature is lowered, however, a point will be reached on the vapor-pressure curve of the fuel that corresponds to the concentration of fuel in air at the rich limit. With still further reduction in temperature, the saturated mixtures will be flammable until a temperature is reached that corresponds to the vapor concentration for the lean limit. The two temperatures are referred to as the rich and lean temperature limits of flammability (at a given pressure). The range of temperatures corresponding to flammable saturated mixtures is lower for volatile fuels, such as 100/130 gasoline or JP-3, than for the less volatile JP-1 or JP-4. The temperature limits are discussed in reference 15.

It is not clear whether the temperature limits of flammability of saturated mixtures have any application to flowing mixtures of fuel droplets in air. It is perhaps conceivable that a spray of fuel droplets might come to equilibrium in the moving air stream if the turbulence level were sufficiently high to effect very rapid heat transfer and mixing of the vapor and air. Even if equilibrium were attained, however, the situation would be complicated by the effects of fuel droplets on the flammability of the vapor fuel - air - fuel droplet mixture, as well as by the effects of velocity and turbulence.

Mists and sprays. - Very little work has been done on the flammability of vapor fuel - air - liquid fuel mixtures. There are obvious difficulties in the measuring of flammability limits in quiescent mixtures because of the need to prepare reasonably stable mists, in which the droplets will not settle out before the ability to sustain flame propagation can be tested. In addition, it is necessary to characterize the average droplet size. Reference 16 (p. 40) reports measurements of the flammability of mists of JP-1 formed by chilling vapor fuel - air mixtures to condense some of the fuel. The average droplet size, measured immediately after formation, was 10 microns at 32° F. Under these conditions, the flammability

limits were at fuel-air ratios of 0.043 (lean limit) and 0.23 (rich limit). Considering the difference in temperature, the limits of JP-1 mists are similar to the limits of JP-1 vapor-air mixtures at 300° F given in table III-III (fuel-air ratios, 0.037 and 0.31). More specifically, an estimate of the effect of the 268° F temperature difference on the limits, based on the temperature effects on limits of homogeneous mixtures (to be discussed in a subsequent section), shows that the lean limit of the mist corresponds very closely to that of the vapor. The rich limit of the mist, however, is at a lower concentration than would be estimated from the data on homogeneous mixtures. It may be concluded that, at least with these small droplet sizes, the propagating flame is able to vaporize and consume the fuel without much penalty on the range of flammability.

Reference 16 (p. 43) also reports tests of the flammability of JP-1 fuel spray formed in a two-fluid nozzle (fuel and air) and ignited in a glass test chamber. The spray was found to propagate flame in the upstream direction down to a lean limit of 0.0394. It is not clear that this was a true limit of flammability, because of the uncertain effects of velocity, turbulence, and droplet size. For example, in other tests on the ignitibility of sprays, it was observed that individual drops were ignited on passage through a spark, and that as the fuel flow was increased, these merged into a long continuous flame at a fuel-air ratio of about 0.006; this value is much below the lean flammability limit (ref. 17). Such observations emphasize the need to define a criterion for the flammability of liquid sprays.

In any event, from the meager information available, it seems clear that flames can propagate in vapor fuel - air - liquid fuel mixtures at over-all fuel-air ratios similar to those found for the limits of homogeneous vapor-air mixtures.

The observations that are sometimes made of burning at extremely lean or rich over-all fuel-air ratios may be a result of the existence of regions in which the mixture is actually within the flammable range; these regions may serve as sources of piloting combustion.

Diluents. - As increasing amounts of an incombustible gas or vapor are added to the atmosphere, the flammability limits of a gaseous fuel in the atmosphere approach one another, and finally meet. Inert diluents, such as carbon dioxide, nitrogen, or argon, merely replace part of the oxygen in the mixture, but they do not all have the same extinctive power: it is found that the order of efficacy is the same as that of the heat capacities of these three gases:

$$CO_2 > N_2 > A$$

For example, the minimum percentage of oxygen that will permit flame propagation in mixtures of methane, air, and carbon dioxide is 14.6 percent by volume; if nitrogen is the diluent, more is required to reduce the oxygen to 12.1 percent, and in the case of argon, still more is needed to reduce the oxygen to 9.8 percent (ref. 13, p. 49).

Other types of diluent are far more effective than the inert gases. Certain halogen-containing organic compounds, in particular, have very powerful effects. Figure III-14 is a plot of the lean and rich limits of flammability of gasoline in atmospheres of air plus several diluents. The compositions given are volume percentages of the total mixture. It is seen that methyl bromide and chlorobromomethane (ref. 18) are much more effective extinguishants than nitrogen, exhaust gas, or carbon dioxide (ref. 10, p. 764); that is, smaller concentrations are required to prevent flame propagation in any mixture of gasoline vapor and air. Reference 19 contains a thorough discussion of this subject.

Inasmuch as the halogenated compounds are in an entirely different class of efficacy from the other three gases shown in figure III-14, it is believed that they exert their extinctive action by interfering with the chemical reactions of flame propagation, rather than by absorbing heat or diluting the mixture.

Figure III-14 also shows that the rich limits are more sensitive to diluents than the lean limits. For example, as much as 15 percent added nitrogen has no appreciable effect on the lean side of the curve, but reduces the rich limit from 7.4 to 5.4 volume percent gasoline vapor.

Temperature. - In view of the accelerating effect of increased temperature on chemical reactions, it is reasonable to expect that the limits of flammability should be broadened if the temperature is increased. That is, the lean limit should lie at a lower concentration, and the rich limit at a higher one. This is experimentally found to be the case. The limits change linearly with temperature. For example, the lean limit of n-pentane decreased from 1.53 volume percent at room temperature to 1.22 percent at 570° F, so that the lean limit decreased at a rate of about 6.1×10^{-4} volume percent per °F. The rich limit increased at a higher rate, approximately 17×10^{-4} volume percent per °F (ref. 13, p. 63). These data were obtained with downward flame propagation, but upward propagation leads to analogous results (ref. 14). The figures quoted for n-pentane appear to be characteristic of other hydrocarbon fuels. Thus, increases in the temperature of homogeneous hydrocarbon-air mixtures produce widened limits of flammability; however, the effects are relatively small.

Velocity and turbulence. - Most of the flammability-limit studies discussed previously have been concerned with quiescent, homogeneous mixtures. Information on the flammability limits of flowing streams of mixture is of considerable practical interest, but very few such observations have been made. It is known that mixtures may be circulated slowly through a flame tube by means of a fan in an external by-pass without any effect on the limits (ref. 20). This observation cannot be considered to apply to the fast streams in high-speed combustors.

A flame burning in a laminar stream cannot propagate upstream against normal components of the flow velocity greater than the laminar burning velocity; in this sense, such a stream might be nonflammable. If the stream is turbulent, the overall burning rate is increased, as described in chapter IV, and the flame may be able to propagate. It therefore appears that the effects of velocity in laminar streams are of little practical value. The effects of turbulence and of velocity in turbulent streams are the important ones, because the flow in practical combustors is invariably turbulent and has a mean velocity greater than the laminar burning velocity.

Only a few experiments have been made to elucidate the effects of turbulence on the limits. It has been reported that the lean limits of methane and ethane are somewhat extended by a suitable amount of turbulence produced by a fan or by stream velocity; that is, flames will propagate in turbulent mixtures that are too lean to sustain propagation in the quiescent condition (ref. 13). However, the turbulence was not characterized, and in the case of the mixtures stirred by a fan, it is possible that true turbulence, that is, completely random disturbances, may not have existed. An opposite effect was found for propane-air mixtures in a different experiment. In this experiment, an axial rotor as long as the flame tube was rotated at various speeds. Above 850 rpm, the lean limit was markedly narrowed (ref. 21); no attempt was made to characterize the turbulence.

A more meaningful experiment is the one described in reference 8 and discussed previously in connection with homogeneous quenching. In that case, the range of

fuel concentrations capable of propagating a flame was narrowed by an increase in flow velocity. At flow velocities between 12 and 50 feet per second, however, the lean limit was extended. In the experiment of reference 8, the flow disturbances were due to pipe turbulence; it is believed that the fluctuations were more likely to be random and thus constitute true turbulence than in the case of experiments employing fans or rotors.

In reference 8 it is suggested that the narrowing of the limits with increase in velocity may be due to the fact that turbulent intensity also increases, so that the flame zone is more diluted with cold unburned mixture. However, a different interpretation is also possible. Karlovitz has observed the stability of turbulent burner flames stabilized on the burner port by a small annular pilot flame (ref. 22). It was found that at sufficiently high flow velocities, broken-off flames were obtained such that a flame burning in one part of the combustible mixture would not propagate through the mixture. The situation is roughly similar to the experiment of reference 8. The explanation given in reference 22 is that flame propagation is arrested by the high velocity gradients across the flame front.

It is not yet possible to draw definite conclusions about the effects of velocity and turbulence on the flammability limits. Various observers have reported contradictory results; it may be that a suitable type of turbulence broadens the limits up to a certain level of turbulent intensities and narrows the limits at higher intensities. In view of the recent work (ref. 8), it is tentatively suggested that, in high-speed combustors employing homogeneous fuel-air mixtures, the flammable range of homogeneous mixtures is reduced by increase in velocity and turbulence. It would, however, be unsafe to apply this idea to the case of heterogeneous mixtures.

Effects of Variables on Flammability Limits at Nonatmospheric Pressures

All the flammability limits discussed thus far have been at atmospheric pressure. Less work has been carried out at pressures above and below 1 atmosphere.

The behavior of the limits at elevated pressures is somewhat surprising, and has not been completely explained. For the simple hydrocarbons, ethane, propane, butane, and pentane, it appears that the rich limits extend linearly with increasing pressure at a rate of about 0.13 volume percent per atmosphere increased pressure above atmospheric; the lean limits, on the other hand, are at first extended slightly, but between 1.3 and 2.5 atmospheres, they pass through a minimum concentration and are thereafter narrowed as pressure is increased to 6 atmospheres (ref. 13, p. 56).

For flammability limits at reduced pressures, most of the older work indicated that the rich and lean limits converge as the pressure is reduced until a pressure is reached below which no flame can propagate (ref. 13, p. 3). However, as pointed out in the discussion of quenching, it has been found that this behavior is due to wall quenching by the tube in which the experiments are conducted (ref. 5). The limits are actually as wide at low pressure as at 1 atmosphere, provided the tube is sufficiently wide, and provided an ignition source can be found that will ignite the mixtures. For example, recent work, (ref. 17) in which a 4-inch tube was used, has shown this to be true for gasoline vapor - air mixtures down to pressures less than 1 inch of mercury. Consequently, the limits obtained at reduced pressures are not generally true limits of flammability, since they are influenced by the tube diameter and are therefore not physicochemical constants of a given fuel. These low-pressure limits might better be termed limits of flame propagation, and should be accompanied by a specification of the tube diameter.

Hydrocarbon type. - Investigations have been conducted at the NACA Lewis laboratory to measure the low-pressure limits of flame propagation of a large number of fuels. The experiments were carried out in a flame tube 2 inches in diameter, using a hot wire as the igniter. The apparatus was not provided with a plenum, so the flames did not propagate at constant pressure; however, all the limits were determined in the same manner, and the data are consistent. The results are contained in references 14 and 23.

It was found that both the lean and rich limits are virtually unaffected by decrease in pressure from 1 atmosphere to about 10 inches of mercury. This result is in agreement with the data of figure III-8. Furthermore, the relative order of concentrations of the limits for the various fuels is the same as at atmospheric pressure. Therefore, table III-I, which gives the limits at 1 atmosphere for several pure compounds, also qualitatively describes the results at pressures down to 10 inches of mercury. Further decrease in pressure introduces the quenching effect of the walls, and causes both lean and rich limits to converge quite rapidly. The limits finally meet at a minimum pressure, below which flame cannot propagate in homogeneous mixtures in a 2-inch tube. This minimum was found to be about 1.3 inches of mercury for most of the fuels investigated.

The relative order of the rich limits for a series of fuels was not the same at pressures below 6.5 inches of mercury as above that pressure. This change occurred through a peculiar behavior of the limit curves. Several typical examples for normal paraffins in air are shown in figure III-15. The rich side of the curve contains an additional lobe; this type of pressure-limit curve was found for all hydrocarbon fuels except methane (refs. 14 and 23). It has been suggested that the lean lobe corresponds to the limits of propagation of normal flames, while the rich lobe is due to "cool flames" which are capable of propagating in rich hydrocarbon-air mixtures by means of a different mechanism (ref. 23).

Petroleum fuels. - Reference 16 reports the effect of reduced pressure on the limits of flame propagation of several petroleum fuels. The data were obtained in a closed 2-inch-diameter tube, in an apparatus similar to the one described in reference 23. However, in the tests of reference 16, a spark-ignition source was used in place of a hot wire. In reference 23, it is stated that doubt exists as to the possibility of initiating cool flames with a spark source; the data of reference 16 support this idea, for the curves do not show cool-flame lobes such as those in figure III-15. Curves are presented in figures III-16(a) and (b) for 100/130 grade aviation gasoline and for JP-3 fuel. The data were obtained at 77° to 81° F with fuel-air mixtures prepared only from the first 20 percent of vapor that distilled from the multicomponent petroleum fuels. Therefore, the percentages of heavy vapors in the mixtures were small. It should also be noted that the previous history of the fuels must have had an effect on the results, as discussed previously in connection with the limits of flammability of petroleum fuels at atmospheric pressure. In view of the uncertain average molecular weight of the combustible vapors, the data in figure III-16 are plotted in terms of volume percent combustible in air.

The facts that a closed flame tube was used in these experiments, and that the type of spark-ignition source affected the results, indicate that the data of figure 16 are of value mainly for comparative purposes. It is believed that they are not true flammability-limit data. However, it is interesting to note that flame propagation may occur at pressures less than 1 inch of mercury, and that the roughly vertical portions of the curves lie at fuel concentrations similar to the true flammability limits at 1 atmosphere of pure normal paraffin fuels in the butane-heptane range.

Significance of Flammability Limits

Limits of flame propagation. - The significance of the observations discussed in the foregoing sections must necessarily be considered in terms of the experimental conditions. The true limits of flammability, which are physicochemical constants of the fuel at a given temperature and pressure, are not affected by the size and shape of the vessel or by the igniter. As has been pointed out, measurement of these true flammability limits has been confined mainly to atmospheric pressure, because at lower pressures the quenching influence of the walls occurs. The limits at lower pressures are therefore properly termed limits of flame propagation, and may be related to quenching distances. That is, limits of flame propagation at low pressures occur in mixtures that are actually flammable, and in sufficiently large vessels, it appears that flame may propagate in these mixtures down to very low pressures.

In addition, it is not yet certain that true limits of flammability may be measured in any but homogeneous mixtures of fuel vapor and air, because of the difficulty of defining precisely the physical state of heterogeneous mixtures of liquid and vapor fuel with air.

The limits of flame propagation at reduced pressure have already been discussed, and the relation to quenching has been described. The true limits of flammability, determined for homogeneous mixtures at atmospheric pressure, remain to be considered.

True flammability limits. - If a flame is to propagate through a mixture, it is evident that each layer of fresh gas just ahead of the flame must be ignited so that the flame overtakes it just as the chemical reactions of combustion reach the state characteristic of the flame. It is therefore reasonable that the true limits of flammability should occur at fuel concentrations such that just sufficient energy is transmitted from the flame to the gas ahead to allow this continuous ignition to take place. Dilution of the limit mixture by fuel at the rich limit, or air at the lean limit, would upset the balance, and flame would propagate only if aided by some external energy supply such as the ignition source.

It was pointed out previously that diffusion of active particles and conduction of heat from the flame zone to the cold gas are probably both important in the process of flame propagation. It is not yet established which of these two mechanisms will be more successful in explaining the observed combustion phenomena. Regardless of the mechanism of energy transfer, however, it is logical to expect that the limit concentration should be related to the amount of chemical enthalpy (heat of combustion) available in the mixture for transfer to the unburned gas. This expectation is experimentally verified, at least in the case of the lean flammability limits of hydrocarbon fuels. On the average, it is found that lean-limit mixtures of most hydrocarbons have a combustion heat release of 10.4 kilocalories per mole of fuel-air mixture (ref. 14). Also, Egerton and Powling (ref. 24) have shown a very striking correlation between the heat of combustion of the fuel and the reciprocal of the lean-limit concentration (ref. 10, p. 334). Similar correlations between the heat of combustion and the rich flammability limits have not been so successful. However, it has been found that the calorific values of rich-limit mixtures are approximately the same for several hydrocarbon fuels (ref. 13, p. 12). The same general ideas of flammability limits may therefore apply to both rich and lean limits.

The foregoing discussion implies that there may be a characteristic temperature associated with the limit flames of each fuel. It will be recalled that increased initial mixture temperature widens the limits, so that the heat of combustion per mole of mixture is decreased. If there is a characteristic limit flame

temperature, the decrease in heat of combustion should be just balanced by the gain in heat content due to the higher initial temperature. This is found to be approximately true for several hydrocarbons, and may explain the linear dependence of limits of flammability on initial mixture temperature that is usually observed (ref. 13, p. 12).

The general ideas of flammability limits discussed have not as yet been implemented with a useful theory. The theoretical approach of Lewis and von Elbe (ref. 10, p. 369) has not led to a means of calculating the limits from basic physical and chemical properties of fuel-air mixtures. The ideas expressed in reference 25 have been somewhat more successful. In this work, it is pointed out, both on the basis of the thermal theory of flame propagation of Zeldovich and from experimental evidence, that the burning velocity does not fall to zero in a limit mixture. Consequently, there must be some factor that prevents the propagation of slower flames in mixtures more dilute than the limit mixtures. It was suggested that this factor is the loss of heat due to radiation. The radiation in question is chiefly infrared. On the basis of necessarily crude calculations, which were not described in detail in the reference, it was estimated that radiation makes it impossible for a flame to propagate in carbon monoxide mixtures at a velocity less than 0.065 foot per second. The lean limit of carbon monoxide in air was calculated to be between 10 and 13.5 percent carbon monoxide by volume, and the rich limit between 81 and 87.5 percent. These figures may be compared with those of reference 13, which gives the limits as 12.5 and 74 percent, respectively. The agreement is quite striking in this case; so far as is known, the theory has not been extended to other fuels. In view of the fact that data on the absolute energies emitted as infrared radiation from gas mixtures at elevated temperatures are required for the calculations, it would appear that a full evaluation of this theory would be a difficult task.

IGNITION

Ignition of gases is usually considered the process of producing a propagating flame in a combustible mixture. There are many methods used to generate this flame; the following are discussed in the succeeding sections: heated surfaces, flames, hot gases, chemical methods, shock waves, capacitance sparks, and inductance sparks. The information available on most of these methods is too voluminous to permit detailed discussions of apparatus and results in this report, hence, only perfunctory descriptions of apparatus will be given and only the more important trends will be discussed.

As an aid in understanding the succeeding discussion of the ignition process the following definitions are offered:

(1) Ignition temperature: The ignition temperature is defined as the lowest temperature at which the heat lost from the gas is overbalanced by the heat generated by chemical reaction. At this temperature, the rate of chemical reaction increases and results in the temperature being increased to the flame temperature. However, when it is desired to determine ignition temperatures, it becomes necessary to employ various types of apparatus which in themselves do not give the true temperature of the gas but rather a temperature of part of the apparatus. Hence, temperatures reported hereinafter for various ignition methods are equipment temperatures.

(2) Ignition limits: Ignition limits of a mixture are those proportions of fuel in air or oxygen that are just capable of permitting flame in a portion of the mixture for a specific ignition method. Because ignition is considered as the process of initiating a propagating flame, ignition is limited by the limits of flammability previously discussed.

(3) Ignition lag: Ignition lag is the time between the introduction of the mixture to the ignition source and the first indication of ignition.

Ignition by Heated Surfaces

The most important methods used to obtain basic data on surface ignition temperatures of fuels are: (1) crucible methods, static and dynamic; (2) heated surfaces of various geometries; (3) adiabatic compressions method, and (4) bomb method.

The crucible methods have been the ones most widely used to obtain ignition temperatures of liquid fuels. In this method, a drop of fuel is dropped through an opening into a heated container containing either quiescent or flowing air or oxygen (depending upon whether static or dynamic tests are to be made). The crucible temperature and ignition lag are determined at the instant the drop bursts into flame. The disadvantages are that the mixture composition is not obtained and that the heat of vaporization must be supplied by the crucible. The ignition temperature is the surface temperature of the crucible. This method has been derived from methods described in references 26 and 27 and yields ignition temperatures which are among the lowest found in the literature.

The dynamic heated-tube method (ref. 28) utilizes concentric quartz or pyrex tubes in which the flammable vapor and supporting atmosphere are flowing and are separately heated. The flammable vapor is metered into the large tube containing the supporting atmosphere by means of a small orifice in the end of the small tube. The measured ignition temperature is the mixture temperature at which flame appears after a measured time lag. The mixture composition is controllable in this method.

The adiabatic-compression method was originally developed by Tizard and Pye (ref. 29) to eliminate the effects of the surface on ignition temperature. The apparatus was constructed with a piston that moved forward very rapidly to compress a volume of fuel-air mixture in a cylinder; the piston was locked at the end of the stroke. Reasonable calculations showed that the time required for any appreciable heat loss from the gas to the cylinder walls was much greater than the observed ignition lags. The ignition lags depend upon the temperature reached in the compression process; the temperature is calculated from the compression ratio, as determined from a pressure record.

The original intention of Tizard and Pye, that the ignition temperatures obtained by the adiabatic-compression method should be those for homogeneous gas-phase ignition, does not appear to have been fulfilled. The experiments of reference 29 showed that, although the ignition lags were only of the order of 10^{-3} second up to a few tenths of a second, significant heat transfer to the cylinder walls occurred. Lewis and von Elbe, in a discussion of the adiabatic-compression method, point out that all experimenters have found it necessary to condition the walls of the reaction chamber in order to obtain consistent results (ref. 10, p. 162). This fact plainly indicates a wall effect on the ignition temperatures. Furthermore, strong evidence for a wall effect has been obtained in photographs taken through the end of the compression chamber fitted with a window; the pictures show that luminous spots appear first at the surface of the cylinder and grow inward (ref. 10, p. 163). Thus, ignition definitely does not occur uniformly throughout the compressed mixture. For these reasons, it appears that the adiabatic-compression method, like the other methods under discussion, gives some sort of apparatus temperature rather than an absolute ignition temperature.

The bomb method (ref. 30) utilizes an evacuated chamber heated to a known temperature. The flammable mixture is introduced into the chamber and time lag measured. The chamber has possible catalytic effects, and errors may result because of the fact that the mixture must be heated before ignition can occur.

Data from all these methods cannot be compared because of the difference in experimental apparatus and technique. However, data from one source can be used to show the trends of different variables.

Mixture composition. - The effect of mixture composition on the surface ignition temperature of electrically heated nickel strips (ref. 31) is shown in figure III-17. The approximately linear relations show that the ignition temperature increases as the percentage of fuel in the fuel-air mixture increases and as the strip width decreases. This trend of increasing temperature with increasing proportions of fuel does not hold for all fuels. Figure III-18(a) shows that, for some hydrocarbons of the paraffin series, the temperature decreases with increasing fuel proportions (refs. 30 and 32), although it might be expected that the curves will eventually turn back up at richer mixtures. Gasoline shows a trend similar to the paraffin hydrocarbons (figs. III-18(a) and (b)).

A fuel may exhibit two ignition temperatures at certain oxygen-fuel ratios (ref. 33). For example, figure III-19 shows the ignition temperatures for n-octane and 2,2,4-trimethylpentane as a function of oxygen-fuel ratio. For the case of 2,2,4-trimethylpentane, the temperature gradually decreases with increasing oxygen-fuel ratio. However, with the n-octane fuel and, for example, an oxygen-fuel ratio of 8, an ignition region is found between 465° and 605° F, a nonignition region between 605° and 865° F, and another ignition region above 865° F. Hence, there are two types of ignition: (1) a low-temperature ignition that is substantially constant regardless of fuel concentration, and (2) a high-temperature ignition that is affected by fuel concentration. The readily ignited hydrocarbons, such as cetane, heptane, decane, and decahydronaphthalene, exhibit zones of nonignition above the minimum ignition temperature (ref. 34). Reference 35 shows that mixtures of air and straight-chain paraffins containing three or more carbon atoms exhibit zones of nonignition. Oxidation-resistant hydrocarbons such as benzene, toluene, and 2,2,4-trimethylpentane exhibit no zones of nonignition. The phenomena of zones of nonignition may be due to chain-making and -breaking mechanisms.

Ignition lag. - The ignition temperature of a flammable depends upon the time interval between the introduction of the flammable to the ignition source and actual appearance of flames. Figure III-20 shows the effect of this lag on the ignition temperature of a gasoline-oxygen mixture (ref. 36). The temperature decreases almost hyperbolically with increasing ignition lag. The minimum ignition temperature is reached when the temperature no longer decreases with increasing lag. This same trend is observed with other fuels and other types of ignition source (except sparks).

The importance of ignition lag in ignition by heated surfaces is indicated in figure III-20. The times shown are unreasonably long compared with the residence time of a fuel in a combustion chamber. Therefore, for such applications, the surface temperature must be markedly increased or else some means provided to prolong contact between fuel and surface.

Heated spheres and rods. - Heated spheres shot into the combustible have also been used as ignition sources, with the results shown in figure III-21. Ignition temperature decreased as the diameter of the sphere increased because of the greater surface area. In this study (ref. 37), the criterion for setting up a theory was that the rate of heat generated by reaction should be greater than that lost by conduction. It is shown that for a specific sphere velocity,

$$\frac{T - T_0}{r} = Ke^{-E/RT} \tag{8}$$

where

E apparent energy of activation

K constant

R gas constant

r sphere radius

T heated sphere temperature

T_0 mixture temperature

Because of the ignition criterion that considered heat losses by conduction only, the equation does not contain any factor relating to the duration of contact of the fuel with the ignition source.

Heated rods have been used as ignition sources for high-velocity gas streams (ref. 38) as shown in figure III-22(a). High mixture velocities correspond to short ignition lags; thus, the ignition temperature of a flammable mixture increases with increasing velocity of the mixture. These data have been correlated (fig. III-22(b)) in accordance with the following equation:

$$\frac{d}{U} e^{-\frac{E}{RC}\left[\frac{U}{d(T - T_0)}\right]} = K \tag{9}$$

where

C,K constants

d heated rod diameter

E energy of activation of mixture

R gas constant

T heated rod temperature

T_0 flowing mixture temperature

U velocity past heated rod

Turbulence. - Data on the effect of turbulence on ignition are not extensive and the little information that is available does not include quantitative measurements of turbulence. Reference 31 shows that mild turbulence decreases the ignition temperature; however, an opposite trend is reported in reference 32. In reference 32, the ignition temperature was increased approximately 30° F by stirring the mixture (fig. III-23).

Surface condition and composition. - The condition of the heated surface may affect ignition in that the scale or ash forms an insulating coating which requires the whole material to be heated to a much higher temperature for ignition than would otherwise be necessary. A gas film (e.g., absorbed water or carbon dioxide vapor) may act in the same manner.

The composition of the ignition surface affects the ignition temperature (refs. 31 and 39) of flammable mixtures. The effects of various surfaces are shown in figure III-24. Differences shown for the various surfaces are probably due to thermal conductivity, catalytic activity, or oxidation properties. Except for molybdenum and platinum, the surface temperature increases with the amount of fuel in the mixture. Molybdenum oxidizes rapidly at these ignition temperatures which probably explains the trend opposite to other metals. Platinum is catalytically active and the results may be explained on that basis. With platinum, a reaction of fuel and oxygen takes place with liberation of heat at the surface. This heat affects the temperature gradient in such a manner that less heat will flow from the heated surface, thereby inhibiting ignition. The rate of the catalytic reaction attains a maximum at stoichiometric mixture composition, causing the heat flow from the surface to be minimum. Therefore, to compensate for the smaller heat flow, it is necessary to raise the surface temperature higher in order to obtain ignition, as shown by the peak in figure III-24.

This effect of type of surface upon the ignition temperature depends upon the particular method of ignition used. For example, reference 40 shows that in the dynamic-bomb method of ignition changing the metal surfaces has substantially no effect on the ignition temperature. Glass surfaces, however, ignite flammables at lower temperatures (ref. 41).

Surface area. - The effect of increasing the surface area of a heated plate (ref. 32) is shown in figure III-25, in which an increase in area lowers the ignition temperature. Increasing the area from which heat may be transferred increases the amount of heat output and correspondingly lowers the ignition temperature. The curve appears to approach a minimum temperature below which it is impossible to obtain ignition regardless of area.

Small wires can cause ignition when heated electrically to incandescence. In the case of platinum, difficulties are caused, however, by combustion without flame that takes place on the surface of the wires. This combustion causes the wire to have a temperature higher than when surrounded by air instead of a flammable mixture. The mixture near the wire becomes heated and convection currents are set up. Ignition of the mixture occurs only if the heated portion of the mixture remains in contact with the wire for a period corresponding to a time greater than the ignition lag. This convective effect is greater with stoichiometric mixtures (those that have the highest thermal energies) and consequently results in higher ignition temperatures at these mixtures.

The limiting minimum diameters of heated wires capable of igniting methane-air mixtures are approximately 0.0079 and 0.0355 inch for platinum and iron wires, respectively (ref. 42). For smaller wires it is assumed that a layer is formed on the wire by oxygen molecules and sufficient heat cannot be conducted through the layer.

Heated particles (friction and fusion sparks) can cause ignition under certain circumstances. However, in general, they are ineffective ignition sources and have little practical importance in high-speed combustors.

Fuel composition. - Variations in molecular structure and molecular weight affect the ignition temperatures of flammable mixtures to a large degree, as shown in references 43 and 44, both using crucible methods. Ignition temperatures for more than 100 organic liquids are reported in reference 43 and for 94 pure hydrocarbons and 15 commercial fluids in reference 44. Portions of these data are plotted in figures III-26(a) and (b), where spontaneous ignition temperatures are shown as functions of the number of carbon atoms per molecule for several types of compound. These figures show that the lowest molecular weight compounds have the

highest ignition temperatures and that, for a given number of carbon atoms, the n-paraffins and n-olefins have substantially lower ignition temperatures than do branched paraffins and aromatics.

Ignition temperatures for several aircraft fuels and lubricants are listed in the following table. These data were taken from reference 44 and from unpublished NACA work in which a crucible method, substantially the same as that of reference 44, was used.

Fuel or lubricant	Spontaneous ignition temperature, °F
100/130 Grade aviation gasoline	844
Low-volatility aviation gasoline	900
Unleaded 62-octane motor gasoline	568
Kerosene	480
Grade JP-3 jet fuel	
Sample A	484
Sample B	502
Grade JP-4 jet fuel	484
Grade JP-5 jet fuel	
Sample A	473
Sample B	477
SAE No. 10 lube oil	720
SAE No. 60 lube oil	770

The ignition temperatures for the jet fuels are among the lowest found for hydrocarbons.

There is no exact relation between octane number and ignition temperature, but references 39 and 45 indicate that ignition temperatures of unleaded fuels generally increase with increasing octane number. Data from references 34, 41, and 46 show that the effect of decreasing fuel quality or cetane number is to increase the ignition temperature (fig. III-27). Addition of tetraethyl lead also increases the ignition temperature (ref. 34).

Pressure. - The effect of pressure on the ignition temperature of methane-air mixtures as determined by a dynamic heated-tube method is shown in figure III-28(a) (ref. 28) and its effect on the bomb-ignition temperature for four liquid hydrocarbons is shown in figure III-28(b) (ref. 47). Ignition temperatures decreased continually with increasing pressure over the pressure range investigated, which was to 30 atmospheres in reference 47. The effects of increasing pressure on crucible-method ignition temperatures are shown in the following table for JP-4 and JP-5 fuels (unpublished NACA data):

Pressure, atm	Ignition temperature, °F	
	JP-4	JP-5
1	484	477
5	376	415
9	378	408

A considerable decrease in ignition temperature is seen when pressure is increased from 1 to 5 atmospheres. Further increases to 9 atmospheres had little effect.

Diluents. - The effect of adding diluents to flammable mixtures is to increase the ignition temperatures, because the amount of oxygen is correspondingly reduced (ref. 33). However, in the low-temperature type of ignition previously described, the effect of diluents is negligible, the ignition temperature remaining substantially constant.

Ignition by Flames

The energy required to initiate the chemical reactions characteristic of a propagating flame may be supplied to a fuel-air mixture by means of flames. Two separate situations may be considered:

(1) A pilot flame is immersed in the fuel-air mixture. Whether or not the mixture will be ignited depends upon the mixture composition, duration of contact between flame and mixture, size and temperature of the flame, pressure, turbulence level, and the nature and amount of diluents.

(2) A flame is propagating in one portion of a fuel-air mixture, separated from a second portion by a constriction. Whether or not the flame will pass through the constriction and ignite the second portion depends on the factors that govern flame quenching by walls. Among the important variables are the pressure, temperature, mixture composition, nature and amount of diluents, and the size and shape of the opening between the two regions of combustible mixture.

There is no extensive reliable literature on ignition by flames, nor have all the variables mentioned been studied. The succeeding sections describe some of the important facts that have been established.

Pilot flames. - Two basic sets of experiments have been conducted on the ignition of homogeneous fuel-air mixtures by means of immersed flames. In both cases, methane was the fuel and the methane-air mixtures were quiescent. The experimental technique involved exposure of the mixture to a small pilot flame for varying short intervals of time by means of a shutter, and the shortest contact time that permitted ignition was measured. The work is described by Morgan in reference 48 (p. 44).

The first experiments established the minimum contact times for ignition as a function of methane concentration in air for pilot flames of various lengths. The results are shown in figure III-29. Mixtures slightly richer than stoichiometric could be ignited with the shortest contact times, and increasing the length of the pilot flame reduced the time required. The flame temperature was the same in all cases; thus, an increase in heat-release rate appears to improve the incendivity of pilot flames. The other interesting result of this work is the very short contact times required. A flame 0.59 inch long was capable of igniting a range of methane-air mixtures with contact times of only 0.003 to 0.004 second.

In the second series of experiments, the size of the pilot flame was kept constant, but the temperature was varied by adjustment of the mixture. In this way, it was found that the minimum contact time for ignition of methane-air mixtures by a pilot flame burning at 3215° F was only about one-sixth the time required with a flame at 2770° F.

These two series of tests therefore established the importance of both pilot heat and pilot flame temperature in the ignition of quiescent mixtures.

Propagating flames through constrictions. - It is apparent from a previous discussion of flame quenching by walls that, if the quenching distance is known, the possibility of a flame propagating in one portion of a mixture passing through a constriction and igniting a second portion can be determined. All evidence indicates that, if the flame succeeds in passing through the constriction, ignition of the second portion is automatically insured. It is therefore appropriate to consider the factors that affect quenching distance in connection with this type of flame ignition; see FLAME QUENCHING.

Ignition by Hot Gases

Ignition by hot gases generally applies to the case in which fuel is injected into hot air. The mixing process is an essential part of the sequence of events leading to ignition. In addition, the chemical nature and physical state of the fuel, and the temperature, pressure, and composition of the hot gas will influence ignition.

In this section, some of the factors governing ignition of fuels injected into hot air streams are discussed. The criterion for ignition in these cases is the appearance of flame. Oxidation is accelerated by increased temperature; therefore, the time lag, or ignition lag, from the instant of fuel injection until the flame appears is a function of the air temperature. In addition, some of the experiments showed that the relative amounts of fuel and air affect the temperature required for ignition after a given ignition lag. It is therefore evident that it is meaningless to quote an ignition temperature for a fuel, unless the fuel-air ratio and the time lag before ignition are also specified.

One of the major difficulties in the measurement of such ignition temperatures is that a mixing process is superimposed on the results. In the older work, the fuel concentration varied from point to point in the apparatus, and there was no attempt to determine the concentration at the point where flame first appeared. In addition, there was often a chance for the fuel to undergo thermal cracking because of prolonged contact with hot surfaces before it was introduced into the air stream.

Consequently, ideal ignition experiments of this type should be free of surface effects, and mixing of the fuel and air should be nearly instantaneous, or else the effects of mixing should be determined. Even if these requirements are met, however, the experimental technique still affects the results; this point is discussed more fully in a following section.

Two types of recent experiment are discussed:

(1) Injection of gaseous fuel into hot air, with very rapid mixing

(2) Injection of gaseous or liquid fuel into a stream of air plus hot products of combustion from a "slave" burner, with no special attempt to secure rapid mixing

Heated air. - A spontaneous-ignition apparatus that overcomes some of the experimental objections to the measurement of ignition temperatures has been designed and used to study the ignition of propane by hot air (ref. 49). The work so far has been limited to the effects of propane and oxygen concentration at 1 atmosphere static pressure.

The propane and the air were very rapidly mixed in a specially designed chamber; the mixing time with the low flow rates used was 6×10^{-3} second or less. Consequently, it is believed that no significant thermal cracking of the fuel occurred before it was mixed with the air. The mixture was allowed to flow upward in a glass flame tube, and the ignition lag was measured by means of a photocell that responded to light from the flame, or by a pressure pickup that recorded a pulse when ignition occurred. By means of several electric heating elements, conditions were controlled so that the mixture, mixing chamber, and flame tube were all the same temperature. The flame tubes were 36 inches long, and 1 or 2 inches in diameter.

The results did not depend appreciably on the flame-tube diameter (ref. 49). There was, however, an effect of flow rate: curves of ignition lag against flow rate, at constant temperature and propane concentration, showed minimums for ignition lag. The flow rate corresponding to the minimum lag shifted to higher values for richer mixtures.

Nevertheless, the data of reference 49 definitely show that ignition lag decreases as propane concentration increases. Typical data, in the form of a logarithmic plot, are shown in figure III-30. The ignition lags vary from 0.3 to 8 seconds, over a range of propane concentrations of 3 to 40 percent by volume, and a range of temperature from 1014° to 1360° F. The straight lines of figure III-30 show that the dependence of ignition lag on propane concentration may be expressed by the following equation:

$$1/t = \text{Constant}[C_3H_8]^b \tag{10}$$

where

b constant

$[C_3H_8]$ propane concentration

t ignition lag, sec

The value of the exponent b may be determined from the slopes of the lines of figure III-30. These slopes have an average value of -0.93, so that the exponent b in equation (10) may be approximated by unity.

Reference 49 also describes experiments in which the oxygen concentration was varied independently of the propane concentration. In this way, it was found that there is a slight dependence of ignition lag on oxygen concentration. The following equation expresses the combined effects of propane and oxygen concentrations on the ignition lags at a given temperature:

$$1/t = \text{Constant}[C_3H_8][O_2]^{1/4} \tag{11}$$

Reference 49 showed that the temperature dependence of ignition lag is not of the simple Arrhenius type; the data indicate that the activation energy is not constant over the range of temperatures studied. However, the ignition-lag data could be reasonably well expressed (within 30 percent) by the following equation, which accounts for all the variables studied:

$$t[C_3H_8][O_2]^{1/4} = 0.030 + 5.4 \times 10^{-9} \exp(26100/T) \tag{12}$$

where

$[C_3H_8]$, $[O_2]$ concentrations in mole fractions

T temperature, $^{\circ}R$

The preceding experiment is subject to apparatus variables that appear to be inevitable, even though some of the objections to the measurement of spontaneous ignition temperatures have been removed. If the essential processes are assumed to take place in the gas phase, ignition cannot occur until the rate of heat release from the preignition reactions (or perhaps the rate of production of certain active particles) overcomes the rate of loss to the walls of the test section and to the air or inert gas that precedes the fuel-air mixture through it. Such a transfer must occur even though the walls are maintained at the same temperature as the entering stream of mixture, for the oxidation reactions release heat even before ignition takes place, so that the temperature of the stream rises as it progresses through the flame tube. Consequently, gradients in temperature and in concentration will exist between the center of the tube and the walls, and the diameter of the test section should have some effect on the results. The material of the walls might also be of some importance. In addition, the flow rate should affect the ignition lags at a given spontaneous ignition temperature, since it influences the heat transfer to the walls. Similar considerations apply if processes at the wall are assumed to be controlling. There is also the possibility that both gas-phase and surface reactions are important, perhaps in different ranges of concentration and temperature.

It is shown in reference 49 that some of the results can be qualitatively explained both in terms of gas-phase reactions, using a reaction mechanism based on low-temperature oxidation studies, and in terms of a postulated surface reaction between adsorbed oxygen and propane. In the latter case, it would be expected that the ignition lags should depend upon the diameter of the flame tube; however, as has been pointed out, there was little difference between the ignition lags measured in 1- and 2-inch tubes. Reference 49 suggests that the explanation may lie in the fact that, whereas the smaller tube with its larger surface-volume ratio gives greater concentrations of reactants per unit volume of gas, the smaller tube also provides a larger relative area for loss of heat or destruction of active particles.

Concerning the other variables, the data of reference 49 show that ignition lag depends upon flow rate. The possible effects of wall material were not investigated. It appears to be impossible to eliminate these variables entirely. Until their separate influences are quantitatively understood, it will be very difficult to assign fundamental significance to measurements of spontaneous ignition temperatures, that is, to use the measurements as a means of investigating the basic chemical reactions that lead to spontaneous ignition.

Recently, studies with propane fuel have been conducted in a different apparatus over a higher range of spontaneous ignition temperatures (unpublished NACA data). Ignition lags from 7 to 50 milliseconds were measured at temperatures from 1375° to 1600° F. Hot air was passed into an unheated duct fitted with a movable water spray near the exhaust end. The water flow was adjusted so that all of the water was just vaporized under the conditions of the test. Propane was introduced into the stream from the end of a coil immersed in the incoming air; therefore, the fuel mixed with the air at essentially constant temperature. Ignition was detected by a sharp increase in the exhaust temperature, and the ignition lag could be varied by changing the position of the water quench. The results did not appear to depend upon the flow rate. The ignition-lag - spontaneous-ignition-temperature data followed an Arrhenius type of relation; the apparent activation energy was about 43 kilocalories per mole.

Vitiated air. - Mullins (ref. 50) has provided some data on short ignition lags obtained under rather specialized conditions. The objective was to simulate the situation in current types of turbojet combustors. In this case, no flame holders are provided in the combustors, and the fuel must be ignited by spraying it into a primary zone of air plus hot products of combustion introduced by recirculation from the flame zone. In the apparatus described in reference 50, the air was heated by addition of the hot exhaust from a "slave" combustion chamber situated upstream of the test section. The fuel was injected through a nozzle; both vapor and liquid fuels were studied. The ignition lag was determined from the known flow rate and a measurement of the distance from the nozzle to the point at which the spontaneously ignited flame stabilized in a gradually tapering diffuser downstream of the injection nozzle.

Such an experiment must be subject to the effects of evaporation, mixing, drop size, drop-size distribution, and turbulence. In addition, the air supply is vitiated by the added combustion products, so that the oxygen concentration varies below 21 percent, as a function of the temperature required in the air stream. Mullins has attempted to account for many of these effects in reference 51, which describes the results of studies on the ignition lags of kerosene-air mixtures. Several physical variables were examined, with the following results:

(1) Fuel-air ratio and velocity had negligible effects on ignition lag.

(2) At a given air temperature, the lag increased about 1 percent per 3-micron increase in spray Sauter mean diameter.

(3) The lag decreased 15 percent per 140° F increase in fuel preheat.

(4) The lag decreased 25 percent if the fuel was prevaporized.

(5) Only slight changes were noted when the induction zone was in the wake of a baffle that induced coarse turbulence.

Studies concerning the effects of air vitiation made with pure hydrocarbon fuels showed that the spontaneous ignition temperature for a given time lag was about 120° F above that for air (ref. 52). In the case of liquid fuels, it was necessary to set the conditions so that the spray was evaporated before it penetrated to the walls of the duct. Furthermore, in reference 51, a nozzle size and an injection pressure were standardized such that the spray Sauter mean diameter was about 100 microns.

The basic measurement was the length of the induction zone, that is, the distance downstream of the nozzle at which the flame stabilized in the 3° diffuser. It might be objected that the results were affected by propagation of the flame upstream into the hot mixture, or that the continuous presence of the flame influenced the length of the induction zone by radiation. To test these possibilities, experiments were conducted in which the flow of fuel was intermittent (ref. 51). The flashes from ignited mixture appeared 1 to 3 inches downstream of the corresponding continuous flame-front position. This result would seem to indicate that the continuous presence of the flame did have some effect, but it was pointed out that intermittent operation may not have allowed time for the nozzle to develop its normal spray. Therefore, the difference between continuous and intermittent ignition lags may have been due to a difference in spray characteristics. In any event, the discrepancies were small in absolute magnitude, although percentagewise they were as high as 15 percent.

Subject to the preceding experimental variables, Mullins' work provides the only measurements of the very short ignition lags of interest in present turbojet

combustors. The measurements covered the range of 1/2 to 30 milliseconds ignition lag. Typical data for kerosene, taken from reference 51, are shown in figure III-31. The effects of pressure were also studied, and figure III-31 includes lines for pressures from 9.88 to 29.92 inches of mercury. At a given temperature, the ignition lag for kerosene under the particular set of spray and stream conditions was found to be proportional to the reciprocal of the pressure. Different pressure dependencies were found for other fuels. Figure III-31 also includes a line for a gaseous hydrocarbon fuel, "calor gas", composed of C_4 hydrocarbons (ref. 52).

From the experimental data, activation energies were calculated and corrected for the effect of air vitiation, so that the results corresponded to pure air. The activation energy for ignition of kerosene was calculated to be 45.5 kilocalories per mole; for "calor gas", 52 kilocalories per mole.

There are several striking differences between the experiments discussed:

(1) In reference 49, it was found that the ignition-lag data for propane did not follow an Arrhenius-type plot; hence, a constant activation energy was not obtained. However, the empirical equation (12) used to express the data includes an exponential term $e^{26100/T}$. This temperature dependence is much less than found in references 51 and 52; the analogous exponential terms, with activation energies of 45.5 and 52 kilocalories per mole, would be $e^{41200/T}$ or $e^{47200/T}$. Although different fuels are involved, other experience would indicate that the temperature coefficients for propane and "calor gas", in particular, should agree more closely.

(2) Reference 51 reported no effect of fuel concentration on ignition lag, whereas in reference 49, it was found that the lag at a given temperature was proportional to the inverse of the propane concentration.

(3) The data of reference 49 indicated a low order of dependence of ignition lag on oxygen concentration, while reference 53 reported that the lag varied inversely as the square of the oxygen concentration.

It is impossible at present to ascertain the reasons for these discrepancies, because the experiments are so different and the effects of variables are incompletely understood. The need for caution in the interpretation of spontaneous ignition measurements is emphasized. In the present stage of knowledge, the safest procedure for practical application of the data to high-speed combustors is to choose an experiment that most nearly matches the actual conditions. For example, the work of Mullins provides measurements suitable for such application to present types of turbojet combustor. More basic experiments, such as those of reference 49, will eventually lead to a better understanding of ignition by hot gases.

Ignition by Chemical Means

The use of chemical methods for the ignition of high-speed combustors presents some attractive possibilities. Such an expedient might make it feasible to eliminate the electrical systems that are used at present, and to substitute more compact apparatus for chemical ignition. Furthermore, the ignition energy required of the spark may become larger than can be provided in the current systems under severe operating conditions, particularly under conditions of low static pressure and high velocity. The electrical apparatus must be made correspondingly large to insure ignition under such conditions. On the other hand, there are certain chemical compounds in which large amounts of easily released chemical energy may be stored in compact form.

The possibility of chemical ignition in practical combustors is still largely speculative, for very few actual tests have been made. Consequently, only a brief discussion of two methods of chemical ignition, and the laboratory evidence that offers encouragement of their eventual application, will be presented. The methods referred to are: (1) ignition by means of spontaneously flammable compounds, and (2) catalytically induced ignition by means of finely divided platinum or palladium. The more obvious expedients, such as the use of squibs and flares, will not be considered in the category of chemical igniters because they, in turn, must be started by electrical means. In other words, the discussion will be limited to cases in which the mere presence of an added chemical substance in a fuel-air mixture leads to ignition.

Spontaneously flammable compounds. - There is a fairly large number of chemical compounds of the type MR_x that have the property of bursting into flame when exposed to air. In the preceding expression, M denotes a metal atom, R an alkyl group (usually methyl or ethyl), and x depends upon the valence of the metal. Among the more common metals, the lower alkyls of boron, aluminum, and zinc are gases or liquids, and are perhaps of greatest practical interest. The specific compounds, their melting points, and boiling points are listed in the following table:

Compound	Formula	Boiling point, °F	Melting point, °F
Trimethyl boron	$B(CH_3)_3$	-4.4	-259
Triethyl boron	$B(C_2H_5)_3$	203	-135.1
Trimethyl aluminum	$Al(CH_3)_3$	266	59.0
Triethyl aluminum	$Al(C_2H_5)_3$	405	------
Dimethyl zinc	$Zn(CH_3)_2$	111.2	-20.5
Diethyl zinc	$Zn(C_2H_5)_2$	243.5	-22.0

The methods of preparation and handling of these materials are not especially difficult. The prime necessity is the exclusion of air. Additional information is included in reference 54.

The metal alkyls listed seem to burst into flame spontaneously because they readily yield free radicals and atoms by decomposition or on reaction with oxygen, even at room temperature. Thus, a chain reaction is set up; the reaction rapidly accelerates and causes the material to ignite under suitable conditions. As would be expected, the liquids burn most readily when their vapors are mixed with air, sometimes with explosive violence. However, a small pool of trimethyl aluminum burns gently when exposed to air, and is sometimes extinguished by formation of an oxide scum that prevents access of air to the surface. All the materials yield solid oxides on complete burning; this feature should be noted in considering their practical use as igniters.

Inasmuch as the spontaneously flammable metal alkyls readily produce free radicals, and, in addition, release heat on oxidation, it is reasonable to expect that their presence in a fuel-air mixture should induce oxidation of the fuel, and, under suitable conditions, lead to ignition. Available literature substantiates this expectation. The ignition of n-butane by dimethyl zinc (ref. 55) and by triethyl boron (ref. 56) was studied. The experiments were conducted in spherical glass bulbs, in a thermostat at 68° F or less. The dimethyl zinc or triethyl boron vapor was admitted to the evacuated bulb to the desired pressure. Butane was then either admitted separately, followed by rapid addition of oxygen, or a butane-oxygen mixture was added rapidly.

A minimum partial pressure of dimethyl zinc of about 0.59 inch of mercury was required to induce explosion in the butane-oxygen - dimethyl zinc mixtures (ref. 55). A series of tests at a total pressure of 7.88 inches of mercury, all with 0.98 inch of mercury of dimethyl zinc, and with varying amounts of oxygen and butane, showed that explosion could be induced over a wide range of composition. An ignition lag was observed and it was concluded (ref. 55) that, when the rate of oxidation of dimethyl zinc becomes sufficiently high, free radicals such as CH_3, CH_3O, and CH_3OO are liberated. These initiate a chain reaction in the mixture, heat is released faster than it can be conducted away, and an explosion results.

The studies indicated that triethyl boron was even more reactive than dimethyl zinc. Reference 56 reported that flashes occurred immediately on introduction of oxygen into a bulb of triethyl boron vapor down to pressures as low as 0.083 inch of mercury. There was no measurable induction period. When a stoichiometric butane-oxygen mixture was admitted to a bulb of triethyl boron vapor to a total pressure of 0.94 inch of mercury, no reaction occurred with 0.039 inch of the vapor present. With 0.117 inch, a violent explosion took place; and with 0.197 or 0.394 inch, there was merely a faint flash. Thus, although triethyl boron appears to be a more vigorous chemical igniter, there may be limits to the induced oxidation.

Aluminum borohydride $Al(BH_4)_3$ is a volatile liquid (b.p., 112° F) that has been reported (ref. 57) to ignite spontaneously on exposure to room air. The work described in reference 58 extended the observations to the ignition of the vapor. As in the preceding experiments, the explosions were observed when oxygen was rapidly introduced to a bulb of aluminum borohydride vapor. It was found that with dry oxygen, no explosion occurred at 68° F; with moist oxygen, explosion took place immediately. Inasmuch as aluminum borohydride is known to undergo rapid hydrolysis, it appears that this reaction is requisite to low-temperature explosion.

In a subsequent paper, the induced oxidation of hydrocarbons by aluminum borohydride was reported (ref. 59). As might be inferred from the results described in the previous paragraph, n-butane was not affected in dry aluminum borohydride - n-butane - oxygen mixtures. However, if the mixture was moist, immediate explosion occurred at 68° F under suitable conditions. When an unsaturated hydrocarbon fuel was used, explosion could be obtained in dry mixtures; 1-butene exploded after an ignition lag, and 1,3-butadiene exploded immediately.

Thus, aluminum borohydride is able to induce ignition of hydrocarbons at room temperature, but only if a suitable small amount of water is present, or in dry mixtures if the hydrocarbon is unsaturated. However, as reference 58 points out, the need for moisture or unsaturated fuel is eliminated if the temperature of the mixture is increased. Presumably, thermal dissociation provides the necessary chain initiators at the elevated temperatures in dry mixtures.

Experiments to explore the value of aluminum borohydride as a practical igniter are described in reference 60. Encouraging results were obtained when 1 to 2 cubic centimeters of the material was injected into a single tubular turbojet-engine combustor.

The evidence is conclusive that several spontaneously flammable compounds are capable of igniting hydrocarbons. The particular materials discussed do not complete the list of materials that may be of use. In view of the fact that one of the materials, aluminum borohydride, has shown promise in practical tests, it is suggested that further research is warranted on this type of chemical ignition.

Catalytic metals. - It has often been observed that finely divided metals can promote reaction between substances that are otherwise inert to one another. The metal acts as a catalyst, that is, it greatly accelerates the rate of reaction

between materials that appear to be unreactive at ordinary temperatures and pressures. For example, a stoichiometric mixture of hydrogen and oxygen may be stored indefinitely at room temperature without visible reaction, even though it is a thermodynamically unstable system. The reason is that the rate of reaction is undetectably small under the storage conditions. However, if a bit of platinum or palladium black is added, the reaction is catalyzed on the metal surface, which quickly glows red-hot and ignites the mixture.

The catalysis of hydrocarbon-air mixtures has also been observed, and these facts suggest the possibility of an igniter of great simplicity. It should only be necessary to place some platinum or palladium black at a suitable point in the combustor, and ignition would then follow whenever a fuel-air mixture contacted the catalyst.

The possibility of using catalytic ignition in practical combustors has not been thoroughly explored. One report (ref. 61) described a catalytic igniter for the hydrogen-air pilot of a 6-inch ram-jet engine. Palladium was precipitated on asbestos fiber, and a wad of this catalytic material was placed in each of four conical pilots. Hydrogen from an auxiliary tank was used as the pilot fuel. The hydrogen-air mixture was ignited by contact with the catalyst, and burned in the flared portion of the pilot body. This flame, in turn, ignited the main stream of mixture, which was propene and air. In laboratory tests, ignition was found to occur smoothly and with no appreciable time lag with a hydrogen flow of 2 cubic feet per minute. The results definitely confirmed the feasibility of this type of ignition in the ram-jet configuration for which it was designed.

Reference 62 reported tests of a different sort in a 1-inch-diameter burner tube. In this case, platinum black was mixed with platinized asbestos and magnesium chips, and the mixture placed in a cavity adjacent to the main stream. The fuel-air mixture contacted the catalyst, and the resultant heating ignited the magnesium chips. These produced a hot flame that was easily capable of igniting the main fuel-air stream. The effectiveness of the igniter varied with the fuel, in the following order: methyl alcohol > methyl alcohol - gasoline > gasoline alone. In some tests, ignition was obtained without the aid of magnesium chips, but the time lag before ignition was longer and the results were more erratic.

The idea of catalytic ignition is most attractive because such a system is self-energizing; it depends only upon the presence of a fuel-air mixture to activate the catalyst. The results of the two experiments described indicate that the method may have practical merit, particularly in systems where especially reactive fuels such as hydrogen are to be employed. However, further work is needed to determine the useful life of a catalyst charge and its susceptibility to catalyst poisoning.

Ignition by Shock Waves

The possibility of ignition of fuel-air mixtures by shock waves may readily be seen by a brief examination of the properties of the waves. It is not within the scope of this discussion to present the details of the formation and propagation of shocks; many excellent references may be consulted on these subjects (for example, ref. 10, p. 590).

A shock wave travels through a gas at a velocity greater than the local sound velocity. As the gas flows through the wave, it undergoes abrupt increases in pressure and temperature. The temperature is considerably greater than that obtained by adiabatic compression, in which case the assumption is made that the piston moves so slowly that equilibrium always exists; this condition is met in

practical cases as long as the piston velocity is small compared with the average molecular velocity. In the case of a shock wave, the piston head is the wave itself, and, as already stated, its velocity is high. Consequently, the compression is accompanied by the degradation of kinetic energy into random molecular motion, that is, thermal energy.

An idea of the properties of shock waves may be obtained from the following table (ref. 10, p. 594). The quantities in the table were calculated from the appropriate hydrodynamic equations, for shock waves in air at an initial temperature of 32° F.

Ratio of pressure behind shock wave to initial pressure	Shock wave velocity, ft/sec	Temperature behind shock, °F	Temperature resulting from adiabatic compression to same pressure ratio, °F
2	1,483	145	135
5	2,290	408	307
10	3,209	810	468
50	7,050	3,610	970
100	9,910	6,490	1250
1000	30,200	33,900	2620
2000	42,300	51,700	3270

The extremely high temperatures produced in the shock are sufficient to indicate the potential of shock waves as ignition sources, particularly when the temperatures in the table are compared with the spontaneous ignition temperatures that have been quoted previously. In addition, the shock contains free atoms and radicals that can promote rapid chemical reaction; shocks are often observed to be luminous, even in inert gases.

Thus far, only shock waves in noncombustible gases have been considered. If the gas is a combustible mixture, a mathematical analysis of the hydrodynamic processes that occur when a wave of chemical reaction sweeps through the mixture shows that two different types of process satisfy the conservation laws. In one case, the pressure and density behind the wave are both lower than those ahead of the wave; this is called a deflagration, and constitutes the usual flame with which this chapter is concerned. In the other case, pressure and density increase behind the wave; this is a detonation. (For a complete discussion see ref. 63.)

Ordinary flames propagating in tubes are often observed to accelerate and transform to detonation waves if the tube is long enough and the mixture is within the concentration limits of detonability. The processes involved are not yet completely understood. It may be sufficient to state that the detonation wave is a shock wave that continuously ignites the mixture into which it propagates, and is sustained at a velocity very much greater than the normal burning velocity by the energy released in combustion.

It is therefore seen that the possibility of ignition by shock waves is established by the very existence of the phenomenon of detonation. In the situation just described, however, flame is present initially. Recent studies have shown that ignition by shock waves can be accomplished without the presence of a preliminary, slowly propagating flame. In general, the technique has been to employ a shock tube, in which an inert gas at high pressure is separated by a diaphragm from a combustible mixture. When the diaphragm ruptures, a shock wave with a strength

dependent on the bursting pressure and the properties of the inert gas travels into the combustible mixture. The properties of this incident shock may be calculated from shock-tube theory, and the shock of minimum strength required to ignite the mixture can be determined. The technique has been used by Shepherd (ref. 64) with methane-oxygen, methane-air, and ethene-oxygen mixtures, and by Fay (ref. 65) with hydrogen-oxygen mixtures. In general, ignition resulted in a detonation if the mixtures were within the concentration range of detonability, as might be expected. However, the incident shock did not by any means need to be as strong as the detonation that resulted from it. For example, reference 64 showed that methane-oxygen mixtures could be ignited by shocks in which the calculated temperature was 410° to 482° F; the calculated temperature in reference 65 for a $2H_2$-O_2 mixture was 266° to 680° F. Ranges of temperature are given because the results depended somewhat upon the experimental arrangement, and the technique has not yet been sufficiently refined to eliminate all extraneous effects. Nevertheless, the indicated ignition temperatures are in a strikingly lower range than those determined by methods previously discussed, especially when the very short lags associated with shock-wave ignition are considered.

The favorable results of shock-ignition experiments, and the fact that a detonation wave is essentially a continuous ignition by a shock wave, have led to a suggested engine utilizing the principle (ref. 66). In such an engine, which might be a form of ram jet, the injectors would be moved into the diffuser upstream of the normal shock. The shock would ignite the mixture and combustion would be completed in a combustion chamber smaller than that required in present-day ram-jet engines. The exit nozzle would be used as a throttle to control the position of the shock igniter. The engine would be self-starting, and flame holders would not be required. Reference 66 should be consulted for further analysis of the characteristics of a shock-ignition ram jet and a discussion of its advantages and disadvantages.

It should be pointed out, however, that the principle need not necessarily be utilized in the form described in reference 66. Although further experimental work is needed, it appears that shock waves have a high potential for ignition of combustible mixtures, and may be found useful in other than ram-jet configurations.

Ignition by Capacitance Sparks

Probably the most important mode of ignition insofar as aircraft are concerned is electrical discharges, such as sparks and glow or arc discharges. These sparks or discharges permit the interchange of energy from an electrical circuit to a gas in a relatively efficient manner and in a minute volume compared with heated surfaces, flames, or hot gases. Complete control can be exercised over the amount of energy and the duration of the discharge. Although spark ignition has been the subject of many investigations and has found wide use in practical applications, there is still much to be learned about the mechanism whereby stored energy is converted to flame. The most complete summary available on spark ignition is that of reference 67.

There are three types of discharges that have been used to obtain ignition: capacitance sparks, inductance sparks, and capacitance sparks of long duration. The rate at which energy is released is different for these sparks and accounts for the difference in igniting ability.

Capacitance sparks are produced by the discharge of charged condensers into a gas. The duration of such a discharge may be extremely short (<0.01 microsec) for low energies and can be as high as 100 microseconds for larger energies (>1 j) because of inherent properties of the circuitry. The appearance of the spark is

bright and the spectrum of the spark corresponds to that of the gas in which the spark occurs. The current is high because of the low impedance of the spark gap. Inductance sparks are obtained from transformers, ignition coils, and magnetos, or when an inductive circuit is interrupted by opening contacts. Because inductance sparks usually are generated by high-impedance sources, the current is low; hence, the sparks have a weak appearance. The duration is long and the spectrum corresponds to the vapor of the metal electrodes. Capacitance sparks of long duration are produced when resistance is added to a capacitance discharge ignition system, the duration being controlled by the relative values of resistance and capacitance. When resistance is added, the characteristics of the discharge, that is, current, duration, and appearance, become very similar to those of an inductance spark. Because of losses in the resistance, such sparks are only useful for fundamental research. The energy at the gap must be measured by oscillographic or calorimetric methods.

The energy in a capacitance spark as obtained from the discharge of a capacitance is calculated by the following equation:

$$j = \frac{1}{2} c \left(v_2^2 - v_1^2\right) \tag{13}$$

where

c capacitance of condenser, farads

j energy obtained from capacitance, joules

v_1 voltage remaining on condenser at instant spark ceases, volts

v_2 voltage on condenser just before spark occurs, volts

This equation gives the energy released from the condenser, which may be higher than that actually dissipated in the spark gap because of losses in the circuit unless extreme care is taken to minimize them. Usually v_1 is small compared with v_2, and hence may be neglected. However, in systems using large capacitors and relatively low voltage, v_1 can be important.

In the succeeding discussion of the effects of variables on ignition by capacitance sparks, the following definitions will aid in consideration of the results:

(1) Minimum spark-ignition energy: The minimum spark-ignition energy of a flammable mixture is the total energy dissipated in the weakest spark that will just cause ignition.

(2) Quenching distance: The quenching distance is the electrode spacing marking the farthest penetration of the flame-quenching effect of the solid material. At this spacing, the ignition energy is a minimum; below this spacing, the energy increases.

(3) Electrostatic sparks: Electrostatic sparks are those sparks generated by friction, impact, pressure, cleavage, induction, successive contact and separation of unlike surfaces, and transference of fluids. They are the same as capacitance sparks, the only difference being in the manner in which the energy is generated. Data for electrostatic ignition energies would be the same as those determined for capacitance-spark ignition energies.

(4) Breakdown voltage of spark gap: The breakdown voltage of a spark gap is the lowest voltage that may be applied to a spark gap and yet cause a spark to be formed. This voltage should be distinguished from the spark discharge voltage, which is the voltage appearing across the spark gap during the life of the spark or discharge.

(5) Spark discharge: A spark occurs upon the electrical breakdown of a gas. It marks a transition from a nonself-sustaining discharge (sometimes called dark discharge) to one of several types of self-sustaining discharge, and usually takes place with explosive suddeness. The most important of the self-sustaining discharges are the glow and arc discharges. The type of discharge that results upon spark breakdown of a gap depends upon the gas pressure, the gap length and shape, the nature of the applied voltage, and the constants of the external circuit.

(6) Glow discharge: The glow discharge is a self-sustained discharge characterized by a glow over a considerable portion of the cathode electrode, low current, high voltage drop in the region close to the cathode electrode, small current densities at the cathode electrode, and generally a weak appearance.

(7) Arc discharge: The arc discharge is a self-sustained discharge characterized by an intense spot at the cathode electrode, high current, low voltage drop at the cathode region, large current densities at the cathode electrode, and generally strong appearance. It is the only type of discharge capable of supporting high currents.

In discussing the parameters that affect the energy required for ignition using capacitance sparks, an attempt has been made to disregard much of the older data which, it is believed, do not contribute to the subject of spark ignition in the light of present knowledge. For example, the bulk of the older work has been completed using electrode spacings shorter than the quenching distance, and many deductions using such information are erroneous, as pointed out in reference 10. Therefore, such information is used only where necessary to show a trend, and it is indicated that such data were obtained within the quenching distance. The important test conditions are included and will generally be found in the figures.

Mixture composition. - The effect of mixture composition on minimum ignition energy of quiescent mixtures (refs. 11 and 68) is shown in figures III-32 and -33 for three electrode configurations, various spacings, three fuels, and two pressures. The curves show that well-defined upper and lower ignition limits exist and that a minimum value of energy is required at a fuel composition of the order of stoichiometric. For most fuels, the minimum falls on the rich side of stoichiometric. For example, the following table (obtained from ref. 69) shows the minimum points of the curves for a number of different hydrocarbon fuels ignited at atmospheric pressure with the same electrodes used to obtain the data in figure III-32:

Flammable	Fuel in fuel-air mixture, percent by volume	Percent fuel in fuel-air mixture / Percent fuel in stoichiometric fuel-air mixture	Least energy, millijoule
Methane	8.45	0.88	0.28
Ethane	6.61	1.17	.25
Propane	5.07	1.26	.26
n-Butane	4.53	1.47	.26
n-Hexane	3.64	1.71	.24
n-Heptane	3.36	1.82	.25
Cyclopropane	6.34	1.45	.18
Cyclohexane	3.94	1.75	.24
Benzene	4.67	1.75	.21
Diethyl ether	5.30	1.57	.19

Data in figure III-33 for benzene are higher than shown in the table because the electrode spacing was within the quenching distance.

The effect of mixture composition on the minimum spark-ignition energy of flowing propane-air mixture at 3 inches of mercury absolute with a long-duration capacitance spark (ref. 70) is shown in figure III-34. The general trend is the same as for quiescent mixtures; however, the energy levels increase with velocity as described in a subsequent section.

The data show that, under proper conditions of fuel-air ratio, the energy required can be extremely low. Any departure from this fuel-air ratio requires higher ignition energies that tend toward infinity as the flammability limit is approached. The extreme importance of locating spark plugs in the proper mixture zone in a combustor is indicated.

Fuel type. - The type of fuel has a definite influence on the minimum ignition energy as shown in the appendix. Reference 71 presents analysis of a number of fuels with respect to molecular weight and arrangement of compounds with the following conclusions:

(1) Hydrocarbon ignition energies decrease in the order: alkanes, alkenes, and alkynes.

(2) An increase in chain length or chain branching increases ignition energy.

(3) Conjugation generally lowers the ignition energy.

(4) For long chains, the effect of structural variation is small, but for short chains, the effects are much larger.

(5) Negative substituent groups result in increasing ignition energy in the order: mercaptan, alcohol, chloride, and amine. The effects of chlorine and amine groups are particularly large.

(6) Primary amines increase ignition energy more than secondary or tertiary amines.

(7) Ethers and thioethers increase ignition energy.

(8) The peroxide group lowers the ignition energy greatly.

(9) Esters and ketones increase ignition energy greatly, but aldehydes raise ignition energy only slightly.

(10) Ignition energies for compounds containing three-membered rings are very low, particularly when oxygen is in the ring.

(11) Saturated compounds containing six-membered rings have relatively high ignition energies, but those of five-membered rings are about average.

(12) Ignition energies for aromatics are similar to those for linear hydrocarbons containing the same number of carbon atoms.

Basic studies of ignition of fuel mists or sprays in air, a very important aspect of fuel type, have not appeared in the literature because of problems associated with wetting of electrodes, energy absorbed by heat of vaporization, measurement of drop size, partial vaporization of droplets, and volatility of fuel. These

variables may affect the energy to such an extent that theories and empirical correlations formulated for gaseous fuel mixtures may not be applicable to liquid fuels.

Electrode spacing. - The effect of electrode spacing for various electrode configurations on the minimum spark-ignition energy (refs. 11 and 12) is shown in figures III-10 and -11. With the unflanged electrodes and irrespective of pressure, as the spacing is increased from low values, the energy required decreases. At atmospheric pressure, the energy remains constant with further increase in spacing. Eventually, the energy will rise again at much larger spacings. This constant energy portion is not observed at low pressure. With flanged electrodes, a spacing can be found below which ignition cannot be obtained regardless of the energy supplied. This spacing defines the quenching distance that has been previously described.

The quenching distance also varies with composition, as shown in figure III-32. The shape of the curve roughly parallels that of the energy curve. The data show that to obtain easiest ignition, electrode spacing must be changed as the fuel-air ratio is changed.

Electrode type. - Varying the electrode material has no significant effect on the ignition energy of a flammable mixture with capacitance sparks of short duration. Ignition of gaseous mixtures by sparks from platinum, nickel, zinc, aluminum, lead, brass, and steel electrodes was unaffected by electrode material (refs. 48 and 72). However, it is shown in reference 12 that, with long-duration capacitance sparks, there may be an indirect effect of electrode material. In this reference, it is shown that ignition energies can be different for the different materials, depending upon the type of discharge produced. Figure III-35 shows that stainless steel electrodes which produced a glow discharge had ignition energies 50 percent higher than cadmium electrodes which produced a discharge starting as an arc discharge and changing to a glow discharge. If the type of discharge was a glow discharge, varying the electrode material had a negligible effect.

The effect of electrode configuration is also shown in figure III-11. It may be concluded that the effect of electrode size is negligible at the quenching distance (0.65 in. at this condition). At spacings less than the quenching distance, the larger electrodes require more energy than the smaller electrodes because of the increased area for quenching to take place.

Condenser voltage. - The effect of condenser voltage on the ignition energy of a flammable mixture is negligible. That is, the ignition energy required is unaffected by increasing the condenser voltage as long as the capacitance is reduced to maintain the same stored energy. Reference 73 reports that the voltage could be varied from 1.6 to 5.8 kilovolts without changing the ignition energy required.

Spark duration. - The effect of increasing the spark duration in the range of 125 to 25,000 microseconds (ref. 70) is to increase the energy required approximately as a power function of the spark duration (fig. III-36). This increase is due to the energy being distributed over a larger volume. However, at extremely short spark durations (2 microsec), the energy is considerably higher than that of the majority of the longer-duration sparks. Reference 12 suggests that the increased energy is due to the energy distribution along the spark length.

Oscillation frequency. - Some references (for example, ref. 74) have stated that electrical processes are more important in the spark-ignition process than any thermal processes. The research used as a basis for this viewpoint is that

described in reference 75, in which the igniting power of a spark generated by a condenser-inductor combination increased with decreasing oscillation frequency of the current wave of the spark. However, as pointed out by Lewis and von Elbe in reference 10, the tests were run under questionable conditions, that is, all the work was carried out with electrode spacings shorter than the quenching distance. Hence, some sort of quenching test was conducted that gave no information regarding electrical processes. Reference 73 reports the addition of inductance to the apparatus in an attempt to determine the effect of oscillation frequency on ignition. At the quenching distance, no effect of reasonable inductance addition was found. Hence, in the light of the recent work, it must be concluded that inductance has no effect on ignition. One qualification might be added. In some cases where high-energy ignition systems are being used, the addition of inductance might change the duration of the discharge and so affect the ignition energy required.

Sparking rate. - The effect of sparking rate is described briefly in reference 76, in which an induction coil was used to produce sparks. However, the sparks produced were a series of capacitance sparks from a characteristic capacitance in the circuit. The first spark caused ignition if ignition occurred at all. The passage of two to ten additional sparks had no effect. This was believed to be because of somewhat lower voltage (and energy) in sparks following the first. These tests were conducted with spacing within the quenching distance and are therefore open to question. It is conceivable that, if the sparking rate is sufficiently high and sparks following the first could be generated in the heated zone left by the first spark, some effect could be observed.

Mixture velocity. - Increasing the velocity of flow of a combustible past the electrodes increases the energy required for ignition (ref. 70), as shown in figure III-37. Over the range of velocities indicated (5 to 54 ft/sec), the energy increases approximately linearly with velocity. At higher velocities (ref. 77), the energy increases much more rapidly (fig. III-38).

The velocity causes the spark to be blown downstream, thereby lengthening the spark path and causing the energy to be distributed over a much larger volume. Such distribution is dependent upon the gas velocity and spark duration. A theory has been proposed in reference 78 to correlate the parameters of density, velocity, spark duration, electrode spacing, fuel constants, and energy. This theory is based on the idea that the total energy H of the spark may not be the important factor in ignition of flowing gases with long-duration sparks. The spark is considered to move downstream at stream velocity U in the form of a square-cornered U. The legs of the U will be continuously lengthening, but the length L (corresponding to electrode spacing) will remain constant. It is considered that this length L is a line source of ignition, moving at mean stream velocity and is the important part of the spark. The energy in this line source H_L is calculated by making certain assumptions as to the manner in which and the rate at which the energy goes into the spark. The energy is calculated as follows:

$$H_L = \frac{LH}{2Ut_s} \log \frac{2Ut_s + L}{L} \tag{14}$$

where

H total ignition energy, joules

H_L energy in line source, joules

L electrode spacing, ft

t_s spark duration, sec

U gas velocity, ft/sec

The energy H_L heats a cylindrical volume of the combustible of length L and radius r. The radius r of this volume is found by assuming the requirement of ignition is that r must be of such size that the rate of heat generated in the volume must be equal to the rate of heat lost by conduction. An equation relating the rate of heat generated and rate of heat lost determines the critical size of r. Once r is determined, the amount of heat required to heat the volume of radius r and length L to flame temperature can be calculated. This heat should be equal to the heat H_L from the spark resulting in

$$\frac{L_q U t_s}{pLH} \propto \log \frac{2Ut_s + L}{L} \tag{15}$$

for electrode spacings equal to or less than quenching distance L_q; or

$$\frac{Ut_s}{pH} \propto \log \frac{2Ut_s + L}{L} \tag{16}$$

for electrode spacing greater than L_q. A plot of equations (15) and (16) is shown in figure III-39 for data obtained from references 70 and 78. Hence, from this analysis, it may be concluded that only a portion of the spark length is important in ignition of flowing gases by long-duration sparks. Energy in the remainder of the spark is dissipated without any help to the ignition process.

Turbulence. - If a turbulence promoter such as a wire screen is placed upstream of the electrodes in a flowing combustible gas (ref. 77), the energy required increases with the wire size of the turbulence promoter and with decreasing distance from turbulence promoter to electrodes (fig. III-38). The energy increases with those factors that increase the intensity of turbulence. The idea of a line source of ignition has been applied to turbulent ignition data similar to those shown in figure III-39 (ref. 78). All the concepts considered in the previous section were used except that the rate of heat loss was assumed to depend upon the intensity of turbulence. From this analysis, it was shown that at constant pressure,

$$\frac{H}{Ut_s} \log \frac{2Ut_s + L}{L} \propto f(\sqrt{\overline{u^2}}) \tag{17}$$

where

$f\sqrt{\overline{u^2}}$ function of intensity of turbulence, ft/sec

A plot of this relation is shown in figure III-40. Hence, the energy in the line source of ignition is shown to depend directly upon the intensity of turbulence. The effect of scale of turbulence was shown to be negligible at this condition.

Pressure. - Pressure has a pronounced effect on the ignition of a flammable mixture (ref. 73), as shown in figure III-41, in which the minimum ignition energy increases with decreasing pressure. For most fuels, the energy varies inversely as the bth power of pressure, where b is approximately 2. If the pressure is reduced sufficiently, a pressure will be reached (minimum ignition pressure) below

which ignition is limited by some factors of the apparatus such as electrode spacing, size of ignition chamber, or available energy. Whether there is an ultimate limiting pressure has not been determined. Therefore, all the following data are apparatus-limited.

Figure III-42 shows the energy increasing as the pressure decreases toward the minimum ignition pressure in tests (ref. 79) with constant electrode spacing. This curve is a combination of two separate effects, pressure effect and quenching effect. That is, as the pressure is reduced, the electrode spacing is effectively moved farther within the quenching distance, since the quenching distance increases with decreasing pressure. Different fuels exhibit different minimum pressures, as shown in figure III-42 and the following table (ref. 79):

Fuel	Minimum ignition pressure[a], in. Hg abs
Hydrogen	0.45
Methane	.75
1,3-Butadiene	.83
2-Butene	1.14
n-Butane and isobutane	1.14
Benzene	1.10
2,4-Dimethyl-1,3-pentadiene	1.30
n-Nonane	1.30

[a]Obtained with capacitance spark; temperature, 75° to 85° F; electrode spacing, 0.110 in. (less than quenching distance); energy, 8.64 j; ref. 79.

Lower pressures than these could have been obtained if the tests had been conducted in apparatus of sufficiently large size so that quenching could not occur. The importance of apparatus size has been emphasized in the quenching discussions.

Pressure limits for some of the petroleum fuels in air at room temperature have been determined as follows:

Fuel	Reference	Minimum ignition pressure,[a] in. Hg abs
100/130 Grade aviation gasoline	16	0.63
115/145 Grade aviation gasoline	16	1.50
Grade JP-3 jet fuel	16	1.50
Grade JP-4 jet fuel	80	.51

[a]Obtained with capacitance spark; temperature, 78° F; electrode spacing, 1.0 in.

Minimum ignition pressures are also a function of the mixture composition (ref. 79), as shown in figure III-43. The lowest pressure occurs at about 7.5 percent mixture ratio and on the lean side of stoichiometric for methane. Hydrogen also has the minimum on the lean side (ref. 79). For heavier hydrocarbons, such as propane and n-butane, the lowest pressure occurs on the rich side of stoichiometric. This phenomenon may be due to relative differences in diffusivities of air and the fuels. Air has a diffusivity less than hydrogen and methane and greater than propane and n-butane.

In determining the effect of pressure on ignition energy, consideration must be given to the choice of electrode spacing to be used, since the quenching distance is also a function of the pressure (ref. 71). This is demonstrated in figure III-44, which shows that the quenching distance increases with decreasing pressure. A complete relation between electrode spacing, pressure, and minimum ignition energy is shown in figure III-45.

The fact that the electrode spacing for minimum ignition energy increases with decreasing pressure may be explained by assuming that a certain spark-ignition energy can initially ignite a certain mass of flammable mixture. If the pressure is decreased, the mass occupies a larger volume, and hence the electrode spacing must be increased so that the spark will be of sufficient size to ignite the larger volume.

In the determination of minimum ignition pressures, capacitance sparks of high energy have been used to overcome the quenching effect of the electrodes (ref. 79). Figure III-46 shows the effect of electrode spacing and energy on minimum ignition pressure for n-butane and 2,2,4-trimethylpentane. The data show that the higher the energy, the less the effect of spacing on pressure. The energy of 8.64 joules that has been used (figs. III-46(a) and (b)) with a spacing of 0.110 inch ignites at pressures close to the minimum of the curves, and consequently, not much is gained by the wider spacing, although the optimum spacing would be greater than 1 inch.

Temperature. - The effect of increasing the temperature is to lower the minimum ignition energy, as shown in the following table taken from reference 81:

Fuel	Temperature, °F	Ignition energy,[a] millijoule
Carbon disulfide	77	0.76
	212	.5
n-Heptane	77	14.5
	212	6.7
	340	3.2
Isooctane	77	27.0
	212	11.0
	340	4.8
n-Pentane	-22	45.0
	-4	14.5
	77	7.8
	212	4.2
	340	2.3
	347	2.5
Propane	-40	11.7
	-22	9.7
	-4	8.4
	77	5.5
	135	4.2
	180	3.6
	212	3.5
	399	1.4
Propene oxide	77	2.4
	212	1.5
	360	.9

[a]Determined with capacitance spark, atmospheric pressure, and flanged electrodes.

From these data, a correlation was obtained relating energy and initial temperature of the mixture. This relation was of the form

$$H = Be^{CT} \tag{18}$$

where H is ignition energy, B and C are constants which are different for the various compounds, and T is the initial temperature.

The minimum ignition pressure is not affected greatly by changing the temperature from -50° to 300° F (ref. 79). Figure III-47 shows a slight linear decrease in pressure with an increase in temperature in this range. This decrease is in the proper direction to be the result of decreased quenching caused by increased temperature, as discussed previously.

Diluents. - The addition of a diluent to a combustible gas has a marked effect on the minimum ignition energy (ref. 73). It should be expected that the minimum ignition energy is dependent upon the absorptive and conductive qualities of any additive that might be present in the fuel, as well as upon the fuel itself. This is shown to be true in figure III-48(a). If the nitrogen in a methane-air mixture is replaced with helium, the energy increases; if replaced by argon, the energy decreases. With the exception of the methane-oxygen-argon mixtures, the minimum ignition energies increase with increasing diffusivity of the mixture according to reference 82.

The quenching distance curves (fig. III-48(b)) are similar to the energy curves.

The effects of diluents on minimum ignition pressure of mixtures of n-butane and oxygen with argon, nitrogen, carbon dioxide, and helium (ref. 79) are shown in figure III-49. In all cases, mixtures containing argon are the most easily ignited; mixtures containing carbon dioxide are the least easily ignited. Humidity, which might be considered as a diluent, would replace some of the oxygen, and would thus cause higher ignition energies. This effect has not been determined experimentally. The effect, if any, is probably small and can be neglected in most cases.

Ignition by Inductance Sparks

The difference between inductance sparks and capacitance sparks has been explained previously. The energy stored in an inductance is

$$j = \frac{1}{2} li^2 \tag{19}$$

where

i current in circuit at instant of sparking, amp

j energy, joules

l inductance, henry

Mixture composition, pressure, and temperature. - The effect of mixture composition, pressure, and temperature on minimum ignition energy with inductance sparks is similar to that obtained with capacitance sparks. However, with inductance sparks, much of the data have been obtained using the current in the primary of a transformer as an indication of the energy in the spark gap. Since this method does not give actual energies, the data are practically useless to both the

ignition-system designer and to the researcher. Also, much of the data have been obtained with spacings less than the quenching distance. For this reason, no further discussion will be given concerning these variables. References 83 to 89 give most of the information on inductance sparks.

Electrode spacing. - As shown in figure III-50, the minimum electrode spacing composition curve is very similar to those obtained with the capacitance spark (fig. III-48(b)). The quenching distances with inductance sparks appear to be slightly lower than those obtained with capacitance sparks.

Electrode material. - The available data on inductance sparks indicate that, unlike capacitance sparks, ignition energies of flammables are affected by changes in electrode materials. Electrodes of platinum, nickel, copper, aluminum, and iron have been used to ignite ethane-air and carbon monoxide - air mixtures (ref. 85). It was shown that decreasing density of the electrode material generally decreased the amount of energy required to ignite the flammable mixture. No separation of the types of discharge, that is, arc or glow, was made; therefore, no comparison can be made with the results obtained with the long-duration capacitance sparks.

Circuit inductance and voltage. - The energy stored in an inductance is determined by a simple relation with inductance and current; however, there are two factors that can be present which may cause errors in calculations. These factors are the type of inductance used and the circuit voltage. Sometimes, in order to obtain large energies, it is necessary to use inductances with metal cores, in which case some energy losses occur in the core material, as can be concluded from the following table (ref. 86):

Number of layers in inductance-core winding	Core of coil	Circuit inductance, henry	Circuit current, amp	Ignition energies,[a] millijoules
14	Air	0.01	0.35	0.6
14	Straight iron bar	.07	.15	.8
14	Rectangular iron frame	.56	.09	2.3

[a]Ignition of coal gas and air at atmospheric pressure and temperature.

Hence, the effect of type of inductance (if losses are present) is higher readings than are actually present in the spark.

The effect of circuit voltage in the case of sparks generated by opening contacts through which current is flowing is current flowing after the energy in the inductance is dissipated. The amount of extraneous energy caused by this after-current increases with the circuit voltage. Therefore, since the actual ignition energy in the spark gap is the sum of the stored energy plus the extraneous energy, any ignition energy values based on calculated stored energy will be too low. This effect is shown in the following table from reference 87:

Circuit potential, volts	Circuit inductance, henry	Circuit current, amp	Spark-ignition energy,[a] millijoules
4	0.0214	0.77	6.35
220	.0214	.35	1.30
4	.012	1.025	6.30
220	.012	.4	.96

[a]Ignition of 8.5 percent by volume mixture of methane in air at atmospheric pressure and temperature.

Current type. - Whether the current is alternating or direct appears to have no effect on ignition with inductance sparks (ref. 88).

SIGNIFICANCE OF BASIC QUENCHING, FLAMMABILITY, AND IGNITION DATA IN RELATION TO AIRCRAFT PROPULSION PROBLEMS

The data herein presented show the environmental conditions under which ignition and flame propagation in hydrocarbon-air mixtures may be obtained. With a fuel-air mixture contained in an apparatus large enough to preclude quenching, there are practically no limits to the conditions under which ignition and flame propagation may be obtained except the concentration limits of flammability. Hence, if proper mixtures can be produced in an aircraft combustor, there should be no basic limitation insofar as ignition and flammability are concerned in the over-all aircraft propulsion problem. However, practical limitations arise at present because of the finite size of combustors, the presence of turbulent flow, and the limited energy available from ignition sources.

There are some areas in which more work is needed. The quenching, flammability, and ignition of fuel sprays and mists have not yet been studied sufficiently. The effects of velocity and turbulence on flammability are still somewhat in doubt. Only a limited amount of research has been done in the promising field of chemical ignition.

As yet, there is no unified theory that is able to predict quantitatively the limits imposed on combustion by quenching, flammability, and ignition, from a knowledge of the basic physical and chemical properties of a combustible mixture. However, some qualitative ideas can be presented on the basis of present knowledge. The ideas are discussed under the three main types of work described in this chapter. Correlations between fundamental combustion properties and combustor performance, which at present must largely take the place of a general quantitative theory, will be given in subsequent chapters.

Quenching

The quenching effect of walls is always present when a flame is enclosed by a duct. If flame propagation is to occur, the dimensions of the volume to be burned must be larger than the quenching distance at the lowest presssure and most unfavorable fuel-air ratio encountered. Even if the flame is stabilized and is in no danger of being quenched by the walls, the dead space still exists and may be appreciable under some conditions. Thus, it should be noted that the full cross section of the chamber is not available for heat release.

In some current tubular-combustor turbojet engines, only two of the chambers are fitted with spark plugs. The remaining chambers must be ignited by the spread of flame through cross-fire tubes. Altitude starting performance should therefore be adversely affected by quenching of the igniting flame if the cross-fire tubes are too narrow. This has experimentally been found to be the case.

Recent work indicates that homogeneous gas-phase quenching may also occur because of turbulent motion. Thus, it is possible that measures taken to increase turbulence and thereby improve mixing or extend the residence time of the fuel in the combustor may actually result in no change or even a decrease in combustor performance.

Flammability

A self-sustained flame cannot exist in a mixture unless the fuel concentration is within the flammable range under the given conditions. Consequently, excessive dilution of the burning zone with either fuel or air must be avoided. It should again be pointed out, however, that flames sustained by a continuous ignition source such as a pilot may sometimes exist at over-all fuel-air ratios outside the range of flammability.

The effects of diluents must also be considered. For example, if it is required to burn fuel in an atmosphere containing exhaust products, substitution of carbon dioxide and water vapor for some of the oxygen originally present will narrow the flammable range. If the exhaust products are hot, the increased temperature may tend to compensate for this narrowing. Such questions might arise, for example, if a pilot flame is required to burn in the presence of recirculation from the main combustion zone of the combustor, or in the case of an afterburner.

Ignition

Ignition in the high-speed combustor can be accomplished by any of the methods discussed; however, practical considerations may make some of them infeasible. For example, ignition by electrically heated surfaces is very inefficient compared with ignition by electrical discharges. Not only must the mass of the heated surface be raised to the required temperature but also a larger volume of gas must be heated because of the longer times required to attain ignition.

Flames or hot gases can be effective ignition sources, but there must be available an additional ignition source to produce the flame or hot gas in the first place. In aircraft at adverse starting conditions, it may be just as difficult to ignite the pilot as it would be to ignite the main combustible. Ignition by electrical discharge or by chemical means, therefore, appears to be the most feasible method, although chemical ignition has not been adequately investigated.

The ideal environmental conditions for ignition by electrical discharges are as follows:

(1) High pressure

(2) High temperature

(3) Low gas velocity and turbulence

(4) Location of spark in zone of best mixture composition

(5) Gaseous fuel-air mixture

(6) Electrode spacing maintained at quenching distance

(7) Optimum spark duration

Obviously, it would be impossible to satisfy all these requirements in an actual combustor, but any attempt to satisfy as many as possible would result in lower ignition energies and lower-weight ignition systems.

Whether capacitance or inductance sparks are the better for ignition is a point for consideration. The data presented herein show that capacitance sparks can readily be varied over a tremendous energy range, whereas inductance sparks may possibly be limited to those applications where low energy is required. On the other hand, if the data on the effect of spark duration using long-duration sparks are used as an indication of what might happen with inductance sparks, there may be some instances where inductance sparks are superior to capacitance sparks.

It would appear, then, that a choice between the two systems would depend upon the actual energy required. Design and operation of the ignition systems producing these two types of sparks might be the important factor in selecting the type of spark to be used.

The fact that there is a minimum contact time, or ignition lag, for ignition by heated surfaces, hot gases, or pilot flames, introduces the possibility of an effect of such ignition sources on the combustion efficiency of combustors that utilize them. If the flow rate in a given burner is fixed, 100 percent combustion efficiency can be obtained only if there is sufficient residence time for the mixture to be ignited and for the flame to consume the mixture as rapidly as it flows into the chamber. The consumption time depends upon the burning velocity under the given conditions. Therefore, if the required time for contact with the ignition source is excessively long, insufficient time for burning may remain before the mixture leaves the burner, that is, only part of the fuel may be consumed, and the combustion efficiency may fall below 100 percent.

REFERENCES

1. Harris, Margaret E., Grumer, Joseph, von Elbe, Guenther, and Lewis, Bernard: Burning Velocities, Quenching, and Stability Data on Nonturbulent Flames of Methane and Propane with Oxygen and Nitrogen. Third Symposium on Combustion and Flame and Explosion Phenomena, The Williams & Wilkins Co. (Baltimore), 1949, pp. 80-89.

2. Friedman, Raymond, and Johnston, W. C.: Pressure Dependence of Quenching Distance of Normal Heptane, Iso-Octane, Benzene, and Ethyl Ether Flames. Jour. Chem. Phys., vol. 20, no. 5, May 1952, p. 919.

3. Friedman, Raymond: The Quenching of Laminar Oxyhydrogen Flames by Solid Surface. Third Symposium on Combustion and Flame and Explosion Phenomena, The Williams & Wilkins Co. (Baltimore), 1949, pp. 110-120.

4. Friedman, Raymond, and Johnston, W. C.: The Wall-Quenching of Laminar Propane Flames as a Function of Pressure, Temperature, and Air-Fuel Ratio. Jour. Appl. Phys., vol. 21, no. 8, Aug. 1950, pp. 791-795.

5. Simon, Dorothy M., Belles, Frank E., and Spakowski, Adolph E.: Investigation and Interpretation of the Flammability Region for Some Lean Hydrocarbon-Air Mixtures. Fourth Symposium (International) on Combustion, The Williams & Wilkins Co. (Baltimore), 1953, pp. 126-138.

6. Berlad, Abraham L.: Flame Quenching by a Variable-Width Rectangular-Slot Burner as a Function of Pressure for Various Propane-Oxygen-Nitrogen Mixtures. NACA RM E53K30, 1954.

7. Wohl, Kurt: Quenching, Flash-Back, Blow-Off - Theory and Experiment. Fourth Symposium (International) on Combustion, The Williams & Wilkins Co. (Baltimore), 1953, pp. 68-89.

8. Starkman, E. S., Haxby, L. P., and Cattaneo, A. G.: A Study of Free Flames in Turbulent Streams. Fourth Symposium (International) on Combustion, The Williams & Wilkins Co. (Baltimore), 1953, pp. 670-673.

9. von Elbe, Guenther, and Lewis, Bernard: Theory of Ignition, Quenching and Stabilization of Flames of Nonturbulent Gas Mixtures. Third Symposium on Combustion and Flame and Explosion Phenomena, The Williams & Wilkins Co. (Baltimore), 1949, pp. 68-79.

10. Lewis, Bernard, and von Elbe, Guenther: Combustion, Flames, and Explosions of Gases. Academic Press, Inc., 1951.

11. Lewis, Bernard, and von Elbe, Guenther: Ignition and Flame Stabilization in Gases. Trans. A.S.M.E., vol. 70, no. 4, May 1948, pp. 307-314; discussion, pp. 314-316.

12. Swett, Clyde C., Jr.: Spark Ignition of Flowing Gases. II - Effect of Electrode Parameters on Energy Required to Ignite a Propane-Air Mixture. NACA RM E51J12, 1951.

13. Coward, H. F., and Jones, G. W.: Limits of Flammability of Gases and Vapors. Bull. 503, Bur. Mines, 1952.

14. Spakowski, Adolph E.: Pressure Limits of Flame Propagation of Pure Hydrocarbon-Air Mixtures at Reduced Pressures. NACA RM E52H15, 1952.

15. Barnett, Henry C., and Hibbard, R. R.: Fuel Characteristics Pertinent to the Design of Aircraft Fuel Systems. NACA RM E53A21, 1953.

16. Jones, G. W., et al.: Research on the Flammability Characteristics of Aircraft Fuels. WADC Tech. Rep. 52-35, Wright Air Dev. Center, Wright-Patterson Air Force Base, June 1952. (Contract AF 33(038)50-1293E.)

17. Damon, Glenn H.: Monthly Report on Contract AF-18(600)151: Flammability Characteristics of Aircraft Fuels. U.S. Dept. Interior, Bur. Mines, Pittsburgh (Pa.), May 6, 1952, p. 5.

18. Moran, H. E., Jr., and Bertschy, A. W.: Flammability Limits for Mixtures of Hydrocarbon Fuels, Air, and Halogen Compounds. Rep. No. NRL 4121, Naval Research Lab., Washington (D.C.), Feb. 25, 1953.

19. Fryburg, George: Review of Literature Pertinent to Fire-Extinguishing Agents and to Basic Mechanisms Involved in Their Action. NACA TN 2102, 1950.

20. Burgoyne, J. H., and Williams-Leir, G.: The Influence of Incombustible Vapours on the Limits of Inflammability of Gases and Vapors in Air. Proc. Roy. Soc. (London), ser. A, vol. 193, July 21, 1948, pp. 525-539.

21. Belles, Frank E.: A Preliminary Investigation of Wall Effects on Pressure-Inflammability Limits of Propane-Air Mixtures. NACA RM E50J10a, 1950.

22. Karlovitz, Bela: Open Turbulent Flames. Fourth Symposium (International) on Combustion, The Williams & Wilkins Co. (Baltimore), 1953, pp. 60-67.

23. DiPiazza, James T., Gerstein, Melvin, and Weast, Robert C.: Flammability Limits of Hydrocarbon-Air Mixtures. Reduced Pressures. Ind. and Eng. Chem., vol. 43, no. 12, Dec. 1951, pp. 2721-2725.

24. Egerton, Alfred, and Powling, J.: The Limits of Flame Propagation at Atmospheric Pressure. I. The Influence of "Promoters." Proc. Roy. Soc. (London), ser. A, vol. 193, May 27, 1948, pp. 172-190.

25. Zeldovich, Y. B.: Theory of Combustion and Detonation of Gases. Tech. Rept. No. F-TS-1226-IA (GDAM A9-T-45), Air Materiel Command, 1949. (Trans. by Brown Univ.)

26. Moore, Harold: Spontaneous Ignition Temperatures of Liquid Fuels for Internal Combustion Engines. Jour. Soc. Chem. Ind., vol. XXXVI, no. 3, Feb. 15, 1917, pp. 109-112.

27. Anon: The Spontaneous Ignition Temperatures of Liquid Fuels. Engineering, vol. CIX, Jan. 30, 1920, pp. 151-152.

28. Dixon, H. B., and Higgins, W. F.: On the Ignition-Point of Gases at Different Pressures. Memoirs and Proc. Manchester Literary and Phil. Soc. (Manchester Memoirs), vol. LXX, 1925-26, pp. 29-36.

29. Tizard, H. T., and Pye, D. R.: Experiments on the Ignition of Gases by Sudden Compression. Phil. Mag. and Jour. Sci. vol. XLIV, no. 259, July 1922, pp. 79-121.

30. Mason, Walter, and Wheeler, Richard Vernon: The Ignition of Gases. Pt. IV. Ignition by a Heated Surface. Mixtures of the Paraffins with Air. Jour. Chem. Soc. Trans. (London), vol. CXXV, pt. II, 1924, pp. 1869-1875.

31. Guest, P. G.: Ignition of Natural Gas-Air Mixtures by Heated Surfaces. Tech. Paper 475, Bur. Mines, 1930.

32. Glendinning, W. G.: Possible Cause of Aircraft Fires on Crash. R. & M. No. 1375, British A.R.C., Jan. 1930.

33. Dykstra, F. J., and Edgar, Graham: Spontaneous Ignition Temperature of Liquid Hydrocarbons at Atmospheric Pressure. Ind. and Eng. Chem., vol. 26, no. 5, May 1934, pp. 509-510.

34. Sortman, Charles W., Beatty, Harold A., and Heron, S. D.: Spontaneous Ignition of Hydrocarbons. Zones of Nonignition. Ind. and Eng. Chem., vol. 33, no. 3, Mar. 1941, pp. 357-360.

35. Townend, D. T. A.: The Present Era in Combustion. Chem. and Ind. (London), no. 44, Nov. 10, 1945, pp. 346-351.

36. Moore, Harold: Spontaneous Ignition-Temperatures of Liquid Fuels. The Auto. Eng., vol. X, no. 138, May 1920, pp. 199-204.

37. Silver, Robert S.: The Ignition of Gaseous Mixtures by Hot Particles. Phil. Mag. and Jour. Sci., vol. 23, no. 156, ser. 7, Apr. 1937, suppl., pp. 633-657.

38. Mullen, James W., II, Fenn, John B., and Irby, Moreland R.: The Ignition of High Velocity Streams of Combustible Gases by Heated Cylindrical Rods. Third Symposium on Combustion and Flame and Explosion Phenomena, The Williams & Wilkins Co. (Baltimore), 1949, pp. 317-329.

39. Masson, Henry James, and Hamilton, William F.: A Study of Auto-Ignition Temperatures. III - (a) Mixtures of Pure Substances, (b) Gasolines. Ind. and Eng. Chem., vol. 21, no. 6, June 1929, pp. 544-549.

40. Frank, Charles E., and Blackham, Angus U.: Spontaneous Ignition of Organic Compounds. Ind. and Eng. Chem., vol. 44, no. 4, Apr. 1952, pp. 862-867.

41. Thompson, Norman J.: Auto-Ignition Temperatures of Flammable Liquids. Ind. and Eng. Chem., vol. 21, no. 2, Feb. 1929, pp. 134-139.

42. Couriot, et Meunier, Jean: Action d'un conducteur électrique incandescent sur les gas qui léntourent. Comptes Rendus, T. 145, Dec. 9, 1907, pp. 1161-1163.

43. The Associated Factory Mutual Fire Insurance Cos.: Properties of Flammable Liquids, Gases, and Solids. Ind. and Eng. Chem., vol. 32, no. 6, June 1940, pp. 880-884.

44. Jackson, Joseph L.: Spontaneous Ignition Temperatures of Pure Hydrocarbons and Commercial Fluids, NACA RM E50J10, 1950. (See also Ind. and Eng. Chem., vol. 43, no. 12, Dec. 1951, p. 2869.)

45. Heron, S. D., and Beatty, Harold A.: Aviation Fuels - Present and Future Development. Proc. of Ninth Mid-Year Meeting of Am. Petroleum Inst., sec. 111, vol. 20M(III), pub. by A.P.I. (New York), 1939.

46. Edgar, Graham: Ignition Temperatures of Aircraft Combustible Liquids. SAE Jour. (Trans.), vol. 45, no. 1, July 1939, p. 294.

47. Tausz, J., and Schulte, F.: Determination of Ignition Points of Liquid Fuels Under Pressure. NACA TM 299, 1925.

48. Morgan, J. D.: Principles of Ignition. Isaac Pitman & Sons, Ltd. (London), 1942.

49. Jackson, Joseph L., and Brokaw, Richard S.: Variation of Spontaneous Ignition Delays with Temperature and Composition for Propane-Oxygen-Nitrogen Mixtures at Atmospheric Pressure. NACA RM E54B19, 1954.

50. Mullins, B. P.: Studies on the Spontaneous Ignition of Fuels Injected into a Hot-Air Stream: General Introduction and Pt. I - The Development of a Combustion Test Rig for Measuring the Ignition Delay of Fuels. Rep. No. R.89, British N.G.T.E., Aug. 1951.

51. Mullins, B. P.: Studies on the Spontaneous Ignition of Fuels Injected into a Hot-Air Stream: Pt. II - The Effect of Physical Factors Upon the Ignition Delay of Kerosine-Air Mixtures. Rep. No. R.90, British N.G.T.E., Sept. 1951.

52. Mullins, B. P.: Studies on the Spontaneous Ignition of Fuels Injected into a Hot-Air Stream: Pt. IV - Ignition Delay Measurements on Some Gaseous Fuels At Atmospheric and Reduced Static Pressures. Rep. No. R.96, British N.G.T.E., Oct. 1951.

53. Barr, J., and Mullins, B. P.: Concerning Combustion in Vitiated Atmospheres. Rep. No. R.44, British N.G.T.E., June 1949.

54. Krause, Erich, and Grosse, Aristid: Die Chemie der metall-organischen Verbindugen. Gebrüder Borntraeger (Berlin), 1937. (Reproduced by Edwards Bros., Inc. (Ann Arbor), 1943.)

55. Badin, Elmer J., Walters, David R., and Pease, Robert N.: The Ignition of n-Butane by the Spontaneous Oxidation of Zinc Dimethyl. Jour. Am. Chem. Soc., vol. 69, no. 11, Dec. 4, 1947, pp. 2586-2588.

56. Brokaw, Richard S., Badin, Elmer J., and Pease, Robert N.: Wall Effects in the Oxidation of Boron Triethyl Vapor. Ignition of n-Butane. Jour. Am. Chem. Soc., vol. 70, no. 5, May 1948, pp. 1921-1922.

57. Schlesinger, H. I., Sanderson, R. Thomas, and Burg, A. B.: Metallo Borohydrides. I. Aluminum Borohydride. Jour. Am. Chem. Soc., vol. 62, no. 12, Dec. 1940, pp. 3421-3425.

58. Badin, Elmer J., Hunter, Paul C., and Pease, Robert N.: The Spontaneous Ignition of Aluminum Borohydride Vapor in Oxygen. Jour. Am. Chem. Soc., vol. 71, no. 8, Aug. 1949, p. 2950.

59. Brokaw, Richard S., Badin, Elmer J., and Pease, Robert N.: The Oxidation of Butene-1 Induced by Aluminum Borohydride. Jour. Am. Chem. Soc., vol. 72, no. 4, Apr. 1950, pp. 1793-1795.

60. Straight, David M., Fletcher, Edward A., and Foster, Hampton H.: Aluminum Borohydride as an Ignition Source for Turbojet Combustors. NACA RM E53G15, 1953.

61. Anon.: Survey of the Bumblebee Activities. Rep. No. 34, Appl. Phys. Lab., The Johns Hopkins Univ., Mar. 1946. (Contract NOrd 7386 with Bur. Ord. Navy Dept.)

62. Seabright, H.: An Investigation of Catalytic Ignition and Flame Holders. Rep. No. M-46-1. Airplane Div., Eng. Dept., Curtiss-Wright Corp., Sept. 26, 1946. (Air Materiel Command, Contract W33-038-ac-14161 and Bur. Aero. Contract NOa(s)-8275.)

63. Evans, Marjorie W.: Current Theoretical Concepts of Steady-State Flame Propagation. Chem. Rev., vol. 51, no. 3, 1952, pp. 363-429.

64. Shepherd, W. C. F.: The Ignition of Gas Mixtures by Impulsive Pressures. Third Symposium on Combustion and Flame and Explosion Phenomena, The Williams & Wilkins Co. (Baltimore), 1949, pp. 301-316.

65. Fay, James A.: Some Experiments on the Initiation of Detonation in $2H_2$-O_2 Mixtures by Uniform Shock Waves. Fourth Symposium (International) on Combustion, The Williams & Wilkins Co. (Baltimore) 1953, pp. 501-507.

66. Rand, Frank F., Jr.: The Shock Ignition Engine. Aero. Eng. Rev., vol. 11, no. 10, Oct. 1952, pp. 22-27; 62.

67. Hazard, Herbert R.: A Review of Research on Spark Ignition. Tech. Rep. No. 15037-1, Battelle Memorial Inst., Mar. 13, 1952. (Contract AF 33(038)-12656, E.O. No. 460-35 S.R.-8.)

68. Guest, P. G.: Apparatus for Determining Minimum Energies for Electric Spark Ignition of Flammable Gases and Vapors. R.I. 3753, Bur. Mines, May 1944.

69. Blanc, M. V., Guest, P. G., von Elbe, Guenther, and Lewis, Bernard: Ignition of Explosive Gas Mixtures by Electric Sparks. Pt. III. Minimum Ignition Energies and Quenching Distances of Mixtures of Hydrocarbons and Ether with Oxygen and Inert Gases. Third Symposium on Combustion and Flame and Explosion Phenomena, The Williams & Wilkins Co. (Baltimore), 1949, pp. 363-367.

70. Swett, Clyde C., Jr.: Spark Ignition of Flowing Gases. I - Energies to Ignite Propane - Air Mixtures in Pressure Range of 2 to 4 Inches Mercury Absolute. NACA RM E9E17, 1949.

71. Calcote, H. F., Gregory, C. A., Jr., Barnett, C. M., and Gilmer, Ruth B.: Spark Ignition - Effect of Molecular Structure. Ind. and Eng. Chem., vol. 44, no. 11, Nov. 1952, pp. 2656-2660; discussion, pp. 2660-2662.

72. Boyle, A. R., and Llewellyn, F. J.: The Electrostatic Ignitibility of Various Solvent Vapour-Air Mixtures. Jour. Soc. Chem. Ind., vol. 66, no. 3, Mar. 1947, pp. 99-102.

73. Blanc, M. V., Guest, P. G., von Elbe, Guenther, and Lewis, Bernard: Ignition of Explosive Gas Mixture by Electric Sparks. I. Minimum Ignition Energies and Quenching Distances of Mixtures of Methane, Oxygen, and Inert Gases. Jour. Chem. Phys., vol. 15, no. 11, Nov. 1947, pp. 798-802.

74. Jost, Wilhelm: Explosion and Combustion Processes in Gases. First ed., McGraw-Hill Book Co., Inc., 1946.

75. Finch, G. I., and Thompson, H. H.: The Effect of Frequency on the Condensed Discharge Ignition of Carbonic Oxide-Air Detonating Gas. Proc. Roy. Soc. (London), vol. CXXXVI, no. A823, Nov. 3, 1931, pp. 343-348; discussion, pp. 349-351.

76. Paterson, Clifford C., and Campbell, Norman: Some Characteristics of the Spark Discharge and Its Effect in Igniting Explosive Mixtures. Proc. Phys. Soc. (London), vol. XXXI, Dec. 1918-Aug. 1919, pp. 168-227; discussion pp. 227-228.

77. Swett, Clyde C., Jr., and Donlon, Richard H.: Spark Ignition of Flowing Gases. III - Effect of Turbulence Promoter on Energy Required to Ignite a Propane-Air Mixture. NACA RM E52J28, 1953.

78. Swett, Clyde C., Jr.: Spark Ignition of Flowing Gases. IV. Theory of Ignition in Nonturbulent and Turbulent Flow Using Long-Duration Discharges. NACA RM E54F29a, 1954.

79. Lakin, W. P., Thwaites, H. L., Skarstrom, C. W., and Baum, A. W.: Fourth Annual Rep. on Fundamental Studies of Combustion. Rep. No. RL-5M-48(69), Esso Labs, Res. Div., (Standard Oil Dev. Co.), Nov. 30, 1948. (Contract N6-ori-109.)

80. Lewis, Bernard: Monthly Report on Contract AF-18(600) 151: Flammability Characteristics of Aircraft Fuels. U.S. Dept. Interior, Bur. Mines, Feb. 10, 1953.

81. Fenn, J. B.: Lean Flammability Limit and Minimum Spark Ignition Energy. Ind. and Eng. Chem., vol. 43, no. 12, Dec. 1951, pp. 2865-2868.

82. Scull, Wilfred E.: Relation Between Inflammables and Ignition Sources in Aircraft Environments. NACA Rep. 1019, 1951. (Supersedes NACA TN 2227.)

83. Wheeler, Richard Vernon: The Ignition of Gases. Pt. III. Ignition by the Impulsive Electrical Discharge. Mixtures of the Paraffins with Air. Jour. Chem. Soc. Trans. (London), vol. CXXV, pt. II, 1924, pp. 1858-1867.

84. Wheeler, Richard Vernon: The Ignition of Gases. Pt. I. Ignition by the Impulsive Electrical Discharge. Mixtures of Methane and Air. Jour. Chem. Soc. Trans. (London), vol. CXVII, pt. II, 1920, pp. 903-917.

85. Thornton, W. M.: The Reaction Between Gas and Pole in the Electrical Ignition of Gaseous Mixtures. Proc. Roy. Soc. (London), vol. XCII, no. A634, ser. A, Oct. 1, 1915, pp. 9-22.

86. Morgan, John David: The Ignition of Explosive Gases by Electric Sparks. Jour. Chem. Soc. Trans. (London), vol. CXV, 1919, pp. 94-104.

87. Morgan, J. D.: The Thermal Theory of Gas Ignition by Electric Sparks. Phil Mag. and Jour. Sci., vol. 49, no. 290, ser. 6, Feb. 1925, pp. 323-336.

88. Wheeler, R. V.: The Electric Ignition of Firedamp: Alternating and Continuing Currents Compared. Paper No. 20, Safety in Mines Res. Board (London), 1926.

89. Allsop, G., and Guenault, E. M.: The Incendivity of Electric Sparks in Relation to the Characteristics of the Circuit. Third Symposium on Combustion and Flame and Explosion Phenomena, The Williams & Wilkins Co. (Baltimore), 1949, pp. 341-353.

TABLE III-I. - FLAMMABILITY LIMITS IN AIR AT ATMOSPHERIC PRESSURE AND ROOM TEMPERATURE[a]

Fuel	Lean limit		Rich limit	
	Volume percent	Stoichiometric fuel-air ratio, percent	Volume percent	Stoichiometric fuel-air ratio, percent
n-Paraffins				
Methane	5.3	53.5	14	156
Propane	2.2	53.8	9.5	251
Butane	1.9	60.1	8.5	288
Pentane	1.5	58.2	7.8	323
Hexane	1.2	55.2	7.5	368
Heptane	1.2	63.9	6.7	378
Octane	1.0	60.3	----	---
Isoparaffins				
2,2-Dimethylpropane	1.4	54.2	7.5	201
2-Methylpentane	1.2	55.2	7.0	342
2,2,4-Trimethylpentane	1.1	66.3	----	---
2,2,3,3-Tetramethylpentane	.8	53.9	4.9	345
Olefins				
Ethene	3.1	45.8	32	676
Propene	2.4	52.8	10.3	247
1-Butene	1.6	46.8	9.3	294
Aromatics				
Benzene	1.4	50.9	7.1	275
Toluene	1.4	61.1	----	---
Ethylbenzene	1.0	50.7	----	---

[a]Ref. 13.

TABLE III-II. - TYPICAL DISTILLATION DATA FOR AIRCRAFT FUELS[a]

A.S.T.M. distillation D86-52, Percentage evaporated	Temperature, °F			
	AN-F-48, 100/130	MIL-F-5616, JP-1	MIL-F-5624A	
			JP-3	JP-4
Initial point	105	338	113	148
10	144	362	169	218
20	162	366	198	255
30	178	369	218	288
40	191	373	236	319
50	202	377	254	349
60	210	381	270	378
70	219	387	293	409
80	225	393	324	441
90	236	404	388	475
End point	299	424	473	561

[a]Ref. 15.

TABLE III-III. - FLAMMABILITY LIMITS OF AIRCRAFT FUELS AT 300° F

Fuel	Flammability limits			
	Fuel-air ratio[a]		Volume percent[b]	
	Lean	Rich	Lean	Rich
100/130 gasoline	0.041	0.27	1.17	7.27
JP-1	.037	.31	.71	5.65
JP-3	.037	.30	.93	7.08

[a]Ref. 16.
[b]Estimated.

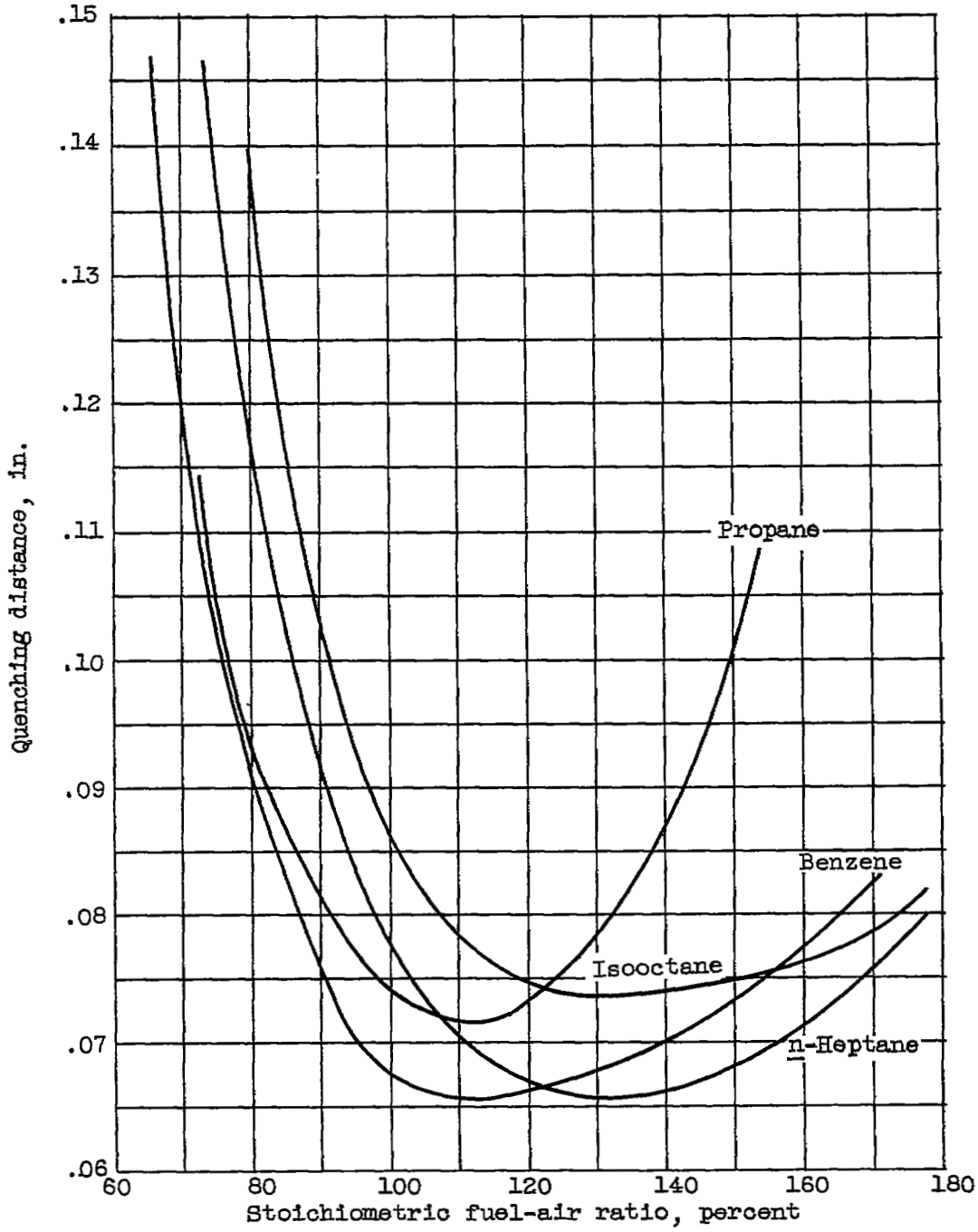

Figure III-1. - Variation of quenching distance with hydrocarbon type. Pressure, atmospheric; temperature, 212° F (by permission from ref. 2).

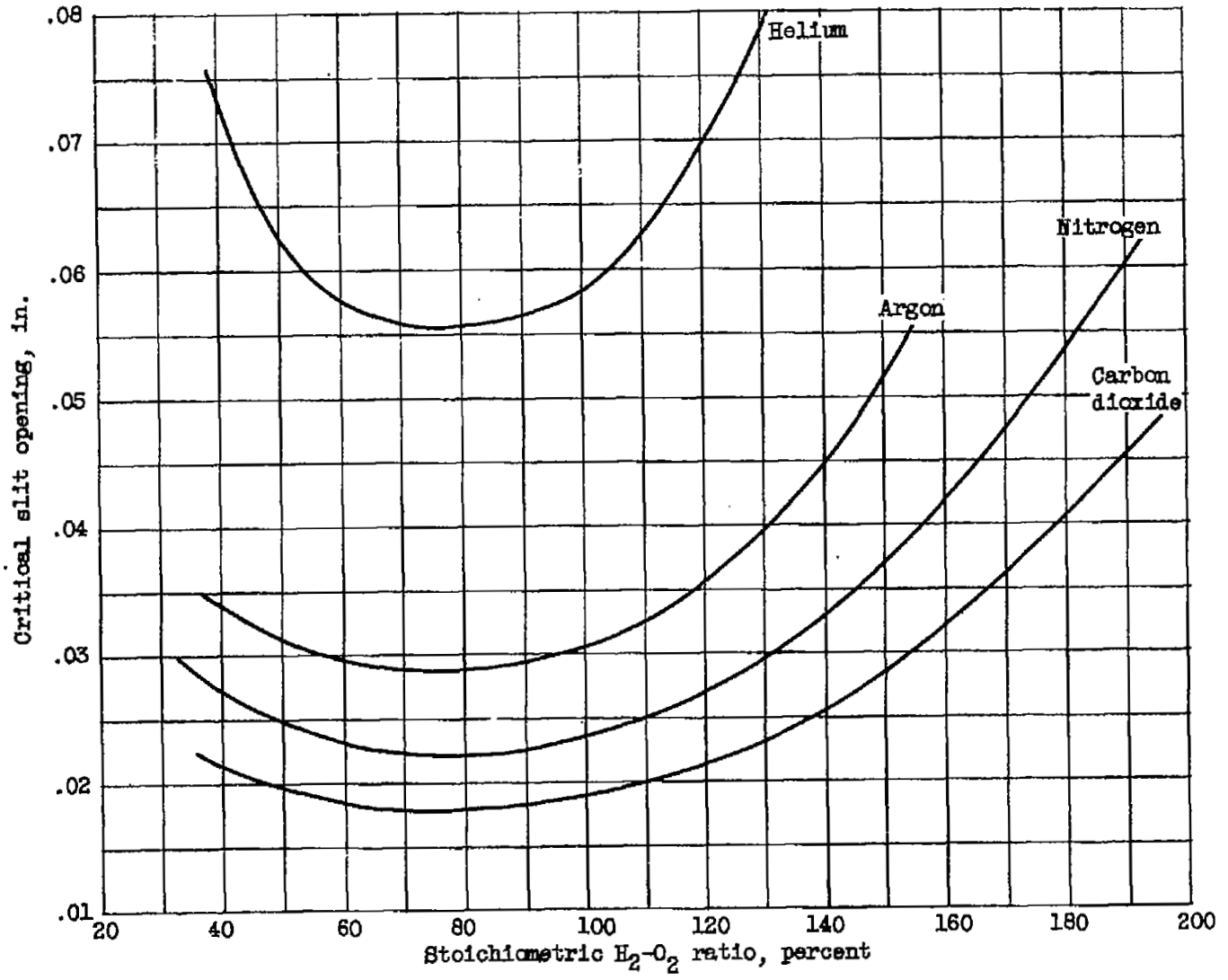

Figure III-2. - Effects of various inert gases on quenching distance (ref. 3).

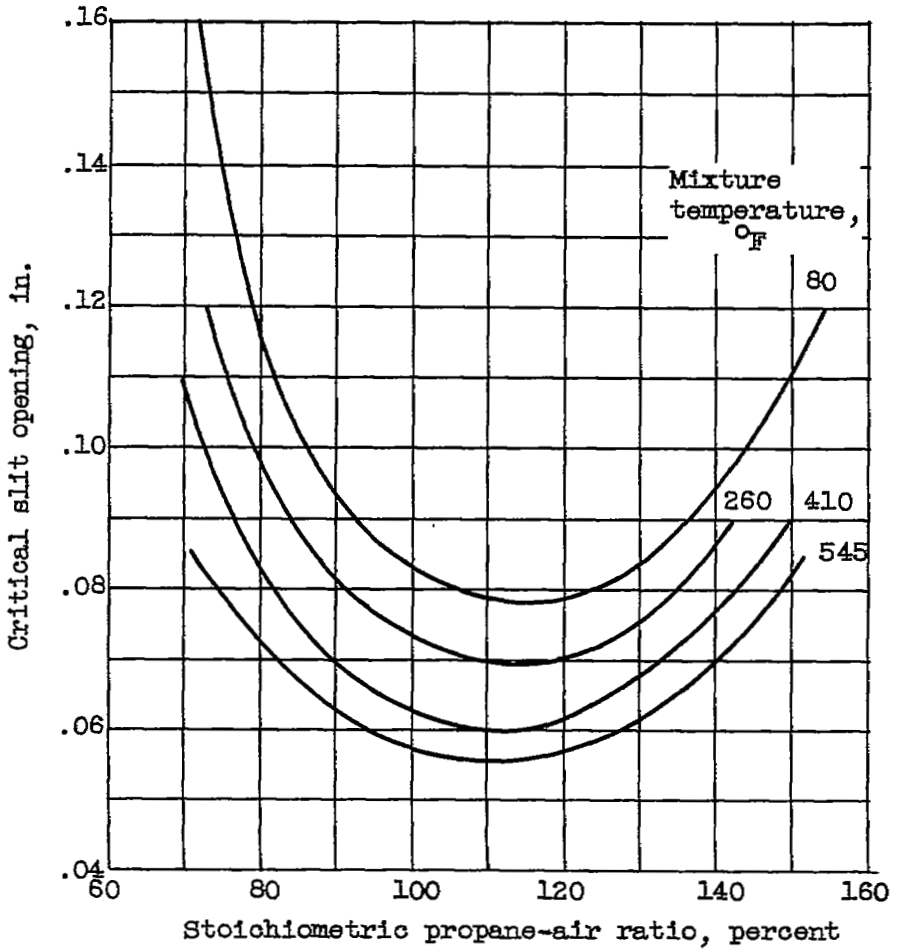

Figure III-3. - Effect of temperature on quenching distance. Pressure, 29.02 inches of mercury absolute (by permission from ref. 4).

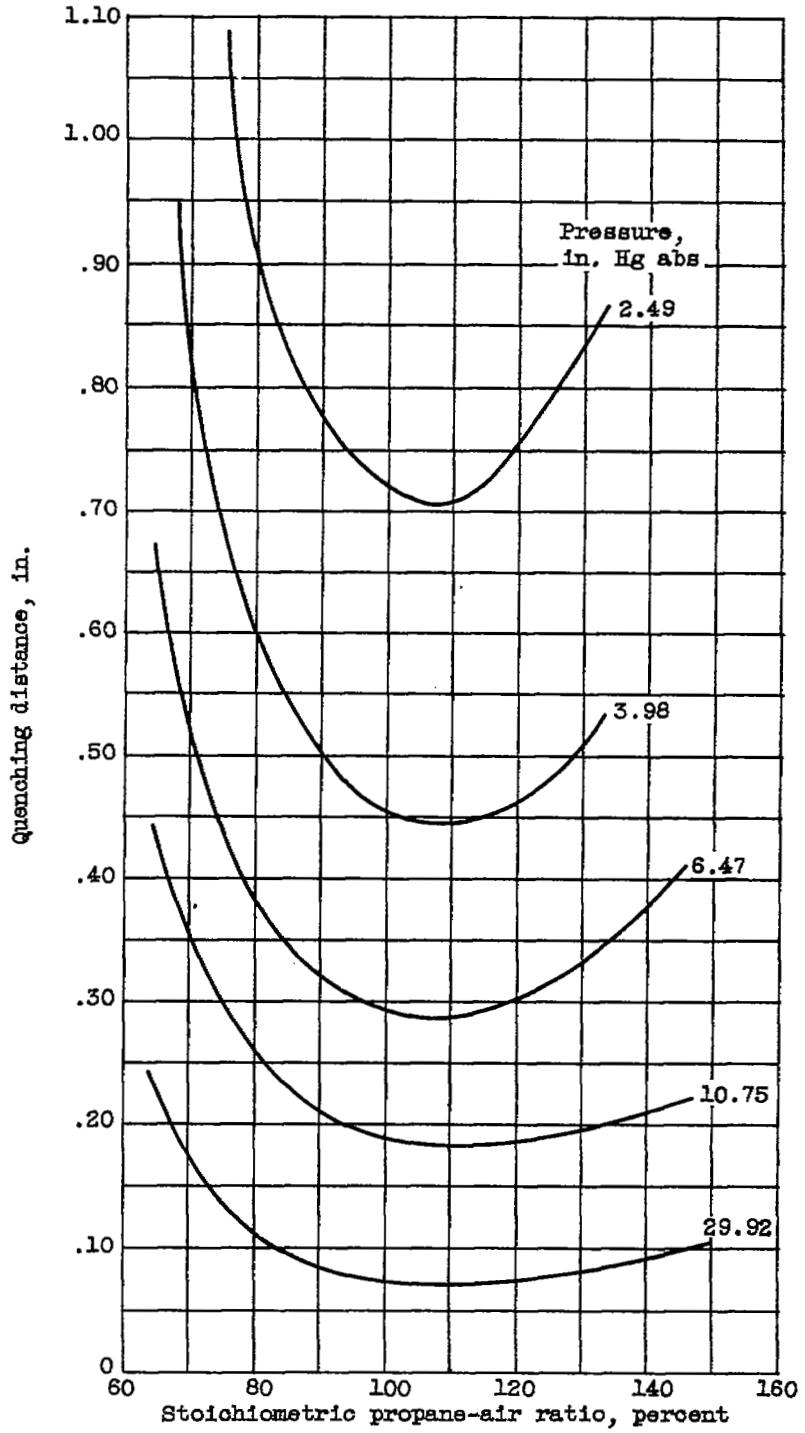

Figure III-4. - Effect of pressure on quenching distance of propane-air flames. Ambient temperature, about 75° F (by permission from ref. 4).

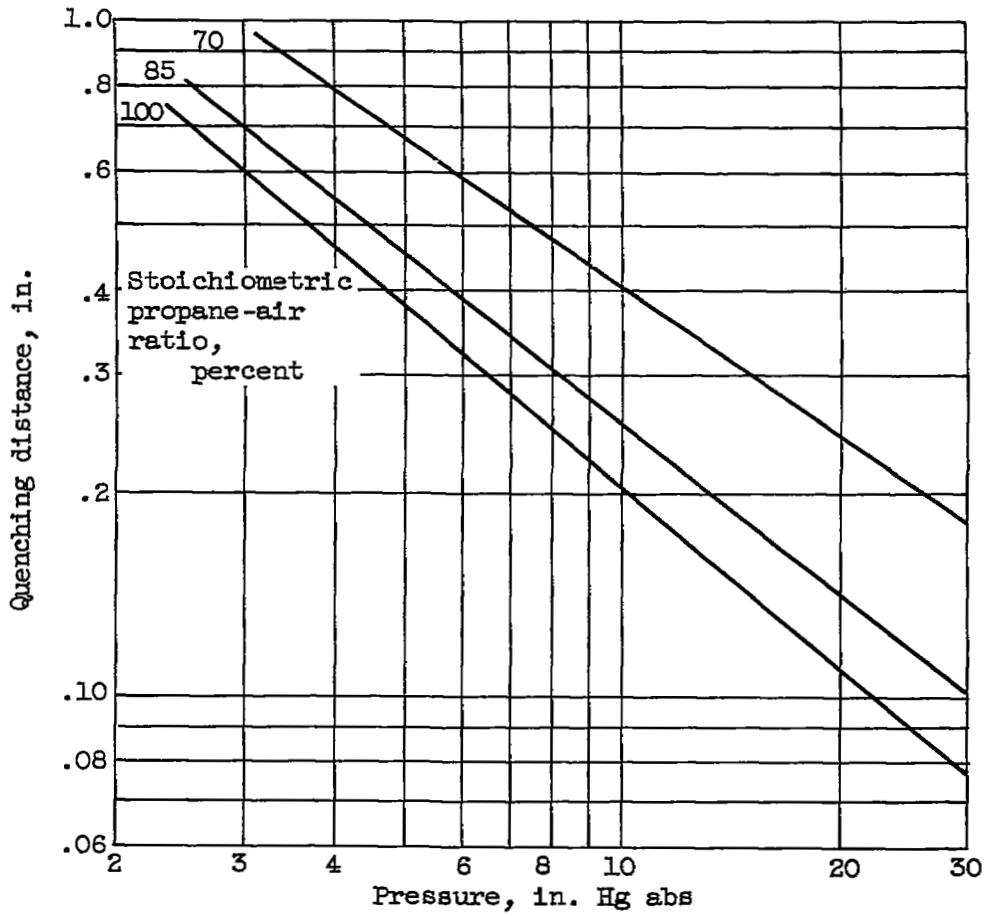

Figure III-5. - Pressure dependence of quenching distance of propane-air flames (ref. 4).

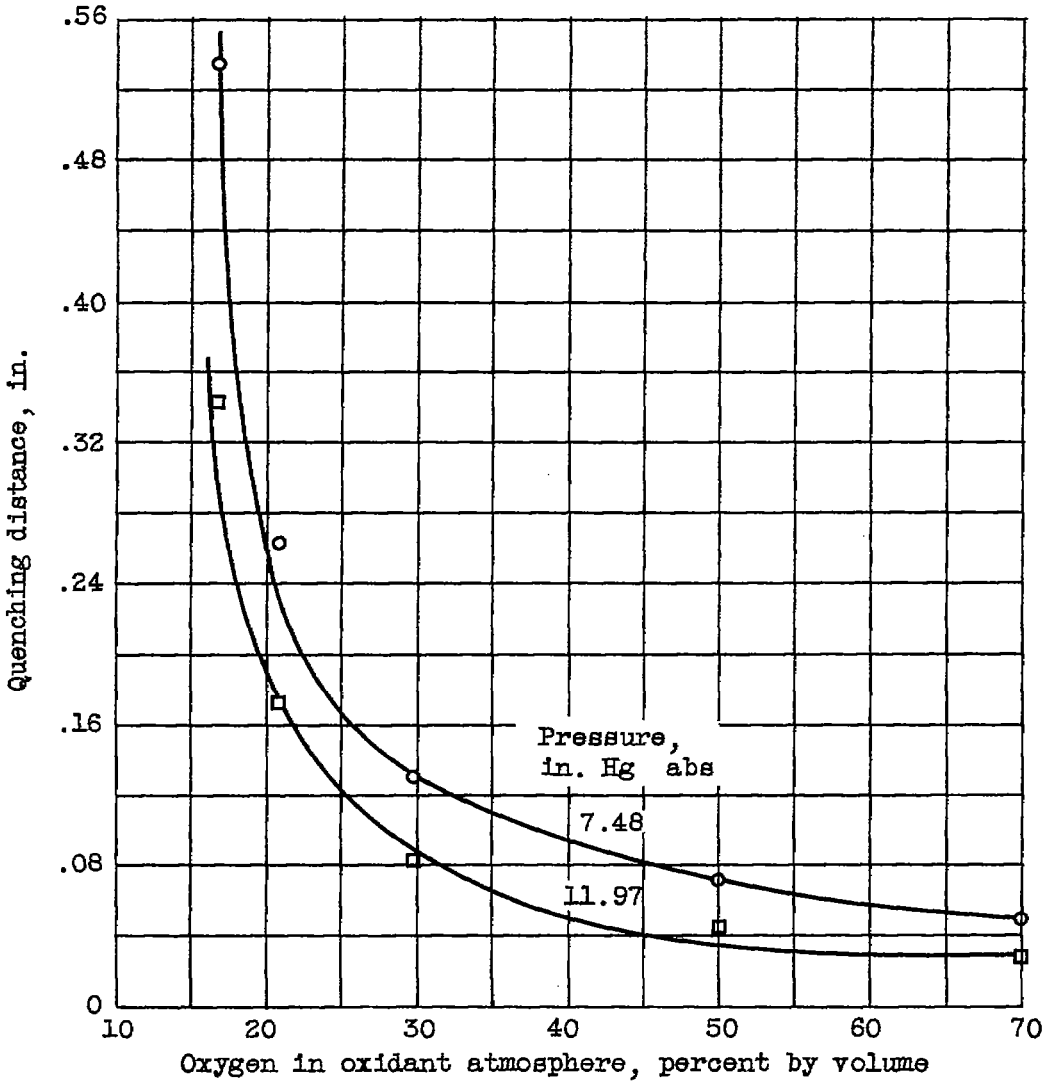

Figure III-6. - Effect of oxygen concentration in oxidant on quenching distances of stoichiometric propane-oxygen-nitrogen mixtures (ref. 6).

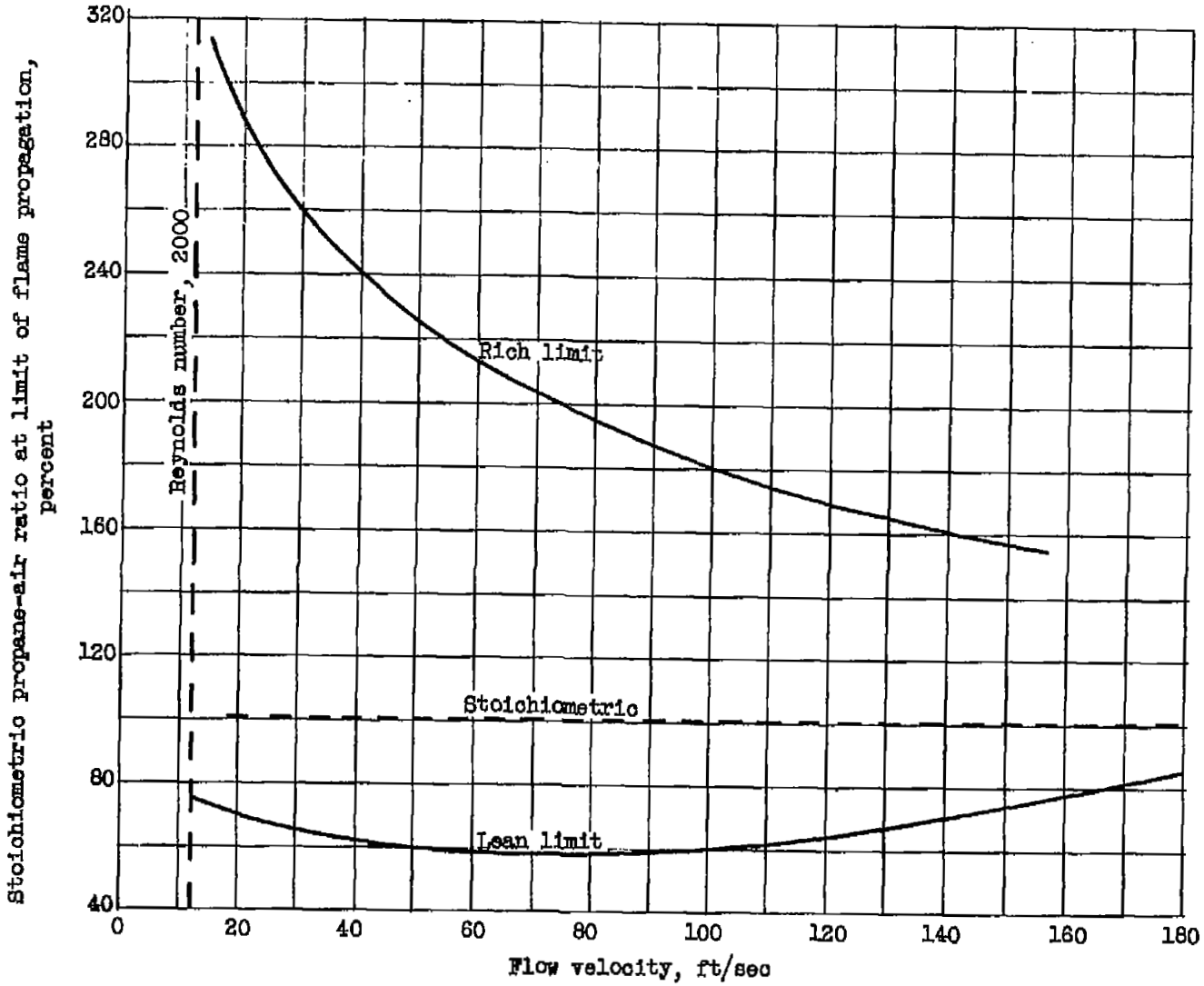

Figure III-7. - Effect of flow velocity on limits of flame propagation in propane-air mixtures. Static pressure, 30.7 inches of mercury absolute (ref. 8).

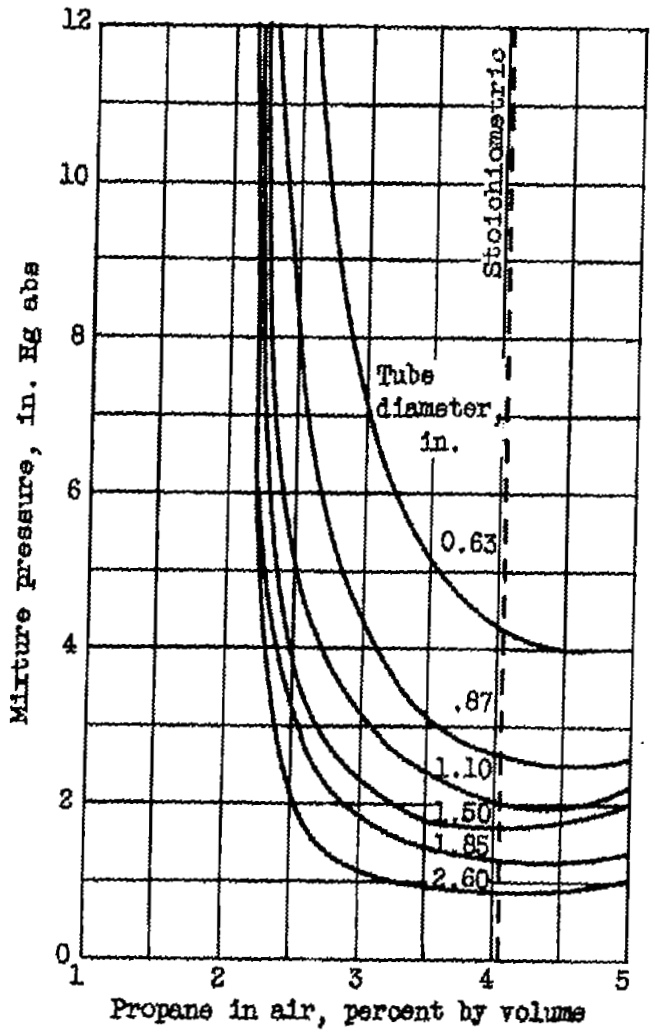

Figure III-8. - Effect of tube diameter on low-pressure limits of flame propagation (ref. 5).

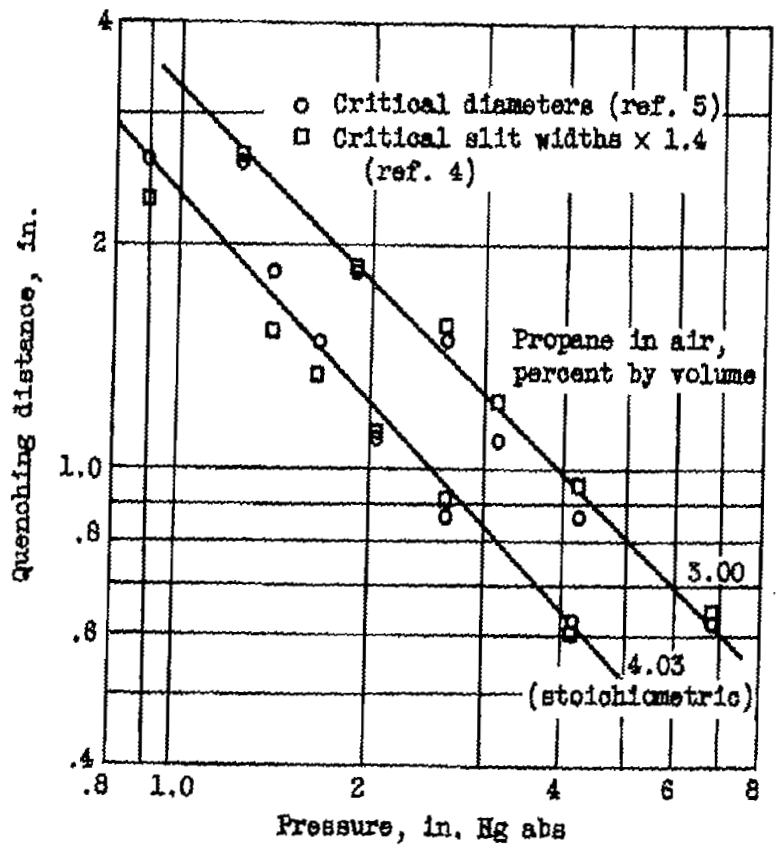

Figure III-9. - Relation of quenching distance and low-pressure limits of flame propagation.

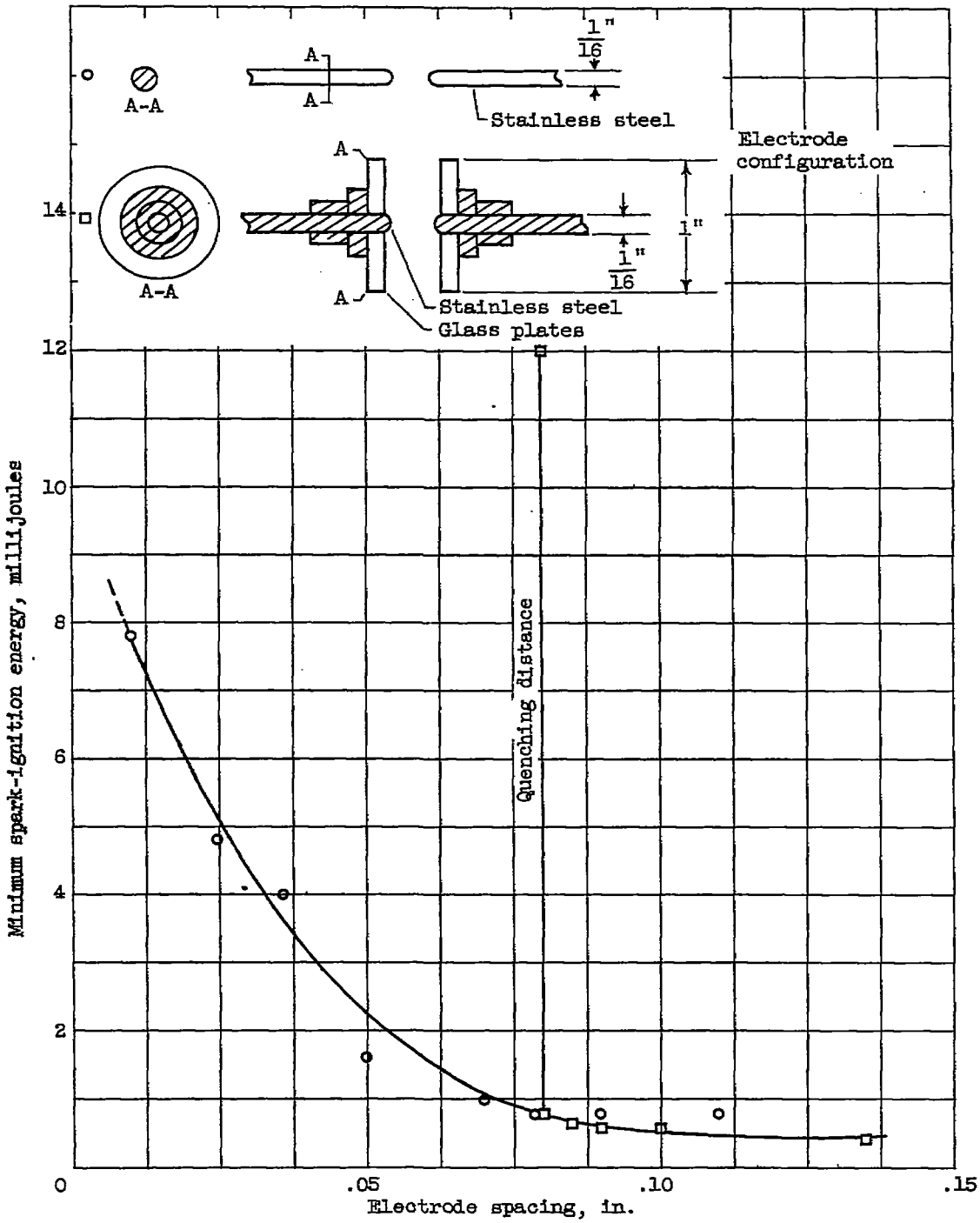

Figure III-10. - Effect of varying spark-gap lengths on minimum spark-ignition energy of 8.5 percent by volume mixture of natural gas and air. Capacitance spark; pressure, atmospheric; temperature, 77° F (ref. 11).

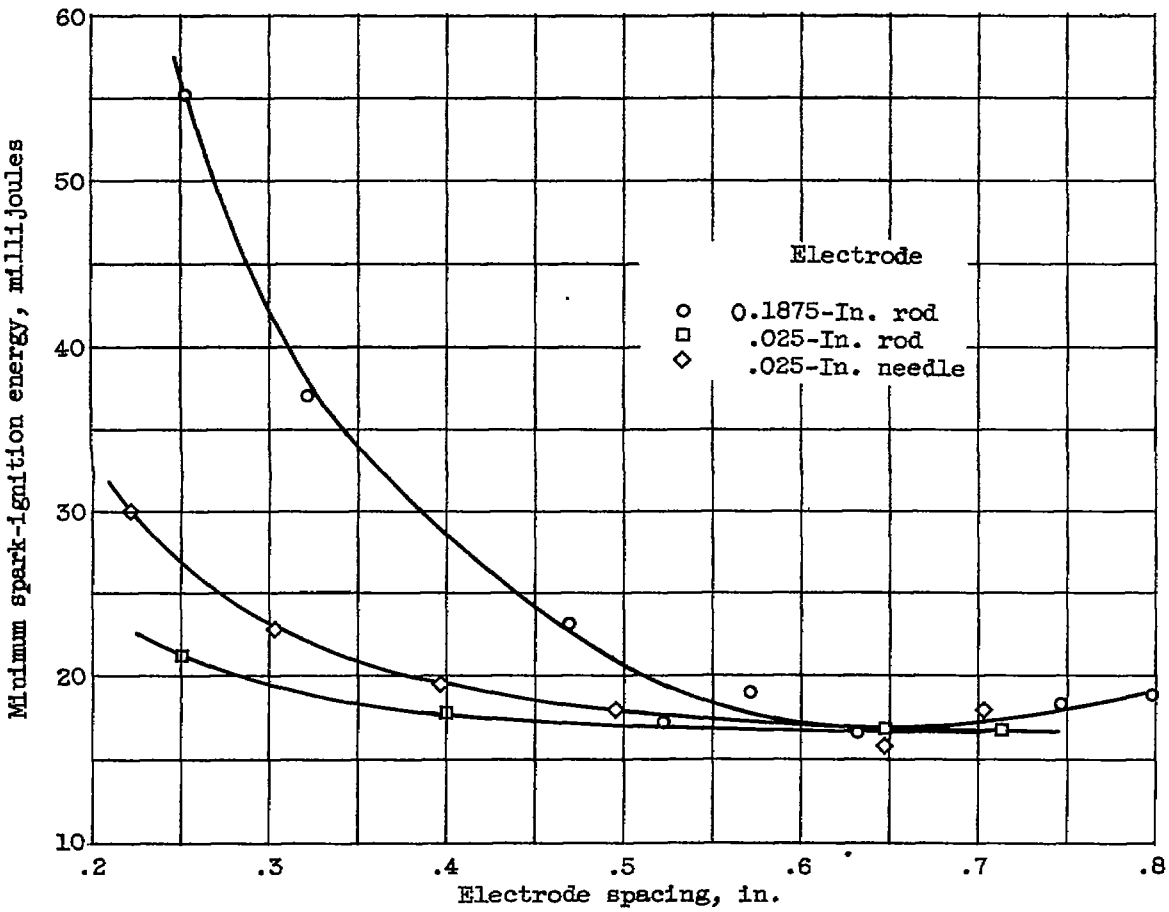

Figure III-11. - Effect of electrode configuration and electrode spacing on minimum spark-ignition energy of flowing 5.2 percent by volume mixture of propane in air. Long-duration (600 microsec) capacitance spark; pressure, 3 inches of mercury absolute; temperature, 80° F (ref. 12).

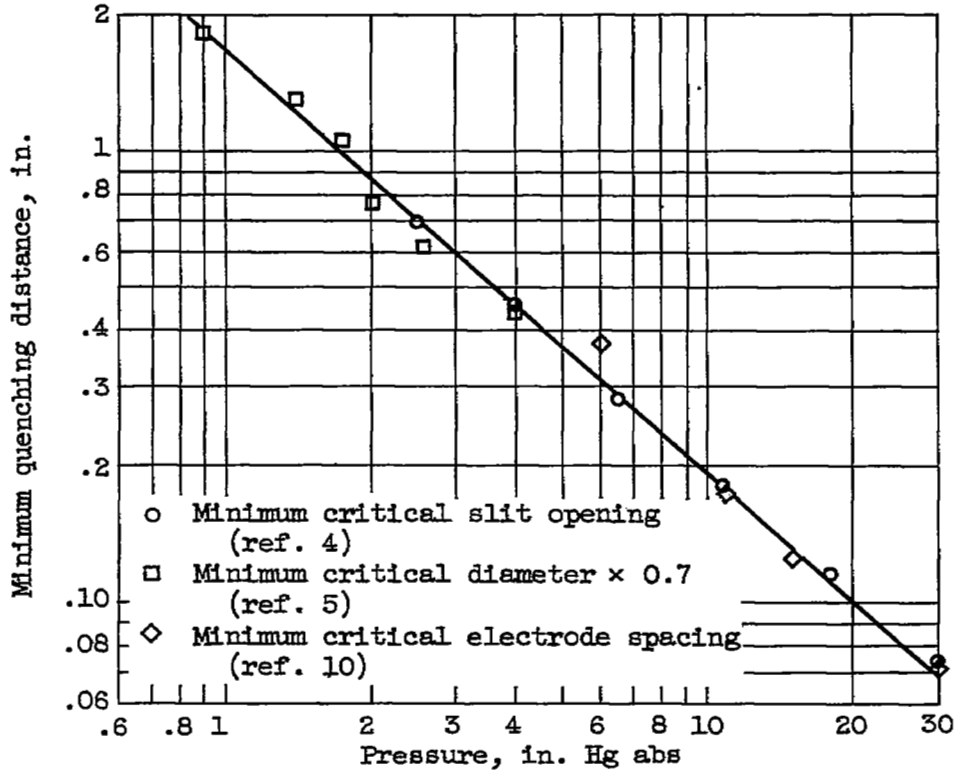

Figure III-12. - Minimum quenching distance at various pressures. Propane in air, approximately 110 percent stoichiometric (ref. 5).

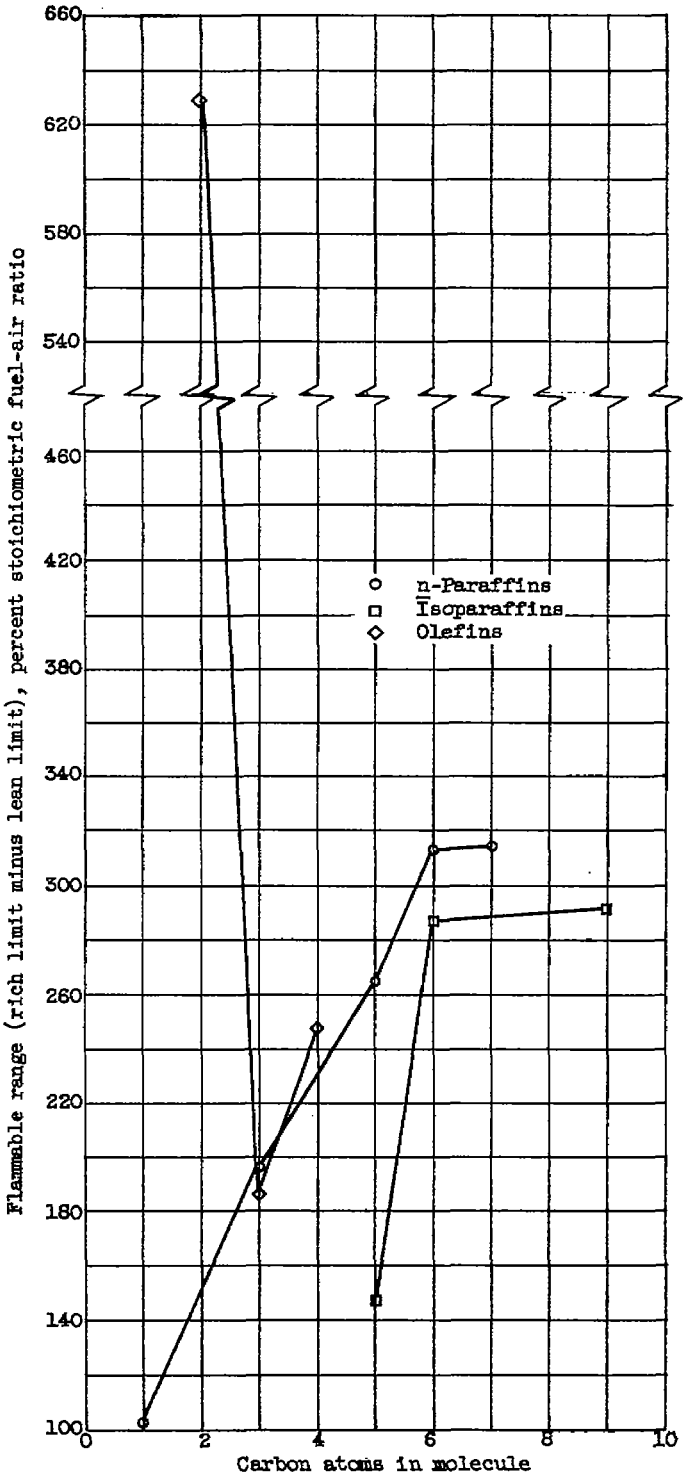

Figure III-13. - Effect of hydrocarbon type on flammable range of pure fuels (ref. 13).

[redacted]

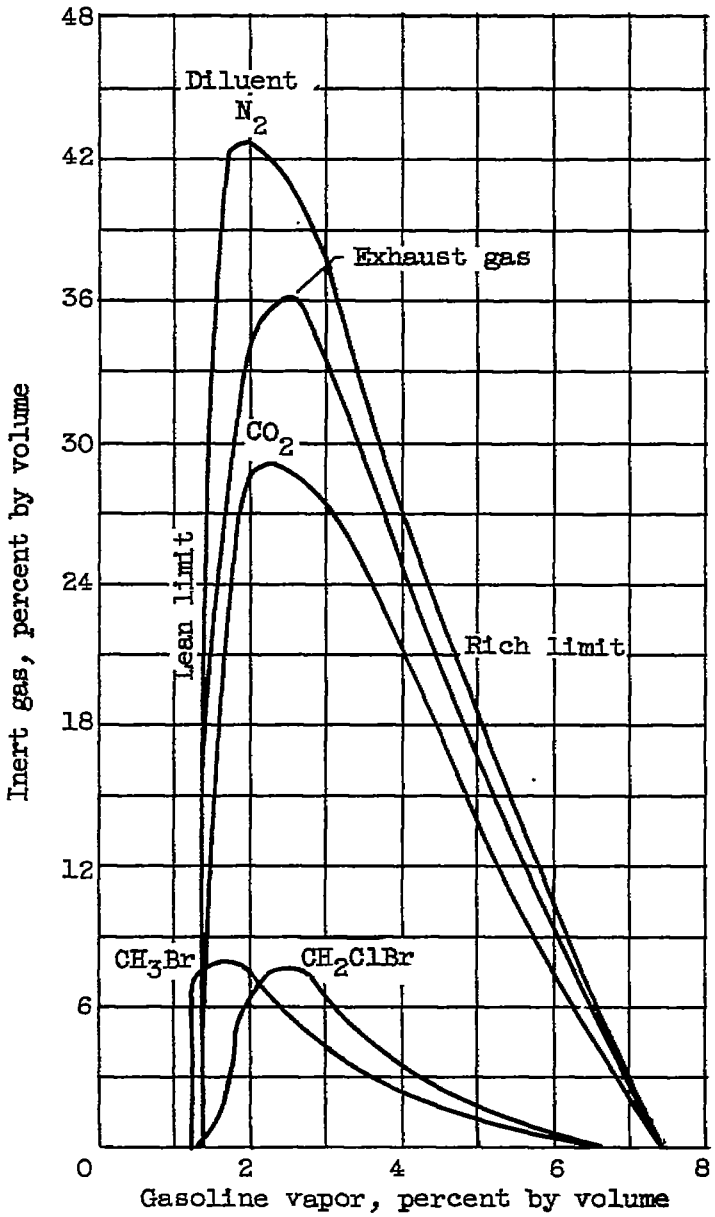

Figure III-14. - Effect of diluents on flammability limits of gasoline (refs. 10 and 18).

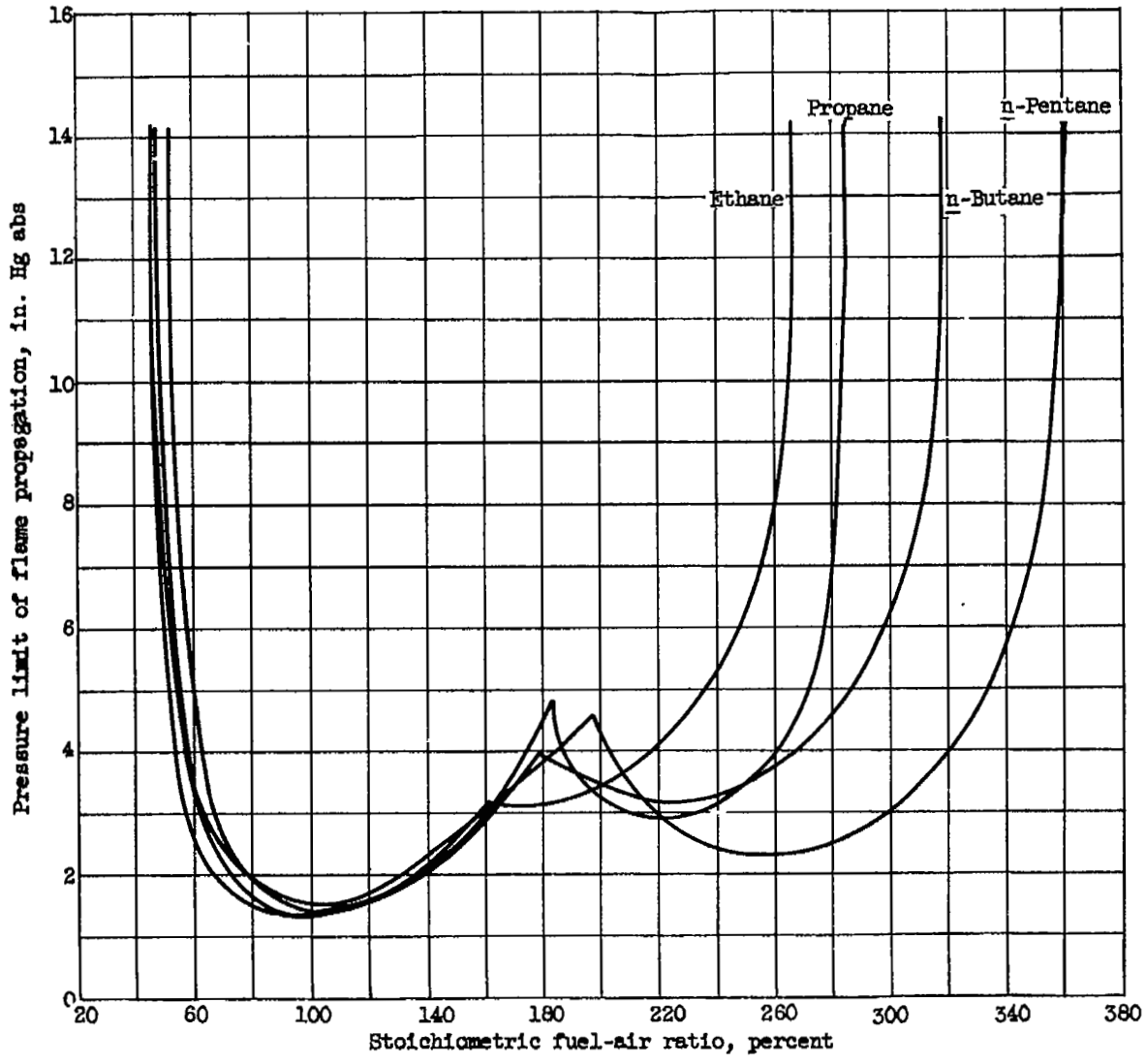

Figure III-15. - Low-pressure limits of flame propagation of normal paraffins in air in 2-inch tube (by permission from ref. 23).

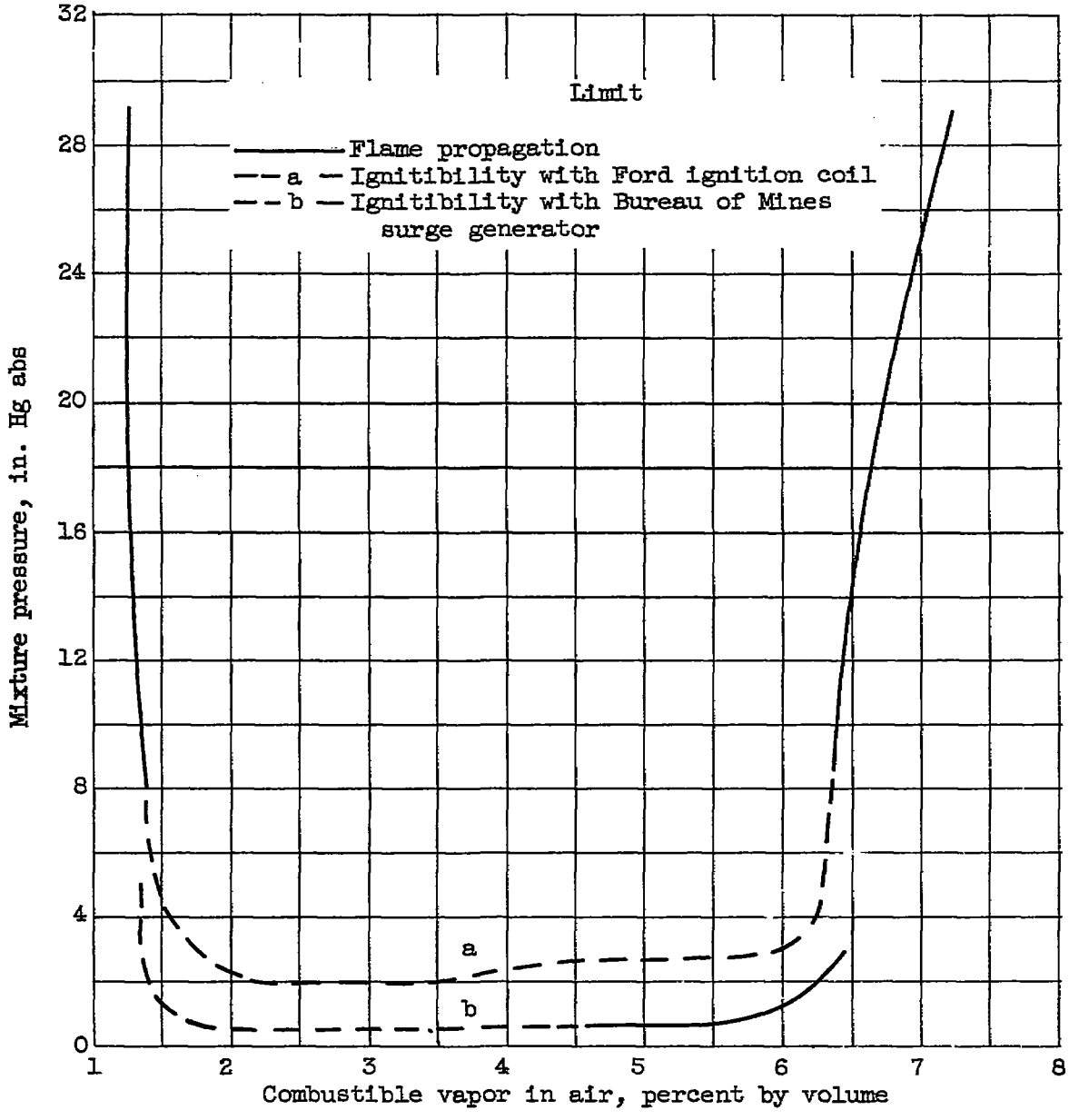

(a) 100/130 Grade aviation gasoline. Temperature, 78° ±1° F.

Figure III-16. - Limits of flame propagation of petroleum fuels at reduced pressures in closed 2-inch-diameter tube (ref. 16).

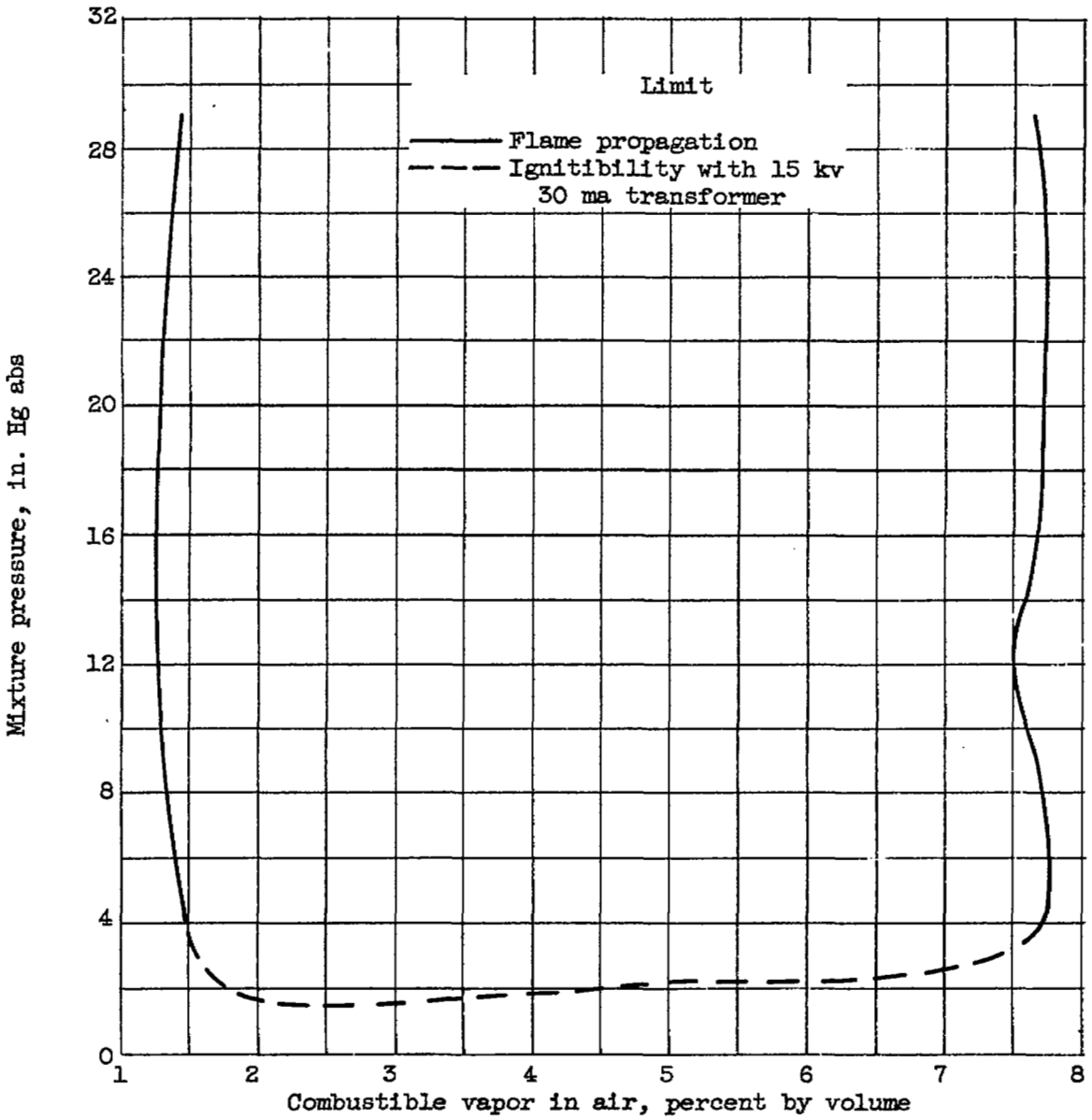

(b) Aviation jet fuel grade JP-4. Temperature, 79° ±2° F.

Figure III-16. - Concluded. Limits of flame propagation of petroleum fuels at reduced pressures in closed 2-inch-diameter tube (ref. 16).

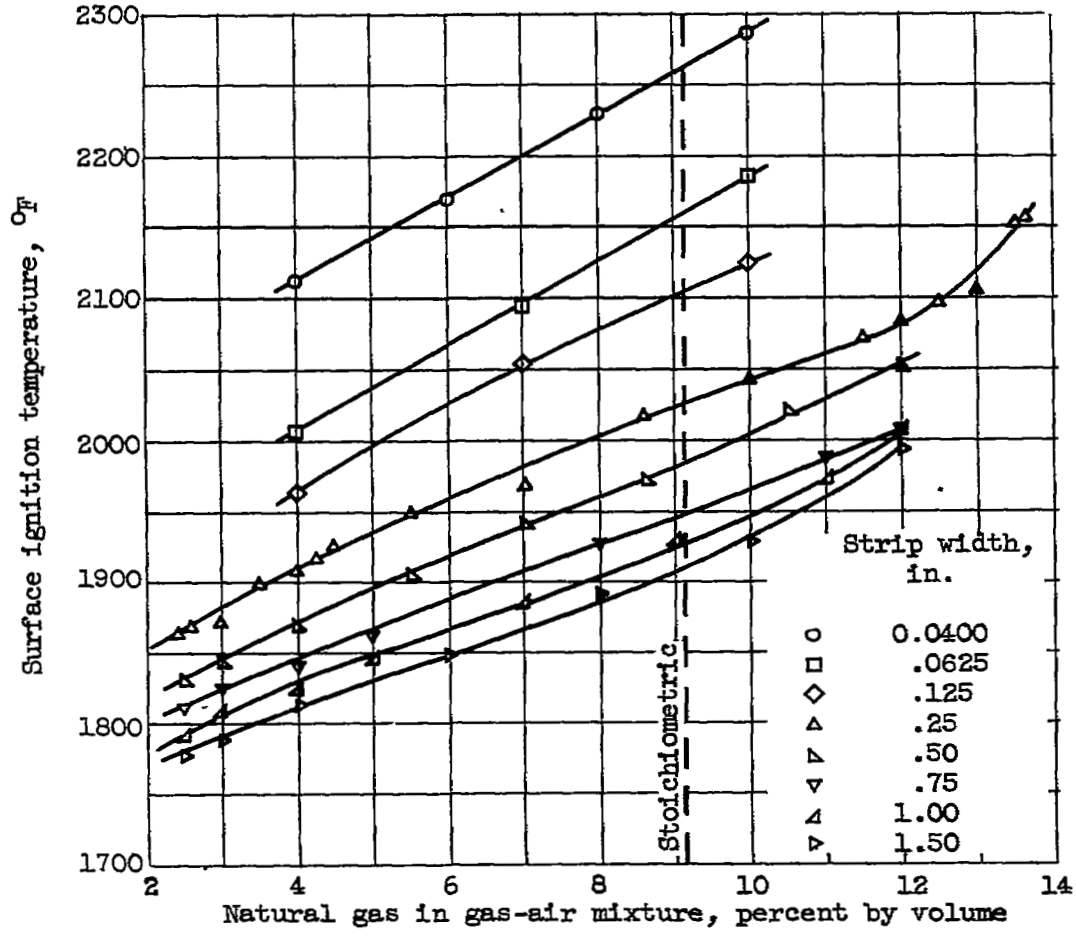

Figure III-17. - Effect of mixture composition on surface ignition temperature of various quiescent natural gas - air mixtures. Ignited by electrically heated nickel strips cut from sheet of No. 18 B and S gage commercial nickel. Length of strips, $4\frac{1}{4}$ inches (ref. 31).

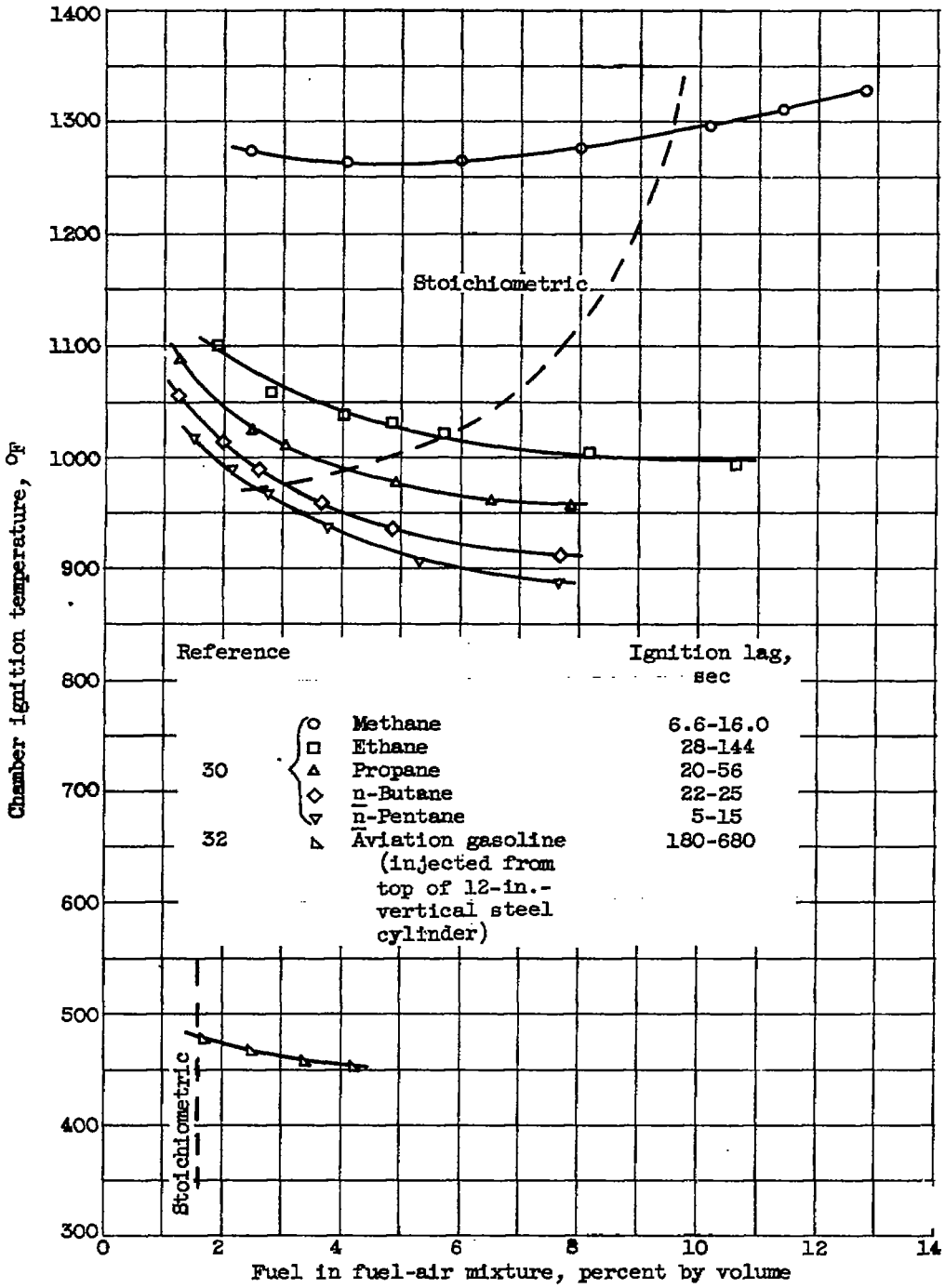

(a) Bomb method (except as noted).

Figure III-18. - Effect of mixture composition upon ignition temperatures of different fuels.

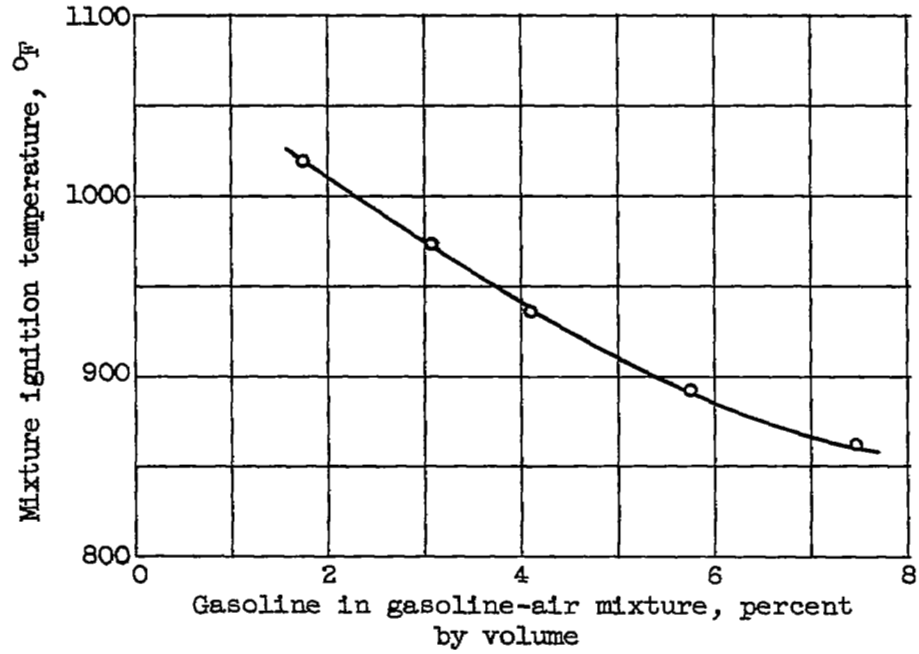

(b) Dynamic heated-tube method (by permission from ref. 33).

Figure III-18. - Concluded. Effect of mixture composition upon ignition temperatures of different fuels.

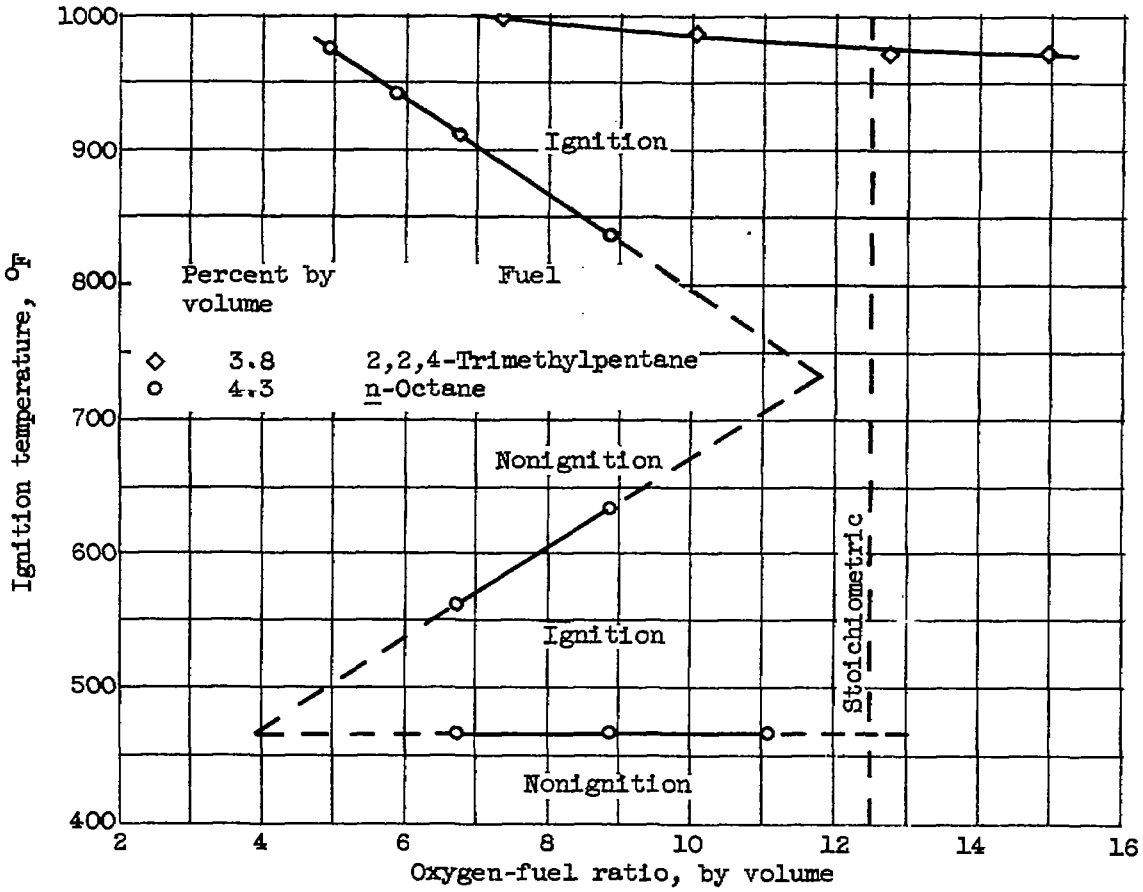

Figure III-19. - Ignition characteristics of n-octane and 2,2,4-trimethylpentane in mixtures of fuel, oxygen, and nitrogen. Dynamic heated-tube method of ignition; supporting atmosphere flow, 230 cubic centimeters per minute at atmospheric pressure and temperature (by permission from ref. 33).

[redacted]

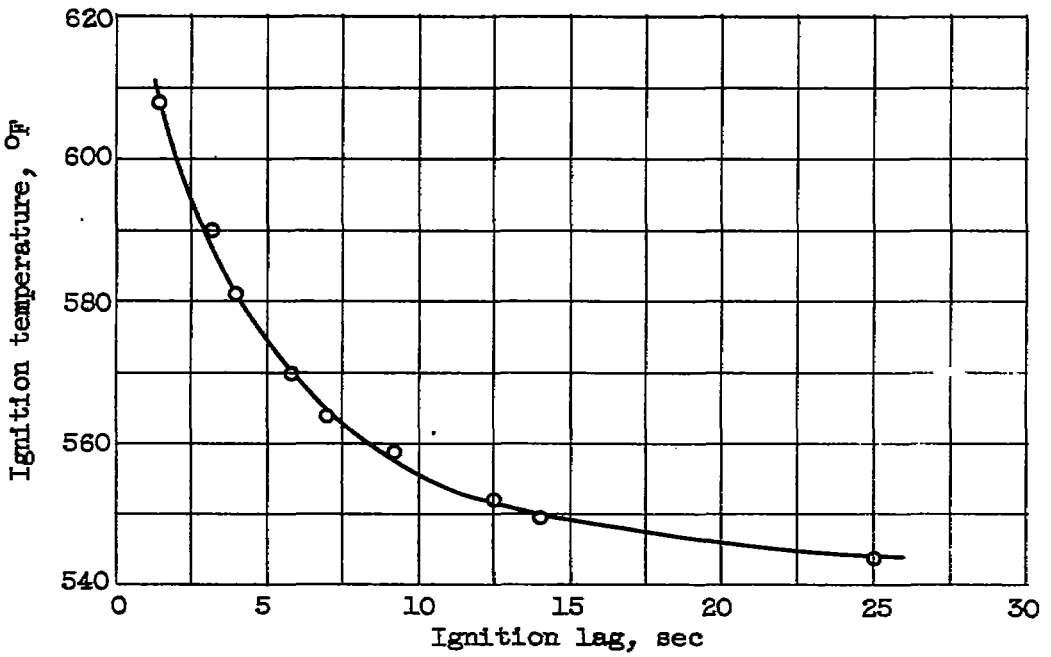

Figure III-20. - Variation of ignition temperature of gasoline in oxygen with varying ignition lags as determined by dynamic-drop method in platinum crucible (ref. 36).

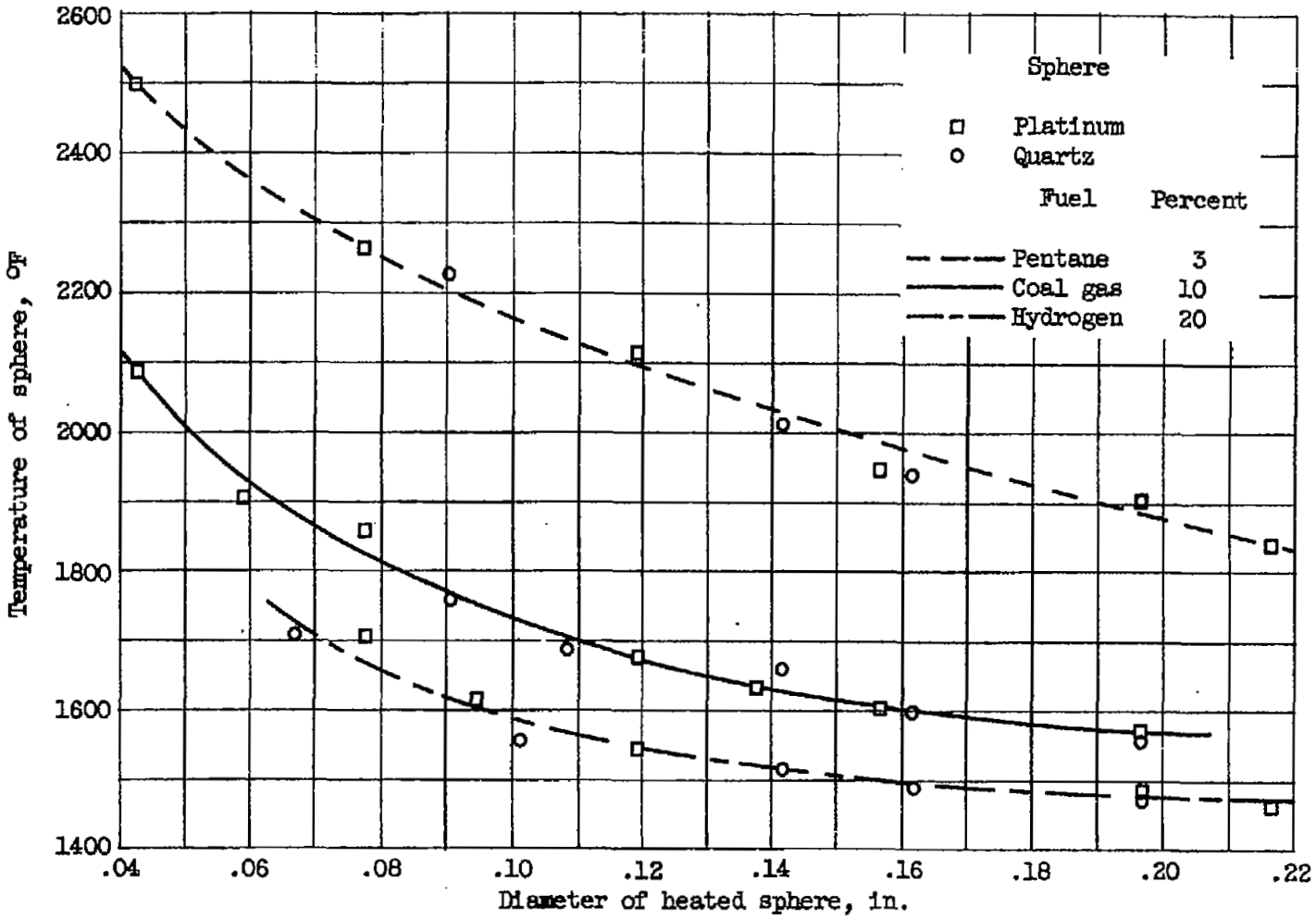

Figure III-21. - Effect of sphere diameter upon ignition of three gas-air mixtures ignited by quartz and platinum spheres shot into mixture at average velocity of 13.12 feet per second (ref. 37).

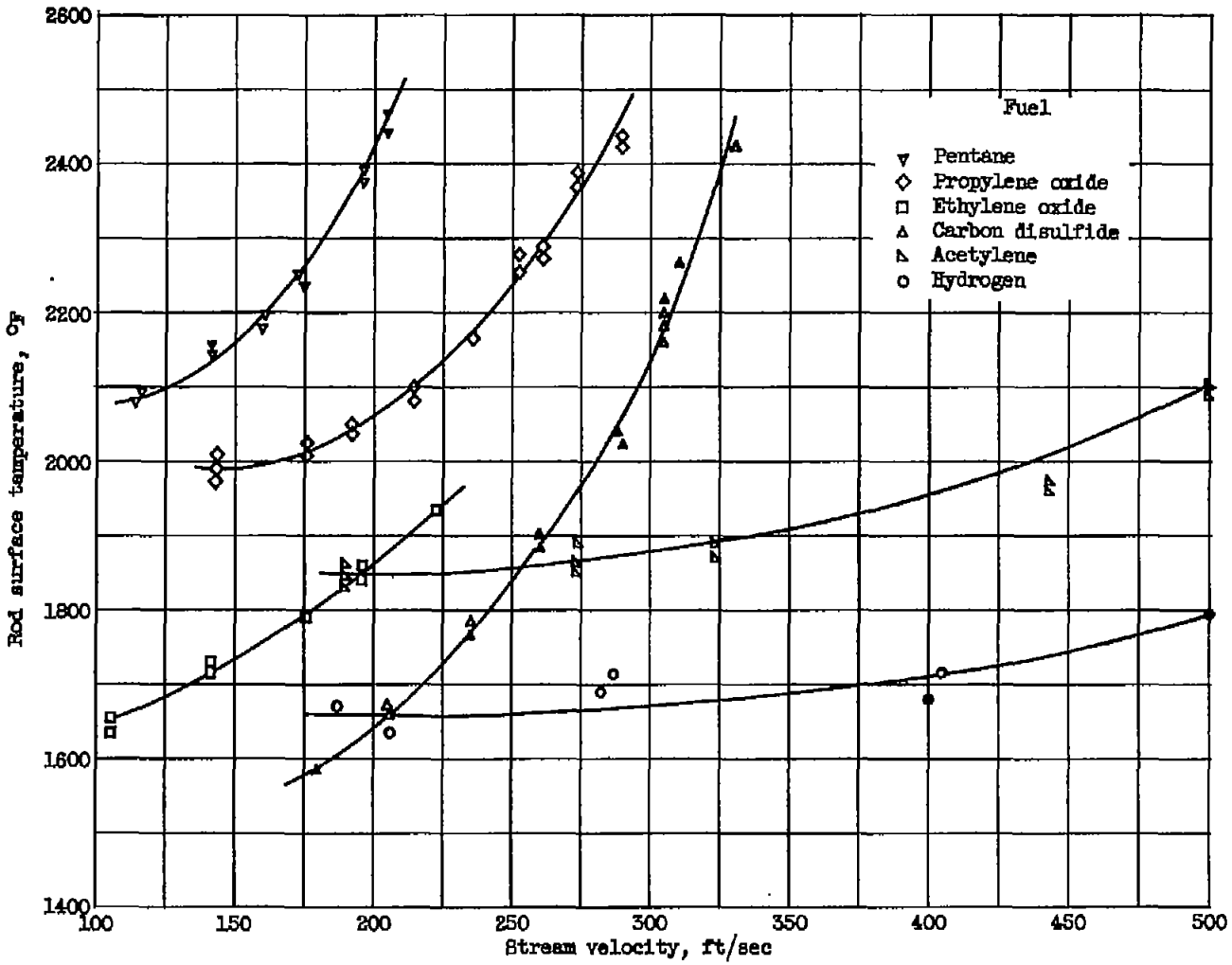

(a) Experimental data.

Figure III-22. - Variation of ignition temperature of various fuels in air with gas-stream velocity. Ignition by 1/4-inch heated rods; stoichiometric mixtures; atmospheric pressure; temperature, 155° F (ref. 38).

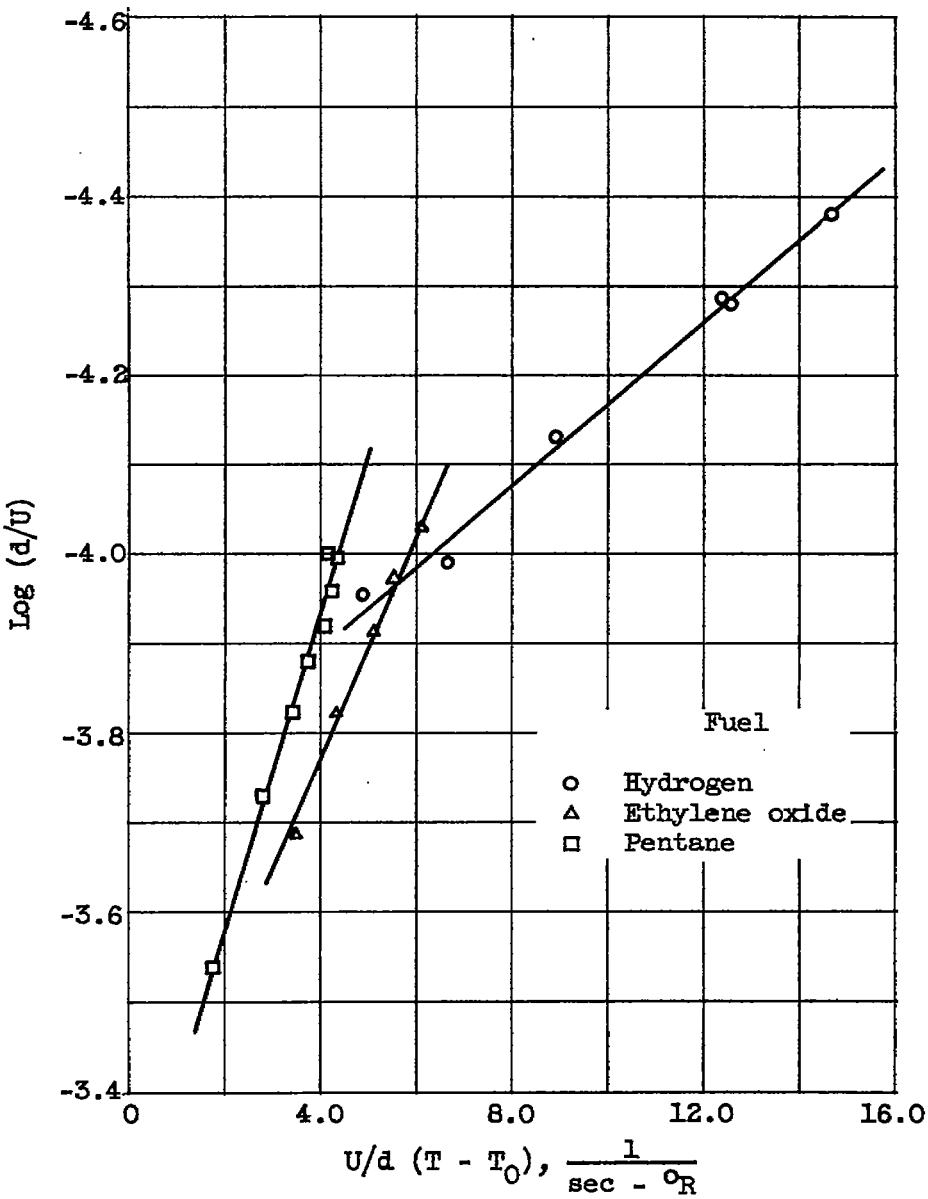

(b) Data correlation.

Figure III-22. - Concluded. Variation of ignition temperature of various fuels in air with gas-stream velocity. Ignition by 1/4-inch heated rods; stoichiometric mixtures; atmospheric pressure; temperature, 155° F (ref. 38).

[redacted]

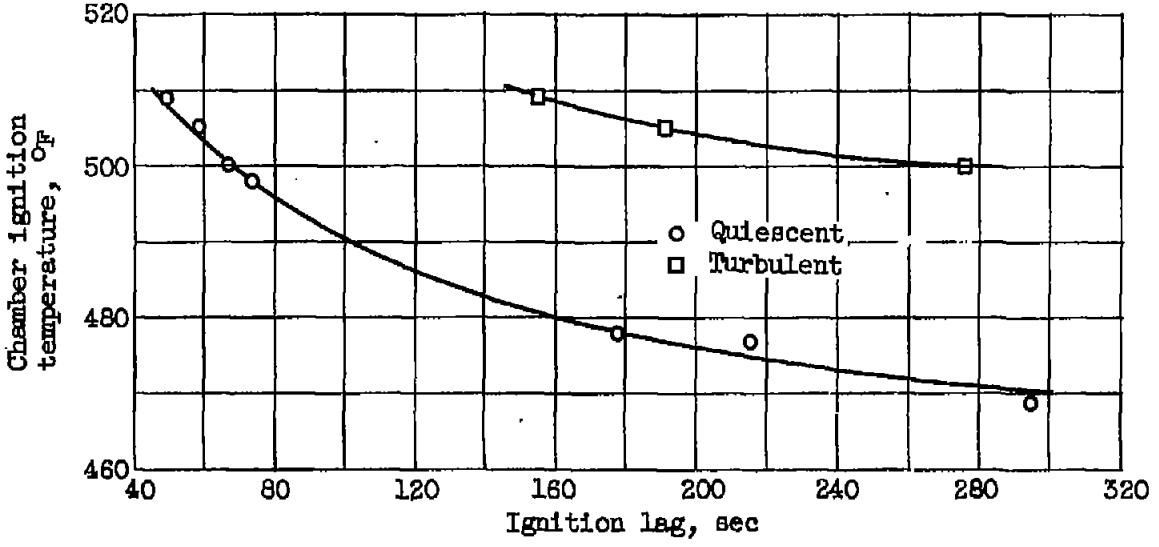

Figure III-23. - Influence of mild turbulence upon minimum ignition temperature of liquid aviation gasoline injected into 12-inch-diameter 12-inch-vertical steel cylinder (ref. 32).

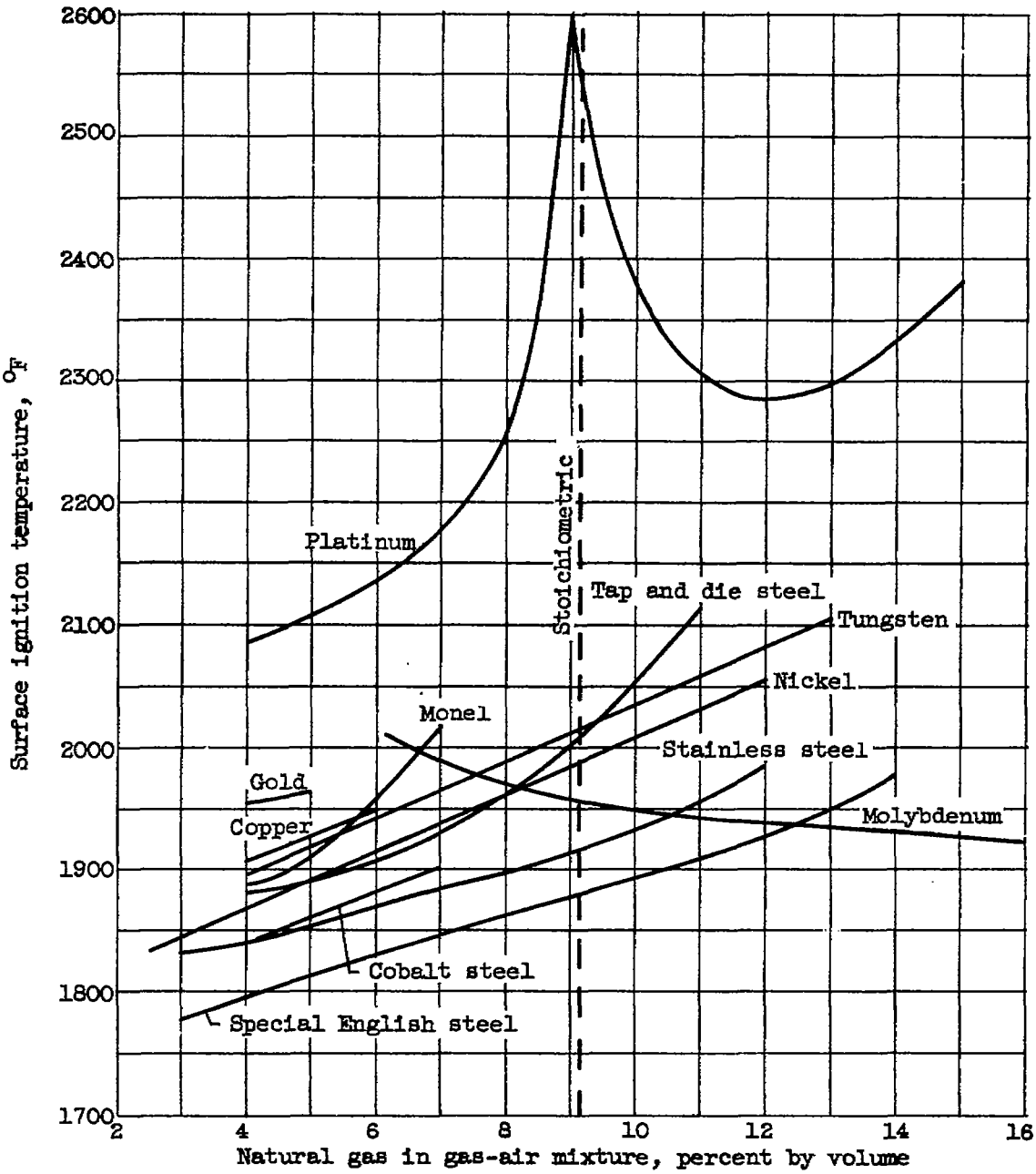

Figure III-24. - Effect of fuel composition on surface ignition temperature. Ignition of natural gas by electrically heated metal strips; size of metal strips, 4.25 by 0.50 by 0.04 inches (ref. 31).

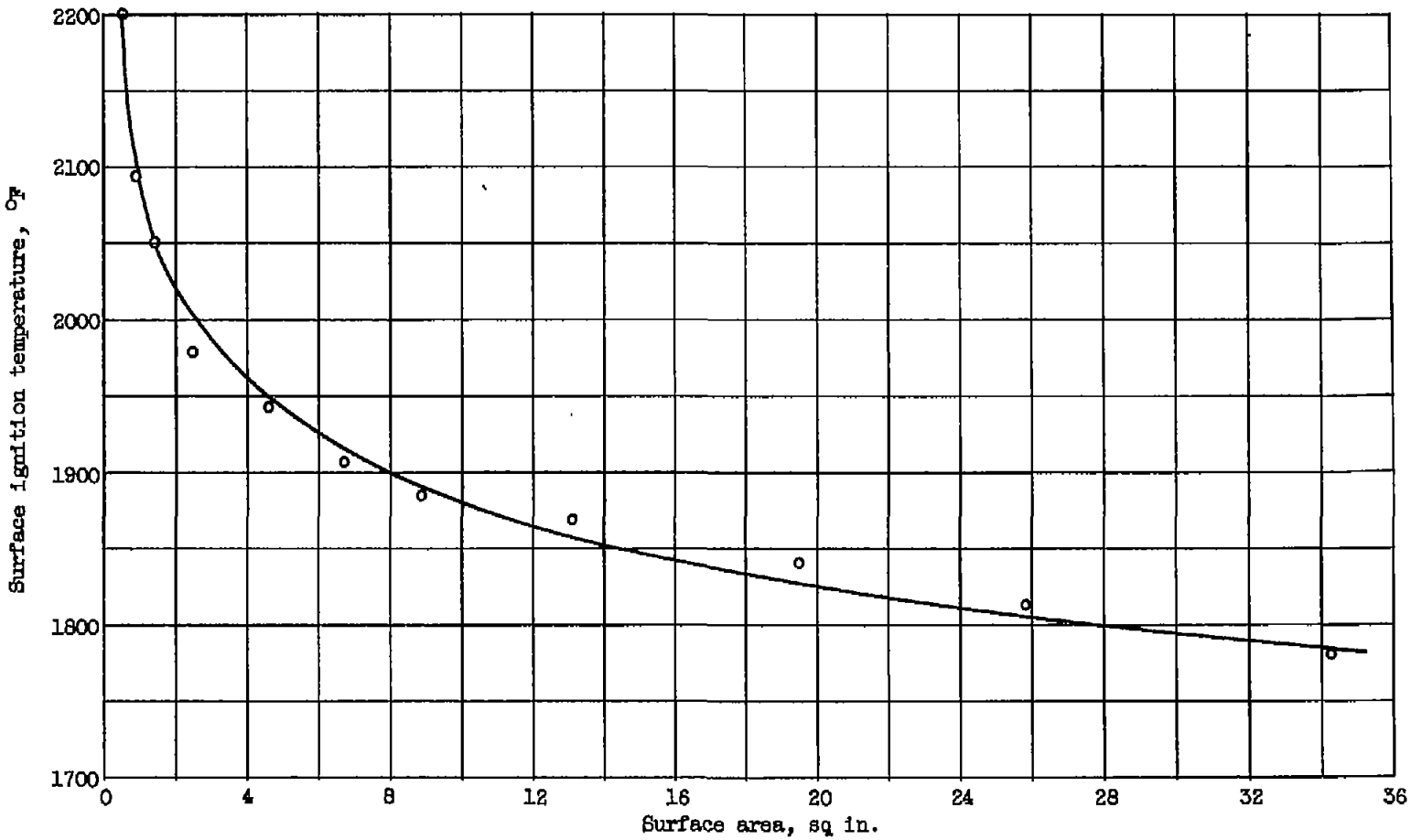

Figure III-25. - Effect of surface area on surface ignition temperature of quiescent mixture of 7 percent natural gas and air. Nickel igniting surface electrically heated (ref. 32).

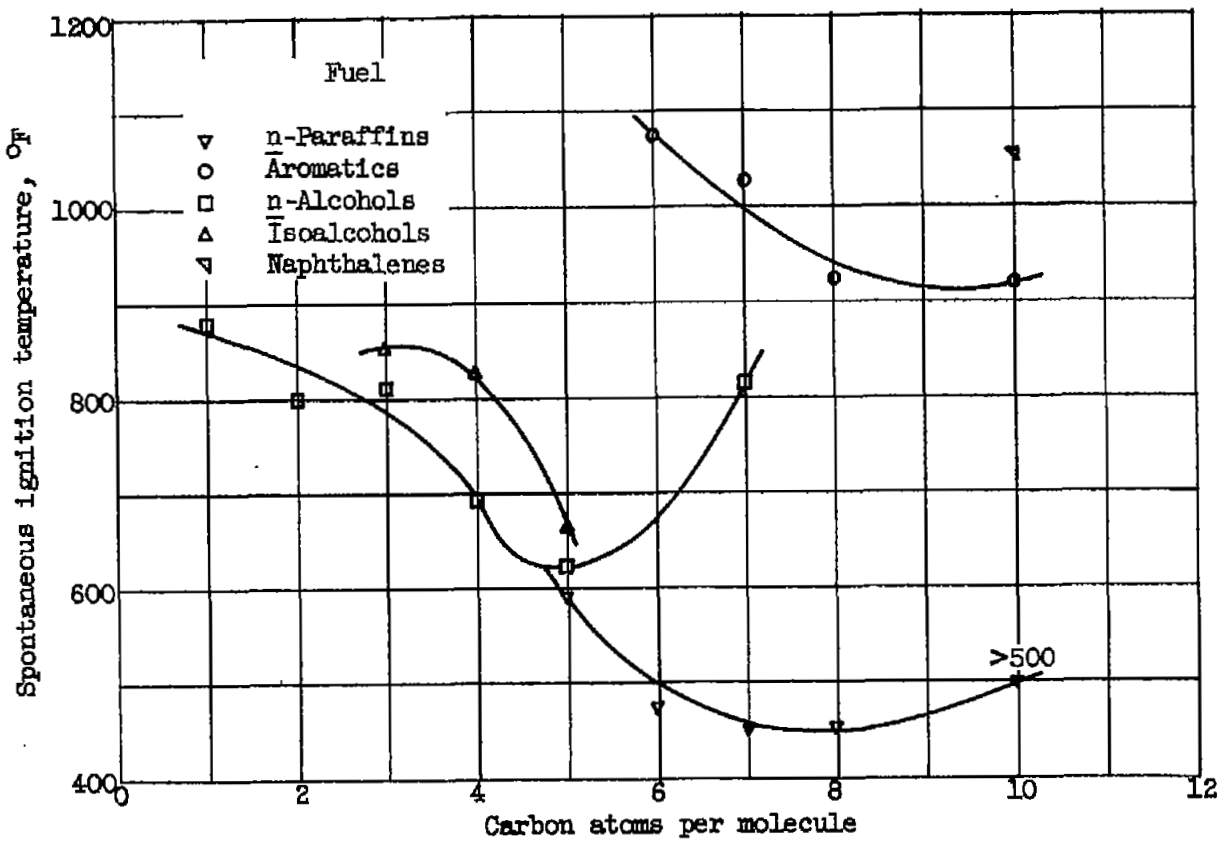

(a) By permission from reference 43.

Figure III-26. - Effect of number of carbon atoms per molecule on spontaneous ignition temperatures of various liquid fuels.

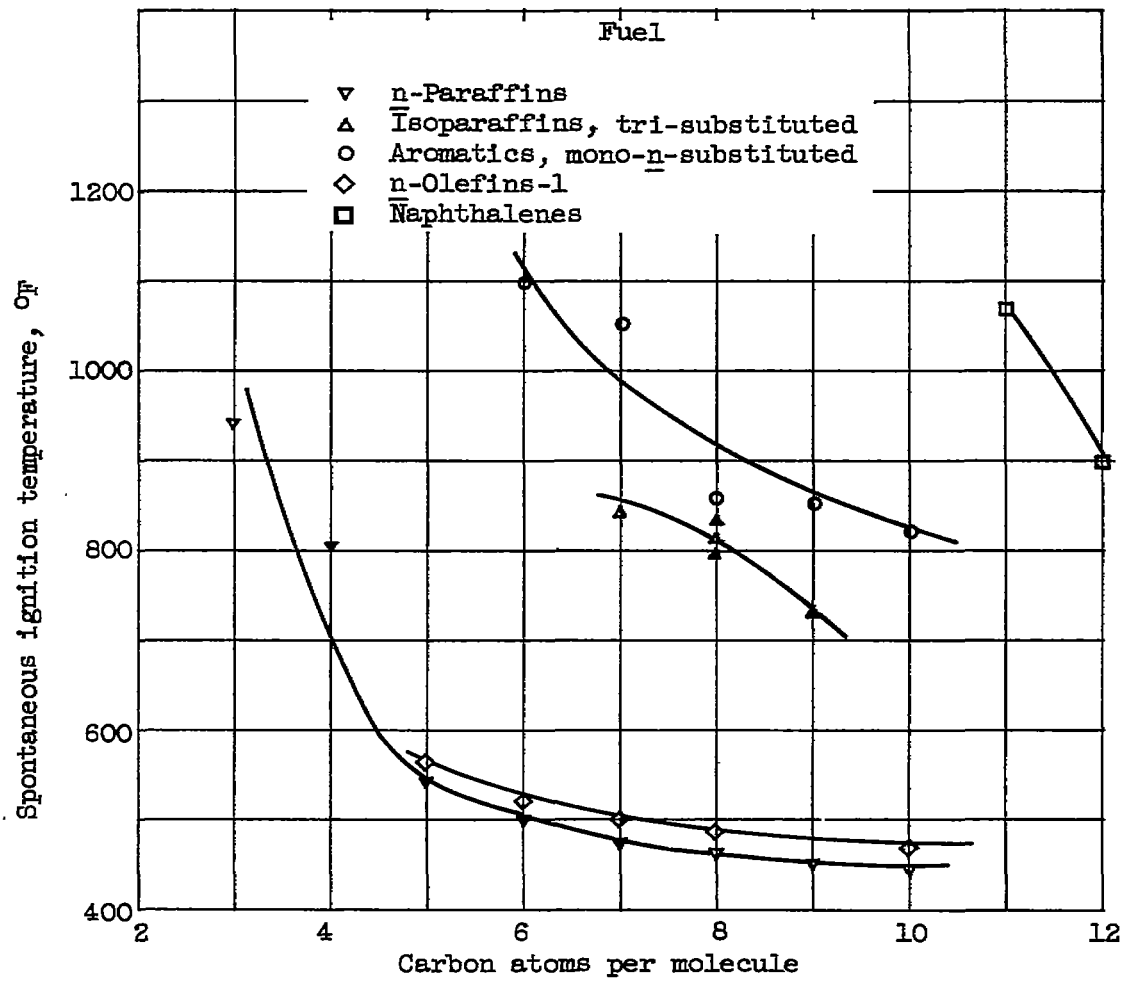

(b) Reference 44.

Figure III-26. - Concluded. Effect of number of carbon atoms per molecule on spontaneous ignition temperatures of various liquid fuels.

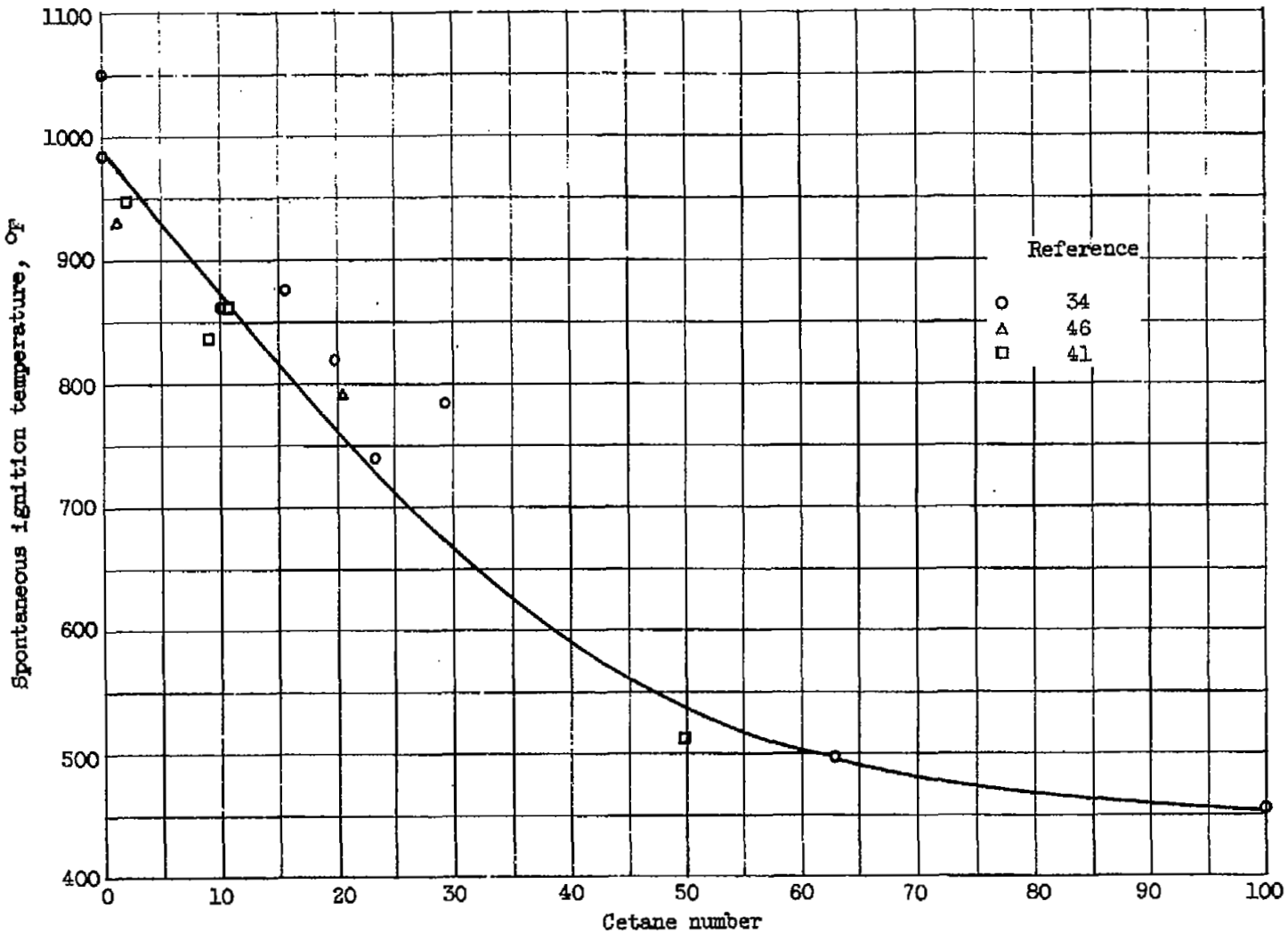

Figure III-27. - Effect of cetane number on spontaneous ignition temperature of various fuels in air. (Cetane numbers are converted A.S.T.M.-CFR octane numbers.)

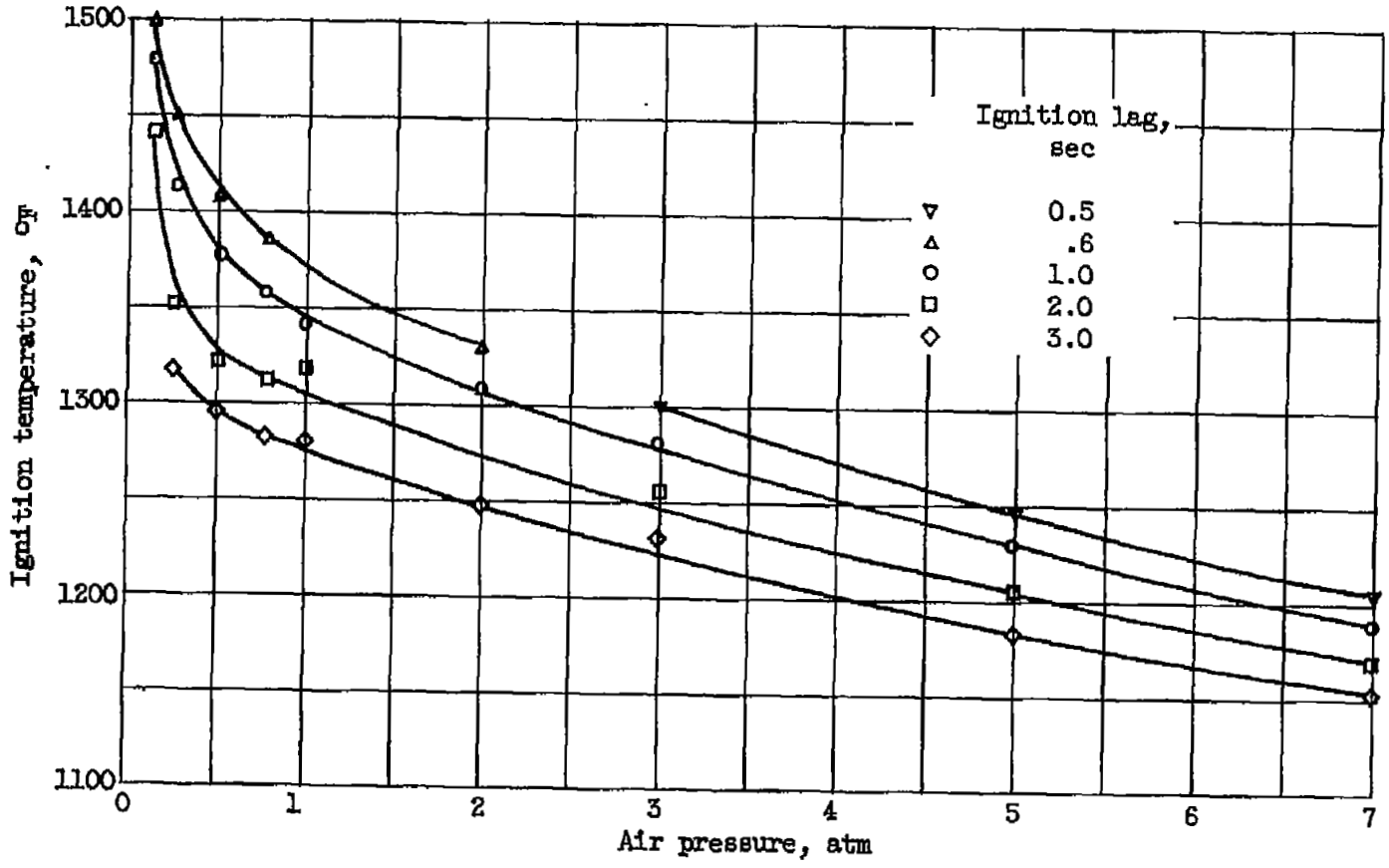

(a) Ignition of methane in air using dynamic heated-tube method (ref. 28).

Figure III-28. - Effect of air pressure on ignition temperature.

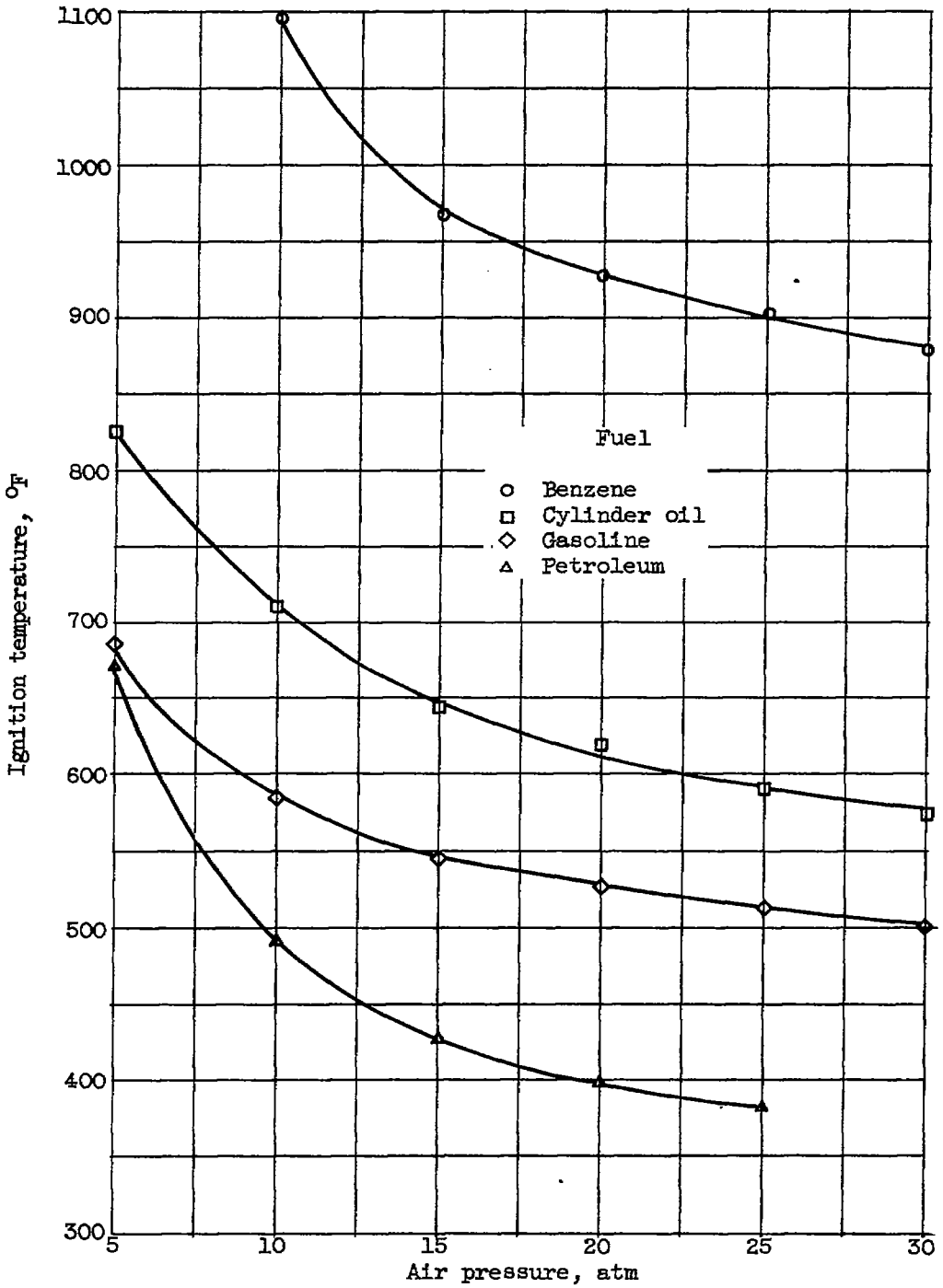

(b) Bomb ignition with fuel sprayed in (ref. 47).

Figure III-28. - Concluded. Effect of air pressure on ignition temperature.

[redacted]

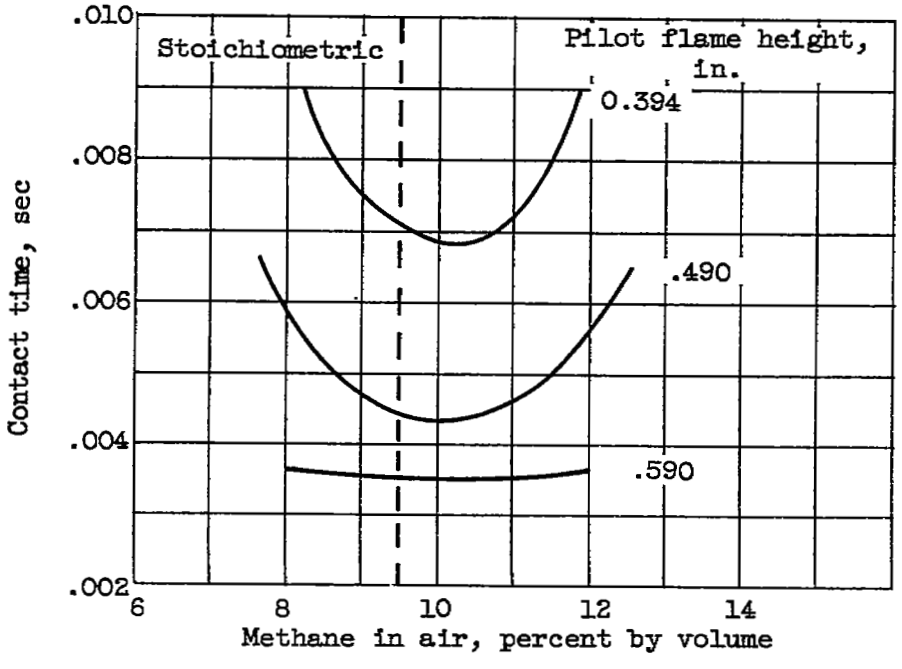

Figure III-29. - Effects of pilot-flame contact time and size on ignition (ref. 48, p. 45).

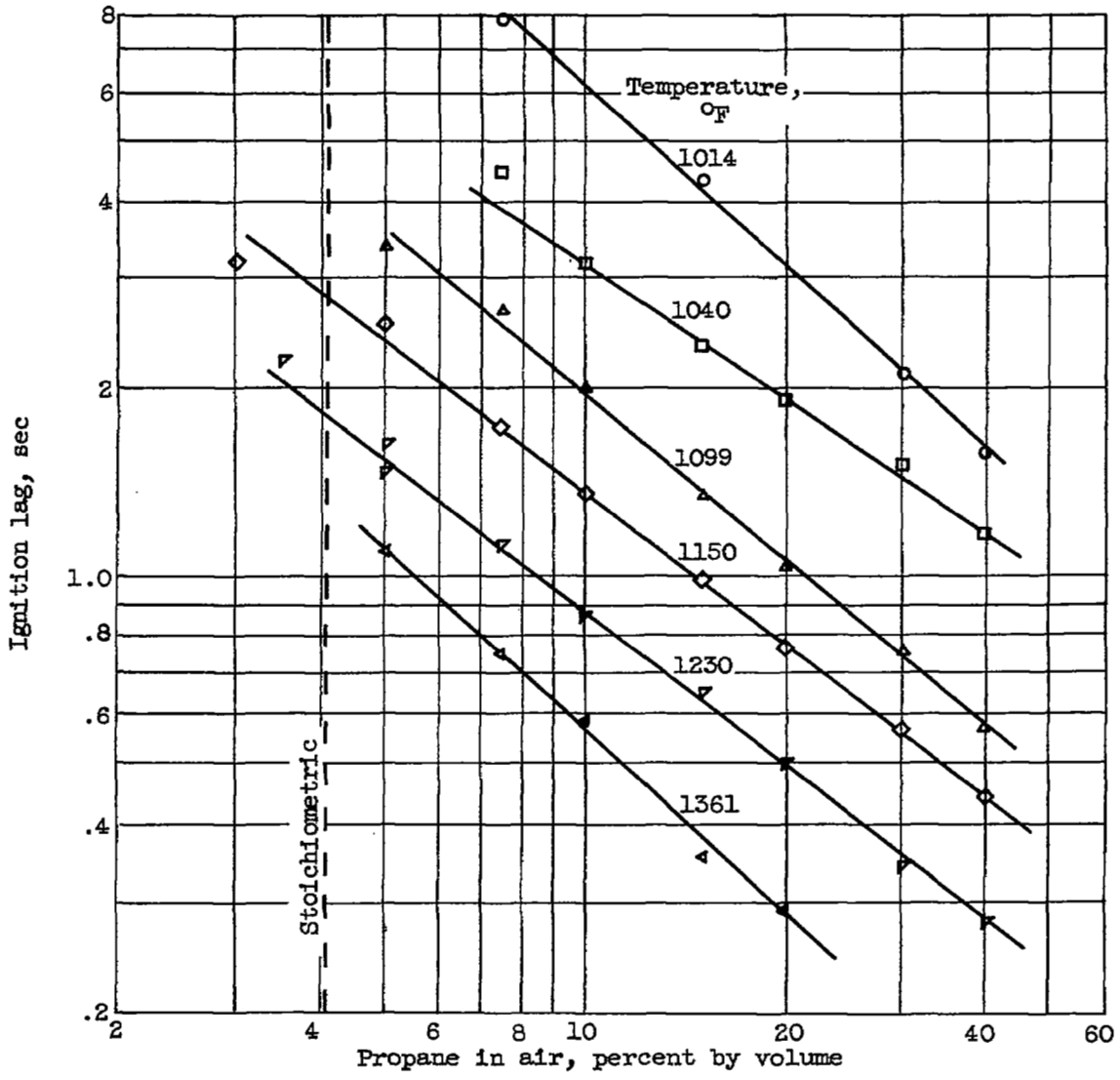

Figure III-30. - Effect of propane concentration and temperature on ignition lags of propane-air mixtures. 1-Inch tube; flow rate approximately that for minimum ignition lag (ref. 49).

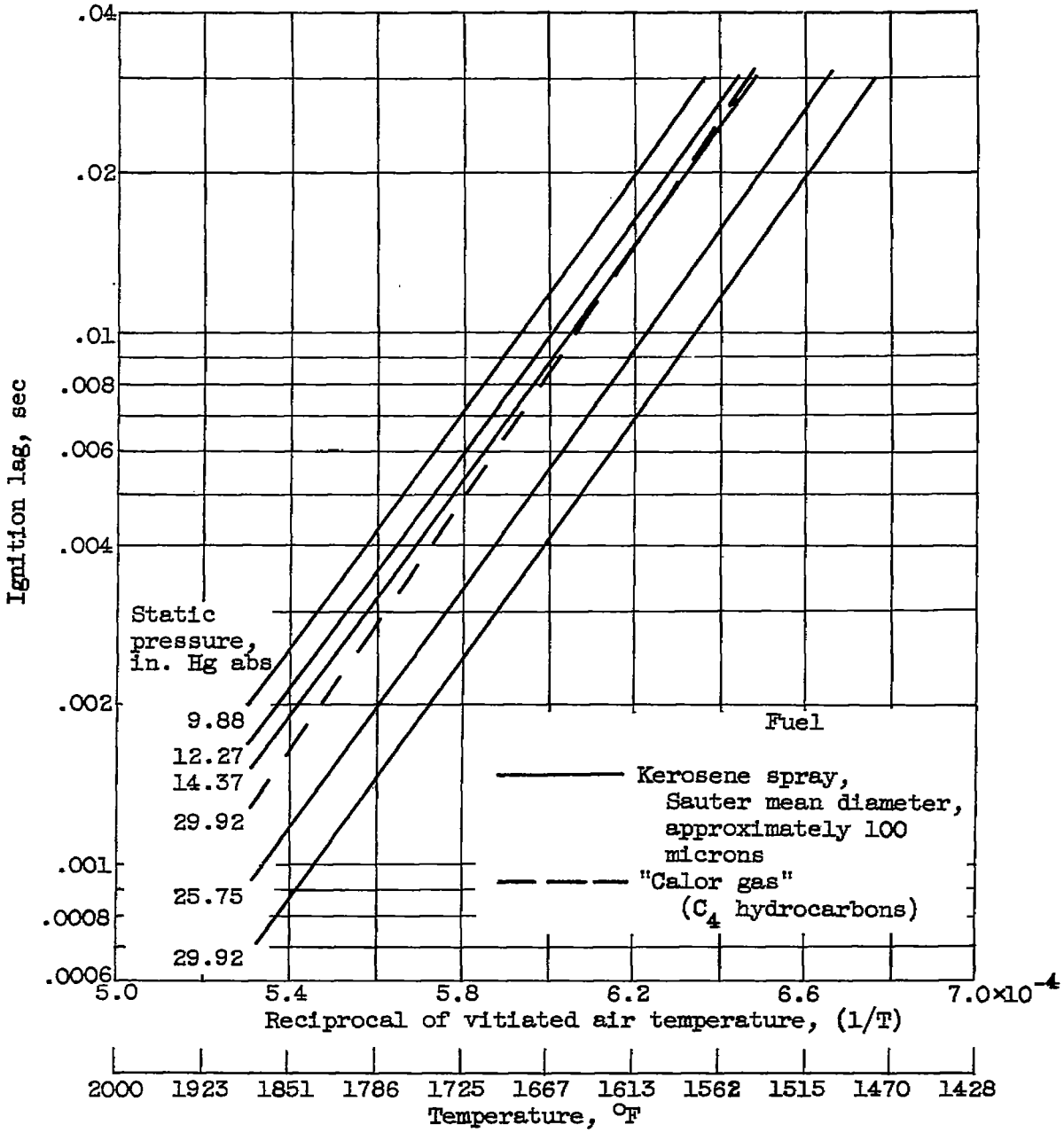

Figure III-31. - Ignition lags on injection of fuel into hot vitiated air stream (refs. 51 and 52).

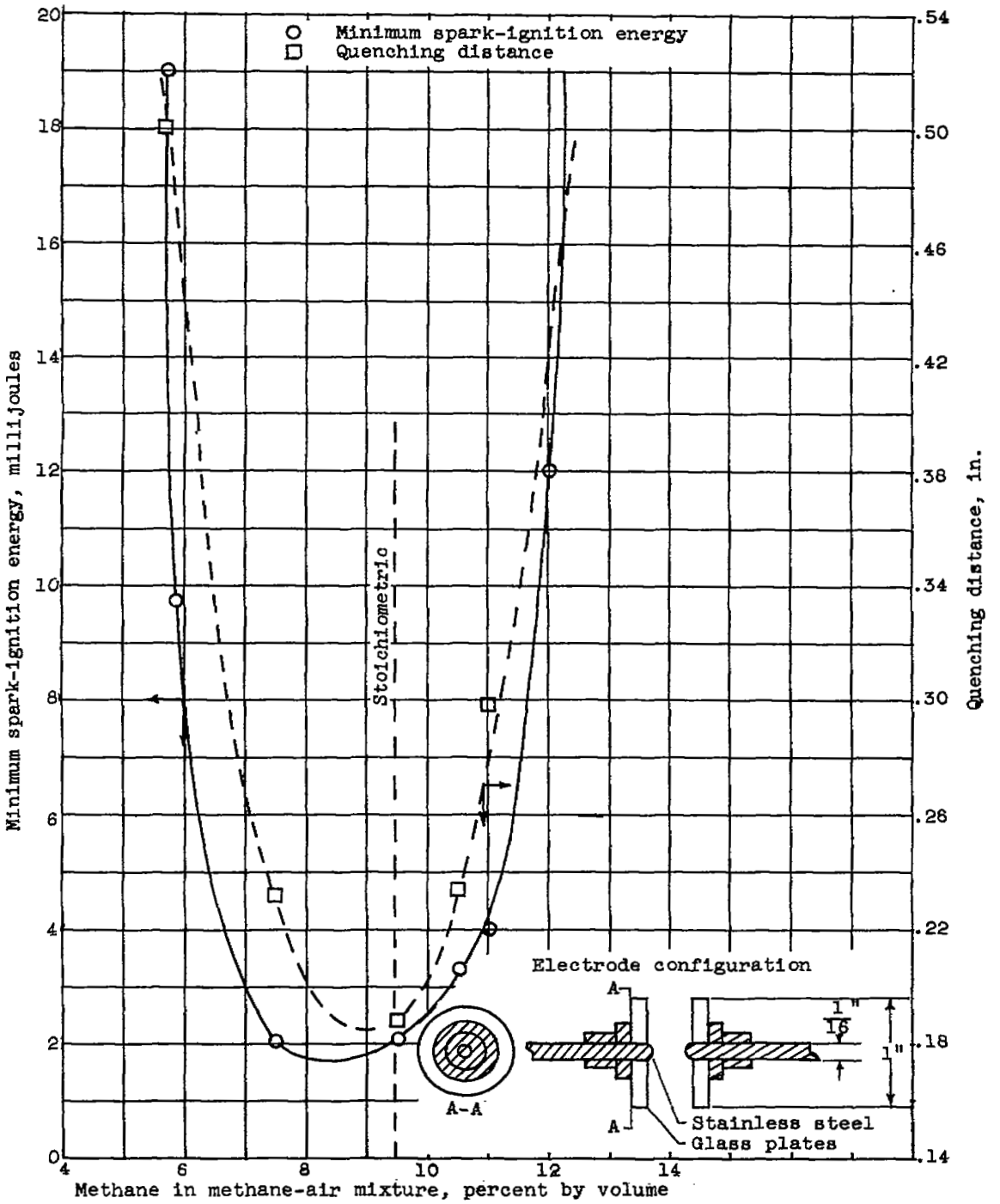

Figure III-32. - Effect of mixture composition on minimum spark-ignition energy and quenching distance of methane-air mixtures. Capacitance spark; pressure, 9.98 inches of mercury absolute; temperature, 77° F (ref. 11).

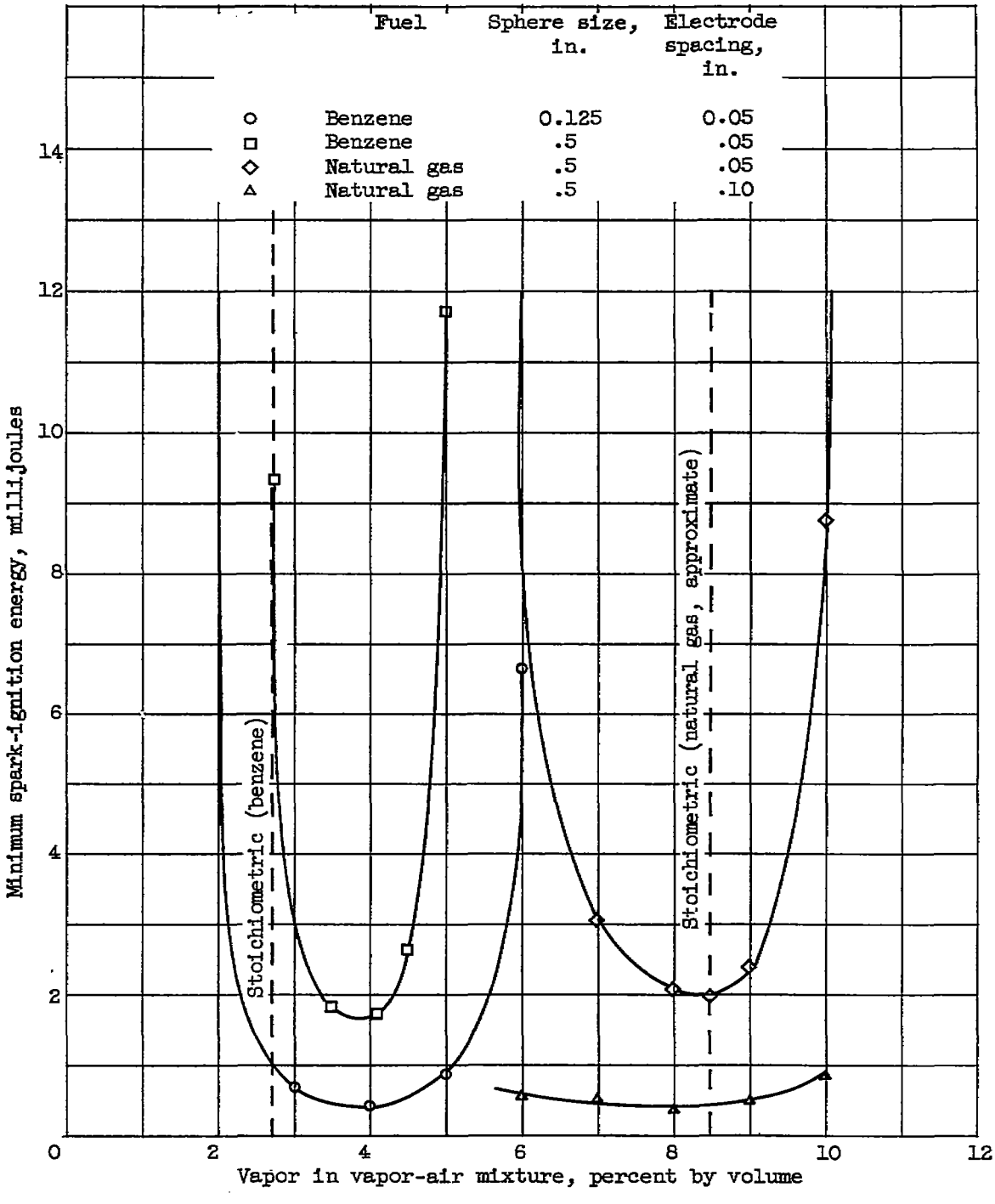

Figure III-33. - Effect of mixture composition on minimum spark-ignition energy of benzene-air and natural gas - air mixtures. Capacitance spark; pressure, atmospheric; room temperature; electrode spacing not maintained at quenching distance; electrodes, stainless steel spheres (ref. 68).

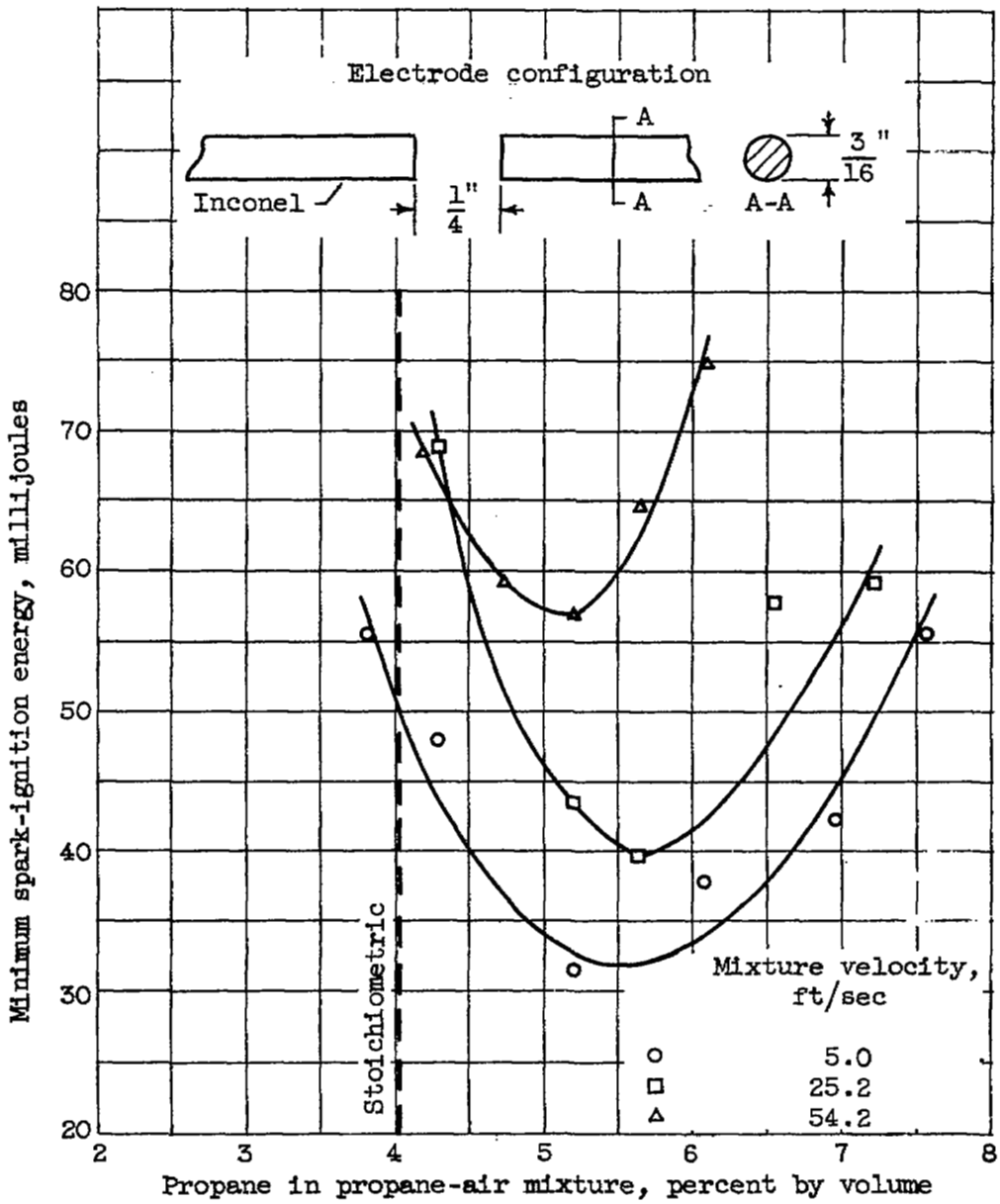

Figure III-34. - Effect of mixture composition and velocity on minimum spark-ignition energy of flowing propane-air mixtures. Long duration (600 to 900 microsec) capacitance spark; pressure, 3 inches of mercury absolute; electrode spacing, 0.25 inch (within quenching distance); temperature, 80° F (ref. 70).

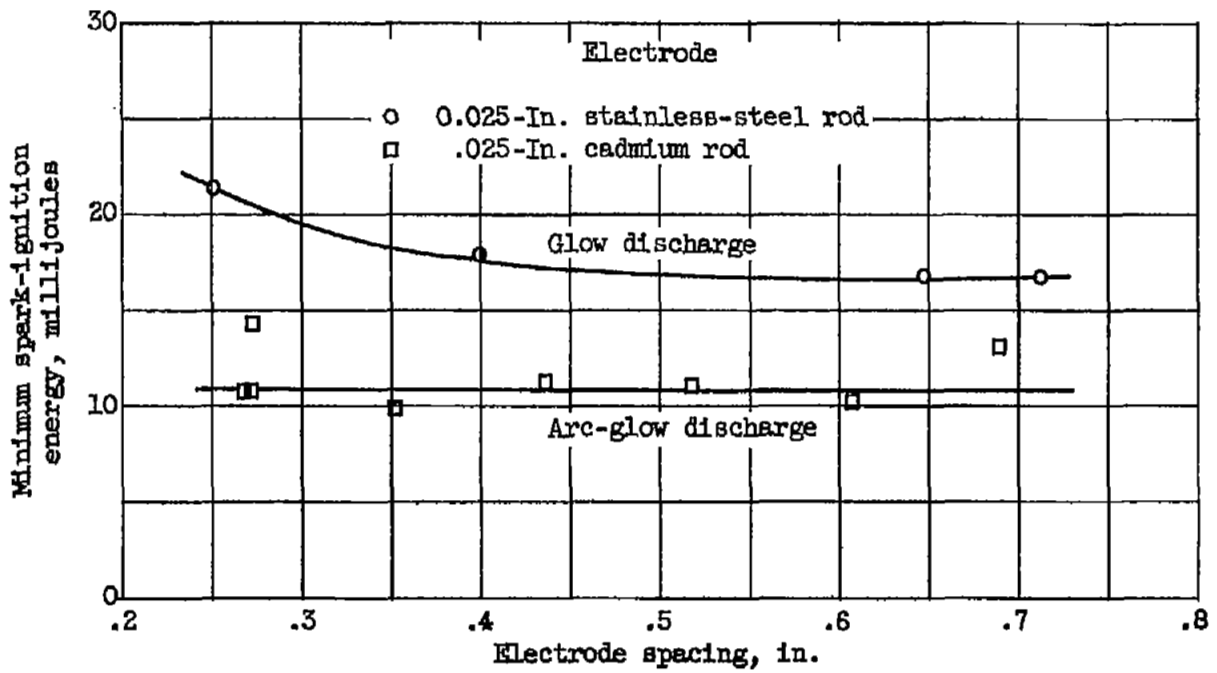

Figure III-35. - Effect of electrode material and electrode spacing on minimum spark-ignition energy of flowing 5.2 percent by volume mixture of propane in air. Long-duration (600 microsec) capacitance spark; pressure, 3 inches of mercury absolute; temperature, 80° F (ref. 12).

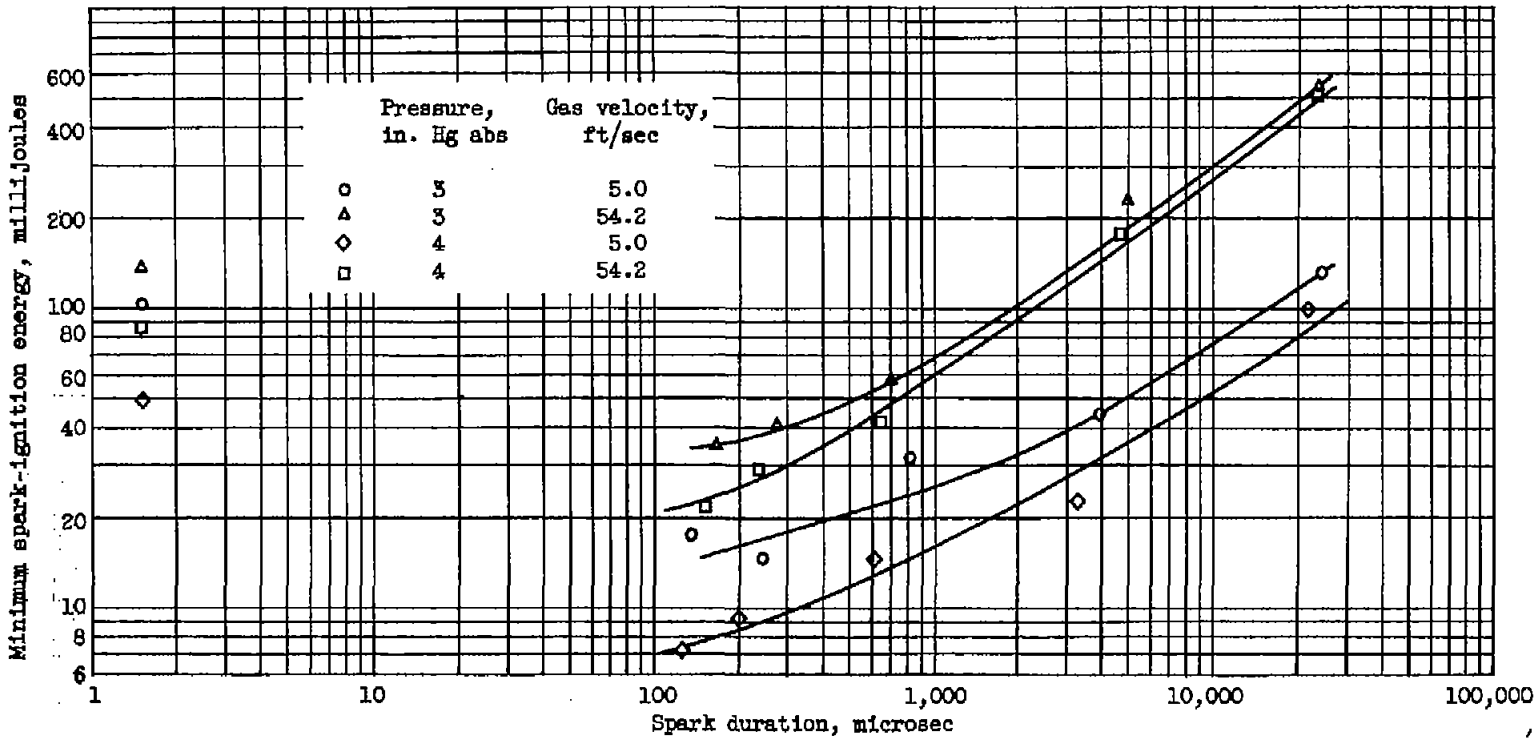

Figure III-36. - Effect of spark duration on minimum spark-ignition energy of flowing 5.2 percent by volume mixture of propane in air. Long-duration capacitance spark; temperature, 80° F; electrode spacing, 0.25 inch (within quenching distance) (ref. 70).

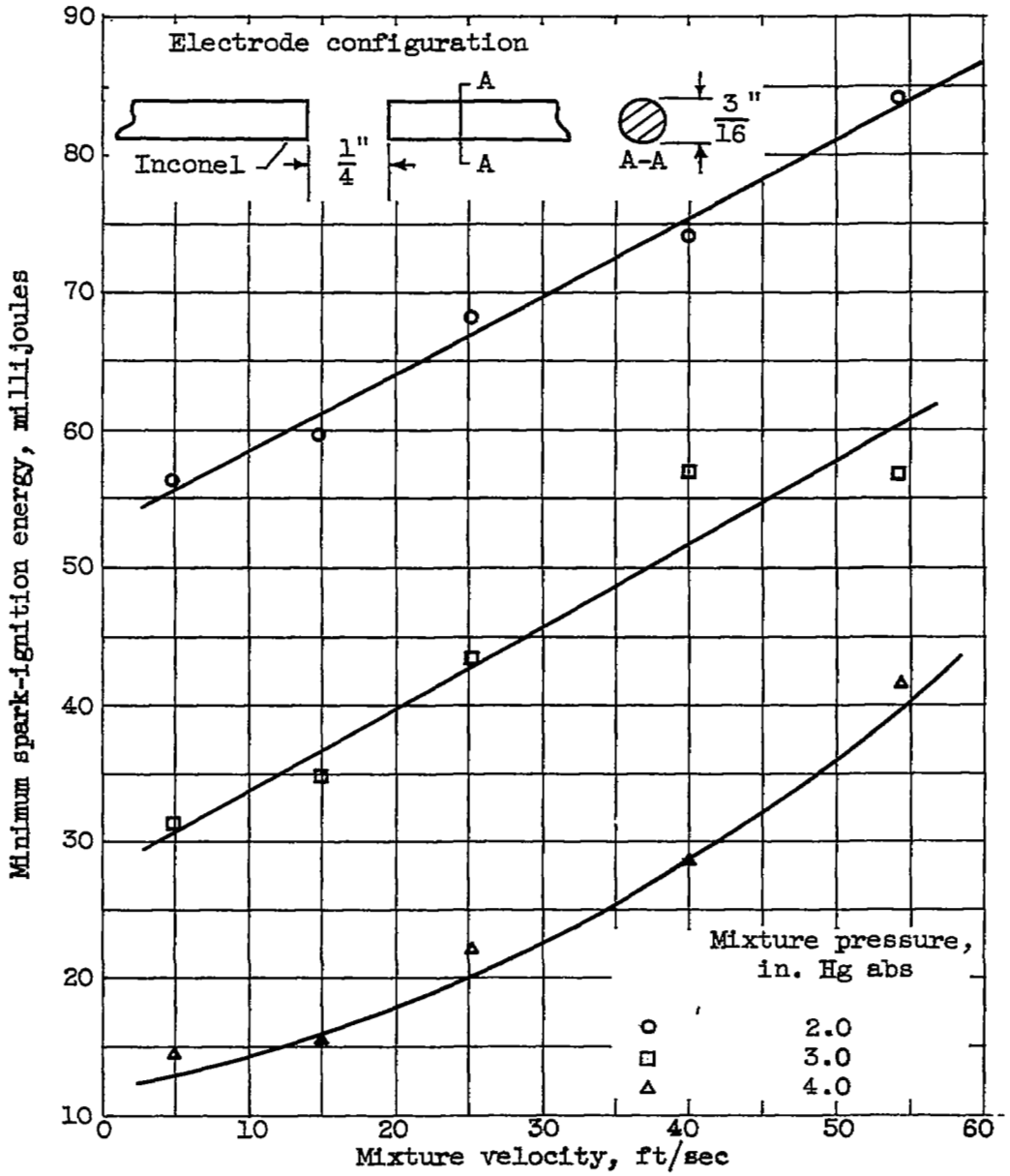

Figure III-37. - Effect of mixture velocity and pressure on minimum spark-ignition energy of flowing 5.2 percent by volume mixture of propane in air. Long-duration (600 microsec) capacitance spark; temperature, 80° F; electrode spacing, 0.25 inch (within quenching distance)(ref. 70).

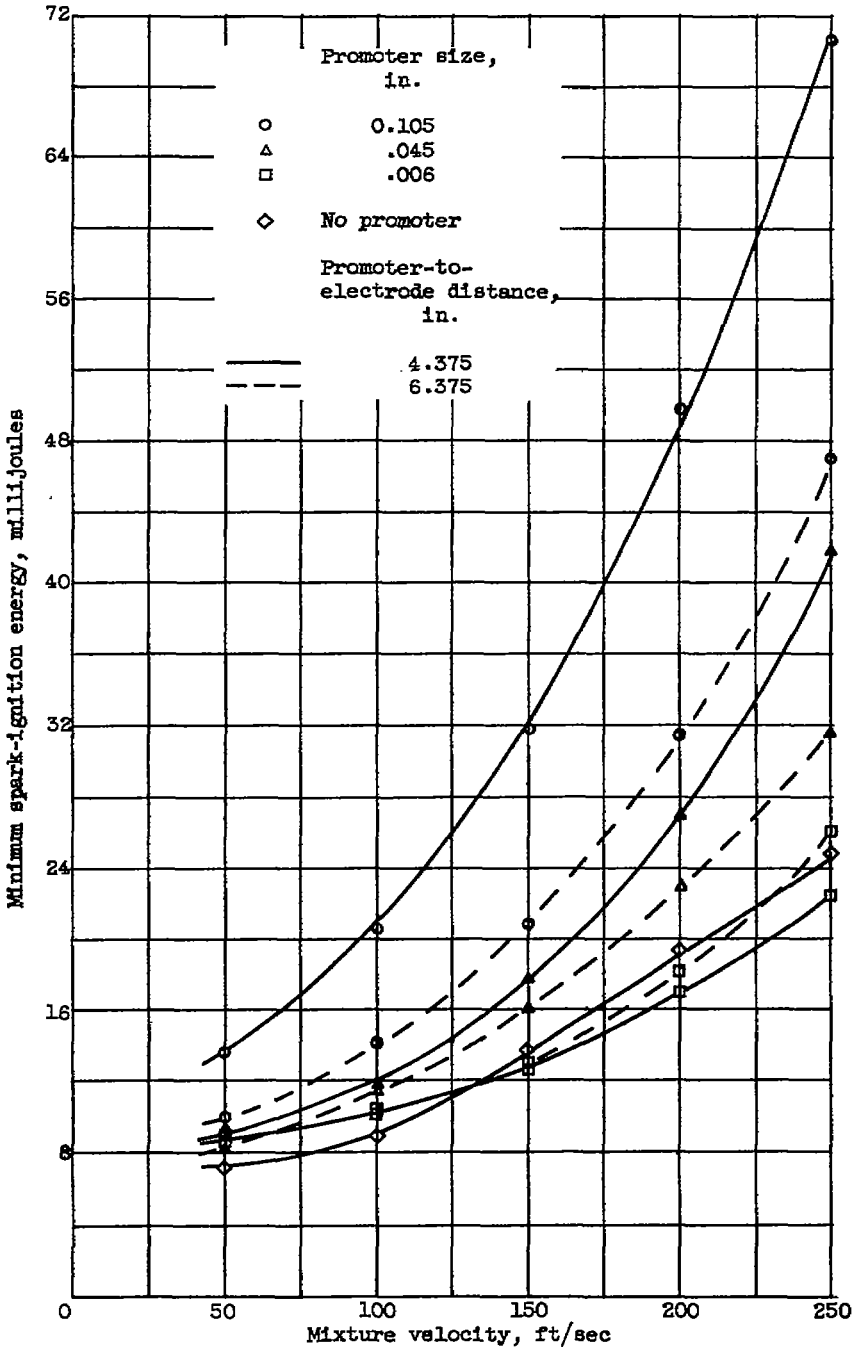

Figure III-38. - Effect of mixture velocity, promoter size, and distance from promoter to spark electrodes on minimum spark-ignition energy of 5.2 percent by volume mixture of propane in air. Long duration (approx. 500 microsec) capacitance spark; pressure, 5 inches of mercury absolute; temperature, 80° F; electrode spacing, 0.37 inch (quenching distance) (ref. 77).

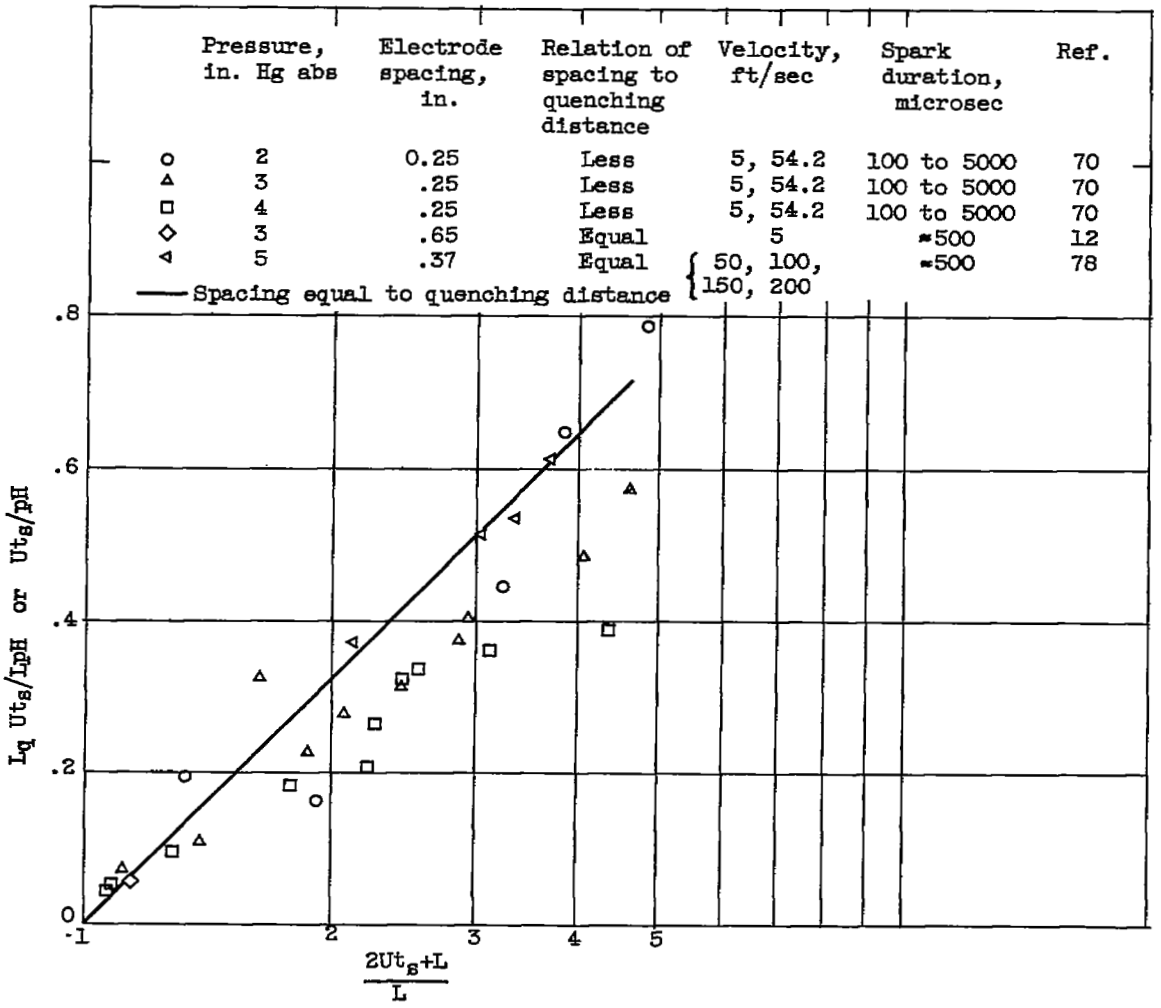

Figure III-39. - Correlation of nonturbulent-flow ignition-energy data. Fuel, propane; fuel-air ratio, 0.0835.

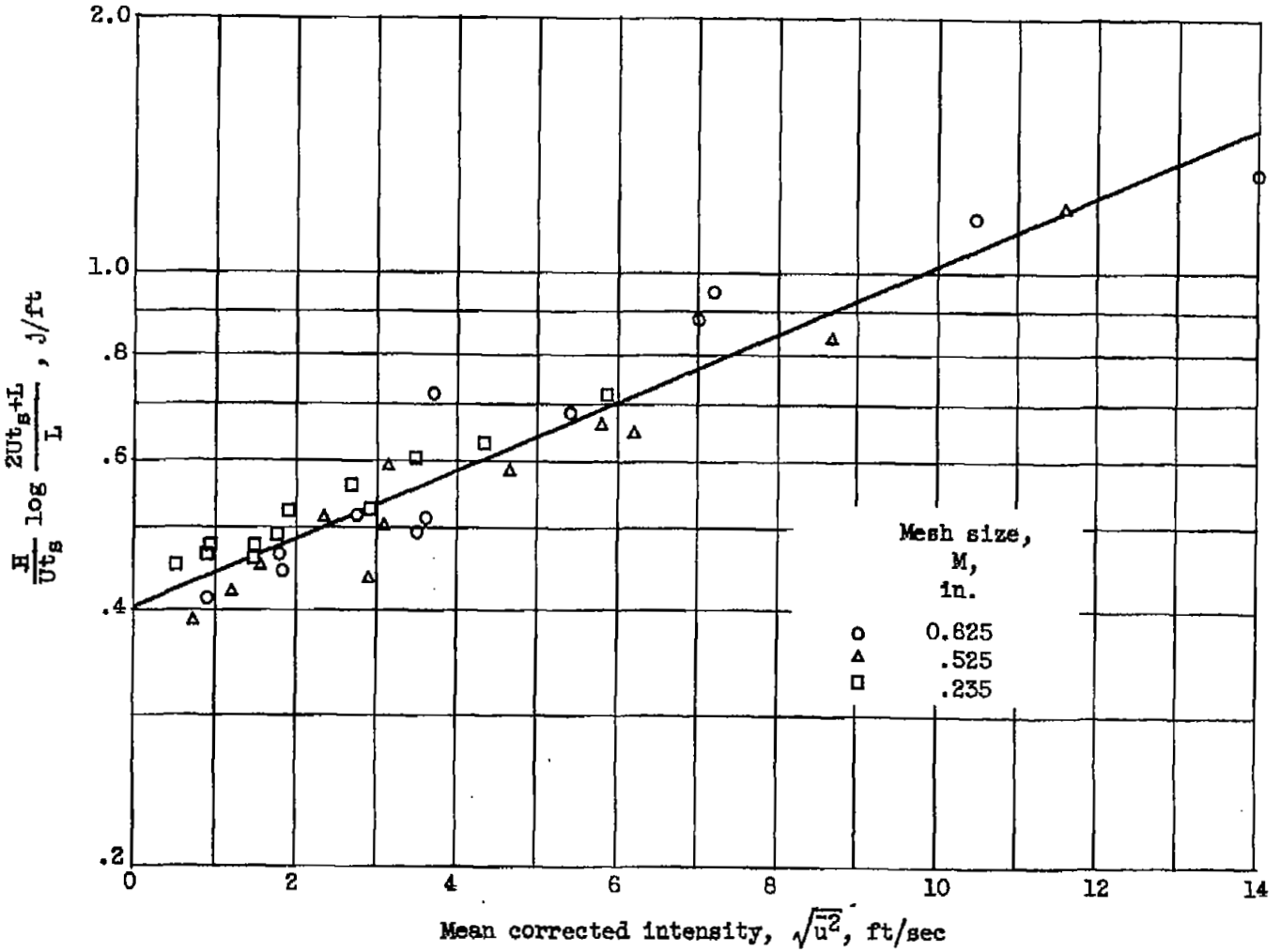

Figure III-40. - Correlation of ignition energy with velocity, spark duration, electrode spacing, and intensity of turbulence. Pressure, 5.0 inches of mercury absolute; velocity, 50 to 200 feet per second; propane-air ratio, 0.0835 by weight; spark duration, approximately 500 microseconds; electrode spacing, 0.37 inch (ref. 77).

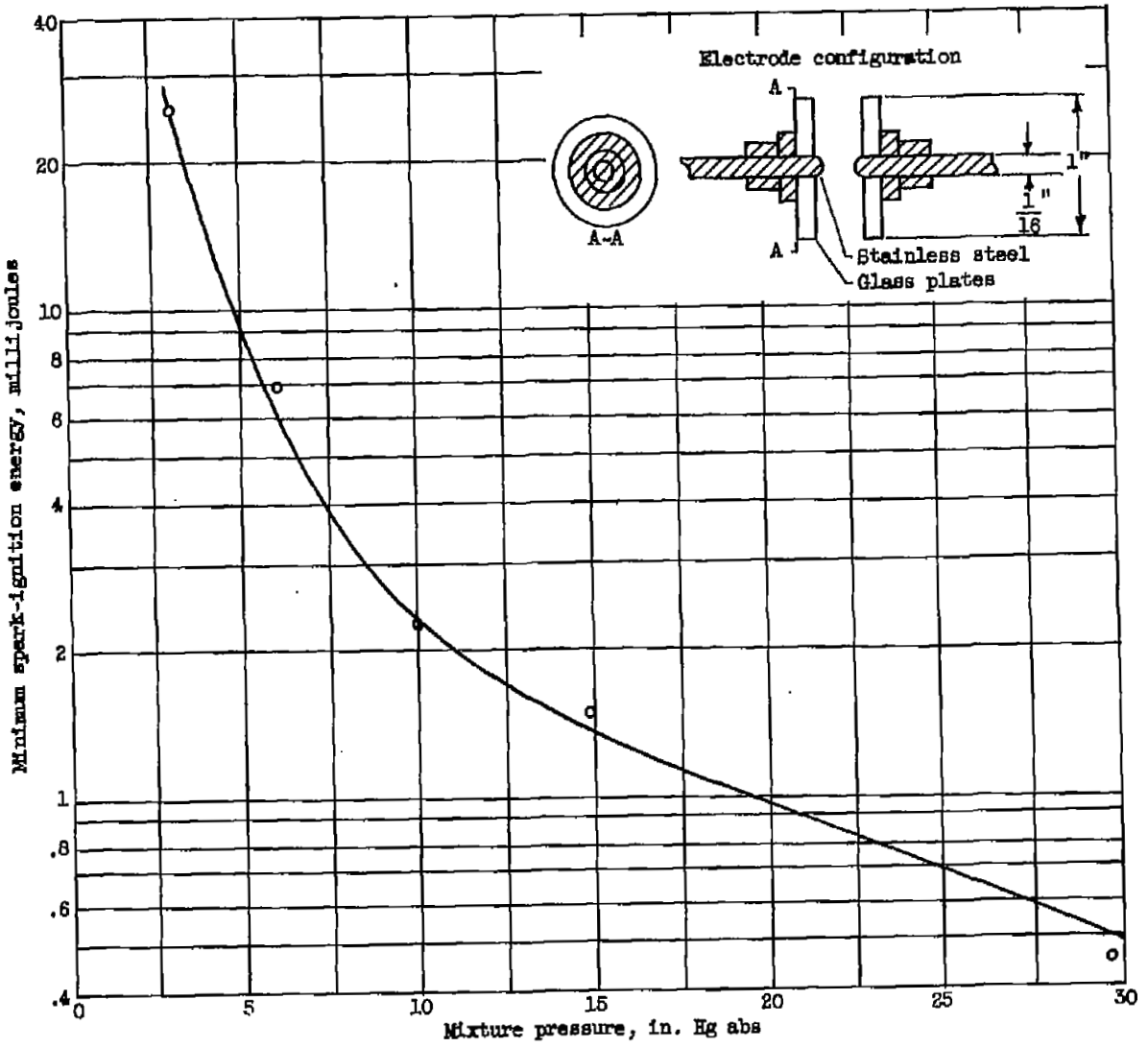

Figure III-41. - Effect of varying pressure of 8.5 to 9.5 percent by volume mixture of methane and air on minimum spark-ignition energy. Capacitance spark; temperature, 77° F (ref. 73).

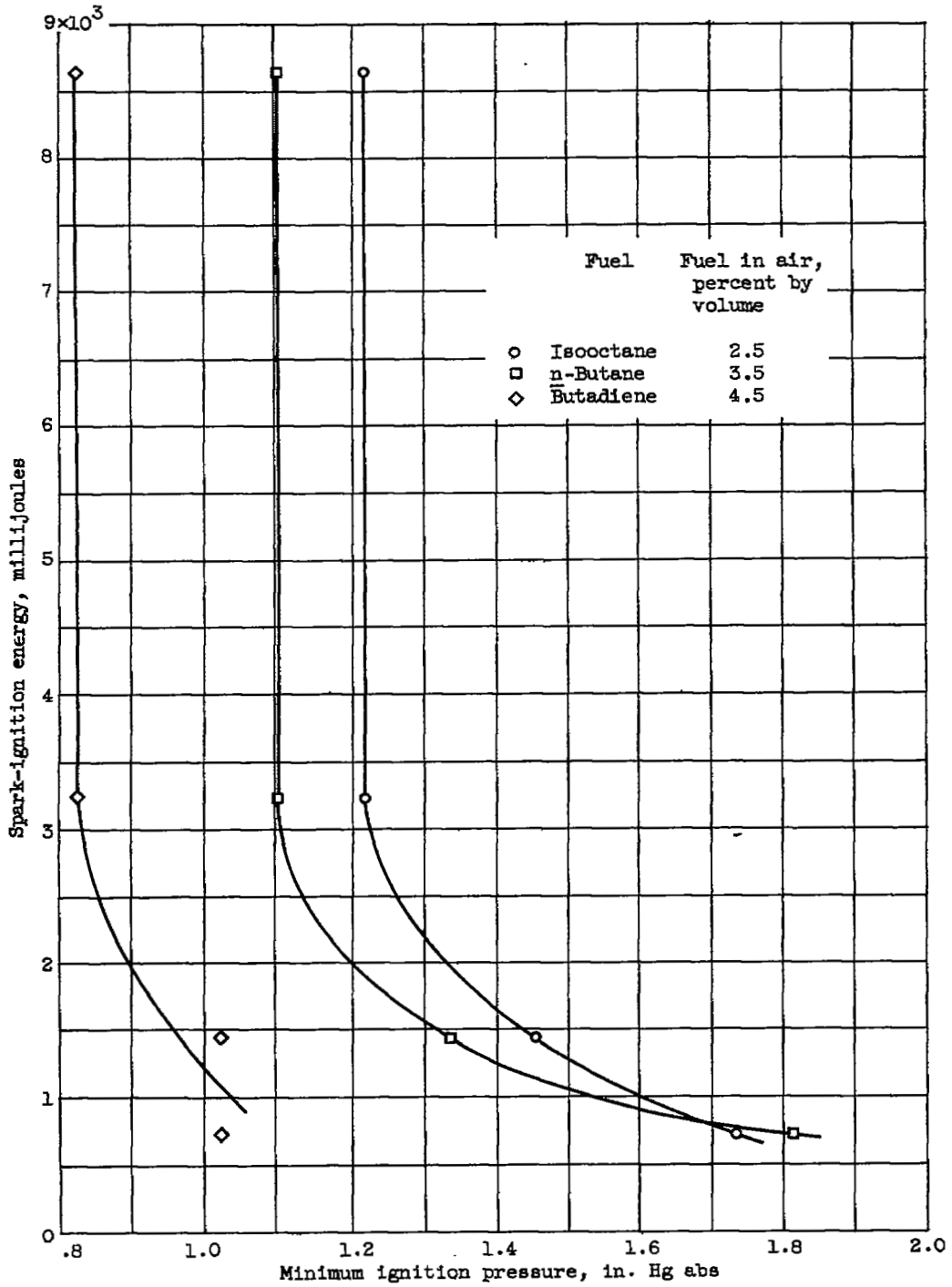

Figure III-42. - Effect of mixture pressure on minimum spark-ignition energy of one electrode configuration. Capacitance spark; electrode spacing, 0.11 inch (within quenching distance); spark voltage, 600 volts; mixtures slightly richer than stoichiometric (ref. 79).

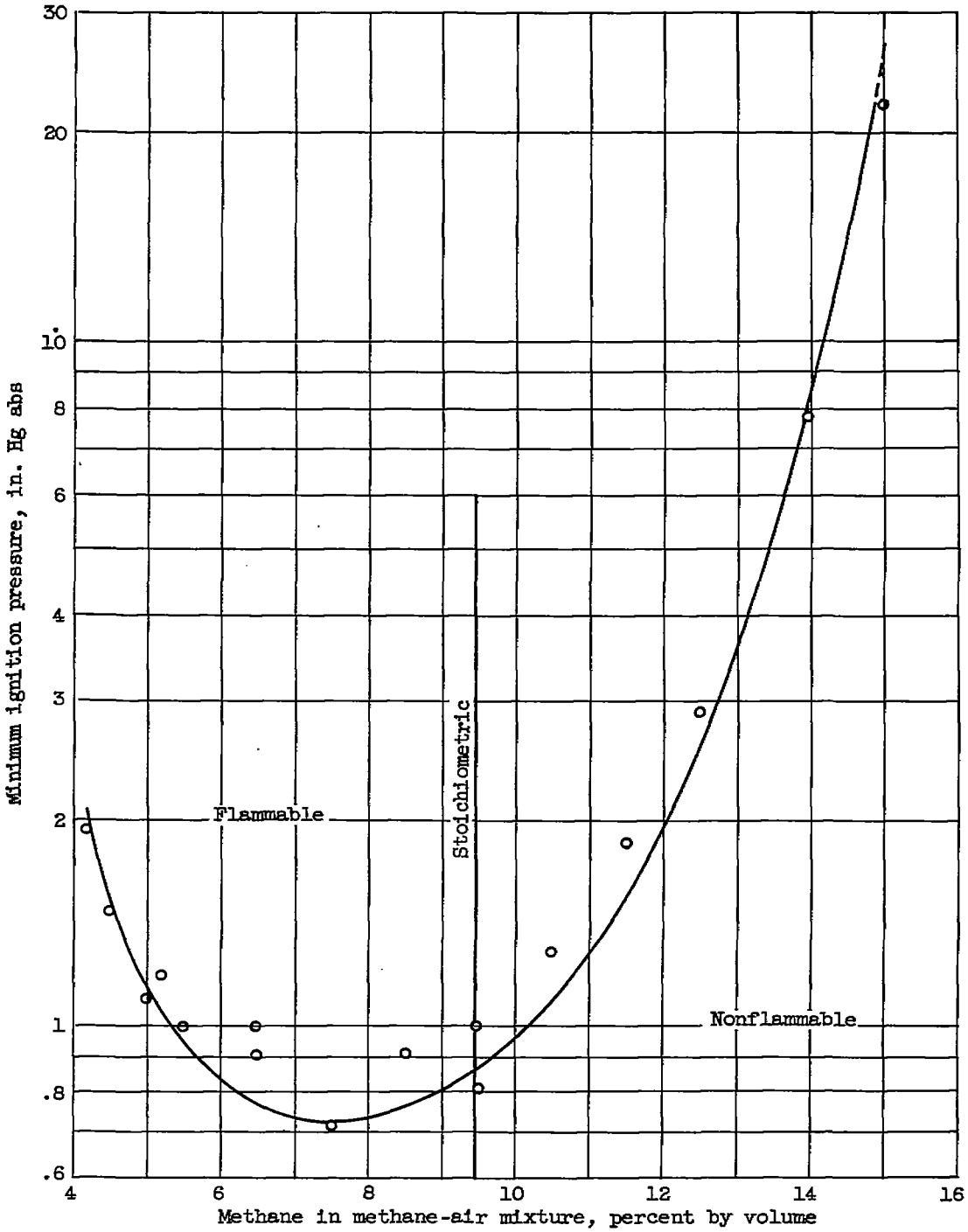

Figure III-43. - Effect of mixture composition on minimum ignition pressure of methane-air mixtures. Capacitance spark; temperature, 78° to 87° F; electrodes, spark plug; electrode spacing, 0.11 inch (within quenching distance); ignition energy, 8640 millijoules (ref. 79).

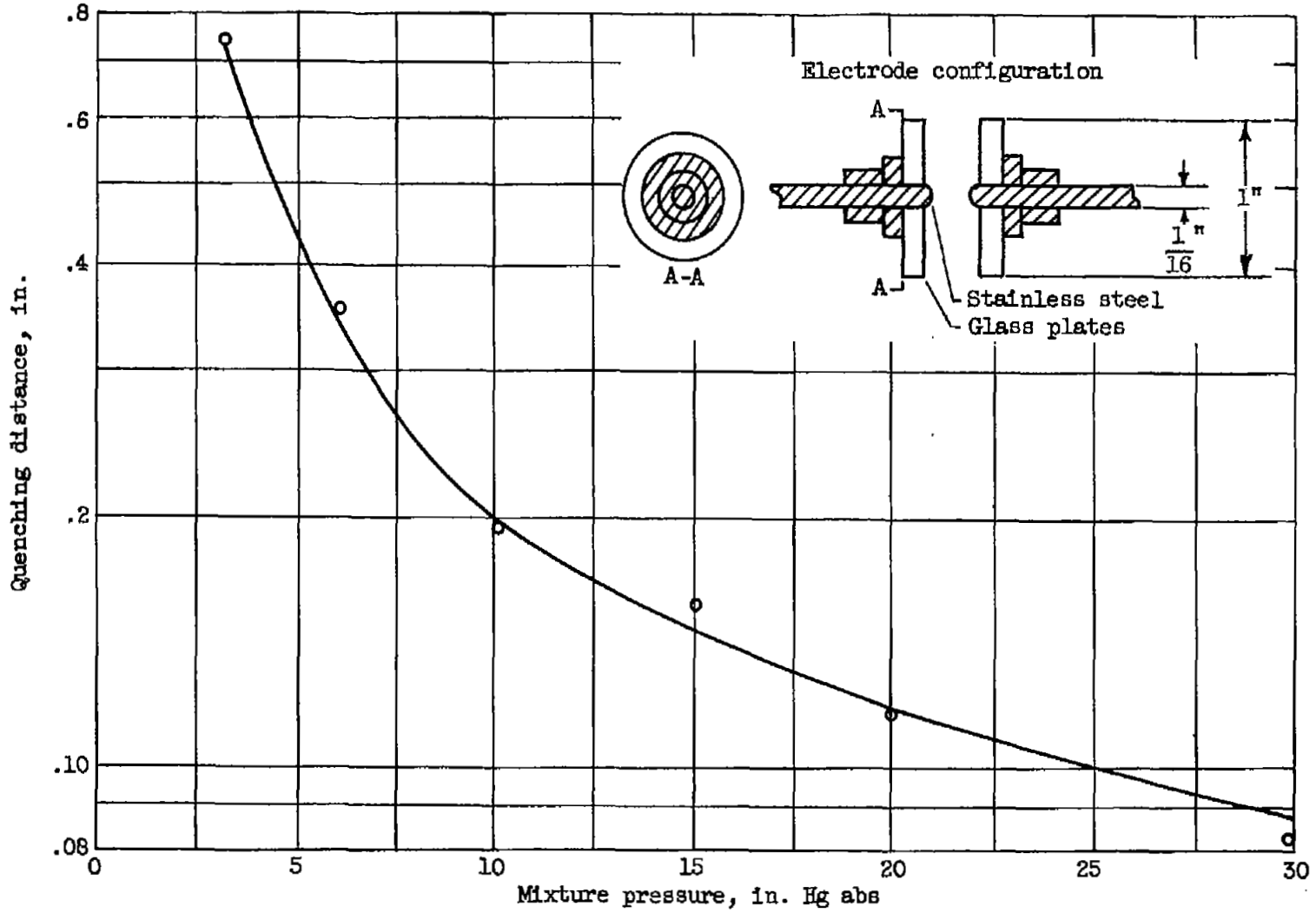

Figure III-44. - Effect of mixture pressure of 8.5 to 9.5 percent by volume mixture of methane and air on quenching distance of one electrode configuration. Capacitance spark; temperature, 77° F (by permission from ref. 73).

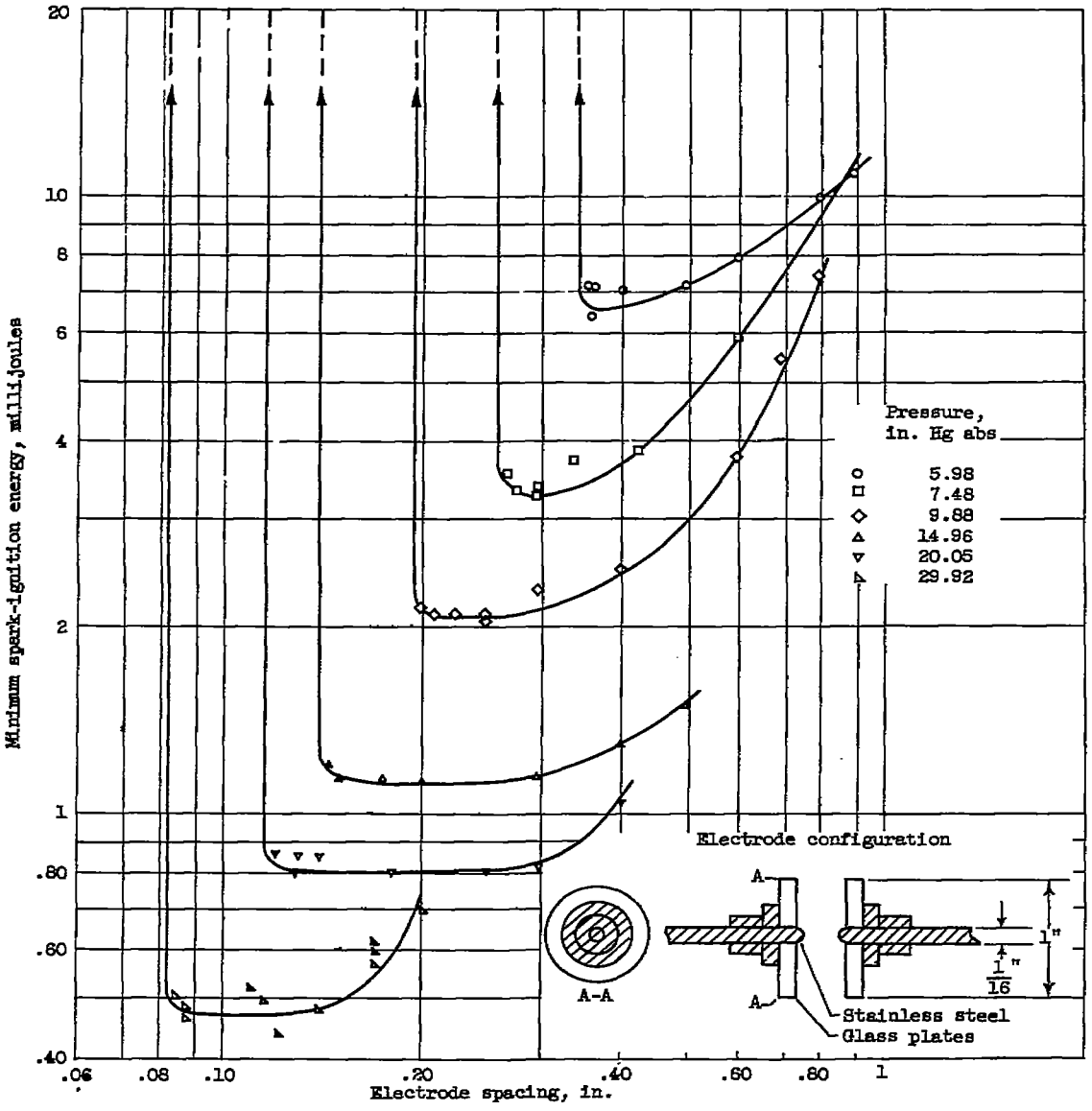

Figure III-45. - Effect of electrode spacing and pressure on minimum spark-ignition energy of 9.5 percent by volume methane in air. Capacitance spark; temperature, 77° F (by permission from ref. 73).

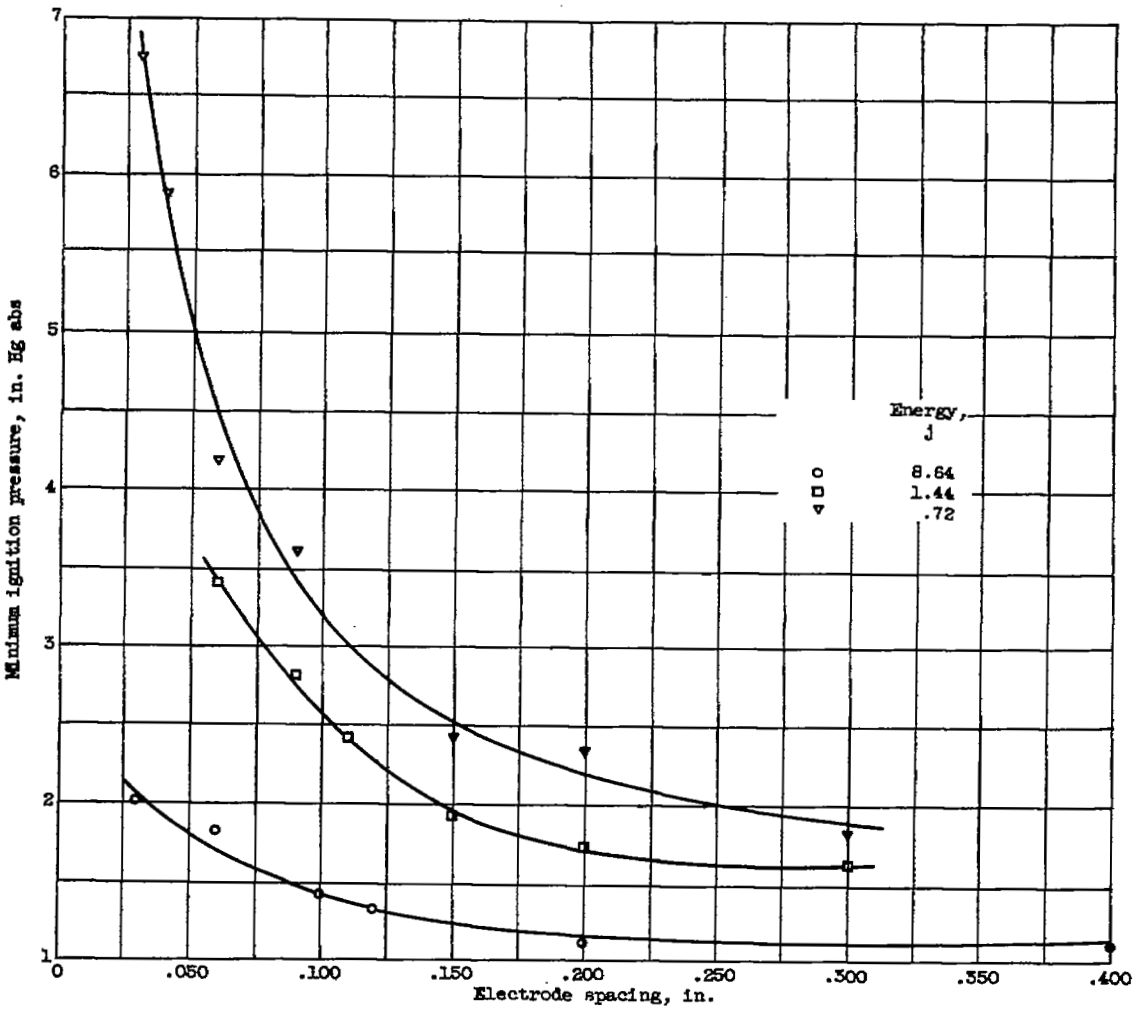

(a) n-Butane, 3.5 percent by volume.

Figure III-46. - Effect of electrode spacing on minimum ignition pressure. Capacitance spark; temperature, 70° to 75° F; spark plug electrodes (ref. 79).

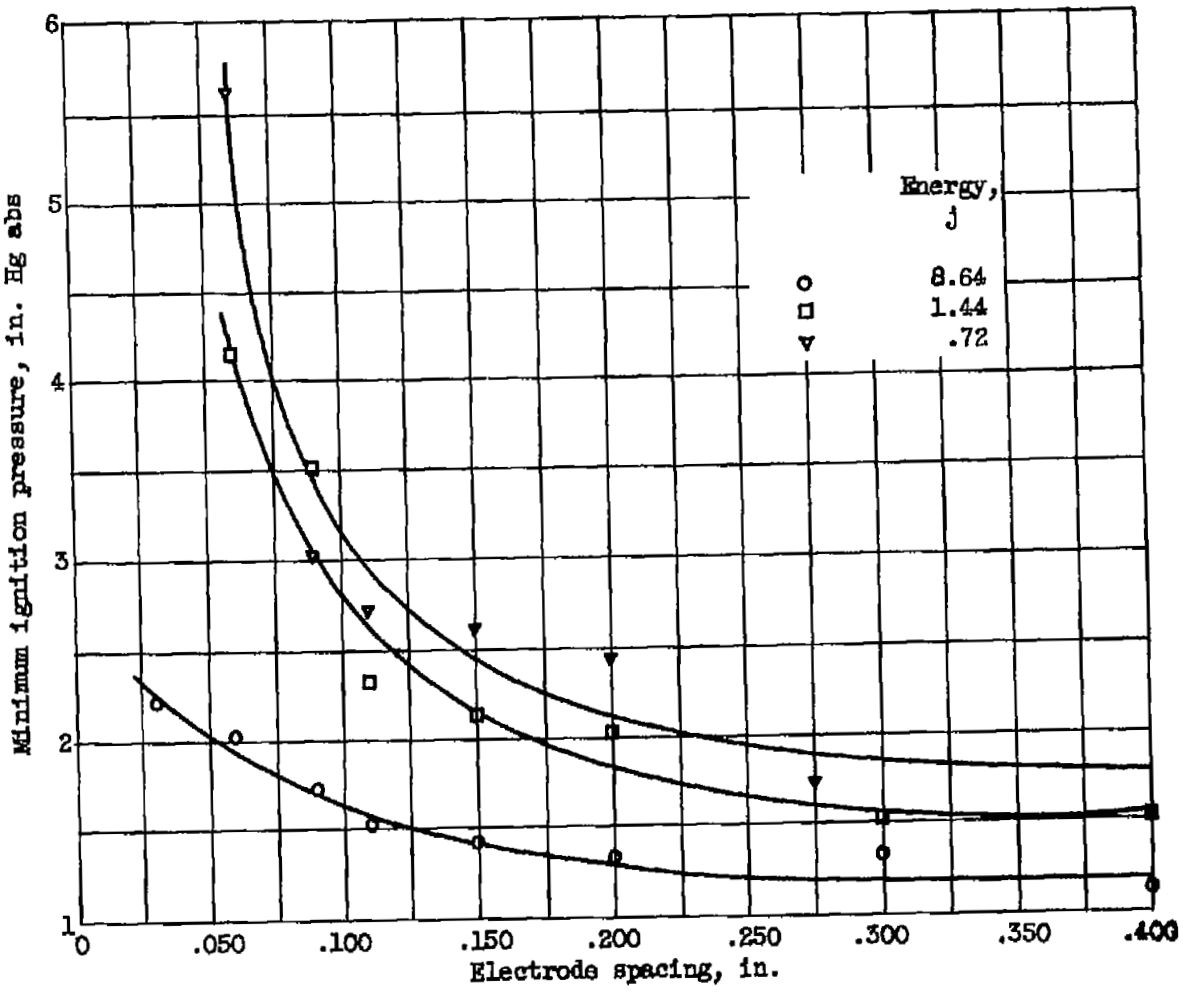

(b) 2,2,4-Trimethylpentane, 2.5 percent by volume.

Figure III-46. - Concluded. Effect of electrode spacing on minimum ignition pressure. Capacitance spark; temperature, 70° to 75° F; spark plug electrodes (ref. 79).

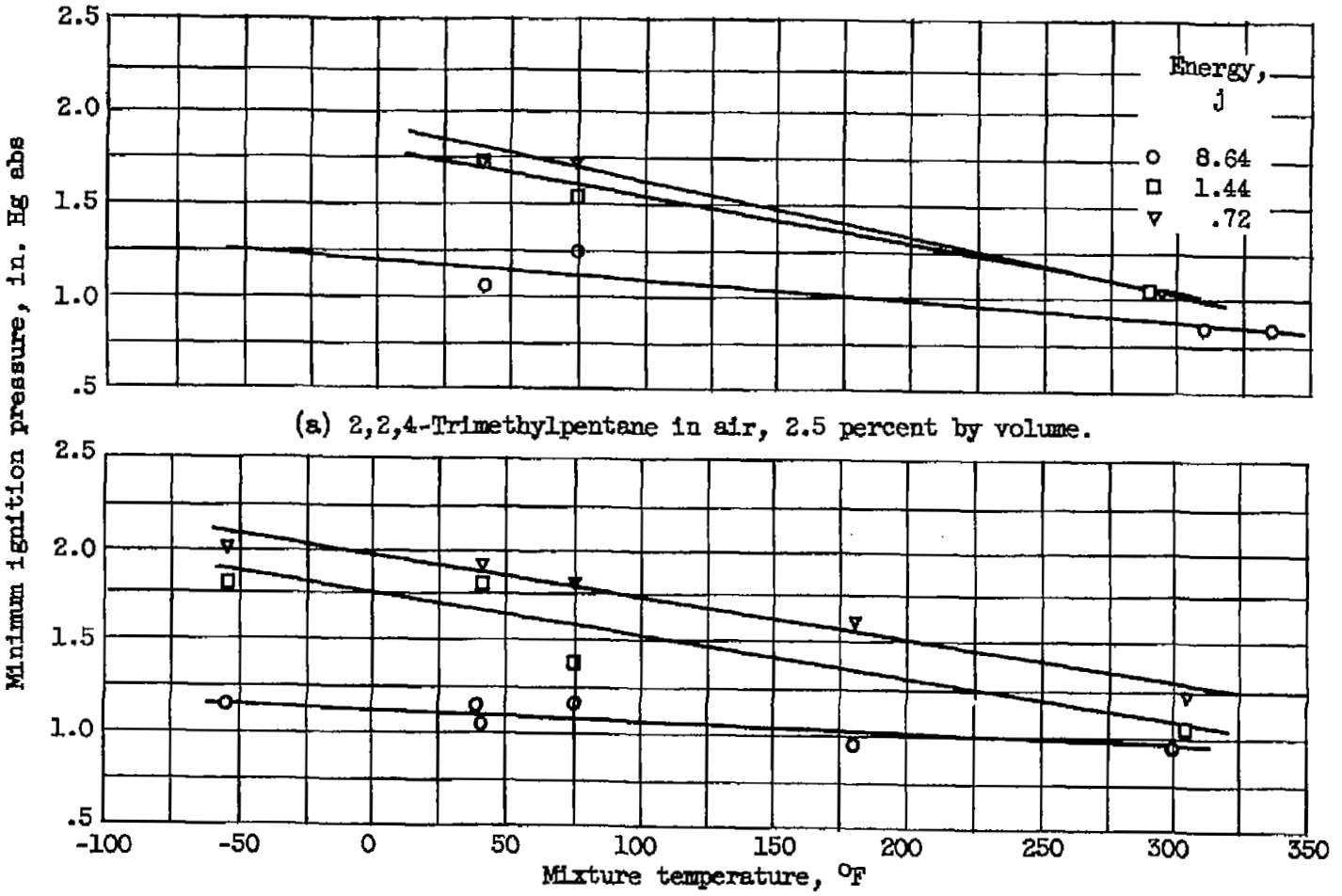

(a) 2,2,4-Trimethylpentane in air, 2.5 percent by volume.

(b) n-Butane in air, 3.5 percent by volume.

Figure III-47. - Effect of mixture temperature on minimum spark-ignition pressure of 2,2,4-trimethylpentane - and n-butane - air mixtures. Capacitance spark; spark plug electrodes; electrode spacing, 0.11 inch (within quenching distance)(ref. 79).

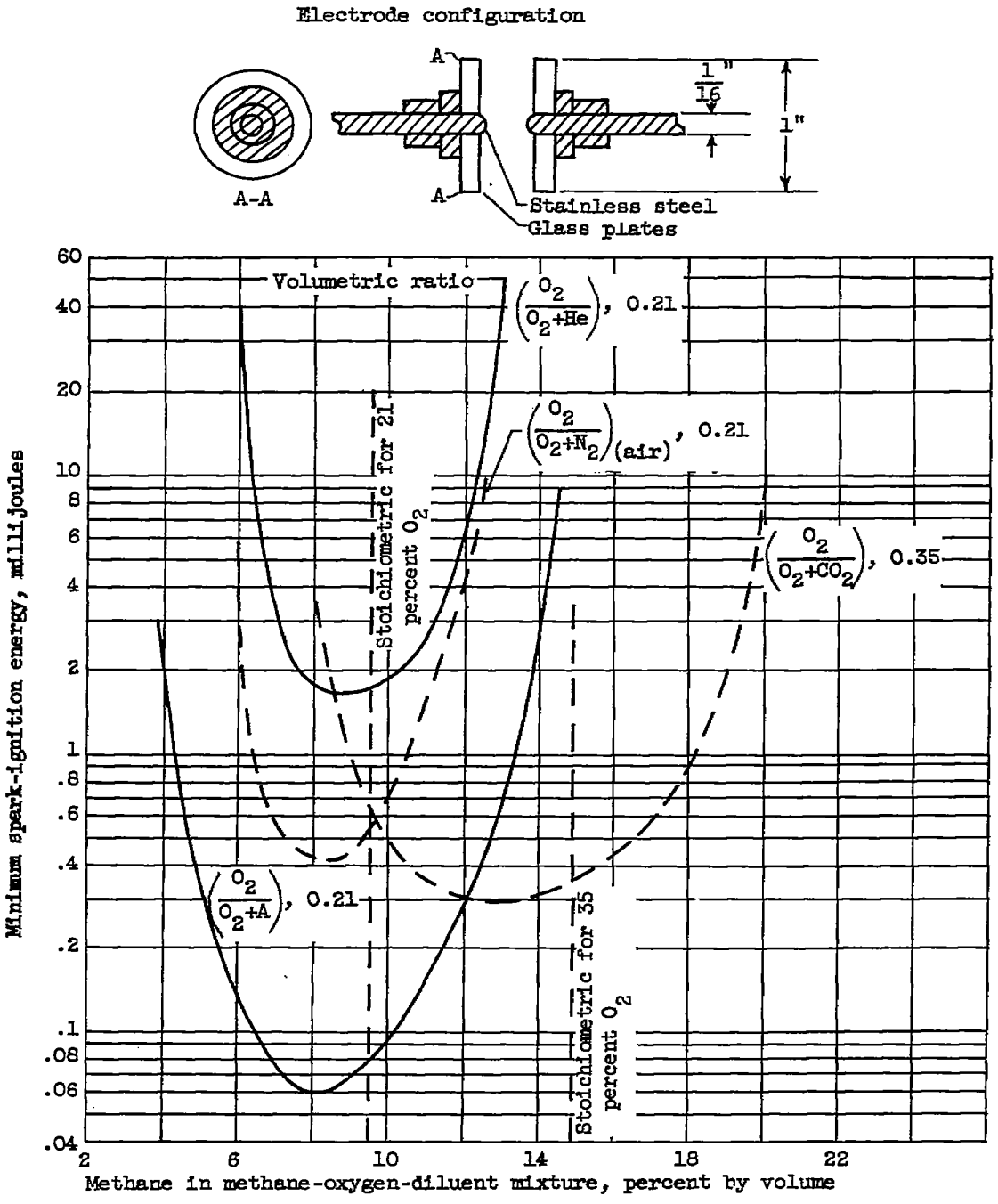

(a) Minimum spark-ignition energy.

Figure III-48. - Effect of diluents on minimum spark-ignition energy and quenching distance of methane-oxygen-diluent mixtures. Capacitance spark; pressure, atmospheric; temperature, 77° F (by permission from ref. 73).

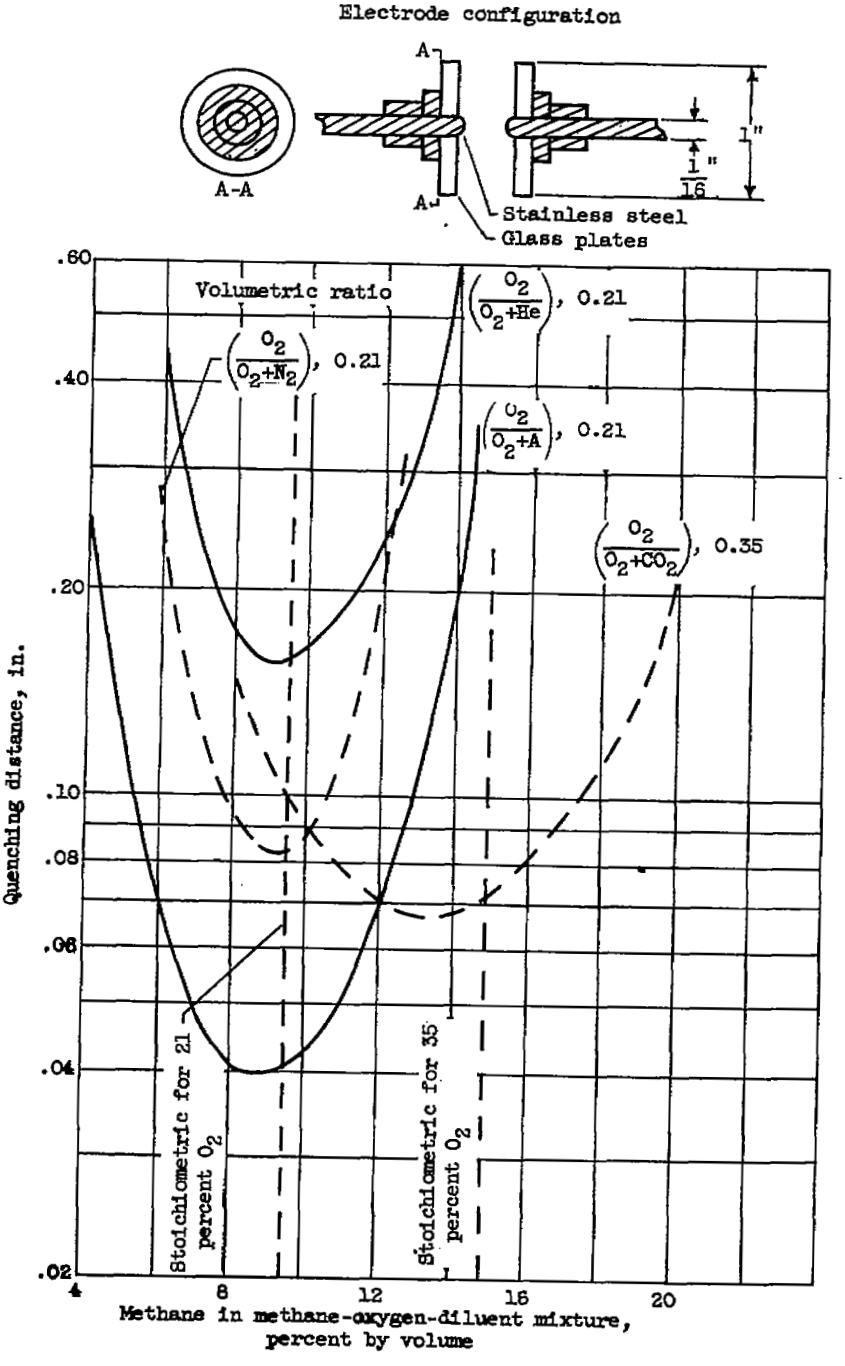

(b) Quenching distance.

Figure III-48. - Concluded. Effect of diluents on minimum spark-ignition energy and quenching distance of methane-oxygen-diluent mixtures. Capacitance spark; pressure, atmospheric; temperature, 77° F (by permission from ref. 73).

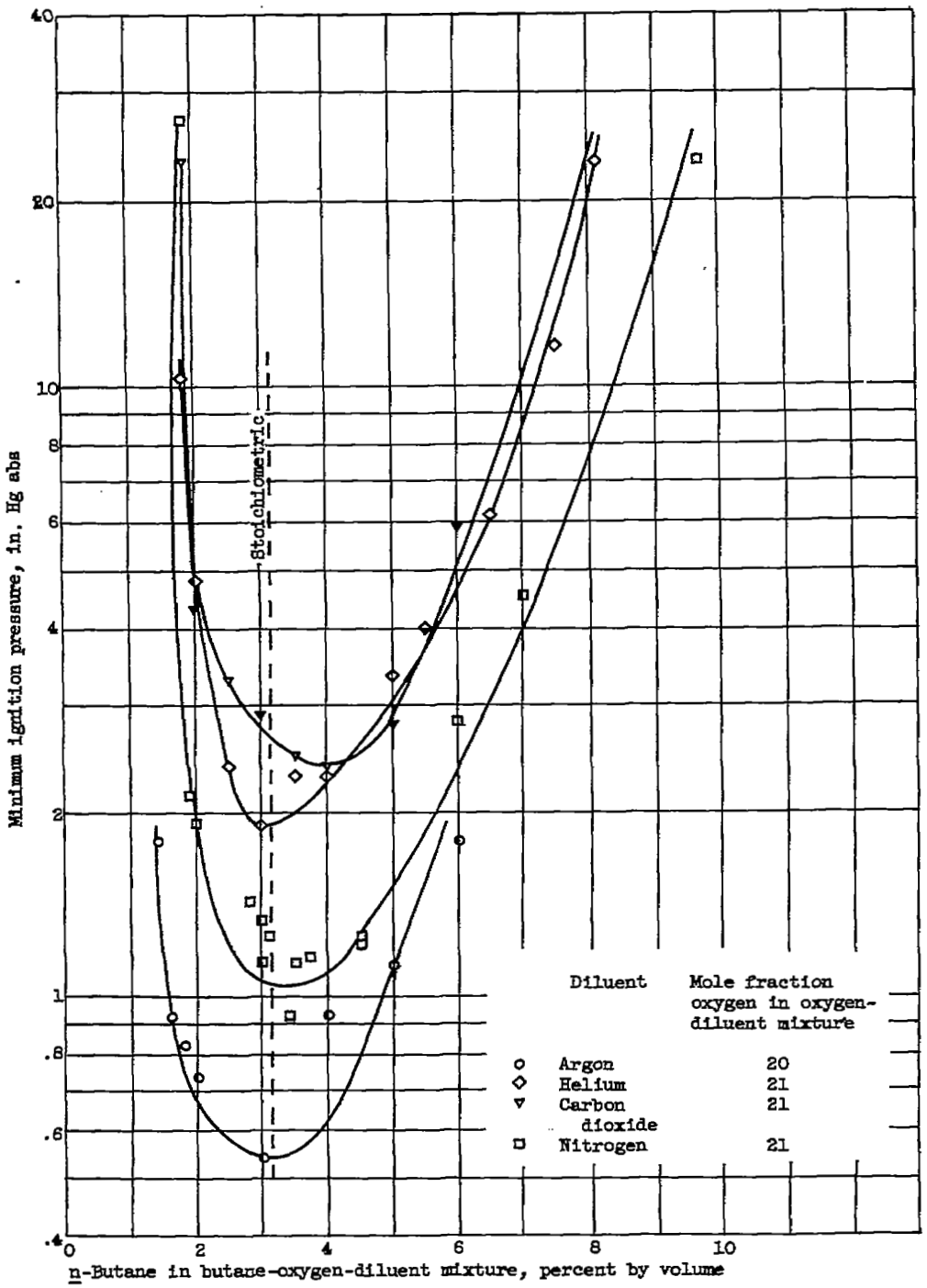

Figure III-49. - Effect of diluent on minimum ignition pressures of n-butane-oxygen-diluent mixtures. Capacitance spark; temperature, 74° to 82° F; electrode spacing, 0.11 inch (within quenching distance); ignition energy, 8640 millijoules (ref. 79).

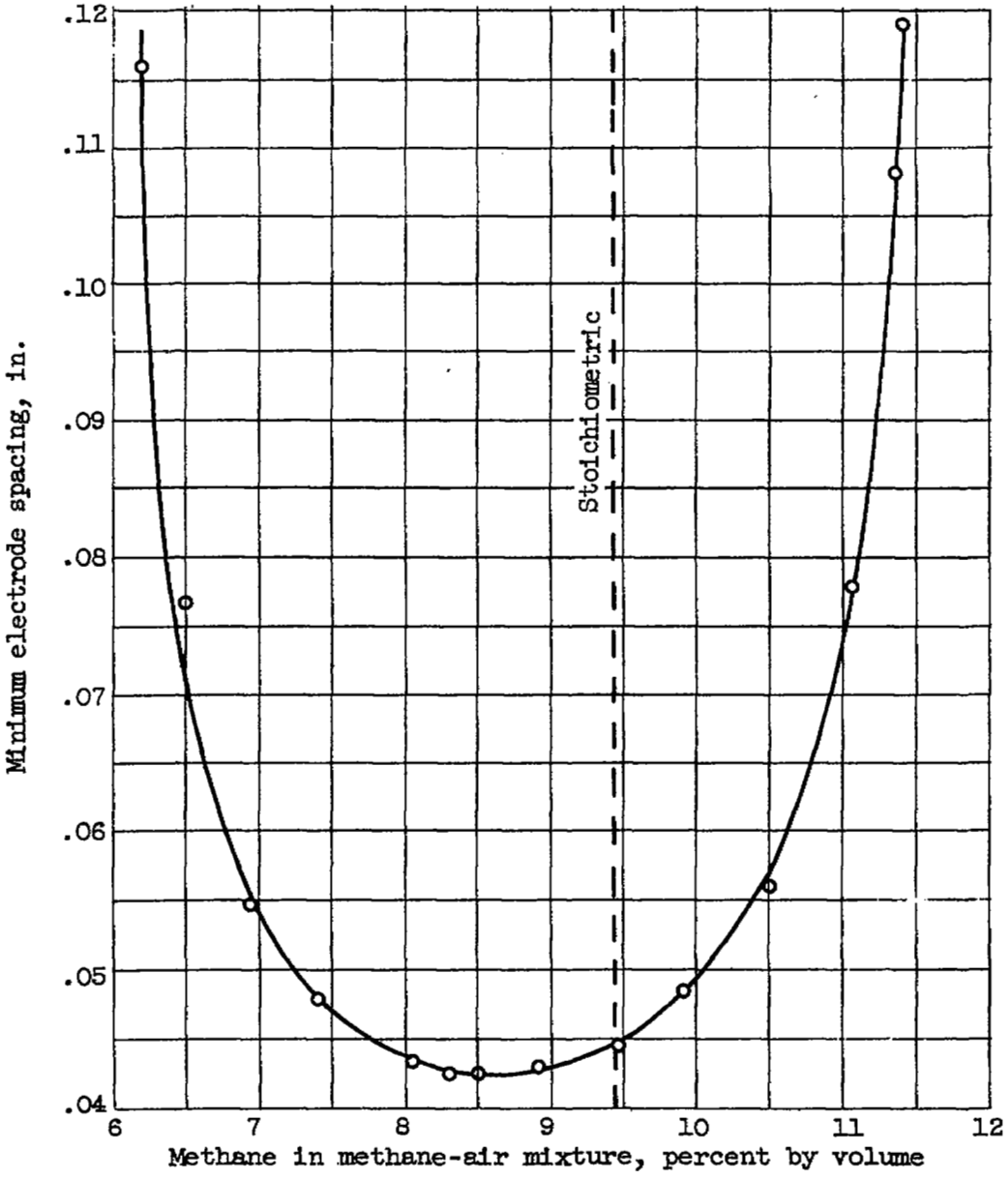

Figure III-50. - Effect of mixture composition on minimum electrode spacing in ignition of methane-air mixture. Inductance spark; atmospheric pressure and temperature; electrode configuration, 0.394-inch-diameter platinum disk and sharply pointed platinum cone; primary circuit current, 1.0 ampere (ref. 84).

CHAPTER IV

LAMINAR FLAME PROPAGATION

By Gordon L. Dugger, Dorothy M. Simon, and Melvin Gerstein

INTRODUCTION

The ultimate goal of fundamental studies in laminar flame propagation is a complete knowledge of the chemical kinetics of the flame reactions. With a knowledge of the kinetics, the effects of variables on the propagation rate could be predicted, and the problems of combustion-chamber design could be approached with greater confidence. Unfortunately, however, the experimental problems involved in the study of kinetics at high temperatures are yet to be solved. Consequently, current studies of the combustion process are necessarily conducted in terms of the laminar flame velocity, minimum ignition energy, flammability limits, and quenching distance. Theoretical interrelations that are in accord with the experimental results indicate these to be fundamental properties of the mixture when properly measured. Correlations between some of these properties and engine performance parameters show that the results of such studies may be of considerable practical value in the aircraft propulsion field.

In this chapter, an attempt is made to summarize available information on laminar flame propagation. Characteristics of laminar flames - the structure of the combustion wave and the relation of direct, schlieren, and shadow photography to that structure - are considered. Also discussed are methods of measuring flame velocity, along with effects of physical and chemical variables on flame velocity. A brief survey of the theory of laminar flame propagation is presented, with particular emphasis on the Semenov (thermal mechanism) and Tanford-Pease (active-particle-diffusion mechanism) equations for flame velocity. A discussion of the more significant experimental evidence in the controversy concerning thermal against diffusional mechanisms is also included. Finally, experimental data and methods of predicting flame velocity are summarized with respect to their significance and application to practical problems of combustion.

SYMBOLS

The following symbols are used in this chapter:

A	cross-sectional area
a	exponent
B,B'	dimensionless quantities
b	exponent
C	constant
c_p	specific heat
D	diffusion coefficient
E	activation energy

G	mass-flow rate
H	enthalpy
h	height of luminous cone
I	rate of production by chemical reaction
K	flame velocity coefficient
K_H	empirical proportionality factor
$\overline{K_\Sigma}$	average proportionality constant
k	specific rate constant
l	length of curve
dl	length of flame boundary
M	molecular weight
m	ratio of moles of reactants to moles of products
N	number of C-H bonds
N_c	Avogadro number
n	concentration
P	steric factor
p	pressure
Q	heat of reaction
R	universal gas constant
r	radial distance
dr	distance between flow lines
S	surface area
s	slant height
T	temperature
t	time
U	velocity
V	volumetric flow rate
X	mole fraction

x	distance
Z	collision number
α	angle between direction of approach flow and burning surface
γ	ratio of specific heats
δ	reaction-zone thickness
ε	expansion ratio of gas mixture
$\varkappa$	thermal conductivity
μ	viscosity
ρ	density
σ	collision diameter
φ	equivalence ratio
ψ	molar ratio, $O_2/(O_2 + N_2)$
ω	reaction rate

Subscripts:

am	ambient
av	average
cir	circumscribed
d	diffusion
e	equilibrium
eff	effective
F	flame
f	fuel
g	gas
i	i^{th} species
ig	ignition
ins	inscribed
j	j^{th} species
l	linear
m	mean

max	maximum
O	oxygen atom
O_2	oxygen molecule
o	initial conditions
r	reactant
rel	relative
t	tube
tot	total
w	weighted

CHARACTERISTICS OF LAMINAR FLAMES

A flame is a rapid, self-sustaining chemical reaction occurring in a discrete reaction zone. Reactants may be introduced into this reaction zone, or the reaction zone may move into the reactants, depending on whether the unburned gas velocity is greater or less than the flame velocity. The flame velocity, which is also called burning velocity or normal combustion velocity, is the velocity at which unburned gas moves through the combustion wave in the direction normal to the wave surface. This definition refers to the velocity of unburned gas relative to the flame front as determined at some point beyond the influence of the flame, that is, at a point where the gas velocity has not yet been altered by either heat conduction from the flame or the pressure field set up as a result of the thrust pressure of the flame. It is obvious that different types of flame photography and different methods of measurement and computation from flame photographs would give different results, depending on how closely the photographs and measurements approximate the true relation between the reference gas velocity and the flame front.

The preheating of the gas by heat conduction from the flame reaction zone is best understood by considering the temperature profile for a laminar flame and the relation of each type of photography to some point in the temperature profile as determined by theoretical considerations and experimental evidence. The bending of unburned gas flow lines due to the pressure field receives less attention than the preheating effect in this report, since its effect on flame velocity measurements is generally less important.

Temperature Profile

Three experimental techniques have been used recently to determine temperature profiles:

(1) Traversing with fine thermocouple (refs. 1 and 2)

(2) Traversing with very fine slit of light and determining flame temperature from refractive index (ref. 3)

(3) Tracing curved path of stroboscopically illuminated dust particle and computing temperature from measurements of its direction and velocity (refs. 4 and 5)

Friedman (ref. 2) used a ceramic-coated thermocouple made by gas-welding 0.0012-centimeter platinum and platinum - 10-percent-rhodium wires to traverse a very lean propane-air flame (flat flame on 25-cm burner; mass air-propane ratio, 29.2; flame thickness, ~2 cm; pressure, 0.0594 atm). The resulting temperature profile had a shape similar to that of figure IV-1. The significance of such a temperature profile is as follows: At the point x_o, the temperature of the unburned gas has just begun to increase because of the heat conducted from the flame reaction. The temperature rises rapidly until the equilibrium flame temperature T_F is reached at a point x_F. These boundaries are not defined exactly, since the limiting values T_o and T_F are approached asymptotically; but the convergence is very rapid, so that the boundaries can be defined within narrow limits of T.

Consider first the part of the profile in which the temperature rises from T_o to a temperature T_3, which marks the inflection point of the T,x curve. This portion of the curve is convex toward the x-axis $\left(\frac{\partial^2 T}{\partial x^2} > 0\right)$, which means that a mass element in this region gains heat by conduction from the hotter elements downstream faster than it loses heat to the cooler elements upstream. There is little chemical reaction in this region; hence, little heat is evolved. Calculations of reference 6 show that 14 percent of the heat release occurs before reaching the luminous zone, which is generally considered to begin at some point beyond (T_3,x_3). Consequently, this region may be called the preheat zone. The mass element expands in volume, causing an acceleration of the unburned gas. On passing T_3, the mass element changes from a heat sink to a heat source, and the curve is concave toward the x-axis $\left(\frac{\partial^2 T}{\partial x^2} < 0\right)$. The temperature of the element continues to rise because of the heat evolution from the chemical reaction, and this region between T_3 and T_F may therefore be called the reaction zone.

The inflection point T_3 may be called the ignition temperature, but it is distinguished from the spontaneous ignition temperature determined in a static system (see ch. III and the appendix), where the ignition delay time may be 10^3 to 10^6 times the period required for the element to traverse the preheat zone of a stationary flame. The temperature T_3 may be calculated by numerical integration of theoretical equations for simple decomposition flames such as the ethylene oxide flame (ref. 7) or determined approximately by careful temperature traverse of the reaction zone by one of the methods mentioned previously.

The relation of direct, shadow, and schlieren images to the temperature profile is discussed in the following sections. While differences in the flame areas determined by these three types of flame photographs are pertinent to any method for measuring flame velocity, most of the discussion is given in terms of the inner cone of a Bunsen burner flame illustrated in the following sketch:

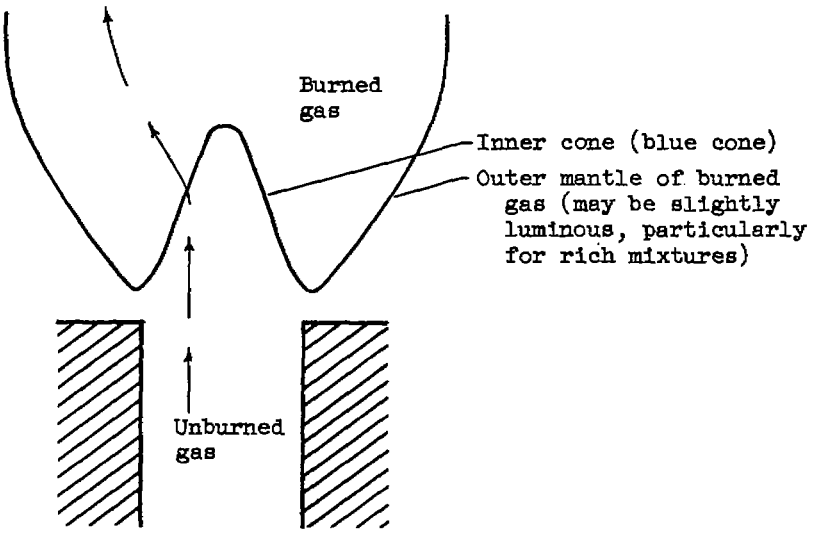

Relation of Various Images to Temperature Profile

Luminous zone. - Direct photography, or direct observation, reveals the luminous zones of the flame. Flame velocity measurements from direct photographs (fig. IV-2(a)) are based on the zone of most intense illumination, which in the case of Bunsen flames is the bright inner cone, sometimes called the blue cone (see preceding sketch). Early workers in the combustion field (see reviews in refs. 8 and 9) presumed that the width of this luminous zone represented the distance between the initiation of combustion and its completion and that flame velocity measurements were properly based on the inner edge of this zone. It has since been established that the entire luminous zone (inner cone) lies at a temperature very near the maximum, or flame temperature, as represented by the region (4) adjacent to inflection point (3) in figure IV-1 (refs. 1, 10, and 11). Before reaching this zone of high heat release but small temperature gradient, the gases experience preheating that causes expansion and bending of the flow lines. As a result, a flame surface chosen at any point in the luminous zone is too large for flame velocity measurements, which are traditionally referred to the unburned gas flow.

Therefore, direct photographs, which are the easiest type to obtain provided the flame is sufficiently luminous, produce a surface larger than the cold gas surface and may indicate erroneously low flame velocities.

Schlieren image. - When schlieren photography (refs. 1, 4, 8, and 10 to 13) is used, a surface is found that has a temperature much nearer that of the unburned gas. The schlieren method also has the advantage of a sharply defined surface (fig. IV-2(b)) as compared with the less distinct inner edge of the luminous zone or the comparatively fuzzy outer edge of the shadow cast by the cone (fig. IV-2(c)). In the most common use of the schlieren method for flame velocity measurements, the flame is placed in the parallel-beam section of a z-type, two-mirror (or lens) schlieren system. A knife edge, placed at the focus of the second mirror, is advanced into the image of the finite light source so that it cuts out approximately half the light. The light passing the knife edge penetrates the objective lens of the camera, which brings the flame image into focus. The density gradients in the flame cause the light rays, which are parallel as they leave the first mirror, to be refracted. Light rays refracted in a direction perpendicular to the knife edge by a positive density gradient are bent away from the knife edge, and an increase in illumination at the corresponding point in the flame-image plane results. On the other hand, a negative density gradient results in decreased illumination. Thus, the brightest portion of the flame image corresponds

to the maximum optical density gradient, which for all practical purposes may be identified with the mass density gradient. Since the density ρ is inversely proportional to the absolute temperature T, it follows that

$$\frac{d\rho}{dx} \sim -\frac{1}{T^2}\frac{dT}{dx}$$

This expression shows that the maximum of the density gradient (flame cone edge given by schlieren image) does not coincide with the maximum of the temperature gradient represented by inflection point (3) in figure IV-1, but occurs at a considerably lower temperature represented by point (1).

Experimental verification of the applicability of the schlieren surface for measuring flame velocity, insofar as the bending of flow lines due to temperature is concerned, has been obtained in several ways. Broeze (ref. 11) investigated the temperature gradient near the schlieren boundary by introducing smoke into the unburned gas. Ammonium chloride, which decomposes at 320° C, and zinc oxide, which sublimes at 1800° C, were used. The ammonium chloride track disappeared about 1 millimeter before it reached the luminous zone in a butane-air flame at atmospheric pressure. The point of disappearance coincided with the edge of the schlieren image. The zinc oxide smoke showed a sharp drop in density about 0.1 millimeter beyond the schlieren edge. Thus, the temperature gradient is very steep in this vicinity. Lewis and von Elbe (ref. 8, p. 254) similarly found the preheat zone of a natural gas flame to be approximately 1 millimeter thick by using stannic chloride hydrate smoke, which disappears by dissociation of the hydrate beginning at about 83° C and reappears as stannic acid after passing the reaction zone. Klaukens and Wolfhard (ref. 1) studied the reaction zone of flat acetylene-air flames at low pressures using luminous and schlieren photographs and thermocouple traverses, with qualitatively similar results. For a flame at 15 millimeters of mercury, the maximum density gradient corresponded to a temperature of 200° C, whereas the maximum luminosity corresponded to a temperature near the maximum temperature. Reference 4, reporting studies of the tracks of stroboscopically illuminated particles of magnesium oxide, and reference 13 added further confirmation. The majority of investigators believe that schlieren photography gives the image best suited for flame velocity measurements.

Shadow image. - Shadow photography (fig. IV-2(c)) has been used considerably in recording flame velocity data. The optical setup for a shadow system is simpler than that for a schlieren system. In the simplest form, a point source of light is placed on one side of the flame and the film is placed on the other side. Shadow photographs are also obtained by the parallel-beam method, in which case the camera is focused on a plane between the flame and the second mirror (real shadow image of the flame).

Formerly, many investigators based their flame velocity measurements on the inside edge of the shadow cast by the cone, but it has since been demonstrated that the outside edge of the shadow should be used. In reference 14, calculations were made of refractions of parallel rays for a simple flame model in which the flame surface of the inner cone was considered as a discontinuity between the cold unburned gas and the hot burned gas within the outer mantle. Constant refractive indices of 1.0003 for the unburned gas and the external atmosphere and 1.00004 for the burned gas were assumed. The calculations showed that the flame deflected the rays in such a way that a caustic curve of high light intensity was formed. The distance of the caustic (represented by the sharp demarcation between black and white at the inner edge of the shadow in fig. IV-2(c)) from the flame axis decreased with increasing distance of the shadowgraph object plane from the flame in a manner similar to that observed experimentally; whereas, the outer edge of the shadow corresponded closely to the position

of the discontinuity in refractive index represented by the flame cone. Hence, flame velocities based on the inner edge of the shadow are erroneously high, but the error decreases as the distance between the flame and the shadow object plane decreases and approaches zero at zero distance.

Reference 14 states that the schlieren image of a flame is exactly coincident with the outer edge of the shadow cone obtained with parallel light; therefore, the two methods should give the same values for flame velocity. However, the outer edge of the shadow is not clearly defined, whereas the inner edge is very sharply defined. The desirability of using this sharply defined surface has led some investigators to take shadowgraphs at several distances from the flame and extrapolate back to zero distance (refs. 14 and 15), while others have computed correction factors for fixed positions (refs. 14 and 16).

In summary, it may be said that the schlieren image represents a surface near the start of the preheat zone, whereas the luminous zone represents a region in the reaction zone at temperatures just below the flame temperature.

FLAME VELOCITY

Methods of Measuring

Stationary flame or burner. - The first attempt to measure flame velocity was made by Bunsen (see ref. 17, p. 66), who determined the flow velocity through a burner at which the flame would just flash back, so that the flame velocity was equal to the flow velocity. This method is accurate only for the case of a flat flame, which in turn is obtained only when the stream velocity is constant over the burner-mouth cross section. Flat-flame burners have been developed (refs. 18 and 19) but can be used only for flame velocities less than 15 or 20 centimeters per second. Therefore, these burners are of little interest for most flame velocity studies, although the flat flame is ideal for studying flame structure, and the method may be useful in defining lean flammability limits.

The majority of the burner methods employ the inner flame cone (fig. IV-2) obtained above vertical tubes or convergent nozzles, which give a more nearly conical inner cone and give the same results as cylindrical tubes when comparable methods of measurement are used (refs. 4 and 10). Tubes employed in such studies are of the order of 1 centimeter in diameter and are more than 40 diameters in length to ensure laminar flow. It is generally found that the mean approach-stream velocity does not affect the results as long as the flow is laminar and that burner diameter has no effect until the quenching diameter is approached (e.g., refs. 8, p. 459, and 16 and 20; for contrary results, see ref. 21).

The methods of measurement of burner flames are variations or modifications of either the total-area method (ref. 22) or the angle method (ref. 23). In the former, an average flame velocity for the entire cone is obtained by dividing the volumetric flow rate of the unburned gas by the surface area of the cone:

$$U_F = \frac{V}{S_F} = \frac{U_{o,m}A_t}{S_F} \tag{1}$$

where

A_t cross-sectional area of tube, cm^2

S_F surface area of flame cone, cm^2

U_F flame velocity, cm/sec

$U_{o,m}$ space mean velocity of approach flow in tube, cm/sec

V volumetric flow rate of unburned gas, cm^3/sec

The area S_F is usually computed by assuming the flame cone to be a right cone. In the early studies, S_F was often computed from the height of the luminous cone h and the radius of either the burner tube or the actual flame base r_t by the equation

$$S_F = \pi r_t \sqrt{r_t^2 + h^2} \tag{2a}$$

One simple method of computing S_F avoids the necessity of choosing between the burner diameter and the actual flame diameter, which varies with both method of photography and approach-flow conditions (ref. 24):

$$S_F = \frac{\pi A_F l}{h} \tag{2b}$$

where

A_F area of projected image of flame measured by planimeter, cm^2

l length of curve that generates S_F when rotated about tube axis (corresponds to slant height of right cone), cm

When the assumption of a right conical shape becomes poor, graphical methods may be used (e.g., ref. 25).

In the angle method, a local flame velocity is computed from the local approach velocity U_o and the angle α between the direction of the approach flow and the burning surface:

$$U_F = U_o \sin \alpha \tag{3}$$

The approach velocity U_o is usually computed for a given position along the flame by assuming that the approach-velocity distribution follows the Poiseuille equation (ref. 8, p. 248)

$$U_o = \frac{2V(r_t^2 - r^2)}{\pi r_t^4} = \frac{2U_{o,m}(r_t^2 - r^2)}{r_t^2} \tag{4}$$

where

r radial distance from tube axis to flame surface, cm

r_t tube radius, cm

In some instances where convergent nozzles have been used, apparent flame velocities have been computed on the assumption that the approach velocity U_o was constant over

the entire cone and equal to $U_{o,m}$ (e.g., ref. 24). Such an assumption could result in significant errors, since local velocities over the central portion of a nozzle may be as much as 20 percent higher than $U_{o,m}$ because of the boundary-layer effect (ref. 16).

The chief advantage of burner methods is that the equipment is simple, flexible, relatively inexpensive, and is easily adapted for measurements at varying temperatures and pressures and with imposed flow disturbances (ref. 26). Burner methods have also been adapted for convenient use with normally liquid fuels (ref. 27). Furthermore, there are obvious advantages in having a readily observed stationary flame. One disadvantage of burner methods is that diffusional interchange with the surrounding atmosphere alters the fuel-oxidant ratio, so that the flame velocity observed may not represent the measured fuel-air ratio. Diffusion may also lead to instability, evidenced by a fluted or polyhedral flame (refs. 28 and 29). This instability might be remedied in some cases by using a split-flame (Smithells separator) burner, which allows the gases of the outer mantle to burn on an outer concentric tube (ref. 30); however, such a modification complicates the photography. Other problems result from the complex flame shape, which directly complicates the area method and indirectly affects the angle method.

The main objections to the area method are as follows:

(1) The flame velocity near the base of the cone is reduced by the quenching action of the burner rim, and the flame velocity in the region of the tip is increased by accelerated heat and active-particle transfer that results from the small radius of curvature. Hence, the average flame velocity may not be equal to the flame velocity for a plane flame.

(2) Some small amount of gas may escape through the dead space (fig. IV-2(a)) between the flame base and the burner rim, tending to make the measured U_F too large.

(3) The method makes the choice of the proper surface (inside visible, outside shadow, or schlieren) to be used for computation very important, particularly for small flames.

The errors due to (1) are minimized if the method is restricted to gas mixtures and flow rates that yield nearly conical flame shapes and to burner tube diameters above approximately 1 centimeter (refs. 10 and 20). The error due to (2) is probably small, as evidenced by the lack of a discernible separation between flame base and burner rim in most schlieren photographs. These errors may be reduced somewhat but not eliminated by using only a frustum area from the middle portion of the cone (ref. 8, p. 464). The volumetric flow passing through this portion of the flame is computed by assuming Poiseuille flow (eq. (4)) up to the chosen flame surface. The flame velocity is therefore computed by:

$$U_F = \frac{2U_{o,m}(r_2 - r_1)\left(1 - \frac{r_2^2 - r_1^2}{2r_t^2}\right)}{s} \tag{5}$$

where

r_1, r_2 radii of upper and lower bases of frustum, cm

s slant height of frustum, cm

The frustum-area method still requires the choice of the proper surface in order to eliminate flow-line bending due to temperature rise. In addition, since only a part of the cone is considered, it may be even more important to consider the redistribution of unburned gas flow due to the pressure field set up by the flame (refs. 8, p. 257, and 31 and 32). The volumetric flow computed by equation (4) does not correspond to the surface computed. Even disallowing the differences of (1) and (2), the result is different from that obtained if the total area is used. Further refinement may be made by using a rectangular burner in which the larger dimension is at least three times the smaller dimension, thus reducing the effect of flame curvature when the flame is viewed parallel to the larger dimension (ref. 33).

In the angle method, the bendings of the flow lines due to (1) the temperature rise and (2) the pressure field are again the main problems, whether the more common cylindrical tubes or rectangular tubes are used. The temperature-rise problem is again solved by choosing the proper surface corresponding to a low temperature. The pressure-field problem might be solved by using the particle-track method. The latter method is a good solution, provided that the approach-flow conditions are measured far enough upstream to avoid pressure-field effects and are then properly related to a point on the flame surface. Inertia effects connected with the particles must also be taken into account. Investigators who have used the particle-track method apparently did not take full advantage of its possibilities with respect to the pressure-field effects. Although reference 8 (pp. 254-257) presents photographs showing the bending of flow lines due to the pressure effect, dr and $U'_{o,m}$ were probably not measured far enough upstream when flame velocities were computed from the equation

$$U_F = U'_m \frac{dr}{dl} \tag{6}$$

where

dl length of flame boundary between flow lines, cm

dr distance between flow lines at a point far enough upstream to avoid distortion due to pressure, cm

U'_m mean velocity for stream tube bounded by the two flow lines considered, computed for Poiseuille flow at plane where dr is measured, cm/sec

In reference 4, the angle between the direction of the particle track ahead of the preheat zone and the surface of the luminous zone was determined at the point where the track intersects the luminous zone, but measurements probably were not made far enough upstream to determine the direction of the particle track.

A stationary flame method that is of interest by analogy to flames supported on a flame holder is the inverted flame or V-flame method (ref. 8, p. 268 and refs. 34 to 36). In this method, the flame burns above the end of an axially mounted wire in the form of an inverted cone or above a horizontal wire or rod over the tube port in the form of a two-dimensional V. An apparent flame velocity may be determined by measuring the flame angle near the flame holder and relating it to a local velocity within the tube at that distance from the axis (ref. 35 used eqs. (3) and (4)). The velocities obtained in such a manner are far from true flame velocities, because the flame thrust causes a strong outward deflection of the flow lines in the unconfined unburned gas approaching the flame. Better values for flame velocity could be determined from inverted-cone or V-flames by the particle-track methods described previously.

Gross (ref. 36) used the V-flame in connection with a stationary flame method that employs an entirely different approach. Flame pressures were measured by traverses of the flame front of a V-flame with a total-pressure tube connected to a micromanometer. Flame temperatures were measured with a platinum and platinum - 10-percent-rhodium thermocouple. Flame velocities were then computed by combining the equation for conservation of momentum across a plane, steady-state combustion wave

$$p_o - p_F = \rho_o U_F^2\left(\frac{\rho_o}{\rho_F} - 1\right) \tag{7}$$

and the total pressure for incompressible, inviscid flow

$$p_t = p + \left(\frac{\rho U^2}{2}\right) \tag{8}$$

to obtain the equation for flame velocity

$$U_F = \frac{\rho_F}{\rho_o - \rho_F}\sqrt{\frac{2}{\rho_o}\left[-\left(\frac{\rho_o}{\rho_F} - 1\right)\left(p_{tot,o} - p_o\right) - \frac{\rho_o}{\rho_F}\left(p_{tot,F} - p_{tot,o}\right)\right]} \tag{9}$$

where

p static pressure, dynes/cm^2

p_{tot} total (stagnation) pressure, dynes/cm^2

ρ density, g/cm^3

The disadvantages of the method arise from the effects of the total-pressure tube on the flow and the flame, the corrections that must be applied to total-pressure measurements at low velocities, and the difficulties in calibrating, operating, and maintaining an ultrasensitive pressure meter.

Others (refs. 8 and 37) have computed flame velocities from equation (7) by assuming p_F to be equal to the ambient pressure in the room. Vasilesco (ref. 37) points out, however, that p_F is in reality smaller than p_{am} and that corrections must be added to the measured value of $p_o - p_{am}$ (the correction may be several times the magnitude of the measured $p_o - p_{am}$). Thus, agreement between values computed from equation (2a) and from equation (7) for $p_F = p_{am}$ that were reported by von Elbe and Mentser for acetylene flames (ref. 8, p. 266) may be a fortuitous result of the choice of the method of equation (2a) for the calculation of flame velocities.

All things considered, the total-area method with schlieren photography is the most easily executed and reproduced burner method and is probably as accurate as the more complicated methods.

Transparent tube. - If a horizontal, transparent tube having an inside diameter greater than the quenching diameter and a length of the order of 1 meter is filled with a homogeneous combustible gas mixture, which is then ignited (preferably by another small flame) at one end of the tube, a flame will travel through the tube. By placing suitable orifices at both ends of the tube to reduce reflected pressure waves, a uniform linear flame movement over a good portion of the tube and a flame

of constant shape for that portion may be obtained (ref. 38). The linear velocity of uniform movement is determined either by timing the passage of the flame between two detectors such as photocells or ionization gaps or by photographing it with a rotating drum or movie camera. The flame velocity is calculated by a total-area method from the equation

$$U_F = (U_l - U_g)\, A_t/S_F \tag{10}$$

where

U_g velocity of unburned gas ahead of flame (determined by allowing gas pushed out of tube to blow a soap bubble, ref. 38), cm/sec

U_l linear velocity of uniform flame movement, cm/sec

The setup required for the tube method is simple and inexpensive, with the possible exception of the timing devices; the method requires very small quantities of fuel compared with burner methods. The method is inferior to the burner method for absolute flame velocities because of the greater difficulty in determining S_F from the more complex flame shapes, which, partly because of the necessity of using direct photography, are rather arbitrarily defined. Wall effects are also unknown or difficult to ascertain. Since the measurements are made in a quiescent mixture in a transparent tube, the method is less readily adapted for measurements at pressures or temperatures other than room conditions than is the burner method.

The tube method shares with the bomb and soap-bubble methods the advantage that the flame is not exposed to an external atmosphere, and as a result determinations may be made over a slightly wider range of compositions (ref. 39). It is believed that relative flame velocities or trends indicated by the method are as good as those obtained by other methods when a consistent and reasonable means of determining S_F is used by a single investigator (provided that wall effects, particularly chemical effects, may be neglected). To this end, a simplified equation for determining S_F for the flames, which usually take the shape of semiellipsoids, was presented in reference 40:

$$S_F = \frac{2\pi(r_{cir}r_{ins} + r_{ins}r_t + r_{cir}r_t)}{3} \tag{11}$$

where

r_{cir} radius of circumscribed circle about projected flame image, cm

r_{ins} radius of inscribed circle, cm

Soap-bubble or constant-pressure bomb. - In the soap-bubble method (refs. 41 to 43), a homogeneous combustible mixture is used to blow a soap bubble around a pair of spark electrodes. The mixture is spark-ignited, and the growth of both the sphere of flame and the soap bubble is recorded by a rotating drum or movie camera. The flame velocity is calculated from

$$U_F = \frac{U_l}{\varepsilon} = \frac{U_l r_o^3}{r_{fin}^3} \tag{12}$$

where

r_{fin} final radius of sphere of burned gas, cm

r_o initial radius of soap bubble, cm

ε expansion ratio of gas mixture

The method is simple in principle and offers (ideally, at least) the desirable feature of a spherical flame shape. Since the final flame diameter is rather large (10 to 20 cm), the type of photography used to define the flame surface is less important than with burner or tube methods. On the other hand, the experimental difficulty in determining r_{fin} is considerable because of afterburning and the possibility of nonspherical flame growth due to (1) gravity effects when slow-burning mixtures such as paraffin hydrocarbon - air are used or (2) nonisotropic propagation (wrinkled surface) when very fast-burning mixtures such as hydrocarbon-oxygen are used (ref. 43). The spark-ignition system should be investigated to avoid effects of spatial velocity (ref. 43). Water soap bubbles cannot be used where water has an appreciable effect on the flame velocity; in this case special glycerin solutions may be used for the bubble (refs. 42 and 43). In either case, diffusion through the confining film and the effects of the components of the film on the burning process must be considered. A recent improvement of the method is the use of an inert atmosphere around the bubble to eliminate afterburning (ref. 42). The method may be used at various pressures by placing the soap-bubble equipment within a large pressure-controlled chamber.

Constant-volume bomb. - In the constant-volume bomb method (refs. 8, 44, and 45), the combustible mixture is ignited in the center of a rigid spherical vessel of the order of 30 centimeters in diameter. Photographs of the growing sphere of flame and one or more continuous pressure records are obtained simultaneously. As the flame progresses, the expansion of the burned gas causes both the pressure and temperature of the unburned gas to increase because of adiabatic compression. The temperature increase causes the flame velocity to increase continuously from the center toward the walls.

The flame velocity may be calculated by two methods. In the first, for any instantaneous flame diameter observed from the photographs, the volume occupied by the burned gas before combustion is calculated with the aid of the pressure record. The equation for U_F derived from the differential equation for adiabatic compression is (ref. 44)

$$U_F = \left(1 - \frac{r_b^3 - r_F^3}{3p\gamma r_F^2}\frac{dp}{dr_F}\right)\frac{dr_F}{dt} \tag{13}$$

p static pressure at time t, dynes/cm^2

r_b bomb radius, cm

r_F flame radius at time t from photograph, cm

γ ratio of specific heats in unburned gas at instantaneous conditions T and p

In this method, two differential quotients are required, and U_F is obtained as a difference of quantities of comparable magnitude, so that errors in these differential quotients and other data are magnified. A 10 to 15 percent scatter in data may result (ref. 8, p. 476).

The second method uses only the pressure record, from which r_F is calculated and may be compared with the observed r_F as a check:

$$U_F = \frac{dr_o}{dt}\left(\frac{r_o}{r_F}\right)^2\left(\frac{p_o}{p}\right)^{\frac{1}{\gamma}} \tag{14}$$

where

$$r_o = r_b\left(\frac{p - p_o}{p_e - p_o}\right)^{1/3} \tag{15}$$

and

$$r_F = r_b\left[1 - \left(\frac{p_o}{p}\right)^{\frac{1}{\gamma}}\left(\frac{p_e - p}{p_e - p_o}\right)\right]^{1/3} \tag{15a}$$

where

p_e final equilibrium pressure after gas has burned, dynes/cm^2

p_o initial static pressure before ignition, dynes/cm^2

Lewis and von Elbe (ref. 8, p. 499) present an example of a CO-O_2-H_2O flame for which the calculated r_F is consistently about 1 percent higher than that observed. They state that even this small difference is partially due to the error in observed r_F, which results from the use of direct photography to locate the flame front.

The experimental advantages of the bomb method are that it allows good control over the initial temperature, pressure, and humidity of the unburned gas and it requires only small amounts of gases. Its disadvantages are that the apparatus is complex, the calculations are lengthy and are dependent on very rapid, accurate pressure measurements, and the flame velocity varies continuously during a run. The spark gap width and energy must be properly matched to obtain spherical flames (ref. 45). While the pressure-record method largely eliminates errors due to convection currents for slow-moving flames, there is still difficulty with nonisotropic propagation with very fast flames or in mixtures that show diffusion instability (tendency of flame front to break into cells because of concentration gradients set up by preferential diffusion of the lighter components of the mixture).

The bomb method, using only the pressure record, may prove to be the most accurate method for determining flame velocities; as such it could be used to establish absolute values of flame velocities, which could in turn be used to appraise the accuracy of simpler burner methods.

Evaluation of methods. - Since there are large differences in flame velocities reported by various investigators for the same fuel-oxidant mixture at the same conditions (table IV-I), the engineer who wishes to compare data from various sources must use caution. For a given experimental method, particularly the various burner methods, measurements that are made from schlieren photographs are probably nearer the true flame velocity than measurements based on direct or shadow photographs. Of the methods for measuring flame velocity, the constant-volume bomb method (using the pressure record only) may prove to be most precise (~1 percent). In general, Bunsen burner methods are the simplest, cheapest, most versatile, and most productive. Of the various burner methods, the total-area method is probably the simplest, has a precision at least as good as the other methods, and has an accuracy comparable with most of them. The tube, soap-bubble, and bomb methods are particularly good under conditions where their disadvantageous characteristics are unimportant for very small quantities of gases. Unless otherwise stated, a precision of ±5 percent is about the average to be expected when a single method is used by a single investigator; this fact should be kept in mind when considering relative changes in flame velocities or comparisons for various fuels such as those given in the appendix.

Effects of Chemical Variables

In the present survey, flame velocities are reported as relative values referred to some standard fuel-oxidant mixture or condition. This is done in the belief that in many cases one investigator using a given experimental technique may correctly determine the trend or relative change in flame velocity as one particular variable is changed, even though some characteristic of his technique makes the absolute values questionable. Except when otherwise noted, a reference flame velocity of 100 is assigned the fuel-air mixture that has the composition for maximum flame velocity, an initial temperature of 25° C, and an initial pressure of 1 atmosphere.

Fuel-oxidant ratio. - As the fuel-oxidant ratio is increased, flame velocity passes through a maximum at an equivalence ratio φ (fuel-oxidant ratio divided by stoichiometric fuel-oxidant ratio) between 1.0 and 1.3, as shown by figures IV-3 to -5 and the appendix. The curve of flame velocity against equivalence ratio is more or less symmetrical about this maximum, for which the equivalence ratio will be called φ_{max}. This φ_{max} is somewhat a function of the method of measurement; the φ_{max} determined by the tube method is usually larger than that determined by the burner method (e.g., compare data from refs. 46 and 47). The value of φ_{max} tends to shift from slightly rich back toward stoichiometric as either the initial mixture temperature or the percentage of oxygen in the oxidant is increased (or diluent decreased) as shown by figures IV-4 (ref. 16) and IV-5 (ref. 48).

The flame velocity near the lean flammability limit ($\varphi \sim 0.5$ to 0.6) is of the order of 1/4 to 1/3 the maximum (refs. 18 and 39). Flame velocity determinations with hydrocarbons are limited on the rich side because the flame shapes become irregular or unusual with either open or confined flames (e.g., refs. 29 and 39; flame instabilities are discussed further in ch. VI).

It may be noted in figure IV-3 that the fractional change in flame velocity with equivalence ratio is the same for three fuels for equivalence ratios smaller than φ_{max}. If a logarithmic scale were used for φ, it would be seen that a linear relation between U_F and $\log \varphi$ exists for $\varphi < 1$:

$$U_F/U_{F,max} = 2.6 \log \varphi + 0.94 \tag{16}$$

An interesting variation of the preceding relation is the plot of the logarithm of the total bond dissociation energy of the fuel per unit volume of mixture against flame velocity illustrated by figure IV-6 (ref. 49). It may be seen that the correlations are linear for lean mixtures and that the lines extrapolate to the lean limit of flame propagation (zero flame velocity) in a 1-inch flame tube. The advantage in using the total bond dissociation energy rather than simply φ is that the maximum flame velocities of all three fuels may be estimated by extrapolating the linear portions of their curves to a common value of the total bond dissociation energy, 1.75 kilocalories per liter. However, both the slopes of the lines and the energy for $U_{F,max}$ depend somewhat on the method of measurement of U_F; the data presented were obtained by the tube method.

A correlation was also observed between the equivalence ratio for maximum flame velocity and the total bond dissociation energy of the fuel. Table IV-II (ref. 49) shows that, for the C_4 and C_6 hydrocarbons tested, the total bond dissociation energy per unit volume of the hydrocarbon-air mixture corresponding to the mixture giving the maximum flame velocity (tube method) is nearly constant, with an average deviation of only 0.9 percent from the average value. This deviation is less than 1/3 of that obtained by simply assuming that the maximum will occur at an average equivalence ratio of 1.15. It may be noted that the average total bond dissociation energy of 1.96 (kcal/liter) for φ_{max} is different from the 1.75 that gave maximum flame velocities from the linear extrapolation in figure IV-6, because the data in that figure began to deviate from the straight line before φ_{max} was reached.

An avenue of experimental study that may clarify the reaction kinetics of flames is the determination of flame velocities for fuel-oxygen-nitrogen systems in which the concentrations are varied in such a way that constant flame temperatures are maintained. If the effective mean reaction-zone temperature T_m is also constant and the reaction mechanism does not change with composition, the true effects of fuel and oxygen concentrations on flame velocity and hence on the over-all reaction rate might be expressed by

$$U_F^2 \propto f\left(\frac{dX_f}{dt}\right) \propto X_f^a X_{O_2}^b \tag{17}$$

where

a,b empirical exponents expressing reaction order of fuel and oxygen, respectively

X_f mole fraction of fuel in unburned gas

X_{O_2} mole fraction of oxygen in unburned gas

The exponent a is determined by studying mixtures for which $\varphi \geq 1$, and the exponent b is determined when $\varphi \leq 1$. In the former case, X_{O_2} is practically constant; whereas, in the latter case, X_f is practically constant.

In reference 50, flame velocities were determined at constant calculated adiabatic flame temperatures for hydrogen-, carbon monoxide-, and methane-oxygen-nitrogen systems. The empirical equation for H_2-O_2-N_2 for X_{O_2}/X_f between 0.8 and 8 at 2000° K is

$$U_F = 7650\ X_f^2\ X_{O_2} + 54 \tag{18}$$

This equation has the form of equation (17) except for the constant 54. An equation of a different form was reported for methane-oxygen-nitrogen for X_{O_2}/X_f between 0.3 and 0.7 at 2000° K:

$$U_F = 13.3\ \ln\left(\frac{X_{O_2}}{X_f}\right) + 14.9 \tag{19}$$

No empirical equations were reported for H_2-O_2-N_2 at 2250° K or for CO-O_2-N_2 at 2000° K.

Zeldovich (ref. 51) reports experiments with lean CO-O_2-N_2 mixtures in which the carbon monoxide concentration was held constant and the O_2-N_2 ratio was varied so that the flame temperatures were essentially constant. The flame velocity, and hence the reaction rate, was found to vary by less than a factor of 1.5 when X_{O_2} was varied from 0.20 to 0.72. Similar experiments with lean mixtures show that flame velocity is proportional to the square root of the carbon monoxide concentration in the reaction zone.

In summary, the flame velocity passes through a maximum $U_{F,max}$ at a fuel-oxidant ratio slightly richer than stoichiometric. For lean hydrocarbon-air mixtures, flame velocity and equivalence ratio may be related by an equation such as

$$\frac{U_F}{U_{F,max}} = 2.6 \log \varphi + 0.94 \tag{16}$$

The logarithm of the total bond dissociation energy of the fuel per unit volume of mixture was found to correlate both the flame velocities of lean mixtures of a given fuel with air and the equivalence ratios for maximum flame velocities of various fuels. Studies of the effects of fuel and oxygen concentration on flame velocity at constant flame temperature may be of importance in understanding flame reaction kinetics; to date, very little work has been done on this particular phase.

Molecular structure of hydrocarbon. - In references 38, 40, 46, and 52, a systematic study was made of the effect of molecular structure on maximum flame velocity using the improved tube method (eq. (10)) except for the higher-molecular-weight, normally liquid fuels, for which a schlieren image total-area (eq. (2b)) burner method was used. Figure IV-7 shows the effect of the number of carbon atoms in the straight chain for alkanes, alkenes, alkynes, alkadienes and allenes. The effect of methyl substitution on alkane, alkene, alkyne, and alkadiene molecules having four carbon atoms in the straight chain is shown in figure IV-8. In general, increased chain length or methyl substitution decreases flame velocity, except for the alkanes, which are not appreciably affected by either. These two figures also emphasize the effect of unsaturation: The flame velocity increases in the order alkanes < alkenes < alkadienes (for which isolated ≈ conjugated < cumulated double bonds) < alkynes.

The effects of cycloalkane ring size and of side-chain-substituent size in a given cycloalkane are shown in figure IV-9, and the effects of alkyl substitution

in a benzene ring are shown by data in the appendix. The fact that the three- and four-membered cycloalkanes have flame velocities greater than the corresponding alkanes, whereas the five- and six-membered rings have flame velocities near the corresponding alkanes, is in keeping with the general chemical behavior associated with ring compounds. Small, saturated rings generally exhibit some double-bond character, but large ones do not. Cyclopropane had a flame velocity 13 percent higher than its isomer, propene; and spiropentane (two three-membered rings joined together by one C-C bond) had a flame velocity (see appendix) 13 percent higher than the fastest isomeric pentadiene flame; this indicates that three-membered rings are somewhat more effective than double bonds. The addition of alkyl groups to aromatic rings showed no definite trend, sometimes reducing flame velocity, sometimes not affecting it.

Some effects of type of oxygen linkage in oxygen-containing compounds are also suggested, but not well established, by data in the appendix. It appears that flame velocity increases with the type of linkage in the order esters < ethers < alcohols < aldehydes and ketones < alkyl oxides. This suggested order is based primarily on data from reference 52, with the position of alcohols and esters suggested by the data of reference 47. Other measurements from reference 47 are in conflict with the suggested order. The measurements were based on the inner edge of the shadow cast by the Bunsen cone, using only the upper part of the cone. In general, the agreement between relative values given by references 40 and 47 is good, as shown by figure IV-10. The maximum flame velocities determined for fuels other than those of references 38, 40, 46, and 52 have been put on a relative basis and are included in the appendix.

In reference 53, an empirical correlation is obtained in which the maximum flame velocity of a hydrocarbon burning with air is calculated from the sum of the contributions of the various H-C bonds in the fuel molecule according to

$$U_F = N_A K_A + N_B K_B + N_C K_C + \ldots \tag{20}$$

where N_A, N_B, N_C, N_D, N_E, N_F, N_G, and N_H are the numbers of methane, primary, secondary, tertiary, alkene, alkyne, cyclohexyl, and aromatic C-H bonds, respectively, per unit volume of hydrocarbon-air mixtures; and K_A, K_B, K_C, . . . are the flame velocity coefficients of these bonds. For the special cases of C-H bonds on carbon atoms placed alpha to (next to) the alkyne C≡C bond, a factor equal to 0.96 was introduced into terms representing these alpha bonds. Flame velocity coefficients established from 34 hydrocarbons gave an average deviation in predicted flame velocity of 1.9 percent. In the evaluation of these coefficients, ethene was excluded, since its coefficient deviated by more than 5 times the average. These coefficients, based on an experimental reference flame velocity of 100 for propane, are given in table IV-III. Inasmuch as the coefficients are averaged for 34 hydrocarbons, the computed value for propane is 97.7 compared with the experimental reference velocity of 100.

The general effects of molecular structure may be summarized as follows: Increased straight-chain length, chain branching, side-chain substitution, or ring size of cycloalkanes (except for cyclopropane-cyclobutane reversal) tends to decrease flame velocity; whereas unsaturation tends to increase flame velocity; all these effects become smaller as the size of the molecule is increased. The flame velocities of oxygen-containing compounds are believed to follow the order esters < ethers < alcohols < aldehydes and ketones < alkyl oxides.

Additives, antiknocks, and fuel blending. - Reference 54 reports the effects on flame velocity of small additions (<3 percent) of other fuels to rich city gas - air mixtures. The compounds studied as additives (acetone, acetaldehyde, benzaldehyde, diethyl ether, benzene, and carbon disulfide) were chosen from those which

displayed oxidation phenomena in low-temperature oxidation and hence were expected to decrease the induction period and increase flame velocity. Despite apparent differences in oxidation properties, all compounds changed the flame velocity (luminous-cone total-area method, using skirted burner) in exactly the same way that dilution with excess fuel would, on the basis of oxygen requirement. There was no phenomenon equivalent to the effect of aldehyde on reaction rate in the low-temperature oxidation of hydrocarbons.

In propane-air-additive (isooctane, benzene, acetone, methylethyl ketone, carbon monoxide, acetaldehyde, diethyl ether, oxygen, hydrogen, and nitrogen) mixtures, however, reference 55 states that the small but distinct changes in flame velocity were not strictly additive. Additive concentrations amounting to 5 to 30 percent of the total fuel were used; in many cases, the flame velocity of the binary mixture was greater than that of either component. The reference also states that the change in theoretical flame temperature does not sufficiently explain the results, but that a near-linear correlation with $(6.5X_H + X_{OH} + X_O)_F$ was obtained.

Studies with moist carbon monoxide (ref. 8, p. 463, and ref. 17, p. 121) show that its flame velocity is raised appreciably by the addition of small amounts of hydrogen or hydrogen-containing fuels (or water vapor, see later discussion). For example, the replacement of 1.5 percent of the carbon monoxide by hydrogen raised the flame velocity of a moist carbon monoxide - air flame by 40 percent or a moist carbon monoxide - oxygen flame by 45 percent; in both cases, this increase was considerably greater than that expected by a simple mixing rule. Even fuels with flame velocities smaller than the moist carbon monoxide caused a marked increase; for example, 1 percent of hexane increased the flame velocity 29.5 percent. On the other hand, carbon disulfide, which contains no hydrogen, had the opposite effect.

It might be expected that common antiknock additives would especially decrease flame velocity, but such is not the case in constant-pressure combustion. Tetraethyl lead had no effect on the flame velocities (measured approximately by a ballistic impulse meter) of isooctane-air mixtures at temperatures up to 500° C, or on n-butane up to 300° C (ref. 56). Above 300° C, the flame velocity of n-butane was markedly diminished by preflame oxidation, which in turn was suppressed by the addition of tetraethyl lead. The conclusion was that the antiknock effect of tetraethyl lead must not be ascribed to a decreased flame velocity. However, in an internal combustion engine it is believed (ref. 57) that, toward the end of the piston travel when the pressure is rising rapidly, the inhibiting effect of tetraethyl lead is very great. The addition of 0.36 percent tetraethyl lead or 5 percent ethyl nitrate had no effect on the flame velocities (cone height, burner method) of 20 fuels of various types at room temperature (ref. 58). Likewise, iron pentacarbonyl did not appreciably decrease the flame velocities of ether - carbon monoxide flames (ref. 17, p. 122).

When two fuels A and B are blended in various proportions, the maximum flame velocity of the blend is generally greater than that which would be computed from the maximum flame velocities of the individual fuels by a simple mixing rule:

$$U_{F,blend} = X_A U_{F,A} + X_B U_{F,B} \tag{21}$$

where X_A and X_B are the mole fractions of A and B in the fuel blend. Reference 59 found that flame velocities of various binary mixtures of any two of the fuels methane, ethene, acetylene, carbon monoxide, and hydrogen were greater than those obtained by the simple mixing rule. As an example, figure IV-11 for hydrogen plus carbon monoxide is presented. In reference 60, a similar result was found for propane plus carbon monoxide; the maximum flame velocity occurred with a fuel mixture of 96 percent dry carbon monoxide and 4 percent propane (35 percent total fuel mixed with air) and was 63 percent greater than the value obtained from equation (21).

For the correlation of flame velocities of mixed fuels, reference 61 presents an equation which is simplified in reference 62 to the form

$$\sum_j \frac{X_{f,j}}{X'_{f,j}} = 1 \quad (j = 1,2,3, \ldots n) \tag{22}$$

where

$X_{f,j}$ mole fraction of jth fuel in multifuel mixture with air that has flame velocity U_F

$X'_{f,j}$ mole fraction of jth fuel in its binary mixture with air that has same flame velocity U_F as multifuel mixture

Thus, for a mixture of two fuels and air, a plot of $(X_{f,1}/X'_{f,1})$ against $(X_{f,2}/X'_{f,2})$ should give a straight line with intercepts (1,0) and (0,1). Reference 62 presents studies of ternary mixtures of propane, air, and either ethene or hydrogen sulfide. Equation (22) was found to be valid for propane plus ethene but invalid for propane plus hydrogen sulfide, as shown by figure IV-12. According to reference 62, the data represented by figure IV-12 show that hydrogen sulfide is an effective flame velocity inhibitor; such a statement is misleading, since the addition of similar quantities of nitrogen to propane-air mixtures causes comparable decreases in flame velocity, as can be computed from the data of reference 48.

Water vapor: The pronounced promoting effect of water vapor on the flame velocity of carbon monoxide has been observed by many investigators. For 45 percent carbon monoxide in air, the flame velocity passes through a maximum after approximately 5 volume percent water has been added, at which point the flame velocity is 2.1 times the value for 0.7 percent water (ref. 17, p. 121, and ref. 63). Heavy water (deuterium oxide) increases the flame velocity of carbon monoxide by a smaller amount than the same percentage of ordinary water (ref. 64). This effect is discussed later in connection with studies of deuterated acetylene.

With hydrocarbons, water vapor has a slight inhibiting effect; for a butane-air mixture containing 2.8 volume percent water, the flame velocity is approximately 8 to 10 percent lower than that for a similar mixture containing 0.08 percent water (ref. 65).

Inert diluents: A decrease in the percentage of nitrogen in the primary air with which a fuel burns causes a marked increase in flame velocity for a given equivalence ratio. For example, the effect of increasing the molar ratio $O_2/(O_2 + N_2)$, hereinafter called ψ, is shown in figure IV-5 from reference 48. Reference 66 reports that, for flame velocities of propane-, ethene-, and isooctane-oxygen-nitrogen mixtures measured by a schlieren total-area method, the maximum flame velocity is a linear function of ψ for the ranges studied. These data are presented in figure IV-13. Additional data on maximum flame velocities of fuel-oxygen-nitrogen systems are reported in references 8 (pp. 460-467), and 43, and are plotted in figure IV-14 as relative flame velocity, referred to the value with air for which $\psi = 0.21$, against ψ.

Figure IV-14 shows that the relative flame velocity of hydrocarbon-oxygen-nitrogen mixtures continues to increase markedly as ψ is increased to 1.0, but that there is some tendency for the rate of increase to diminish in the region $\psi = 0.5$ to 1.0. The effect appears to decrease as chain length or unsaturation of the hydrocarbon increases. The effect of ψ on U_F is apparently much smaller for hydrogen or carbon monoxide flames. On the assumption that a linear relation between $U_{F,rel}$

and ψ should be obtained for a limited range of ψ in the vicinity of 0.21, which is the region most likely to be of interest for air-breathing engines that might be subject to local oxygen enrichment or vitiation, empirical equations of the form

$$U_{F,rel} = B(\psi - C) \tag{23}$$

have been computed where possible. These are summarized in table IV-IV, in which are also included equations of the form

$$U_{F,rel} = B'T_o^b(\psi - C_{av}) \tag{24}$$

for propane-, ethene-, and isooctane-oxygen-nitrogen mixtures from reference 66.

The effect of changing the diluent from nitrogen to an equal volume of another inert gas is of interest in that the variations in specific heats (and hence flame temperatures), thermal conductivities, and diffusion coefficients of the diluents allow somewhat more critical tests of the various approximate theoretical equations for flame velocity (table IV-V). Table IV-VI shows maximum flame velocities, relative to an arbitrary value of 100 with nitrogen as the inert gas, for several fuels burning with primary air in which the nitrogen has been replaced by an equal volume of argon, helium, or carbon dioxide (refs. 8, 17, and 67 to 72). In all cases the flame velocity increases as the diluent is changed from carbon dioxide to nitrogen to argon to helium. As the ratio $O_2/(O_2 + \text{inert})$ increases, the effect of changing the diluent is smaller, because the common value of 100 for $O_2/(O_2 + \text{inert}) = 1$ is approached.

Effects of Physical Variables

Pressure. - From the contradictory data reported in the literature, it appears that the accurate measurement of the pressure dependence of flame velocity is very difficult and that at present all reported pressure effects must be questioned. Some recent measurements (table IV-VII, from ref. 73) indicate that the flame velocities of stoichiometric methane-, propane-, and ethene-air mixtures are independent of pressure, whether measured by the constant-volume bomb method or the slot-burner (luminous) method. References 74 and 75 report the flame velocities of acetylene burning with oxygen, oxygen and argon, or air (pressures > 10 mm Hg) and of propane and air (pressure > 20 mm Hg) to be independent of pressure. The flame velocities were measured by a luminous-cone angle method, and the burner diameter was increased in proportion to the pressure decrease. Reference 76 confirms the independence of flame velocity of pressure using the soap-bubble method. It is believed (ref. 76) that earlier results obtained by a burner method, which showed a pressure effect, were probably less reliable.

On the other hand, reference 77 reports that, even though the burner diameters were varied, there was a pressure effect such that the flame velocities of propane-air and ethene-air mixtures were inversely proportional to the logarithm of pressure in the range 1/3 to 1 atmosphere. The propane-air curves of reference 77 are reproduced in figure IV-15 and, for various tube diameters, approach a common upper envelope.

Many other investigators also report pressure effects. In general, the majority find flame velocity to be inversely proportional to pressure raised to a power between 0.1 and 0.5. The pressure dependences indicated by some of the more recent studies (refs. 19 and 73 to 81) are summarized in table IV-VIII. However, until the effect of apparatus on the measurement of the pressure dependence of flame velocity is more clearly resolved, it is assumed that flame velocity is independent of pressure in the range of interest for jet-engine combustion chambers.

Temperature. - The initial temperature of the unburned gas mixture has an appreciable effect on flame velocity. As an example, data for propane-air obtained by a shadowgraph total-area method are presented in figure IV-4. The relative effects of initial temperature on the maximum flame velocity of methane-, propane-, and ethene-air flames are shown in figure IV-16. References 16, 37, 52, 54, 66, and 82 to 89 present extensive studies of the temperature effect. A summary of these effects is given in table IV-IX. The only references that are purposely omitted from table IV-IX are those covering too small a temperature range to be significant, investigating nonhydrocarbon fuels not likely to be of interest, or containing results that are questionable or contradictory to the more extensive studies. Where possible, an empirical equation of the form

$$U_{F,rel} = B + CT_o^b \tag{25}$$

is given. The relative flame velocities computed from these equations are referred to an arbitrary value of 100 at 25° C. The flame velocity is a function of T_o raised to a power between 1.4 and 2.1; the exponent varies with the temperature range covered and with the fuel. Since propane is a fairly representative paraffin hydrocarbon, most blends containing a preponderance of paraffin hydrocarbons would be reasonably well represented by the equation

$$U_{F,rel} = 25 + 0.00085\ T_o^2 \tag{26}$$

for the temperature range 200° to 615° K. For the smaller temperature range 290° to 420° K (or 520° to 760° R), it might be assumed that $U_F \propto T_o^{1.4}$. Alternatively, the percentage change of maximum flame velocity could be determined from the propane curve (fig. IV-16).

A method of empirical prediction for ethene, as well as methane and propane, and hence useful for both paraffinic and olefinic fuels, is demonstrated in reference 16. A very good linear correlation between computed adiabatic equilibrium hydrogen atom concentration p_H and flame velocity exists for each of the three fuels. These correlations indicate that, if for any similar fuel, maximum flame velocities are known for any two initial temperatures, the maximum flame velocity at any other temperature can be computed. The equations for temperatures from 200° to 615° K for methane, propane, and ethene, respectively, are

$$U_{F,rel} = 2.91\times10^5\ p_H - 50 \tag{27}$$

$$U_{F,rel} = 2.89\times10^5\ p_H - 75 \tag{28}$$

$$U_{F,rel} = 1.33\times10^5\ p_H - 97 \tag{29}$$

Electric fields. - Laminar flame velocity does not seem to be affected by electric fields. In reference 90, longitudinal direct- and alternating-current fields were applied to propane-air flames. The potential was applied between the burner rim and a spherical electrode placed in the burned gas near the flame. The direct-current field (4000 v) caused a 5 percent decrease in the surface area of the luminous cone. The simple periodic disturbances of the flame surface caused by the alternating-current field (0 to 6000 v at 400 cps) had no detectable effect on the total surface area. The surface area, and hence the flame velocity, was independent of the amplitude and phase of the disturbance.

Reference 91 presents measured velocities of burner flames of butane and air in transverse electric fields (electrodes on either side of the flame; 0 to 15,000 v potential). The flame cone was deflected toward the negative electrode. Local flame velocities were computed from the particle-track method of equation (6): it was found that the flame velocity increased on the side of the cone near the positive electrode and decreased on the negative side by as much as 50 percent of the original value. The average flame velocity (total-area method) was probably not changed appreciably. The observed variations in local flame velocity were in the direction to be expected if positive ions played an active role in flame propagation.

Acoustical and mechanical disturbances. - The effect of sound on propane-air burner flames was also studied in reference 90. No change in flame surface area, and hence no change in flame velocity, was observed. Reference 92 likewise reports no effect of sound (12.7 kc and known intensity) on the surface area of propane-air flames. In reference 25, however, flame velocity was increased by 7 or 8 percent, and sound of medium intensity was most effective.

Reference 93 reports investigation of vibrating flames of methane, city gas, propane, or ethene that traveled through transparent tubes of various lengths and diameters against gas velocities slightly smaller than the flame velocities. With carefully selected compositions and flow rates, flames were obtained that, after traveling partway down the tube, became saucer-shaped so that they were flat over the major portion of the cross section. Consideration of (1) the circulation of unburned gas ahead of the flame indicated by the curling and uncurling of the flame edges toward the unburned gas, (2) the lack of vibration at the point where coupling of an oscillatory heat source and a vibrating gas column should have been optimum, and (3) photographic evidence that waves in the unburned gas receded from the flame front at an essentially constant rate, led to the conclusion that variations in flame velocity were small.

Reference 26 states that disadvantages in the methods used in generating electrical and acoustical disturbances in reference 90 were (1) no allowance for a measurement of the initial amplitude of the flow disturbance introduced into the flame, and (2) complication of acoustical disturbances by resonance effects. A mechanical disturbance, which could be applied locally to the flame and the amplitude of which could be measured accurately, was obtained with a wire that touched the flame and vibrated perpendicular to the flame front surface. The resulting distortion of the flame surface was similar to that obtained with the alternating-current field or the sound. The surface area of the periodically disturbed flames, and hence the flame velocity, was unaffected.

THEORIES OF LAMINAR FLAME PROPAGATION

The phenomenon of laminar flame propagation can be described by the use of the basic equations of fluid dynamics, modified to account for the liberation and conduction of heat and for changes in chemical species within the reaction zone. (An excellent review of the theoretical concepts of laminar flame propagation as of 1951 is given by ref. 8, pp. 337-351; see also ref. 9.) The formulation of the problem requires equations of continuity for each chemical component, of state, and of conservation of energy, momentum, and total mass. In order to solve these equations for a unique flame velocity (eigen value), the following simplifying assumptions are made:

(1) The flame is one-dimensional.

(2) The flame is steady with respect to time.

(3) Velocity gradients may be neglected; hence, viscosity terms in the momentum and energy equations may be ignored.

(4) Pressure is essentially constant across the flame front, so that the equation for conservation of momentum may be ignored.

(5) The effect of gravity is negligible.

(6) The loss of energy by radiation is negligible.

In order to solve the mass and energy equations, boundary conditions must be selected. The hot boundary for the flame reaction zone is assumed to be the condition of thermodynamic equilibrium at the adiabatic flame temperature $T = T_F$ at $x = x_\infty$. The selection of a cold boundary with respect to the chemical reaction involved in these equations requires some justification, because the reaction rate never falls to zero if it follows an Arrhenius type relation

$$\omega \propto \exp(-E/RT) \tag{30}$$

where

E activation energy, cal/mole

R universal gas constant, 1.987 cal/(°K)(mole)

ω reaction rate, (molecules of reactant)/(cm^3)(sec)

However, some reasonable approximation for a cold-boundary condition must be found. The choice of this cold-boundary condition is intimately related to the question of whether or not a unique flame velocity exists in an essentially adiabatic system.

Consider a tube of infinite extent, adiabatically isolated from the surroundings and without heat-absorbing walls, filled with combustible mixture as follows:

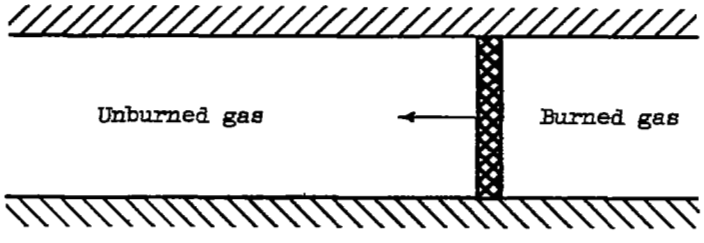

A flat flame is shown moving into the unburned gas. Since the pipe is of infinite length, the unburned gas far from the flame will be changing in composition and temperature because of the finite (albeit extremely slow) rate of exothermic reaction, even at T_o. Only if the increase in temperature and change in composition exactly compensate with respect to flame velocity effects would a constant flame velocity be possible. Zeldovich (ref. 51) has shown, and it may be seen by comparison of the effect of initial temperature with the effect of dilution on flame velocity (see previous data sections), that such compensation does not occur for carbon monoxide flames. This suggests that in an infinite, adiabatic system a unique flame velocity

does not exist. However, the reactions at T_o are very slow, and there is, therefore, a very long period of flame travel before a measurable change in flame velocity would occur. If the equations for flame propagation including a time dependence were set up and solved for short periods of time, the ignition temperature as a boundary condition should not be required. If a steady state is assumed, as is usually done, an ignition temperature is required in the infinite system.

Suppose, however, that there is a mixing chamber a short distance from the flame, as follows:

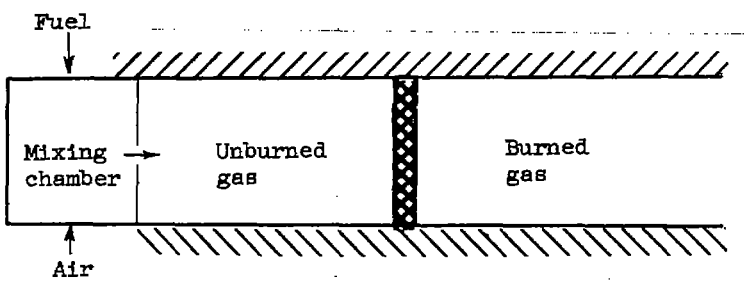

The problem of slow reaction at an infinite time is thus eliminated, but the presence of the mixing chamber in the neighborhood of (even several meters from) the flame means that a small but finite transfer of heat to the mixing chamber and a small but finite back-diffusion of products must occur. Hirschfelder (ref. 94), whose comprehensive equations are presented hereinafter, has indicated that the temperature drop to the mixing chamber need only be 10^{-6} °K but that the heat transfer is required to describe a steady-state flame with a unique flame velocity. This kind of cold-boundary condition closely approximates the conditions under which experimental observations are made, and accounts, at least in part, for the apparent existence of a steady-state flame when theoretically such a flame does not exist.

When the temperature profile for a laminar flame (fig. IV-1) was discussed, it was pointed out that there is a temperature T_3 at which the chemical reaction becomes appreciable to the extent that a mass element of gas changes from a heat sink to a heat source. As will be shown in the following sections, most of the simplified equations for flame velocity are obtained by assuming the temperature T_3 to be the cold boundary for the reaction zone. With this assumption, the energy equation can be integrated for the preheat zone (T_o to T_3) and the reaction zone (T_3 to T_F) and solved for flame velocity by equating the two integrals at the T_3 boundary, where dT/dx must be the same for both zones.

Comprehensive Equations

The following equations are formulated in reference 95 to describe the steady-state, one-dimensional flame:

Continuity equations:

For each component:

$$\frac{d}{dx}\left[\frac{n_i(U + U_{d,i})}{N_c}\right] = I_i \quad (i = 1,2,3, \ldots j) \tag{31}$$

For the total:

$$\left(\sum_i \frac{n_i M_i}{N_c}\right) U = \rho U = \rho_o U_F = G = \text{constant} \tag{32}$$

Energy equation:

$$\frac{d}{dx}\left(\varkappa \frac{dT}{dx}\right) - \frac{d}{dx}\left[\sum_i \frac{n_i M_i H_i (U + U_{d,i})}{N_c}\right] = 0 \tag{33}$$

Equation of state:

$$n = \sum_i n_i = N_c p/RT \tag{34}$$

where

G mass-flow rate, $g/(cm^2)(sec)$

H_i enthalpy of ith species, cal/g

I_i rate of production by chemical reaction of ith species, g-mole/(cm^3)(sec)

N_c Avogadro number, 6.025×10^{23}, molecules/g-mole

n total concentration, molecules/cm^3

$\varkappa$ thermal conductivity, cal/(cm^2)(sec)(^oK/cm)

It is assumed that the cold boundary is terminated by a flame holder that has two properties; it prevents back-diffusion of product molecules into the gases outside the cold boundary of the flame front, and it extracts an amount of heat q_o from the flame:

$$q_o = -\varkappa\left(\frac{dT}{dx}\right)_o \tag{35}$$

Since equations (31) to (33) are formulated in terms of individual chemical species, it is necessary to identify each chemical species occurring during the combustion reaction and to know the enthalpy, molecular weight, and other properties of the species. It is also necessary to know the specific rates of chemical production for a sufficient number of species so that the rest may be calculated from the chemical equations relating the various species. In order to determine these chemical kinetic factors, the scheme of reaction occurring in the flame and the rate constants for each independent step in the scheme must be established. But this information is completely lacking for hydrocarbon-air flames; indeed, few homogeneous, low-temperature chemical reactions have been incontrovertibly established. The comprehensive equations of Hirschfelder and Curtiss have been solved by approximate methods for only a few of the simplest flames - for example, the azomethane (ref. 95) and ethylene oxide (ref. 7) decomposition flames and the ozone flame (ref. 94).

Although the comprehensive theory of laminar flames is necessary for an understanding of flame propagation, it is currently impossible to use it to predict flame

velocities of hydrocarbons or the effects of changes in experimental variables without making further simplifying assumptions. It is desirable to develop simpler equations for these purposes, even if some of the theoretical exactness is lost. Some of the approximate equations, which usually emphasize only one process of the total mechanism such as the heat-conduction process or the active-particle diffusion process, have proven quite satisfactory for the prediction of flame velocity.

Approximate Equations

Thermal mechanism. - Both the early flame velocity equations of Mallard and LeChatellier, Nusselt, Jouguet and Crussard, Daniell, and Damköhler and the equations more recently reported by Bechert, Bartholomé and Emmons, Harr, and Strong are based on thermal concepts (ref. 9). The original, frequently quoted Mallard-LeChatelier equation was obtained simply by equating the sensible heat gain in the preheat zone to the heat conducted from the reaction zone at the T_3 boundary:

$$\bar{c}_p(\rho_o U_F)(T_3 - T_o) = \varkappa\left(\frac{dT}{dx}\right)_3 \tag{36}$$

where it was assumed that

$$\left(\frac{dT}{dx}\right)_3 \approx \frac{T_F - T_3}{x_F - x_3} \tag{37}$$

hence,

$$U_F = \frac{\varkappa}{\bar{c}_p\rho_o(x_F - x_3)}\,\frac{T_F - T_3}{T_3 - T_o} \tag{38}$$

where

$\bar{c}_p$ mean specific heat from T_o to T_3, cal/(g)(°K)

Assumption (37) regards the T,x curve as linear in the reaction zone with a slope equal to that at x_3 as determined by approaching x_3 through the preheat zone. It involves the chemical reaction rate only indirectly through the reaction zone thickness $(x_F - x_3)$. All authors since Mallard and LeChatelier have included some consideration of the reaction rate. The early equations included an ignition temperature; however, it is not easy to determine the proper ignition temperature to use in such equations (see previous discussion of T_3 and fig. IV-1).

Zeldovich and Frank-Kamenetsky have derived an equation for flame velocity for which the beginning basic equations were quite comprehensive. In its final simplified and approximate form, it includes diffusion of molecules but not free radicals and atoms. As a result, it emphasizes the thermal mechanism. Semenov (ref. 96) has presented the derivation of this equation in detail. Because this equation, hereinafter called the Semenov equation, has been widely used in the correlation of experimental flame velocities of hydrocarbons, its derivation is discussed briefly.

In the Semenov derivation, an ignition temperature is used only as a mathematical device for approximate computation. Semenov assumes that this ignition temperature,

above which nearly all the reaction occurs, is near the flame temperature, because the chemical reaction rate is an exponential function of the temperature according to equation (30). By approximations, the ignition temperature is entirely eliminated from the final equation, thus making the equation more useful than the previous ones. The following assumptions, in addition to that regarding ignition temperature and those stated heretofore for the comprehensive theory, are used:

(1) Diffusion is important only as it affects energy balance.

(2) Flame velocity may be described in terms of an over-all chemical reaction; equations are set up in terms of zero-order, first-order (monomolecular), or second-order (bimolecular) reactions.

(3) Specific heat c_p and thermal conductivity $\varkappa$ are constant.

(4) Thermal diffusivity $\varkappa/c_p\rho$ is equal to molecular diffusivity D.

(5) Total number of molecules is constant.

The basic equations, which may be compared with the corresponding exact equations (32) to (34), are as follows:

Continuity equation:

$$D\rho \frac{d^2n'}{dx^2} - G \frac{dn'}{dx} + \omega = 0 \tag{32a}$$

$$n' = (n_{r,o}\rho_o) - (n_r/\rho)$$

Energy equation:

$$\frac{\varkappa}{c_p} \frac{d^2T}{dx^2} - G \frac{dT}{dx} + \omega \frac{Q}{c_p} = 0 \tag{33a}$$

$$G = \rho U = \rho_o U_F$$

Equation of state:

$$\frac{\rho}{\rho_o} = \frac{T_o}{T} \tag{34a}$$

where

D diffusion coefficient, cm^2/sec

n_r concentration of reactant, $molecules/cm^3$

Q heat of reaction, cal/molecule of reactant

The energy equation consists of three terms, the first representing the heat gained by a mass element through conduction from a hotter element downstream, the

second the loss of heat through mass transfer, and the third the heat evolved by the chemical reaction. In the preheat zone x_o to x_3, it is assumed that no chemical reaction occurs; and in the reaction zone x_3 to x_F, it is assumed that the net energy loss due to mass transfer may be neglected in comparison with the chemical reaction and heat conduction terms. With these assumptions, the equation is solved for U_F by integrating over the preheat and reaction zones separately and establishing the condition of continuity by equating dT/dx at $x = x_3$ for the two zones. The result is

$$U_F = \sqrt{\frac{2\varkappa}{n_{r,o}\rho_o\bar{c}_p(T_F - T_o)} \int_0^{T_F} \omega \, dT} \tag{39}$$

In order to evaluate the reaction-rate integral in equation (39), an Arrhenius-type temperature relation is assumed. It is generally assumed that the over-all reaction is bimolecular and second-order with respect to fuel and oxygen. Following the Semenov derivation, the rate integral is evaluated as follows:

$$\int_0^{T_F} \omega \, dT = \int_0^{T_F} n_f n_{O_2} PZ \exp(-E/RT) \tag{40a}$$

$$\approx n_{f,eff} \, n_{O_2,eff} \, PZ \frac{RT_F^2}{E} \exp(-E/RT_F) \tag{40b}$$

where

n_f fuel concentration, molecules/cm^3

$n_{f,eff}$ effective mean fuel concentration in reaction zone, molecules/cm^3

n_{O_2} oxygen concentration, molecules/cm^3

$n_{O_2,eff}$ effective mean oxygen concentration in reaction zone, molecules/cm^3

P steric factor

Z collision number; number of molecular collisions/(cm^3)(sec) when the concentration is one molecule of each type per cm^3

Semenov states that the approximation for the exponential term obtained from equations (40a) and (40b) is satisfactory for $RT_F/E \leq 0.1$.

Approximate solutions must be obtained for the effective concentration terms. The relation between concentration and temperature is first established for a zero-order reaction as follows: A new variable, $\theta = c_p(T - T_o)/Q$, is introduced into the energy equation to give

$$\frac{\varkappa}{c_p}\frac{d^2\theta}{dx^2} - G\frac{d\theta}{dx} + \omega = 0 \tag{41}$$

which is formally identical with the continuity equation (32a), because by assumption (4), $\varkappa/c_p = D\rho$. It can be shown that the boundary conditions of these equations coincide at x_o and x_F. If $n' = \theta$ for the entire interval, a relation between concentration and temperature is obtained:

$$c_pT + n_rQ = c_pT_o + n_{r,o}Q = c_pT_F \tag{42}$$

Equation (42) means that the sum of chemical and thermal energies is constant throughout the flame (a condition that holds only where assumption (4) is valid). Following the approximation technique used by Semenov, this relation is modified for $n_{f,eff}$ and $n_{O_2,eff}$ for the bimolecular reaction as follows:

For rich mixtures, $\varphi > 1$:

$$n_{f,eff} = n_{f,o}\frac{T_o}{T_f}\left(1 - \frac{1-\beta}{\varphi}\right);\ n_{O_2,eff} = n_{O_2,o}\frac{T_o}{T_F}\beta \tag{43}$$

For lean mixtures, $\varphi < 1$:

$$n_{f,eff} = n_{f,o}\frac{T_o}{T_F}\beta;\ n_{O_2,eff} = n_{O_2,o}\frac{T_o}{T_F}\left[1 - \varphi(1-\beta)\right] \tag{44}$$

where

$$\beta = \frac{RT_F^2}{E(T_F - T_o)} \tag{45}$$

and

$$n_{O_2,o} = \frac{n_{f,o}}{\varphi}\left(\frac{n_{f,o}}{n_{O_2,o}}\right)_{st} \tag{46}$$

where

$(n_{f,o}/n_{O_2,o})_{st}$ stoichiometric fuel-oxygen ratio

Corrections may now be applied to some of the assumptions as follows: Assumption (3) is corrected by the use of a mean value of $\varkappa/c_p$ for the preheat zone, and it is assumed that physical properties in the reaction zone may be represented by their values at T_F. For the bimolecular reaction, assumptions (4) and (5) are corrected by inserting the factors $(\varkappa/c_p\rho D)_F^2$ and m^2, respectively, under the square root sign; m is the ratio of moles of reactants to moles of products in the stoichiometric reaction. These correction factors and equations (34a), (40b), (43) or (44), and (45) are substituted into the flame velocity equation (39). After collecting terms, the resulting equation for rich mixtures is:

$$U_F = \frac{C\beta}{c_{p,F}D_F}\sqrt{\frac{2\varkappa_F^3 PZn_{f,o}\left(1 - \frac{1-\beta}{\varphi}\right)}{\rho_o^3 c_p \varphi(n_{f,o}/n_{O_2,o})_{st}}\exp\left(\frac{-E}{RT_F}\right)} \tag{47}$$

For lean mixtures, the term $\left[1 - (1 - \beta)/\varphi\right]$ is replaced by $\left[1 - \varphi(1 - \beta)\right]$, and for stoichiometric mixtures it becomes simply β.

All the factors in equation (47) except P and E can be estimated by extrapolation of thermodynamic tables (refs. 97 and 98) and by use of the following equations:

$$c_p = \sum_i c_{p,i}X_i \tag{48}$$

$$\varkappa = \left(c_p' + \frac{5}{4R}\right)\frac{\mu}{M} \tag{49}$$

$$D = 1.336\,\frac{\mu}{\rho} \tag{50}$$

$$Z = \left(\frac{\sigma_f + \sigma_{O_2}}{2}\right)\sqrt{8\pi\frac{R}{N_c}T\left(\frac{M_f + M_{O_2}}{M_f M_{O_2}}\right)} \tag{51}$$

where

c_p' molar heat capacity, cal/(g-mole)(°K)

μ viscosity, poises

σ collision diameter, cm

The values of μ for combustion-product mixtures were determined by the additive volume rule analogous to equation (47) and were within 1 percent of values calculated by the method of reference 99.

For lack of better knowledge, low-temperature activation energies reported in the literature for the appropriate hydrocarbon oxidation may be substituted for E. For example, the following activation energies (kcal/g-mole) were used for burning-velocity predictions in references 49 and 16: methane, 51 (ref. 100); propane, 38 (ref. 17); and ethene, 40 (ref. 101). In reference 49, the steric factor P was calculated from each experimental flame velocity. These values of P were then averaged to give $\overline{P}$ for the group of data under consideration. The ratio of predicted to experimental flame velocity was calculated as $(\overline{P}/P)^{1/2}$ for each point.

Figures IV-17 and -18 illustrate the agreement between experimental flame velocities and the relative values obtained by multiplying the experimental values by $(\overline{P}/P)^{1/2}$. The relative predictions are satisfactory for these three- to sevenfold increases in flame velocity that result from changes in initial temperature or O_2/N_2 ratio. The accuracies of these and other predictions for methane, ethene, and propane are indicated in table IV-X by the average percent deviation of $(\overline{P}/P)^{1/2}$ from unity for each of the data ranges studied.

Equation (46) may be further simplified for particular purposes by making additional assumptions. For example, in order to predict the effect of initial mixture temperature on flame velocity, the nontemperature-dependent terms may be eliminated to give (ref. 16)

$$U_F \propto \sqrt{T_o^2 T_F^{4.9} \exp(-E/RT_F)/(T_F - T_o)^3} \tag{52}$$

Here it is assumed that the physical properties of the combustion-zone mixture have essentially the same temperature dependences as the same properties have for air; these temperature dependences for air are estimated (ref. 102) as follows: $\kappa \propto T^{0.84}$; $c_p \propto T^{0.09}$; $n_{f,o} \propto \rho \propto T^{-1}$; and $D \propto \mu/\rho \propto T^{1.67}$. The temperature dependence of Z has been neglected; Semenov actually did not consider Z, and it does not greatly affect the results of equation (52). Relative flame velocities (ref. 49) predicted by equation (52) are almost as good as those obtained with the more tedious procedure of equation (47).

Thus, the Semenov equation, which is based primarily on a thermal mechanism but is more comprehensive than earlier thermal theory equations, gives satisfactory relative predictions for flame velocities as either the initial temperature or the ratio O_2/N_2 is varied over a wide range or equivalence ratio is varied over a narrower range (table IV-X).

Diffusional mechanism. - Several approximate equations for burning velocity have been derived in which the diffusion of atoms and free radicals has been considered of major importance. These equations are based to some degree on speculation, but they do follow from considerations of flame structure and the possible influence of a small concentration of reaction-chain initiators on the rate of the chemical reaction and subsequently on the process of flame propagation.

The reasoning for a diffusional mechanism begins with the assumption that potential oxidation chain carriers such as hydrogen and oxygen atoms and hydroxyl radicals are present in the flame front (zone of maximum temperature) in the thermodynamic equilibrium concentration for the flame temperature (ref. 103). Because some of these particles, especially hydrogen atoms, diffuse rapidly, it is further assumed that the concentration of chain carriers in the colder unburned gas ahead of the flame front is increased by diffusion to a value far greater than the thermodynamic equilibrium concentration for that region (e.g., table IV-XI, from ref. 104). A concentration profile similar to that shown in figure IV-19 is obtained. Even in the cold gas these active particles react rapidly, because chemical reactions involving atoms and free radicals generally have low energies of activation; that is, the reaction rate is not very dependent on the temperature. Therefore, these active particles could serve as initiators of the oxidation reaction. Since the concentration of active particles reaching the unburned gas by diffusion must be related to the maximum concentration in the flame front, the conclusion is that flame velocity should be related to the equilibrium concentrations at the adiabatic flame temperature.

It is difficult to measure the concentration of hydrogen atoms in a flame zone, but hydroxyl radicals [OH] may be observed spectroscopically. By use of this method, it was found in reference 105 that the relative concentration of hydroxyl radicals remained high in the unburned gas ahead of the visible flame zone (fig. IV-20). Reference 106 shows that the width of the reaction zone for several hydrocarbon-air and -oxygen flames as determined from the temperature profiles of the flames is roughly equal to the limit of diffusion of hydrogen atoms from the flame front into the unburned gas. Measurements and calculations such as those of table IV-XI substantiate the assumption that the concentrations of active particles that diffuse ahead of the flame may be large enough to be important.

From studies of the slow oxidation of hydrocarbons (ref. 8, pp. 94-202), it seems probable that the chemical reaction in the flame follows a chain mechanism. As previously stated, the activation energies of reactions between fuel molecules and chain carriers are low (usually 10 kcal or less, ref. 107). Hence, the assumption that the introduction of a few chain carriers into relatively cool gas could initiate the flame reaction may also be valid. The diffusion model of flame propagation thus qualitatively follows known features of the structure of the flame and the oxidation reaction. Tanford and Pease (refs. 104, 108, and 109) have derived an approximate equation for flame velocity based on the diffusion model. In addition to the assumptions listed for the comprehensive theory, the following simplifications and assumptions were made:

(1) Chain branching does not occur.

(2) The rate-controlling step (or steps) in the chemical chain reaction is the reaction of an active particle, such as the hydrogen atom, with a fuel molecule; for example,

$$H + CH_4 \rightarrow \text{products} \tag{53}$$

(3) The number of active particles is calculated from the linear continuity equation

$$D_i\left(\frac{d^2n_i}{dx^2}\right) + U_F\left(\frac{dn_i}{dx}\right) + I_i = 0 \tag{54}$$

where

I_i rate of production of the active species regardless of reaction order of process, molecules/(cm^3)(sec)

(4) The rate of formation of combustion products per unit area of flame surface can be written as the integral of a sum of a number of terms, one for each active particle:

$$\frac{d(\text{product})}{dt} = \int_{x_0}^{x_\infty}\left(\sum_i k_i \frac{\partial n_i}{\partial x}\right) n_f dx \tag{55}$$

where

k_i specific rate constant for reaction between i^{th} active species

(5) Through each unit area of flame surface, the unburned gas is converted at the flame velocity to products of complete combustion, so that another expression for product formation is:

$$\frac{d(\text{product})}{dt} = n_{tot,o}X_pU_F \tag{56}$$

where

$n_{tot,o}$ total number of molecules per cm^3 at initial conditions

X_p mole fraction of potential combustion product in unburned gas

(6) The fuel concentration, combustion-zone temperature, and diffusion coefficient are expressed as constant mean values, $n_{f,m}$, T_m, and D_m, respectively. The ratio T_m/T_o is called θ_m, and T_m is arbitrarily assigned the value $0.7\ T_F$.

Complete details of the derivation are given in reference 109. The continuity equation (54) is solved for n_i, which is then differentiated to give $\partial n_i/\partial x$. By equating the two simplified expressions for product formation under (4) and (5), substituting for $\partial n_i/\partial x$, and making the indicated integration, there is obtained the square-root law for flame velocity:

$$U_F = \left(\frac{n_{tot,m}X_{f,o}}{\theta_m^2 X_p}\sum_i \frac{k_i X_{i,F} D_{i,m}}{B_i}\right)^{1/2} \tag{57}$$

where

B_i dimensionless factor (near unity) that allows for radical recombination

$D_{i,m}$ diffusion coefficient for i^{th} species into unburned gas at mean combustion-zone temperature, cm^2/sec

$X_{f,o}$ mole fraction of fuel in unburned gas

$X_{i,F}$ calculated mole fraction of ith active species at equilibrium flame temperature T_F

θ_m $0.7\ T_F/T_o$

Tanford and Pease have substituted $D_{i,o}$ for $D_{i,m}/\theta_m^2$, thus assuming that the diffusion coefficient is proportional to the square of absolute temperature.

For predicting relative flame velocities of hydrocarbons, equation (57) has been modified (ref. 49) as follows: The active particles are considered to be H, OH, and O. It is assumed that D_i varies with the 1.67 power of absolute temperature and that $B_O = B_{OH} = 1$. It is further assumed that the specific rate constants k_i of equation (55) can be replaced by a weighted mean specific rate constant k_w representing all three active particles so that

$$\sum_i k_i X_{i,F} D_{i,m}/B_i \approx k_w\left(\frac{X_{H,F}D_{H,o}}{B_H} + X_{OH,F}D_{OH,o} + X_{O,F}D_{O,o}\right)\theta_m^{1.67} \tag{58}$$

where the recombination factor B_H is calculated by (ref. 109)

$$B_H = 1/2\left[1 + \sqrt{1 + \frac{24{,}000(D_{H,O}\theta_m^{1.67})}{U_F^2\theta_m^4}\,0.5X_{O,o} + 3700\ X_{H,F}}\right] \tag{59}$$

The required flame temperature and active-particle concentrations are calculated, assuming adiabatic thermal equilibrium, by the method of reference 110. Diffusion

coefficients are computed by the Stefan-Maxwell equation (ref. 111) to be 1.78 for H, 0.28 for OH, and 0.4 for O at 298° K. The quantities $n_{t,m}$, $X_{f,o}$, $X_{O_2,o}$, and X_p are calculated from a knowledge of the over-all oxidation process and the initial fuel and oxygen concentrations.

With these modifications and substitutions, equation (57) has been used in two ways with comparable success. In the first case, k_w was treated as a semiempirical constant independent of temperature; it was calculated for each flame velocity from equation (57). The average k_w for the group of data under consideration was called $\bar{k}_w$, and the ratio of predicted to measured flame velocity was calculated as $(\bar{k}_w/k_w)^{1/2}$. The mean deviation of this factor from unity is given in table IV-X. In the second method, the Arrhenius rate expression

$$k_w = P_w Z_w e^{-E_w/RT_m} \tag{60}$$

was substituted. The two unknowns P_w and E_w in this expression were calculated simultaneously from the flame velocity data in which the initial temperature was varied. The resulting $\bar{E}_w$ was used for the prediction of burning velocities for the same hydrocarbon under other experimental conditions. For each set of experimental data a new $\bar{P}_w$ was calculated (table IV-X).

Fairly satisfactory predictions of maximum burning velocity for hydrocarbon-air mixtures in which the molecular structure (chain length, branching, saturation, etc.) of the hydrocarbon is varied may be made by either the Tanford and Pease equation (first method, $\bar{k}_w$ independent of temperature, ref. 112) using an average empirical rate constant for all compounds except acetylene and ethene, or by a simplified form of the Semenov equation using an average steric factor and a constant activation energy of 40 kilocalories per gram-mole for all compounds except acetylene and ethene (ref. 113). Examples of these predictions are shown in the following table:

Hydrocarbon in air	Burning velocity, cm/sec		
	Measured	Calculated by Tanford-Pease eq. (ref. 112)	Calculated by Semenov eq. (ref. 113)
Methane	33.8	33.9	40.2
Propane	39.0	37.7	39.0
Hexane	38.5	37.3	37.2
2-Methylbutane	36.6	37.1	38.8
2,3-Dimethylbutane	36.3	37.0	39.1
2,2,3-Trimethylbutane	35.9	36.6	37.0
Propene	43.8	45.3	48.9
1-Hexene	42.1	41.7	42.0
2-Ethyl-1-butene	39.3	40.7	41.7
Propyne	69.9	61.3	64.9
1-Hexyne	48.5	48.6	46.0
Cyclohexane	38.7	37.4	38.3
Benzene	40.7	40.4	44.5

Miscellaneous approximate equations. - Other equations for burning velocity that are either based on a diffusional mechanism or include a diffusion concentration have been derived by Van Tiggelen, Gaydon and Wolfhard, and Manson. Details of these derivations and references to the original papers are given in reference 9. The final burning velocity equations are stated below:

Van Tiggelen:

$$U_F = \frac{4T_o}{\pi}\sqrt{\frac{2R(\xi - \xi')}{3MT_m}} \tag{61}$$

where

M molecular weight of active particles

T_m mean temperature of reaction zone

ξ probability of occurrence of chain-branching reaction

ξ' probability of occurrence of chain-breaking reaction

Gaydon-Wolfhard:

$$U_F = \frac{D_m T_o}{2\delta T_m} \tag{62}$$

where

δ reaction-zone thickness, cm

Manson:

$$U_F = \sqrt{\frac{\rho_F}{\rho_o(\rho_o - \rho_F)}\,\frac{pX_H T_o}{2T_F}} \tag{63}$$

where

p pressure, dyne/cm^2

X_H mole fraction of hydrogen atoms in burned gas

The Manson equation is derived from an aerodynamic model of the combustion process (eq. (7)) and does not include chemical kinetics. The flame chemistry enters only through pX_H, which has been substituted for the flame pressure drop. It is interesting to compare flame velocities predicted by this equation with the Semenov and Tanford-Pease predictions. In reference 49, equation (63) was used to predict flame velocities in two ways: (1) an empirical proportionality factor K_H was evaluated for each set of experimental data (table IV-X), or (2) the effects of all types of active particles were considered by substituting

$$\left(X_H + X_{OH}\frac{D_{OH}}{D_H} + X_O\frac{D_O}{D_H}\right) \tag{64}$$

for X_H in equation (63). In this case, again an average proportionality constant designated as $\overline{K}_\Sigma$ was used for each set of experimental data (see table IV-X).

Table IV-X and the other work reported in reference 49 show that burning-velocity predictions from either form of the Manson equation are not as consistent as those from the Semenov or the Tanford-Pease equation. The average deviation of the predicted velocities from measured values is about the same for the Semenov equation and for the Tanford-Pease equation (method (2)) using an empirical activation energy.

Neither the Tanford-Pease equation nor the Semenov equation gives as good predictions of burning velocity when the empirical factor determined with one variable is used to predict the effects of other variables. When the empirical factor calculated for ethene flames from equivalence-ratio data was used in the Semenov equation to predict flame velocities over the ranges of initial temperature and oxygen concentration covered experimentally, the predicted velocities differed from the measured velocities by an average of 14 percent. The maximum deviation was 24 percent. Similarly, an average rate constant $\overline{k}_w$ calculated from the ethene-air data over a range of concentrations used with the Tanford-Pease equation gave burning-velocity predictions for ethene-air mixtures at various initial temperatures that deviated from the measured burning velocities by -9 to 13 percent with an average deviation of 6 percent. Predicted flame velocities for various oxygen concentrations with the same $\overline{k}_w$ differed from experimental values by 8 to 22 percent with an average deviation of 12 percent.

In conclusion, if sufficient burning-velocity data are available to evaluate the necessary empirical constants, fairly good predictions of burning velocity can be made by semitheoretical methods for hydrocarbon-oxygen-nitrogen systems in which the following are varied: (1) molecular structure of hydrocarbon, (2) equivalence ratio, (3) initial mixture temperature, or (4) the oxygen concentration in the oxygen-nitrogen part of the mixture.

Evaluation of thermal and diffusional mechanisms. - Correlations of measured burning velocities with values predicted by approximate theoretical equations or with parameters from these equations have been presented from time to time as evidence that either a thermal or a diffusional mechanism of flame propagation is operative. For example, approximate equations based on a thermal mechanism generally indicate a relation between flame velocity and thermal conductivity, whereas those based on a diffusional mechanism generally indicate a relation between flame velocity and equilibrium concentrations and diffusion coefficients of the active particles. Many such correlations are reported in the literature. These include studies of the following variables: (1) mixture composition (or equivalence ratio), (2) molecular structure of the fuel, (3) initial mixture temperature, (4) pressure, (5) fuel additives, (6) isotope substitution of deuterium for hydrogen in the fuel, and (7) change of inert diluent. The correlations based on diffusional mechanisms are summarized in table IV-V; references to the original papers in which these correlations were given and to figures showing representative examples (figs. IV-21 to -23) are also given.

The generality of the correlations between flame velocity and active-particle concentrations indicates a need for a critical study of the physical significance of the diffusion concept. Judgment or understanding of the physical significance is difficult for several reasons:

(1) Equations for heat conduction are mathematically similar to those for diffusion, so that burning-velocity equations based on either a thermal or a diffusion mechanism of flame propagation are similar in form.

(2) The calculated equilibrium concentrations of active particles depend strongly on the temperature of the flame. Moreover, these calculated concentrations may not represent the concentrations that exist in the flame.

(3) All the equations that may be used to test the experimental data are based on broad simplifying assumptions, and the validity of many of these assumptions varies for different combustion systems.

(4) The chemical kinetic factors that occur in the equations have not been independently determined (and probably will not be determined for many years).

(5) Thermal and transport properties of mixtures at high temperatures and diffusion coefficients for atoms and free radicals used in the equations are questionable.

(6) The precision of burning-velocity measurement is usually 2 to 5 percent, while the accuracy is probably much less.

Many detailed studies of various combustible systems have been published (table IV-V), and experiments have been designed with the purpose of distinguishing between the two mechanisms. Two such experiments are studies of the effects on burning velocity of the change in diluent from argon to helium (e.g., ref. 114) and of substitution of a deuterated hydrocarbon for a hydrogenated one (ref. 129). In the former case the flame temperature remains essentially constant, while diffusion coefficients and thermal conductivities change. In the latter case the major change is in the most important type of chain carrier, which is usually the hydrogen atom but which, on the substitution of a deuterated compound, becomes the deuterium atom. Critical examination of all such experiments shows that diffusion effects do not give unique explanations of the experimental data; only two experimental investigations appear to favor one mechanism over the other. Both indicate that diffusion may be more important than heat conduction:

(1) Nonhydrogen-containing combustible systems to which water or hydrogen are added show increased burning velocities, while hydrogen-containing systems are not greatly affected. The increased burning velocity is explicable on the basis of free-radical diffusion. For one of the two nonhydrogen-containing systems studied ($CO-O_2$), the burning-velocity effect on addition of water (refs. 64 and 115) is also explicable on a conduction mechanism basis (ref. 115). The other system ($C_2N_2-O_2-A$, ref. 116) is not so easily explained on a thermal basis.

(2) Changes in burning velocity caused by interchanging argon and helium as diluents are closer to the predictions of diffusion theories than those of thermal theories, as shown by table IV-XII (ref. 114). In this table, the ratio of flame velocity of a mixture containing helium to that of a mixture containing an equal volume of argon is compared with the ratio of the square roots of the thermal conductivities of these mixtures and with the ratios of the square roots of the diffusion coefficients of various active particles. The ratios of diffusion coefficients are closer to the flame velocity ratio than is the ratio of thermal conductivity for all the fuels listed except hydrogen.

Neither of these pieces of evidence is very strong, and both are subject to criticism as to the validity of the criteria used to judge which mechanism is operative. It is probable that both heat conduction and the diffusion of atoms and free radicals contribute to the propagation of flame, and that both concepts are needed to explain flame behavior. A better understanding of the mechanism of laminar flame propagation in the future will result from the further development of the comprehensive theory and the investigation of the chemical kinetics of flames.

APPLICATION OF LAMINAR FLAME RESEARCH TO PRACTICAL COMBUSTION PROBLEMS

A high flame velocity contributes to maximum heat release per unit volume and enables an air-breathing engine to operate at high throughput rates without blow-out. (It has been suggested, however, that in some cases a high flame velocity may contribute to instability in the region near a flame holder through increased shear; see ch. VI.) The chemical factors that are important in obtaining a high flame velocity are the fuel-oxygen ratio, the molecular structure of the fuel, and the mole fraction of oxygen in the air used. The only physical factor that has an established and appreciable effect on the laminar flame velocity is the initial mixture temperature. (The effects of flow parameters on turbulent flame velocity are discussed in ch. V.) The effects of these factors and of less important factors are summarized in the following paragraphs.

As the fuel-oxygen ratio is increased from the lean flammability limit, the flame velocity increases by a factor of 3 or 4 to a maximum value at a fuel-oxygen ratio that is 1.0 to 1.2 times the stoichiometric ratio and then decreases to give a rather symmetrical pattern about the maximum. This shows the importance of proper mixture preparation as discussed in chapter I. Between the lean flammability limit and the stoichiometric mixture, the flame velocity may be related to the fraction of stoichiometric fuel-oxygen ratio by an equation such as

$$\frac{U_F}{U_{F,max}} = 2.6 \log \varphi + 0.94$$

which holds for ethene-, propyne-, and pentane-air mixtures. Empirical methods based on the bond dissociation energy of the fuel are reported by which $U_{F,max}$ and the corresponding φ may be predicted.

The maximum flame velocities of all hydrocarbons with air at 25° C and 1 atmosphere fall in the range 30 to 80 centimeters per second, with the exception of acetylene at 142 centimeters per second. Within this range, the following molecular structural features contribute to high flame velocity: short chain length or small cycloalkane ring size, unsaturation, and minimum chain branching. The effects of unsaturation and branching become smaller as the chain length increases. Aromatic compounds generally have flame velocities equal to or smaller than the saturated hydrocarbons (alkanes, $U_F \sim 40$ cm/sec), and chain branching has less effect on them. Alkyl oxides (e.g., propylene oxide) have higher flame velocities than their parent alkenes; aldehydes and ketones are generally intermediate between alkanes and alkenes; and alcohols and ethers are near the alkanes.

An empirical equation has been developed for the flame velocities of aliphatic hydrocarbons based on the number of various types of carbon-hydrogen bonds. The flame velocity of a mixture of hydrocarbons is related to the individual flame velocities through

$$\sum_j \frac{X_{f,j}}{X'_{f,j}} = 1$$

No additives, including antiknock compounds, have been found which will increase flame velocity beyond the mixing effect given by the preceding equation for constant-pressure combustion. Water decreases the flame velocity of hydrocarbons somewhat, but not as much as an equal quantity of nitrogen.

A factor that could enter the jet combustion picture either through deliberate oxygen enrichment (e.g., for a pilot flame) or through vitiation of the combustion air (as in tail-pipe burning) is the oxygen-nitrogen ratio, or more generally, the oxygen-inert ratio. For hydrocarbon-oxygen-nitrogen mixtures, there is a linear increase in maximum flame velocity as the mole ratio $O_2/(O_2 + N_2)$ is increased from 0.15 to 0.35. Empirical equations are presented for a number of hydrocarbons. If the nitrogen is replaced by an equal volume of carbon dioxide, argon, or helium, the flame velocity of the mixture increases in the order carbon dioxide < nitrogen < argon < helium.

The flame velocity can also be increased several times by increasing the initial mixture temperature, according to a relation such as that for propane-air in the range 200° to 615° K:

$$U_{F,rel} = 25 + 0.00085\ T_o^2$$

This shows the advantage that could be obtained with a fuel injector that would inject hot gaseous fuel into hot primary air. For the smaller temperature range 290° to 420° K (or 520° to 760° R), it appears that $U_F \propto T_o^{1.4}$ would be a reasonable assumption for many hydrocarbons, with the power increasing toward 2.0 as the high end of the temperature range is increased.

At present, it appears that pressure has a negligible effect on flame velocity; at most, $U_F \propto p^{-0.5}$. Electric fields and acoustical and mechanical disturbances also have little or no effect.

Considerable advances have been made in recent years in the theory of the propagation of a one-dimensional steady-state flame. Comprehensive equations have been presented that take into account all the chemical species involved in the flame reactions with the necessary reaction rates and diffusion rates for each species. These comprehensive equations have been solved by numerical integration for the simplest kinds of flames, but the present state of knowledge does not allow their solution for the flame velocities of complex hydrocarbon flames. Instead, various simpler, approximate equations for the laminar flame velocity have been presented. Most of these approximate equations consider flame propagation to occur through a mechanism that is based primarily on either the conduction of heat from the flame to the unburned gas (thermal mechanism) or the diffusion of active reaction centers into the unburned gas (diffusional mechanism). This chapter has shown that both types of equations, as represented by the Semenov and Tanford-Pease equations, can be used to predict, generally within 10 or 20 percent, the relative changes in flame velocity caused by changing the important chemical and physical factors.

The question is repeatedly raised as to whether heat conduction or active-particle diffusion is more important in laminar flame propagation. Since both types of equations usually give equally good relative predictions of flame velocity for the chemical and physical factors that are of interest to engine applications, the question remains unsolved. There are two experimental investigations, neither of which can be considered final, that appear to favor a diffusional mechanism. One shows that the addition of water or hydrogen to nonhydrogen-containing combustible mixtures increases flame velocities, while hydrogen-containing systems are not greatly affected; the other shows that changes in the flame velocity caused by interchanging argon and helium as inert diluents are closer to the predictions of diffusional equations than to those of thermal equations. It is probable that both heat conduction and active-particle diffusion contribute to the propagation of any flame; both are included in the comprehensive equations.

Another use of the equations describing laminar flame propagation and of some of the recent experimental investigations that is of interest in engine applications is the calculation of maximum heat-release rates in laminar flames. Zeldovich (ref. 51) and Avery and Hart (ref. 117) have used thermal equations to calculate heat-release rates of 10^{10} and 10^{9} (Btu/(ft^3)(hr)(atm^2)) for carbon monoxide and butane flames, respectively. Avery and Hart point out that a heat-release rate of approximately 10^{8} (Btu/(ft^3)(hr)) has been achieved at 1 atmosphere in a ram-jet engine and that this indicates the possibility that combustion rates under ram-jet conditions of maximum heat release may be determined by kinetic factors rather than mixing times. Friedman and Burke (ref. 6) have used an energy equation analogous to equation (35) together with their experimental temperature profile to calculate the heat-release rate as a function of distance through a lean propane-air flame at 0.06 atmosphere, with the results shown in figure IV-24.

Empirical relations for the effects of such factors as the ratio $O_2/(O_2 + N_2)$ and the initial temperature have already found use in correlations of engine performance. These and other correlations for engine combustion efficiency and stability which include terms for the chemical reaction rates are discussed in subsequent chapters.

REFERENCES

1. Klaukens, H., and Wolfhard, H. G.: Measurements in the Reaction Zone of a Bunsen Flame. Proc. Roy. Soc. (London), vol. A193, July 21, 1948, pp. 512-524.

2. Friedman, Raymond: Measurement of the Temperature Profile in a Laminar Flame. Fourth Symposium (International) on Combustion, The Williams & Wilkins Co. (Baltimore), 1953, pp. 259-263.

3. Dixon-Lewis, G.: Temperature Distribution in Flame Reaction Zones. Fourth Symposium (International) on Combustion, The Williams & Wilkins Co. (Baltimore), 1953, pp. 263-267.

4. Andersen, J. W., and Fein, R. S.: Measurements of Normal Burning Velocities and Flame Temperatures in Bunsen Flames. Jour. Chem. Phys., vol. 17, no. 12, Dec. 1949, pp. 1268-1273.

5. Fristrom, R. M., Prescott, R., Neumann, R. K., and Avery, W. H.: Temperature Profiles in Propane-Air Flame Fronts. Fourth Symposium (International) on Combustion, The Williams & Wilkins Co. (Baltimore), 1953, pp. 267-274.

6. Friedman, Raymond, and Burke, Edward: Measurement of Temperature Distribution in a Low-Pressure Flat Flame. Jour. Chem. Phys., vol. 22, no. 5, May 1954, pp. 824-830.

7. Gerstein, Melvin, McDonald, Glen E., and Schalla, Rose L.: Decomposition Flame Studies with Ethylene Oxide. Fourth Symposium (International) on Combustion, The Williams & Wilkins Co. (Baltimore), 1953, pp. 375-383.

8. Lewis, Bernard, and von Elbe, Guenther: Combustion, Flames and Explosions of Gases. Academic Press, Inc. (New York), 1951.

9. Evans, Marjorie W.: Current Theoretical Concepts of Steady-State Flame Propagation. Chem. Rev., vol. 51, no. 3, Dec. 1952, pp. 363-429.

10. Wohl, Kurt, Kapp, N. M., Coon, D. C., Jr., and Fulmer, R. F.: Methods of Determining Burning Velocities and Stability Measurements of Tube and Nozzle Flames. Meteor Rep. UAC-49, Res. Dept., United Aircraft Corp., Dec. 1950. (Proj. Meteor, U.S. Navy BuOrd Contract NOrd 9845 with M.I.T.)

11. Broeze, J. J.: Theories and Phenomena of Flame Propagation. Third Symposium on Combustion and Flame and Explosion Phenomena, The Williams & Wilkins Co. (Baltimore), 1949, pp. 146-155.

12. Linnett, J. W.: Methods of Measuring Burning Velocities. Fourth Symposium (International) on Combustion, The Williams & Wilkins Co. (Baltimore), 1953, pp. 20-35.

13. Guenoche, H.: Note on the Application of Optical Methods to Stationary Flames. Rev. Inst. Francais Petrole, vol. 6, no. 2, Feb. 1951, pp. 60-63.

14. Grove, J. R., Hoare, M. F., and Linnett, J. W.: The Shadow Cast by a Bunsen Flame, Its Production and Usefulness. Trans. Faraday Soc. (London), vol. 46, pt. 9, Sept. 1950, pp. 745-755.

15. Andersen, J. W., and Fein, R. S.: Measurement and Correlation of Burning Velocities of Propane-Air Flames. Rep. CM-552, Dept. Chem., Naval Res. Lab., Univ. Wisconsin, July 20, 1949. (BuOrd Contract NOrd 9938 Task WIS-1-G.)

16. Dugger, Gordon L.: Effect of Initial Mixture Temperature on Flame Speed of Methane-Air, Propane-Air, and Ethylene-Air Mixtures. NACA Rep. 1061, 1952. (Supersedes NACA TN's 2170 and 2374.)

17. Jost, Wilhelm: Explosion and Combustion Processes in Gases. McGraw-Hill Book Co., Inc., 1946.

18. Powling, J.: A New Burner Method for the Determination of Low Burning Velocities and Limits of Inflammability. Fuel, vol. XXVIII, no. 2, 1949, pp. 25-28.

19. Egerton, Alfred, and Sen, D.: Flame Propagation: The Influence of Pressure on the Burning Velocities of Flat Flames. Fourth Symposium (International) on Combustion, The Williams & Wilkins Co. (Baltimore), 1953, pp. 321-328.

20. Culshaw, G. W., and Garside, J. E.: A Study of Burning Velocity. Third Symposium on Combustion and Flame and Explosion Phenomena, The Williams & Wilkins Co. (Baltimore), 1949, pp. 204-209.

21. Caldwell, Frank R., Broida, Herbert P., and Dover, Jerome J.: Combustion in Bunsen Flames. Ind. and Eng. Chem., vol. 43, no. 12, Dec. 1951, pp. 2731-2739.

22. Gouy, M.: Recherches Photométriques sur les Flammes Colorées. Ann. de Chim. et de Phys., T. XVIII, 1879, pp. 5-101.

23. Smith, Francis A., and Pickering, S. F.: Measurements of Flame Velocity by a Modified Burner Method. Res. Paper RP900, Jour. Res. Nat. Bur. Standards, vol. 17, no. 1, July 1936, pp. 7-43.

24. Corsiglia, John: New Method for Determining Ignition Velocities of Air and Gas Mixtures. Am. Gas Assoc. Monthly, vol. XIII, no. 10, 1931, pp. 437-422.

25. Hahnemann, H., and Ehret, L.: Effect of Intense Sound Waves on a Stationary Gas Flame. NACA TM 1271, 1950.

26. Markstein, G. H.: Interaction of Flame Propagation and Flow Disturbances. Third Symposium on Combustion, Flame and Explosion Phenomena, The Williams & Wilkins Co. (Baltimore), 1949, pp. 162-167.

27. Calcote, Hartwell F.: Accurate Control and Vaporizing System for Small Liquid Flows. Anal. Chem., vol. 22, no. 8, Aug. 1950, pp. 1058-1060.

28. Behrens, H.: Flame Instabilities and Combustion Mechanism. Fourth Symposium (International) on Combustion, The Williams & Wilkins Co. (Baltimore), 1953, pp. 538-545.

29. Garside, J. E., and Jackson, B.: The Formation and Some Properties of Polyhedral Burner Flames. Fourth Symposium (International) on Combustion, The Williams & Wilkins Co. (Baltimore), 1953, pp. 545-552.

30. Kurz, Philip F.: Flame Stability on Bunsen-Smithells Burners. Tech. Rep. 15036-17, Battelle Memorial Inst., Feb. 1953. (Contract AF 33(038)-12656, E.O. No. 460-35, S.R.-8.)

31. Ball, George A.: Combustion Aerodynamics - A Study of a Two-Dimensional Flame. Dept. Eng. Sci. and Appl. Phys., Harvard Univ., July 1951. (Army Ord. Dept. Contract No. W19-020-ORD-6509.)

32. Fabri, J., Siestrunck, R., and Fouré, C.: On the Aerodynamic Field of Stabilized Flames. Fourth Symposium (International) on Combustion, The Williams & Wilkins Co. (Baltimore), 1953, pp. 443-450.

33. Singer, J. M.: Burning-Velocity Measurements on Slot Burners; Comparison with Cylindrical Burner Determinations. Fourth Symposium (International) on Combustion, The Williams & Wilkins Co. (Baltimore), 1953, pp. 352-358.

34. Morrison, R. B., and Dunlap, R. A.: Measurement of Flame Speeds with the V-Flame. Rep. UMM-21, Aero. Res. Center, Eng. Res. Inst., Univ. Mich., May 1948. (AAF Contract W33-038 ac 14222, Proj. MX-794.)

35. Pilcher, J. M., Miesse, C. C., Jensen, R. A., and Terrill, F. B.: Study of Flame Speeds. Battelle Memorial Inst., Thirty-Sixth Progress Report to Hdq., AMC, Mar. 2-May 1, 1950. (Contract AF 33 (038)-2038.)

36. Gross, Robert A.: Aerodynamics of a Two-Dimensional Flame. Combustion Tunnel Lab. Interim Tech. Rep. No. 2, Div. Appl. Sci., Harvard Univ., June 1952. (Contract No. DA-19-020-ORD-1029, Army Ord. Dept.)

37. Culshaw, G. W., and Garside, J. E.: Recent Studies of Aerated Burner Flames. Inst. Gas Eng. Inst. (London) Gas Res. Fellowship Rep., 1946-1947. (Reviews papers from period 1943-1946, including those of Delbourg, Heiligenstaedt, and Vasilesco.)

38. Gerstein, Melvin, Levine, Oscar, and Wong, Edgar L.: Fundamental Flame Velocities of Pure Hydrocarbons. I - Alkanes, Alkenes, Alkynes, Benzene, and Cyclohexane. NACA RM E50G24, 1950. (See also Jour. Am. Chem. Soc., vol. 73, no. 1, Jan. 1951, pp. 418-422.)

39. Simon, Dorothy M., and Wong, Edgar L.: Flame Velocities over a Wide Composition Range for Pentane-Air, Ethylene-Air, and Propyne-Air Flames. NACA RM E51H09, 1951.

40. Levine, Oscar, and Gerstein, Melvin: Fundamental Flame Velocities of Pure Hydrocarbons. III - Extension of Tube Method to High Flame Velocities - Acetylene-Air Mixtures. NACA RM E51J05, 1951.

41. Stevens, F. W.: A Constant Pressure Bomb. NACA Rep. 176, 1923. (See also NACA Reps. 280, 305, 337, and 372.)

42. Strehlow, R. A., and Stuart, Joseph G.: An Improved Soap Bubble Method of Measuring Flame Velocities. Fourth Symposium (International) on Combustion, The Williams & Wilkins Co. (Baltimore), 1953, pp. 329-336.

43. Simon, Dorothy M., and Wong, Edgar L.: An Evaluation of the Soap-Bubble Method for Burning Velocity Measurements Using Ethylene-Oxygen-Nitrogen and Methane-Oxygen-Nitrogen Mixtures. NACA TN 3106, 1954. (See also Jour. Chem. Phys., vol. 21, no. 5, May 1953, pp. 936-937.)

44. Flock, Ernest F., Marvin, Charles F., Jr., Caldwell, Frank R., and Roeder, Carl H.: Flame Speeds and Energy Considerations for Explosions in a Spherical Bomb. NACA Rep. 682, 1940.

45. Manton, John, von Elbe, Guenther, and Lewis, Bernard: Burning-Velocity Measurements in a Spherical Vessel with Central Ignition. Fourth Symposium (International) on Combustion, The Williams & Wilkins Co. (Baltimore), 1953, pp. 358-363.

46. Gerstein, Melvin, Levine, Oscar, and Wong, Edgar L.: Fundamental Flame Velocities of Hydrocarbons. Ind. and Eng. Chem., vol. 43, no. 12, Dec. 1951, pp. 2770-2772.

47. Anon.: Survey of Bumblebee Activities. Bumblebee Series Rep. No. 113, Appl. Phys. Lab., Johns Hopkins Univ., Nov. 1949. (Contract NOrd 7385 with Bur. Ord., U.S. Navy.)

48. Dugger, Gordon L., and Graab, Dorothy D.: Flame Velocities of Propane- and Ethylene-Oxygen-Nitrogen Mixtures. NACA RM E52J24, 1953.

49. Dugger, Gordon L., and Simon, Dorothy M.: Prediction of Flame Velocities of Hydrocarbon Flames. NACA Rep. 1158, 1954. (Supersedes NACA RM E52J13.) (See also Fourth Symposium (International) on Combustion, The Williams & Wilkins Co., 1953, pp. 336-345.)

50. Nicol, D. L., Fedde, P., Katz, S., and Linden, H. R.: Study of Fundamentals of Combustion. Rep. No. 2, Inst. Gas Tech. Center (Chicago), Jan. 1951. (Contract NONR-04100, Office Naval Res., Dept. Navy.) (See also other reps. same series, same title, including: Nicol, D. L., Flanigan, O., and Shomaker, J., Rep. No. 3, May 1952; Searight, E. F., Sickafoose, R. D., Nicol, D. L., and Peck, R. E., Rep. No. 5, Mar. 1952.)

51. Zeldovich, Y. B.: Theory of Combustion and Detonation of Gases. Tech. Rep. F-TS-1226-IA (GDAM A9-T-45), Air Materiel Command, 1949. (Trans. by Brown Univ.)

52. Wagner, Paul, and Dugger, Gordon L.: Flame Propagation. V. Structural Influences on Burning Velocity. Comparison of Measured and Calculated Burning Velocity. Jour. Am. Chem. Soc., vol. 77, no. 1, Jan. 5, 1955, pp. 227-231.

53. Hibbard, R. R., and Pinkel, B.: Flame Propagation. IV. Correlation of Maximum Fundamental Flame Velocity with Hydrocarbon Structure. Jour. Am. Chem. Soc., vol. 73, no. 4, Apr. 1951, pp. 1622-1625.

54. Leason, D. B.: The Effect of Organic Additions on Ignition Velocity. Pt. I - Review of Previous Work and the Effect on Rich Towns Gas-Air Mixtures. Rep. E.62, Div. Aero., Australian Council Sci. and Ind. Res. (Melbourne), Nov. 1948.

55. Leason, D. B.: The Effect of Gaseous Additions on the Burning Velocity of Propane-Air Mixtures. Fourth Symposium (International) on Combustion, The Williams & Wilkins Co. (Baltimore), 1953, pp. 369-375.

56. Smittenberg, J., and Kooijman, P. L.: Tentative Investigation into the Influence of Tetra-Ethyl-Lead on the Flame Velocity in Hydrocarbon - Air Mixtures, Ignited by Electric Sparks. Rec. des Travaux Chim. des Pays-Bas, T. 59, 1940, pp. 591-600.

57. Egerton, A. C.: General Statement as to Existing Knowledge on Knocking and Its Prevention. The Science of Petroleum, Oxford Univ. Press, 1938, p. 2924.

58. Sachsse, H., und Bartholome, E.: Beiträge zur Frage der Flammengeschwindigkeit. Zs. f. Elek., Bd. 53, Nr. 4, Aug. 1949, pp. 183-190.

59. Ubbelohde, von L., and Hofsass, M.: Über die Entzündungsgeschwindigkeit im Innenkegel der Bunsenflamme. Jour. Gasbel., Jahrg. 56, Nr. 51, Dec. 20, 1913, pp. 1253-1262.

60. Walker, P. L., Jr., and Wright, C. C.: Stability and Burning Velocity of Bunsen Flames with Propane-Carbon Monoxide Mixtures. Fuel, vol. XXXI, 1952, pp. 45-49.

61. Payman, W.: The Propagation of Flame in Complex Gaseous Mixtures. Jour. Chem. Soc., vol. 115, Dec. 1919, pp. 1436-1462.

62. Kurz, Philip F.: Influence of Hydrogen Sulfide on Flame Speed of Propane-Air Mixtures. Ind. and Eng. Chem., vol. 45, no. 10, Oct. 1953, pp. 2361-2366.

63. Fiock, Ernest F., and King, H. Kendall: The Effect of Water Vapor on Flame Velocity in Equivalent $CO-O_2$ Mixtures. NACA Rep. 531, 1935.

64. McDonald, Glen E.: Measurement of Uniform Flame Movement in Carbon Monoxide - Air Mixtures Containing Either Added D_2O or H_2O. NACA RM E50C10, 1950.

65. Kapp, N. M., Snow, B., and Wohl, K.: The Effect of Water Vapor on the Normal Burning Velocity and on the Stability of Butane-Air Flames Burning Above Tubes in Free Air. Meteor Rep. UAC-30, Res. Dept., United Aircraft Corp., Nov. 1948. (U.S. Navy, Bur. Ord. Contract NOrd 9845 with M.I.T.)

66. Dugger, Gordon L., and Grabb, Dorothy D.: Flame Velocities of Hydrocarbon-Oyxgen-Nitrogen Mixtures. Fourth Symposium (International) on Combustion, The Williams & Wilkins Co. (Baltimore), 1953, pp. 302-310. (See also NACA TN 2680 and NACA RM E52J24.)

67. Clingman, William H., Brokaw, Richard S., and Pease, Robert N.: Burning Velocities of Methane with Nitrogen-Oxygen, Argon-Oxygen, and Helium-Oxygen Mixtures. Fourth Symposium (International) on Combustion, The Williams & Wilkins Co. (Baltimore), 1953, pp. 310-313.

68. Coward, H. F., and Payman, W.: Problems in Flame Propagation. Chem. Rev., vol. 21, no. 3, Dec. 1937, pp. 359-366.

69. Caldwell, F. R., Ruegg, F. W., and Olsen, L. O.: Seventy-Second Report of Progress on the Combustion Chamber Research Program for the Quarter ending Dec. 31, 1951. Rep. 1B111, U.S. Dept. Commerce, Nat. Bur. Standards, Jan. 30, 1952.

70. Mellish, C. E., and Linnett, J. W.: The Influence of Inert Gases on Some Flame Phenomena. Fourth Symposium (International) on Combustion, The Williams & Wilkins Co. (Baltimore), 1953, pp. 407-420.

71. Badin, Elmer J., Stuart, Joseph G., and Pease, Robert N.: Burning Velocities of Butadiene-1, 3 with Nitrogen-Oxygen and Helium-Oxygen Mixtures. Jour. Chem. Phys., vol. 17, no. 3, Mar. 1949, pp. 314-315.

72. Friedman, Raymond: The Quenching of Laminar Oxyhydrogen Flames by Solid Surfaces. Third Symposium on Combustion and Flame and Explosion Phenomena, The Williams & Wilkins Co. (Baltimore), 1949, pp. 110-120.

73. Lewis, Bernard, et al.: Research of Flame and Ignition Phenomena. Semi-Annual Prog. Rep., James Forrestal Res. Center, Princeton Univ., Apr. 1, 1953, pp. 81-91. (Office Naval Res. Contract N6-ori-105, Task Order 111, NR-098-038.)

74. Wolfhard, H. G.: Die Eigenschaften stationareer Flammen im Unterdruck. Zs. f. Tech. Phys., Nr. 9, 1943, pp. 206-211.

75. Hubner, H. J., and Wolfhard, H. G.: Combustion at High Altitudes. Library Trans. No. 125, British R.A.E., Nov. 1946.

76. Pickering, H. S., and Linnett, J. W.: Burning Velocity Determinations. VII - The Burning Velocities of Some Ethylene + Oxygen + Nitrogen Mixtures. Trans. Faraday Soc., vol. 47, pt. 10, Oct. 1951, pp. 1101-1103; discussion, pp. 1104-1106.

77. Cullen, R. E.: A Non-Dimensional Correlation of Flame Propagation at Subatmospheric Pressures. Trans. A.S.M.E., vol. 75, no. 1, Jan. 1953, pp. 43-49.

78. Wohl, Kurt, and Kapp, Numer M.: Flame Stability at Variable Pressures. Meteor Rep. UAC-42, Res. Dept., United Aircraft Corp., Oct. 1949. (Proj. METEOR, Bur. Ord. Contract NOrd 9845 with M.I.T.)

79. Ribaud, G., and Gaudry, H.: Effect of Pressure on the Speed of Propagation of Flame at Constant Speed and under Constant Pressure in Various Combustible Gas Mixtures (Propane, Benzine, and City Gas). Tech. Phys., USSR, vol. 3, no. 11, 1936, pp. 18-23.

80. Garner, F. H., Ashforth, G. K., and Long, R.: Effect of Pressure on Burning Velocities of Benzene-Air, Heptane-Air and 2,2,4-Trimethylpentane-Air Mixtures. Fuel, vol. XXX, 1951, p. 17.

81. Linnett, J. W., and Wheatley, P. T.: Effect of Pressure on Velocity of Burning. Nature, vol. 164, no. 4166, Sept. 3, 1949, pp. 403-404.

82. Albright, R. E., Heath, D. P., and Thena, R. H.: Flame Velocities of Liquid Hydrocarbons. Ind. and Eng. Chem., vol. 44, no. 10, Oct. 1952, pp. 2490-2496.

83. Ubbelohde, L., and Dommer, O.: Zur Kenntis der Verbrennung im Innenkegel der Bunsen flamme. Jour. Gasbel, vol. 57, no. 31, Aug. 1914, pp. 757-765; 781-787; 805-810.

84. Passauer, H. Eisenstein: Verbrennungsgeschwindigkeit und Verbrennungstemperatur bei Vorwärmung von Gas und Luft. Das Gas-und Wasserfach, Jahrg. 73, Heft 17, Apr. 26, 1930, pp. 393-397.

85. Dugger, Gordon L.: Effect of Initial Mixture Temperature on Flame Speed of Methane-Air, Propane-Air, and Ethylene-Air Mixtures. NACA Rep. 1061, 1952. (Supersedes NACA TN's 2170 and 2374.)

86. Sachsse, Hans: Über die Temperaturabhängigkeit der Flammengeschwindigkeit und das Temperaturgefälle in der Flammenfront. Zs. f. Phys. Chem., Bd. 180, Heft 4, Abt. A, Oct. 1935, pp. 305-313.

87. Dugger, Gordon L., Weast, Robert C., and Heimel, Sheldon: Flame Velocity and Preflame Reaction in Heated Propane-Air Mixtures. Ind. and Eng. Chem., vol. 47, no. 1, Jan. 1955, pp. 114-116.

88. Johnston, W. C.: Measured Flame Velocities of Fuels at Low Pressures. SAE Jour., vol. 55, no. 12, Dec. 1947, pp. 62-65.

89. Tamman, G., and Thiele, H.: Speeds of Combustion in Gas Mixtures. Zs. anorg. all gem. Chem., vol. 192, 1930, pp. 65-89.

90. Polanyi, M. L., and Markstein, G. H.: Phenomena in Electrically and Acoustically Disturbed Bunsen Burner Flames. Tech. Rep. 5, Proj. Squid, Cornell Aero Lab., Sept. 15, 1947.

91. Calcote, Hartwell F.: Electrical Properties of Flames. Burner Flames in Transverse Electric Fields. Third Symposium on Combustion and Flame and Explosion Phenomena, The Williams & Wilkins Co. (Baltimore), 1949, pp. 245-253.

92. Loshaek, Sam, Fein, R. S., and Olsen, H. L.: The Effect of Sound on the Normal Velocity and Stability Limits of Laminar Propane-Air Flames. Rep. CM-553, Dept. Chem., Naval Res. Lab., Univ. Wisconsin, July 9, 1949. (Navy BuOrd Contract NOrd 9938.)

93. Kaskan, W. E.: An Investigation of Vibrating Flames. Fourth Symposium (International) on Combustion, The Williams & Wilkins Co. (Baltimore), 1953, pp. 575-591.

94. Hirschfelder, J. O., Curtiss, C. F., and Campbell, Dorothy E.: The Theory of Flames and Detonations. Fourth Symposium (International) on Combustion, The Williams & Wilkins Co. (Baltimore), 1953, pp. 190-211.

95. Hirschfelder, J. O., and Curtiss, C. F.: Theory of Propagation of Flames. Pt. 1 - General Equations. Third Symposium on Combustion and Flame and Explosion Phenomena, The Williams & Wilkins Co. (Baltimore), 1949, pp. 121-127.

96. Semenov, N. N.: Thermal Theory of Combustion and Explosion. III - Theory of Normal Flame Propagation. NACA TM 1026, 1942.

97. Hirschfelder, J. O., Bird, R. B., and Spotz, Ellen L.: Viscosity and Other Physical Properties of Gases and Gas Mixtures. Trans. A.S.M.E., vol. 21, no. 8, Nov. 1949, pp. 921-937.

98. Rossini, Frederick D., et al.: Selected Values of Properties of Hydrocarbons. Circular C461, Nat. Bur. Standards, Nov. 1947.

99. Bromley, L. A., and Wilke, C. R.: Viscosity Behavior of Gases. Ind. and Eng. Chem., vol. 43, no. 7, July 1951, pp. 1641-1648.

100. Chamberlain, G. H. N., et Walsh, A. D.: L'oxydation lente de l'éther diisapropylique dans l'intervalle de températures 360°-460° C. Revue de L'Institut Francais du Pétrole et Annales des Combustibles Liquids, T. IV, Nr. 7, July 1949, pp. 301-313; discussion, pp. 314-318.

101. Linnett, J. W., and Hoare, M. F.: Burning Velocities in Ethylene-Air-Nitrogen Mixtures. Third Symposium on Combustion and Flame and Explosion Phenomena, The Williams & Wilkins Co. (Baltimore), 1949, pp. 195-204.

102. McAdams, W. H.: Heat Transmission. Second ed., McGraw-Hill Book Co., Inc., 1942, pp. 391-411.

103. Tanford, Charles, and Pease, Robert N.: Equilibrium Atom and Free Radical Concentrations in Carbon Monoxide Flames and Correlation with Burning Velocities. Jour. Chem. Phys., vol. 15, no. 7, July 1947, pp. 431-433.

104. Tanford, Charles: The Role of Free Atoms and Radicals in Burner Flames. Third Symposium on Combustion and Flame and Explosion Phenomena, The Williams & Wilkins Co. (Baltimore), 1949, pp. 140-146.

105. Gaydon, A. G., and Wolfhard, H. G.: Spectroscopic Studies of Low Pressure Flames; Temperature Measurements in Acetylene Flames. Proc. Roy. Soc. (London), ser. A, vol. 194, no. A1037, Aug. 12, 1948, pp. 169-184.

106. Gaydon, A. G., and Wolfhard, H. G.: The Influence of Diffusion on Flame Propagation. Proc. Roy. Soc. (London), ser. A, vol. 196, 1949, pp. 105-113.

107. Steacie, E. W. R.: Atomic and Free Radical Reactions. Reinhold Pub. Co. (New York), 1946.

108. Tanford, Charles, and Pease, Robert N.: Theory of Burning Velocity. II - The Square Root Law for Burning Velocity. Jour. Chem. Phys., vol. 15, no. 12, Dec. 1947, pp. 861-865.

109. Tanford, Charles: Theory of Burning Velocity. I - Temperature and Free Radical Concentrations Near the Flame Front, Relative Importance of Heat Conduction and Diffusion. Jour. Chem. Phys., vol. 15, no. 7, July 1947, pp. 433-439.

110. Huff, Vearl N., Gordon, Sanford, and Morrell, Virginia E.: General Method and Thermodynamic Tables for Computation of Equilibrium Composition and Temperature of Chemical Reactions. NACA Rep. 1037, 1951. (Supersedes NACA TN's 2113 and 2161.)

111. Jeans, James: An Introduction to the Kinetic Theory of Gases. Cambridge Univ. Press (London), 1940, p. 207.

112. Simon, Dorothy Martin: Flame Propagation - Active Particle Diffusion Theory. Ind. and Eng. Chem., vol. 43, no. 12, Dec. 1951, pp. 2718-2721.

113. Walker, P. L., Jr., and Wright, C. C.: Hydrocarbon Burning Velocities Predicted by Thermal Versus Diffusional Mechanisms. Jour. Am. Chem. Soc., vol. 74, no. 15, Aug. 5, 1952, pp. 3769-3771.

114. Mellish, C. E., and Linnett, J. W.: The Influence of Inert Gases on Some Flame Phenomena. Fourth Symposium (International) on Combustion, The Williams & Wilkins Co. (Baltimore), 1953, pp. 407-420.

115. Hoare, M. F., and Linnett, J. W.: The Mechanism of Flame Propagation. Jour. Chem. Phys., vol. 16, no. 8, Aug. 1948, pp. 747-749.

116. Brokaw, Richard S., and Pease, Robert N.: The Effect of Water on the Burning Velocities of Cyanogen-Oxygen-Argon Mixtures. Jour. Am. Chem. Soc., vol. 75, no. 6, Mar. 20, 1953, pp. 1454-1457.

117. Avery, W. H., and Hart, R. W.: Combustor Performance with Instantaneous Mixing. Ind. and Eng. Chem., vol. 45, no. 8, Aug. 1954, pp. 1634-1637.

118. Harris, Margaret E., Grumer, Joseph, von Elbe, Guenther, and Lewis, Bernard: Burning Velocities, Quenching, and Stability Data on Nonturbulent Flames of Methane and Propane with Oxygen and Nitrogen - Applications of Theory of Ignition, Quenching, and Stabilization to Flames of Propane and Air. Third Symposium on Combustion and Flame and Explosion Phenomena, The Williams & Wilkins Co. (Baltimore), 1949, pp. 80-89.

119. Linnett, J. W.: Methods of Measuring Burning Velocities. Fourth Symposium (International) on Combustion, The Williams & Wilkins Co. (Baltimore), 1953, p. 31.

120. Bartholomé, E.: Die Flammengeschwindigkeit in stationär brennenden Flammen. Die Naturwissenschaften, Jahrg. 36, Heft 6, 1949, pp. 171-175.

121. Bartholomé, E.: Die Flammengeschwindigkeit in sehr heissen Flammen. Zs. f. Elektrochemie, Bd. 54, Heft 3, 1950, p. 169.

122. Sachsse, H., und Bartholomé, E.: Beiträge zur Frage der Flammengeschwindigkeit. Zs. f. Elektrochemie, Bd. 53, Heft 4, 1949, pp. 183-190.

123. Simon, Dorothy Martin: Flame Propagation. III. Theoretical Consideration of the Burning Velocities of Hydrocarbons. Jour. Am. Chem. Soc., vol. 73, no. 1, Jan. 1951, pp. 422-425.

124. Walker, P. L., Jr., and Wright, C. C.: Prediction of Hydrocarbon Burning Velocities by Modified Semenov Equation. Jour. Am. Chem. Soc., vol. 75, no. 5, Feb. 5, 1953, pp. 750-751.

125. Gaydon, A. G., and Wolfhard, H. G.: Low-Pressure Flames and Flame Propagation. Fuel, vol. XXIX, no. 1, Jan. 1950, pp. 15-19.

126. Manson, N.: Effect of Pressure on the Fundamental Burning Velocity in Gaseous Mixtures. Fuel, vol. XXXII, 1953, pp. 186-195.

127. Wheatley, P. J., and Linnett, J. W.: Burning Velocity Determinations. Pt. 8 - Some Acetylene + Oxygen + Inert Gas Mixtures. Trans. Faraday Soc., vol. 48, 1952, pp. 338-345.

128. Manson, N.: On the Theory of Burning Velocities in Gas Mixtures. Jour. Chem. Phys., vol. 17, no. 9, Sept. 1949, pp. 837-838.

129. Friedman, Raymond, and Burke, Edward: Burning Velocities. Ind. and Eng. Chem., vol. 43, no. 12, Dec. 1951, pp. 2772-2776.

TABLE IV-I. - COMPARISON OF MAXIMUM FLAME VELOCITIES DETERMINED BY VARIOUS METHODS

[Propane-air at 25° C and 1 atm.]

Method	Type of photography	Tube diam., cm	Equivalence ratio for max. U_F	Max. flame velocity, cm/sec	Reference
Burner:					
Total area (eq. (2b))	Schlieren	1.26	1.06	{43.0, 40.7}	49
Angle, r/r_t in const. velocity range	Schlieren	1.358	1.08	[a]43.2	118
Total area	Shadow, outer edge	1.57	1.12	40.2	16
Total area	Shadow, inner edge with extrapolation to flame axis	1.27 (tube or nozzle)	1.03	[a]45.5	4,15
Total area	Shadow, inner edge	1.57	1.12	45.4	16
Frustum area including cone tip	Shadow, inner edge	----	(1.05)	46.7	47
Frustum area, rectangular burner	Direct, inner luminous edge	0.65×2.55	[b]1.0	[a]41.2	
Frustum area	Direct	1.36	1.07	[a]41.5	119
Frustum area	Direct	0.94	1.05	[a]46.3	8
Total area (eq. (2b))	Direct, center of luminous zone	1.57	1.1	38	16
Angle, at 0.36 to 0.51 r_t	Direct	1.36	1.06	[a]43.3	119
Angle, at common point	Combination of direct and shadow	----	----	[a]48.5	
Particle track	Stroboscopic direct	1.27 (nozzle)	1.05	[a]45.0	4,15
Tube:					
Total area	Direct	2.5	1.14	[a]39.0	38
Bomb:					
Pressure record	None	15-cm sphere	[b]1.0	40.6	45
Flame record	Direct		[b]1.0	40.4	45

[a]Exact temperature not specified but assumed to be ~25° C.

[b]These determinations for stoichiometric mixtures do not represent maximums, but are probably lower than the maximums by no more than 2 cm/sec.

TABLE IV-II. - BOND DISSOCIATION ENERGIES FOR C_4 AND C_6 HYDROCARBONS

AT CONCENTRATION FOR MAXIMUM FLAME VELOCITY

[Tube method; ref. 49.]

Hydrocarbon	Equivalence ratio for maximum U_F, φ_{max}	Deviation of φ_{max} from average φ_{max}, percent	Dissociation energy of hydrocarbon, $\frac{kcal}{g\text{-}mole}$	Dissociation energy of mixture at φ_{max}, $\frac{kcal}{liter}$	Deviation from average, percent
Butane	1.09	5.5	1250	1.93	2.0
Hexane	1.16	.9	1791	2.00	1.5
2-Methylpropane	1.11	3.6	1257	1.94	1.5
2,2-Dimethylbutane	1.12	2.5	1821	1.97	
1-Butene	1.17	1.7	1133	1.98	.5
1-Hexene	1.16	.9	1680	2.02	2.5
Isobutene	1.14	.9	1147	1.97	
2-Methyl-1-pentene	1.19	3.4	1603	1.99	1.0
1-Butyne	1.17	1.7	1016	1.95	1.0
1-Hexyne	1.21	5.0	1564	1.97	.0
4-Methylpentyne	1.18	2.5	1574	1.95	1.0
Benzene	1.34	14.2	1305	1.96	.5
Average	1.15	3.29	----	1.96	0.9

TABLE IV-III. - EMPIRICAL COEFFICIENTS FOR CALCULATING MAXIMUM

FLAME VELOCITY FROM HYDROCARBON STRUCTURE

[Ref. 53.]

Type C-H Bond	Coefficient[a], $cm/(sec)(bond/cm^3)$
Methane	$K_A = 90\times10^{-19}$
Primary	$K_B = 109$
Secondary	$K_C = 122$
Tertiary	$K_D = 116$
Cyclohexyl	$K_G = 129$
Alkene	$K_E = 207$
Aromatic	$K_H = 216$
Alkyne	$K_F = 574$

[a]Relative to propane.

TABLE IV-IV. - VALUES OF EMPIRICAL EQUATIONS[a] FOR EFFECT OF ψ ON RELATIVE MAXIMUM FLAME VELOCITY[b]

[Pressure, 1 atm.]

Fuel	T_o, °K	Range of ψ, $\frac{O_2}{(O_2 + N_2)}$	B	C	B'	b	C_{av}	Method and reference[c]
Methane	Room	0.21-0.50	1290	0.135				1
		.18- .50	1550	.144				2
		.21- .50	1520	.143				3
		.20- .50	1420	.140				4
Propane	311	0.17-0.50	1420	0.140	1.79	1.16	0.133	5
	422	.17- .50	1195	.126				
	Room	.21- .42	1290	.135				4
Isooctane	311	0.21-0.50	1172	0.125	0.381	1.40	0.120	5
	422	.21- .50	1056	.115				
Ethene	311	0.17-0.35	1085	0.118	1.23	1.18	0.113	5
	422	.17- .35	981	.108				
	Room	.21- .50	1100	.12				3
Acetylene	Room	0.11-0.24	770	0.08				4
Hydrogen	Room	0.13-0.25	620	0.05				1
Carbon monoxide	Room	0.13-0.25	600	0.04				1

[a] $U_{F,rel} = B(\psi - C)$; $U_{F,rel} = B'T_o^b(\psi - C_{av})$.

[b] $U_{F,rel}$ is maximum flame velocity (with respect to equivalence ratio) relative to arbitrary value of 100 for $\psi = 0.21$ and $T = 298°$ K.

[c] Method and reference:
1. Cone-height, total-area method of eq. (2a); ref. 8, pp. 459-466.
2. Luminous-cone, frustum-area method of eq. (5); ref. 8, p. 467.
3. Soap-bubble method; ref. 39.
4. Schlieren image (line of maximum intensity obtained with horizontal knife edge), special angle method with nozzle burner; ref. 69.
5. Schlieren-image (outer edge of image obtained with horizontal knife edge), total-area method of eq. (26); ref. 66.

TABLE IV-V. - SUMMARY OF BURNING-VELOCITY CORRELATIONS

Type of data	Combustion system	Correlations with diffusion theories				Correlations with thermal theories	
		U_F vs. active-particle concentrations	Reference	Equation	Reference	Equations and properties	Reference
Range of mixture concentrations	$CO-O_2-N_2$ plus H_2O or H_2	U_F vs. p_H, nonlinear	103	Tanford-Pease	104, 108	U_F vs. $\left(\frac{T_F-T_o}{T_{1g}-T_o}\right)$	115
	$C_2N_2-O_2-A$ plus H_2O or D_2O	U_F^2 vs. p_{OH}, linear	116	Tanford-Pease	116		
	$H_2-O_2-N_2$			Tanford-Pease	104		
	$CH_4-O_2-N_2$			Tanford-Pease	104		
	$C_2H_4-O_2-N_2$	U_F vs. $6.5\ p_H+p_O+p_{OH}$, nonlinear	66, 101, 39	Tanford-Pease	49	U_F vs. $\left(\frac{T_F-T_o}{T_{1g}-T_o}\right)$	101
			Fig. IV-23	Manson	49	Semenov eq.	49
	$C_3H_8-O_2-N_2$	U_F vs. $6.5\ p_H+p_O+p_{OH}$, nonlinear	66	Tanford-Pease		Semenov eq.	49
		U_F vs. $\sqrt{6.5\ p_H+p_O+p_{OH}}$, nonlinear	Fig. IV-22	Manson	49		
	$C_3H_4-O_2-N_2$	U_F vs. $6.5\ p_H+p_O+p_{OH}$, nonlinear	39 Fig. IV-23	Tanford-Pease	39	Semenov eq.	Unpub.
	$C_5H_{12}-O_2-N_2$ (pentane)	U_F vs. $6.5\ p_H+p_O+p_{OH}$, nonlinear	39 Fig. IV-23	Tanford-Pease	39	Semenov eq.	Unpub.
	$C_8H_{18}-O_2-N_2$ (2,2,4-trimethylpentane)	U_F vs. $6.5\ p_H+p_O+p_{OH}$, nonlinear	66	Tanford-Pease	49	Semenov eq.	49
		U_F vs. $\sqrt{6.5\ p_H+p_O+p_{OH}}$, nonlinear	66	Manson	49		

TABLE IV-V. - Continued. SUMMARY OF BURNING-VELOCITY CORRELATIONS

Type of data	Combustion system	Correlations with diffusion theories				Correlations with thermal theories	
		U_F vs. active-particle concentrations	Reference	Equation	Reference	Equations and properties	Reference
Series of compounds at maximum burning velocity	Paraffins, olefins, diolefins, acetylenes, and benzene in air	U_F vs. p_H	120, 121, 122	Tanford-Pease	112	U_F vs. T_F	112, 120, 122
		U_F vs. 6.5 $p_H+p_O+p_{OH}$, nonlinear	112, 123	Manson	49	Semenov eq.	113, 124
	Nonhydrocarbons in air	U_F vs. 6.5 $p_H+p_O+p_{OH}$	111				
Different initial temperatures	CH_4-O_2-N_2	U_F vs. p_H, linear	16	Tanford-Pease	49	Semenov eq.	49
		U_F vs. 6.5 $p_H+p_O+p_{OH}$, linear	Fig. IV-21 16	Manson	49		
	C_2H_4-O_2-N_2	U_F vs. p_H, linear	16	Tanford-Pease	49	Semenov eq.	49
			Fig. IV-21	Manson	49		
	C_3H_8-O_2-N_2	U_F vs. p_H, linear	16	Tanford-Pease	49, 16	Semenov eq.	49
		U_F vs. 6.5 $p_H+p_O+p_{OH}$, linear	Fig. IV-21 16	Manson	49		
Additives	C_3H_8-O_2-N_2 plus various compounds[a]	U_F vs. 6.5 $p_H+p_O+p_{OH}$, nearly linear	55				
Pressure dependence of burning velocity	Various hydrocarbons in air or oxygen			Tanford-Pease	103	Semenov eq.	
				Gaydon-Wolfhard	106, 125		
				Manson	126		

[a]Isooctane, benzene, acetone, methylethyl ketone, carbon monoxide, acetaldehyde, diethyl ether, oxygen, hydrogen, and nitrogen.

TABLE IV-V. - Concluded. SUMMARY OF BURNING-VELOCITY CORRELATIONS

Type of data	Combustion system	Correlations with diffusion theories				Correlations with thermal theories	
		U_F vs. active-particle concentrations	Reference	Equation	Reference	Equations and properties	Reference
Isotope substitution	C_2H_2 or C_2D_2			Tanford-Pease	6	Damköhler eq.	6
Change of diluent	$CO-O_2$-A or He		Table IV-XII	Ratio of $\sqrt{D}$ calculated	114, 127	Ratio of $\sqrt{\alpha}$ calculated	114, 127
	H_2-O_2-A or He		Table IV-XII	Ratio of $\sqrt{D}$ calculated	119, 114, 127	Ratio of $\sqrt{\alpha}$ calculated	119, 114, 127
	CH_4-O_2-A or He		Table IV-XII	Tanford-Pease Ratio of $\sqrt{D}$ calculated	67 49	Ratio of $\sqrt{\alpha}$ calculated	49
	$C_2H_2-O_2$-A or He		Table IV-XII	Ratio of $\sqrt{D}$ calculated	114, 127	Ratio of $\sqrt{\alpha}$ calculated	114, 127
	$CH_4-O_2-N_2$ or A			Tanford-Pease	67		
	Butadiene-O_2-N_2 or He			Tanford-Pease Manson	71 128		

TABLE IV-VI. - MAXIMUM FLAME VELOCITIES

[Relative to arbitrary value of 100 for nitrogen with primary air in which nitrogen was replaced by indicated inert gas.]

Fuel	Reference	Method	$\frac{O_2}{O_2+inert}$	$U_{F,rel}$ with inert gas		
				Argon	Helium	CO_2
Methane	69	Shadow total-area	0.21	231	327	
	17, p. 2	Spatial velocity in tube	.21	270	320	
	68	Tube, area	.21	[a]231	[a]321	
	67 for A, He	Schlieren	.21	185	300	
		total-area	.30	155	260	24
			.40	140	200	26
	8, p. 465 for CO_2	Cone-height	.60	115	150	54
		total-area	.80	105	115	76
Propane	67	Schlieren	0.21	180	280	
		total-area	.32	140	235	
			.42	120	160	
			.57	110	150	
Ethene	70	Soap-bubble	0.21	151	217	
Butadiene	71		0.21		332	
Acetylene	70	Soap-bubble	0.21	146	225	26
	67	Schlieren	.11	190	340	
		total-area	.21	145	215	
Hydrogen	68	Spatial velocity in tube	0.21	135	[b]135	
	72	Cone-height total-area	.12	[c]115	[c]275	
	8, p. 460	Cone-height	.21			50
		total-area	.30			68
			.50			85
			.80			96
Carbon monoxide containing 1.5 percent H_2, 1.35 percent H_2O	8, p. 462	Cone-height total-area	0.21			52
			.40			70
			.60			86
			.80			94

[a]No nitrogen value was given; these are based on relative value for argon from ref. 69.

[b]Same value was also given for neon; results seem questionable in view of ref. 72.

[c]No nitrogen value was given for this inert concentration; relative values are based on interpolated nitrogen value from ref. 8, p. 460.

TABLE IV-VII. - FLAME VELOCITY MEASUREMENTS OF STOICHIOMETRIC HYDROCARBON-AIR MIXTURES

[Constant-volume bomb and rectangular-burner, inner-luminous-edge, frustum-area methods; ref. 73.]

Fuel	Pressure, mm Hg	Flame velocity, cm/sec		
		Bomb method		Burner method
		Pressure record	Flame record	
Methane	253			38.1
	380			37.8
	532	36.0	36.3	
	760	36.6	36.4	37.0
Propane	253			39.9
	523	40.2	40.5	
	760	40.6	40.4	41.2
Ethene	38	62.5	63.0	
	76	62.7	62.9	
	152	63.0	63.5	
	380	62.8	63.3	
	760	63.1	63.0	
	1140	62.3	62.5	

TABLE IV-VIII. - EFFECT OF PRESSURE ON FLAME VELOCITY

System	φ	Pressure range, atm	Approximate pressure dependence	Method and reference[a]
Methane-air	1.00	0.7 -1.0	None	1
	1.00	.33-1.0	None	2
	1.00	.25-1.0	$p^{-0.24}$	3
	or φ_{max}	1.0 -6.3	$p^{-0.45}$	3
	1.46	.25-6.3	$p^{-0.5}$	3
	.60- .65	.26- .66	$p^{-0.49}$	4
Propane-air	1.00	0.7 -1.0	None	1
	1.00	.33-1.0	None	2
	φ_{max}	.03-1.0	None	5
	1.00		log p	6
	.56	.26- .66	$p^{-0.30}$	4
	φ_{max}	1-5	None	7
Butane-air	φ_{max}	0.25-1.0	$p^{0.17}$	3
n-Heptane-air	1.00	0.53-0.99	$p^{-0.36}$	8
Isooctane-air	1.00	0.53-0.92	$p^{-0.39}$	8
Ethene-air	1.00	0.33-1.0	log p	6
	1.00	.05-1.5	None	1
	1.08-1.24	.30- .80	None	9
	1.4	.35-1.0	$p^{-0.39}$	10
	.46	.26- .66	$p^{-0.31}$	4
Acetylene-air	φ_{max}	0.01-1.0	None	11
	0.33	.26- .66	$p^{-0.47}$	4
Acetylene-O_2	φ_{max}	0.01-1.0	None	11
Benzene-air	1.00	0.40-0.92	$p^{-0.31}$	8

[a]Methods and references:
1. Constant-volume bomb, pressure record or flame record; ref. 73.
2. Rectangular burner, luminous cone, frustum-area; ref. 73.
3. Burner, inner edge of luminous zone, total area; no effect of tube diameter from 1 to 2 cm; ref. 78.
4. Flat flame burner, luminous zone, total area; ref. 19.
5. Burner, luminous cone, angle; ref. 75.
6. Burner, luminous cone, angle; ref. 77.
7. Spatial velocity in tube (drum camera); ref. 79.
8. Ref. 80.
9. Soap-bubble; ref. 76.
10. Burner; ref. 81.
11. Burner, luminous cone, angle; ref. 74.

TABLE IV-IX. - EFFECT OF INITIAL MIXTURE TEMPERATURE ON LAMINAR FLAME VELOCITY

[Empirical equations for flame velocity relative to arbitrary value of 100 at 25° C; pressure, 1 atm. Calculations can only be made when B, C, and b are given.]

Fuel	Oxidant	T_o range, °K	$U_{F,rel} = B + CT_o^b$			Method and reference[a]
			B	C	b	
Methane	Air	293-703			1.70	1
		293-			2.00	2
		141-615	24	0.47×10^{-3}	2.11	3
	Oxygen	273-1273	30		[c]~1.70	4
Ethane	Oxygen	273-773	23		[c]2.00	4
Propane	Air[d]	322-411	(e)	38.0×10^{-3}	1.38	5
	Air	307-615	(e)	5.32	1.72	6
		200-617	25	.85	2.00	3
		307-867				7
	Oxygen	273-773	32		[c]2.00	4
Isooctane	Air[d]	311-422		11.9×10^{-3}	1.40	5
Decane	Air	367-411	(e)	7.39×10^{-3}	1.67	8
1-Decene	Air	367-411	(e)	1.99×10^{-3}	1.90	8
Benzene	Air	311-395	(e)	3.95×10^{-3}	1.78	8
Toluene	Air	318-422	(e)	28.90×10^{-3}	1.43	8
Ethene	Air	293-			2.00	2
	Air[d]	322-411	(e)	23.4×10^{-3}	1.47	5
	Air	307-615	(e)	12.6	1.565	6
		200-617	16	4.05	1.74	3
Acetylene	Air	417-590			[f]1.80	9
Hydrogen	Air	293-			2.00	2
Carbon monoxide	Air (dry)	293-733			2.00	1
	Air (dry)	291-873	0	4.8×10^{-3}	1.75	10
	Air (dry)	293-			2.00	2
	Air (moist)	293-			2.00	2
Natural gas	Air	332-756			2.00	9
City gas	Air	293-				2
		293-773			[g]1.74	11
Coke oven gas	Air	283-673			1.64	12

[a]Methods and references:
1. Luminous-cone-height total-area by eq. (2a); ref. 83.
2. Luminous-cone-height total-area by eq. (2a); ref. 84.
3. Inner or outer edge of cone shadow, total-area by eq. (2b); ref. 16.
4. Luminous-cone-height total-area by eq. (2a); ref. 86.
5. Outer edge of schlieren cone (horizontal knife edge advanced downward), total-area by eq. (2b); ref. 66.
6. Inner or outer edge of cone shadow, total-area by eq. (2b); ref. 85.
7. Outer edge of schlieren cone (horizontal knife edge advanced downward), total-area by eq. (2b); ref. 87.
8. Luminous-cone angle at 0.5 r_t; ref. 52.
9. Schlieren; ref. 88.
10. Luminous-cone total-area; ref. 89.
11. Luminous-cone total-area; ref. 37.
12. Luminous-cone-height total-area by eq. (2b); ref. 37.

[c]These constants based on authors' belief that Sachsse had not corrected his flame velocities for expansion due to preheating. All Sachsse's curves are for lean fuel-oxygen mixtures.

[d]Same relation successfully used empirically for $O_2/(O_2 + N_2) = 0.25$ to 0.50; ref. 54.

[e]Deliberately equated to zero to simplify expression for engine application.

[f]Range of data too limited and/or data scatter too great to rely on results.

[g]Preheated only air.

TABLE IV-X. - PERCENTAGE AVERAGE DEVIATION IN RATIO OF PREDICTED TO MEASURED FLAME VELOCITY

Hydrocarbon	Concentration, equivalence ratio	$\frac{O_2}{O_2 + N_2}$, mole fraction	Initial temperature, °K	Burning-velocity range, cm/sec	Average deviation[a]				
					Semenov equation (bimolecular) using $\bar{P}$	Tanford-Pease equation		Manson equation	
						$\bar{k}_w$	$\bar{E}_w$ from T_o data	Using $\bar{k}_H$	Using $\bar{k}_\Sigma$
Methane	Stoichiometric ±0.20	0.21	307	25-36	7.4	5.7	7.0	23.6	1.8
	Max. burning velocity	0.21	200-615	19-133	2.7	7.8	0.8	10.3	10.1
Propane	Stoichiometric ±0.20	0.21	302	25-40	4.0	0.6	---	15.1	1.2
	Max. burning velocity	0.21	200-615	23-141	2.1	6.1	---	10.0	13.0
		0.17-0.50	422	33-305	12.4	5.2	---	12.7	13.0
Ethene	Stoichiometric ±0.20	0.21	298	58-65	5.0	3.7	3.3	10.1	1.8
	Max. burning velocity	0.21	200-615	35-196	1.8	5.8	1.8	12.0	13.8
		0.17-0.35	422	69-287	3.0	4.6	---	6.8	5.3

[a]Average deviation from unity of $(\bar{C}/C)^{1/2}$ where C is remaining "constant" unknown quantity in flame velocity equation. For example, for the Semenov equation, C is steric factor P, and percent average deviation is calculated $\frac{\sum_1^n \left|(P/P)^{1/2} - 1\right|}{n} \times 100$, where n is number of data points.

TABLE IV-XI. - HYDROGEN ATOM CONCENTRATION IN COMBUSTION ZONE OF MOIST CARBON MONOXIDE - OXYGEN FLAMES

[Ref. 104.]

x, cm	Local mixture temperature, °K	H atom, mole fraction	
		Local equilibrium	Diffusion (eq. (54))
0	2930	2.4×10^{-3}	2.40×10^{-3}
.002	2630	8.5×10^{-4}	2.37
.004	2330	2.3×10^{-4}	2.34
.006	2030	4.0×10^{-5}	2.32
.008	1740	4.4×10^{-6}	2.29
.010	1460	2.2×10^{-7}	2.26

TABLE IV-XII. - COMPARISONS FOR FLAMES WITH ARGON AND HELIUM AS INERT

[Ref. 114.]

Fuel	Fuel, percent	Inert, percent	Ratio: $\frac{\text{Property with He as inert}}{\text{Property with A as inert}}$				
			U_F	$\sqrt{\varkappa}$	$\sqrt{D_H}$	$\sqrt{D_{OH}}$	$\sqrt{D_O}$
C_2H_2	8	73	1.61	2.69	1.30	1.39	1.41
	10	71	1.54	2.67	1.28	1.38	1.39
	13	69	1.55	2.64	1.27	1.35	1.37
$CO(H_2O)$	50	20	1.09	1.37	1.06	1.07	1.08
	37	40	1.28	1.95	1.13	1.15	1.18
CH_4	10	71	1.39	2.65	1.29	1.39	1.41
H_2	21	68	2.40	1.94	1.32	1.47	1.51
C_2H_4	6	75	1.42	2.71	1.24	1.42	1.44
	7.7	73	1.43	2.70	1.23	1.40	1.43
	10	71	1.46	2.68	1.22	1.38	1.41

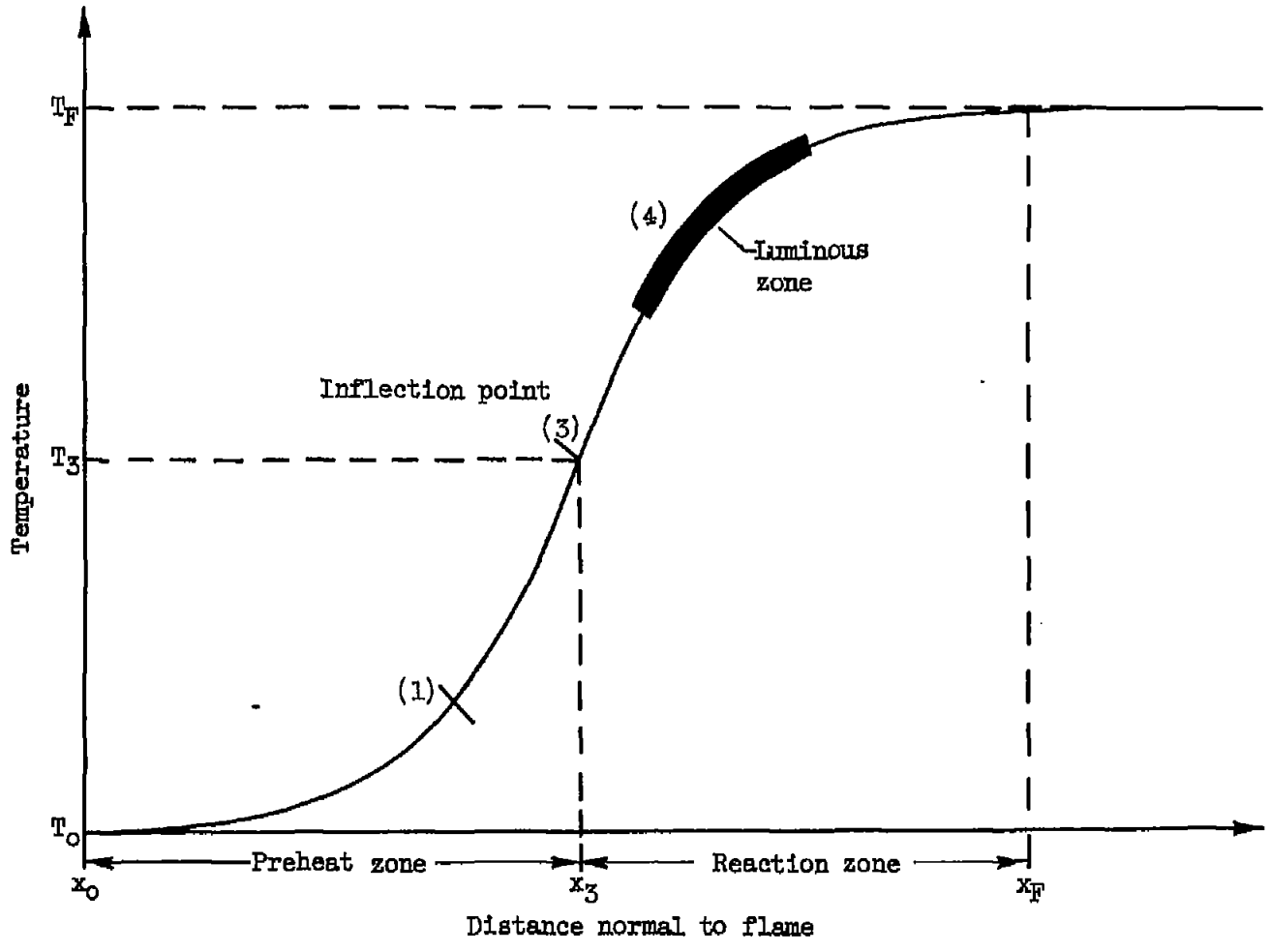

Figure IV-1. - Qualitative temperature-distance diagram for stationary flame.

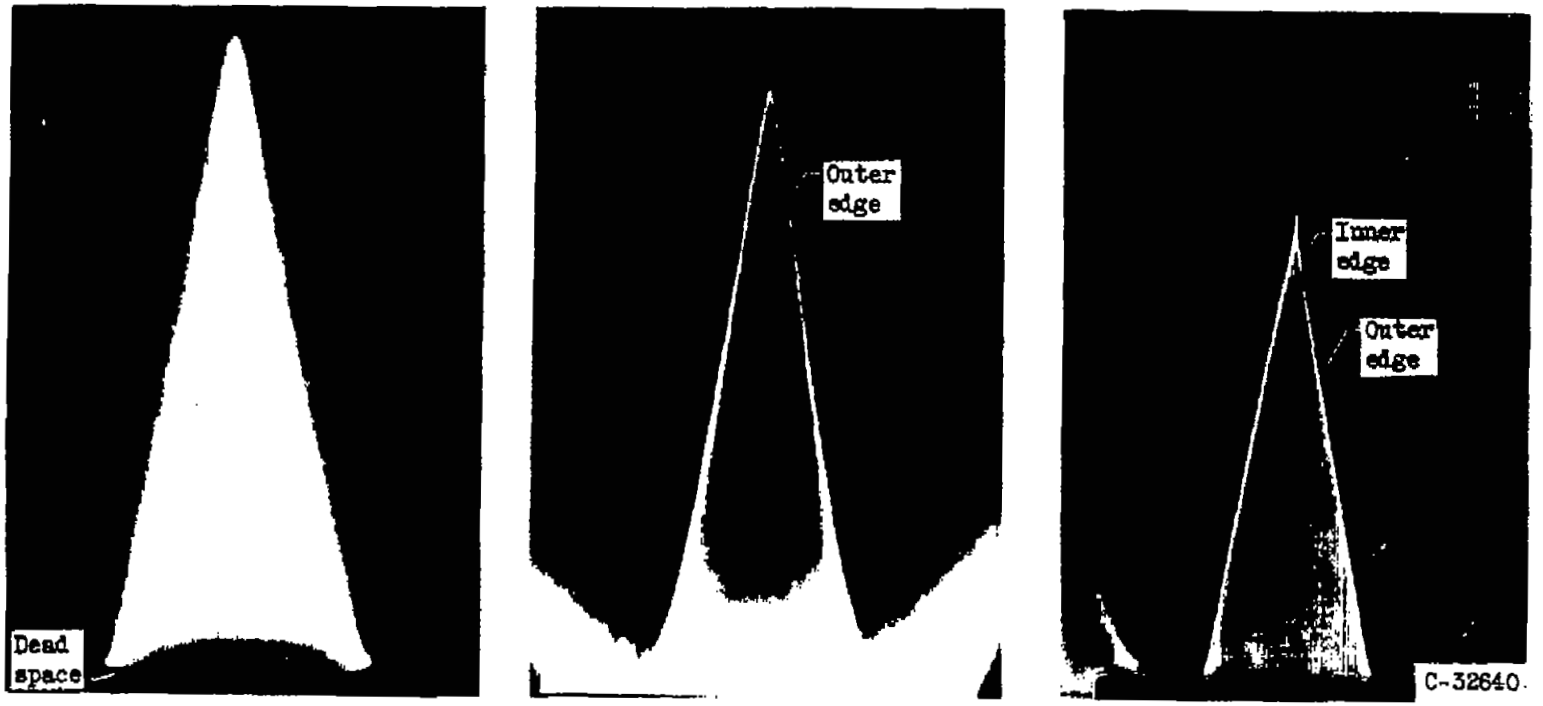

(a) Direct. (b) Schlieren. (c) Shadow.

Figure IV-2 - Typical photographs of laminar Bunsen flames.

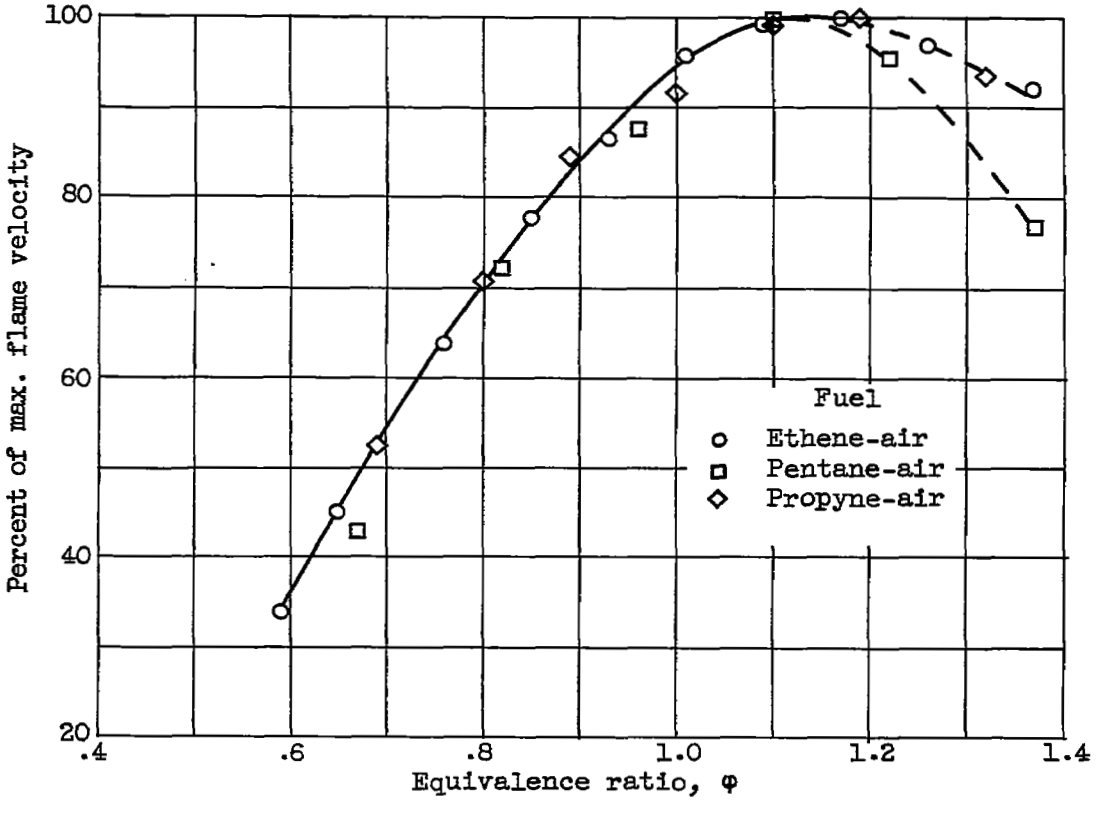

Figure IV-3. - Change in relative flame velocity with equivalence ratio at 25° C and 1 atmosphere (ref. 39).

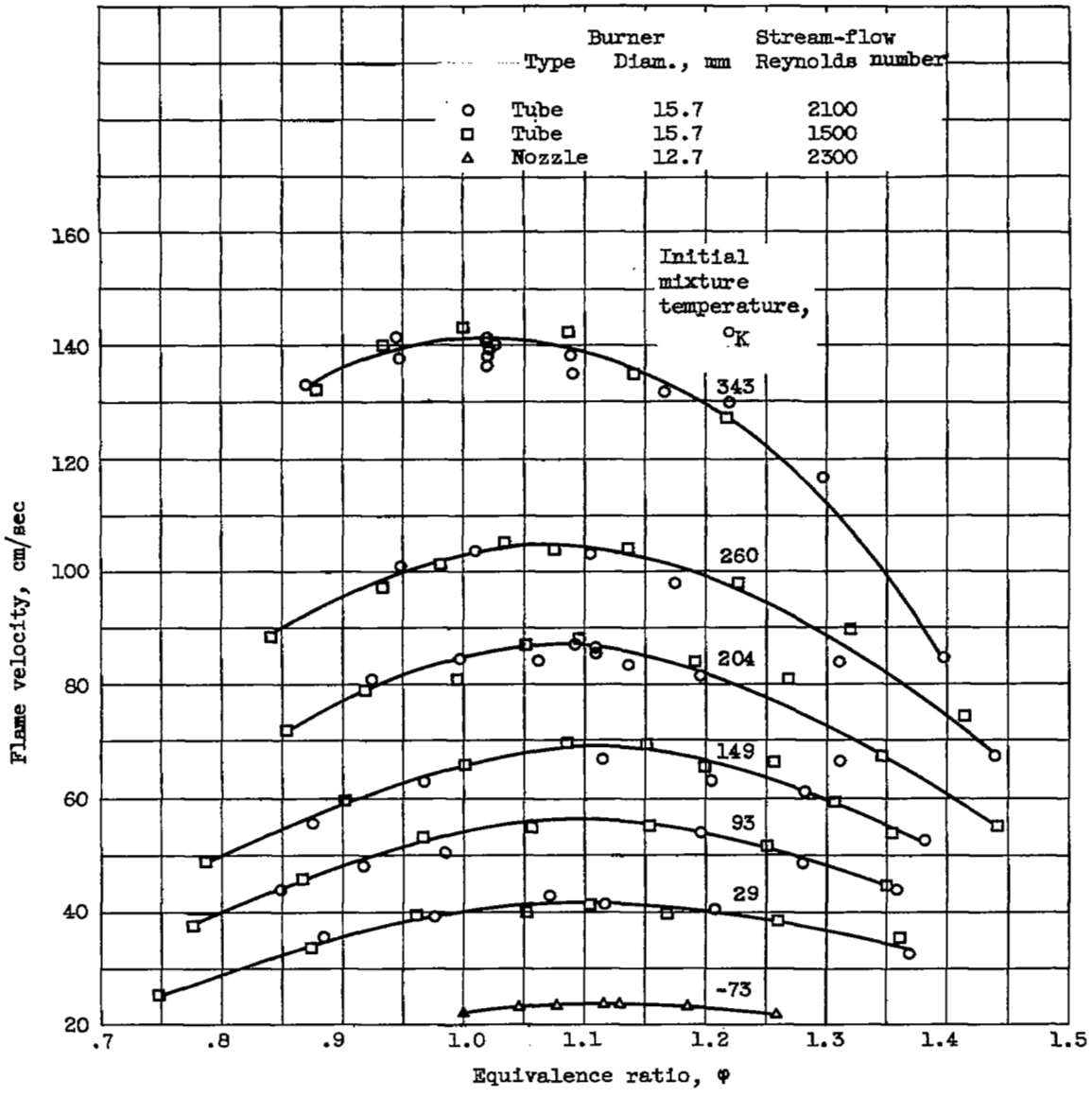

Figure IV-4. - Flame velocity as function of equivalence ratio at various initial mixture temperatures for propane-air flames at 1 atmosphere, measured by outer-shadow-edge total-area burner method (ref. 16).

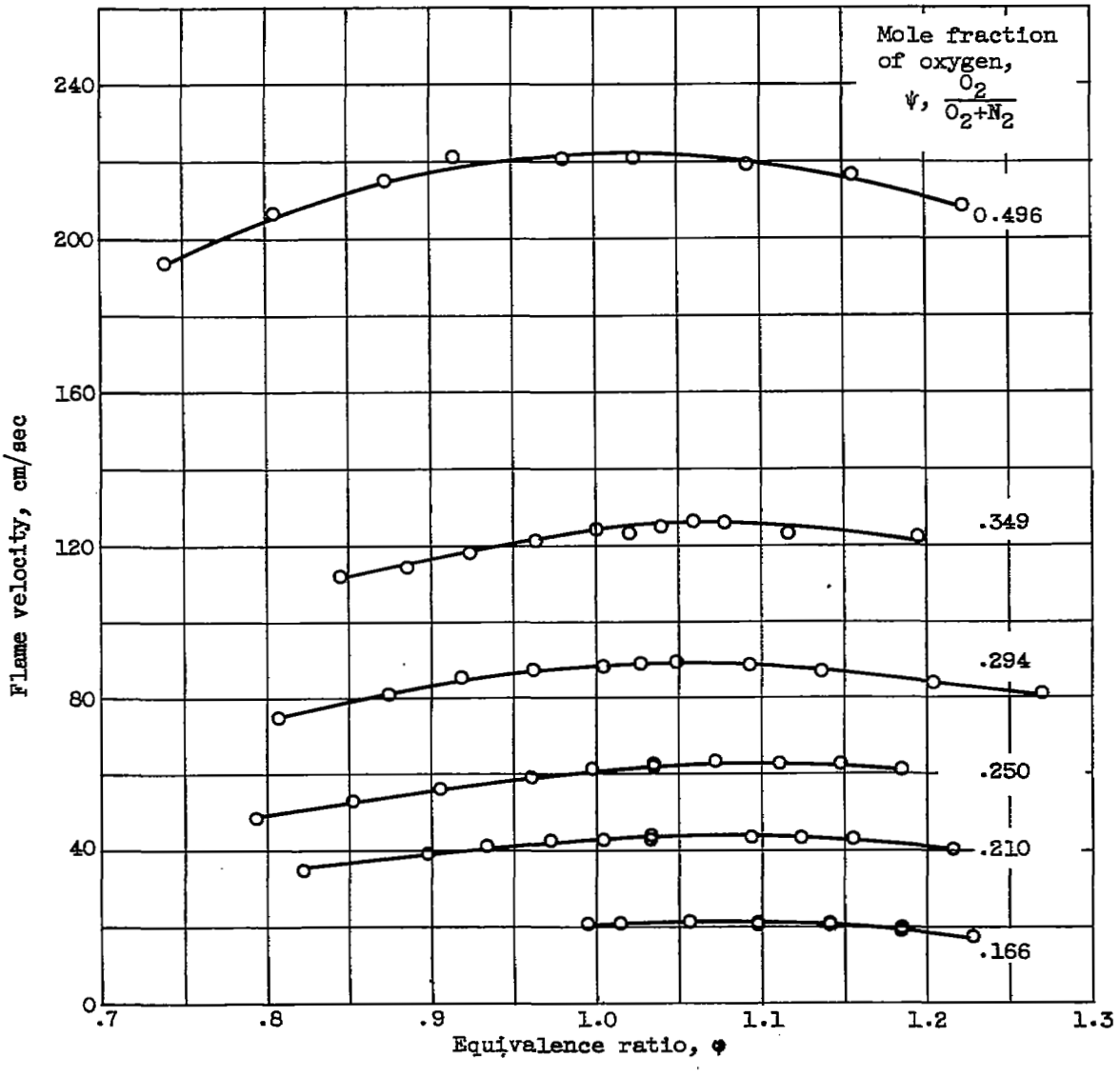

Figure IV-5. - Flame velocity as function of equivalence ratio over range of oxygen concentrations for propane-oxygen-nitrogen mixtures at 311° K, measured by schlieren total-area burner method (ref. 48).

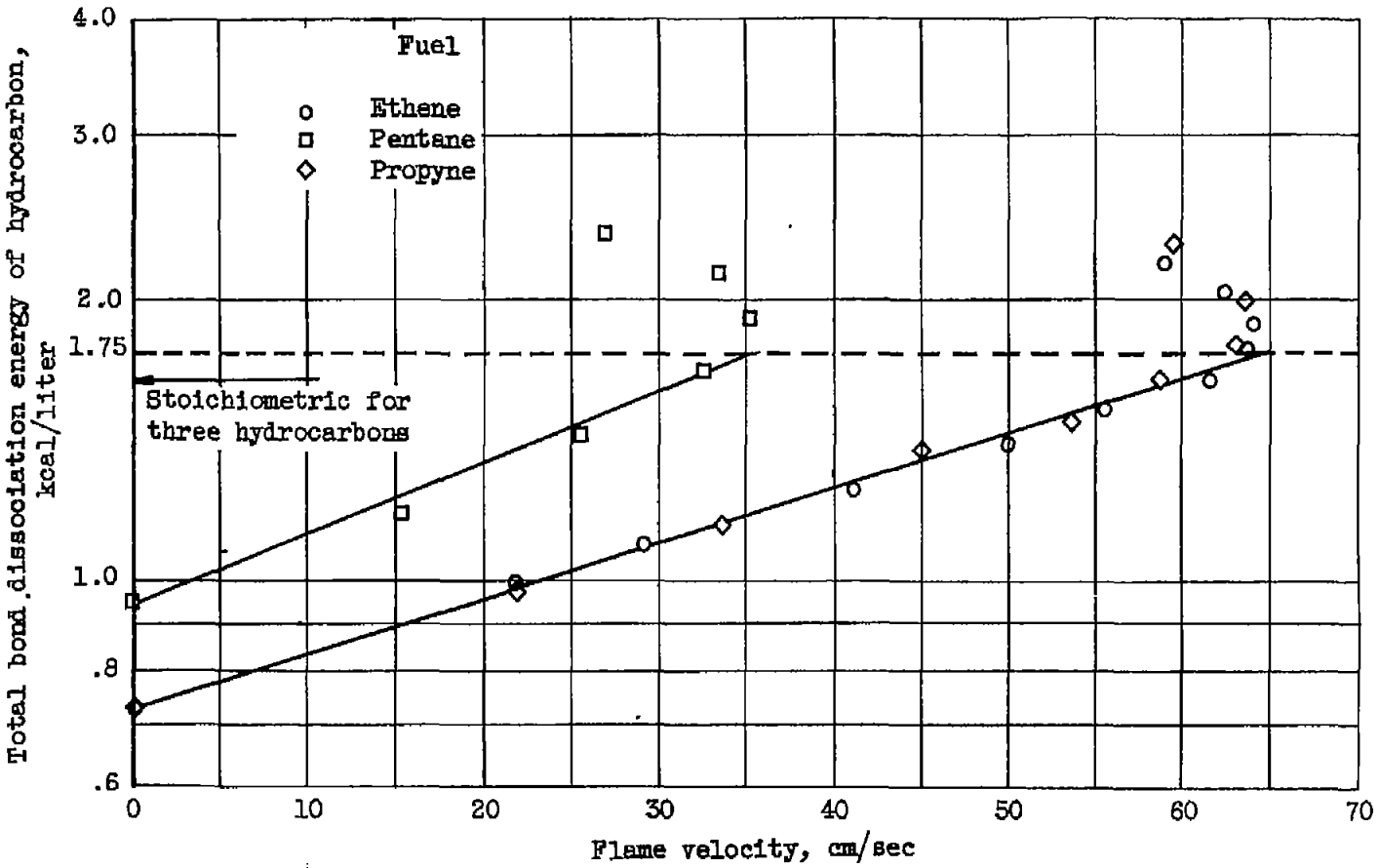

Figure IV-6. - Empirical correlation for equivalence ratio data. Tube method (ref. 49).

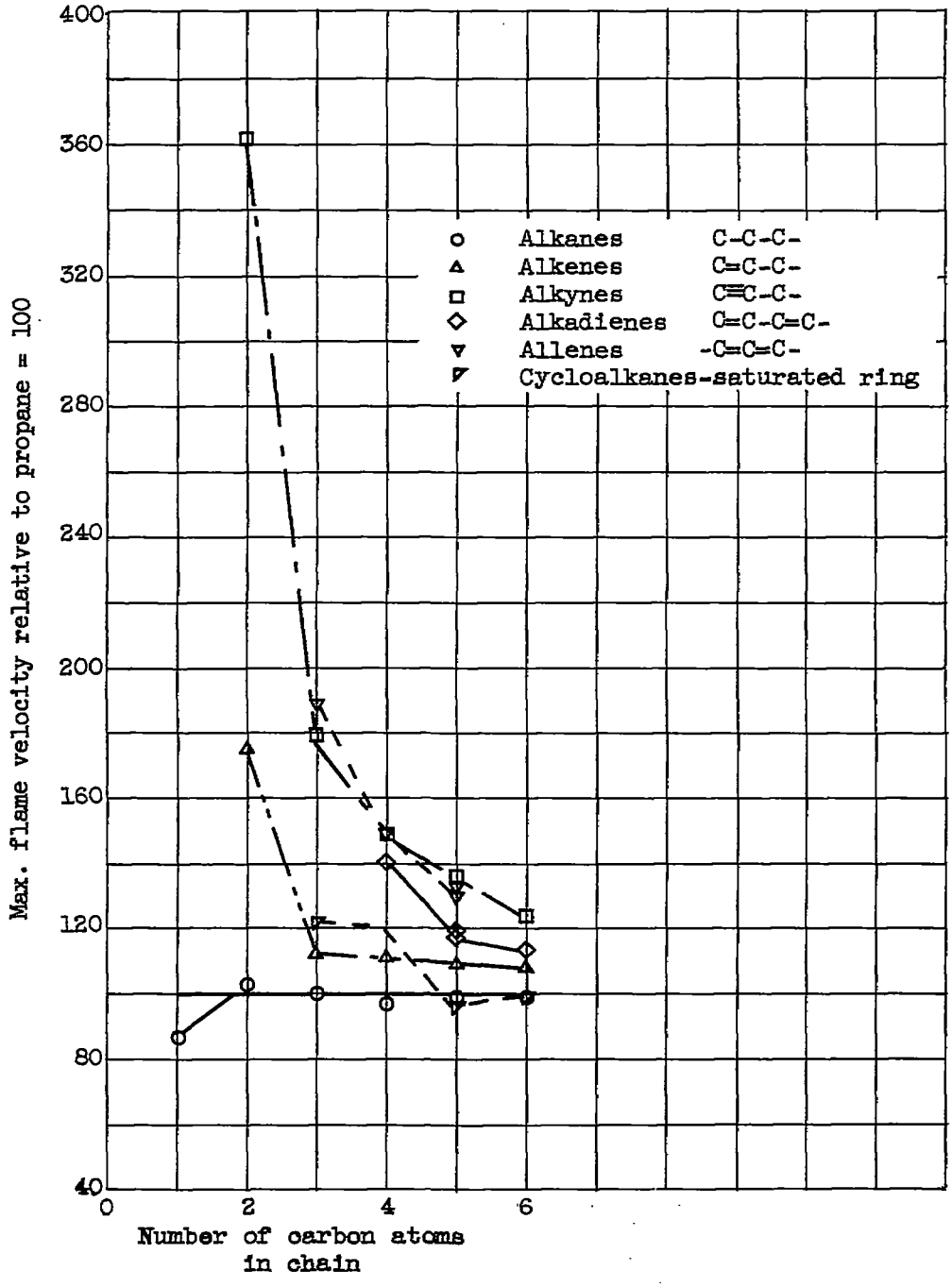

Figure IV-7. - Effect of chain length and saturation on relative flame velocities of straight-chain (or non-substituted ring) hydrocarbons at 25° C and 1 atmosphere (by permission from refs. 38, 40, and 46).

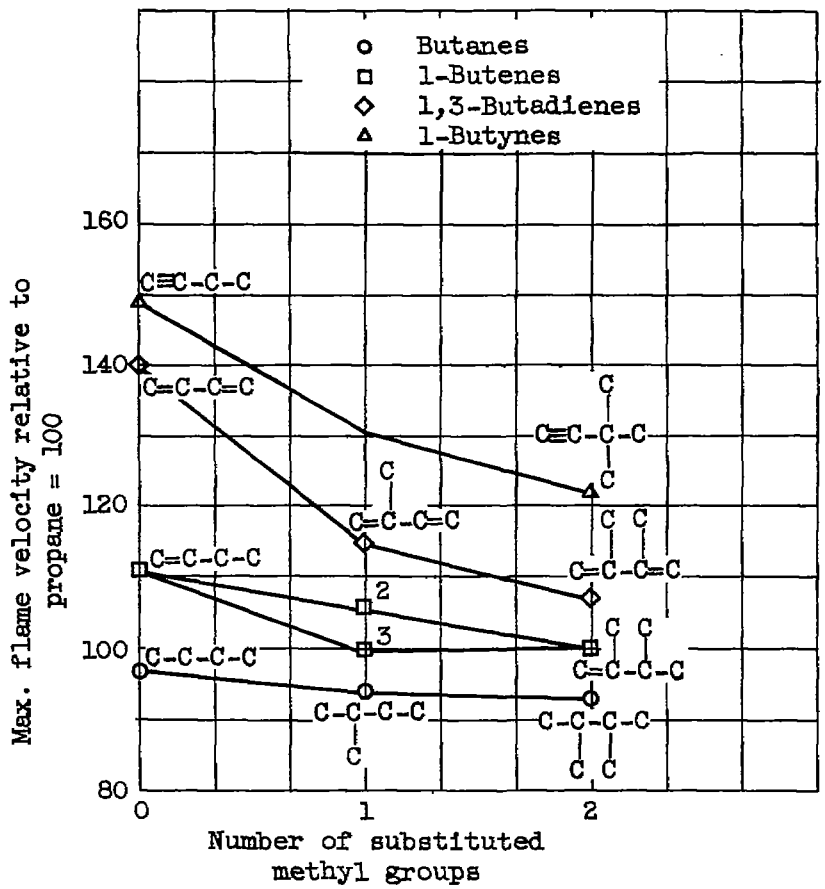

Figure IV-8. - Effect of methyl substitution on relative flame velocities of four-carbon-atom, straight-chain hydrocarbons (by permission from ref. 46).

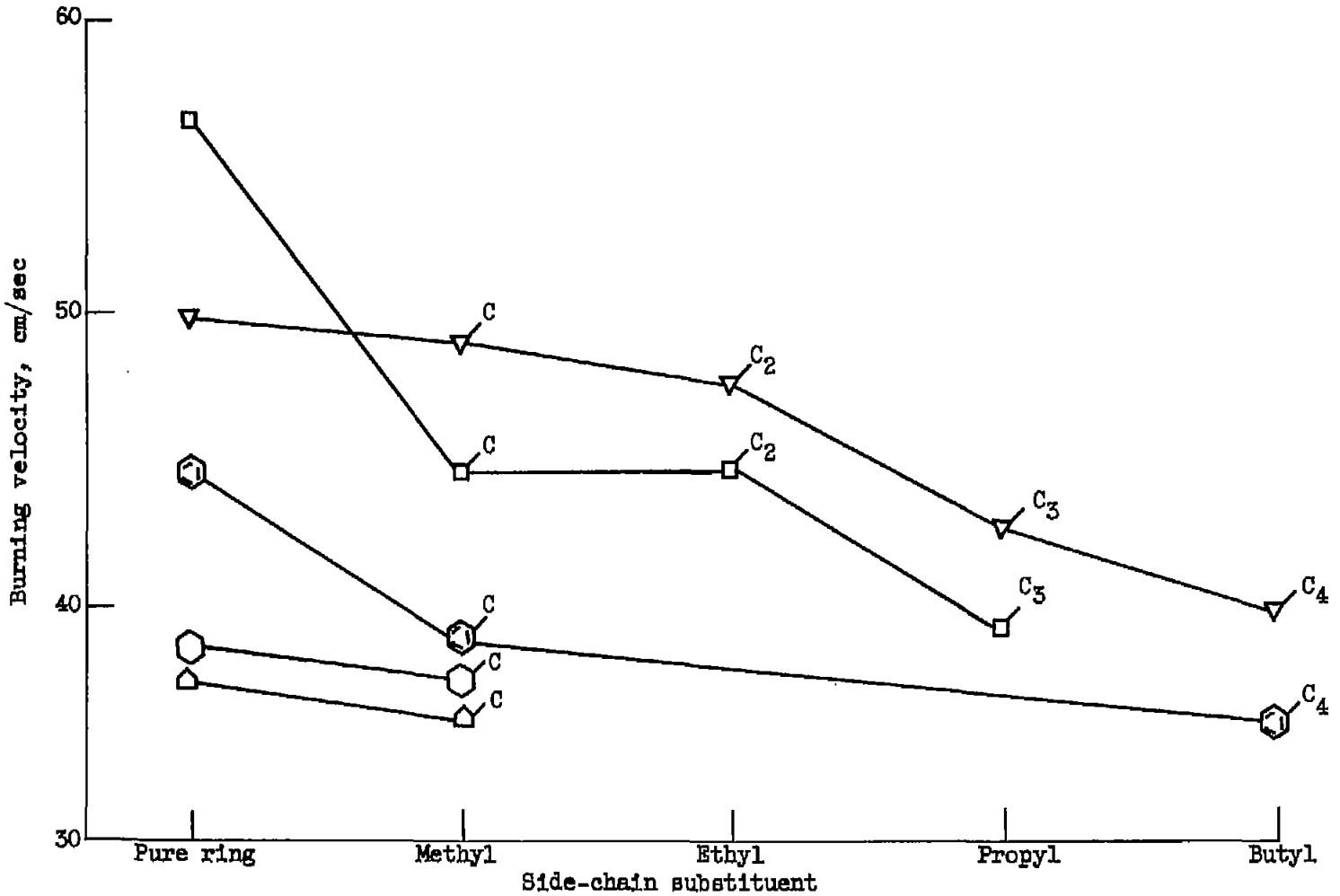

Figure IV-9. - Effects of ring size and substitution on burning velocity trends in cyclic hydrocarbons (by permission from ref. 52).

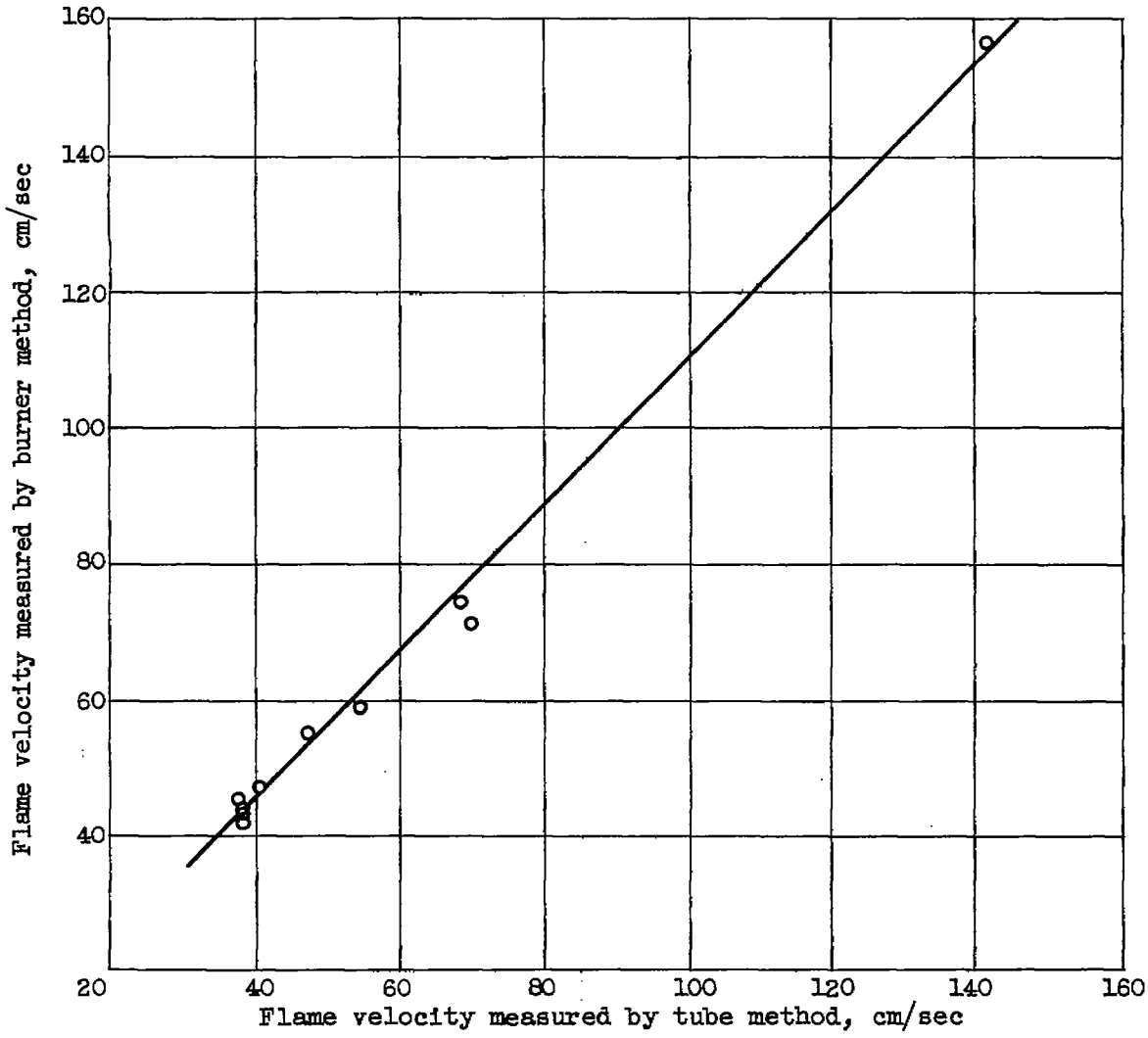

Figure IV-10. - Comparison of flame velocities measured by the inner-shadow-edge burner method (ref. 47) with values measured by tube method (ref. 40).

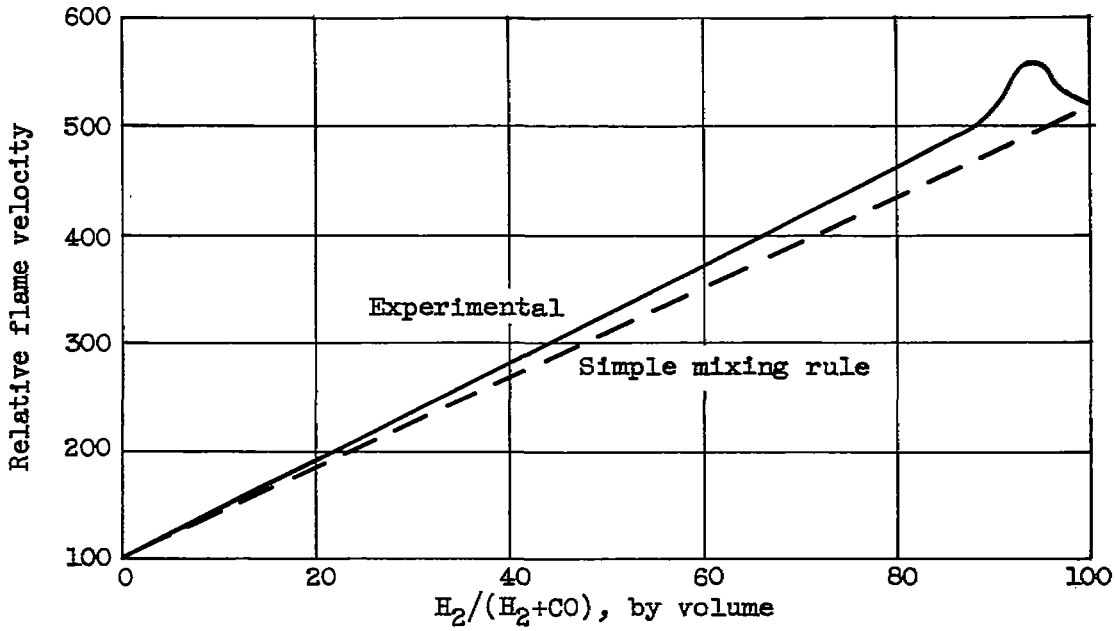

Figure IV-11. - Comparison of experimental data with simple mixing rule for flame velocities of hydrogen - carbon monoxide mixtures (ref. 59).

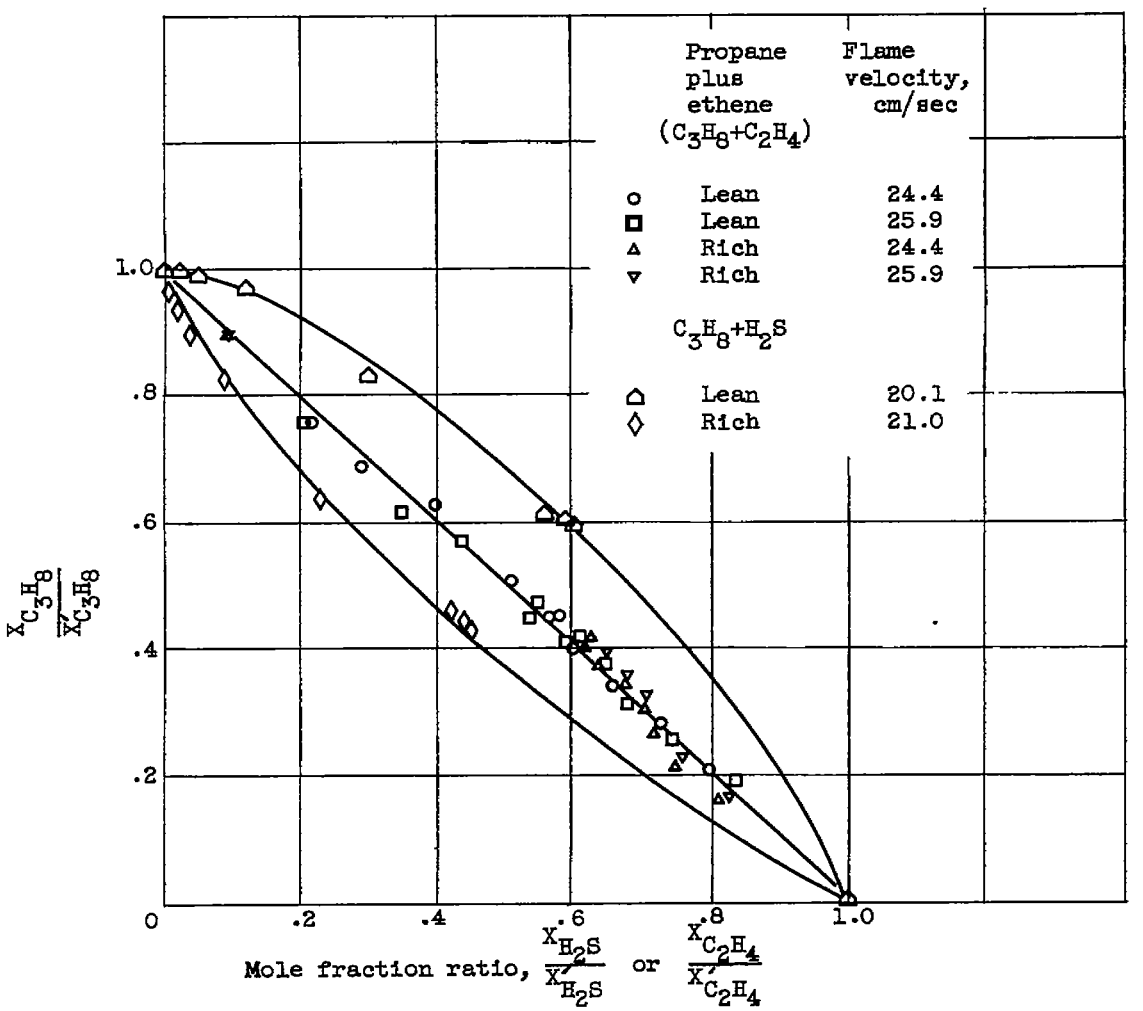

Figure IV-12. - Relation between $\frac{X_{C_3H_8}}{X'_{C_3H_8}}$ and $\frac{X_{H_2S}}{X'_{H_2S}}$ and between $\frac{X_{C_3H_8}}{X'_{C_3H_8}}$ and $\frac{X_{C_2H_4}}{X'_{C_2H_4}}$ for lean and rich binary fuel mixtures at constant flame velocity levels (reprinted by permission from ref. 62).

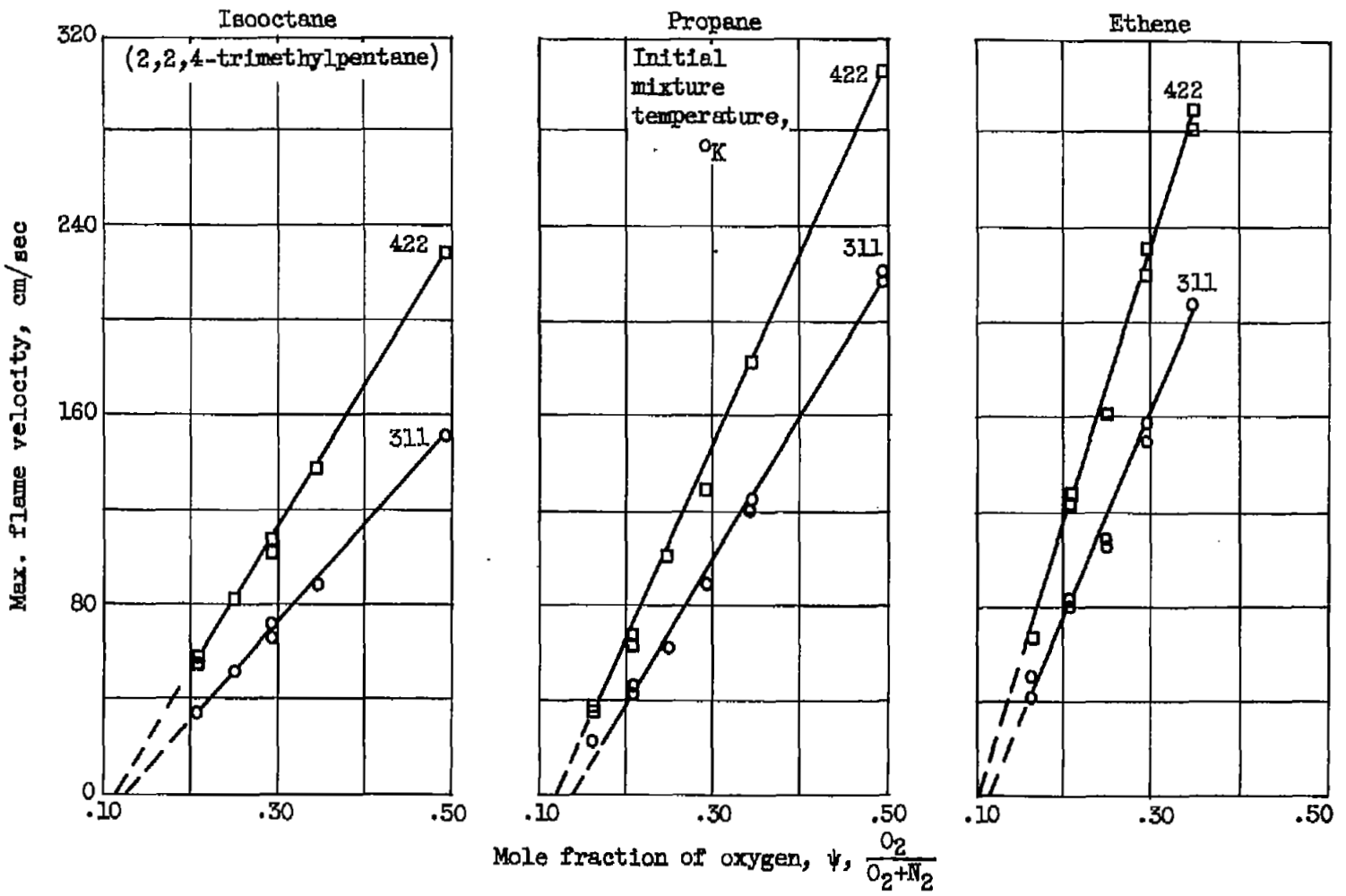

Figure IV-13. - Effect of oxygen concentration on maximum flame velocities; schlieren total-area method (ref. 66).

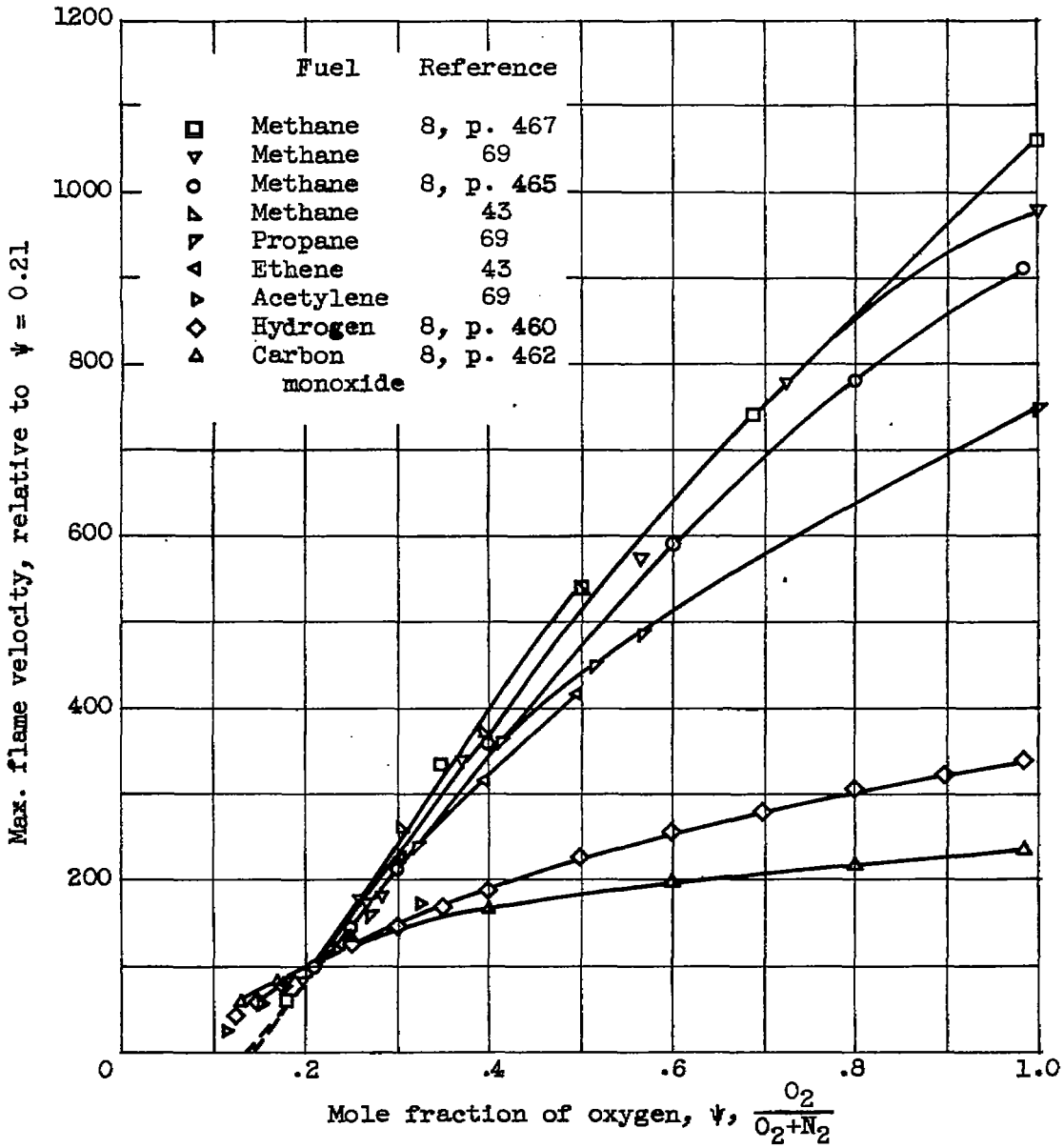

Figure IV-14. - Effect of oxygen concentration on relative flame velocities of various fuel-oxygen-nitrogen systems at room temperature and atmospheric pressure.

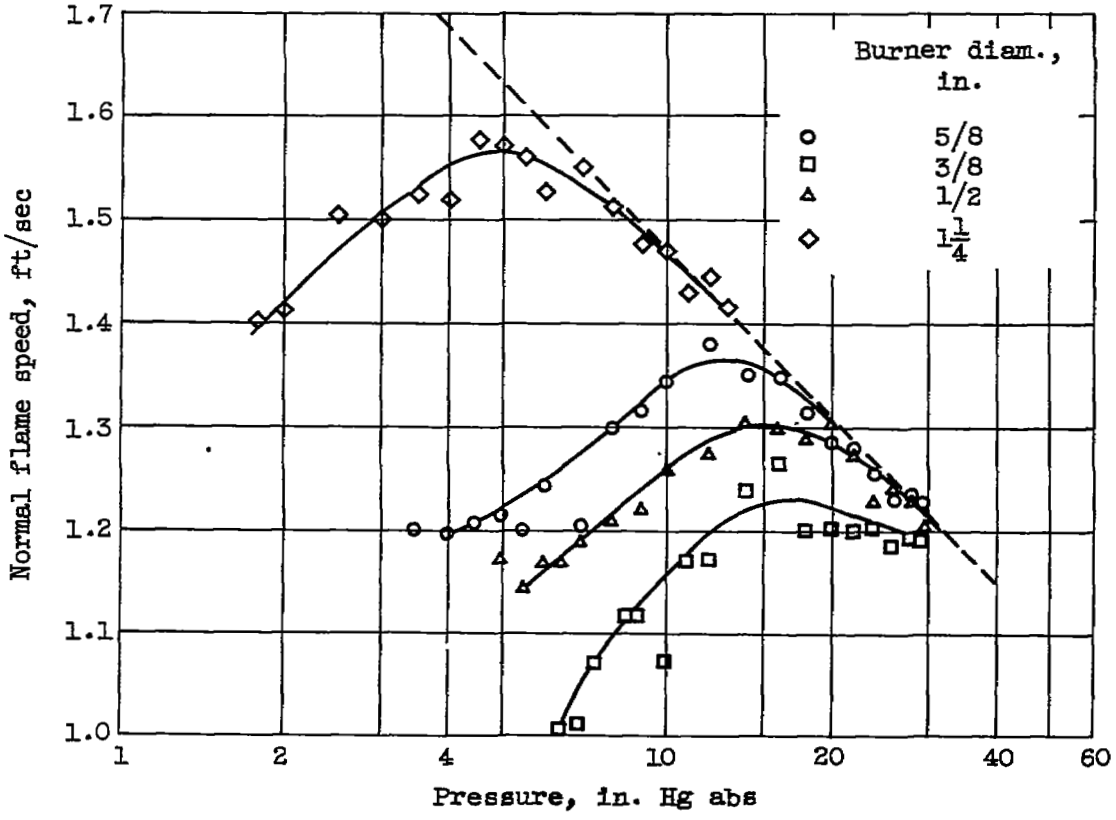

Figure IV-15. - Variation of normal flame speed with pressure for propane-air Bunsen flames. Fuel-air ratio, 0.067 (ref. 77).

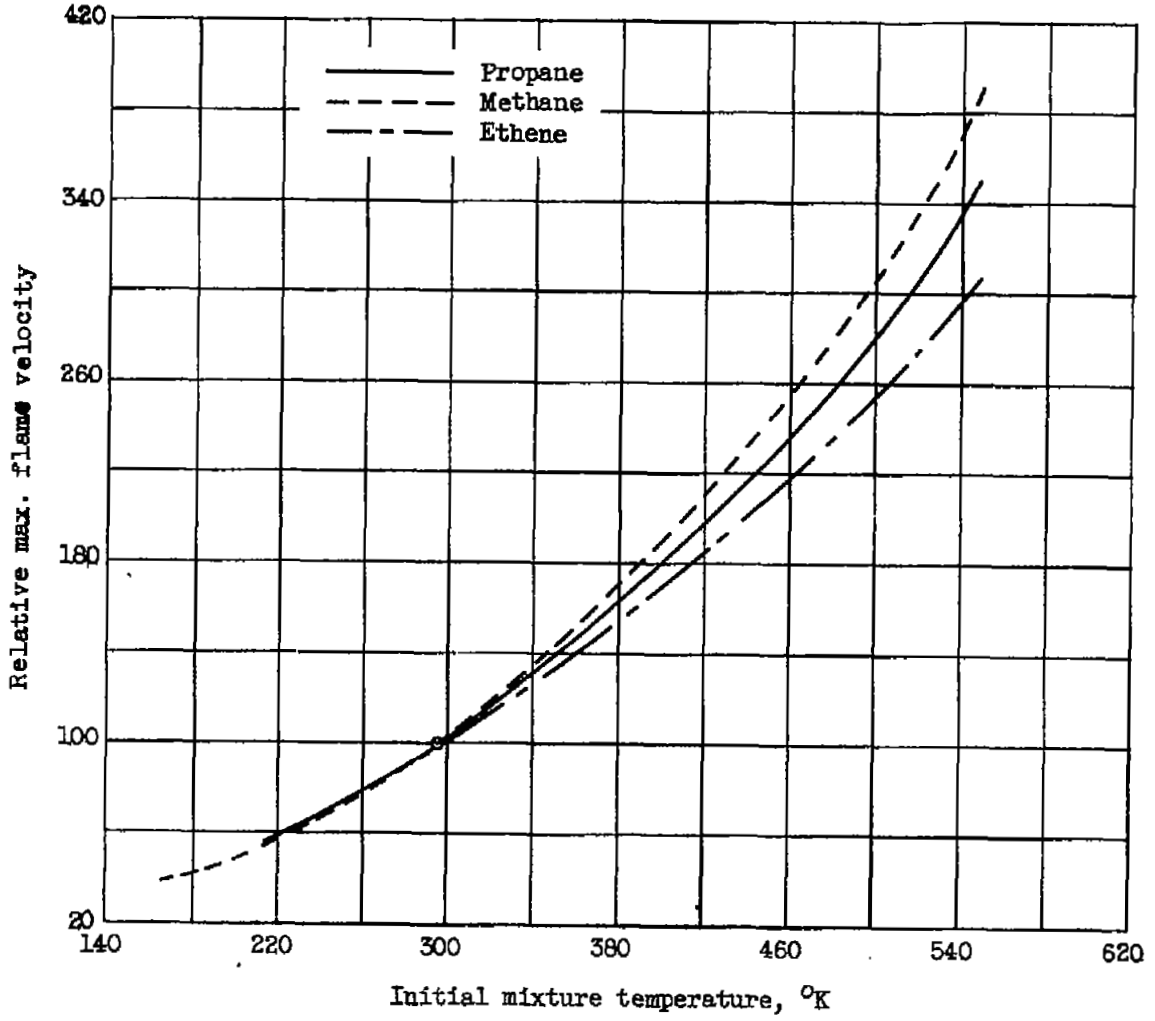

Figure IV-16. - Relative maximum flame velocity referred to maximum flame velocity at 25° C, with initial mixture temperature (ref. 16).

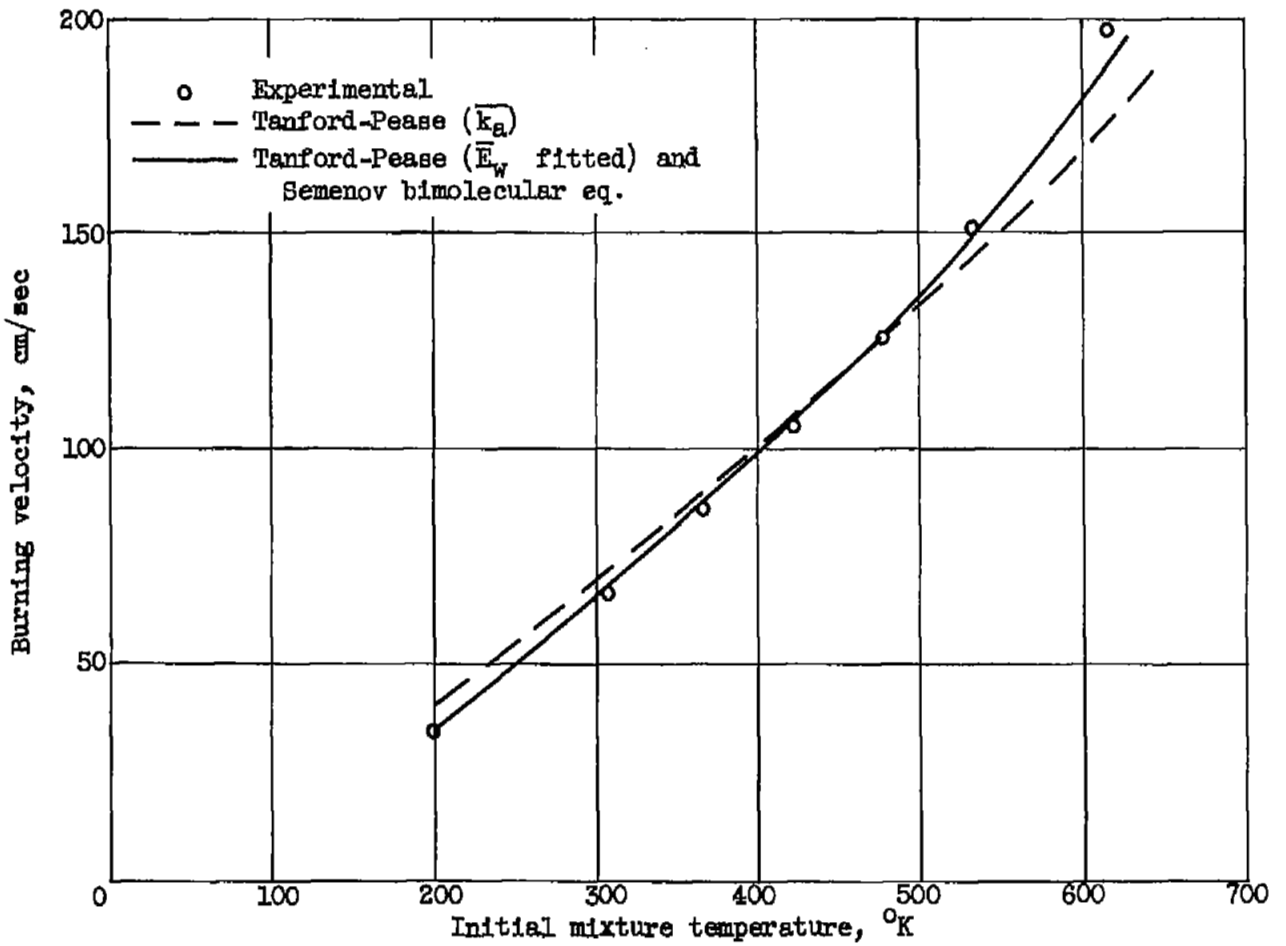

Figure IV-17. - Comparison of measured and calculated burning velocities for ethene-air mixtures at different initial temperatures (data of ref. 16 and calculations of ref. 49).

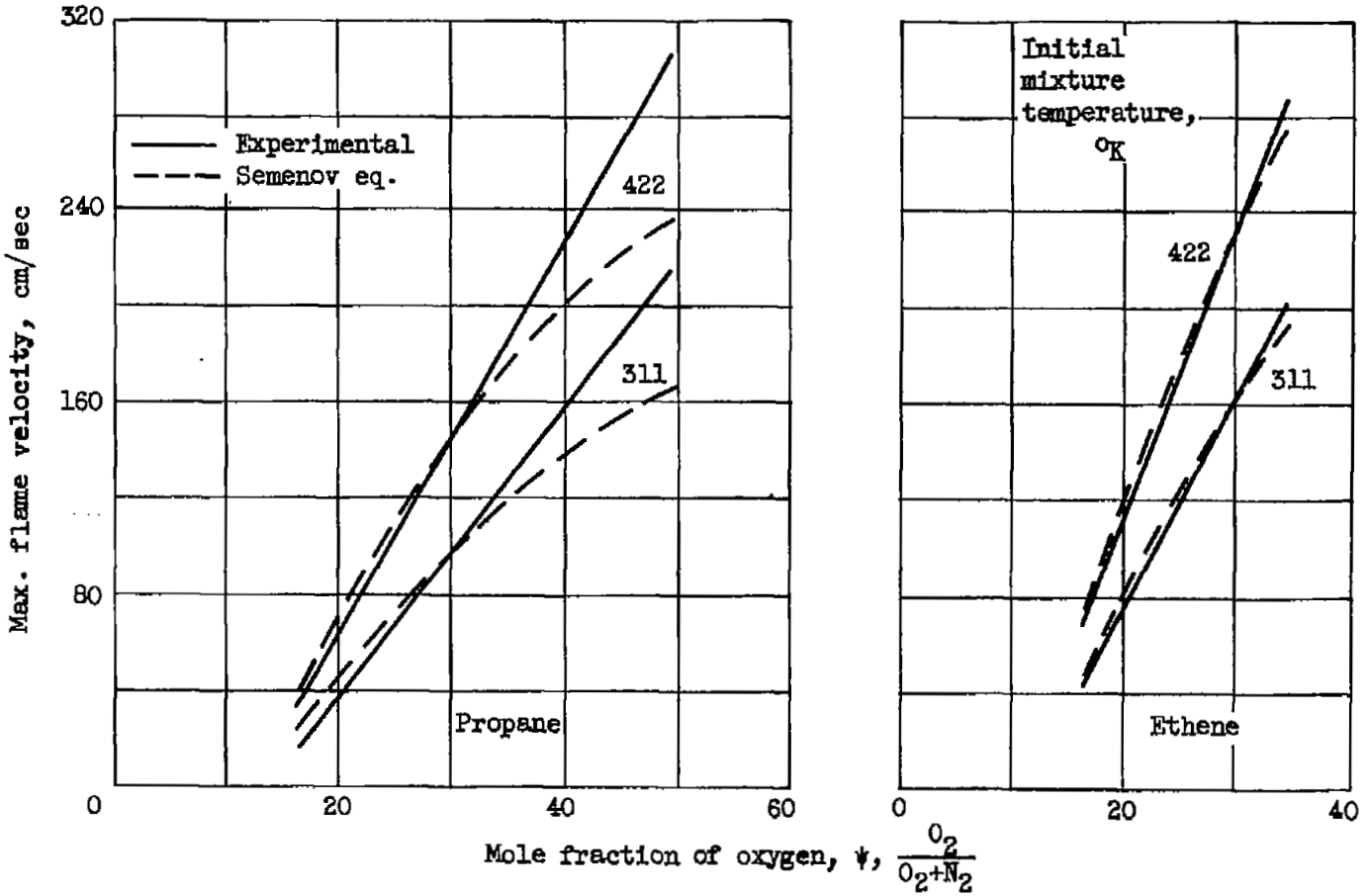

(a) Semenov bimolecular equation.

Figure IV-18. - Comparison of predicted and experimental results (ref. 66).

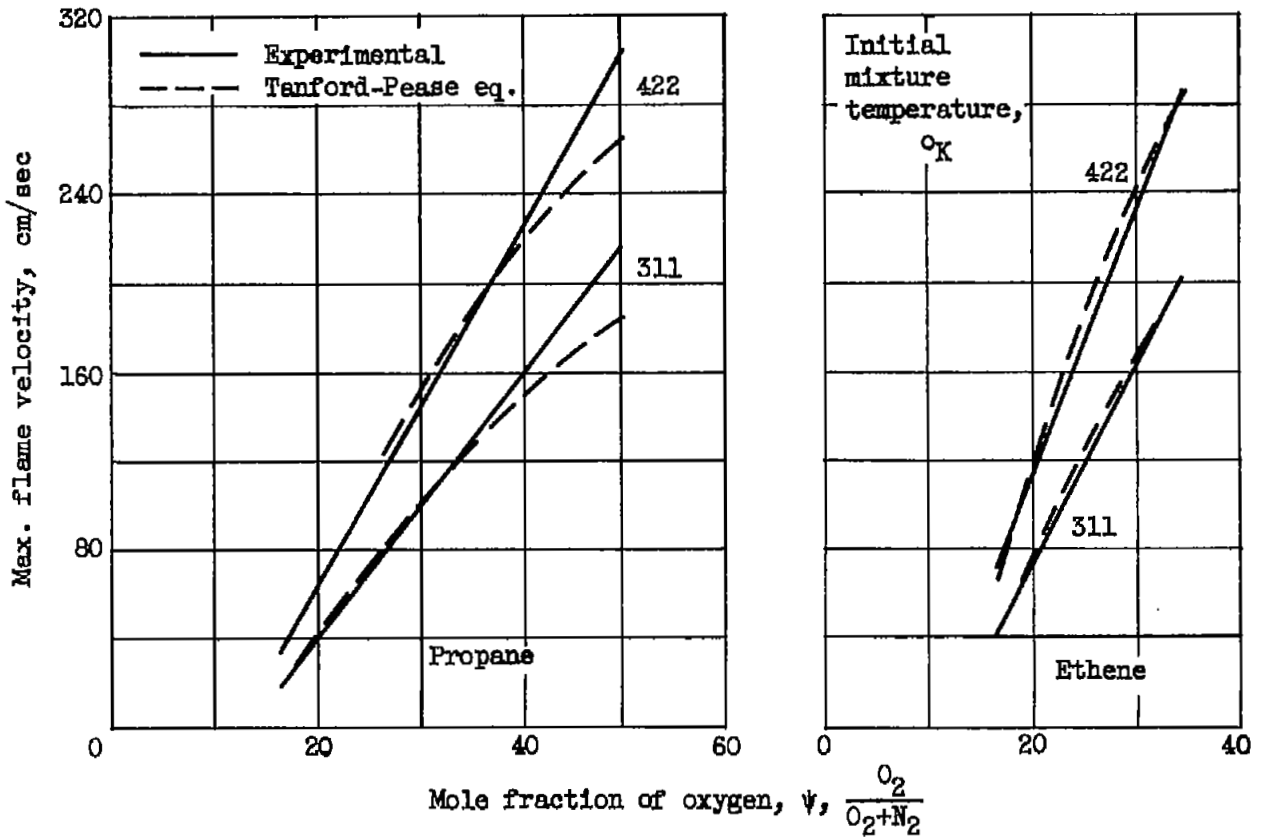

(b) Tanford-Pease Equation.

Figure IV-18. - Concluded. Comparison of predicted and experimental results (ref. 66).

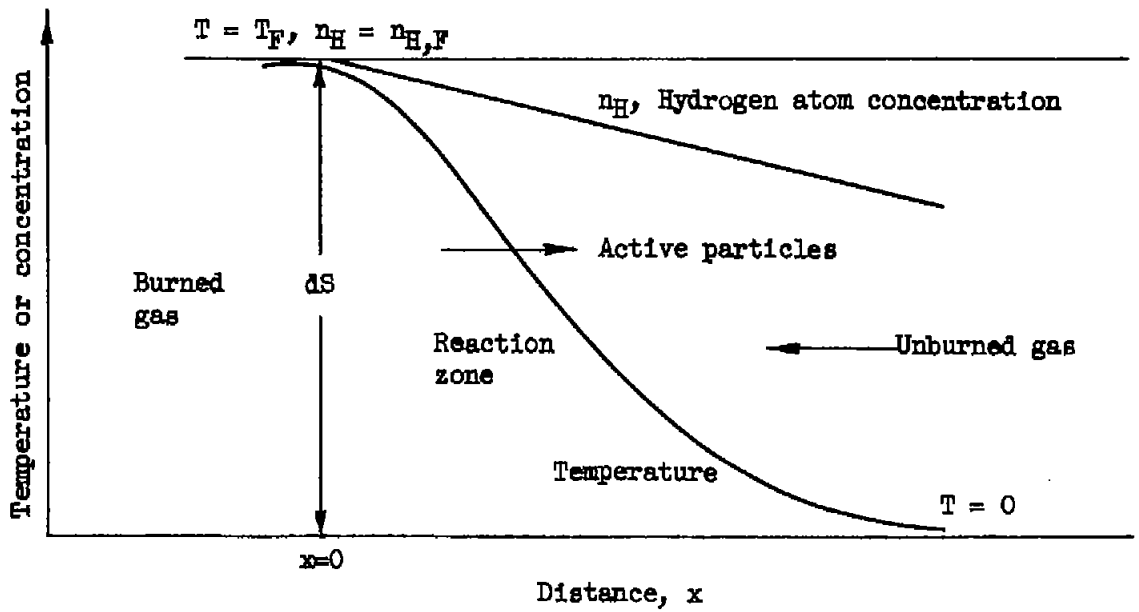

Figure IV-19. - Model of structure of flame front (ref. 104).

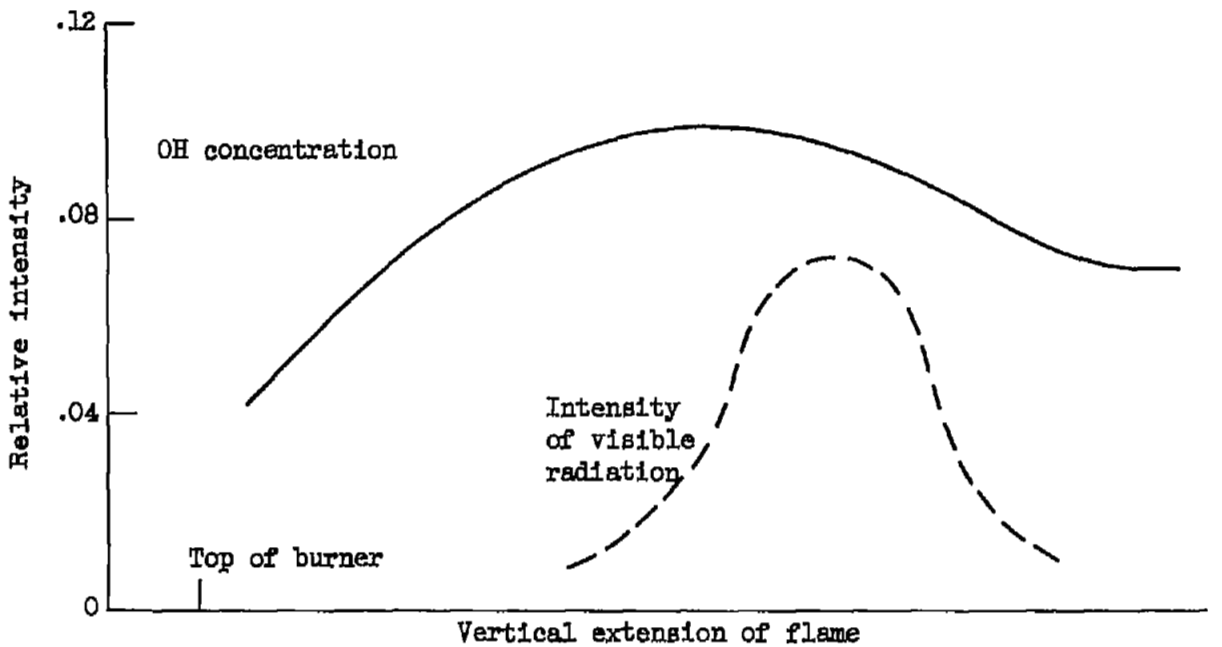

Figure IV-20. - Measured hydroxyl radical concentration in acetylene-air flame. Pressure, 66 millimeters of mercury (ref. 105).

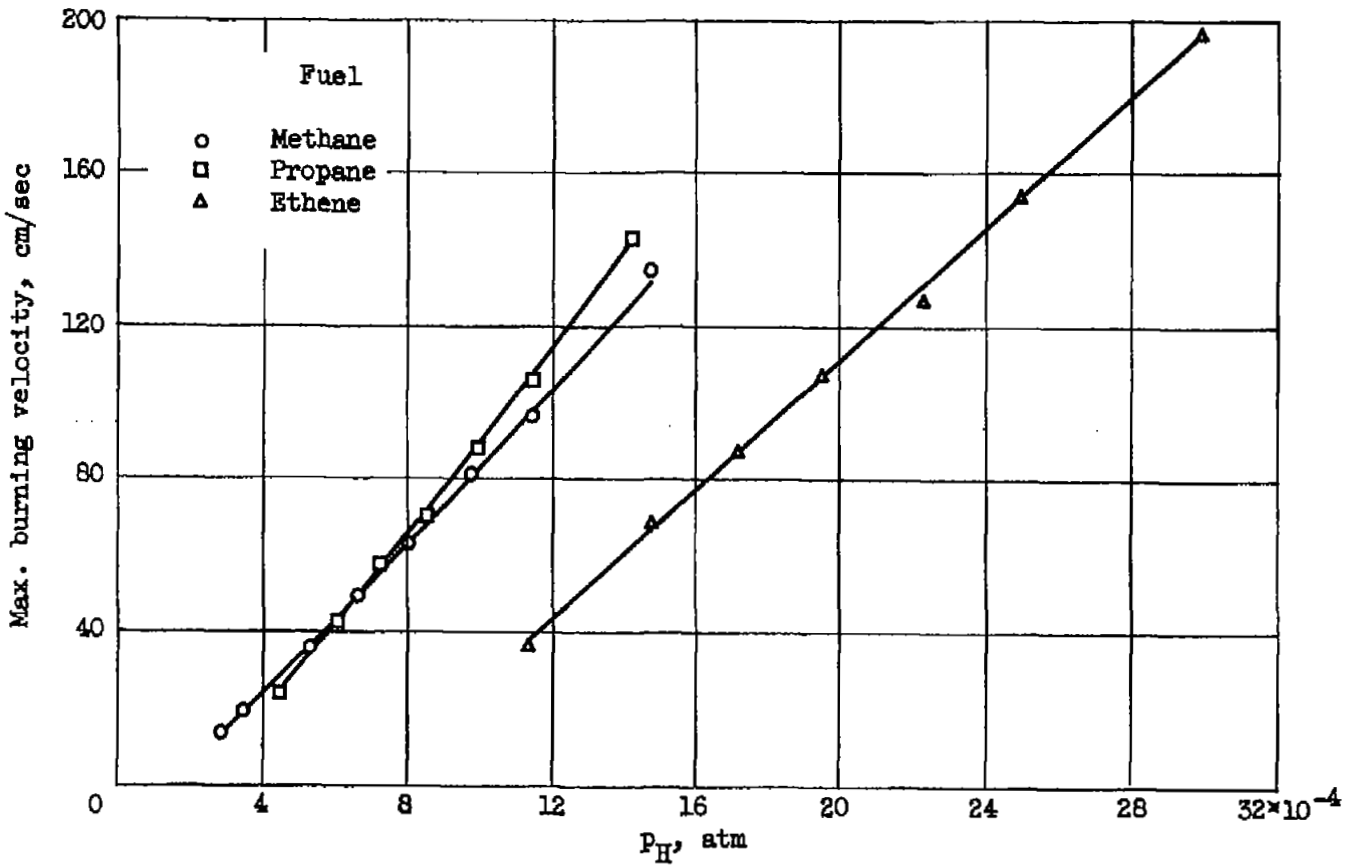

Figure IV-21. - Variation of burning velocity with hydrogen atom concentration for flames of different initial mixture temperature (ref. 16).

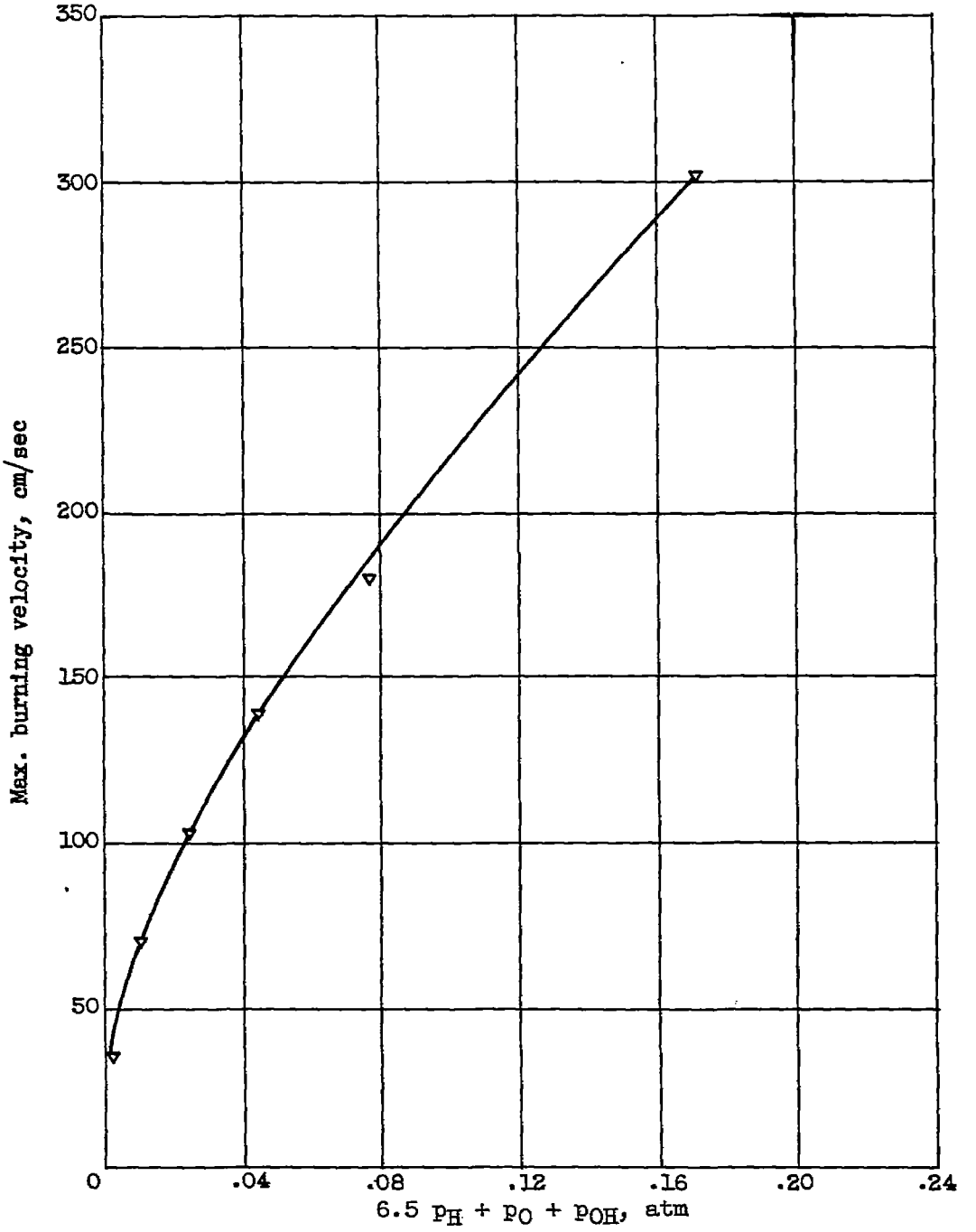

Figure IV-22. - Correlation of maximum burning velocity with relative diffusion concentration of active particles for propane-oxygen-nitrogen mixtures. Variable oxygen concentration of atmosphere (ref. 66).

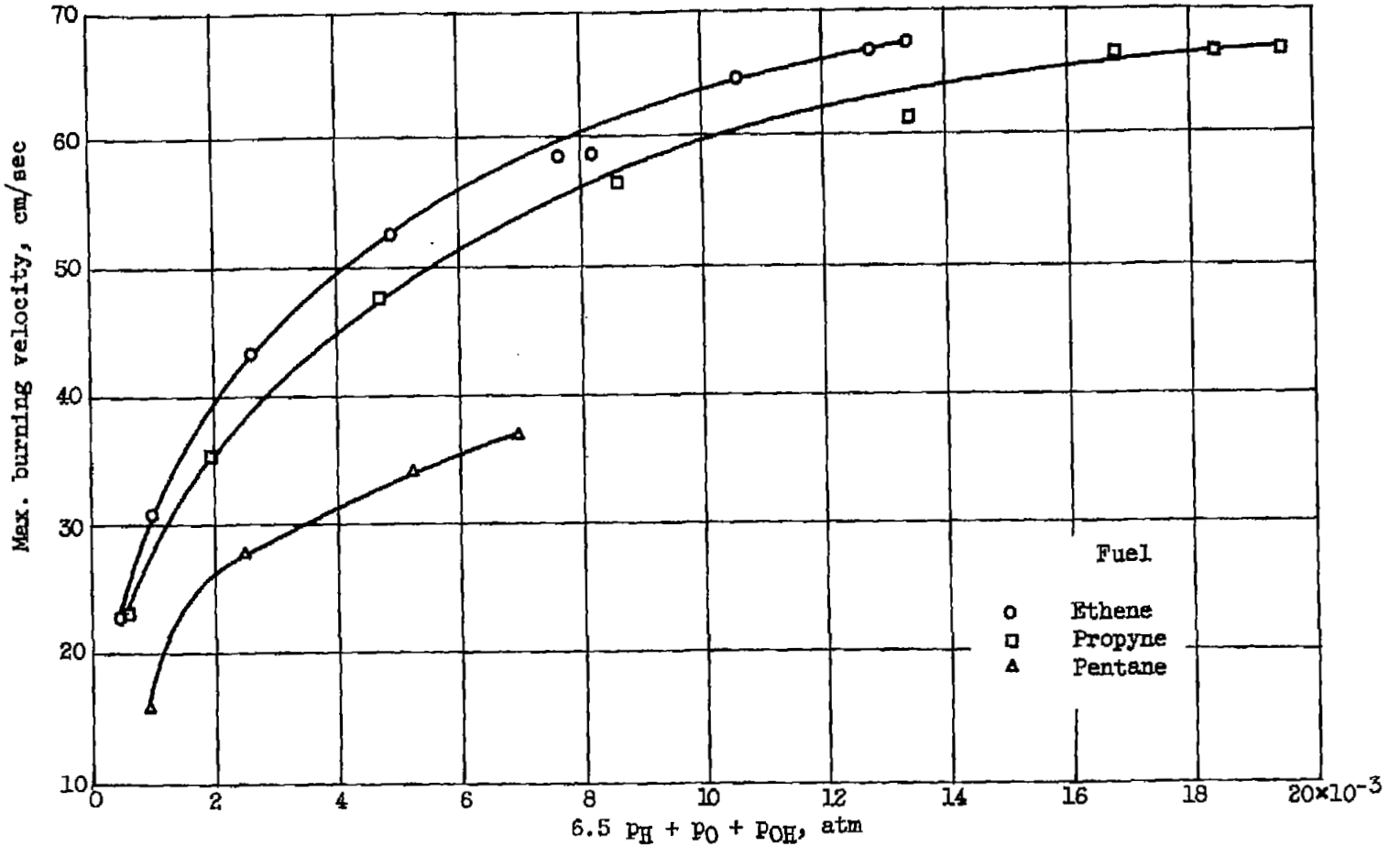

Figure IV-23. - Variation of burning velocity with relative diffusion concentration of active particles for three hydrocarbons in air for range of hydrocarbon concentrations (ref. 39).

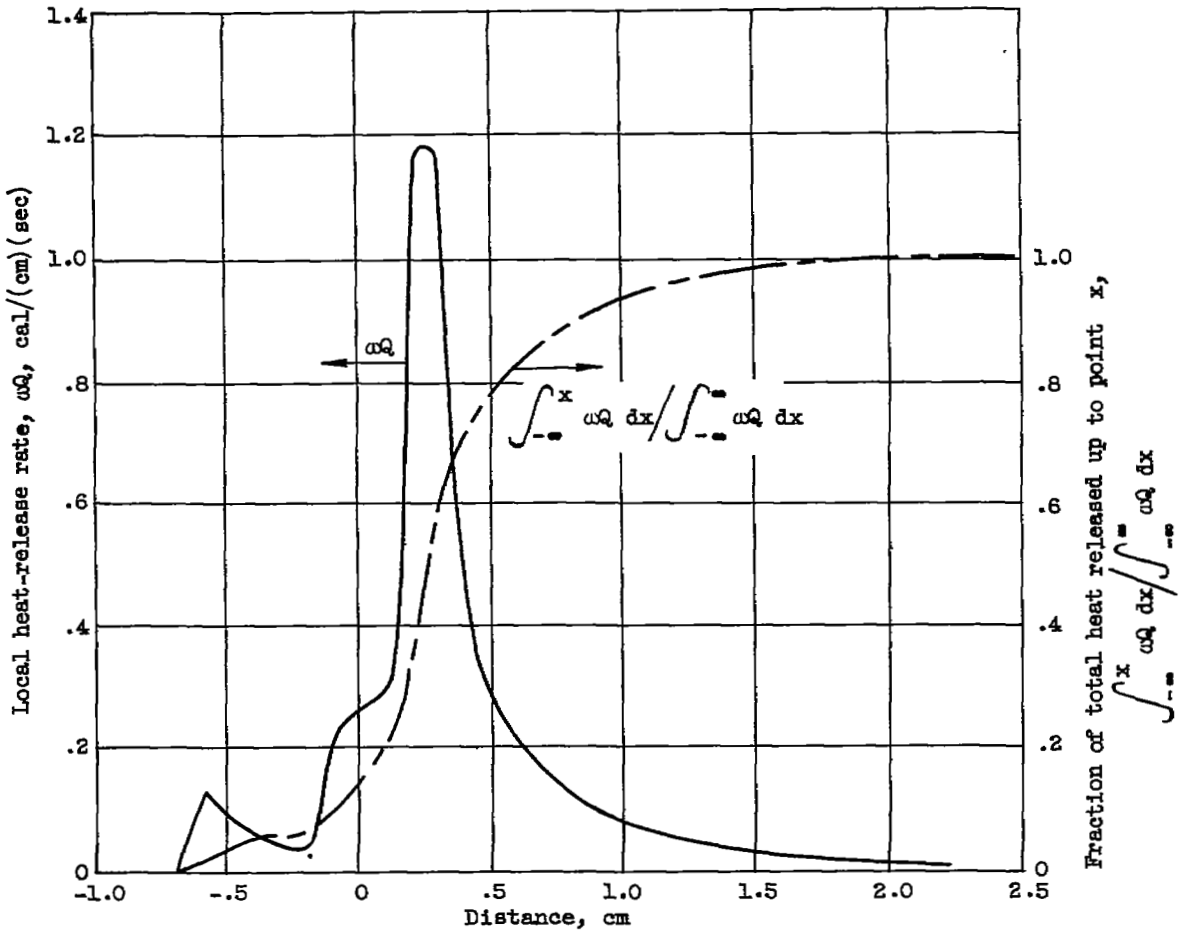

Figure IV-24. - Local and integrated heat-release rates as functions of distance through flame. Beginning of luminous zone designated by x = 0; mass air-propane ratio, 29.2; absolute pressure, 0.0594 atmosphere; initial temperature, 46° C; 25-centimeter flat-flame burner (reprinted by permission from ref. 6).

CHAPTER V

TURBULENT FLAMES

By Melvin Gerstein and Gordon L. Dugger

INTRODUCTION

The previous chapter is concerned with laminar flames in which a smooth, discrete flame zone exists. Such smooth flames (e.g., fig. IV-2) occur when the unburned gas flow is laminar and undisturbed (ref. 1). Small flow disturbances may distort the flame surface (ref. 2) and influence the rate of flame propagation somewhat, but the discrete reaction zone remains. If, however, the unburned gas flow is made turbulent, a diffuse, brushy flame results, and the rate at which the combustible mixture is consumed increases greatly. The turbulent flame, unlike the laminar one, is often accompanied by noise and rapid fluctuations of the flame envelope.

For the laminar flame, it is possible to define a flame velocity that, within reasonable limits, is independent of the experimental apparatus. It would be equally desirable to define a propagation velocity for turbulent flames that would be independent of the experimental apparatus and depend only on the fuel-air mixture and some easily identified properties of the flow. Such is not yet the case, however, and the numerical values of turbulent propagation velocities depend not only on the experimental technique but also on the concept of turbulent flames assumed by the investigator. Similarly, the theoretical concepts of turbulent flames are not as well defined as laminar flame theories. These points should be kept in mind during consideration of this chapter, in which the current status of knowledge in the field of turbulent flame propagation is discussed.

SYMBOLS

The following symbols are used in this chapter:

A cross-sectional area

a constant

b constant

C constant

c_p specific heat

d diameter

E energy

F fraction of fuel

h height of perturbation

K constant

l scale of turbulence

l_1 Lagrangian scale

l_2 Eulerian scale

R correlation factor

Re Reynolds number

r radius

S surface area of cone

T temperature

t time

U velocity

U' turbulent component of turbulent flame velocity

u velocity fluctuations

u' intensity of turbulence, $\sqrt{\overline{u^2}}$

v' rms fluctuating velocity in y-direction

x distance

Y duct half-width

$\overline{Y}$ mean displacement

y flame half-width

δ flame thickness

ε eddy diffusivity

κ thermal conductivity

ν kinematic viscosity

ρ density

τ reaction time

ω chemical reaction rate

Subscripts:

b burned gas

F flame

L laminar

max maximum

o initial conditions

t tube

tot total

u unburned gas

CHARACTERISTICS OF TURBULENT FLAMES

The nature of turbulent flames has been studied, using the photographic techniques developed for laminar flames (ch. IV). Unlike the laminar flame, however, the flame surface is very complex, and it is difficult to locate the various surfaces that were used to characterize laminar flames. A brief description of the characteristics of some turbulent flames is given in the following sections.

Bunsen Flames

The turbulent Bunsen flame has probably received the most attention. Laminar and turbulent Bunsen flames are compared in figure V-1, which compares time exposures of the luminous zones of a laminar and a turbulent flame. The diffuse appearance of the time exposure of the luminous turbulent flame zone is due to the rapid oscillations of a wrinkled flame front, which can be seen in instantaneous schlieren photographs (ref. 1). Superposition of the schlieren photograph on the luminous photograph shows that the random fluctuations of the instantaneous flame front are contained within the luminous envelope (ref. 1, p. 481).

Flame height. - As long as the approach flow of unburned gas toward an open flame remains laminar, an increase in the average stream velocity is maintained according to equation (1) of chapter IV. The cone height increases correspondingly, and for a perfectly conical flame the relation between cone height and average stream velocity is given by the solid line in figure V-2. When the flow becomes turbulent, however, the flame becomes turbulent and the mean flame height (fig. V-3) no longer increases in the same manner; greater quantities of fuel-air mixture are consumed in a turbulent flame than would be consumed in a laminar flame of the same height. The dotted curve in figure V-2 represents the mean flame heights measured (ref. 3) for turbulent flames burning under conditions comparable with those used to calculate the laminar curve except for the nature of the flow. The variation of the mean flame height with flow velocity and tube diameter for three fuels, propane, ethene, and acetylene are shown in figure V-4 from reference 3. The mean height of the flame and the width of the burner port can be used to estimate a lower limit to the flame volume required under a particular set of conditions. Any reduction in available space should lead to inefficient burning.

Brush width. - A time exposure of the turbulent flame surface appears as a brush of increasing width from base to tip as shown in figure V-3. The distance between the inner and outer boundaries of the flame brush at the tip of the flame has been called the brush width. In reference 3, the brush width as a function of flow velocity and tube diameter was measured for propane and acetylene flames. The data are plotted against Reynolds number in figure V-5. At low Reynolds numbers (below 2000) where the flow and flame become laminar, the distance between the inner and outer boundaries should approach the thickness of the luminous zone of a laminar flame, of the order of 0.1 millimeter (ref. 1, pp. 238, 254). Only flow velocity and tube diameter were varied in this study, density and viscosity remaining roughly constant.

Flames in Tubes

Only a limited amount of basic work has been done on the velocity and structure of turbulent flames in tubes. Many investigators have noted that a laminar flame in a tube can become oscillatory and finally become diffuse and wrinkled like a turbulent burner flame. In an experiment in which the gas velocity ahead of the flame was measured, it was found that the turbulent flame appeared when the gas flow ahead of the flame had a Reynolds number exceeding 2000 (ref. 4). In the case of flames propagating toward the closed end of a tube, a turbulent circulatory motion is set up ahead of the flame, creating a turbulent flame. In all cases, the spatial rate of flame propagation increases when the turbulent flame appears.

3517

Flames Supported on Rods (V-Flames)

A technique that has created considerable interest because of its similarity to flames supported on flame holders is the V-flame method in which the flame is supported on a rod. Essentially, the V-flame measures the ability of the flame to spread from the sheltered zone near the stabilizer into the unburned gas flowing past it. The greater the burning rate, the wider the flame will grow at a given distance from the flame holder. The flame width, then, is a measure of the burning rate.

TURBULENT FLAME VELOCITY

Measurement

Open burner flames. - The earliest measurements of a turbulent flame velocity were those of reference 5, in which it was assumed that the inner boundary of the turbulent flame represented a zone of maximum burning rate or the turbulent flame velocity, while the outer boundary represented the zone of slowest burning rate or the laminar flame velocity. The surface areas corresponding to these zones were measured, and flame velocities were calculated by a total-area method using equation (1) of chapter IV. The flame velocity calculated from the inner surface is a maximum value and corresponds to the hypothetical condition that at any instant all the flame exists along this surface. As is evident from instantaneous schlieren photographs of turbulent flames, only part of the flame exists at the inner surface at any instant.

In consideration of the fluctuating nature of a turbulent flame, a line, such as the dotted line in figure V-3, might be drawn somewhere between the inner and outer boundaries to indicate a mean flame surface about which the instantaneous flame front oscillates. It might be considered the most probable position of any given increment of flame front. In reference 3, the line was drawn midway between the inner and outer boundaries; such a surface does not give a mean surface area. In reference 6, the locus of maximum light intensity determined from densitometer measurements on the time exposure was used. Since the extreme boundaries of a turbulent flame are quite diffuse, this method of determining a mean boundary is more precise and more readily reproduced. The flame velocity so obtained is intermediate between the minimum and the maximum of reference 5; there is no simple relation between the maximum flame velocity of reference 5 and the turbulent flame velocity of reference 6, because the dimensions of the flame brush change as flow conditions change (fig. V-5).

References 3 and 5 report flame velocities computed by a total-area method based on surface-of-revolution formulas (ch. IV, eq. (2b)); whereas, in reference 6, an angle method was used (ch. IV, eq. (3)). It is important to note, however, that none

of these methods of computing turbulent flame velocity corresponds to that for computing the laminar flame velocity, which is defined as the flow velocity of unburned gas perpendicular to the instantaneous flame surface. The calculated turbulent flame velocity corresponds to the flow velocity of unburned gas perpendicular to a time-average position of the flame, and the instantaneous flame surface area does not enter the calculation. No precise measurements have been made of the velocity normal to the actual flame surface, although the laminar flame velocity does enter many of the proposed theoretical relations discussed in this chapter.

In reference 7, an attempt was made to estimate the total area of a turbulent flame from the height and diameter of the perturbations visible on a spark photograph. It was found that

$$d = 5.0\ L \tag{1}$$

where

d diameter of perturbation

L average eddy diameter (called turbulent wind in ref. 7)

and

$$h = \frac{0.266\ u'_{tot}}{U_{F,L}} \tag{2}$$

where

h height of perturbation

u'_{tot} total rms fluctuating velocity

Flames in tubes. - In reference 8, spatial velocities of turbulent flames in tubes were measured. The ratio of turbulent to laminar spatial velocity in a tube is equivalent to the ratio obtained with a Bunsen burner with the additional assumption that the mean flame boundary has the same meaning in both cases.

Spherical flames. - Analogous to the use of the soap-bubble or constant-volume bomb method for laminar flame velocities, spherical flames have been used to study turbulent flame velocity. In reference 9, a single spark was used to ignite a turbulent mixture flowing through a 4- by 4-inch duct, thus creating a sphere of flame that expanded into the flowing unburned gas mixture. Just as in the soap-bubble method, the spatial rate of propagation of the mean spherical surface multiplied by an expansion ratio resulted in a flame velocity. In the soap-bubble and constant-volume bomb experiments, the required expansion ratios could be measured, but in the free-stream method used in reference 9, a theoretical expansion ratio was used which was based on the equilibrium flame temperature. The ratio of turbulent to laminar spatial velocities, assuming the same expansion ratio applies for both cases, should then be equivalent to the flame velocity ratio obtained in tube and Bunsen flames.

Flames supported on rods (V-flames). - The turbulent V-flame may be used to determine the flame velocity in a manner analogous to the laminar V-flame (ch. IV). Consider the sketch in figure V-6 (ref. 10). The total length of burning surface of one side of the V-flame is $\overline{OS}$, the approach-stream velocity is U_o, and the duct

half-width is Y. Consider the flame segment $\overline{OS'}$, which extends from the flame holder to the point where the flame half-width is y. The unburned gas that enters segment $\overline{OS'}$ originally had a stream tube half-width y_o and velocity U_o in the approach stream. In this two-dimensional system, y, y_o, and $\overline{OS'}$ are representative of areas; and, since the pressure drop due to combustion is small, the density of the unburned gas may be assumed constant. Hence, the product yU is constant for conservation of mass. By analogy to equation (1) of chapter IV, the average turbulent flame velocity for the segment is

$$U_{F,T} = y_o U_o / \overline{OS'} \tag{3}$$

3517

The fraction of fuel F burned in segment y is

$$F = \frac{y_o U_o}{Y U_o} = \frac{y_o}{Y} \tag{4}$$

Therefore,

$$U_{F,T} = FY\ U_o / \overline{OS'} \tag{5}$$

The flame half-width y was considered a differential width dy with corresponding increments in pressure and unburned and burned gas velocities in reference 10; this concept was used in the writing of differential equations for the over-all mass balance, over-all force balance, and force balances on the burned and unburned gases. These equations were solved by a stepwise method for finite increments in order to obtain curves of y/Y against F (fig. V-7). Flame widths y were measured from the outer edge of the luminous flame zone from a time exposure of the turbulent V-flame. The values of F were then read from figure V-7, and the average turbulent flame velocities were calculated by equation (5).

Dependence of flame velocity on location of measurement. - As with the laminar flame (ch. IV), the turbulent flame velocity may vary from point to point. Figure V-8 shows the ratio of turbulent to laminar flame velocity $U_{F,T}/U_{F,L}$ plotted against the fraction of the tube radius r/r_t. The flame velocity ratio increases from unity at the tube rim ($r/r_t = 1$) to the order of 4 at $r/r_t = 0.7$. These changes are considered further in the discussion of flame-induced turbulence. The effects of chemical and physical variables on $U_{F,T}$ discussed hereinafter apply to average velocities determined by total-area methods.

Effects of Chemical Variables

Fuel concentration. - Reference 5 reports measurements of the effect of fuel concentration on the turbulent flame velocities of propane-oxygen mixtures. The results are shown in figure V-9, where the dotted curve represents measurements based on the outer boundary of the flame brush, whereas the solid curves are based on the inner boundary. According to reference 5, these velocities represent laminar and turbulent flame velocities, respectively. The dashed curve shows laminar flame velocities measured from the inner boundary of the luminous zone of a laminar flame. As would be expected if the outer boundary of the turbulent flame brush does represent a laminar flame velocity, all the points computed from it, irrespective of tube size or flow characteristics, fall on a single curve. The dashed curve representing laminar flame velocity based on the inner boundary of the luminous zone might be

expected to fall above the dotted curve because of the finite thickness of the luminous zone. The turbulent flames show a rapidly increasing velocity from rich mixtures toward stoichiometric. Unfortunately, leaner flames were unstable and could not be studied. It should be noted that the higher flame velocities in figure V-9 were measured with higher flow velocities, so that the increase in flame velocity was not due to changes in fuel-oxidant ratio alone; and, as will be evident in the discussion of the effect of flow velocity on turbulent flame velocity, the increases in flame velocity from rich to stoichiometric mixtures were greater than the would be expected from the effect of fuel-oxidant ratio alone.

In reference 3, a more complete study was made of the effect of fuel concentration on ethene-air flames on a 3/8-inch burner using flow velocity (expressed in terms of Reynolds number) as a parameter. The data are shown in figure V-10. The curves indicate a maximum slightly richer than stoichiometric, the maximum not shifting appreciably with Reynolds number.

Reference 11 reports a slight shift of the maximum toward richer mixtures at higher turbulence levels for butane flames. The turbulence was produced by screens for most of the cases shown in figure V-11.

The V-flame data of reference 10 presented in figure V-12 also show a maximum at fuel-air ratios near the laminar maximum. The effect of velocity is not quite as clear-cut as that of reference 3 because of the 50-foot-per-second curve falling above the 100-foot-per-second curve. The flames were turbulent, although, in these cases, the approach flow was laminar. The turbulence in the flame was attributed to a flame-generated turbulence, the effect increasing with increasing velocity. This point is discussed in a subsequent section in this chapter. The results are relatively independent of stabilizer size and shape and are insensitive to the introduction of turbulence-producing screens just below the stabilizer.

Fuel type. - It is shown in reference 3 that for propane-, ethene-, and acetylene-air flames the turbulent flame velocities were empirically correlated by the expression showing a direct proportionality to laminar flame velocity (table V-I). Thus, turbulent flame velocity, under the conditions studied, might be expected to vary with hydrocarbon structure in the same way that laminar flame velocity does. This is also in agreement with the theoretical treatments of references 6, 10, and 12.

Effects of Physical Variables

Pressure. - There is no adequate information on the effects of pressure on turbulent flame velocity. However, the problem is considered in reference 13, in which turbulent hydrogen-oxygen flames at a pressure of 14.6 atmospheres were studied. The burner diameter and the height of the equivalent cone defined by the angle of the turbulent flame near the burner rim in equation (2a) of chapter IV were used to obtain an equivalent cone area. An equivalent flame velocity for the turbulent flame was then computed from this area by equation (1) of chapter IV. Since $U_{F,T}/U_{F,L}$ approaches 1 near the rim (fig. V-8), these flame velocities would be near the laminar flame velocities.

A comparison of these computed velocities at a pressure of 14.6 atmospheres with laminar flame velocities at 1 atmosphere is shown in figure V-13. It is difficult to discuss quantitatively the effect of pressure, since the flames were small and the measurements are necessarily less reliable than those obtained for slower flames.

Temperature. - The effect of initial air temperature on turbulent flame velocity of coke-oven gas-air mixtures was measured by Heiligenstaedt (ref. 14), whose curves are replotted in terms of $U_{F,T}/U_{F,L}$ in figure V-14. The inner flame surface was used and assumed to be a right circular cone. Although three distinct curves for the three temperatures appear in the figure, indicating a small negative temperature dependence of $U_{F,T}/U_{F,L}$, Reynolds number correlates the data to within 10 percent over the range 10° to 400° C. Heiligenstaedt reported the turbulent flame velocity to increase approximately as the 1.6 power of the absolute initial temperature:

$$U_{F,T} \propto T_o^{1.6} \tag{6}$$

According to Delbourg (ref. 14), for town gas - air flames,

$$\frac{U_{F,T}}{U_{F,L}} \propto \frac{T_o^{1.65}}{T_o^{1.74}} \propto T_o^{-0.09} \tag{7}$$

Thus, for both of these examples the ratio of turbulent to laminar flame velocity is practically independent of initial temperature.

Velocity and turbulence promotion. - Several investigators have studied the effect of flow velocity on turbulent flame velocity. Tube diameter was also varied in these investigations, and the results were usually presented in terms of Reynolds number. Since for most of the studies density and viscosity were constant, the use of Reynolds number as a correlating parameter must be questioned. However, the results of Heiligenstaedt for various initial temperatures (hence various densities and viscosities) indicate that Reynolds number may be a meaningful parameter when plotted against the ratio of turbulent to laminar flame velocity (fig. V-14). He found $U_{F,T}/U_{F,L} \propto Re$ at Reynolds numbers above 10,000. Delbourg (ref. 12), who used the Bunsen burner technique and the inner flame boundary, shows the change of flame velocity as Reynolds number increases from 1000 to about 35,000. His results in figure V-15 on a double logarithmic scale show that, at Reynolds numbers to about 2000, the laminar flame velocity is obtained and is independent of Reynolds number. Between 2000 and 4000 he found a transition region showing a rapid increase in the ratio $U_{F,T}/U_{F,L}$, followed by a linear change in the ratio from 4000 to 35,000 such that $U_{F,T}/U_{F,L} = 0.088\ Re^{0.4}$. The variation of $U_{F,T}/U_{F,L}$ with Reynolds number for propane-oxygen flames as measured in reference 5 is shown in figure V-16; the results indicate that, for Reynolds numbers between 2000 and 5000, $U_{F,T}/U_{F,L} \propto Re^{0.5}$, and for larger Reynolds numbers, $U_{F,T}/U_{F,L} \propto Re$ in agreement with Heiligenstaedt. The results of reference 3 for acetylene-, ethene-, and propane-air are shown in figure V-17. Empirical equations for the curves are given in table V-I.

Although velocity and Reynolds number are related to the intensity and scale of turbulence in pipe flow, the turbulence is not isotropic. Several investigators have used screens of known characteristics to produce turbulence in the unburned gas. In reference 15, a rectangular Bunsen burner was used; the ratio of turbulent to laminar flame velocity and the intensity of turbulence in the narrow dimension of the burner were correlated. The results are shown in figure V-18. In reference 16, a similar technique but a symmetrical burner was used; the results are correlated with the turbulence intensity along the direction of flow. A tube method was used in reference 8; the spatial velocity as a function of distance from the turbulence-producing screen was measured. Since the intensity of turbulence varies with distance from the

screen, the results (fig. V-19) show the variation of flame speed with intensity of turbulence. In reference 9, the expanding spherical flame was used, with screens to create turbulence; a variation was obtained, as shown in figure V-20. The author found a very low laminar flame velocity of only 0.59 foot per second which is unexplained as yet. A distribution of flame velocities was obtained which the author associated with the random nature of turbulence. The curves illustrate the data obtained as a function of the fraction of the measurements giving a given flame velocity. It should be noted that in all these experiments the turbulence level was based on measured or calculated intensities in the absence of flame. Except for the experiments of reference 8, in which the intensity was considered at each point in the tube, the measurements were made at the initiation point of the flame (the lip of the burner for Bunsen flames or the ignition point for spherical flames), and hence the flame propagated into regions of varying turbulence.

The empirical equations for the variations of turbulent flame velocity with turbulence intensity in the approach stream are given in table V-II. Since Reynolds number can be related to intensity by the equation $Re \propto u'$ (ref. 5), the data of references 3, 5, and 12 can also be compared. The comparison of turbulent burning velocities by different investigators is difficult, however, because of the varied techniques used to study the flame and the different interpretations of the location of the flame surface. For example, in reference 5, in which the innermost boundary of the flame brush was used, turbulent burning velocities were considerably higher than those of reference 3, in which a mean flame surface was used. In deciding which of several relations to use, it is best at present to choose the one obtained in the experiment that most closely resembles the condition for which the data will be used. For approximate estimates of turbulent burning velocity, the expression of reference 3 is recommended for its convenience.

THEORIES OF TURBULENT FLAME PROPAGATION

The increased rate of burning of a fuel-air mixture in a turbulent flame compared with a laminar flame may be due to any one or a combination of three processes: (1) The turbulent flow may distort the flame so that the surface area is markedly increased, while the normal component of the burning velocity remains the laminar flame velocity. (2) Turbulence may increase the rate of transport of heat and active species, thus increasing the actual burning velocity normal to the flame surface. (3) Turbulence may rapidly mix the burned and unburned gas in such a way that the flame becomes essentially a homogeneous reaction, the rate depending on the ratio of burned to unburned gas produced in the mixing process. The first two processes have received the major emphasis in the consideration of turbulent Bunsen burner, tube, and V-flames, while the third process has been considered for some combustor systems.

Turbulent Flames

Damköhler theory. - Damköhler (ref. 5) pioneered in theoretical considerations of turbulent flames. He considered separately the cases of large-scale (greater than the flame thickness δ), small-intensity turbulence, and small-scale ($< \delta$), large-intensity turbulence. He readily admitted that both situations existed in most flames, the large-scale turbulence being of greater importance in combustor applications. Damköhler points out that the eddy diffusivity ε alone may not be sufficient to describe the effects of turbulence on flames, since $\varepsilon = lu'$ and both l and u' may have different influences on flame propagation. It is necessary, therefore, to know both the scale and intensity of turbulence.

In the case of large-scale, low-intensity turbulence, Damköhler suggests that the flame will be wrinkled but that the laminar transport processes will remain virtually unaffected. This is not unreasonable if large-scale turbulence is considered

to consist of large eddies, within which the molecular processes of heat transfer and diffusion take place independent of the movement of the eddy as a whole. Damköhler suggests the following picture:

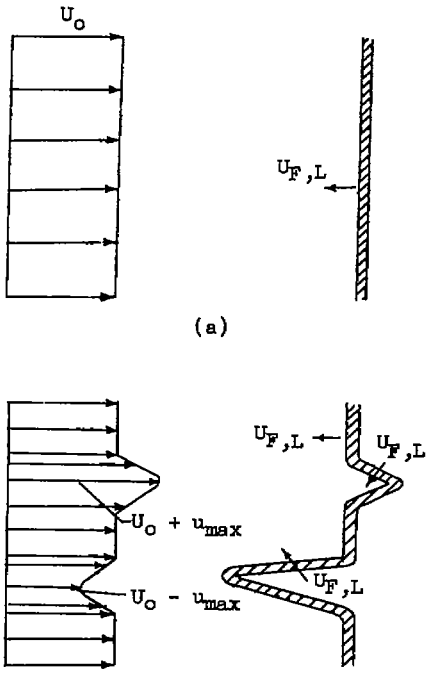

In the case of a laminar flat flame with constant $U_o = U_{F,L}$, the situation in (a) is obtained. If velocity fluctuations u are introduced, however, the velocity at some points will be $U_o + u$, and a conical Bunsen-like flame retaining a normal flame velocity $U_{F,L}$ will be obtained. Where $U_o - u$ exists, a local flash-back will occur. In the case of flash-back, the flame surface area continues to increase so that the spatial rate of flame movement increases with time, and hence the distortion is greater where the velocity fluctuation is negative. In order to reverse the flash-back, the flow velocity must exceed $U_o + u$. The velocity fluctuations thus produce a wrinkled flame.

Equation (1) of chapter IV shows that for a constant $U_{F,L}$ the flame area will be proportional to the flow velocity; hence, the mean flow through the turbulent flame $U_{F,T} \propto u'$, where $u' = \sqrt{\overline{u^2}}$; or, if l is constant as is true for tube flow, $U_{F,T} \propto \varepsilon$. Since $\varepsilon \propto Re$, it follows, according to Damköhler, that $U_{F,T} \propto Re$ for large-scale, low-intensity turbulence. Because of the complex nature of the wrinkling, Damköhler concludes that the exact relation between Reynolds number and $U_{F,T}$ cannot be written, but only the proportionality. As is evident from figure V-16, the turbulent flame velocity measured by Damköhler using the inner luminous surface is linear with Reynolds number at the higher Reynolds numbers. Since the higher Reynolds numbers were produced in tubes of large diameter, they do represent large-scale turbulence in which l/δ varies from 2.7 to 2.1. Actually, the equation representing the straight portion is of the form $U_{F,T} = a\ Re + b$, and Damköhler attributed the the term b to small-scale turbulence. For a different interpretation of the same data, see the discussion of Delbourg's theory.

In order to explain the influence of small-scale turbulence on flame velocity, Damköhler investigated the change in diffusion and heat transfer with Reynolds number, since the small-scale turbulence is assumed to produce no roughening of the flame surface. In thermal mechanisms of flame propagation, the flame velocity is related to transport properties by the following relation from equation (39) of chapter IV:

$$U_{F,L} \propto \sqrt{\frac{\varkappa_L}{c_p \rho_o}} \tag{8}$$

3517 Since $\varkappa_L/c_p\rho_o \approx \nu$, it follows that $U_{F,L} \propto \sqrt{\nu}$. In turbulent flow, ε determines the turbulent heat-transfer coefficient so that

$$\varepsilon = \frac{\varkappa_T}{c_p \rho_o} \tag{9}$$

can be used in turbulent flame equations. The ratio of turbulent to laminar flame velocities would then be given by

$$\frac{U_{F,T}}{U_{F,L}} = \sqrt{\frac{\varkappa_T}{\varkappa_L}} = \sqrt{\frac{\varepsilon}{\nu}} \tag{10}$$

Damköhler points out that equation (10), unlike the relations for large-scale turbulence, shows the direct dependence of the flame velocity ratio and not merely proportionality. It should be remembered, however, that this is true only if the remaining terms in equation (39) of chapter IV are not influenced by turbulence.

Equation (10) would permit the calculation of turbulent flame velocities for small-scale turbulence. Since the value of ε changes across the burner diameter, however, and only a mean flame velocity was measured by Damköhler, a direct comparison was not possible. Damköhler constructed a hypothetical inner flame cone using equation (10) and an equation for the radius and height for laminar flames. He then calculated a mean turbulent flame velocity from the constructed flame shape. The dotted line in figure V-16 indicates reasonable agreement between his calculated and experimental results.

Shelkin theory. - Shelkin (ref. 17) expanded on Damköhler's model of turbulent flame propagation but, in general, came to similar conclusions. He assumed from the early thermal theories that the flame velocity could be represented by

$$U_{F,L} = \sqrt{\frac{\varkappa_L}{\tau}} \tag{11}$$

where τ is the reaction time.

In the turbulent case, molecular and turbulent heat transfer would be combined so that

$$U_{F,T} = \sqrt{\frac{\varkappa_L + \varkappa_T}{\tau}} \tag{12}$$

which assumes that τ is unchanged in small-scale, high-intensity turbulence. Rearranging,

$$U_{F,T} = \sqrt{\frac{\varkappa_L}{\tau}\left(1 + \frac{\varkappa_T}{\varkappa_L}\right)} = U_{F,L}\sqrt{1 + \frac{\varkappa_T}{\varkappa_L}} \tag{13}$$

may be written. If it is assumed that $\varkappa_L + \varkappa_T = c_p\rho_o\varepsilon$, Damköhler's equation is obtained.

For large-scale turbulence, Shelkin also assumes that only the flame area changes. He assumes that the flame breaks into cones and that the ratio of the turbulent flame velocity to laminar flame velocity will be equal to the ratio of the surface area of the average cone to the area of its base. The height of the cone is taken to be proportional to the intensity of turbulence u' (see fig. V-2 for the variation of cone height with velocity) and is given by $lu'/U_{F,L}$. The surface area of the cone is then

$$S = \frac{1}{2}\pi l\sqrt{\left(\frac{l}{2}\right)^2 + \left(\frac{lu'}{U_{F,L}}\right)^2} \tag{14}$$

while the area of the base is $\epsilon A = \pi(l/2)^2$. Hence the ratio becomes, after rearranging,

$$\frac{U_{F,T}}{U_{F,L}} = \frac{S}{A} = \sqrt{1 + \left(\frac{bu'}{U_{F,L}}\right)^2} \tag{15}$$

($b = 2$ for a cone, but Shelkin prefers the arbitrary constant b.) This reduces to Damköhler's equation when $(bu'/U_{F,L})^2 >> 1$ or when $u' > U_{F,L}$; hence, Shelkin concludes that Damköhler's equation applies for large-scale, high-intensity turbulence. For very large intensities, Shelkin suggests that the flame breaks up into small islands and that the rate of burning depends only on the rate of mixing so that $U_{F,T} \propto u'$ and is completely independent of $U_{F,L}$. While this is evidently not the case for burner flames (see fig. V-17), it is reasonable that some combustor conditions may exist where mixing processes control the burning rate.

Scurlock (ref. 10) combines both of Shelkin's equations so that for small-scale turbulence equation (13) is approached, for large-scale turbulence equation (15) is approached, and both are important where the scale of turbulence is of the order of the flame thickness. Scurlock's equation is

$$\frac{U_{F,T}}{U_{F,L}} = \sqrt{\left[1 + \left(\frac{2u'}{U_{F,L}}\right)^2\left(\frac{l/\delta}{C_1 + l/\delta}\right)\right]\left[1 + \left(\frac{\varkappa/c_p\rho_o}{Cu'l}\right)\left(\frac{1}{1 + l/C_2\delta}\right)\right]} \tag{16}$$

Delbourg theory. - Delbourg (ref. 12) investigated in greater detail the regime that Damköhler and Shelkin attributed to small-scale turbulence where the flame speed changes because of changes in the transport properties. Delbourg, like Shelkin, introduces an over-all thermal conductivity $\varkappa = \varkappa_L + \varkappa_T$ composed of laminar and turbulent components. Delbourg uses essentially a thermal approach to calculate turbulent flame velocity. Delbourg writes an energy equation analogous to the integrated form of the energy equation (33a) of chapter IV for laminar flames, and a continuity equation analogous to equation (32a) of chapter IV.

In order to simplify integration, Delbourg assumes that the chemical reaction rate ω is directly proportional to temperature rather than the usual Arrhenius

reaction rate and uses mean values for the thermal conductivity $\varkappa$ and specific heat c_p. Delbourg's assumptions lead to the following equation for laminar flame:

$$U_{F,L} = \frac{C_L T_o}{\rho_o c_p} \varkappa_L \frac{T_F - T_3}{T_3 - T_o} \tag{17}$$

By analogy, he writes for turbulent flames

$$U_{F,T} = \frac{C_1 T_o}{\rho_o c_p} \varkappa \frac{T_F - T_3}{T_3 - T_o} \tag{18}$$

where C_1 represents the nontemperature-dependent terms in the turbulent reaction rate, and, like $\varkappa$, may be considered to be composed of a turbulent and a laminar component:

$$C_1 = C_T + C_L \tag{19}$$

Some changes in the equations are necessary to obtain a solution in terms of measurable quantities. From equation (9), the turbulent component of thermal conductivity is proportional to the eddy diffusivity:

$$\varkappa_T \propto \varepsilon \tag{20}$$

and for tube flow,

$$\varepsilon = f\left(\frac{y}{r}\right) Re^{7/8} \tag{21}$$

Since $\varkappa_T$ is therefore a function of radius, it is difficult to relate the calculations to the measured average flame velocity. A turbulent flame velocity based on an average across the tube may be defined:

$$\overline{U}_{F,T} = \overline{U}_o \frac{A_t}{S_F} \tag{22}$$

where

A_t cross-sectional area of tube

S_F surface area of flame

By numerical integration of the differential equations relating the surface area of the turbulent flame to measurable quantities, Delbourg gets

$$\frac{\overline{U}_{F,T}}{U_{F,L}} = 0.0128\ Re^{0.4} \tag{23}$$

which is in reasonable agreement with his experimental relation

$$\frac{U_{F,T}}{U_{F,L}} = 0.088\ Re^{0.4} \tag{24}$$

As shown in figure V-21, Delbourg points out that Damköhler's data are in agreement, since they may be represented by an equation

$$\frac{U_{F,T}}{U_{F,L}} = 0.07\ Re^{0.4} \tag{25}$$

Delbourg states that the ratio $U_{F,T}/U_{F,L}$ is relatively independent of the fuel-air mixture.

Karlovitz theory. - Karlovitz and coworkers (ref. 6) studied a model much like Damköhler's for large-scale turbulence. They consider the effect produced as an eddy passes through a laminar flame front. The time of contact between the eddy and the flame is given by $t = l/U_{F,L}$. During this contact period the flame is distorted, since the element of flame in contact with the eddy is advanced a distance $\sqrt{\overline{x^2}}$ in the time t because of the contact with the eddy. The turbulent movement velocity is then

$$U'_{F,T} = \frac{\sqrt{\overline{x^2}}}{t} \tag{26}$$

The value of $\sqrt{\overline{x^2}}$ is determined from the equation

$$\sqrt{\overline{x^2}} = \left\{2u'^2\ t_o \left[t - t_o\left(1 - e^{-t/t_o}\right)\right]\right\}^{\frac{1}{2}} \tag{27}$$

where $t_o = l/u'$.

Substituting these relations in equation (26), there results the general equation

$$(U'_{F,T})^2 = 2U_{F,L}\ u' \left[1 - \frac{U_{F,L}}{u'}\left(1 - e^{-u'/U_{F,L}}\right)\right] \tag{28}$$

which, for $t/t_o << 1$ (low-intensity turbulence), reduces to

$$U'_{F,T} = u' \tag{29}$$

and, for $t/t_o >> 1$ (high intensity), reduces to

$$U'_{F,T} = (2U_{F,L}\ u')^{1/2}$$

or (30)

$$\frac{U'_{F,T}}{U_{F,L}} = \left(2\ \frac{u'}{U_{F,L}}\right)^{1/2}$$

Karlovitz found that equation (30) represents the general equation (28) over most of the range. If it is assumed that $u' \propto Re$, then Karlovitz's results are in qualitative agreement with Delbourg's Re variation, but Karlovitz shows a dependence of the ratio on laminar flame velocity.

Equations (28), (29), and (30) give only a part of the turbulent flame movement, however. Karlovitz suggests that the turbulent motion described by $U'_{F,T}$ proceeds forward and backward with equal velocity but produces no net movement of the entire flame. There must be added to the turbulent movement the one-directional flame movement that results from laminar flame propagation so that the turbulent flame velocity is

3547

$$U_{F,T} = U'_{F,T} + U_{F,L} \tag{31}$$

The equations for turbulent flame velocity thus become:

General equation:

$$\frac{U_{F,T}}{U_{F,L}} = 1 + \left\{\left(\frac{2u'}{U_{F,L}}\right)\left[1 - \left(1 - e^{-u'/U_{F,L}}\right)\frac{U_{F,L}}{u'}\right]\right\}^{\frac{1}{2}} \tag{32}$$

For $t/t_o << 1$:

$$\frac{U_{F,T}}{U_{F,L}} = 1 + \frac{u'}{U_{F,L}} \tag{33}$$

For $t/t_o >> 1$:

$$\frac{U_{F,T}}{U_{F,L}} = 1 + \left(\frac{2u'}{U_{F,L}}\right)^{1/2} \tag{34}$$

Leason theory. - Leason (ref. 8) also considers the effect produced when an eddy passes through a flame. The physical picture, which is based on an eddy containing a sinusoidal velocity profile, is illustrated in figure V-22. Leason obtains from the geometric consideration alone the relation

$$\frac{U_{F,T}}{U_{F,L}} = \left[1 + \left(\frac{2u'}{U_o}\right)^2\right]^{1/2} \tag{35}$$

which would be the same as Shelkin's relation for a cone (eq. (15), b = 2) if the U_o in the brackets were replaced by $U_{F,L}$. Leason found that the area extension alone did not account for all of the flame velocity increase with turbulence. Therefore, he added a diffusivity factor similar to Damköhler's, except that it takes into account the statistical property of the turbulent flow. The use of the entire spectrum of turbulence intensities, of course, greatly complicates the equations, but the good agreement obtained by Leason between his modified equation and his experiments is shown in figure V-23. Inasmuch as Leason does not give the complete development of his equations, it is difficult to evaluate the results.

Scurlock and Grover theory. - Scurlock and Grover (ref. 18) developed in detail the processes that can produce wrinkling of the flame surface in turbulent flow. Only large-scale turbulence is considered, and it is assumed that the laminar flame velocity within the wrinkled flame remains unchanged. In the manner of Shelkin (ref. 17) and Leason (ref. 8), Scurlock and Grover assume that the passage of an eddy through the undisturbed flame front produces the wrinkling. A sketch of the assumed wrinkled flame shape after the passage of a certain time is given; note the similarity to figure V-22(c) from Leason's model:

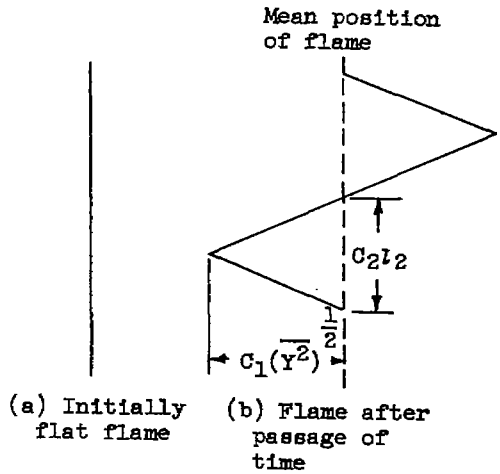

It is assumed that the average height of the wrinkles is proportional to the root-mean-square displacement $(\overline{Y^2})^{1/2}$ of a flame element from the mean flame front position and that the average base width of these wrinkles is proportional to the Eulerian scale l_2. Considering the wrinkle either as an infinitely long prism with the cross section corresponding to one of the wrinkles in the sketch, or as a cone with height and base diameter as shown, would give the ratio of wrinkled area (turbulent flame) to base area (laminar flame):

$$\frac{A_T}{A_L} = \frac{U_{F,T}}{U_{F,L}} = \left[1 + C_3\left(\frac{\overline{Y^2}}{l_2^{\,2}}\right)\right]^{1/2} \tag{36}$$

where $C_3 = 4C_1^{\,2}/C_2^{\,2}$. This has the same form as Shelkin's equation (see eq. (15)), but the root-mean-square displacement and Eulerian scale have been used instead of the turbulence intensity and laminar flame velocity.

According to the preceding picture of a turbulent flame, the ratio of the turbulent to laminar flame velocities will depend on both $\overline{Y^2}$ and l_2. Scurlock and Grover describe three effects believed to be important in determining $\overline{Y^2}$. These are:

(1) Eddy diffusion associated with turbulence in the unburned gases which tends to increase $\overline{Y^2}$

(2) Propagation of the flame into the unburned gases, which tends to reduce $\overline{Y^2}$

(3) Flame-generated instability and shear and eddy diffusion, which are associated with the density decrease across a flame and which tend to increase $\overline{Y^2}$

The process of eddy diffusion resulting from turbulence in the approach flow can be considered alone if $U_{F,L}$ is assumed small so that $U_{F,L}/u'$ approaches zero and if the density change across the flame is ignored. Under these conditions, the mean displacement at any time t can be calculated from the equation

3517

$$\frac{d(\overline{Y^2})}{dt} = 2(u')^2 \int_0^t R_t \, dt \tag{37}$$

(See ch. II for a more detailed discussion of calculations of the mean displacement.) In the actual flame, however, the flame has moved a distance $y = U_{F,L}\, t$, so that the simple displacement previously calculated does not apply. Consideration must also be given to the change of flame position. Scurlock and Grover accomplish this by means of a mixed (time and position) correlation factor R_{ty} such that

$$\frac{d(\overline{Y^2})}{dt} = 2(u')^2 \int_0^t R_{ty} \, dt = 2(u')^2 \int_0^t R_t R_y \, dt \tag{38}$$

For very short diffusion times, $R_t R_y \approx 1$ and equation (38) reduces to

$$\frac{d\overline{Y^2}}{dt} \approx 2(u')^2 \, t \tag{39}$$

or

$$\overline{Y^2} = (u't)^2 \tag{40}$$

For long diffusion times,

$$\overline{Y^2} = 2u' l_1' t \tag{41}$$

where

$$l_1' = u' \int_0^\infty R_t R_y \, dt = u' T_o \tag{42}$$

It is much more difficult to evaluate the equation for intermediate times. Scurlock and Grover derive the equation

$$\overline{Y^2} = 2u' l_1' t \left[1 - \frac{l_1'}{u't}\left(1 - e^{-u't/l_1'}\right)\right] \tag{43}$$

and suggest that l_1' can be calculated from the equation

$$l_1' = \frac{l_1}{1 + \frac{U_{F,L}}{2u'}} = \frac{l_2}{2 + \frac{U_{F,L}}{u'}} \tag{44}$$

It should be noted that the consideration of eddy diffusion alone predicts that the area increases rapidly and reaches no limiting value with increasing time. The rate of area increase is reduced by decreasing u', by increasing $U_{F,L}$, and by increasing l_2.

The tendency for a flame to flatten and decrease the flame surface was treated by Karlovitz and coworkers (ref. 6). Scurlock uses an essentially similar treatment. Consider a single wrinkle in the flame and the effect of laminar flame propagation.

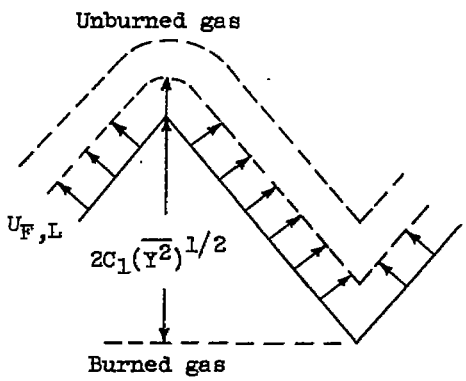

As illustrated, the presence of a constant velocity tends to flatten the flame, thus reducing the area ratio A_T/A_L. If the mean depth of the wrinkle is $C_1(\overline{Y^2})^{1/2}$, the distance between the heads of two wrinkles, one facing toward the unburned gas and the other toward the burned gas, is $2C_1(\overline{Y^2})^{1/2}$. The rate of change of this quantity with time consists of two terms, a positive term representing the rate of movement of the apex into the unburned gas and equal to $U_{F,L}$, and a negative term representing a decrease in the protrusion of the negative apex into the burned gas and given by $-U_{F,L}(1 + C_2\,\overline{Y^2}/l_2^2)^{1/2}$. The change in displacement due to flame propagation may thus be obtained from

$$\frac{d(\overline{Y^2})^{1/2}}{dt} = -\,C_3U_{F,L}\left\{\left[1 + C_2\left(\frac{\overline{Y^2}}{l_2^2}\right)\right]^{1/2} - 1\right\} \tag{45}$$

The negative sign indicates the reduction in $\overline{Y^2}$ due to the flame propagation.

The last effect considered by Scurlock and Grover is the increased displacement due to flame-generated disturbance resulting from the decreased density of the burned gas compared with the unburned gas. A sketch is presented in figure V-24 showing the shear regions that generate turbulence in a rod-stabilized flame. In region 1, the unburned gas velocity exceeds the velocities in the sheltered eddy region behind

the stabilizer. In region 2, the unburned gases, which have been accelerated, still have lower velocities than the burned gases. Finally, the burned gases are completely mixed and a uniform velocity results. They write momentum balances between the unburned gases and the gases exiting in nonuniform flow from the combustion zone (shear region 2 in fig. V-24), and between the unburned gases and the gases exiting in uniform flow after complete mixing (burned gases of region 3 in fig. V-24). From these two momentum balances they solve for half the difference in the squares of the velocities of unmixed and mixed burned gases; this quantity represents the maximum kinetic energy that would be available for the turbulence generation from this source. Assuming that this energy is equally divided among the three directions to produce an isotropic turbulence intensity u_F',

$$\frac{1}{3} E = \frac{1}{2} u_F'^2 \tag{46}$$

or

$$u_F' = \left(\frac{2E}{3}\right)^{1/2} \tag{47}$$

The value of u_F' so calculated may be combined with u_o' of the approach stream to give the total intensity u' in the flame as follows:

$$u' = \sqrt{(u_o')^2 + (u_F')^2} \tag{48}$$

The combined displacement for the three effects can then be calculated from the sum of equations (43) and (45) wherein u' is calculated by equation (48).

A comparison of the shape and thickness of turbulent flames resulting from a consideration of the three processes influencing $\overline{Y^2}$ is shown in figure V-25. The curves of $U_{F,T}/U_{F,L}$ against initial velocity calculated from a combination of the three effects agree well in shape with the data of reference 3, although the theory does not predict the strong effect of scale (as indicated by the dependence of $U_{F,T}/U_{F,L}$ on the tube diameter) found in reference 3. Scurlock and Grover suggest that the discrepancy may be in the fraction of the kinetic energy of the burned gases, which is converted into turbulence having a scale dependence.

The theories of turbulent flame velocity consider small-scale turbulence as a means of increasing the heat-transfer and diffusion characteristics of the system, while large-scale turbulence increases the surface area of the flame. The latter condition is probably of the most interest in practical applications. The theories are not yet sufficiently advanced to be of great value in predicting turbulent flame velocities. It appears, at this time, that more reliable estimates may be made using the empirical relations listed in tables V-I and -II.

Flame-Induced Turbulence

The theoretical studies presented attempt to relate the turbulent flame velocity to the intensity and scale of the approach-stream turbulence. While Damköhler, Delbourg, and Leason met with some success in this regard, some of the observations by Scurlock and Karlovitz require additional explanations.

If the turbulent flame velocity is strongly dependent on the approach-stream turbulence, it would be expected that changes in the intensity of turbulence should be reflected in the flame velocity. Scurlock (ref. 10) found in his V-flame experiments that the insertion of screens in the approach flow had a negligible effect on the measured flame velocity. He explains this phenomenon by suggesting a model in which the approach-stream turbulence merely is added to a much stronger turbulence produced by the flame itself. As burning begins at the stabilizer, as shown in figure V-24, the unburned gas around it must either expand or accelerate. Since the gas flow is enclosed in a tunnel, the unburned gases accelerate, producing shear forces between the burned and unburned gas and creating a highly turbulent flow. If the shear forces become sufficiently great, as may occur at very high velocities, the flame may not be able to transfer heat and active particles at a sufficient rate to propagate. This suggests that too much turbulence can be detrimental to flame propagation and is consistent with experimental observations of flame stability (ch. VI).

Karlovitz (ref. 6) subsequently found it necessary to consider flame-induced turbulence for open flames as well. Since he used an angle method to determine turbulent flame velocity, he was able to measure flame velocity as a function of the distance from the tube edge. Using equation (32) to calculate turbulence intensities from his measured turbulent flame velocities, Karlovitz found that the calculated u' agreed with the u' measured by a hot-wire anemometer only at the burner rim, and, as shown in figure V-26, the calculated u' is considerably greater than the measured intensity at other points. It was mentioned previously that the expansion of the burned gas may either accelerate the unburned gas or cause it to expand. In the closed pipe, a velocity increase was suggested. With the open flame, Karlovitz suggests that the expansion of the burned gas from the flame, which is oriented at random angles, produces random fluctuations in the unburned gas, thus increasing the turbulence intensity. The turbulence intensity increases as the burning proceeds from the base to the tip of the flame. Karlovitz computes the maximum flame-generated turbulence from an equation based on the expansion ratio, where

$$u' = \left(\frac{1}{\sqrt{3}}\right)\left(\frac{\rho_u}{\rho_b} - 1\right) U_{F,L} \tag{49}$$

The calculated flame-generated turbulence is shown in figure V-26, and it is evident that this could account for the discrepancy between calculated and measured turbulence intensities.

APPLICABILITY OF TURBULENT FLAME STUDIES TO JET-ENGINE COMBUSTION

One of the characteristics that the turbulent flames considered in this chapter have in common is the apparent existence of a continuous flame surface. While islands of flame may be broken away from the main body of flame under high flow conditions, such flames have not received much study. The flames existing in practical combustors may or may not have a continuous surface. It appears reasonable that a flame burning from a flame holder, at least under conditions of moderate flow velocity, should resemble the V-flames discussed herein. There is no analogy, however, between these flames and the highly broken-up flame in a turbojet combustor. Nevertheless, if these islands of flame behave as individual burning spheres, each such sphere may retain the burning characteristics of the turbulent flames discussed in this chapter.

Despite the uncertainty in the prediction of turbulent burning velocity, the flame dimensions included herein may be used to compute the space requirements for combustion under a given flow condition. It may be assumed, for example, that the envelope of a turbulent Bunsen flame represents the minimum volume necessary for complete combustion of the mixture flowing into the flame. Correlations based on this and analogous concepts are presented in subsequent chapters.

REFERENCES

1. Lewis, Bernard, and von Elbe Guenther: Combustion, Flames and Explosions of Gases. Academic Press, Inc., 1951.

2. Kaskan, W. E.: An Investigation of Vibrating Flames. Fourth Symposium (International) on Combustion, The Williams & Wilkins Co. (Baltimore), 1953, pp. 575-591.

3. Bollinger, Lowell M., and Williams, David T.: Effect of Reynolds Number in Turbulent-Flow Range on Flame Speeds of Bunsen Burner Flames. NACA Rep. 932. 1949. (Supersedes NACA TN 1707.)

4. Levine, Oscar, and Gerstein, Melvin: Fundamental Flame Velocities of Pure Hydrocarbons. III - Extension of Tube Method to High Flame Velocities - Acetylene-Air Mixtures. NACA RM E51J05, 1951.

5. Damköhler, Gerhard: The Effect of Turbulence on the Flame Velocity in Gas Mixtures. NACA TM 1112, 1947.

6. Karlovitz, Béla, Denniston, D. W., Jr., and Wells, F. E.: Investigation of Turbulent Flames. Jour. Chem. Phys., vol. 19, no. 5, May 1951, pp. 541-547.

7. Hottel, H. C., Williams, G. C., and Levine, R. S.: The Influence of Isotropic Turbulence on Flame Propagation. Fourth Symposium (International) on Combustion, The Williams & Wilkins Co. (Baltimore), 1953, pp. 636-644.

8. Leason, D. B.: Turbulence and Flame Propagation in Premixed Gases. Fuel, vol. XXX, no. 10. Oct. 1951, pp. 233-238; discussion, pp. 238-239.

9. Mickelsen, William R.: The Propagation of a Free Flame Through a Turbulent Gas Stream. M. S. Thesis, Case Inst. of Tech., 1933.

10. Scurlock, A. C.: Flame Stabilization and Propagation in High-Velocity Gas Streams. Meteor Rep. 19, M.I.T., May 1948. (Contract NOrd 9661.)

11. Wohl, Kurt, Shore, L., von Rosenberg, H., and Weil, C. W.: The Burning Velocity of Turbulent Flames. Fourth Symposium (International) on Combustion, The Williams & Wilkins Co. (Baltimore), 1953, pp. 620-635.

12. Delbourg, M. P.: Influence of the Turbulence on the Mechanism of the Reactions of Combustion in the Gaseous Phase. Trans. from Reveu de L'Institute Francaise de Petrole et annales des combustibles liquids, vol. 4, Sept. 1949, pp. 530-538.

13. Edse, Rudolph: Studies on Burner Flames of Hydrogen-Oxygen Mixtures at High Pressures. Tech. Rep. 52-59, Flight Res. Lab., Wright Air Dev. Center, Wright-Patterson Air Force Base, Apr. 1952. (RDO No. R-467-1.)

14. Culshaw, G. W., and Garside, J. E.: Recent Studies of Aerated Burner Flames. Inst. Gas Eng. (London), Inst. Gas Res. Fellowship Rep. 1946-1947. (Reviews papers from period 1943-1946, including those of Delbourg, Heiligenstaedt, and Vasilesco.)

15. Wright, F. H.: Measurements of Flame Speed and Turbulence in a Small Burner. Prog. Rep. No. 3-21, C.I.T., June 6, 1950.

16. Wohl, K., et al.: Investigation of the Basic Problems Associated with Gaseous Combustion. Proj. Squid Semi-Annual Prog. Rep., James Forrestal Res. Center, Princeton Univ., Apr. 1, 1953, pp. 61-73. (Office Naval Res. Contract N7-ori-105, Task Order III, NR-098-038.)

17. Shelkin, K. I.: On Combustion in a Turbulent Flow. NACA TM 1110, 1947.

18. Scurlock, A. C., and Grover, J. H.: Propagation of Turbulent Flames. Fourth Symposium (International) on Combustion, The Williams & Wilkins Co. (Baltimore), 1953, pp. 645-658.

3517

TABLE V-I. - EXPERIMENTAL RELATIONS BETWEEN TURBULENT FLAME VELOCITY AND REYNOLDS NUMBER

Mixture	Reynolds number range	Relation	Reference
Propane-oxygen	2,000-5,000 5,000-40,000	$U_{F,T} \propto Re^{0.5}$ $U_{F,T} = C_1 + C_2 Re$	5
Town gas - air	2,000-40,000	$U_{F,T} \propto U_{F,L}\, Re^{0.4}$	12
Propane-air[a] Ethene-air[a] Acetylene-air[a]	3,000-40,000	$U_{F,T} = U_{F,L}\,(0.18 d_t^{0.26} Re^{0.24})$	3

[a]Fuel-oxidant ratio for maximum turbulent flame velocity.

TABLE V-II. - EXPERIMENTAL RELATIONS BETWEEN TURBULENT FLAME VELOCITY AND TURBULENCE INTENSITY

Mixture	Relation	Reference
Propane-air	$U_{F,T} \propto v'(U_o)$	15
Butane-air Stoichiometric 1.25 Stoichiometric 1.50 Stoichiometric	 $U_{F,T} = U_{F,L}\,[1 + 0.02\, U_o(u'/U_o + 0.04)]$ $U_{F,T} = U_{F,L}\,[1 + (24 + 0.0147\, U_o)(u'/U_{T,o} + 0.01)]$ $U_{F,T} = U_{F,L}\,[1 + (77 + 0.0406\, U_o)(u'/U_o + 0.01)]$	16
Propane-air; stoichiometric	$U_{F,T} = U_{F,L}\left[1 + 26.2\,(u'/U_o) + 1.40\,(U_o/24)^{1.12}\right]$	11

3517

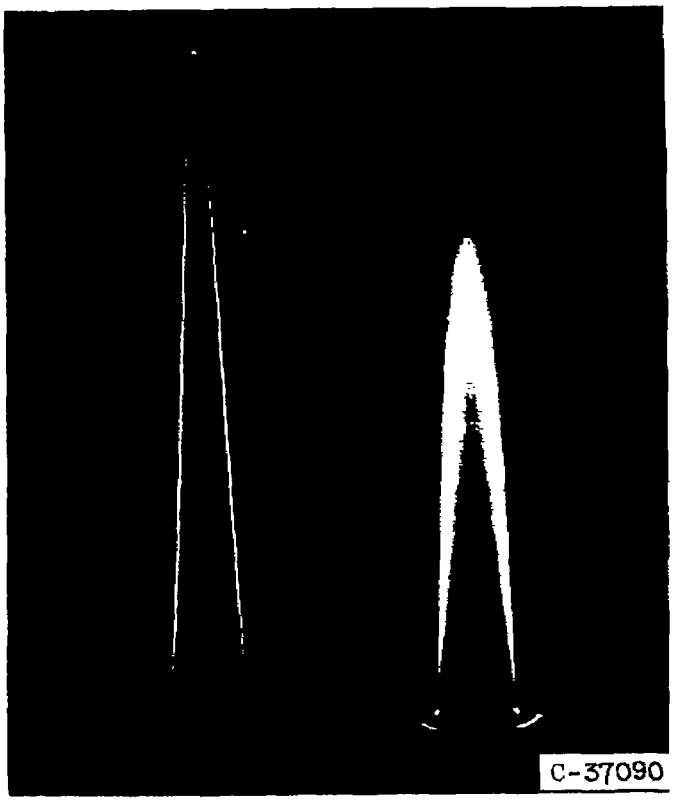

Laminar Turbulent

Figure V-1. - Comparison of direct photographs of a laminar and turbulent flame at the same flow rate, fuel-air ratio, and burner size.

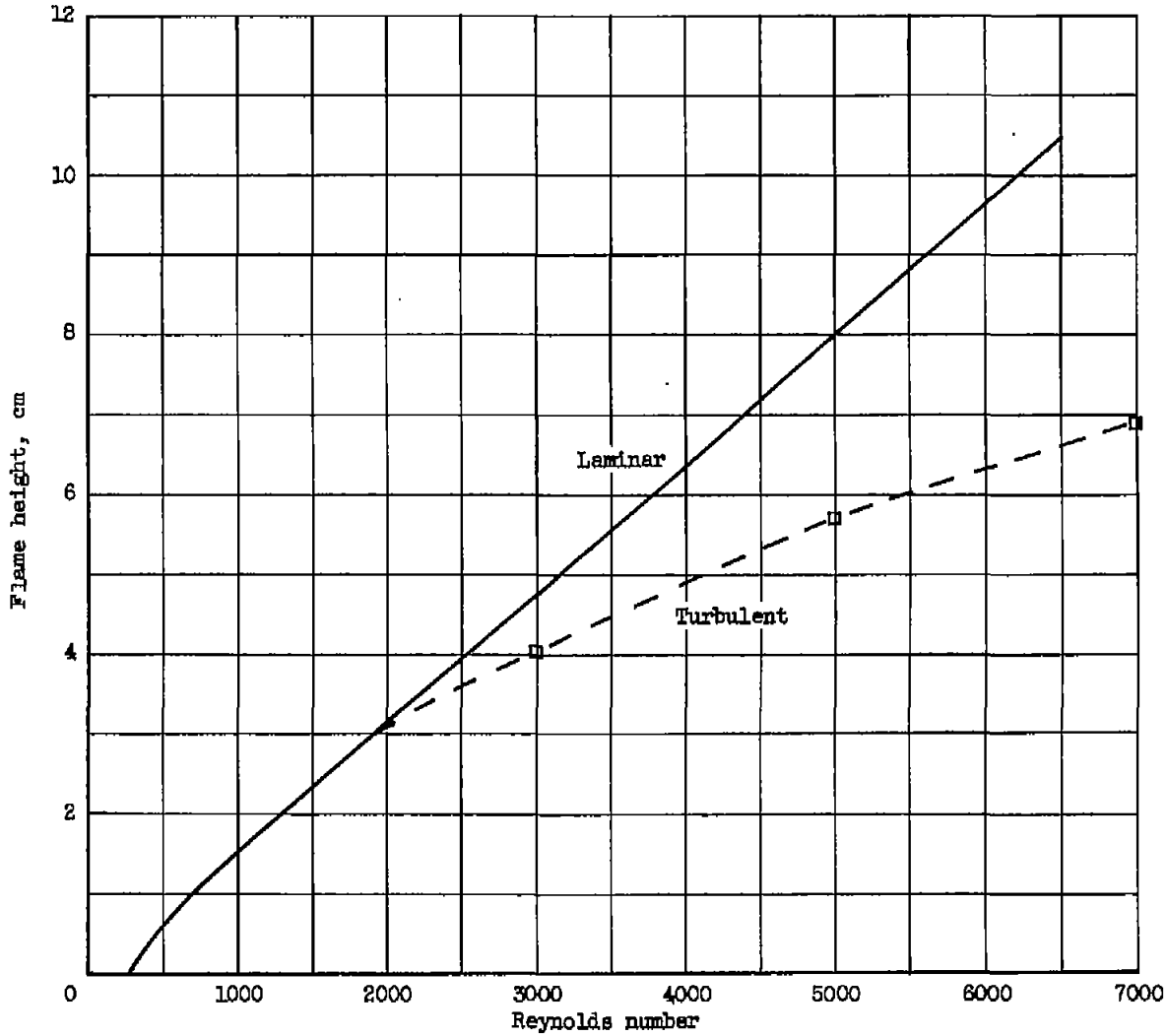

Figure V-2. - Effect of Reynolds number of approach flow on cone heights of laminar and turbulent flames.

3517

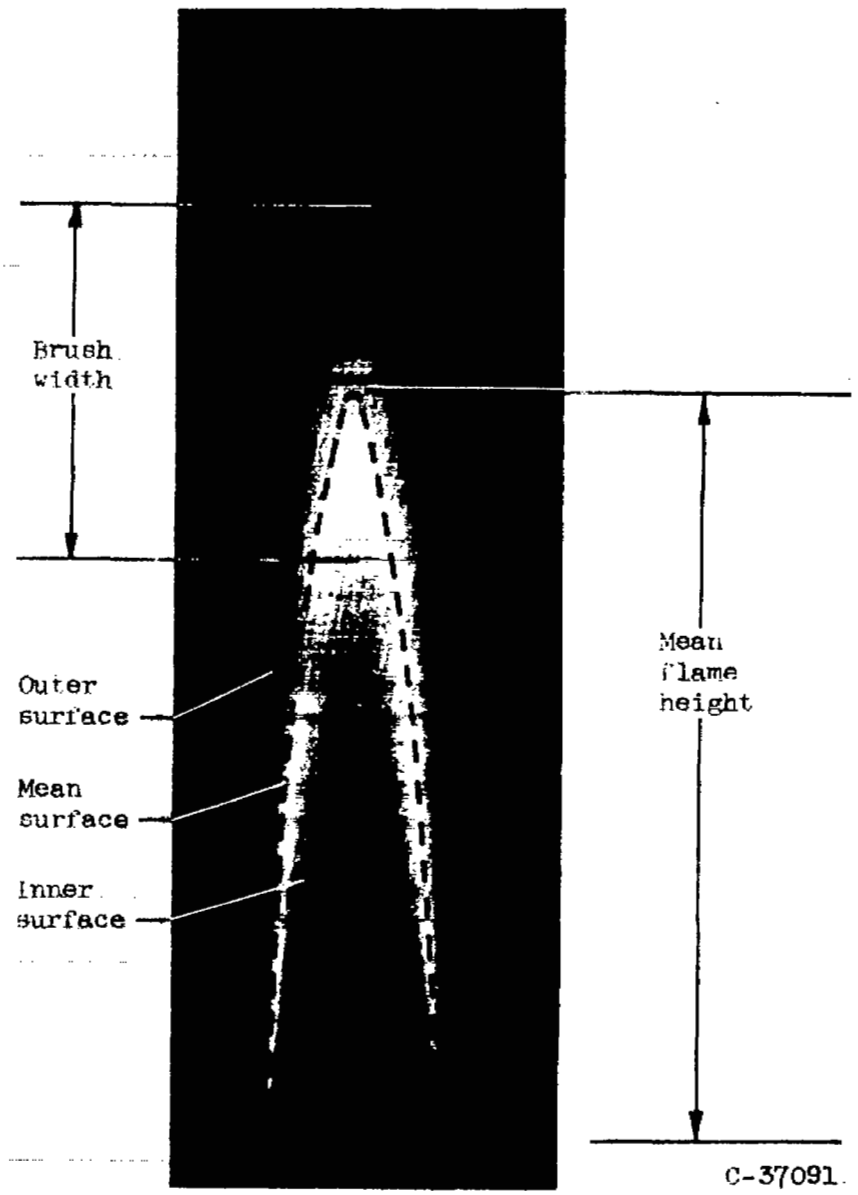

Figure V-3. - Time exposure of luminous turbulent flame showing boundaries of flame brush and mean surface about which instantaneous flame front oscillates (ref. 3).

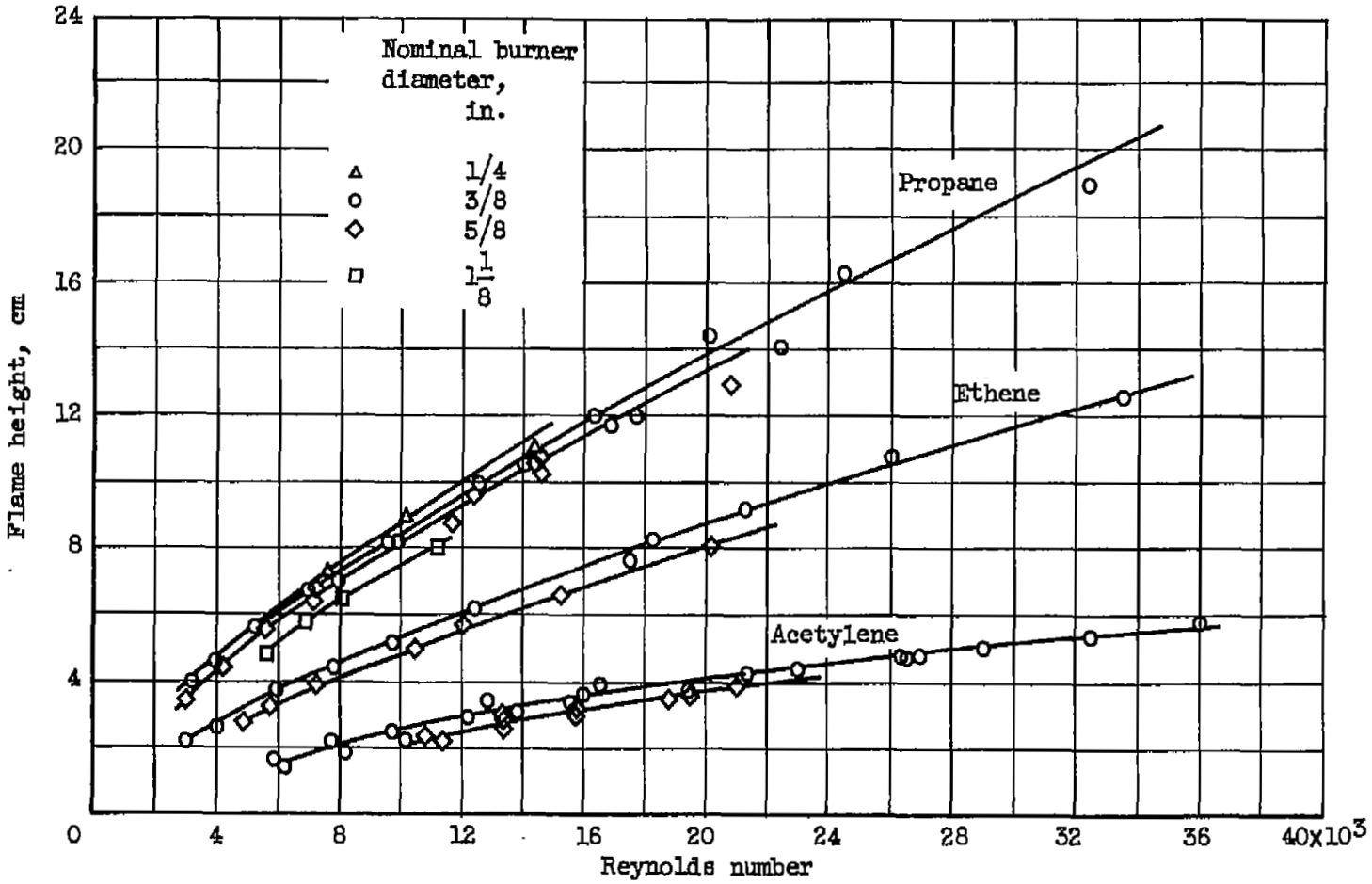

Figure V-4. - Variation of mean flame height with Reynolds number for hydrocarbon-air flames. Constant density and viscosity (ref. 3).

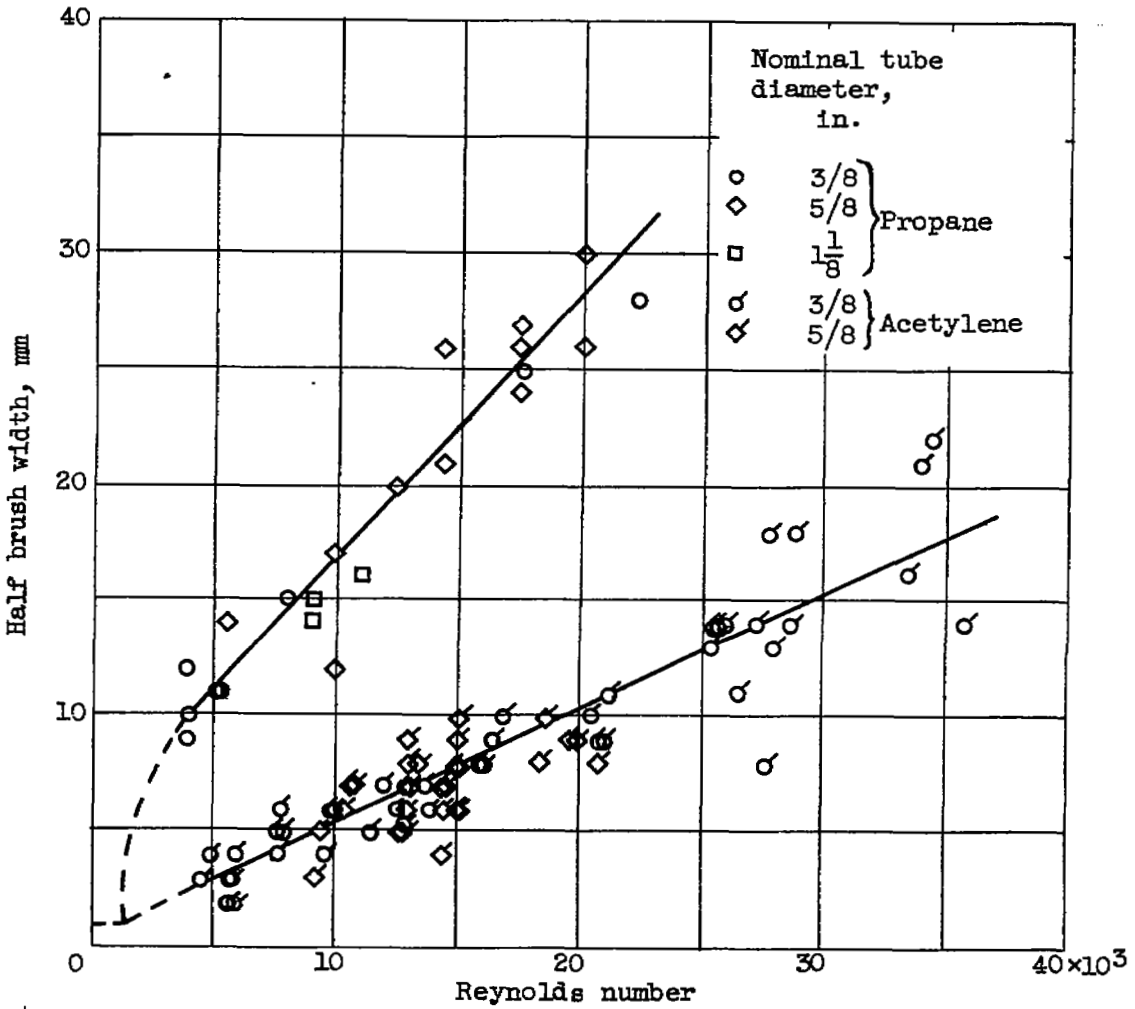

Figure V-5. - Variation of half brush width with Reynolds number. Constant density and viscosity (ref. 3).

3517

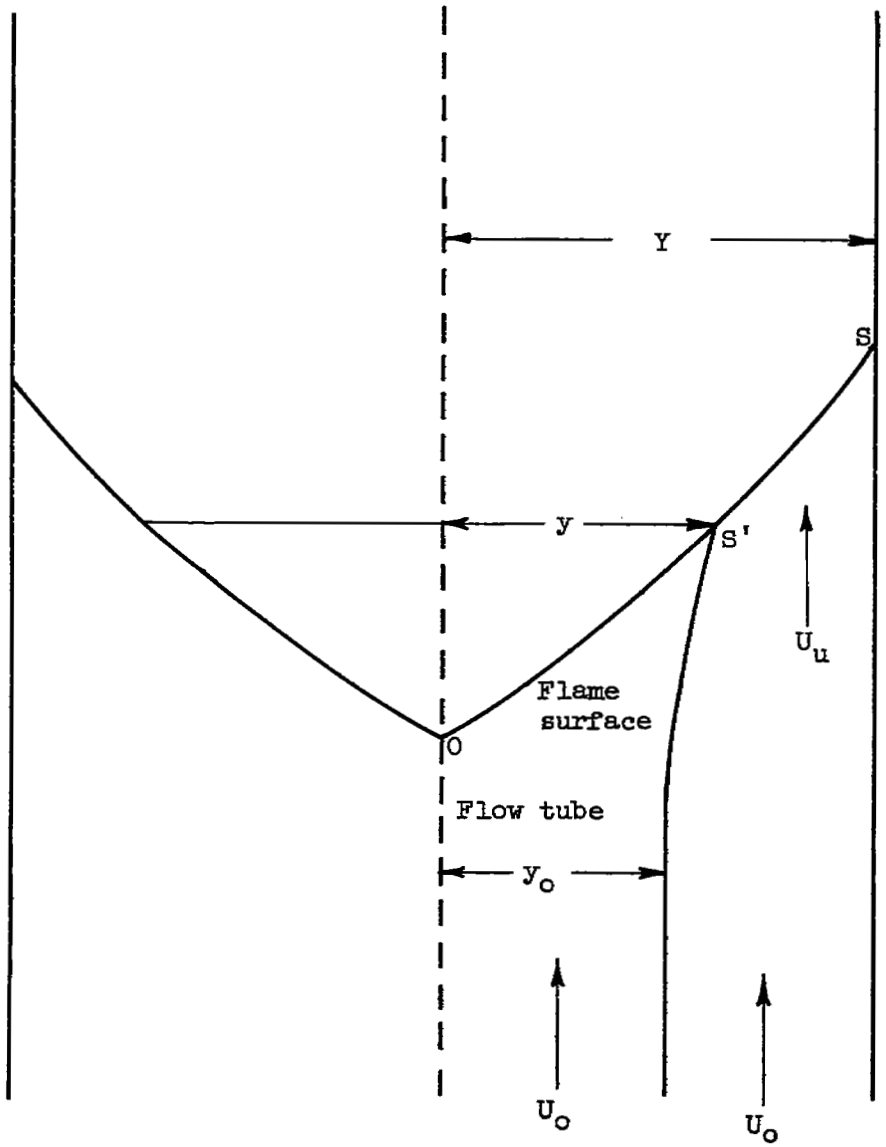

Figure V-6. - Sketch of V-flame showing quantities used in calculating flame velocity (ref. 10).

3517

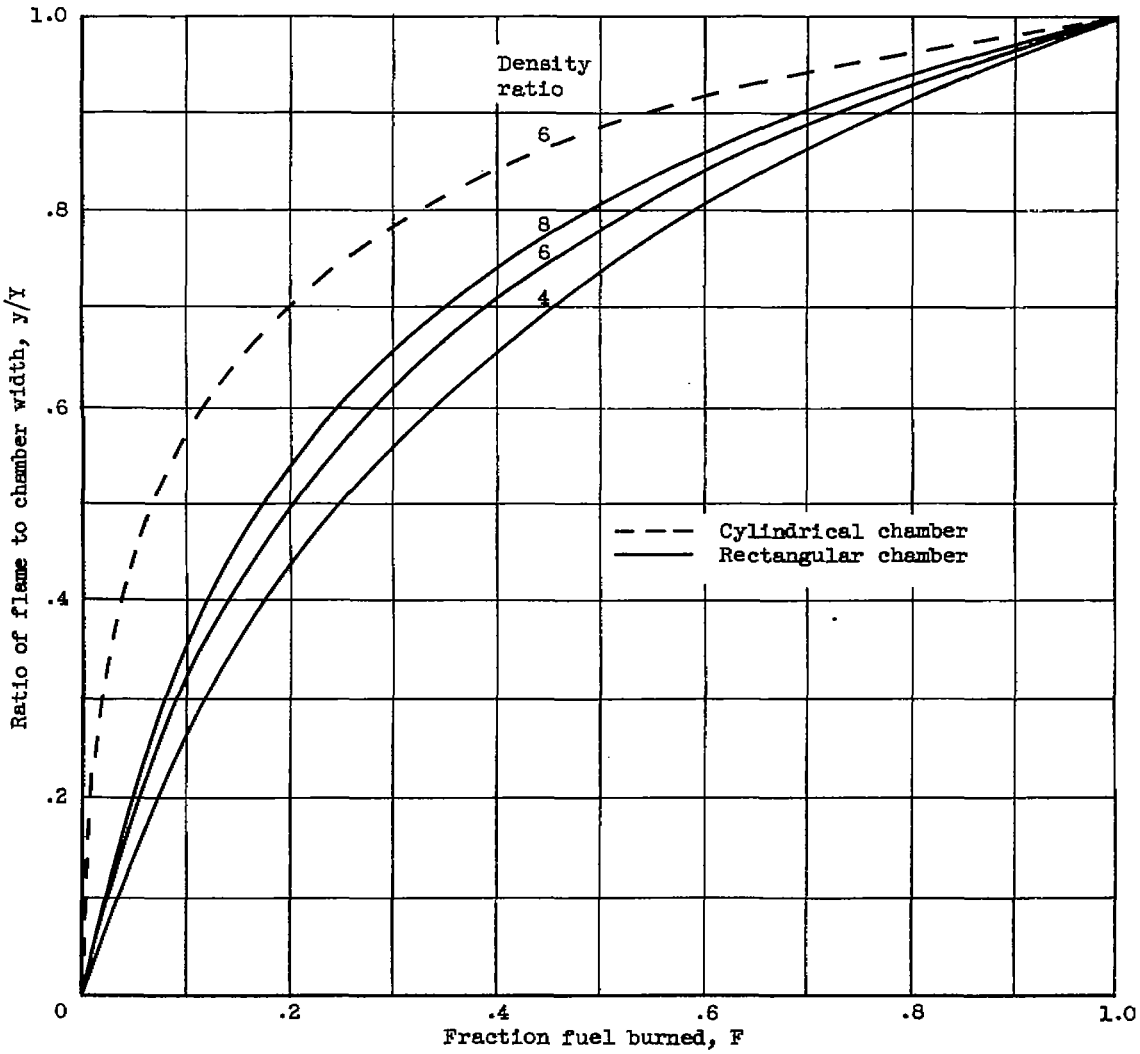

Figure V-7. - Calculated variation in ratio of flame width to chamber width with fraction of fuel burned up to point of measurement of flame width (ref. 10).

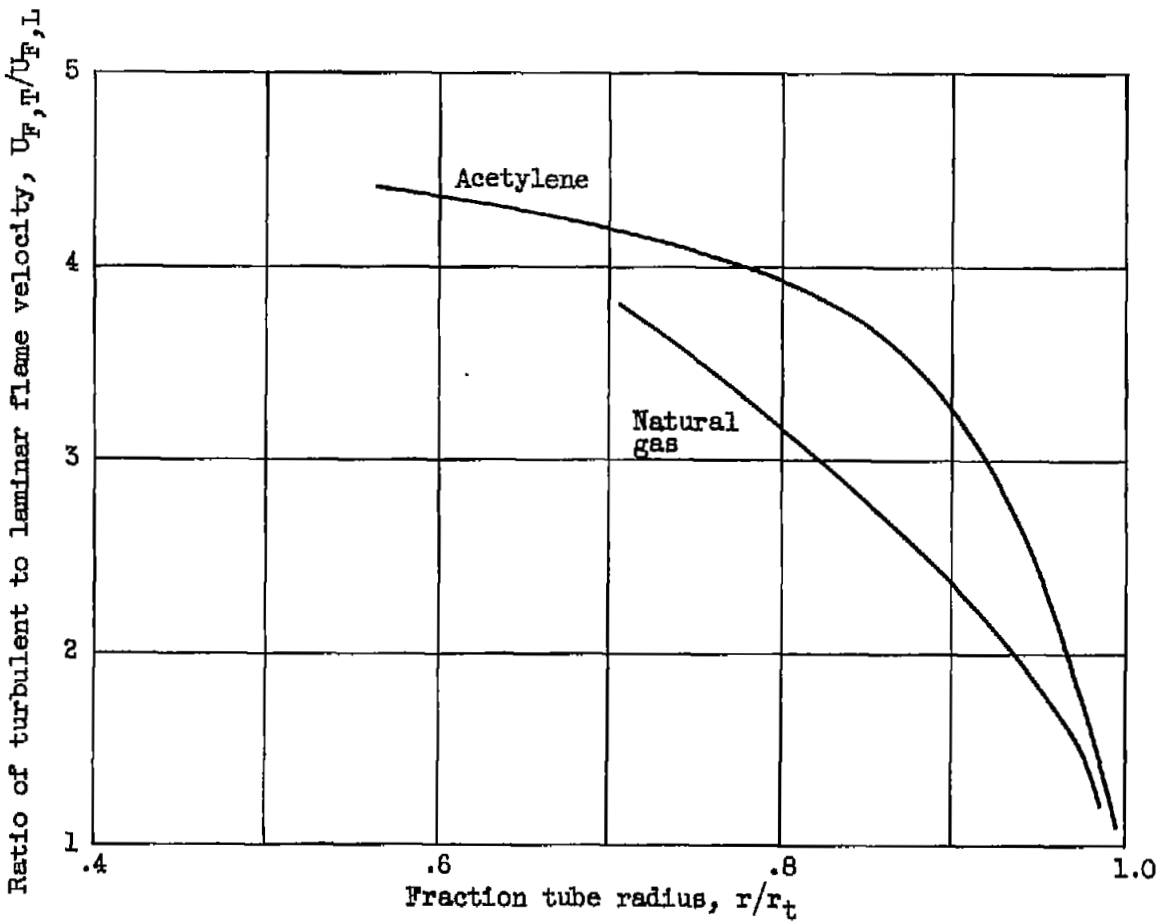

Figure V-8. - Variation in ratio of turbulent to laminar flame velocity with fraction of radial distance from tube axis to rim, for stoichiometric acetylene-air and natural gas - air flames. Reynolds number, 25,000 (ref. 6).

3517

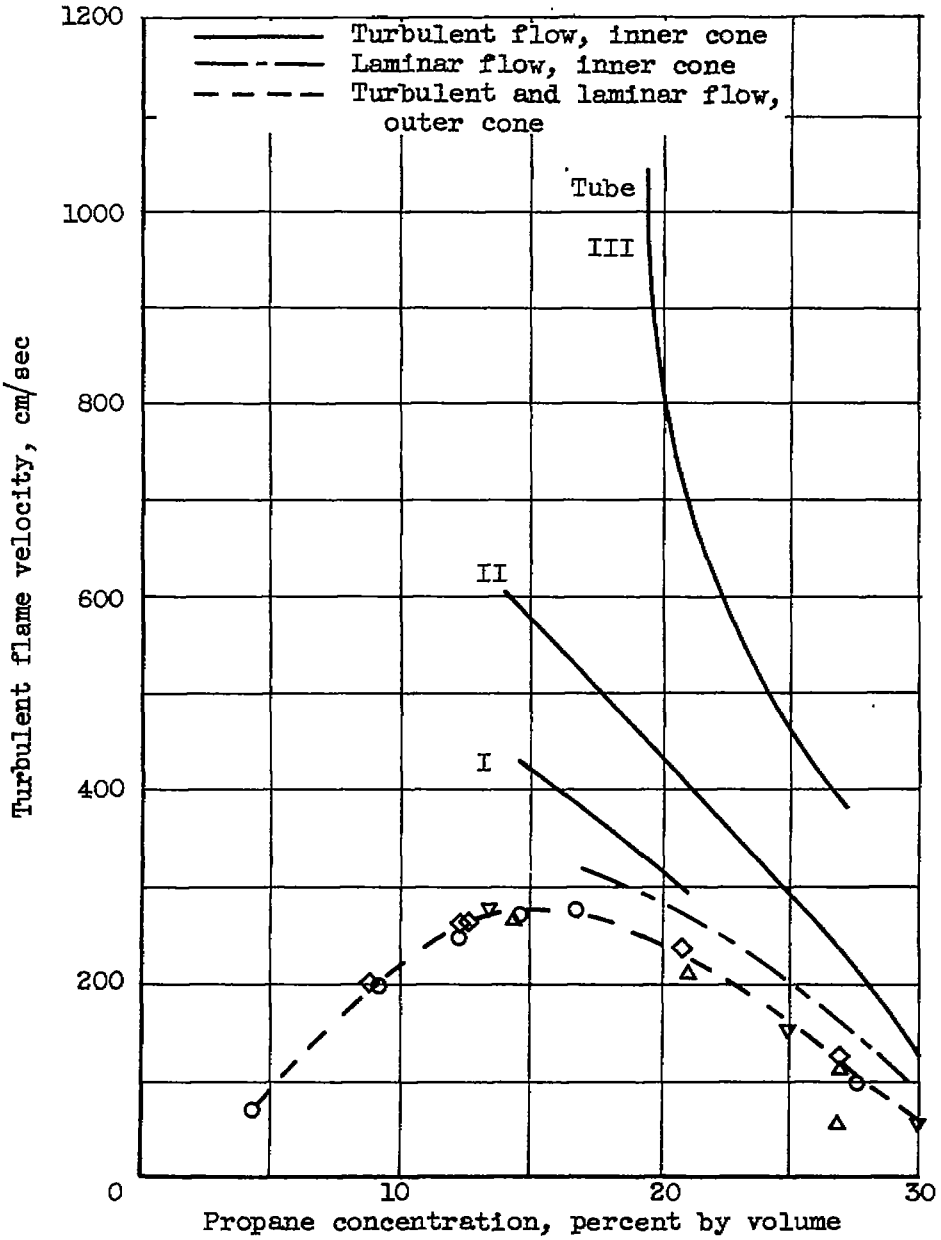

Figure V-9. - Effect of fuel concentration on laminar and turbulent flame velocities of propane-oxygen mixtures (ref. 5).

3547

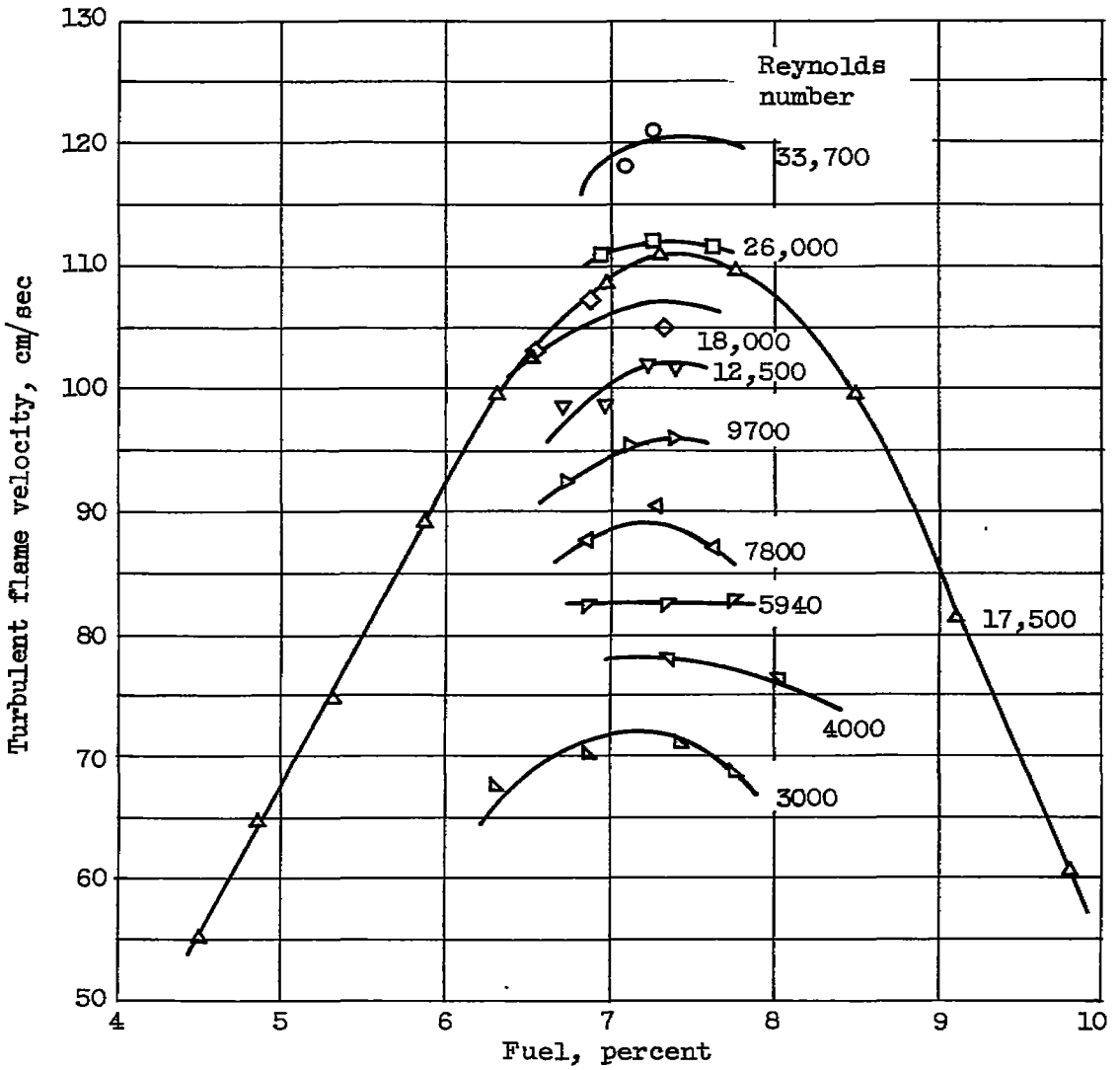

Figure V-10. - Effect of fuel concentration on turbulent flame velocity of ethene-air mixtures at various Reynolds numbers. Constant density and viscosity; 3/8-inch burner (ref. 3).

3517

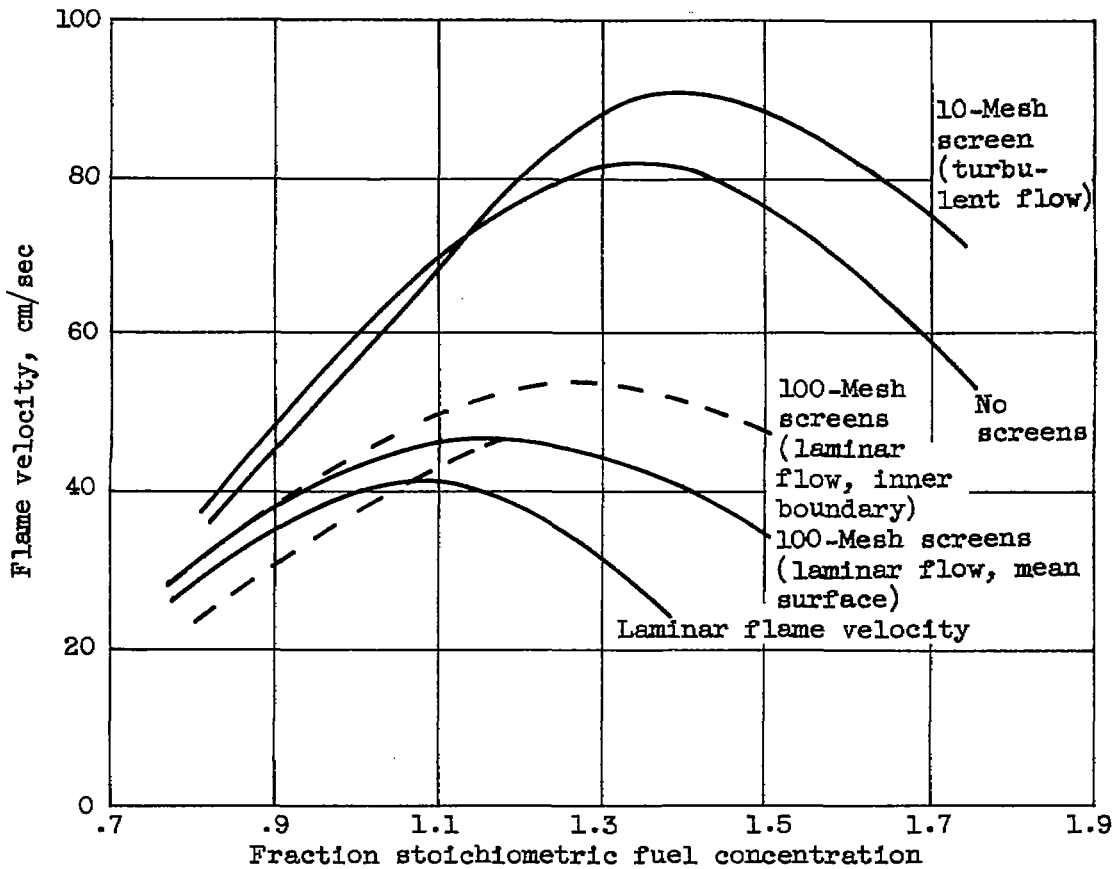

Figure V- 11. - Variation of flame velocity of butane-air mixtures with volume fraction of stoichiometric fuel concentration for various degrees of turbulence. Turbulent flames held by pilot flame on 2.55-centimeter burner at 540 centimeters per second; Reynolds number, 8800 (ref. 11).

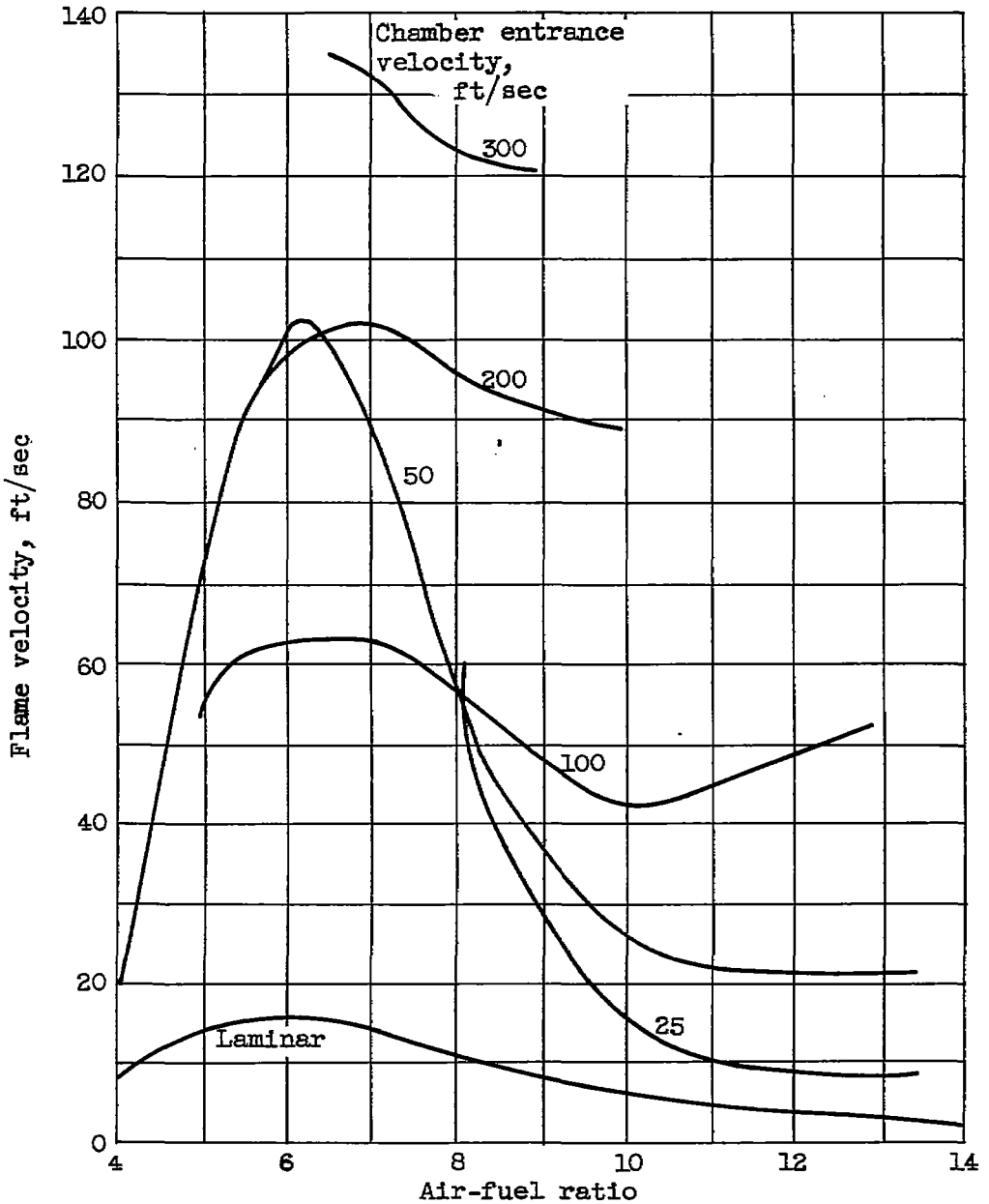

Figure V-12. - Effect of air-fuel ratio on turbulent flame velocity of Cambridge city gas - air mixtures measured from confined V-flames at various chamber entrance velocities (ref. 10).

3517

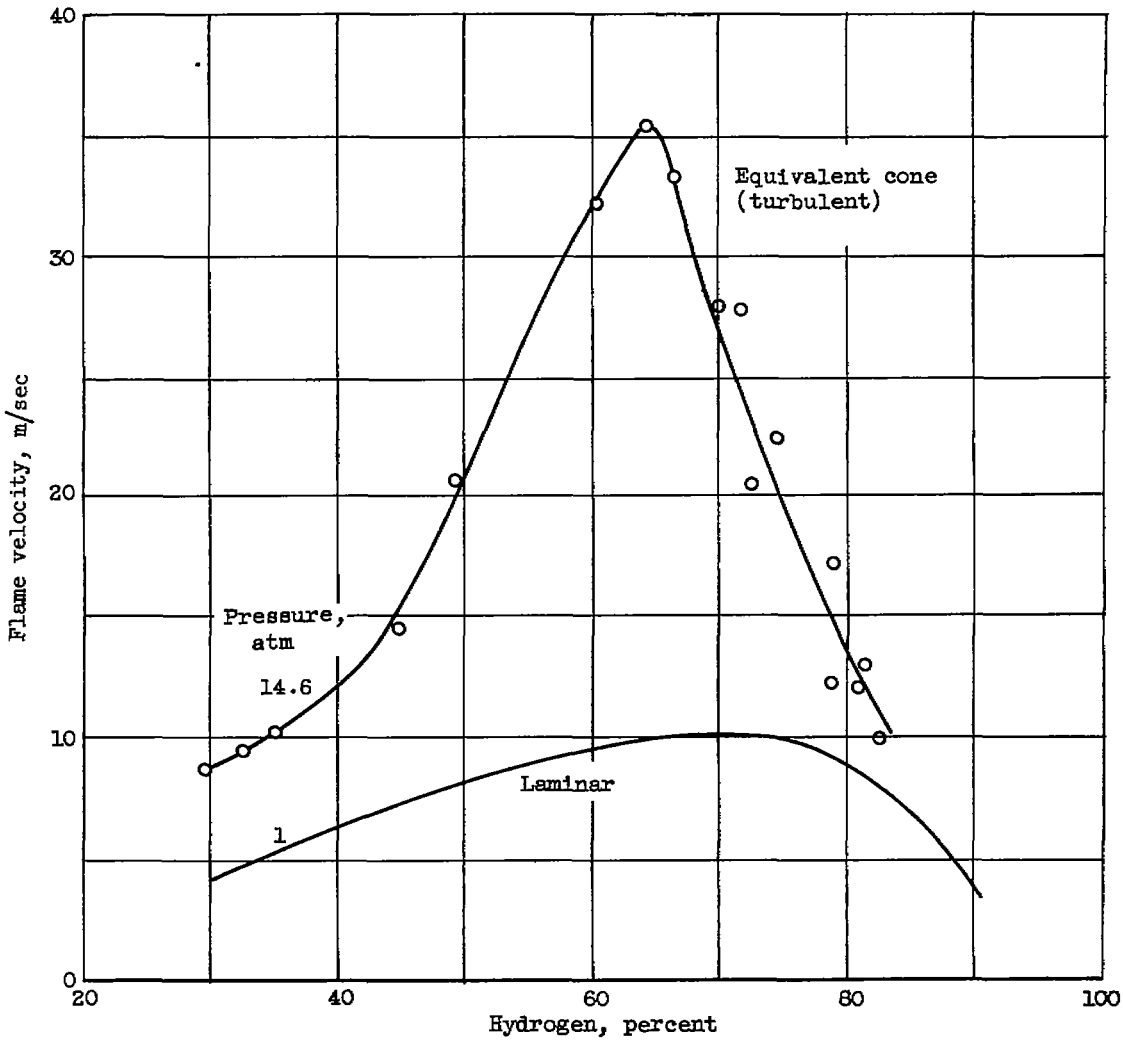

Figure V-13. - Comparison of equivalent cone flame velocity with laminar flame velocity. Hydrogen-oxygen flames on 0.3-millimeter burner (ref. 13).

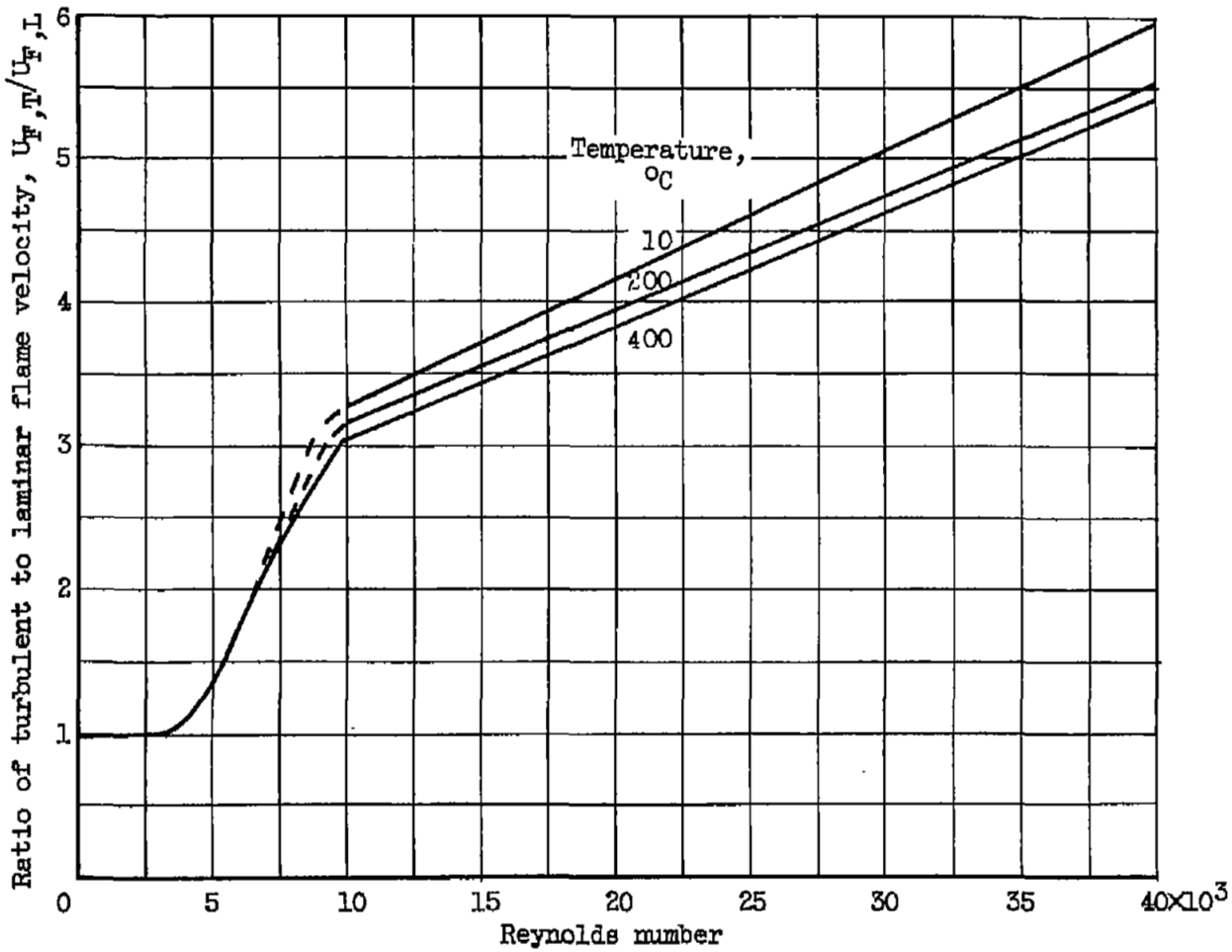

Figure V-14. - Effect of Reynolds number on ratio of turbulent to laminar flame velocity for coke-oven gas-air flames (ref. 14).

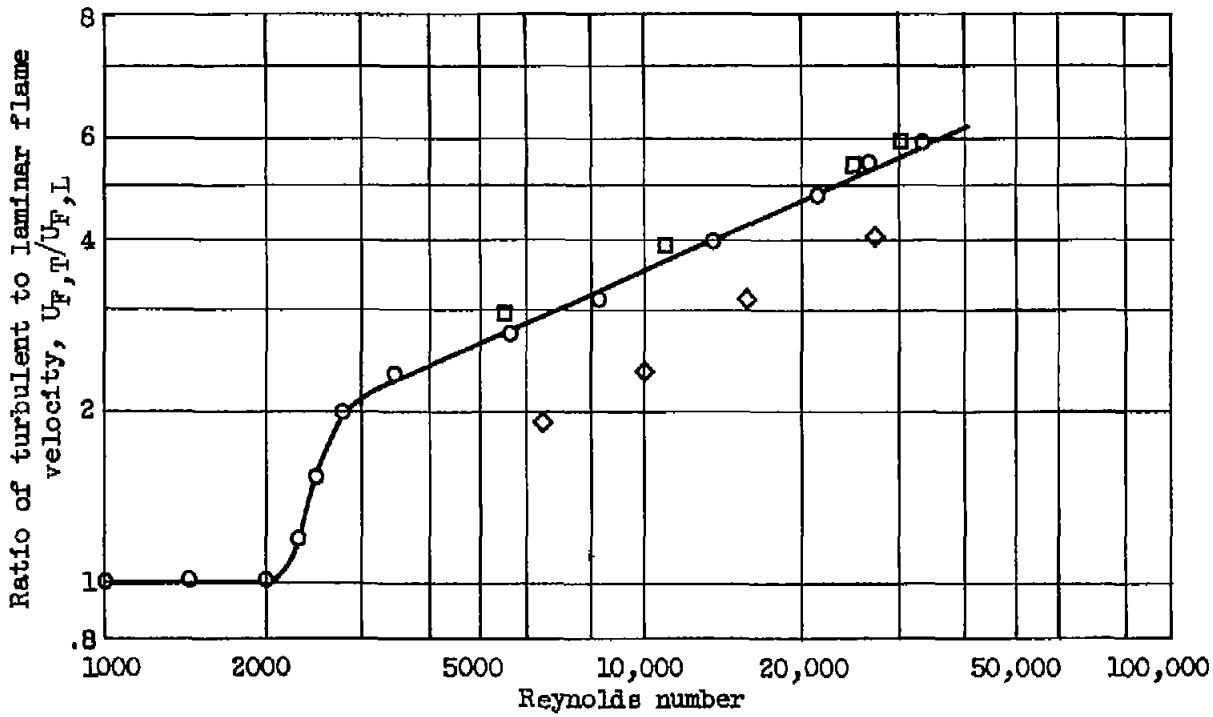

Figure V-15. - Effect of Reynolds number on ratio of turbulent to laminar flame velocity for town gas - air flames. Constant density and viscosity (ref. 14). Symbols indicate points of constant fuel-air ratio unspecified by reference.

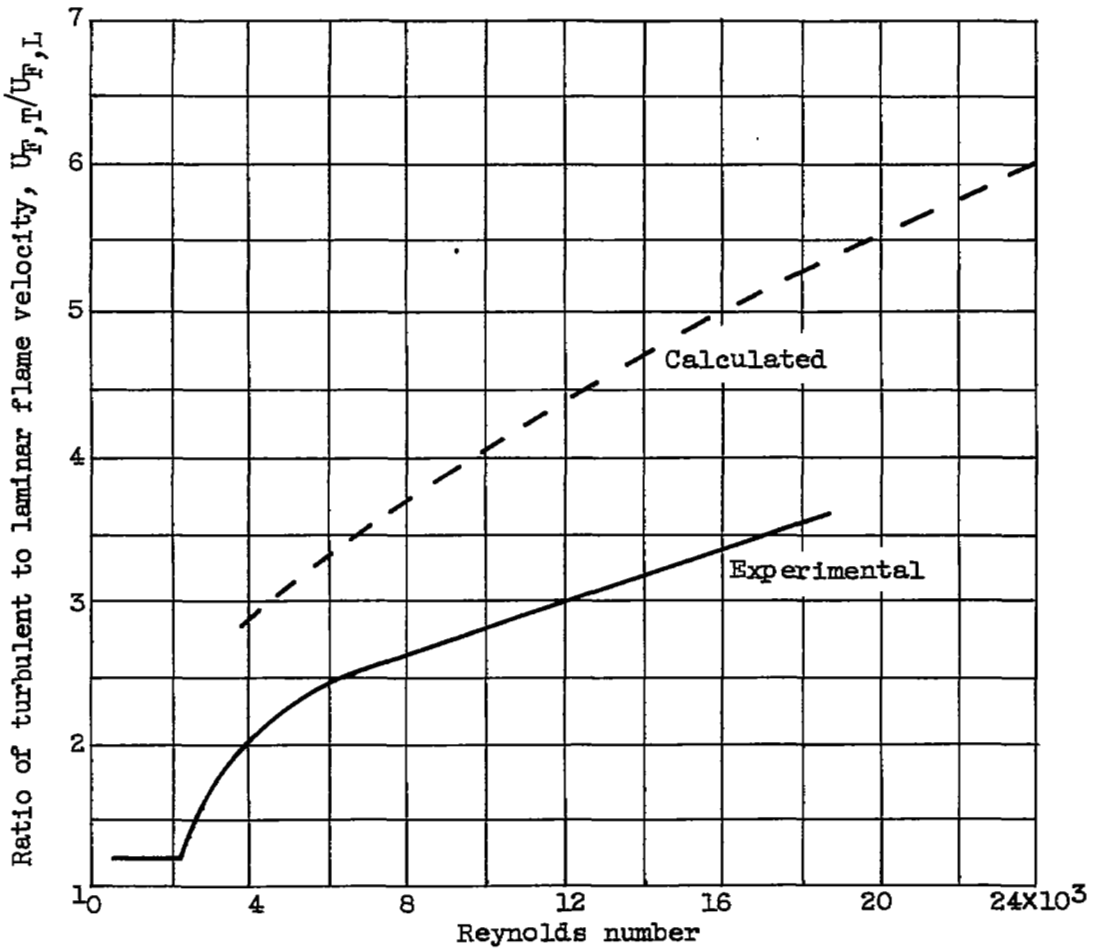

Figure V-16. - Effect of Reynolds number on ratio of turbulent to laminar flame velocity for propane-oxygen flames. Constant density and viscosity (ref. 5).

3517

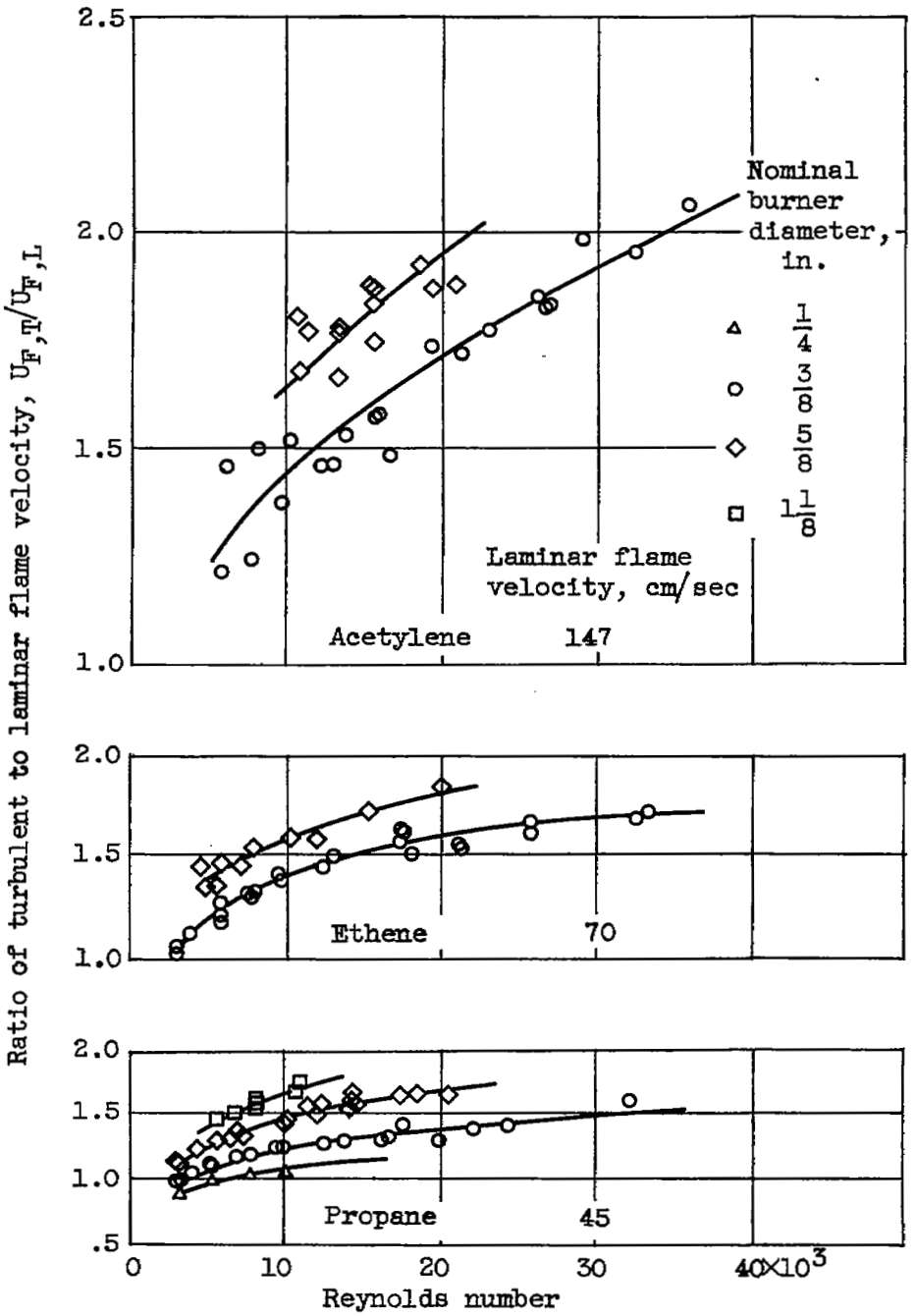

Figure V-17. - Effect of Reynolds number on ratio of turbulent to laminar flame velocity for hydrocarbon-air flames. Constant density and viscosity (ref. 3).

3517

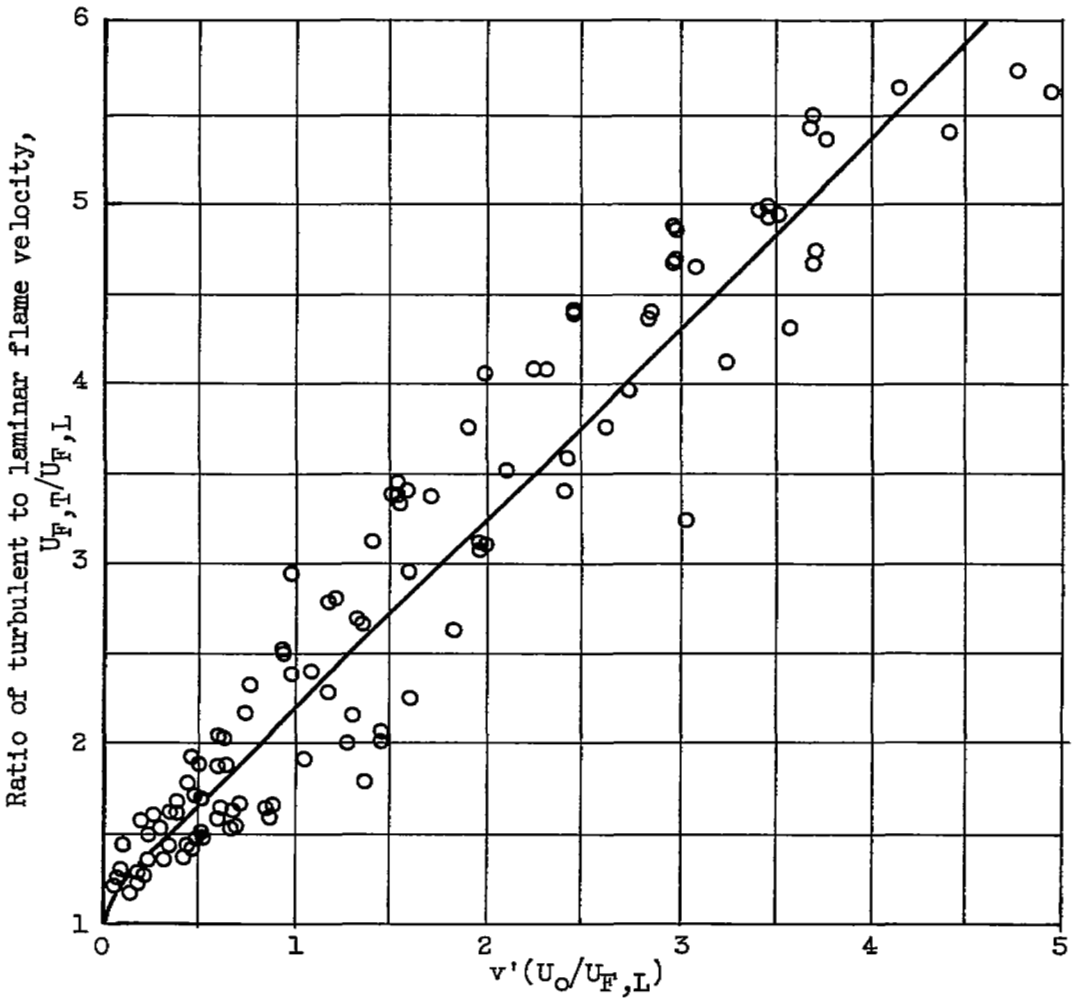

Figure V-18. - Variation of ratio of turbulent to laminar flame velocity with parameter $v'(U_o/U_{F,L})$. Propane-air flames on various rectangular nozzles at various fuel-air ratios and velocities (ref. 15).

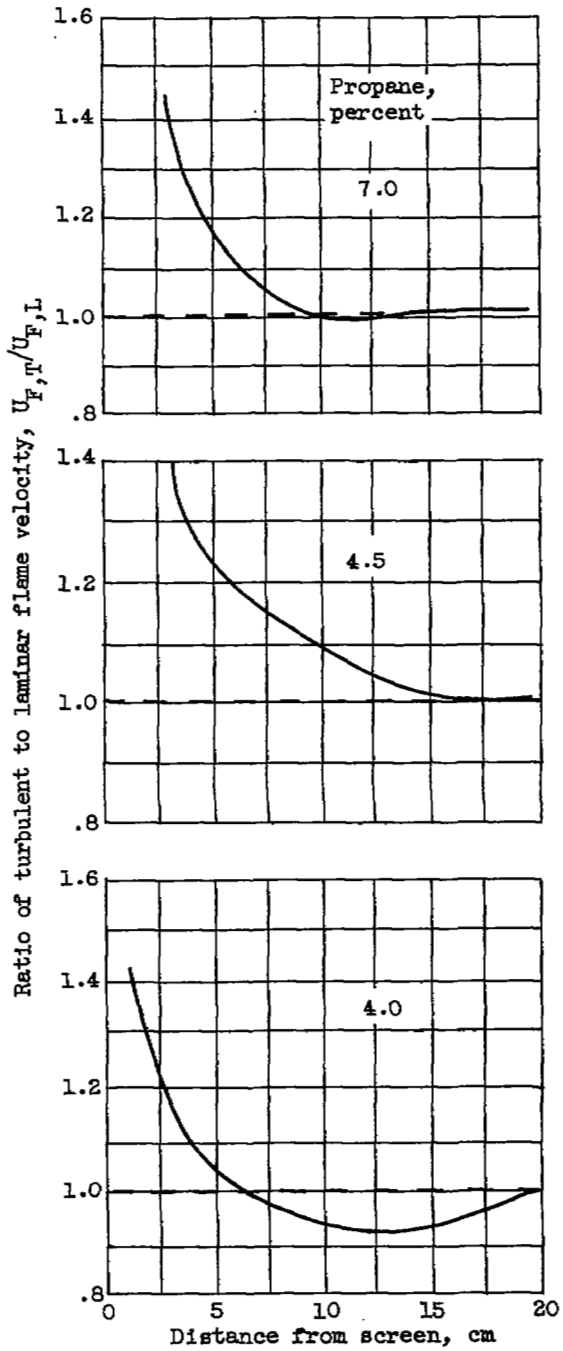

Figure V-19. - Variation of turbulent to laminar flame velocity ratio with distance from 6.0-millimeter-mesh, 1.5-millimeter-wire-diameter screen. Propane-air flames inside 5.4-centimeter tube moving against flow velocity of 58.8 centimeters per second (ref. 8).

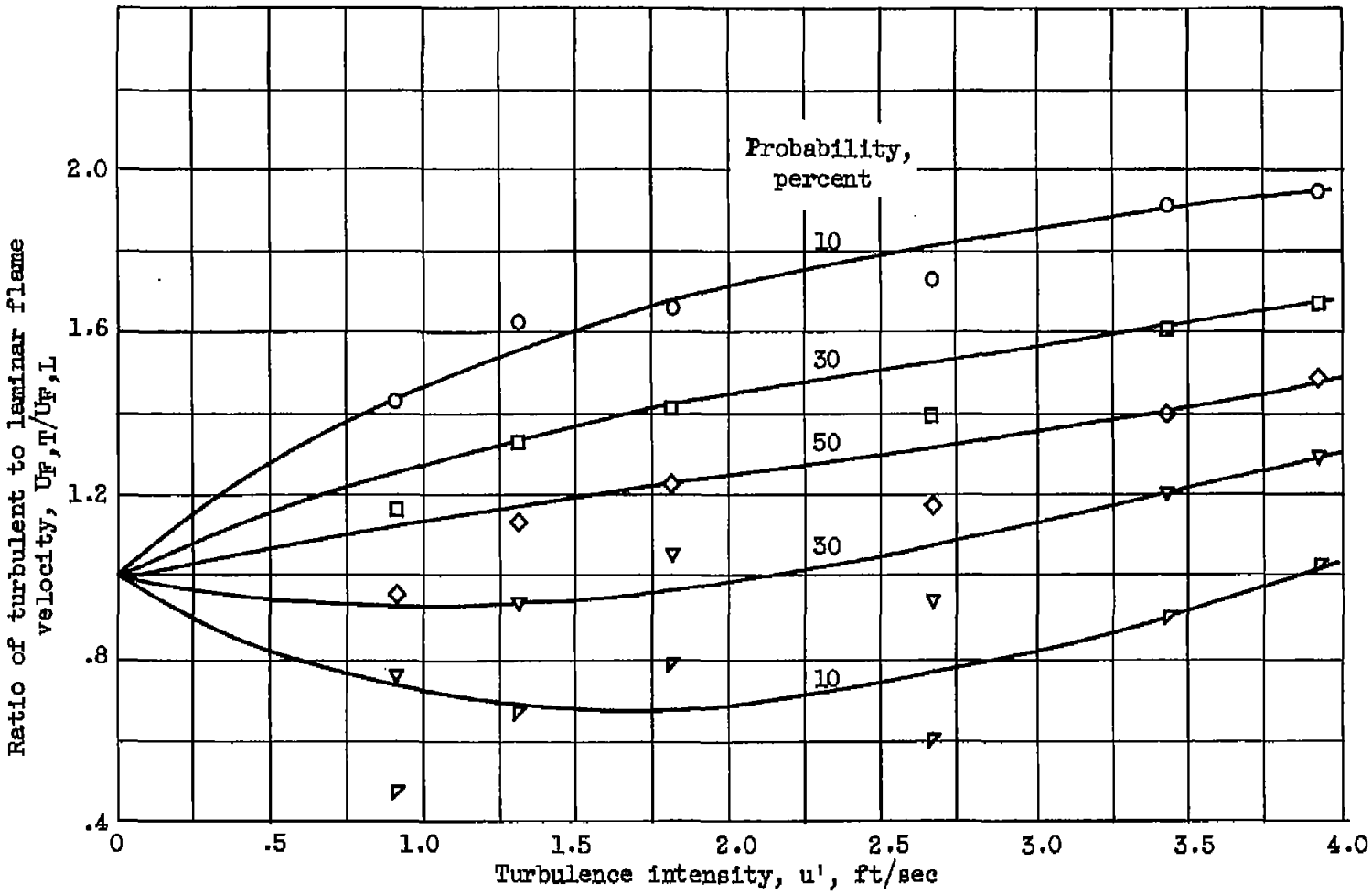

Figure V-20. - Variation of ratio of turbulent to laminar flame velocity with turbulence intensity for various probability percentages (ref. 9).

3517

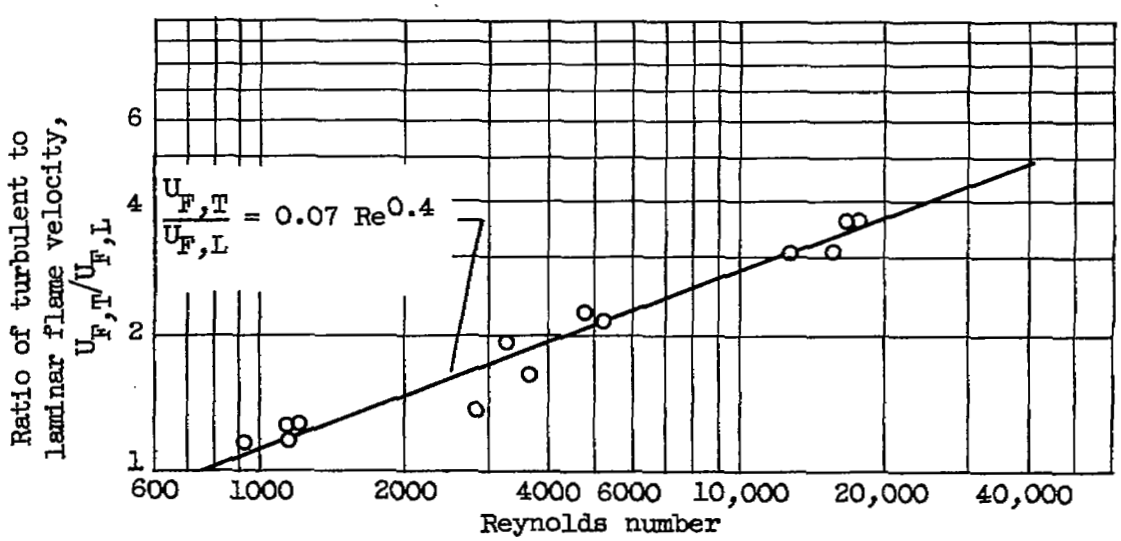

Figure V-21. - Variation of ratio of turbulent to laminar flame velocity with Reynolds number. Data of reference 5; equation of reference 12.

3517

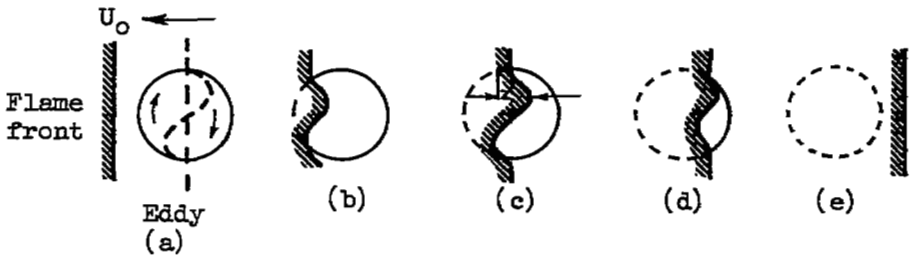

Figure V-22. - Passage of eddy through flame (ref. 8).

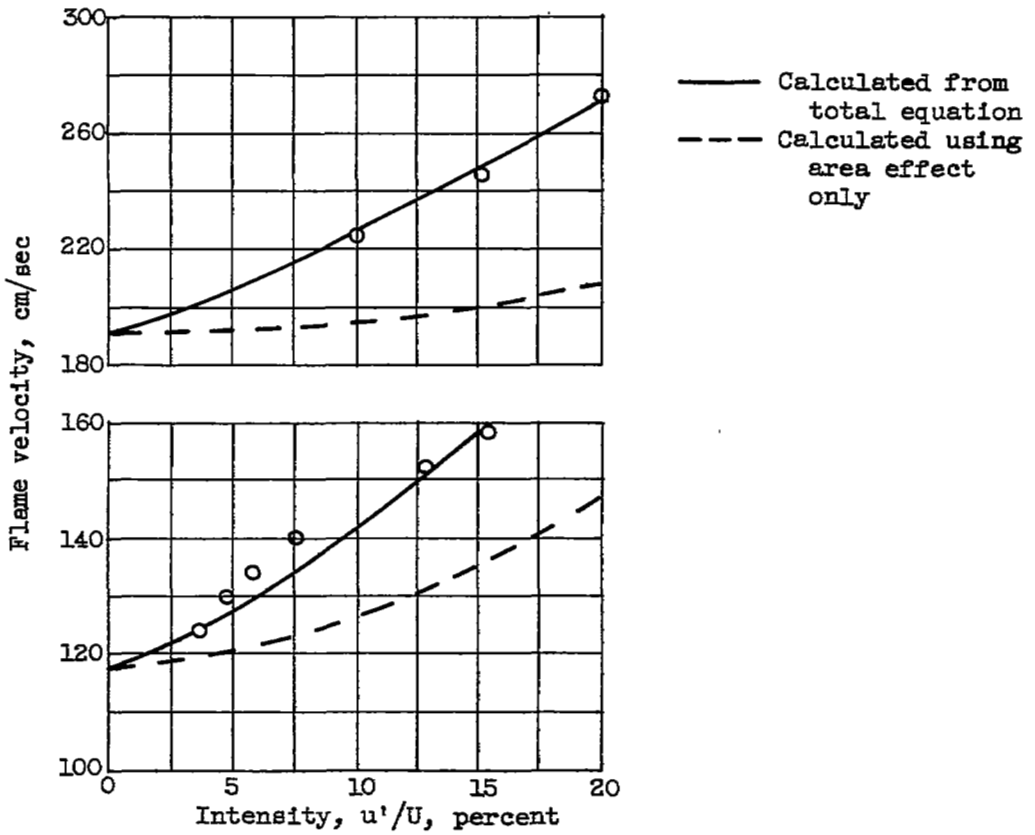

Figure V-23. - Comparison of theoretical curves with experimental data (ref. 8).

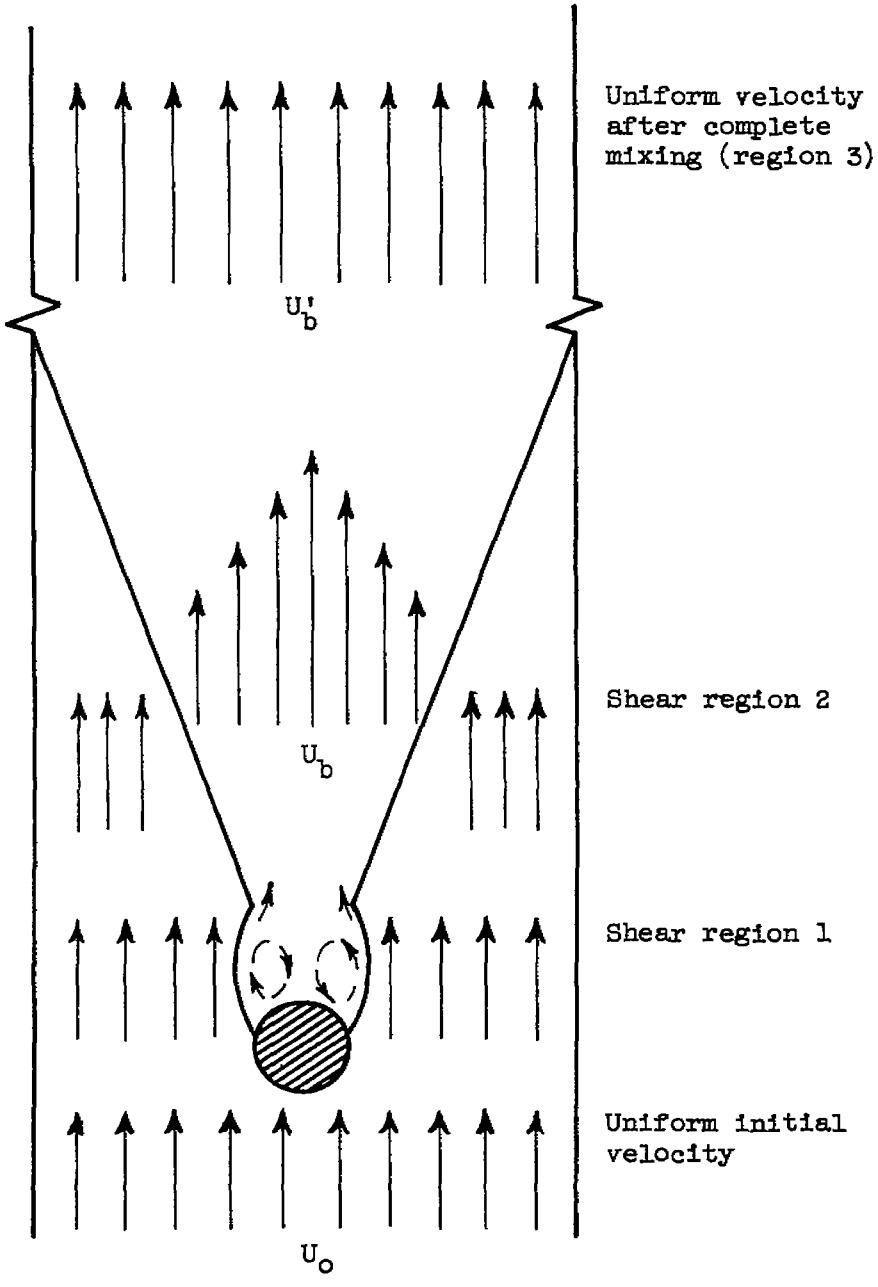

Figure V-24. - Shear regions generating turbulence in a rod-stabilized flame (ref. 10).

3547

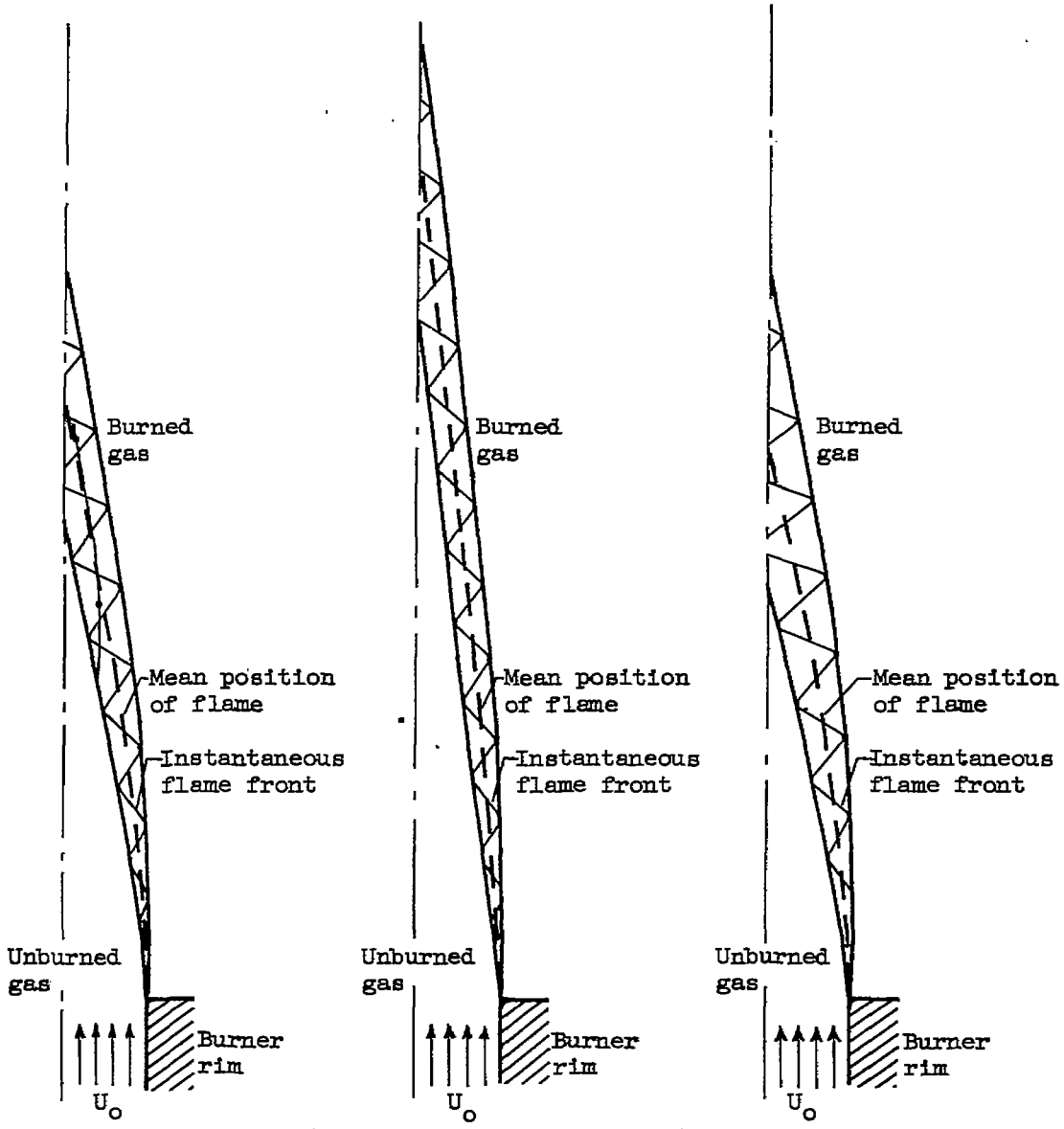

(a) First effect only.

(b) First and second effects only.

(c) First, second, and third effects.

Figure V-25. - Schematic diagrams of stabilized unconfined flames disturbed by turbulence, assuming 100 percent conversion of available energy to turbulence (ref. 10).

3517

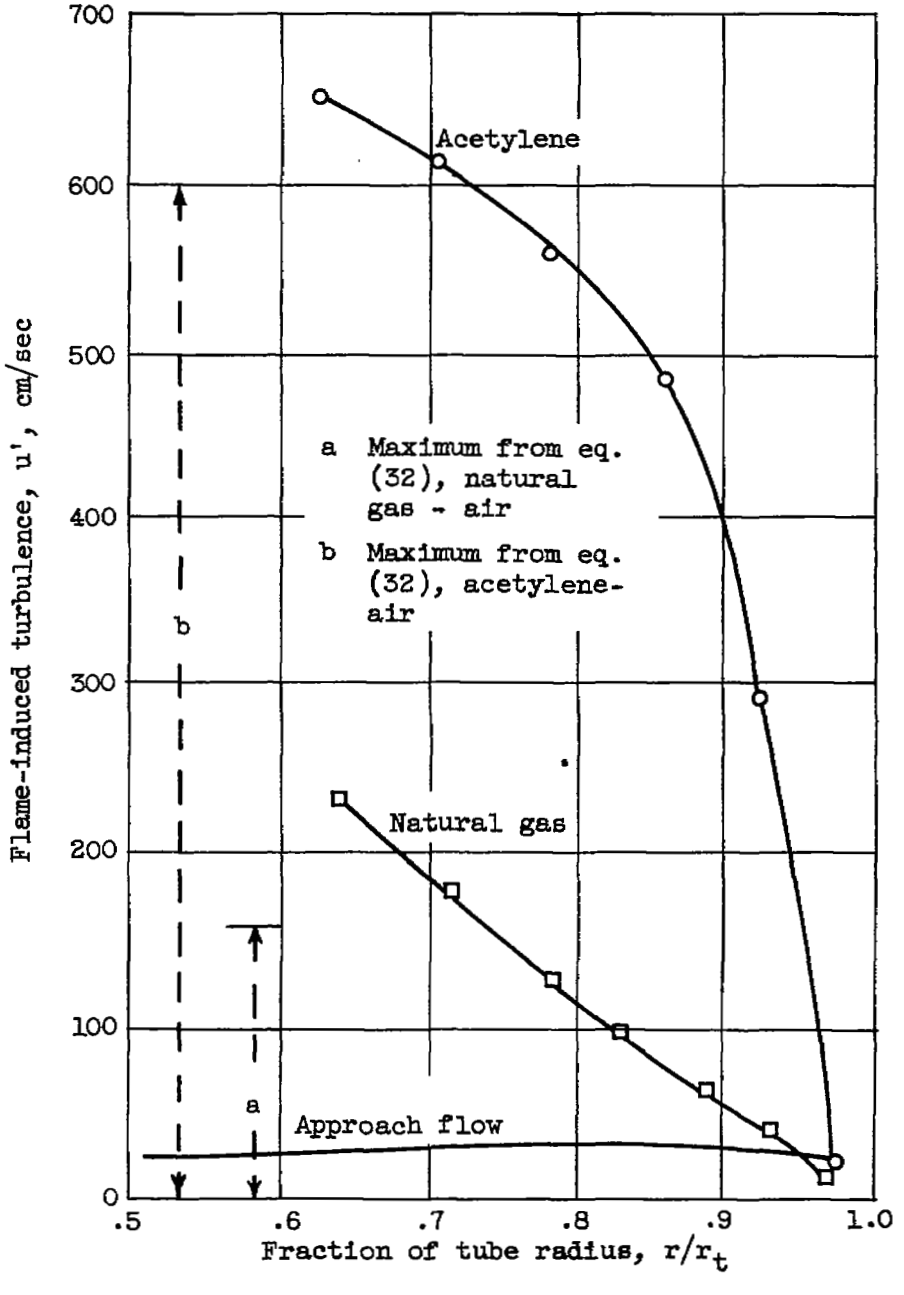

Figure V-26. - Variation of flame-induced turbulence with fraction of tube radius as calculated from experimental flame velocities (ref. 6).

CHAPTER VI

FLAME STABILIZATION

By Gordon L. Dugger and Melvin Gerstein

INTRODUCTION

The discussion of flame stabilization presented in this chapter is limited to studies of open flames burning from the ends of cylindrical tubes or nozzles and of confined flames burning from single flame holders in small, ram-jet-type combustion chambers. The description, definition, and significance of critical boundary velocity gradients, penetration distances, and eddy stabilization are given. Also included are experimental data and correlations of the effects of various flow parameters and chemical factors on flame stability. Some instability phenomena connected with the propagation of nonturbulent flames are discussed. Finally, theoretical treatments for the prediction of critical boundary velocity gradients and for stabilization in the recirculation zone behind bluff bodies (eddy stabilization) are considered.

SYMBOLS

The following symbols are used in this chapter:

A	area
a	constant
B	ratio of rod diameter to tube diameter
b	exponent
C	collision concentration
c	exponent
c_p	specific heat
D	diffusion coefficient
d	diameter
d^*	characteristic dimension of flame holder
E	activation energy
F	friction factor
f	fuel-air ratio
G	mass-flow rate
g	boundary velocity gradient

H	heat-supply rate
K	property of multifuel mixture
k	constant
M	molecular weight
m	exponent
p	pressure
q	percent of stoichiometric oxidant
R	universal gas constant
Re	Reynolds number
r	radius
T	temperature
T_3	ignition temperature
U	fundamental velocity
V	volume
X	mole fraction
x	distance
y	fraction of stoichiometric fuel concentration
Z	collision factor
δ	reaction-zone thickness
ε	fraction of entering fuel
$\varkappa$	thermal conductivity
μ	absolute viscosity
ν	kinematic viscosity
ρ	density
φ	equivalence ratio
ψ	volumetric ratio

Subscripts:

a	air
av	average
b	blow-off

c	cell
F	flame
f	fuel
fb	flash-back
i	i^{th} fuel
j	j^{th} fuel
L	laminar
m	mixture
o	initial conditions
p	penetration
r	rod
req	required
s	sheltered zone
st	stoichiometric

3072

STABILITY DIAGRAMS: VELOCITY-CONCENTRATION LIMITS

Open Flames with Secondary Air

The velocity-concentration regions for the various stability phenomena typical of open burner flames with secondary (ambient) air, which have been studied by a number of investigators (e.g., refs. 1 to 3), are schematically illustrated in figure VI-1. When the approach velocity to a seated open flame is decreased until the flame velocity exceeds the approach velocity over some portion of the burner port, the flame flashes back into the burner. This flash-back always occurs in the unshaded area under the flash-back curve in figure VI-1. If, on the other hand, the approach velocity is increased until it exceeds the flame velocity at every point, the flame will either be extinguished completely when the conditions fall in the unshaded region to the left of the blow-off curve or, for fuel-rich mixtures, it will be lifted above the burner until a new stable position in the gas stream above the port is reached as a result of turbulent mixing with and dilution by secondary air. The lift curve is a continuation of the blow-off curve beyond a critical percentage of the fuel gas at point A. The blow-out curve corresponds to the gas velocity required to extinguish a lifted flame. Once the flame has been lifted above the port, the approach velocity must be decreased to well below the lift velocity before the flame will drop back and be reseated on the burner rim. Between fuel concentrations A and B, the blow-out of the lifted flame occurs at a lower velocity than the flame blow-off from the port. Such a lifted flame, at constant composition, can be produced only by ignition from above the port.

Flames Deprived of Secondary Air

Burner flames may be deprived of secondary air either by surrounding the flame with an annular flow of an inert gas (ref. 4, p. 287) or by splitting the flame

(Smithells separator-type burner) so that the outer mantle burns above an outer concentric tube, thus depriving the inner cone of access to the secondary air (ref. 5). In either case, blow-off curves pass through a maximum near the stoichiometric concentration (fig. VI-2) and therefore are similar in shape to flame velocity curves (e.g., fig. IV-3). The decrease in blow-off velocity with increasing concentration on the rich side is not observed with open flames having access to secondary air, because, as a rich mixture is diluted by secondary air through molecular and eddy diffusion, the flame velocity is kept high and the blow-off velocity continues to increase. For the same reason, lifted flames do not occur in the absence of secondary air. Flash-back is, of course, unaffected by secondary air. The blow-off behavior of confined flames burning from flame holders is similar, as illustrated by figure VI-3 for a hydrocarbon fuel burning from flame holders of various diameters (ref. 6). These flame holders were mounted across the 1-inch dimension of a 1- by 4- by 12-inch combustion chamber. 3072

Another type of stability diagram that eliminated the effect of flame-holder diameter for rich blow-off from spherical flame holders in a 1-inch free jet at atmospheric pressure is demonstrated in reference 7. Fuel mass flow was plotted against air mass flow, as shown in figure VI-4, in which the rich curves form a common envelope.

MECHANISMS OF FLAME STABILIZATION

Critical Boundary Velocity Gradient

Flames stabilized on burner. - The conditions for stability may be described in terms of laminar flow, regardless of whether the flow in the tube is laminar or turbulent, because in either case there is a laminar sublayer at the stream boundary (ref. 1). Any point of equality between flow velocity and flame velocity must lie within the laminar sublayer, because the gas velocity at the boundary between the sublayer and the turbulent core is greater than the flame velocity. The velocity gradient in this region near the stream boundary where stabilization must occur may be assumed constant if the width of the region is small compared with the tube diameter. In reference 3 (p. 282), curves for flash-back of natural gas flames indicate that this assumption is satisfactory for correlating flash-back data obtained with tube diameters larger than the flame-quenching diameter. The critical boundary velocity gradients for flash-back and blow-off have been used quite successfully both to correlate flash-back or blow-off data obtained with burners of various sizes and shapes (ref. 3, pp. 282-302, and ref. 8) and to correlate turbulent with laminar blow-off data (e.g., refs. 2 and 9).

The interaction of the flame velocity and the critical boundary velocity gradient for a Bunsen flame can be understood by reference to figure VI-5. Figure VI-5(a) illustrates how the flame position shifts with increasing gas flow, the flow increasing from flame position A to C. As the flame moves away from the burner port, the fringe of the flame moves closer to the stream boundary. The reason for this can be seen by considering also curves A, B, and C of figure VI-5(b), which represent the variation of flame velocity with distance from the stream boundary for flame positions A, B, and C. In all these curves, the flame velocity is constant far from the stream boundary, but at smaller distances the solid burner rim exerts a quenching effect on the flame by extracting heat and destroying reactive chain carriers, and the flame velocity decreases. At some small distance from the stream boundary, the quenching becomes complete and the flame velocity falls to zero. The height of the flame fringe above the rim (fig. VI-5(a)) has been called the dead space above the rim. As the flame moves up from position A to position B or C, the loss of heat and active particles diminishes, the region of constant flame velocity extends closer to the stream boundary, and the fringe of the flame approaches the

stream boundary. For lean mixtures, there is a limit to this movement toward the stream boundary, because there is superimposed on the quenching effect a flame velocity reduction due to the diffusion of external (secondary) air into the unburned gas. This diluting effect increases as the flame moves away from the burner. Thus, flame velocity curve C may represent the limit of approach of the flame fringe toward the stream boundary for a lean mixture. For a rich mixture, secondary-air dilution may increase the flame velocity; for a very rich mixture, a stable lifted flame may be obtained several tube diameters above the port (fig. VI-6; note that the base of the flame is at the point of turbulent break-up of the laminar jet issuing from the port; the turbulent eddy diffusion is required to mix sufficient secondary air with the very rich mixture so that a nearly stoichiometric mixture results). Conversely, curve A of figure VI-5(b) may represent the limit due to quenching to which a stable flame can approach the burner rim.

For any flame velocity curve between the limiting curves A and C (fig. VI-5(b)), there will be a gas flow for which the straight line representing the boundary velocity gradient is tangent to the flame velocity curve (lines 2 to 4). Any line such as 1, which represents a smaller gradient than line 2, will intersect curve A, and there will be a region where the flame velocity exceeds the gas velocity. As a result, the flame will flash back into the tube. Any gradient larger than line 4 will cause the gas velocity to be everywhere greater than the flame velocity, and the flame will blow off. Hence, gradients 2 and 4 are called the critical boundary velocity gradients for flash-back and blow-off, respectively.

The critical boundary velocity gradients for Bunsen flames are calculated from equations for the frictional drag imposed by a wall. For fully developed laminar flow through a long cylindrical tube (Reynolds number < 2100), the critical boundary velocity gradient may be found by differentiating the Poiseuille equation (ref. 3, p. 279), which gives

$$g = 8U_{av}/d_t \tag{1}$$

The more general equation, which holds for any either laminar or turbulent flow, is

$$g = F\rho U_{av}^2/2\mu = FU_{av}Re/2d_t \tag{2}$$

where

F friction factor from empirical Fanning equation (ref. 9)

For the laminar flow condition through long cylinders considered in equation (1), $F = 16/Re$. The following expressions are given in reference 8 for the friction factor in laminar flow through various types of burners:

Type of burner	Friction factor, F =	Equation
Short circular port (orifice)	$8.5/Re^{0.85}$	(3)
Long square channel	$18.9/Re^{1.11}$	(4)
Long rectangular channel	$40.2/Re^{1.27}$	(5)
Long triangular channel	$29.8/Re^{1.29}$	(6)

In all these cases, the diameter used in computing Re is the hydraulic diameter, that is, twice the cross-sectional area of the channel divided by the perimeter.

For turbulent flow in long, smooth, cylindrical tubes, several equations have appeared in the literature. The empirical equation of Blasuis (see ref. 9) is used in references 2 and 8 to 10. For $3000 < Re < 100,000$, this equation gives

$$F = 0.080/Re^{0.25} \tag{7}$$

Others (e.g., ref. 1) have used the empirical equation of Koo (see ref. 11), which for the range $5000 < Re < 200,000$ gives

$$F = 0.046/Re^{0.2} \tag{8}$$

For flow in the transition region between laminar and turbulent flow ($2100 < Re < 3000$ to 5000), there is no available equation for F. Some estimate of F is obtained from arbitrary curves connecting the curves for laminar and turbulent flow (ref. 11). 3072

Flames supported on wires or rods. - A mechanism similar to that for burner flames can be applied with some success to flames supported on wires or rods, but the correlations are not as good as those for burner flames, and other mechanisms have been proposed. Nevertheless, it is of interest to examine this theory for supported flames. Lewis and von Elbe (ref. 3, p. 245) visualize the stabilization as shown in figure VI-7. In figure VI-7(a), the concept of the flow around a wire located coaxially with the flow is shown. Just above the wire, there is a region of zero flow velocity followed by a gradient to the stream flow. At position A above the wire, the condition shown in figure VI-7(b) exists, in which the flame velocity is everywhere lower than the flow velocity and a stable flame cannot exist. The flame would thus be forced upward, away from the wire. At a position more remote from the wire, such as position B, both the flow velocity and the flame velocity in this region increase, the flame velocity increasing more rapidly than the flow velocity, so that ultimately a point of tangency exists as shown in figure VI-7(c), which corresponds to condition of stability. The increase in flame velocity is limited, however, since it presumably will approach laminar flame velocity when the quenching action of the wire is reduced, but the flow velocity can be increased so that ultimately the flow velocity exceeds the flame velocity at all points and the flame blows off, as shown by the curves of figure VI-7(d). As long as the wire does not heat up and is smaller than twice the dead space in diameter, Lewis and von Elbe predict that the velocity gradient for blow-off is independent of wire diameter. However, larger wires produce a large sheltered region, so that a higher flow velocity and a higher boundary velocity gradient are reached before blow-off occurs.

The critical boundary velocity gradients for flames anchored at the end of an axially mounted wire or rod may be calculated by differentiating the equation for flow through an annular space, which gives (ref. 3, p. 289)

$$g_b = \frac{2U_{av}}{r_t} B \left[\frac{-2 + \dfrac{1 - \dfrac{1}{B^2}}{\ln B}}{1 - B^4 + \dfrac{(B^2 - 1)^2}{\ln B}} \right] \tag{9}$$

Penetration distance. - An arbitrarily defined quantity that has been used to illustrate the effects of wall quenching and secondary-air dilution (e.g., refs. 1, 3 (p. 285), 9, 10, and 12) is the penetration distance x_p:

$$x_p = U_F/g_{fb} \tag{10}$$

This ratio of fundamental flame velocity to critical boundary velocity gradient represents the distance from the burner wall at which the local stream velocity is equal to the fundamental flame velocity (fig. VI-8). The penetration distance is to be distinguished from the small dead space at the wall (fig. VI-8(a)) or the dead space above the rim (fig. VI-8(b)) where quenching is complete and the luminous zone assumes a position parallel to the gas-flow lines. For the case of flash-back, this distance approximates the depth of penetration of the quenching effect of a single wall, that is, the distance from the wall at which the local flame velocity becomes smaller than the fundamental flame velocity of the mixture as a result of quenching. In the case of blow-off, secondary-air dilution also affects the penetration distance; for a lean mixture, secondary-air dilution would tend to decrease the flame velocity and thus decrease the penetration distance, whereas for very rich mixtures, it would have the opposite effect. (The maximum flame velocity generally occurs with a mixture slightly richer than stoichiometric.) The subject of penetration distance is discussed further in the theoretical section of this chapter.

3072

Stabilization by Eddies

While the mechanism of Lewis and von Elbe is reasonable for supported flames as well as for burner flames, some of the characteristics of supported flames are not as well described as is desirable. Supported flames do not always blow off as the theory suggests, but often a small residual flame remains in the wake of the support. Lewis and von Elbe have, in fact, shown that this region is not characterized by a linear velocity gradient but that eddies are formed just after the support. These are shown schematically in figure VI-9, in which the eddies are apparently stabilized by the flame, since for a given flow the eddy is smaller with ignition than without. Reference 13 suggests that these eddies act as a source of heat and active radicals and thus provide a constant ignition source to stabilize the flame. The nature of these eddies and the flow around them will determine when blow-off occurs, because an equilibrium will be set up between the production of heat in the eddies, its transfer to the surrounding flow, and the ignition requirements. This subject is also discussed later in this chapter.

EFFECT OF VARIABLES ON STABILITY LIMITS

Flow Variables at Constant Pressure and Temperature

Characteristic dimension of burner or flame holder. - A number of investigators have found that flash-back and blow-off limits of open flames burning from tubes or nozzles at room conditions are independent of tube diameter when plotted as fuel concentration (or equivalence ratio) against the critical boundary velocity gradient. Lewis and von Elbe (ref. 3, pp. 282-300) plotted flash-back limit data for natural gas - air, hydrogen-air, hydrogen-oxygen, acetylene-oxygen, methane-oxygen-nitrogen, and propane-oxygen-nitrogen flames in this manner. They found the critical boundary velocity gradients for flash-back g_{fb} to be independent of tube diameter as long as the diameter was somewhat larger than the quenching diameter but not so large that flash-back was preceded by a severe tilting of the flame, in which case the limit was not clearly distinguished.

The critical boundary velocity gradients for blow-off g_b of natural gas - air mixtures in the laminar flow region were also independent of diameter both for ordinary Bunsen flames and for some inverted flames stabilized at the ends of wires mounted in the axes of the tubes. Successful correlations were obtained with g_b for several other fuel-oxygen-nitrogen mixtures in laminar flow. Reference 2 presents a correlation extending from the laminar-flow range well into the turbulent-flow range on a continuous curve for propane-air flames for a range of tube diameters

as shown in figure VI-10. This figure shows that the curves for the small tubes deviate toward higher velocity gradients only above a propane mole fraction of 0.15. Reference 1 also presents continuous curves from laminar into turbulent flow for butane-air flames. Furthermore, it was shown that the hydrogen-air data of reference 3 (pp. 292-293) when properly calculated gave a similar smooth curve extending into the turbulent region.

For blow-off limits of simple, single flame holders in small combustion chambers, various investigators have found correlations with a parameter U_{av}/d^{*b} plotted against fuel concentration, where d^* is the characteristic dimension of the flame holder and b is an empirical exponent (table VI-I). For example, in reference 13, a correlation was obtained for $b = 0.45$ with rods varying in diameter from 0.016 to 0.498 inch (some of which were downstream of turbulence-producing screens) for city gas - air flames in a two-dimensional combustion chamber 1 by 3 inches in cross section (fig. VI-11). Reference 6 reports the data of figure VI-3 to be correlated with $b = 0.5$ for equivalence ratios below 1.5. However, it was found in reference 14 that $b = 0.18$ gave the best correlation for new data on rod-stabilized city gas - air flames, and that, for lean hydrogen-air flames and for propane and city gas flames in certain ranges of velocity and concentration, b is negative. 3072

Axially mounted cylinders and cones in high-velocity streams (200 to 900 ft/sec) near the open end of a 6-inch pipe were used in reference 15, in which a correlation was observed with diameter for $b = 1.0$, when a high-boiling mixture of paraffins and naphthenes was used. DeZubay (refs. 16 and 17) used disks mounted with the diameter normal to the flow in a cylindrical duct. He obtained a correlation with $b = 1.0$ for naphtha, 0.85 for propane, and 0.74 for hydrogen. DeZubay pointed out that, in the case of reference 13 (and the same comment would apply to refs. 6 and 18), the projected flame-holder area was proportional to the characteristic dimension d^*, because in all cases the flame holder extended across a duct of fixed width. On the other hand, for DeZubay's data (or those of ref. 15), the projected area is proportional to the diameter squared. Hence, all the correlations except those recently reported in reference 14 are close to $U_{av,b}/A^{1/2}$. These and other empirical correlations (refs. 6, 7, 13, and 15 to 19) involving the characteristic dimension d^* are summarized in table VI-I.

On the other hand, Barrère and Mestre (ref. 20) recently showed a lack of correlation with characteristic dimension, because, for a cylinder, a 90° gutter, and a flat plate, each having a projected width of 5 millimeters, three different sets of velocity-concentration curves were obtained. Gerstein (ref. 20) suggests that for greater generality the correlating parameter should account for differences in flow about obstacles of different shapes. The dimension sought may be, for example, the lateral width of the vortex formed behind the obstacle. In cold flow, a cylinder with a projected width of 0.75 inch has a vortex width of 1.09 inches, whereas a flat plate of the same projected width produces a vortex 1.30 inches wide under the same flow conditions (ref. 21). The use of these relative vortex widths would bring the data of reference 20 for the cylinder and the flat plate together. Unfortunately, such agreement based on cold-flow vortex widths may be fortuitous, because the flame does influence the flow (ref. 22). (Reference 13 reports the stability limits for a given size flame holder to be unaffected by chamber width for ratios of simulated chamber width to stabilizer characteristic dimensions from 10 to 79.) In general, then, the velocity-concentration limits for open burner flames, or for open flames supported at the end of axially mounted wires, may be correlated by the critical boundary velocity gradient. For confined flames supported on flame holders, an empirical correlation of the type

$$U_{av,b}/A^c = f(\varphi) \tag{11}$$

may be applicable, where c is of the order of 1/2; for greater generality, a function of some length or area associated with the flow about the obstacle might be used in place of $A^{1/2}$.

Turbulence. - It has already been noted that blow-off data for open flames on tubes of various diameters are correlated by a single curve of critical boundary velocity gradient against fuel concentration for both laminar and turbulent flow. Turbulent flash-back is not ordinarily encountered in laboratory experiments, but, with very-high-velocity flames (e.g., H_2-O_2 flames, ref. 23) in large-diameter tubes, or at increased pressure, it may occur (ref. 12). The g_{fb} for turbulent flames is always greater than that for a laminar flame of the same mixture, because the laminar boundary layer at the wall within which stabilization must occur becomes smaller.

3072

Scurlock (ref. 13) produced known turbulence in the approach stream of confined flames by means of screens. As the intensity of turbulence was increased, blow-off velocities decreased (fig. VI-12). The effect of turbulence of given scale and intensity decreased with increase in the ratio of flame-holder diameter to turbulence scale. Contradictory results are reported in reference 19, which states that placing a flame holder farther from the source of turbulence (closer to the combustion-chamber exit), where the intensity and frequency of turbulence are smaller, decreased the stability limits.

Boundary-layer thickness. - In reference 24, the thickness of the boundary layer on a flame holder was varied by removing part of the layer by suction through grooves in the flame holder. It was reported that both the data of reference 24 and other data show no effect on blow-off velocity as long as both the approach flow and the boundary layer are laminar. If the approach stream is turbulent, a thin boundary layer may be penetrated to favor blow-off. When the boundary layer itself is turbulent, blow-off is accelerated in the same manner as it is promoted by upstream turbulence, but the effect may be more severe because of the absence of the laminar buffer layer between the combustible mixture and the recirculation zone. An increase in the flame-wedge angle at the farthest upstream point of flame holding increased the flame-holding ability. In reference 7, the effect of boundary-layer removal from the flame holder (approximately 1 percent of the total flow) was studied; it was found that flame heights were drastically reduced and blow-off velocities were halved.

Reference 25 reports that, for stream velocities of 80 to 180 feet per second, the theoretically complete removal of the boundary layer markedly decreased the blow-off velocity of a fuel-lean flame and slightly decreased the blow-off velocity of a fuel-rich flame. It was also observed that blowing air into the boundary layer decreased the stability of lean flames and increased the stability of rich flames. A stable pilot was obtained by blowing propane into the boundary layer, even when the mainstream fuel concentration was zero.

In summary, boundary-layer removal has no effect when both the approach flow and the boundary layer are laminar; when the laminar boundary layer becomes very thin because of approach-stream turbulence, or when the boundary layer itself becomes turbulent, its removal reduces stability. Lean flames are affected more than rich flames.

Electric fields. - Reference 26 reports that longitudinal electric fields, either alternating current at 400 cps or direct current with the positive electrode in the burned gas, approximately doubled the blow-off velocity of a given propane-air burner flame as the voltage was increased from zero to 2000 volts. The rate of increase of the blow-off limits decreased rapidly after 2000 volts.

Reference 27 confirms the preceding longitudinal direct-current field results in a study with butane-air flames. In the apparatus of reference 27, the downstream electrode was a platinum ring around the outer tube or skirt of a split-flame burner, and therefore the blow-off curves obtained were typical of confined flames. The inner flame cone was subjected to a direct-current field of zero to 18,000 volts, which caused a current through the flame of zero to 100 microamperes. Further results obtained for a positive field (positive downstream electrode) were as follows: (1) Concentration limits could be widened 200 percent, (2) dead space could be reduced 70 percent, and (3) flame pressure could be more than doubled. When the downstream electrode was made negative and the direct-current voltage was increased, it was found that (1) concentration limits narrowed at low voltages, but the same widening obtained with positive fields was obtained at the higher voltages; (2) velocity limits increased in an erratic manner; (3) dead space passed through a maximum (at highest voltages the flame vibrated rapidly and then became "derby" shaped); and (4) flame pressure decreased and then increased with increasing voltage. 3072

With a transverse electric field of 15,000 volts, the concentration limits were narrowed by 43 percent with a flow rate of 61 cubic centimeters per second, regardless of whether or not the flame was deprived of secondary air by using a quartz mantle (ref. 28). As stated previously, the inner cone and the flow lines inside the cone were strongly deflected toward the negative electrode. The addition of alkali salts had little effect on the deflection of the flow lines.

Acoustical disturbances. - Reference 26 reports that strong acoustical disturbances decrease the blow-off stability limits of propane-air flames. In certain cases, an increase in sound intensity caused a seated burner flame to lift above the port, but when the sound intensity was again decreased, the flame blew out. The eddy motion in the emerging gas jet caused by the sound had stabilized the flame.

Pressure and Temperature Variation

Pressure. - Reference 29 has already been mentioned with regard to flame velocity. The data are actually presented on what might be considered stability diagrams for velocity-pressure limits for stoichiometric acetylene-oxygen and propane-oxygen flames. For a given mixture, a different velocity-pressure curve for each burner nozzle diameter was obtained, as shown in figure VI-13 for propane-air flames. Each of these curves consists of a blow-off branch to the upper left and a flash-back branch to the right. The lower part of each curve, which has a negative slope and connects the blow-off and flash-back portions, represents the extinction limit where the flame dies out because of its inability to supply enough heat or active radicals to a sufficient volume of gas to continue the propagation.

The curves of figure VI-13 were obtained by varying pressure along a constant volumetric flow line such as AB until either flash-back, blow-off, or extinction occurred. The narrowing of the flash-back extinction neck in the curves at lower velocities was more pronounced for acetylene-air flames. In this neck region, flat flames were obtained, and the computed flame velocity dropped below the non-pressure-dependent value obtained when this region was avoided. The minimum of each curve represents a minimum propagation velocity for the mixture, which apparently is not greatly affected by pressure or tube diameter. The limiting pressure for combustion of a given mixture at a given velocity was inversely proportional to tube diameter. In other words, the blow-off extinction curves of figure VI-13 may be brought together by plotting critical velocity against the product pd_t (see also ref. 12). This is analogous to the use of the correlating parameter U/pd_t for blow-off from spherical or disk-shaped flame holders (table VI-I).

Reference 30 presents the extinction curve for stoichiometric propane-air flames burning from Bunsen tubes or from round-end rods mounted axially in tubes. The extinction velocity was proportional to p^{-2}. The length of the extinction curve was increased by means of longitudinal electric fields, which displace blow-off curves toward higher velocities as discussed previously. Reference 31 reports that the critical velocity gradient for flash-back g_{fb} increased pressure for methane-air from 1/4 to 1 atmosphere, or $g_{fb} \propto p^{0.6 \text{ to } 0.8}$. This order of magnitude of the pressure effect qualitatively agrees with the varying slope of the flash-back curves of figure VI-13. Since the data of reference 31 showed flame velocity $U_F \propto p^{-0.24}$ for methane, the penetration distance was approximately inversely proportional to pressure. The critical velocity gradient for blow-off g_b also increased with pressure (ref. 31). While the blow-off data were more erratic than the flash-back data for methane, g_b was approximately proportional to pressure for both methane and butane in the range 1/4 to 1 atmosphere.

It has already been stated that the contradictory reports on the effect of pressure on flame velocity may very probably be ascribed to apparatus effects. It is equally likely that the results of studies of stability limits and structure of open flames at various pressures are subject to unknown apparatus effects. Reference 15 reports that, for cylindrical flame holders mounted axially near the end of a 6-inch pipe, pressure changes between 1 and 3 atmospheres had little effect on blow-off limits from large-diameter flame holders (2.87 in.). References 7 and 16 report blow-off results for smaller disks or spheres to be correlated by a parameter including pressure in the denominator (table VI-I).

Mixture temperature. - The effects of initial mixture temperature on the flash-back and blow-off limits of open flames of methane and air (ref. 9) and propane and air (ref. 10) have been studied recently. In these studies, the burner rim temperature was not much different from the mixture temperature. The critical average stream velocity for blow-off of propane-air flames (ref. 10) from a 15.6-millimeter tube increased with approximately the square of the absolute temperature, whether the stream flow was laminar or turbulent. The effect of temperature on the flash-back velocity was an even more pronounced increase, so that there was a relative decrease in the flow range for stable flames as shown by figure VI-14. Empirical equations for maximum flash-back velocity and for turbulent blow-off velocity at the same equivalence ratio, 1.12, which was also close to the equivalence ratio for maximum flame velocity (ref. 10), took the same form as empirical maximum flame velocity equations. For the temperature range 306° to 617° K, these were:

For maximum flash-back velocity,

$$U_{av} = 100 + 1.15\times10^{-9}\ T_o^{4.2} \tag{12}$$

For turbulent blow-off velocity,

$$U_{av} = 100 + 4.5\times10^{-3}\ T_o^{1.9} \tag{13}$$

Neither critical boundary velocity gradient, critical mass flow, nor critical stream-flow Reynolds number entirely eliminated the effect of temperature on these stability limits. Of these three parameters, the critical Reynolds number (using only one tube diameter) most nearly eliminated the temperature effect, particularly for blow-off limit, as shown in figure VI-15. The penetration distance decreased with temperature for flash-back and increased for blow-off. A comparison of twice the penetration distance x_p with reported values of the quenching distance between parallel plates $x_{||}$ showed the ratio $2x_p/x_{||}$ to be 0.6 to 0.7. The suggestion was made that this

ratio was less than 1 because a minimum space was required for the occupancy of the flame itself in traveling through a tube or between parallel plates. Approximately the same value of $2x_p/x_{||}$ was observed in reference 3 (p. 285) for natural gas - air flames at room conditions. The prediction of the effect of initial mixture temperature on critical boundary velocity gradients is discussed in the theoretical section hereinafter.

Other investigations have also reported critical average velocities to be proportional to T_o to a power equal to or greater than 1. It was found in reference 32 that $U_{av} \propto T_o$ for flash-back of coke-oven gas flames when only the air was preheated. This reference reports the temperature exponents to be 1.63 and 1.3 for laminar and turbulent flash-back, respectively, of city gas - air flames. References 33 and 34 give $U_{av} \propto T_o$ for blow-off of liquid-vapor-oxygen mixtures.

The effect of approach-stream temperature on blow-off from cylindrical flame holders in two-dimensional ducts has been studied in references 6 and 18. The data, which cover temperatures ranging from 610° to 960° R (339° to 533° K), were correlated reasonably well by plotting $U_{av}/d_t^{0.5}\,T_o^{1.2}$ against equivalence ratio. The temperature exponent was believed (ref. 6) to be representative of the effect of temperature on flame velocity as shown by the data of reference 35. On the basis of the larger temperature exponents reported from the majority of flame velocity investigations (table VI-I), the correlation is regarded as strictly empirical, particularly since the penetration distance for open flames has been shown to vary with temperature.

In general, then, stability limits for either open or confined flames are proportional to initial temperature to some power greater than 1, probably ~2 for blow-off of open-burner flames, >2 for flash-back of open flames, and ~1.2 for blow-off of rod-stabilized confined flames. Undoubtedly, the exponents vary with concentration and fuel type and are influenced by such factors as wall temperature and water vapor.

Liquid fuel. - In references 33 and 34, the blow-off, flash-back, and lift curves of open flames were determined for a variety of liquid fuels burning with air or oxygen at initial mixture temperatures ranging from 125° to 535° F. Insufficient heat was added to completely vaporize the fuel. The stability curves were quite similar to those for completely gaseous systems, except for low T_o and high concentrations when a large part of the fuel remained in the liquid state. For a given lean mixture and given burner geometry, the blow-off velocity was proportional to T_o. Both ordinary burners (diam. approx. 0.1 to 0.2 in.) and skirted (split-flame) burners (skirt diam. of order of 1 in.) were studied. With very rich mixtures, lifted flames were stabilized near the skirt exit by a vortex flow of secondary air when the skirt length beyond the burner exit was approximately 3 inches; with longer skirts, the hot skirt itself stabilized the flame.

Reference 36 reports studies of the stability of rod-stabilized flames using liquid fuel. It was found that flames could be supported in much leaner mixtures for sprays than for gaseous mixtures. This was attributed to the fuel-concentrating action of the stabilizer. Increasing the volatility of the fuel and decreasing the drop size in the spray tended to shift the stability curves toward the rich side, these changes tending to approach more closely the conditions for gaseous mixtures.

Vapor fuel concentration in the eddy region near the stabilizer may be higher than that in the free stream when liquid spray injection is used. The vapor concentration in the eddy depends on the collection efficiency of drops from the free stream onto the stabilizer and the heat transfer between the flame, the stabilizer,

and the liquid. Increased air velocity moved the lean and rich blow-out limit toward the lean side for sprays, as contrasted to gaseous systems where the lean blow-out limit moves to the rich side as velocity is increased and the rich blow-out moves toward leaner fuel-air ratios. Stable combustion of sprays was possible at much leaner fuel-air ratios than was possible with gaseous fuels. It was suggested (ref. 36) that flame extinction occurs in two ways: As the spray fuel-air ratio becomes rich because of increasing the fuel flow, more of the liquid fuel reaching the flame holder sloughs off without burning. The sensible heat carried by the liquid fuel cools the flame holder and reduces the vapor concentration to a point where flame can no longer be stabilized. As the spray fuel-air ratio becomes lean, less fuel impinges on the flame holder and the flame-holder temperature rises. Ultimately, the flame holder becomes dry and the flame-holder temperature rises sharply. At this point, an insulating film of fuel vapor surrounds the flame holder, reducing the heat transfer to the surrounding spray. Again, the rate of vaporization decreases and the flame blows out.

3072

Flame-holder temperature. - Reference 13 reports stability limits to be widened considerably as flame-holder temperature is increased. This was confirmed in reference 37, in which, for lean mixtures, the mass air-fuel ratio at blow-off was linearly related to flame-holder temperature for velocities of 30 feet per second or greater, but was independent of flame-holder temperature at velocities below 20 feet per second. On the other hand, little change was observed (ref. 6) in the limits for a flame holder that was allowed to seek its equilibrium temperature (various mixture temperatures and velocities to 600 ft/sec) as compared with a water-cooled flame holder. Flash-back and blow-off velocities for burner flames may also be increased by heating the burner lip, thus decreasing the thermal gradient associated with the penetration distance.

Increasing flame-holder temperature may have a deleterious effect on the stabilization of flames supported by fuel sprays (ref. 36). In fact, the flame may actually be extinguished by adding sufficient heat to the flame holder. While the addition of heat to the stabilizer may assist vaporization for small heat additions, ultimately, sufficient heat may be added to produce either a too-rich region near the stabilizer or a film of vapor fuel which, as for lean blow-out, reduces heat transfer from the stabilizer to the liquid fuel.

Chemical Variables

Fuel type. - It was observed in reference 1 that curves of critical boundary velocity gradients g_b against percent of stoichiometric oxidant concentration were nearly the same for propane, butane, and Pittsburgh natural gas (largely methane). However, gases with higher flame velocities - Newark city gas, hydrogen, and acetylene-oxygen - showed much higher values of g_b, and therefore penetration distances were smaller; for example, hydrogen had a penetration distance of 0.00033 centimeter compared with 0.076 centimeter for propane, both fuels burning with 130 percent of stoichiometric air. In other words, the quenching effect of the wall is much smaller for the higher-velocity flames. Since the g_b curves on semilog paper were nearly linear, reference 1 suggests the empirical equation

$$g_b = a\ 10^{-kq}/100 \tag{14}$$

where q is percent of stoichiometric oxidant (volume basis) and a and k are constants that must be determined for each fuel gas. A similar effect for flames held on disks in a circular duct was point out by DeZubay (ref. 17). He noted that the exponent b in the blow-off parameter U/d^{*b} decreased as molecular weight decreased from naphtha to propane to hydrogen, but this is also the order of increasing flame velocity.

Additives and fuel blending. - Reference 38 reports studies of the stability of mixed fuels with vortex burners having (1) radial fuel injection from the axis, or (2) radial fuel injection from the periphery. In each type, the mixing of fuel and air occurred in the burner with tangential air admission. Mixing was rapid and uniform. The flame was seated in a divergent nozzle at the open end of the burner (pressure-recovery section). These vortex burners are reported to be useful for studying flame stability of both slow- and fast-burning mixtures with a single burner. The following mixing equation was found to apply for a common blow-off velocity (to be exact, a hold velocity, which is one flow increment less than the blow-off velocity) as well as for a common flame velocity for all studies of binary hydrocarbon mixtures (e.g., propane-propene and propane-ethane):

$$\sum_j X_j/X_j^* = 1 \tag{15}$$

where

X_j mole fraction of jth fuel in multifuel mixture with air which has a given blow-off limit

X_j^* mole fraction of jth fuel in binary mixture of j with air which has the same blow-off limit

It was concluded that the combustion mechanisms for the various hydrocarbons must therefore be compatible and that all hydrocarbons burn according to the same mechanism for the initial, rate-determining steps.

Propane-hydrogen (refs. 38 and 39) and methane-hydrogen (ref. 40) were also investigated. A simple linear mixing rule such as

$$K = \sum_j X_i K_i \tag{16}$$

cannot be used to determine stability limits of these binary mixtures of hydrocarbons with hydrogen, but equation (15) can be used to determine blow-off limits for lean hydrocarbon-hydrogen mixtures (ref. 38). A significant result of the studies is that a small addition of hydrogen to a hydrocarbon, particularly for rich over-all mixtures, widens the stability range because the blow-off velocity increases much faster than the flash-back velocity (refs. 39 and 40).

References 40 to 42 also report studies of mixtures of methane, propane, or hydrogen with carbon monoxide. For the hydrocarbon - carbon monoxide mixtures, the critical velocities or velocity gradients for flash-back or blow-off pass through a maximum for low hydrocarbon - carbon monoxide ratios for a given over-all equivalence ratio. It appears that these ratios for maximum limits are such that the equivalence ratio with respect to the hydrocarbon is of the same order as that with respect to carbon monoxide. With hydrogen - carbon monoxide or hydrocarbon-hydrogen mixtures, such maximums do not occur. While the simple linear mixing rule (eq. (16)) does not apply for averaging critical boundary velocity gradients of single gases to obtain critical gradients of binary mixtures, it does work reasonably well when binary mixtures such as $CO + CH_4$ and $H_2 + CH_4$ are combined to determine the critical boundary velocity gradient of the ternary mixture $CO + H_2 + CH_4$.

Hydrogen sulfide decreases the flame stability of hydrocarbons just as it decreases the flame velocity, and the extent of the decrease becomes greater as the over-all equivalence ratio is increased. However, lean mixtures of H_2-H_2S follow equation (15) (ref. 38). Equation (15) was also tested for isobutane-ethene mixtures

deprived of secondary air (ref. 4). It was found to apply for lean mixtures, but the indicated summation was less than 1 for rich mixtures.

Water vapor. - The addition of 2.5 percent water vapor to the primary air decreased the blow-off, lift, and drop-back limits of butane flames (ref. 43). The blow-off velocities of rich mixtures decreased approximately 5 percent and the blow-off velocities for lean mixtures decreased by 10 to 30 percent. The addition of water vapor to the secondary air had less effect, although some decrease was noted at higher concentrations and velocities. Similarly, the addition of water vapor to the primary air decreased the flash-back and blow-off velocities of methane flames, but the water content of the secondary air had little effect (ref. 41). For carbon monoxide flames, water in either the primary or the secondary air increased the blow-off velocity, but the flash-back velocity gradient was not affected by water in the secondary air, as would be expected (ref. 41).

3072

Diluent concentration. - The effect of diluent concentration is presented in terms of the volumetric ratio $\psi = O_2/(O_2 + N_2)$ by Lewis and von Elbe (ref. 3, pp. 299-302) for methane- and propane-oxygen-nitrogen mixtures. As ψ increases from 0.21 (air) to 1.0 for CH_4-O_2-N_2 mixtures, both flash-back and blow-off velocity gradients increase approximately a hundredfold for concentrations near stoichiometric and a thousandfold for lean flames. The values of g_b increase somewhat more than those of g_{fb}, so that a slight widening of the stability range results. It might be noted that the corresponding maximum flame velocity increase is only of the order of 10 (fig. IV-13), so that penetration distance near stoichiometric decreases by a factor of the order of 10.

THERMAL THEORIES OF FLAME STABILIZATION

Burner Flames - Critical Boundary Velocity Gradients

Lewis and von Elbe (ref. 3, pp. 379-390 and 425-429) have obtained approximate theoretical equations by which g_{fb} and g_b may be calculated if flame velocities and minimum ignition energies are known. These equations were obtained by considering the flow line for which the stream velocity and flame velocity are equal and integrating the energy equation for a plane combustion wave. To accomplish the integration for the reaction zone, this zone was subdivided into an adiabatic and an isothermal zone, and it was assumed that $dT/dx = (T_F - T_3)/(x_F - x_3)$ for the adiabatic zone. Ignition-energy data were used to determine the inflection-point temperature T_3. Agreement between calculated and experimental g_b curves for methane-air at room conditions was satisfactory with regard to the curve shape, but calculated values were low by a factor of 2 to 10. Calculated flash-back and quenching limits for propane-air did not even show the correct trends in all cases.

More recently, satisfactory relative predictions of critical boundary velocity gradients at various initial mixture temperatures T_o were obtained for methane-air flames by solving equation (10) for g (ref. 9):

$$g = \frac{U_F}{x_p} \tag{17}$$

It was assumed that

$$U_F \propto \frac{T_F - T_3}{T_F - T_o} \tag{18}$$

from the Mallard-LeChatelier equation (see ch. IV, eq. (38)), where T_F is the calculated adiabatic flame temperature and T_3 is the ignition temperature for the flame reaction zone. (In ch. IV, the factor $\varkappa/c_p\delta$ was assumed to be independent of temperature.) It was further assumed that, for flash-back,

$$x_{p,fb} \propto T_3 - T_o \tag{19}$$

and for blow-off,

$$x_{p,b} \propto \sqrt{D_o} \propto T_o^{3/4} \tag{20}$$

where D_o is the diffusion coefficient for secondary air diffusing into unburned gas at T_o. Assuming T_3 to be independent of T_o, the value of T_3 was calculated for every pair of experimentally determined gradients for a given fuel-air mixture at two temperatures by

$$\frac{g_1}{g_2} = \frac{f(U_F)_1 f(x_p)_1}{f(U_F)_2 f(x_p)_2} \tag{21}$$

and equations (18) and (19) or (20). This procedure gave an equation for T_3 that was cubic for flash-back or quadratic for blow-off. The values of T_3 (largest of the real roots) from various pairs of gradients were averaged, and the average value was used to compute gradients for the temperature range studied.

An approach that avoids the necessity of determining T_3 and that takes into account approximately the variations in thermal properties and reaction rate (which in turn is related to the reaction-zone thickness δ) is suggested in reference 10. This approach employs the modified form of the Semenov equation (bimolecular reaction) for flame velocity (ch. IV):

$$U_F \propto \sqrt{T_o^2 T_F^{4.9} \frac{\exp(-E/RT_F)}{(T_F - T_o)^3}} \tag{22}$$

For flash-back it is assumed that

$$x_{p,fb} \propto (T_F - T_o) \tag{23}$$

The latter assumption is in keeping with the Semenov approach for flame velocity, because Semenov assumed that T_3 was always near T_F and varied with T_F because of the exponential variation of the reaction rate with temperature. Equations (22) and (23) can be substituted for U_F and $x_{p,fb}$ in equation (21) by using activation energies from low-temperature oxidation studies in the literature. This substitution permits direct solution for the ratio of any two values of g_{fb}. It might be argued that the use of activation energies from low-temperature oxidation studies is subject to question, but such activation energies have been used successfully for flame velocity predictions (ch. IV) and must suffice until more appropriate values are measured.

Critical boundary velocity gradients for flash-back (referred to the gradient at 306° K) have been calculated from the data of reference 10 using 38 kilocalories per mole for E for propane and adiabatic flame temperatures as follows:

Initial temperature, °K	Critical boundary velocity gradient for flash-back, sec^{-1}	
	Calculated	Measured
306	----	680
422	1200	1190
506	1720	1710
617	2620	3500

Equation (20) for the penetration distance for blow-off may be oversimplified even for fuel-lean flames, because it neglects the role of wall-quenching and assumes that secondary-air diffusion occurs at T_o only. Actually, the secondary air must either travel through the dead space, where the temperature varies from T_o to some value near T_F, or through the burned gas (fig. VI-8(b)). Since T_F, for many fuel-air mixtures, increases approximately 1/2° for each °K that T_o is increased, it follows that any temperature between T_o and T_F increases less rapidly than T_o, so that it might be more reasonable to assume that the square root of the diffusion coefficient varies with $T_o^{1/4}$. Hence, taking the effect of wall quenching into account in the same manner as flash-back,

$$x_{p,b} \propto T_o^{1/4}(T_F - T_o) \tag{24}$$

In spite of these arguments, however, equation (20) gave somewhat better results for propane-air at an equivalence ratio of 1.12 (ref. 10), as can be seen from the following table:

Initial temperature, °K	Critical boundary velocity gradient for blow-off, sec^{-1}		
	Eqs. (20) to (22)	Eqs. (21), (22), and (24)	Measured
306	-----	------	4,000
422	5,400	6,500	5,300
506	6,600	8,900	7,300
617	8,400	13,000	10,400

In summary, either the method of reference 9 or the method suggested in reference 10 appears to give satisfactory predictions of the effect of temperature on critical boundary velocity gradients, but the latter method is less tedious and somewhat more desirable theoretically because it uses the Semenov approach with regard to ignition temperature.

Flames Supported on Flame Holders - Eddy Stabilization

Reference 13 suggests that, on a thermal basis alone, the quantity of energy required from the stabilizer would be increased by (1) increasing the approach-stream velocity U_o, (2) increasing the difference between the ignition temperature and the approach-stream temperature $T_3 - T_o$, (3) increasing the thickness of the preignition zone, or (4) increasing the heat capacity per unit volume. If, as in the early thermal theories, the thickness of the preignition zone is assumed proportional to the thermal diffusivity $\varkappa/\rho c_p$ divided by the laminar flame velocity, then the required heat-supply rate can be written as

$$H_{req} \propto \frac{U_o \varkappa}{U_{F,L}} (T_3 - T_o) \tag{25}$$

At blow-off, the heat required is infinitesimally greater than the heat supplied from the sheltered zone, which is given by

$$H_s \propto \left[\left(\frac{dU_o}{\nu}\right)^c \varkappa/d_r\right] d_r(T_F - T_o) \tag{26}$$

where c is a constant and where the bracketed term includes the factors affecting the heat-transfer coefficient from heated cylinders. In the two-dimensional duct, the area for heat transfer is proportional to the rod diameter d_r. Equating H_{req} and H_s, a relation of the form

$$U_b/d_r^b = f(\varphi) \tag{27}$$

is obtained, where the new exponent b on the rod diameter replaces $c/(1 - c)$. This type of correlation is demonstrated in table VI-I.

In reference 44, a quantitative relation was obtained by considering the recirculation zone behind a flame holder to be a steady-state reactor of volume V. If a homogeneous unburned gas mixture of fuel-air mass ratio f enters this volume at a rate such that the air mass-flow rate is W_a (in g/sec), and a fraction ε of the entering fuel is burned within the volume, then the fuel burned is $W_a f \varepsilon$. This quantity must be equal to the fuel consumed by chemical reaction. Reference 44 states that a second-order reaction is required to account for the observed effect of pressure (stability correlates with p^{-1}, table VI-I). The actual ratio-limiting reactions are unknown, but their concentrations can be assumed proportional to the mass air and fuel concentrations C_a and C_f, respectively. The collision factor Z combines the collision number, the steric factor, and the concentration proportionality constants. Thus, the material balance can be written

$$W_a f = VC_aC_fZ \exp(-E/RT) \tag{28}$$

Now C_a and C_f can be related to the initial fuel concentration and the initial temperature through f and ε; with the appropriate substitutions, equation (28) can be written as

$$\frac{W_a}{Vp^2} = \frac{Z \exp(-E/RT)}{T^2} \frac{(1-\varepsilon)(1-\varepsilon y)}{\varepsilon \psi} \tag{29}$$

where

T adiabatic flame temperature corresponding to fraction burned

y fraction of stoichiometric fuel concentration if mixture is lean, unity if mixture is rich

ψ $(Rf/M + R/29)^2$

M molecular weight of fuel

If W_a/Vp^2 from equation (29) is plotted against ε, curves such as those sketched in figure VI-16 are obtained for various concentrations using a given activation energy. (The equation is actually triple-valued in part, but only the values indicated by the solid curves are of practical interest.) A blow-out curve of W_a/Vp^2 against concentration can be obtained by cross-plotting the maximum of such curves

against concentration; the maximum could be obtained directly by setting the derivation of equation (29) equal to zero, solving for ε and by trial and error, and substituting values of ε and T into equation (29) to obtain values of W_a/Vp^2.

The air mass flow W_a into the recirculation zone is proportional to the velocity U, to the stream density, which in turn is proportional to the static pressure p, and to some function of the diameter d. The zone volume V depends almost entirely on some function of d. Hence,

$$\frac{W_a}{Vp^2} \propto \frac{U}{d^b p} \tag{30}$$

which has the same form as the correlating factor used by DeZubay and others if $b = 0.85$ or some such value (table VI-I). From DeZubay's data, Z was estimated to be 4×10^{12} cubic centimeters per gram mole (ref. 16) for E of 40 kilocalories per gram mole. These values are reasonable and are comparable with those obtained from classical kinetics. For a stoichiometric mixture, these values give a maximum value of W_a/Vp^2 of 40 g/(sec)(cm^3)(atm^2), which corresponds to $\varepsilon = 0.72$ and a heat-release rate of 190 calories per cubic centimeter per second, or 77 million Btu per cubic foot per hour. These data are used in reference 15 to calculate a flame-front thickness of 0.022 centimeter. It is stated that, since a reported value of the flame-front thickness of a propane flame is 0.05 centimeter, or more than twice as great as the calculated value of reference 15, the flame fronts in the recirculation zone must overlap. Thus, a state of homogeneity would be approached, or, in other words, the calculated results are not inconsistent with the original assumption of homogeneity. The general conclusion is that under certain conditions combustion appears to proceed homogeneously as a second-order chemical reaction. The gross features of flame stabilization behind flame holders in high-velocity air streams are explained by this hypothesis.

NONISOTROPIC FLAMES

Stationary open flames were long considered evidence that the laminar combustion wave is dynamically stable. Analyses of flame propagation (ch. IV) customarily start with the assumption of a steady-state, one-dimensional flame front. Many investigators had occasionally observed nonisotropic flames, usually in the form of polyhedral open flames, in which the ordinarily smooth cone breaks up into several (usually three to eight) petal-like sides, convex toward the unburned gas and separated by dark ridges. These polyhedrons could be made to remain stationary or to rotate at variable speeds, depending on composition and flow rate. However, the appearance of such flames was generally considered an abnormal phenomenon. The reasons and conditions for such instabilities received little attention before the recent studies of cellular or filamented flames in tubes (refs. 45 to 47) and studies of polyhedral open flames (refs. 32, 45 to 48, 50, and 51). Nonisotropic propagation has also been observed with spherical flames (ref. 52).

Cell Formation and Surface Break-up of Open Flames

Reference 48 reports that very lean hydrogen-air or H_2-O_2-CO_2 flames burning on a 1.36-centimeter nozzle separated into several filaments that rose from the burner rim and failed to combine into a closed cone tip. The number of filaments increased (or conversely, the size of the filaments decreased) with O_2/CO_2 ratio, with fraction of stoichiometric volume percent fuel (between 0.05 and 0.28, depending on the

absence or presence of CO_2), and with flow rate (fig. VI-17). The use of a 3.08-centimeter glass filter (sintered glass) as a burner enabled smaller, more clearly defined, parabloid-shaped filaments to be obtained, which were evenly distributed over the filter surface. No effect of filter porosity was observed. Nonisotropic structure was also observed in lean methane-plus-hydrogen flames and rich flames of various hydrocarbons. The manner of soot formation in rich, polyhedral flames of hydrocarbon-air mixtures was particularly noted; with benzene, carbon issued from the flame exclusively as a narrow stream at the tip, whereas with acetylene, it appeared in a luminous region that surrounded the cone uniformly, except for a dark region at the tip and a cup-shaped region of increased luminosity rising from the rim. Rich, polyhedral flames of other hydrocarbons (e.g., butane, heptane) exhibited intermediate behavior; oxygen-enrichment shifted the behavior of some of these toward the benzene type.

In reference 50, regions of polyhedral flames were mapped on flow rate - pressure diagrams for various rich propane- and butane-air mixtures and lean hydrogen-air mixtures. A typical diagram for a propane-air mixture is shown in figure VI-18. At constant pressure and composition within the region for polyhedral flames, the number of polyhedron sides increased with increasing flow rate. Upon the addition of 1 to 7 percent hydrogen, which by itself only exhibits instabilities in lean mixtures, to rich propane-air air mixtures, the over-all equivalence ratios at which polyhedral flames occur were reduced, other conditions being fixed. Adding hydrogen to rich carbon monoxide - air mixtures, which would otherwise exhibit no polyhedral flames at any composition, also produced polyhedral flames.

The most generally accepted explanation of nonisotropic structure in rich open flames of hydrocarbons and of soot formation at the tip is the preferential diffusion of the oxygen molecules, which are lighter than the fuel molecules, to the valleys, where the propagation is faster. In lean hydrogen or hydrogen-methane flames, the fuel becomes the lighter component and diffuses preferentially. In either case, it is the diffusion of combustion products into the unburned gas that sets up the concentration gradients leading to this preferential diffusion. Some investigators also believe in the necessity of the presence of hydrogen (refs. 48 and 50), and Behrens (ref. 48) points to the role of thermal diffusion in producing the observed soot filaments. Markstein (ref. 45) used a different attack - an aerodynamic treatment into which he incorporated the assumption that all transport phenomena could be described to a first approximation by a linear relation between flame velocity and reciprocal radius of curvature of the flame front. This aerodynamic treatment included the effect of gravity. It appears that the diffusion-kinetics against aerodynamic-instability question is yet unresolved.

Cellular Flames in Tubes

Nonisotropic structure of flame propagating through tubes was particularly evident in flammability-limit studies (ref. 43 and ch. III). Markstein (refs. 45 to 47) has made more definitive studies insofar as cell diameter d_c, molecular weight of fuel, and pressure effects are concerned by studying near-stoichiometric flames traveling downward through larger tubes (10-cm diam.) at low velocities. The low spatial velocities were obtained by reducing the flame velocity through the addition of nitrogen and letting the flame travel against a small, unburned gas flow. For hydrocarbons in the molecular weight range 42 to 114, $d_c \propto M^{-1/3}$. For n-butane-air-nitrogen mixtures at pressures from 1/3 to 1 atmosphere, $d_c \propto M^{-3/4}$. Both of these effects were determined for equivalence ratios between 1.2 and 1.4.

Contrary to the results of reference 50, Markstein found that the addition of hydrogen to rich mixtures of higher hydrocarbons suppressed cell structure, whereas addition to lean mixtures gave nonisotropic structure with small cell sizes. He also

observed that a 90 percent carbon monoxide - 10 percent butane fuel, burning rich, gave the same structure as butane. Reference 47 presents the relation between flame structure and vibratory movement with rich methane-n-butane-air-nitrogen mixtures. In this study, it was found that, for a given equivalence ratio, average cell size increased with methane concentration until a noncellular structure was reached. Discussion of oscillatory combustion may be found in chapter VIII.

SIGNIFICANCE OF FLAME STABILIZATION TO JET-ENGINE COMBUSTION

3072

High-output combustors require the stabilization of flame at velocites of several hundred feet per second. In the past decade, ram-jet engine performance has been boosted dramatically at ever-increasing inlet-air velocities, but many of the gains were accomplished by cut-and-try methods. In order to understand the interaction of flame and flow by which flame stabilization is accomplished, it is helpful not only to study small-scale ram-jet-type combustion chambers, but also to analyze open or confined flames on Bunsen-type burners. These burner experiments, which allow more rigid control and separation of operating variables, add to the basic understanding of such factors as wall quenching and secondary-air dilution. The experimental results reviewed in this chapter, together with some of the major theoretical concepts emphasized in recent years, are summarized in the following paragraphs.

For open flames burning above channels of simple geometric shape, including cylindrical tubes containing axially mounted rods, blow-off or flash-back limits for various lengths of the characteristic dimension of a given type of channel are correlated by means of the critical boundary velocity gradient, that is, the linear velocity gradient near the flame-holding solid surface or the stream boundary. For confined flames supported on flame holders, the stabilization process is dependent on a recirculation zone behind the flame holder; and, since the size of the recirculation zone is related to a characteristic dimension of the flame holder, the concentration-velocity limits are also related to flame-holder dimensions. From experimental results in the literature (and from theoretical considerations mentioned hereinafter), it appears that a quantity such as $U_{av,b}/A^c$ against a concentration parameter may correlate blow-off limit data, where A is the projected area of the flame holder and c is an exponent of the order of 1/2. For greater generality, a more direct function of the recirculation-zone size should be used instead of A^c, because obstacles of different shapes are known to produce vortices of different sizes.

The use of the vortex size rather than the obstacle size may also correct for effects that occur when the size of the obstacles is no longer small compared with the duct size. As the size of the obstacle is increased, a point is reached at which the vortex size begins to decrease; as the obstacle size approaches the duct size, the vortex may be considerably smaller than the obstacle, and reduced stability may result. Thus, the previous expression applies only for small stabilizers in large ducts as long as A refers to obstacle dimensions. The use of obstacles that block an appreciable fraction of the duct cross section (greater than 60 percent) may also be undesirable from other considerations. The pressure drop would, of course, be high, and the unburned gas velocities past the flame holder would be high. The latter effect would make flame-spreading from the sheltered zone difficult, and only a small fraction of the mixture near the flame holder would burn. In a practical design, the use of small flame holders located at various places within the duct might alleviate both the reduction in eddy size and the flame-propagation problem. Empirical correlations based on characteristic dimensions of flame holders are summarized in table VI-I.

For open flames, blow-off limits under conditions where there is turbulence in the approach stream are correlated with nonturbulent limits by the critical boundary velocity gradient, because in all cases the point of stabilization occurs within the laminar boundary layer. Contradictory results are reported on the effect of approach-stream turbulence on blow-off of confined flames from flame holders. When turbulence intensity was increased by means of various screens, a stability decrease resulted, but another investigation reported that the stability limits decreased when turbulence intensity was decreased by moving the flame holder downstream. Partial removal of a laminar boundary layer has little effect on blow-off from flame holders, unless the approach flow is so turbulent that the laminar sub-layer is very thin. Lean flames are affected by boundary-layer removal more than rich flames. Blowing a gaseous fuel into the boundary layer through slots in a flame holder may provide good pilot flames.

3072

A 2000-volt axial electric field, either alternating current at 400 cps or direct current with the positive electrode in the burned gas can double the blow-off velocity and triple the stable concentration range for burner flames. On the other hand, a transverse direct-current field of 15,000 volts decreased concentration limits of butane flames by 43 percent. Strong acoustical disturbances decrease stability (see also ch. VIII).

For burner flames, the effect of pressure is related to tube diameter d_t; that is, $U_{av,b}/pd_t$ is a function of concentration. An analogous situation is encountered with confined, supported flames; for example, for disk-shaped flame holders of diameter d, $U_{av,b}/p^{0.95}d^{0.85}$ was related to fuel-air ratio for propane flames. This type of correlation is substantiated by theoretical considerations. Scurlock arrived at the generality $U_{av,b}/d^b = f(\text{concentration})$ by considering the heat transferred between the eddy region behind the flame holder and the mainstream. In reference 15, $W_a/Vp^2 \propto U_{av,b}/d^b p = f(\text{concentration})$ was obtained, where W_a is the air mass flow entering the recirculation zone behind the flame holder, and V is the volume of that zone, which is considered to be a homogeneous, second-order reaction zone. The $f(\text{concentration})$ results from considering the second-order reaction and a certain fraction of the fuel within the zone being burned to produce a certain adiabatic reaction temperature. (The initial mixture temperature could also be included through its effect on this reaction-zone temperature.)

The blow-off velocity of open flames increases with approximately the square of the absolute initial mixture temperature; the exact exponent varies with concentration and fuel type and may be influenced by such factors as wall temperature and water vapor. The flash-back velocity is even more temperature-dependent, so that a decrease in relative stability range occurs as temperature is increased. The relative effect of temperature on critical boundary velocity gradients may be predicted by considering the effects of temperature on flame velocity and penetration distance (wall quenching and/or secondary-air dilution effect) on a thermal basis. Empirical correlations indicate that blow-off from flame holders may depend on a lower power of the initial mixture temperature; the parameter $U_{av,b}/d^{1/2}T_o^{1.2}$ correlated data for a hydrocarbon blend. At this point, it might be noted that the effects of flame-holder area, pressure, and temperature might be combined in a correlating parameter such as $U_{av,b}/A^c pT_o^m$ where c and m may be of the order of 0.5 and 1.2, respectively.

Liquid-vapor-air mixtures obtained by partial vaporization of liquid fuels generally gave Bunsen burner stability curves similar to those for gaseous systems. Blow-off limits can be increased appreciably by heating the flame holder; blow-off and flash-back velocities of burner flames are also increased by heating the burner

rim. Therefore, a heated flame holder, which might, in turn, be used to preheat fuel, would be advantageous in a high-speed engine.

The effect of fuel type on flame velocity was discussed in chapter IV; as might be expected, the blow-off and flash-back velocity gradients are greater for fuels with high flame velocities. Disk-stabilized, confined flames became less dependent on the disk diameter for fuels of higher flame velocity. Blow-off velocities of mixed fuels generally follow the relation

3072

$$\sum_j \frac{X_j}{X_j^*} = 1$$

where X_j is the mole fraction of the jth fuel in the total mixture having a certain blow-off velocity, and X_j^* is the mole fraction of the jth fuel in its binary mixture with air that has the same blow-off velocity.

Added water vapor decreases stability velocities; 2.5 percent water in the primary air reduced the blow-off velocities of butane flames by approximately 5 percent for lean mixtures and up to 30 percent for rich mixtures. Decreasing the diluent concentration in a combustible mixture greatly increases blow-off and flash-back velocities; for example, the critical boundary velocity gradients for methane-oxygen mixtures are two to three orders of magnitude greater than those for methane-air mixtures. This indicates that oxygen-enrichment of the inlet air is another method of obtaining very stable flames or pilot flames.

Also reviewed in this chapter were certain instability phenomena observed in bench-scale equipment and, for the most part, with laminar flames. The break-up of open laminar flames into cells or polyhedral shapes is believed by some investigators to be diffusion-kinetics process, while others treat it primarily as an aerodynamic instability.

In final summary, most of the experimental results for the stability of burner flames can be explained on the basis of the interaction between flame velocity and flow velocity in terms of the critical boundary velocity gradient. For confined flames, stabilization occurs through the recirculation zone behind a flame holder that is bluff or nonstreamlined on its downstream end. All the gross features of this latter type of stabilization appear to be explained by an assumption that the recirculation zone behaves as a volume of homogeneous, second-order reaction.

REFERENCES

1. Wohl, Kurt, Kapp, Numer, M., and Gazley, Carl: The Stability of Open Flames. Third Symposium on Combustion and Flame and Explosion Phenomena, The Williams & Wilkins Co. (Baltimore), 1949, pp. 3-21.

2. Bollinger, Lowell M., and Williams, David T.: Experiments on Stability of Bunsen-Burner Flames for Turbulent Flow. NACA Rep. 913, 1948. (Supersedes NACA TN 1234.)

3. Lewis, Bernard, and von Elbe, Guenther: Combustion, Flames and Explosion of Gases. Academic Press, Inc., 1951.

4. Garside, J. E., Hall, A. R., and Townend, D. T. A.: The Stability of Aerated Burner Flames. Trans. Inst. Gas Eng., vol. 91, 1941-1942, pp. 81-110.

5. Kurz, Philip F.: The Stability of Isobutane-Ethylene Flames on a Bunsen Burner Shielded to Exclude Ambient Air. Tech. Rep. No. 15036-18, Battelle Memorial Inst., Feb. 27, 1953. (Contract AF 33(038) - 12653, E.O. No. 460-35, S.R.-8.)

6. Haddock, Gordon W.: Flame-Blowoff Studies of Cylindrical Flame Holders in Channeled Flow. Prog. Rep. No. 3-24, Jet. Prop. Lab., C.I.T., May 14, 1951.

7. Weir, Alexander, Jr., Rogers, Donald E., and Cullen, Robert E.: Blowoff Velocities of Spherical Flameholders. Rep. UMM 74, Willow Run Res. Center, Eng. Res. Inst., Univ. Michigan, Sept. 1950. (USAF Contract W33-038-ac-21100, Proj. MX-772.)

8. Grumer, Joseph, Harris, Margaret E., and Schultz, Harold: Flame Stabilization on Burners with Short Ports or Noncircular Ports. Fourth Symposium (International) on Combustion, The Williams & Wilkins Co. (Baltimore), 1953, pp. 695-701.

9. Grumer, Joseph, and Harris, Margaret E.: Flame-Stability Limits of Methane, Hydrogen, and Carbon Monoxide Mixtures. Ind. and Eng. Chem., vol. 44, no. 7, July 1952, pp. 1547-1559.

10. Dugger, Gordon L.: Flame Stability of Preheated Propane-Air Mixtures. Ind. and Eng. Chem., vol. 47, no. 1, Jan. 1955, pp. 109-114.

11. McAdams, William H.: Heat Transmission. Second ed., McGraw-Hill Book Co., Inc., 1942, pp. 117-120.

12. Wohl, Kurt; Quenching, Flash-Back, Blow-Off - Theory and Experiment. Fourth Symposium (International) on Combustion, The Williams & Wilkins Co. (Baltimore), 1953, pp. 68-89.

13. Scurlock, A. C.: Flame Stabilization and Propagation in High-Velocity Gas Streams. METEOR Rep. 19, M.I.T., May 1948. (Contract NOrd 9661.)

14. Scurlock, A. C., Grover, J. H., and Barnes, W. P.: Turbulent Flames, Flame Stability, and Rough Burning. Semi-Annual Prog. Rep., Proj. Squid, James Forrestal Res. Center, Princeton Univ., Apr. 1, 1953. (Office Naval Res. Contract N7-ori-105, Task Order III, NR-098-038.)

15. Longwell, J. P., Chenevey, J. E., Clark, W. W., and Frost, E. E.: Flame Stabilization by Baffles in a High Velocity Gas Stream. Third Symposium on Combustion and Flame and Explosion Phenomena, The Williams & Wilkins Co. (Baltimore), 1949, pp. 40-44.

16. DeZubay, E. A.: Characteristics of Disk-Controlled Flame. Aero. Digest, vol. 61, no. 1, July 1950, pp. 54-56; 102-104.

17. Longwell, J. P.: Flame Stabilization by Bluff Bodies and Turbulent Flames in Ducts. Fourth Symposium (International) on Combustion, The Williams & Wilkins Co. (Baltimore), 1953, pp. 90-97.

3072

18. Caldwell, F. R., Ruegg, F. W., and Olsen, L. O.: Seventy-first Report on Progress on the Combustion Chamber Research Program for the Quarter Ending Sept. 30, 1951. Rep. 1B106, U. S. Dept. Commerce, Nat. Bur. Standards, Oct. 29, 1951. (NAer Order 01183.)

19. Williams, Glenn C., and Shipman, C. W.: Some Properties of Rod-Stabilized Flames of Homogeneous Gas Mixtures. Fourth Symposium (International) on Combustion, The Williams & Wilkins Co. (Baltimore), 1953, pp. 733-742.

20. Barrère, M., et Mestre, A.: Stabilisation des Flammes par des Obstacles. Selected Combustion Problems - Fundamentals and Aeronautical Applications, Butterworths Scientific Publications (London), 1954, pp. 426-446. (Comments by Melvin Gerstein, p. 524.)

21. Younger, George G., Gabriel, David S., and Mickelsen, William R.: Experimental Study of Isothermal Wake-Flow Characteristics of Various Flame-Holder Shapes. NACA RM E51K07, 1952.

22. Nickolson, H. M., and Field, J. P.: Some Experimental Techniques for the Investigation of the Mechanism of Flame Stabilization in the Wakes of Bluff Bodies. Third Symposium on Combustion and Flame and Explosion Phenomena, The William & Wilkins Co. (Baltimore), 1949, pp. 44-68.

23. Edse, Rudolph: Studies on Burner Flames of Hydrogen-Oxygen Mixtures at High Pressures. Tech. Rep. 52-59, Flight Res. Lab., Wright Air Dev. Center, Wright-Patterson Air Force Base, Apr. 1952. (RDO No. R-467-1.)

24. Putnam, Abbott A., and Landry, Bertrand A.: The Effect of Boundary-Layer Thickness on Flame Stability. Tech. Rep. 15033-1, Battelle Memorial Inst., Dec. 15, 1952. (Contract No. AF 33(038)-12656, E.O. No. 460-35 S.R.-8.)

25. Hottel, Hoyt C., et al.: High Output Combustion. Semi-Annual Prog. Rep., Proj. Squid, James Forrestal Res. Center, Princeton Univ., Oct. 1, 1953, pp. 97-125. (Office Naval Res. Contract N7-ori-105, Task Order III, NR-098-038.)

26. Polanyi, M. L., and Markstein, G. H.: Phenomena in Electrically and Acoustically Disturbed Bunsen Burner Flames. Tech. Rep. 5, Proj. Squid, Cornell Aero. Lab., Sept. 15, 1947.

27. Calcote, Hartwell F., and Pease, Robert N.: Electrical Properties of Flames - Burner Flames in Longitudinal Electric Fields. Ind. and Eng. Chem., vol. 43, no. 12, Dec. 1951, pp. 2726-2731.

N-140304

28. Calcote, Hartwell F.: Electrical Properties of Flames - Burner Flames in Transverse Electric Fields. Third Symposium on Combustion and Flame and Explosion Phenomena, The Williams & Wilkins Co. (Baltimore), 1949, pp. 245-253.

29. Hubner, H. J., and Wolfhard, H. G.: Combustion at High Altitudes. Library Trans. No. 125, British R.A.E., 1946.

30. Putnam, Abbott A., and Smith, Robert L.: On the Extinction Limit of Laminar Flames. Fourth Symposium (International) on Combustion, The Williams & Wilkins Co. (Baltimore), 1953, pp. 708-714.

31. Wohl, Kurt, and Kapp, Numer M.: Flame Stability at Variable Pressures. Meteor Rep. UAC-42, Res. Dept., United Aircraft Corp., Oct. 1949. (Proj. METEOR, Bur. Ord. Contract NOrd 9845 with M.I.T.)

32. Culshaw, G. W., and Garside, J. E.: Recent Studies of Aerated Burner Flames. Inst. Gas. Eng. (London), Inst. Gas. Res. Fellowship Rep. 1946-1947. (Reviews papers from period 1943-1946, including those of Delbourgh, Heiligenstaedt, and Vasilesco.)

33. Browning, James A., and Thorpe, Merle L.: Flame Stability of Liquid-Vapor Oxygen Mixtures. Tech. Memo. Dart-1, Proj. Squid, Thayer School of Eng., Dartmouth College, Feb. 11, 1952. (Contract N-onr-438, Task Order 1, NR 090172.)

34. Browning, James A., and Thorpe, Merle L.: Flame Stability of Liquid-Vapor Mixtures. Tech. Memo. Dart 2, Proj. Squid, Dartmouth College, Oct. 1, 1952. (Contract No-ori-105, T.O. III, NR-098-038.)

35. Sachsse, Hans: Über die Temperaturabhängigkeit der Flammengeschwindigkeit und das Temperaturgefälle in der Flammenfront. Zs. f. Phys. Chem., Bd. 180, Heft 4, Abt. A, Oct. 1935, pp. 305-313.

36. May, Walter G., and Maddocks, Frank E., Jr.: Flame Stabilization in Air/Fuel-Spray Mixtures at High Velocity. Meteor Rep. No. 54, Fuels Res. Lab., M.I.T., Apr. 1950.

37. Russi, M. J., Cornet, I., and Cornog, R.: The Influence of Flame Holder Temperature on Flame Stabilization. Fourth Symposium (International) on Combustion, The Williams & Wilkins Co. (Baltimore), 1953, pp. 743-748.

38. Kurz, Philip F.: Flame-Stability Studies with Mixed Fuels. Ind. and Eng. Chem., vol. 45, no. 9, Sept. 1953, pp. 2072-2078.

39. Reiter, S. H., and Wright, C. C.: Stability of Burner Flames with Propane-Hydrogen Mixtures. Ind. and Eng. Chem., vol. 42, no. 4, Apr. 1950, pp. 691-694.

40. Grumer, Joseph, and Harris, Margaret E.: Flame-Stability Limits of Methane, Hydrogen, and Carbon Monoxide Mixtures. Ind. and Eng., Chem., vol. 44, no. 7, July 1952, pp. 1547-1559.

41. Walker, P. L., Jr., and Wright, C. C.: Stability of Burner Flames for Binary and Tertiary Mixtures of Methane, Carbon Monoxide and Water Vapour. Fuel, vol. XXXI, no. 1, Jan. 1952, pp. 37-44.

3072

42. Walker, P. L., Jr., and Wright, C. C.: Stability and Burning Velocity of Bunsen Flames with Propane-Carbon Monoxide Mixtures. Fuel, vol. XXXI, no. 1, Jan. 1952, pp. 45-49.

43. Kapp, N. M., Snow, B., and Wohl, K.: The Effect of Water Vapor on the Normal Burning Velocity and on the Stability of Butane-Air Flames Burning above Tubes in Free Air. Meteor Rep. UAC-30, United Aircraft Corp., Nov. 1948. (U.S. Navy Bur. Ord. Contract NOrd 9845 with M.I.T.)

3072

44. Longwell, John P., Frost, Edward E., and Weiss, Malcom A.: Flame Stability in Bluff Body Recirculation Zones. Ind. and Eng. Chem., vol. 45, no. 8, Aug. 1953, pp. 1629-1633.

45. Markstein, George H.: Instability Phenomena in Combustion Waves. Fourth Symposium (International) on Combustion, The Williams & Wilkins Co. (Baltimore), 1953, pp. 44-59.

46. Markstein, George H.: Experimental and Theoretical Studies of Flame-Front Stability. Jour. Aero. Sci., vol. 18, no. 3, Mar. 1951, pp. 199-209.

47. Markstein, G. H., and Somers, L. M.: Cellular Flame Structure and Vibratory Flame Movement in N-Butane-Methane Mixtures. Fourth Symposium (International) on Combustion, The Williams & Wilkins Co. (Baltimore), 1953, pp. 527-535.

48. Behrens, Hans: Untersuchung über Aussehen und Gestalt von Brennerflammen. Zs. Phys. Chem., Bd. 196, Sept. 1950, pp. 78-101.

49. Garside, J. E., and Jackson, B.: The Formation and Some Properties of Polyhedral Burner Flames. Fourth Symposium (International) on Combustion. The Williams & Wilkins Co. (Baltimore), 1953, pp. 545-552.

50. Jost, W., Krug, Joachim, and Sieg, L.: Observations on Disturbed Flames. Fourth Symposium (International) on Combustion, The Williams & Wilkins Co. (Baltimore), 1953, pp. 535-537.

51. Simon, Dorothy M., and Wong, Edgar L.: Burning Velocity Measurement. Jour. Chem. Phys., vol. 21, no. 5, May 1953, pp. 936-937.

TABLE VI-I. - CORRELATING PARAMETERS FOR CONCENTRATION LIMITS OF BLOW-OFF FROM FLAME HOLDERS

Flame holder mounted in chamber	Correlating parameter	Flame holder	Characteristic dimension, d*, in.	Mixture velocity, ft/sec	Pressure, atm	Approach temperature, °R	Fuel	Calming-chamber screens and contraction ratio	Reference
Transverse, in 1" by 3"	$U/d^{0.45}$	Uncooled rods or gutters	0.016-0.498	60-300; Approach	1.0	520-600; Mixture	Cambridge city gas; propane	200-Mesh; 20:1 ($\mu'/U = 0.004$)	13
Transverse, in 1" by 4"	$U/d^{0.5}$ $U/T_o^{1.2}$	Cooled cylinders	0.035-0.494 .127	60-740; Approach 60-600; Approach	1.0 1.0	610; Mixture 606-970	Hydrocarbon blend (C_6-C_8)	150-Mesh; 28:1	6
Transverse, in $1\frac{1}{2}$" by 3"	$U/d^{0.5}T^{1.2}$	Cooled or uncooled rods	0.187-0.375	120-850; Approach	1.0	660, 860; Mixture	Gasoline		18
Axial, in 6" pipe	U/d	Uncooled rods, cones, annuli, or gutters	0.75-3.5	200-950; Past baffle	1.0	760; Inlet air	Naphtha (C_5-C_8)	(Fully developed pipe turbulence)	15
Axial, in 4" pipe	$U/d^{0.85}p^{0.95}$ U/d $U/d^{0.74}$	Disks	0.25-2.0	40-550; Past baffle	0.2-1.0	550; Mixture	Propane Naphtha Hydrogen	Fine mesh; 4:1	16 17 17
Axial	$U/d^{0.5}$ U/d	Disks Spheres			1.0 1.0				19 19
Axial, above $\frac{3}{8}$" to $1\frac{1}{4}$" nozzle	U/p (given d)	Spheres	0.0625-0.189	65-350; Approach		100; Inlet air	Propane	100-Mesh 576:1	7

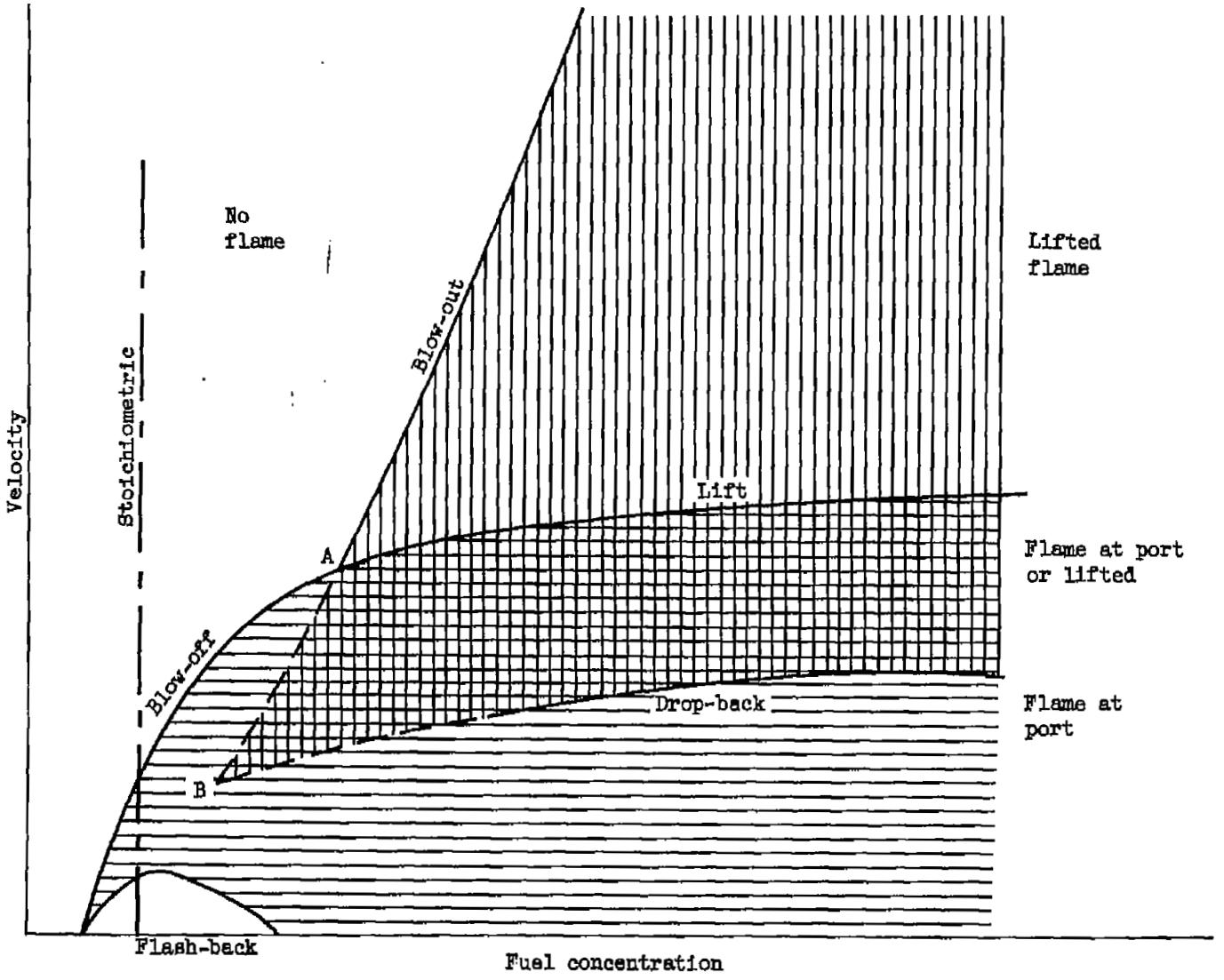

Figure VI-1. - Characteristic stability diagram for open flames (ref. 1).

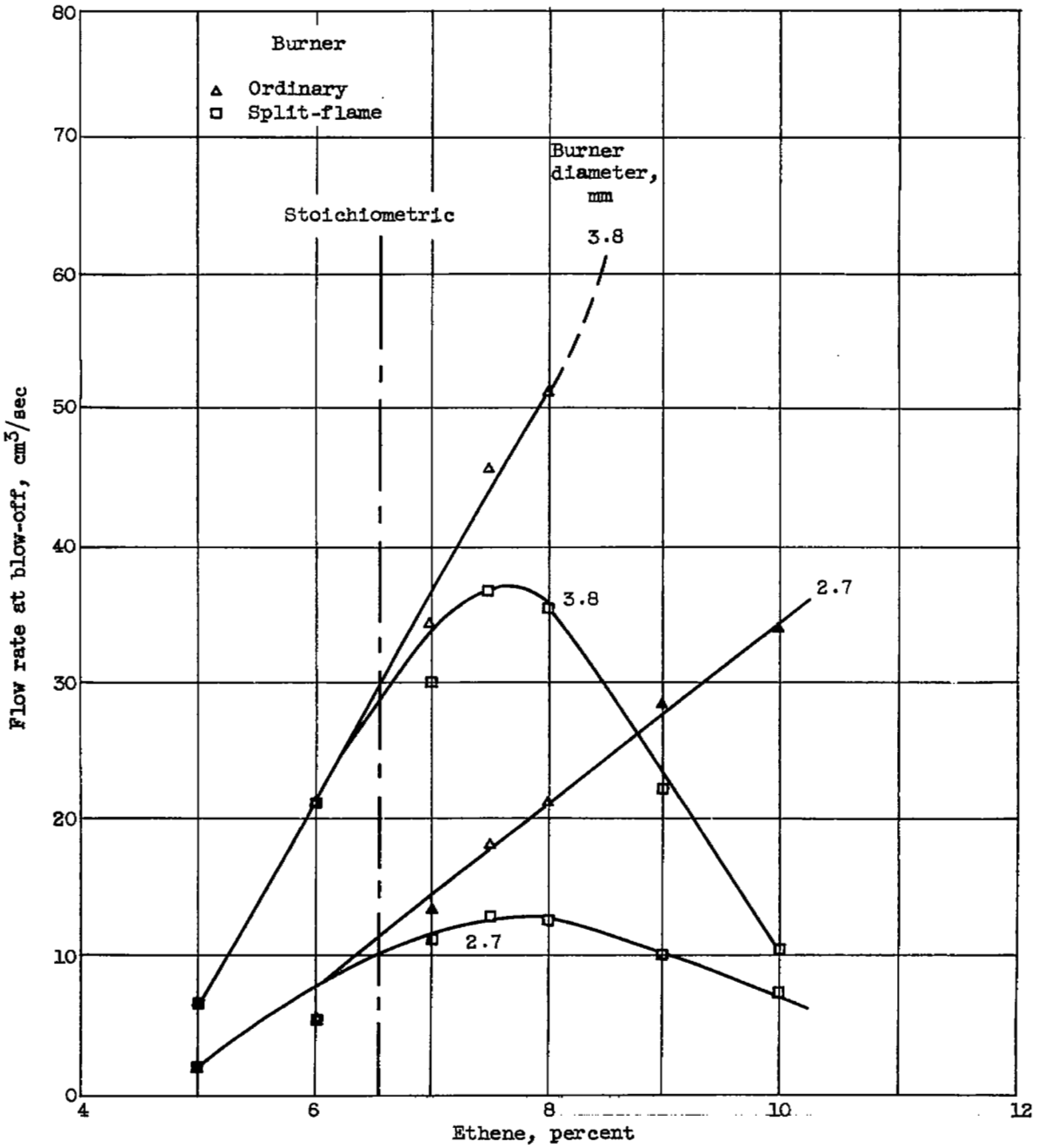

Figure VI-2. - Comparison of blow-off curves obtained with split-flame (Smithells) burners with those obtained on ordinary single-tube burners. Ethene-air mixtures saturated with water vapor at 20° C (ref. 5).

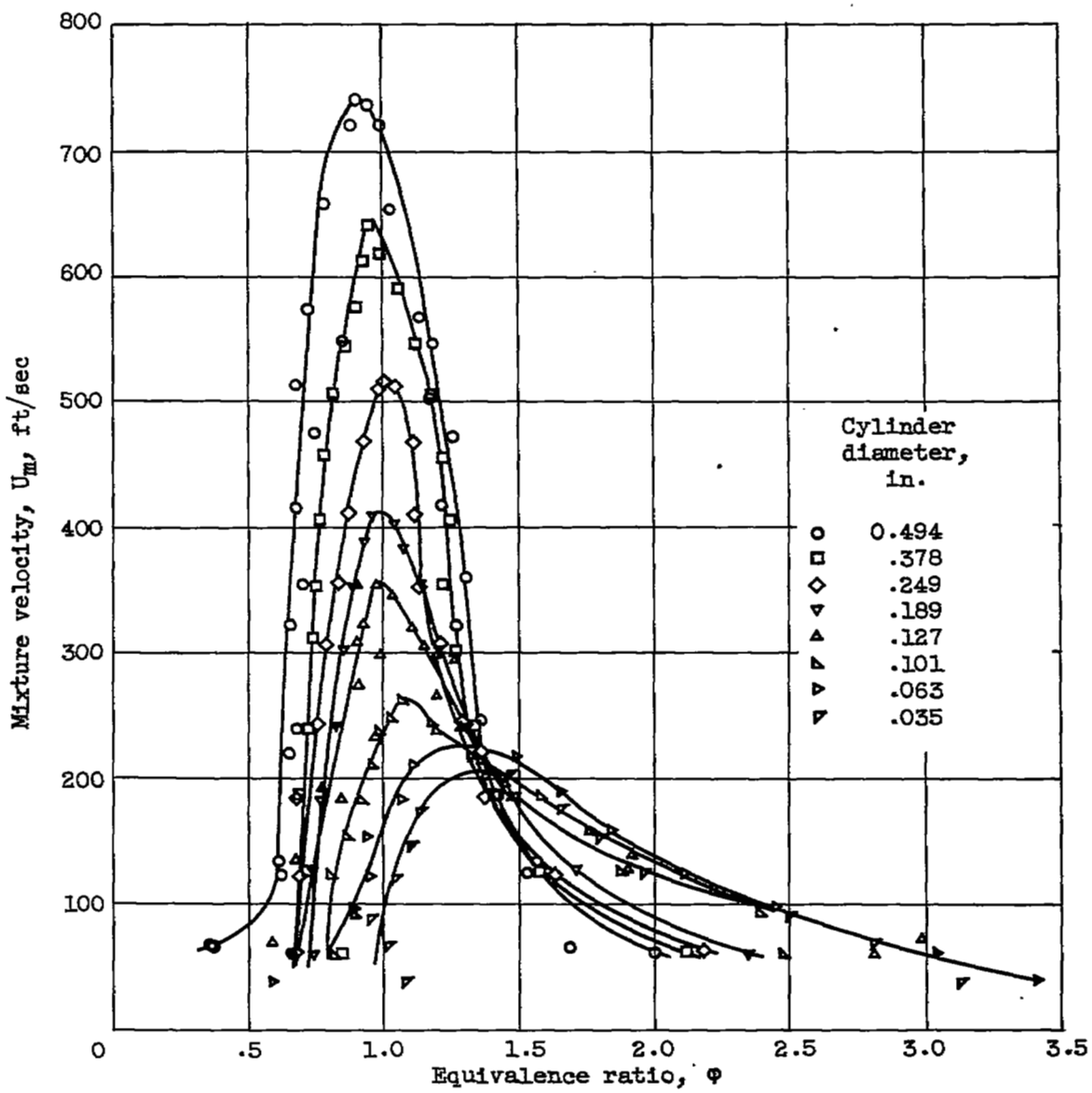

Figure VI-3. - Flame blow-off limits for cylinder sizes from 0.035 to 0.494 inch in diameter. Fuel, hydrocarbon blend (commercial paint thinner); mixture stagnation temperature, 150° F; static pressure, approximately 1 atmosphere (ref. 6).

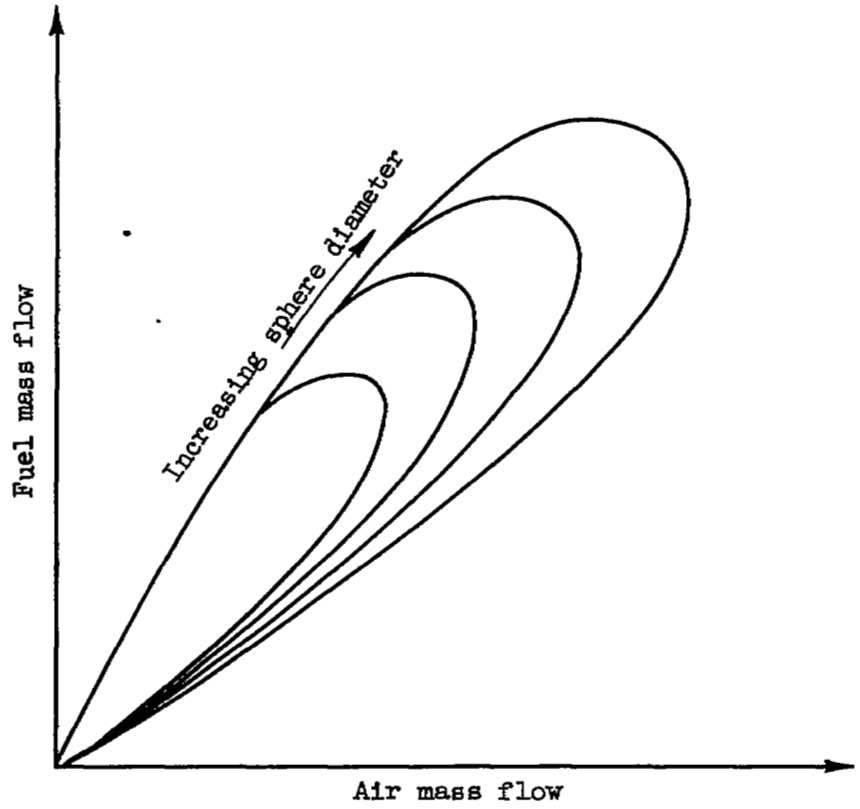

Figure VI-4. - Blow-off from spherical flame holders in 1-inch free jet at atmospheric pressure (ref. 7).

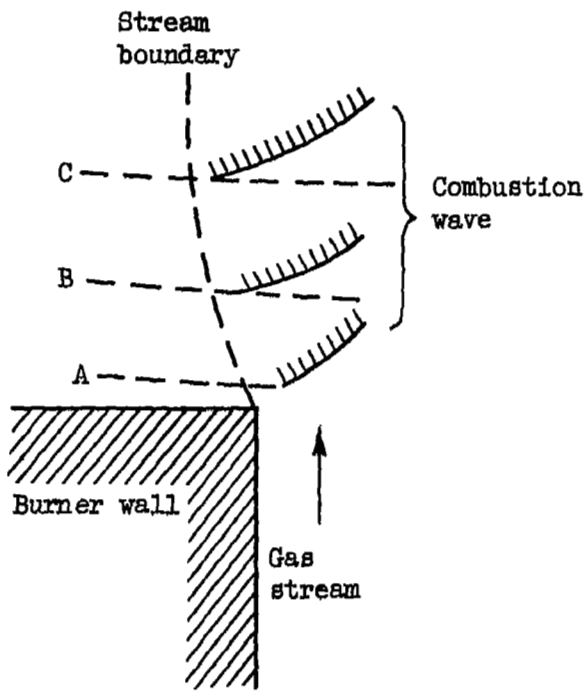

(a) Location of flame with respect to burner at various distances above port.

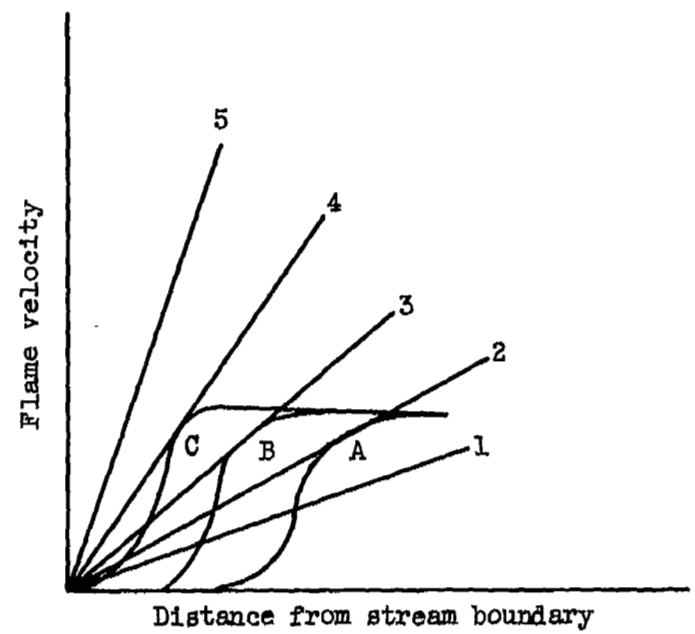

(b) Relation between flame and stream velocity as function of distance from stream boundary.

Figure VI-5. - Interaction of flame velocity and critical boundary velocity gradient. Bunsen flame (ref. 3, p. 244).

Figure VI-6. - Lifted turbulent burner flame (ref. 3).

3072

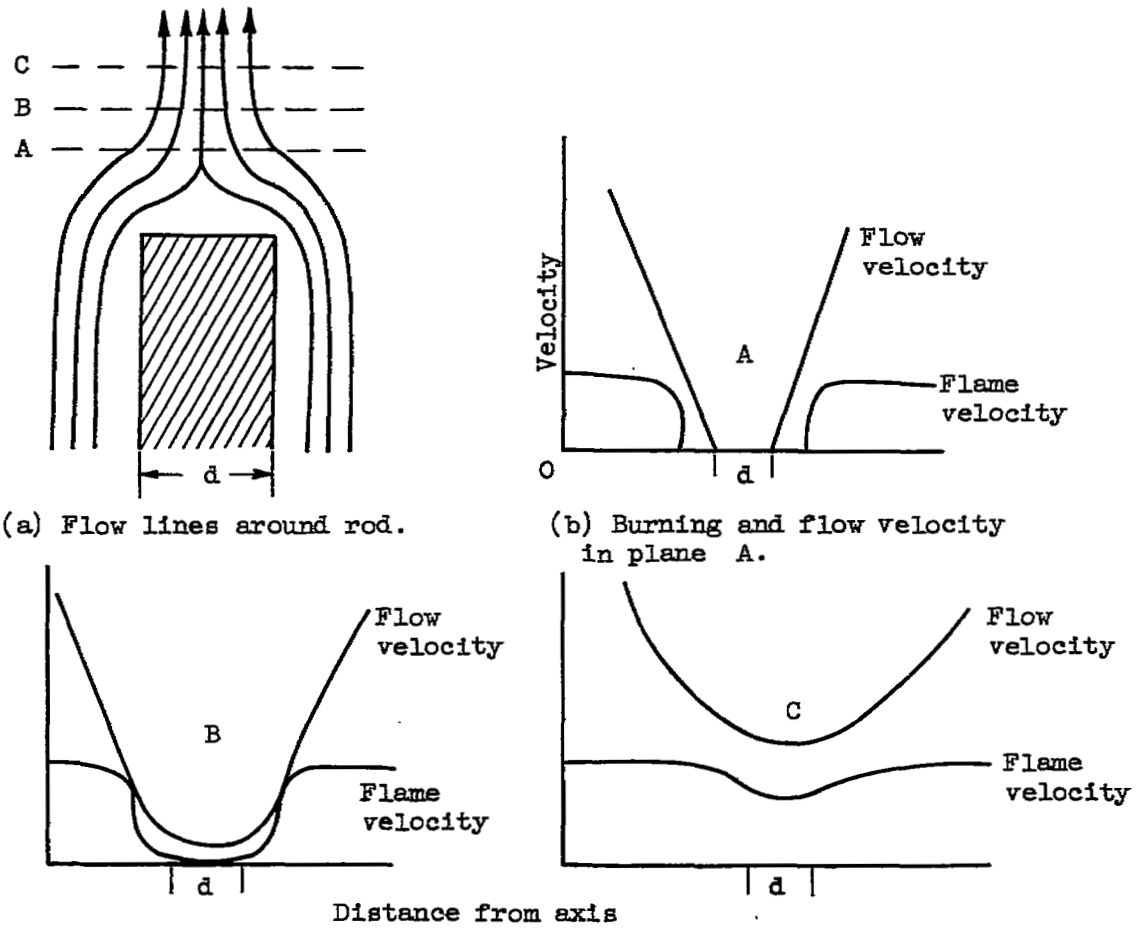

(a) Flow lines around rod.

(b) Burning and flow velocity in plane A.

(c) Burning and flow velocity in plane B.

(d) Burning and flow velocity in plane C.

Figure VI-7. - Stabilization of combustion wave by rod (ref. 3, p. 246).

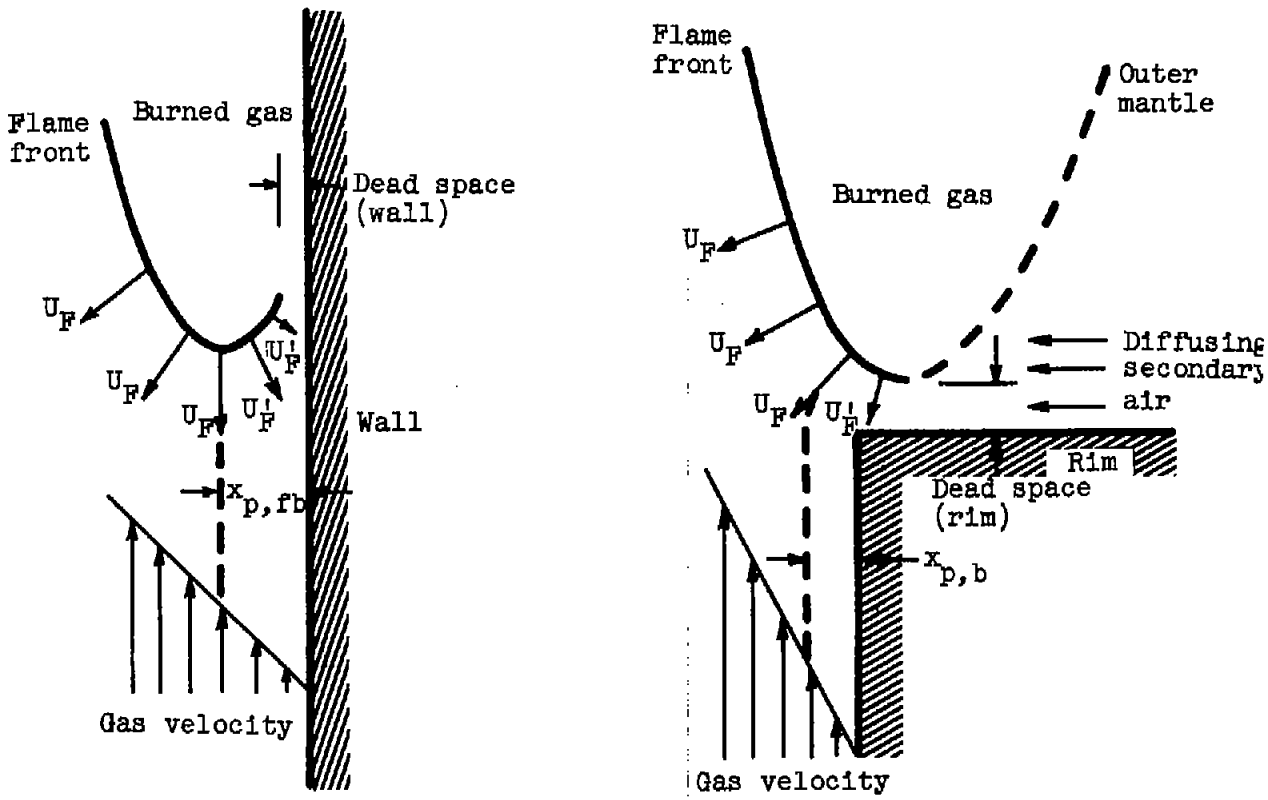

(a) Flash-back.

(b) Blow-off.

Figure VI-8. - Relation between flame- and gas-velocity curves at stability limits. For flash-back, tube diameter is considered to be at least twice the quenching distance (primes refer to nonadiabatic conditions) (by permission from ref. 10).

3072

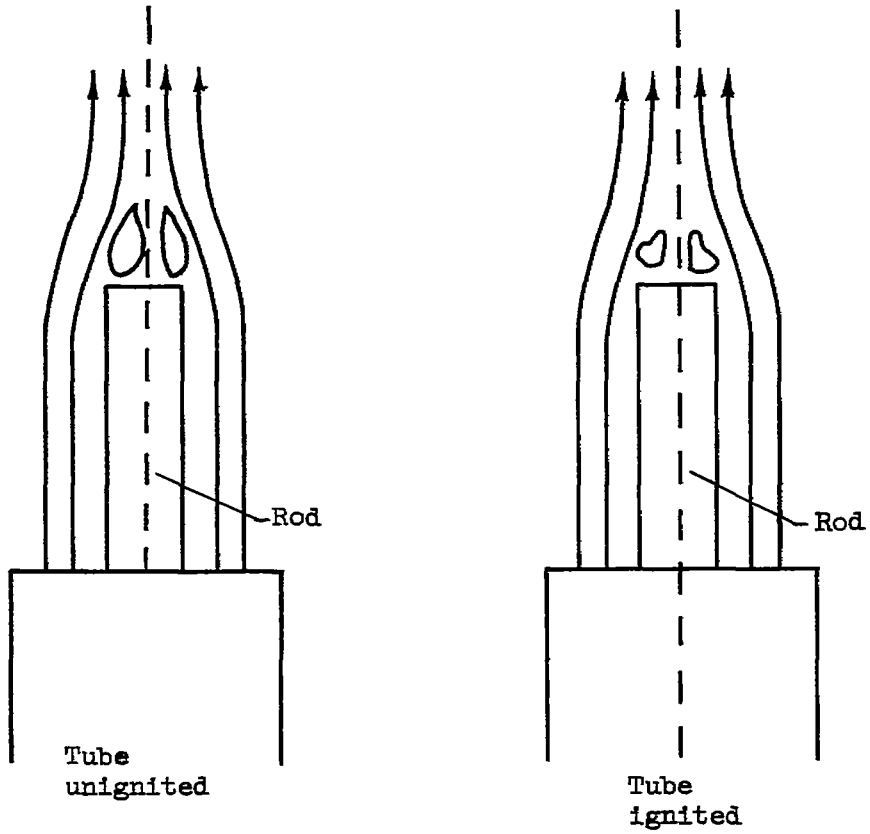

Figure VI-9. - Flow lines around axially placed rod with and without flame (ref. 3, p. 269).

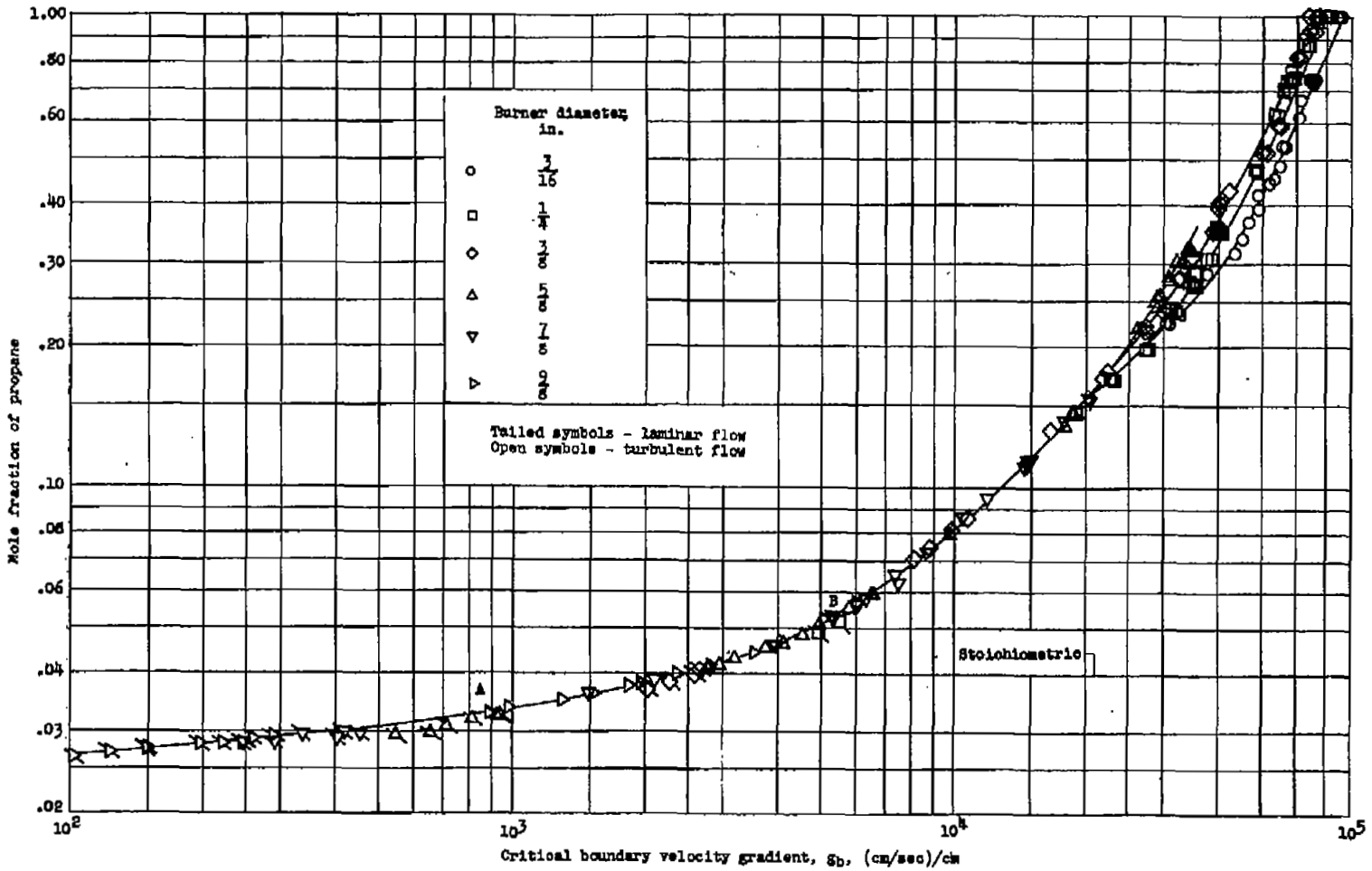

Figure VI-10. - Variation of fuel-air ratio with velocity gradient at tube wall for blow-off of seated propane-air flames (ref. 2).

3072

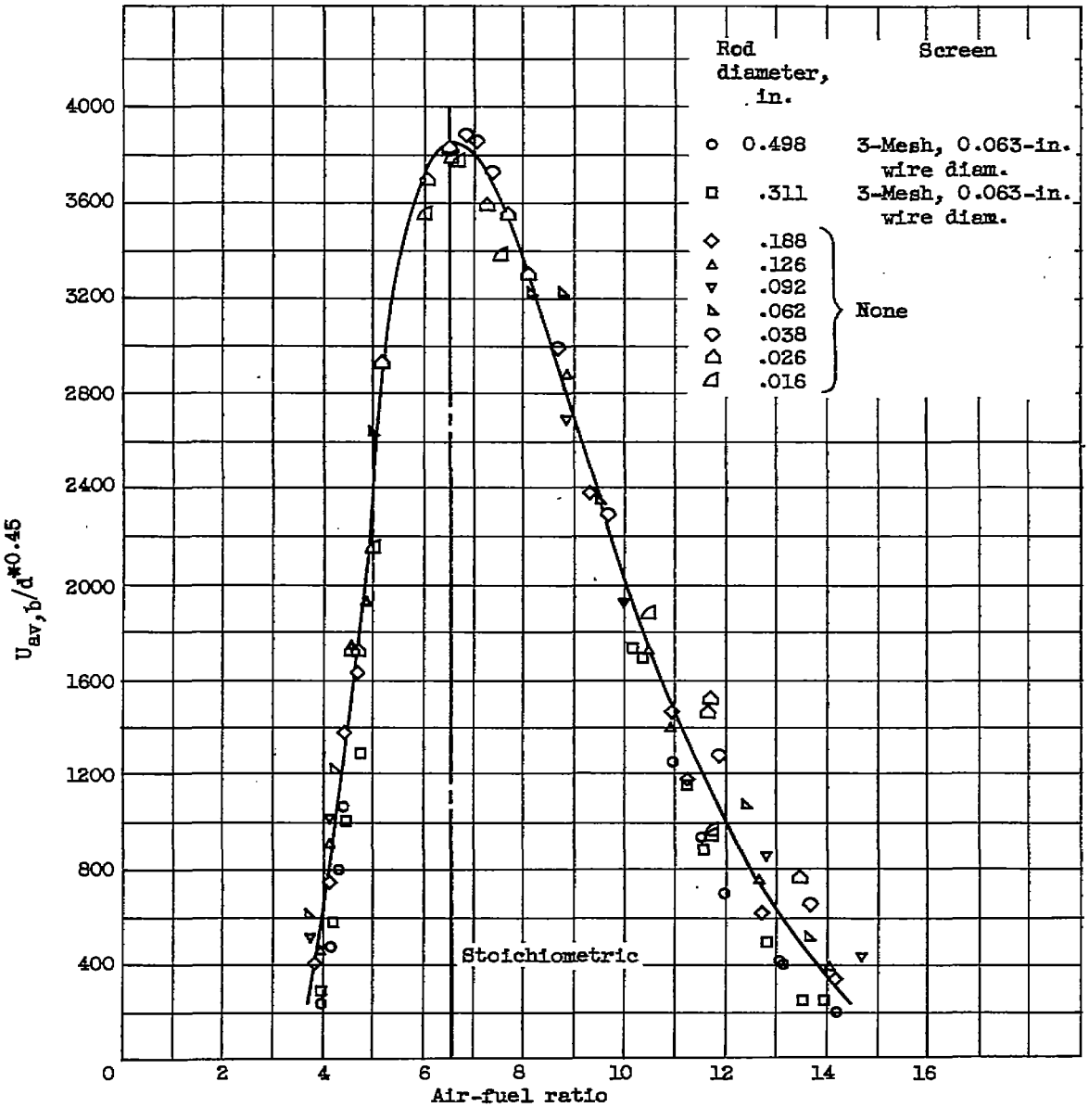

Figure VI-11. - Correlation of rod stabilizer blow-out limit data. Fuel, city gas; stabilizers 9 inches from chamber entrance (ref. 13).

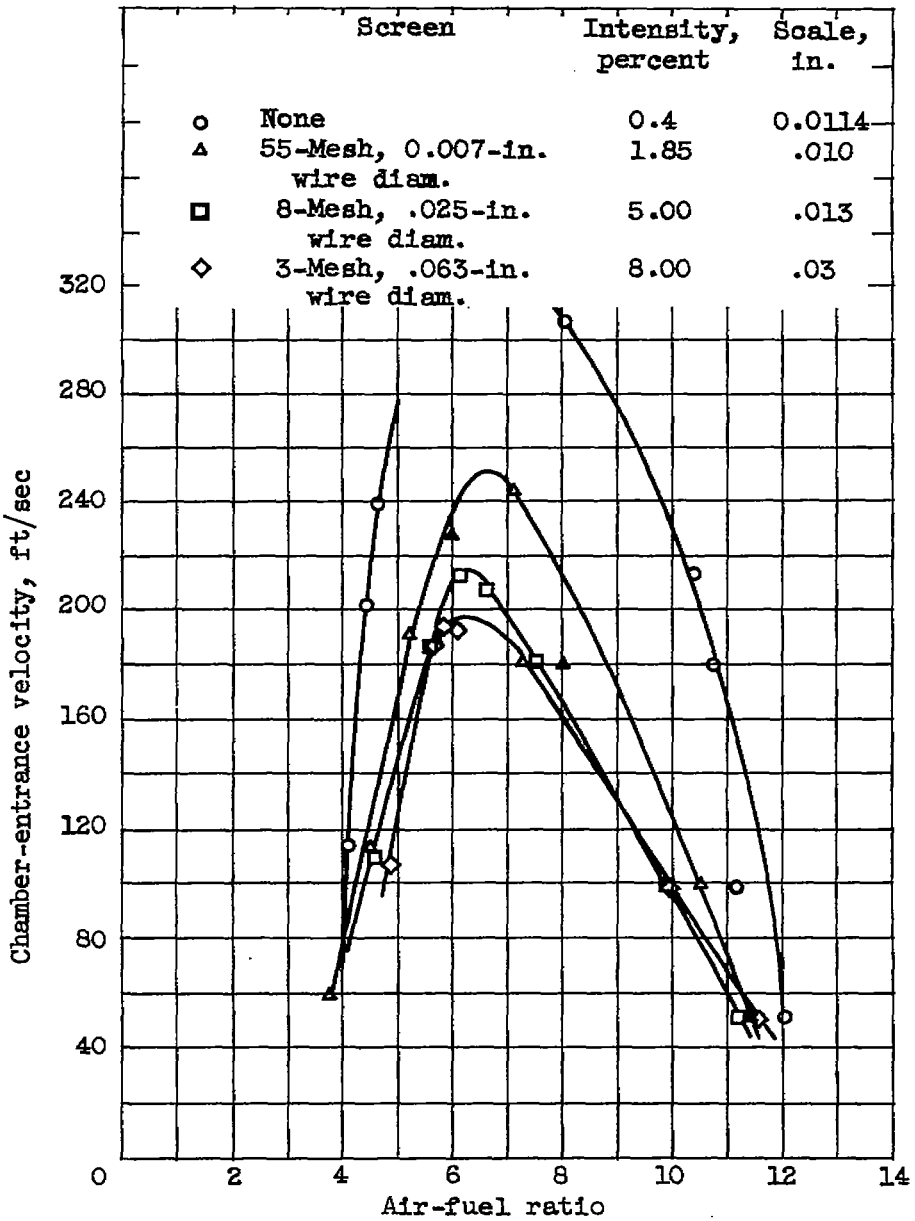

Figure VI-12. - Effect of approach-stream turbulence on rod stabilizer blow-off limits of Cambridge city gas - air flames. Screens 2 inches upstream of 0.038-inch rod in 1- by 3-inch chamber (ref. 13).

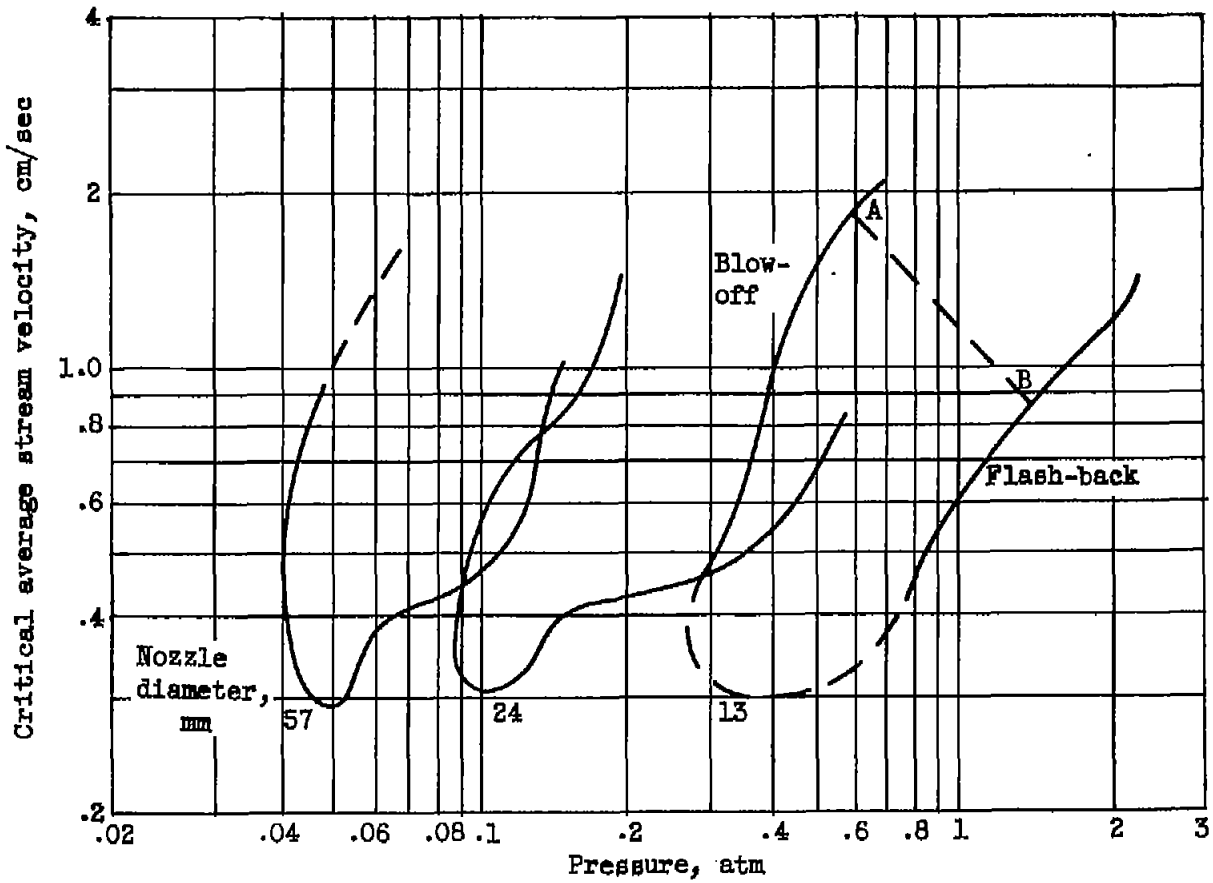

Figure VI-13. - Effect of pressure and burner nozzle diameter on stability limits of stoichiometric propane-air flames at room temperature (ref. 29).

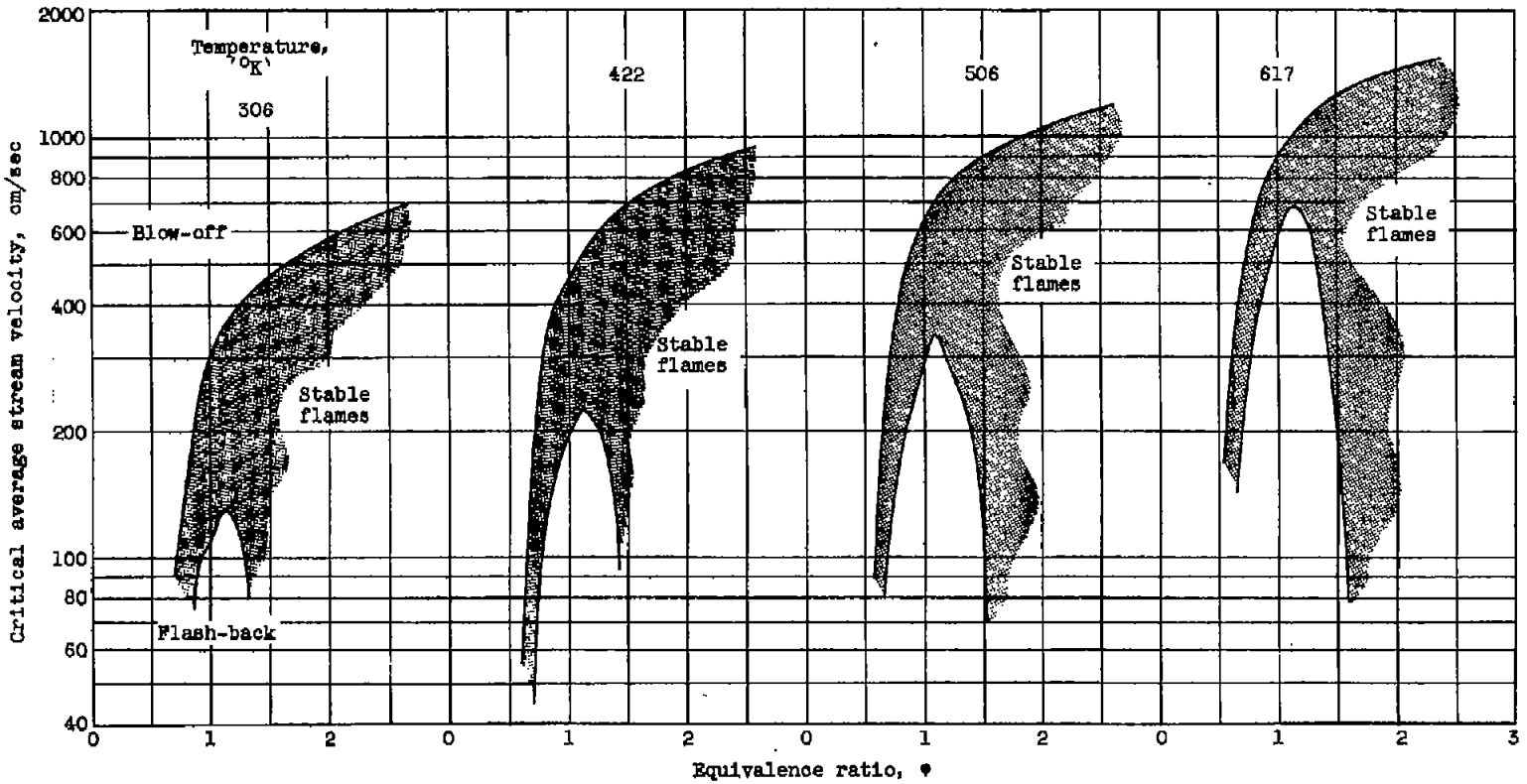

Figure VI-14. - Effect of initial mixture temperature on stable flame region for propane-air flames on 15.6-millimeter burner at atmospheric pressure (by permission from ref. 10).

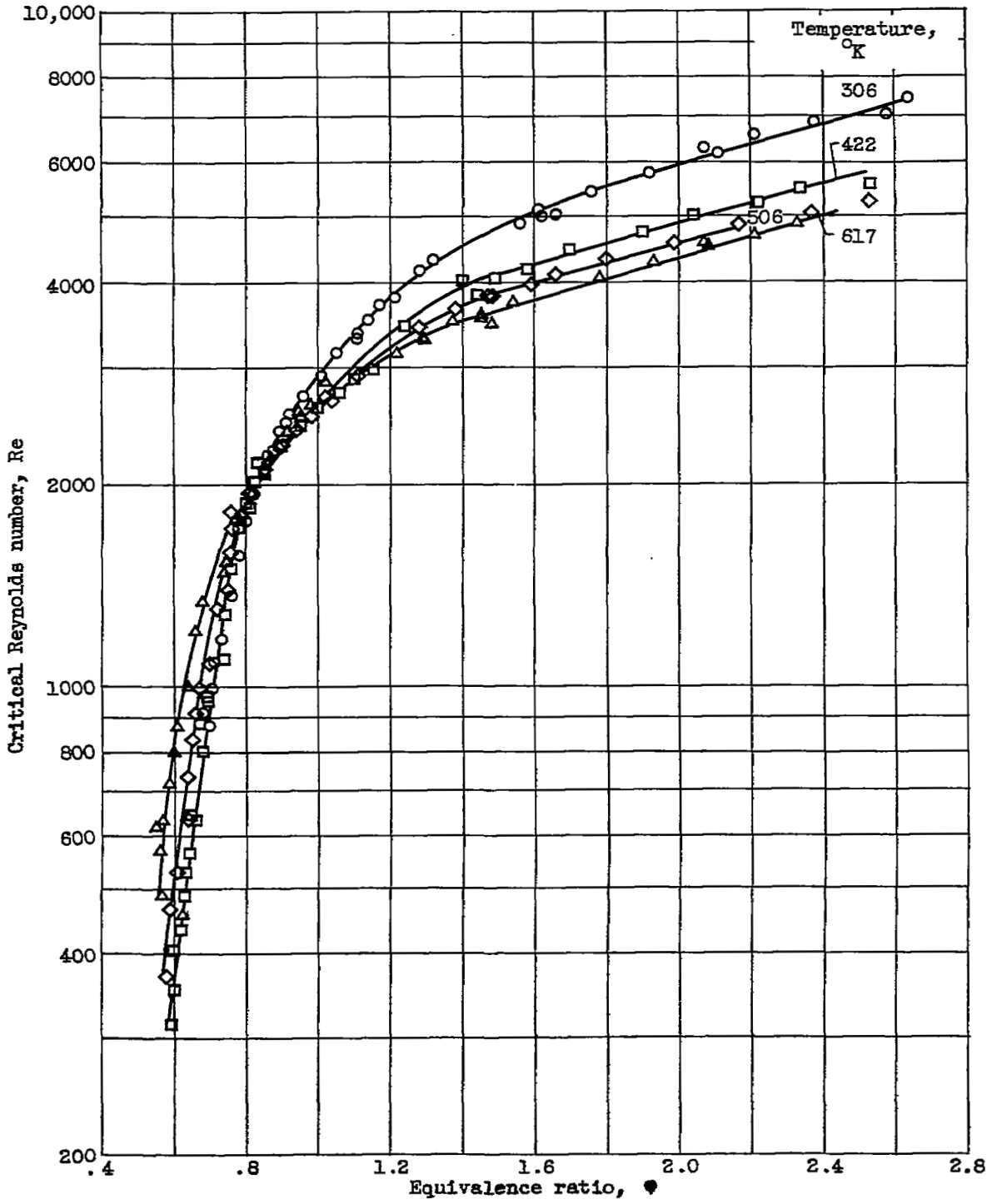

Figure VI-15. - Effect of initial mixture temperature on critical Reynolds number for blow-off (by permission from ref. 10).

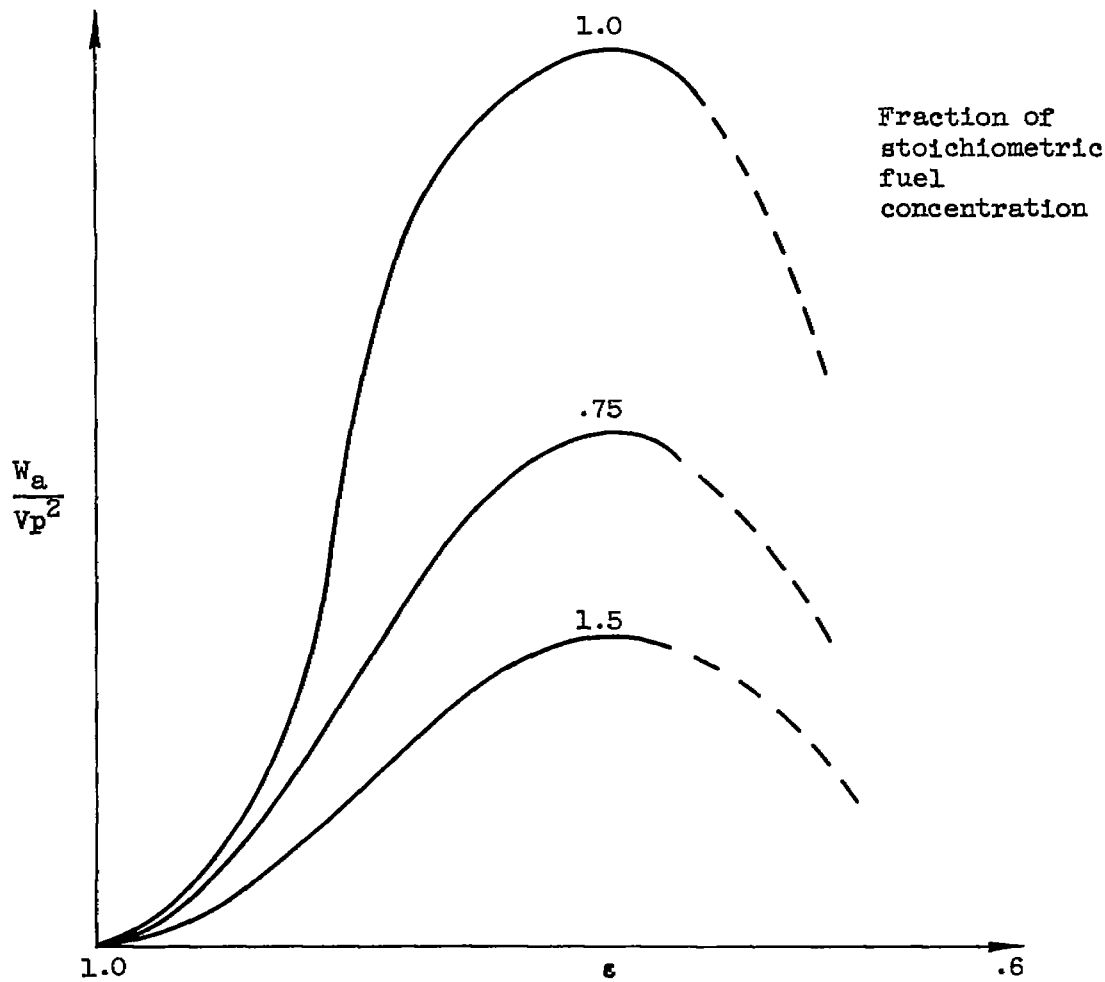

Figure VI-16. - Variation of W_a/Vp^2 with ε.

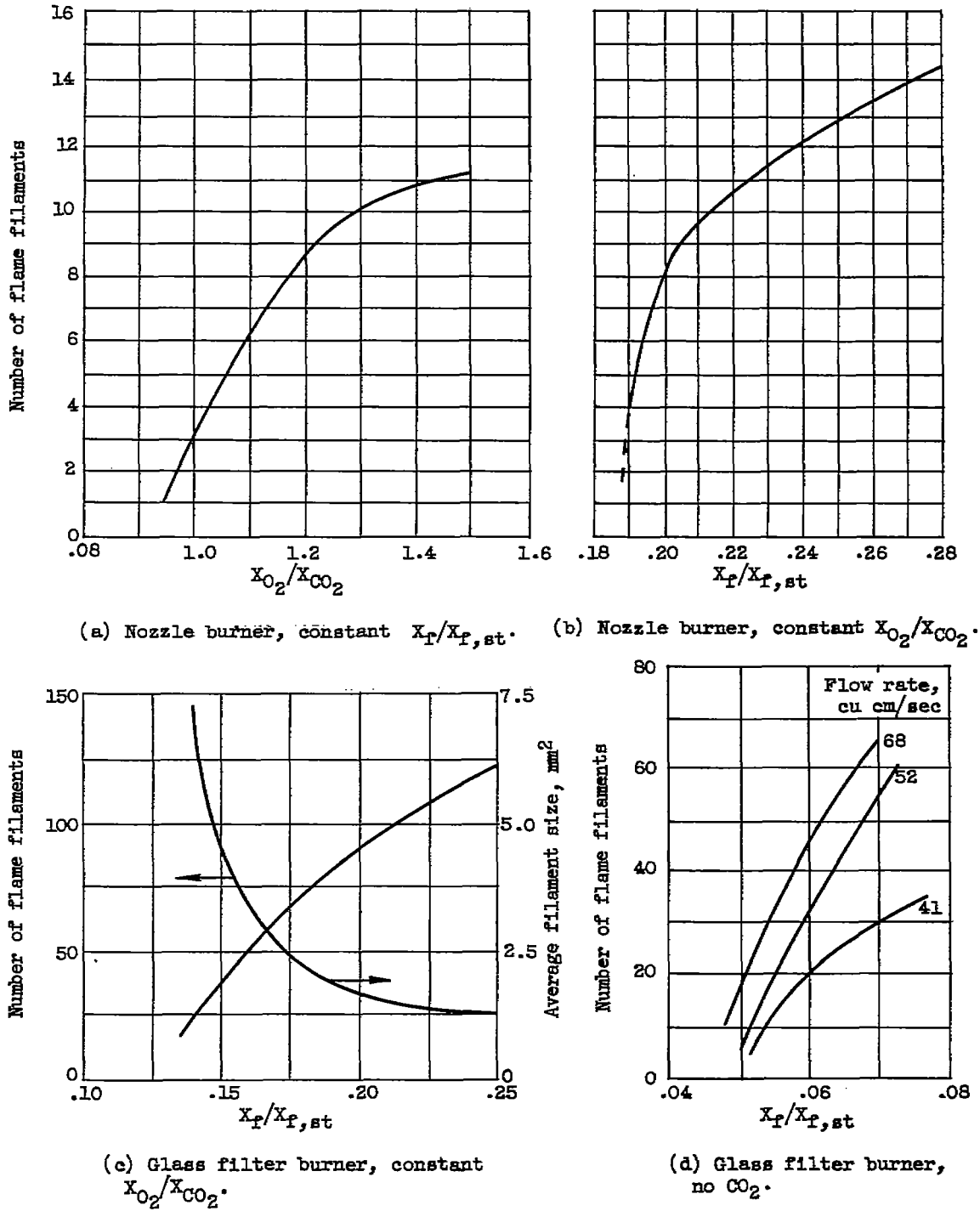

(a) Nozzle burner, constant $X_f/X_{f,st}$.

(b) Nozzle burner, constant X_{O_2}/X_{CO_2}.

(c) Glass filter burner, constant X_{O_2}/X_{CO_2}.

(d) Glass filter burner, no CO_2.

Figure VI-17. - Number of flame filaments for lean hydrogen burner flames at various H_2-O_2-CO_2 concentrations (expressed in mole fractions X), on 1.36-centimeter nozzle or a 3.08-millimeter sintered glass filter (ref. 48).

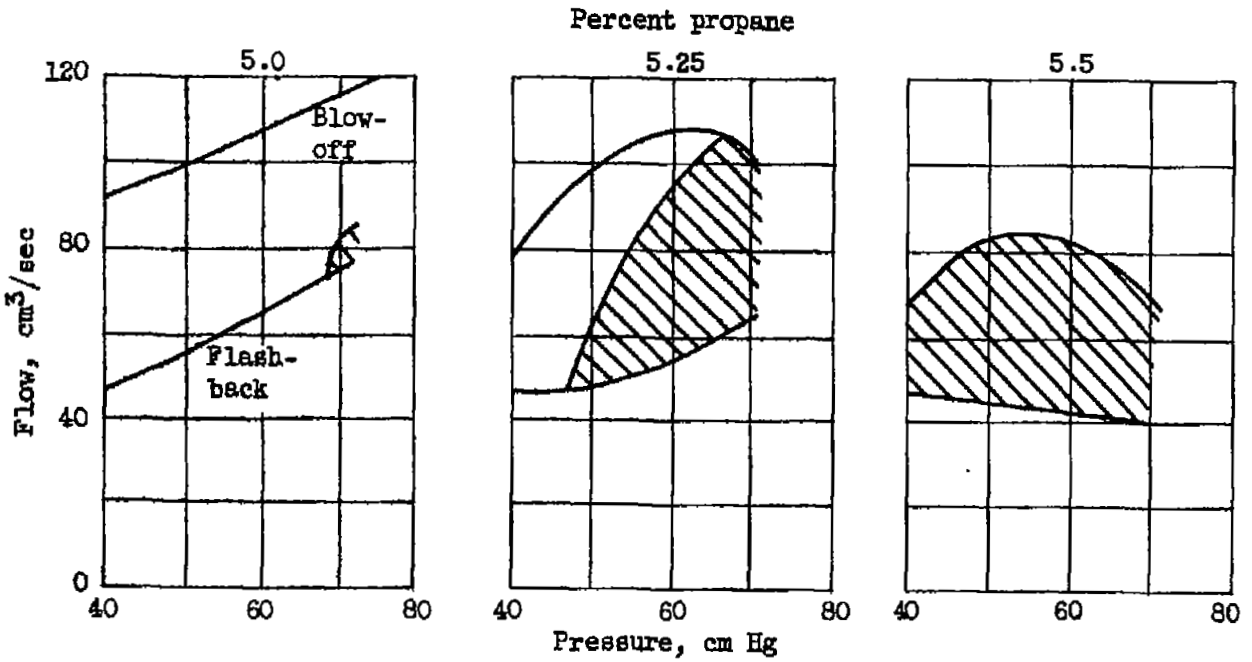

Figure VI-18. - Regions of polyhedral flames (shaded areas) of propane-air mixtures at reduced pressure. Split-flame burner (ref. 50).

[redacted]

CHAPTER VII

DIFFUSION FLAMES

By Richard S. Brokaw and Melvin Gerstein

INTRODUCTION

3092

The previous chapters consider combustion occurring in systems in which the fuel and air are homogeneously distributed. Chapter II discusses the preparation of such mixtures. If the mixing occurs rapidly compared with the combustion reactions, or well ahead of the flame zone, burning may be considered solely in terms of homogeneous processes. There are systems, however, in which mixing is slow compared with the reaction rates, so that the mixing time controls the burning rate. This is true for so-called diffusion flames in which the fuel and oxidant come together in a reaction zone through molecular and turbulent diffusion. The fuel may be in the form of a gaseous jet or a liquid surface; the distinctive characteristic of a diffusion flame is that the burning rate is determined by the rate at which the fuel and oxidant are brought together in proper proportions for reaction. Between the extremes in which the chemical reaction rate on the one hand and the mixing rate on the other control the burning rate, there is the region in which the chemistry and mixing have similar rates and must be considered together. This middle region has received very little attention in fundamental studies because of its complexity, but is considered in some of the practical systems discussed in subsequent chapters.

SYMBOLS

The following symbols are used in this chapter:

A	constant
B	constant
B'	transfer number
C	concentration
c_p	specific heat at constant pressure
D	diffusion coefficient
d	diameter
G	mass flow per unit area
g	acceleration due to gravity
h	specific enthalpy
i	stoichiometric number of moles of oxygen per mole of fuel
J_0,J_1	Bessel functions of the first kind
K	constant

[redacted]

k	constant
L	height of plate
l_1	scale of turbulence
M	molecular weight
m	mass
n	exponent
P	total pressure
Pr	Prandtl number, $c_p\mu/\varkappa$
p	partial pressure
Q	volume flow rate
R	universal gas constant
R'	drop distribution parameter
Re	Reynolds number
r	radial distance
T	temperature
t	time
U	velocity
u'	intensity of turbulence
W	total mass flow
w	stoichiometric weight of oxygen per unit weight of fuel
X	mole fraction
x	distance from drop center
$\bar{x}$	size constant
y	longitudinal distance
α	parameter
β	evaporation constant
δ	half-thickness of port
ϵ	eddy diffusivity
θ	parameter
$\varkappa$	thermal conductivity
μ	viscosity
ρ	density
τ	concentration parameter

Subscripts:

A drop surface

a air

B burning

C surrounding atmosphere

c combustion

F flame

f fuel

j jet

L laminar

l liquid

P products

s secondary flow

st stoichiometric

T turbulent

v vaporization

0 initial conditions

GASEOUS DIFFUSION FLAMES

Gaseous diffusion flames occur upon ignition of a jet of fuel entering either quiescent air or an air stream. The resulting flame emits heat and light and appears to have a discrete reaction zone, the appearance of which depends on the conditions of burning. Gaseous diffusion flames are most commonly encountered in simple home and industrial burners, but may exist in any system where fuel and air are admitted separately, and where the mixing processes are slow compared with chemical reaction rates. Typical ways in which the fuel and oxidant are caused to interact are shown in figure VII-1 (ref. 1, p. 99). Most of the basic work on diffusion flames has been done with the concentric tube arrangement (c), since it has the simplest geometry. Arrangement (a) has been used for some spectroscopic studies of flames, which are discussed herein.

Appearance

The shape of a laminar flame burning from a jet of fuel depends on the relative quantity of air supplied. If an excess of air is present, the flame is a closed, elongated figure. Such flames occur when a jet of fuel is admitted into a large volume of quiescent air or when two laminar coaxial jets are used, the inner containing fuel and the outer containing an excess of air. If the air supply in the outer tube is reduced below the stoichiometric proportions, a fan-shaped, underventilated flame is produced.

Under certain limiting flow conditions, the flame can assume a more complex structure. Flame shapes obtained in concentric-tube hydrocarbon diffusion flames (fig. VII-1(c)) for various fuel and air flows are classified in reference 2. These flame zones are illustrated in figure VII-2. Zone 1 indicates a normal, overventilated diffusion flame and zone 2 indicates the underventilated flame. The dotted line separating zones 1 and 2 denotes the smoke point, smoke appearing as the fuel flow is increased (see ch. IX). Zone 3 illustrates overventilated flames having a meniscus shape without the yellow glow usually associated with diffusion flames. The shaded areas are essentially zones of unstable flames. In the lower part of zone 4, there appear flames that oscillate from side to side, called lambent flames in reference 2, and in the upper part of zone 4, rich, tilted flames appear. In the lower part of zone 5 are found toroidal-shaped flames, called vortex flames, and in the upper part of zone 5, lean, tilted flames appear. In zone 6, the flame has begun to move away from the burner base and corresponds to the lifted flames discussed in chapter VI.

If either the fuel flow or the air flow is made turbulent, a brushy, rough flame results. At flows near the critical transition from laminar to turbulent, only the upper portion of the flame is turbulent, the flame near the burner port retaining the appearance of a laminar flame. Typical changes in the appearance of a gaseous diffusion flame as the fuel-flow velocity is increased are shown in figure VII-3. The line separating the laminar portion of the flame from the turbulent portion is called the break point. When the break point closely approaches the nozzle, further increases in velocity have very little effect on either the total flame height (measured from the burner port) or the break point, although the noise intensity increases. The quantitative variation of flame height with flow velocity is treated in a subsequent section.

Structure

Unlike the flame of premixed gases, which has a very narrow reaction zone, the diffusion flame has a wide region over which the composition of the gas changes. These changes are principally due to the interdiffusion of reactants and products, since the actual reaction apparently takes place rapidly in a narrow zone. The diffusion flame is thus better suited for studies of the temperatures and concentration profiles. Some of the results obtained for both laminar and turbulent flames are discussed herein.

Laminar flames. - In reference 3, the distribution of combustion products in a laminar diffusion flame was measured. A probe was placed along the axis of the burner and gas samples at various heights were removed. The measurements for a cylindrical carbon monoxide flame are shown in figure VII-4, in which the CO, CO_2, and N_2 concentrations are shown as a function of height above the port.

Reference 4 reports measurements of H_2, O_2, and N_2 concentrations in a hydrogen-air diffusion flame at various heights and radial distances in the flame. The results are shown in figure VII-5. The measurable O_2 concentration shown in the fuel side of the flame front is attributed to air entering the sampling tube because of flame movement. The structure of the diffusion flame suggested from the analysis is illustrated in figure VII-6, which may be considered generally typical for laminar, gaseous diffusion flames. The figure shows the fuel gas concentration at the burner center line dropping to zero at the flame front, while the O_2 rises from zero at the flame front to its value in the ambient stream. The concentration of products is a maximum at the flame front. The oxygen and fuel are considered to reach the flame front in stoichiometric proportions and to react to form products instantaneously. In the most theoretical treatments, a simplified picture of the reaction has

been assumed in which only one diffusing gas is considered. Instead of treating both fuel and oxygen varying from their initial concentrations to zero at the flame front, the fuel, for example, is treated as negative oxygen. In the case of the reaction $2H_2 + O_2 \rightarrow 2H_2O$, each mole of hydrogen is equivalent to 1/2 mole of oxygen. One of the dashed curves in figure VII-6 represents the reflected fuel curve corrected for the stoichiometric ratio. Thus, it is possible to consider only the diffusion of oxygen from its initial concentration through zero at the flame front to the proper negative value in the unburned fuel. In a similar manner, the other dashed curve illustrates the condition in which the oxygen is considered in terms of its fuel equivalent.

The actual flame is not as simple as the previous discussion may suggest, since, in addition to the molecular species that have been studied by conventional sampling and gas analysis, free atoms and radicals are present. A flat flame in an apparatus similar to that shown in figure VII-1(a) was used in reference 5, in which the distribution of various species in the flame was studied by a spectroscopic method. In addition, a sodium line reversal method was employed to measure flame temperature. The results are given for a H_2-O_2 flame in figure VII-7(a). The temperature profile is shown, in addition to a qualitative intensity distribution for OH and O_2 as determined by both emission and absorption spectroscopy. The relatively flat temperature profile has a maximum of about 2800° C, which agrees closely with calculated adiabatic flame temperatures for the stoichiometric reaction. A similar set of curves for CH_4-O_2 flames may be seen in figure VII-7(b). In addition to OH and O_2, the C_2, CH, and continuous emission are shown. Similar curves are shown for NH_3-O_2 flames in reference 5, while additional curves for H_2-O_2 and NH_3-O_2 along with C_2H_4-O_2 and CO-O_2 are given in reference 6. The general characteristics are similar.

Turbulent flames. - The distribution of reactants and products in a turbulent diffusion flame of H_2-air is studied in reference 7. The situation is somewhat more complex than in the laminar flame. Unfortunately, the results are influenced by the confining duct, so that the curves can be applied only qualitatively to open flames. The data are shown in figure VII-8 for various heights and radial positions. The O_2 and H_2 concentrations were measured, while the H_2O concentration was calculated. The general appearance of the H_2 and O_2 curves resembles that of a laminar flame, although there is considerably more overlapping of the H_2 and O_2 in the vicinity of the flame front. This result is consistent, however, with the oscillating nature of the turbulent flame, which results in the apparent thickening of the reaction zone when a time-average, rather than instantaneous, position is considered.

Theory

The theories of the burning of premixed fuel-oxidant systems discussed in chapters IV and V consist essentially of analyses of the factors such as diffusion, heat transfer, and reaction mechanisms as they affect the rate of the homogeneous reaction taking place. "Homogeneous" is used in the sense that fuel and oxidant molecules are intimately mixed in the unburned gas, although concentration and temperature gradients exist in the reaction zone. Inasmuch as the primary mixing process of fuel and oxidant appears to dominate the burning process in diffusion flames, the theories emphasize the rates of mixing in deriving the characteristics of diffusion flames. Since laminar and turbulent mixing processes are usually treated differently, the theories of laminar and turbulent diffusion flames are also separated in the following discussion. Only those mixing processes directly involved in setting up the equations for the flame are considered, since the general subject of mixing is treated in chapter II.

Laminar flames. - The basic equations for the theoretical treatment of laminar, gaseous diffusion flames to determine flame length and other properties were established by Burke and Schumann in 1928 (ref. 3). Later work has extended the range of the treatment. Burke and Schumann used an experimental model corresponding to figure VII-1(c), which is reproduced to aid in defining some of the terms:

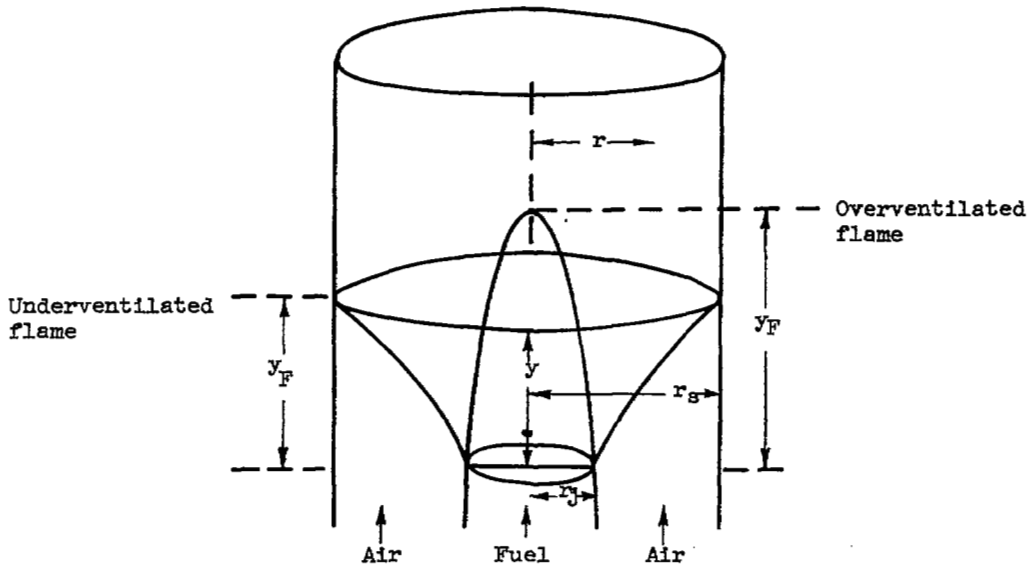

The basic assumptions which Burke and Schumann made in setting up the problem are listed and discussed to facilitate reference to the assumptions. Additional assumptions to facilitate solutions of various equations are considered as they arise.

(1) At the port position, the velocities of the air and the fuel are assumed constant, equal, and uniform across their respective tubes so that the molar ratio of fuel flow to air flow is given by $r_j^2/(r_s^2 - r_j^2)$.

(2) The velocity of the fuel and air up the tube in the region of the flame is the same as the velocity at the port. That this is not actually true has been shown for premixed V-flames in chapter IV.

(3) The coefficient of interdiffusion of the two gas streams is constant. Since diffusion coefficient increases with temperature, as would the gas velocity assumed constant in (2), Burke and Schumann suggest that these two effects may minimize the errors introduced by the assumptions.

(4) The interdiffusion of the two gas streams is entirely radial. This is a reasonable assumption for tall flames.

(5) The mixing of the two streams occurs by diffusion only. In other words, recirculation eddies and radial flow components are assumed absent.

(6) The flame front is a geometric surface where fuel and oxygen meet in stoichiometric proportions and react to give reaction products.

(7) The oxygen is considered the negative fuel. In the reaction Fuel + $iO_2 \rightarrow$ Products, each mole of fuel is equivalent to i moles of oxygen. The oxygen concentration C_{O_2} may then be replaced by its stoichiometric equivalent in terms of fuel C_{O_2}/i, which is the number of moles of fuel that would be completely burned by C_{O_2} moles of oxygen. Since zero concentration of reactants at the flame front is desirable, the oxygen is treated as negative fuel so that the fuel concentration ranges from its value in the unreacted jet C_f to the equivalent value of oxygen in the unreacted air $-C_{O_2}/i$. This has been shown in figure VII-6 by reflecting the oxygen concentration curve in the horizontal axis and plotting C_{O_2}/i, where $i = 1/2$ for the stoichiometric H_2-O_2 flame. Burke and Schumann consider the concentration in terms of partial pressures, which are proportional to the molal concentrations discussed.

3092

(8) The tube containing the fuel flow has a negligible thickness.

The assumptions made reduce the problem to one of diffusion of a single gas having a certain initial distribution and subject to certain boundary conditions. In cylindrical coordinates, Fick's law of diffusion gives the equation describing the concentration as a function of time and coordinates:

$$\frac{\partial p}{\partial t} = D\left(\frac{\partial^2 p}{\partial r^2} + \frac{1}{r}\frac{\partial p}{\partial r}\right) \tag{1}$$

From assumptions (1) and (2), t can be replaced by vertical distance, since

$$t = y/U_j \tag{2}$$

and there results

$$\frac{\partial C}{\partial y} = \frac{D}{U_0}\left(\frac{\partial^2 C}{\partial r^2} + \frac{1}{r}\frac{\partial C}{\partial r}\right)\frac{\partial p}{\partial y} = \frac{D}{U_j}\left(\frac{\partial^2 p}{\partial r^2} + \frac{1}{r}\frac{\partial p}{\partial r}\right) \tag{3}$$

which now contains the height and radius. The boundary conditions can be stated on the basis of the burner port at $y = 0$. At this point,

$$y = 0 \begin{array}{|c|c|} \hline p = p_f & 0 \leq r \leq r_j - \delta \\ \hline p = \frac{p_{O_2}}{i} & r_j + \delta \leq r \leq r_s \\ \hline \end{array} \tag{4}$$

The half-thickness of the port δ has been assumed negligibly small. Also,

$$\frac{\partial p}{\partial r} = 0 \begin{cases} r = 0 \\ r = r_s \end{cases} \tag{5}$$

The solution of equation (3) with the boundary conditions (4) and (5) is

$$p = P\frac{r_j^2}{r_s^2} - \frac{p_{O_2}}{i} + \frac{2r_j P}{r_s^2}\sum \frac{1}{k}\frac{J_1(kr_j)J_0(kr_s)}{[J_0(kr_s)]^2} e^{-\frac{Dk^2 y}{U_j}} \tag{6}$$

where

k constant that assumed all positive roots of the equation $J_1(kr_s) = 0$

P $p_f + \frac{p_{O_2}}{i}$

For further discussion of the solution of equation (3), see reference 8. General methods of solution of equations of this type are discussed in reference 9.

The equation for the flame front is obtained by setting $p = 0$ at $r = r_F$, so that equation (6) becomes at the flame front

$$\sum \frac{1}{k} \frac{J_1(kr_j)J_0(kr_F)}{[J_0(kr_s)]^2} e^{-\frac{Dk^2y}{U_j}} = \frac{r_s^2 p_{O_2}}{2r_s iP} - \frac{r_j}{2} \tag{7}$$

The shape of the flame front can be obtained by plotting the values of r_F and y that satisfy equation (7). The height of the flame y_F is given by the value of y when $r_F = 0$ for an overventilated flame and $r_F = r_s$ for an underventilated flame. The results of a typical calculation are illustrated in figure VII-9 for an overventilated and an underventilated flame for which it was assumed $r_j = 1/2$ inch, $r_s = 1$ inch, $D = 0.0763$ square inch per second, and $U_j = 0.610$ inch per second, which corresponds to a fuel flow of 1 cubic foot per hour. The calculated shapes agree well with the observed flame shapes. A similar treatment was used (ref. 3) to calculate the flame shape for a flat diffusion flame on a burner resembling that of figure VII-1(a).

The properties of diffusion flames are also calculated in reference 8, in which the analysis was begun with equation (1), and essentially the same assumptions except assumption (1) were used. The fuel and air velocities were not required to be equal, although it was required that the air velocity be constant over the annulus and the fuel velocity over the inner tube, and that no momentum transfer occur during diffusion (assumption (2)). Solution of the equation of reference 8 gives

$$\sum \frac{1}{k} \frac{J_1(kr_j)J_0(kr_F)}{[J_0(kr_s)]^2} e^{-\frac{Dk^2y}{U_j}} + \frac{iU_j}{p_{O_2}U_s} e^{-\frac{Dk^2y}{U_j}} = \frac{r_s^2 - r_j^2}{2r_j} - \frac{iU_j}{p_{O_2}U_s}\frac{r_j}{2} \tag{8}$$

Comparison of equations (7) and (8) shows the similarity. The principal difference is the addition of two terms containing the ratio U_j/U_s, which was assumed equal to 1 by Burke and Schumann.

The analysis was also begun with equation (1) in reference 4, in which the characteristics of the flame burning on a jet of fuel discharging into still air were computed. Essentially the same assumptions as those of reference 3 were used, except assumptions (1) and (2), which no longer apply. Unlike the assumption of reference 3, in which the oxygen is considered negative fuel, the analogous position that fuel is negative oxygen is taken in reference 4. The oxygen concentration curve would then follow the dashed line in figure VII-6 on the fuel side of the flame front where the fuel concentration has been replaced by $-ip_f$. The oxygen partial pressure varies in an air flame from 0.21 to $-ip_f$. The solution of reference 4 was obtained in terms of a generalized dimensionless concentration C_m defined as

$$C_{m,F} = \frac{1 + \left(\frac{C_a}{C_f}\right)_j}{1 + \left(\frac{C_a}{C_f}\right)_{st}} \tag{9}$$

and a dimensionless time parameter θ defined by the equation

$$\theta = \frac{4Dt}{8r_j^2} \tag{10}$$

3092

The solution of equation (7) is (ref. 4)

$$C_{m,F} = 1 - e^{-\frac{1}{4\theta_F}} \tag{11}$$

where

$$\theta_F = \frac{1}{4 \ln \left\{ \left[1 + \left(\frac{C_a}{C_f}\right)_{st}\right] \Big/ \left[\left(\frac{C_a}{C_f}\right)_{st} + \left(\frac{C_a}{C_f}\right)_j\right] \right\}} \tag{12}$$

Also, from equations (10) and (11),

$$\ln (1 - C_m) = \frac{r_j^2}{2Dt} \tag{13}$$

If the volume flow rate Q is introduced, where

$$Q = \pi U_j r_j^2 \tag{14}$$

there results

$$U_j t = \frac{Q}{4\pi D[- \ln(1 - C_{m,F})]} \tag{15}$$

In equation (15), the value of t is yet undetermined. A form based on dimensional analysis and experimental data was used in reference 4.

In reference 10, t was treated somewhat differently. Equation (15) was simplified to (see ref. 1)

$$U_j t = \frac{Q\left(\frac{1}{C_{m,F}} - \frac{1}{2}\right)}{4\pi D} \tag{16}$$

and t was replaced by $y_F/U_{0,f}$, which assumes that the port velocity remains unchanged to the flame tip. The flame length is then given by

$$y_{F,L} = \frac{Q\left(\frac{1}{C_{m,F}} - \frac{1}{2}\right)}{4\pi D} = \frac{Q\theta_F}{\pi D} \tag{17}$$

which is in agreement with the result of reference 3.

While the laminar diffusion flame theories discussed in the previous paragraphs have considered the general characteristics of the flame, they have not considered the detailed phenomena occurring in the flame region. These theories have considered the flame as a discontinuity, while in the actual case the flame has a thickness that depends on the relative rates of chemical reaction and mixing. The details of flame structure are considered in reference 11, in which an Arrhenius type of reaction-rate expression is used. At remote points from the reaction zone, the curves of concentration and temperature are not appreciably altered, but the sharp break assumed by the earlier theories at the instantaneous reaction zone becomes a rounded curve for a finite reaction time:

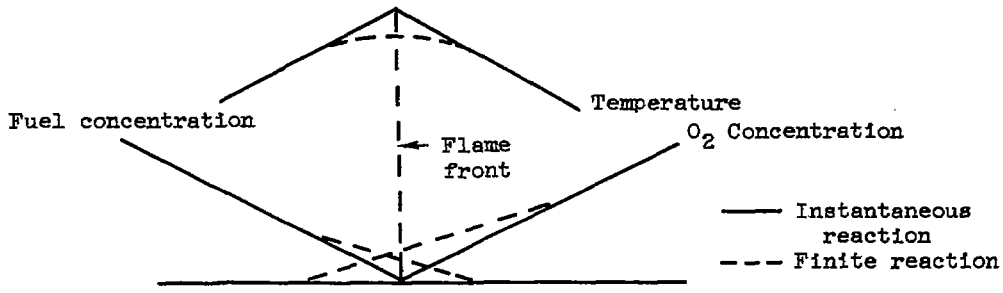

Under the usual condition of burning in a laminar diffusion flame, the simplified flame diagram used by Burke and Schumann and others is adequate. If the flow conditions are altered so that the flame zone becomes thin compared with its length, the diffusion processes may be sufficiently rapid that the chemical reaction rate becomes important, and the more complicated treatment of reference 11 is necessary. Such may well be the case near the extinction limits. Equation (8) may be used for calculating the dimensions and concentration gradients in a diffusion flame, while the simpler equation (17) is useful for estimating relative flame heights.

Turbulent flames. - The theoretical treatment of turbulent diffusion flames is less advanced than that of the laminar diffusion flame because of the much more complicated mixing process involved. There have been essentially two approaches to the problem: the first uses the laminar diffusion flame equations, but replaces the molecular diffusion coefficient by an eddy diffusivity, and the second uses equations based on the mixing of turbulent jets and derives a new set of equations. Since the first treatment follows directly from the previous discussions, it is discussed first.

The eddy diffusivity ε that will replace the molecular diffusion coefficient is given by

$$\varepsilon = l_1 u' \tag{18}$$

For fully developed turbulent flow inside the burner tube, l_1 is proportional to the tube diameter, and the intensity of turbulence is approximately proportional to the mean flow velocity at the axis, so that

$$\varepsilon \propto U_0 r_f \tag{19}$$

can now be inserted into equation (17), for example, to give

$$y_{F,T} = \frac{Q\theta_F}{\pi\varepsilon} \propto \frac{Q\theta_F}{\pi U_j r_j} \tag{20}$$

Substituting Q from equation (14), there results

$$\frac{y_{F,T}}{r_j} \propto \theta_F \tag{21}$$

which indicates that $y_{F,T}/r_j$ is nearly constant in the turbulent region. A similar result is shown in reference 12 for flat flames (fig. VII-1(a)).

In reference 7, the diffusion flame is described by use of the cold-jet mixing process. The details of this mixing process are discussed in chapter II. In this section, only the application of turbulent mixing to diffusion flames will be considered. Therefore, only the distance required to produce a stoichiometric mixture is of concern here, for, as in the laminar flame, this equiconcentration surface is considered to be the flame front. In the case of simple turbulent mixing, the axial distance at which a given concentration is reached (e.g., stoichiometric) is found to depend only on diameter and not on velocity. Thus, $y_{F,T}/r_j$ would be a constant, in agreement with the results obtained previously. A consideration of the actual mixing process in the presence of buoyancy due to density differences and in the presence of chemical reaction is quite complex. The problem is treated in reference 7, in which the following equation is obtained:

$$\frac{y_{F,T}}{r_j} = \frac{10.6}{\tau}\sqrt{\frac{T_F}{\alpha T_j}\left[\tau + (1 - \tau)\frac{M_s}{M_j}\right]} \tag{22}$$

where

$$\tau = \left[\frac{(C_f + C_a)_j}{(C_f + C_a)_j + C_{a,s}}\right]_{st}$$

and

$$\alpha = \left[\frac{(C_f + C_a)_j + C_{a,s})}{C_p}\right]_{st}$$

As with the previous treatments, the ratio $y_{F,T}/r_j$ depends only on the stoichiometry and thermodynamics of the system and is independent of velocity and diameter. Although obtained by a less rigorous treatment than the equations for laminar diffusion flames, equation (22) reflects the same type of controlling process and is one of the most readily used equations for predicting the relative flame heights of turbulent gaseous diffusion flames.

Effect of Variables on Flame Height

Laminar flames. - Within the region designated normal flames (zones 1 and 2 of fig. VII-2), the flame height varies with changes in fuel flow. For a given fuel flow, the shorter flame indicates a greater burning rate per unit volume of space than the higher flame, so that flame height is often used in diffusion flames as a

measure of burning rate. A study was made of the effect of various factors that can influence the flame height of diffusion flames containing some premixed primary air (ref. 13). The apparatus was essentially that of figure VII-1(c), except that the secondary air was supplied by natural rather than forced convection. The effects of port velocity, port diameter, and primary air - gas ratio on the flame height were investigated. While a discussion of the addition of primary air overlaps previous discussions (chs. IV and V), it should be recalled that even so-called premixed flames with primary gases richer in fuel than stoichiometric have an outer flame zone that is a diffusion flame. It was found in reference 13 that flame height increased with increasing port diameter and primary gas velocity, and the results for Cambridge city gas are represented by the equation

$$y_{F,L} = K_1 \log U_j + K_2 \log r_j + K_3 \tag{23}$$

where

K_1, K_2, K_3 constants that depend on primary air - gas ratio

The quantity of secondary gas supplied to the flame had little effect on the flame height, provided there was sufficient secondary air for combustion of 75 percent of the fuel (ref. 13).

The results of Gaunce quoted in reference 4 for Cambridge city gas flames with no primary air, burning on a 0.125-inch port, are shown in figure VII-10. It was found in reference 4 that the data of reference 13, the laminar portion of the data of Gaunce for Cambridge city gas, and the data of reference 4 for carbon monoxide could be empirically correlated, using only two empirical constants depending on fuel type and air-gas ratio. The equation is

$$y_{F,L} = K_1 \log Q\theta_f + K_2 \tag{24}$$

The values of K_1 and K_2 used are given in the following table, and the effectiveness of the correlation is shown in figure VII-11, where straight lines are obtained when $\log Q\theta_f$ is plotted against flame height:

Fuel	(C_a/C_f)	K_1	K_2
City gas	0	1.39	5.09
City gas	1.29	1.87	5.93
CO	0	1.39	4.91

For the calculation of θ_f, it was assumed that $(C_a/C_f)_{st} = 2.38$ for carbon monoxide and from 4.3 to 4.8 for city gas, depending on the composition. Equation (17), derived theoretically, shows that $y_{F,L}$ should increase as U_j and the product $Q\theta_F$ increase, but fails to show the logarithmic form that is found empirically to fit the experimental data.

Data similar to those of reference 4 for city gas were obtained in reference 10 for a mixture of 50 percent city gas and 50 percent air by volume and for butane. The laminar portions of the flame-height curves for 100 percent city gas fit the empirical equation

$$y_{F,L} = \frac{1}{\frac{0.206}{\sqrt{Q}} + \frac{0.354}{Q}} \tag{25}$$

where Q is in cubic centimeters per second and $y_{F,L}$ is in centimeters.

Diameter does not appear in this equation, since flame height was independent of port diameter at the low flows necessary for laminar flow. Actually, the experimental curves do show a slight effect of tube diameter. A larger diameter effect is found when a mixture of 50 percent city gas and 50 percent air is used. These data fit the empirical equation

$$\frac{y_{F,L}}{r_j} = \frac{2}{\frac{0.275}{\sqrt{U_j}} + \frac{2.47}{U_j}} \tag{26}$$

where U is in centimeters per second. It was found (ref. 10) that 100 percent butane and butane - primary air flames follow a very simple relation with flow rate for tubes:

$$y_{F,L} = \frac{K_1}{\sqrt{QX_f}} \tag{27}$$

where

X_f mole fraction of fuel in jet

The data are shown in figure VII-12 for a 0.4-inch-diameter port. The empirical coefficient decreases slightly for large changes in port diameter:

Port diameter, in.	K_1
0.180	10.4
.290	9.9
.40	9.7
1.03	9.1
1.99	8.3

Since the empirical equations of reference 10 bear little resemblance to equation (17), it is suggested therein that the assumptions of constant D and constant U_j may be in error. Since D changes more rapidly than U_j, the total change may be represented by a change in D alone, which results in

$$y_{F,L} = \left(\frac{Q\theta_F}{\pi D}\right)^{1/2} \tag{28}$$

Combining all the effects yields the following form of the theoretical equation:

$$y_{F,L} = \frac{1}{\sqrt{\frac{1}{2}\frac{\pi k}{Q\theta_F} + \frac{1}{2}\frac{\pi D}{Q\theta_F}}} \tag{29}$$

which has the same form as equation (25). In general, the measurements and correlations that have been presented were determined for flames that ranged initially from 4 to 6 inches upwards to about 25 inches.

Reference 8 presents some measurements of flames from 0.2 to about 1.5 inches in length. The effect of fuel flow on flame height is shown in figure VII-13. In the region of low fuel velocities, the flame heights are independent of the air velocity in agreement with the data of reference 13 but at higher fuel flows the points for the lower air flows of 0.9 and 1.74 inches per second rise above the

other data. The lines in the figure were calculated from equation (8), and it is seen that reasonably good agreement is obtained for the higher air velocities. The proper trend in flame height is predicted for the air flows of 0.9 and 1.74 inches per second, but the theory predicts a greater separation of the 3.45- and 5.13-inch-per-second data than was found experimentally. Equation (8) contains the parameters $y_{F,L}/U_j$ and U_j/U_s, which suggests that these quantities may be useful in correlating the experimental data. The first of these has the dimension of time, while the second is proportional to the fuel-air ratio. A plot of $y_{F,L}/U_j$ against fuel-air ratio is shown in figure VII-14 along with the line obtained theoretically from equation (8). Reasonably good correlation and agreement with theory are obtained.

3092

The change in flame height with flow velocity and tube diameter represents the principal studies on laminar diffusion flames. Only a little work has been done on the effect of pressure on flame height. It was found in reference 8 that pressure changes of 10 to 1 atmospheres had practically no effect on flame height. The theory (eq. (8)) predicts that flame height should be independent of pressure. Reference 3 also found flame height to be insensitive to temperature and pressure. Theoretically, this independence of flame height results from the fact that pressure and temperature affect the flow velocity and diffusion coefficient in opposite directions, thus canceling their effects.

The rather simple form of equation (24) and its success in correlating the data for different systems make it appear the most useful for calculating laminar flame heights where the empirical constants are known. The difficulty of applying the theoretical equations and the uncertainty of some of the assumptions limit their use in predicting absolute flame heights.

Turbulent flames. - It has been shown in figure VII-10 that, at certain critical flows, the tip of the flame becomes turbulent and that the turbulent portion increases with increasing flow rate. The break points of city gas, hydrogen, and propane flames were measured in reference 7. The total flame heights, which are relatively constant, were also measured and are shown along with the break points in figure VII-15. It is evident that both the total flame heights and break-point heights are relatively insensitive to flow rate in the fully developed turbulent flame, which agrees with equation (22). The break points for two gases of differing diffusion coefficients are shown in figure VII-16, where the ratio of break-point height to port diameter is plotted against the product of diffusion coefficient and flow velocity. Again, there is a drop in break-point height with flow velocity until a critical velocity occurs, after which there is little change. Break points for unignited and ignited ethene systems were studied in reference 14, in which it was found that the break point was higher for the ignited stream. The flow velocity range can be increased somewhat by the use of a pilot, and reference 1 shows that the flame height increases somewhat with flow velocity under these conditions; an increase of flow velocity from 200 to 1200 feet per second causes about a 5-inch increase in flame height in the presence of a pilot.

Flame heights of 100 percent city gas flames (fig. VII-17(a)) and 50 percent city gas - 50 percent air flames (fig. VII-17(b)) in the turbulent regime were measured in reference 10. The data are represented approximately by

$$\frac{y_{F,T}}{r_j} = \frac{2}{0.00775 + 3.80/U_0} \tag{30}$$

for 100 percent city gas where U is centimeters per second; and

$$\frac{y_{F,T}}{r_j} = \frac{2}{0.0132 + 3.23/U_0} \tag{31}$$

for 50 percent city gas - 50 percent air, again in metric units. Reference 15 shows that diffusion flames containing jets of powdered coal in air have flame heights similar in magnitude to those of gaseous fuels.

A comparison of several equations for the length of turbulent diffusion flames is made in figure VII-18, where flame height is plotted against the stoichiometric concentration for five fuels. Each point represents a single fuel while the lines are calculated from the equations shown in the figure. Wohl's equation is shown as a broken line; a curve derived in reference 15 in which $y \propto \log \tau$ is shown as a dot-dash line; while the equation of reference 1, represented as a family of lines for various molecular-weight ratios, is illustrated by the thin lines. Black dots on these lines indicate the range of $C_{m,F}$ of interest. It is apparent that, for fuels of widely differing molecular weight, the molecular-weight ratio is necessary, although Wohl's equation can be made to agree with equation (22) to within about 30 percent if hydrogen is omitted. The proposed function of reference 15 cannot fit different fuel types unless a different empirical constant is used for each fuel.

3092

Stability

The diffusion flame, like the premixed flame, has certain regions of stability beyond which burning cannot occur. These have already been indicated in figure VII-2 by the boundary separating the various flame zones from the extinction region. While the phenomenon of flash-back is, of course, not possible for diffusion flames, the extinction curve does not extend to either zero fuel flow or zero air flow. As the fuel flow is decreased, the flame becomes smaller and smaller until the quenching action of the nozzle wall is sufficient to prevent propagation. Thus, a lower boundary is set to the fuel flow. As the fuel flow is increased, the flame length increases. At critical fuel flows, however, the processes of flame lift and blow-off occur entirely analogously to the Bunsen flame. In fact, the blow-off of rich Bunsen flames (see ch. VI) may well depend on the characteristics of the outer-mantle diffusion flame. Some typical data on the lifting and ultimate blow-off of a butane diffusion flame (ref. 10) are illustrated by figure VII-19. The solid line shows the location of the flame base as the flow velocity is increased and lift occurs. The dotted line, on which typical flames are shown, illustrates the path of the flame bases as the butane flow velocity is reduced and the flame resettles. This type of hysteresis in the lift curves also occurs with premixed gases (see ch. VI). The ultimate point, at a flow velocity of about 300 milliliters per second, corresponds to complete blow-off. The data of reference 2 are for rather short laminar flames, but the phenomenon of lift is illustrated for turbulent flames by the dotted curve of figure VII-10, which shows the location of the bottom of lifted flames and their corresponding total flame height.

The stability range of diffusion flames of ethene issuing from carburetor-type jets into still air is reported in reference 14. The results showing the stability region as a function of jet diameter and Reynolds number may be seen in figure VII-20. The range of gas flow over which the flame is stable increases only slightly with increasing jet diameter. Above a certain diameter, the range over which the lifted flame persists widens rapidly, as the jet size increases, because of the rapid decrease in blow-off tendency on larger jets. On small jets, the lift and blow-off limits coincide. The phenomenon of lift is explained in reference 14 by a comparison of the break points of ignited and unignited streams and the height of the base of the lifted flame. In figure VII-21, the height to turbulence or the

break point or the height to the base of a lifted flame is plotted against Reynolds number - essentially flow velocity. Curves A and B connect the data for the height to turbulence in the unignited and ignited streams, respectively. Note that the height to turbulence occurs at higher Reynolds numbers for the ignited gas stream. The stabilization was attributed in reference 14 to heat addition from the flame. Curve C represents the height between the top of the burner and the base of the lifted flame. Curve D represents the height to turbulence in the fuel jet of a lifted flame. At a flow rate immediately before lift, the break point in the gas stream lies well within the flame envelope. At the actual lift point, the flame is stabilized by eddies formed at the break point and the base of the flame is at the same height as the height to turbulence (point X in fig. VII-21). After the flame has lifted, the heating effect of the flame on the gas stream is removed so that the break point returns to that of an unignited jet, shown by the dotted line connecting curve D and point X. As the flow rate is reduced, the break point follows the curve D, while the flame base follows curve C. When they meet at point Y, the flame suddenly resettles on the port, and the break point rises to point Z on curve B. This description accounts for the hysteresis in the lift curves noted previously.

Within the region in which the flame seat is located at the port, the length of the flame has been shown to increase regularly with flow velocity (fig. VII-10). However, reference 2 reports that, under some conditions, flame vibrations may appear. To the eye, there appears a double flame that may correspond to the maximum and minimum positions of the vibrating flame as sketched in figure VII-22(a). Stroboscopic pictures of the flame (fig. VII-22(b)) showed that the vibration consisted of a progressive necking of the flame; this can lead to the formation of an island of flame which, separated from the seated flame, burns itself out. The butane flame vibrations have a frequency of about 8 cps that is relatively independent of the flow. Modifications of the fuel supply system change the vibration frequency so that frequencies from 3 to 20 cps have been measured. Hydrogen gives a frequency of about 200 cps; in a few cases, the butane frequency can be equally high. Similar frequencies were found (ref. 16) for the rate of flicker of diffusion flames; hence, it appears that the phenomena are related. In reference 2, the vibrations are related to the phase lag Δt between the occurrence of maximum fuel flow in the oscillating flow and the appearance of maximum flame height. If the phase lag is small compared with the half-period of the vibration ($\Delta t << t_{1/2}$), the flame flickers; if $\Delta t = t_{1/2}$, the flame height rises to a maximum and suddenly drops to its initial value; if $\Delta t > t_{1/2}$, flame necking and ultimate breaking off of islands of flame can occur.

LIQUID DIFFUSION FLAMES

Single Drop Combustion

When a single drop of liquid fuel burns, it is surrounded by a diffusion flame as illustrated in figure VII-23. Fuel is evaporated from the liquid interface and diffuses to the flame front, while oxygen moves from the outside air to the burning surface. The rate at which the drop evaporates and burns is determined by the rate of heat transfer from the flame front to the liquid surface. As in the case of gaseous diffusion flames, chemical processes are assumed to occur so rapidly that burning rates are determined solely by mass- and heat-transfer rates.

Theory. - Flame structure: Spalding (refs. 17 and 18) and Graves (ref. 19) consider a double-film model for combustion of a liquid fuel. One film separates the drop surface from the flame front; a second separates the flame front from the surrounding atmosphere. The distributions of temperature and of fuel, oxygen, and product concentrations as a function of distance through the combustion zone are as follows:

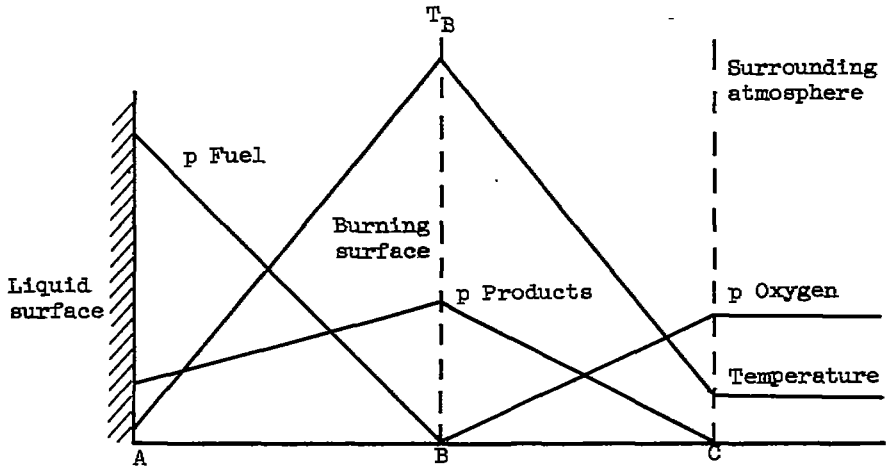

In steady-state combustion, the liquid surface is assumed to be at a temperature a few degrees below the normal boiling point of the fuel, as surveys of the temperature fields in burning liquids indicate (ref. 20). In the AB region, fuel evaporates at the drop surface and diffuses to the flame front, where it is consumed. Heat conducted from the flame front serves to vaporize the fuel and heat it to the burning temperature T_B. (It is assumed that there is no chemical reaction of the fuel before it reaches the flame front.) In the BC region, oxygen diffuses to the flame front, and combustion products and heat are transported to the surrounding atmosphere. The position of the C surface is determined by convection (natural or forced).

Burning temperature: By equating fuel flow to oxygen diffusion and heat conduction in the BC region, the burning temperature may be determined. For oxygen diffusion, with the fuel and oxygen flowing in opposite directions,

$$G_f = \frac{W_f}{4\pi x^2} = -\frac{W_{O_2}}{4\pi x^2 \, w} = \frac{DP}{w \, RT} \frac{M_{O_2}}{P + \left(\frac{X_P}{X_{O_2}} - 1\right) p_{O_2}} \frac{dp_{O_2}}{dx} \tag{32}$$

where

w weight of oxygen consumed in combustion of unit weight of fuel (stoichiometric relation)

X_P/X_{O_2} number of moles of products formed per mole of oxygen consumed

The term $(X_P/X_{O_2} - 1)$ takes some account of the fact that there will be a net gas motion if $X_P/X_{O_2} \neq 1$. The expression is applicable to the steady-state diffusion of both components of a binary mixture (ref. 21) and neglects the presence of a stagnant inert gas. For heat flow in BC,

$$\frac{W_f}{4\pi x^2}\left[h_c - (h_P - h_{P,C}) + \left(h_{O_2} - h_{O_2,C}\right)\right] = -\kappa_{BC}\frac{dT}{dx} \tag{33}$$

where

h_c specific lower heat of combustion of liquid fuel at temperature of surrounding atmosphere

h_{O_2} specific enthalpy of oxygen referred to unit quantity of fuel

h_P specific enthalpy of products referred to unit quantity of fuel

The term in the brackets is the heat that must be transported to the point x in the combustion of unit quantity of fuel. Eliminating the fuel flow from equations (32) and (33) and integrating will give

$$\frac{\varkappa_{BC}w}{D\rho_{O_2}}\int_{T_C}^{T_B}\frac{dT}{h_c-\left(h_P-h_{P,C}\right)+\left(h_{O_2}-h_{O_2,C}\right)}\approx\frac{1}{\left(\frac{X_P}{X_{O_2}}\right)-1}\ln\left[1+\frac{p_{O_2,C}}{P}\left(\frac{X_P}{X_{O_2}}-1\right)\right]\simeq p_{O_2,C}/P \tag{34}$$

if $p_{O_2,C}$ is small and $X_P/X_{O_2} \sim 1$. The factor $\varkappa_{BC}w/D\rho_{O_2}$ is considered independent of temperature.

Integrating the left side of equation (34) by introducing mean specific heat c_p for products and oxygen results in

$$\frac{\varkappa_{BC}w}{D\rho_{O_2}\left(c_{p,P}-c_{p,O_2}\right)}\ln\left[1-\frac{\left(c_{p,P}-c_{p,O_2}\right)(T_B-T_C)}{h_c}\right]\approx\frac{\varkappa_{BC}w}{D\rho_{O_2}}\frac{T_B-T_C}{h_c}\approx\frac{p_{O_2,C}}{P}$$

or

$$T_B-T_C\approx\frac{D\rho_{O_2}}{\varkappa_{BC}}\frac{h_c}{w}\frac{p_{O_2,C}}{P} \tag{34a}$$

Unfortunately, the error introduced by expansion of the logarithm is in the opposite direction from the expansion of equation (34), and predicted burning temperatures are too high. Nonetheless, equation (34a) is useful for showing qualitatively the factors that influence the burning temperatures.

Equation (34) permits a more reliable calculation of the burning temperature. It has been used (ref. 18) to obtain burning temperatures for kerosene drops in atmospheres of varying temperature and oxygen concentration, with carbon dioxide and water assumed to be the sole combustion products. Preferential diffusion of water with respect to carbon dioxide was also neglected. The calculations of reference 19 for isooctane burning in atmospheres of various oxygen concentrations neglected preferential product diffusion and employed the simplified form of equation (34) valid for low oxygen partial pressure or $X_P/X_{O_2} \sim 1$; however, equilibrium dissociation of products was taken into consideration. In figure VII-24, burning temperatures of references 18 and 19 are compared for similar conditions. Burning temperatures for isooctane calculated from equation (34a) are also shown. It is to be noted that these temperatures are higher than the adiabatic flame temperatures for corresponding isooctane vapor-oxygen-nitrogen mixtures (ref. 22). Drop burning temperatures may be greater because there is no net flow of inert gas (nitrogen) through

the burning zone and because the oxygen is preheated to the combustion temperature by the hot reaction products. The fact that the reaction zone must have a finite thickness will give rise to lower burning temperatures than those calculated from equation (34).

Burning rate: For the AB region, heat and fuel flow may be equated analogously to equation (33) (directions of fuel and heat flow are opposite):

$$\frac{W_f}{4\pi x^2} = \frac{\varkappa_{AB}}{h_v + h_l + h_f - h_{f,A}} \frac{dT}{dx} \tag{35}$$

where

h_f specific enthalpy of fuel vapor

h_l heat necessary to raise unit mass of fuel to vaporization temperature

Integrating over the AB region gives

$$\frac{W_f}{4\pi}\left(\frac{1}{x_A} - \frac{1}{x_B}\right) = \int_{T_A}^{T_B} \frac{\varkappa_{AB}\, dT}{h_v + h_l + h_f - h_{f,A}} = A \tag{36}$$

The term h_l is included because of the assumption that the bulk of the drop remains at the initial temperature during combustion. If the entire drop rapidly reaches the surface temperature during the first stages of combustion, h_l should be omitted. The factors determining the drop interior temperature are discussed in reference 23.

If equation (33) is rearranged and integrated over the BC region,

$$\frac{W_f}{4\pi}\left(\frac{1}{x_B} - \frac{1}{x_C}\right) = \int_{T_C}^{T_B} \frac{\varkappa_{BC}\, dT}{h_c - \left(h_P - h_{P,C}\right) + \left(h_{O_2} - h_{O_2,C}\right)} = B \tag{37}$$

From equations (36) and (37), the mass burning rate is found to be

$$W_f = \frac{4\pi A}{\left(\frac{1}{x_A} - \frac{1}{x_B}\right)} = \frac{4\pi\,(A+B)}{\left(\frac{1}{x_A} - \frac{1}{x_C}\right)} \tag{38}$$

In the burning-rate equation, the variation of thermal conductivities with temperature is considered.

Godsave's burning-rate equation (refs. 24 and 25) may be obtained from the first part of equation (38) by using a mean value for the thermal conductivity in the AB region and letting $h_f - h_{f,A} = c_{p,f}(T - T_A)$.

$$W_f = \frac{4\pi A}{\left(\frac{1}{x_A} - \frac{1}{x_B}\right)} = \frac{4\pi\overline{\varkappa_{AB}}}{c_{p,f}} \ln\left[1 + \frac{c_{p,f}(T_B - T_A)}{(h_l + h_v)}\right] \Bigg/ \left(\frac{1}{x_A} - \frac{1}{x_B}\right) \tag{38a}$$

For a liquid sphere, the relation

$$\frac{dm}{dt} = - W_f = 4\pi\rho_l x_A^2 \frac{dx_A}{dt} \tag{39}$$

gives the mass burning rate in terms of the change of radius with time.

Experimentally (refs. 19 and 25 to 28), mass burning rates of single fuel drops are found to be proportional to the drop radius. Variation of drop diameter with time is given by

$$d^2 = d_0^2 - \beta t \tag{40}$$

where d_0 is the initial drop diameter, $d = 2x_A$ is the diameter at any subsequent time, and the constant β is the evaporation constant. The rate of change of radius with time may be obtained from equation (40):

$$\frac{dx_A}{dt} = - \frac{\beta}{8x_A} \tag{41}$$

From equations (38), (39), and (41) it follows that

$$\beta = \frac{2W_f}{\pi\rho_l x_A} = \frac{8}{\rho_l} \frac{(A+B)}{1 - \frac{x_A}{x_C}} \tag{42}$$

Note that β will be constant if x_A/x_C is constant or if $x_C = \infty$ (drop burning in the absence of convection). Equation (42) has been successfully used to predict evaporation constants for the combustion of single fuel drops.

Combustion in quiescent air. - Evaporation constants of single drops (initial diameter 1000 to 1500 microns) of various liquid fuels burning in quiescent air have been obtained by Godsave (refs. 25 and 26) using a motion picture technique. By the same method, Graves (ref. 19) has studied the combustion of isooctane drops in various oxygen-nitrogen atmospheres. Plots of square of drop diameter against time were found to be linear (see eq. (40)). Figure VII-25 shows a typical plot for isooctane burning in an atmosphere containing 34.9 percent oxygen. In table VII-I, experimental and calculated (ref. 29) values of evaporation constants for combustion in air determined by Godsave are presented. Although values for jet fuels were not determined, evaporation constants of about 10×10^{-6} square foot per second (similar to kerosene) are to be expected. Evaporation constants from reference 19 for isooctane are contained in table VII-II.

The combustion of suspended single droplets of decane, tetralin, furfuryl alcohol, and amyl acetate was studied in reference 28, and drop lifetimes were measured at pressures between 1 and 20 atmospheres. Lifetimes were found to be very nearly proportional to the square of the initial drop diameter for a given pressure and fuel, in agreement with equation (40). Evaporation constants were not determined as such, but droplet lifetimes were consistent with evaporation constants of the order of 10×10^{-6} square foot per second (similar to those of tables VII-I and -II). With increasing pressure, volumetric burning rates increased approximately with the fourth root of the pressure. (The effect on mass burning rates may be somewhat less, since the density of the fuel drop may be lower at higher pressures because of higher drop-surface temperatures.) It was observed that at the higher pressures the distance between flame front and drop surface decreased, which might

be expected with a higher burning rate (see eq. (38a)). This is probably a result of a decrease in film thickness under natural convection at high pressure, as suggested by reference 30. In contrast, vaporization rates in the absence of combustion decrease when pressure is raised (ref. 31).

In addition, reference 28 reports investigations of the burning of free droplets (150 to 700 microns initial diam.) in air at 1310° F and atmospheric pressure. In these experiments, drops of uniform size produced by feeding liquid fuel onto the center of a rotating disk were projected into a furnace, and droplet lifetimes were recorded by means of a drum camera. In this regime also, lifetimes were found to be proportional to the square of the initial drop diameter; it is not surprising that burning rates were somewhat faster at the higher temperature.

3092

Equation (38a) has been used (ref. 29) to calculate evaporation constants for benzene, tert-butylbenzene, and n-heptane combustion. The diameter of the burning surface was evaluated from photographs, and allowance was made for estimated heat transfer by radiation. The assumed burning temperature of 3100° F seems too low; calculations (refs. 18 and 19, see fig. VII-24) would suggest 4300° F as a more reasonable estimate. Results of Godsave's calculations (ref. 29) are shown in table VII-I, and while the agreement may in part be due to fortuitous choice of T_B, $c_{p,f}$, and $\overline{x}_{AB}$, the values are of the correct order of magnitude and suggest that Godsave's equation (eq. (38a)) is useful for estimating hydrocarbon burning rates. Accordingly, equation (38a) has been used to calculate variations in evaporation constants for the series of compounds investigated by Godsave. Burning temperatures were estimated by employing equation (34a) to convert variations in h_c/w into equivalent variations in oxygen concentrations; burning temperatures could then be estimated from the isooctane curve of reference 19. Mean heat capacities and thermal conductivities were taken at 2200° F; the latter was taken as the mean of the thermal conductivities of air and the fuel. The position of the burning surface with respect to the drop was taken from Godsave's determinations (ref. 29). (For isooctane and ethyl alcohol, the value of n-heptane was employed, since no measurements were made.)

Evaporation constants so calculated were found to be, on the average, 26 percent higher than experimental values; therefore, they have been reduced by this amount and tabulated in table VII-I. It is suggested in reference 26 that, unless otherwise indicated, the experimental evaporation constants are precise to 10 percent; reduced calculated values agree with the reliable values to within this margin. Accuracy of this type of experiment may be poor. Since the isooctane-air value of reference 19 is some 20 percent higher than that of reference 26, the 26 percent correction factor does not prove that the calculations are in error by this amount.

Evaporation constants for isooctane combustion in the absence of convection ($x_C = \infty$) were calculated in reference 19. The transport properties of air were assumed in the BC region, and preferential diffusion among combustion products was neglected. Figure VII-26 shows three curves calculated assuming:

(a) Thermal conductivity of isooctane in region between drop and burning surfaces; dissociation of products

(b) Thermal conductivity of isooctane; no dissociation

(c) Thermal conductivity of air; no dissociation

The experimental determinations of reference 19 are also plotted.

However, it must be noted that these calculations are for no convection. Equations (36) and (37) may be employed to calculate the position of the burning surface with respect to the drop. The result is

$$\frac{x_B}{x_A} = \frac{A + B}{A\left(\frac{x_A}{x_C}\right) + B} \tag{43}$$

For an isooctane drop burning in air in the absence of convection, values of the integrals A and B (ref. 19) predict $x_B/x_A = 18.5$. On the other hand, for n-heptane, the measurement (ref. 29) shows that $x_B/x_A \sim 3$. (Because of convection, the burning surface is highly distorted from a spherical shape; the value of ref. 29 must be regarded as a minimum, see fig. VII-23.) With the same value assumed for isooctane, $x_A/x_C \sim 0.3$ (from eq. (43)). Observed evaporation constants should be diminished by 30 percent to yield values applicable in the absence of convection (eq. (43)). Measured values so reduced have also been plotted in figure VII-26 to indicate the range for experimental constants in the absence of convection. 3092

It would appear, therefore, that the essential features governing the rate of combustion for single drops in quiescent air are well understood. Uncertainties in the proper selection of transport properties for the calculation, as well as experimental uncertainties, cause difficulties in drawing conclusions from figure VII-26 on the relative merits of the various assumptions of reference 19. However, the calculation that considers product dissociation seems preferable, since it presents a more realistic picture of the state of combustion products, particularly at higher temperatures. In general, burning rates of hydrocarbons are very similar. Rates are increased by factors tending to increase the burning temperature and the thermal conductivity in the region between the flame and drop surfaces. Decreases in latent heat of vaporization and film thickness also cause increases in evaporation constant.

Combustion in air streams. - The principal work on combustion from liquid surfaces in moving air streams has been conducted by Spalding (refs. 32 and 33), with spill-type burners in which the fuel (for most experiments, kerosene) was circulated over the surface of the burner and collected. Both vertical flat-plate and spherical burners were employed (the latter simulates a drop of liquid fuel). Variation of the fuel-flow rate permitted variation in the amount of heat absorbed by the fuel. The burners were of such a size that the effect of natural convection must be considered. Experiments on burning from spheres under forced convection (ref. 33) were also carried out.

Spalding (refs. 33 and 34) presents without complete derivation the following equation in terms of dimensionless groups for combustion from a vertical flat plate under laminar natural convection:

$$\frac{G_f L c_p}{\varkappa} = f_1(B',Pr)\left(\frac{gL^3 c_p{}^2 \rho^2}{\varkappa^2}\right)^{1/4} = f_1(B',Pr)\left[Pr^2\left(\frac{gL^3\rho^2}{\mu^2}\right)\right]^{1/4} \tag{44}$$

where

B' $\left[\left(m_{O_2} h_c/w\right) + c_p\left(T_C - T_A\right)\right] \Big/ \left(h_l + h_v\right)$

m_{O_2} weight of oxygen per unit weight of gas mixture in atmosphere

Values of specific heat, density, thermal conductivity, and viscosity to be employed are not specified; however, for his calculations, Spalding used the room-temperature properties of air. It might be noted that the group $gL^3\rho^2/\mu^2$ is a part of the Grashof number. The function $f_1(B',Pr)$ is approximated by $0.769 \ln(1 + B')$ when $Pr = 0.71$ (air).

For forced convection from a flat plate in a longitudinal laminar gas stream, the following formula is given:

$$\frac{G_f L}{\mu} = f_2(B',Pr)\, Re^{1/2} \tag{45}$$

For $Pr = 0.71$, the function $f_1(B',Pr)$ is approximated by $0.646 \ln(1 + B')$.

It is stated that, in general, mass-transfer rates (burning rates) can be predicted approximately from existing heat-transfer data by the relation

$$G_f = \left(\frac{H}{c_p}\right) \ln(1 + B') \tag{46}$$

where H is the heat-transfer coefficient determined in an experiment without combustion or mass transport.

Equation (46) is similar to equation (38a), which, when based on a burning rate per unit area, yields

$$G_f = \frac{W_f}{4\pi x_A^2} = \frac{1}{c_{p,f}} \frac{x_B \overline{\varkappa_{AB}}}{x_A(x_B - x_A)} \ln\left[1 + \frac{c_{p,f}(T_B - T_A)}{h_v + h_l}\right] \tag{47}$$

The term $(x_B/x_A)\,[\varkappa_{AB}/(x_B - x_A)]$ might be replaced by a heat-transfer coefficient.

By introducing the burning temperature from equation (34a),

$$\frac{c_{p,f}(T_B - T_A)}{h_v + h_l} = \frac{\left[\frac{c_{p,f}\rho_{O_2} D}{\varkappa_{BC}} \frac{h_c}{w} \frac{p_{O_2,C}}{P} + c_{p,f}(T_C - T_A)\right]}{h_v + h_l} \cong \frac{\left[\frac{h_c}{w} \frac{p_{O_2,C}}{P_t} + c_{p,f}(T_C - T_A)\right]}{h_v + h_l} \cong B' \tag{48}$$

since $c_p\rho D/\varkappa \sim 1$, and for air $p_{O_2,C}/P \sim m_{O_2}$. Thus, the relation between equations (46) and (47) may be seen.

Natural convection: Spalding's experiments on combustion in natural convection employed a flat-plate burner 2.5 inches high and 2.08 inches wide and a 1.5-inch-diameter spherical burner. Upon variation of the fuel-flow rate over the burner, the heat absorbed by the liquid could be as high as 4000 Btu per pound of fuel burned. This permitted a much wider variation of $h_v + h_l$ than could be obtained by burning single drops of fuels of different heats of vaporization and boiling points.

Data for both the plate and spherical burners were well correlated by equation (44). For combustion from a sphere, the diameter was used as the characteristic dimension in place of the plate height. This procedure is justified with the statement that heat-transfer data by natural convection from plates, spheres, or

cylinders are well correlated by a single relation, so that the same might be expected to hold true for combustion results. Most of the experiments were on kerosene combustion, but data on gas oil, gasoline, and heavy naphtha were predicted equally well by equation (44). Equations (44) and (46) are considered equally good for estimating burning rates by natural convection.

Forced convection: For most of his experiments on forced convection, Spalding employed a 1-inch-diameter spherical burner, with kerosene, gasoline, ethyl alcohol, and benzene as fuels. Experimental burning rates were 10 to 15 percent higher than theory for a flat-plate burner according to equation (45), but were an equal amount lower than the predictions of equation (46). Data were not as reproducible as results on natural convection. A calculation based on equation (46) gives an estimate of 5 milliseconds as the lifetime of a 100-micron jet-fuel droplet burning in a 400° F air stream when the velocity of the drop relative to the air stream is 50 feet per second. In the absence of convection, the lifetime would be 12 milliseconds.

A more exact treatment of combustion from a flat plate in forced convection is reported in reference 35, in which a Prandtl number of 1 is assumed. The results of this calculation appear to agree with experiment somewhat better than equation (45) or (46).

During experiments on combustion from spheres in air streams, it was observed that at a critical air velocity the leading half of the envelope flame surrounding the sphere was extinguished. Spalding attributes this extinction phenomenon to chemical limitations on the combustion rate. As the air velocity is increased, the boundary layer becomes thinner, and mass transport to the flame front is increased. Since chemical reaction rates at the burning surface are finite, the reaction zone thickens and its temperature falls. Eventually, a point is reached at which the chemical reaction rate can no longer keep pace with the rate at which fuel and oxygen are supplied to the burning zone, and the flame is extinguished. Spalding conducted extinction experiments under forced convection on spheres of varying diameter (0.275 to 1.025 in.). It was predicted that at extinction the air velocity (expressed in diam/sec) and the distance of the flame from the sphere surface on the upstream side should be constant for spheres of varying diameter. This was found to be the case, within 10 percent, for the 3.7-fold variation in sphere diameter studied.

Another method of studying combustion by convection is that employed in reference 36, in which fuel droplets (about 300 to 600 microns initial diameter) fall through a heated furnace at their terminal velocities. Quantitative data on evaporation in high-temperature atmospheres were obtained by this technique, but only a few qualitative observations on residues from burning residual fuel oil droplets are presented.

In general, Spalding's equations appear to predict well experimental burning rates under natural and forced convection. However, drop sizes encountered in fuel sprays are 3 or more orders of magnitude smaller than the spherical burners used by Spalding, and no other quantitative data on burning under convection are available. Therefore, it is difficult to assess the value of his equations for application to the combustion of small droplets.

Fuel Sprays and Mists

The mode of combustion of the droplets in a burning fuel spray might be considered in terms of two extremes. In the first instance, the droplet may burn as a diffusion flame in the local atmosphere surrounding it. In this event, its combustion will be governed by the factors considered in the preceding section. On the

other hand, the droplet might evaporate and mix by diffusion with the air in the preheat zone of an established flame front. The burning of the spray would in this case be determined by the same considerations that apply to the combustion of gaseous fuel-air mixtures.

Theory of combustion. - The evaporation or burning of liquid fuel sprays has been examined theoretically in reference 37. It was assumed that the evaporation or burning rates of individual drops are proportional to the drop diameters (as observed experimentally), that the evaporation constant is the same for all drops, and that all drops have the same available time for burning. The fuel spray drop-size distribution was represented by the Rosin-Rammler relation

3092

$$R' = e^{-\left(\frac{d}{\bar{x}}\right)^n} \tag{49}$$

where R' is the volume or weight fraction of the spray composed of drops greater in diameter than d. The constants $\bar{x}$ and n are known as the size and distribution constants, respectively. The more uniform the drop size, the higher the value of n; if all drops were of the same size, n would be infinite. In practice, it has been found that atomizing nozzles give sprays having values of n between 2 and 4. Mean diameters that determine the evaporation rate of the injected spray and of the spray in steady-state burning (where injection and evaporation rates are equal) have been evaluated. The specific volume in steady burning, which is the volume of unevaporated fuel divided by the volume of fuel introduced per second, has also been calculated.

Incomplete evaporation of the spray for limited evaporative time was considered. The results are shown in figure VII-27, where the fraction of the spray unevaporated is plotted against time in units of $\beta/\bar{x}^2$ for sprays in which the distribution constant is 2, 3, or 4. The dotted line illustrates the behavior of a single fuel droplet, or a spray in which all drops are the same size ($n = \infty$). Note that in the early stages sprays of low distribution constant n evaporate most rapidly (since more small droplets are present). Later, however, sprays of uniform size distribution (large n) are favored, since they have fewer large drops (which evaporate more slowly). In general, it was concluded (ref. 37) that the size constant $\bar{x}$ is the most important factor in determining the evaporation or burning rate of sprays. The distribution constant has a much smaller effect, although a large value of n favors more complete evaporation, despite the fact that the initial evaporation rate of the injected spray will be lower. In appendix C of reference 19, the relations of reference 37 were applied to the case of a fuel spray burning in a duct where heat release changes the average velocity along the duct. In this manner, the author calculated what the effect of evaporation rate on combustion efficiency should be.

The foregoing considerations are applicable if the burning of a fuel spray may be represented as an integration of the burning of single drops.

Experimental observation. - The observations of reference 38 on a kerosene spray burning in still air give some information as to the manner in which the fuel droplets are consumed. It was observed that a flame front was established about 1 inch from the spray nozzle. As indicated in calculations, at this point small drops (size of the order of 10 microns) were at rest with respect to the air stream, which was moving with a velocity of about 0.7 to 1.0 foot per second (compatible with normal burning velocities). It was concluded that, in the period of about 0.1 second which the small drops spent in transit from the nozzle to the flame front (for larger drops, this time was even shorter), very little evaporation was possible. With the preheat zone of the kerosene flame assumed to be approximately 0.1 inch thick, calculations

on heat transfer to small drops indicated that this thickness was sufficient to allow evaporation and mixing with air in the preheat zone. Larger drops (size of the order of 100 microns) could pass through the flame front without being completely vaporized.

Some confirmation for this analysis was provided by observations on kerosene droplets in the approach streams of premixed Bunsen flames. For a butane-air flame, droplets (sizes 9 to 30 microns) disappeared before reaching the luminous inner cone of the flame. However, when an acetylene-air flame was used, conditions for vaporization were not as favorable, because of a narrower preheat zone and higher gas stream velocity. Some droplets escaped evaporation in the preheat zone; large droplets (of the order of 80 microns) completed evaporation definitely above the inner cone.

Limits of flammability: There are some experimental data on limits of flammability and rate of flame propagation in fuel sprays and mists. With fuel sprays, it is difficult to achieve mixtures which are macroscopically homogeneous; that is, mixtures in which fuel-air ratio and drop-size distribution do not vary throughout the mixture.

Early experiments on the flammability limits of condensed mists are reported in reference 39. Drop diameters were of the order of 10 microns. Lean limits for the three fuel mists studied are compared with limits for the corresponding vapors in table VII-III, which shows that the limits are the same (the effect of temperature on the lower limit is small). Under comparable conditions, lower limits for hydrocarbon vapors fall in the fuel-air ratio range 0.030 to 0.040 (ref. 40); therefore, the values in table VII-III are reasonable.

The results of similar experiments (ref. 41) are presented in table VII-IV. While drop sizes were not measured, they must have been small to permit the formation of stable mists. Lean limits are again in the region anticipated for hydrocarbon vapors. On the other hand, rich limits occurred at somewhat lower fuel-air ratios than are usually observed for heavy hydrocarbon vapors. This fact is perhaps not too surprising, since the rich limit is more susceptible to slight effects, such as direction of flame propagation (e.g., for hexane with upward propagation, the rich limit is 0.242; with downward propagation, the limit is 0.112 (ref. 40)). The percentage of nitrogen or carbon dioxide that must be added to air to render mists of cutting oil number 3 nonflammable were: nitrogen, 30 percent; carbon dioxide, 22 percent. These values are somewhat smaller than the equivalent figures for hydrocarbon vapors (for n-heptane, the amounts required are: nitrogen, 42 percent; carbon dioxide, 29 percent), and suggest that the combustion of mists is more easily suppressed.

On the other hand, the spray flammability test of reference 42 does not indicate this difference. In this test, fuel was introduced as a spray into a cylinder $2\frac{3}{8}$ inches in diameter and 15 inches long, through which an oxygen-nitrogen mixture was flowing. The spray flammability limit was defined by the minimum volume percent of oxygen for which ignition took place. In table VII-V, spray flammability limits for a number of hydrocarbons are listed, and minimum oxygen concentrations for combustion of hydrocarbon vapors are also included for purposes of comparison. While the empirical nature of the spray flammability test is stressed, it is of interest to note that these limits correspond closely to the values for hydrocarbon vapors. It is impossible to say whether the higher limits for lubricating oils were real or whether they were due to a failure of the spray to deliver sufficient fuel to the ignition region of the apparatus when more viscous oils were tested.

The limits of flammability in air of condensed mists of JP-1 fuel were 0.043 (lean limit) and 0.23 (rich limit)(ref. 43). In a spray apparatus, the lean limit was 0.0394. In general, lean limits for condensed mists and fine sprays seem to be the same as limits for the corresponding vapors; rich limits for mists may be somewhat lower.

Rate of flame propagation: Spatial flame speeds were determined (ref. 39) for condensed mists and the equivalent vapor mixtures, and the results are contained in table VII-VI. Although flame speeds for vapors were higher, the experiments on vapors were conducted at higher temperatures. Therefore, mist flame speeds were increased to values that might be anticipated at the vapor experiment temperature, with the flame speed assumed to increase as the 1.4 power of the absolute temperature, as is the case for isooctane (ref. 22). These corrected mist flame speeds, tabulated in table VII-VI, have in most instances the same values as vapor. It should be noted that some of the spatial flame speeds are quite large, suggesting that the propagating flames were not laminar. Presumably, conditions were the same in both mist and vapor mixtures, so that the comparison is still permissible.

In conclusion, flammability limits and flame velocities for mists and fine sprays (drop diameters of the order of 10 microns) apparently correspond closely to those of vaporized fuel-air mixtures. This result is compatible with the idea that small droplets can vaporize and mix with air in the preheat zone of an established flame front. For larger drops (order of 100 microns), the experiments of reference 38 suggest that this is not the case. At the present time, there does not appear to be information on limits and flame speeds for systems in which these larger drops are uniformly dispersed through the combustible mixture.

APPLICABILITY OF RESEARCH DATA ON DIFFUSION FLAMES TO JET-ENGINE COMBUSTOR DESIGN

In this chapter, the present status of knowledge of the burning of gaseous and liquid fuels as diffusion flames is reviewed. For simple systems (simple fuel jets, or single drops of liquid fuels), combustion properties may be quite successfully predicted from mixing rates; chemical reaction rates are not considered. Mixing rates are, in turn, determined by mass- and heat-transport processes. Current understanding of the burning of complex gas jets and fuel sprays is far less complete. Fine fuel sprays and mists appear to be similar to premixed fuel-air systems, while for coarser sprays behavior intermediate between that of diffusion and premixed flames might be expected. The application of the data of this chapter to combustor performance is therefore somewhat limited. Another limitation exists because of the high heat-release rates required by aircraft combustion systems. The high velocities may result in conditions that more nearly approach the extinction regions of the flames where chemical reaction rates appear to be important. The extinction of diffusion flames has received somewhat less attention than normal burning and appears to be a fruitful field for future research.

REFERENCES

1. Hottel, H. C.: Burning in Laminar and Turbulent Fuel Jets. Fourth Symposium (International) on Combustion, The Williams & Wilkins Co. (Baltimore), 1953, pp. 97-113.

2. Barr, John: Diffusion Flames. Fourth Symposium (International) on Combustion, The Williams & Wilkins Co. (Baltimore), 1953, pp. 765-771.

3. Burke, S. P., and Schumann, T. E. W.: Diffusion Flames. Ind. and Eng. Chem., vol. 20, no. 10, Oct. 1928, pp. 998-1004.

4. Hottel, H. C., and Hawthorne, W. R.: Diffusion in Laminar Flame Jets. Third Symposium on Combustion and Flame and Explosion Phenomena, The Williams & Wilkins Co. (Baltimore), 1949, pp. 254-266.

5. Wolfhard, H. G., and Parker, W. G.: A New Technique for the Spectroscopic Examination of Flames at Normal Pressures. Proc. Phys. Soc., sec. A, vol. 62, Nov. 1949, pp. 722-730.

6. Wolfhard, H. G., and Parker, W. G.: A Spectroscopic Investigation into the Structure of Diffusion Flames. Proc. Phys. Soc., sec. A, vol. 65, Jan. 1952, pp. 2-19.

7. Hawthorne, W. R., Weddell, D. S., and Hottel, H. C.: Mixing and Combustion in Turbulent Gas Jets. Third Symposium on Combustion and Flame and Explosion Phenomena, The Williams & Wilkins Co. (Baltimore), 1949, pp. 266-288.

8. Barr, J., and Mullins, B. P.: Concerning Combustion in Vitiated Atmospheres. Rep. No. R.44, British N.G.T.E., June 1949.

9. Gray, Andrew, Mathews, G. B., and MacRobert, T. M.: A Treatise on Bessel Functions and Their Applications to Physics. Second ed., MacMillan and Co. (London), 1931, p. 78.

10. Wohl, Kurt, Gazley, Carl, and Kapp, Numer: Diffusion Flames. Third Symposium on Combustion and Flame and Explosion Phenomena, The Williams & Wilkins Co. (Baltimore), 1949, pp. 288-300.

11. Zeldovich, Y. B.: On the Theory of Combustion of Initially Unmixed Gases. NACA TM 1296, 1951.

12. Sawai, Ikutaro, Kunugi, Masanga, and Jinno, Hiroshi: Turbulent Diffusion Flames. Fourth Symposium (International) on Combustion, The Williams & Wilkins Co. (Baltimore), 1953, pp. 806-814.

13. Rembert, E. W., and Haslam, R. T.: Factors Influencing Length of a Gas Flame Burning in Secondary Air. Ind. and Eng., Chem., vol. 17, no. 12, Dec. 1925, pp. 1236-1238.

14. Scholefield, D. A., and Garside, J. E.: The Structure and Stability of Diffusion Flames. Third Symposium on Combustion and Flame and Explosion Phenomena, The Williams & Wilkins Co. (Baltimore), 1949, pp. 102-110.

15. Yagi, Sakae, and Saji, Kenjiro: Problems of Turbulent Diffusion and Flame Jet. Fourth Symposium (International) on Combustion, The Williams & Wilkins Co. (Baltimore), 1953, pp. 771-781.

16. Chamberlin, D. S., and Rose, A.: Flicker of Luminous Flames. Ind. and Eng. Chem., vol. 20, no. 10, Oct. 1928, pp. 1013-1016.

17. Spalding, D. B.: Combustion of Liquid Fuel in a Gas Stream - I. Fuel, vol. XXIX, no. 1, Jan. 1950, pp. 2-7.

18. Spalding, D. B.: Combustion of Fuel Particles. Fuel, vol. XXX, no. 6, June 1951, pp. 121-130.

19. Graves, Charles C.: Burning Rates of Single Fuel Drops and Their Application to Turbojet Combustion Process. NACA RM E53E22, 1953.

20. Khudyakov, G. N.: The Temperature Field of a Liquid Burning from a Free Surface and the Flame Over It. Chem. Abs., vol. 46, no. 22, Nov. 25, 1952, p. 10844e. (Abs. from Izvest. Akad. Nauk S.S.S.R., Otdel, Tekh. Nauk, vol. 1951, pp. 1015-1024.)

21. Sherwood, Thomas K.: Absorption and Extraction. McGraw-Hill Book Co., Inc., 1937, p. 9.

22. Dugger, Gordon L., and Graab, Dorothy D.: Flame Speeds of 2,2,4-Trimethylpentane-Oxygen-Nitrogen Mixtures. NACA TN 2680, 1952.

23. Godsave, G. A. E.: The Burning of Single Drops of Fuel. Pt. IV. The Flow of Heat and Carbon Residue Formation in Drops of Fuel. Rep. No. R.125, British N.G.T.E., Oct. 1952.

24. Godsave, G. A. E.: The Burning of Single Drops of Fuel. Pt. I. Temperature Distribution and Heat Transfer in the Pre-Flame Region. Rep. No. R.66, British N.G.T.E., Mar. 1950.

25. Godsave, G. A. E.: Studies of the Combustion of Drops in a Fuel Spray - The Burning of Single Drops of Fuel. Fourth Symposium (International) on Combustion, The Williams & Wilkins Co. (Baltimore), 1953, pp. 819-830.

26. Godsave, G. A. E.: The Burning of Single Drops of Fuel. Pt. II. Experimental Results. Rep. No. R.87, British N.G.T.E., Apr. 1951.

27. Kumagai, Seiichiro, and Isoda, Hiroshi: Combustion of Fuel Droplets. Nature, vol. 166, no. 4235, Dec. 30, 1950, p. 1111.

28. Hall, A. R., and Diederichsen, J.: An Experimental Study of the Burning of Single Drops of Fuel in Air at Pressures up to Twenty Atmospheres. Fourth Symposium (International) on Combustion, The Williams & Wilkins Co. (Baltimore), 1953, pp. 837-846.

29. Godsave, G. A. E.: The Burning of Single Drops of Fuel. Pt. III. Comparison of Experimental and Theoretical Burning Rates and Discussion of the Mechanism of the Combustion Process. Rep. No. R.88, British N.G.T.E., Aug. 1952.

30. Spalding, D. B.: Combustion of a Single Droplet and of a Fuel Spray. Selected Combustion Problems - Fundamentals and Aeronautical Applications, Butterworths Scientific Pub.(London), 1954, pp. 340-351.

31. Ingebo, Robert D.: Study of Pressure Effects on Vaporization Rate of Drops in Gas Streams. NACA TN 2850, 1953.

32. Spalding, D. B.: Experiments on the Burning and Extinction of Liquid Fuel Spheres. Fuel, vol. XXXII, no. 2, Apr. 1953, pp. 169-185.

33. Spalding, D. B.: Combustion of Liquid Fuel in a Gas Stream, Pt. II. Fuel, vol. XXIX, no. 2, Feb. 1950, pp. 25-32.

34. Spalding, D. B.: The Combustion of Liquid Fuels. Fourth Symposium (International) on Combustion, The Williams & Wilkins Co. (Baltimore), 1953, pp. 847-864.

35. Emmons, Howard W.: The Film Combustion of Liquid Fuel. Interim Tech. Rep. No. 6, Combustion Aero. Lab., Harvard Univ., June 1953. (Contract No. DA-19-020-ORD-1029, Army Ord. Dept.)

36. Topps, J. E. C.: An Experimental Study of the Evaporation and Combustion of Falling Droplets. N.G.T.E. Memo. No. M.105, British M.O.S., Feb. 1951 (See also Jour. Inst. Petroleum, vol. 37, no. 333, Sept. 1951, pp. 535-553.)

37. Probert, R. P.: The Influence of Spray Particle Size and Distribution in the Combustion of Oil Droplets. Phil. Mag., ser. 7, vol. XXXVII, no. 265, Feb. 1946, pp. 94-105.

38. Wolfhard, H. G., and Parker, W. G.: Combustion Processes in Flames. Pt. II. Evaporation Process in a Burning Kerosene Spray. Rep. Chem. 437, British R.A.E., Dec. 1947. (See also Jour. Inst. Petroleum, vol. 35, no. 302, Feb. 1949, pp. 118-125.

39. Haber, F., und Wolff, H.: Über Nebelexplosionen. Zs. Angew. Chem., Jahrg. 36, Nr. 55, July 18, 1923, pp. 373-377.

40. Coward, H. F., and Jones, G. W.: Limits of Flammability of Gases and Vapors. Bull. 503, Bur. Mines, 1952.

41. Burgoyne, J. H., and Richardson, J. F.: The Inflammability of Oil Mists. Fuel, vol. XXVIII, no. 1, Jan. 1949, pp. 2-6.

42. Sullivan, M. V., Wolfe, J. K., and Zisman, W. A.: Flammability of the Higher Boiling Liquids and Their Mists. Ind. and Eng. Chem., vol. 39, no. 12, Dec. 1947, pp. 1607-1614.

43. Jones, G. W., et al.: Research on the Flammability Characteristics of Aircraft Fuels. WADC Tech. Rep. 52-35, Wright Air Dev. Center, Wright-Patterson Air Force Base, June 1952. (Contract AF 33(038)50-1293E.)

3092

TABLE VII-I. - EVAPORATION CONSTANT FOR VARIOUS FUELS

BURNING IN AIR

Fuel	Evaporation constant, β, ft^2/sec		
	Experimental (refs. 25 and 26)	Calculated (ref. 29)	Calculated (c)
Petroleum ether (100° to 120° C)	10.6×10^{-6}	----	----
Kerosene	10.3	----	----
Diesel fuel	8.5	----	----
Ethyl alcohol	8.7	----	8.6×10^{-6}
Benzene	10.4	10.6×10^{-6}	9.6
Toluene	[a]7.1	----	9.6
Ethylbenzene	9.3	----	9.2
o-Xylene	8.5	----	8.9
p-Xylene	8.3	----	9.1
Isopropylbenzene	8.4	----	8.7
Pseudocumene	[b]9.4	----	8.4
n-Butylbenzene	[b]9.3	----	8.2
tert-Butylbenzene	8.3	10.3	8.3
tert-Amylbenzene	8.4	----	7.8
n-Heptane	10.4	11.6	10.4
Isooctane	10.2	----	10.1

[a]Experimental value believed to be too low.

[b]Experimental value believed to be too high.

[c]Calculated using equation (38a) and a correction factor of 0.79.

TABLE VII-II. - EVAPORATION CONSTANT FOR ISOOCTANE

IN VARIOUS OXYGEN-NITROGEN ATMOSPHERES[a]

Oxygen in atmosphere, percent	Evaporation constant, β, ft^2/sec
17.0	11.5×10^{-6}
20.9 (air)	12.3
24.9	13.5
34.9	15.4

[a]Ref. 19.

TABLE VII-III. - COMPARISON OF LOWER LIMITS OF FLAMMIBILITY OF MIST AND VAPOR[a]

[Vessel, 3 in. diam., 20 in. long.]

Fuel	Mist			Vapor	
	Fuel as vapor, percent	Temperature, °F	Lean-limit fuel-air ratio	Temperature, °F	Lean-limit fuel-air ratio
Petroleum (180° to 220° C)	41	75	0.037	140	0.036
Tetralin	[b]7	84	.035	212	.035
Quinolin	[b]1	97	.056	230	.054

[a]Ref. 39.

[b]From estimated fuel vapor pressure.

3092

TABLE VII-IV. - LIMITS OF FLAMMABILITY OF OIL MISTS[a]

[Tube diam., $1\frac{7}{8}$ in.]

Fuel	Fuel-air ratio	
	Rich limit	Lean limit
Cutting oil no. 1	0.033	0.118
Cutting oil no. 2	.043	.134
Cutting oil no. 2, distilled once	.043	.214
Cutting oil no. 3	.038	----
Sperm quenching oil	.035	.159
Diesel oil	.038	----

[a]Ref. 41.

3092

TABLE VII-V. - SPRAY FLAMMABILITY LIMITS COMPARED WITH MINIMUM OXYGEN CONCENTRATIONS FOR COMBUSTION OF HYDROCARBON VAPORS IN OXYGEN-NITROGEN MIXTURES

Fuel (liquid)	Spray flammability limit[a], percent O_2 in O_2-N_2	Fuel (vapor)	Min. O_2 concentration for fuel vapor combustion[b], percent O_2 in O_2-N_2
Benzene	12	Benzene	11.2
n-Hexadecane	12	Methane	12.1
Cumene	12	Propane	11.4
Aviation hydraulic fluid AN-VV-O-366B	12	Pentane	12.1
		Hexane	11.9
Naval lubricating oil N.S. 2135	34		

[a]Ref. 20.
[b]Ref. 18.

TABLE VII-VI. - SPATIAL FLAME SPEEDS OF MIST AND VAPOR[a]

Fuel	Mist				Vapor		Mist flame speed corrected to temperature of vapor experiment
	Fuel-air ratio	Fuel as vapor, percent	Temperature, °F	Flame speed, ft/sec	Temperature, °F	Flame speed, ft/sec	
Petroleum (180° to 220° C)	0.044	34	75	3.6	140	4.3	4.2
	.061	30	93	16	140	18	18
	.072	33	99	19	140	22	21
Tetralin	0.040	[b]6	84	2.3	212	2.6	3.1
	.080	[b]3	113	3.6	212	6.2	4.5

[a]Ref. 39.
[b]Calculated from estimated fuel vapor pressure.

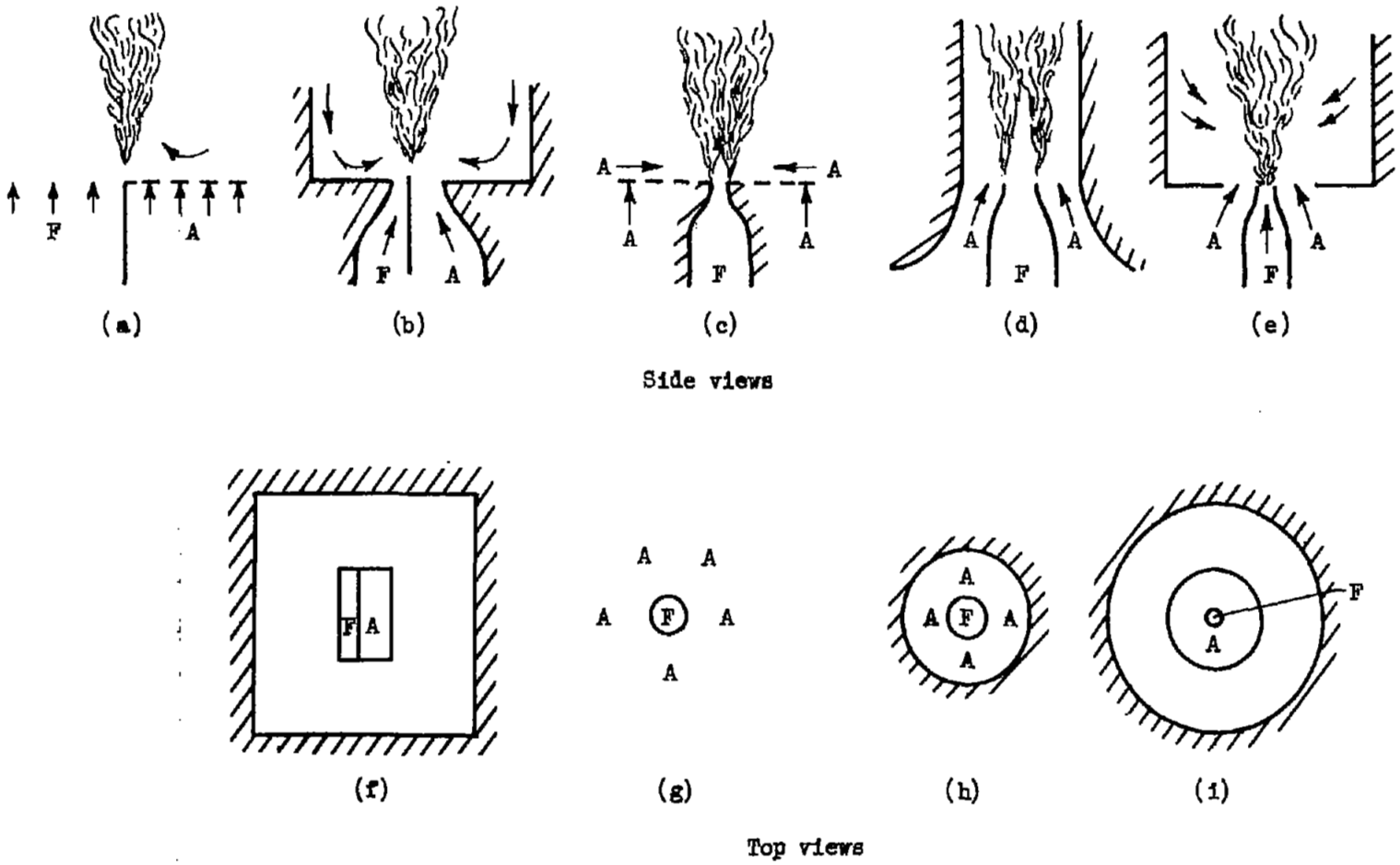

Figure VII-1. - Various configurations used to obtain gaseous diffusion flames (ref. 1).

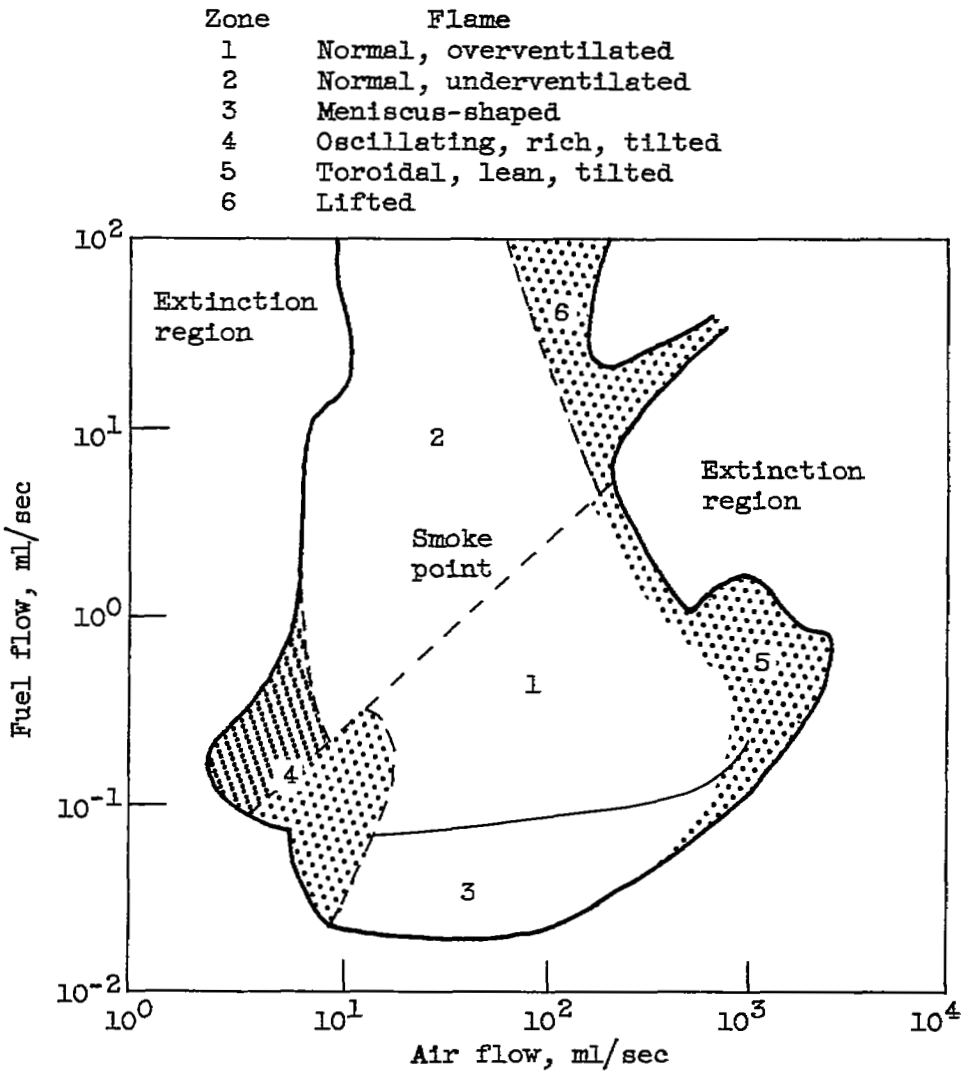

Figure VII-2. - Flame zones for gaseous diffusion flames (ref. 2, p. 766).

[redacted]

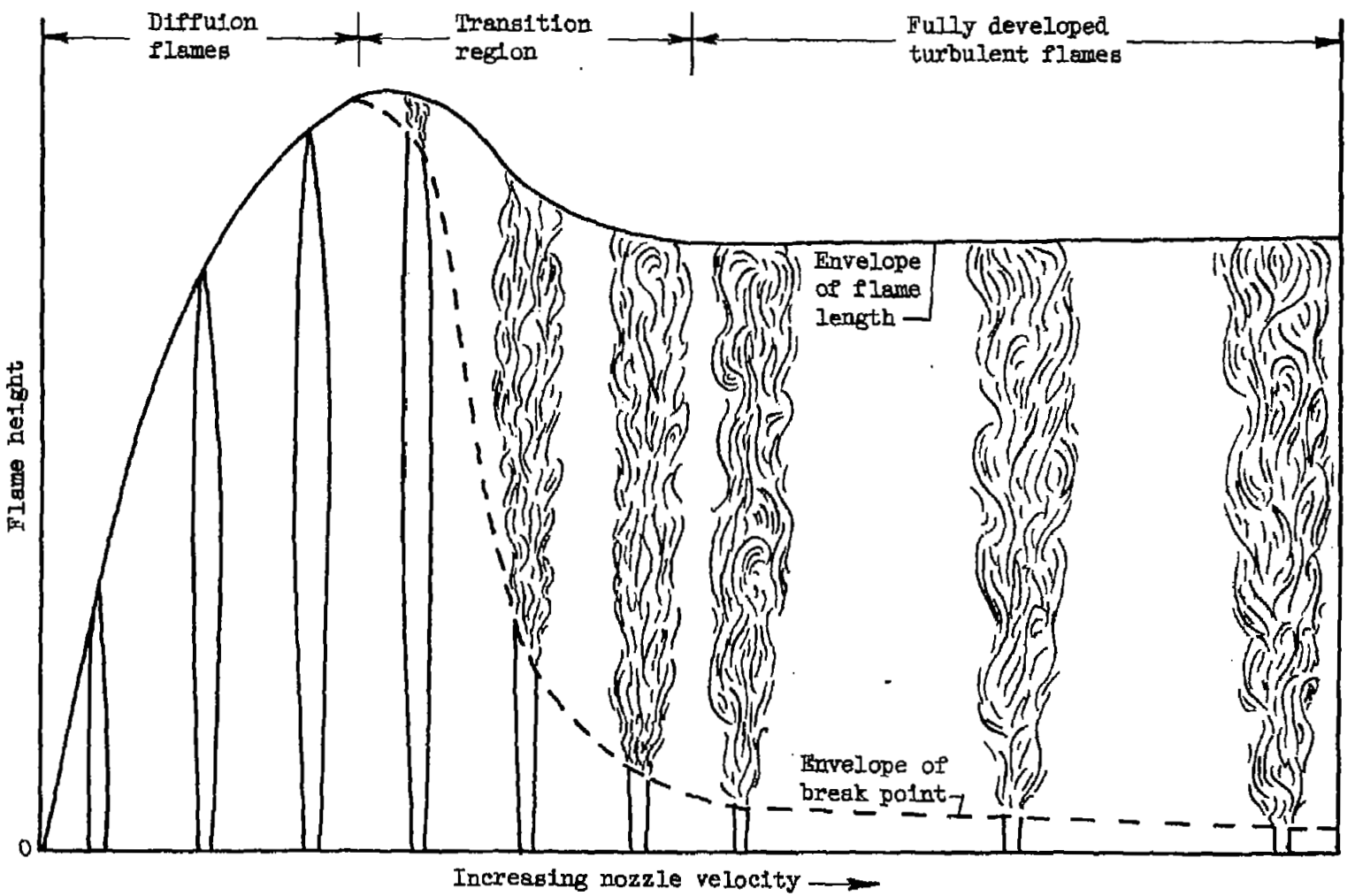

Figure VII-3. - Progressive change in flame type with increase in nozzle velocity (ref. 4.).

[redacted]

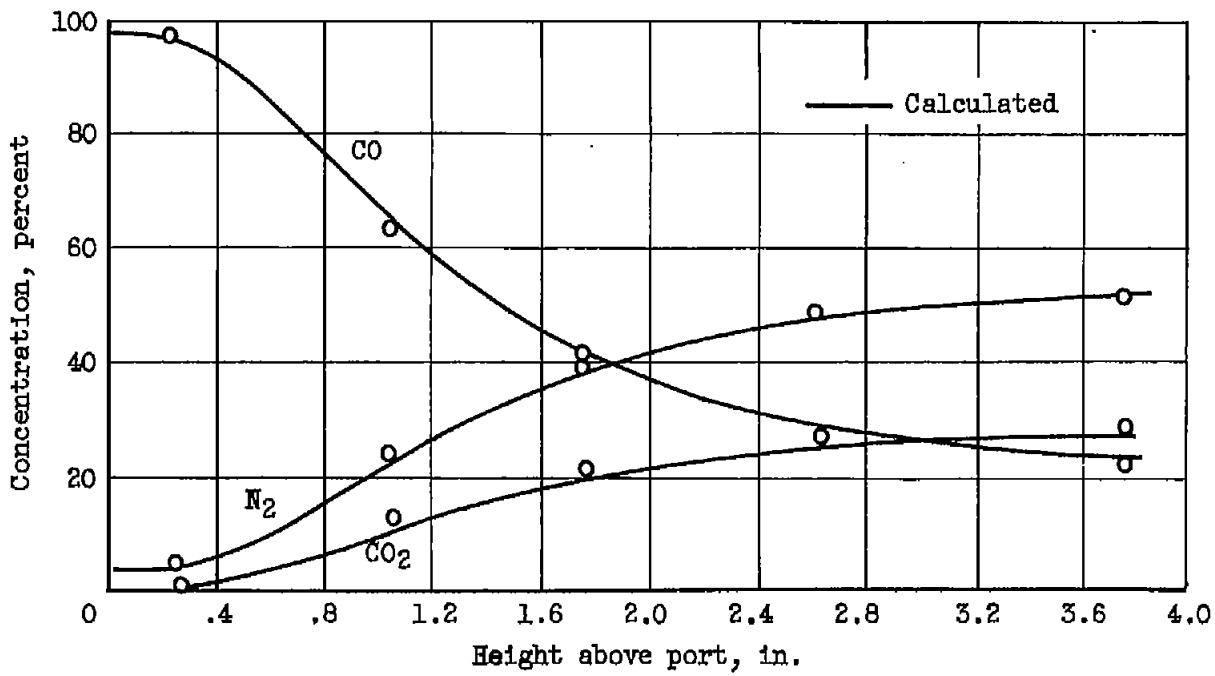

Figure VII-4. - Concentrations of carbon monoxide, nitrogen, and carbon dioxide on axis of cylindrical carbon monoxide flame (by permission from ref. 3).

3092

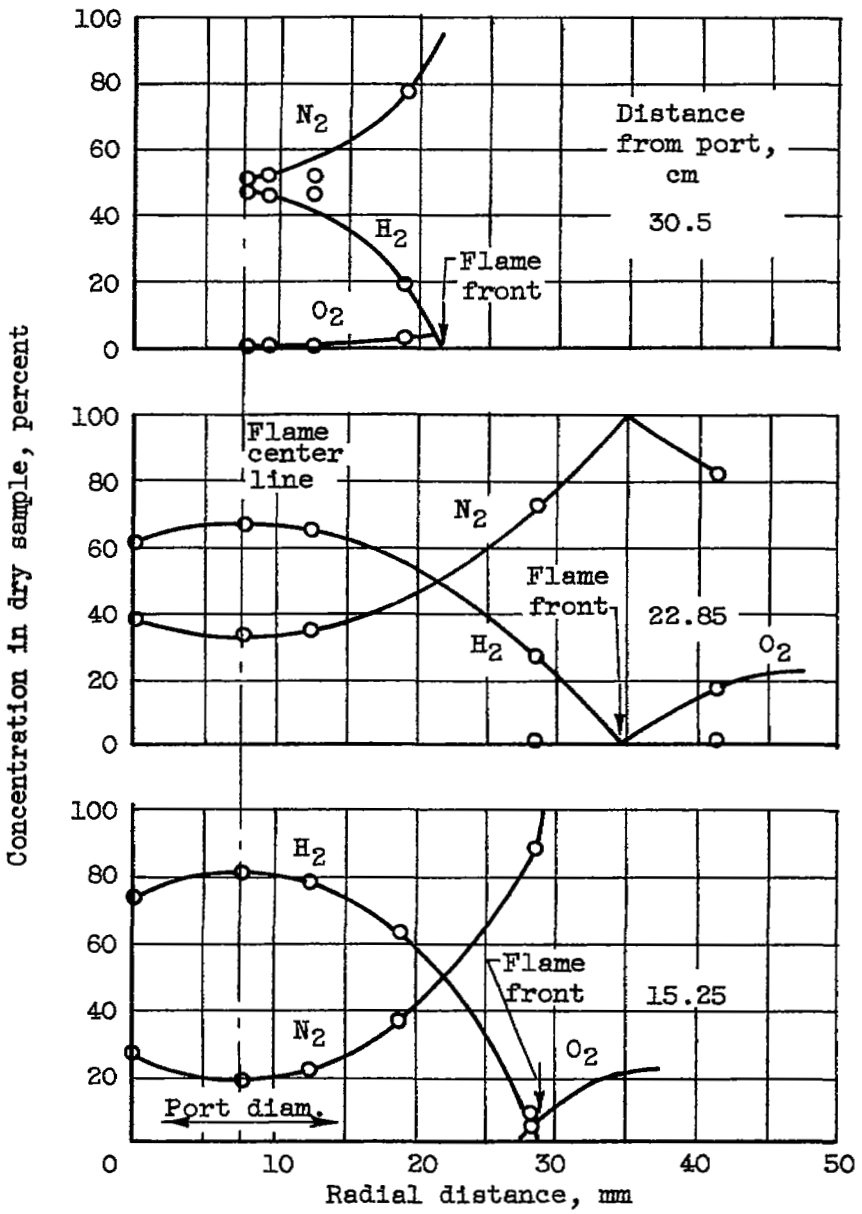

Figure VII-5. - Composition of hydrogen diffusion flame. Nozzle diameter, 1/4 inch; nozzle velocity, 108 feet per second (ref. 4).

[redacted]

3092

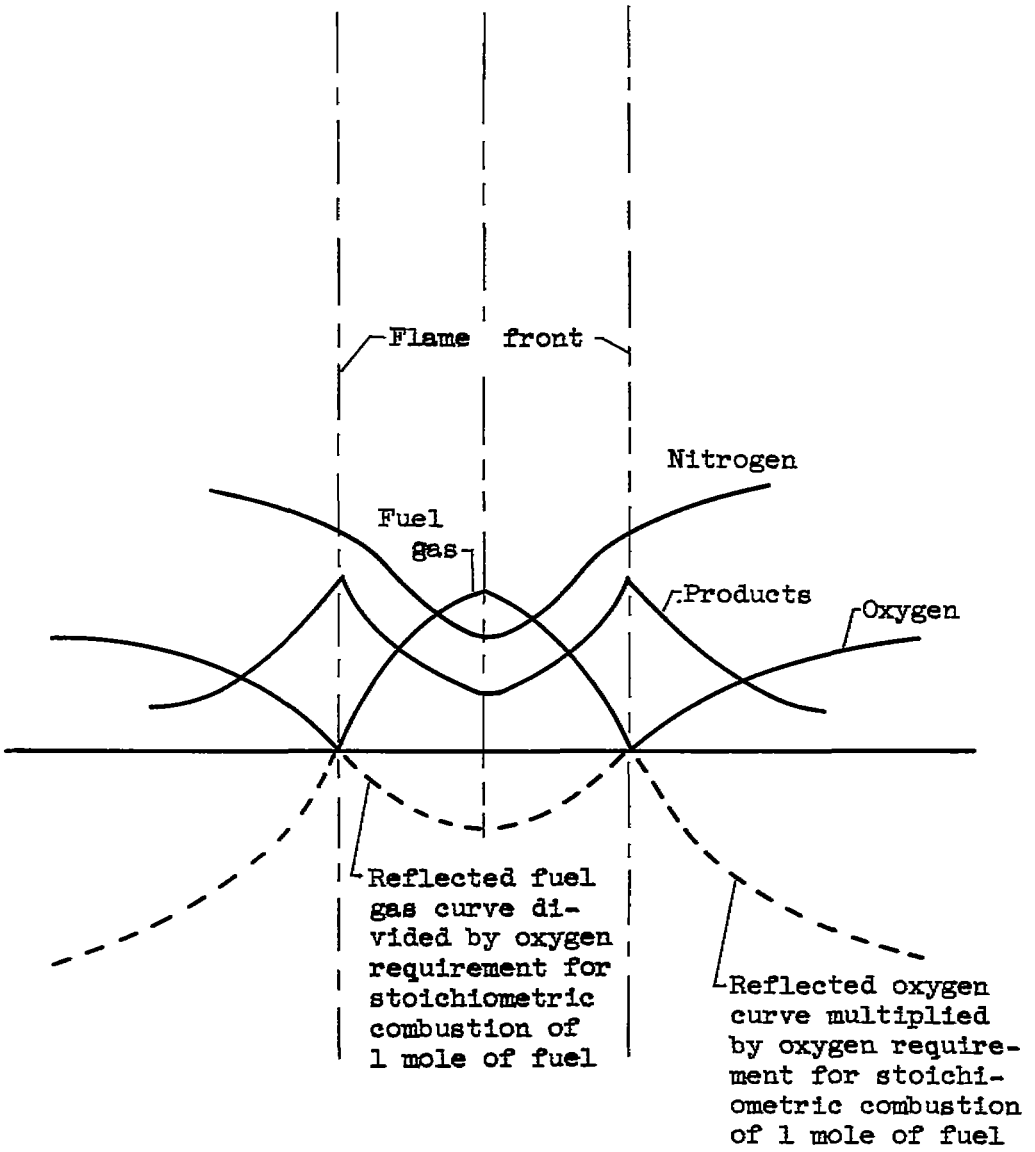

Figure VII-6. - Simplified diagram of concentration profiles in typical laminar diffusion flame (ref. 4).

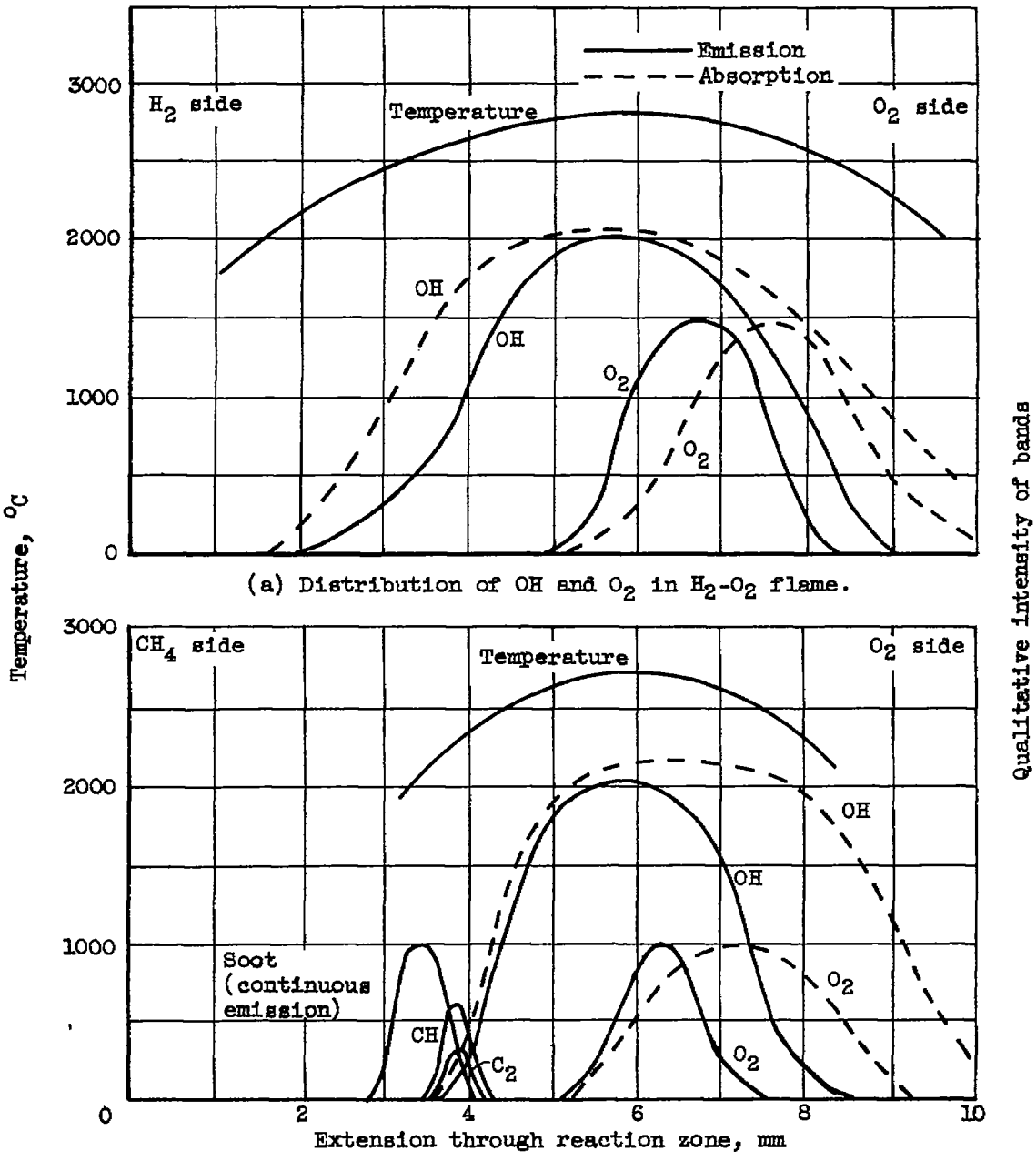

(a) Distribution of OH and O_2 in H_2-O_2 flame.

(b) Distribution of OH, O_2, CH, C_2, and soot in CH_4-O_2 flame.

Figure VII-7. - Temperature profile and distributions of various species in flat diffusion flames (ref. 5).

3092

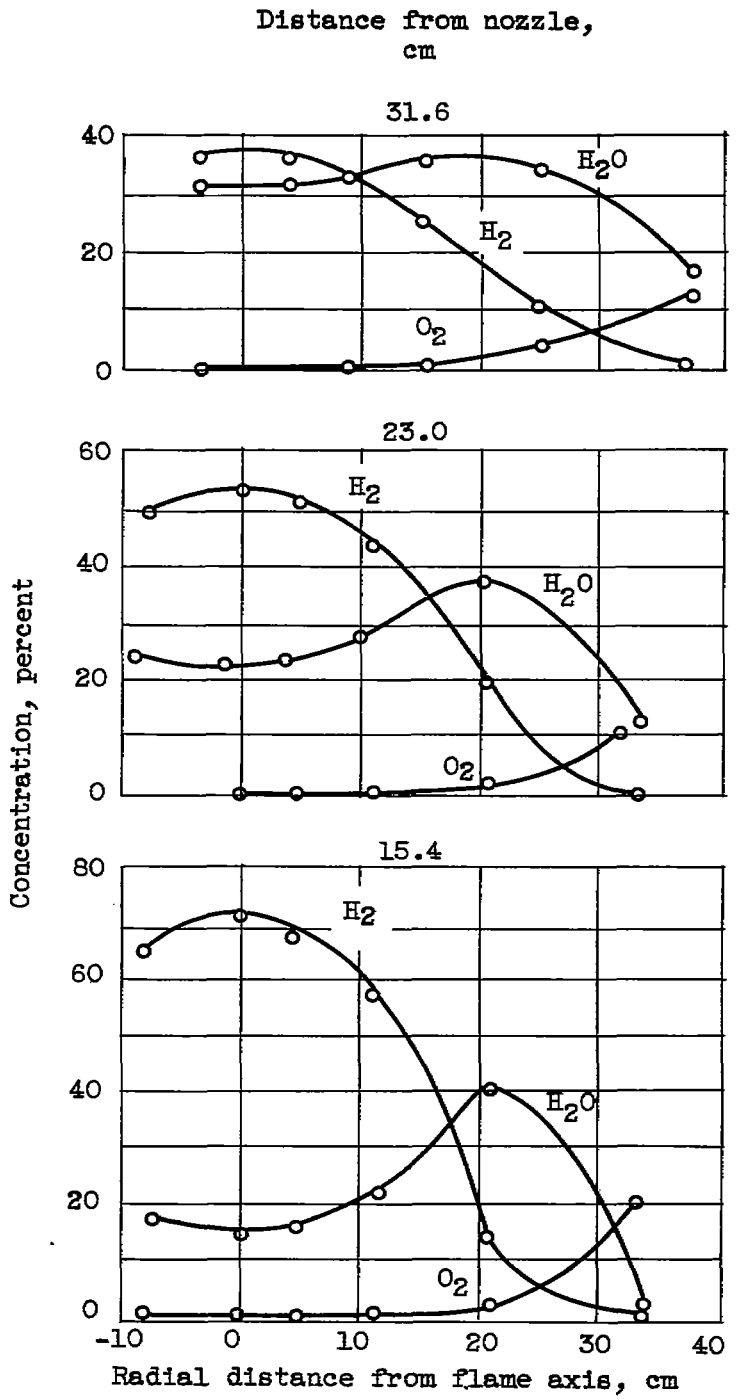

Figure VII-8. - Concentration profiles in hydrogen-air flame. 3/16-Inch nozzle; no primary air; flow velocity, 162 feet per second (ref. 7).

[redacted]

3092

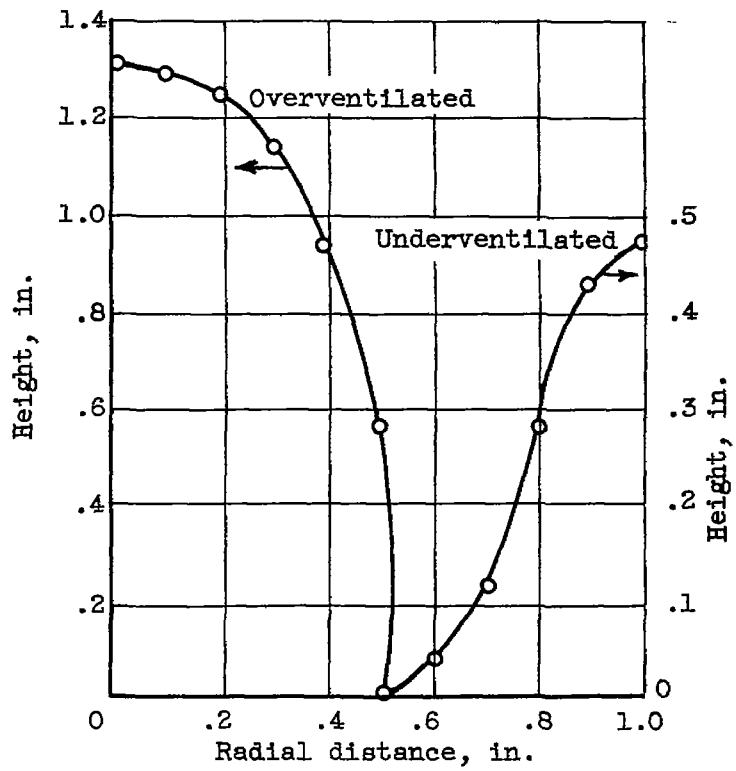

Figure VII-9. - Calculated flame shape using equation (6) for underventilated and overventilated flame (by permission from ref. 3).

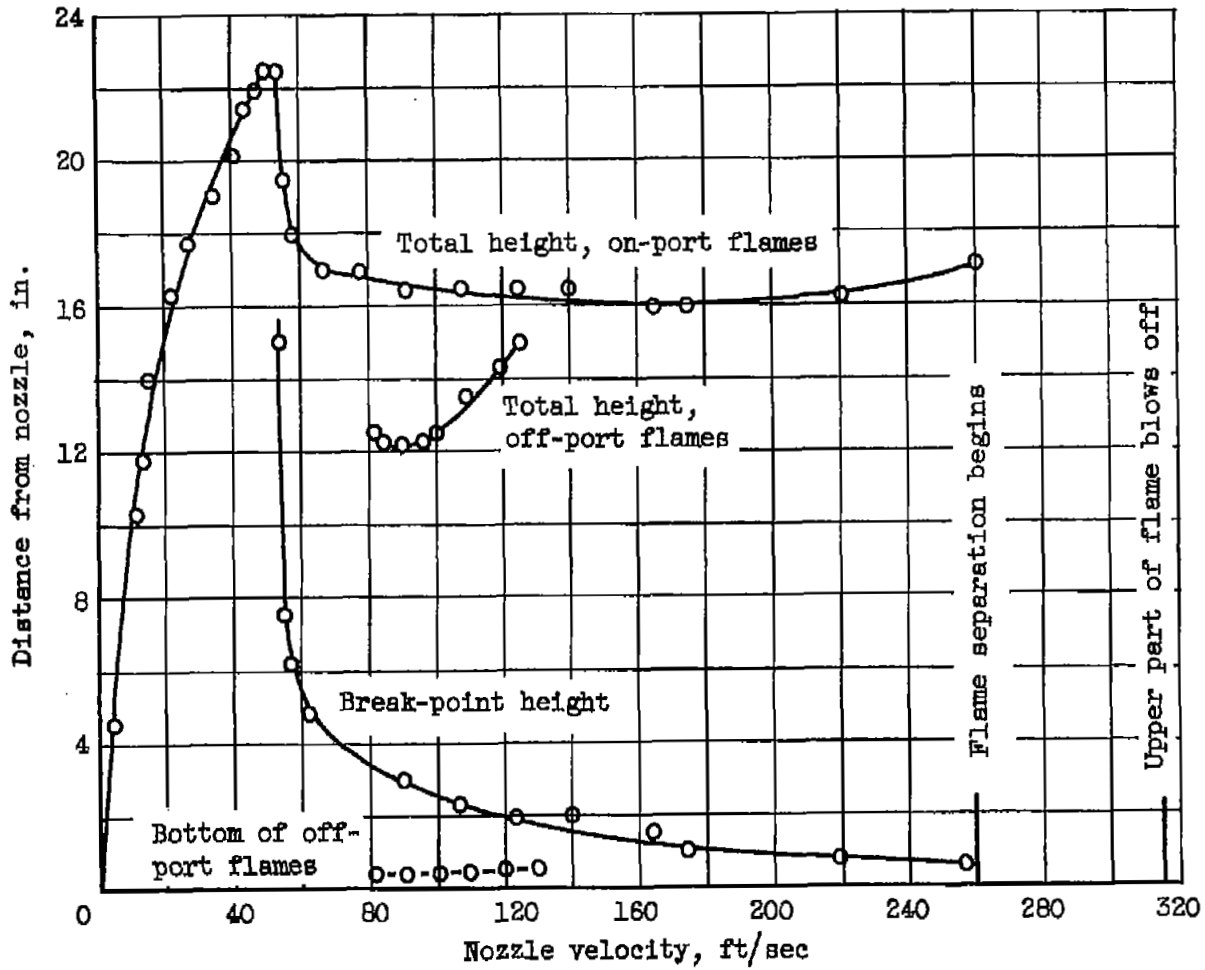

Figure VII-10. - Effect of nozzle velocity on flame height of city gas flames. Molecular weight, 19.7; no primary air; air requirement, approximately 4.5; nozzle diameter, 1/8 inch (ref. 4).

3092

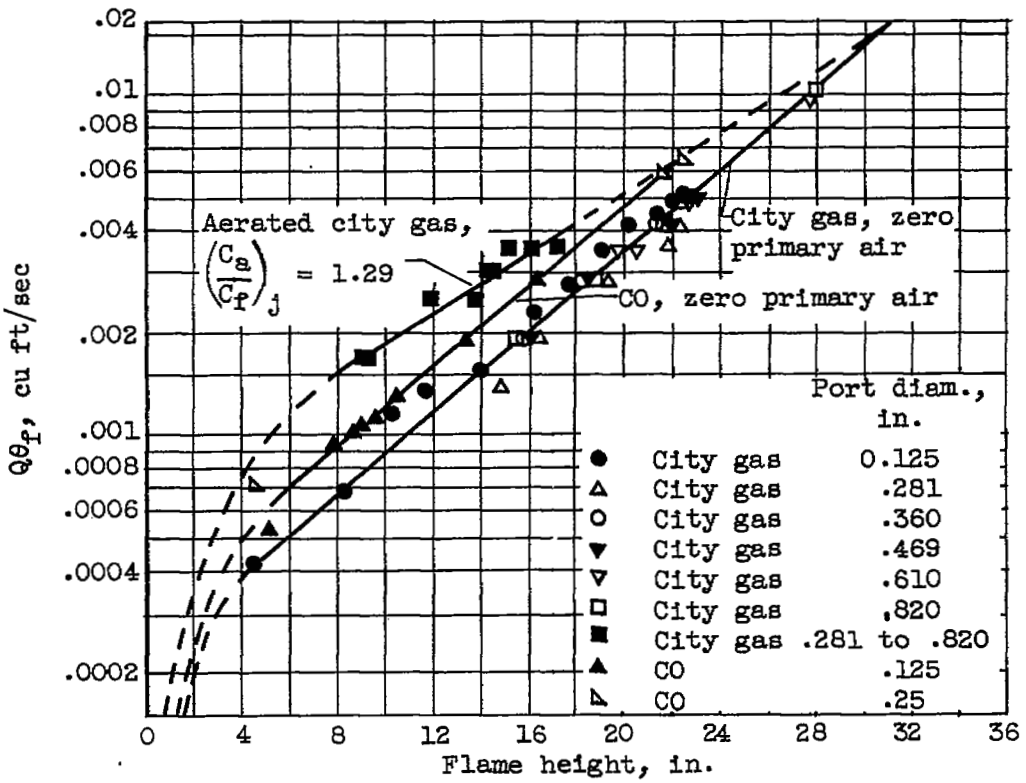

Figure VII-11. - Correlation of data on height of diffusion flames (ref. 4).

[redacted]

3092

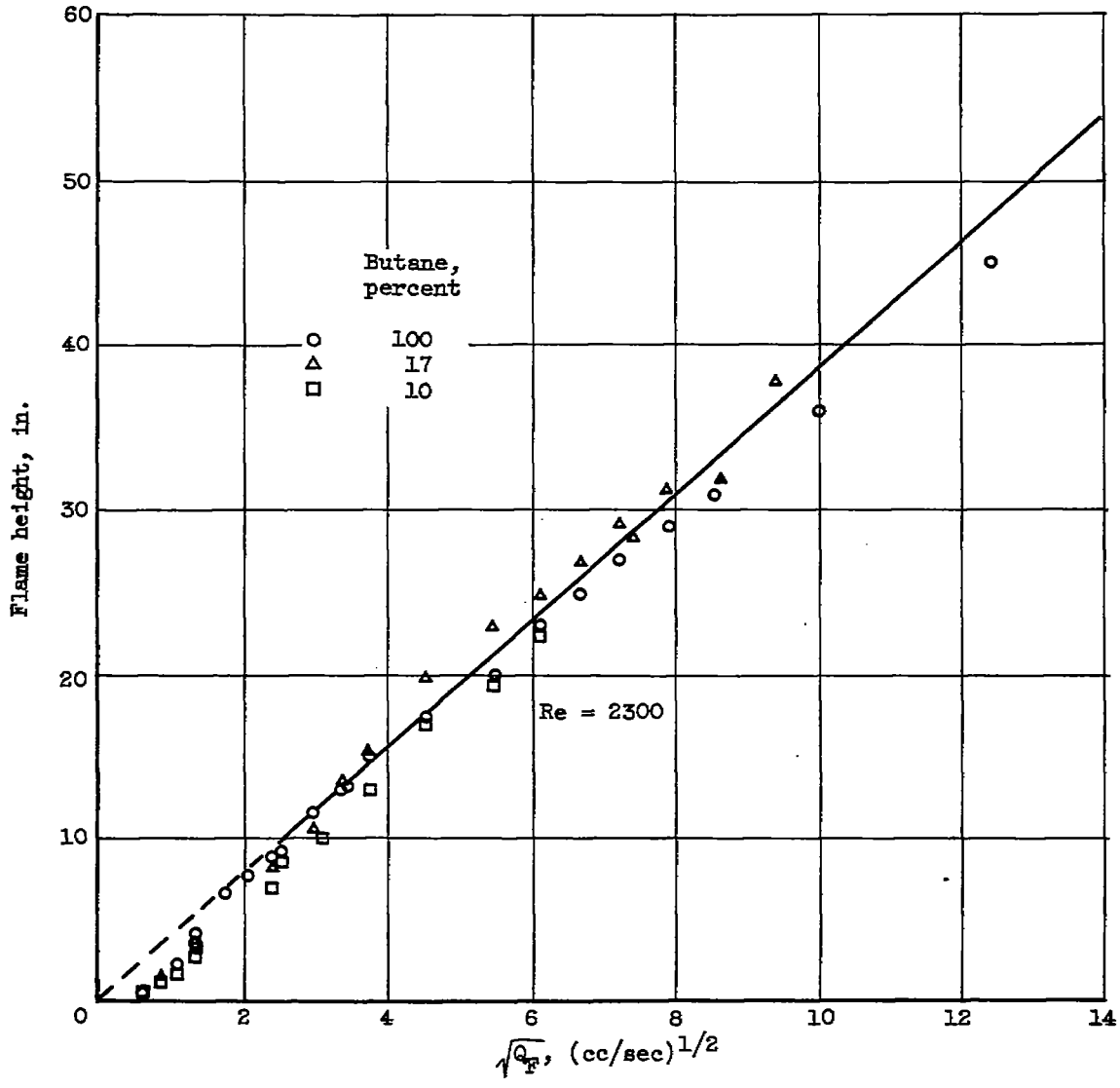

Figure VII-12. - Heights of butane-air flames in free air. Burner tube inside diameter, 0.4 inch (ref. 10).

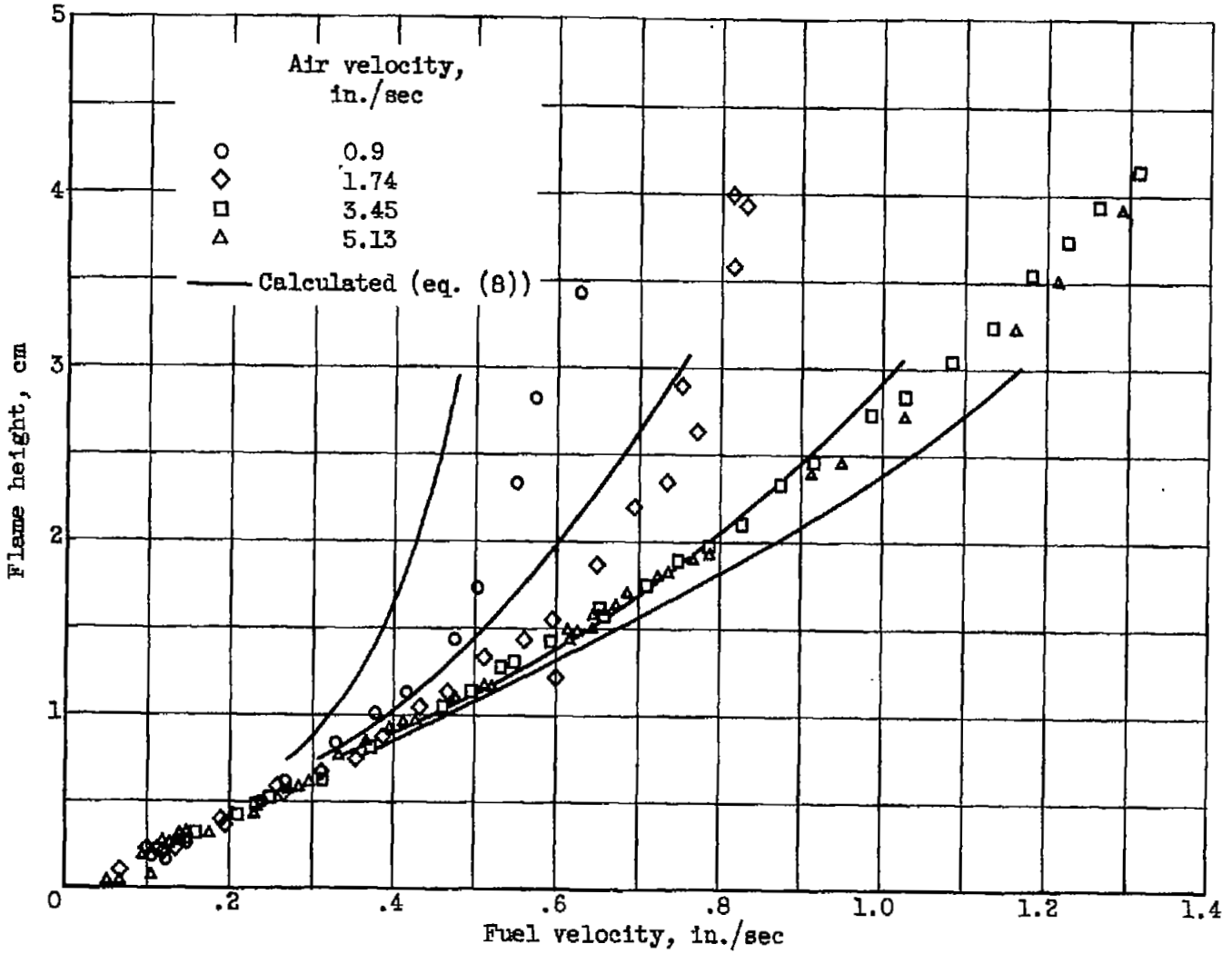

Figure VII-13. - Effect of fuel and air velocity on flame height (ref. 8).

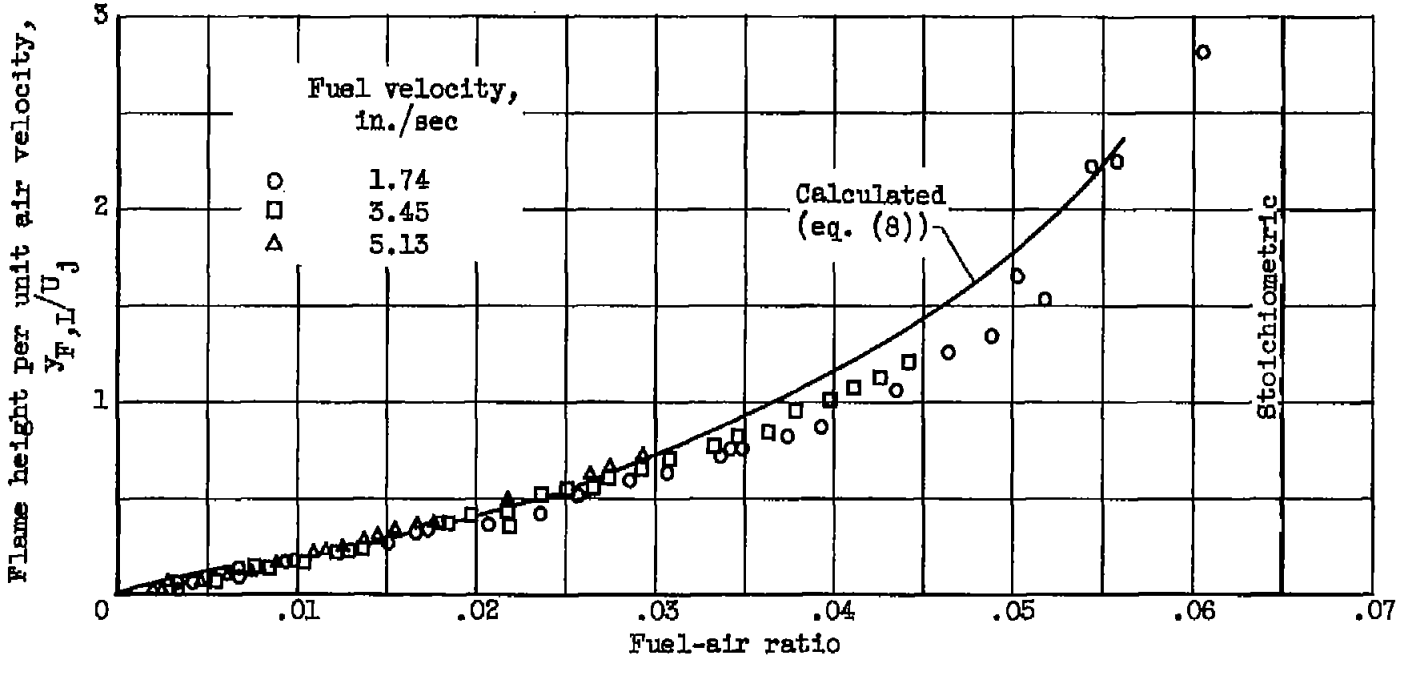

Figure VII-14. - Correlation of effect of air and fuel velocity on flame height (ref. 8).

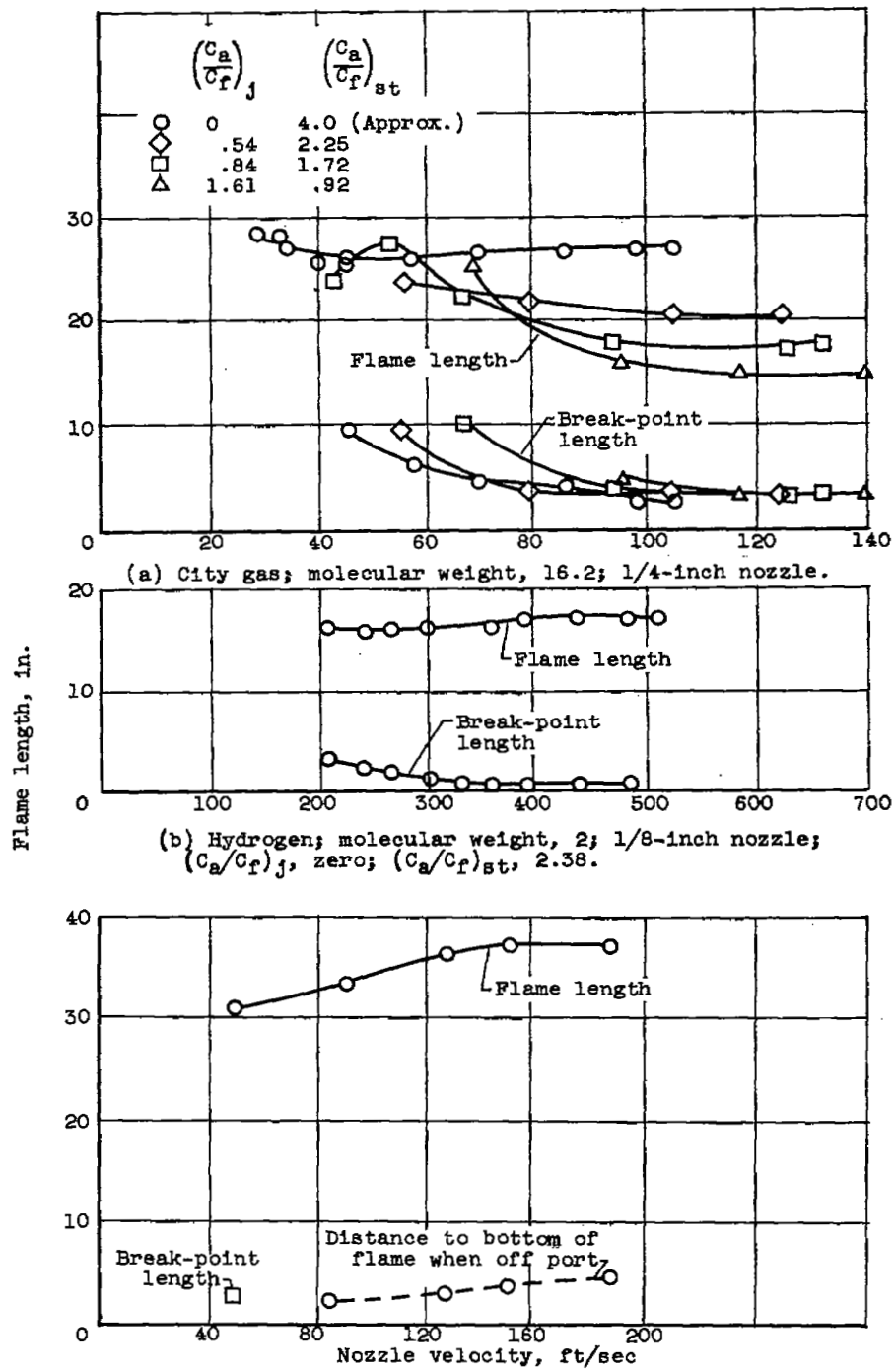

(a) City gas; molecular weight, 16.2; 1/4-inch nozzle.

(b) Hydrogen; molecular weight, 2; 1/8-inch nozzle; $(C_a/C_f)_j$, zero; $(C_a/C_f)_{st}$, 2.38.

(c) Propane; molecular weight, 43.2; 1/8-inch nozzle; $(C_a/C_f)_j$, zero; $(C_a/C_f)_{st}$, 2.33.

Figure VII-15. - Visible flame-length characteristics. Unconfined flames; rounded nozzles (ref. 7).

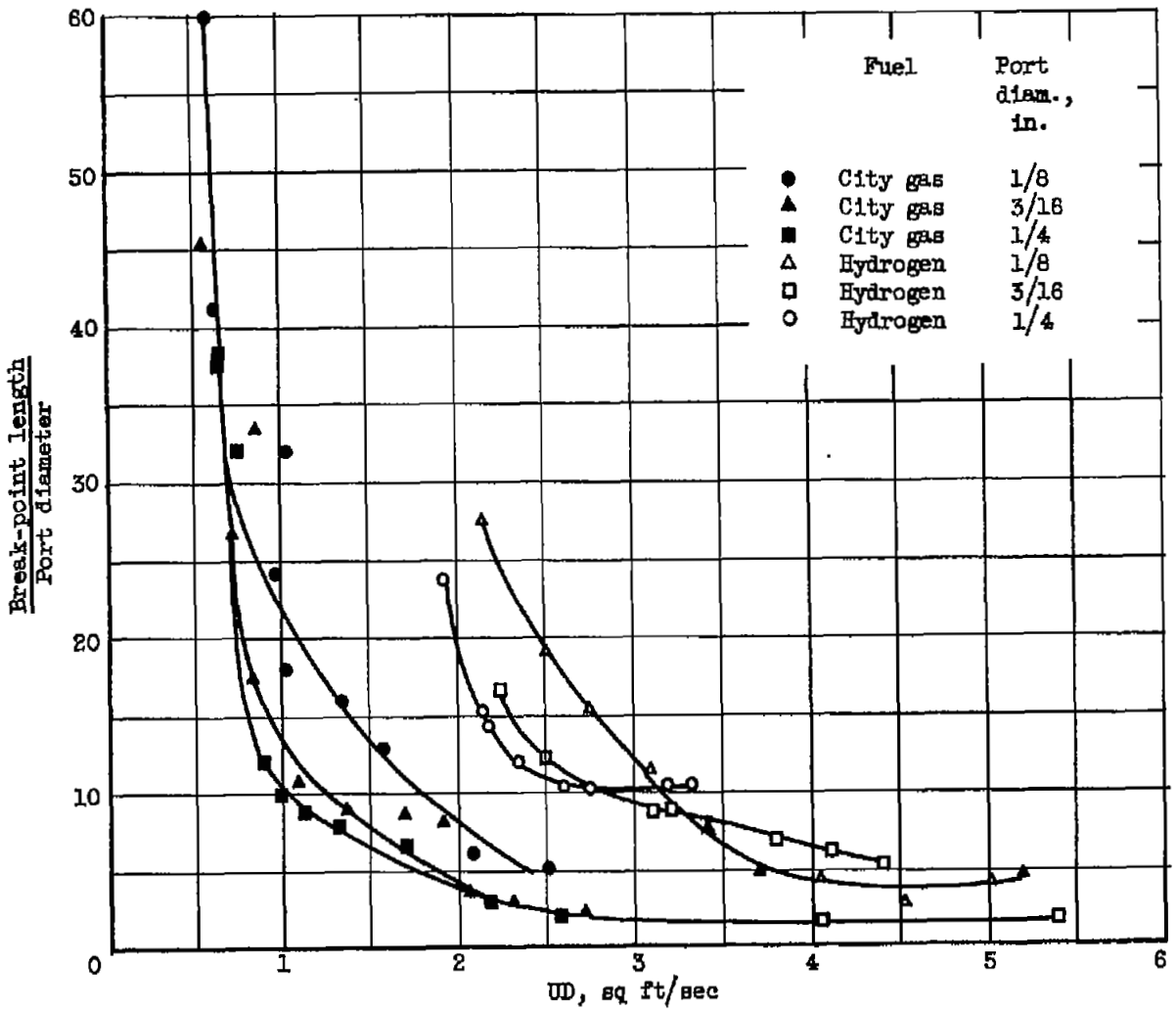

Figure VII-16. - Break-point lengths for hydrogen and city gas (molecular wt., 19.7) flames (nonpremix) (ref. 7).

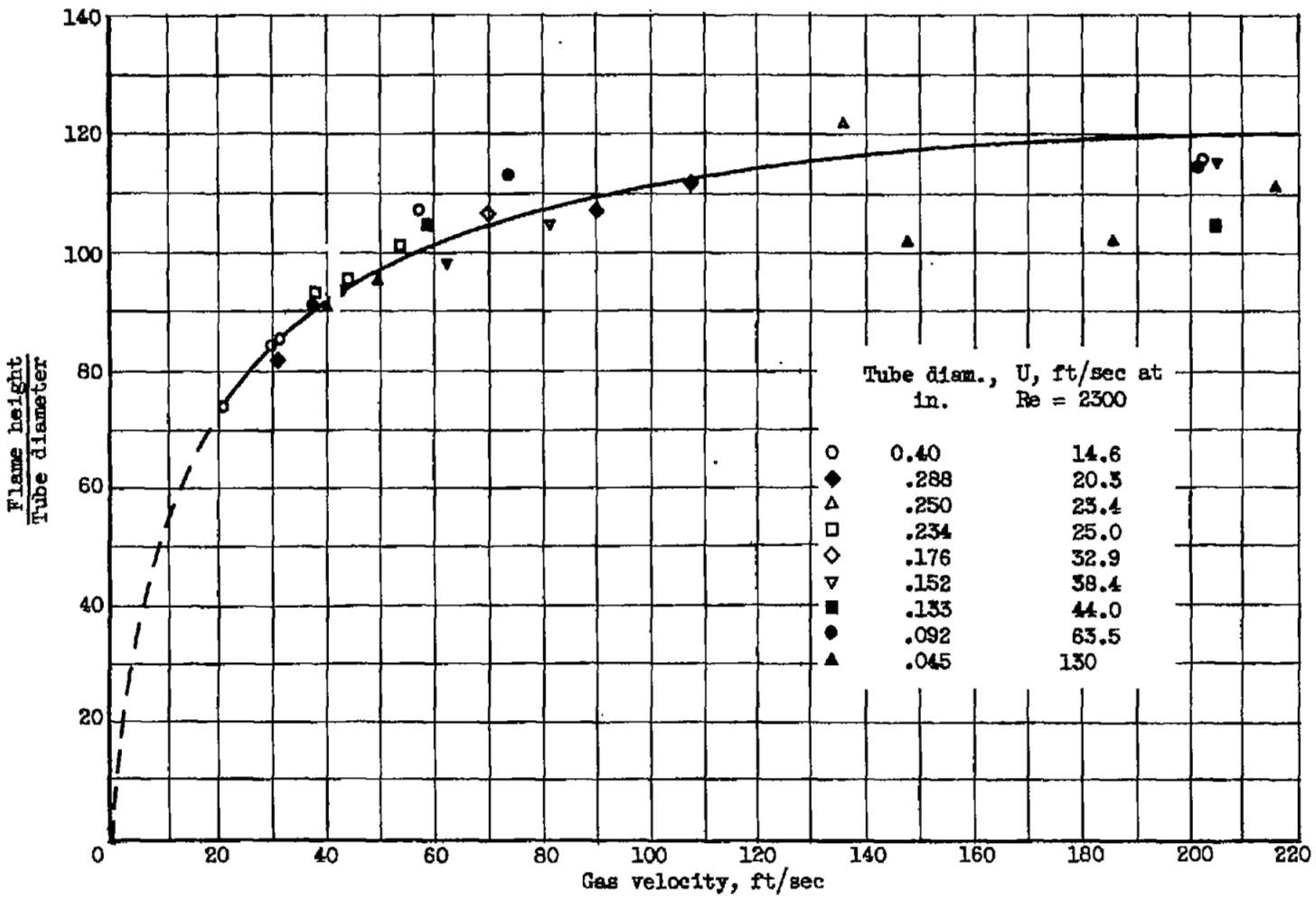

(a) City gas concentration, 100 percent.

Figure VII-17. - Effect of velocity on ratio of flame height to tube diameter in turbulent region of city gas flames in free air (ref. 10).

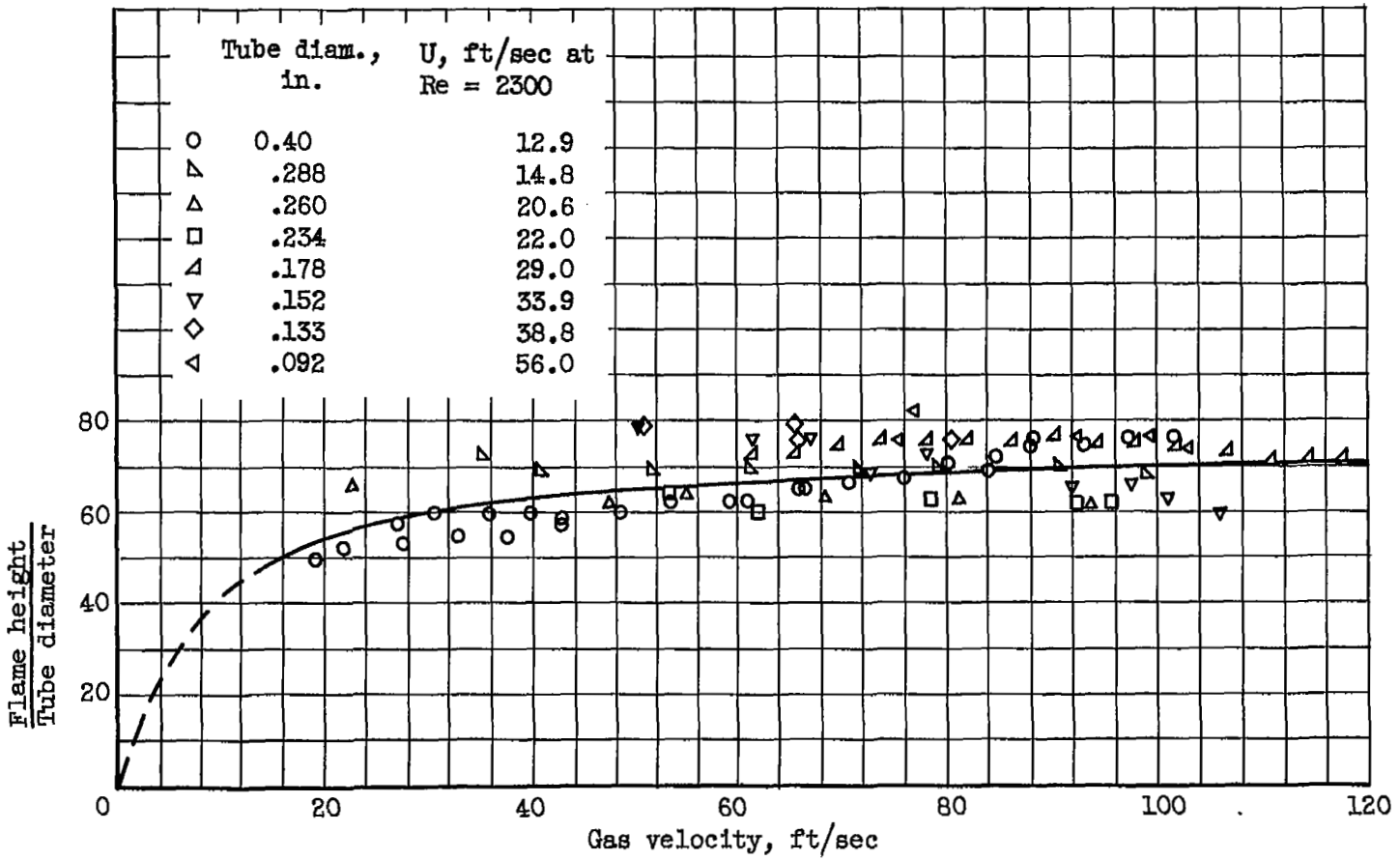

(b) City gas concentration, 50 percent.

Figure VII-17. - Concluded. Effect of velocity on ratio of flame height to tube diameter in turbulent region of city gas flames in free air (ref. 10).

3092

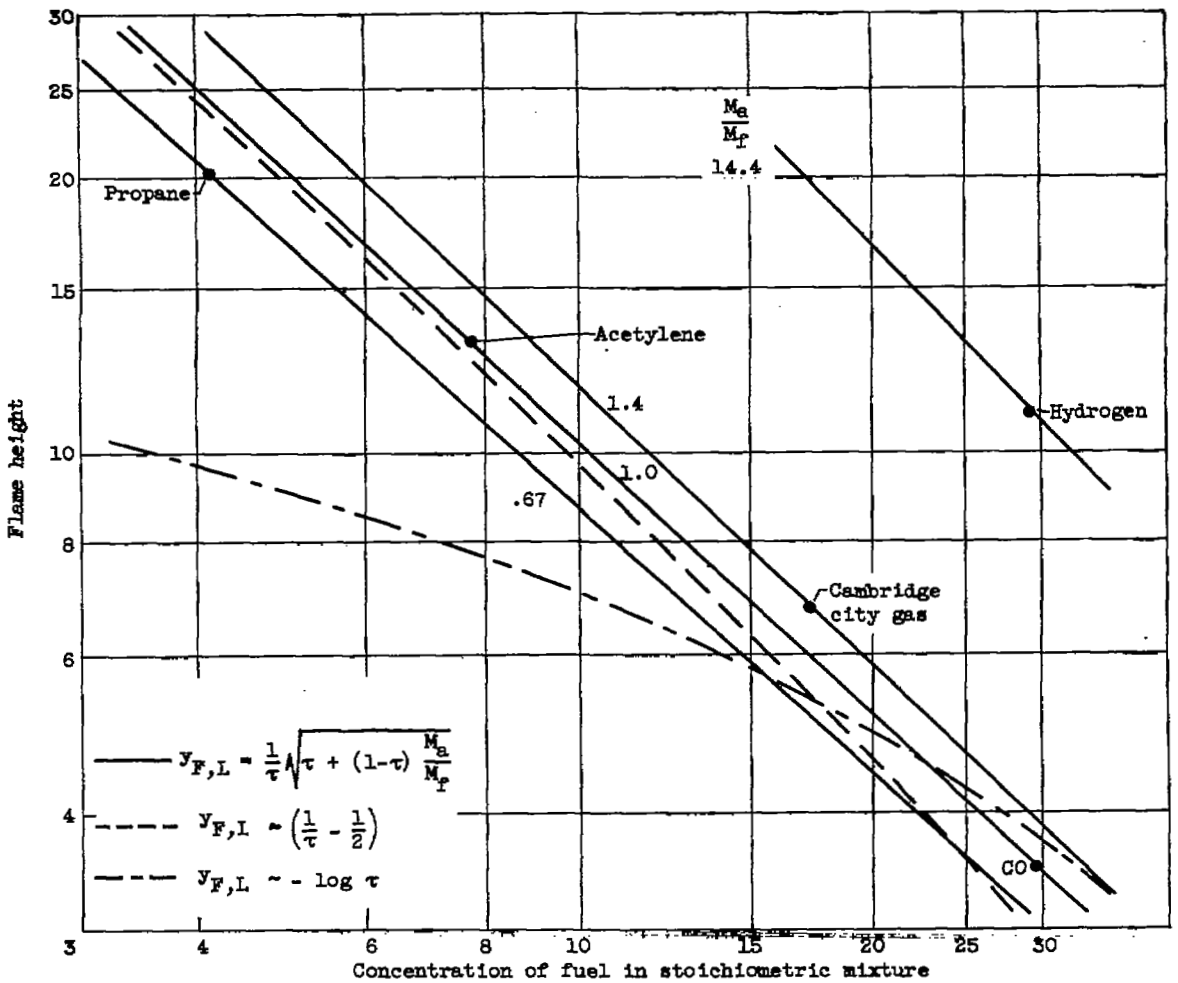

Figure VII-18. - Comparison of calculated curves and experimental data for five fuels (ref. 1).

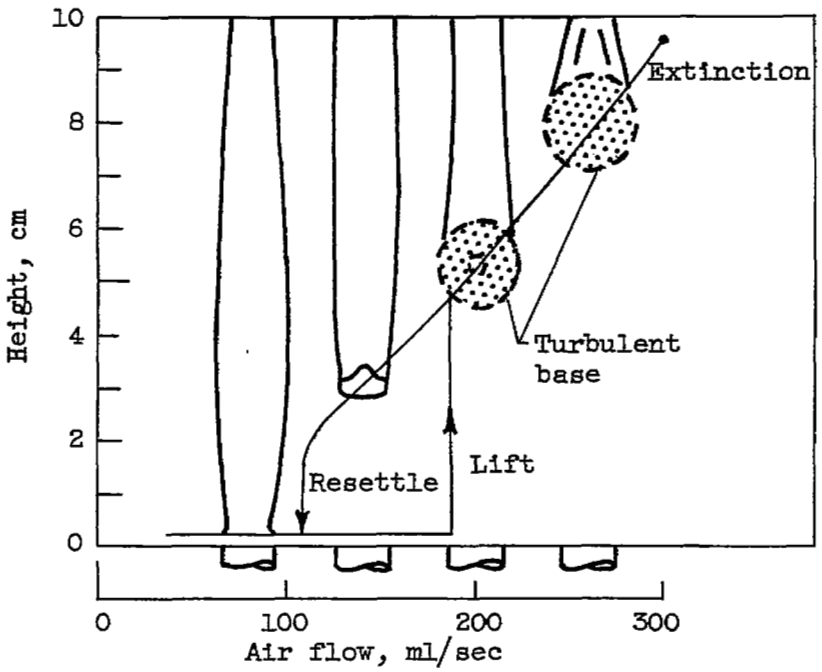

Figure VII-19. - Flame lifting. Butane flow, 10 millimeters per second (ref. 10).

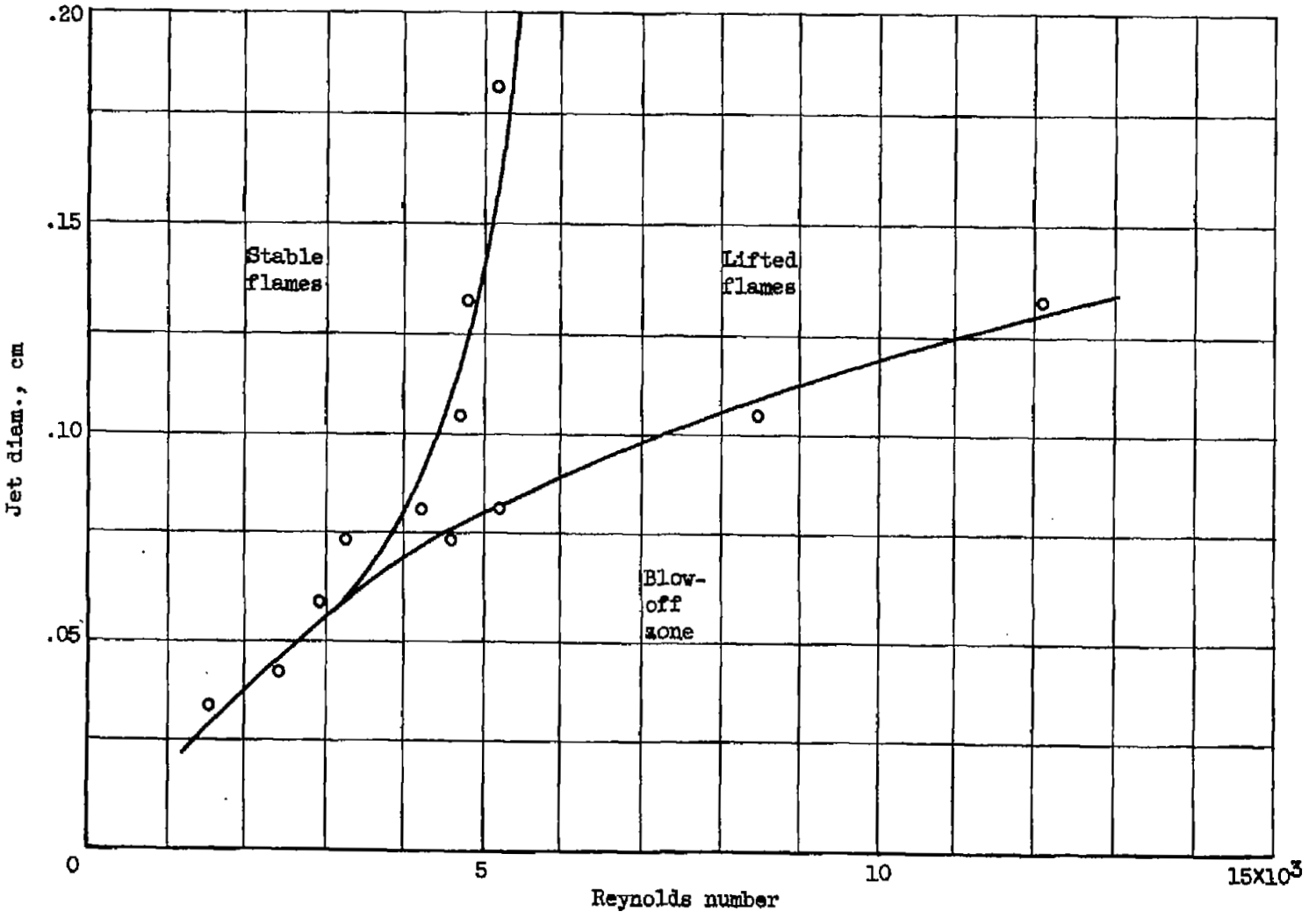

Figure VII-20. - Stability ranges of diffusion flames on carburetor-type jets (ref. 14).

3092

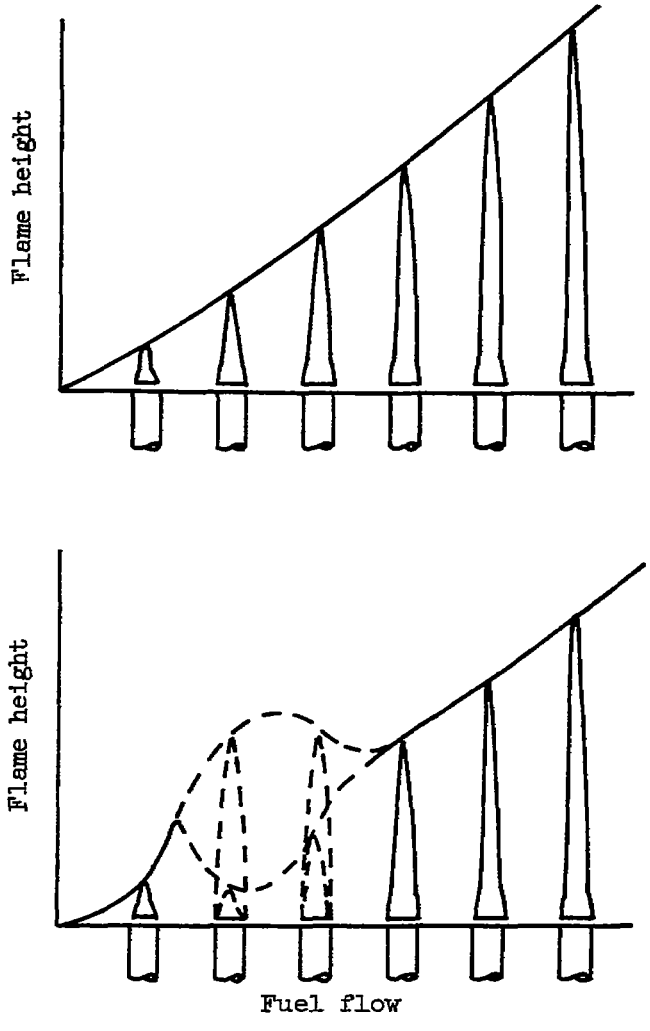

(a) With and without oscillations.

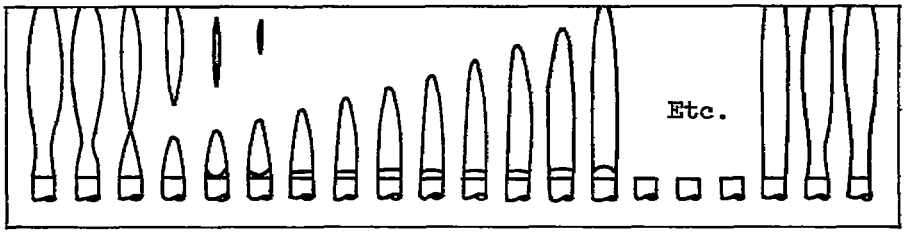

(b) Instantaneous changes in flame appearance.

Figure VII-21. - Effect of fuel flow on flame height (ref. 2).

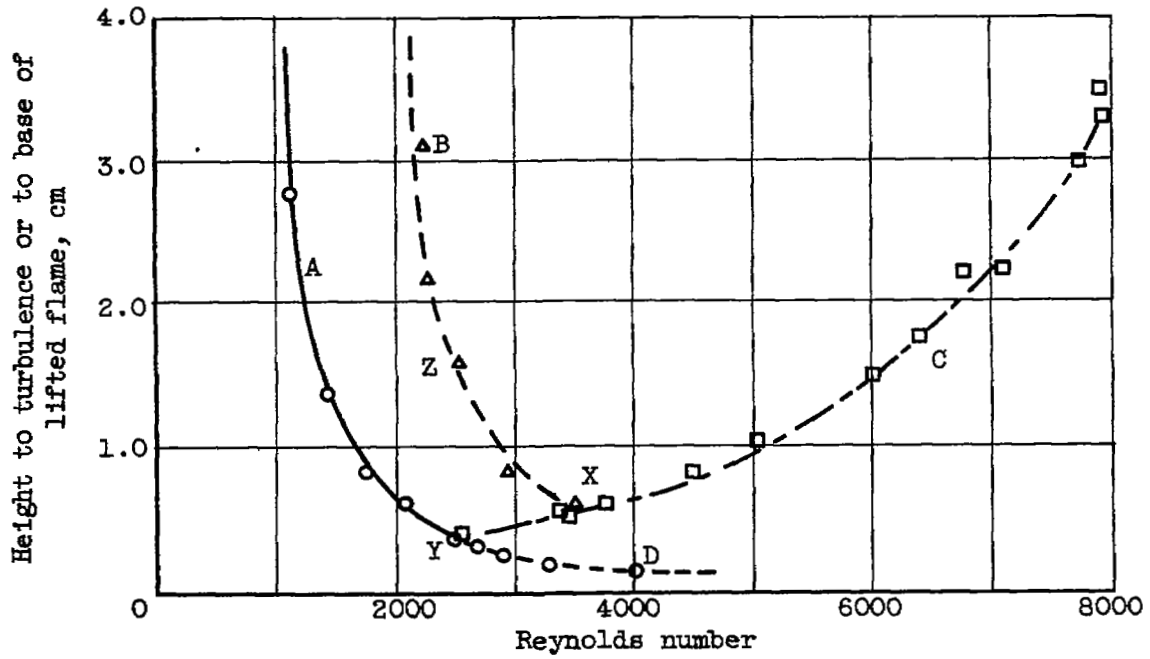

Figure VII-22. - Diffusion flame stability diagram showing: A, height to turbulence in unignited jet; B, height to turbulence in presence of seated flame; C, height to flame base of lifted flame; and D, height to turbulence in presence of lifted flame (ref. 14).

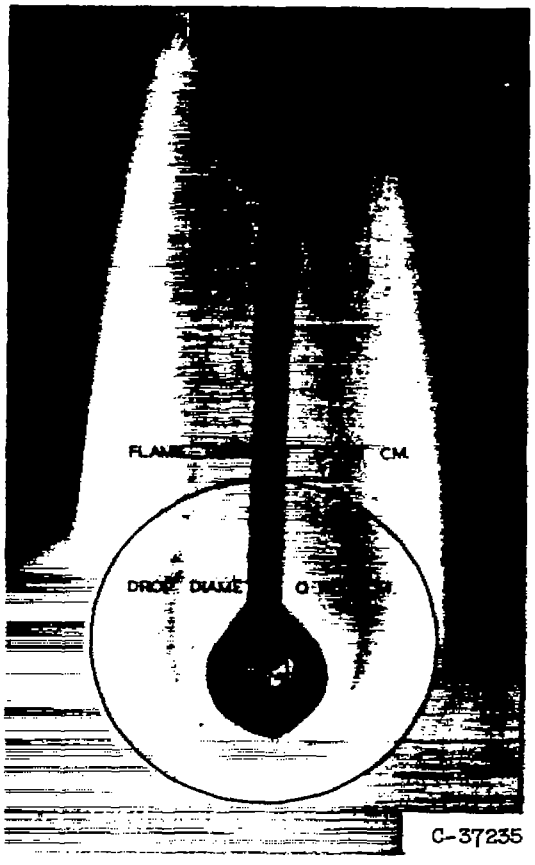

Figure VII-23. - Burning benzene drop (ref. 29).

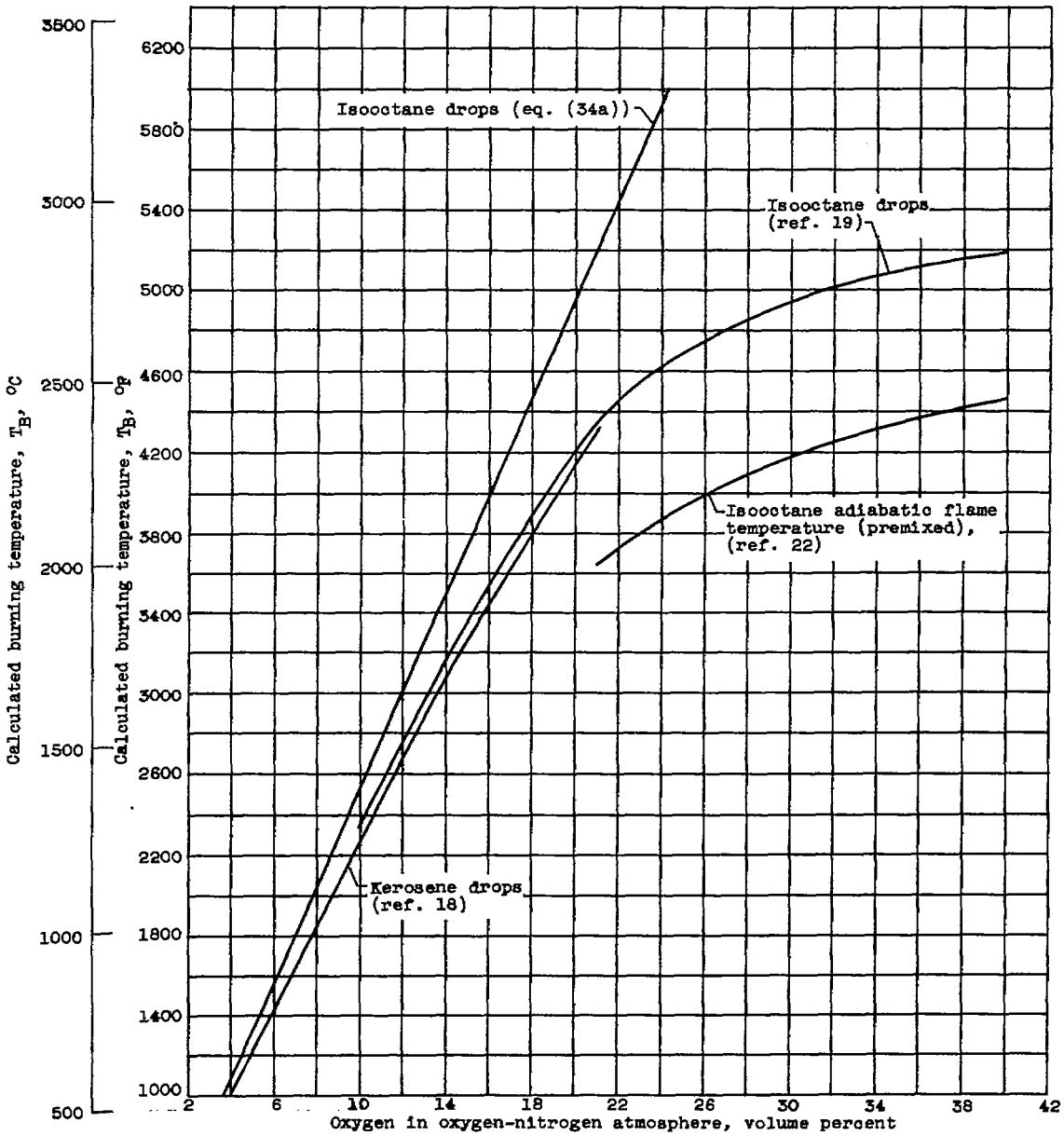

Figure VII-24. - Calculated burning temperatures. Initial temperature, 77° F.

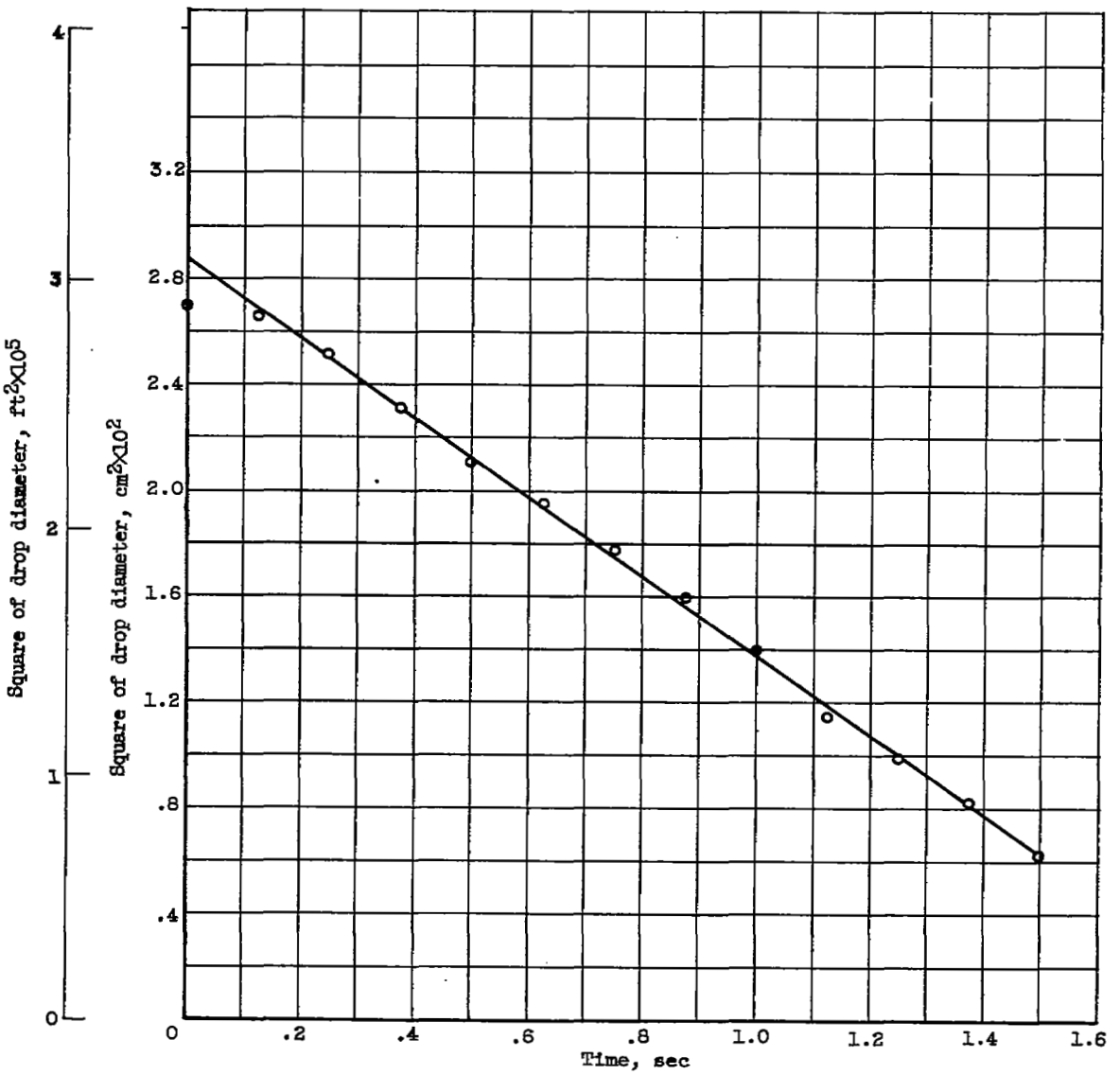

Figure VII-25. - Time variation in diameter for drop of isooctane burning in oxygen-nitrogen atmosphere containing 34.9 percent oxygen (ref. 19).

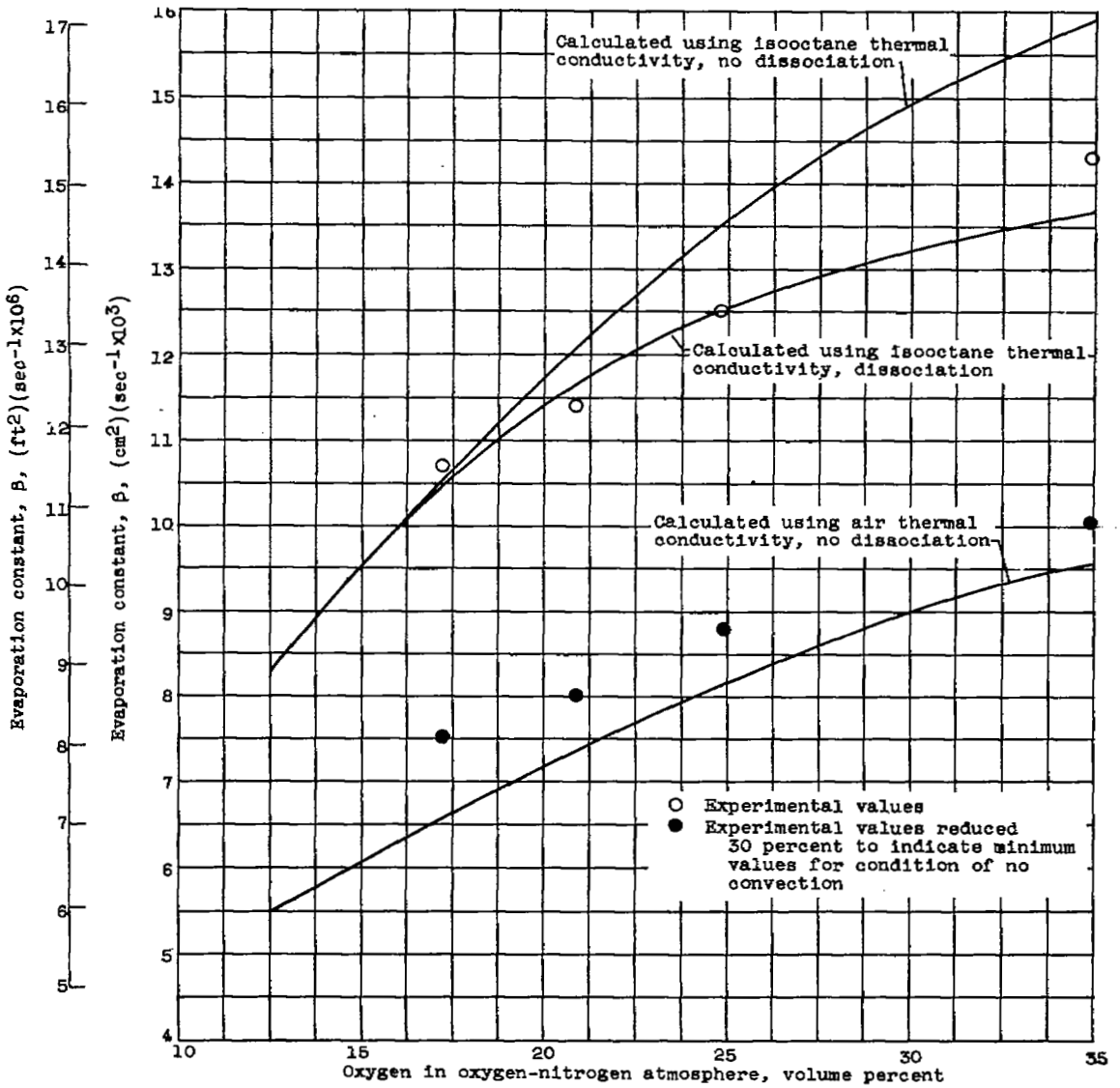

Figure VII-26. - Comparison of calculated and experimental evaporation constants for isooctane drops (ref. 19).

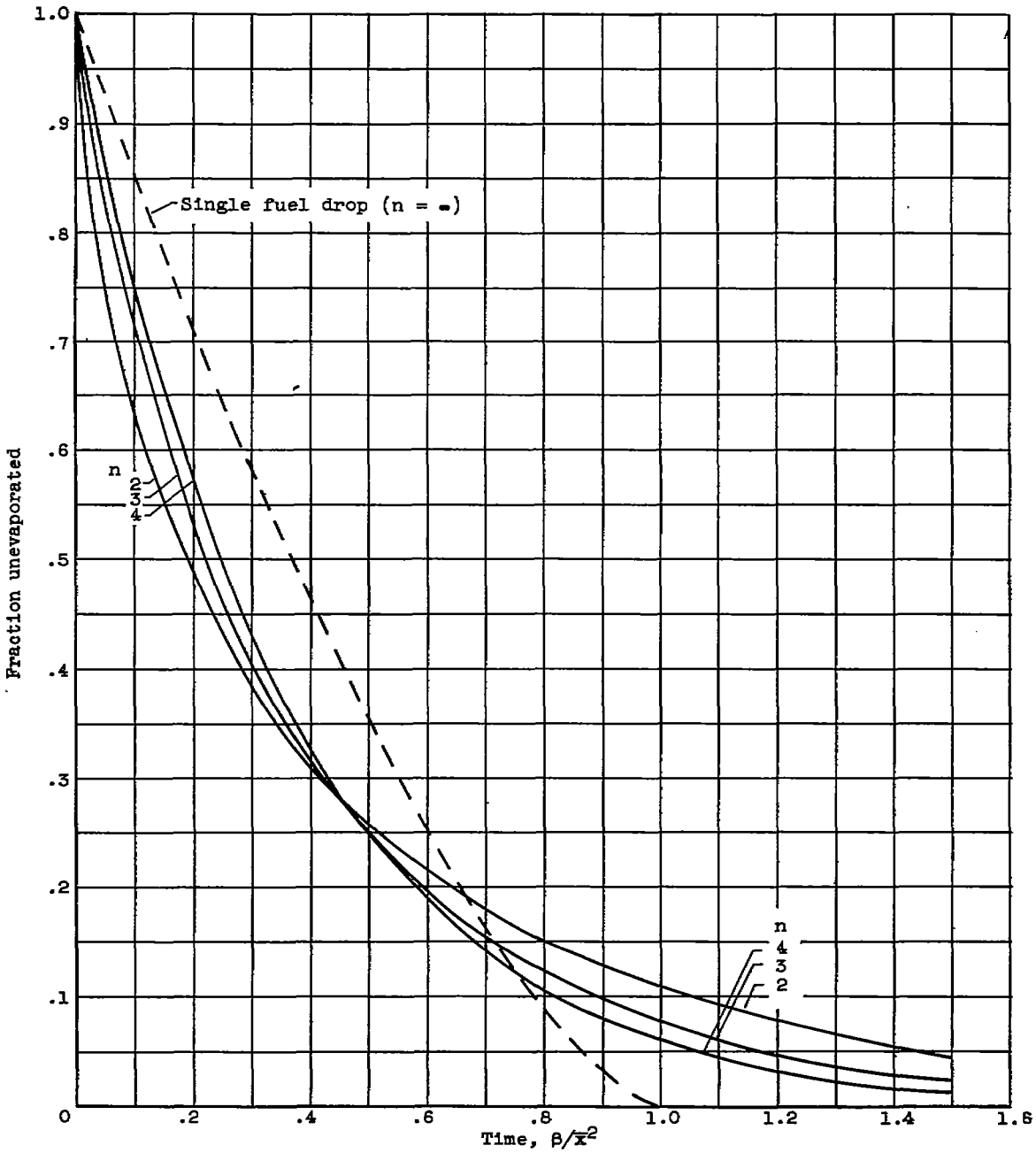

Figure VII-27. - Evaporation of fuel spray (ref. 37).

[redacted]

CHAPTER VIII

OSCILLATIONS IN COMBUSTORS

By Perry L. Blackshear, Jr. and Warren D. Rayle

INTRODUCTION

3137

High-performance jet-engine combustors designed for steady-flow operations frequently and sometimes unexpectedly exhibit periodic flow oscillations, which are usually audible. The frequencies of these sounds range from the 20 to 30 cps buzz of a ram-jet engine to the 1000 to 3000 cps screech of a high-performance afterburner. Some type of combustion oscillation may occur at any point within the engine operating range. These combustion oscillations are accompanied by excursions in pressure and velocity within the combustion chamber. Some observers report beneficial effects due to these velocity and pressure excursions evidenced by a noticeable increase in the combustion efficiency within the combustor. Still more observers report deleterious effects, such as a restricted range of operating conditions or the actual destruction of combustor component parts.

Some modes of combustor oscillation exhibit distribution of pressure and velocity perturbation that can best be described by solutions of the wave equation for an idealized, homogeneous, stationary medium in an enclosure having the dimensions of the combustor. Other oscillations, where the implied wavelength is long compared with the dimension of the enclosure, can better be described by use of a lumped-constant analysis, analogous to the treatment given the Helmholtz resonator. In these analyses, the wave and the enclosure have been the primary elements; the flame and the flow processes have been given cursory treatment. There are types of combustor oscillation, however, where such treatment will not adequately describe the phenomena, but where the combustor components must be considered. Examples of such oscillations might include those involving aeolian tones, modulation of fuel flow or fuel distribution, and recurrent detonation.

Regardless of the system employed to describe the pressure and velocity distribution within the engine, a few general remarks may be made concerning the importance of the flame and the flowing stream in maintaining the oscillation. Any oscillation, whatever its nature, requires a source of energy for its continued existence. Two sources of energy are available in the combustor: (1) the kinetic energy in the flowing gas, and (2) the chemical energy released in the combustion process. Of these two sources, the chemical energy is far greater. However, this energy can only be made available to drive the oscillation through a time-varying work cycle, while the kinetic energy is immediately available for driving the oscillation by means of any of a number of thermodynamic or aerodynamic processes that alternately store and release this energy.

The interaction of the combustion and flow processes within the oscillatory system is complex. The flame zone is not anchored spatially but can move with and be disturbed by the oscillating gas. Meanwhile, the local reaction rates within this mobile zone vary in some manner with the time-varying pressures and temperatures. These local rate variations act as sources of acoustic waves whose combined effect is to drive the oscillation.

In this chapter, the analyses that have been found useful in identifying modes of combustor oscillation are summarized. The manner in which departure from the

assumed ideal condition affects mode identification is discussed, and methods whereby an identified mode may be controlled or eliminated are suggested. An effort is made to formulate a coherent picture of the interaction between the oscillation and the combustion and flow processes in an engine on the basis of the little that is known about such interactions.

MODES OF OSCILLATION

The Burner as a Resonant Room

3137

In almost every case of burner resonance encountered in practice, a portion of the engine containing the fuel in reaction can be assumed separated from the rest of the universe by some acoustic barrier. The resulting enclosure can be treated as a resonant room having certain peculiar acoustic properties. For example, the space between the compressor and the turbine in a turbojet constitutes such a room. In a similar manner, the space between the inlet diffuser and the exhaust nozzle of a ram jet constitutes such a room. The theoretical treatment delineating the modes of resonance possible in a room of a given geometry is available in a number of standard acoustic texts (refs. 1, 2, and others). The rather concise breakdown of the application of these acoustic treatments to a rocket engine given in reference 3 serves as a basis for the following discussion.

The general solution to the wave equation for a cylindrical room closed at both ends with rigid, nondissipative walls is

$$p = \sum_{m,n,n_z} J_m\left(\frac{\pi\alpha_{m,n}r}{R}\right)\cos\left(\frac{n_z\pi z}{L}\right)\left[K_1\cos\left(m\theta + \omega t - \varphi_1\right) + K_2\cos\left(m\theta - \omega t - \varphi_2\right)\right] \tag{1}$$

where

J_m	Bessel function of first kind of order m
K_1,K_2 φ_1,φ_2	arbitrary constants
L	length of enclosure, ft
m,n,n_z	indices
p	perturbation pressure
R	radius of enclosure, ft
r,z,θ	cylindrical coordinates, ft, ft, radians
t	time, sec
$\alpha_{m,n}$	constant, (see table VIII-I)
ω	frequency, radians/sec

A mode of oscillation then can be obtained by giving the constants m, n, and n_z integral values. Since the wave equation is linear, a combination of different modes may exist simultaneously. The frequency for any mode of oscillation in the cylindrical room is given by the formula

$$f = \frac{a}{2}\sqrt{\frac{n_z^2}{L^2} + \frac{\alpha_{m,n}^2}{R^2}} \tag{2}$$

where

3157

a sonic velocity, ft/sec

f frequency, cps

It is of interest to consider three of the simplest modes possible in the cylindrical room. If $m = n = 0$, the mode is the purely longitudinal organ-pipe type of oscillation. For $m = n_z = 0$, the mode of oscillation is purely radial with the gas oscillating back and forth from wall to center of the cylinder uniformly along the length of the cylindrical room. For $n = n_z = 0$, the mode is a purely transverse oscillation where for $m = 1$ the gas sloshes back and forth across a diameter, again uniformly along the length of the cylindrical room. Sketches of the pressure distribution and particle motion for these three simplest cases are given in figure VIII-1. The higher modes of oscillation possible can be computed from equations (1) and (2) with the help of the values of $\alpha_{m,n}$ given in table VIII-I for the first several modes of transverse and radial oscillations for which n_z may or may not be equal to zero.

A similar treatment may be given the annular room (ref. 3) and the rectangular room (refs. 1 and 2). Reference 3 points out the fact, usually omitted by standard acoustic texts, that the transverse mode of oscillation may occur as a traveling wave as well as a standing wave. The pressure distribution for the traveling wave is obtained from equation (1) by taking $K_1 = 0$, $K_2 \neq 0$; or $K_1 \neq 0$, $K_2 = 0$. Figure VIII-2 gives a comparison of the pressure and particle-motion distribution of standing and traveling waves for the first transverse mode.

On the basis of the preceding discussion, it is now of interest to consider the methods whereby such modes of oscillation may be experimentally identified. If the modes actually correspond to the simple solutions of the cylindrical wave equation as discussed herein, for a purely transverse mode, the pressure would undergo a maximum excursion near the wall and go through zero excursion at the center line of the duct. The pressure on opposite sides of the burner would be out of phase for odd transverse modes and in phase for even transverse modes.

If the transverse mode were a standing wave, the oscillatory pressure about a circumference would reach a maximum at the nodal point, vanish at an antinodal point, and so forth. On either side of the antinodal line, the pressure oscillation would everywhere be in phase. If the transverse mode were a traveling wave, the amplitude about the circumference would be everywhere the same, and the phase difference between two points of circumference would be an integral multiple of their angular displacement. A radial wave would have the pressure distribution shown in figure VIII-1. The phasing would be such that the pressure at the center of the duct would be 180° out of phase with the pressure at the wall for odd modes and in phase for even modes.

In both the transverse and radial modes, there would be no change in pressure and phase along the axis of the cylindrical room. In the purely longitudinal mode, however, there should be no change in amplitude or phase across the diameter or around the periphery, whereas there would be a change in amplitude along the axis and a 180° shift in phase every time an antinodal plane was crossed. In selecting a reliable characteristic for the identification of the mode, deviations resulting from the too-radical departure from the assumed ideal homogeneous stationary medium may be considered.

The presence of steady flow through the burner would probably have its greatest effect on the longitudinal resonance. Strong velocity gradients might occur in a radial direction. These would tend to diffract longitudinal waves and concentrate their energy in the region of low effective sound speed. 3137

Temperature gradients would tend to affect almost all the modes of oscillation. For example, reference 4 gives a theoretical effect of an assumed temperature distribution upon the first transverse mode of oscillation in a cylindrical duct. Reference 5 discusses the effect of a sharp temperature discontinuity upon longitudinal oscillation. Reference 6 gives an experimental demonstration of the effect of sharp temperature gradients on the first transverse mode of oscillation in a cylindrical duct. The discussions in references 4 and 6 indicate that, where the gas in one section of a cylindrical duct is executing a uniformly transverse motion, at a temperature gradient, there will be phase shifts and a propagation of the oscillatory motion in the longitudinal direction. Therefore, although the wave equation solution for a transverse standing wave may adequately describe the transverse gas motion, there will be a longitudinal component of the gas motion in the pressure propagation direction. Thus, it would seem that the only possible confusion that could be caused by neglect of velocity and temperature gradients would lie in the identification of a longitudinal mode by a longitudinal pressure survey. Usually, consideration of the frequency alone leads to a rather wide choice of possible modes of oscillation, since sound speed is rarely known accurately.

In burner oscillations, amplitudes are reached that far exceed the values commonly referred to as infinitesimal, for which the wave equation in its linear form applies. Reference 6 shows that for these high amplitude waves almost any wave form tends toward the saw-tooth wave form because of the differing acoustic velocity in the compressed and rarefied gas. This tendency toward saw-tooth form would not necessarily change the frequency of oscillation, since even for waves of as much as 2 atmospheres peak-to-peak amplitude, the apparent propagation rate of a train of waves does not differ appreciably from sound speed. There would be an effect, however, in that the waves constituting either a standing or traveling wave oscillation would be asymmetrical. A very simple way of demonstrating this effect is by considering equation (1) for the case where $m = n = 0$. Since a sum of solutions of the form thus obtained is also a solution of the wave equation, an equation describing a standing wave system composed of saw-tooth waves may be derived:

$$p = \sum_{n_z=1}^{\infty} (-)^{n_z+1} \frac{K_0}{n_z} \cos \frac{n_z \pi z}{L} \cos \frac{n_z \pi a t}{L} \tag{3}$$

where

K_0 arbitrary constant

p pressure

z axial distance, ft

The rather unusual properties exhibited by this standing wave system include an amplitude at the antinode one-half the value at the node; the frequency of the oscillation measured at this point appears to be doubled. Similarly, the phase obtained by measuring the time between pressure peaks will differ from point to point in the region between a node and antinode when the wave is saw-tooth and will vanish when the wave is sinusoidal.

This same treatment cannot be applied directly to the transverse modes, since higher harmonics are not multiples of the fundamentals. In reference 4, the transverse waves of finite amplitude were investigated by retaining the second-order terms in the wave equation. The conclusion was that to second order the waves were smooth and permanent, and no difficulty should arise in basing identification on first-order terms alone. In practice, a rather careful study must be made to ascertain amplitude and frequency distribution about a circumference in order to distinguish between standing and traveling transverse waves. However, the primary aim of mode identification is to give a clue to the best manner in which damping may be applied; therefore, a rigorous determination as to whether a transverse mode is traveling or standing is not important, since the damping of both waves would be the same.

Once the mode has been identified, appropriate damping can be applied by acoustic treatment either of the outer shell, the core of the combustor, or the terminating end of the combustor by various methods suggested in references 1 and 2. Further mention of damping methods is made in a subsequent section. Reference 7 demonstrates the suppression of identified transverse modes in a screeching afterburner by installation of a perforated liner downstream of the flame holder.

The Burner as a Helmholtz Resonator

Both ram-jet engines and turbojet afterburners ordinarily include a subsonic diffuser of smaller cross section than that of the combustion chamber. This geometry is analogous to that of the Helmholtz resonator. A mode of resonance should then be possible wherein the gas in the diffuser oscillates back and forth and that in the combustion chamber undergoes pressure fluctuations. Such a mode of resonance would be less probable in the afterburner, since the pressure drop across the turbine ensures a nearly constant flow of gas into the afterburner.

Like any other form of oscillation, the Helmholtz type requires that energy be available to sustain it. In the ram-jet engine, there are three mechanisms by which the available energy may be applied. The most obvious one is that depending on a time-varying heat-release rate within the combustor. Another relies on a variable pressure recovery of the supersonic diffuser, thus using the kinetic energy of the incoming air to drive the oscillation. Still a third might employ a time-varying temperature or temperature profile at the exhaust nozzle; this would not necessarily imply a varying heat-release rate for the whole combustor.

The effectiveness of varying heat release as a driving mechanism can be easily analyzed. Assume first that the diffuser is of constant area and has a pressure recovery independent of mass flow. Let the temperature rise across the combustion zone be constant; the heat-release variation is produced by variation of mass flow through the (nonstationary) combustion zone. Assume a choked exhaust nozzle and neglect the pressure drop in the combustion chamber. Then, if the density of the hot gas is

$$\rho_h = \rho_c \frac{T_c}{T_c + \Delta T_c} \tag{4}$$

the linear differential equation for the gas motion is found to contain the damping term

$$\left[\frac{\gamma - 1}{2}\left(2\Delta T_C + T_C\right) + \Delta T_C - \left(\frac{q}{Q}\right)\left(\frac{P_C}{p}\right)\gamma\Delta T_C\right]\frac{du}{dt} \tag{5}$$

where

P_C mean combustor pressure

p perturbation combustor pressure

Q mean heat-release rate

q perturbation heat-release rate

T_C mean temperature of gas entering combustor

ΔT_C temperature rise across combustor

γ ratio of specific heats, c_p/c_v

ρ_c, ρ_h densities of gas before and after combustion

For maximum instability, q is assumed to be in phase with p. Instability results, then, only if

$$\frac{qP_C}{Qp} > \frac{1}{2\gamma}\left[(\gamma - 1)\left(2 + \frac{T_C}{\Delta T_C}\right) + 2\right] \tag{6}$$

It is readily seen that, for realistic values of ΔT_C, the criterion becomes nearly

$$\frac{qP_C}{Qp} > 1 \tag{7}$$

The case of Helmholtz oscillation driven by a variable diffuser pressure recovery is treated by reference 8. For isothermal flow, a differential equation is derived to describe the gas motion. It may be written as

$$K_1\frac{d^2u}{dt^2} + K_2\frac{du}{dt} + K_3u = 0 \tag{8}$$

where

$$K_1 = \frac{W_C W_d}{m_2\gamma P A_1} \tag{8a}$$

$$K_2 = \frac{W_C}{\gamma P a_2 M_2}\left(\frac{\gamma - 1}{2}\frac{W_d}{W_C}\frac{m}{m_2}\frac{a_2}{A_1}M_2 - \frac{dP}{dm_2}\right) \tag{8b}$$

$$K_3 = \frac{1}{a_2 M_2}\left(1 - \frac{\gamma + 1}{2\gamma}\frac{m}{P}\frac{dP}{dm_2}\right) \tag{8c}$$

The frequency of oscillation may then be expressed as

$$f = \frac{1}{2\pi}\left[\frac{K_3}{K_1} - \left(\frac{K_2}{K_1}\right)^2\right]^{1/2} \tag{9}$$

3137

where

A_1 area of diffuser inlet, sq ft

a_2 sonic velocity at diffuser exit, ft/sec

f frequency, sec^{-1}

M_2 Mach number of flow at diffuser exit

m total mass flow (mean), slugs/sec

m_2 mass-flow rate (mean) of gas through oscillatory area at diffuser exit, slugs/sec

P total pressure in combustion chamber, lb/sq ft abs

u perturbation velocity, ft/sec

W_c mass of gas in combustion chamber, slugs

W_d mass of oscillating gas in diffuser, slugs

The system is seen to be oscillatory if the quantity K_2 is less than zero. The theoretical frequencies and stability regions are reported in reference 8 to agree reasonably well with experimental values.

When heat is added in the combustion chamber, the analysis becomes more complex. In this case, reference 8 assumes a constant rate of heat release. This part of the investigation, then, includes oscillations driven by a time-varying temperature profile at the exhaust nozzle and by a variable diffuser pressure recovery. The effect of heat addition is to further reduce the region of stable operation for a given configuration. A typical result is presented in figure VIII-3 (ref. 8). This figure shows stability regions computed for isothermal as well as combustion conditions. The oscillation frequencies predicted were found in reference 8 to be considerably lower than those observed. The observed frequencies were sufficiently high that the possibility of standing-wave resonance should be considered.

The third factor by which a Helmholtz oscillation may be driven is a variable exhaust temperature. Since the exhaust is usually choked, an increase in gas temperature produces a decrease in mass flow. The analysis of reference 8 does not deal with this effect alone. However, since the heat-release rate is assumed constant, the variation in exhaust temperature with mass flow can be considered to account for the decreased stability accompanying combustion (fig. VIII-3).

In the actual engine, the stability depends on all three factors. Potential instability with respect to one may be overcome by the effects of the others. The analyses available are necessarily simplified, a mathematically rigorous treatment being impossible for a real engine. The stability criteria should nevertheless be indicative.

Departures from the idealized condition will affect both the actual stability region and the actual frequencies. The effect of through-flow has been included in the analyses; the effects of finite sound level, spatial temperature gradients, and nonlinear performance of exhaust and diffuser have not been completely discussed. Insofar as the stability criteria are concerned, the ultimate amplitude of the oscillation is probably not important. The criteria merely state that under certain conditions infinitesimal disturbances will be amplified. It is possible that additional instability will result from finite disturbances, or triggers; the effect of flow disturbance on heat release cannot be expected to remain linear at high amplitude. 3137

To prevent the Helmholtz-type oscillation, the driving forces must be reduced or opposed. The driving force due to varying diffuser pressure recovery can be reversed by using a diffuser with an appropriate characteristic, that is, a diffuser whose pressure recovery decreases as the mass flow increases. The driving due to varying heat release can be reduced or reversed by (1) reducing the sensitivity of the combustion process to velocity or pressure fluctuations, and (2) bringing any residual perturbations as far as possible out of phase with the burner pressure. The driving by varying exhaust temperature can be altered by (1) making the exhaust temperature insensitive to velocity and pressure fluctuations, and (2) controlling the residence time of the hot gas and hence the phasing of the reflected pressure.

According to reference 8, the least oscillation should be found for a configuration employing a long diffuser and a small combustion-chamber volume. The reduction of the sensitivity of the combustion process might result from (1) removing the flame holder from the high-velocity perturbation region, and (2) using a fuel whose reaction rate is little affected by variation of pressure and temperature.

Damping by the use of tuned resonators attached to the combustion chamber has been proposed and experimentally investigated. Reference 9 showed that such a resonator, tuned from 43 to 64 cps, was effective in suppressing pulsations in a ram-jet engine. These pulsations, without the resonator present, occurred at about 20 cps. Suppression of pulsations was obtained over a small part of the diffuser operating range.

Control by viscous damping seems impractical, though theoretically a large friction loss in the diffuser would be effective. Another theoretical possibility would be to contrive a pressure-sensitive exhaust nozzle so that its effective area would increase with pressure.

Systems of Oscillation with Nonacoustic Elements

It was found in reference 10 that vortices shed from a bluff object in a duct could excite longitudinal resonance in the duct. The frequency of vortex shedding from a cylindrical rod is given as

$$f = 0.185 \frac{v}{D} \tag{10}$$

where

D rod diameter, ft

f frequency, sec^{-1}

v stream velocity, ft/sec

The length of the duct in this case could be varied until the frequency of vortex shedding and that of a mode of resonance in the duct coincided, at which time a rather large amplitude oscillation would ensue. The separation of the boundary layer from a rod is but one of the forms of separation that can occur in the complex interior of a jet-engine combustor and that can interact with the gross flow to excite either a longitudinal, a radial, or a transverse mode of oscillation of the burner enclosure.

3137

When the frequency of vortex shedding coincides with the frequency of the supported cylindrical rod, the ensuing vibration is greatly amplified. This is the source of the musical note in the aeolian harp and is given a rather general investigation by Strouhal (discussed in ref. 2).

Another form of oscillation involving nonacoustic elements is discussed in reference 11. A flow disturbance in the combustion chamber created a pressure pulse that traveled upstream and modulated the rate of fuel flow from a fuel injector. The modulated fuel-air mixture then traveled downstream at stream velocity, arrived at the combustion chamber, caused a change in pressure in the combustion chamber, and sent a corresponding pressure pulse upstream to repeat the cycle. The frequency of oscillation for this type of nonacoustic vibration is given as

$$f = \left[2\left(\frac{d}{v} + \frac{d}{a - v}\right)\right]^{-1} \tag{11}$$

where

a sonic velocity, 1280 ft/sec

d distance from igniter to injector, ft

v stream velocity, ft/sec

Also discussed in reference 11 is a type of oscillation involving recurrent detonation originating in the boundary layer of a duct filled with a combustible mixture. The frequency of this type of oscillation can be determined from equations (1) and (2) of reference 2.

All these types of oscillations would be affected by the acoustic damping discussed previously; however, special treatment may be given these types of oscillations. For example, the physical structure of the offending strut can be modified either in its rigidity or in its size and location so that its natural frequencies differ from the excitable frequencies of the burner enclosure. For the second type of oscillation, the injection pressure can be increased to render the fuel-injection system relatively insensitive to small fluctuations in the combustor pressure. The oscillation involving recurrent detonation was controlled in reference 11 by the injection of chain-breaking additives in the boundary layer of the combustion chamber immediately downstream of the flame holder.

Reference 12 uses a quasi one-dimensional plane wave theory to express pressure-time relations in a buzzing ram jet. This isothermal pulsation is assumed to be triggered by flow separation in the diffuser. The consequent momentary reduction in mass flow is accompanied by a shift in the location of the normal shock and by

pressure and rarefaction waves that propagate into the combustor. These waves are reflected back and forth between the exhaust and the diffuser as the engine pressure slowly regains its original value. Then the cycle repeats.

The characteristic of this type of instability is the nonsinusoidal nature of the perturbation of the inlet mass flow. For as much as 70 percent of the cycle this flow is constant. At any station in the combustion chamber, the pressure first undergoes a sharp decrease, then climbs slowly back to its original value, at the same time being modulated by the reechoing pressure-rarefaction couplets. Various predicted pressure-time curves are shown by reference 12 to correspond amazingly well with experimental ones (fig. VIII-4).

This type of pulsation is not combustion-driven. It is of interest as a representative of nonsinusoidal vibration systems, analogous to the electronic relaxation oscillator. These systems differ from the sinusoidal oscillators in that not even an infinitesimal disturbance is needed to start the cycle.

3137

INTERACTIONS

Elements Disturbed by Velocity and Pressure Oscillations

The nature of steady flow through diffusers, around obstructions, through perforated liners, and particularly through the flame zone is poorly understood. Any attempt to describe processes that occur when pressure and velocity oscillations are superimposed on the steady flow may appear presumptuous. The fact remains, however, that in the real combustor real oscillations do exist. Even though discussing the effects of these oscillations on the processes that take place in a combustor may be considered sheer speculation, it is felt that to speculate is potentially more profitable than to ignore.

There are a number of possible effects that combustor oscillations may have on the boundary layers existing in the various component parts of the burner. Some of the effects can be extremely violent, such as the increase in heat-transfer rate to the outer shell during screeching burning (ref. 13). A possible explanation for this effect is given in reference 3, which states that the velocity of the gas adjacent to the wall is increased during screech by means of the transverse mode of oscillation.

There is no clear-cut demonstration of the effect of oscillations on the overall build-up and separation of a boundary layer on a straight wall. In some theoretical studies of boundary-layer growth, the amplification of disturbances of a sinusoidal nature has been considered as a possible explanation for the transition from a laminar to a turbulent boundary layer (ref. 14). Since, in most cases, the boundary layer in the combustion chamber will already be turbulent, the possible intermittent separation and attachment of a boundary layer should be considered. The synchronizing of the shedding of a bound vortex on a rod with duct oscillations has already been cited (ref. 10). Reference 15 states that, when a flame is seated on the rod, the vortices no longer shed but become bound and, in most cases, symmetric. The literature is not in unanimous agreement on this point. Reference 16 indicates that, near blow-out, vortex shedding with combustion does occur. With combustor oscillations, there certainly seems to be evidence of something resembling vortex shedding in the wake of a flame holder, as can be seen from the excellent schlieren photographs of a ram-jet flame during screech in reference 13.

Of general interest regarding the influence of flow fluctuations on a vortex train in the wake of a cylinder with and without combustion is reference 17. Here, the following velocity profile is examined for neutral stability:

$$U = fk \operatorname{sech}^2 (\Phi y) \tag{12}$$

where

f, Φ functions of viscosity, distance, and initial stream momentum

k constant of integration

U velocity

y distance perpendicular to direction of flow

Equation (12) was found (ref. 18) to represent profiles of mixing plane jets and wakes. It was found that the disturbance vortices (for unsymmetric disturbances) formed two trains a distance h apart, alternately aligned as in the Kármán vortex street. The relation between h and the distance λ between vortices in a single train is given in reference 17 as

$$\frac{h}{\lambda} = \frac{2}{\pi} \tanh^{-1} \frac{1}{2\Phi k}$$

whereas, for the Kármán street,

$$\frac{h}{\lambda} = \frac{1}{\pi} \tanh^{-1} \frac{1}{\sqrt{2}}$$

or the two agree if

$$\Phi k = \frac{1}{\sqrt{2}} \pm \frac{1}{2}$$

Since vortex occurrence in wakes is possibly connected to the stability of a mean wake profile, the problem can be further simplified by an approximation of the profile with a broken-line V-profile (ref. 2) and a study of the effect of density variations. It is found that the wavelength of the neutral disturbance of the V-profile is the same as for equation (12) when the V is of comparable width, and that reducing the density of the wake gases has a stabilizing influence, but does not render the profile completely stable, at wavelengths large compared with the profile width. This is in qualitative agreement with the data of reference 15. The interaction, then, is this: Acoustic oscillations supply the initial amplitude to a flow disturbance in a wake, which subsequently grows, decays, or remains unchanged, depending on the wavelength of the disturbance.

In reference 5, a study was made of the superimposed steady and time-varying flow through a 1/2-inch-diameter thick-plate orifice. The thickness of the time-varying flow boundary layer depended on the Reynolds number of the steady component of the flow. The time-varying flow profile through the orifice was essentially that computable from the potential flow theory, except for a thin boundary layer that depended on the Reynolds number of the steady flow, as shown in figure VIII-5.

The effects of pressure and velocity oscillations on fuel flow and on mixing rates depend largely on the types of oscillations involved and the location and design of the fuel-injection systems. The pressure pulsations may directly modulate the fuel-flow rate during the oscillation. The major effect on the mixing rate, however, will be that of the time-varying velocity, which will be most strongly felt when the oscillation contains radial or transverse components.

Most studies to establish the fundamental nature of flame-stabilizing elements have recognized that flow oscillations greatly affect the performance of flame stabilizers. Reference 15 reported that, when resonance was encountered, blow-out velocity data could not be reproduced. The possibility of duct resonance in the study reported in reference 15 was removed by placing the flame stabilizer near the exhaust of the test duct so that only a small portion of the stabilized flame remained enclosed in the duct. A number of investigators have mentioned the fact that increasing duct length appears to increase the instability of a burning engine. This trend is illustrated by unpublished NACA data in figure VIII-6, which shows blow-out limits for several different velocities as a function of tail-pipe length and fuel-air ratio. The factor affecting both the flame stability and the heat-release rate is the previously mentioned tendency of the time-varying flow to follow potential flow streamlines. This tendency is shown by the sequence of photographs in figure VIII-7. Thus, a velocity disturbance at the flame holder, rather than separating at the downstream edge and allowing for a sheltered zone where recirculation may occur, will cause a penetration of this sheltered zone by an amount dependent upon the amplitude of the disturbance. The effect of this potential flow about the flame holder, then, will be (1) to hinder the recirculation in the wake of the flame holder by an inclusion of cold gas, and (2) to extend the flame-front area at the flame holder, this extension then flowing downstream at about stream velocity.

It is felt that the wrinkling of a flame front at a flame holder is one of several ways in which the flame area or the heat release may be varied during an oscillation. The sequence of photographs (ref. 5) in figure VIII-7 shows the time history of a wrinkle from its generation at a flame holder to its disappearance at the flame tip.

Reference 19 points out that the stability of a hot-cold interface is markedly affected by the accelerations occurring during acoustic resonance. The effect of acceleration is to destabilize if the acceleration vector has the same direction as the density gradient (refs. 20 and 21).

Data of reference 19 show that a flat flame breaks periodically into cellular flamelets in a resonating tube in phase with the gas acceleration. The phase relation required by the Rayleigh criterion for driving standing waves by heat addition is thus met. The oscillations and the cells occurred in all fuel-air mixtures tested, but amplitudes were greatest in those mixtures in which cells formed spontaneously, that is, in downward propagating flames that were unstable in spite of the stabilizing effect of gravity.

To treat this problem theoretically, a periodically varying acceleration was substituted for the gravity acceleration in the flame-front stability equations (ref. 19), and remarkably good agreement with experiment was achieved. The same sort of substitution can be made in the stability analyses of references 20 and 21, in which a continuous-velocity distribution is assumed parallel to a sequence of discontinuities in densities.

One general conclusion might be drawn from these stability considerations; the flame front can be desensitized if the density gradients are not parallel to probable acceleration vectors. Some of the oscillations encountered in jet engines reach such violence that it is possible that large reaction-rate changes accompany the oscillations. Whatever the direct cause of the increase in reaction rate, the oscillation is certainly conducive to high performance in some cases. For example, reference 6 showed that during a screech condition the combustion efficiency for a simulated afterburner was 92 to 98 percent, dropping to 65 percent with the cessation of screech. The effects of oscillations on nozzle and diffuser performance are to date unknown.

A few general remarks may be made about the location of the disturbed elements. It has been shown that in some cases a velocity fluctuation causes the sensitive element to be disturbed; whereas, in other cases the pressure fluctuation is responsible. Thus, if the oscillation consists of a standing wave, the maximum pressure variations will be found in those parts of the burner where the velocity fluctuations are least, and vice versa. In this case, the resonance may be reduced by judicious location of the sensitive elements far from their exciters. Such a remedy is not available, however, if the mode of oscillation is one in which traveling waves dominate.

3137

Effects of Feedback Loops on Pressure and Velocity

In general, any self-excited oscillation may be considered to involve a feedback loop, that is, a means by which the effect of a given signal is ultimately to generate another such signal. When very-high-frequency oscillations (wavelengths on the order of a burner diameter) are involved, the signal will probably be acoustic throughout the cycle and will therefore travel at velocities of 1200 to 3000 feet per second. At lower frequencies, the feedback loop may comprise such elements as variation of gas composition, which will be transported at stream velocities.

If the oscillation is assumed to be combustion-driven, each cycle will include a variation of heat release that may be either local or over-all. This variation will, in turn, produce pressure and velocity waves moving upstream at a speed $a_1 (1 - M_1)$, and downstream at $a_2 (1 + M_2)$. A composition and a temperature irregularity will also be generated and will move downstream at a velocity $a_2 (M_2)$. The problem then becomes one of defining the possible methods whereby these waves can produce subsequent changes in the heat-release rate.

If the gas velocity is sonic at the exhaust, an impinging pressure wave will reflect, and a pressure wave will then propagate upstream. A momentary increase in temperature, on the other hand, will be transformed into a rarefaction wave traveling upstream. These waves may affect the heat release as they pass through the combustion zone by modifying the pressure and temperature therein, or they may have an indirect effect after passing through the combustion zone. In the latter case, the effect of sound waves traveling upstream from the combustion zone may be considered, regardless of whether the waves originate in the time-varying combustion or whether they have already reflected from the exhaust nozzle. Such waves may affect the subsequent heat-release rate in many ways, among which are (1) changing the flame area as the wave passes the flame holder, (2) changing the velocity profile upstream of the flame holder, (3) altering the local fuel-air ratio as the wave passes the fuel injectors, (4) altering the mass-flow rate into the diffuser, and (5) reflection from the inlet diffuser followed by any of the aforementioned interactions.

This summary of possible interaction is intended to be suggestive rather than exhaustive. Additional signal channels such as the shedding of vortices, mechanical vibration, and modulation of fuel spray or fuel evaporation characteristics should be noted.

The fundamental frequency for any loop can be determined as the reciprocal of the time required for the signal to travel the loop:

$$f = \left(\sum \frac{L_i}{V_i}\right)^{-1} \tag{13}$$

where

L_i length of loop segment, ft

V_i velocity of signal in loop segment, ft/sec

Although it is impossible to assign a given loop definitely to a known frequency, it is possible to eliminate from consideration those channels requiring unduly long or short intervals. Some caution is necessary; if various channels are simultaneously active, the frequency need not be the fundamental of all and may not be the fundamental of any. It is highly probable that, with the multiplicity of potential feedback loops, many may contribute to any given frequency of oscillation. It is likely that the mode of resonance selected by the burner will be that for which the energy released from the individual feedbacks is greatest.

All the feedback loops considered have one element in common; the signal is carried upstream as an acoustic wave. This suggests the possibility of controlling these oscillations either by damping this wave or by desensitizing the elements it will affect. One method of damping might be to provide channels of varying acoustic length from the flame holder to the region of interest, so that the original wave would be broken down into a series of smaller waves arriving one after another.

The case of oscillation of very high frequency can be considered analogous, except that the signal may be propagating transversely for much of the cycle.

SIGNIFICANCE OF RESONANCE STUDIES IN DESIGN OF JET-ENGINE COMBUSTORS

Design Criteria Based on Mode of Resonance

The application of results of resonance investigations to the design of jet-engine combustors is somewhat limited because of the opposing requisites for good combustion and less resonance. From acoustic considerations, the features of current combustors are more likely to produce than to reduce resonance. Current designs are symmetrical, smooth, hard, and uniform. On the other hand, less resonance would be anticipated if no two surfaces reflected waves alike, absorbed waves alike, nor had parallel walls. The optimum combustor design must necessarily be a compromise between the two extremes.

In the actual design of the combustor, the simplest rule to apply would be to acoustically soften those parts of the combustor where possible modes of oscillation would have pressure maximums. Thus, for the longitudinal wave, the softened part of the burner should be at the terminations and at the walls near the terminations. For transverse modes of oscillation, the wall surrounding the region where the transverse oscillation might occur would be indicated. If the walls are softened by use of some sound-absorbing material such as filaments of glass or steel wool behind a perforated shell, it might be well to place such sound-absorptive material in a random distribution of patches, random both in size of patch and in location upon the wall.

If the flame is driving the oscillations, and it appears that this is the case in a large number of instances, it is well to keep the flame away from regions where the pressure goes through its maximum excursion. This means that the maximum reaction zone should be kept away from pressure loops in the standing wave: away from the terminating ends of the combustor in the case of longitudinal standing wave, and away from the wall in the case of transverse standing wave. If the combustor is of such a nature that stratification of hot and cold gases is implicit in the design, such hot and cold patches might be sized and spaced to act as sources of wave interference.

After measures to reduce oscillations have been applied, it may be found that a given combustor still oscillates at particular operating conditions. If the mode of this oscillation can be identified, corrective measures specific to that mode may then be applied. Table VIII-II gives a summary of corrective measures for specific modes of oscillation.

Design Criteria Based on Sensitivity of Disturbed Elements

If a component part of the combustor such as the flame holder is a sensitive element in the feedback loop causing the self-excited oscillation, at least one design criterion can be employed. If the element is sensitive to velocity or pressure, it can be moved from the locus of maximum velocity or pressure excursion. Other remedies equally as obvious would be either to desensitize the sensitive element completely or to shift its sensitivity to a frequency range that does not correspond to a possible mode of oscillation in the combustor. Some sensitive elements can be desensitized. For example, a fuel-injection nozzle that can be influenced by pressure pulses could be desensitized by increasing the pressure drop across the injector. A fuel-air mixture could be desensitized by the selection of either a new fuel or a fuel additive that would cause a diminished response of the combustion process to disturbances in pressure and temperature.

The Future for Combustion Oscillation

There is an ever-growing group of workers who believe that combustor oscillation has evidenced such impressive advantages that a far more profitable course to follow would be to study the control and use rather than the elimination of oscillation. Measurements indicate that a work cycle over and above the steady-state work cycle is involved in the oscillatory motion; therefore, there is clearly a large quantity of energy added to the gas in part in the form of additional mixing. Combustors designed to operate at low over-all fuel-air ratios have been shown to perform best if the combustion occurs in mixtures near stoichiometric with the combustion products subsequently diluted with the remainder of the air. The screech cycle might well be used to expedite this mixing. It is not clear how much of this extra energy is directly available for producing thrust.

References 6 and 13 show that in the case of screech the maximum pressure amplitude in a transverse oscillation occurred in a very short region relative to the over-all length of the combustor. If the burner were strengthened only in this region to allow for continuous operation without shell failure, the increased combustion efficiencies accompanying screech might be retained without a prohibitive weight penalty.

In recent years, the pulse jet has not been considered a high-priority propulsive unit. Consequently, propulsive units employing intermittent combustion have not been the subject of intensive investigation. In view of the multiplicity of possible modes of oscillation in cavities of various shapes, it might be concluded that some high-frequency combustor oscillation exists that offers advantages over and above those of the pulse jet or the ram jet. Oscillations in combustors have appeared in many forms since the advent of jet propulsion. It would seem a safe guess that still more and different appearances lie ahead. A great deal of work on momentum and mass transport, combustion, and allied subjects in a nonsteady, nonhomogeneous flow field is needed before the current and future oscillations in combustors can be intelligently handled.

REFERENCES

1. Morse, Philip M.: Vibration and Sound. McGraw-Hill Book Co., Inc., 1936.

2. Rayleigh: The Theory of Sound. Vol. II. Dover Pub., 1945.

3. Smith, R. P., and Sprenger, D. F.: Combustion Instability in Solid-Propellant Rockets. Fourth Symposium (International) on Combustion, The Williams & Wilkins Co. (Baltimore), 1953, pp. 893-906.

4. Moore, Franklin K., and Maslen, Stephen H.: Transverse Oscillations in a Cylindrical Combustion Chamber. NACA TN 3152, 1954.

5. Blackshear, Perry L., Jr.: Driving Standing Waves by Heat Addition. NACA TN 2772, 1952.

6. Blackshear, Perry L., Jr., Rayle, Warren D., and Tower, Leonard K.: Experimental Determination of Gas Motion Accompanying Screeching Combustion in a 6-Inch Simulated Afterburner. NACA RM E53I28, 1953.

7. Harp, James L., Jr., Velie, Wallace W., and Bryant, Lively: Investigation of Combustion Screech and a Method of Its Control. NACA RM E53L24b, 1954.

8. Sterbentz, William H., and Evvard, John C.: Criterions for Prediction and Control of Ram-Jet Flow Pulsations. NACA RM E51C27, 1951.

9. Fox, Jerome L.: Preliminary Investigation of Helmholtz Resonators for Damping Pressure Fluctuations in 3.6-Inch Ram Jet at Mach Number 1.90. NACA RM E51C05, 1951.

10. Shonerd, David E.: Studies of Flame-Front Oscillations. Jet Propulsion Laboratory, California Institute of Technology Report No. 3-18, 1952.

11. Fenn, J. B., Forney, H. B., and Garmon, R. C.: Burners for Supersonic Ram-Jets. Ind. and Eng. Chem., vol. 43, no. 7, July 1951, pp. 1663-1671.

12. Trimpi, Robert L.: An Analysis of Buzzing in Supersonic Ram Jets by a Modified One-Dimensional Non-Stationary Wave Theory. NACA RM L52A18, 1952.

13. Bragdon, Thomas A., Lewis George D., and King, Charles H.: Interim Report on Experimental Investigation of High Frequency Oscillations in Ramjet Combustion Chambers. M.I.T. Meteor Rep. UAC-53, Res. Dep., United Aircraft Corp., Oct. 1951. (BuOrd Contract NOrd 9845.)

14. Lees, Lester: The Stability of the Laminar Boundary Layer in a Compressible Fluid. NACA Rep. 876, 1947. (Supersedes NACA TN 1360.)

15. Scurlock, A. C.: Flame Stabilization and Propagation in High-Velocity Gas Streams. Meteor Rep. 19, M.I.T., May 1948. (Contract NOrd 9661.)

16. Nicholson, H. M., and Field, J. P.: Some Experimental Techniques for the Investigation of the Mechanism of Flame Stabilization in the Wakes of Bluff Bodies. Third Symposium on Combustion and Flame and Explosion Phenomena, The Williams & Wilkins Co. (Baltimore), 1949, pp. 44-68.

17. Savic, P.: On Acoustically Effective Vortex Motion in Gaseous Jets. Phil. Mag., ser. 7, vol. 32, Sept. 1941, pp. 245-252.

3137

18. Bickley, W. G.: The Plane Jet. Phil. Mag., ser. 7, vol. 23, no. 156, Apr. 1937, pp. 727-731.

19. Markstein, George H.: Instability Phenomena in Combustion Waves. Fourth Symposium (International) on Combustion, The Williams & Wilkins Co. (Baltimore), 1953, pp. 44-59.

20. Taylor, G. I.: Effect of Variation in Density on the Stability of Superposed Streams of Fluid. Proc. Roy. Soc. (London), ser. A, vol. 132, Aug. 1, 1931, pp. 499-524.

21. Goldstein, S.: On the Stability of Superposed Streams of Fluids of Different Densities. Proc. Roy. Soc. (London), ser. A, vol. 132, Aug. 1, 1931, pp. 524-548.

3137

3137

TABLE VIII-I. - VALUES OF $\alpha_{m,n}$ FOR THE LOWER RADIAL, TRANSVERSE, AND COMPOUND MODES

m	Values of α for n of				
	0	1	2	3	4
0	0.0000	1.2197	2.2331	3.2383	4.2411
1	.5861	1.6970	2.7140	3.7261	4.7312
2	.9722	2.1346	3.1734	4.1923	5.2036
3	1.3373	2.5513	3.6115	4.6428	5.6624
4	1.6926	2.9547	4.0368	5.0815	6.1103

TABLE VIII-II. - SUGGESTED METHODS FOR CONTROLLING VARIOUS TYPES OF OSCILLATION

Type of oscillation	Control possibilities
Resonance:	
All modes	Use of a fuel whose burning rate is not responsive to pressure and velocity fluctuations Absorption by tuned resonators
Longitudinal	Absorption of sound at burner terminals Stratification of flow to give transverse variation of acoustic speed
Radial	Absorption of sound at burner wall or burner center Diffraction and reflection from temperature variations (transverse) Noncircular burner cross section Nonconstant cross-sectional area Diffraction of sound at burner wall by corrugations, etc. Nonreactive layer at wall and center
Transverse	Nonconstant cross-sectional area Absorption of sound at burner walls Nonreactive layer near wall
Helmholtz	Diffuser design for negative pressure recovery against flow slope Long diffuser Small combustion chamber Controlled residence time
Nonacoustic feedback:	
Modulated fuel flow	Increased injection pressure Increased mixing length
Modulated fuel-air ratio	Increased mixing length Location of fuel injectors away from time-varying velocities
Vortices shed from upstream obstruction	Streamlining of obstructions Location of obstructions farther upstream Location of obstructions out of line with flame holder
Flow separation modulation	Design to prevent separation Removal of separation wake from reaction zone
Relaxation oscillation	Supercritical operation
Detonation in boundary	Nonreactive boundary layer Addition of chain-breaking substance to boundary
Temperature distribution reflections (exhaust)	Extra mixing for flat exhaust-temperature profile

[redacted]

3137

3137

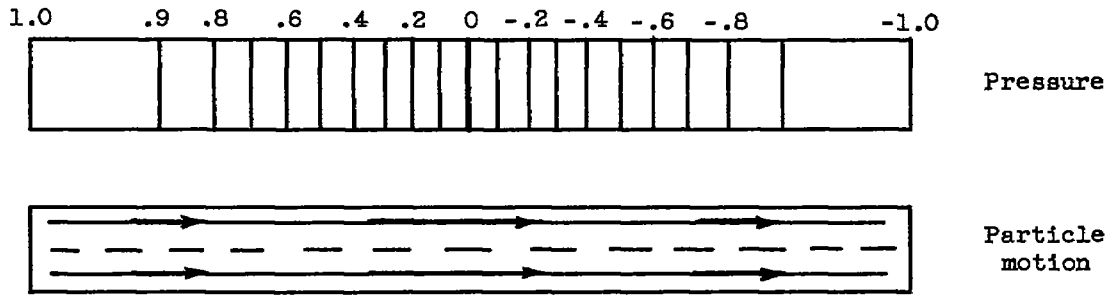

(a) First longitudinal mode.

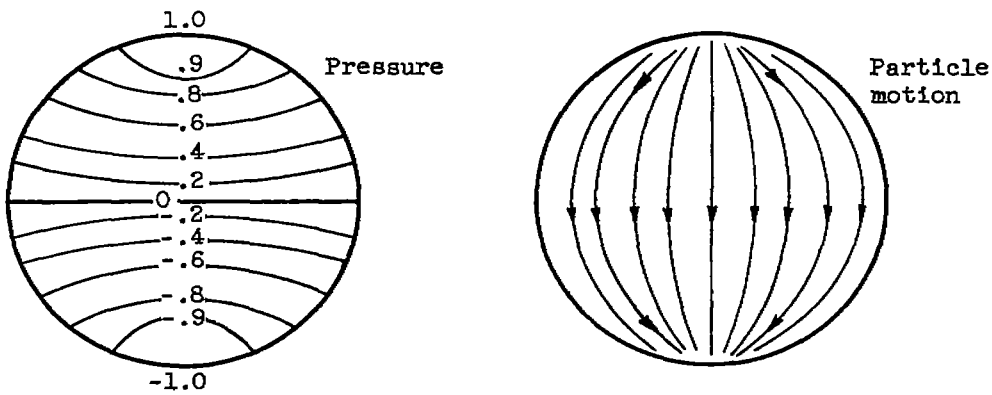

(b) First transverse mode.

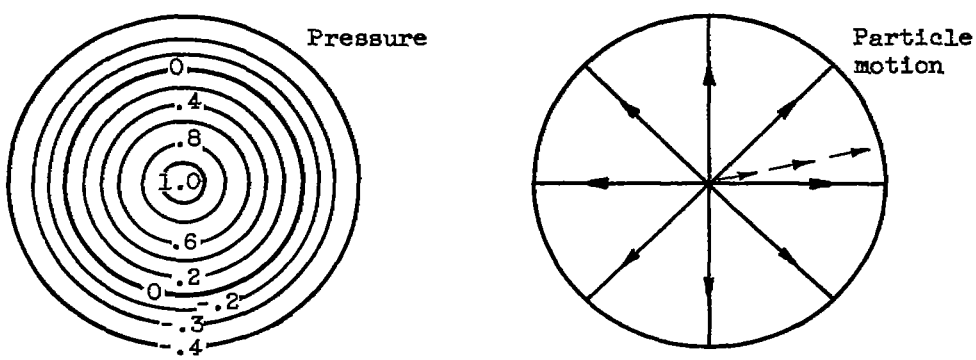

(c) First radial mode.

Figure VIII-1. - Pressure contours and particle motions for fundamental modes of cylindrical duct (ref. 6).

3137

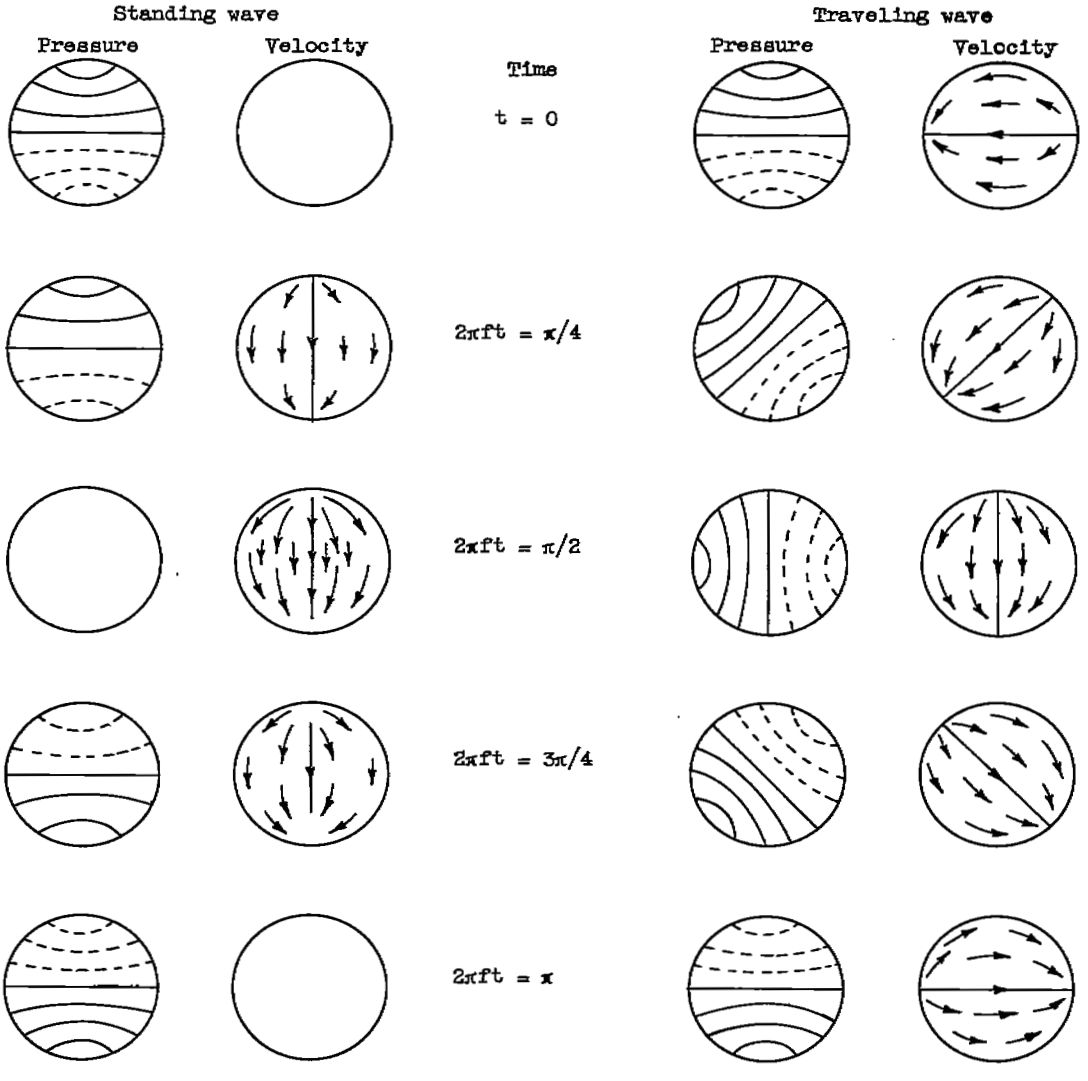

Figure VIII-2. - Distribution of pressure and velocity for standing and traveling transverse waves through half a cycle.

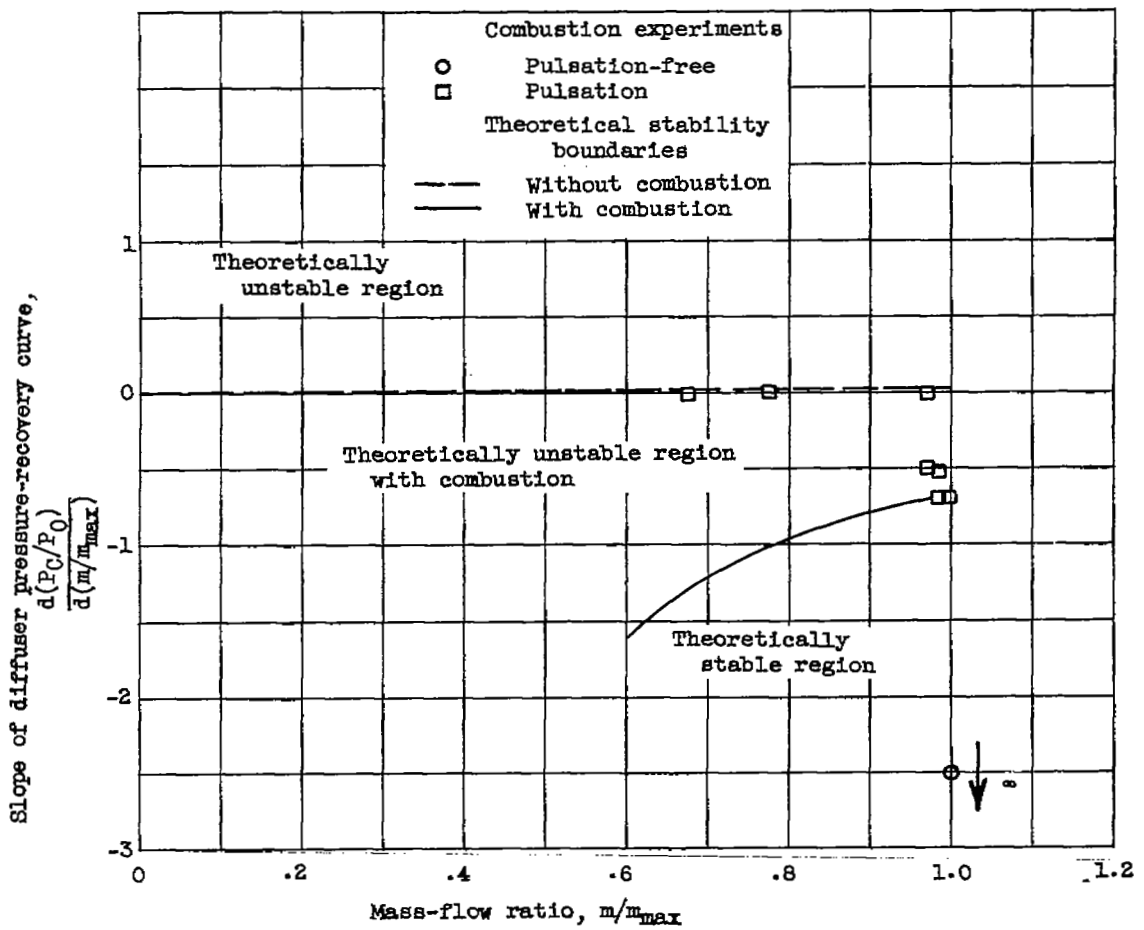

Figure VIII-3. - Theoretical and experimental stability conditions of 16-inch ram jet using gasoline as fuel. Free-stream Mach number, 1.77 (ref. 8).

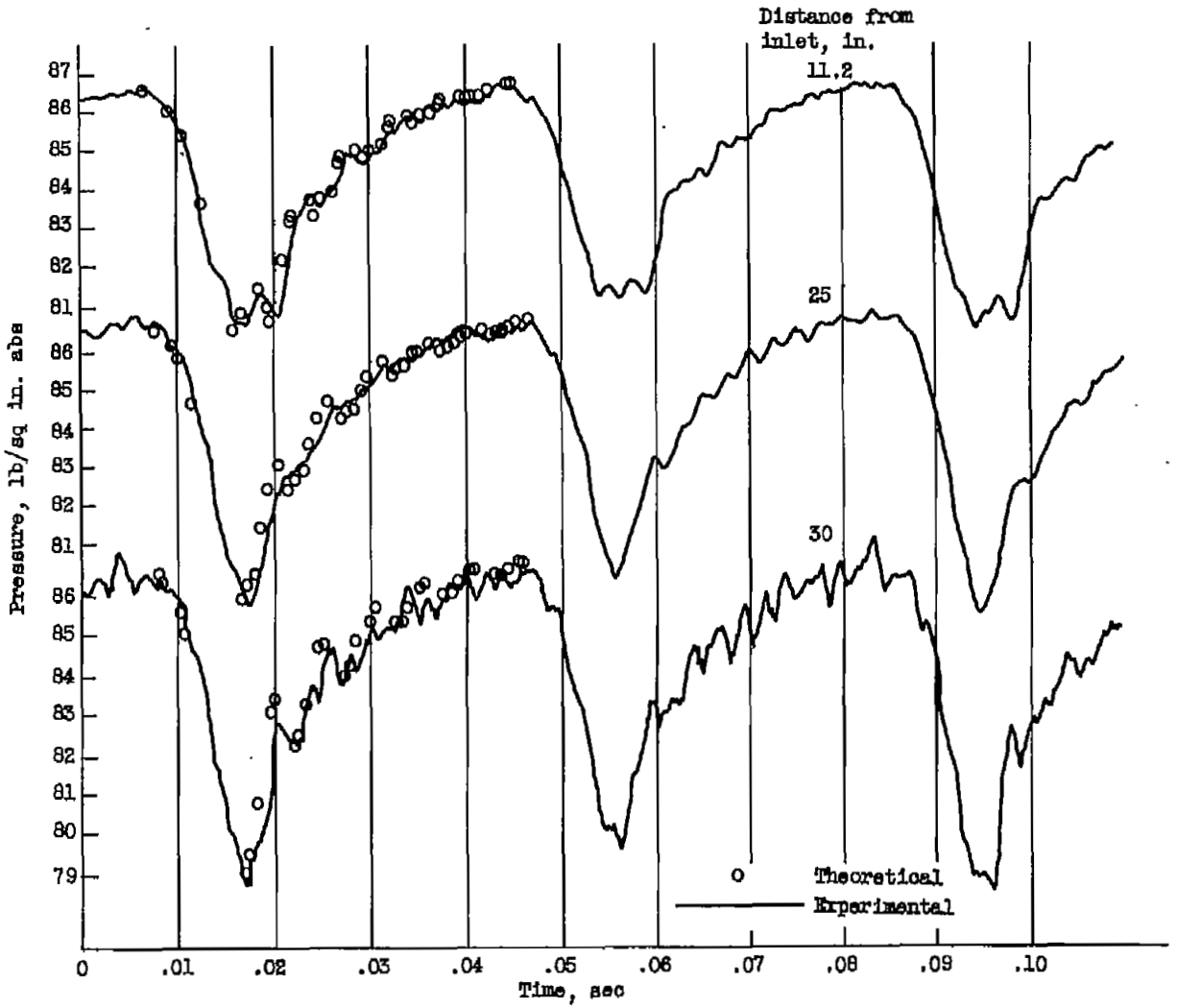

Figure VIII-4. - Theoretical and experimental pressure traces for a simulated ram jet 34 inches long, 3 cycles after onset of diffuser buzz without burning (ref. 12).

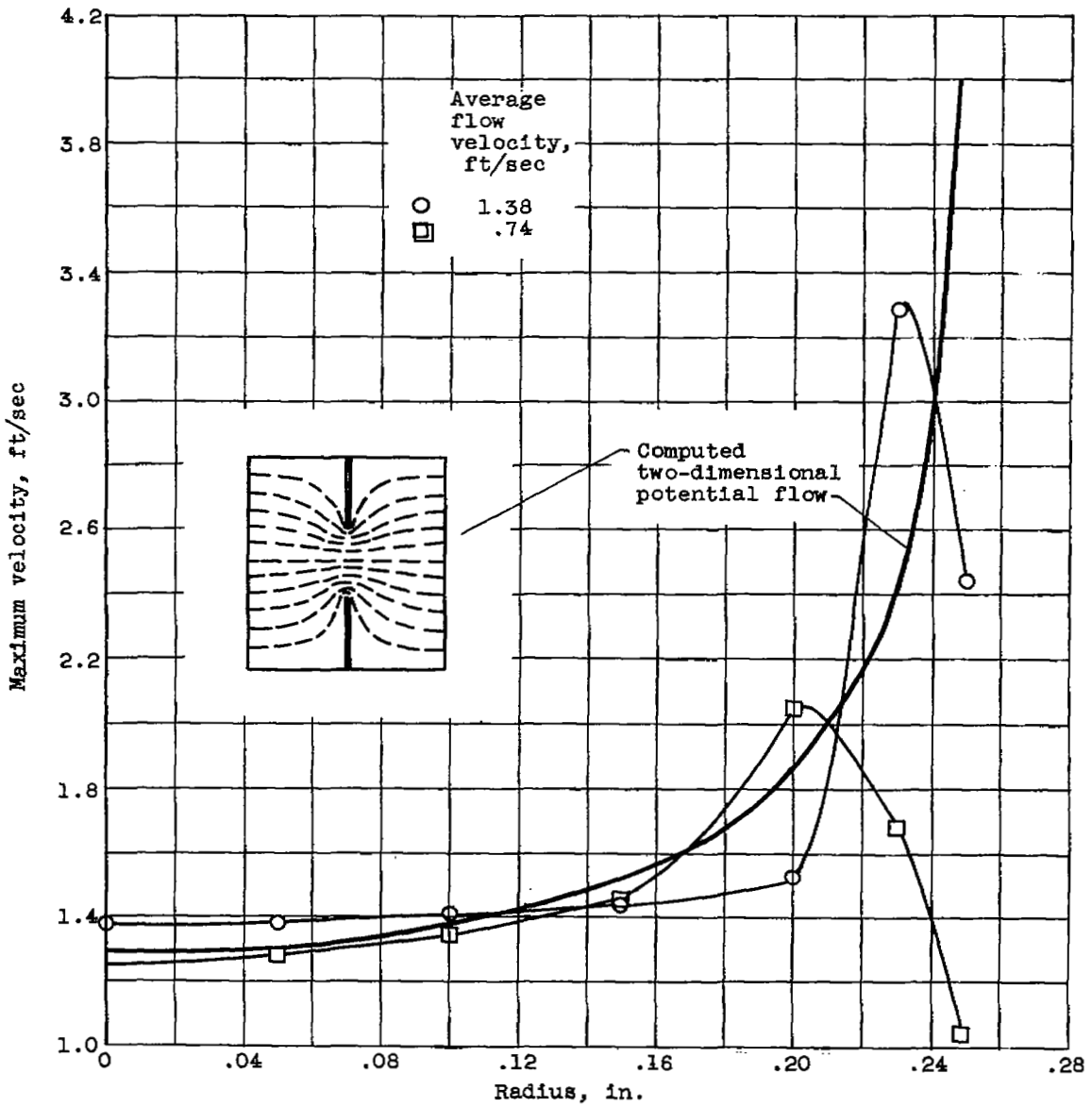

Figure VIII-5. - Comparison of measured time-varying flow through flame holder with two-dimensional potential flow (ref. 5).

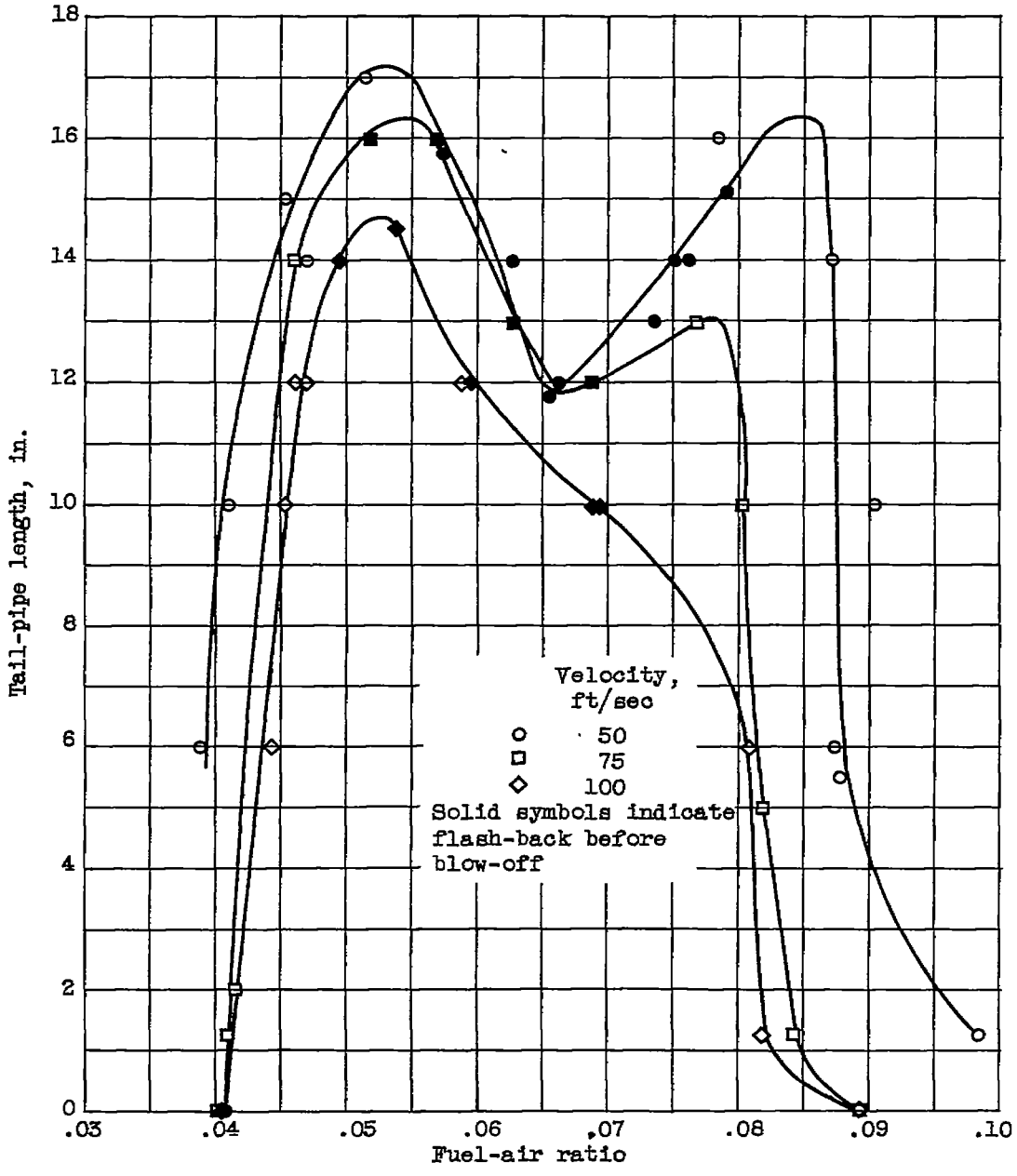

Figure VIII-6. - Blow-off limits for 1-inch-diameter ram-jet engine (unpublished NACA data).

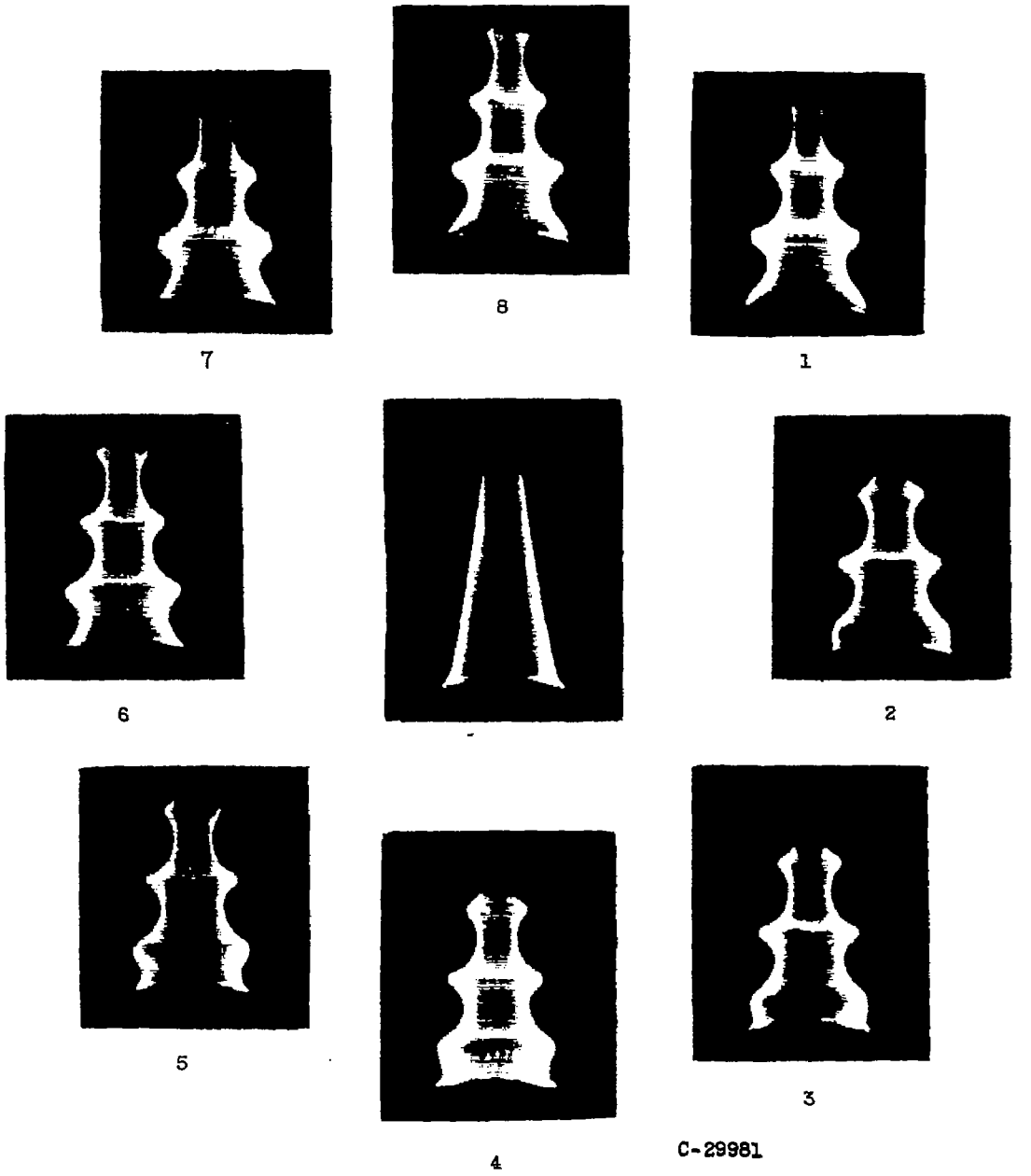

Figure VIII-7. - Sequence of flame shapes for one cycle at intervals o. Time increases clockwise; frequency, 329 cps; velocity, 1.378 feet per secc fuel-air ratio; 0.080 (ref. 5).

CHAPTER IX

SMOKE AND COKE FORMATION IN THE COMBUSTION OF HYDROCARBON-AIR MIXTURES

By Rose L. Schalla and Robert R. Hibbard

INTRODUCTION

There has been no consistent usage of the terms smoke, soot, carbon, carbon deposits, or coke in referring to the solid products arising from the incomplete combustion of hydrocarbon fuels. In studies of single combustors and engines, the solids discharged with the exhaust gases are usually called smoke, and those deposited in the combustion chamber are usually called carbon, carbon deposits, or coke. Since the so-called carbon and carbon deposits are not chemically pure, the word carbon is restricted herein to the pure element. Therefore, in connection with the bench-scale experiments in this chapter, smoke is defined as the solid product sometimes formed in the gas phase during the incomplete combustion of hydrocarbon fuels, and coke designates the solid product formed in the liquid phase from the thermal breakdown or incomplete oxidation of hydrocarbons. This distinction between coke and smoke is not as easily made in combustor studies, especially in regard to coke. The deposits that adhere to combustor walls appear to consist of carbonaceous materials formed in both gas and liquid phase. Therefore, for combustor work, smoke is defined as the solid discharged with the exhaust gases and coke as the material that adheres to the combustor walls.

Deposition of coke and formation of smoke are both undesirable in the operation of turbojet combustors. Of the two factors, coke deposition presents the more serious problem because of its adverse effect on combustor performance and life. Excessive smoke has no effect on the engine but does offer a military tactical problem, in that the presence of a smoke trail facilitates aircraft detection in combat. Under very severe conditions, smoke may hamper landing-field operations or become a nuisance to civilians. The loss in fuel heating value attributable to smoke and coke is unimportant, even under the worst conditions. For example, the heaviest coke deposits found in single combustor tests in reference 1 amounted to only 26.7 grams for 1240 pounds of fuel, or a loss of combustion efficiency of 0.004 percent due to coke deposits. Similar calculations have not been made for the loss due to smoke, but reference 2 concludes that there is no loss in combustion efficiency attributable to smoke.

In continuous-combustion engines, the tendency to form coke or smoke varies more among petroleum-derived fuels than does any other combustion property except volatility. There is very little difference in the fundamental flame velocity, minimum ignition energy, flammability limits, quenching distance, flame temperature, or heat of combustion for various batches of fuel supplied under a single specification or even for fuels meeting different specifications. However, wide differences may occur in the coking and smoking tendencies, as well as the volatility, of jet fuels.

In addition to coke and smoke considerations, the effect of fuel composition on flame radiation may also be important. Carbon is the only solid that can be formed in the combustion of hydrocarbons; and this solid can, under some burning conditions, greatly affect the amount of radiation emitted by a flame. Radiative heat transfer is an important consideration in engine design and, along with coking and smoking tendencies, becomes increasingly important with high-compression engines.

The control of coke and smoke and of heat-transfer factors in turbojet engines has been accomplished by proper combustor design and by the control of certain fuel

properties. However, in this field of combustion research, a fruitful laboratory study of fundamental factors may yield an understanding that would facilitate engine design. Many investigations have been conducted on both the fuel and the flame environmental factors contributing to smoke and coke. The greater part of this work has dealt with burning in the gas phase and therefore with the formation of smoke. From such work, the fuel factors affecting smoking tendency have been fairly well defined. Relatively little has been done on a laboratory scale regarding coke formation because of the difficulties in simulating the engine conditions in which liquid fuel impinges on hot metal in the presence of flame and flowing gases. This chapter summarizes the laboratory phases of smoke and coke formation and describes the properties of these materials, the effect of variables on the formation of smoke and coke, and the chemical mechanisms proposed for their formation.

3090

PHYSICAL AND CHEMICAL NATURE OF SMOKE AND COKE

Smoke

Luminous hydrocarbon flames, distinct from so-called nonluminous ones, emit a yellow radiation which has a black-body energy-wavelength distribution. This black-body distribution can be emitted only by solids. The only possible solid products from hydrocarbon combustion are either carbon or materials containing very high percentages of carbon. The presence of such materials in luminous flames is confirmed by the deposits formed on a cold probe passed through such a flame. Under some conditions, the solids are released from luminous flames as smoke.

These materials are formed during the combustion of hydrocarbons only when the system is fuel-rich, either over-all or locally. Therefore, the most familiar types of solid-forming combustion processes are the candle or wick-lamp diffusion flames, where fuel alone is released locally and burns after diffusive mixing with oxygen. These hydrocarbon diffusion flames are always luminous at atmospheric pressure and are often smoky. Premixed fuel-oxidant systems, such as the Bunsen burner, are not luminous unless they are operated fuel-rich over-all. For example, in reference 3 premixed benzene-air flames were found to be luminous only when the equivalence ratio exceeded 1.4 and to be smoky only at higher ratios.

The smoke released during smoky combustion is not pure carbon but has been shown by chemical analysis to be a combination of carbon, hydrogen, and oxygen. A typical analysis (ref. 3) shows 96.2 percent carbon and 0.8 percent hydrogen, with the remainder believed to be oxygen. Similar results have been obtained in the analysis of carbon blacks, which are the products of smoky combustion in diffusion flames.

Hydrocarbon-derived smoke is crystalline on a submicroscopic scale. X-ray diffraction studies show the basic element to be a crystallite with a major edge length of about 20 angstroms (ref. 4). The atomic structure consists of several layers of distorted hexagonal lattices, with the lattice substantially the same as that found in the graphite form of carbon. The distortion is believed to be due to the presence of about 1 atom of hydrogen for every 10 atoms of carbon, and the preceding elemental analysis has approximately this hydrogen-to-carbon atom ratio.

When the same smoke was examined by electron microscopy (ref. 3), these crystallites were shown to be agglomerated into nearly spherical particles of 0.01 to 1.0 micron (100 to 10,000 A) diameter. These spheres, produced in a burner under a single set of conditions, were quite uniform in diameter and clung together to form an open, lace-like structure.

Although the turbojet combustor operates with an over-all fuel-lean mixture, a large amount of the burning reaction takes place in locally fuel-rich regions.

These regions are present because all the fuel enters the upstream end of the combustor, whereas the air-entry holes are distributed along the full length of the combustor. Flame in the rich upstream end is highly luminous under many operating conditions, and the environment in this region should be conducive to the formation of large amounts of smoke. Since only small amounts of smoke, if any, are exhausted from most turbojet engines, it appears that much of the smoke probably produced in the upstream end of the combustor is consumed in passage through the burner.

In reference 3, the capacity of laboratory flames in the burning of smoke was studied, and a stream of smoke, freshly produced by a diffusion flame, was easily burned by a secondary Bunsen flame. High concentrations of smoke can be consumed in this manner. This is apparently confirmed by electron micrographs of turbojet combustion smoke, in which the particles look like partially eroded spheres (ref. 3). Their appearance suggests that spherical smoke particles are generated in the engine primary zone and that these particles are largely burned away in passing through the engine.

3090

Coke

The coke found in turbojet combustors varies in nature from soft, fluffy material to hard, brittle deposits. Typical analyses of these types (ref. 5) show the soft coke to contain 80.0 percent carbon and 2.0 percent hydrogen, and the hard coke to contain 92.4 and 1.6 percent of carbon and hydrogen, respectively. The remainder is believed to be mostly oxygen and a small amount of sulfur. Unpublished NACA data show that the sulfur content of combustor cokes varies with the sulfur content of the fuel. For example, coke-deposition tests were run on a fuel containing 0.05 percent sulfur and on the same fuel to which alkyl disulfides were added to raise the sulfur content to 1.00 percent. The amount of coke formed was substantially the same for both fuels, but the sulfur contents of the cokes were 0.7 and 2.4 percent, respectively. Unpublished NACA data also show that combustor cokes contain 25 to 50 percent of material that is soluble in carbon disulfide. This soluble material contains aromatic rings and a considerable amount of carbonyl oxygen, as indicated by infrared examination of the extract.

X-ray diffraction studies indicate that combustor coke has some of the crystalline character described for smoke. Electron microscopy (ref. 5) indicates that the soft coke consists of nearly spherical particles imbedded in an amorphous matrix. However, the hard coke is a vitreous material with no perceptible microstructure.

Soft combustor coke may be made up of a large amount of true smoke formed in the gas phase and bound to the combustor by tars formed during the liquid-phase pyrolysis of fuels. Hard combustor coke may be largely the product of the liquid-phase degradation of fuel but may contain some smoke trapped in this product. Possible mechanisms of coke formation are discussed in a subsequent portion of this chapter.

EFFECT OF OPERATING VARIABLES ON SMOKING TENDENCY

Burner Geometry

Diffusion flames. - The two principal types of apparatus used to study the smoking tendency of diffusion flames are the wick lamp and the conical or open-cup burner. Of these two methods, the wick lamp has been used more extensively; however, the exact design of this lamp has varied appreciably from one investigation to another. The Davis factor lamp was one of the earliest wick lamps to be developed (1926). This lamp was later modified (ref. 6) and used for smoking-point determinations as recently as 1952 (ref. 7). In 1935 a test lamp (ref. 8) was standardized

by the Institute of Petroleum Technologists (I.P.T.) and has been employed by several investigators (refs. 9 and 10). This I.P.T. lamp is used in the current U.S. military fuel procurement specifications and is now being cooperatively tested by the American Society for Testing Materials. The fairly simple lamp shown in figure IX-1 is a combination of the Davis apparatus and the I.P.T. lamp (used in ref. 11). A comparison of the data obtained with the various wick lamps and accessory equipment indicates that smoking tendencies depend on the geometry of the apparatus and that no simple comparison can be made between smoke-point data obtained with different lamps.

The conical or open-cup lamp is often referred to as the wickless lamp, since the flame burns directly from the top of a pool of liquid fuel contained in a shallow funnel or cup-shaped vessel. Development of the wickless burner is described in reference 12 and similar burners have been used for investigations reported in references 13 and 14.

The main advantage of the wickless lamp is that it can be used for the comparison of less smoky fuels, since flame heights up to 450 millimeters may be measured; whereas, the Davis wick lamp is limited to 102, and the I.P.T. lamp to about 50 millimeters. A comparison of the I.P.T. lamp and the wickless lamp (ref. 10) shows that the smoking points of various fuels measured by the two methods gave a fair correlation, but the correlation appeared logarithmic rather than linear. Reference 10 reports that the wickless lamp is much more difficult to operate than the I.P.T. lamp and recommends that it be used only when the range of the I.P.T. lamp is exceeded.

With all types of diffusion burners, the flame is enclosed by a glass tube that acts as a chimney and keeps the flame erect and stable. The size and position of this chimney greatly influence the smoking point of the flame.

The general procedure in using any of these lamps is to increase the fuel flow until the flame just begins to smoke. The smoke point may be detected visually, or an ice-cooled porcelain surface may be placed above the flame to collect and indicate the presence of smoke. A measure of the smokiness of the fuel may be made in several ways. The technique usually employed is to measure the maximum height to which the flame will burn without smoking; however, in two investigations (refs. 3 and 10), measurements were made of the maximum rate at which fuel can be burned without smoking. A comparison of the two techniques (ref. 10) indicates that the maximum burning rate is readily obtained and is more reproducible than the smoke-height test. It also represents more closely the information desired by the test, namely, the relative amount of fuel that can be burned under standardized conditions before smoke becomes a problem. Only when illumination is concerned does the height of the flame become a significant factor. The smoke-height test, however, is somewhat more convenient to use and therefore has been adopted in the A.S.T.M. procedure. Another method (ref. 13) is to pass a light beam through the chimney in which the smoke is issuing from the flame. A photoelectric cell indicates the amount of light absorbed and, consequently, a measure of the smokiness of the fuel. Also, the smoke issuing from various aromatic fuels burning at a given fuel flow has been collected and weighed (ref. 14). The greater the amount of smoke collected, the higher the smoking tendency of the fuel.

As previously stated, the smoke point is generally determined by measuring the maximum height or maximum fuel rate at which the flame will burn without smoking. The higher the flame or the greater the fuel-flow rate, the lower the tendency for that fuel to smoke. Consequently, the smoking tendency is an inverse function of the flame height or fuel flow. Reference 15 defines smoking tendency S_t as equal to a constant k over the maximum flame height h (in millimeters) and assigns the value of 320 to k:

$$S_t = \frac{k}{h}$$

The value of k is unimportant in the following discussion, but the distinction between maximum flame height and the concept of smoking tendency should be noted.

Bunsen flames. - The smoking tendencies of Bunsen flames are reported in references 3, 13, and 16. In reference 16 a continuous-flow apparatus was used in which steady streams of both volatile and nonvolatile fuels could be mixed with air either as vapors or as mist droplets, according to their vapor pressures. The fuel-air mixture was passed up a vertical tube after generation and burned on top in primary air only. The composition of the mixture was determined by analyzing the exhaust gases.

3090

In the investigations reported in references 3 and 13 the fuel was metered from a burette and mixed with metered air. The premixed fuel and air were then burned from a tube surrounded by a glass tube chimney. The effect of varying the burner-tube inside diameter from 6 to 9 millimeters was investigated in reference 3, and showed that the smoking tendency was slightly reduced as the burner-tube diameter was decreased. The influence of chimney length, diameter, and position with respect to the flame was also reported in reference 3. Increasing the chimney length from 120 to 500 millimeters caused a reduction in smoking tendency. Changes in the diameter and position of the chimney gave varied results, depending on the convection in the chimney. In general, all chimney variables that reduced smoke formation did so by generating a flue effect which tended to flow more air around the flame. If the burner tube was ducted so that a controlled secondary-air flow could be passed by the flame, the smoking tendency was reduced as the secondary-air flow was increased.

Fuel-Air Ratio

Diffusion flames. - The effect of over-all fuel-air ratio on the smoking tendency of laminar diffusion flames has been investigated by two different techniques. In reference 14, the air supply past the flame was maintained constant and the smoke issuing from the flame was collected at various increasing fuel flows. A plot of the smoke deposit against the fuel-air ratio is shown in figure IX-2. Since the air flow was constant, the ordinate is essentially a measure of the fuel flow. As shown in this figure, the initial increase in fuel flow produces a sharp increase in the amount of smoke collected. As higher fuel flows are reached, the amount of smoke produced appears to level off.

In another controlled-air study with diffusion flames (ref. 3), the air-flow rate past the flame was increased by gradual steps, and a determination was made of the maximum rate at which the fuel could be burned without smoking at each given air flow. In figure IX-3, the maximum fuel rate for smoke-free burning is plotted against the air-flow rate for eight pure hydrocarbon fuels. With initial increases in air flow, the maximum smoke-free fuel flow increases proportionally, but eventually a limiting fuel flow is reached at which further increases in air flow past the flame do not permit more fuel to burn smoke-free.

Bunsen flames. - The effect of fuel-air ratio on smoke formation from Bunsen flames is reported in reference 13. A measure of the smoke density of the fuel was made by passing a light beam through the chimney in which the smoke was issuing from the flame. A photoelectric cell indicated the amount of light absorbed as a measure of the smoke formation. In this burner, the paraffins, cycloparaffins, and olefins, with the exception of triisobutylene, could not be made to smoke even at

the maximum fuel-air ratio that would support combustion. Figure IX-4 shows the variation of smoke (percent light absorbed) against the fuel-air ratio for kerosene and aromatic and dicyclic compounds. The air flow premixed with the fuel was held constant at 4.1±0.1 liters per minute, and the fuel flow was increased to give the fuel-air ratios indicated. The aromatic and dicyclic compounds began to smoke at approximately stoichiometric fuel-air ratios. Within experimental error, smoke formation from a Bunsen flame appears to be a linear function of the fuel-air ratio.

Temperature

Diffusion flames. - An investigation (ref. 9) of the effect of ambient temperature on the smoke point of five fuels burning as diffusion flames at three temperatures (0°, 70°, and 90° F) showed the smoke point to be independent of temperature in the range between 0° and 90° F. Nor did the preheating of gases burning as diffusion flames to 375° F change the smoking tendency (ref. 3).

Bunsen flames. - In references 3 and 16 the effect of temperature on the smoking tendency of Bunsen flames was studied. The fuel-air ratio at which incandescent carbon was first observed, and also the fuel-air ratio at which smoke actually issued from the flame were determined (ref. 3). Over a temperature range of 82° to 842° F, the point at which smoke issued from a premixed benzene flame was independent of temperature. However, the first appearance of yellow incandescent carbon in the flame occurred at slightly higher fuel-air ratios as the temperature was increased over this range.

In reference 16, only the appearance of yellow incandescent carbon in the flame was used to measure the effect of temperature on propane, propene, benzene, and kerosene flames. Over a temperature range of -40° to 925° F, incandescent carbon in the flame appeared at slightly higher fuel-air ratios as the temperature was increased.

Pressure

Diffusion flames. - Studies of the effect of pressure on smoke formation from diffusion flames are reported in references 3, 9, and 17. The investigation of reference 17 was limited to acetylene; and that of reference 9 to petroleum fractions. The work of both reference 9 and 17 was conducted at pressures below atmospheric; and in both investigations, the tendency to smoke decreased with decreasing pressure. In reference 3 are reported smoking tendencies for six pure hydrocarbons, a JP-4 fuel, and two blends of n-octane and toluene over a pressure range of about 0.5 to 4 atmospheres. For two of the pure hydrocarbons, 1-octene and n-octane, the pressure range was extended to 9 and 12 atmospheres, respectively. Ethane and ethene were studied over a pressure range of 4 to 22 atmospheres. The maximum relative rate at which all fuels could be burned without smoking decreased consistently with increasing pressure. Typical results are shown in figure IX-5. The data in reference 3 show that the product of the smoke-free fuel flow and the pressure is a constant, or, in other words, that the smoke-free fuel flow is inversely proportional to the pressure. Since diffusion coefficients are also inversely proportional to the pressure, it was concluded that the rate of diffusion and, consequently, the rate of mixing of fuel and air may account for the variation in smoke formation with pressure.

Bunsen flames. - In a spectroscopic study of a premixed ethene flame (ref. 18), it was observed that smoke started to form as the pressure was increased. In reference 19 (p. 170), the formation of smoke from an acetylene-oxygen flame at various

pressures was studied, and it was concluded that the effect of pressure on smoke formation from Bunsen flames is probably slight. The effects that reference 18 observed were attributed to changes in experimental parameters such as mass flow and the influence of the burner wall. Since the results of the diffusion-flame study (ref. 3) indicate that the increase in smoke formation with pressure results from the decreases in diffusion coefficients with pressure, the smoke formation from a Bunsen flame, which contains all its oxygen, should be independent of pressure if outside diffusion effects are eliminated.

3090

EFFECT OF FUEL VARIABLES ON SMOKING TENDENCY

Effect of Hydrocarbon Type on Diffusion Flames

One of the first studies to indicate the importance of fuel type on smoke formation is reported in reference 20. The influence of fuel type on smoke has been more extensively investigated, and data have been reported for pure liquid hydrocarbons (refs. 3, 7, 12, 14, and 15) and pure gaseous hydrocarbons (ref. 3). Since each investigator employed a different apparatus, no absolute or standardized values are available; however, certain consistent trends have become apparent. For the pure hydrocarbon compounds, the smoking tendency among the four major homologous series varies as follows: aromatics > alkynes > monoolefins > n-paraffins.

The magnitude of the variations in smoking tendency among the aromatic, olefin, and paraffin series is illustrated in the following table:

Reference	Ratio of smoking tendency		
	Aromatic to olefin	Olefin to paraffin	Aromatic to paraffin
12	6.2	2.61	16.2
3	13.6	2.34	31.8
7	15.7	1.51	23.7

The smoking tendency of the average aromatic is reported to be from 6.2 to 15.7 times greater than for the olefins, and 16.2 to 31.8 times greater than for the paraffins. The smoking tendency of the olefins is about twice that of the paraffins. The lack of quantitative agreement becomes readily apparent from examining the values in the table. The variations within the aromatic, alkyne, olefin, and paraffin series are discussed in the following paragraphs.

Aromatics. - As the preceding table indicates, the aromatic compounds have the greatest smoking tendency of the various classes of fuels. With benzene as a reference, the smoking tendency generally increases with the addition of a side chain of one or two carbon atoms; but with a sufficiently long side chain, the smoking tendency is reduced. The total range of flame heights among the aromatic compounds, however, is very small. For example, most investigators report the smoke-point flame height of benzene to be between 5 and 10 millimeters. The aromatics of higher smoking tendency have flame heights ranging down to about 3 millimeters; and those of lesser smoking tendency, up to 12 millimeters. The total range of 3 to 12 millimeters is not very great compared with an average paraffin such as hexane with a flame height of 150 millimeters. The experimental error, percentagewise, in measuring flames as small as 3 to 12 millimeters is very large. Since the aromatics have an essentially uniform smoke point, it is difficult to make a satisfactory differentiation among the various aromatic structures.

Hunt (ref. 7) attempted to overcome this difficulty by studying blends containing 20 percent of various aromatics in n-dodecane. This procedure increased the flame height of the benzene blend to 66 millimeters. Blends of about 30 other aromatic and naphthalene compounds were studied in this manner; flame heights ranged from 36 to 81 millimeters. Differences in smoke heights were thus magnified sufficiently to eliminate most experimental errors and permit a definite distinction to be made in smoke points among various aromatic structures. In figure IX-6, the variations in flame heights for 20 percent blends of 30 aromatic compounds are plotted against the number of carbon atoms in the compound. Figure IX-6 emphasizes that substitution on the benzene ring may cause an increase or decrease in the smoke point, depending on the nature of the substituted group. Naphthalene and substituted naphthalene compounds definitely exhibit a greater tendency to smoke than the aromatics.

Alkynes. - Smoke-point data for the alkynes are limited. Reference 3 reports the smoking tendency for acetylene, 1-propyne, 1-pentyne, and 1-hexyne. The smoking tendencies decreased slightly with increasing chain length and were of about the same order of magnitude as for the aromatics. Comparison of 1-octyne and 1-dodecyne (ref. 7) showed a decrease in smoking tendency with increasing chain length; however, the smoking tendency for these two alkynes was appreciably less than for the aromatics.

Monoolefins. - All the investigators have reported the monoolefins to be appreciably less smoky than the aromatics but of higher smoking tendency than the n-paraffins. From the data of reference 3, the smoking tendency is reported to increase from ethene to butene. References 3, 12, and 15 indicate that, with olefins of five or more carbon atoms, the smoking tendency decreases with increasing chain length. Data from reference 7 indicate that the smoking tendency is essentially constant for all the olefins above five carbon atoms. The effect of the position of the double bond, in the one and two position only, is reported by reference 7 where 2-heptene is shown to have a slightly higher smoking tendency than 1-heptene; however, the difference is less than 6 percent. 1-Octene and 2-octene showed the same smoking tendency (ref. 7).

Diolefins. - Diolefins (refs. 3 and 15) have appreciably higher smoking tendencies than the monoolefins. The smoking tendency of 1,3-butadiene is higher than most aromatics (ref. 3). As the chain is lengthened, the smoking tendency decreases.

Cycloolefins. - Cyclohexene has a somewhat higher smoking tendency than 1-hexene (ref. 3). Cyclopentene, however, has an appreciably higher smoking tendency than cyclohexene or 1-pentene, and forms almost as much smoke as the aromatics.

Paraffins. - The n-paraffins are consistently reported to have a lower smoking tendency than any of the other homologous series. The smoking tendency increases with increasing chain length. From ethane to hexane, the increase in smoking tendency is over 100 percent (ref. 3); while, for compounds of 6 to 15 carbon atoms, the increase is generally about 10 percent.

If the paraffin chain is branched, the smoking tendency increases markedly. In fact, a highly branched compound such as isooctane (2,2,4-trimethylpentane) has a higher smoking tendency than a monoolefin of corresponding number of carbon atoms (ref. 7). 2,2-Dimethylpropane has a smoking tendency almost as great as 1-pentene (ref. 3). The smoke points for several isomeric paraffins are plotted and compared with similar data for n-paraffins and n-olefins in figure IX-7 (ref. 7).

Cycloparaffins. - Cycloparaffins produce more smoke than the n-paraffins; the smoking tendency decreases with increasing ring size from three to six carbon atoms (ref. 3). The addition of a short side chain to the ring increases the smoking

tendency; but, as the length of the side chain is increased, the smoking tendency is reduced slightly. Cyclopentane with a side chain of 10 carbon atoms (decylcyclopentane) has about the same smoking tendency as cyclopentane (ref. 7).

Summary. - The smoking tendency decreases as follows: aromatics > alkynes > olefins > n-paraffins:

(1) All the aromatics have a fairly uniform and extremely high smoking tendency. From an average of three investigations, the aromatics are about 12 times as smoky as the olefins and about 24 times as smoky as the n-paraffins.

(2) The alkynes lie between the aromatics and the monoolefins, with the smoking tendency decreasing with increasing chain length.

(3) The smoking tendency of the monoolefins increases from ethene to butene and then decreases with increasing chain length. The olefins are about 1/12 as smoky as the aromatics, but about twice as smoky as the n-paraffins. Branching, ring formation, and additional double bonds increase the smoking tendency.

(4) The n-paraffins have a lower smoking tendency than any of the other homologous series. The smoking tendency increases with increasing chain length, branching, and ring formation.

Hydrocarbon blends and refinery streams. - The smoke points of two component blends of pure hydrocarbons are reported in references 7, 9, and 10. As an example of such blending smoke-point data, figure IX-8 shows the smoke points for 0 to 100 percent blends of sec-butylbenzene and of α-methylnaphthalene in n-dodecane (ref. 7). Although the smoke points of the two pure aromatics differ by only 2 millimeters, the blending curves are different. For example, at a 20 percent aromatic concentration, the smoke point of the sec-butylbenzene blend is about 74, whereas that of the α-methylnaphthalene blend is only 37. The marked effect of the aromatic on the smoke point of paraffins is also apparent. For example, a 20 percent addition of the aromatic reduces the flame height of n-dodecane by about 50 percent or greater. When the concentration of α-methylnaphthalene is 50 percent, the smoke point of the blend is substantially that of the pure aromatic.

Smoking tendencies for various refinery fractions are reported in references 9 to 11, 15 and 20. The early studies were used to evaluate the illumination quality of kerosene-type fuels burning in lamps. The major interest in smoke-point data in the last several years has resulted from the demand for clean-burning jet fuels. The smoking points of 48 jet fuels and the fuel-inspection data for these fuels are reported in reference 9. Reference 11 reports the flame-height smoke point for jet fuels to be about 15 to 30 millimeters, compared with 6 or 7 millimeters for aromatics and 77 millimeters for commercial isoheptane.

Effect of Hydrocarbon Type on Bunsen Flames

Measurements of variations in smoke formation of various hydrocarbons are reported in references 13 and 16. Since in reference 13 the paraffins, cycloparaffins, and olefins could not be made to smoke even at the maximum fuel-air ratio that would support combustion, these fuels appear to be less smoky than the aromatics and other fuels shown in figure IX-4. In general, the smoking tendency of the fuels shown in figure IX-4 are in the same relation to each other as in diffusion-flame studies. The aromatics show a fairly uniform smoking tendency, as was the case in diffusion flames.

Reference 16 reports determination of the critical fuel-air ratio that would just cause a yellow streak of incandescent carbon to appear in Bunsen flames of various hydrocarbon and oxygenated compounds. The appearance of this yellow streak in the flame, of course, occurs at considerably lower fuel-air ratios than the actual emission of smoke. The results of reference 16 are shown in figure IX-9, where the critical air-fuel ratio is plotted against the number of carbon atoms in the compound. The higher the position of a fuel on this plot, the greater is its tendency to form an incandescent streak of carbon.

The values for the aromatics, instead of being decidedly worse than the other fuels, are similar to the paraffins, isoparaffins, and olefins. The order of these last three series is the reverse of that observed in diffusion studies. The order of decalin with respect to the substituted naphthalenes and the aromatics differs from the Bunsen work of reference 13 (see fig. IX-4). The variation with respect to the data in figure IX-4 may be explained by the fact that the appearance of yellow incandescent carbon in the flame and not the emission of smoke was measured in reference 16. It is probable that these two types of measurements would not be directly proportional. If they are, however, the effect of fuel type on smoke formation as measured by Bunsen and diffusion flames appears appreciably different.

3090

Methods of Correlating Smoking Tendency with Hydrocarbon Structure in Diffusion Flames

Several methods of predicting or explaining the variation of smoking tendency among different fuel types have been proposed. An equation based on the oxygen requirements of diffusion flames was developed in reference 15 to predict the maximum smoke-free flame height h (the constants apply only for this particular apparatus):

$$h = \frac{(x + 3)^2}{36.1\ xy + 54.9 - 26.65\ x^2} \tag{1}$$

where

x molecular volume of combustion products

y molecular volume of oxygen

While this equation predicts qualitative trends among the various series quite accurately, it does not predict the magnitude by which one series differs from another as reported experimentally. Some of the trends within the series - for example, the effect of branching and ring formation - would not be predicted by the equation. Modification of the equation to fit the apparatus in use may be of some practical value for making qualitative comparison, but, with respect to theory, the equation does not explain the effect of differences in fuel type such as branching.

The relation between the tendency to smoke and the carbon-hydrogen ratio of the compound is discussed in reference 12. It is indicated that, in general, compounds of high C-H ratio show a higher smoking tendency than compounds of low C-H ratio. This particular correlation, which gives good qualitative agreement, has been used in predicting combustor coke deposition (ref. 21). Like equation (1), however, it does not explain the differences resulting from such factors as branching and ring formation; consequently, in reference 12 the smokiness of the hydrocarbon molecule is attributed to its compactness.

References 3 and 22 suggest that smoking tendencies may be related to the relative ease of removal of hydrogen atoms compared to the stability of the carbon chain or skeleton of the molecule. A true measure of the stability of the carbon skeleton is difficult to obtain but can be represented to some extent by the carbon-carbon bond strengths. A comparison of the stability as measured by bond strengths is shown in figure IX-10 and appears to give good qualitative agreement with the smoking tendencies. If all the factors contributing to the stability of the carbon chain could be evaluated and assessed, the agreement might be better.

3090

Effect of Nonhydrocarbon Components

Diffusion flames. - Petroleum-derived fuels may contain small quantities of organic sulfur, nitrogen, and oxygen compounds. The maximum amount of sulfur permitted by the current military fuel specifications is 0.2 percent for JP-1, 0.4 percent for JP-3 and JP-4, and 0.5 percent for JP-5. Concentration limits for nitrogen and oxygen are not specified but are not likely to exceed 0.1 and 0.5 percent, respectively.

Smoke-point data for some sulfur compounds are reported in reference 7, and for some nitrogen compounds, in references 7 and 12. Both the alkyl-substituted sulfur compounds (mercaptans and disulfides) and the alkyl-substituted nitrogen compounds (amines) have smoking tendencies somewhat higher than their hydrocarbon analogs. The aryl mercaptans and sulfides have smoking tendencies substantially the same, and the aryl amines appreciably lower than their parent hydrocarbons.

A thorough study of oxygen-containing compounds is reported in reference 12. In general, increasing the oxygen content results in decreasing smoking tendency. Compounds containing high percentages of oxygen, such as methyl acetate, smoke only at very great flame heights. Methyl alcohol cannot be made to smoke at all; and, at equal oxygen concentration, the general order for increasing tendency to smoke is n-primary alcohols, n-primary nitroparaffins, propionates, acetates, lactates, and formates.

In general, the concentrations of sulfur, nitrogen, and oxygen are so low in conventional hydrocarbon fuels that the presence of these impurities does not measurably affect the smoking tendency of the fuel.

Bunsen flames. - Aryl amines and oxygenated compounds were investigated in Bunsen flames in reference 16. The results are shown in figure IX-9. The values for the aryl amines are not appreciably different from those of their hydrocarbon analogs. The oxygenated compounds show increasing air-fuel ratio with increasing number of carbon atoms in the molecule, the alcohols requiring a higher air-fuel ratio than aldehydes or ketones of a similar number of carbon atoms.

Effect of Additives

Diffusion flames. - Relatively little information is available on the effect of additives on the smoking characteristics of hydrocarbon flames. This effect may differ between diffusion and Bunsen type flames. Additions of the order of 5 percent of sulfur trioxide are required to measurably reduce the smoking tendency of a diffusion flame (ref. 23), but as little as 0.1 percent of this gas will change a nonluminous Bunsen flame to a luminous one (ref. 19, p. 173). However, the actions of sulfur dioxide and hydrogen sulfide are similar in both type flames; and, with concentrations of the order of 5 percent, slight reductions in smoking tendency of diffusion flames and decreases in the luminosity for Bunsen flames were observed

(ref. 19, p. 173). Reference 23 proposes that the oxides of sulfur reduce smoke formation in a diffusion flame by being first converted to S_2 molecules which then react with carbon to form CS.

A few other substances, such as nitric oxide, nitrogen dioxide, diethyl peroxide, and tetraethyl lead, have been tested as additives but have produced no striking effects in regard to smoke formation from diffusion flames (ref. 19, p. 173). In general, no additive is known which, when used in small concentrations, will measurably change the smoking tendencies of hydrocarbon diffusion flames.

Bunsen flames. - In reference 18, which used the first appearance of incandescent carbon in the flame as a measure of smoking tendency, no additive was found that had any significant effect on the fuel-air ratio in concentrations under 1 percent by weight. Addition in quantities over 10 percent by weight may have an appreciable effect. Halogenated compounds, sulfuric acid, and sulfur trioxide increase the fraction of stoichiometric air required to inhibit carbon formation; nitrogen peroxide, carbon monoxide, tetraethyl lead, methyl alcohol, methylethyl ketone, and amyl nitrate have the opposite effect; sulfur dioxide, carbon dioxide, and water have no effect; carbon disulfide has no effect on kerosene flames but increases the fraction of stoichiometric air required in benzene flames. Sulfur dioxide, though having no effect on the critical air-fuel ratio, appears to reduce the amount of carbon formed in flames of rich mixtures.

THEORIES OF SMOKE AND COKE FORMATION

Smoke

In the preceding sections it was proposed that the relative ease of removal of hydrogen atoms from the molecule as compared with the breaking of carbon bonds is responsible for the variations in smoking among different fuel types burning as diffusion flames. This proposal suggests that the thermal and oxidative dehydrogenation processes, which occur very early in the burning process, influence the further course of smoke formation. The thermal dehydrogenation probably occurs as soon as the fuel enters a laminar diffusion flame, because the fuel is heated to temperatures of the order of 1500° F or higher before coming in contact with oxygen. Active decomposition particles, then, further promote dehydrogenation processes.

Other investigators have considered the importance of dehydrogenation reactions and tend to support this proposal. For example, the energy requirements for removal of a hydrogen atom from an acetylene molecule by a free hydrogen atom,

$$H + C_2H_2 \rightarrow H_2 + C_2H$$

were considered in reference 24. This reaction has an activation energy of only 5 kilocalories per mole, which indicates that it could easily occur. Activation energies for the reaction of hydrogen atoms with various other hydrocarbon compounds are of similar magnitude (ref. 25).

It was observed in reference 26 that suppression of the hydrogen-atom concentration in flames accompanies the suppression of smoke formation. Thus, smoke formation could be prevented by reactions that consume hydrogen atoms or render them ineffective. Reference 27 suggests that smoke formation could be suppressed by carbon monoxide and nitrogen, which serve as nuclei for the recombination and removal of hydrogen atoms. Reference 14 reports that, in addition to hydrogen atoms, other atoms and radicals such as those found in the pyrolysis of halogen compounds also increase smoke formation. All these active species probably promote polymerization

reactions leading to smoke by stripping hydrogen from the fuel molecules. Even if halogen atoms react with and remove some of the hydrogen atoms, the concentration of fuel molecules is so much greater than the concentration of the short-lived hydrogen atoms that the dehydrogenation process predominates. It is therefore proposed that the removal of hydrogen atoms from the fuel molecules both by thermal processes and by active atoms is probably the initial process involved in the formation of smoke.

The steps that might occur after total or partial dehydrogenation are controversial. Since aromatics have the greatest smoking tendencies, and since the graphite structure of carbon particles resembles the molecular structure of the multiringed homologs of benzene, the formation of smoke by a build-up of aromatic ring structures has been suggested (ref. 28). This theory is not opposed to the initial step of hydrogen removal, since the fuels would have to lose some hydrogen atoms before a polymerization of the rings might begin. However, absorption spectroscopic examinations of a benzene flame in the ultraviolet region (ref. 17) indicate that benzene is consumed in the lowest portion of the flame and that an appreciable gap exists between the disappearance of benzene and the appearance of smoke particles. No intermediate aromatic products, which should be readily detectable in the ultraviolet, are found in this region. The absence of aromatic intermediates in this gap is evidence against the ring-building theory.

Thorp, Long, and Garner (ref. 29) analyzed the smoke from a flat benzene flame and found diphenyl to be present, thus supporting the aromatic-ring-building theory; but in later work (ref. 30) they did not find diphenyl present in the products of the soots from paraffinic or naphthenic fuels. Consequently, it is unlikely that carbon formation in hydrocarbon diffusion flames occurs through diphenyl, the polyphenyls, or the polycyclic aromatics as intermediate compounds (ref. 30).

Parker and Wolfhard (ref. 17) reject the aromatic-ring-building theory; but they have proposed as mechanisms for smoke formation (1) the formation of large molecules that may graphitize from within, or (2) an increase in the concentration of moderately high-molecular-weight hydrocarbons until the saturation vapor pressure is reached, at which time condensation occurs to form a mist of droplets that form nuclei and graphitize. Observations on the physical nature of smoke (ref. 31) show that the first mechanism is improbable. Frazee and Anderson (ref. 24) object to both mechanisms, on the basis of prohibitive energy requirements and other considerations. Porter (ref. 32) concludes from considerations based on the time available for polymerization and on the nature of the smoke formed that the droplet-formation mechanism or polymerization mechanisms in general do not contribute to smoke formation to any significant extent in ordinary diffusion flames.

Porter (ref. 32) believes, instead, that fuels in combustion waves first decompose to form lower-molecular-weight hydrocarbons such as acetylene as a result of both thermal decomposition and partial oxidation. By rapid adiabatic photolysis he obtained rates of liberation of heat and active particles in a reaction vessel comparable with those which occur in flames. A rapid quenching resulted in the retention of a fraction of all stable intermediates. Complete analysis of the products showed no higher hydrocarbons. Porter therefore proposes a series of reactions:

$$C_2H_6 \rightarrow C_2H_4 \rightarrow C_2H_2 \rightarrow \text{carbon}$$

Previously, Tropsch and Egloff (ref. 33) showed that acetylene is a product of the pyrolysis of pure hydrocarbons. They passed ethane rapidly through a heated tube for various contact times and found that ethene, acetylene, and carbon were formed. This experiment simulates the reactions that might occur in the lowest portion of a diffusion flame where the fuel is heated before coming into contact with oxygen.

Since acetylene may be the last stable product to appear before smoke formation, the final step in the mechanism of smoke formation would be that leading from acetylene to smoke. If all hydrogen atoms were removed from the C_2H_2 molecule, the mechanism for the final step in the formation of smoke would be that of the polymerization of C_2 radicals. Such a mechanism was at one time considered a plausible and promising explanation of smoke formation (e.g., ref. 18). However, the theory of smoke formation via C_2 has now been rejected by numerous authors (refs. 17, 24, and 32).

A mechanism based on simultaneous polymerization and dehydrogenation is proposed in reference 32 to account for the steps between acetylene and smoke. The reaction is exemplified by the following equation:

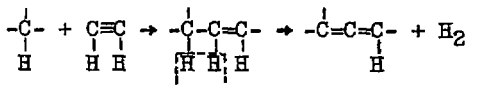

Transient diene structures like those indicated were also deemed important in reference 30.

Analogous to the work of reference 32 is the indication in reference 24 that a mechanism involving free radicals or atoms is important in the formation of smoke. The activation-energy requirements for such free-radical reactions were considered, and the following values were reported:

	Energy, kcal/mole
$C_2H + C_2H_2 \rightarrow C_4H_3 \rightarrow C_4H + H_2$	~58
$C_2H + C_2H_2 \rightarrow C_4H_2 + H$	~29
$C_2H_2 + C_2H_2 \rightarrow C_4H_3 + H$	~60

Reference 24 indicates that the first equation is of the type suggested by Porter and proposes that, while the reaction is feasible and may occur to some extent, its activation energy is much higher than that for the reaction shown in the second equation. The third equation shows a possibility for the use of the energy of combination in initiating reactions perhaps more effectively than by purely thermal means. At particularly high temperatures, more than one reactive radical or hydrogen atom could result from a step such as the second equation, and chain-branching might result. Steps such as these can occur with molecules containing larger and larger numbers of carbon atoms, leading eventually to formation of carbon nuclei and even to growth of a particle.

In summary, the general mechanism of smoke formation, based on the information currently available, probably proceeds as follows:

(1) Some hydrogen atoms are removed from the fuel molecule by thermal processes. The hydrogen atoms, in turn, cause further dehydrogenation of the molecule. The more readily the hydrogen atoms are removed as compared with the breaking of carbon bonds, the greater is the probability of smoke formation.

(2) After these initial dehydrogenation steps, the fuel molecules probably continue to decompose to smaller molecules and fragments of molecules. Acetylene is reported to be the last stable product to appear before smoke formation. Various authors have shown that a breakdown to smaller products must occur rather than an immediate growth to polymers or aromatic ring structures.

(3) Although a breakdown to small fragments and relatively small molecules takes place, the formation of smoke through polymerization of C_2 radicals has been rejected. It has been proposed that in the final stages the small molecules such as acetylene and hydrocarbon fragments undergo a simultaneous polymerization and dehydrogenation to form smoke.

Coke

3090

As previously mentioned, both the chemical and physical nature of hard combustor coke and the location of these deposits on the combustor liner suggest that this material is formed by the liquid-phase degradation of fuel residues. In reference 5 it was concluded that this hard coke "is largely a petroleum coke resulting from liquid phase cracking, subsequent pyrolysis, and final coking of the fuel from the spray nozzle as it impinges on the hot liner wall," and that soft combustor coke consists of smoke mixed with the residue from the degradation of fuel in the liquid phase. If it is assumed that combustor coke is largely the product of hydrocarbon-cracking reactions in the liquid phase, then the literature on the cracking of petroleum should apply to this problem.

Reference 34 on the formation and properties of petroleum coke is of interest, since it describes quite fully the later stages in the reactions yielding this product. This reference cites earlier work that proposes the following sequence of reactions: paraffins → olefins → aromatics with side chains → condensed ring systems → asphaltenes → carboids. The last reaction is then expanded to include the series of: asphalt → pitch → semipitch → asphaltic coke → carboid coke (→ graphite). It is of little importance whether the earlier stages of the over-all coking reaction proceed as indicated, since all commercial jet fuels contain aromatics in sufficient quantity to yield very easily the amount of coke found in combustors. These aromatics would be relatively nonvolatile, and this class of compounds would be concentrated in the liquid residues on combustor walls. The conversion of these residues to the various asphaltic and coke-like products is accomplished at temperatures of the order of 850° to 1475° F, and these products resemble combustor cokes in many ways (ref. 5).

The temperature at which combustor coke is formed cannot be determined by a comparison with the properties of petroleum cokes formed at different temperatures. The hydrogen-to-carbon ratio of hard combustor coke (ref. 4) is about the same as that found in reference 34 for petroleum coke formed at about 1380° F. However, the high concentration in combustor coke of solvent soluble materials suggests a much lower temperature of formation, of the order of 750° to 925° F. Probably, this lower temperature range is more nearly the temperatures at which the fuel was degraded, and the observed low hydrogen-to-carbon ratio is the result of the trapping of smoke in the coke deposits. True smoke has a comparatively low hydrogen-to-carbon ratio and would reduce this ratio to that found in the coke samples (ref. 4).

Combustor coke is produced in the presence of oxygen and flame; petroleum coke results from the decomposition of hydrocarbons alone. Because of these dissimilarities in formation, the determination of the conditions for the production of combustor coke may not be based on those for petroleum coke. The literature on the cracking of hydrocarbons in the presence of small amounts of air or oxygen might be more applicable. The presence of oxygen certainly accelerates the formation of high-molecular-weight, asphaltic materials from lower-molecular-weight hydrocarbons. Asphalt is made commercially by blowing residual petroleum fractions with air at temperatures from 425° to 600° F; the liquid hydrocarbon is converted to semisolids by this treatment (ref. 35).

A direct attempt to simulate combustor conditions in the formation of coke with a bench-scale apparatus is reported in reference 36. In this work, fuel was allowed to drip on a heated metal plate, and the evaporated fuel vapors were ignited by a small pilot flame. The amount of coke deposited was determined by weighing the metal plate before and after the test. Residues similar to combustor coke were formed at plate temperatures of about 600° F, and the amount of deposits decreased to substantially zero at about 1000° F. This test was developed primarily as a fuel evaluation test and has not been used to propose a mechanism for coke formation, although it does indicate that the formation of coke may be minimized with high metal temperatures.

In summary, it appears probable that combustor coke is formed by degradation, in the liquid phase, of the less volatile fuel components. This coke probably contains considerable quantities of gas-phase-produced smoke that is trapped therein. The degradation of fuel is accelerated by oxygen, and coke may be produced at temperatures in the 750° to 950° F range.

3090

EFFECT OF SOLIDS ON RADIANT HEAT TRANSFER

Information concerning radiant heat transfer from flames is necessary for the evaluation of problems such as combustor-wall cooling, application of flame-immersed fuel vaporizers, and the rate of evaporation of fuel droplets. This section deals with the effect of the solid products of combustion on the radiant power or the emissivity of flames. The solid products that become attached to the combustor walls (coke) may also influence radiant heat transfer to these walls by increasing the surface emissivity. However, this latter effect is not believed to be of much importance, since the emissivity of the usual materials of construction is quite high at high temperatures and would not be greatly increased by coke deposits.

Nonluminous flames emit two types of radiation. These are (1) electronic emission by radicals in the ultraviolet and visible region, and (2) molecular emission by water and carbon dioxide in the infrared. The electronic emission comprises a very small fraction of the total radiant power from combustion processes, and its effect on radiant heat transfer can be ignored. Luminous flames yield, in addition to the preceding types of radiation, a black-body radiation that arises from the hot solids present in such flames. A large fraction of this black-body radiation is in the near infrared. A further discussion of the radiation from both types of flames can be found in reference 37.

The radiant power from a combustion zone increases sharply as the flame is changed from a nonluminous to a luminous type. This change may be accomplished by increasing the pressure, the fuel-air ratio, or the smoking tendency of the fuel. As an example of the effect of pressure, a study of the radiation from flames in a turbojet combustor (ref. 38) showed that the radiant power increased rapidly with pressure and to a lesser degree with changes in fuel-air ratio. Pressures ranged from 20 to 95 inches of mercury absolute, and the total radiation from a luminous flame was several times greater than that from a nonluminous flame. Increases in fuel-air ratio that changed nonluminous flames to luminous ones were studied in a laboratory burner (ref. 39) and in a small furnace (ref. 40). A fourfold increase in radiant power was observed with acetylene fuel in the laboratory burner and a two- to threefold increase with natural gas in the furnace. In reference 41, the character of the fuel fed to an industrial furnace was varied. The addition of small amounts of fuels of high smoking tendencies, such as benzene or tar, increased the emissivity of the flame from 0.15 to 0.4. In general, the emissivity or radiant power from a flame increases several times as the flame becomes luminous because of the presence of solid products of combustion.

Fairly accurate calculations of the rate of radiant heat transfer can be made for nonluminous flames with the method and charts of reference 42. These require, as input variables, the combustion-chamber geometry, reaction stoichiometry, pressure, and temperature. Similar calculations cannot be made on a theoretical basis alone for luminous flames. These require the experimental measurement of at least two flame properties to determine emissivity. In reference 42, two-color optical pyrometry was used to determine red and green brightness temperatures, which were then used in the calculation of emissivity. In reference 38, a total-radiation pyrometer and a red-filtered optical pyrometer were used to supply the necessary experimental data. Once emissivities are known, the calculation of radiant heat-transfer rates is similar for both luminous and nonluminous flames.

In summary, radiant heat transfer is greatly increased by the presence of solid combustion products. Quantitative determinations of the radiant power from luminous flames require, at present, experimental measurements of the flame in question. However, it is possible that further research plus a backlog of experience on various types of combustors may eventually permit estimates of radiant heat transfer from luminous flames based on theory alone.

SIGNIFICANCE OF BASIC SMOKE AND COKE STUDIES IN DESIGN OF JET-ENGINE COMBUSTORS

The factors relating to the formation of solid carbon during the combustion of hydrocarbons in simple laboratory flames have been reviewed. Some of the major conclusions resulting from the study of laboratory flames that are pertinent to combustor design may be summarized as follows:

1. Smoke is formed only in systems containing a fuel-rich region. Coke and smoke will not result from the combustion of premixed fuel-air systems if the mixture strength is maintained near stoichiometric. Therefore, any combustor design that minimizes or eliminates the presence of local fuel-rich regions should also minimize or eliminate the smoking and coking tendency of the combustor. It is recognized that fuel-lean operation reduces combustor stability and altitude efficiencies. Therefore, compromises must be made in combustor design to obtain satisfactory performance in regard to both burner stability and efficiency and to freedom from coking.

2. Increasing pressure increases the carbon-forming tendency of hydrocarbon flames. Therefore, the problems of smoke and coke, and also of radiant heat-transfer effects, increase with increasing combustion-chamber pressure.

3. There are pronounced differences in the smoking tendencies of the various hydrocarbon fuels. Of the hydrocarbon types commonly found in petroleum-derived fuels, aromatics have by far the greatest smoking tendencies. However, there are large differences among the various classes of aromatics. The problems of controlling smoke and coke in turbojet engines can be lessened by limiting the aromatic concentrations in fuels and especially by limiting the concentrations of the more objectionable types of aromatics.

REFERENCES

1. Wear, Jerrold D., and Douglass, Howard W.: Carbon Deposition from AN-F-58 Fuels in a J33 Single Combustor. NACA RM E9D06, 1949.

2. Butze, Helmut F.: Effect of Inlet-Air and Fuel Parameters on Smoking Characteristics of a Single Tubular Turbojet-Engine Combustor. NACA RM E52A18, 1952.

3. Schalla, Rose L., Clark, Thomas P., and MacDonald, Glen E.: Formation and Combustion of Smoke in Laminar Flames. NACA Rep. 1186, 1954. (Supersedes NACA RM's E51E15, E52G24, E52I22, E52I26, E53E05, E53J12, and E54E03.)

4. Biscoe, J., and Warren, B. E.: An X-Ray Study of Carbon Black. Jour. Appl. Phys., vol. 13, no. 6, June 1942, pp. 364-371.

5. Clark, Thomas P.: Examination of Smoke and Carbon from Turbojet-Engine Combustors. NACA RM E52I26, 1952.

6. Terry, John B., and Field, Edward: The Smoke Tendency of Refined Kerosene and Its Determination. Ind. and Eng. Chem. (Anal. ed.), vol. 8, no. 4, July 15, 1936, pp. 293-295.

7. Hunt, Russell A., Jr.: The Relation of Smoke Point to Molecular Structure. Ind. and Eng. Chem., vol. 45, no. 3, Mar. 1953, pp. 602-606.

8. Anon.: Standard Method of Testing Petroleum and Its Products. Third ed., Inst. Petroleum Tech. (London), 1935, pp. 133-136.

9. Krynitsky, J. A., Garrett, W. D., and McLean, C. A.: Factors Affecting the Use of a Smoke Lamp for Evaluating Jet Fuels. NRL Rep. 4068, Naval Res. Lab., Oct. 16, 1952.

10. Jezl, J. L.: Smoking Tendencies of Fuels. Rep. No. D-1016, Res. and Dev. Dept., Sun Oil Co., Feb. 14, 1950.

11. Busch, Arthur M.: Correlation of Laboratory Smoke Test with Carbon Deposition in Turbojet Combustors. NACA RM E9K04, 1950.

12. Clarke, A. E., Hunter, T. G., and Garner, F. H.: The Tendency to Smoke of Organic Substances on Burning, Pt. I. Jour. Inst. Petroleum, vol. 32, no. 274, Oct. 1946, pp. 627-642.

13. Ebersole, Earl R., and Barnett, Henry C.: Smoking Characteristics of Various Fuels as Determined by Open-Cup and Laboratory-Burner Smoke Tests. NACA WR E-190, 1945. (Supersedes NACA MR's E5F20 and E5I12.)

14. Sacks, W., and Ziebell, M.T.I.: Carbon Formation in Flames of Aromatic Hydrocarbons. Lab. Rep: LR-30, Nat. Aero. Est. (Canada), June 25, 1952.

15. Minchin, S. T.: Luminous Stationary Flames: The Quantitative Relationship Between Flame Dimensions at the Sooting Point and Chemical Composition, with Special Reference to Petroleum Hydrocarbons. Jour. Inst. Petroleum Technologists, vol. 17, 1931, pp. 102-120.

16. Street, J. C., Thomas, A., and Williams, R. A.: Carbon Formation in Pre-Mixed Flames. Rep. K.113, Aero-Engine Lab., Thornton Research Center, Sept. 1953. (Contract No. 6/ENGS/4668/CB.11(a).)

17. Parker, W. G., and Wolfhard, H. G.: Carbon Formation in Flames, Pt. III. Jour. Chem. Soc. (London), Aug. 1950, pp. 2038-2044; discussion, pp. 2045-2049.

18. Smith, E. C. W.: The Emission Spectrum of Hydrocarbon Flames. Proc. Roy. Soc. (London), ser. A, vol. 174, no. A956, Jan. 12, 1940, pp. 110-125.

19. Gaydon, A. G., and Wolfhard, H. G.: Flames. Chapman and Hall (London), 1953.

20. Kewley, J., and Jackson, J. S.: The Burning of Mineral Oils in Wick Fed Lamps. Jour. Inst. Petroleum Tech., vol. 13, 1927, pp. 364-397.

21. Jonash, Edmund R., Wear, Jerrold D., and Hibbard, Robert R.: Relation Between Fuel Properties and Combustion Carbon Deposition. NACA RM E52B14, 1952.

22. Schalla, Rose L., and McDonald, Glen E.: Variation in Smoking Tendency Among Hydrocarbons of Low Molecular Weight. Ind. and Eng. Chem., vol. 45, no. 7, July 1953, pp. 1497-1500.

23. Wolfhard, H. G., and Parker, W. G.: Influence of Sulfur on Carbon Formation in Diffusion Flames. Fuel, vol. 29, no. 10, Oct. 1950, pp. 235-240.

24. Frazee, J. D., and Anderson, Robbin C.: Carbon Formation and Reaction in Flames in Acetylene. Abs. of papers presented at meeting of Am. Chem. Soc., Chicago (Ill.), Sept. 6-11, 1953.

25. Steacie, E. W. R.: Atomic and Free Radical Reactions. Reinhold Pub. Corp. (New York), 1946.

26. Arthur, J. R.: Some Reactions of Atomic Hydrogen in Flames. Nature, vol. 165, no. 4197, Apr. 8, 1950, pp. 557-558.

27. Iyengar, M. S., Vaidyeswaran, R., and Datar, D. S.: Studies on Carbon Formation in Flames. Pt. I. Suppression of Carbon Deposit Formation in Flames of Some Organic Compounds by Carbon Dioxide and Nitrogen. Jour. Sci. Ind. Res. (India), vol. 11B, 1952, pp. 455-457.

28. Rummel, Kurt, and Veh, Paul O.: Radiation of Luminous Flames. I - Literature, Working Hypotheses and Preliminary Tests. Arch. Eisenhuttenw., vol. 14, 1941, pp. 489-499.

29. Thorp, N., Long, R., and Garner, F. H.: Carbon Formation in Benzene-Oxygen Diffusion Flames. Fuel, vol. 30, no. 11, Nov. 1951, p. 266.

30. Garner, F. H., Long, R., and Thorp, N.: Carbon Formation in Hydrocarbon Diffusion Flames. Fuel, vol. 32, 1953, pp. 116-117.

31. Grisdale, R. O.: The Formation of Black Carbon. Jour. Appl. Phys., vol. 24, no. 9, Sept. 1953, pp. 1082-1091.

32. Porter, George: Carbon Formation in the Combustion Wave. Fourth Symposium (International) on Combustion, The Williams & Wilkins Co. (Baltimore), 1953, pp. 248-252.

33. Tropsch, Hans, and Egloff, Gustav: High-Temperature Pyrolysis of Gaseous Paraffin Hydrocarbons. Ind. and Eng. Chem., vol. 27, no. 9, Sept. 1935, pp. 1063-1067.

34. Berry, A. G. V., and Edgeworth-Johnstone, R.: Petroleum Coke Formation and Properties. Ind. and Eng. Chem., vol. 36, no. 12, Dec. 1944, pp. 1140-1144.

35. Puller, H. B., et al.: Blown Asphalt. Vol. IV. Sci. of Petroleum, Oxford Univ. Press, 1938, pp. 2700-2705.

36. Rogers, J. D., and Jones, D. R.: Combustion Characteristics of Gas Turbine Fuels. Prog. Rep. No. 27, Calif. Res. Corp., Dec. 31, 1949. (Contract W-33-038ac-9083, AMC Proj. MX-587.)

37. Berlad, A. L., and Hibbard, R. R.: Effect of Radiant Energy on Vaporization and Combustion of Liquid Fuels. NACA RM E52I09, 1952.

38. Topper, Leonard: Radiant Heat Transfer from Flames in a Single Tubular Turbojet Engine. NACA RM E52F23, 1952.

39. Haslam, R. T., and Boyer, M. W.: Radiation from Luminous Flames. Ind. and Eng. Chem., vol. 19, no. 1, Jan. 1927, pp. 4-6.

40. Sherman, Ralph A.: Radiation from Luminous and Non-Luminous Natural-Gas Flames. Trans. A.S.M.E., vol. 56, no. 3, Mar. 1934, pp. 177-185.

41. Ribaud, G.: Heat Transmission by Radiation in Industrial Furnaces. Chem. Abs., vol. 42, no. 7, Apr. 10, 1948, p. 2145d. (Abs. from Energie, vol. 31, 1947, pp. 57-67; 92-94.)

42. Hottel, Hoyt C.: Section on Heat Transfer. Chemical Engineers' Handbook, Third ed., John H. Perry, ed., McGraw-Hill Book Co., Inc., 1950, pp. 483-498.

3090

3090

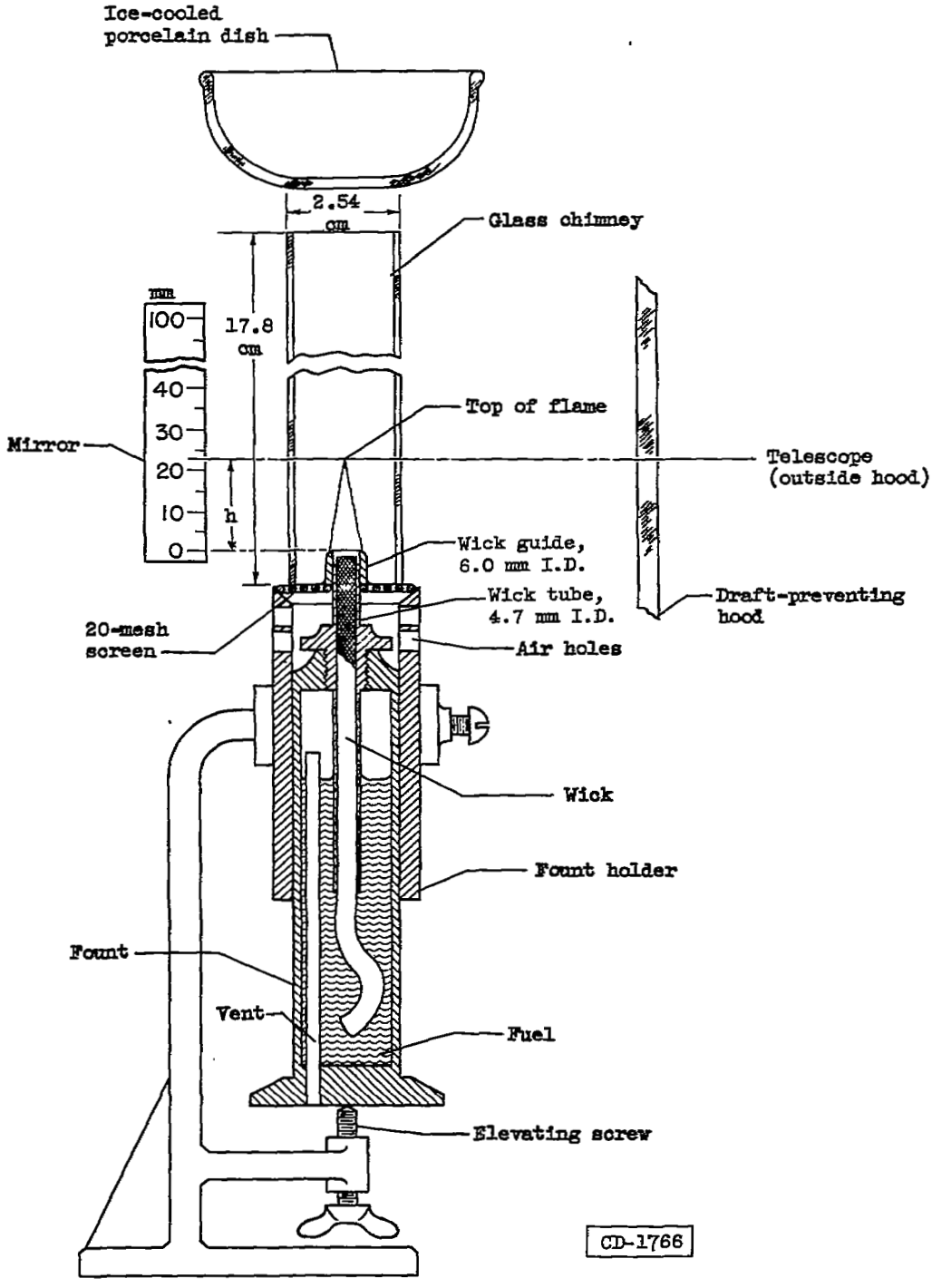

Figure IX-1. - NACA modified Davis factor lamp (ref. 11).

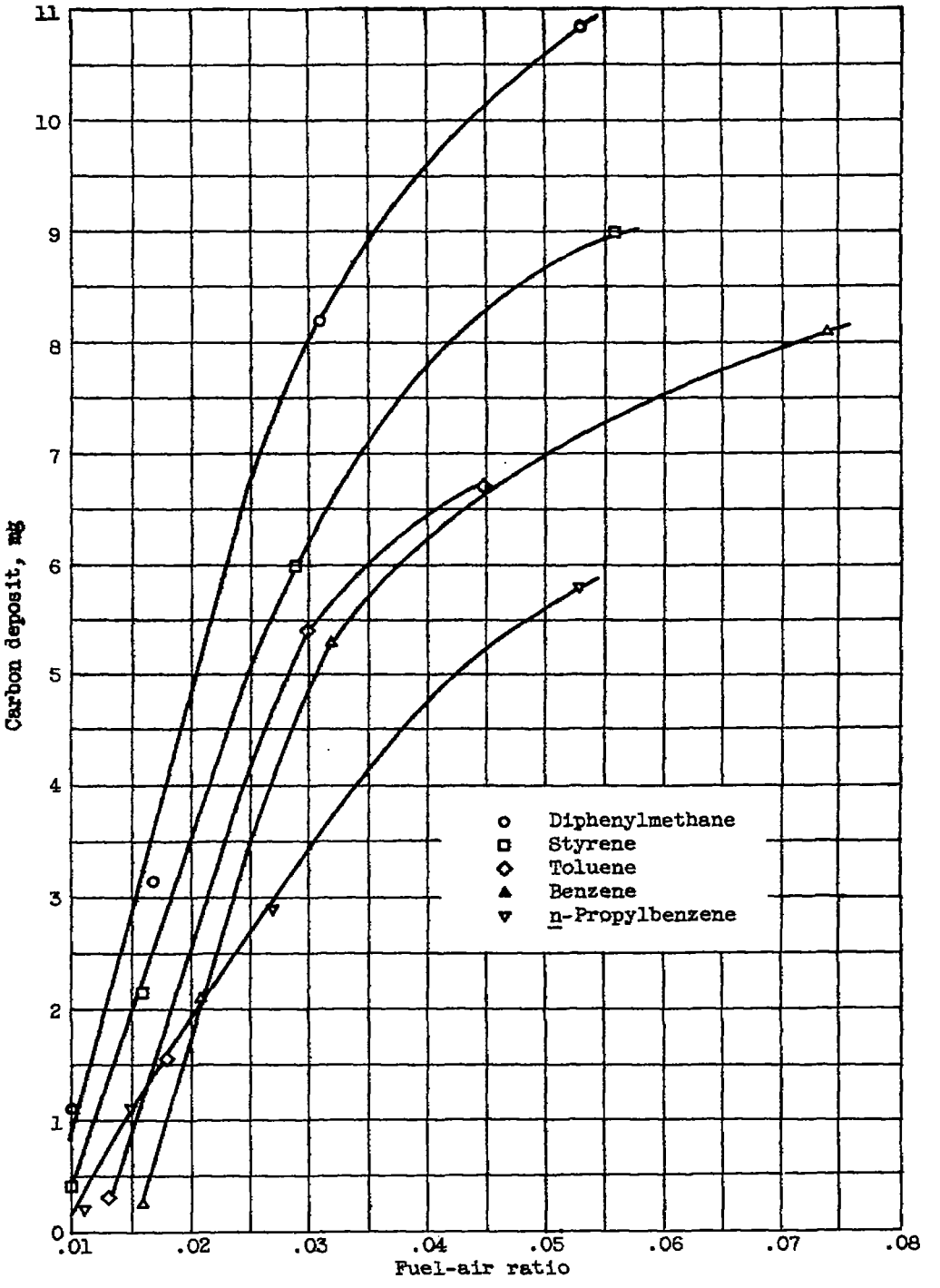

Figure IX-2. - Variation of carbon deposit with fuel-air ratio for several fuels burning as diffusion flames. Air flow past flame, 10 liters per minute (ref. 14).

3090

3090

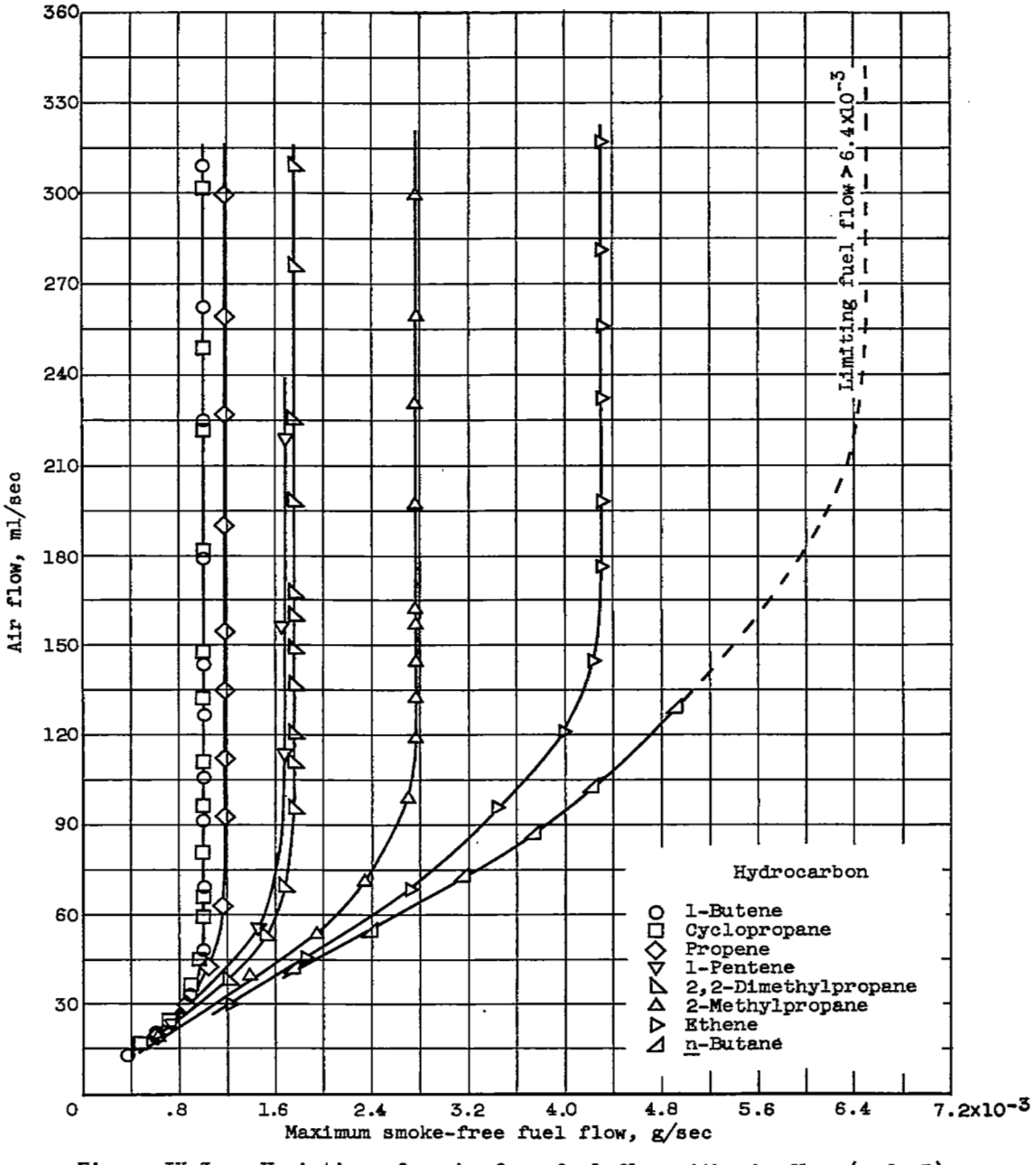

Figure IX-3. - Variation of smoke-free fuel flow with air flow (ref. 3).

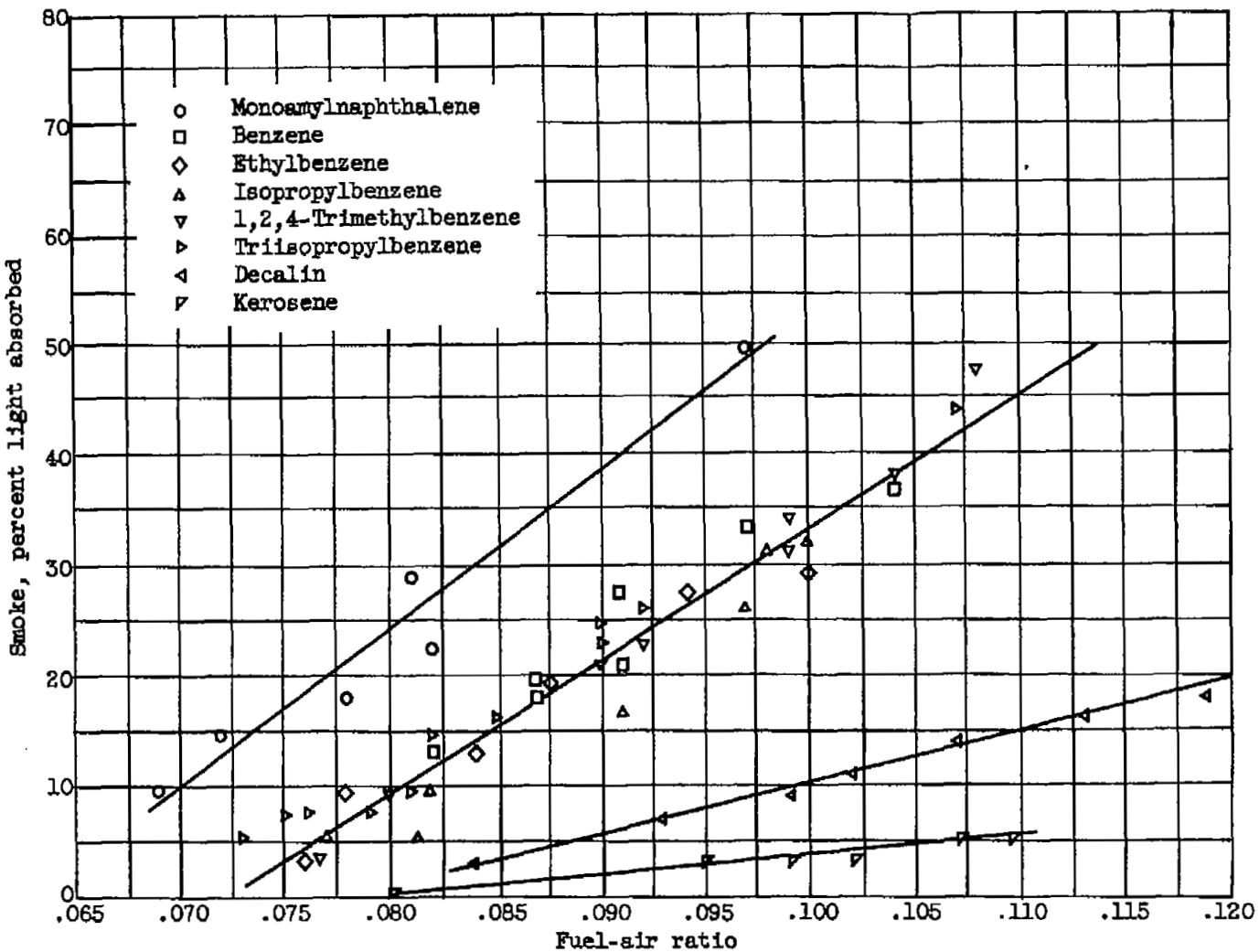

Figure IX-4. - Variation of smoke with fuel-air ratio for several fuels burning as Bunsen flames. Air flow, 4.1 liters per minute (ref. 13).

3090

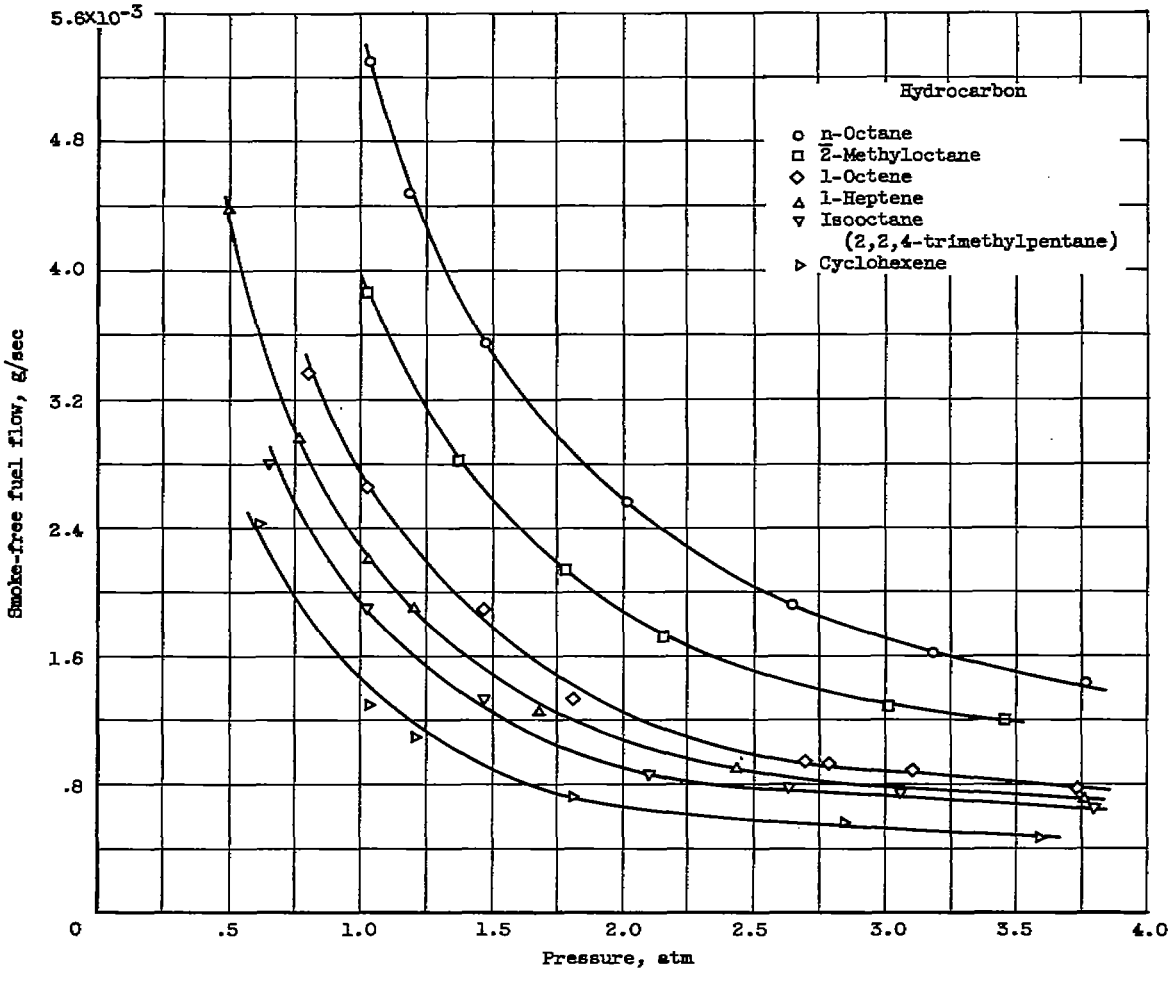

(a) Six hydrocarbons at pressures to 4 atmospheres.

Figure IX-5. - Variation of smoke-free fuel flow with pressure (ref. 3).

[redacted]

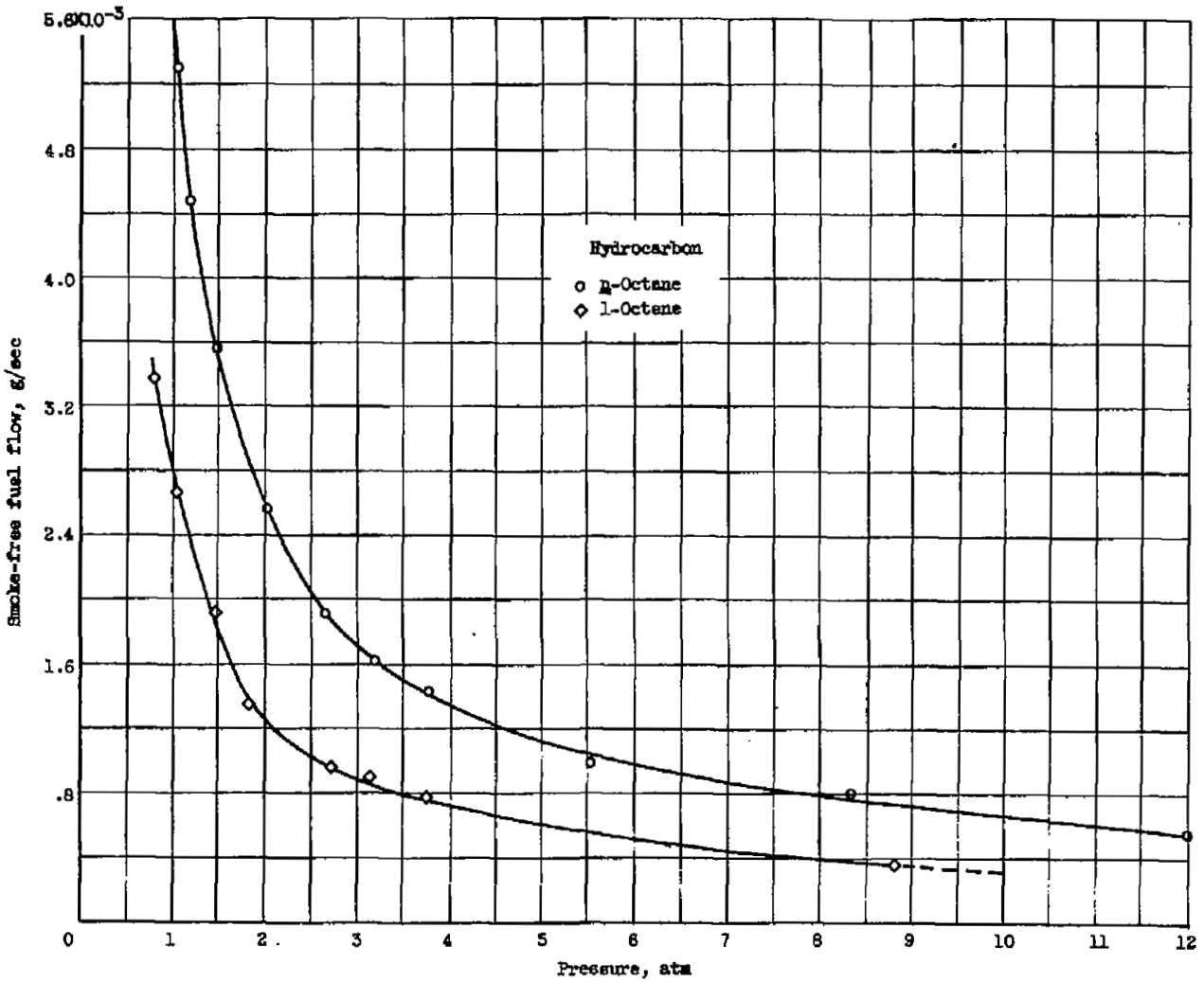

(b) Two hydrocarbons at pressures to 12 atmospheres.

Figure IX-5. - Continued. Variation of smoke-free fuel flow with pressure (ref. 3).

3090

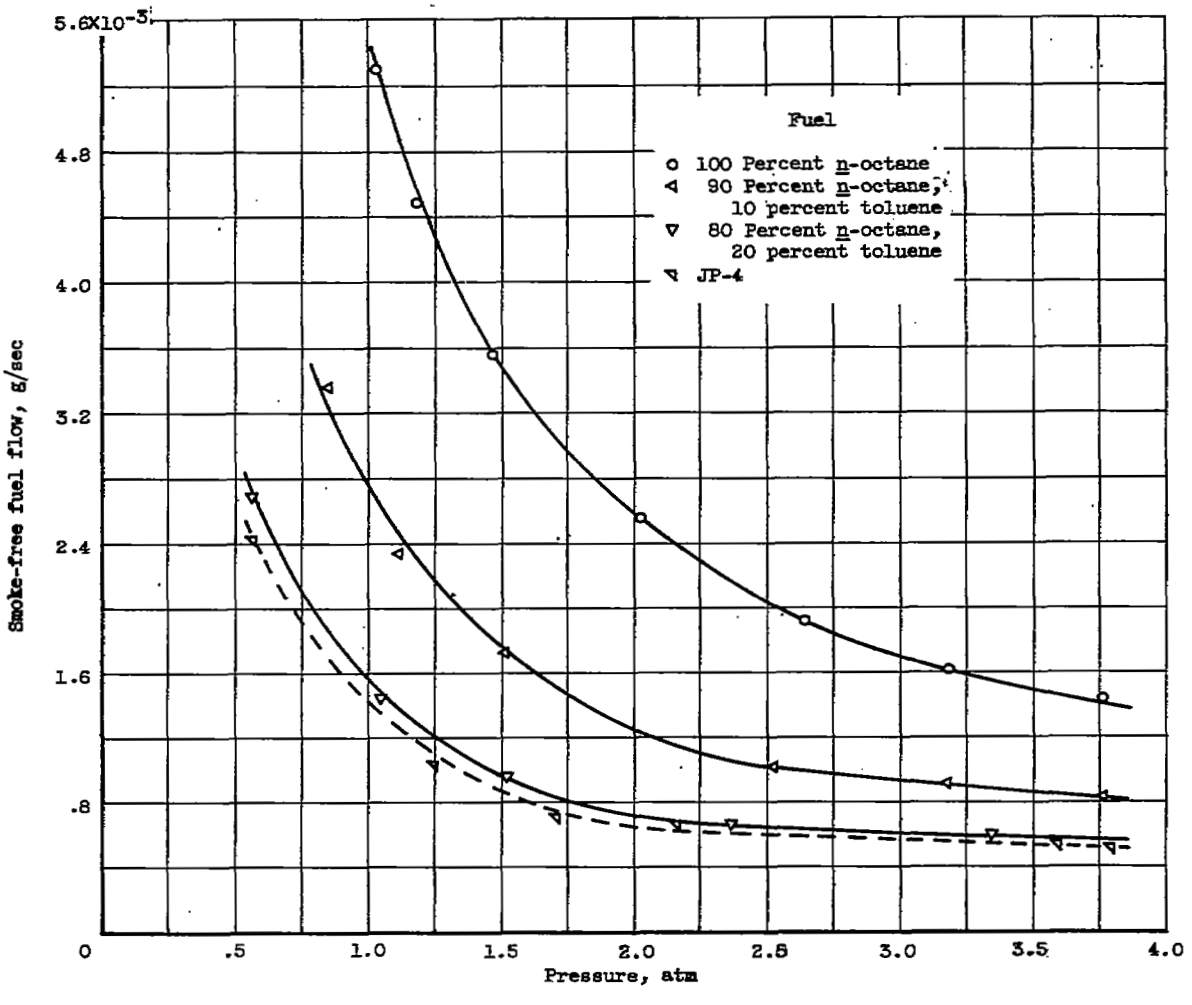

(c) Various fuels and blends at pressures to 4 atmospheres.

Figure IX-5. Concluded. Variation of smoke-free fuel flow with pressure (ref. 3).

[redacted]

3090

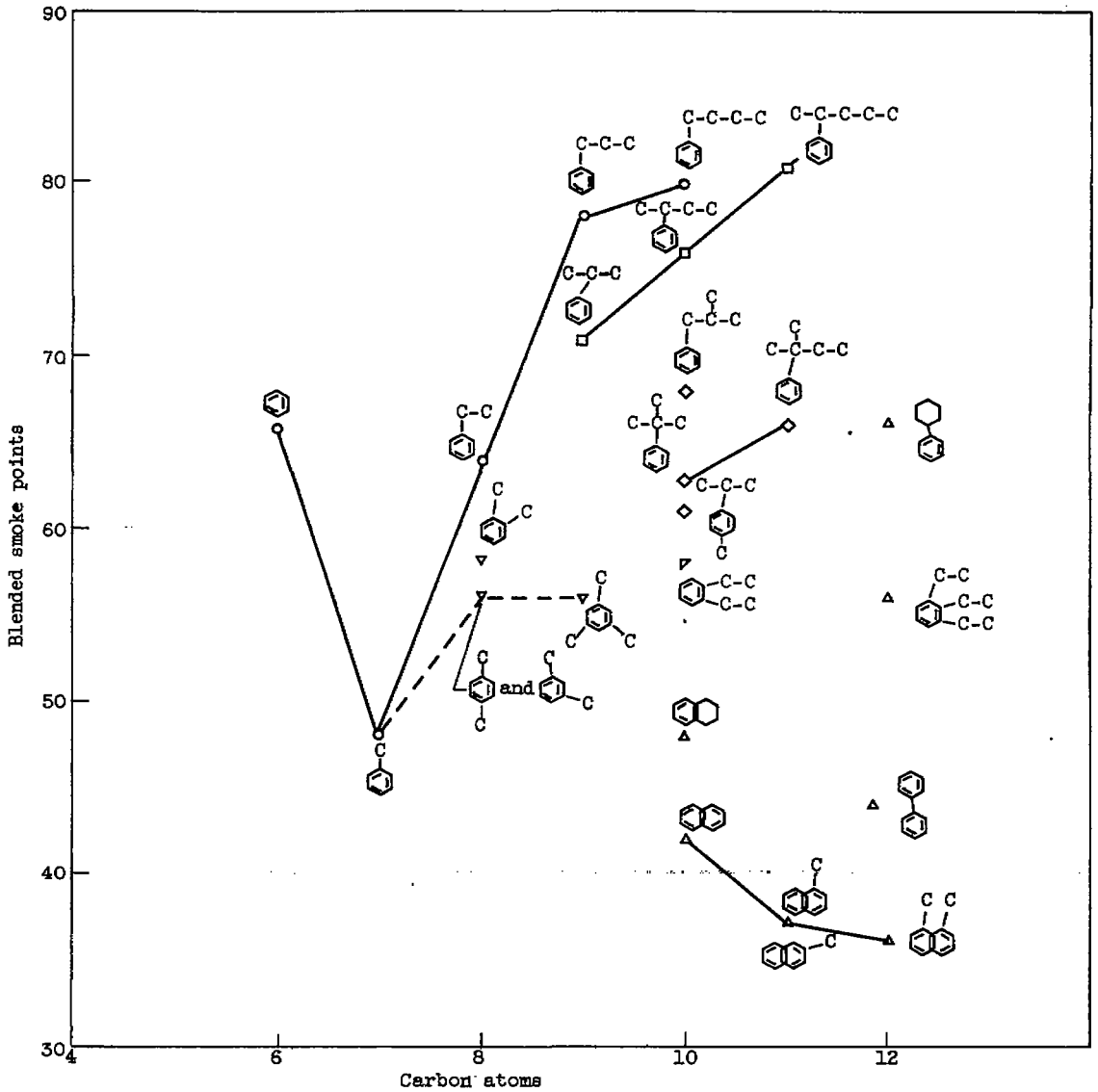

Figure IX-6. - Relation between molecular structure and smoking tendency for aromatics as determined in a modified Davis factor lamp (by permission from ref. 7). (20-Volume-percent blends of aromatic with n-dodecane.)

3090

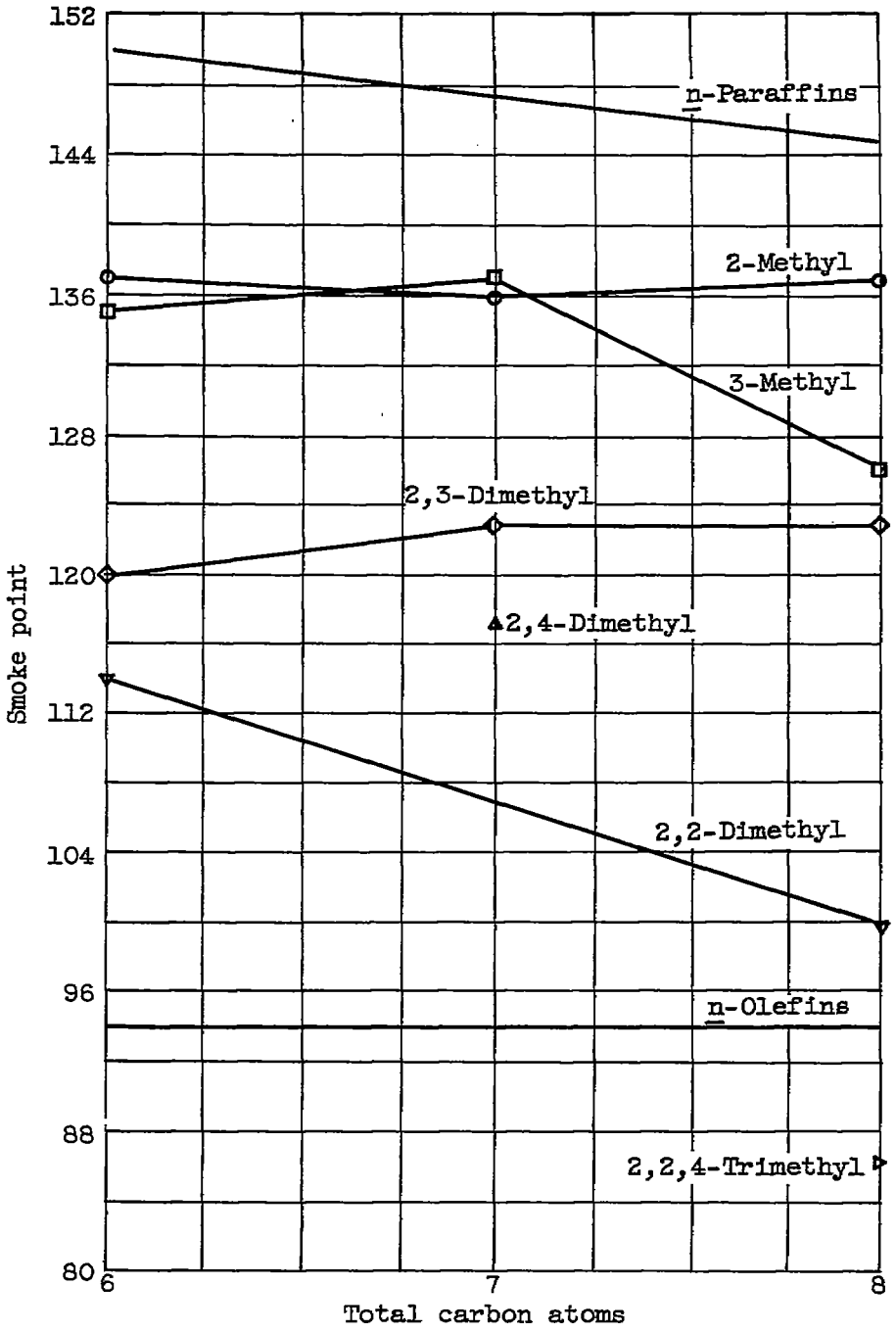

Figure IX-7. - Relation of molecular structure and smoking tendency for paraffins and olefins as determined in a modified Davis factor lamp (by permission from ref. 7).

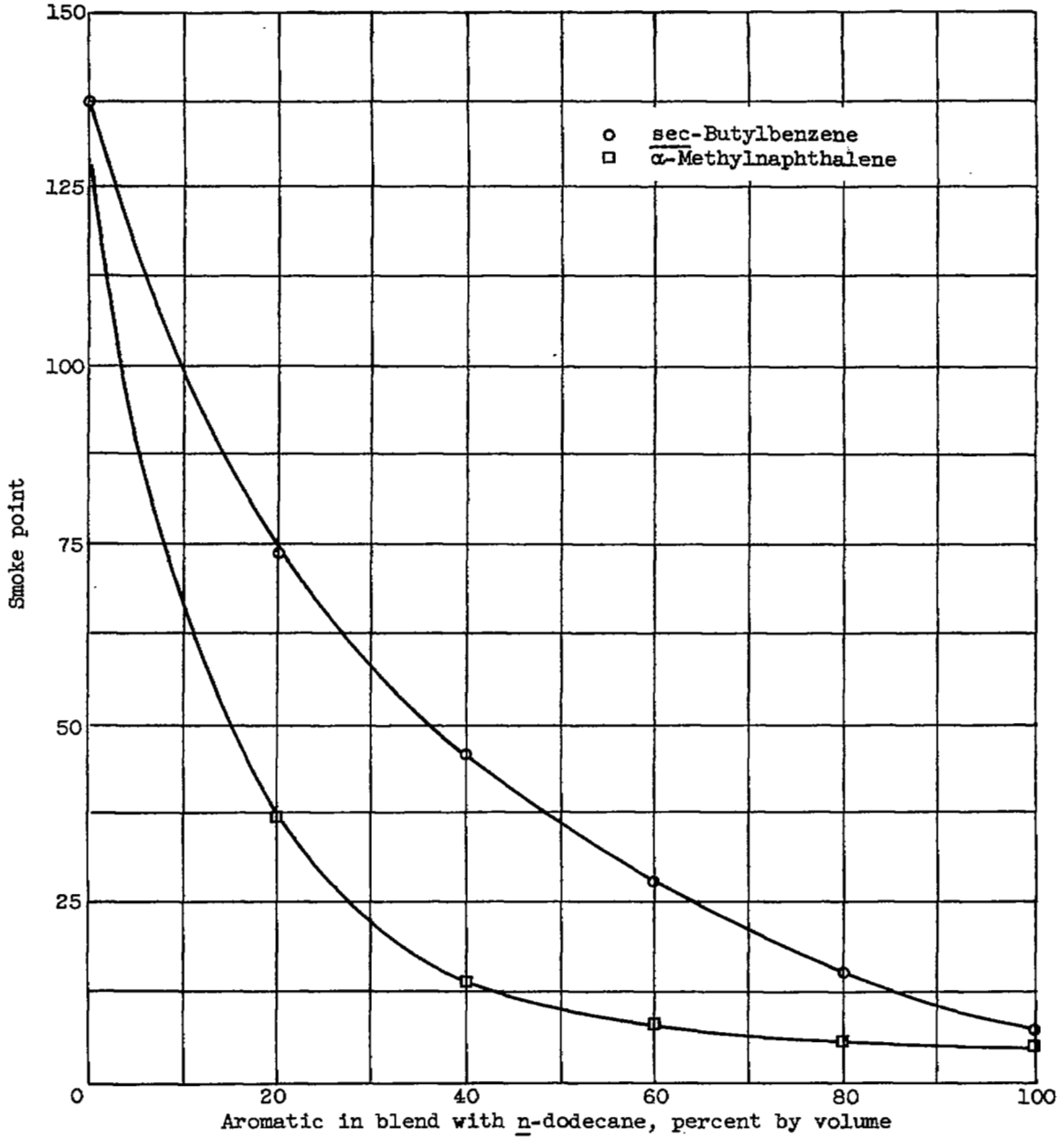

Figure IX-8. - Relation of blend composition and smoking tendency as determined in a modified Davis factor lamp (by permission from ref. 7).

3090

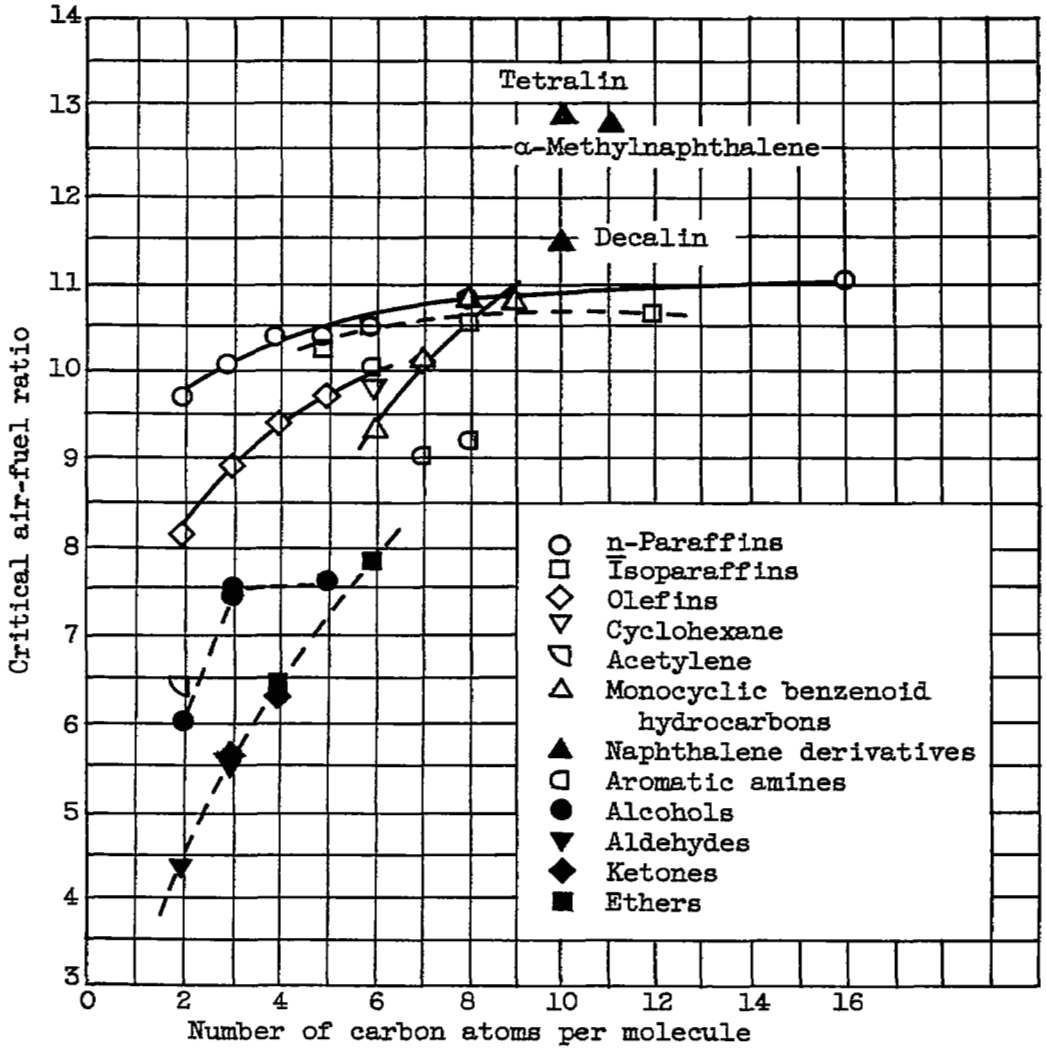

Figure IX-9. - Critical air-fuel ratio for carbon formation as a function of molecular weight and fuel type (ref. 16).

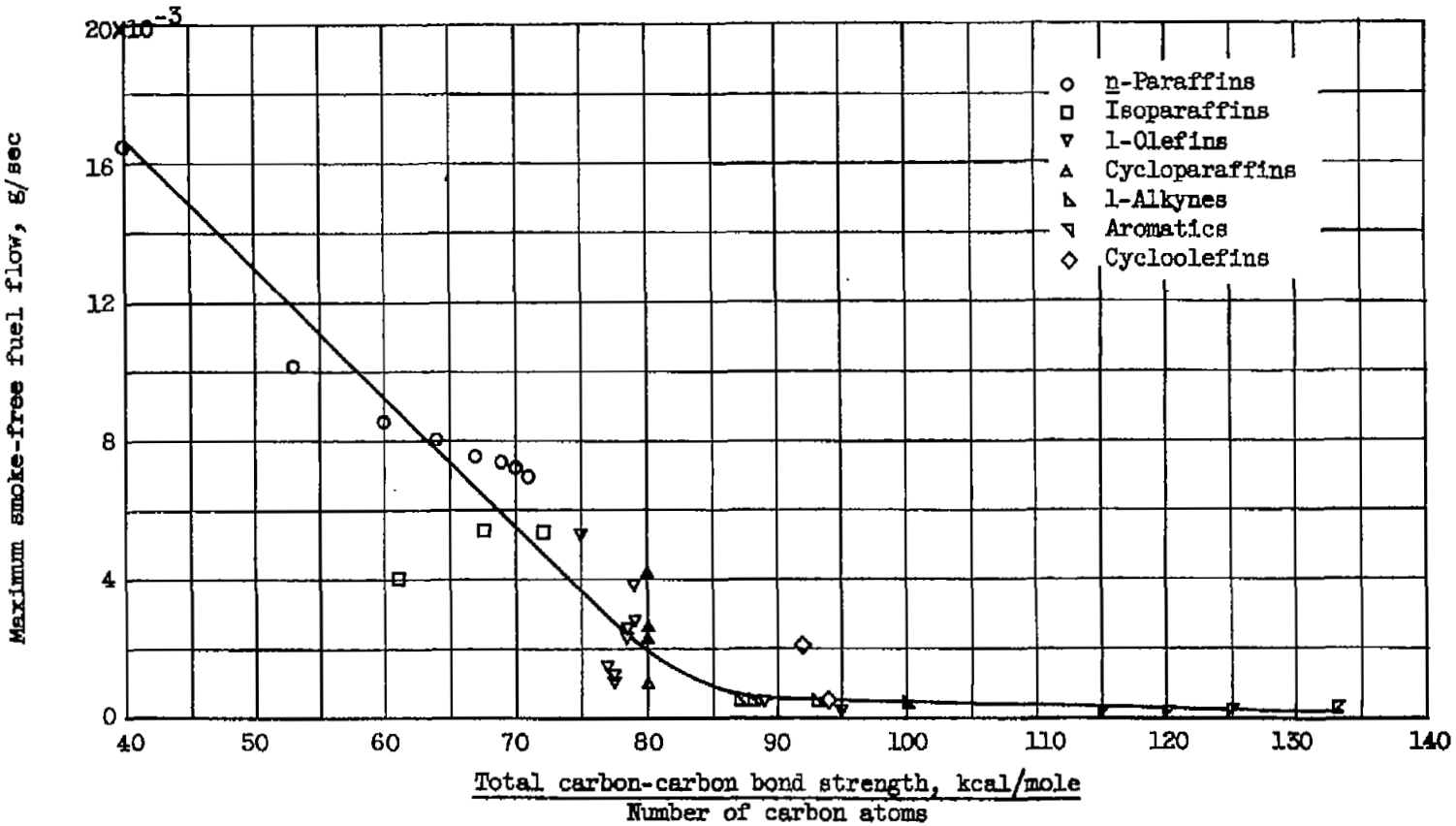

Figure IX-10. - Variation of maximum smoke-free fuel flow with total carbon-carbon bond strength per number of carbon atoms (by permission from ref. 22).

APPENDIX - PHYSICAL AND COMBUSTION PROPERTIES OF SELECTED FUELS

Data according to various investigators have been compiled and are presented in table I. Column headings are explained as follows:

Sp. gr. - Specific gravities were obtained from reference 1, except as noted. Values from reference 1 are 60°/60° F, while those from reference 2 are generally 20°/4° C.

B.p. - Normal boiling points at 1 atmosphere were taken from reference 1, except as noted.

ΔH_{vap}. - Heats of vaporization were obtained from reference 1, except as noted.

ΔH_c. - Heats of combustion of gaseous fuel to give gaseous products are from reference 1.

Stoich. mixt. - Stoichiometric mixtures are given, as mole fraction of fuel (volume percent/100) and as fuel-air ratio by weight.

Flammability limit. - Flammability limits in percent of stoichiometric fuel-air ratio, in most cases obtained with upward propagation in a 2-inch tube closed at both ends, are from reference 3, except as noted.

Spon. ig. temp. - Spontaneous ignition temperatures were determined by the modified A.S.T.M. drop test in reference 4, except as noted. Minus signs following values indicate that slightly lower values have been reported.

f/a for max. U_F. - Fuel concentrations in percent stoichiometric fuel-air ratio for maximum burning velocity were determined at 77° F and atmospheric pressure (ref. 5).

Max. U_F (ref). - Maximum burning velocities relative to propane, which are arbitrarily rated 100 for each experimental method (see table II for absolute values for propane for each method), were obtained from reference 5. Burning velocities were, in most cases, measured by the NACA tube method (see ref. 6).

T_F at f/a for max. U_F. - Adiabatic flame temperatures were calculated at the stoichiometric fuel-air ratio for maximum burning velocity according to the method of reference 7. Values were obtained from reference 5.

Min. ig. energy. - Minimum ignition energies at stoichiometric fuel-air ratios and the absolute minimum ignition energies that occur at some richer concentration were obtained from reference 8, except as noted. In most cases, 1/8-inch rod electrodes (unflanged) and capacitance sparks were used; pressure was 1 atmosphere.

Quench. dist. - Quenching distances between parallel plates at stoichiometric fuel-air ratios, and absolute quenching distances through which no flame will pass regardless of concentration were estimated from log-log correlations between ignition energy and quenching distance (based on data from refs. 9 and 10 and information received from Experiment, Inc.) and minimum ignition energies included herein, except when taken from references 9 and 10.

TABLE I. - PHYSICAL AND COMBUSTION

[Numbered superscripts

Fuel	Molecular wt.	Sp. gr.	B.p., °F	ΔH_{vap}, Btu/lb	ΔH_c, gas-gas, Btu/lb	Stoich. mixt. By vol.	Stoich. mixt. By wt.
Acetaldehyde	44.1	0.783[2]	-70[2]	245[2]		0.0772	0.1280
Acetone	58.1	.792[2]	134[2]	224[2]		.0497	.1054
Acetylene	26.0	.621[2]	[b]-119		20,734	.0772	.0755
Acrolein	56.1	.841[2]	127[2]			.0564	.1163
Acrylonitrile	53.1	.797[2]	173[2]			.0528	.1028
Allene (propadiene)	40.1		-30		19,921	.0497	.0728
Ammonia	17.0	[e].817	-28[2]	590[2]		.2181	.1645
Aniline	93.1	1.022[2]	364[2]	187[16]		.0263	.0872
Benzene	78.1	.885	176	169	17,446	.0271	.0756
,n-butyl-	134.2	.865	362		17,984	.0153	.0721
,sec-butyl-	134.2	.866	344			.0153	.0721
,tert-butyl-	134.2	.871	336			.0153	.0721
,1,2,-diethyl-	134.2	.884	362			.0153	.0721
,1,3-diethyl-	134.2	.868	358			.0153	.0721
,1,4-diethyl-	134.2	.866	363			.0153	.0721
,1,2-dimethyl- (o-xylene)	106.2	.885	292	149	17,723	.0195	.0734
,1,3-dimethyl- (m-xylene)	106.2	.869	282	147	17,716	.0195	.0734
,1,4-dimethyl- (p-xylene)	106.2	.866	281	146	17,719	.0195	.0734
,ethyl-	106.2	.872	277	146	17,767	.0195	.0734
,isobutyl-	134.2	.858	343			.0153	.0721
,isopropyl- (cumene)	120.2	.866	306	134	17,873	.0171	.0727
,1-methyl-2-ethyl-	120.2	.885	329	139	17,864	.0171	.0727
,1,-methyl-3-ethyl-	120.2	.869	322	138	17,853	.0171	.0727
,1-methyl-4-ethyl-	120.2	.866	324	137	17,848	.0171	.0727
,1-methyl-3,5-diethyl-	148.2	.867	393			.0138	.0717
,nitro-	123.1	1.199[2]	412[2]	142[16]		.0324	.1429
,propyl-	120.2	.867	319	137	17,887	.0171	.0727
,1,2,3-trimethyl- (hemimellitene)	120.2	.899	349	143	17,825	.0171	.0727
,1,2,4-trimethyl- (pseudocumene)	120.2	.880	337	140	17,809	.0171	.0727
,1,3,5-trimethyl- (mesitylene)	120.2	.870	328	140	17,802	.0171	.0727
,vinyl- (styrene)	104.1	.911	293		17,598	.0205	.0755

[a]Tube open at lower end.

[b]Sublimes.

[c]Flanged electrodes.

[d]0.0225-Inch stainless-steel electrodes; spark duration, 1 millisec.

[e]Measured at -110° F.

[f]Measured at elevated temperatures by Bunsen burner schlieren total-area method and extrapolated to room temperature.

3560

PROPERTIES OF FUELS

indicate references.]

Flammability limit, percent of stoich.		Spon. ig. temp., °F	f/a for max. U_F, percent of stoich.	Max. U_F(rel)	T_F at f/a for max. U_F, °R	Min. ig. energy, 10^{-5} joule		Quench. dist., in.	
Lean	Rich					Stoich.	Abs. min.	Stoich.	Abs. min.
						37.6		0.09	
a_{59}[11]	a_{233}[11]	1042[12]	131	117[13]	3820	115		.15	
a_{31}[11]		581[12]	133	362[6]		c_3		.03	
a_{48}[11]	a_{752}[11]	532[12]	~100	144[14]		$c_{17.5}$		.06	
a_{87}[11]		898[12]	105	109[13]	4430	c_{36}	d_{16}[15]	.09	0.06
			121	189[13]	4430				
		1204[12]							
		1100-							
43	336	1097-	108	f_{104}[13]	4150	55	$d_{22.5}$[17]	.11	.07
		821	108	f_{84}[13]	4185				
		836							
		891	105	f_{85}[13]	4175				
		759							
		851							
		844							
		934-	108	f_{80}[13]	4205				
45	307	1045							
		1048							
a_{50}[11]		860							
		853							
52	352	873							
		836							
		905							
		902							
		861							
		900[12]							
		853							
		895							
		970	109	f_{84}[13]	4180				
		1039							
		914[12]							

TABLE I. - Continued. PHYSICAL AND

[Numbered superscripts

Fuel	Molecular wt.	Sp. gr.	B.p., °F	ΔH_{vap}, Btu/lb	ΔH_c, gas-gas, Btu/lb	Stoich. mixt. By vol.	Stoich. mixt. By wt.
Benzyl alcohol	108.1	1.050[2]	401[2]			0.0240	0.0923
Biphenyl	154.2	1.180[2]	490[2]			.0141	.0772
,2-butyl-	210.3					.0101	.0745
,2-ethyl-	182.3					.0118	.0756
,2-methyl-	168.2	1.010[2]	500[2]			.0129	.0763
,2-propyl-	196.3					.0109	.0750
1,2-Butadiene (methylallene)	54.1	[g].658	52		19,567	.0366	.0714
1,3-Butadiene (divinyl, vinylethylene)	54.1	[g].627	24		19,153	.0366	.0714
,2,3-dimethyl-	82.1	.731	156			.0240	.0701
,2-methyl- (isoprene)	68.1	.686	93		19,003	.0290	.0706
n-Butane	58.1	[g].584	31	166	19,655	.0312	.0649
,2-cyclopropyl-	98.2					.0195	.0679
,2,2-dimethyl-	86.2	.654	122	131	19,299	.0216	.0659
,2,3-dimethyl-	86.2	.666	136	136	19,338	.0216	.0659
,1,1-diphenyl-	210.3					.0101	.0744
,2-methyl- (isopentane)	72.1	.625	82	146	19,451	.0255	.0654
,2,2,3-trimethyl-	100.2	.695	178	124	19,241	.0187	.0661
Butanone (methylethyl ketone)	72.1	.805[2]	175[2]	191[2]		.0366	.0951
1-Butene	56.1	[g].601	21	168	19,475	.0337	.0679
,2-cyclopropyl-	96.2					.0205	.0698
,2,3-dimethyl-	84.2	.683	132		19,159	.0227	.0679
,2-ethyl-	84.2	.694	148		19,198	.0227	.0679
,2-methyl-	70.1	.656	88		19,252	.0271	.0678
,3-methyl- (α-isoamylene)	70.1	.633	68		19,297	.0271	.0678
,2,3,3-trimethyl-	98.2	.710	172		19,092	.0195	.0679
trans-2-Butene	56.1	[g].610	34	174	19,389	.0337	.0679
2,3-dimethyl-2-butene	84.2	.713	164		19,135	.0227	.0679
2-methyl-2-butene	70.1	.668	101		19,214	.0271	.0678
3-Buten-1-yne (vinylacetylene)	52.1	.687[2]	41[2]			.0402	.0756
n-Butyl chloride	92.6	.884[2]	172[2]			.0324	.1075
1-Butyne	54.1	[g].650	47		19,590	.0366	.0714
,3,3-dimethyl-	82.2					.0240	.0702

[a]Tube open at lower end.

[b]Sublimes.

[c]Flanged electrodes.

[d]0.0225-Inch stainless-steel electrodes; spark duration, 1 millisec.

[g]Saturation pressure.

COMBUSTION PROPERTIES OF FUELS

indicate references.]

Flammability limit, percent of stoich.		Spon. ig. temp., °F	f/a for max. U_F, percent	Max. U_F(rel)	T_F at f/a for max. U_F, °R	Min. ig. energy, 10^{-5} joule		Quench. dist., in.	
Lean	Rich					Stoich.	Abs. min.	Stoich.	Abs. min.
		802[12]							
		1071							
		811							
		840							
		936							
		845							
			117	149[18]	4355				
[a]53[11]	[a]340[11]	784[12]	119	140[18]	4275	[c]23.5	12.5	0.07	0.05
			119	112[18]	4170				
		824[12]	118	119[18]	4220				
54[19]	330[19]	807-	113	97	4060	76[9]	26[9]	.12	.07
			129	102					
55[19]	351[19]	824	113	92	4055	164	[d]25[15]	.18	.07
55[19]	372[19]	790	113	93	4055				
		863							
50[19]	359[19]	800-	114	94	4055	[c]96	[d]21[15]	.14	.07
58[19]	358[19]	849	116	92	4035	100		.14	
			100	92[14]		53	28	.10	.08
53[19]	353[19]	830[12]	116	111	4175				
			115	109[13]	4215				
		697	131	101[13]	3970				
		615	117	101	4110				
			115	100	4135				
		706	115	106	4150				
		721							
[a]52[11]	[a]307[11]								
		764	115	95[13]	4115				
			109	193[13]	4520	8.22		.04	
						[c]124		.15	
			120	149[18]	4345				
			121	122[18]	4210				

3560

TABLE I. - Continued. PHYSICAL AND

[Numbered superscripts

Fuel	Molecular wt.	Sp. gr.	B.p., °F	ΔH_{vap}, Btu/lb	ΔH_c, gas-gas, Btu/lb	Stoich. mixt. By vol.	Stoich. mixt. By wt.
2-Butyne	54.1	0.697	81		19,440	0.0366	0.0714
d-Camphor	152.2	.990[2]	[b]399[2]			.0153	.0818
Carbon disulfide	76.1	1.263[2]	115[2]	151[2]		.0652	.1841
Carbon monoxide	28.0		-310[2]	91		.2950	.4064
Cyanogen	52.0	.866[2]	-5[2]	186[16]		.0947	.1887
Cyclobutane	56.1	.703[2]	55[2]			.0337	.0679
,ethyl-	84.2					.0227	.0679
,isopropyl-	98.2					.0195	.0679
,methyl-	70.1	.693[2]	97[2]			.0271	.0678
,methylene-	68.2					.0290	.0707
Cyclohexane	84.2	.783	177	154	18,846	.0227	.0679
,ethyl-	112.2	.792	269	133	18,816	.0171	.0679
,methyl-	98.2	.774	214	139	18,797	.0195	.0679
,1-methyl-2-tert-butyl-	154.3					.0125	.0679
Cyclohexene	82.1	.810[2]	181[2]			.0240	.0701
Cyclopentadiene	66.1	.805[2]	109[2]			.0312	.0738
Cyclopentane	70.1	.751	121	167	19,001	.0271	.0678
,methyl-	84.2	.754	161	148	18,930	.0227	.0679
,n-propyl-	112.2	.781	268		18,907	.0171	.0679
Cyclopentene	68.1	.772[2]	112[2]			.0290	.0706
Cyclopropane	42.1	[e].720	-30[2]			.0444	.0679
,cis-1,2-dimethyl-	70.1					.0271	.0678
,trans-1,2-dimethyl-	70.1					.0271	.0678
,ethyl-	70.1					.0271	.0678
,methyl-	56.1	[i].691	41[2]			.0337	.0679
,1,1,2-trimethyl-	84.2					.0227	.0679
trans-Decalin (decahydronaphthalene)	138.2	.874	369			.0142	.0692
n-Decane	142.3	.734	345	119	19,175	.0133	.0666
1-Decene	140.3	.745	339		19,094	.0138	.0679
Diethyl ether	74.1	.714[2]	94[2]	151[2]		.0337	.0896
Dihydropyran	84.1					.0312	.0939
Diisopropyl ether	102.2	.726[2]	154[2]			.0227	.0824

[a]Tube open at lower end.

[c]Flanged electrodes.

[d]0.0225-Inch stainless-steel electrodes; spark duration, 1 millisec.

[e]Measured at -110° F.

[f]Measured at elevated temperatures by Bunsen burner schlieren total-area method and extrapolated to room temperature.

[h]Dry air; 0.97 percent hydrogen in carbon monoxide.

[i]Measured at -4° F.

[redacted]

3560

COMBUSTION PROPERTIES OF FUELS

indicate references.]

Flammability limit, percent of stoich.		Spon. ig. temp., °F	f/a for max. U_F, percent	Max. U_F(rel)	T_F at f/a for max. U_F, °R	Min. ig. energy, 10^{-5} joule		Quench. dist., in.	
Lean	Rich					Stoich.	Abs. min.	Stoich.	Abs. min.
			120	132	4320				
		871							
a18[11]	a1120[11]	248[12]	~102	127[14]		1.5		0.02	
a34[11]	a676[11]	1128[12]	~170	h100[14]					
		1562[12]							
			115	145[13]	4155				
a55[11]	a376[11]		115	115[13]	4125				
			135	100[13]	3900				
			118	114					
			123	132					
48	401	518	117	99[18]	4050	138	d22.3[17]	.16	0.07
a54[11]	a420[11]	507							
45	359	509	125	96[18]	3935		d27[15]		.07
		597							
				103		c86		.13	
			100	101[14]		67		.11	
		725	117	96[18]	4075	c83		.13	
43	368	614	122	92[18]	4010				
		545[12]							
			121	104					
a58[11]	a276[11]	928[12]	113	122[18]	4190	c24	c23	.07	.07
			116	119[13]	4170				
			118	119[13]	4160				
			125	122[13]	4125				
			116	126[13]	4170				
			115	112[13]	4155				
		521-	109	f79[13]	4000				
45	356	449	105	f94[13]	4115				
36	392	471	112	f96[13]	4135				
a55[11]	a2640[11]	366[20]	115	102[13]	4055	49	d28[15]	.10	.08
						c56		.11	
						114		.15	

[redacted]

TABLE I. - Continued. PHYSICAL AND

[Numbered superscripts

Fuel	Molecular wt.	Sp. gr.	B.p., °F	ΔH_{vap}, Btu/lb	ΔH_c, gas-gas, Btu/lb	Stoich. mixt. By vol.	Stoich. mixt. By wt.
Dimethoxymethane	76.1	0.856[2]	111[2]			0.0497	0.1381
Dimethyl ether	46.1		-11[2]			.0652	.1115
Dimethyl sulfide	62.1	.846[2]	100[2]			.0444	.1001
Di-tert-butyl peroxide	146.2					.0179	.0923
Divinyl ether	70.1	.774[2]	102[2]			.0402	.1017
Ethane	30.1		-128	210	20,416	.0564	.0624
,1,1-diphenyl-	182.3	1.006[2]	522[2]			.0118	.0756
Ethene	28.1		-155	208	20,276	.0652	.0680
Ethyl acetate	88.1	.901[2]	171[2]			.0402	.1279
Ethyl alcohol	46.1	.789[2]	173[2]	368[2]		.0652	.1115
Ethylamine	45.1	.706[2]	62[2]	263[16]		.0528	.0873
Ethylene oxide	44.1	1.965[2]	51[2]	250[2]		.0772	.1280
Ethylenimine	43.1	.832[2]	132[2]			.0605	.0962
Furan	68.1	.936[2]	90[2]	172[2]		.0444	.1098
,tetrahydro-	72.1		149[2]			.0366	.0951
,thio- (thiophene)	84.1	1.064[2]	183[2]			.0337	.1017
n-Heptane	100.2	.688	209	136	19,314	.0187	.0661
,3,3-dimethyl-	128.3	.730	279	118		.0147	.0665
1-Heptene	98.2	.702	201		19,202	.0195	.0679
1-Heptyne	96.2	.738	212		19,262	.0205	.0698
Hexadecane	226.4	.777	548	98	19,052	.0085	.0671
1-Hexadecene	224.4	.785	544		19,000	.0086	.0679
1,5-Hexadiene	82.1	.697	139			.0240	.0701
n-Hexane	86.2	.664	156	144	19,391	.0216	.0659
,2,3-dimethyl-	114.2	.717	240	126	19,236	.0195	.0789
1-Hexene	84.2	.678	146		19,262	.0227	.0679
1-Hexyne	82.1	.721	161		19,334	.0240	.0701
3-Hexyne	82.1	.726[2]				.0240	.0701
Hydrogen	2.0		-423[2]	194[2]	51,571	.2950	.0290
Hydrogen sulfide	34.1		-79[2]	237[2]		.1224	.1650

[a]Tube open at lower end.

[c]Flanged electrodes.

[d]0.0225-Inch stainless-steel electrodes; spark duration, 1 millisec.

[f]Measured at elevated temperatures by Bunsen burner schlieren total-area method and extropolated to room temperature.

3560

COMBUSTION PROPERTIES OF FUELS

indicate references.]

Flammability limit, percent of stoich.		Spon. ig. temp., °F	f/a for max. U_F, percent	Max. U_F(rel)	T_F at f/a for max. U_F, °R	Min. ig. energy, 10^{-5} joule		Quench. dist., in.	
Lean	Rich					Stoich.	Abs. min.	Stoich.	Abs. min.
[a]50[11]	[a]330[11]	662[12]	119	117[13]	4010	42 [c]45 [c]76 [c]65		0.09 .09 .12 .11	
		680[12]							
50[19]	272[19]	882[12] 909	112	103	4040	[c]42	[d]24[17]	.09[9]	0.07[9]
41[19] [a]61[11]	>610[19] [a]236[11]	914[12] 907[20] 738[12]	115 ~100	175 83[14]	4275	9.6 142	48	.05 .17	.10
		804[20]	125 100	234[13] 101	4340	240 10.5 48	6.2	.21 .05 .10	.04
						22.5 54 [c]60		.07 .11 .11	
53	450	477-626	122	99	3985	[c]115	[d]24[15]	.15	.07
		505							
		446 464	108	[f]95[13]	4115	[c]93.1		.13	
			118	113					
51	400	501-820[12]	117	99	4030	95[9]	23[9]	.14	.07
52	393	521	118 124	108 124 116[18]	4115 4200 4150				
		1060-[12] 554[12]	-170	679[14]		2.0 [c]7.7	1.8	.025[10] .04	.024[10]

TABLE I. - Continued. PHYSICAL AND

[Numbered superscripts

Fuel	Molecular wt.	Sp. gr.	B.p., °F	ΔH_{vap}, Btu/lb	ΔH_c, gas-gas, Btu/lb	Stoich. mixt. By vol.	Stoich. mixt. By wt.
Isopropyl alcohol	60.1	0.785[2]	180[2]	286[2]		0.0444	0.0969
Isopropylamine	59.1	.690[2]	93[2]			.0383	.0817
Isopropyl chloride	78.5	.859[2]	96[2]			.0422	.1199
Isopropyl mercaptan	76.2	.836[2]	154[2]			.0337	.0922
dl-Limonene	136.2	.842[2]	351[2]	125[16]		.0147	.0706
Methane	16.0		-259	219	21,502	.0947	.0581
,diphenyl-	168.2	1.001[2]	503[2]			.0129	.0763
Methyl alcohol	32.0	.793[2]	148[2]	473[2]		.1224	.1548
Methyl formate	60.1	.975[2]	89[2]	203[2]		.0947	.2181
Naphthalene, 1-ethyl-	156.2	1.012	498			.0138	.0756
,1-methyl-	142.2	1.025	472			.0153	.0764
n-Nonane	128.3	.722	303	124	19,211	.0147	.0665
,2-methyl-	142.3	.732	332			.0133	.0666
n-Octane	114.2	.707	258	129	19,256	.0165	.0663
,2,3-dimethyl-	142.3	.742	327			.0133	.0666
,4-ethyl-	142.3	.744	334			.0133	.0666
,2-methyl-	128.3	.718	290	123		.0147	.0665
,3-methyl-	128.3	.725	292	123		.0147	.0665
,4-methyl-	128.3	.724	288	123		.0147	.0665
1-Octene	112.2	.719	250		19,157	.0171	.0679
1,2-Pentadiene (ethylallene)	68.1	.698	113		19,444	.0290	.0706
cis-1,3-Pentadiene	68.1	.696	111		19,018	.0290	.0706
trans-1,3-Pentadiene (piperylene)	68.1	.681	108		19,016	.0290	.0706
,2-methyl-(cis or trans)	82.1	.724	169			.0240	.0701
1,4-Pentadiene	68.1	.666	79		19,190	.0290	.0706
2,3-Pentadiene	68.1	.700	119		19,399	.0290	.0706
n-Pentane	72.1	.631	97	154	19,499	.0255	.0654
,2,2-dimethyl-	100.2	.678	175	125	19,235	.0187	.0661
,2,3-dimethyl-	100.2	.699	194	130	19,265	.0187	.0661
,2,4-dimethyl-	100.2	.677	177	127	19,253	.0187	.0661

[c]Flanged electrodes.

[d]0.0225-Inch stainless-steel electrodes; spark duration, 1 millisec.

[f]Measured at elevated temperatures by Bunsen burner schlieren total-area method and extrapolated to room temperature.

[j]Unpublished NACA data.

3560

COMBUSTION PROPERTIES OF FUELS

indicate references.]

Flammability limit, percent of stoich.		Spon. ig. temp., °F	f/a for max. U_F, percent	Max. U_F(rel)	T_F at f/a for max. U_F, °R	Min. ig. energy, 10^{-5} joule		Quench. dist., in.	
Lean	Rich					Stoich.	Abs. min.	Stoich.	Abs. min.
		852[20]	100	89[14]		65		0.11	
		.	114	68[13]	4030	200[22]		.19	
						155[22]		.17	
						[c]87		.13	
		505							
46[19]	164[19]	1170-[12]	106	87	4025	33[9]	29[9]	.10[9]	0.08[9]
		962	107	[f]77[13]	4280				
[j]48	[j]408	878[20]	~101	122[14]		21.5	[d]14[15]	.07	.06
						[c]62		.11	
		898							
		1017							
47	434	453							
		418							
51	425	464-							
		447							
		458							
		440							
		442							
		450							
46	384	493							
			119	133[18]	4285				
			120	119[18]	4205				
			119	117[18]	4230				
			115	100[13]	4220				
			115	119[18]	4270				
			119	130[18]	4280				
54	359	544	115	99	4050	[c]82	[d]22[15]	.13	.07
			119	89[18]	4040				
69	437	640	119	94[18]	3995				
			117	92	4025				

TABLE I. - Continued. PHYSICAL AND

[Numbered superscripts

Fuel	Molecular wt.	Sp. gr.	B.p., °F	ΔH_{vap}, Btu/lb	ΔH_c, gas-gas, Btu/lb	Stoich. mixt. By vol.	Stoich. mixt. By wt.
n-Pentane, 2,4-dimethyl-3-ethyl-	128.3	0.742	278	119		0.0147	0.0665
,3,3-dimethyl-	100.2	.698	187	127	19,255	.0187	.0661
,2-methyl-	86.2	.658	140	139	19,356	.0216	.0659
,3-methyl-	86.2	.669	146	140	19,369	.0216	.0659
,2,2,3,3-tetramethyl-	128.3	.761	284	118		.0147	.0665
,2,3,3,4-tetramethyl-	128.3	.759	287	117		.0147	.0665
,2,2,3-trimethyl-	114.2	.720	230	121	19,212	.0165	.0663
,2,2,4-trimethyl- (isooctane)	114.2	.696	211	117	19,197	.0165	.0663
,2,3,3-trimethyl-	114.2	.730	239	123	19,226	.0165	.0663
1-Pentene	70.1	.646	86		19,346	.0271	.0678
,2-methyl-	84.2	.687	141		19,185	.0227	.0679
,4-methyl-	84.2	.669	129		19,225	.0227	.0679
,2,3,4-trimethyl-	112.2	.733	226			.0171	.0679
,2,4,4-trimethyl- (diisobutylene)	112.2	.719	215			.0171	.0679
cis-2-Pentene	70.1	.661	99		19,308	.0271	.0678
,2,4,4-trimethyl-	112.2	.726	221			.0171	.0679
,3,4,4-trimethyl-(cis or trans)	112.2	.743	234			.0171	.0679
trans-2-Pentene	70.1	.653	97		19,280	.0271	.0678
1-Pentyne	68.1	.695	104		19,436	.0290	.0706
,4-methyl-	82.2					.0240	.0702
2-Pentyne	68.1	.716	133		19,338	.0290	.0706
,4-methyl-	82.2					.0240	.0702
α-Pinene	136.2	.858[2]	309[2]			.0147	.0706
Propadiene (see Allene)							
Propane	44.1	[g].508	-44	183	19,929	.0402	.0640
,2-cyclopropyl-	84.2					.0227	.0679
,1-deutero-	45.1					.0402	.0655
,1-deutero-2-methyl-	59.1					.0312	.0660
,2-deutero-2-methyl-	59.1					.0312	.0660
,2,2-dimethyl- (neopentane)	72.1	.597	49	136		.0255	.0654
,1,1-diphenyl-	196.3					.0109	.0750
,2-methyl- (isobutane)	58.1	[g].563	11	158	19,593	.0312	.0649

[a]Tube open at lower end.

[c]Unflanged electrodes.

[d]0.0225-Inch stainless-steel electrodes; spark duration, 1 millisec.

[g]Saturation pressure.

[j]Unpublished NACA data.

[redacted]

3590

COMBUSTION PROPERTIES OF FUELS

indicate references.]

Flammability limit, percent of stoich.		Spon. ig. temp., °F	f/a for max. U_F, percent	Max. U_F(rel)	T_F at f/a for max. U_F, °R	Min. ig. energy, 10^{-5} joule		Quench. dist., in.	
Lean	Rich					Stoich.	Abs. min.	Stoich.	Abs. min.
		734							
60[19]	372[19]	585	115	94	4050				
		580	116	94	4040				
[a]54[11]	[a]344[11]	845							
		818							
		816							
48	360	837-806	117	89[18]	4020	[c]29	28[17]	0.08	0.07
[j]47	[j]370	569-	114	109	4165				
		582	124	102	4025				
		580	117	104	4130				
		495							
		788				[c]175		.18	
[j]49	[j]345		124	111[13]	4035	[c]82	[d]18[15]	.13	.06
		587							
		626							
			122	136	4265				
			120	115[18]	4220				
			115	132[13]	4280				
			125	117[13]	4160				
		506							
51[19]	283[19]	940-	114	100	4050	31[23]	25[23]	.08[9]	.07[9]
			118	109					
			110	86					
			110	86[13]					
			110	86[13]					
54[19]	283[19]	853		85	4060	[c]157		.17	
		870							
60[19]	321[19]	890-	110	90	4065				

[redacted]

TABLE I. - Concluded. PHYSICAL AND

[Numbered superscripts

Fuel	Molecular wt.	Sp. gr.	B.p., °F	ΔH_{vap}, Btu/lb	ΔH_c, gas-gas, Btu/lb	Stoich. mixt. By vol.	Stoich. mixt. By wt.
Propene	42.1	[g]0.522	-54	188	19,683	0.0444	0.0679
,2-cyclopropyl-	82.2					.0240	.0702
,2-methyl-	56.1	[g].600	20	169	19,346	.0337	.0679
Propionaldehyde	58.1	.807[2]	120[2]			.0497	.1054
n-Propyl alcohol	60.1	.804[2]	207[2]	295[2]		.0444	.0969
n-Propyl chloride	78.5	.890[2]	117[2]			.0422	.1199
Propylene oxide (1,2-epoxypropane)	58.1	.831[2]	95[2]			.0497	.1054
1-Propyne	40.1		-10		19,849	.0497	.0728
Silane, n-butyl-	88.2					.0255	.0800
,diethyl-	88.2					.0255	.0800
,ethyl-	60.1					.0402	.0872
,isobutyl-	88.2					.0255	.0800
,methyl-	46.1	[l].620	-70[2]			.0564	.0956
,tetramethyl-	88.2	.645[2]	80[2]			.0255	.0800
,trimethyl-	74.2					.0312	.0828
,vinyl-	58.1					.0444	.0937
Spiropentane	68.1					.0290	.0706
1-Tetradecene	196.4	.775	484		19,022	.0099	.0679
Tetrahydropyran	86.1	.854[2]	179[2]			.0290	.0893
Tetralin (tetrahydronaphthalene)	132.2	.971[2]	405[2]			.0158	.0738
Toluene (methylbenzene)	92.1	.872	231	156	17,601	.0227	.0743
Triethylamine	101.2	.723[2]	193[2]			.0210	.0753
Turpentine (mainly α-pinene)							
Vinyl acetate	86.1	.932[2]	162[2]			.0444	.1388
Gasoline, 73-octane							
Gasoline, 100-octane							
Jet fuel, grade JP-1[m]	150	.81			[n]18,500	.013	.068
Jet fuel, grade JP-3[m]	112	.76			[n]18,700	.017	.068
Jet fuel, grade JP-4[m]	126	.78			[n]18,700	.015	.068
Jet fuel, grade JP-5[m]	170	.83			[n]18,500	.011	.069

[c]Flanged electrodes.

[d]0.0225-Inch stainless-steel electrodes; spark duration, 1 millisec.

[f]Measured at elevated temperatures by Bunsen burner schlieren total-area method and extrapolated to room temperature.

[g]Saturation pressure.

[j]Unpublished NACA data.

[k]Estimated from explosion curves.

[l]Measured at -71° F.

[m]Properties are given for average quality jet fuels.

[n]Lower heating valve; i.e., liquid to gas.

[redacted]

3560

COMBUSTION PROPERTIES OF FUELS

indicate references.]

Flammability limit, percent of stoich.		Spon. ig. temp., °F	f/a for max. U_F, percent	Max. U_F(rel)	T_F at f/a for max. U_F, °R	Min. ig. energy, 10^{-5} joule		Quench. dist., in.	
Lean	Rich					Stoich.	Abs. min.	Stoich.	Abs. min.
48	272	1036-	114	112	4210	28.2		0.08	
			119	115					
			114	96					
			131	126[13]	3855	49		.10	
		812[20]							
						108[22]		.15	
47[19]			128	179[13]	4170	20[23]	[d]14[15]	.07	0.06
			119	179	4450	16[23]	11.5[23]	.06	.05
				[j]~380					
		[j,k]~491	123	285[25]					
		[j,k]~455		>285[25]					
				[j]~330					
		[k]~266[24]		[j]~640					
		[k]~846[24]	119	154[25]					
		[k]~594[24]	119	236[25]					
		[k]~207[24]	123	[j]690					
			120	154					
		463							
			~90	105[14]		121	[d]22[15]	.15	.07
		794	101	[f]84[13]	4175				
43	322	1054-	105	[f]90[13]	4220				
						115[22]		.15	
		486[12]							
						[c]120		.15	
		570[12]							
		800-950							
		[j]480							
		[j]502							
		468[12]							

3560

TABLE II. - EXPERIMENTAL BURNING VELOCITIES OF

PROPANE-AIR MIXTURES

Method	Maximum burning velocity, ft/sec	Stoichiometric fuel-air ratio for maximum burning velocity, percent	Reference
Tube	1.28	113	26
Bunsen burner schlieren	1.41	106	27
Bunsen burner shadowgraph	1.53	110	14

APPENDIX REFERENCES

1. Rossini, Frederick D., et al.: Selected Values of Physical and Thermodynamic Properties of Hydrocarbons and Related Compounds. Carnegie Press (Pittsburgh), 1953.

2. Hodgman, Charles D., ed.: Handbook of Chemistry and Physics. Thirty-fifth ed., Chem. Rubber Pub. Co., 1953-1954.

3. Spakowski, Adolph E.: Pressure Limits of Flame Propagation of Pure Hydrocarbon-Air Mixtures at Reduced Pressure. NACA RM E52H15, 1952.

4. Jackson, Joseph L.: Spontaneous Ignition Temperatures - Commercial Fluids and Pure Hydrocarbons. Ind. and Eng. Chem., vol. 43, no. 12, Dec. 1951, pp. 2869-2870.

5. Simon, Dorothy Martin: Flame Propagation. III. Theoretical Considerations of the Burning Velocities of Hydrocarbons. Jour. Am. Chem. Soc., vol. 73, no. 1, Jan. 1951, pp. 422-425.

6. Levine, Oscar, and Gerstein, Melvin: Fundamental Flame Velocities of Pure Hydrocarbons. III - Extension of Tube Method to High Flame Velocities - Acetylene-Air Mixtures. NACA RM E51J05, 1951.

7. Huff, Vearl N., Gordon, Sanford, and Morrell, Virginia E.: General Method and Thermodynamic Tables for Computation of Equilibrium Composition and Temperature of Chemical Reactions. NACA Rep. 1037, 1951. (Supersedes NACA TN's 2113 and 2161.)

8. Calcote, H. F., Gregory, C. A., Jr., Barnett, C. M., and Gilmer, Ruth B.: Spark Ignition - Effects of Molecular Structure. Ind. and Eng. Chem., vol. 44, no. 11, Nov. 1952, pp. 2656-2660.

9. Blanc, M. V., Guest, P. G., von Elbe, Guenther, and Lewis, Bernard: Ignition of Explosive Gas Mixtures by Electric Sparks. III. Minimum Ignition Energies and Quenching Distances of Mixtures of Hydrocarbons and Ether with Oxygen and Inert Gases. Third Symposium on Combustion and Flame and Explosion Phenomena, The Williams & Wilkins Co. (Baltimore), 1949, pp. 363-367.

10. Lewis, Bernard, and von Elbe, Guenther: Combustion, Flames and Explosions of Gases. Academic Press, Inc. (New York), 1951, pp. 408-414.

11. Coward, H. F., and Jones, G. W.: Limits of Flammability of Gases and Vapors. Bull. 503, Bur. Mines, 1952.

12. Scott, G. S., Jones, G. W., and Scott, F. E.: Determination of Ignition Temperatures of Combustible Liquids and Gases. Anal. Chem., vol. 20, no. 3, Mar. 1948, pp. 238-241.

13. Wagner, Paul, and Dugger, Gordon L.: Flame Propagation. V. Structural Influences on Burning Velocity. Comparisons of Measured and Calculated Burning Velocity. Jour. Am. Chem. Soc., vol. 77, no. 1, Jan. 5, 1955, pp. 227-231.

14. Calcote, Hartwell F., Barnett, Charles M., and Irby, Moreland R.: The Burning Velocity of Various Compounds by the Bunsen Burner Method. Paper presented at meeting Am. Chem. Soc. (Atlantic City), Sept. 18-23, 1949.

UNCLASSIFIED

15. Metzler, Allen J.: Minimum Spark-Ignition Energies of 12 Pure Fuels at Atmospheric and Reduced Pressure. NACA RM E53H31, 1953.

16. Perry, John J., ed.: Chemical Engineers' Handbook. Third ed., McGraw-Hill Book Co., Inc., 1950, p. 216.

17. Metzler, Allen J.: Minimum Ignition Energies of Six Pure Hydrocarbon Fuels of the C_2 and C_6 Series. NACA RM E52F27, 1952.

18. Simon, Dorothy M.: Flame Propagation - Active Particle Diffusion Theory. Ind. and Eng. Chem., vol. 43, no. 12, Dec. 1951, pp. 2718-2721.

19. DiPiazza, James T., Gerstein, Melvin, and Weast, Robert C.: Flammability Limits of Hydrocarbon-Air Mixtures. Reduced Pressures. Ind. and Eng. Chem., vol. 43, no. 12, Dec. 1951, pp. 2721-2725.

20. The Associated Factory Mutual Fire Insurance Cos.: Properties of Flammable Liquids, Gases, and Solids. Ind. and Eng. Chem. (Ind. ed.), vol. 32, no. 6, June 1940, pp. 880-884.

21. Jost, Wilhelm: Explosion and Combustion Processes in Gases. McGraw-Hill Book Co., Inc., 1946.

22. Fenn, John B.: Lean Flammability Limit and Minimum Spark Ignition Energy. Ind. and Eng. Chem., vol. 43, no. 12, Dec. 1951, pp. 2865-2868.

23. Calcote, H. F., et al.: Minimum Spark Energy Correlation with Ramjet and Turbojet Burner Performance. TP-36, Experiment, Inc. (Richmond, Va.), Mar. 1950. (Final Rep. No. 1 to Bur. Aero. under Contract NOa(s) 10115.)

24. Schalla, Rose L.: Explosion and Combustion Properties of Alkylsilanes. I. Temperature-Composition Limits of Explosion for Methyl-, Dimethyl-, Trimethyl-, Tetramethyl-, and Vinylsilanes at Atmospheric Pressure. NACA RM E53L01, 1954.

25. Gerstein, Melvin, Wong, Edgar L., and Levine, Oscar: Flame Velocities of Four Alkylsilanes. NACA RM E51A08, 1951.

26. Gerstein, Melvin, Levine, Oscar, and Wong, Edgar L.: Flame Propagation. II. The Determination of Fundamental Burning Velocities of Hydrocarbons by a Revised Tube Method. Jour. Am. Chem. Soc., vol. 73, no. 1, Jan. 1951, pp. 418-422.

27. Dugger, Gordon L., and Grabb, Dorothy D.: Flame Velocities of Propane- and Ethylene-Oxygen-Nitrogen Mixtures. NACA RM E52J24, 1953.

UNCLASSIFIED
~~CONFIDENTIAL~~

NACA-Langley - 4-1-55 - 350

~~CONFIDENTIAL~~

UNCLASSIFIED

NASA Technical Library
3 1176 01435 7306

UNCLASSIFIED

~~CONFIDENTIAL~~